universität wien

DISSERTATION

Titel der Dissertation

"Geochemical, mineralogical, and petrographic investigations of the Eyreville drill cores from the Chesapeake Bay impact structure"

Verfasserin

Mag. Kateřina Bartošová

angestrebter akademischer Grad

Doktorin der Naturwissenschaften (Dr. rer. nat.)

Wien, im Januar 2010

Studienkennzahl lt Studienblatt:	A 091 426
Dissertationsgebiet lt. Studenblatt:	Erdwissenschaften
Betreuer:	Prof. Dr. Christian Koeberl

PREFACE:

The thesis summarizes three years of work at the Department of Lithospheric Research, University of Vienna, on the Eyreville drill cores that were obtained from the ICDP-USGS Deep Drilling Project at the Chesapeake Bay Impact Structure. For the studies, 166 drill core samples were collected. The first task was a detailed description, as well as geochemical analyses of all samples. As the Chesapeake Bay project was international, interaction with the other scientific teams was essential. The cooperation with the research group of the Natural History Museum in Berlin was especially fruitful. The detailed analyses of the sampled impactites resulted in several papers that were published in the Geological Society of America Special Paper 458 in 2009 (which constitutes the first joint publication of the international research team on the Eyreville drill cores) and are part of this thesis. The results also contributed to the construction of the detailed geologic column that was established by the USGS scientific team.

My investigations focused mainly on the impact breccia interval. Chapter 6 presents petrographic observations of the impact breccia samples on macro- and microscopic scale. These analyses, together with core observations and comparison of matrix, clast, and melt contents, form the basis for a detailed core stratigraphy. The impact breccia interval was subdivided into several units and their formation is discussed. Detailed descriptions of melt particles and shock metamorphic features are also included.

Chapter 7 deals with the impact breccia from a geochemical point of view. In this study, analyses of our samples were completed with data from samples analyzed by the Berlin group. Trends in chemical composition versus depth as well as contents of siderophile elements were studied. Geochemical mixing calculations were performed to model the contribution of the target rocks into forming of the impact breccia interval.

Appendix 1 is a paper by W. U. Reimold et al. (me as second author), which presents detailed observations of the Exmore breccia. In this paper, analyses of more than 100 samples are discussed. My contributions included detailed petrographic analyses, macro- and microscopic description, as well as modal point counting and geochemical data of the Vienna sample suit. I also summarized the general results of my observations and provided several photographs for the paper. Combining of data from both Berlin and Vienna sample suits enabled to subdivide the Exmore breccia interval as well as suggest its formation mechanisms.

Appendix 2, a paper by R. T. Schmitt et al. (me as second author), summarizes geochemical investigations of more than 300 samples from the Eyreville cores (from both Vienna and Berlin sample suites). The paper presents chemical data obtained by X-ray fluorescence (performed at the Natural History Museum in Berlin) and instrumental neutron activation analysis (INAA, performed at the Department of Lithospheric

Research, University of Vienna). Average compositions of the main lithologies as well as trends with depth in the core are discussed. I was primarily involved with the INAA analyses and provided the petrographic characteristics of the Vienna sample suite.

Appendix 3 presents platinum group element (PGE) analyses of mainly the impact breccia samples by I. McDonald et al. (me as second author). Based on initial geochemical analyses, I selected impact breccia samples with enhanced siderophile element contents for detailed PGE investigations. Also, several samples of target rocks were analyzed for comparison. I provided petrographic details for all studied samples. The PGE data did not suggest presence of an extraterrestrial component and thus did not reveal the nature of the Chesapeake impactor.

Other chapters of the thesis comprise first author papers submitted to the journal *"Meteoritics and Planetary Science"* (accepted or under review) that present further detailed investigations of the impactite samples. Chapter 8 presents studies of melt particles from the impact breccia interval. Based on previous investigations by optical microscope, selected thin sections were analyzed by electron microprobe and microRaman spectrometry to obtain information on chemical composition and mineral phases. Melt particles were grouped into several categories and their precursors are discussed.

Chapter 9 discusses shock metamorphism effects in the impact breccia interval. Mainly planar deformation features (PDFs) were investigated. Using optical microscopy, proportions of shocked quartz grains in clasts of different lithologies were counted and changes with depth and differences among the lithologies are discussed. Crystallographic orientations of PDFs in several clasts were determined using the universal stage.

Chapter 10 is focused on the gravelly sand interval. Detailed petrographic studies, including modal point counting, were complemented by bulk rock X-ray diffraction analyses. Additionally, clay fraction components were separated and determined by X-ray diffraction. Chemical analyses of all samples were performed. The results are presented in the context of previous investigations and the formation of the gravelly sand interval is discussed.

ACKNOWLEDGEMENTS:

I thank my supervisor Christian Koeberl for supervising the thesis, encouragement, assisting me with writing scientific papers, providing me with the opportunity to attend many international conferences and workshops, and financial support through his FWF grant.

I thank W. Uwe Reimold (Museum of Natural History, Berlin, Germany) for valuable help, many discussions, and successful cooperation on many scientific papers.

All the work would have been much more difficult without the support of my colleagues. Here I want to thank to my dear colleague and friend Ludovic Ferrière, who helped me especially in my first months in Vienna. Most of my knowledge about impact cratering I gained from him and from the literature he passed along to me. Later we cooperated on several abstracts and manuscripts.

I thank Dieter Mader for his assistance in many aspects. He helped especially with the geochemical analyses (INAA and mass spectrometry) as well as interpretation of the chemical data. Further his frequent IT-support, and help with translations from and to German language (including the thesis abstract) is very much appreciated.

I would like to thank following persons for help with various analytical methods:

M. Bichler, H. Böck, E. Klapfer, H. Schachner, G. Steinhauser, J. Sterba, and M. Villa (Atominstitut Vienna) for the irradiations of samples for INAA.

F. Brandstätter (Natural History Museum, Vienna) for assistance with SEM-EDX analyses.

P. Czaja and L. Hecht (Museum of Natural History, Berlin, Germany) for technical assistance with the electron microprobe in Berlin.

R. T. Schmitt (Museum of Natural History, Berlin, Germany), S. Farrell-Turner (Wits Univ., Johannesburg, South Africa), and P. Nagl and P. McDonald (Univ. Vienna) for XRF analyses.

S. Gier (Univ. Vienna) for XRD analyses.

E. Libowitzky (Univ. Vienna) for assistance with microRaman spectroscopy.

W. Füzi, L. Slawek, and S. Hrabe (Univ. Vienna) for thin section preparations.

I thank F. Brandstätter, H. Dypvik, L. Ferrière, S. Gier, L. Hecht, J. W. Horton, C. Koeberl, E. Libowitzky, D. Mader, I. McDonald, W. U. Reimold, R. T. Schmitt, and G. N. Townsend for cooperation on scientific papers, including important help and discussions.

I thank P. Claeys, L. E. Edwards, B. M. French, S. Goderis, R. L. Gibson, G. S. Gohn, J. Morrow, G. Osinski, C. W. Poag, M. Poelchau, and A. Wittmann for interesting discussions and/or review of some of the papers that are part of this thesis.

I thank also the staff of the university, namely F. Mikysek and A. Vogt for secretarial help and N. Irnberger for the printing of conference posters.

Colleagues and students from our small Impact Cratering Group are thanked for support, encouragement, help, and friendly discussions, namely Tsolmon Amgaa, Miruts Hagos, Andre Dunford, Tamara Goldin, Ana Cernok, Liang Chen, Bettina Schenk, and Ildiko Gyollai.

The work on the Eyreville drill core project was supported by the Austrian FWF grant P18862-N10 to Christian Koeberl.
I thank the SYNTHESYS (DE-TAF-5452) for supporting my work at the Museum of Natural History in Berlin.

The drilling at Eyreville was supported by ICDP, USGS, and NASA. We appreciate the work of general contractor DOSECC and drilling operator Major Drilling, USA. The help of the staff at the USGS National Center, Reston, during the sampling process is appreciated.

I thank the Planetary Studies Foundation, Sokendai, and the Barringer Family Fund for student travel grants that enabled me to attend international conferences.

Finally I would like to thank my family. I thank my parents for support and encouragement during all my studies. I want to thank to my brother-in-law and his family, who let me share a flat with them during my studies in Vienna and made me feel like being at home. Special thanks belong to my dear husband for his support and immense love and patience.

ABSTRACT:

The late Eocene Chesapeake Bay impact structure is 35.3 Myr old and ~85 km in diameter. Three stacked cores (A, B, and C) were drilled to a total depth of 1766 m in years 2005–2006 at Eyreville Farm, Northampton County, Virginia, USA, located in the central moat of the impact structure. The project was a joint International Continental Drilling Program (ICDP) and U.S. Geological Survey (USGS) collaboration. This thesis presents investigations of 166 samples of impactites from Eyreville cores A and B. All samples were described macro- and microscopically and their major and trace element composition was determined. Further work was focused on the impact breccia interval (1397–1551 m depth) and the overlying gravelly sand interval (1371–1397 m depth).

The impact breccia interval consists mostly of suevite, but two thin layers of impact melt rock were found in the upper part of the interval and large blocks of cataclastic gneiss occur in the lower part. The impact breccia interval has been divided into six subunits based on the differences in content of matrix, melt, and clasts of different lithologies. Generally the abundance of lithic clasts increases and amount of melt particles decreases with increasing depth. The bottom part is a ground surge breccia, whereas towards the top the fallback material becomes more abundant and is dominant in the uppermost part of the interval. Various shock metamorphic and related effects were noted in the impact breccias, including rare planar fractures (PFs) and abundant planar deformation features (PDFs) in quartz, common “toasted” appearance of quartz, occasional ballen silica, rare PDFs in feldspar, and kink banding in mica.

Shock metamorphic effects were studied in detail. The proportion of shocked quartz grains (grains displaying PFs and/or PDFs) was investigated in clasts of different lithologies from the impact breccia interval. No linear trend with depth was found, although the highly shocked clasts become generally less abundant with depth. More important differences were found among clasts of different lithologies, e.g., mostly minimally shocked clasts from the crystalline basement versus abundant highly shocked clasts from the overlying sedimentary rocks. In addition, the crystallographic orientations of PDFs were determined (using universal stage measurements) in quartz grains of several clasts.

The polymict impactites show a decrease in the SiO_2 content and slight increases of the TiO_2, Al_2O_3, and Fe_2O_3 abundances, with depth. This is in agreement with an increase of the schist/gneiss component with depth. Siderophile element concentrations are lower than in, e.g., the target schists, and do not indicate the presence of an extraterrestrial component. Geochemical harmonic least square mixing (HMX) calculations suggest that the main components of the polymict impactites of the impact breccia interval are basement-derived rocks (gneiss/schist) together with a significant sedimentary component

(probably derived mainly from the Cretaceous Potomac Formation) and possibly a pegmatite/granite and amphibolite component.

Melt particles were grouped into six different types, primarily based on their appearance under optical microscope (e.g., color, shape, inclusions). Some common melt types occur over a wide depth range, whereas other types are found only in the impact melt rock intervals. Several melt particles of each type were analyzed by electron microprobe. Average composition of each melt type was determined and possible precursors were discussed. The observations, including HMX calculations, suggest a predominance of sedimentary precursors. Mineral phases in the melt (i.e., undigested clasts, quench crystals, as well as secondary phases) were analyzed by electron microprobe and microRaman spectrometry.

The gravelly sand interval of the Eyreville drill core consists of grayish, poorly sorted and poorly consolidated sand. The matrix comprises 30 to 40 vol% and includes clasts of mostly mono- and polycrystalline quartz and less abundant K-feldspar. Other minerals are only accessory. The main clay fraction components are smectite and kaolinite. The gravelly sand is non-marine, as indicated by the absence of marine microfossils and glauconite. The composition is very silica-rich (>80 wt% of SiO_2). Results of our investigations are in agreement with the hypothesis that the gravelly sand interval was formed by an avalanche during the crater modification and the material originated from the non-marine Potomac Formation.

The Eyreville core impactites represent a complex series of depositional events following the shallow-marine Chesapeake Bay impact event. Probably all the lithologies in the core are allochthonous. The deposition mechanism of the impactites changed from ground-surge to fallout, which was soon interrupted by rock avalanches and resurge of the ocean water with sediments. Shock metamorphism effects are present in the impact and resurge breccias, but the allochthonous crystalline blocks are unshocked.

ZUSAMMENFASSUNG:

Der ICDP-USGS Eyreville Bohrkern wurde in den Jahren 2005-2006 im zentralen Graben der spät-Eozänen Chesapeake Bay Impaktstruktur, nahe der Eyreville Farm (Northampton County, Virginia, USA) erbohrt. Die vorliegende Dissertation präsentiert petrografische und geochemische Analysen von 166 Impaktgesteinsproben der Eyreville-Bohrkerne A und B. Weiters wurden speziell die Intervalle der Impaktbrekzien und der kieseligen Sande des Bohrkerns detailliert untersucht.

Das Impaktbrekzien-Intervall besteht hauptsächlich aus Sueviten, aber es kommen auch zwei dünne Lagen Impaktitschmelzen und große kataklastische Gneisblöcke vor. Dieses Intervall wurde auf Grund der Unterschiede im Matrix-, Schmelzen- und Klastengehalt in sechs Untereinheiten unterteilt. Im Liegenden der Impaktbrekzien kommt eine Dichtestrom-Brekzie vor, wohingegen gegen das Hangende Rückfall (fall-back)-Material häufiger wird. Es wurden verschiedene schockmetamorphe und ähnliche Effekte verzeichnet. In den Gesteinsbruchstücken (Klasten) wurde die Häufigkeitsverteilung geschockter Quarzkörner ermittelt, sowie mittels Universal-Drehtisch die Orientierung der Schocklamellen dieser Quarzkörner bestimmt. Mit zunehmender Tiefe verringert sich die Häufigkeit der stark geschockten Klasten; weiters zeigen Klasten unterschiedlicher Lithologien unterschiedliche Schockintensitäten. Die Zusammensetzung der polymikten Impaktite zeigt mit zunehmender Tiefe einige Unterschiede. Die Konzentration der siderophilen Elemente weist auf keine Präsenz einer extraterrestrischen Komponente hin. Geochemische Mischungsberechnungen lassen vermuten, dass die Hauptkomponenten der polymikten Impaktite aus grundgesteinsbezogenen Gneisen/Schiefern und einer signifikanten sedimentären Komponente bestehen. Basierend auf optischen und elektronenmikroskopischen Beobachtungen, sowie Elektronenmikrosonden-Analysen, konnten die Schmelzpartikel in sechs unterschiedliche Typen gruppiert werden. Diese Beobachtungen, zusammen mit den Mischungsberechnungen, legen einen vorwiegend sedimentären Vorläufer der Schmelzen nahe.

Das Intervall der kieseligen Sande besteht aus schlecht sortierten unkonsolidierten Sanden, hauptsächlich zusammengesetzt aus Quarzen, Kalifeldspäten, Smektiten und Kaoliniten. Die Untersuchungsergebnisse bestätigen die Entstehung der kieseligen Sande aus einer vom Impakt induzierten Gesteinslawine, bestehend aus Material der nichtmarinen Potomac-Formation.

CONTENTS:

Preface I
Acknowledgements III
Abstract V
Zusammenfassung VII

CHAPTER 1: IMPACT CRATERING 1
1.1 History of impact research 1
1.2 General introduction to impact cratering 2
1.3 Crater morphology 4
1.3.1 Simple craters 4
1.3.2 Complex craters 5
1.3.3 Multiring basins 6
1.4 Impact crater formation 6
1.4.1 Contact and compression stage 7
1.4.2 Excavation stage 7
1.4.3 Modification stage 8
References 10

CHAPTER 2: SHOCK METAMORPHIC AND GEOCHEMICAL SIGNATURES IN TARGET ROCKS AND MINERALS 13
2.1 Introduction 13
2.2 Classification of impactites 16
2.2.1 Proximal impactites 16
2.2.1.1 Shocked rocks 16
2.2.1.2 Impact breccias 16
2.2.1.2.1 Monomict impact breccia 16
2.2.1.2.2 Lithic (impact) breccia 17
2.2.1.2.3 Suevite 17
2.2.1.2.4 Dyke breccias 18
2.2.1.3 Impact melt rocks 19
2.2.2 Distal impactites 20
2.2.2.1 Consolidated – Tektites and microtektites 20
2.2.2.2 Unconsolidated - Airfall beds 22
2.2.3 Impactites from multiple impacts 22
2.3 Shock metamorphism effects 23
2.3.1 Shatter cones 23
2.3.2 Shock metamorphism effects in quartz 24
2.3.2.1 Planar microstructures 24
2.3.2.1.1 Planar fractures (PFs) 24
2.3.2.1.2 Planar deformation features (PDFs) 24
2.3.2.2 Mosaicism 25
2.3.2.3 Changes in physical characteristics 26
2.3.3 Shock metamorphism effects in other minerals 26
2.3.4 High-pressure polymorphs 27
2.3.4.1 High pressure polymorphs of quartz 27
2.3.4.2 High pressure polymorphs of other minerals 27
2.3.5 Diaplectic glasses 28
2.3.6 Impact melts 28

2.3.7 Other associated features 30
2.3.7.1 Toasted quartz 30
2.3.7.2 Ballen silica 31
2.4 Geochemical signatures of impact structures 31
2.4.1 Siderophile elements and platinum group elements (PGE) 32
2.4.2 The Os isotopic system 32
2.4.3 The Cr isotopic system 32
References 34

CHAPTER 3: CHESAPEAKE BAY IMPACT STRUCTURE 39
3.1 Introduction 39
3.2 Geology of the Atlantic Coastal Plain 39
3.3 Discovery of the Chesapeake Bay impact structure 42
3.4 Size and structure of the Chesapeake Bay impact structure 42
3.5 Geochemical studies and dating of the Chesapeake Bay impact structure 45
3.6 North American tektites 46
3.7 Deep drilling at the Chesapeake Bay impact structure 46
3.8 Eyreville drill core 49
References 52

CHAPTER 4: LATE EOCENE IMPACTS AND CLIMATE CHANGES 59
4.1 The Late Eocene period and Eocene impacts 59
4.2 Late Eocene global ejecta 60
4.3 Late Eocene climate changes 61
4.4 Late Eocene extinctions 63
4.5 Massignano Eocene/Oligocene (E/O) global stratigraphic section and point (GSSP) 63
4.6 Extinctions after Chesapeake Bay (and Popigai) impact? 65
References 67

CHAPTER 5: METHODOLOGY 71
5.1 Samples 71
5.1.1 Sampling of the Eyreville drill cores 71
5.1.2 Samples documentation and database 72
5.1.3 Bulk rock powder preparation 73
5.1.4 Thin section preparation 73
5.2 Analytical methods 73
5.2.1 X-ray fluorescence (XRF) 73
5.2.1.1 Sample preparation 74
5.2.1.2 XRF Analysis 74
5.2.1.3 Data processing 75
5.2.1.3 Loss on ignition 75
5.2.1.4 Details on XRF measurements presented in the thesis 76
5.2.2 Instrumental neutron activation analysis (INAA) 77
5.2.2.1 Sample preparation 77
5.2.2.2 Irradiation 78
5.2.2.3 Detection 79
5.2.2.4 Data processing 79
5.2.2.5 Details on INAA measurements presented in the thesis 79
5.2.3 Optical microscopy 81

5.2.4 Universal stage measurements 82
5.2.4.1 Mounting the U-stage 82
5.2.4.2 Measuring the orientation of the c-axis 82
5.2.4.3 Determining of PDF orientations 83
5.2.4.4 Plotting the results of the measurements 83
5.2.5 X-ray diffraction (XRD) 84
5.2.5.1 XRD analysis by a diffractometer 85
5.2.5.2 Evaluation of results 86
5.2.5.3 Details on XRD analyses presented in the thesis 86
5.2.5.4 Clay fraction sample preparation 87
5.2.6 Scanning electron microscopy with energy dispersive X-ray spectrometry (SEM-EDS) 87
5.2.6.1 Electron-specimen interaction 88
5.2.6.2 Electron microscope 88
5.2.6.3 Energy dispersive spectrometry (EDS) 89
5.2.6.4 Details on SEM-EDS measurements presented in the thesis 90
5.2.7 Electron microprobe (EMP) 91
5.2.7.1 Wavelength dispersive spectrometry (WDS) 91
5.2.7.2 Details on EMP measurements presented in the thesis 91
5.2.8 Raman spectroscopy 92
5.2.8.1 Raman scattering 92
5.2.8.2 MicroRaman spectrometer 93
5.2.8.3 Details on microRaman measurements presented in the thesis 94
5.2.9 Mass spectrometry 94
5.2.9.1 Gas source mass spectrometry 94
5.2.9.2 Magnetic sector mass spectrometer 94
5.2.9.3 Faraday cup detector 95
5.2.9.4 Carbon stable isotope analysis 95
5.2.9.5 Details on carbon isotopic ratio measurements presented in the thesis 96
References 97

CHAPTER 6:
Petrographic and shock metamorphic studies of the impact breccia section (1397 – 1551 m depth) of the Eyreville drill core, Chesapeake Bay impact structure, USA (K. Bartosova, L. Ferrière, C. Koeberl, W.U. Reimold, and S. Gier)
101

CHAPTER 7:
Geochemistry of the impact breccia section (1397 – 1551 m depth) of the Eyreville drill core, Chesapeake Bay impact structure, USA (K. Bartosova, D. Mader, R. T. Schmitt, L. Ferrière, C. Koeberl, W.U. Reimold, and Franz Brandstätter)
133

CHAPTER 8:
Melt in the impact breccias from the Eyreville drill core, Chesapeake Bay impact structure, USA (K. Bartosova, L. Hecht, C. Koeberl, E. Libowitzky, and W.U. Reimold)
171

CHAPTER 9:
Shock-metamorphism investigations of quartz grains in clasts from impact breccia of the Eyreville drill core, Chesapeake Bay impact structure, USA (K. Bartosova and C. Koeberl)
231

CHAPTER 10:
Petrography, mineralogy, and geochemistry of deep gravelly sand in the Eyreville B core, Chesapeake Bay impact structure (K. Bartosova, S. Gier, J.W. Horton Jr., C. Koeberl, D. Mader, and H. Dypvik)
257

CHAPTER 11: CONCLUSIONS 307

APPENDIX 1:
Petrographic observations on the Exmore breccia, ICDP-USGS drilling at Eyreville, Chesapeake Bay impact structure, USA (W.U. Reimold, K. Bartosova, R.T. Schmitt, B. Hansen, C. Crasselt, C. Koeberl, A. Wittmann, and D.S. Powars)
309

APPENDIX 2:
Geochemistry of impactites and crystalline basement-derived lithologies from the ICDP-USGS Eyreville A and B drill cores, Chesapeake Bay impact structure, Virginia, USA (R. T. Schmitt, K. Bartosova, W.U. Reimold, D. Mader, A. Wittmann, C. Koeberl, and R.L. Gibson)
353

APPENDIX 3:
Search for a meteoritic component in impact breccia from the Eyreville core, Chesapeake Bay impact structure: Considerations from platinum group element contents (I. McDonald, K. Bartosova, and C. Koeberl)
415

APPENDIX 4: SAMPLE LIST 427

Curriculum Vitae 431
List of publications 433

CHAPTER 1: IMPACT CRATERING

1.1 History of impact research

Impact cratering is a relatively young field of geology. Although some impact craters are relatively young, well-preserved, and exposed on the Earth's surface (e.g., the famous Barringer Meteor Crater, Arizona, USA), it took a long time before their real origin was recognized. Only in the second half of the 20th century it was generally accepted that asteroidal and cometary impacts are common and important events in the solar system.

The formation of features now known as impact craters was previously explained by generally accepted geological processes as volcanism and related processes. Similarly, although meteorite falls were observed many times in the history, their origin was mysterious for a long time. It was thought that meteorites were formed within the upper atmosphere (hypothesis preferred by, e.g., Aristotle or even Alexander von Humboldt) or that they were of lunar volcanic origin (explanation by, e.g., Georg C. Lichtenberg). In 1794 Ernst F. F. Chladni published an important book, where he proposed that meteor stones and iron masses entered the atmosphere from cosmic space (Marvin, 2007). This was a new daring idea because at that time it was believed that "1) fragments of rock and metal do not fall from the sky, and 2) no small bodies exist in space beyond the Moon" (Marvin, 2007). The first controversy was overcome by more eye-witnessed meteorite falls. Also chemical and mineralogical analyses of the meteorites by Edward C. Howard and Jacques-Louis de Bournon showed that the meteorites are different from the Earth's crustal rocks (Marvin, 2007). Later, it was discovered that the solar system is not so "empty" as it had been thought and that besides planets there are many small bodies. First asteroid – Ceres – was discovered on the 1st of January 1801 by Giuseppe Piazzi. Today, thank to the development of space exploration, it is well known that impact craters are very abundant on other planets and cosmic bodies, although the distance complicates their investigations. But also these craters, for example on the Moon, were first thought to be of volcanic origin. Today it is generally accepted that most of the craters on bodies of the Solar System are of impact origin (Reimold and Koeberl, 2008), although on some planets and moons (e.g., Venus and Mars) volcanic craters occur as well.

Recent events prove that impact cratering is an important geologic process that continues to shape the surfaces of planets in our solar system. The multiple impact of fragments of comet Schumacher-Levy 9 on Jupiter in 1994 provided further evidence that impacts need to be seriously considered as common events in the solar system. There are also two very recent small craters, for which the meteorite fall was observed - Sterlitamak and Carancas. The youngest crater, the Carancas crater in Peru, formed on the 15th of September 2007 and has only 14.2 m in diameter (Fig. 1-1; Kenkmann et al., 2009). The Sterlitamak crater formed in 1990 in the Bashkortostan Republic, European Russia, and is

~9.4 m in diameter; 325 kg of the octahedrite projectile have been recovered from the crater (Ivanov and Petaev, 1992).

Fig 1-1. Carancas impact crater in Peru, 14.2 m in diameter. From www.wanderingstarmeteorites.com.

1.2 General introduction to impact cratering

Today, impact cratering is accepted by large majority of the scientific community as an important geological process that influenced the formation of the Earth. And not only the Earth, but all the solar system was shaped by impacts of asteroids but also by collisions of larger bodies, especially in its early history. Even the Earth's Moon is most probably the results of a gigantic collision between Earth and another large body of about Mars-size (e.g., Canup and Asphaug, 2001).

Impact crater formation differs from other geological processes by extreme pressure-temperature (p-T) conditions and by a very short time scale (Melosh, 1989) compared to typical geologic time intervals. Under these extreme conditions shock metamorphic features and high pressure polymorphs (see chapter 2 of the thesis), which cannot be a result of any other geological process, are formed. These special imprints, together with possible presence of a meteoritic component, serve as unambiguous evidence of impact origin (Koeberl, 2002; Reimold, 2007).

Today, almost 180 impact craters are known on Earth (Earth Impact Database, 2009; Fig. 1-2). The distribution of the so far discovered craters is influenced by several factors. In general, young craters and large craters are more probable to be preserved and discovered. Most abundant craters can be found on stable cratons formed by old crust not much changed by destructive geological processes (e.g., tectonics, erosion). Accessibility and level of geological exploration of an area plays an important role (French, 1998; Reimold, 2007). All these criteria explain why there are so many impact craters known in, e.g., Scandinavia, but, on the other hand, so few in, e.g., the Amazon rainforest.

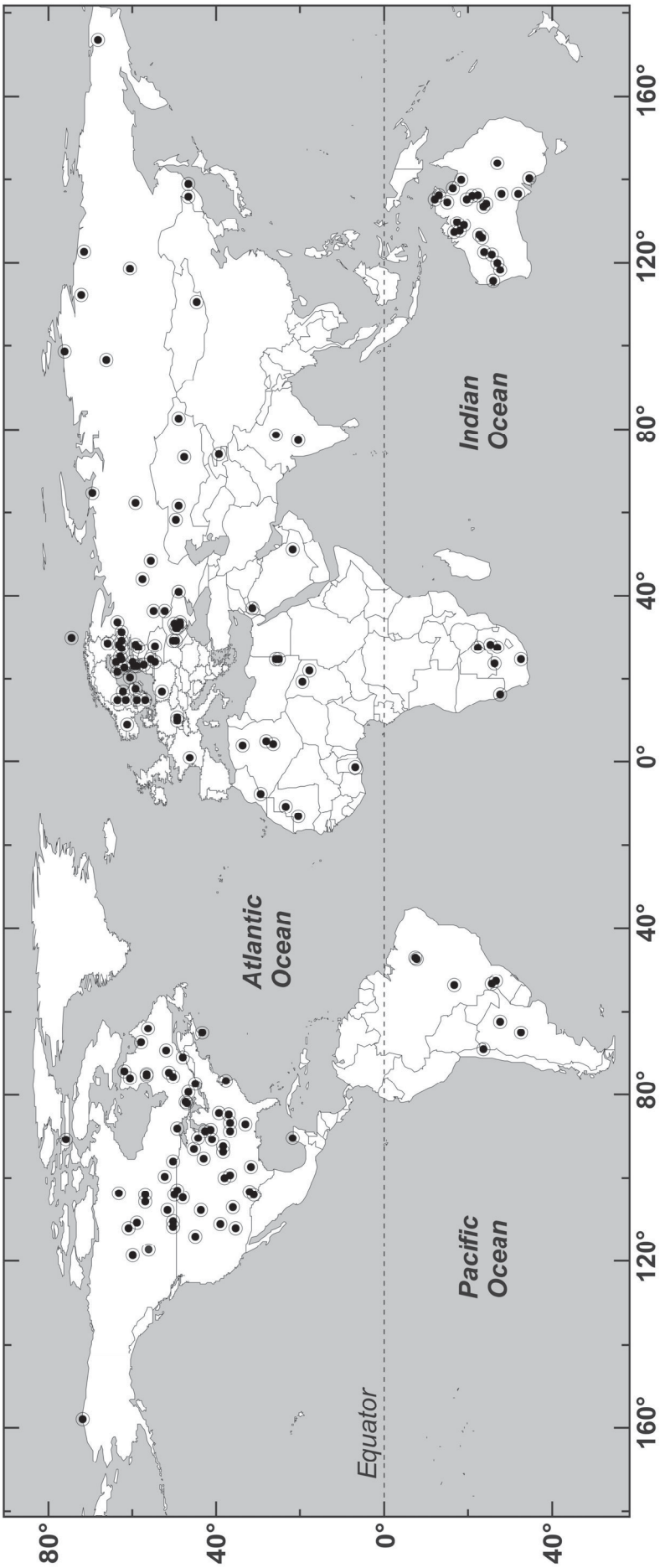

Fig. 1-2. World map showing distribution of known impact structures. Updated from Ferrière (2008).

Another striking disproportion is that most of the impacts are found on continents, whereas two thirds of the Earth's surface are covered by oceans. Only a few impacts are located on continental shelves, such as the Mjølnir or Montagnais impact structures, and also the large Chicxulub and Chesapeake Bay impact structures (Gersonde et al., 2002). The known oceanic impacts are scarce because the ocean floor is not easily accessible and thus not much explored, but also because only very large impactors can penetrate through the deep water column and make an imprint on the ocean floor (Gersonde et al., 2002). Artemieva and Shuvalov (2002) calculated that no crater is formed when the water depth/impactor diameter ratio is >4. Furthermore, the ocean crust is relatively young.

1.3 Crater morphology

The size and shape of an impact crater results from several factors including size, mass, and velocity of the impactor, obliquity of the impact, and properties of the target. The target can have different strength according to the lithology in the area. It can be relatively homogeneous (e.g., granitic rocks of a stable craton) or layered (e.g., layers of sediments on top of a crystalline basement. If the target area is covered by water (e.g., continental shelf), further modification of the crater formation is the result.

The basic two groups of impact craters are simple and complex craters (Melosh, 1989; French, 1998). The different resulting shapes of the craters depend first of all on the crater size (diameter). The size limit is slightly different for different target rocks and is valid only for Earth impact craters. The crater shapes and sizes on other bodies of the solar system are different due to differences in gravity and atmosphere (Cintala and Grieve, 1998; Reimold and Koeberl, 2008).

1.3.1 Simple craters

Simple craters have a so called "bowl shape" (Fig. 1-3). The crater depth is commonly about one fourth of the crater diameter (Grieve, 1987). As mentioned above, the changeover diameter between simple and complex crater is not uniform. In sedimentary targets the transition between simple and complex craters it at about 2 km, in crystalline targets about 4 km (Grieve, 1987). The craters are usually filled with impact breccia (French, 1998) and many also contain post-impact (typically lake) sediments. Examples of simple impact craters are the Meteor Crater in the USA, Brent in Canada, or Tswaing in South Africa (Fig. 1-4).

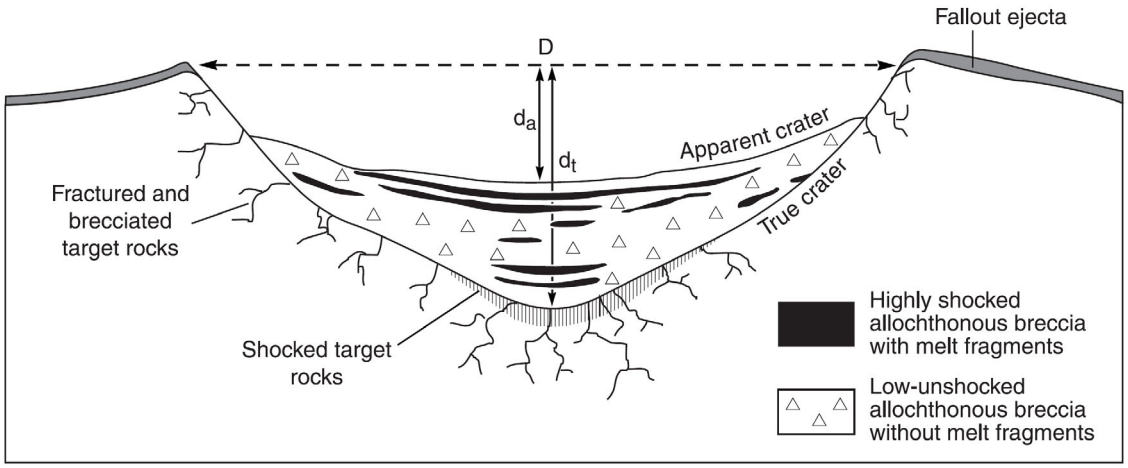

Fig. 1-3. Cross section of a simple impact structure and location of impactite types. From French (1998).

Fig. 1-4. Panoramic view of Tswaing impact crater (220 kyr old, 1.13 km in diameter; Earth Impact Database, 2009). The typical bowl shape of this simple impact crater has been modified by erosion of the rim and deposition of lake sediments in the crater.

1.3.2 Complex craters

Complex craters are characterized by a flat floor, central uplift, and inward collapse around the rim (Fig. 1-5; Grieve, 1991). As mentioned above, complex craters on Earth are craters with a diameter larger than 2-4 km. In the central uplift, the basement rocks are elevated. The stratigraphic uplift is about one tenth of the final diameter of the structure (Grieve et al., 1981; French, 1998). Complex craters are filled with impact breccias and melt rocks, but also by material slumped or transported to the crater from outside. There are several types of the complex craters, depending on the crater diameter. These are (with increasing crater diameter) central-peak structures, central-peak-basin structures, and peak ring basin structures (French, 1998). The crater shapes have been studied in more detail on other cosmic bodies, e.g., on the Moon, where the impact craters are well exposed and preserved. However, these can not be easily compared to Earth, as the transient diameters between the different types on Earth and Moon differ (mostly due to different gravity; French, 1998).

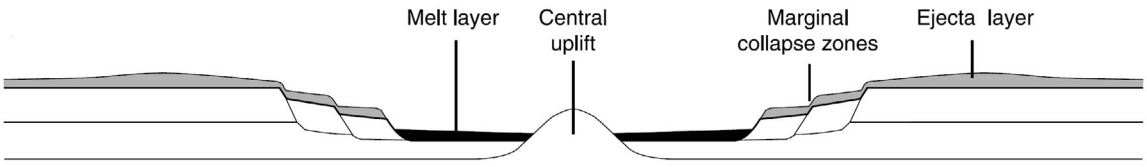

Fig. 1-5. Cross section of a complex impact structure with a central uplift. This type of central-peak morphology is typical for terrestrial impact structures 2-25 km in diameter. From French (1998).

1.3.3 Multiring basins

The largest and most energetic impacts form even more complicated impact structures, so called multiring basins. These structures have two or more interior rings in addition to the outer rim and have diameters of hundreds of km. Multiring basins date mostly from an Early history of the solar system and are observed on planets with well-preserved ancient surfaces. On Earth, the transient diameter at which multiring basins should start to form is about 100 km. The largest craters on Earth are mostly deeply eroded and it is not yet established if any multiring basin exists on Earth. Possible candidates are the largest terrestrial impact structures: Chicxulub in Mexico (Morgan and Warner, 1999), Sudbury in Canada, and Vredefort in South Africa (Reimold and Koeberl, 2008). The formation of the multiring basins is not yet well understood and it is not clear if, for example, in addition to a large diameter also special target properties are necessary (French, 1998).

1.4 Impact crater formation

An impact of an asteroid or a comet is a very energetic and nearly instantaneous (at least compared to the geological time scale) event. There are many factors that influence the crater formation. The resulting size of the impact crater is first of all dependent on the mass and velocity of the impactor. The velocities of these cosmic bodies hitting the Earth range from 10 to 72 km/s, depending also on the direction of their approach – consequently the velocity of the Earth is added or subtracted from the impactor velocity (Melosh, 1989).

Small bodies usually disintegrate in the atmosphere and the fragments reach the Earth's surface at low speed. These objects penetrate only a short distance into the target and form small so-called penetration craters. The projectile survives the impact and can be found in the small crater. Example of these penetration craters are the many pits made by meteorites of the Sikhote-Alin meteorite shower in 1947 (French, 1998). Large objects like asteroids or comets are not much decelerated by the atmosphere and hit the Earth at cosmic velocities. The limit size for these impactors that reach the Earth surface at cosmic velocities is about 50 m for stony objects and 20 m for iron impactors. These impacts produce shock waves that progress radially into the target. The pressure can reach up to hundreds of GPa and the target is set into motion, thus excavating the crater (French,

1998). Our knowledge about the crater formation is based on geological observations, laboratory experiments, and computer modeling. The impact crater formation is a complex process that has several stages (Fig. 1-6; Grieve, 1987; Melosh, 1989; French, 1998).

1.4.1 Contact and compression stage

This stage of the impact formation starts when the impactor gets into first contact with the ground. The impactor is stopped by the solid rock and its kinetic energy is nearly instantaneously transferred to the target by shock waves (Melosh, 1989). The shock waves are transmitted into the target and a complementary shock wave is reflected back into the impactor (French, 1998). The shock waves rapidly loose their energy while passing into the target due to heating, deformation, acceleration, as well as due to the expanding area of the shock front. The peak shock wave pressure decreases exponentially with the distance from the impact point, as suggested by geological observations (e.g., Dressler et al., 1998) and computer modeling (Melosh, 1989). The peak pressure can reach more than 100 GPa at the impact point (French, 1998). In the center of the impact area, a large volume of rocks (including the impactor) are melted or vaporized. With increasing distance from the impact crater the peak shock pressure decreases to about 1–2 GPa and the waves become elastic or seismic waves and their velocity drops to the sound velocity (Kiefer and Simonds, 1980; French, 1998). When the reflected shock wave passes back through the projectile, it is reflected again and a release wave is formed. This wave unloads the high pressure and causes melting or vaporization of the projectile. Then this release wave proceeds into the target, also unloading the pressure and melting the target rock. The point when the release wave reaches the projectile/target boundary is the end of the compression stage. The contact/compression stage is very short, it takes usually less than one second. The time depends on the size of the projectile, but even for small impactors does not exceed a few seconds. The impactor is vaporized into the plume or melted and mixed into the impact breccias (French, 1998).

1.4.2 Excavation stage

At the end of contact/compression stage the shock waves pass from the projectile in hemispherical envelopes. During the excavation stage the release wave passes through the target. The center of this hemisphere lies below the original target surface and the shock waves that travel upward are reflected from the surface as rarefaction waves. Near the surface this release wave is connected with fracturing of the target rock. The target rocks are accelerated outward and transient crater is excavated. The upper part of the target moves outward and upward and lower part of the target outward and downward. The transient crater expands and transient crater rim is formed. An ideal transient crater has a bowl shape and a structurally uplifted rim. The maximum depth of the transient crater is

about one third of the diameter. The growth of the transient crater stops when the shock and release waves cannot eject and displace any more rocks. The excavation stage is also relatively short; it takes ~6 s for a 1-km-diameter crater and less than two minutes even for the largest craters on Earth. In case of a simple crater, the transient crater shape is not much different from that of the final crater (Melosh, 1989; French, 1998).

1.4.3 Modification stage

The excavation stage ends when the transient crater reaches its maximum size. The shock waves have decayed by this point and usual geologic forces (most important gravity) start to modify the transient crater. The main part of the modification stage ends also in a few minutes; however, the modification stage has no clear end limit (French, 1998). The processes of uplift and collapse gradually change into usual geological processes. In a case of impact to a marine shelf the modification stage includes resurge of the water column back into the crater and following tsunami waves. Also hydrothermal processes initiated by the impact heat continue after the impact event (Naumov, 2005).

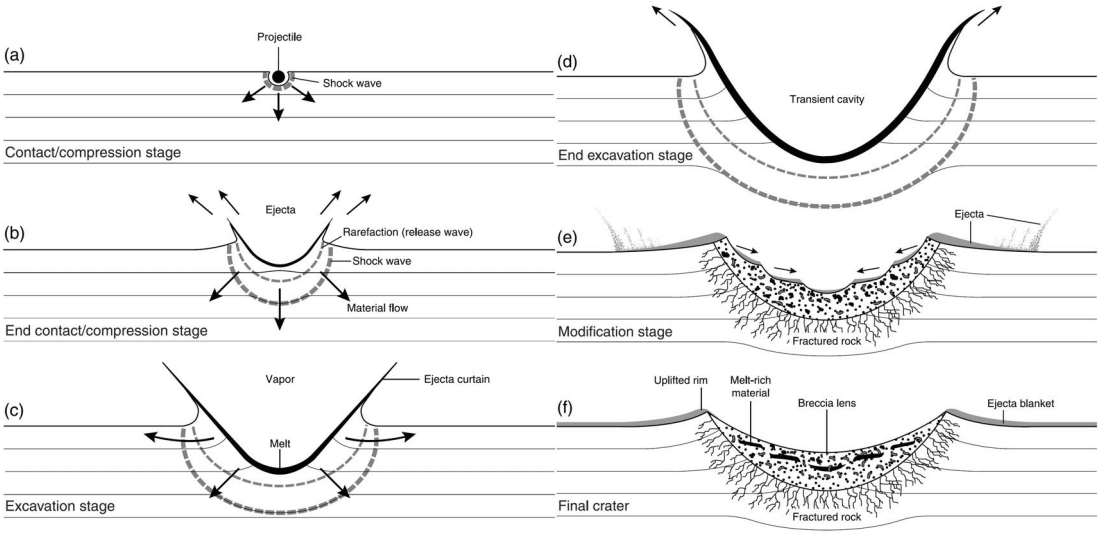

Fig. 1-6. Cross-section diagrams showing simple crater formation in a layered target. a) Contact/compression stage: penetration of projectile, radiation of shock wave. b) Start of excavation stage: expansion of shock wave, development of rarefaction wave, interaction of rarefaction wave with ground surface to accelerate near-surface material upward and outward. c) Middle of excavation stage: continued expansion of shock wave and rarefaction wave, development of melt in expanding transient cavity, ejecta flow from the opening crater. d) End of excavation stage: transient cavity reaches maximum extent, melt-lined transient crater forms, near-surface ejecta curtain reaches maximum extent, crater rim develops. e) Start of modification stage: walls of transient crater collapse and together with near-crater ejecta form breccia lens within crater. f) Final simple crater: a bowl-shaped crater, partially filled with complex breccias and bodies of impact melt. From French (1998).

References:

Artemieva N. A. and Shuvalov V. V. 2002. Shock metamorphism on the ocean floor (numerical simulations). *Deep-Sea Research II* 49: 959–968.

Canup R. M. and Asphaug E. 2001. Origin of the Moon in a giant impact near the end of the Earth's formation. *Nature* 412: 708–712.

Cintala M. J. and Grieve R. A. F. 1998. Scaling impact melting and crater dimensions: Implications for the lunar cratering record. *Meteoritics and Planetary Science* 33: 889–912.

Dressler B. O., Sharpton V. L., and Schuraytz B. C. 1998. Shock metamorphism and shock barometry at a complex impact structure: Slate Islands, Canada. *Contributions to Mineralogy and Petrology* 130: 275–287.

Earth Impact Database. 2009. http://www.unb.ca/passc/ImpactDatabase/ (accessed in December, 2009)

Ferrière L. 2008. *Shock metamorphism and geochemistry of impactites from the Bosumtwi impact structure: A case study of shock-induced deformations and transformations in quartz and associated methodology.* Ph.D. thesis, University of Vienna, Vienna, Austria, 279 p.

French B. M. 1998. *Traces of catastrophe: A handbook of shock-metamorphic effects in terrestrial meteorite impact structures.* LPI contribution No. 954, Lunar and Planetary Institute, Houston. 120 p.

Gersonde R., Deutsch A., Ivanov B. A., and Kyte F. T. 2002. Oceanic impacts – a growing field of fundamental geoscience. *Deep-Sea Resarch II* 49: 951–957.

Grieve R. A. F. 1987. Terrestrial impact structures. *Annual Review of Earth and Planetary Science* 15: 245–270.

Grieve R. A. F. 1991. Terrestrial impact: The record in the rocks. *Meteoritics* 26: 175-194.

Grieve R. A. F., Robertson P. B., and Dance M. R. 1981. Constraints on the formation of ring impact structures, based on terrestrial data. *Proceedings of the Lunar and Planetary Science Conference*. New York and Oxford: Pergamon Press. p. 37–57.

Ivanov B. A. and Petaev M. I. 1992. Mass and impact velocity of the meteorite formed the Sterlitamak crater in 1990. *Lunar and Planetary Science* 23: 573–574.

Kenkmann T., Artemieva N. A., Wünnemann K., Poelchau M. H., Elbeshausen D. and Nunez del Prado H. 2009. The Carancas meteorite impact crater, Peru: Geologic surveying and modeling of crater formation and atmospheric passage. *Meteoritics and Planetary Science* 44: 985–1000.

Kieffer S. W. and Simonds C. H. 1980. The role of volatiles and lithology in the impact cratering process. *Review of Geophysics and Space Physics* 18: 143–181.

Koeberl C. 2002. Mineralogical and geochemical aspects of impact craters. *Mineralogical Magazine* 66: 745–768.

Marvin U. B. 2007. Ernst Florens Friedrich Chladni (1756-1827) and the origins of modern meteorite research. *Meteoritics and Planetary Science* 42: Supplement, B1–B68.

Melosh H. J. 1989. *Impact cratering—A geological process.* New York: Oxford University Press. 245 p.

Morgan J. and Warner M. 1999. Chicxulub: The third dimension of a multi-ring impact basin. *Geology* 27: 407–410.

Naumov M. V. 2005. Principal features of impact-generated hydrothermal circulation systems: mineralogical and geochemical evidence. *Geofluids* 5: 165–184.

Reimold W. U. 2007. The impact crater bandwagon (Some problems with the terrestrial impact cratering record). *Meteoritics and Planetary Science* 42: 1467–1472.

Reimold W. U. and Koeberl C. 2008. Catastrophes, extinctions and evolution: 50 years of impact cratering studies. *Golden Jubilee Memoir of the Geological Society of India* 66: 69–110.

CHAPTER 2: SHOCK METAMORPHIC AND GEOCHEMICAL SIGNATURES IN TARGET ROCKS AND MINERALS

2.1 Introduction

Formation of an impact crater is associated with unique conditions, i.e., extremely high temperature and mainly pressure that can not be obtained in any other geological process (Fig. 2-1; French et al., 1998; French and Koeberl, 2010). The material influenced by a shock wave is subjected to what is collectively called “impact metamorphism” Stöffler and Grieve (2007). Shock metamorphism, a more general term that can be used also for artificial hypervelocity impacts or explosions, is defined as "all changes in rocks and minerals resulting from the passage of transient, high-pressure shock waves" (French, 1968). Shock metamorphism and related effects cause characteristic changes, deformation, phase transitions, melting, and vaporization in target rocks and minerals. Shock metamorphic effects in rocks and minerals are generally formed above the so-called Hugoniot elastic limit, which is in the order of several GPa for silicate minerals. Typical pressures of shock metamorphism are between 5 and 100 GPa for solid state effects and melting, and above 100 GPa for vaporization (Stöffler and Grieve, 2007). Impactites are formed during all stages of the crater formation: compression stage, excavation stage (including ballistic transport), and modification stage. Consequently, the shock metamorphosed material commonly displays disequilibrium and is mixed with unshocked material (Stöffler and Grieve, 2007).

Some of the shock metamorphism effects serve as unambiguous evidence of an impact origin of a structure (Koeberl, 2002; Reimold, 2007). Also, traces of the meteoritic material, in some cases even pieces of the meteorite, can be preserved in the impact crater (e.g., Koeberl, 1998, 2002; Maier et al., 2006). These can be used not only as impact evidence, but also to recognize the type of the impactor.

The identification of an impact crater is not always straightforward. Not every crater contains all the possible evidence of an impact origin. In very young and small craters (e.g., the recent Carancas crater in Peru; Kenkmann et al., 2009), and also in some larger simple craters (e.g., Barringer crater), pieces of the actual impactor can be preserved. On the other hand, in these small craters the shock pressure might not be high enough to form the characteristic shock metamorphic features (Kenkmann et al., 2009). In large craters, the projectile is usually completely melted or vaporized. Only some traces can be found in the target rocks, most commonly the impact melt rocks. But there are some exceptions. In the large Morokweng impact structure (70 km in diameter; Earth Impact database, 2009) up to 25-cm-sized pieces of the meteorite were found in the impact melt rock (Maier et al., 2006). In large craters, the shock pressures and temperatures are high enough to create

other typical shock metamorphic features, such as deformations in minerals, high pressure polymorphs, and impact melts.

Recently, new techniques, especially the remote sensing data, are used to search for new possible impact structures. This is a very powerful modern method; however, not every circular structure is an impact crater. Circular morphology can be a result of other geological processes (Reimold, 2007; e.g., volcanism, salt diapir). Every suspected impact structure has to be confirmed by unambiguous mineralogical and/or geochemical evidence (Reimold and Koeberl, 2008).

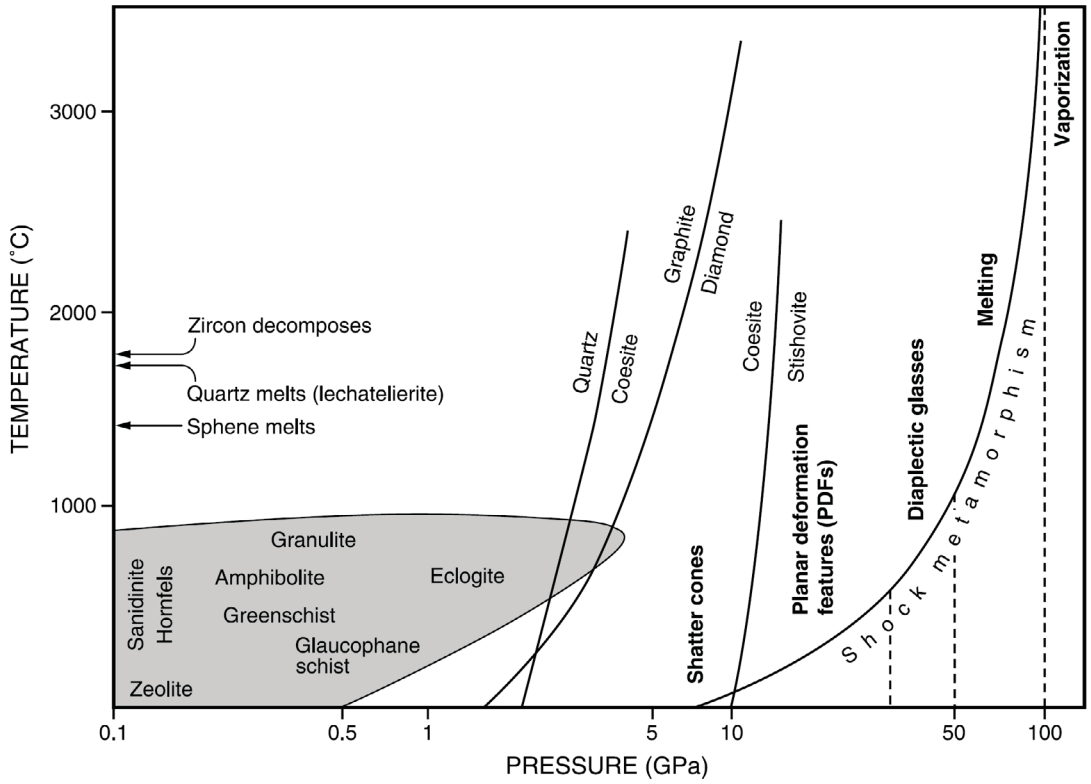

Fig. 2-1. Pressure-temperature diagram comparing conditions of normal crustal metamorphism (grey field) and shock metamorphism. Note the logarithmic horizontal scale. The exponential curve "Shock metamorphism" indicates the approximate post-shock temperatures produced by specific shock pressures in granitic crystalline rocks. The phase transition curves for minerals are valid for static equilibrium conditions and may vary widely under shock conditions. From French (1998).

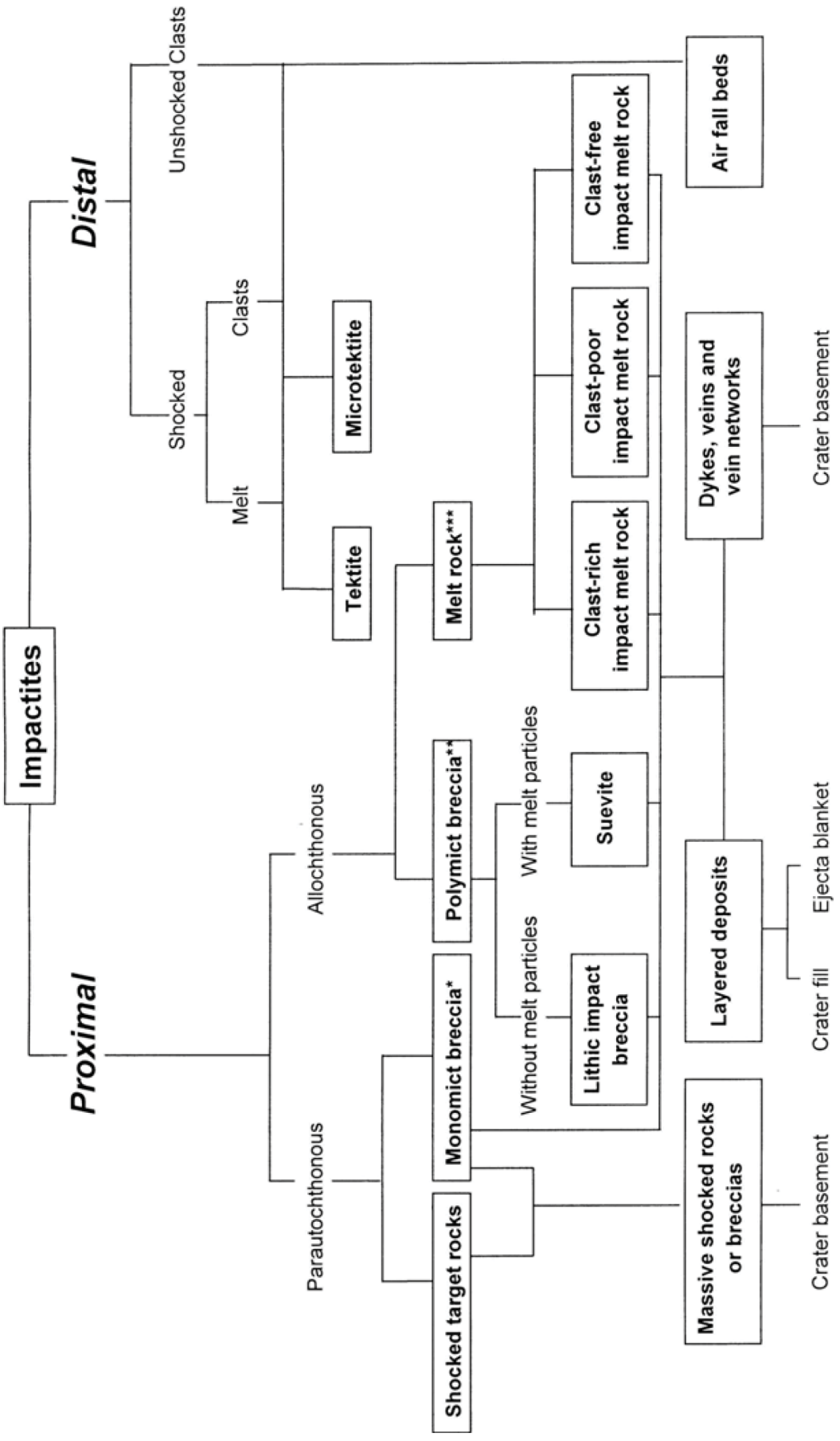

Fig. 2-2. Impactite classification scheme according to Stöffler and Grieve (2007).

2.2 Classification of impactites

A detailed classification of impactites has been published by Stöffler and Grieve (2007; Fig. 2-2). Although some nomenclature problems of this classification scheme have been discussed (Reimold et al., 2008), it is today the latest and most widely accepted classification and is used throughout the papers that are part of the thesis and also in the following text.

Impactites are all rocks affected by a hypervelocity impact. The term is applicable to terrestrial and extraterrestrial rocks, as well as meteorites, and includes shocked rocks, impact breccias, impact melt rocks, (micro)tektites, and impactoclastic airfall beds (Stöffler and Grieve, 2007). The criteria used for classification are degree of shock metamorphism, texture, and lithological components. Additional criteria include the occurrence (distance) with respect to the parent crater and geological and structural setting (Stöffler and Grieve, 2007).

2.2.1 Proximal impactites

2.2.1.1 Shocked rocks

Shocked rocks are all rocks affected by impact metamorphism. They are defined as "non-brecciated rocks, which show unequivocal effects of shock metamorphism, exclusive of whole rock melting" (Stöffler and Grieve, 2007). They are further classified according to progressive stages of shock metamorphism. Detailed classification of shocked rocks at different stages of metamorphism, based on numerous previous studies, is presented in Stöffler and Grieve (2007). The definition of progressive stages of shock metamorphism depends on texture (porosity) and mineralogical composition of the material shocked, therefore the shock classification is different for different lithologies (Stöffler and Grieve, 2007).

2.2.1.2 Impact breccias

Impact breccias are subdivided into groups according to the degree of mixing of target rocks and the melt content. Lithic breccias and suevites are polymict breccias, except for single lithology targets. Dyke breccias also belong to this group.

2.2.1.2.1 Monomict impact breccia

Monomict impact breccia is a "cataclasite produced by impact and displaying weak or no shock metamorphism". It occurs in the (par)autochthonous floor of an impact crater or (up to the size of blocks and megablocks) within allochthonous (polymict) impact breccias (Stöffler and Grieve, 2007). Monomict breccias are characteristic of crater basement but also as constituents of the polymict breccias, commonly in a form of brecciated displaced

megablocks. However, in some cases the cataclastic nature of a rock within or near an impact crater can also be a pre-impact tectonic feature, or can be formed during the later modification stage of the crater. This has been discussed, e.g., for the crystalline basement derived rocks from the Eyreville drill core from the Chesapeake Bay impact structure (Gibson et al., 2009).

2.2.1.2.2 Lithic (impact) breccia

Lithic impact breccia (Fig. 2-3) is a "polymict impact breccia with clastic matrix containing shocked and unshocked mineral and lithic clasts, but lacking cogenetic impact melt particles" (Stöffler and Grieve, 2007). The term is synonymous with, and supersedes, fragmental breccia. Clasts of different parts of the target are displaced and mixed. Rarely the lithic breccia can be monomict, if the target is composed of just a single lithology (Stöffler and Grieve, 2007).

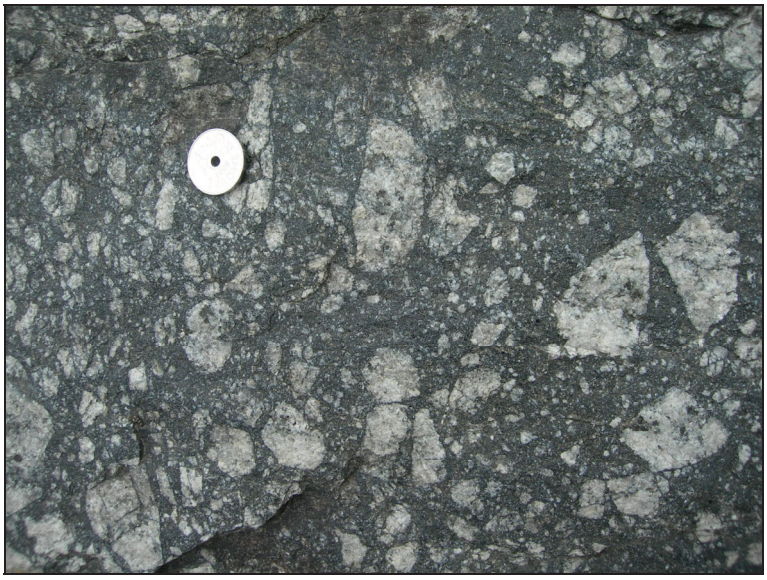

Fig. 2-3. Gardnos breccia – lithic breccia from Gardnos impact crater, Norway. The photograph shows granitic and quartzitic clasts in dark matrix.

2.2.1.2.3 Suevite

Suevite (Fig. 2-4) is a "polymict impact breccia with particulate matrix containing lithic and mineral clasts in all stages of shock metamorphism including cogenetic impact melt particles which are in a glassy or crystallized state" (Stöffler and Grieve, 2007). The name was first established for the Ries suevite and originates from the Latin name for the province Schwaben – Suevia. The Ries suevite remains the classical example of this lithology, although later the name was used for similar melt-bearing rocks from other impact structures. But also the texture of the Ries suevite has recently been discussed and it was suggested that the matrix, originally thought to be clastic, might be largely composed of melt products (Osinski, 2008).

Recent studies of drill cores of some impact structures have opened new questions. The breccias from Bosumtwi impact crater are generally melt poor and only in some thin sections the melt particles were found. Consequently, it has been discussed whether or not a lower limit for the melt abundance in suevites should be established (Reimold et al., 2008). The Eyreville core from the Chesapeake Bay impact structure revealed related scale problems of the nomenclature (Reimold et al., 2008). In the lower part of the impact breccias only a small fraction of the samples contains microscopic melt particles. This part of the core was consequently classified as polymict impact breccia (Horton et al., 2009), whereas the single samples are more specifically classified as suevite or lithic impact breccia (Reimold et al., 2008).

Fig. 2-4. Suevite from the Eyreville drill core, Chesapeake Bay impact structure. Note the light yellowish melt particles.

2.2.1.2.4 Dyke breccias

A breccia dyke is a "dyke formed in the (par)autochthonous basement or in displaced megablocks of impact craters consisting of impact breccia (polymict breccias such as impact melt rock, suevite, lithic breccia or more rarely monomict breccia)" (Stöffler and Grieve, 2007). Dyke breccias can be related to all major phases of crater formation. Stöffler and Grieve (2007) report that pseudotachylites are formed during the compression stage, because they often occur as clasts within later formed breccia dykes, and propose a new name for these rocks: shock veins and vein networks. During the compression and excavation stage injection of dykes of polymict lithic breccias takes place. Last generation of dykes (polymict or monomict breccias) is produced during the modification stage (Stöffler and Grieve, 2007).

An important type of a dyke breccia is a pseudotachylitic breccia. Impact pseudotachylite is defined as "dyke-like breccia formed by frictional melting in the basement of impact craters, resulting often in irregular vein-like networks. Typically it contains unshocked and shocked mineral and lithic clasts in a fine-grained aphanitic matrix" (Stöffler and Grieve, 2007). The impact-produced pseudotachylitic breccias are

very complicated rocks that are still widely debated and are not well understood (e.g., Reimold, 1995). The well-known pseudotachylitic breccias from Vredefort (Fig. 2-5) are discussed to have formed by shock melting, friction melting, decompression melting, or if they could represent influx of impact melt from the crater floor (Reimold, 2008).

Fig. 2-5. Example of extremely large pseudotachylitic breccia dykes from Vredefort Dome, South Africa (author for scale).

2.2.1.3 Impact melt rocks

Impact melt rock (Fig. 2-6) is a "crystalline, semihyaline or hyaline rock solidified from impact melt and containing variable amounts of clastic debris of different degree of shock metamorphism" (Stöffler and Grieve, 2007). The term impact melt rock should replace the previously used term impact melt breccia. Impact melt rocks are further subdivided into three groups according to the clast content: clast-rich, clast-poor, and clast-free impact melt rock. Impact melt rocks can form large melt bodies/sheets within the impact crater, as for example in the Popigai, Mistastin, or Brent impact structures (Grieve and Cintala, 1992).

Fig. 2-6. Impact melt rock from the Rochechouart impact structure.

2.2.2 Distal impactites

2.2.2.1 Consolidated – Tektites and microtektites

Tektites are "impact glasses formed at terrestrial impact craters from melt ejected ballistically and deposited as aerodynamically shaped bodies in a strewn field outside the continuous ejecta blanket" (Stöffler and Grieve, 2007). Another definition by Neuendorf et al. (2005) characterizes a tektite as "a jet-black to greenish or yellowish body of silicate glass of non-volcanic origin found in several widely separated areas of the Earth's surface and generally bearing no relation to the associated geologic formations." The main characteristics of tektites have been summarized by Montanari and Koeberl (2002): "1) they are glassy (amorphous); 2) they are fairly homogeneous rock (not mineral) melts; 3) they contain abundant lechatelierite; 4) they occur in geographically extended strewn fields (not just at one or two closely related locations); 5) they are distal ejecta and do not occur directly in or around a source crater, or within typical impact lithologies (e.g., suevitic breccias, impact melt breccias); 6) they are very poor in water (except some microtektites) and have a very small extraterrestrial component; and 7) they seem to have formed from the uppermost layer of the target surface."

The size of tektites ranges from sub-millimeter to centimeter or rarely decimeter sizes. The sub-mm tektites are called microtektites and are generally found in deep sea sediments. The term tektite originates from Greek tèktos and was first proposed by Franz Suess in 1900 for small corroded silicate glass nodules from southern Bohemia (Fig. 2-7).

Fig. 2-7. A moldavite, about 2.5 cm long. Moldavites are often used in jewelry.

The origin of tektites was not understood for a long time. Geochemical investigations, mainly of moldavites and the target lithologies from the Ries crater (Koeberl et al., 1985), have shown, that the tektites were formed from melted uppermost target material. However, the exact process of their formation is still not completely understood (von Engelhardt, 1987; Melosh, 1989; Stöffler et al., 2002; Montanari and Koeberl, 2000).

Several types of tektites have been distinguished. These are splash-form tektites (formed by solidification of rotating liquids), aerodynamically shaped tektites (shaped during reentry of the solidified tektite into the atmosphere), Muong Nong-type tektites (generally larger, with abundant vesicles, irregular shapes, and layered), and microtektites (sub-mm-sized spherules found in deep sea sediments) (e.g., French, 1998; Montanari and Koeberl, 2000).

There are four known tektite strewn fields (Fig. 2-8). Central European tektites (moldavites) are associated with the Ries crater, the Ivory Coast tektites with the Bosumtwi crater, and the North American tektites (bediasites and georgiaites) with the Chesapeake Bay impact structure (e.g., Koeberl et al., 1996; Deutsch and Koeberl, 2006). No impact structure has been associated with the Australasian strewn field (Hartung and Koeberl, 1994; Glass and Koeberl, 2006). Tektites have been extensively studied by, e.g., O'Keefe (1963), Glass (1967, 1990), Koeberl (1986, 1990, 1994), and Taylor and Koeberl (1994).

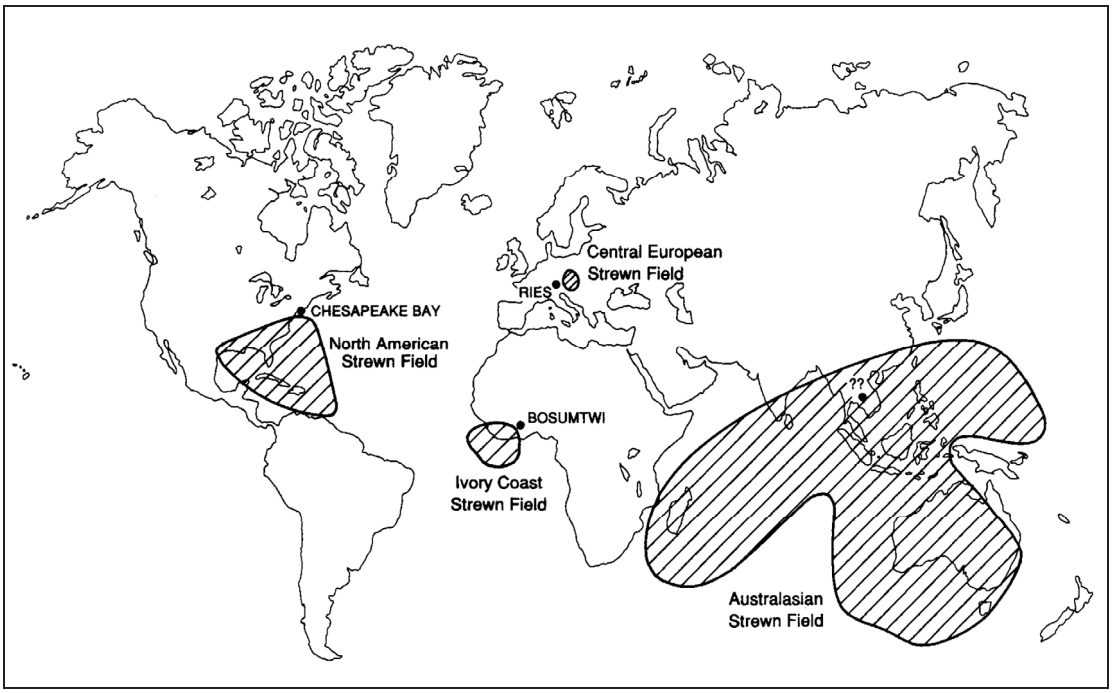

Fig. 2-8. Location of the four tektite strewn fields on Earth. Positions of the known source craters (Chesapeake Bay, Ries, and Bosumtwi craters) and the suspected crater location for the Australasian strewn field are shown. From Montanari and Koeberl (2000).

2.2.2.2 Unconsolidated - Airfall beds

Impactoclastic airfall bed is a "pelitic sedimentary layer containing a certain fraction of shock-metamorphosed material, e.g., shocked minerals and melt particles, which has been ejected from an impact crater and deposited by interaction with the atmosphere over large regions of a planet or globally" (Stöffler and Grieve, 2007).

2.2.3 Impactites from multiple impacts

Impactites from multiple impacts are typical for planetary bodies with thin or no atmosphere and low endogenic activity and have been described from e.g., Moon and meteorites. These impactites are subdivided into two main groups: unconsolidated clastic impact debris (*impact regolith*) and consolidated clastic impact debris (*shock lithified impact regolith*). The lithified impact regolith can be further subdivided into *regolith breccia* - with matrix melt and melt particles and *lithic breccia* –without matrix melt and melt particles (Stöffler and Grieve, 2007).

2.3 Shock metamorphism effects

2.3.1 Shatter cones

Shatter cone (Fig. 2-9) is a "striated cup-and cone structure resulting from hypervelocity impact; the structure occurs on the cm- to m-scale" (Stöffler and Grieve, 2007). It was first described at the Steinheim impact crater in Germany. Today, shatter cones are known from many impact craters. They are the only macroscopically visible shock features (French and Koeberl, 2010). In rare cases, meter-sized, so-called megacones, can develop (French, 1998). However, the shatter cones must be carefully examined, especially when they should serve to confirm the impact origin of a geological structure, as they can be confused with some other similar structures, e.g., ventifacts (formed by wind erosion) or sedimentary cone-in-cone structures (Reimold, 2007). The criteria for shatter cone identification are listed in, e.g., French and Koeberl (2010).

Shatter cones are best developed in fine-grained rocks, e.g., carbonates or shales. They occur typically in the central part of a crater, below the crater floor, usually in the central uplift. Shatter cones are formed at relatively low pressures, from about 2 GPa (French, 1998). However, some shatter cones can also be associated with shock metamorphism effects, such as planar deformation features (Dressler, 1990).

Fig. 2-9. Shatter cones at Vredefort Dome.

2.3.2 Shock metamorphism effects in quartz

2.3.2.1 Planar microstructures

Planar microstructures is a term comprising shock-induced planar fractures and planar deformation features (Stöffler and Grieve, 2007). Planar structures are crystallographically oriented, i.e., parallel to rational crystallographic planes. Bravais indices (hkil), mineralogical indices equivalent to Miller indices, describing crystallographic planes in trigonal and hexagonal crystal system (e.g., Cracknell, 1969), are used to characterize the orientations of the planar microstructures in quartz crystals.

2.3.2.1.1 Planar fractures (PFs)

Planar fractures are "fractures occurring in shocked minerals, as multiple sets of planar fissures parallel to rational crystallographic planes, which are usually not observed as cleavage planes under normal geological (non-shock) conditions" (Stöffler and Grieve, 2007). Planar fractures are typically 5–10 μm wide with spacing 15–20 μm or more (French, 1998; Stöffler and Langenhorst, 1994). They are generally parallel to planes with low Bravais indices (Stöffler, 1972). Planar fractures are not intersected by planar deformation features (PDFs) and form kind of boundaries for the PDFs. This suggests that PFs are formed earlier than PDFs (Stöffler and Langenhorst, 1994). Planar fractures form at relatively low pressures, about 5–8 GPa, and can rarely occur in quartz from non-impact settings (French, 1998). Thus, planar fractures can not be used to confirm a meteorite impact structure, unless they are accompanied by other unambiguous evidence.

2.3.2.1.2 Planar deformation features (PDFs)

Planar deformation features are "submicroscopic amorphous lamellae occurring in shocked minerals as multiple sets of planar amorphous lamellae (optical discontinuities under the petrographic microscope), parallel to rational crystallographic planes; indicative of shock metamorphism" (Stöffler and Grieve, 2007). The term is synonymous with, and supersedes deformation lamellae, planar elements, planar features, and shock lamellae. Compared to PFs, PDFs are more narrow (<2–3 μm) and more closely spaced (2–10 μm), and are formed of highly deformed or amorphous quartz (Engelhardt and Bertsch, 1969; French, 1998; Stöffler and Langenhorst, 1994).

Four categories of PDFs have been distinguished: 1) non-decorated, fine optical discontinuities barely visible in the optical microscope; 2) homogeneous PDFs which differ slightly in optical orientation and decreased refractive index from the host crystal; 3) PDFs filled with glass and high-pressure polymorphs, and 4) decorated PDFs with fluid and gas inclusions (Engelhardt and Bertsch, 1969). Planar deformation features are parallel to crystallographic planes, mostly (0001), $\{10\bar{1}3\}$, and $\{10\bar{1}2\}$. Depending on

shock intensity, up to 10 or more PDF sets can occur in one quartz grain (Stöffler and Langenhorst, 1994). Based on the proportions of the PDF sets with different crystallographic orientations in grains within one sample, it is possible to estimate what peak shock pressure the sample experienced (e.g., Grieve et al., 1996).

Although presence of PDFs is an unambiguous evidence of an impact origin, PDFs should be identified with special care (Reimold, 2007). PDFs in sets have to be planar (Fig. 2-10) and their observations should be completed by U-stage (or spindle stage) and/or TEM measurements, to determine their crystallographic orientations.

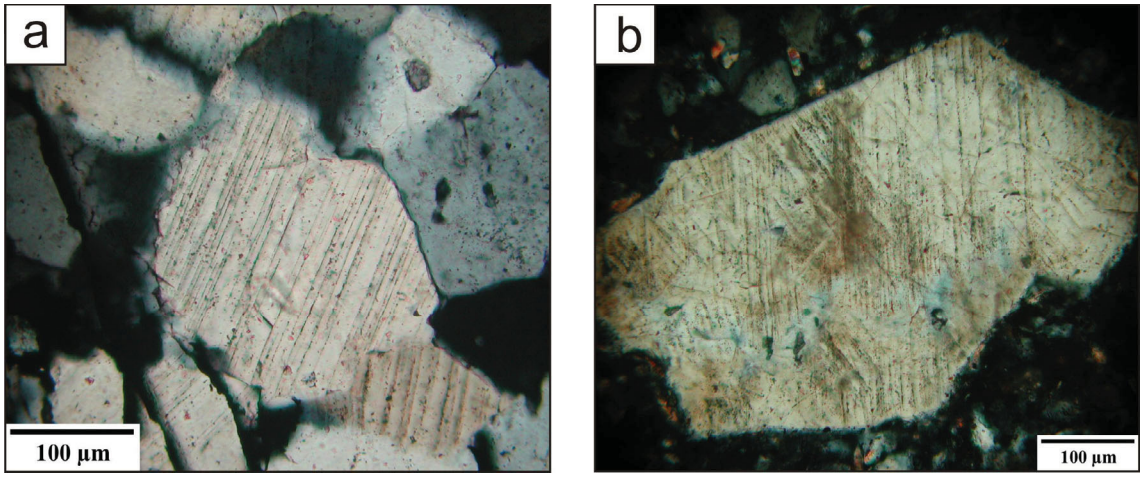

Fig. 2-10. PDFs in quartz grains from suevite from the Eyreville drill core, Chesapeake Bay impact structure, USA. Cross-polarized light. a) One set of PDFs. b) Two sets of PDFs.

2.3.2.2 Mosaicism

Mosaicism is a "general disorientation of a crystal structure as a result of shock metamorphism resulting in marked, highly irregular 'mottled' extinction under the petrographic microscope" (Stöffler and Grieve, 2007). This feature is a result of formation of mutually disoriented domains in the crystal structure. Mosaicism is formed during plastic deformation by dynamic compression (Stöffler, 1972). Weak mosaicism can also be the result of endogenic tectonic processes. Mosaicism differs from undulatory extinction (caused by tectonic deformation) in that the homogeneously extinguishing domains are very small, usually submicroscopic (Stöffler and Langenhorst, 1994).

2.3.2.3 Changes in physical characteristics

Shock metamorphism causes changes in physical characteristic of the material (mineral). Especially density and optical characteristics as refractivity and birefringence are affected. The normal refractive indices as well as birefringence of quartz decrease with increasing shock intensity. This trend continues until the refractive index of diaplectic glass (1.468) is reached (Stöffler and Langenhorst, 1994). There are also changes in density of shocked quartz – the density increases with increasing shock pressure. The transition density, where quartz becomes isotropic, was found to be 2.280 g/cm^3 (Stöffler and Langenhorst, 1994).

2.3.3 Shock metamorphism effects in other minerals

Although shock metamorphism is probably most easily identified and also most widely studied in quartz, shock metamorphic effects have been found also in other minerals. Planar microstructures have been described from pyroxene, amphiboles, olivine, as well as accessory minerals, e.g., apatite, sillimanite, cordierite, garnet, scapolite, and zircon (Stöffler, 1972; French, 1998). Aside from quartz, PDFs have been mostly studied in feldspars, although in feldspars one should be careful not to confuse PDFs with cleavage or twinning, typical for feldspars. There are only rare observations of PDFs in mafic minerals. These minerals form PDFs only in a limited range of pressure; the necessary pressure is much higher than in, e.g., quartz, and close to the pressure of whole rock melting (French, 1998). Another type of shock deformation are kink bands that are typical for mica (Fig. 2-11), but can also be found in other minerals, e.g., feldspar, olivine, pyroxene, and graphite (French, 1998; Stöffler, 1972). However, kink banding is not a shock diagnostic feature, as it can be formed also by tectonic deformation (French, 1998; French and Koeberl, 2010). Mosaicism, typically described in quartz, has been noted also in, e.g., plagioclase.

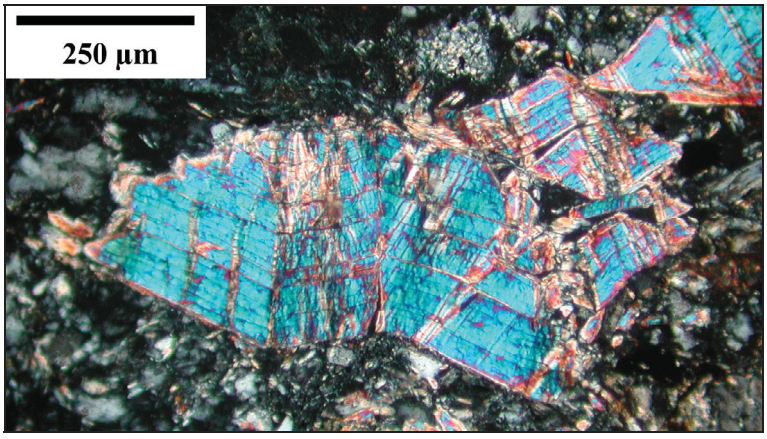

Fig. 2-11. Kink banding in mica. Muscovite clasts in suevite from the Eyreville core, Chesapeake Bay impact structure.

2.3.4 High-pressure polymorphs

Due to the extremely high pressures, high pressure polymorphs of minerals are commonly found in impact structures. Occurrence of high pressure polymorphs, such as coesite, stishovite, and diamond in near crustal rocks, especially as a disequilibrium assemblage with other chemically equivalent minerals, can be used as impact evidence (French, 1998).

2.3.4.1 High pressure polymorphs of quartz

High pressure polymorphs of quartz, coesite, and stishovite have been reported from several impact structures. Under static equilibrium conditions, stishovite is formed under higher pressures (above ~10 GPa) than coesite (above ~2 GPa; Fig. 2-1; French et al., 1998). In contrast, during shock metamorphism, stishovite is formed at lower pressures than coesite. This is because stishovite is formed during shock compression, while coesite crystallizes during pressure release (Stöffler and Langenhorst, 1994). Stishovite and coesite can be found in rocks shocked at 12–45 GPa and 30–60 GPa, respectively, on condition that secondary thermal metamorphism is absent (Stöffler and Langenhorst, 1994). This is especially important for stishovite, which is unstable above 400 °C. Coesite can be observed in the optical microscope as fine-grained, colorless to brownish aggregates with high refractive index, commonly embedded in diaplectic quartz glass. Stishovite can not be identified microscopically. Identification of both polymorphs needs chemical separation followed by, e.g., X-ray diffraction (Stöffler and Langenhorst, 1994), or microRaman spectroscopy on thin sections.

Coesite is typically found in impactites, but it can also form at static conditions in deep rocks and be brought to the surface by tectonic processes. However, the different mineral assemblages clearly distinguish these cases. Coesite has been reported from, e.g., Barringer crater (Chao, 1960), Ries crater (Shoemaker and Chao, 1961), and the Vredefort impact structure (Martini, 1991); stishovite was also found in these impact craters. Recently, coesite has been detected also in the suevite from the Chesapeake Bay impact structure (Horton et al., 2009).

2.3.4.2 High pressure polymorphs of other minerals

Other important high pressure polymorphs known from impact structures are diamonds. Diamonds are formed by shock pressure in the impact structures, where graphite is present in the target rocks. Classical occurrence is known from the Popigai impact structure (Masaitis et al., 1972). Another occurrence is reported from, e.g., the Ries crater (Rost et al., 1978) and Ukrainian craters – Ilyinets, Zapadnaya, and Obolon (Gurov et al., 1995). Detailed studies by, e.g., Koeberl et al. (1997) have shown that the diamonds preserve the crystallographic habit and twinning of the original graphite. Also, trace element and isotopic composition suggest a graphite precursor. Diamonds occur also deep in the Earth

mantle and can be brought to the surface by kimberlites. But these diamonds can be distinguished from impact diamonds by the mineral assemblage and structure (French, 1998).

Other high pressure polymorphs associated with shock metamorphism are, e.g., jadeite (polymorph of plagioclase), majorite (polymorph of pyroxene), ringwoodite (polymorph of olivine), and reidite (polymorph of zircon; Glass et al., 2002; Horton et al., 2009).

2.3.5 Diaplectic glasses

Diaplectic glass is an "amorphous form of crystals ('solid state glass') resulting from shock wave compression and subsequent pressure release of single crystals or polycrystalline rocks; most commonly observed in tectosilicates" (Stöffler and Grieve, 2007). The name originates from the Greek diaplesso – to destroy by striking or beating. Diaplectic glass, mostly studied for quartz, is formed in a pressure regime where post-shock temperature does not reach the melting temperature (about 35–50 GPa; Stöffler and Langenhorst, 1994). Diaplectic glass has a higher degree of long range order compared to glass quenched from a melt (Stöffler, 1972). At higher pressure, >50 GPa, lechatelierite is formed from quartz (Stöffler and Langenhorst, 1994). Also diaplectic feldspar glass and rare diaplectic glasses of other minerals are known (French and Koeberl, 2009).

2.3.6 Impact melts

Impact melt is a "melt formed by shock melting of rocks in impact craters" (Stöffler and Grieve, 2007). At pressures higher than about 45 GPa (for feldspar; French, 1998) to 50 GPa (for quartz; Stöffler and Langenhorst, 1994), mineral melts are formed. At even higher pressures, >60 GPa, whole-rock melts occur (French, 1998). Lechatelierite occurs commonly in sandstone and quartzite target lithologies. In highly shocked crystalline rocks, feldspar glass can be present, but not lechatelierite, because its formation requires pressures higher than the pressure at which all such rock is melted (Stöffler and Langenhorst, 1994)

Melt occurs commonly as melt particles in suevite or as glass bombs in ejecta (Fig. 2-12); classical examples are found in the Ries crater. In some impact structures, large sheets of impact melt rocks occur. A typical example is the Popigai impact structure, but also many other (see also the section about Impact melt rocks of this chapter).

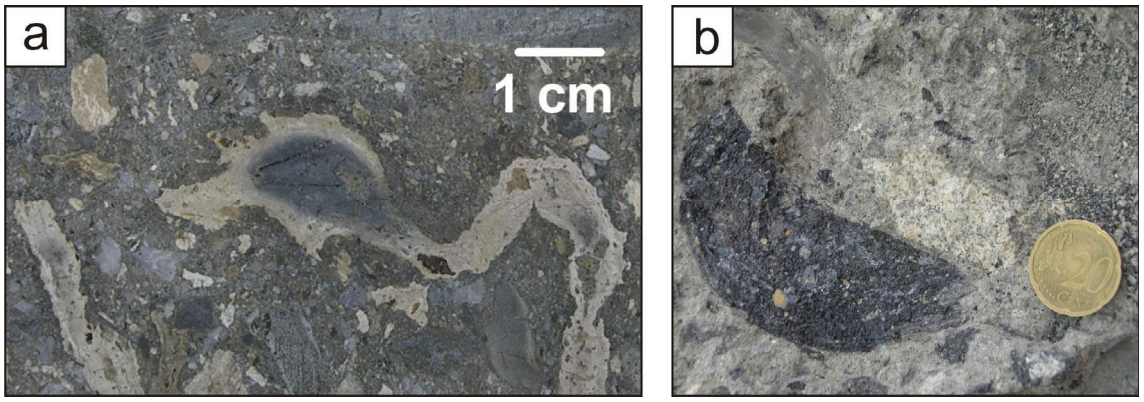

Fig. 2-12. a) Large melt particles (light colored) in suevite from the Eyreville drill core, Chesapeake Bay impact structure. b) A glass bomb (dark gray) from fallout suevite at Otting, Ries crater.

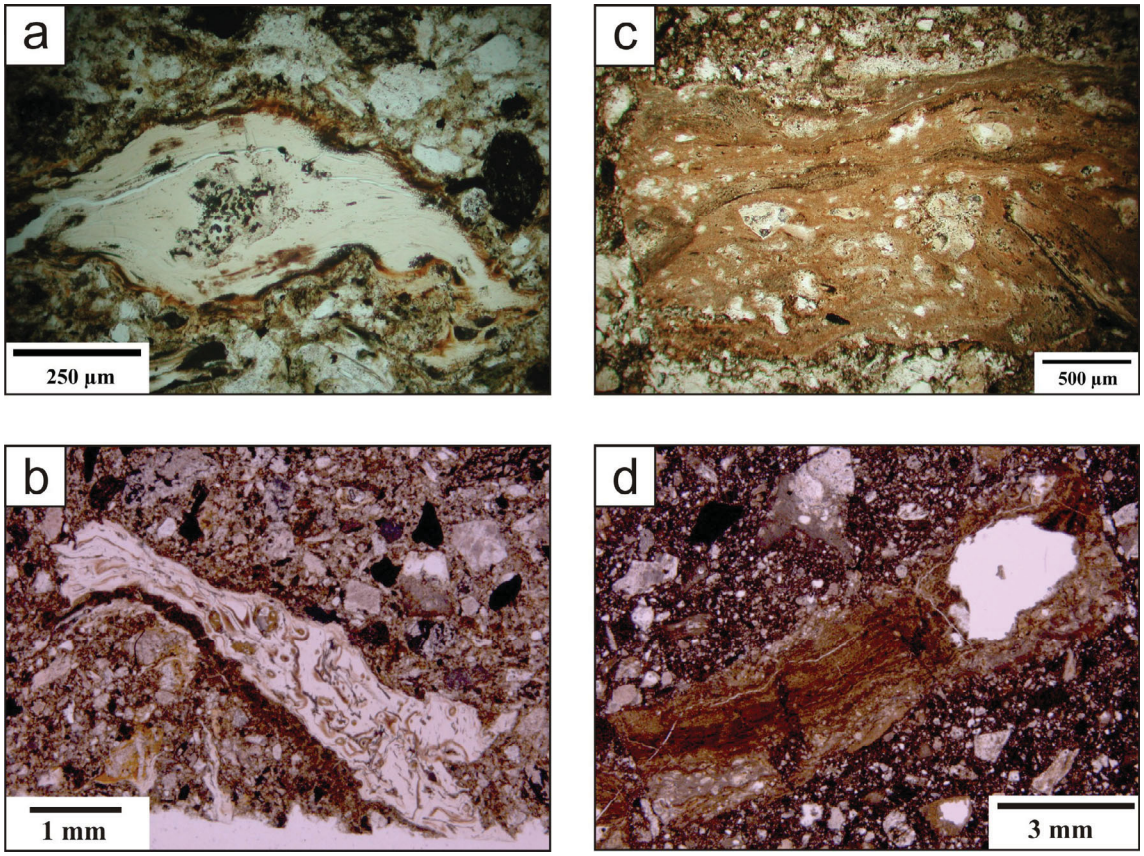

Fig. 2-13. Microphotographs of melt particles from suevite from the Eyreville drill core, Chesapeake Bay impact structure, USA. Plane polarized light. a), b) Clear to brownish melt particles. c), d) Melt particles altered to phyllosilicate minerals, with abundant undigested clasts.

Melt particles commonly have vesicular texture, flow texture (schlieren), and can contain undigested mineral grains or quench crystals (commonly pyroxene and plagioclase). The shapes of the particles are mostly oval, amoeboid, or shard-like. In different processes of formation, precursors, and subsequent alteration, different types of melt particles can be formed, even within one impact crater (e.g., Stöffler et al., 2004,

Bartosova et al., 2009). Examples of melt particles from the Chesapeake Bay impact structure are shown in Fig. 2-13.

2.3.7 Other associated features

Other typical features associated with impact metamorphism include toasting and ballen silica. These are, however, associated with post-shock processes rather than with the high shock pressures.

2.3.7.1 Toasted quartz

The term toasted quartz (Fig. 2-14) was first used by Short and Gold (1993, 1996), as this special texture reminded the authors of "toasted bread". They described the colors as orange-brown to gray-brown in plane polarized light and deeper reddish brown with reduced birefringence in cross polarized light. At high magnification "the alteration consists of tiny specks of unknown identity that often obscure but do not destroy the sets of PDFs" Short and Gold (1993). Later studies by Whitehead et al. (2002) did not identify any compositional cause of the browning. These authors explained the toasted appearance by tiny fluid inclusions predominantly located along decorated PDFs that enhance scattering of the transmitted light. Toasted quartz has been described from e.g., the Charlevoix, Clearwater Lake, Haughton, Mistastin, Lappajärvi, Manicouagan, Popigai, Rochechouart, and Wanapitei impact structures (Whitehead et al., 2002). The list was recently extended by Ferrière (2008). This author observed a vesicular texture of the toasted quartz in back-scattered electron images.

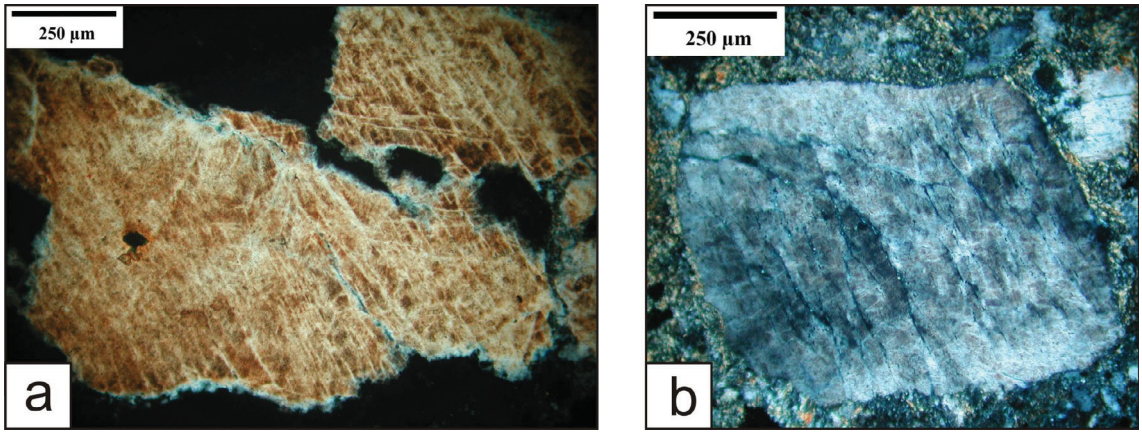

Fig. 2-14. Quartz with toasted appearance from suevite from the Eyreville drill core, Chesapeake Bay impact structure, USA. Cross-polarized light. a) Quartz grain in a conglomerate clast in suevite. b) Single quartz grain in matrix of suevite.

2.3.7.2 Ballen silica

Ballen silica (Fig. 2-15) are microscopic spheroidal features in quartz, diaplectic quartz, or lechatelierite that are formed of α-quartz or α-cristobalite Ferrière et al. (2009). Ballen silica mostly occurs in impact melt rocks, or more rarely in suevites. Different types of ballen silica have been described by Bischoff and Stöffler (1984). Ferrière et al. (2009) have distinguished five different types of ballen silica, based on their internal texture (extinction) and mineralogical composition (i.e., quartz or cristobalite). Ballen silica have been found in rocks from a large number of the known terrestrial impact craters (Ferrière et al., 2009).

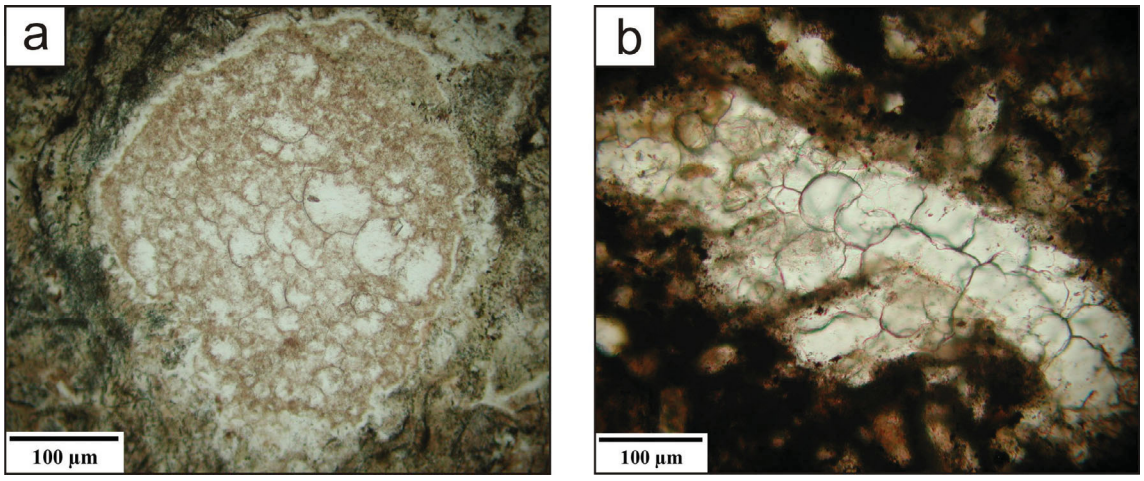

Fig. 2-15. a), b) Microphotographs of ballen quartz from impact melt rock from the Eyreville drill core, Chesapeake Bay impact structure, USA. Plane polarized light.

2.4 Geochemical signatures of impact structures

During an impact, only in small young craters pieces of the meteorite can be preserved (see the Introduction part of this chapter). In most impact structures the impactor is vaporized and small amount of the finely dispersed meteoritic melt or vapor is mixed with the melt or vapor of the target rocks (Koeberl, 2002, 2007). The contribution is generally very small, <<1%, thus the detection of a meteoritic component is very difficult (Koeberl, 2002, 2007). Elements that are very abundant in the meteorites, but generally low in the crustal rocks, are used for the meteoritic component identification. Today, meteoritic material has been identified at about 45 impact structures (French and Koeberl, 2010)

The meteoritic component can be most probably found in impact melt rocks. Also the target rocks must be chemically analyzed for comparison (French and Koeberl, 2009). Further, every meteorite has a different composition. Iron or chondritic meteoritic component can be relatively well resolved, while achondritic meteorites are much more difficult to identify, due to their significantly lower abundance of siderophile elements (Koeberl, 2002, 2007).

2.4.1 Siderophile elements and platinum group elements (PGE)

Impactites with a meteoritic component have generally higher content of Cr, Co, and Ni. However, higher abundances of these moderately siderophile elements can help us to find the best samples for further investigation, but can not be used as evidence of a meteoritic component (Koeberl, 1998, 2007). Also the enrichment in Ir is a good indicator of a meteoritic component, but especially low Ir abundances, without any other supporting chemical data, need to be used with caution (French and Koeberl, 2010). Furthermore, as mentioned above, the contents of these elements should be always compared with the target rock values. Determining of the platinum group element (PGE) abundances and ratios is a much more reliable method. However, identifying of the actual type of the impacting meteorite is not always possible, as the siderophile elements often show fractionation. The fractionation may occur during the early stages of the impact or due to a later hydrothermal alteration (Koeberl, 1998, 2002).

2.4.2 The Os isotopic system

Abundance of Os in meteorites is several orders of magnitude higher than in crustal rocks (Koeberl, 2002, 2007). The isotope ^{187}Os forms by β^- decay of ^{187} Re. Re/Os ratio in meteorites is about 0.1, whereas in the crustal rocks the Re/Os ratios is generally higher than 10. The amount of the radiogenic isotope ^{187}Os is normalized to the abundance of the non-radiogenic isotope ^{188}Os. Because old crustal rocks have high Re and low Os abundances, their $^{187}Os/^{188}Os$ ratio increases rapidly in time; average upper crustal ratio is 1–1.2. Meteorites have low $^{187}Os/^{188}Os$ ratio (about 0.11–0.18) that changes only slightly in time (due to relatively low Re abundance). Due to high Os concentration in meteorites, even small addition of meteoritic matter can cause significant change in the Os isotopic ratio of the impactites (Koeberl and Shirey, 1993; Koeberl, 2002, 2007). One potential problem is that Os isotopic ratio of mantle rocks is similar to the ratio in meteorites. However, because Os concentrations in mantle rocks are much lower than in meteorites, much higher amount of mantle component would be required to make the same isotopic signature. Consequently, this component would be easily identified by petrographic or geochemical studies (Sr and Nd isotopes). Unfortunately, the Os isotopic system can not be used for identification of the projectile type (Koeberl, 2002).

2.4.3 The Cr isotopic system

Another geochemical method of detecting a meteoritic component uses the relative abundance of ^{53}Cr isotope, which is the daughter isotope of ^{53}Mn. The $^{53}Cr/^{52}Cr$ ratio is used. Terrestrial rocks do not show any variation in the $^{53}Cr/^{52}Cr$ ratio (Koeberl, 2002, 2007). Most meteorite types, in contrast, show variable excess of ^{53}Cr in comparison to terrestrial samples (Shukolyukov and Lugmair, 2000). With chromium isotopic data the

presence of meteoritic component can be confirmed, and furthermore also the meteorite type can be estimated. However, compared to the Os isotopic method, the Cr isotopic analysis is less sensitive and the analytical procedure is more complicated and time-consuming (Koeberl, 2002).

References:

Bartosova K., Ferrière L., Koeberl C., Reimold W. U., and Gier S. 2009. Petrographic and shock metamorphic studies of the impact breccia section (1397–1551 m depth) of the Eyreville drill core, Chesapeake Bay impact structure, USA. In *The ICDP-USGS deep drilling project in the Chesapeake Bay impact structure: Results from the Eyreville core holes,* edited by Gohn G. S., Koeberl C., Miller K. G., and Reimold W. U. *Geological Society of America Special Paper* 458: 317–348.

Bischoff A. and Stöffler D. 1984. Chemical and structural changes induced by thermal annealing of shocked feldspar inclusions in impact melt rocks from Lappajärvi crater, Finland. *Journal of Geophysical Research* 89: B645–B656.

Chao E. C. T., Shoemaker E. M, and Madsen B. M. 1960. First natural occurrence of coesite. *Science* 132: 220–222.

Cracknell A. P. 1969. *Crystals and their structures.* Great Britain: Pergamon Press Ltd. 231 p.

Deutsch A. and Koeberl C. 2006. Establishing the link between the Chesapeake Bay impact structure and the North American tektite strewn field: The Sr-Nd isotopic evidence. *Meteoritics and Planetary Science* 41: 689–703.

Dressler B. 1990. Shock metamorphic features and their zoning and orientation in the Precambrian rocks of the Manicouagan Structure, Quebec, Canada. *Tectonophysics* 171: 229–245.

Earth Impact Database. 2009. http://www.unb.ca/passc/ImpactDatabase/ (accessed December 2009)

Engelhardt W. v. and Bertsch W. 1969. Shock-induced planar deformation structures in quartz from the Ries crater, Germany. *Contributions to Mineralogy and Petrology* 20: 203–234.

Ferrière L. 2008. *Shock metamorphism and geochemistry of impactites from the Bosumtwi impact structure: A case study of shock-induced deformations and transformations in quartz and associated methodology.* PhD thesis, University of Vienna, Vienna, Austria. 279 p.

Ferrière L., Koeberl C., and Reimold W. U. 2009. Characterisation of ballen quartz and cristobalite in impact breccias: new observations and constraints on ballen formation. *European Journal of Mineralogy* 21: 203–217.

French B. M. 1968. Shock metamorphism as a geological process. In *Shock metamorphism of natural materials*, edited by French B. M., Short N. M. Baltimore, MD: Mono Book Corporation. p. 1–17.

French B. M. 1998. *Traces of catastrophe: A handbook of shock-metamorphic effects in terrestrial meteorite impact structures.* LPI contribution No. 954, Lunar and Planetary Institute, Houston. 120 p.

French B. M. and Koeberl C. 2010. The convincing identification of terrestrial meteorite impact structures: What works, what doesn't, and why. *Earth Science Reviews* 98: 123–170.

Gibson R. L., Townsend G. N., Horton J. W. Jr., and Reimold W. U. 2009. Pre-impact tectonothermal evolution of the crystalline basement-derived rocks in the ICDP-USGS Eyreville B core, Chesapeake Bay impact structure. In *The ICDP-USGS deep drilling project in the Chesapeake Bay impact structure: Results from the Eyreville core holes,* edited by Gohn G. S., Koeberl C., Miller K. G., and Reimold W. U. *Geological Society of America Special Paper* 458: 235–254.

Glass B. P. 1967. Microtektites in deep sea sediments. *Nature* 214:372–374.

Glass B. P. 1990. Tektites and microtektites: key facts and inferences. *Tectonophysics* 171: 393–404.

Glass B.P. and Koeberl C. 2006. Australasian microtektites and associated impact ejecta in the South China Sea and the Middle Pleistocene supereruption of Toba. *Meteoritics and Planetary Science* 41: 305–326.

Glass B. P., Liu S., and Leavens P. B. 2002. Reidite: An impact-produced high-pressure polymorph of zircon found in marine sediments. *American Mineralogist* 87: 562–565.

Grieve R. A. F. and Cintala M. J. 1992. An analysis of differential impact melt-crater scaling and implication for the terrestrial impact record. *Meteoritics* 27: 526–538.

Grieve R. A. F., Langenhorst F., and Stöffler D. 1996. Shock metamorphism of quartz in nature and experiment: II. Significance in geoscience. *Meteoritics and planetary science* 31: 6–35.

Gurov E. P. Gurova E. P., and Rakitskaya, R. B. 1995. Impact diamonds in the craters of the Ukrainian shield. Abstract. *Meteoritics* 30: 515–516.

Hartung J. and Koeberl C. 1994. In search of the Australasian tektite source crater: The Tonle Sap hypothesys. *Meteoritics* 29: 411–416.

Horton J. W. Jr., Kunk M. J., Belkin H. E., Aleinikoff J. N., Jackson J. C., and Chou I-M. 2009. Evolution of crystalline target rocks and impactites in the Chesapeake Bay impact structure, ICDP-USGS Eyreville B core. In *The ICDP-USGS deep drilling project in the Chesapeake Bay impact structure: Results from the Eyreville core holes,* edited by Gohn G. S., Koeberl C., Miller K. G., and Reimold W. U. *Geological Society of America Special Paper* 458: 277–316.

Kenkmann T., Artemieva N. A., Wünnemann K., Poelchau M. H., Elbeshausen D. and Nunez del Prado H. 2009. The Carancas meteorite impact crater, Peru: Geologic surveying and modeling of crater formation and atmospheric passage. *Meteoritics and Planetary Science* 44: 985–1000.

Koeberl C. 1986. Geochemistry of tektites and impact glasses. *Annual Reviews of Earth and Planetary Science* 14: 323–350.

Koeberl C. 1994. Tektite origin by hypervelocity asteroidal or cometary impact: Target rocks, source craters, and mechanisms. In *Large meteorite impacts and planetary evolution*, edited by Dressler B. O., Grieve R. A. F., and Sharpton V. L. *Geological Society of America Special Paper* 293: 133–151.

Koeberl C 1998. Identification of meteoritic components in impactites. In *Meteorites: Flux with time and impact effects*, edited by Grady M. M., Hutchinson R., McCall G. J. H., and Rothery D. A. Geological Society of London. Special Publication 140: 133–153.

Koeberl C. 1990. The geochemistry of tektites: An overview. *Tectonophysics* 171: 405–422.

Koeberl C. 2002. Mineralogical and geochemical aspects of impact craters. *Mineralogical Magazine* 66: 745–768.

Koeberl C. 2007. The geochemistry and cosmochemistry of impacts. In *Treatise of Geochemistry*, edited by Davis A. Online edition, Vol. 1, Elsevier. p. 1.28.1–1.28.52. doi:10.1016/B978-008043751-4/00228-5.

Koeberl C. and Shirey S. B. 1993. Detection of a meteoritic component in Ivory Coast tektites with rhenium-osmium isotopes. *Science* 261: 595–598.

Koeberl C., Kluger F., and Kiesl W. 1985. Rare earth elemental abundances in some impact glasses and tektites and potential parent materials. *Chemie der Erde* 44: 107–121.

Koeberl C., Poag C. W., Reimold W. U., and Brandt D. 1996. Impact origin of the Chesapeake Bay structure and the source of the North American tektites. *Science* 271: 1263–1266.

Koeberl C., Masaitis V. L., Shafranovsky G. I., Gilmour I., Langenhorst F., and Schrauder M. 1997. Diamonds from the Popigai impact structure, Russia. *Geology* 25: 967–970.

Maier W. D., Andreoli M. A. G., McDonald I., Higgins M. D., Boyce A. J., Shukolyukov A., Lugmair G. W., Ashwal L. D., Gräser P., Ripley E. M., and Hart R. J. 2006. Discovery of a 25-cm asteroid clast in the giant Morokweng impact crater, South Africa. *Nature* 441: 203–206.

Martini J. E. J. 1991. The nature, distribution and genesis of the coesite and stishovite associated with the pseudotachylite of the Vredefort Dome, South Africa. *Earth and Planetary Science Letters* 103: 285–300.

Masaitis V. L., Futergendler S. I., and Gnevushev M. A. 1972. Diamonds in impactites of the Popigai meteorite crater. *Zapiski Vsesoyuznoge Mineralogicheskogo Obshchestva* 101: 108–112 (in Russian).

Melosh H. J. 1989. *Impact cratering—A geological process.* New York: Oxford University Press. 245 p.

Montanari A. and Koeberl C. 2000. Impact stratigraphy. The Italian record. Berlin Heidelberg: Springer. 364 p.

Neuendorf K. K. E., Mehl J. P. Jr., and Jackson J. A. 2005. *Glossary of Geology.* Fifth edition. American Geological Institute, Alexandria, Virginia. United Book Press. 779 p.

O'Keefe J. A. 1963. *Tektites*. Chicago: University of Chicago Press. 228 p.

Osinski G. R., Grieve R. A. F., Collins G. S., Marion C., and Sylvester P. 2008. The effect of target lithology on the products of impact melting. *Meteoritics and Planetary Science* 43: 1939–1954.

Reimold W. U. 1995. Pseudotachylite in impact structures – generation by friction melting and shock brecciation?: A review and discussion. *Earth Science Reviews* 39: 247–265.

Reimold W. U. 2007. The impact crater bandwagon (Some problems with the terrestrial impact cratering record). *Meteoritics and Planetary Science* 42: 1467–1472.

Reimold W. U. and Koeberl C. 2008. Catastrophes, extinctions and evolution: 50 years of impact cratering studies. Golden Jubilee Memoir of the Geological Society of India 66: 69–110.

Reimold W. U., Horton J. W. Jr. and Schmitt R. T. 2008. Debate about impactite nomenclature – recent problems. *Large meteorite impacts and planetary evolution IV*. Conference Program & Abstract Volume, LPI contribution No. 1423. p. 187–188.

Rost R., Dolgov Y. A., and Vishnevsky S. A. 1978. Gases in inclusions of impact glass in the Ries crater, West Germany and finds of high-pressure carbon polymorphs. *Doklady Akademia Nauk SSSR* 241: 695–698 (in Russian).

Shoemaker E. M. and Chao E. C. T. 1961. New evidence for the impact origin of the Ries Basin, Bavaria, Germany. *Journal of Geophysical Research* 66: 3371–3378.

Shukolyukov A. and Lugmair G. W. 1998. Extraterrestrial matter on Earth: Evidence from the Cr isotopes (abstract). In *Catastropjic events and mass extinctions: Impacts and beyond*. LPI Contribution No. 1053; lunar and Planetary Institute, Houston. p. 197–198.

Short N. M. and Gold D. P. 1993. Petrographic analysis of selected core materials from the Manson (Iowa) impact structure (abstract). *Meteoritics and Planetary Science* 28: A436–437.

Short N. M. and Gold D. P. 1996. Petrography of shocked rocks from the central peak at the Manson impact structure. In *The Manson impact structure, Iowa; anatomy of an impact crate,* edited by Koeberl C. and Anderson R. R. *Geological Society of America Special Paper* 302: 245–265.

Stöffler D. 1972. Deformation and transformation of rock-forming minerals by natural and experimental shock processes. I. Behavior of minerals under shock compression. *Fortschritte der Mineralogie* 49: 50–113.

Stöffler D. and Grieve, R. A. F. 2007. Impactites, chapter 2.11. In *Metamorphic rocks: A classification and glossary of terms, recommendations of the International Union of Geological Sciences,* edited by Fettes D. and Desmons J. Cambridge, UK: Cambridge University Press. p. 82-92, 111– 125, and 126–242.

Stöffler D. and Langenhorst F. 1994. Shock metamorphism of quartz in nature and experiment: I. Basic observation and theory. *Meteoritics* 29: 155–181.

Stöffler D., Artemieva N. A., and Pierazzo E. 2002. Modeling the Ries–Steinheim impact event and the formation of the Moldavite strewn field. *Meteoritics and Planetary Science* 37: 1893–1907.

Stöffler D., Artemieva N. A., Ivanov B., Hecht L., Kenkmann T., Schmitt R.T., Tagle R. A., and Wittmann A. 2004. Origin and emplacement of the impact formations at Chicxulub, Mexico, as revealed by the ICDP deep drilling at Yaxcopoil-1 and by numerical modeling. *Meteoritics and Planetary Science* 39: 1035–1067.

Taylor S. R. and Koeberl C. 1994. The origin of tektites: Comment on a paper by J. A. O'Keefe. *Meteoritics* 29: 739–742.

Whitehead J., Spray J. G., and Grieve R. A. F. 2002. Origin of “toasted” quartz in terrestrial impact structures. *Geology* 30: 431–434.

CHAPTER 3: CHESAPEAKE BAY IMPACT STRUCTURE

3.1 Introduction

The late Eocene Chesapeake Bay impact structure is one of the largest and best preserved impact structures on Earth (e.g., Poag et al., 1994, 2004; Gohn et al., 2006a; Earth impact database, 2010). The structure is about 85 km in diameter and about 35.3 Myr old (e.g., Poag et al., 1994, 2004; Horton and Izett, 2005). The formation of the structure by an impact event was confirmed by Koeberl et al. (1996) by their finding of shocked minerals within the crater fill. Analyses of geographic position, age, and chemical and isotopic data led to the conclusion that the Chesapeake Bay impact structure is the likely source of the North American tektites (Koeberl et al., 1996; Deutsch and Koeberl, 2006).

Figure 3-1. Location of the Chesapeake Bay impact structure.

3.2 Geology of the Atlantic Coastal Plain

The Chesapeake Bay impact structure is located along the East coast of the United States (Fig. 3-1). The Atlantic Coastal Plain is a subsiding passive continental margin, where marine transgressions alternated with regressions during Cenozoic. Other processes that influenced the geology (e.g., the sediment supply) of the area include isostatic adjustment, Appalachian tectonics, and paleoclimatic changes (Poag, 1997).

The basement of the Virginia Coastal Plain comprises crystalline rocks that include a variety of plutonic, volcanic, and metamorphic rocks that constitute distal parts of the

Appalachian orogen (Thomas et al., 1989). Most of the Virginia Coastal Plain is underlain by the Chesapeake Block, Archean to Lower Proterozoic in age, which has been interpreted as African rocks accreted to the North American continent (Powars, 2000; Lefort and Max, 1991). The basement surface dips eastward, with a gentle dip between Richmond and Delmarva Peninsula, and then a steeper dip to the east from the Delmarva Peninsula (Poag, 1997).

The crystalline basement is overlain by thick sedimentary deposits of the Atlantic Coastal Plain, which constitute a seaward-thickening wedge of poorly consolidated siliciclastic sands, silts, and clays of both marine and non-marine origin (Poag et al., 2004). Deposition of these sediments began in the Late Jurassic with the opening of the Atlantic Ocean and the beginning of sea floor spreading (Powars, 2000). The 1 to 1.5 km thick pre-impact sediments of the Virginia Coastal Plain are Lower Cretaceous to lowest Upper Eocene in age. Because of similarities of the lithic facies and paucity of biostratigraphic data (pollen is the only biostratigraphic indicator found consistently in the deposits), it is difficult to correlate among and subdivide these deposits (Powars and Bruce, 1999). The following pre-impact formations have been distinguished (from the oldest to the youngest): Potomac Formation, Unnamed Formation, Brightseat Formation, Aquia Formation, Marlboro Clay, Nanjemoy Formation, and Piney Point Formation (Fig. 3-2; e.g., Poag et al., 2004; Gohn et al., 2005).

The Potomac Formation is the oldest (Early to Late Cretaceous) and thickest sedimentary formation of the Virginia Coastal Plain (Poag et al., 2004; Powars and Bruce, 1999; Powars, 2000). It lies unconformably on the crystalline basement. The Potomac Formation is mainly nonmarine (deltaic), siliciclastic, composed of quartz sand and silt (Powars, 2000; Poag et al., 2004). Fining-upward sequences are common (Powars and Bruce, 1999). Only a few upper Cretaceous beds of nonmarine, deltaic, as well as marine origin, 40 to 110 m thick, have been found in the Virginia Coastal Plain. The Brightseat Formation consists of the oldest Cenozoic deposits. There is mainly clayey quartz sand, rarely with glauconite (Poag et al., 2004). The Aquia Formation is of upper Paleocene age and consists of clayey, silty, quartz sands, glauconitic and shell-rich (Poag et al., 2004). Marlboro Clay are thin deposits (~2.5–5.5 m thick) of upper Paleocene age that consist of grey to pale-red plastic clays and reddish silts (Powars and Bruce, 1999; Poag et al., 2004). The Nanjemoy Formation was deposited during the lower Eocene and contains glauconitic sands with clay and silt (Powars, 2000). The youngest pre-impact formation is the Piney Point Formation, which was deposited during the middle Eocene. The Piney Point Formation is poorly sorted, olive gray, clayey, glauconite and fossil-rich. It contains some layers of hard, glauconitic, bioclastic limestone (Poag et al., 2004). The last sedimentary deposits that formed before the impact event were probably some late Eocene marine clays (Poag et al., 2004).

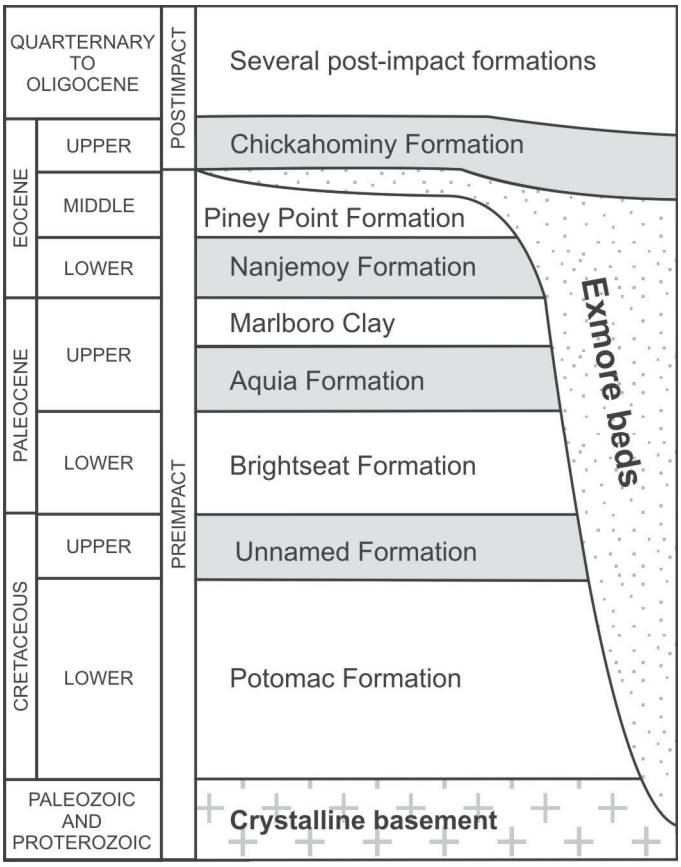

Figure 3-2. Stratigraphic succession of crystalline basement and sedimentary formations in southeastern Virginia. After Poag et al. (2004).

The formation of the crater apparently caused adjustments to the James River structural zone, disrupted the pre-impact sediments, and influenced subsequent sediment deposition and distribution patterns (Powars, 2000). Also the hydrogeology of the Virginia Coastal Plain was highly influenced. The differential flushing of seawater probably caused the formation of the "inland salt-water wedge"; high salinity water is concentrated inside the impact structure (Powars and Bruce, 1999).

Powars and Bruce (1999) reported that "The impact resulted in several regional anomalies: (1) a large crater, partly filled by impact and collapse debris; (2) mixing of Lower Cretaceous, Upper Cretaceous, Paleocene, and lower and upper Eocene sediments with seawater to form an impact tsunami-breccia; (3) a large area of anomalous water quality; (4) transformation of the depositional environment from inner neritic (shallow shelf) to bathyal (deep water) depths, in which fine-grained, low permeability sediments accumulated; and (5) a regional depression that persisted due to post-impact loading and differential compaction".

Marine sedimentation resumed immediately after the impact event and thus the impact structure was well protected from erosion (Poag et al., 2004). The crater's structural depression and subsequent structural adjustments since burial have influenced post-impact deposition and stratigraphic relations within and among formations and resulted in higher subsidence rates in the crater area (Powars and Bruce, 1999) Today the crater is covered by about 200–550 m of sediments (Poag et al., 2004). According to seismic data, most of these deposits dip concentrically into the crater (Powars and Bruce, 1999).

3.3 Discovery of the Chesapeake Bay impact structure

The first hint of an impact structure in the region came from the discovery of impact ejecta, which are part of the North American tektite strewn field. Based on the nature and thickness of impact ejecta recovered in the Deep Sea Drilling Project (especially from DSDP Site 612), approximate locations of the impact site were suggested by Thein (1987) and Koeberl (1989). Site 612 was drilled on the upper continental slope off New Jersey, approximately 330 km northeast of the center of the Chesapeake Bay impact structure (Koeberl, 1989; Koeberl et al., 1996). In 1992, Poag et al. interpreted the Exmore boulder bed in southeastern Virginia as deposits formed by tsunami-like wave generated by an impact event. In 1994, the existence of the Chesapeake Bay impact structure was proposed by Poag et al., based on analyses of core samples and seismic profiles. The impact origin of the Chesapeake Bay structure was confirmed by Koeberl et al. (1996), who found the first evidence of shocked minerals within the crater fill (in the Exmore breccia) at the Chesapeake Bay structure. Koeberl et al. (1996) reported on quartz grains with planar deformation features, including universal stage measurements of their crystallographic orientations. In addition, these authors presented chemical analyses of breccia and clast samples from the Exmore breccia and noted a similarity with the composition of the North American tektites, which suggest that the Chesapeake Bay structure is the source crater of those tektites. Koeberl et al. (1996) further showed that the distribution of gravity anomalies is typical of a complex impact structure and is in good agreement with the seismostratigraphic analyses and their interpretations.

3.4 Size and structure of the Chesapeake Bay impact structure

The Chesapeake Bay impact structure is about 85 km in diameter (Poag et al., 2004). The structure displays a complex crater geometry that has been described as “inverted sombrero” (Powars, 2000; Gohn et al., 2006a; Fig. 3-3). It has a deep inner basin (also called inner crater) with a small central uplift surrounded by a shallower, relatively flat, outer basin (also called annular trough). The central uplift is surrounded by a series of concentric valleys and ridges (Powars and Bruce, 1999). Gravity anomalies have been studied by, e.g., Koeberl et al. (1996), Poag et al. (2004), and Plescia et al. (2009). There is a subcircular negative anomaly above the inner basin and a ring of positive anomalies corresponding with the peak ring (Poag et al., 2004; Fig. 3-4).

The final size of the crater was largely influenced by the target properties. The structure was formed on a continental shelf, in a target with high rheological contrasts. There was a rigid crystalline basement covered with a thick layer of soft, water-saturated sediments. The formation of the final impact structure was also largely influenced by slumping of rocks and resurge of the oceanic water followed by tsunami-like waves. Collins and Wünnemann (2005) suggested that the impact structure would have been

much smaller if it had formed in a strong, homogeneous target. These authors proposed that the diameter of the inner basin, about 28 km (previous estimate 40 km, Poag et al., 2002), might better represent the energy involved in the impact event. Collins and Wünnemann (2005) also suggested that the unusually thick breccia deposit that fills the crater is a consequence of the layer of weak sediments in the upper part of the target.

Shah et al. (2005, 2009) presented detailed gravity and magnetic field data and refined the geophysical signatures of the structure. These authors also discussed the possible occurrence and volume of impact melt. In such a large impact crater as the Chesapeake Bay impact structure, a continuous melt sheet would be expected (Shah et al., 2005, 2009). However, so far, no large bodies of impact melt have been found in the Chesapeake Bay impact structure. Only two thin intervals of impact melt rock have been found in the Eyreville drill core (Horton et al., 2009a; Wittmann et al., 2009a, 2009b). These are probably just small melt pockets, rather than wide-spread melt sheets. Shah et al. (2005) estimated the volume of impact melt distributed around the central peak to be about 0.4–7.5 km^3. New magnetic field measurements and magnetic investigations of the Eyreville drill core suggest possible melt bodies in the western part of the inner basin (Shah et al., 2009). Wittmann et al. (2009a) estimated the total volume of melt in the crater to be 6–10.5 km^3 based on analyzing the melt volume in the Eyreville drill core and extrapolating the result on a circular area of the transient crater (28 km in diameter). These authors also mentioned the possibility that the melt rocks could have been reworked during the ocean resurge (maybe dispersed in a reaction between hot melt and seawater). Wittmann et al. (2009a) further suggested that an impact sheet could be buried at depth (as it is in, e.g., the Chicxulub impact structure).

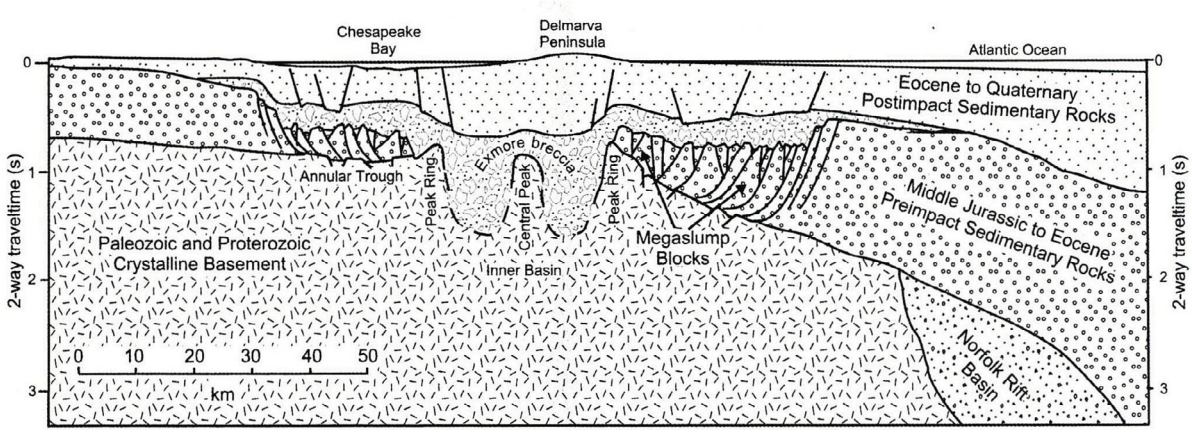

Fig. 3-3. Cross section of the Chesapeake Bay impact structure. Vertically exaggerated scale; 2-way travel time is shown on vertical axis. From Poag et al. (2004).

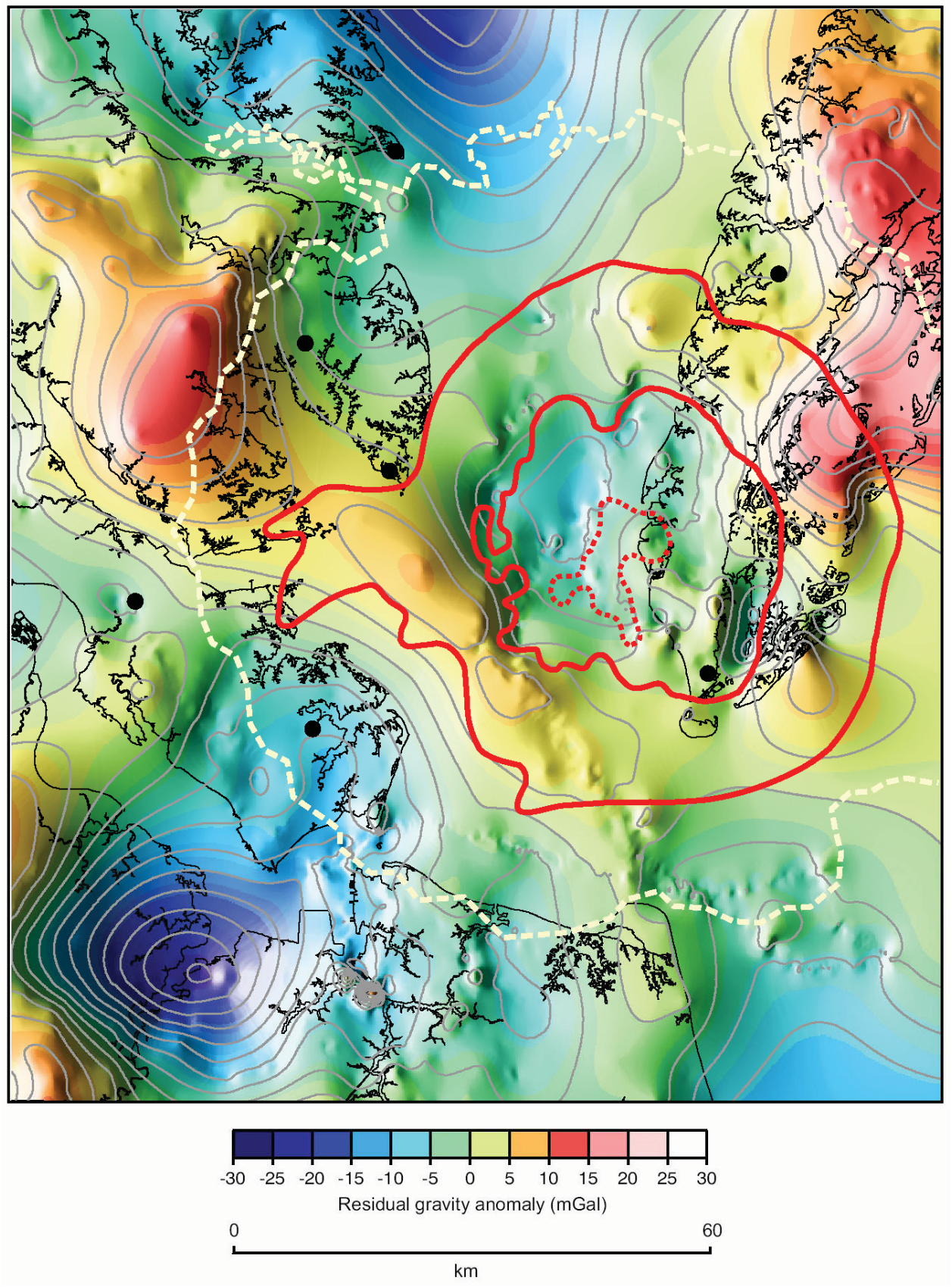

Figure 3-4. Gravity anomalies of the Chesapeake Bay impact structure. From Poag et al. (2004).

3.5 Geochemical studies and dating of the Chesapeake Bay impact structure

The Chesapeake Bay impact structure is buried under post-impact sediments and water, thus, today, samples of impactites are available only from drill cores. Poag et al. (2004) published major and trace element contents for a large suite of clasts of different lithic types (quartz sand, glauconitic sand, clayey sand, silt, clay, cherty breccia) extracted from Exmore breccia samples from the Exmore, Newport News, and Windmill Point cores. The analyzed samples show large variations in both, major and trace element contents. An extensive study of the chemical composition of the main target sediments was also performed by Deutsch and Koeberl (2006). These authors present geochemical data of samples from drill cores and outcrops, including several pre-impact sedimentary formations (Potomac, Aquia, Piney Point, and Nanjemoy Formation; Fig. 3-2), as well as the first post-impact deposit – the Chickahominy Formation. Recently, a large suite of impactite samples from the Eyreville drill core was analyzed by Schmitt et al. (2009; see Appendix 2 of the thesis).

A single rhyolite clast from the Exmore breccia and one monzogranite sample, both taken from the Langley core, were analyzed by Horton and Izett (2005). The granite, apparently derived from the crystalline basement, was cored at a depth of 626.3 m in the Langley core and was dated as being of Neoproterozoic age, 612 ± 10 Ma ($^{206}Pb/^{238}U$ weighted average age of igneous zircons; Horton et al., 2005a). Horton and Izett (2005) also interpreted the age of the impact to be 35.3 ± 0.1 Ma (±1σ), based on $^{40}Ar/^{39}Ar$ dating of North American tektites. Impact age of 35.7–35.8 Ma was obtained by studying the occurrence of calcareous nannofossils by Frederiksen et al. (2005). The same age was suggested by Edwards et al. (2005) based on projecting the base of the Chickahominy Formation into the timescale by Berggren et al. (1995); using zone boundaries and accumulation rates.

Only very small meteoritic component has been found in the Chesapeake Bay impactites and the type of the projectile has not been constrained yet. Lee et al. (2006) analyzed samples from the Sustainable Technology Park testhole and found that the rhenium and platinum-group element (PGE) concentrations of the impact melt rock are 30–270 times higher than those of basement gneiss. This, together with osmium isotopic data, indicated the presence of a very small, but discernable meteoritic component, which could be 0.01–0.1 % by mass, according to mixing calculations (Lee et al., 2006). New analyses of the impactites from the Eyreville drill core detected only very low platinum group element abundances and the chondrite-normalized abundance patterns are non-chondritic (McDonald et al., 2009).

3.6 North American tektites

The distal ejecta had been discovered many years before the Chesapeake Bay impact structure itself. The North American strewn field (see Fig. 2-8) contains tektites, microtektites, shocked minerals, and high pressure minerals (e.g., reidite, coesite, and stishovite; Glass, 1998, 2002). The general location of the source crater of the North American tektites along the east coast of the U.S. was suggested on the basis of the abundance and composition of distal ejecta (Thein, 1987; Koeberl, 1989; Glass, 1989). A possible candidate for the source impact structure was also the Toms Canyon underwater structure – a crater-like feature that has not yet been confirmed as being of impact origin. Poag et al. (1994) infirmed that the North American tektites originated from Toms Canyon, because the structure is too small and shallow and the target rocks are carbonate-dominated. Koeberl et al. (1996) found good agreement in chemical composition between the North American tektites and breccia fragments from the Chesapeake Bay impact structure. Further analyses of Sr and Nd isotopic composition by Whitehead et al. (2000) confirmed that the Chesapeake Bay impact structure is the likely source of the North American tektites. More samples from the Chesapeake Bay impact structure were analyzed by Deutsch and Koeberl (2006). These authors found a correlation of Sr-Nd data and a great similarity in refractory and lithophile element contents, including the rare earth elements (REE), between the tektites and the target rocks (sediments, one Exmore breccia sample, and one granite sample) from the Bayside core from the Chesapeake Bay impact structure. The isotope and compositional data by Deutsch and Koeberl (2006) excluded another possible source crater for the North American tektites, the nearly coeval Popigai impact structure in Russia (see also chapter 4 of the thesis).

3.7 Deep drilling at the Chesapeake Bay impact structure

Previous drilling operations at the Chesapeake Bay impact structure have been summarized in detail by Poag et al. (2004) and Horton et al. (2005b). The most important drill cores in the Chesapeake Bay area are summarized in Table 3-1, and Figs. 3-5 and 3-6. First drill cores in the area were recovered already in 1940s. These drill cores included samples of impact breccias, but their impact origin was not suspected until 1992 (Poag et al., 1992, 2004; Koeberl et al., 1996). The Exmore boulder bed was cored in 1986 in the Exmore corehole (Poag et al., 1992). In the late 1980s and early 1990s Exmore breccia was cored at the Kiptopeke, Newport News Park, and Windmill Point coreholes (Poag et al., 2004).

Four important drill cores were drilled in the years 2000-2002: North, Bayside, and NASA Langley in the annular trough, and Watkins School at the outer margin of the impact structure. The Bayside corehole penetrated the post-impact, impact-generated, and impact-modified sediments and reached the underlying Precambrian crystalline rocks

(Horton et al., 2008). In 2000 the continuously cored NASA Langley core was drilled on the York-James Peninsula in Hampton. The core includes 236 m of upper Eocene-Pleistocene deposits, 390 m of impact-generated deposits, and 9 m of underlying medium-grained Precambrian monzogranite. Based on lithology, sedimentary structure, clast-matrix ratio, and deformation, Gohn et al. (2001) distinguished three units within impact-generated deposits in the NASA Langley core. The lowermost unit - so-called crater unit A - typically consists of feldspathic, medium-grained to gravelly quartz sands and contains minor amounts of dark-colored clay-silt clasts and quartz, quartzite, and chert and granodiorite pebbles. Crater unit B above is a clast-supported sedimentary-clast breccia that has been derived probably from the Cretaceous Potomac Formation. The uppermost crater unit C is a different sedimentary breccia, which is matrix-supported and contains a mixture of clasts derived from the lower Tertiary formations and the Cretaceous Potomac Formation (Gohn et al., 2001). In the samples from the NASA Langley core very rare quartz grains with planar deformation features were found (Horton and Izett, 2005.

TABLE 3-1. IMPORTANT DRILL CORES IN THE CHESAPEAKE BAY AREA

Short name	Detailed name	Year	Depth (m)	Relative location
Putneys Mill	Putneys Mill Corehole	1979	39.6	outside crater
MW4	MW4 Corehole	1980s	299.6	outside crater
Haynesville	USGS Corehole Haynesville No.2	1985	169.5	outside crater
Exmore	USGS Exmore Corehole	1986	416.4	annular trough
Dismal Swamp	Dismal Swamp Corehole	1987	566	outside crater
Jenkins Bridge	Jenkins Bridge Corehole	1987	400.5	outside crater
Fentress	Fentress Corehole	1988	611.1	outside crater
Kiptopeke	Va.Dept.Env.Qual. Kiptopeke Corehole	1989	607.5	inner basin
Newport	Va.Dept.Env.Qual. Newport News Park II Corehole	1990	173.7	outer margin
Windmill	USGS Windmill Point Corehole	1992	226.7	outer margin
Jamestown	Jamestown Corehole	1995	82.9	outside crater
NASA Langley	USGS NASA Langley Corehole	2000	632.7	annular trough
North	USGS North Corehole	2001	430.5	annular trough
Bayside	USGS Bayside Corehole	2001	728.2	annular trough
Watkins School	USGS Watkins School	2002	300.3	outer margin
Cape Charles	USGS STP test hole	2004	823	flank of central uplift
Eyreville	ICDEP-USGS Eyreville Corehole	2005-6	1766.3	central part, moat

Data from Poag et al. 2004, Sanford et al. 2004, Gohn et al. 2006a, D.S. Powars, USGS, pers. comm., 2007)

A deep drilling proposal was put to ICDP for a continuous corehole through the interior of the Chesapeake Bay impact structure in 2003. Subsequently, in 2004 a testhole was drilled by USGS near Cape Charles. This 823 m deep Sustainable Technology Park (STP) testhole was partially cored (with a core diameter of 64 mm). The core consists of 355 m of marine, upper Eocene to Pleistocene sediments, 300 m of sedimentary-clast breccia, and 167 m of crystalline-clast breccias (largely suevitic) and cataclastic gneiss (Horton et al., 2005c; Gohn et al., 2007). The suevite from the STP testhole contains glassy to aphanitic melt. Some melt particles display flow lamination and some have

shapes and textures that suggest compaction of still hot and plastic particles (Horton et al., 2005c). The suevite was albitized and chloritized at lower greenschist facies conditions (Horton et al., 2005c). There are amygdules filled with clay minerals and carbonates in the suevite (Horton et al., 2005c). Clasts in suevite and in brecciated gneiss contain quartz and feldspar grains that show multiple sets of decorated PDFs (Horton et al., 2005c).

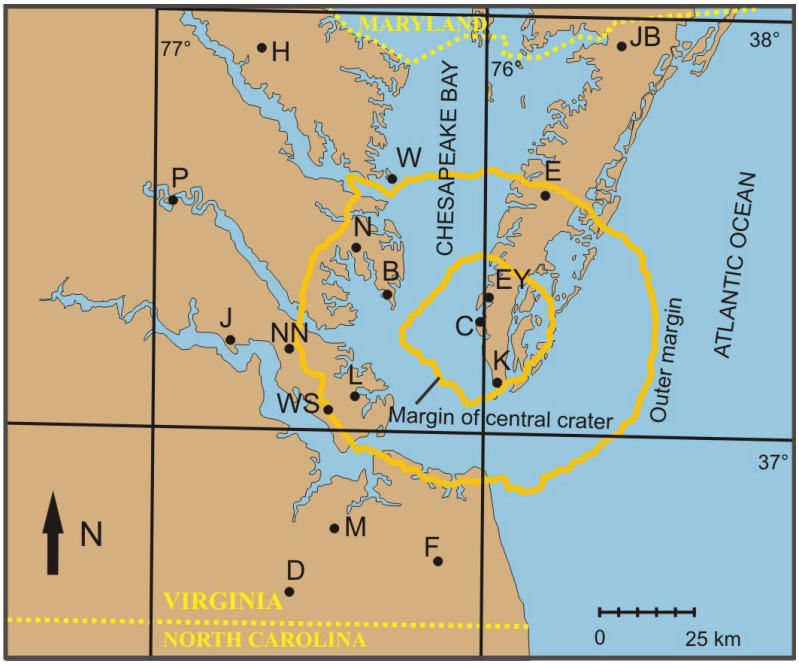

Figure 3-5. Map of Chesapeake Bay (modified from Horton et al., 2005b), showing the location of the Chesapeake Bay impact structure and major core holes. B-Bayside, C-Cape Charles USGS Sustainable Technology Park (STP), D-Dismal Swamp, E-Exmore, EY-Eyreville, F-Fentress, H-Haynesville, J-Jamestown, JB-Jenkins Bridge, K-Kiptopeke, L-USGS-NASA Langley, M-MW4, N-North, NN-Newport News Park 2, P-Putneys Mill, W-Windmill Point, and WS-Watkins School.

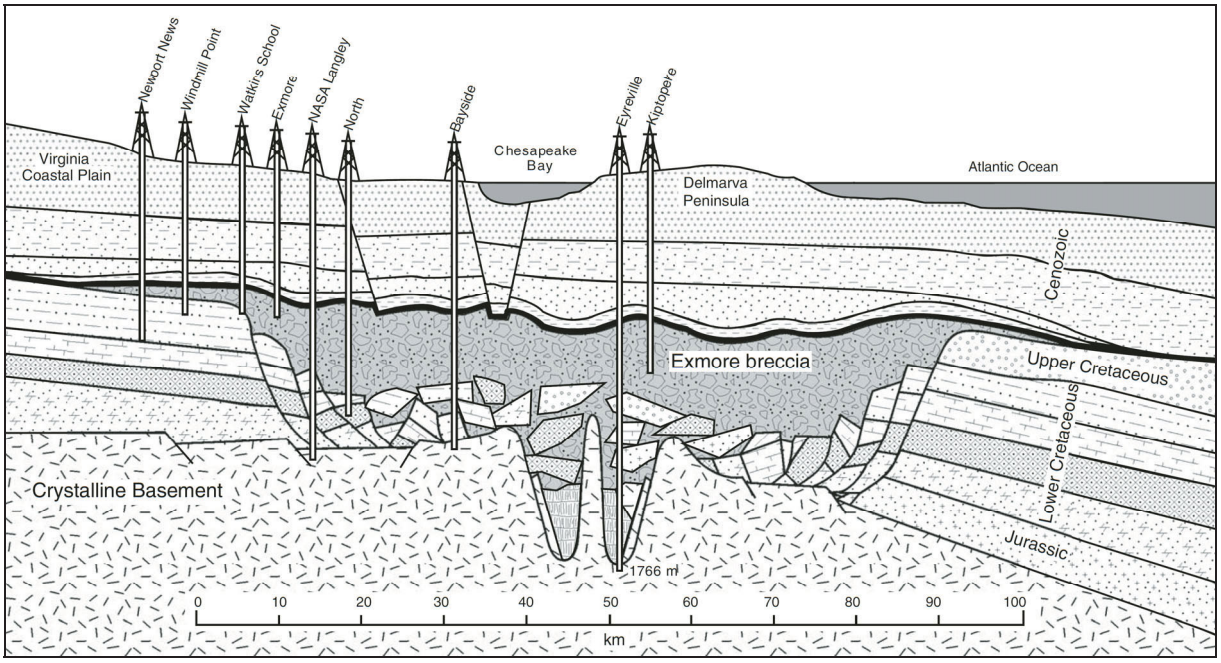

Fig. 3-6. Cross section of the Chesapeake Bay impact structure, showing approximate position of major drill cores (projected to line of section). Vertically exaggerated. From Poag (2009).

3.8 Eyreville drill core

In 2005–2006 three boreholes were drilled as part of the ICDP-USGS Chesapeake Bay Impact Structure Drilling Project at Eyreville Farm in Northampton County, Virginia, USA. Eyreville hole A was cored in 2005 from 125 to 941 m depth (with core diameters of 85 mm and 63.5 mm in the intervals 125.6–591.0 m and 591.0–940.9 m, respectively). Eyreville hole B was cored in 2005 from 738 m to a final depth of 1766 m (with core diameters of 63.5 mm and 47.6 mm in the intervals 737.6–1100.9 m and 1100.9–1766.3 m, respectively). Eyreville hole C was cored in 2006 from the land surface to 140 m depth (with a core diameter of 63.5 mm; Gohn et al., 2006a, 2006b, 2008). More details about the coring operations at Eyreville have been reported in Gohn et al. (2006b).

General information about the drill core has been summarized by Gohn et al. (2009a). A detailed geologic column of the Eyreville drill core was established by Horton et al. (2009a) for the depth interval 1766–1095 m, by Edwards et al. (2009a) for the depth interval 1096–444 m, and by Edwards et al. (2009b) for the post-impact sediments (depth interval 444–0 m). The core is now stored at the USGS in Reston, Virginia.

According to the changes in lithology of the core, the Eyreville drill core has been subdivided into several main sections (Fig. 3-6). The lowermost section of the Eyreville core (1551-1766 m depth) consists of crystalline basement-derived rocks. There are granites and pegmatites alternating with mica schists (Gohn et al., 2006a, 2008, Horton et al., 2009a). It has been suggested by, e.g., Kenkmann et al. (2009) and Horton et al. (2009a) that these crystalline rocks do not represent in situ crater floor, but they are rather parautochtonous blocks derived from the weakly to unshocked material originating at the edge of the transient cavity. The crystalline basement was studied in detail by, e.g., Townsend et al. (2009), Gibson et al. (2009), and Horton et al. (2009a, 2009b).

A section of impact breccia was cored in the depth interval from 1397 to 1551 m. Most of the impact breccia interval consists of suevite. In the upper part of the impact breccia (above 1474 m) there are two intervals of impact melt rock (Wittmann et al., 2009b). In the lower part there are meter-sized blocks of cataclastic gneiss (Horton et al., 2009a). More information about the impact breccia section can be found in, e.g., Horton et al. (2009a, 2009b), Bartosova et al. (2009a, chapter 6 of the thesis), Bartosova et al. (2009b, chapter 7 of the thesis), and Wittmann et al. (2009a, 2009b). A small suevite boulder occurs in gravelly sand between 1393.0 and 1393.4 m depth above the impactite section, and some melt particles (thought to be derived from reworked suevite) are present within the gravelly sand between 1396.4 and 1397.2 m (Horton et al., 2009a). Suevite occurs also in the form of several dike breccia veins in the crystalline basement (Reimold et al., 2007).

Above impact breccia interval there is a thin layer of gravelly sand (1371-1397 m depth). The gravelly sand is very poorly lithified and is probably derived from non-marine

pre-impact sediments (Gohn et al., 2009b). The gravelly sand interval has been extensively studied by, e.g., Gohn et al. (2009b), Self-Trail et al. (2009), Reimold et al. (2009, Appendix 1 of the thesis), and Bartosova et al. (submitted, chapter 10 of the thesis).

A granitic megablock and an amphibolitic block occur embedded in gravelly sand. The smaller amphibolitic block (1376-1390 m depth) is most likely of igneous origin and has been metamorphosed in amphibolite facies (Townsend et al., 2009). The large granitic slab (in the depth interval 1371–1096 m) consists of fine- to coarse-grained granite, in parts gneissic (Townsend et al., 2009; Horton et al., 2009a, 2009b).

Above the granitic megablock, there is the thickest section of the Eyreville drill core (1096–444 m depth), consisting of sedimentary breccias and sediment blocks. This section has been subdivided into an informal lower unit of "sediment boulders and sand" (1095.7–867.4 m) and a newly formalized Exmore Formation (Edwards et al., 2009a). In the Exmore Formation, Edwards et al. (2009a) further distinguished four informal units (from base to top, Fig. 3-6): lower diamicton member (867.4–856.6 m), block-dominated member (856.6–618.2 m), upper diamicton member (618.2–451.0 m), and stratified member (451.0–443.9 m). The diamicton members have been interpreted as resurge debris flows (Gohn et al., 2009b; Ormö et al., 2009). The diamicton members consist of muddy glauconitic quartz sand matrix with polymict sediment clasts, crystalline rock clasts, and mixed-age microfossils (Edwards et al., 2009a; Self-Trail et al., 2009). There are also parts with abundant melt particles and very rare shocked quartz grains (Reimold et al., 2009). The clay mineralogy of the sedimentary breccias has been studied by Larsen et al. (2009) and Ferrell and Dypvik (2009).

The uppermost section of the composite Eyreville drilling consists of 444 m of post-impact sediments that have been extensively studied by, e.g., Edwards et al. (2009b), Poag (2009), Browning et al. (2009), and Kulpecz et al. (2009).

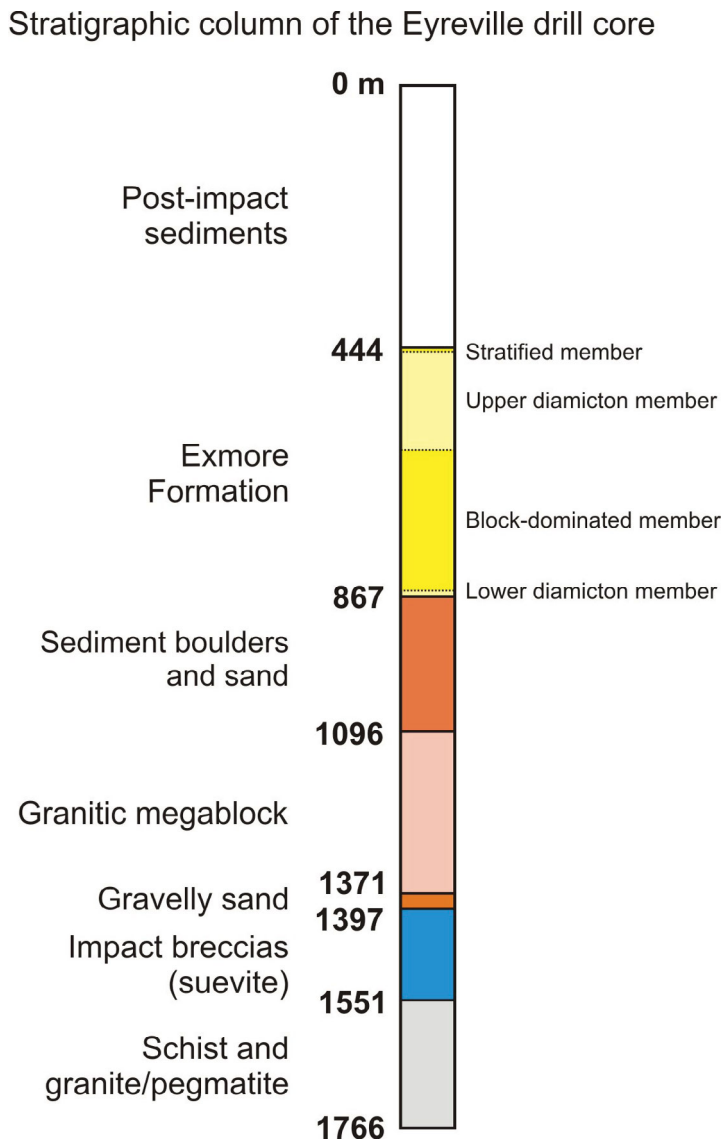

Figure 3-6. Simplified stratigraphic column of the Eyreville drill core showing the main lithologies. Modified from Gohn et al. (2006a, 2008) and Horton et al. (2009a) and Edwards et al. (2009a). Depth is below surface in meters.

References:

Bartosova K., Ferrière L., Koeberl C., Reimold W. U., and Gier S. 2009a. Petrographic and shock metamorphic studies of the impact breccia section (1397 – 1551 m depth) of the Eyreville drill core, Chesapeake Bay impact structure, USA. In *The ICDP-USGS deep drilling project in the Chesapeake Bay impact structure: Results from the Eyreville core holes,* edited by Gohn G. S., Koeberl C., Miller K. G., and Reimold W. U. *Geological Society of America Special Paper* 458: 317–348.

Bartosova K., Mader D., Schmitt R. T., Ferrière L., Koeberl C., Reimold W. U., and Brandstaetter F. 2009b. Geochemistry of the impact breccia section of the Eyreville drill core, Chesapeake Bay impact structure, USA. In *The ICDP-USGS deep drilling project in the Chesapeake Bay impact structure: Results from the Eyreville core holes,* edited by Gohn G. S., Koeberl C., Miller K. G., and Reimold W. U. *Geological Society of America Special Paper* 458: 397–433.

Berggren W. A., Kent D. V., Swisher C. C. III, and Aubry M. P. 1995. A revised Cenozoic geochronology and chronostratigraphy. In *Geochronology, time scales and global stratigraphic correlation*, edited by Berggren W. A., Kent D. V., Aubry M. P., and Hardenbol J. *Society for Sedimentary Geology Special Publication* 54: 129–212.

Browning J. V., Miller K. G., McLaughlin P. P. Jr., Edwards L. E., Kulpecz A. A., Powars D. S., Wade B. S., Feigenson M. D., and Wright J. D. 2009. Integrated sequence stratigraphy of the postimpact sediments from the Eyreville core holes, Chesapeake Bay impact structure inner basin. In *The ICDP-USGS deep drilling project in the Chesapeake Bay impact structure: Results from the Eyreville core holes,* edited by Gohn G. S., Koeberl C., Miller K. G., and Reimold W. U. *Geological Society of America Special Paper* 458: 775–810,

Collins G. S. and Wünnemann K. 2005. How big was the Chesapeake Bay impact? Insight from numerical modeling. *Geology* 33: 925–928.

Deutsch A. and Koeberl C. 2006. Establishing the link between the Chesapeake Bay impact structure and the North American tektite strewn field: The Sr-Nd isotopic evidence. *Meteoritics and Planetary Science* 41: 689–703.

Earth Impact Database. 2010. http://www.unb.ca/passc/ImpactDatabase/ (accessed in January, 2010)

Edwards L. E., Barron J. A., Bukry D., Bybell L. M., Cronin T. M., Poag C. W., Weems R. E., and Wingard G. L. 2005. Paleontology of the Upper Eocene to Quaternary postimpact section in the USGS-NASA Langley core, Hampton, Virginia. *US Geological Survey Professional Paper* 1688: H1–H47.

Edwards L. E., Powars D. S., Gohn G. S., and Dypvik H. 2009a. Geologic columns for the ICDP-USGS Eyreville A and B cores, Chesapeake Bay impact structure: Sediment breccias, 444 to 1,096 m depth. In *The ICDP-USGS deep drilling project in the Chesapeake Bay impact structure: Results from the Eyreville core holes,* edited by Gohn G. S., Koeberl C., Miller K. G., and Reimold W. U. *Geological Society of America Special Paper* 458: 51–90.

Edwards L. E., Powars D. S., Browning J. V., McLaughlin P. P., Miller K. G., Self-Trail J. M., Kulpecz A. A., and Elbra T. 2009b. Geologic columns for the ICDP-USGS Eyreville A and C coreholes, Chesapeake Bay impact structure: Post-impact sediments, 0 to 444 m depth. In *The ICDP-USGS deep drilling project in the Chesapeake Bay impact structure: Results from the Eyreville core holes,* edited by Gohn G. S., Koeberl C., Miller K. G., and Reimold W. U. *Geological Society of America Special Paper* 458: 91–114.

Ferrell R. E. Jr. and Dypvik H. 2009. The mineralogy of the Exmore – Chickahominy boundary section of the Chesapeake Bay Impact structure – the Eyreville core. In *The ICDP-USGS deep drilling project in the Chesapeake Bay impact structure: Results from the Eyreville core holes,* edited by Gohn G. S., Koeberl C., Miller K. G., and Reimold W. U. *Geological Society of America Special Paper* 458: 723–746.

Frederiksen O., Edwards L. E., Self-Trail J. M., Bybell L. M., and Cronin T. M. 2005. Paleontology of the impact-modified and impact-generated sediments in the USGS-NASA Langley core, Hampton, Virginia. *US Geological Survey Professional Paper* 1688: D1–D37.

Gibson R. L., Townsend G. N., Horton J. W. Jr., and Reimold W. U. 2009. Pre-impact tectonothermal evolution of the crystalline basement-derived rocks in the ICDP-USGS Eyreville B core, Chesapeake Bay impact structure. In *The ICDP-USGS deep drilling project in the Chesapeake Bay impact structure: Results from the Eyreville core holes,* edited by Gohn G. S., Koeberl C., Miller K. G., and Reimold W. U. *Geological Society of America Special Paper* 458: 235–254.

Glass B. P. 1998. Upper Eocene tektite and impact ejecta layer on the continental slope off New Jersey. *Meteoritics and Planetary Science* 33: 229–241.

Glass B. P. 2002. Upper Eocene impact ejecta/spherule layers in marine sediments. *Chemie der Erde* 62: 173–196.

Gohn G. S., Clark A. C., Queen D. G., Levine J. S., McFarland E. R., and Powars D. S. 2001. Operational and geological summary for the USGS-NASA Langley corehole, Hampton, Virginia. *USGS Open-File Report* 01-87, 19 p.

Gohn G. S., Powars D. S., Bruce T. S., and Self-Trail J. M. 2005. Physical geology of the impact-modified and impact-generated sediments in the USGS-NASA Langley core, Hampton, Virginia. *US Geological Survey Professional Paper* 1688: C1–C38.

Gohn G. S., Koeberl C., Miller K. G., Reimold W. U., Cockell C. S., Horton J. W. Jr., Sanford W. E., and Voytek M. A. 2006a. Chesapeake Bay impact structure drilled. *EOS, Transactions, American Geophysical Union* 87: 349 & 355.

Gohn G. S., Koeberl C., Miller K. G., Reimold W. U., and the scientific staff of the Chesapeake Bay impact structure drilling project. 2006b. Chesapeake Bay impact structure deep drilling project completes coring. *Scientific Drilling* 2006: 34–37.

Gohn G. S., Sanford W. E., Powars D. S., Horton J. W. Jr., Edwards L. E., Morin R. H., and Self-Trail J. M. 2007. Site report for USGS test holes drilled at Cape Charles, Northampton County, Virginia, in 2004: *U.S. Geological Survey Open-File Report* 2007–1094, 22 p.

Gohn G. S., Koeberl C., Miller K. G., Reimold W. U., Browning J. V., Cockell C. S., Horton J. W. Jr., Kenkmann T., Kulpecz A.A., Powars D. S., Sanford W.E., and Voytek M. A. 2008. Deep drilling into the Chesapeake Bay impact structure. *Science* 320: 1740–1745.

Gohn G. S., Koeberl, C., Miller, K. G., and Reimold W. U. 2009a. Deep drilling in the Chesapeake Bay impact structure – An overview. In *The ICDP-USGS deep drilling project in the Chesapeake Bay impact structure: Results from the Eyreville core holes,* edited by Gohn G. S., Koeberl C., Miller K. G., and Reimold W. U. *Geological Society of America Special Paper* 458: 1–20.

Gohn G. S., Powars D. S., Dypvik H., and Edwards L. E. 2009b. Rock-avalanche and ocean-resurge deposits in the late Eocene Chesapeake Bay impact structure: Evidence from the ICDP-USGS Eyreville cores, Virginia, USA. In *The ICDP-USGS deep drilling project in the Chesapeake Bay impact structure: Results from the Eyreville core holes,* edited by Gohn G. S., Koeberl C., Miller K. G., and Reimold W. U. *Geological Society of America Special Paper* 458: 587–616.

Horton J. W. Jr. and Izett G. A. 2005. Crystalline-rock ejecta and shocked minerals of the Chesapeake Bay impact structure, USGS-NASA Langley core, Hampton, Virginia, with supplemental constraints on the age of impact. In *Studies of the Chesapeake Bay impact structure—The USGS-NASA Langley corehole, Hampton, Virginia, and related coreholes and geophysical surveys*, edited by Horton J. W. Jr., Powars D. S., and Gohn G. S. *US Geological Survey Professional Paper* 1688: E1–E30.

Horton J. W. Jr., Aleinikoff J. N., Kunk M. J., Naeser C. W., and Naeser N. D. 2005a. Petrography, structure, age, and thermal history of granitic coastal plain basement in the Chesapeake Bay impact structure, USGS-NASA Langley core, Hampton, Virginia. In *Studies of the Chesapeake Bay impact structure—The USGS-NASA Langley corehole, Hampton, Virginia, and related coreholes and geophysical surveys*, edited by Horton J. W. Jr., Powars D. S., and Gohn G. S. *US Geological Survey Professional Paper* 1688: B1–B29.

Horton J. W. Jr., Powars D. S., and Gohn G. S. 2005b. Studies of the Chesapeake Bay Impact Structure – Introduction and discussion. US Geological Survey Professional Paper 1688: A1–A24.

Horton J. W. Jr., Gohn G. S., Jackson J. C., Aleinikoff J. N., Sanford W. E., Edwards L. E., and Powars D. S. 2005c. Results from a scientific test hole in the central uplift, Chesapeake Bay impact structure, Virginia, USA (abstract #2003). 36th Lunar and Planetary Science Conference. CD-ROM.

Horton J. W. Jr., Gohn G. S., Powars D. S., and Edwards L. E. 2008. Origin and emplacement of impactites in the Chesapeake Bay impact structure, Virginia, USA. In *The sedimentary record of meteorite impacts*, edited by Evans K., Horton J. W. Jr., King D. T. Jr., and Morrow J. R. *Geological Society of America Special Paper 437*: 73–97.

Horton J. W. Jr., Gibson R. L., Reimold W. U., Wittmann A., Gohn G. S., and Edwards L. E. 2009a. Geologic column for the ICDP-USGS Eyreville B core, Chesapeake Bay impact structure: Impactites and crystalline rocks, 1,096–1,766 m. In *The ICDP-USGS deep drilling project in the Chesapeake Bay impact structure: Results from the Eyreville core holes,* edited by Gohn G. S., Koeberl C., Miller K. G., and Reimold W. U. *Geological Society of America Special Paper* 458: 21–49.

Horton J. W. Jr., Kunk M. J., Belkin H. E., Aleinikoff J. N., Jackson J. C., and Chou I-M. 2009b, Evolution of crystalline target rocks and impactites in the Chesapeake Bay impact structure, ICDP-USGS Eyreville B core. In *The ICDP-USGS deep drilling project in the Chesapeake Bay impact structure: Results from the Eyreville core holes,* edited by Gohn G. S., Koeberl C., Miller K. G., and Reimold W. U. *Geological Society of America Special Paper* 458: 277–316.

Kenkmann T., Collins G. S., Wittmann A., Wünnemann K., Reimold W. U., and Melosh J. H. 2009. A model for the formation of the Chesapeake Bay impact crater as revealed by drilling and numerical simulation. In *The ICDP-USGS deep drilling project in the Chesapeake Bay impact structure: Results from the Eyreville core holes,* edited by Gohn G. S., Koeberl C., Miller K. G., and Reimold W. U. *Geological Society of America Special Paper* 458: 571–586.

Koeberl C. 1989. New estimates of area and mass for the North American tektite strewn field. Proceedings of the 19th Lunar and Planetary Science Conference, Cambridge University Press, New York, p. 745–751.

Koeberl C., Poag C. W., Reimold W. U., and Brandt D. 1996. Impact origin of the Chesapeake Bay structure and the source of the North American tektites. *Science* 271: 1263–1266.

Kulpecz A. A., Miller K. G., Browning J. V., Edwards L. E., Powars D. S., McLaughlin P. P. Jr., Harris A. D., and Feigenson M. D. 2009. Postimpact deposition in the Chesapeake Bay impact structure: Variations in eustasy, compaction, sediment supply, and passive-aggressive tectonism. In *The ICDP-USGS deep drilling project in the Chesapeake Bay impact structure: Results from the Eyreville core holes,* edited by Gohn G. S., Koeberl C., Miller K. G., and Reimold W. U. *Geological Society of America Special Paper* 458: 811–837.

Larsen D., Stephens E. C., and ZivkovicV. B. 2009. Postimpact alteration of sedimentary breccias in the ICDP-USGS Eyreville A and B cores with comparison to the Cape Charles core, Chesapeake Bay impact structure, Virginia, USA. In *The ICDP-USGS deep drilling project in the Chesapeake Bay impact structure: Results from the Eyreville core holes,* edited by Gohn G. S., Koeberl C., Miller K. G., and Reimold W. U. *Geological Society of America Special Paper* 458: 699–722.

Lee S. R., Horton J. W. Jr., and Walker R. J. 2006. Confirmation of a meteoritic component in impact-melt rocks of the Chesapeake Bay impact structure, Virginia, USA - Evidence from osmium isotopic and PGE systematics. *Meteoritics and Planetary Science* 41: 819–833.

Lefort J. P. and Max M. D. 1991. Is there an Archean crust beneath Chesapeake Bay? *Tectonics* 10: 213–226.

McDonald, I., Bartosova, K., and Koeberl, C., 2009, Search for a meteoritic component in impact breccia from the Eyreville core, Chesapeake Bay impact structure: Considerations from platinum group element contents. In *The ICDP-USGS deep drilling project in the Chesapeake Bay impact structure: Results from the Eyreville core holes,* edited by Gohn G. S., Koeberl C., Miller K. G., and Reimold W. U. *Geological Society of America Special Paper* 458: 469–479.

Ormö J., Sturkell E., Horton J. W. Jr., Powars D. S., and Edwards L. E. 2009. Comparison of clast frequency and size in the resurge deposits at the Chesapeake Bay impact structure (Eyreville A and Langley cores): Clues to the resurge process. In *The ICDP-USGS deep drilling project in the Chesapeake Bay impact structure: Results from the Eyreville core holes,* edited by Gohn G. S., Koeberl C., Miller K. G., and Reimold W. U. *Geological Society of America Special Paper* 458: 617–632.

Plescia J. B., Daniels D. L., and Shah A. K. 2009. Gravity investigations of the Chesapeake Bay impact structure. In *The ICDP-USGS deep drilling project in the Chesapeake Bay impact structure: Results from the Eyreville core holes,* edited by Gohn G. S., Koeberl C., Miller K. G., and Reimold W. U. *Geological Society of America Special Paper* 458: 181–193.

Poag C. W. 1997. The Chesapeake Bay bolide impact: A convulsive event in Atlantic Coastal Plain evolution. *Sedimentary Geology* 108: 45–90.

Poag C. W. 2009. Paleoenvironmental recovery from the Chesapeake Bay bolide impact: The benthic foraminiferal record. In *The ICDP-USGS deep drilling project in the Chesapeake Bay impact structure: Results from the Eyreville core holes,* edited by Gohn G. S., Koeberl C., Miller K. G., and Reimold W. U. *Geological Society of America Special Paper* 458: 747–773.

Poag C. W., Powars D. S., Poppe L. J., Mixon R. B., Edwards L. E., Folger D. W., and Bruce S. 1992. Deep Sea Drilling Project Site 612 bolide event: New evidence of a late Eocene impact-wave deposit and a possible impact site, U.S. east coast. *Geology* 20: 771–774.

Poag C. W., Powars D. S., Poppe L. J., and Mixon R. B. 1994. Meteoroid mayhem in Ole Virginny: source of the North American tektite strewn field. *Geology* 22: 691–694.

Poag C. W., Plecsia J. B., and Molzer P. C. 2002. Ancient impact structures on modern continental shelves: The Chesapeake Bay, Montagnais, and Toms Canyon craters, Atlantic margin of North America. *Deep-Sea Research II* 49: 1081–1102.

Poag C. W., Koeberl C., and Reimold W. U. 2004. *The Chesapeake Bay crater: Geology and geophysics of a late Eocene submarine impact structure.* Impact Studies series. Heidelberg: Springer. 522 p.

Powars D. S. 2000. The effects of the Chesapeake Bay impact crater on the geologic framework and the correlation of hydrogeologic units of southeastern Virginia, south of the James River. *US Geological Survey Professional Paper* 1622, 55 p.

Powars D. S. and Bruce T. S. 1999. The effects of the Chesapeake Bay impact crater on the geological framework and correlation of hydrogeologic units of the lower York-James Peninsula, Virginia. *US Geological Survey Professional Paper* 1612: 1–82.

Reimold W. U., Kenkmann T., Gibson R. L., Bartosova K., Schmitt R. T., Hecht L., Koeberl C., and Horton J. W. Jr. 2007. Dike breccias in the deep basement-derived section of the Eyreville B core, Chesapeake Bay impact structure. Geological Society of America, Abstracts with Programs 39(6): 451.

Reimold W. U., Bartosova K., Schmitt R. T., Hansen B., Crasselt C., Koeberl C., Wittmann A., and Powars D. 2009. Petrographic observations on the Exmore Breccia, ICDP-USGS Drilling at Eyreville, Chesapeake Bay impact Structure, USA. In *The ICDP-USGS deep drilling project in the Chesapeake Bay impact structure: Results from the Eyreville core holes,* edited by Gohn G. S., Koeberl C., Miller K. G., and Reimold W. U. *Geological Society of America Special Paper* 458: 655–698.

Sanford W. E., Gohn G. S., Powars D. S., Horton J. W. Jr., Edwards L. E, Self-Trail J. M., and Morin R. H. 2004. Drilling the central crater of the Chesapeake Bay impact structure: a first look. *EOS, Transactions, American Geophysical Union* 85: 369 & 377.

Schmitt R. T., Bartosova K., Reimold W. U., Mader D., Wittmann A., Koeberl C., and Gibson R. L. 2009. Geochemistry of impactites and crystalline basement-derived lithologies from the ICDP-USGS Eyreville A and B drill cores, Chesapeake Bay impact structure, Virginia/USA. In *The ICDP-USGS deep drilling project in the Chesapeake Bay impact structure: Results from the Eyreville core holes,* edited by Gohn G. S., Koeberl C., Miller K. G., and Reimold W. U. *Geological Society of America Special Paper* 458: 481–541.

Self-Trail J. M., Edwards L. E., and Litwin R.J. 2009. Paleontological interpretations of crater processes and infilling of syn-impact sediments from the Chesapeake Bay impact structure. In *The ICDP-USGS deep drilling project in the Chesapeake Bay impact structure: Results from the Eyreville core holes,* edited by Gohn G. S., Koeberl C., Miller K. G., and Reimold W. U. *Geological Society of America Special Paper* 458: 633–654.

Shah A. K., Brozena J., Vogt P., Daniels D., and Plescia J. 2005. New surveys of the Chesapeake Bay impact structure suggest melt pockets and target-structure effect. *Geology* 33: 417–420.

Shah A. K., Daniels D. L., Kontny A., and Brozena J. 2009. Megablocks and melt pockets in the Chesapeake Bay impact structure constrained by magnetic field measurements and properties of the Eyreville and Cape Charles cores. In *The ICDP-USGS deep drilling project in the Chesapeake Bay impact structure: Results from the Eyreville core holes,* edited by Gohn G. S., Koeberl C., Miller K. G., and Reimold W. U. *Geological Society of America Special Paper* 458: 195-208.

Thein J. 1987. A tektite layer in Upper Eocene sediments of the New Jersey continental slope (Site 612, Leg 95). In *Initial reports of the Deep Sea Drilling Project, Leg 95*, edited by Poag C. W., Watts A. B. et al. Washington D.C., U.S: Government Printing Office. p. 565–579.

Thomas W. A., Chowns T. M., Daniels D. L., Neathery T. L., Glower. L. III., Gleason. R. J. 1989. The subsurface Appalachians beneath the Atlantic and Gulf coastal plains. In *Geology of North America: The Appalachian-Ouachita Orogen in the United States,* edited by Hatcher. R. D. Jr., Thomas W.A., and Viele G. W. Boulder. Geological Society of America. F2: 445–458.

Townsend G. N., Gibson R. L., Horton J. W. Jr., Reimold W. U., Schmitt R. T., and Bartosova K. 2009. Petrographic and geochemical comparisons between the crystalline basement-derived section and the granite and amphibolite megablocks of the Eyreville-B core, Chesapeake Bay impact structure, USA. In *The ICDP-USGS deep drilling project in the Chesapeake Bay impact structure: Results from the Eyreville core holes,* edited by Gohn G. S., Koeberl C., Miller K. G., and Reimold W. U. *Geological Society of America Special Paper* 458: 255–276.

Whitehead J., Papanastassiou D. A., Spray J. G., Grieve R. A. F., and Wasserburg, G. J. 2000. Late Eocene impact ejecta: geochemical and isotopic connections with the Popigai impact structure. *Earth and Planetary Science Letters* 181: 473–487.

Wittmann A., Reimold W. U., Schmitt R. T., Hecht L., and Kenkmann T. 2009a. The record of ground zero in the Chesapeake Bay impact crater – suevites and related rocks. In *The ICDP-USGS deep drilling project in the Chesapeake Bay impact structure: Results from the Eyreville core holes,* edited by Gohn G. S., Koeberl C., Miller K. G., and Reimold W. U. *Geological Society of America Special Paper* 458: 349–376.

Wittmann A., Schmitt R.-T., Hecht L., Kring D. A., and Povenmire H. 2009b. Petrology of impact melt rocks from the Chesapeake Bay crater, USA. In *The ICDP-USGS deep drilling project in the Chesapeake Bay impact structure: Results from the Eyreville core holes,* edited by Gohn G. S., Koeberl C., Miller K. G., and Reimold W. U. *Geological Society of America Special Paper* 458: 377–396.

CHAPTER 4: LATE EOCENE IMPACTS AND CLIMATE CHANGES

4.1 The late Eocene period and Eocene impacts

The late Eocene is geologically a very interesting, but still not well understood period. Several impact events and changes in climate and biodiversity, which might be connected, occurred at this time. Two large impact structures that belong to the largest on Earth are of late Eocene age (http://www.unb.ca/passc/ImpactDatabase/index.html). The Popigai impact structure is 100 km in diameter and 35.7 Myr old. The slightly smaller Chesapeake Bay impact structure is 85 km in diameter and 35.3 Myr old (e.g., Koeberl 2009; Poag et al., 2004). Furthermore, there are several smaller impact structures of late Eocene age, although some of them are not yet precisely dated. Impact structures of Eocene (or probably Eocene) age are listed in Table 4-1 and locations of late Eocene impact structures are shown in Fig. 4-1. Late Eocene is also a time of enhanced influx of extraterrestrial material. Farley et al. (1998) concluded that there was a period of about 2.5 Myr, when more extraterrestrial material was deposited on Earth, based on studies of ^{3}He isotopes in Massignano sedimentary section. All these events are possibly a result of a comet shower (Farley at al. 1998, 2009) or asteroid shower (Tagle and Claeys, 2004). Recently, the asteroid shower hypothesis is slightly preferred, as the impactors of Popigai and Wanapitei impact structures have been recognized as L-chondrites (Tagle and Claeys, 2005 and Goderis et al., 2007, respectively). However, for example for the Chesapeake Bay impact structure – the second largest late Eocene crater, the impactor has not yet been identified (McDonald et al., 2009; Goderis et al., 2010), but seems to be of chondritic nature.

TABLE 4-1. LIST OF IMPACT STRUCTURES OF EOCENE AGE

Impact structure	Age	Diameter (km)	Impact structure	Age	Diameter (km)
Chesapeake Bay	35.3 ± 0.1	85	Beyenchime-Salaatin	40 ± 20	8
Popigai	35.7 ± 0.8	100	Logoisk	42.3 ± 1.1	15
Flaxman	> 35	10	Shunak	45 ± 10	2.8
Crawford	> 35	8.5	Ragozinka	46 ± 3	9
Mistastin	37 ± 2.6	28	Chiyli	46 ± 7	5.5
Wanapitei	37.2 ± 1.2	7.5	Kamensk	49 ± 0.2	25
Haughton	39?	23	Gusev	49 ± 0.2	3
Logancha	40 ± 20	20	Goat Paddock	<50	5.1

Data from http://www.unb.ca/passc/ImpactDatabase/index.html and Koeberl (2009).

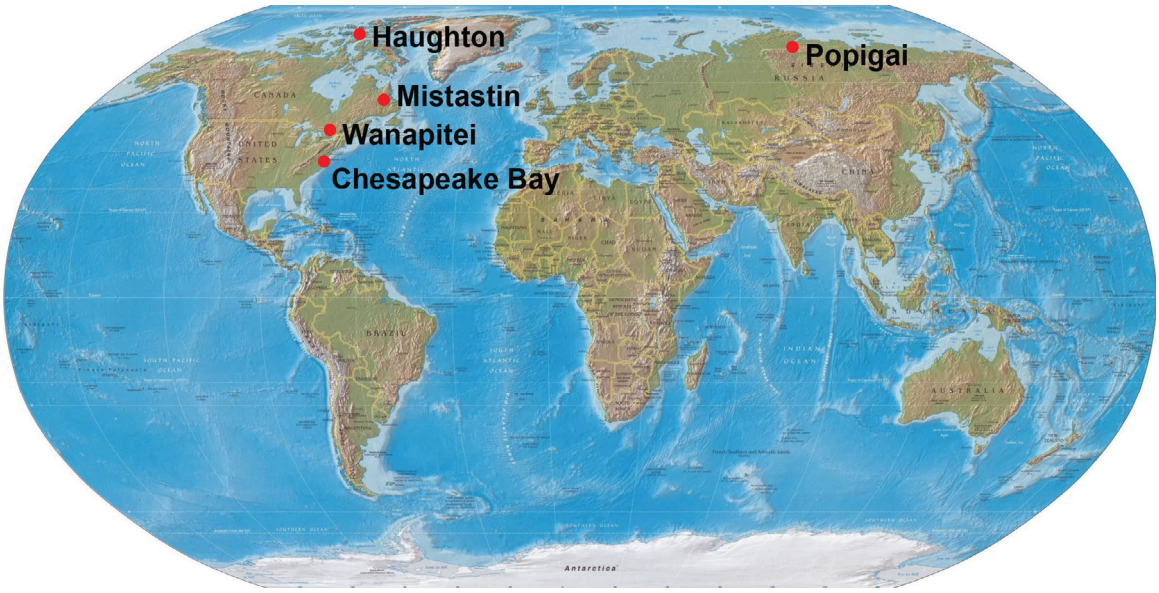

Fig. 4-1. Locations of late Eocene impact structures.

4.2 Late Eocene global ejecta

The Popigai impact structure is located in Siberia, Russia, and the Chesapeake Bay impact structure on the East Coast of the USA. The Chesapeake Bay impactor hit crystalline rocks of the Appalachian orogen, which were – at the time of impact – covered by 1–1.5 km of poorly consolidated Lower Cretaceous to Eocene siliciclastic sediments (Poag et al., 2004). In the case of Popigai impact event, the target rocks were Precambrian gneisses covered by ~1 km of late Precambrian to Paleozoic sediments (sandstones and rare carbonates; e.g., Masaitis 1994, Vishnevsky and Montanari, 1999). Popigai, and possibly also the Chesapeake Bay impact event, are associated with global ejecta layers. There are two closely spaced ejecta layers with Ir and ^{3}He anomalies that have been documented at different localities around the world (Koeberl, 2009). The younger layer is the "North American microtektite layer" that contains microtektites, shocked minerals, and high-pressure polymorphs. It correlates with the North American tektites that have been linked to the Chesapeake Bay impact structure based on the geographic position, and Sr and Nd isotopic data (Glass, 2002; Deutsch and Koeberl, 2006). The older layer is the so-called "clinopyroxene (cpx) spherule layer" (Fig. 4-2), which contains spherules with clinopyroxene and/or Ni- or Cr-rich spinel. Shocked quartz has been found in this layer at Massignano and in deep sea drill cores from the Indian Ocean, from where also coesite has recently been reported (Liu et al., 2009). The cpx spherule layer has been associated with the Popigai impact structure, based on age and Sr and Nd isotopic data (Whitehead et al., 2000; Glass, 2002). Deep-sea core analyses suggested that the Popigai ejecta have a ray-like pattern (Liu et al., 2009; Fig. 4-3). The time span between deposition of these two ejecta layers is estimated to be 5–20 kyr in the deep sea cores (Glass, 2002; Koeberl et al.,

2009), but seems to be about 90 kyr in the Massignano section (Koeberl et al., 2009), casting doubt that this records the same event.

Figure 4-2. Layer with Popigai ejecta (marked by hammer) at the Massignano section.

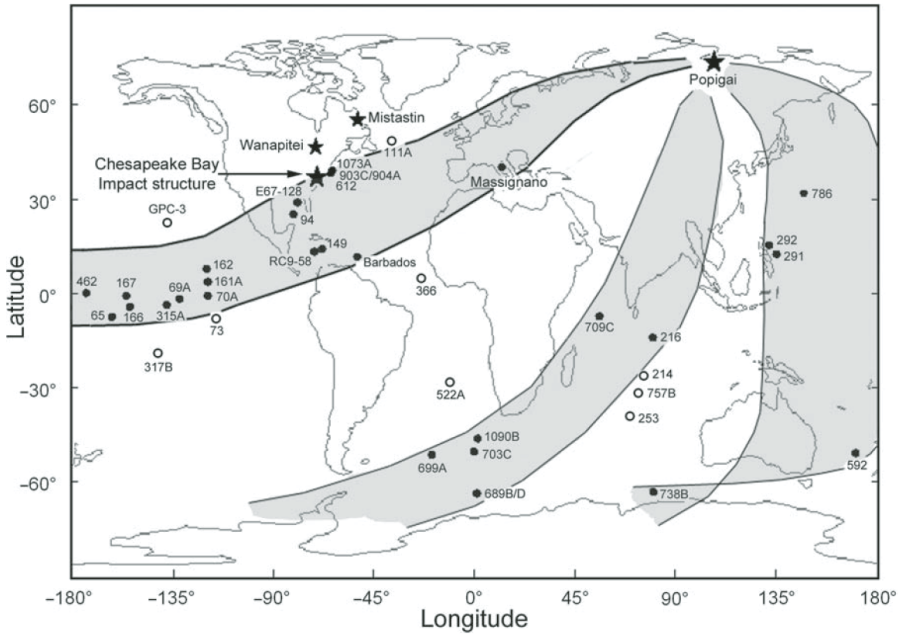

Fig. 4-3. Possible ray-like character of the Popigai ejecta, from Liu et al. (2009).

4.3 Late Eocene climate changes

The late Eocene is associated with extensive climate changes and some extinctions. The geologic record of the climate changes has been extensively studied in the Massignano section in Italy. In the Massignano limestone, three ^{3}He and Ir anomalies have been reported (Montanari et al., 1993, Farley et al., 1998). The anomalies occur at 5.6, 6.2, and

10.3 m of the Massignano section (Fig. 4-4). The first anomaly has been associated with the Popigai event and the second anomaly with the Chesapeake Bay event (Montanari and Koeberl, 2000; Koeberl, 2009). The third anomaly has not been linked to an impact structure yet. The ^{3}He and Ir anomalies are also connected with climatic changes that are reflected in the isotopic composition. The 5.6 m anomaly was followed by increase of $\delta^{18}O$ and $\delta^{13}C$, which has been interpreted as cooling and decrease of bio-productivity by Bodiselitsch et al. (2004). The 6.2 m peak is connected with a decrease of $\delta^{18}O$ and $\delta^{13}C$, explained as warming and increase of productivity. A similar negative excursion and warming was reported for the youngest anomaly (10.4 m; Bodiselitsch et al., 2004, Liu et al., 2009). However, Coccioni et al. (2009) has recently published an opposite interpretation in terms of cooling/warming after the impact events based on studies of foraminiferal assemblages; i.e., warming after the Popigai impact event and cooling after the Chesapeake Bay impact event. Bodiselitsch et al. (2004) suggested that the late Eocene impacts caused a warm pulse, superimposed on the long-term cooling period (decrease of 5-10 °C) that lasted from the middle Eocene into the Oligocene. This pulse supposedly slowed down the cooling, but was followed by a sharp temperature drop (of at least 3 °C for both bottom and surface ocean waters) at the Eocene/Oligocene (E/O) boundary (Zachos et al., 1996; Katz et al., 2008; Miller et al., 2008; Liu et al., 2009). Based of stratigraphic studies of the Alabama St. Stephens quarry Miller et al. (2008) proposed that the increase in $\delta^{18}O$ near the E/O boundary (~33.8 Ma) was mainly due to cooling, whereas the $\delta^{18}O$ increase at the time of Oi1 (~33.55 Ma) event was a result of both cooling and ice growth (sea level fall). Zanazzi et al. (2007) studied continental temperature record of the E/O transition and found a large temperature drop in mean annual temperature of 8.2 ± 3.1 over about 400 kyr. They further propose that the continental temperature drop was delayed by up to 400 kyr in respect to marine changes.

Apparently, the opinions on the late Eocene climatic changes are not uniform and the topic is still discussed. In general, possible mechanisms that could change the climate are the following: Warming can be a result of CO_2 and methane hydrate release during an impact, and consequent greenhouse effect (Bodiselitsch et al., 2004; Coccioni et al., 2009). Cooling can be caused by injection of dust into the atmosphere (e.g., Toon et al., 1997) or by an impact-generated equatorial debris ring that would cast a shadow on the winter hemisphere (Fawcett and Boslough, 2002).

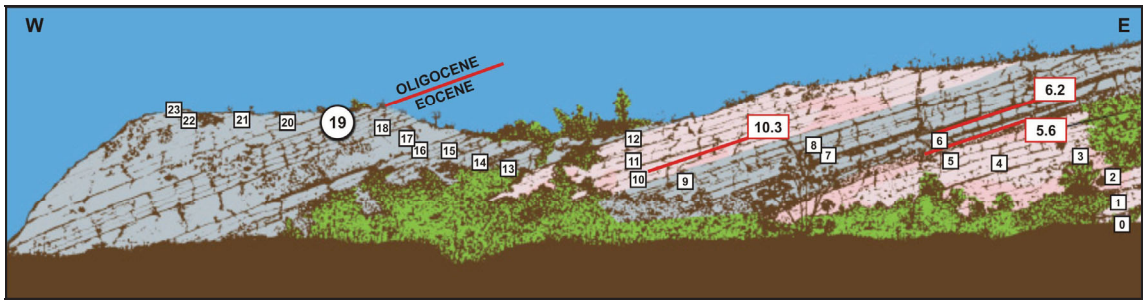

Figure 4-4. Sketch of the Massignano global stratigraphic section and the important markers – the three ^{3}He anomalies at 5.3, 6.2, and 10.3 m and the Eocene/Oligocene boundary at 19 m. Modified from a figure by A. Montanari (for Massignano info-board).

4.4 Late Eocene extinctions

The extinctions in the late Eocene occurred over a long period of time, about 10 Myr, with some peaks at 37–38 Ma, 33 Ma, and smaller peaks at 35 Ma, and 30 Ma (Prothero, 1994). An abrupt forcing, such as meteoritic impact, is not a probable cause of such long period of extinction. More probable reasons are changes in ocean currents, mountain building, and changes in greenhouse gases that all together caused the global cooling (Retallack et al., 2004; Prothero, 1994). There are no significant extinctions associated with the late Eocene ejecta layers (Prothero, 1994). However, Sanfilippo et al. (1985) discussed possible radiolarian extinctions and Coccioni et al. (2000, 2009) reported quantitative changes in calcareous plankton in the sediments from the Massignano section. Naturally, local effects of the impact events have been reported. In the Chesapeake Bay impact structure, so-called dead zone was found in drill cores, implying a hostile environment for organisms for about 1–3 kyr after the impact (Poag, 2002; Poag et al., 2004). No evidence of mass extinction or a world-wide pelagic crisis, analogous to the K/T event, has been reported for the late Eocene impacts (e.g., Montanari and Koeberl, 2000; Coccioni et al., 2009)

4.5 Massignano Eocene/Oligocene (E/O) global stratigraphic section and point (GSSP)

The abandoned quarry at Massignano, near Ancona in Italy (Fig. 4-5) exposes 23 m thick complete sequence of pelagic marly limestones and calcareous marls of upper Eocene to lower Oligocene age. The sediments belong to Scaglia Variegata and Scaglia Cinerea formations (Montanari and Koeberl, 2000). The section at Massignano contains well-preserved benthic and planktonic microfossils and furthermore several layers of biotite-rich volcanic ash, thus provides ideal conditions for stratigraphic correlation (Montanari and Koeberl, 2000). In the stratigraphic studies of late Eocene, there was a discrepancy in dating. Thus the Eocene impact structures appeared to be younger than the E/O boundary, which was incorrectly dated as ~37 Ma. Dating of biotite layers in the sediments at Contessa, Monte Cagnéro, and Massignano enabled to revise the age of the E/O boundary

to 33.7 ± 0.4 Ma (Montanari et al., 1988). Massignano GSSP was established in 1993 (Premoli Silva and Jenkins, 1993).

Fig 4-5. Panoramic view of the Massignano quarry, Monte Conero, Marche region, Italy.

At Massignano, there are three layers with anomalous concetrations of extraterrestrial material, mainly Ir; ^{3}He anomalies cover the whole interval (Montanari et al., 1993; Farley et al., 1998). In the layer at 5.6 m there is material ejected from the Popigai impact, including shocked quartz grains (Fig. 4-6A; Clymer et al., 1996; Langenhorst, 1996), Ni-rich spinels, and microkrystites/cpx spherules (Fig. 4-6B, Pierrard et al., 1998; Glass et al., 2004).

Above the sedimentary layers with the anomalies of extraterrestrial material, at 19 m of the section, is the E/O boundary with the global stratigraphic section and point (GSSP). Some scientists argue that the current E/O boundary criterion, which is based on the local extinction of the tropical planktonic foraminifera genus Hantkenina, represents an isolated event and is not suitable for global correlation (Van Mourik and Brinkhuis, 2005). These authors proposed to establish the Oi1 δ^{18}O benthic isotope event as the base of Oligocene. As this slightly younger event is not well recorded in the Massignano section, it might be necessary to establish a new GSSP for the E/O boundary in the future.

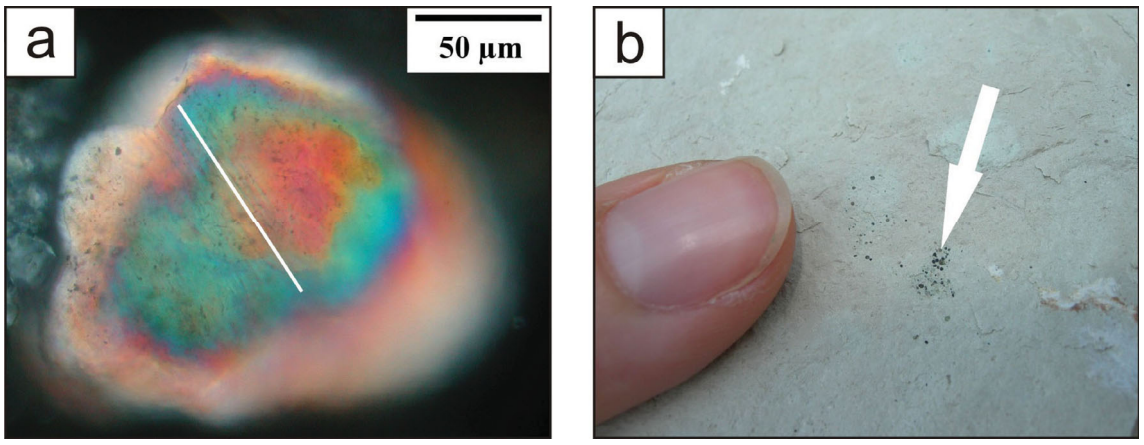

Fig 4-6. Popigai ejecta found in Massignano section. a) Shocked quartz grain from a smear slide. White line shows orientation of the PDF set. Microphotograph in cross polarized light. b) Impact spherules (marked by arrow). Macrophotograph, thumb for scale.

4.6 Extinctions after Chesapeake Bay (and Popigai) impact?

Although some local extinctions were noted (Poag et al., 2004), probably no global rapid climate changes or consequent extinctions are connected with the Chesapeake Bay impact event. Based on computer modeling, Collins and Wünemann (2005) concluded that the Chesapeake Bay impact structure diameter was influenced by the strength differences in the target rocks (i.e., the crystalline basement and unconsolidated siliciclastic sediments). They calculated that the transient crater diameter was only ~28 km and that the final crater diameter would have been probably only ~40 km in diameter if the impactor had hit a different target with absence of strength variations.

Walkden and Parker (2008) suggested that the size of the crater is not the only criteria of its environmental influence. They note that the timing and location of impact is also very important. According to these authors the Popigai impact did not cause significant changes in biodiversity because the impact site was in a cold area with low biodiversity. Walkden and Parker (2008) consider the Chesapeake Bay impact site a potentially vulnerable place with high biodiversity and explain the low actual biotic effect by lower impact energy than expected from the large crater diameter (as explained by Collins and Wünnemann, 2005). The hypothesis by Walkden and Parker (2008) is illustrated in Fig. 4-7.

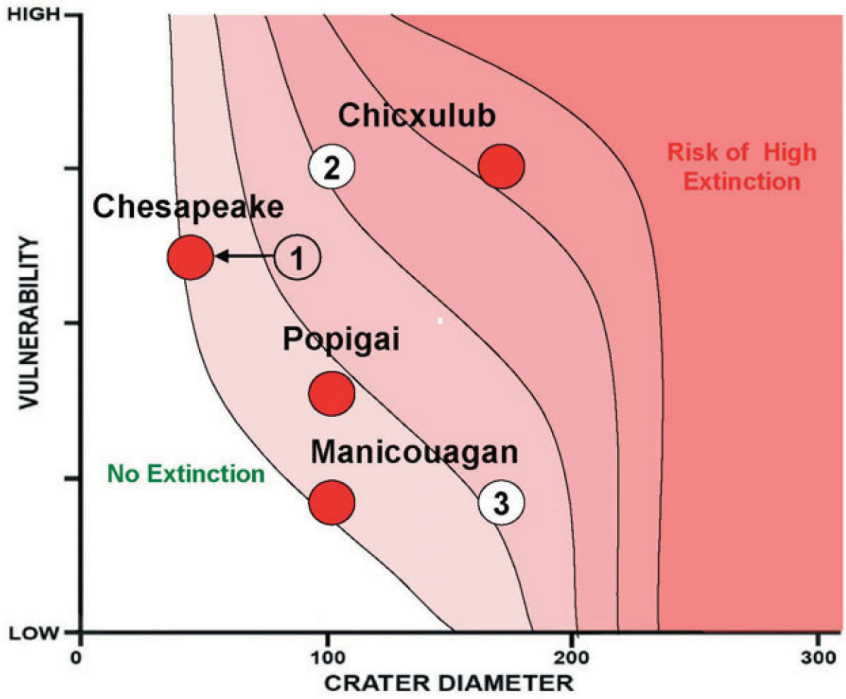

Figure 4-7. Diagram from Walkden and Parker (2008), which shows extinction risk of four large terrestrial craters. There is crater diameter on the horizontal scale and vulnerability (depending on specific place and time) on the vertical scale. The point of Chesapeake Bay structure (1) is repositioned due to the structure's misleading large size. For the Manicouagan (2) and Chicxulub (3) impact structures along with the real parameters (red points) also theoretical points (white points numbered 2 and 3) are shown. These white points show theoretical biotic effects if the impacts (with the same diameter) happened on a site with different vulnerability. For the Popigai impact structure, only the real position is plotted.

References:

Bodiselitsch B., Montanari A., Koeberl C., and Coccioni R. 2004. Delayed climate cooling in the Late Eocene caused by multiple impacts: high-resolution geochemical studies at Massignano, Italy. *Earth and Planetary Science Letters* 223: 283–302.

Clymer A. K., Bice D. M., and Montanari A. 1996. Shocked quartz from the late Eocene: Impact evidence from Massignano, Italy. *Geolo*gy 24: 483–486.

Coccioni R., Basso D., Brinkhuis H., Galeotti S., Gardin S., Monechi S., and Spezzaferri S. 2000. Marine biotic signals across a late Eocene impact layer at Massignano, Italy: evidence for long-term environmental perturbations? *Terra Nova* 12: 258–263.

Coccioni R., Frontalini F., and Spezzaferri S. 2009. Late Eocene impact-induced climate and hydrological changes: Evidence from the Massignano global stratotype section and point (central Italy). In *The Late Eocene Earth—Hothouse, Icehouse, and Impact*, edited by Koeberl C., and Montanari A. *Geological Society of America Special Paper* 452: 97–118.

Collins G. S. and Wünnemann K. 2005. How big was the Chesapeake Bay impact? Insight from numerical modeling. *Geology* 33: 925–928.

Deutsch A. and Koeberl C. 2006. Establishing the link between the Chesapeake Bay impact structure and the North American tektite strewn field: The Sr-Nd isotopic evidence. *Meteoritics and Planetary Science* 41: 689–703.

Farley K. A. 2009. Late Eocene and late Miocene cosmic dust events: Comet showers, asteroid collisions, or lunar impacts? In *The Late Eocene Earth—Hothouse, Icehouse, and Impact*, edited by Koeberl C., and Montanari A. *Geological Society of America Special Paper* 452: 27–35.

Farley K. A., Montanari A., Shoemaker E. M., and Shoemaker C. S. 1998. Geochemical Evidence for a Comet Shower in the Late Eocene. *Science* 280: 1250–1253.

Fawcett P. J. and Boslough M. B. E. 2002. Climatic effects of an impact-induced equatorial debris ring. *Journal of Geophysical Research D: Atmospheres* 107: (D15) 10129–10146.

Glass B. P. 2002. Upper Eocene impact ejecta/spherule layers in marine sediments. *Chemie der Erde* 62: 173–196.

Goderis S., Tagle R., and Claeys P. 2007. Current situation on the characterization of the late Eocene impact structures using platinum group element (PGE) ratios. In *The Late Eocene Earth—Hothouse, Icehouse, and Impact*, edited by Koeberl C., and Montanari A. Ancona, Italy, *Penrose Conference Abstract volume*. p. 27–28.

Goderis S., Hertogen J., Vanhaecke F., and Claeys P. 2010. Siderophile elements from the Eyreville drill cores of the Chesapeake Bay impact structure do not constrain the nature of the projectile. In *Large meteorite impacts and planetary evolution IV*, edited by Gibson R. L. and Reimold W. U. *Geological Society of America Special Paper* 465. In press.

Katz M. E., Miller K. G., Wright J. D., Wade B. S., Browning J. V., Cramer B. S., Rosenthal Y. 2008. Stepwise transition from the Eocene greenhouse to the Oligocene icehouse. *Nature Geoscience* 1: 329–334.

Koeberl C. 2009. Late Eocene impact craters and impactoclastic layers—An overview. In *The Late Eocene Earth—Hothouse, Icehouse, and Impact*, edited by Koeberl C., and Montanari A. *Geological Society of America Special Paper* 452: 17–26.

Langenhorst F. 1996. Characteristics of shocked quartz in late Eocene impact ejecta from Massignano (Ancona, Italy): Clues to shock conditions and source crater. *Geology* 24: 487–490.

Liu S., Glass B. P., Kyte F. T., and Bohaty S. M. 2009. The late Eocene clinopyroxene-bearing spherule layer: New sites, nature of the strewn field, Ir data, and discovery of coesite and shocked quartz. In *The Late Eocene Earth—Hothouse, Icehouse, and Impact*, edited by Koeberl C., and Montanari A. *Geological Society of America Special Paper* 452: 37–70.

Liu Z., Pagani M., Zinniker D., DeConto R., Huber M., Brinkhuis H., Shah S. R., Leckie R. M., and Pearson A. 2009. Global Cooling During the Eocene-Oligocene Climate Transition. *Science* 323: 1187–1190.

Masaitis V. L. 1994. Impactites from Popigai crater, *in* Dressler B. O., Grieve R. A. F., and Sharpton V. L., eds., Large Meteorite Impacts and Planetary Evolution. *Geological Society of America Special Paper* 293: 153–162.

McDonald I., Bartosova K., and Koeberl C. 2009. Search for a meteoritic component in impact breccia from the Eyreville core, Chesapeake Bay impact structure: Considerations from platinum-group element contents. In *The ICDP-USGS deep drilling project in the Chesapeake Bay impact structure: Results from the Eyreville core holes,* edited by Gohn G. S., Koeberl C., Miller K. G., and Reimold W. U. *Geological Society of America Special Paper* 458: 469–479.

Miller K. G., Browning J. V., Aubry M.-P., Wade B. S., Katz M. E., Kulpecz A. A., and Wright J. D. 2008. Eocene Oligocene global climate and sea-level changes: St. Stephens Quarry, Alabama. *Geological Society of America Bulletin* 120: 34–53

Montanari A., Deino A. L., Drake R. E., Turrin B. D., DePaolo D. J., Odin G. S., Curtis G. H., Alvarez W., and Bice D.M. 1988. Radioisotopic dating of the Eocene-Oligocene boundary in the pelagic sequence of the Norhern Apennines. In *The Eocene-Oligocene boundary in the Marche-Umbria basin (Italy)*, edited by Premoli Silva I., Coccioni R., and Montanari A. International Subcommission on Paleogene Stratigraphy, special publication, Eocene/Oligocene Boundary Meeting, Ancona, 1987. F.lli Aniballi Publishers, Ancona. p. 195–208.

Montanari A., Asaro F., Michel H. V., and Kennett J. P. 1993. Iridium anomalies of late Eocene age at Massignano (Italy), and ODP Site 689B (Maud Rise, Antarctic). *Palaios* 8: 420–437.

Montanari A. and Koeberl C. 2000. Impact Stratigraphy, The Italian Record: Springer-Verlag Berlin Heidelberg, 364 p.

Pierrard O., Robin E., Rocchia R., and Montanari A. 1998. Extraterrestrial Ni-rich spinel in upper Eocene sediments from Massignano, Italy. *Geology* 26: 307–310.

Poag C. W. 2002. Synimpact-postimpact transition inside Chesapeake Bay crater. *Geology* 30: 995–998.

Poag C. W., Koeberl C., and Reimold W. U. 2004. *The Chesapeake Bay crater: Geology and geophysics of a late Eocene submarine impact structure*. Impact Studies series. Heidelberg: Springer. 522 p.

Premoli Silva I. and Jenkins D. J. 1993. Decision on the Eocene-Oligocene boundary stratotype. *Episodes* 16: 379–381.

Prothero D.R. 1994. The late Eocene-Oligocene extinctions: *Annual Reviews of Earth and Planetary Science* 22: 145–165.

Retallack G. J., Orr W. N., Prothero D. R., Duncan R. A., Kester P. R., and Ambers C. P. 2004. Eocene-Oligocene extinction and paleoclimatic change near Eugene, Oregon. *GSA Bulletin* 116: 817–839.

Sanfilippo A., Riedel W. R., Glass B. P., and Kyte F. T. 1985. Late Eocene microtektites and radiolarian extinctions on Barbados. *Nature* 314: 613–615.

Tagle R., and Claeys P. 2004. Comet or asteroid shower in the Late Eocene? *Scienc* 23: 492.

Tagle R., and Claeys P. 2005. An ordinary chondrite impactor for the Popigai crater, Siberia. *Geochimica et Cosmochimica Acta* 69: 2877–2889.

Toon O.B., Zahnle K., Morrison D., Turco R. P., and Covey C. 1997. Environmental perturbations caused by the impacts of asteroids and comets. *Reviews of Geophysics* 35: 41–78.

Van Mourik C. A., and Brinkhuis H. 2005. The Massignano Eocene-Oligocene golden spike section revisited. *Stratigraphy* 2: 13–30.

Vishnevsky S. and Montanari A. 1999. Popigai impact structure (Arctic Siberia, Russia): Geology, petrology, geochemistry, and geochronology of glass-bearing impactites. In *Large meteorite impacts and planetary evolution II*, edited by Dressler B. O. and Sharpton V. L. *Geological Society of America Special Paper* 339: 19–59.

Walkden G. and Parker J. 2008. The biotic effects of large bolide impacts: size versus time and place. *International Journal of Astrobiology* 7: 209–215.

Whitehead J., Papanastassiou D.A., Spray J. G., Grieve R. A. F., and Wasserburg, G. J. 2000. Late Eocene impact ejecta: geochemical and isotopic connections with the Popigai impact structure. *Earth and Planetary Science Letters* 181: 473–487.

Zachos J. C., Quinn T. M., and Salamy K. A. 1996. High-resolution (104 years) deep-sea foraminiferal stable isotope records of the Eocene-Oligocene climate transition. *Paleoceanography* 11: 251–266.

Zanazzi A., Kohn M. J., MacFadden B. J., Terry D.O. Jr. 2007. Large temperature drop across the Eocene–Oligocene transition in central North America. *Nature* 445: 639–642.

CHAPTER 5: METHODOLOGY

In total, 166 impactite samples from the Eyreville drill core were studied for this thesis. A variety of analytical methods, from the traditional ones (e.g., optical microscopy) to the more sophisticated modern methods (e.g., electron microprobe and mass spectrometry), were used for the investigations. For the chemical analyses of bulk sample powders, X-ray fluorescence and instrumental neutron activation analysis were performed. Mineral compositions of selected samples were further analyzed by X-ray diffraction, including clay fraction analyses of some gravelly sand samples. For most samples, thin sections were prepared. The thin sections were first studied by optical microscopy and selected thin sections were further analyzed by microRaman spectrometry, scanning electron microscopy with an energy-dispersive X-ray analyzer, and electron microprobe analysis. The orientations of planar deformation features in quartz were determined using an optical microscope with universal stage. The carbon isotopic composition of some carbon rich clasts, as well as calcite veins, was analyzed by gas source mass spectrometry.

5.1 Samples

5.1.1 Sampling of the Eyreville drill cores

The Eyreville core was drilled in the years 2005–2006 in the central moat of the Chesapeake Bay impact structure. The three stacked drill cores (Eyreville A, B, and C), with a total depth of 1766 m are now stored in core boxes (Fig. 5-1) at the USGS in Reston, Washington, USA.

Most of the studied samples were collected at the first sampling party in March 2006 by C. Koeberl. These are samples with numbers CB6-001 to CB6-150. Note that the samples were originally named CK-001 to CK-150; these original numbers can be also found in the core boxes and official USGS sampling lists. The samples were collected to cover the whole core interval (444–1766 m depth), excluding the post-impact sediments. The sampling was denser in the most interesting and non-homogeneous intervals (e.g., impact breccias and Exmore Formation), whereas in the crystalline sections (the granitic megablock and basement-derived schists and pegmatites) the intervals between the samples are larger. Additional samples were taken later to acquire more study material for the core intervals the thesis is focused on. The author of the thesis collected six additional samples (KB-1 to KB-6) from the impact breccia interval, especially the impact melt rocks, in November 2007. Ten additional samples (KB1-09 to KB10-09) were taken from the gravelly sand interval by J. W. Horton in February 2009. The selected core samples were cut by USGS staff and shipped to Vienna. All the samples are mostly half core or quarter core with lengths of about 10 cm; masses are commonly between 100 and 300 g.

As there was a close cooperation with the impact research group of the Natural History Museum in Berlin, their sample suite was in many cases used to compare and complete the observations of our samples. The results of analyses of the Vienna and Berlin samples suites are combined together in several papers (in, e.g., chapter 7 and Appendix 1 and 2 of the thesis).

The samples shipped from the USGS Reston were accompanied by a list, where all the basic data of the samples were summarized. The important attributes were the number of box and slot of the core, and first of all the sample depth. All sample depths used in the thesis and papers are so called "corrected depths". This means that the original core depth was later corrected (due to, e.g., changes in core recovery). The corrections were done by L. Edwards (USGS).

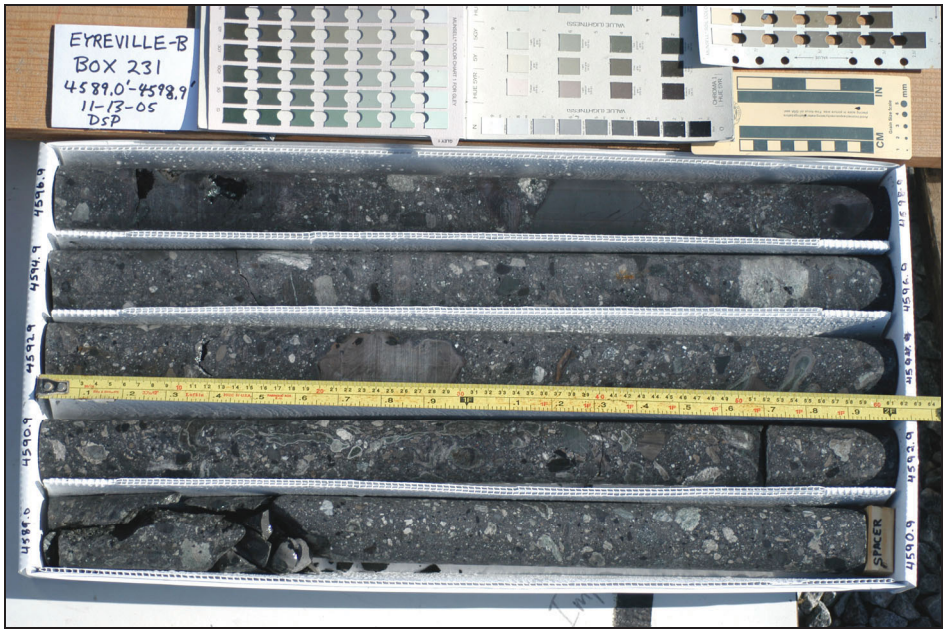

Fig. 5-1. Example of a core box. Eyreville B core, box 231 with five slots. Photo courtesy USGS.

5.1.2 Samples documentation and database

All the samples were first well documented before further analyses were started. Macrophotographs of all samples were obtained. All the photographs can be found on the DVD included in this thesis. The samples were also weighed and macroscopically described in detail, including characterization of color, textures, clasts, and other important features of the samples.

For easier work with the large amount of samples and data, as well as for documentation of the samples, a sample database was created in Microsoft Access. The database contains all most important data about the samples as, e.g., the original data from the sampling. In further tables there are detailed macro- and microscopic descriptions of all samples. The database includes also all photo-documentation (i.e., photographs of hand

samples, as well as of thin sections of all samples) and data from bulk rock chemical analyses. The database with a short user guide is included on the DVD, which is attached to this thesis.

5.1.3 Bulk rock powder preparation

Bulk rock powder of the samples was used for the chemical analyses. About 60 g of each sample were cut. Especially among the impact breccias, samples with large clasts occur. However, we tried to avoid clasts larger than ~1.5 cm. The samples were crushed in polyethylene bags, and some harder specimens (e.g., granites) were further crushed in a jaw-crusher. The crushed samples were then milled to a fine homogeneous powder in a mechanical agate mill. The sample powders were used for X-ray fluorescence and instrumental neutron activation analysis, as well as for X-ray diffraction.

5.1.4 Thin section preparation

For all samples (except for a few very soft clayish samples from the upper parts of the core) thin sections were prepared. For most samples, one thin section was obtained. For the samples of the core intervals studied in greater detail (i.e., the impact breccias and gravelly sand), two to four thin sections were obtained. For the most important samples, polished thin sections that can be used for, e.g., electron microprobe analyses, were prepared. Some samples, especially from the impact breccia, the gravelly sand, and the Exmore Formation interval, were soft and clayish, thus causing difficulties in the thin section preparation. These samples were impregnated with epoxy resin in vacuum before thin section preparation.

5.2 Analytical methods

5.2.1 X-ray fluorescence (XRF)

X-ray fluorescence is a powerful and common method used for bulk chemical analysis. The method can determine precisely the contents of major oxides (SiO_2, TiO_2, Al_2O_3, Fe_2O_3, MnO, MgO, CaO, Na_2O, K_2O, P_2O_5, and SO_3). Also many trace element contents can be analyzed by this method, including Ba, Ce, Co, Cr, Cu, Ga, Mo, Nb, Ni, Pb, Rb, Sc, Sr, Th, U, V, Y, Zn, and Zr.

The principle of the method is irradiation of a sample with X-ray photons. This causes the emission of secondary X-rays that are detected and analyzed. The X-rays, when interacting with a material, can eject electrons from an inner shell (usually K or L) of a sample atom. The free electron position is consequently filled by an electron from a higher energy level. This process is accompanied by emission of secondary X-rays (characteristic X-rays), which have energies corresponding to the difference of the two energy levels, and

are characteristic for each element. A spectrum of an element consists of a few well-defined peaks with characteristic wavelengths. However, the energy excess can be also dissipated by emission of a second Auger electron from an outer shell. Low atomic number atoms favor Auger electron emission and, therefore, XRF is not very sensitive for light elements (with atomic number <10).

5.2.1.1 Sample preparation

Samples for XRF require special preparation. About 15 g of bulk rock powder are necessary for an XRF analysis. The major element oxide content is commonly measured on glass pellets that are made from calcined rock powder fused with lithium tetraborate. Trace elements are measured on pressed powder pellets, made from rock powder mixed with polyvinyl alcohol as a binding agent.

5.2.1.2 XRF Analysis

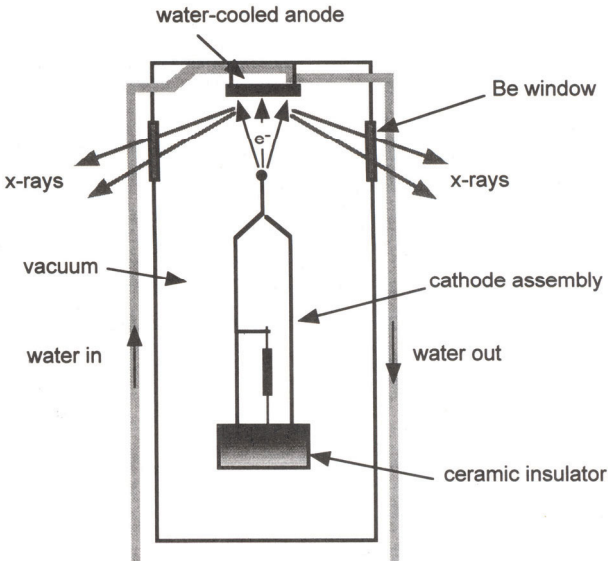

An X-ray analyzer consists of an X-ray source (X-ray tube; Fig. 5-2). An X-ray tube is an evacuated tube with heated tungsten filament and an anode. Electrons emitted from the filament are accelerated along the anode focusing tube by high potential difference. Electrons impinging on the anode produce X-rays that are emitted from the X-ray tube and interact with the sample.

Fig. 5-2. Schematic section of an X-ray tube. From Suryanarayana and Norton (1998).

The secondary X-rays emitted from the sample are collimated to a parallel beam and then spectrally divided. In the conventional wavelength dispersive XRF the X-rays are divided by diffraction on a crystal (according to Bragg's law – see the part about XRD of this chapter). Then the rays are collimated again and detected on a detector. In the energy-dispersive XRF the detector generates an electric pulse with an amplitude proportional to the photon energy for each X-ray photon. The signal is amplified and analyzed by a multi-channel analyzer.

There are several types of detectors used in the X-ray analysis. Gas ionization detectors have relatively low sensitivity and are used to detect low energy X-rays. Most common are the scintillation detectors consisting of a NaI crystal with added Tl. The detector generates an electrical pulse proportional to the energy of detected radiation. The

scintillation detectors are best for detecting high energy X-rays. Semiconductor detectors (Li-drifted Si detectors or high purity Ge detectors) have very good resolution (see also part about INAA of this chapter). Semiconductor detectors are used only in energy-dispersive XRF, as in wavelength-dispersive XRF the energy resolution is performed by the diffraction on a crystal. The scheme of an XRF spectrometer is shown in Fig. 5-3.

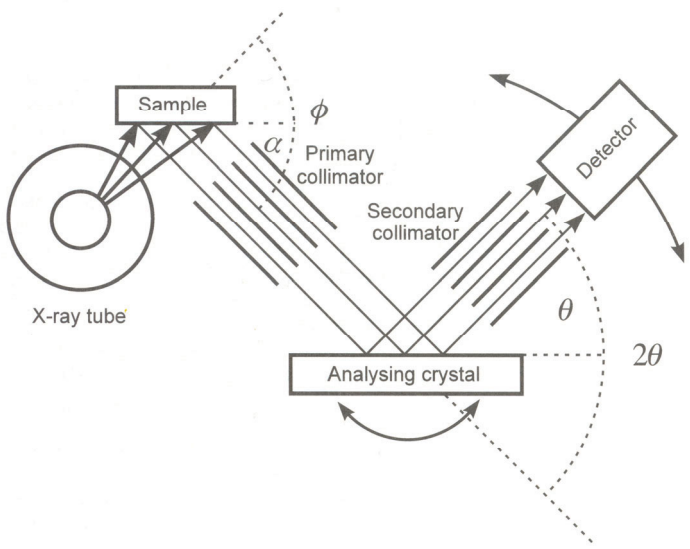

Fig. 5-3. Schematic diagram of configuration of an XRF spectrometer. From Gill (1997).

5.2.1.3 Data processing

The signal of a sample is compared with reference standards to quantify the results. The standards are internationally certified rock reference materials of different compositions (e.g., Serpentine UB-N, Granite GSR-1, Andesite GSR-2, Basalt GSR-3, Sandstone GSR-4, Shale GSR-5, Limestone GSR-6). The precision is maintained by use of monitor samples, which supports instrument stability and ensures repeatability and reproducibility.

Signal intensities of the geostandards are used to establish the calibration curve for each element. However, the correlation between the net count rate and the concentration is linear only for a limited concentration range, as there are some deviations due to inter-element effects. Consequently, corrections of these matrix effects have to be applied. For the trace element analysis, accurate background and line overlap corrected net peak intensities are important.

The XRF precision is commonly better than 0.1 rel% and relative standard deviations are below 1%, even for trace elements.

5.2.1.3 Loss on ignition

The XRF analysis is commonly completed by determining the loss on ignition. The basic principle is measuring of weight loss of a sample after heating. The sample powder is weighted into a porcelain crucible (commonly about 3–5 g) and the exact weight is noted. The sample and the crucible has to be absolutely dry, therefore heating to ~110°C in an

oven (for several hours or overnight) is used before the weighing. Then the crucible with the sample is placed in an oven and heated usually for 3 hours at 950°C. After taking the sample out of the oven the crucible is put in a desiccator. When the crucible with sample is cooled to the room temperature, it is weighted again. The weight after heating is then compared with the original weight. The simple formula is:

$$LOI = [(m_0 - m_t) \times 100] / m_0$$

where m_0 = original sample weight, m_t = sample weight after heating.

5.2.1.4 Details on XRF measurements presented in the thesis

X-ray analyses presented in the thesis were mostly performed at the Natural History Museum in Berlin. The samples were analyzed on a SIEMENS SRS 3000 instrument. More details on the measurement technique can be found in Schmitt et al. (2004). Values of detection limits and standard errors are listed in Table 5-1. Six additional samples of impact breccias (samples KB-1 to KB-6) were analyzed at the University of Witwatersrand, Johannesburg, South Africa. Details of the analytical procedures and accuracies are given in Reimold et al. (1994). Ten additional samples of the gravelly sand were analyzed at the University of Vienna. Here the samples were measured by wavelength dispersive XRF spectrometry on a Philips PW2400 sequential spectrometer. Panalytical ProTrace-software was used. The detection limit was about 0.02 wt% for major element oxides and about 1 ppm for trace elements.

TABLE 5-1. DETECTION LIMITS AND STANDARD ERRORS FOR XRF MEASUREMENTS.

major oxides	detection limit (wt%)	standard error (wt%)	trace elements	detection limit (ppm)	standard error (ppm)
SiO_2	1.0	0.5	V	15	5
TiO_2	0.01	0.01	Cr	15	5
Al_2O_3	0.5	0.1	Co	15	5
Fe_2O_3[§]	0.05	0.05	Ni	15	5
MnO	0.01	0.01	Rb	15	5
MgO	0.01	0.05	Sr	15	5
CaO	0.01	0.05	Zr	15	5
Na2O	0.01	0.05	Ba	30	30
K_2O	0.01	0.05			
P_2O_5	0.01	0.01			
SO_3	0.1	0.1			

Values for the XRF measurements at the Natural History Museum in Berlin. Data from Schmitt et al. (2004).

References used for chapter 5.2.1: Liebhafsky and Pfeiffer (1971), Potts (1987), Vandecasteele and Block (1993), Gill (1997), Jenkins (1999), P. Nagl (Univ. Vienna, written com., 2009).

5.2.2 Instrumental neutron activation analysis (INAA)

The instrumental neutron activation analysis is a sensitive method used for analyzing mostly minor and trace element contents. A large number of trace elements suitable for this analysis comprises Sc, Cr, Co, Ni, Zn, As, Se, Br, Rb, Sr, Zr, Sb, Cs, Ba, Hf, Ta, W, Ir, Au, Th, U, including rare earth elements La, Ce, Nd, Sm, Eu, Gd, Tb. Tm, Yb, and Lu. Also some major element contents (Na, K, and Fe) can be determined.

The basic principle of this method is irradiation of a sample by neutrons, which change the sample atoms into radioactive isotopes that consequently emit γ–rays with characteristic energies. In a neutron capture reaction, the stable isotopes within the sample are transformed to short-lived radioactive isotopes (with the same atomic number but higher mass number). These radioactive isotopes then decay commonly by β-decay combined with emission of X-ray or γ–ray photons. The energies of the emitted photons are characteristic for the specific isotopes. The intensities of the radiation of different energies enable to determine the amount of each isotope. As the radioactive isotopes have different half-lives, the γ-spectrum changes in time and measurement in several cycles is required. The short-lived isotopes have best signals in the first cycles, whereas the long-lived isotopes can be better measured in later cycles of the measurement, after the short-lived isotopes have decayed. The obtained spectra are compared with spectra of several standards that are irradiated and measured together with the samples.

5.2.2.1 Sample preparation

The INAA does not require a complicated sample preparation. Even untreated samples, e.g., small pieces of a meteorite, can be analyzed. However, for the bulk rock analyses, a sample powder is commonly used to ensure that the sample is representative and homogeneous. The sample has to be precisely weighted and sealed in a plastic capsule. The next step of the analysis is the irradiation of the sample with neutrons.

5.2.2.2 Irradiation

Nuclear reactors (mostly using neutrons from ^{235}U fission) are commonly used as neutron sources for INAA. Other possible sources of neutrons are accelerators or radioisotopic emitters, but these have generally much lower neutron fluxes.

For the INAA, commonly thermal neutrons, with low energies (<0.5eV), are used. An important value is the so called neutron capture cross section, which quantifies the probability of the interaction of a neutron with a target nuclide. The neutron capture cross section is mostly larger for thermal neutrons compared to epithermal or fast neutrons, but is also variable for different isotopes. The activity of a nuclide at the end of irradiation can be calculated according to the equation:

$$A = N \times \sigma \times \Phi(1 - e^{-\lambda t_{irr}})$$

where N = number of target nuclides, σ = neutron capture cross section in cm^2, Φ = neutron flux in n cm^{-2} s^{-1}, λ = decay constant of the radionuclide produced, t_{irr} = irradiation time.

5.2.2.3 Detection

The radioactive isotopes formed during the irradiation decay and the energy and intensity of the emitted γ–rays is detected. There are two basic types of interaction between γ–rays and matter. First is the photoelectric effect – the γ–ray is completely absorbed and a photoelectron is emitted. A full peak appears in the spectrum with the energy of the γ–ray less the binding energy of the electron in the absorber atom. The second type of interaction is the Compton effect. In this case only part of the γ–ray energy is transferred to an electron. The γ–ray is not absorbed, but is scattered and its energy is lowered. In case the scattered γ–ray is lost without detection, the difference to the full energy peak is displayed as a Compton continuum about 256 keV below the value of the non-detected full energy peak. Another type of interaction is the electron-positron pair production. This interaction requires a high-energetic γ–ray (>1022 keV, twice the electron rest energy). The unstable positron is immediately annihilated by recombination with an electron and annihilation γ quanta are ejected in opposite directions. Full peak appears in the spectrum if both of them are detected. If one annihilation photon escapes, an escape peak is indicated in the spectrum at 511 keV below the full energy peak, if both photons escape, the double escape peak is indicated by a peak 1022 keV below the full energy peak.

Modern semiconductor Germanium (Ge) detectors are used for INAA. Gamma-rays help to elevate the electrons into the conduction band and leave electron holes in the valence band. The electron-hole pairs are moved in a high-voltage electric field to the opposite-charged electrode. Electric signal, proportional to the energy of the γ–rays, is obtained. The semiconductor detectors have both high efficiency and high energy resolution. There are two types of semiconductor detectors – Li-drifted Ge detectors and high purity Ge detectors. The semiconductor detectors have to be cooled with liquid nitrogen as the conduction caused by thermal excitation has to be minimized. Gamma-ray detectors are placed in a lead shielding and the sample should be positioned in a reproducible way in the detector. The electric signal is amplified in a preamplifier and main amplifier. Then the signal is processed by a digital signal processor and stored in a multichannel analyzer. Every channel stores a signal of certain energy and the signals are combined in the γ-spectrum. The resolution of a detector is a capability to separate adjacent γ-ray lines.

5.2.2.4 Data processing

Determination of absolute concentrations of elements is theoretically possible, but would be complicated as many factors (some not precisely known) influence the final signal. As common in analytical methods, several standards are measured together with the samples and the resulting signals are compared.

Several corrections have to be considered. Geometry correction has to be applied if the measurement geometry (e.g., the distance between sample and detector) is changed between the analyzed samples. As the samples are not measured simultaneously, the decay correction has to be used:

$$f_z = e^{(\ln 2 / t_{1/2})\Delta t}$$

where $t_{1/2}$ = half-life of the indicator nuclide and Δt is the passed time (normative time t_n minus measurement time t_m).

The dead time correction is commonly used during signal processing. When two pulses come in a too short time-span, they can not be detected. Also the difference in measuring times for the individual samples has to be considered. Further, due to the decay, the activity is decreasing during the measurement. This depends on the half-life of the radioactive nuclide. The interval correction f_n is calculated as:

$$f_n = (1 - e^{-(\ln 2 / t_{1/2})t_m}) / (1 - e^{-(\ln 2 / t_{1/2})t_n})$$

where t_m = measurement interval and t_n = normative time.

In case of an inhomogeneous neutron flux a flux correction has to be applied. This can be calculated based on the known position of the samples and standards in the sample batch.

After applying all the corrections, the peak area is obtained and the concentration of an element is calculated according to the equation:

$$ppm_p = P_p W_s / P_s W_p$$

where P_p , P_s are the corrected peak areas of the sample and standard, W_s = weight of the sample (in g), and W_p = weight of the element in the standard (in μg).

5.2.2.5 Details on INAA measurements presented in the thesis

INAA presented in this thesis was performed at the University of Vienna. The rock powders were weighted into polyethylene capsules and sealed. About 130 mg of each sample was used; the amount of standards was ~60–90 mg. In each batch, about 20 samples together with three international standards were packed and the position of the samples in the batch was noted. The following international standards were used: the carbonaceous chondrite Allende (Smithsonian Institution, Washington DC, USA; Jarosewich et al., 1987), granite AC-E (Centre de Recherche Pétrographique et Géochimique, Nancy, France; Govindaraju, 1989), and Devonian Ohio shale SDO-1 (United States Geological Survey; Govindaraju, 1989).

All samples and standards were irradiated in the 250 kW Triga reactor of the Atomic Institute of the Austrian Universities. The irradiation time was commonly 8 h at a neutron flux of 2.10^{12} n cm^{-2} s^{-1}. The measurements were started after a cooling period, which was usually about five days. During this cooling period, the high activity of short-lived isotopes (e.g., ^{24}Na) decays. Four independent high purity Ge detectors are used in the INAA laboratory at the University of Vienna (Fig. 5-4). The detectors have relative efficiencies of 14 to 48 % and energy resolutions of 1.60 to 1.82 keV at 1332 keV (Koeberl, 1993; Mader and Koeberl, 2009).

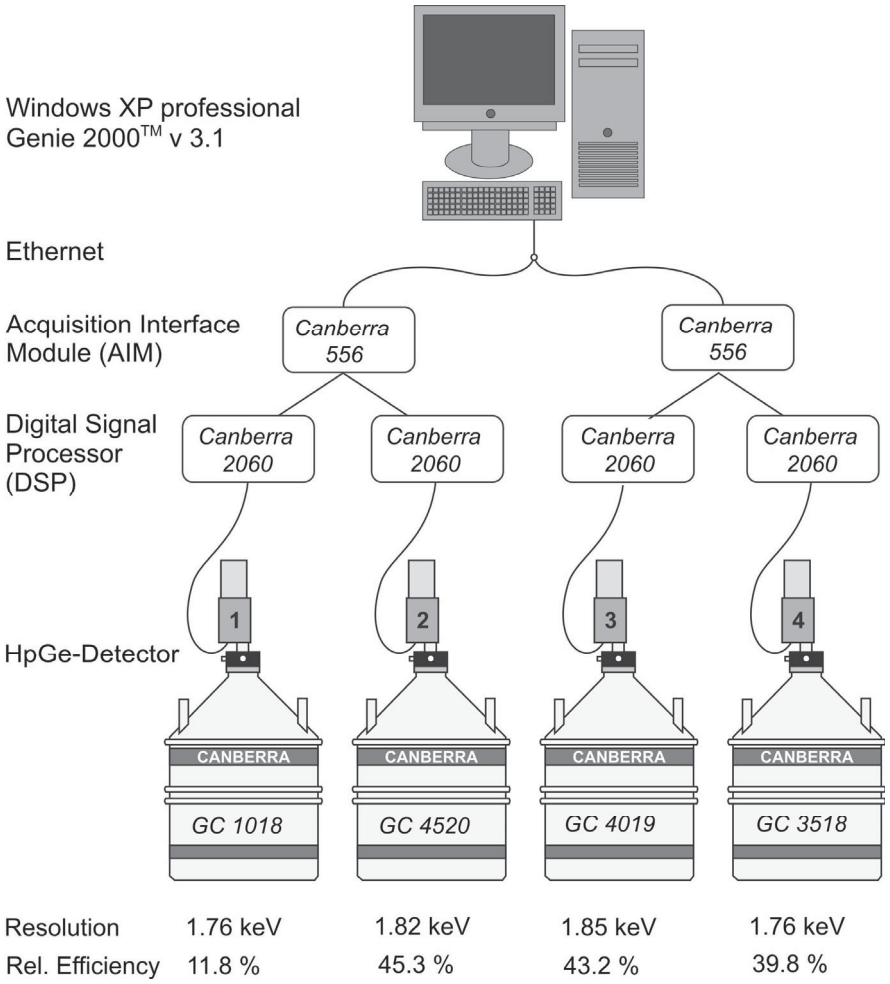

Fig. 5-4. Scheme of the system at the INAA lab at the University of Vienna, Department of Lithospheric research. Modified after Huber (2003).

The measurements are made in three cycles. The first cycle (L1), where the short-lived isotopes are measured, starts about five days after the end of the irradiation. Every sample is measured for about 40–60 minutes, depending on the activity. The second cycle (L2) starts about 10 days after the irradiation and the samples are measured for about 3 hours. The last cycle (L3) starts when most of the short-lived isotopes have decayed, about 5 weeks after the irradiation. In the L3 cycle the samples are measured for about 24 hours. When the measurements are finished, the spectra are calibrated and calculations

comparing samples with the standards are performed. For each element, peaks from different cycles, which have different significance, are compared and corrected. The concentration of an element is calculated as a mean value of the fitting peaks. Typical precisions for the analyzed elements are listed in Table 5-2. The instrumentation of the INAA lab at the University of Vienna has been recently described in detail by Mader and Koeberl (2009).

TABLE 5-2. TYPICAL PRECISION OF INAA AT THE INAA LAB AT THE UNIVERSITY OF VIENNA (IN REL%).

Na (wt%)	2	La	2
K (wt%)	5	Ce	3
Fe (wt%)	4	Nd	5
Sc	2	Sm	2
Cr	3	Eu	2
Co	2	Gd	5
Ni	15	Tb	2
Zn	3	Tm	2
As	10	Yb	2
Se	10	Lu	2
Br	10	Hf	2
Rb	2	Ta	2
Sr	5	W	10
Zr	10	Ir (ppb)	<1 ppb*
Sn	2	Au (ppb)	15
Sb	5	Th	2
Cs	2	U	10
Ba	10		
La	2		
Ce	3		
Nd	5		

Data from Son and Koeberl (2005). Data were obtained by at least 10 replicate analyses of international geological standard reference materials.

* below detection limit of 1 ppb

References used for chapter 5.2.2: Potts (1987), Vandecasteele and Block (1993), Koeberl (1995), Gill (1997).

5.2.3 Optical microscopy

Many basic observations of the samples were performed on thin sections by the optical microscope. The thin sections were examined in transmitted, plane polarized and cross polarized light. The mineral components were determined and the textures and all important features of the samples were described. Also shock metamorphism effects were studied in detail. During the optical microscope examinations thin sections suitable for further analyses were selected. Some thin sections (especially of the impact breccia samples) were examined also under reflected light to determine the opaque minerals.

5.2.4 Universal stage measurements

The orientations of planar deformation features (PDFs) in quartz grains were determined by measurements on optical microscope with a universal stage (U-stage).

5.2.4.1 Mounting the U-stage

The U-stage has to be placed on a stage of an optical microscope, fixed, and well centered. Special objectives have to be used for the U-stage investigations. To investigate a thin section, we assemble the lower glass hemisphere, the circular glass, then the thin section, and the upper glass hemisphere on the top. A drop of glycerin is put between each of these parts. Glass hemispheres with refractive index 1.554 are used for quartz investigations. The main parts of a U-stage are shown in Fig. 5-5.

5.2.4.2 Measuring the orientation of the c-axis

First a quartz grain with PDFs has to be placed in the center of the view (under the cross hairs). All the scales of the microscope and U-stage have to be at 0 positions. Then the right position of the c-axis has to be chosen. In the extinction position of the quartz grain, the c-axis can be oriented either E-W or N-S, but the E-W orientation is necessary for the measurement. The grain has to be put to extinction by turning the inner vertical stage. Then the microscope stage is turned clockwise by about 30°. In this position, the gypsum plate is inserted. If the color of the grain becomes gray/yellow, the position is correct. If the color turns blue/green, the position is wrong. In this case, the microscope stage has to be put back to 0° and the inner vertical stage has to be rotated by 90° to the next extinction position.

When the quartz grain is at the correct precise extinction position, the outer horizontal stage is rotated by about 30°, until the grain comes out of the extinction. Then the inner horizontal stage has to be rotated until the maximum extinction is achieved again. When the parts of the U-stage are at this final position, the azimuth and inclination have to be recorded. For each grain, this measurement has to be repeated, but from a different position of the first extinction (the original position +180°). If the two measurements are too different, it indicates a large error and the measurements need to be repeated.

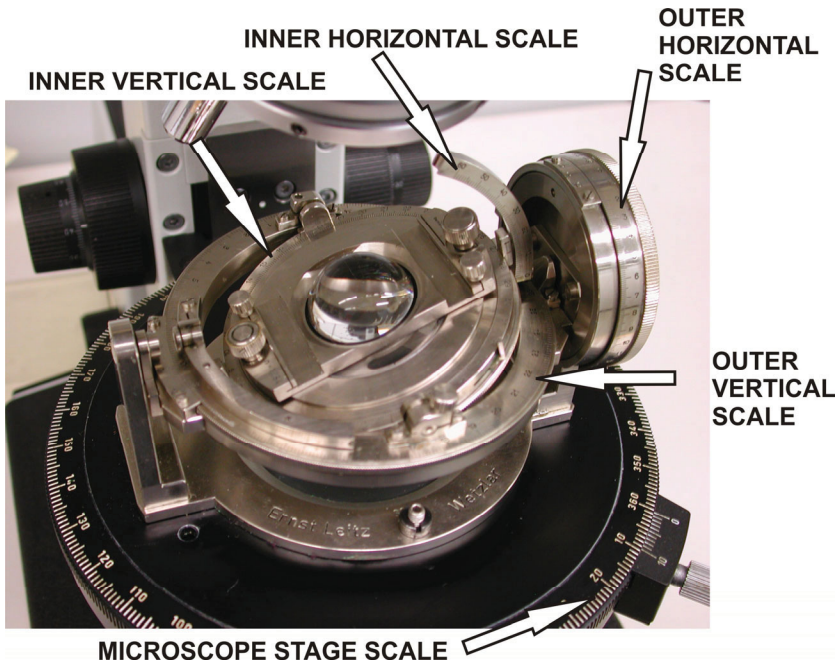

Fig. 5-5. Universal stage mounted on an optical microscope. Arrows show the main parts (scales) of the U-stage.

5.2.4.3 Determining of PDF orientations

After the position of the c-axis of a quartz grain is determined, the orientation of PDF sets can be measured. A PDF set has to be chosen and moved to a position parallel with the N-S cross hair by rotating the inner vertical stage. Then the inner horizontal stage is used to get the PDF set to a position, where it is maximally sharp and narrow. In this final position, azimuth and inclination has to be noted. The same procedure is repeated for each PDF set. Further, for each set two measurements (in two positions with 180° difference) are performed.

5.2.4.4 Plotting the results of the measurements

After the measurement of c-axis and poles normal to PDF planes are finished, the results are plotted into the Wulff net. First the raw results are plotted and then all is transformed so that the c-axis is in the center of the stereoplot. Then the data points are compared with a special stereographic projection template, which displays the orientations of PDF planes within 5° envelopes (Engelhardt and Bertsch, 1969; Stöffler and Langenhorst, 1994). The standard template (e.g., Stöffler and Langenhorst, 1994) has been recently updated by Ferrière (2009). For the measurements presented in the thesis (chapter 9), the updated template (Fig. 5-6), which includes additional PDF orientations, was used.

Details of the U-stage method were described in, e.g., Reinhard (1931) and Emmons (1943). A detailed guide for the U-stage measurements can be found in Ferrière (2008).

References used for chapter 5.2.4: B. French (written notes), Ferrière (2008).

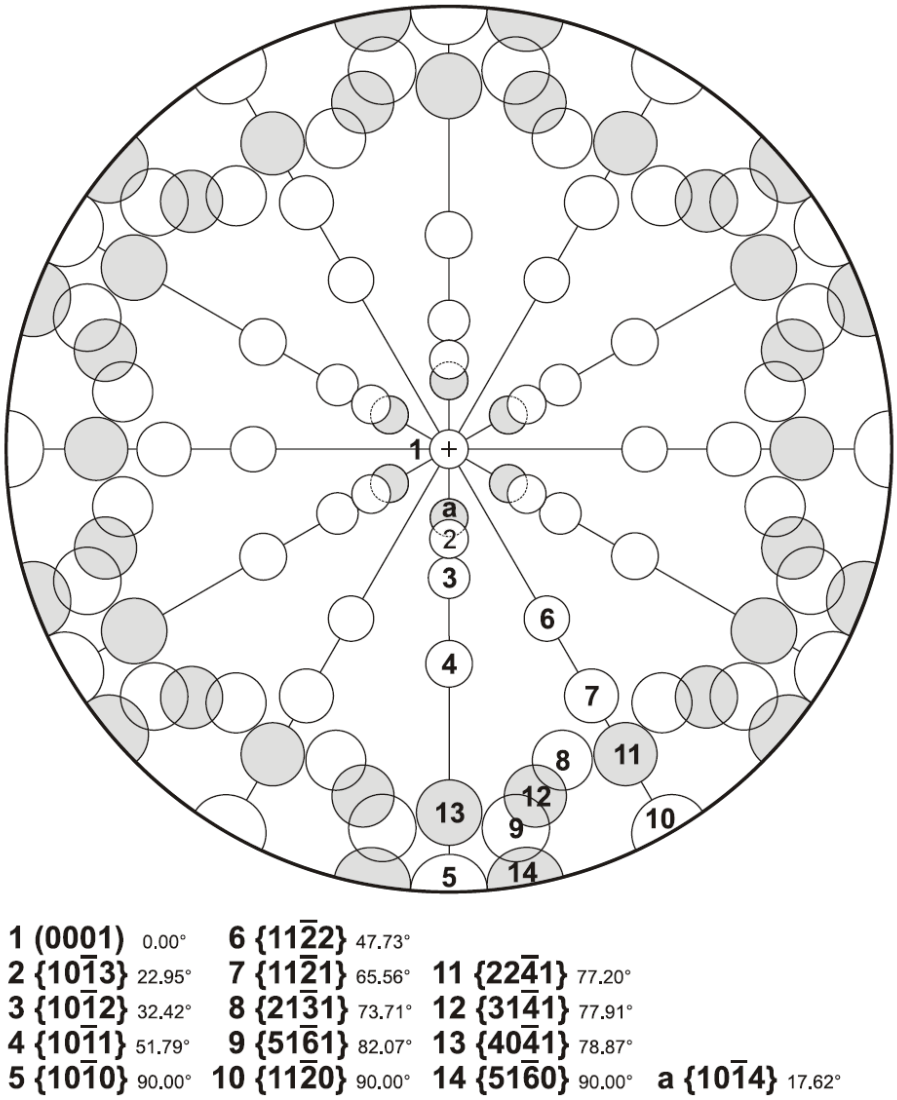

Fig. 5-6. The updated template for evaluating U-stage measurements of the PDF orientations in quartz. C-axis is in the center, the circles mark the positions of common PDF orientations. From Ferrière (2009).

5.2.5 X-ray diffraction (XRD)

X-ray diffraction is a common method used to study the structure of materials. Phase identification as well as determination of crystal cell dimensions can be performed. The method has been evolving and has changed from manual (graphic) evaluation of the results to modern automatic method with digital and graphic output. Several different configurations and sample preparations can be used to study a material. The sample can be a monocrystal, but commonly a fine sample powder is used. There are also several types of instruments used for X-ray diffraction measurements.

The X-ray diffraction is based on irradiating a sample with X-rays. The X-rays (that have wavelengths similar to the crystal cell dimensions), interact with the crystal lattice and diffract. The distances of the lattice planes are then reflected in the peak positions of

the diffractogram. When the X-ray strikes an electron, the electron starts emanating secondary spherical waves. A regular array of waves is produced by a regular array of scatterers. The waves interfere constructively in specific directions which can be determined by Bragg's law (see Fig. 5-7):

$$2\,d\,\sin\Phi = n\,\lambda$$

where d = lattice distance, Φ = diffraction range, n = an integer, order of diffraction, λ = wavelength of the X-rays.

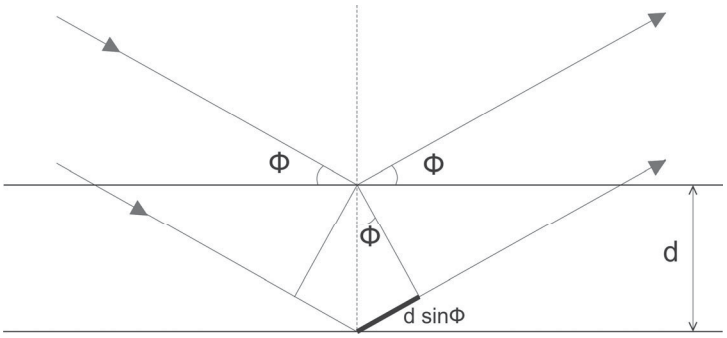

Fig. 5-7. Schematic picture showing X-ray scattering on crystal planes and the parameters of the Bragg's law.

5.2.5.1 XRD analysis by a diffractometer

In the further text, the most common configuration, which was used also for the measurements presented in the thesis, is described. The fine sample powder is pressed into a special sample holder. Monochromatic X-rays, generated in an X-ray tube (see also part about XRF analysis of this chapter) are focused on the sample. The X-rays interact with the sample and diffracted X-rays are detected. The typical configuration of an X-ray diffractometer is shown in Fig. 5-8. The detector moves along a circle around the sample and detects the X-rays. The sample holder and detector are moving simultaneously, but the detector moves with double angle frequency. Before the modern detectors were developed, the X-rays were detected on a film (Debye-Scherrer method). There are several types of detectors. Scintillation detectors were used mostly in older instruments. Solid-state detectors have many advantages, but high costs. Proportional detectors are currently most widely used.

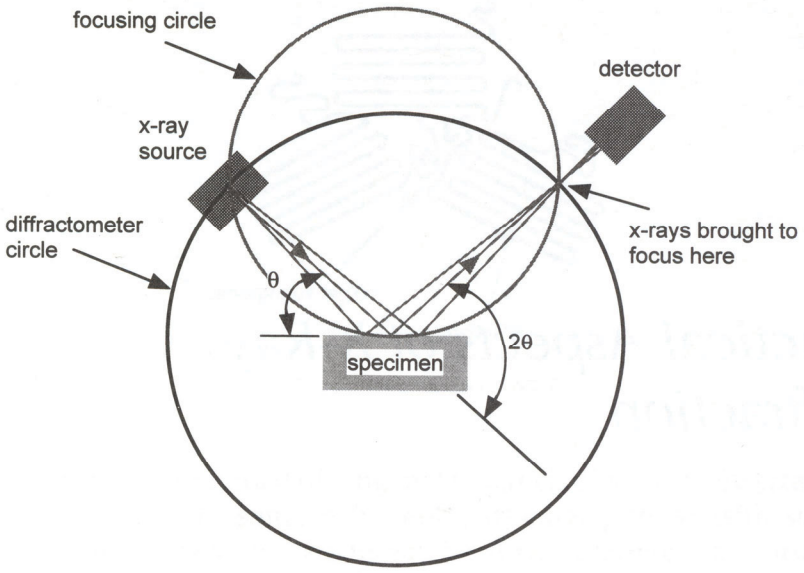

Fig. 5-8. Configuration of an X-ray diffractometer. From Suryanarayana and Norton (1998).

5.2.5.2 Evaluation of results

The result of a measurement is a diffractogram, a diagram with diffraction angle Φ (or more precisely 2Φ) on the horizontal axis and intensity on vertical axis. The distances between lattice planes can be calculated from the position of the peaks according to the Bragg's equation. To identify a mineral, the peak positions and intensities are compared with table values. These can be found in books (e.g., Bayliss et al., 1986; Brindley and Brown, 1980) or today commonly in computer databases. A database is usually part of the evaluation software, where automatic search/match routines can be used.

There are some limitations of the XRD method. These include systematic overlapping due to the collapse of the 3-D reciprocal space on the one dimensional 2Φ axis as well as accidental overlapping because of limited resolution. There is also a considerable background. Non-random distribution of the crystallites in the powder specimen can also occur (preferred orientation).

5.2.5.3 Details on XRD analyses presented in the thesis

The XRD measurements presented in the thesis were performed at the University of Vienna. Fine bulk rock powder was pressed into the sample holder. Diffraction data were collected with a Philips diffractometer (PW 3710, goniometer PW 1820), CuKα radiation, 45 kV, 35 mA, step size of 0.02 degree, and a counting time of 1s per step. Minerals were identified using the Joint Committee on Powder Diffraction Standards database (JCPDS, 1980).

For the separation of the clay fraction (<2 μm) a special preparation (described below) was performed. To distinguish the different clay minerals, further special treatments were performed (according to Moore and Reynolds, 1997). The clay fraction

samples were saturated with 1N KCl-solution and 1N $MgCl_2$-solution by shaking overnight and afterwards washed with distilled water. Also saturation with ethylene glycol and glycerol was used. The samples were analyzed after air-drying, after saturation with Mg-ions, K-ions, ethylene glycol and glycerol, and after heating to 550 °C. The samples were then measured on a PANalytical X´Pert Pro diffractometer, CuK_α- radiation, 40 kV, 40 mA, step size 0.0167 degree, counting time 5 s per step. Minerals were identified according to Moore and Reynolds (1997).

5.2.5.4 Clay fraction sample preparation

Selected samples of the gravelly sand were used for the clay fraction analyses. In order to separate the clay fraction, the samples were crushed into small pieces. Then the samples were put into 15% H_2O_2 to remove the organic material and treated with a 400 W ultrasonic probe for 3 min. After complete removal of organic material and disintegration of the samples, the sample suspension was poured into Atterberg-cylinders and the sedimentation was run for a specific time (24 hours and 33 minutes), to obtain the fraction <2 μm. The samples were dried in an oven and the dry powder was collected. The clay fraction powder was suspended in distilled water (8 mg/ml) and oriented XRD mounts were prepared by pipetting the clay suspensions onto glass slides.

References used for chapter 5.2.5: Liebhafsky and Pfeiffer (1971), Suryanarayana and Norton (1998), Jenkins (1999), Will (2006), Kruger (2002).

5.2.6 Scanning electron microscopy with energy dispersive X-ray spectrometry (SEM-EDS)

Scanning electron microscopy is a powerful method that enables imaging of specimen at submicroscopic scale. Most commonly thin sections are investigated, but also other types of samples can be used. An energy dispersive spectrometer is commonly attached to an electron microscope. This enables qualitative and (semi)quantitative chemical analyses. The sample has to be coated with a conductive layer (commonly graphite or gold) to lead away the electric charge. Graphite is ideal for compositional analysis, whereas gold coating is more suitable for imaging.

Compared to X-rays, electrons are less penetrative, thus not only the diameter, but also depth (i.e., the overall volume) analyzed is much smaller. Electron excitation gives analytical lines of higher intensity with less absorption and enhancement effects. On the other hand, this method has higher background and requires high vacuum

5.2.6.1 Electron-specimen interaction

There are several types of interactions between electrons and the analyzed material (Fig. 5-9). Secondary electrons (SE) are generated in elastic collisions. Their most probable energies are 2–5 eV. The limit between SE and back scattered electrons (BSE) is drawn at 50 eV. Auger electron (AE) production is an alternative to characteristic X-ray emission after ionization of an inner shell. In this case, the energy is transferred to an electron which leaves the specimen, instead of to X-ray quantum. Secondary electrons and Auger electrons are generated only from a very thin surface layer. Characteristic X-rays are generated only in the volume in which the electron ionization energy exceeds ionization energy of the inner shell. The dimensions of the specimen interaction volume depend mostly on the energy of the electron beam and on the atomic number of the specimen. The characteristic X-rays are commonly generated from a pear-shaped volume, typically 2 μm across and 2 μm deep.

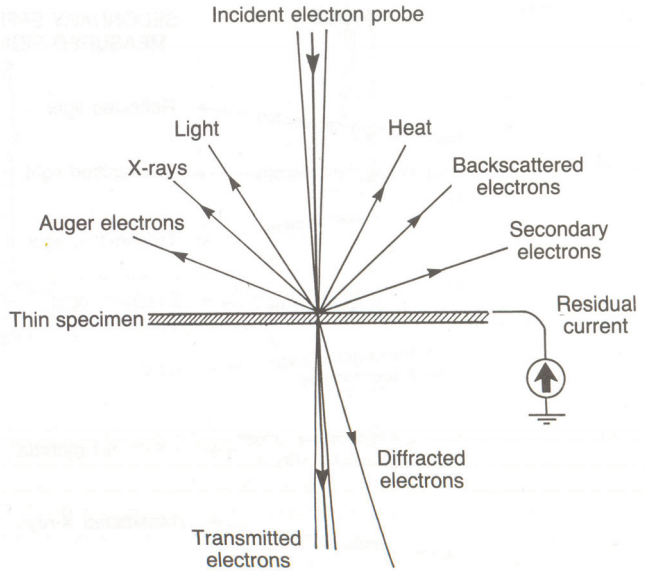

Fig. 5-9. Types of interaction between an electron beam and a specimen. From Potts et al. (1995).

5.2.6.2 Electron microscope

Electrons from a thermo-ionic cathode (commonly a tungsten filament) are accelerated through a voltage difference between cathode and anode (usually 2-30 kV). The electron beam is focused to a small point by electromagnetic lenses. The electrons interact with the specimen and electrons and rays resulting from the reaction are detected. The electron beam may be swept in a raster across the surface to form an image. Secondary electron mode is used for imaging of the surface of a sample as SE originate from the upper few nanometers of the sample. The SE are collected by a positively biased grid. However, SE are also excited by BSE. Therefore, typical BSE contrast is superimposed on every SE photograph. The large depth of field makes a three dimensional appearance of the specimen. Back scattered electrons move on straight trajectories and can be detected by

scintillators, semiconductors, or channel plates. Emission of BSE also depends on the surface tilt, thus surface topography can be imaged. However, more important is the dependence of the backscattering coefficient on the mean atomic number. Thus, phases with different mean atomic numbers can be distinguished in the BSE mode.

5.2.6.3 Energy dispersive spectrometry (EDS)

Two kinds of inelastic interactions are important for the X-ray generation. First is deceleration of the electrons that forms the so-called Bremsstrahlung. This continuous X-ray radiation is present in all spectra as a background. More important are the characteristic X-rays (see also part about XRF of this chapter). The detector is usually a Li-drifted Ge or Si crystal. The pulses are detected by a pulse height analyzer and stored in a multichannel analyzer. As common in this kind of analytical instruments, the detectors have a "dead time", thus X-ray quantum arriving at the detector within about 10 microseconds after the previous one can not be detected. The detector crystals are usually mounted behind an isolating window (made of Be or various polymers). It should be noted that the Be window absorbs X-rays from light elements (lighter than Na). A schematic diagram of a scanning electron microscope with energy dispersive X-ray analyzer is shown in Fig. 5-10.

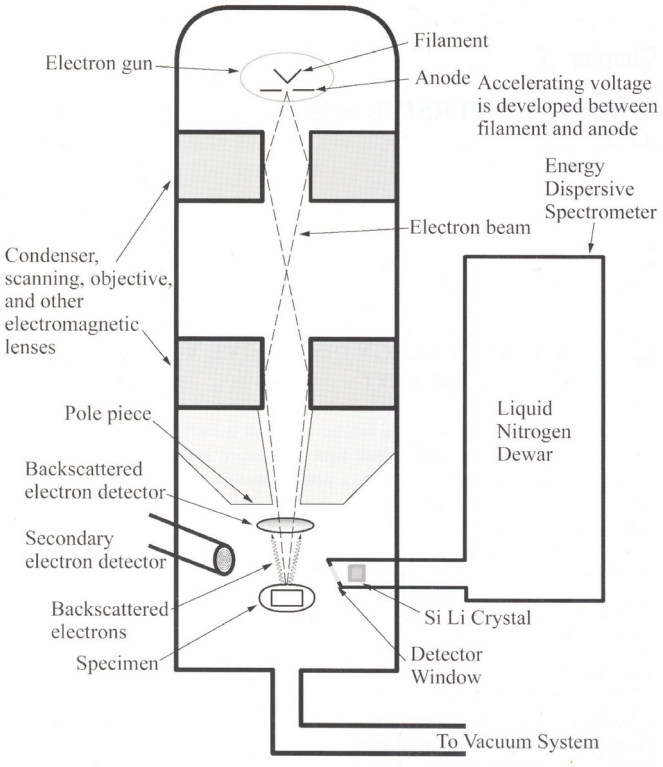

Fig. 5-10 Schematic cross section of an electron microscope with an energy dispersive X-ray spectrometer. From Severin (2004).

5.2.6.4 Details on SEM-EDS measurements presented in the thesis

Polished thin sections were examined on a JEOL JSM 6400 scanning electron microscope with an energy-dispersive X-ray analyzer at the Natural History Museum in Vienna. Secondary electron and backscattered electron modes were used. The compositions of mineral and melt phases were analyzed by KEVEX SuperDry Si(Li) detector linked to a VANTAGE EDS system with operating conditions 15 kV acceleration potential and ~1–2 nA sample current. The following elements were analyzed and results were recalculated to oxide contents (automatically normalized to 100 wt%): Si, Al, Ca, Fe, Mg, K, Na, Ti, Mn, and Cr. The standardless EDX analyses have a precision of ~3 rel% and accuracies of 10 rel%. Detection limits are ~0.2–0.5 wt%. Both focused and defocused beams were used for the measurements.

References used for chapter 5.2.6: Potts (1987), Lee (1993), Reimer (1998), Severin (2004), Goldstein et al. (2007).

5.2.7 Electron microprobe (EMP)

An electron microprobe can analyze chemical composition of very small parts of a sample (thin section). The diameter of the beam can be as small as about 1 μm. The sample interacts with a beam of electrons and the emitted rays are detected. The principle of an EMP (Fig. 5-11) is very similar to an electron microscope and there is considerable overlap in the functions of these instruments. However, the electron microscope, if equipped for chemical analysis, has only an EDS or one WDS detector, whereas a microprobe includes several WDS detectors. The electron microscope also usually does not have beam current regulation. The sample preparation is equivalent to the SEM.

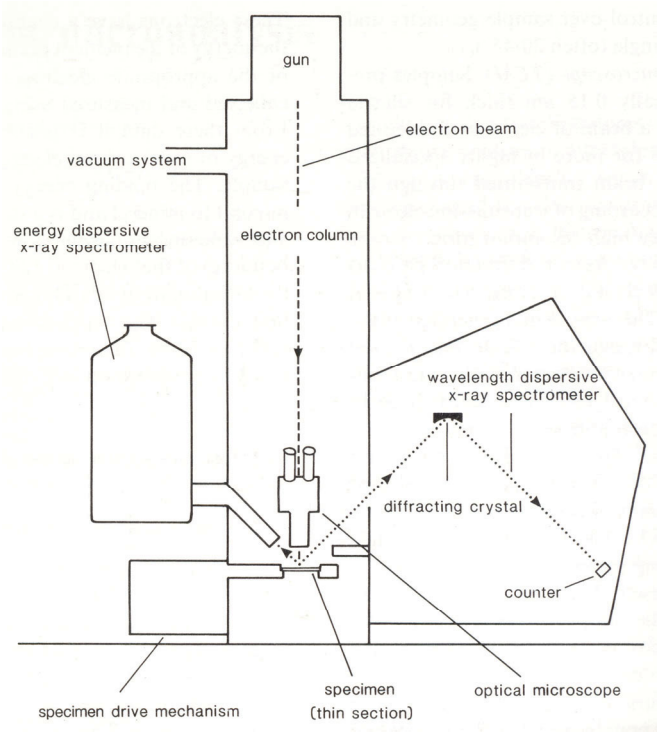

Fig. 5-11. Typical configuration of an electron microprobe. From Potts (1987).

The primary use of an EMP is chemical analyses on sub-microscale. These are again similar to the chemical analyses that can be performed on an electron microscope, but much more precise. The wavelength-dispersive spectrometers are more precise than the energy-dispersive spectrometers, described in the previous chapter. All elements from Be to U can be detected in principle, although not all instruments can measure light elements (with atomic number <10). Qualitative analysis involves identification of spectrum lines, quantitative analysis requires measurement of the line intensities. The detected X-ray lines are compared with standards of known composition.

By scanning the beam in a raster, element distribution maps can be obtained. As the relationship of the intensity of an X-ray line and the concentration of the element depends on the sample composition, matrix corrections have to be applied. Electron microprobe can also produce microimages in SE and BSE mode, similar to scanning electron microscope.

5.2.7.1 Wavelength dispersive spectrometry (WDS)

Wavelength dispersive X-ray spectrometers use crystal diffraction to separate the different wavelengths of the spectrum; the wavelength is varied by moving the crystal. Curved crystals are used in the detectors. There are several crystals needed to cover the full spectrum of wavelengths, thus several WDS are usually fitted to an EMP. WDS can detect only one wavelength at a time and the spectrum is measured sequentially. The X-rays reflected by the crystal are detected by a proportional counter, whereas the X-rays ionize a gas and create electric pulses. The spectrometer is moved in small steps and the digital output is stored. In an EDS the whole spectrum is measured simultaneously. ED analysis is generally quicker, easier, and cheaper, whereas WD analysis has better energy resolution, high count rate capability, and is essential for low concentrations. A combination of the two methods is commonly used.

5.2.7.2 Details on EMP measurements presented in the thesis

Electron microprobe was used for detailed studies and precise chemical analyses of melt particles in suevite. Electron microprobe analyses were performed on a JEOL JXA 8500F at the Museum of Natural History, Berlin. The microprobe was calibrated using Smithsonian international mineral standards. Counting times were 40 s on the peak and 20 s on background. Both focused and defocused beam were used. Defocused beam with a diameter of 20 μm was used to obtain the average composition of each melt particle and for analyses of larger homogeneous phases (acceleration voltage was 20 kV and probe current 20 nA). A focused beam with a diameter of 1–3 μm was used to identify small phases (operating at 15 kV and 15 nA). Following elements were analyzed: S, Na, Fe, K, Ti, Al, Mg, Cr, Ca, Mn, and P. Several element profiles and maps (combining WDS and

EDS analyses) were obtained and photographs in back-scattered electron (BSE) mode were taken.

References used for chapter 5.2.7: Liebhafsky and Pfeiffer (1971), Potts (1987), Reed (1993), Potts et al. (1995), Goldstein et al. (2007).

5.2.8 Raman spectroscopy

Raman spectroscopy is a modern non-destructive method, which has a wide use in geology, as well as in many other fields of science. The method can identify mineral phases based on the molecular vibrations in their structure. The basic principle is the so-called Raman scattering, described below. The sample can be a thin section, but also a small hand specimen. Raman spectrometry is widely used for phase identification (ideal for, e.g., small crystals and inclusions, that can not be easily separated and analyzed by other methods). The sensitivity to short range order enables to study structure of melts and glasses, as well as amorphised minerals. However, not all minerals can be identified by Raman spectroscopy, because some minerals have no first order Raman spectra (e.g., halite), and there are minerals with thermal sensitivity, strong light absorption, or poor transparency. There are also some disturbing effects such as intense luminescence or so-called "Raman background".

5.2.8.1 Raman scattering

Raman effect results from interaction of light and matter. The scattering of light can be elastic, so-called Rayleigh scattering, which does not change the light frequency. Further there are inelastic scatterings, which change the light spectrum. The Raman scattering (Fig. 5-12) is a result of interaction of electromagnetic radiation with vibrational and/or rotational motions of molecules and constitutes the Raman spectrum of a material. Brillouin scattering involves translational motion of molecules, but produces only very small frequency shifts. The molecular motion can have only certain discrete energy states. The interaction of a molecule with electromagnetic radiation thus can be analyzed in terms of an energy-transfer mechanism.

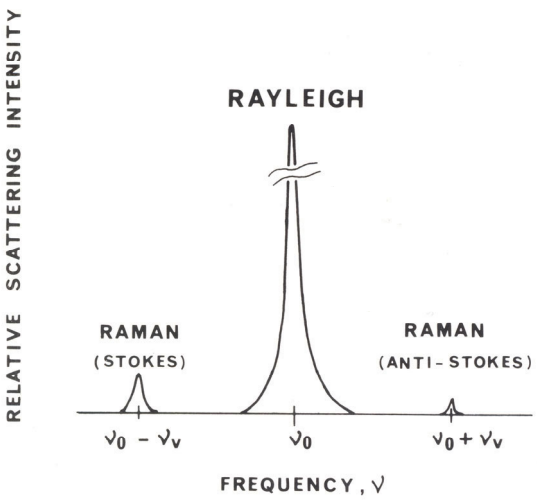

Fig. 5-12. Raman and Rayleigh scattering of excitation at a frequency ν_0. From Turrell and Corset (1996).

In scattering processes at least two quanta act simultaneously in the light-matter system. Simple elastic scattering occurs when a quantum of electromagnetic energy is created and an identical one is annihilated at the same time. In the inelastic Raman scattering the two photons are not identical and the state of the molecule is changed. If the created photon has less energy than the annihilated one, the scattered light has lower frequency. This is so-called Stokes Raman scattering (red shift). An anti-stokes spectrum is produced when the created photon is more energetic (loss of vibrational energy of the sample, blue shift). Raman data are presented as wave-number shift in cm^{-1} from the incident radiation. The Raman shifts are absolute energy differences and are not a function of the wavelength of the original radiation.

5.2.8.2 MicroRaman spectrometer

In Raman spectroscopy, a laser is used as the light source. Wavelengths of visible light are used; common lasers are He-Ne (632 nm), Ar^+ (515 nm), and Kr^+ (406 nm). In microRaman spectroscopy the laser beam is directed into an optical microscope and focused through the objective onto the sample. The scattered light travels back through the same objective into the spectrometer. The frequency components of the collected light are characterized and a radiation detector transforms the optical system output into an electrical signal. Wavelength separation is usually based on diffraction or interference. The dispersion system consists of either conventional gratings or a holographic Rayleigh rejection filter (notch filter). Dispersive double or triple monochromators have good spectral resolution (0.05 cm^{-1}), but cause strong light intensity loss. For this reason, the notch filters are more suitable for the use in geosciences (the only disadvantage is that bands with shifts < ~100 nm are cut off). Charge-coupled device (CCD) array detectors are most widely used for the signal detection. An example of configuration of a microRaman spectrometer is shown in Fig. 5-13.

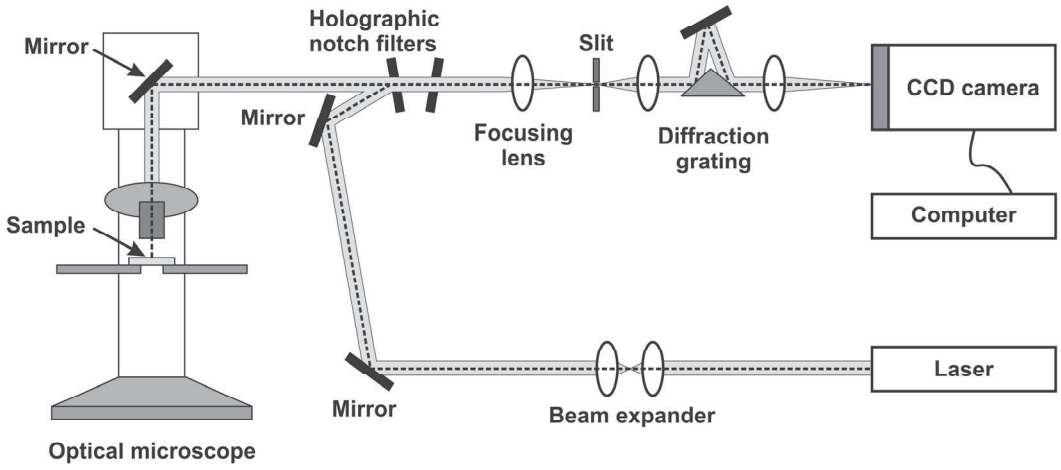

Fig. 5-13. Confocal microRaman spectrometer at the Institute of Mineralogy and Crystallography, University of Vienna is shown. From Ferrière (2008).

5.2.8.3 Details on microRaman measurements presented in the thesis

Raman microspectroscopy was performed at the University of Vienna. The method was used to identify mineral phases in thin sections with high spatial resolution (l–2 μm lateral, 2–3 μm depth, using a 50x/0.75 objective). The measurements were performed on a Renishaw RM1000 confocal edge filter-based microRaman spectrometer with a 17 mW, 632.8 nm HeNe (red) laser and a 20 mW (blue) 488 nm Ar ion laser excitation system with a thermoelectrically cooled charge-coupled device (CCD) array detector, A 1200 lines/mm grating monochromator provided a spectral resolution (apparatus function) of 3–4 cm^{-1} (red) and 5–6 cm^{-1} (blue). Spectra were calibrated with the Rayleigh line and the 520.5 cm^{-1} line of a Si standard. The obtained spectra were compared with libraries from Renishaw and from the RRUFF database (Downs, 2006) using Grams/32 software.

References used for chapter 5.2.8: Turrell and Corset (1996), Laserna (1996), Nasdala et al. (2004).

5.2.9 Mass spectrometry

Mass spectrometry is a powerful method that can distinguish not only the elements, but also different isotopes of an element. Mass spectrometry is based on the fact that ionized atoms can be separated in a magnetic field according to their different mass-to-charge ratio. There are several types of mass spectrometers with different configurations, different sources and detectors, several possible methods of sample preparation and a wide variety of uses. Here the gas source mass spectrometer that was used for carbon stable isotope analyses is schematically described.

5.2.9.1 Gas source mass spectrometry

Gas source mass spectrometry has a wide use in, e.g., the characterization of organic molecules and the petrochemical industry. It is mostly used to determine stable isotope ratios of elements such as H, C, O, N, or S. Furthermore, gas source spectrometry is used for geochronology (e.g., K-Ar or Ar/Ar dating). The gas samples can be released in stepped ignition process and must be chemically purified before the analysis. The gas source mass spectrometer comprises an electron impact ion source, where gas samples are ionized by collision with a stream of electrons, a flight tube with magnetic sector mass analyzer, and an ion collector assembly.

5.2.9.2 Magnetic sector mass spectrometer

Ions from an ion source are accelerated through a potential gradient and collimated by slits. The charged ions enter a strong magnetic field and are separated according to mass and charge. Only positively charged ions are analyzed. Negatively charged and uncharged

ions collide with the instrument walls and are pumped away. In the magnetic field, the trajectory of the ion is ideally circular. The radius of the trajectory can be calculated according to an equation resulting from the balance of the centrifugal force and the magnetic centripetal force:

$$m/z = r^2H^2 / 2V$$

where m = mass of the ion, z = charge of the ion, r = radius, H = magnetic field strength, V = potential gradient. To scan a mass spectrum, it is necessary to vary either the potential gradient or the magnetic field strength (more common). The resolution of a mass spectrometer indicates how well it separates ions close in mass. Abundance sensitivity tells to which extent the tails of the peak at mass m contribute to neighboring peaks at masses (m-1) and (m+1). A simplified scheme of a mass spectrometer is shown in Fig. 5-14.

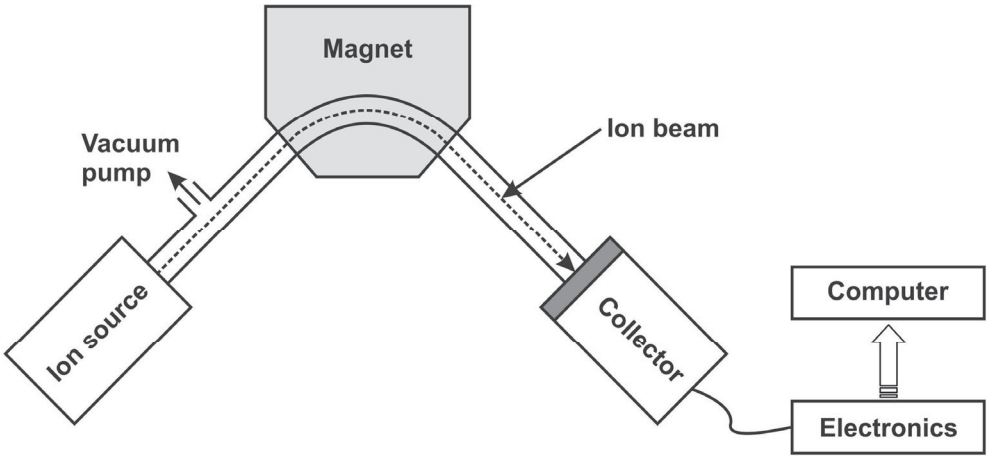

Fig. 5-14. Simplified scheme of a mass spectrometer. From Ferrière, 2008.

5.2.9.3 Faraday cup detector

A Faraday cup is a cup-shaped metal tube connected to an amplifier. It consists of beam-defining slit, an electrode, and an electron repeller plate. Ions entering the Faraday cup charge the electrode and this charge is leaked to earth through a resistor. The ion count rate is proportional to the voltage drop across the resistor. The ions impinging on the electrode can cause emission of secondary electrons and induce errors. The electron repeller (a negatively charged plate) is placed in front of the Faraday cup to suppress this effect. The minimum detectable current is about 10^{-8} – 10^{-14} A. The Faraday cup is a robust detector, with long lifetime. However, the detection limits are generally worse compared to other types of detectors.

5.2.9.4 Carbon stable isotope analysis

The ratio of the stable isotopes $^{13}C/^{12}C$ is analyzed. The sample powder or small chips are combusted in an atmosphere of oxygen to ensure complete oxidation to CO_2. Carbon

dioxide is then measured by a gas source mass spectrometry using a double collector. The same mass of $^{13}C^{16}O^{16}O$ and $^{12}C^{16}O^{17}O$ has to be considered.

5.2.9.5 Details on carbon isotopic ratio measurements presented in the thesis

For the carbon isotopic measurements several carbon-rich clasts (mostly mudstones, dark-colored due to the organic matter content) from the Exmore breccia and impact breccia interval were used. Further a carbonaceous melt particle, carbonate veins, graphitic breccia, and a piece of vitrinite were analyzed. About 0.2 to 5 mg powder of each sample (depending on the carbon content) were drilled out and weighed into tin capsules. The isotopic composition of carbon was measured in the Stable Isotope Laboratory at the Department of Lithospheric Research, University of Vienna, using a Carlo Erba Element Analyzer coupled to a Micromass Optima stable isotope ratio mass spectrometer. Each sample was analyzed at least three times with a precision between 0.13 and 1.33 ‰. The carbon content of the samples was calculated from this data. The following laboratory standards were used: graphite USGS-24 (Coplen et al., 2006) and carbonatite NBS-18 (Verkouteren and Klinedinst, 2004). The accuracy was better than 0.6 ‰ for USGS-24 and better than 0.48 ‰ for NBS-18.

References used for chapter 5.2.9: Potts (1987), Vandecasteele and Block (1993), Gill (1997).

References:

Bayliss P., Erd D. C., Mrose M. E., Sabina A. P. and Smith D. K. 1986. *Mineral powder diffraction file*, Search manual. JCPDS International Centre for Diffraction Data. Printed in USA. 467 p.

Brindley G. W. and Brown G. 1980. *Crystal structures of clay minerals and their X-ray identification*. Mineralogical Society Monograph no. 5. Colchester and London: Spottiswoode Ballantyne Ltd. 495 p.

Coplen T. B., Brand W. A., Gehre M., Gröning M., Meijer H. A. J., Toman B., and Verkouteren R. M. 2006. New guidelines for $\delta^{13}C$ measurements. *Analytical Chemistry* 78: 2439–2441.

Downs R. T. 2006. The RRUFF Project: an integrated study of the chemistry, crystallography, Raman and infrared spectroscopy of minerals. Program and Abstracts of the 19th General Meeting of the International Mineralogical Association in Kobe, Japan. O03–13.

Emmons R. C. 1943. The universal stage (with five axes of rotation). *Geological Society of America Memoir* 8. 205 p.

Engelhardt W. v. and Bertsch W. 1969. Shock induced planar deformation structures in quartz from the Ries crater, Germany. *Contributions to Mineralogy and Petrology* 20: 203–234.

Ferrière L. 2008. *Shock metamorphism and geochemistry of impactites from the Bosumtwi impact structure: A case study of shock-induced deformations and transformations in quartz and associated methodology.* Ph.D. thesis, University of Vienna, Vienna, Austria, 279 p.

Ferrière L., Morrow J. R., Amgaa T., and Koeberl C. 2009. Systematic study of universal-stage measurements of planar deformation features in shocked quartz: Implications for statistical significance and representation of results. *Meteoritics and Planetary Science* 44: 925–940.

Gill R. 1997. *Modern analytical geochemistry: an introduction to quantitative chemical analysis techniques for earth, environmental and materials scientists*. Harlow, England: Addison Wesley Longman Limited. 329 p.

Goldstein J., Newbury D., Joy D., Lyman C., Echlin P., Lifshin E., Sawyer L., and Michael J. 2007. *Scanning electron microscopy and X-ray microanalysis.* Third edition. USA: Springer. 690 p.

Govindaraju K. 1989. 1989 compilation of working values and sample description for 272 geostandards: *Geostandards Newsletter* 13: 1–113.

Huber H. 2003. *Application of gamma, gamma-coincidence spectrometry for the determination of iridium in impact related rocks, glasses, and microtekites.* Ph.D. thesis, University of Vienna, Vienna, Austria, 326 p.

Jenkins R. 1999. *X-ray fluorescence spectrometry.* Second edition. USA: John Wiley & Sons, Inc.. 207 p.

Jarosewich E., Clarke R. S. J., and Barrows J.N. 1987. The Allende meteorite reference sample. *Smithsonian Contributions to Earth Sciences* 27: 1–49.

Koeberl C. 1993. Instrumental neutron activation analysis of geochemical and cosmochemical samples: a fast and reliable method for small sample analysis. *Journal of Radioanalytical and Nuclear Chemistry* 168: 47–60.

Koeberl C. 1995. Neutron activation analysis. In *Methods and instrumentations: results and recent developments*, Advanced mineralogy, Vol 2, edited by Marfunin A. S. Berlin, Heidelberg, New York: Springer. p. 322–329.

Kruger G. 2002. Basic concepts of powder diffraction. In *Powder diffraction*, edited by Gupta S. P. S. and Chatterjee P. Proceedings of the II International School on Powder Diffraction. New Delhi: Allied Publishers Limited. p. 17–19.

Laserna J. J. 1996. *Modern techniques in Raman spectroscopy.* Chichester, England: John Wiley & Sons Ltd. 427 p.

Lee R. E. 1993. *Scanning electron microscopy and X-ray microanalysis.* Engelwood Cliffs, New Jersey: PTR Prentice–Hall, Inc. 458 p.

Liebhafsky H. A. and Pfeiffer H. G. 1971. X-ray techniques. In *Modern methods of geochemical analysis*, edited by Wainerdi R. E. and Uken E. A. New York: Plenum Press. p. 245–270.

Mader D. and Koeberl C. 2009. Using instrumental neutron activation analysis for geochemical analyses of terrestrial impact structures: Current analytical procedures at the University of Vienna Geochemistry activation analysis laboratory. *Applied Radiation and Isotopes* 67: 2100–2103.

Moore D. M. and Reynolds R. C. Jr. 1997. *X-ray diffraction and the identification and analysis of clay minerals*. Oxford: Oxford University Press. 378 p.

Nasdala L., Smith D. C., Kaindl R., and Ziemann M. A. 2004. Raman spectroscopy: Analytical perspectives in mineralogical research. In *Spectroscopic methods in mineralogy*, edited by Beran A. and Libowitzky E. EMU Notes in Mineralogy 6: 281–343.

Potts P. J. 1987. *A handbook of silicate rock analysis*. Glasgow: Blackie. 622 p.

Potts P. J., Bowles J. F. W., Reed S. J. B., and Cave M. R. 1995. *Microprobe techniques in the Earth sciences.* London: Chapman & Hall. 419 p.

Reed S. J. B. 1993. *Electron microprobe analysis*. Second edition. Cambridge: Cambridge University Press. 326 p.

Reimer L. 1998. Scanning electron microscopy, Physice of image formation and microanalysis. Second edition. Heidelberg: Springer. 527 p.

Reimold W. U., Koeberl C., and Bishop J. 1994. Roter Kamm impact crater, Namibia: Geochemistry of basement rocks and breccias. *Geochimica et Cosmochimica Acta* 58: 2689–2710.

Reinhard M. 1931. *Universaldrehtischmethoden*. Basel, Switzerland: Birkhäuser. 118 p.

Severin K. P. 2004. *Energy dispersive spectrometry of common rock forming minerals.* Dordrecht, Netherlands: Kluwer Academic Publishers. 225 p.

Schmitt R. T., Wittmann A., and Stöffler D. 2004. Geochemistry of drill core samples from Yaxcopoil-1, Chicxulub impact crater, Mexico. *Meteoritics and Planetary Science* 39: 979–1001.

Son T. H. and Koeberl C. 2005. Chemical variation within fragments of Australasian tektites. *Meteoritics and Planetary Sciences* 40: 805–815.

Stöffler D. and Langenhorst F. 1994. Shock metamorphism of quartz in nature and experiment: I. Basic observation and theory. *Meteoritics and Planetary Science* 29: 155–181.

Suryanarayana C. and Norton M. G. 1998. *X-ray diffraction, A practical approach.* New York: Plenum Press. 273 p.

Turrell G. and Corset J. 1996. *Raman microscopy, developments and applications.* London: Academic Press Ltd. 463 p.

Vandecasteele C. and Block C. B. 1993. *Modern methods for trace element determination.* Chippenham, Wiltshire, UK: John Wiley & Sons. 330 p.

Verkouteren M. R. and Klinedinst D. B. 2004. *Value Assignment and Uncertainty Estimation of Selected Light Stable Isotope Reference Materials: RMs 8543-8545, RMs 8562-8564, and RM 8566.* NIST Special Publication 260-149. National Institute of Standards and Technology, Gaithersburg, Maryland, USA. 59 p.

Will G. 2006. *Powder diffraction: The Rietveld method and the two-stage method.* Stuertz, Wuerzburg, Germany: Springer. 224 p.

The Geological Society of America
Special Paper 458
2009

Petrographic and shock metamorphic studies of the impact breccia section (1397–1551 m depth) of the Eyreville drill core, Chesapeake Bay impact structure, USA

Katerina Bartosova*
Department of Lithospheric Research, University of Vienna, Althanstrasse 14, A-1090 Vienna, Austria

Ludovic Ferrière
Department of Lithospheric Research, University of Vienna, Althanstrasse 14, A-1090 Vienna, Austria, and
Department of Earth Sciences, University of Western Ontario, 1151 Richmond Street, London, ON, N6A 5B7, Canada

Christian Koeberl
Department of Lithospheric Research, University of Vienna, Althanstrasse 14, A-1090 Vienna, Austria

W. Uwe Reimold
Museum für Naturkunde–Leibniz Institute at Humboldt University Berlin, Invalidenstrasse 43, 10115 Berlin, Germany

Susanne Gier
Department of Geodynamics and Sedimentology, University of Vienna, Althanstrasse 14, A-1090 Vienna, Austria

ABSTRACT

The moat of the 85-km-diameter and 35.3-Ma-old Chesapeake Bay impact structure (USA) was drilled at Eyreville Farm in 2005–2006 as part of an International Continental Scientific Drilling Program (ICDP)–U.S. Geological Survey (USGS) drilling project. The Eyreville drilling penetrated postimpact sediments and impactites, as well as crystalline basement-derived material, to a total depth of 1766 m. We present petrographic observations on 43 samples of suevite, impact melt rock, polymict lithic impact breccia, cataclastic gneiss, and clasts in suevite, from the impact breccia section from 1397 to 1551 m depth in the Eyreville B drill core. Suevite samples have a fine-grained clastic matrix and contain a variety of mineral and rock clasts, including sedimentary, metamorphic, and igneous lithologies.

Six subunits (U1–U6, from top to bottom) are distinguished in the impact breccia section based on abundance of different clasts, melt particles, and matrix; the boundaries between the subunits are generally gradational. Sedimentary clasts are dominant in most subunits (especially in U1, but also in U3, U4, and U6). There

*katerina.bartosova@univie.ac.at

Bartosova, K., Ferrière, L., Koeberl, C., Reimold, W.U., and Gier, S., 2009, Petrographic and shock metamorphic studies of the impact breccia section (1397–1551 m depth) of the Eyreville drill core, Chesapeake Bay impact structure, USA, *in* Gohn, G.S., Koeberl, C., Miller, K.G., and Reimold, W.U., eds., The ICDP-USGS Deep Drilling Project in the Chesapeake Bay Impact Structure: Results from the Eyreville Core Holes: Geological Society of America Special Paper 458, p. 317–348, doi: 10.1130/2009.2458(15).

are two melt-rich subunits (U1 and U3), and there are two melt-poor subunits with predominantly crystalline clasts (U2 and U5). The lower part (subunits U5 and U6), which has large blocks of cataclastic gneiss and rare melt particles, probably represents ground-surge material. Subunit U1 possibly represents fallback material, since it contains shard-like melt particles that were solidified before incorporation into the breccia. The melt-poor, crystalline clast–rich subunit U2 could have been formed by slumping of material, probably from the central uplift or from the margin of the transient crater.

Melt particles are most abundant near the top of the impact breccia section (above 1409 m) and around 1450 m, where the suevite grades into impact melt rock. Five different types of melt particles have been recognized: (1) clear colorless to brownish glass; (2) melt altered to fine-grained phyllosilicate minerals; (3) recrystallized silica melt; (4) melt with microlites; and (5) dark-brown melt. Proportions of matrix and melt in the suevite are highly variable (~2–67 vol% and 1–67 vol%, respectively; the remainder consists of lithic clasts).

Quartz grains in suevite commonly show planar fractures (PFs) and/or planar deformation features (PDFs; 1 or 2 sets, rarely more); some PDFs are decorated. On average, ~16 rel% of quartz grains in suevite samples are shocked (i.e., show PFs and/or PDFs). Sedimentary clasts (e.g., graywacke or sandstone) and polycrystalline quartz clasts have relatively higher proportions of shocked quartz grains, whereas quartz grains in schist and gneiss clasts rarely show shock effects. Rare feldspar grains with PDFs and mica with kink banding were observed. Ballen quartz was noted in melt-rich samples. Evidence of hydrothermal alteration, namely, the presence of smectite and secondary carbonate veins, was found especially in the lower parts of the impact breccia section.

INTRODUCTION

The 85-km-diameter Chesapeake Bay impact structure (Fig. 1) is ~35.3 Ma old (e.g., Poag et al., 1994, 2004; Horton and Izett, 2005; Gohn et al., 2006a). It is a large and well-preserved marine impact structure that displays a complex crater geometry (known as "inverted sombrero"; Gohn et al., 2006a). It has a deep inner crater and a small central uplift structure (Poag et al., 1999) surrounded by a shallower outer basin. The 85-km-diameter outer basin was formed during the crater modification stage. Collins and Wünnemann (2005) suggested that the diameter of the inner basin, ~40 km (Poag et al., 2002), might better represent the energy involved in the impact event. The location of the impact structure on a passive continental margin and the immediate resumption of marine deposition after impact protected the crater from subsequent erosion (Poag et al., 2004, p. 4). Today, the impact crater is buried beneath southern Chesapeake Bay, its surrounding peninsulas, and the continental shelf east of the Delmarva Peninsula (Poag et al., 1994; Poag, 1997). Previous work, based on geographic position, age, and chemical as well as isotopic data, indicates that the Chesapeake Bay impact structure is the source of the North American tektites (Koeberl et al., 1996; Deutsch and Koeberl, 2006).

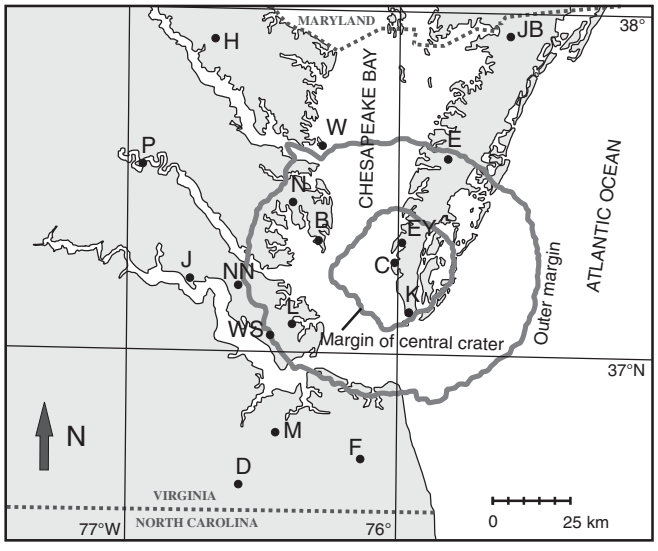

Figure 1. Map of Chesapeake Bay (modified from Horton et al., 2005c), showing the location of the Chesapeake Bay impact structure and major core holes. Locations: B—Bayside, C—Cape Charles U.S. Geological Survey (USGS) Sustainable Technology Park (STP), D—Dismal Swamp, E—Exmore, EY—Eyreville, F—Fentress, H—Haynesville, J—Jamestown, JB—Jenkins Bridge, K—Kiptopeke, L—USGS-NASA Langley, M—MW4, N—North, NN—Newport News Park 2, P—Putneys Mill, W—Windmill Point, and WS—Watkins School.

Geology of the Atlantic Coastal Plain and Discovery of the Chesapeake Bay Impact Structure

The Atlantic Coastal Plain is a subsiding passive continental margin. Marine transgressions have alternated with regressions, and the succession has been modified by isostatic adjustment, Appalachian tectonics, and paleoclimatic changes (Poag, 1997). Crystalline basement rocks beneath the Virginia coastal plain include a variety of plutonic, volcanic, and metamorphic rocks that constitute distal parts of the Appalachian orogen (Thomas et al., 1989). Sedimentary deposits of the Atlantic Coastal Plain constitute a seaward-thickening wedge of poorly consolidated siliciclastic sands, silts, and clays of both marine and nonmarine origin (Poag et al., 2004, p. 47). The ages of these deposits range from Early Cretaceous to Holocene. The pre-impact sediments of the Virginia coastal plain are Early Cretaceous to early late Eocene in age, and they are 1–1.5 km thick. The following pre-impact formations are distinguished (from the oldest to the most recent): Potomac Formation, unnamed Formation, Brightseat Formation, Aquia Formation, Marlboro Clay, Nanjemoy Formation, and Piney Point Formation (Fig. 2; e.g., Poag et al., 2004, p. 49; Gohn et al., 2005). Marine sedimentation resumed immediately after the impact, and today the crater is covered by ~200–550 m of sediments (Poag et al., 2004, p. 51).

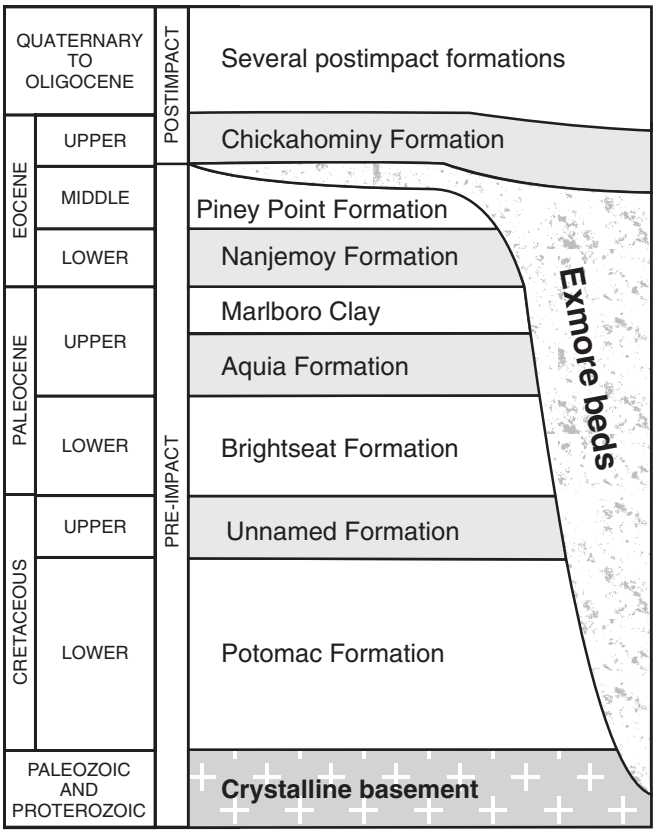

Figure 2. Stratigraphy of mainly pre-impact sedimentary formations in southeastern Virginia (modified from Poag et al., 2004).

Initial evidence of an impact structure in this region came from the discovery of impact ejecta, which are part of the North American tektite strewn field. Approximate inferred locations of the impact site, based on the nature and thickness of impact ejecta at Deep Sea Drilling Project (DSDP) Site 612, were suggested by Thein (1987) and Koeberl (1989). Site 612 was drilled on the upper continental slope off New Jersey, ~330 km northeast of the center of the Chesapeake Bay impact structure (Koeberl, 1989; Koeberl et al., 1996). Poag et al. (1992) interpreted the Exmore boulder bed in southeastern Virginia to have been deposited by a tsunami-like wave generated by an impact event. The existence of the Chesapeake Bay impact structure was proposed by Poag et al. (1994) based on analyses of core samples and seismic profiles. Koeberl et al. (1996) found the first evidence of shocked minerals within the crater fill (the Exmore breccia) at the Chesapeake Bay structure and thus confirmed that the structure is of impact origin. These authors also presented chemical analyses of breccia and clast samples from the Exmore breccia and noted a similarity with the composition of North American tektites, thus providing further evidence that the Chesapeake Bay structure was the source crater of those tektites. Koeberl et al. (1996) also showed that the distribution of gravity anomalies is typical of a complex impact structure and is in good agreement with the structural interpretations derived from seismostratigraphic analyses, i.e., subcircular negative anomaly above the inner basin and a ring of positive anomalies corresponding with the peak ring (Poag et al., 2004, p. 88–89). Shah et al. (2005, this volume) collected more gravity and magnetic field data, refined the geophysical signatures of the structure, and discussed possible volume and occurrence of impact melt.

Previous Deep Drilling at the Chesapeake Bay Impact Structure and Main Observations

Impact breccias were recovered from core holes into the Chesapeake Bay impact structure already in the 1940s, although their impact origin was not suspected until 1992 (Poag et al., 1992, 2004, p. 17–39; Koeberl et al., 1996). The Exmore boulder bed was cored in 1986 in the Exmore core hole (Poag et al., 1992). In the late 1980s and early 1990s, Exmore breccia was cored at the Kiptopeke, Newport News Park, and Windmill Point core holes (Poag et al., 2004, p. 17–39; Fig. 1). The Kiptopeke core hole was the first core drilled in the central part of the crater; however, the drilling did not penetrate the full crater fill, and core recovery was poor in the breccia interval (Poag et al., 2004, p. 216).

In 2000–2002, four major core holes were drilled: North, Bayside, and National Aeronautics and Space Administration (NASA) Langley in the annular trough, and Watkins School at the outer margin of the impact structure. The Bayside core hole penetrated the full thickness of postimpact, impact-generated, and impact-modified sediments and reached the underlying

Precambrian crystalline rocks (Horton et al., 2008). The continuously cored NASA Langley core was drilled on the York-James Peninsula in Hampton in 2000. It penetrated 236 m of Upper Eocene–Pleistocene deposits, 390 m of impact-generated deposits, and reached 9 m of underlying pale red, medium-grained Precambrian monzogranite. Three units were defined within impact-generated deposits in the NASA Langley core on the basis of lithology, sedimentary structure, clast-matrix ratio, and deformation style (Gohn et al., 2001). The lowermost so-called crater unit A typically consists of feldspathic, medium-grained to gravelly quartz sands containing minor amounts of dark-colored clay-silt clasts and quartz, quartzite, and chert pebbles in addition to the granodiorite pebbles. Crater unit B is a clast-supported sedimentary-clast breccia, and the vast majority of its material appears to have been derived from the Cretaceous Potomac Formation. The uppermost crater unit C corresponds to a different sedimentary breccia: it is matrix-supported and contains a mixture of clasts derived from the Lower Tertiary formations as well as from the Cretaceous Potomac Formation (Gohn et al., 2001). Very rare quartz grains and cataclastic crystalline clasts with planar deformation features (PDFs) were reported in the samples from the NASA Langley core by Horton and Izett (2005) and Horton et al. (2005a). No shock metamorphic features were found in the autochthonous granites cored in the NASA Langley and Bayside cores (Horton et al., 2005a).

In 2003, a deep drilling proposal was put to ICDP for a continuous core hole through the interior of the Chesapeake Bay impact structure. Subsequently, in 2004, the USGS drilled a test hole near Cape Charles. This 823-m-deep, partially cored (with a core diameter of 64 mm), Sustainable Technology Park (STP) test hole consists of 355 m of marine, Upper Eocene to Pleistocene sediments, 300 m of sedimentary-clast breccia, and 167 m of crystalline-clast breccias (largely suevitic) and cataclastic gneiss (Horton et al., 2005b; Gohn et al., 2007). According to Horton et al. (2005b), the melt particles in suevite are glassy to aphanitic, and some have flow lamination. Shapes and textures of some melt particles suggest that they were compacted while they were still hot and plastic. Multiple sets of decorated PDFs in quartz and feldspar were observed in clasts in suevite and in brecciated gneiss (Horton et al., 2005b). The suevite was found to be pervasively albitized and chloritized at lower-greenschist-facies conditions. The suevite contains amygdules filled with clay minerals and carbonates (Horton et al., 2005b). A minor meteoritic component was identified by Lee et al. (2006) in impact melt rock clasts in suevite from the STP test hole using osmium isotope ratios and platinum group element analysis (for detailed discussion, see McDonald et al., this volume). Previous drilling operations at the Chesapeake Bay impact structure have been summarized in detail by Poag et al. (2004, p. 17–39) and Horton et al. (2005c).

Eyreville Drill Core

In 2005–2006, three cores were drilled as part of the international ICDP-USGS Chesapeake Bay impact structure drilling project at Eyreville farm, in Northampton County (Virginia). Core hole Eyreville A was cored between 125 and 941 m depths (with core diameters of 85 mm and 63.5 mm in the intervals 125.6–591.0 m and 591.0–940.9 m, respectively). Eyreville B was cored from 738 m to a final depth of 1766 m (with core diameters of 63.5 mm and 47.6 mm in the intervals 737.6–1100.9 m and 1100.9–1766.3 m, respectively). In Eyreville C, postimpact sediments were cored from the land surface to a depth of 140 m (with a core diameter of 63.5 mm; Gohn et al., 2006a, 2006b, 2006c). At Eyreville, the crater fill consists of sedimentary-clast breccia and sedimentary megablocks of the Exmore beds, a granitic and an amphibolitic megablock, gravelly sand, impact breccia, and granite/pegmatite and mica schist (Fig. 3; Gohn et al., 2006a, 2006b). The core is now stored at the USGS in Reston, Virginia. More details about the coring operations at Eyreville have been reported in Gohn et al. (2006c) and Koeberl et al. (2007). A detailed geologic column of the Eyreville drill core was established by Horton et al. (this volume, Chapter 2) for the depth interval 1766–1095 m, by Edwards et al. (this volume, Chapter 3) for the depth interval 1096–444 m, and by Edwards et al. (this volume, Chapter 4) for the postimpact sediments (depth interval 444–0 m).

The deep Eyreville drill core provides a unique opportunity to compare the Chesapeake Bay impact structure with observations reported from other impact structures formed in a shallow-marine environment, such as the Montagnais, Mjølnir, and Lockne impact structures (Dypvik and Jansa, 2003; Lindström et al., 2005, and references therein). As one of the largest craters on Earth, the Chesapeake Bay impact structure can be compared with the Chicxulub impact structure, which also formed on a continental shelf (Kring, 2005).

The impact breccia section constitutes 154 m of the Eyreville B drill core, from 1397.2 to 1551.2 m. There are several suevite units in the impact breccia section, as well as two intervals of impact melt rock in the upper part (Wittmann et al., this volume, Chapter 16) and blocks of cataclastic gneiss in the lower part of the section (Horton et al., this volume). A small suevite boulder occurs in gravelly sand between 1393.0 and 1393.4 m depth above the impactite section, and some melt particles (thought to be derived from reworked suevite) are present within the gravelly sand between 1396.4 and 1397.2 m (Horton et al., this volume). Suevite occurs also in the form of several dike breccia veins in the crystalline basement (Reimold et al., 2007).

This study is based on macroscopic observation of the Eyreville B core and optical microscopic investigation of 43 samples from the impact breccia interval. Detailed petrographic (mineral composition and modal proportions of lithic clasts) and shock metamorphic studies (shock effects in minerals; shapes, textures, and types of melt particles) were carried out to constrain conditions and processes involved in the formation of the impact breccias. Preliminary results were reported in abstracts by Bartosova et al. (2007a, 2007b, 2008).

SAMPLES AND ANALYTICAL METHODS

Forty-three samples were taken from the impact breccia section between 1399.2 m (sample CB6-093) and 1547.4 m (sample CB6-130) depth. These samples include 30 samples of suevite, three samples of impact melt rock, one polymict lithic impact breccia (CB6-128), six samples of cataclasite (CB6-119, CB6-122, CB6-123, CB6-124, CB6-129, and CB6-130), and three conglomerate clasts from suevite (CB6112, CB6-115, and KB-6). All samples are described in detail in the Appendix. The samples are mostly half core, with a diameter of 47.6 mm and lengths of ~100 mm. Samples were selected to encompass the variety of different lithologies occurring in the studied core interval. The spacing between the samples varies according to the lithology of the core. In relatively homogeneous parts, e.g., the cataclastic gneiss blocks, the spacing of the samples is larger (~5 m). In those sections, in which the nature of the impact breccias changes over small distances, or which are petrographically interesting (e.g., melt-rich parts), the distances between samples are smaller (~2 m). Thin sections of all samples were investigated using optical microscopy. In addition, 16 polished thin sections were prepared for electron microscopy.

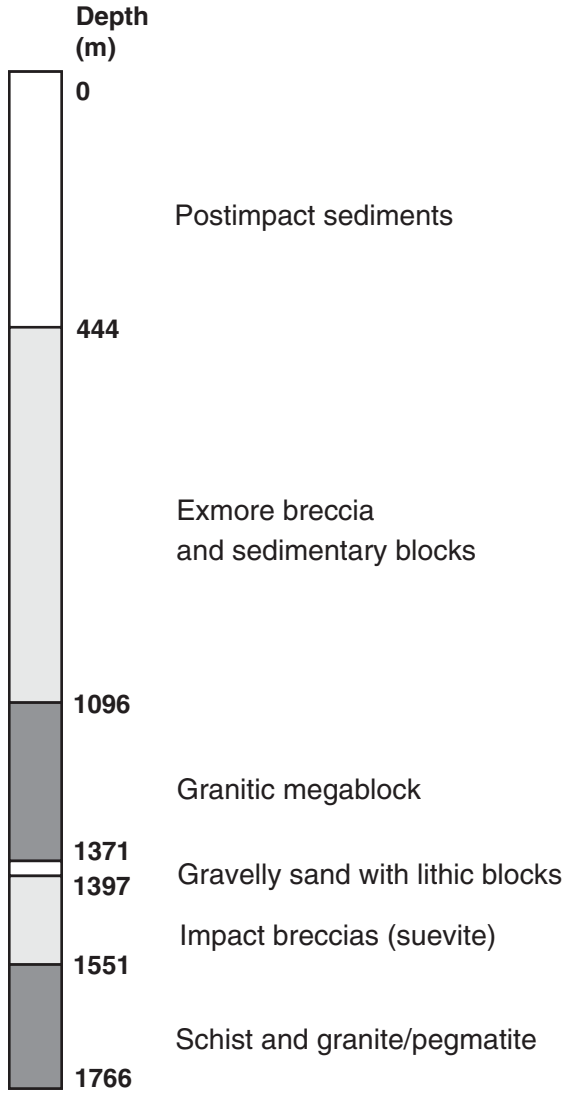

Figure 3. Simplified stratigraphic column showing the Eyreville drill core and its main lithologies (modified from Gohn et al., 2006b; Horton et al., this volume). Column shows depth below surface in meters.

Electron microscopy, including melt particle analyses by energy-dispersive spectrometry (EDX), was done with a JEOL JSM 6400 instrument at the Naturhistorisches Museum, Vienna. Energy-dispersive microchemical analysis was performed using a KEVEX SuperDry Si(Li) detector linked to a VANTAGE EDX system at 15 kV acceleration voltage and a beam current of ~1–2 nA. The standardless EDX analyses have a precision of ~3 rel% and a detection limit of ~0.2–0.5 wt% for major elements. An electron beam with a diameter of ~2 µm was used for identification of minerals. For determining the composition of the melt particles, a defocused beam was used, and larger areas (~50 × 50 µm to 200 × 200 µm) were analyzed.

Modal analysis by point counting was performed on 28 suevite samples to estimate the proportions of the different clast types (i.e., mineral and rock clasts); 155 points per thin section were counted on average. The whole area of a thin section was investigated with 2 mm spacing between each point counted; mineral grains (single grains in matrix) and rock clasts (without distinguishing individual minerals within rock clasts), as well as melt particles, were characterized; grains/clasts of less than 0.2 mm apparent diameter were counted as matrix.

Systematic analysis of the properties of quartz grains in suevite was carried out to determine the following properties: proportion of unshocked and shocked grains, i.e., grains with planar fractures (PFs) and/or with PDFs; number of sets of PDFs per grain; and percentage of grains with "toasted" appearance (brownish cloudy appearance; see, e.g., Short and Gold, 1996; Whitehead et al., 2002; Ferrière et al., 2009a). For this statistical analysis, information for single quartz grains enclosed in matrix and grains occurring within different rock clasts was recorded separately. About 360 quartz grains were analyzed per thin section, on average.

The mineral compositions of seven bulk samples were determined by X-ray diffraction (XRD) at the University of Vienna. This suite included one mafic cataclasite and six suevites, from which clasts larger than ~1.5 cm had been extracted. Diffraction data were collected with a Philips diffractometer (PW 3710, goniometer PW 1820), CuKα radiation (45 kV, 35 mA), step size of 0.02 degrees, and a counting time of 1 s per step. Minerals were identified using the Joint Committee on Powder Diffraction Standards database (JCPDS, 1980). The samples were milled to a fine powder, pressed into the sample holder, and analyzed. Two phyllosilicate-rich samples were also analyzed after treatment with ethylene

glycol to detect expandable clay minerals (see Moore and Reynolds [1997] for more information on the technique).

The focused ion beam (FIB) technique was used for the preparation of a transmission electron microscope (TEM) foil of a quartz grain with PDFs from suevite sample CB6-097 (depth = 1412.8 m) at the GeoForschungsZentrum (GFZ) Potsdam (Germany). A FIB foil of 15 × 7 µm extent and ~100–200 nm thickness was prepared following the method presented by Wirth (2004). TEM studies were performed using a 200 kV Philips CM 20 STEM equipped with a TRACOR Northern energy-dispersive X-ray detector at the Museum of Natural History, Humboldt University, Berlin (Germany). Conventional bright-field imaging techniques were used to observe and characterize microstructural characteristics of PDFs.

In addition, a Renishaw RM1000 confocal edge filter-based microRaman spectrometer with a 20 mW, 632.8 nm He-Ne-laser excitation system, and a thermoelectrically cooled charge-coupled device array detector was used at the Institute of Mineralogy and Crystallography, University of Vienna, for identification of some mineral phases.

RESULTS

The impact breccia section, ~154 m thick, consists of ~110 m of suevite and lithic impact breccia and 44 m of cataclastic gneiss (Fig. 3). Detailed petrographic descriptions of the samples are given in the Appendix.

Suevite and Impact Melt Rock

According to Stöffler and Grieve (2007, p. 198), suevite is "a polymict impact breccia with particulate matrix containing lithic and mineral clasts in all stages of shock metamorphism including cogenetic impact melt particles which are in a glassy or crystallised state." Impact melt rock is "a crystalline, semihyaline or hyaline rock solidified from impact melt and containing variable amounts of clastic debris of different degree of shock metamorphism" (Stöffler and Grieve, 2007, p. 162). In the Eyreville B core, suevite occurs in the 1397.2–1551.2 m depth interval (Fig. 4; Horton et al., this volume). At the top of the impact breccia section, the suevite is melt-rich and grades locally into impact melt rock (Wittmann et al., 2008, this volume, Chapters 16 and 17). The term "melt-rich suevite" is used here when melt constitutes more than ~20 vol% of the rock. In the lower parts of the section, lithic clasts in the suevite become more abundant and larger, and the suevite contains blocks of cataclastically deformed gneiss/schist. Most suevite samples have a grayish, fine-grained, clastic matrix that contains a variety of rock and mineral clasts, melt particles, and secondary minerals (e.g., phyllosilicates and calcite).

Cataclastic Gneiss

Cataclasite is "a fault rock that is cohesive with a poorly developed or absent schistosity, or that is incohesive, characterized by generally angular porphyroclasts and lithic fragments in a finer-grained matrix of similar composition" (Brodie et al., 2007, p. 138). Cataclastic gneiss occurs mostly in the lower part of the studied interval (below 1474 m), as large, monomict, brecciated crystalline basement-derived blocks incorporated into the suevite (Fig. 4). The cataclasite blocks consist of millimeter- to centimeter-sized clasts of fine-grained gneiss or more rarely schist, with some flour-like groundmass of the same material. The main minerals recognized microscopically are quartz, chlorite, muscovite, biotite, K-feldspar, and plagioclase. Additionally, carbonate occurs as irregular patches or filling in fractures. Opaque minerals and other accessories (e.g., sphene, epidote, garnet, and tourmaline) were also noted. Cataclastic gneiss shows both PFs and PDFs in quartz grains, and some of the quartz grains display a toasted appearance. In the cataclasite samples from the lower part of the core (below ~1530 m), shock metamorphic effects are less abundant, and in sample CB6-129 (depth = 1542.7 m), neither PFs nor PDFs were detected. In one portion of the core (1514.5–1521.5 m), the cataclasite appears dark greenish and contains abundant chlorite and amphibole (sample CB6-123; depth = 1514.3 m). The upper part of the impact breccia section (above 1474 m) contains only one larger (~1.5 m) boulder of cataclastic gneiss at ~1433 m depth (Fig. 4).

Stratigraphy of the Impactite Section and Petrographic Description of the Subunits

The detailed stratigraphic column of the impact breccia section presented by Horton et al. (this volume) is shown in Figure 4, where short macroscopic descriptions of the core are also added. Based on macroscopic and microscopic observations of our samples, in addition to our macroscopic study of the drill core, we recognized six subunits of suevite (Fig. 4; Table 1). Our subdivision is not in conflict with that by Horton et al. (this volume), but it is somewhat different, because we have focused our subdivision on distinguishing different types of suevite based on differences in proportions and types of melt particles, clasts, and matrix present. Transitions between subunits are gradational. For detailed information on the different types of melt particles distinguished in suevite and used in the distinction of subunits, see the section "Melt Particles and Melt Matrix" and Table 2.

Figure 4. Geologic column of the impact breccia section from the Eyreville B drill core. The geologic column is modified from Horton et al. (this volume). Positions of the samples for the present study are indicated by lines on the left side; sections U1–U6 are the subunits of suevite identified during our investigations (Table 1). The detailed core descriptions on the right are based mostly on macroscopic observations, and only details based on microscopic studies were added.

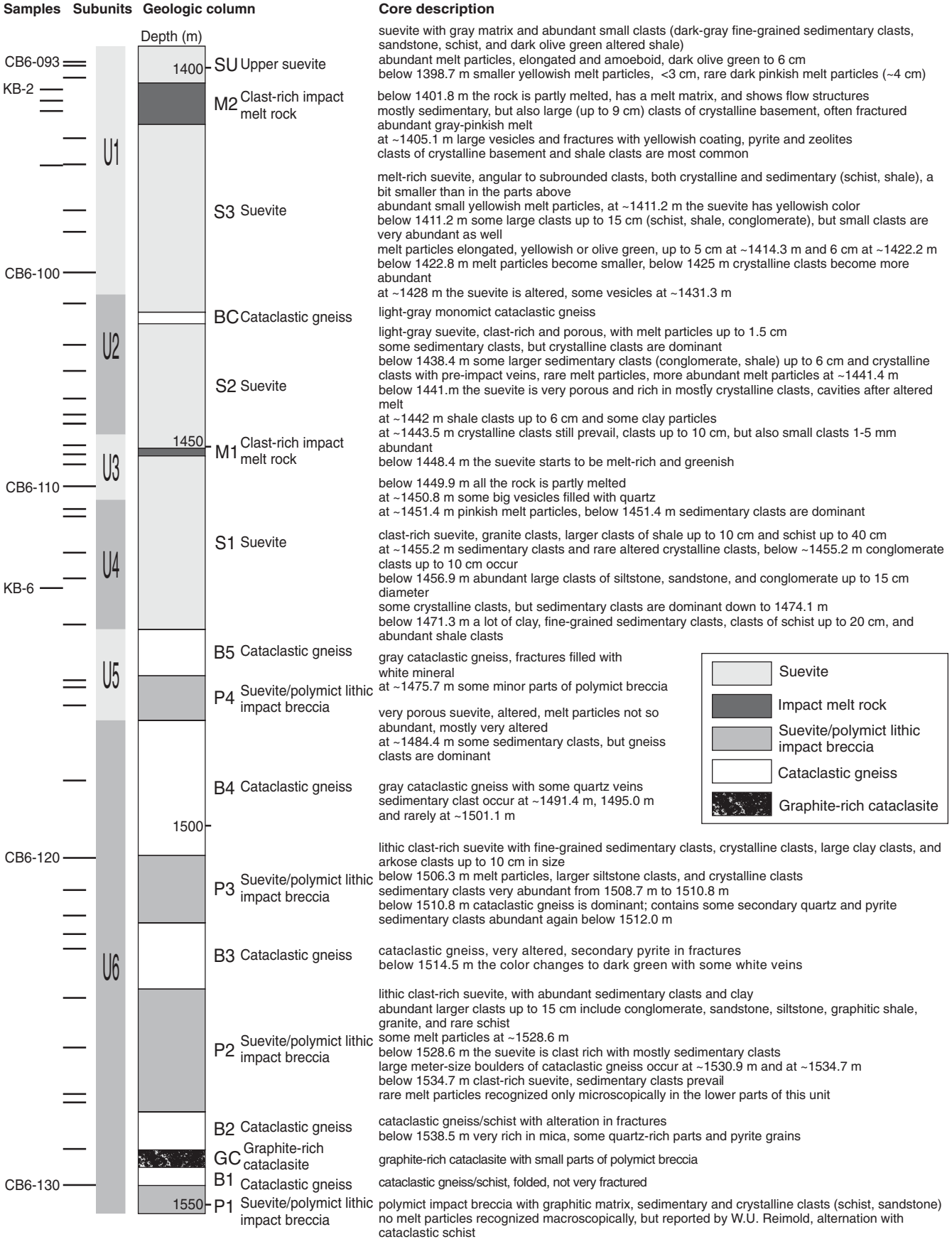
Samples
Subunits
Geologic column
Core description
Depth (m)
CB6-093
KB-2
CB6-100
CB6-110
KB-6
CB6-120
CB6-130
U1
U2
U3
U4
U5
U6
1400
1450
1500
1550
SU Upper suevite
suevite with gray matrix and abundant small clasts (dark-gray fine-grained sedimentary clasts, sandstone, schist, and dark olive green altered shale)
abundant melt particles, elongated and amoeboid, dark olive green to 6 cm
below 1398.7 m smaller yellowish melt particles, <3 cm, rare dark pinkish melt particles (~4 cm)
M2 Clast-rich impact melt rock
below 1401.8 m the rock is partly melted, has a melt matrix, and shows flow structures
S3 Suevite
mostly sedimentary, but also large (up to 9 cm) clasts of crystalline basement, often fractured
abundant gray-pinkish melt
at ~1405.1 m large vesicles and fractures with yellowish coating, pyrite and zeolites
clasts of crystalline basement and shale clasts are most common
melt-rich suevite, angular to subrounded clasts, both crystalline and sedimentary (schist, shale), a bit smaller than in the parts above
abundant small yellowish melt particles, at ~1411.2 m the suevite has yellowish color
below 1411.2 m some large clasts up to 15 cm (schist, shale, conglomerate), but small clasts are very abundant as well
melt particles elongated, yellowish or olive green, up to 5 cm at ~1414.3 m and 6 cm at ~1422.2 m
below 1422.8 m melt particles become smaller, below 1425 m crystalline clasts become more abundant
at ~1428 m the suevite is altered, some vesicles at ~1431.3 m
BC Cataclastic gneiss
light-gray monomict cataclastic gneiss
S2 Suevite
light-gray suevite, clast-rich and porous, with melt particles up to 1.5 cm
some sedimentary clasts, but crystalline clasts are dominant
below 1438.4 m some larger sedimentary clasts (conglomerate, shale) up to 6 cm and crystalline clasts with pre-impact veins, rare melt particles, more abundant melt particles at ~1441.4 m
below 1441.m the suevite is very porous and rich in mostly crystalline clasts, cavities after altered melt
at ~1442 m shale clasts up to 6 cm and some clay particles
at ~1443.5 m crystalline clasts still prevail, clasts up to 10 cm, but also small clasts 1-5 mm abundant
M1 Clast-rich impact melt rock
below 1448.4 m the suevite starts to be melt-rich and greenish
below 1449.9 m all the rock is partly melted
at ~1450.8 m some big vesicles filled with quartz
at ~1451.4 m pinkish melt particles, below 1451.4 m sedimentary clasts are dominant
S1 Suevite
clast-rich suevite, granite clasts, larger clasts of shale up to 10 cm and schist up to 40 cm
at ~1455.2 m sedimentary clasts and rare altered crystalline clasts, below ~1455.2 m conglomerate clasts up to 10 cm occur
below 1456.9 m abundant large clasts of siltstone, sandstone, and conglomerate up to 15 cm diameter
some crystalline clasts, but sedimentary clasts are dominant down to 1474.1 m
below 1471.3 m a lot of clay, fine-grained sedimentary clasts, clasts of schist up to 20 cm, and abundant shale clasts
B5 Cataclastic gneiss
gray cataclastic gneiss, fractures filled with white mineral
P4 Suevite/polymict lithic impact breccia
at ~1475.7 m some minor parts of polymict breccia
very porous suevite, altered, melt particles not so abundant, mostly very altered
at ~1484.4 m some sedimentary clasts, but gneiss clasts are dominant
B4 Cataclastic gneiss
gray cataclastic gneiss with some quartz veins
sedimentary clast occur at ~1491.4 m, 1495.0 m and rarely at ~1501.1 m
lithic clast-rich suevite with fine-grained sedimentary clasts, crystalline clasts, large clay clasts, and arkose clasts up to 10 cm in size
P3 Suevite/polymict lithic impact breccia
below 1506.3 m melt particles, larger siltstone clasts, and crystalline clasts
sedimentary clasts very abundant from 1508.7 m to 1510.8 m
below 1510.8 m cataclastic gneiss is dominant; contains some secondary quartz and pyrite
sedimentary clasts abundant again below 1512.0 m
B3 Cataclastic gneiss
cataclastic gneiss, very altered, secondary pyrite in fractures
below 1514.5 m the color changes to dark green with some white veins
lithic clast-rich suevite, with abundant sedimentary clasts and clay
abundant larger clasts up to 15 cm include conglomerate, sandstone, siltstone, graphitic shale, granite, and rare schist
P2 Suevite/polymict lithic impact breccia
some melt particles at ~1528.6 m
below 1528.6 m the suevite is clast rich with mostly sedimentary clasts
large meter-size boulders of cataclastic gneiss occur at ~1530.9 m and at ~1534.7 m
below 1534.7 m clast-rich suevite, sedimentary clasts prevail
rare melt particles recognized only microscopically in the lower parts of this unit
B2 Cataclastic gneiss
cataclastic gneiss/schist with alteration in fractures
below 1538.5 m very rich in mica, some quartz-rich parts and pyrite grains
GC Graphite-rich cataclasite
graphite-rich cataclasite with small parts of polymict breccia
B1 Cataclastic gneiss
cataclastic gneiss/schist, folded, not very fractured
P1 Suevite/polymict lithic impact breccia
polymict impact breccia with graphitic matrix, sedimentary and crystalline clasts (schist, sandstone)
no melt particles recognized macroscopically, but reported by W.U. Reimold, alternation with cataclastic schist
Suevite
Impact melt rock
Suevite/polymict lithic impact breccia
Cataclastic gneiss
Graphite-rich cataclasite

TABLE 1. MAIN CHARACTERISTICS OF THE SIX SUBUNITS OF THE IMPACT BRECCIA SECTION FROM THE EYREVILLE B DRILL CORE

Subunit:	U1	U2	U3	U4	U5	U6
Depth (m):	1397.2–1430	1430–1448.4	1448.4–1457	1457–1474.1	1474.1–1486.1	1486.1–1551.2
Melt particles	Typically type 1, also type 2	Very rare, mostly type 2	Types 3 and 5 most common	Only type 2	Very rare, only type 2	Rare, types 2 and 5
Clasts	Sedimentary clasts (e.g., siltstone, sandstone, conglomerate) are dominant, also clasts of schist occur	Crystalline basement lithologies are dominant (gneiss, schist, and granite), rare sedimentary clasts	Abundant sedimentary clasts (e.g., siltstone, mudstone, sandstone, graywacke) and some crystalline clasts (e.g., schist and granite)	Various types of lithic clasts (e.g., siltstone, sandstone, conglomerate, schist), commonly larger (~10 cm), sedimentary clasts are dominant	Crystalline clasts (schist, gneiss) are dominant	Sedimentary clasts (e.g., siltstone, shale, sandstone, conglomerate) generally more abundant than crystalline clasts (schist/gneiss and granite), but some crystalline clast–rich parts occur as well
Stratigraphy	Contains section of impact melt rock	Contains cataclastic gneiss boulder	Contains a thin interval of impact melt rock		The upper part (1474.1 to 1480.2 m) consists of cataclastic gneiss	Contains three large blocks of cataclastic gneiss
Notes	Most homogeneous subunit			Proportion of matrix is higher than in subunit U3 above	Similar to subunit U2	Most heterogeneous subunit

Note: See Table 2 for definition of the types of melt particles.

Subunit 1 (U1, 1397.2–1430 m)

Subunit U1 is the most homogeneous subunit with respect to smallest clast sizes. Clasts are smaller in size and the proportion of matrix is larger than in the other subunits. Sedimentary clasts (e.g., siltstone, sandstone, and conglomerate) are dominant, but clasts of schist/gneiss are also present. Large melt particles (up to 5 cm) occur. This suevite is melt-rich and grades into impact melt rock in the interval 1402.2–1407.5 m, where melt with microlites (type 4) is abundant. Clear glass particles (unaltered glass; type 1) with shard-like shapes are common and are typical of this subunit, but the occurrence of clear glass is much more limited in lower subunits. A sample from subunit U1 (CB6-097; depth = 1412.8 m) with small clasts and abundant particles of melt type 1 is shown in Figure 5A.

Subunit 2 (U2, 1430–1448.4 m)

This suevite unit is clast-rich, and the clasts mostly originate from crystalline basement lithologies (gneiss, schist, and granite). Rare sedimentary clasts (e.g., siltstone, shale, and conglomerate) occur. Melt particles (mostly of type 2) are rare and constitute less than 3 vol% in the samples from this subunit. PDFs in quartz grains from polycrystalline quartz clasts and kink-banding in muscovite were observed in samples of this subunit. A sample from subunit U2 (CB6-103; depth = 1440.0 m) with abundant crystalline clasts and rare melt particles is shown in Figure 5B.

Subunit 3 (U3, 1448.4–1457 m)

Subunit U3 consists of melt-rich suevite and contains a thin interval of impact melt rock between 1450.2 and 1451.2 m; the contact with the suevite is gradational. Clasts are difficult to resolve due to partial melting. There are abundant sedimentary clasts (e.g., siltstone, mudstone, sandstone, graywacke) and some crystalline clasts (e.g., schist/gneiss and granite). At ~1455 m depth, there are abundant larger clasts, ~10 cm in size (shale, conglomerate, schist/gneiss). Quartz grains show abundant PFs and PDFs, and ballen quartz also occurs. Melt particles of types 3 and 5 are the most common ones in this unit. A suevite from subunit U3 with abundant melt particles and sedimentary clasts (CB6-109; depth = 1452.3 m) is presented in Figure 5C. A sample transitional between suevite and impact melt rock (CB6-108; depth = 1451.0 m) is shown in Figure 5D.

Subunit 4 (U4, 1457–1474.1 m)

Suevite in subunit U4 contains abundant melt particles, but the proportion of melt is lower and the proportion of matrix is higher than in subunit U3 above (Fig. 6). There are various types of lithic clasts (e.g., siltstone, sandstone, conglomerate, and

TABLE 2. CLASSIFICATION AND MAIN CHARACTERISTICS OF THE DIFFERENT TYPES OF MELT PARTICLES IDENTIFIED IN THE IMPACT BRECCIA FROM THE EYREVILLE B DRILL CORE

Type	1 Clear glass	2 Altered melt	3 Recrystallized silica melt	4 Melt with microlites	5 Dark-brown melt
Color*	Mostly light brown, rarely colorless or greenish	Brown, beige	Colorless, some show brownish patches	Brownish to dark gray	Dark brown to black
Shape	Amoeboid, “flame”-shaped, many are shard-like, with sharp contacts with the matrix	Oval to amoeboid	Amoeboid, some preserve shapes of the clasts, globules	Irregular shapes, forms matrix in impact melt rock intervals or rare single particles	Oval to amoeboid
Texture, vesicles, inclusions, grains	Many have darker brown schlieren, rarely undigested grains or vesicles occur	Commonly fluidal texture, many cracks, contains undigested grains (as quartz)	Some recrystallized into cherty texture, in melt-rich intervals can be recrystallized to ballen quartz	Laths of feldspars and/or pyroxenes, intersertal or microporphyritic texture	Commonly contains undigested grains, mostly quartz grains, some isotropic
Alteration	Fresh, can be partly altered, interestingly, some particles are altered in the middle of the particle	Altered to clay minerals (e.g., smectite), commonly parts removed during thin-section preparation	Some parts altered, brownish	Fresh or slightly altered	Altered, commonly parts removed during thin-section preparation
Interval of most abundant occurrence† (m)	1412.8–1421.7 (CB6-097:CB6-099)	1399.2–1409.3 (CB6-093:CB6-096)	1402.9–1405.7 (KB-2:KB-4) 1449.8–1452.3 (CB6-107:CB6-109)	1402.9–1405.7 (KB-2:KB-4) 1451.01 (CB6-108)	1452.33–1455.22 (CB6-109:CB6-110)
Interval of occurrence† (m)	1399.2–1452.3 (CB6-093:CB6-109)	1399.2–1508.5 (CB6-093:CB6-121)	1399.7–1452.3 (CB6-094:CB6-109)	1402.9–1455.2 (KB-2:CB6-110)	1443.65–1535.40 (CB6-104:CB6-127)
Notes	Shapes suggest solidification before incorporation	Most abundant melt type	Probably recrystallized clasts of quartz and quartz-rich rocks	In some cases, clasts of impact melt and clasts of dolerite are difficult to distinguish from each other	Probably melt of carbon-rich shale or other fine-grained sediment

*Color in plane-polarized light using optical microscope.
†In our samples.

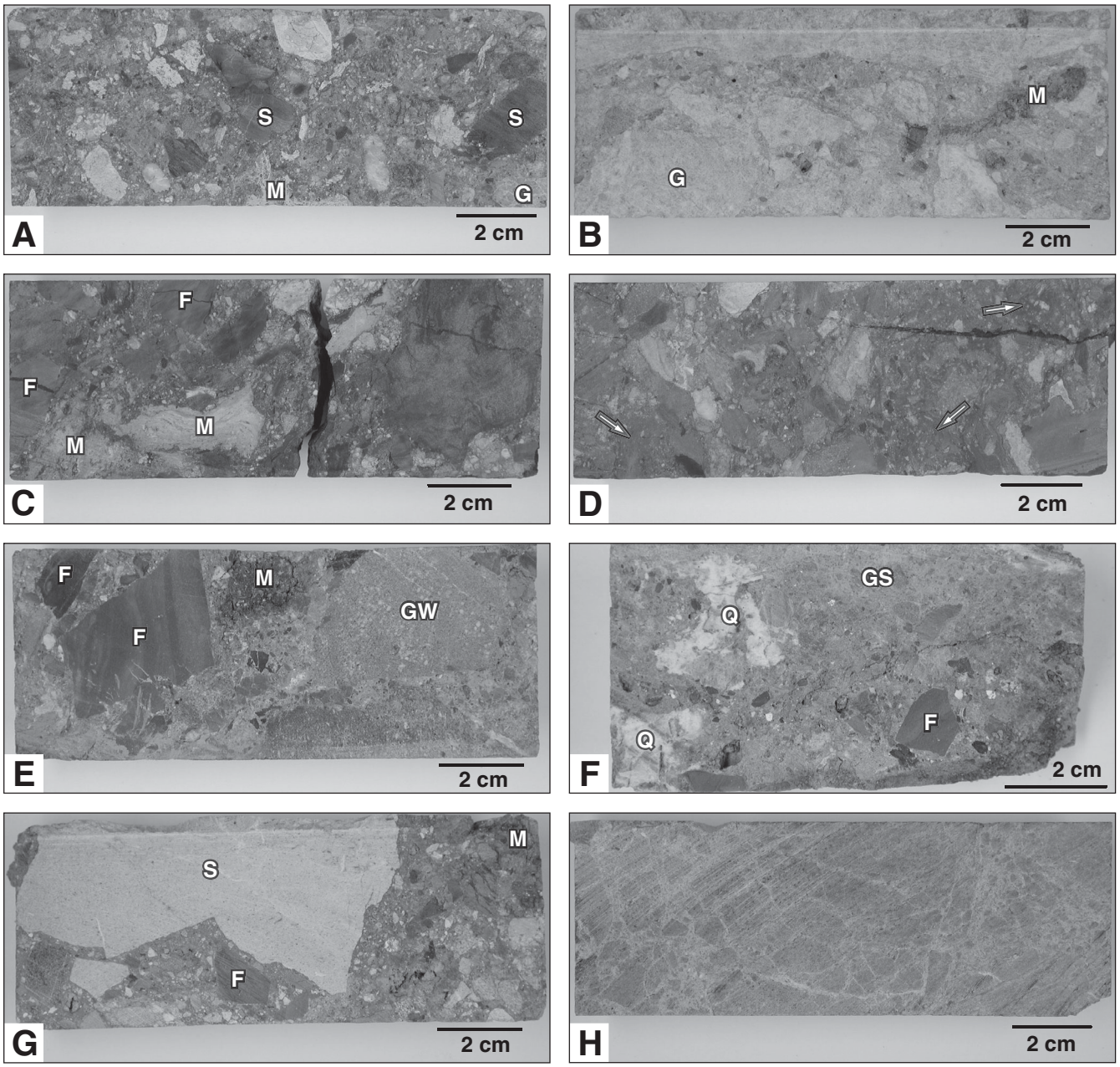

Figure 5. Macrophotographs of samples from the impact breccia section from the Eyreville B drill core, Chesapeake Bay impact structure. (A) Melt-rich suevite sample of subunit U1 with abundant small yellowish melt particles (M—melt type 1) and small fine-grained sedimentary clasts (e.g., S—siltstone) and crystalline clasts (e.g., G—granite; sample CB6-097; depth = 1412.8 m). (B) Suevite sample of subunit U2 with large, mostly crystalline, clasts (e.g., G—granite) and rare melt particles (e.g., M—elongated greenish-gray melt particle; sample CB6-103; depth = 1440.0 m). (C) Suevite sample of subunit U3 with abundant melt particles and sedimentary clasts (e.g., M—melt particles, F—fine-grained sedimentary clasts, such as siltstone and mudstone; sample CB6-109; depth = 1452.3 m). (D) Sample of subunit U3, transitional between suevite and impact melt rock with local melt matrix (e.g., areas marked with arrows), but also with some clastic matrix. All clasts are deformed and partly melted; thus, it is difficult to resolve their nature (sample CB6-108; depth = 1451.0 m). (E) Suevite sample from subunit U4 with large, mostly sedimentary clasts (e.g., GW—large clast of graywacke, F—clasts of fine-grained sediments [siltstone, mudstone]) and relatively abundant melt particles (e.g., M—altered melt particle; sample CB6-114; depth = 1467.4 m). (F) Suevite from subunit U5 with small, mostly crystalline (GS—gneiss), and rare fine-grained sedimentary (F), clasts. The suevite is very porous; some vesicles are filled with secondary quartz (Q; sample CB6-117; depth = 1481.7 m). (G) Suevite sample from subunit U6 with large, mostly sedimentary clasts (e.g., S—large white clast of sandstone, F—small gray fine-grained sedimentary clast) and rare melt particles (e.g., M—altered melt particle; sample CB6-126; depth = 1529.3 m). (H) Sample of cataclastic gneiss (sample CB6-124; depth = 1516.2 m). An intense fracture network is developed, visible as light lines in the picture. The NE-SW lines in the left part of the photograph are only saw cuts.

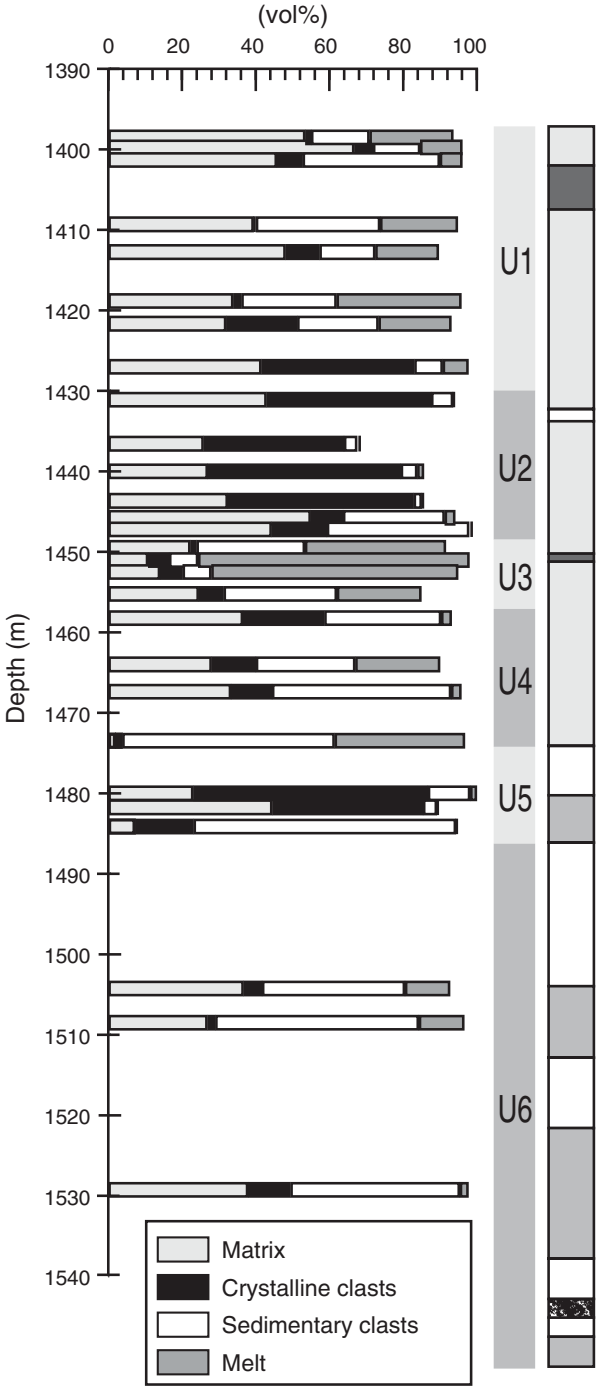

Figure 6. Bar diagram showing the proportions of (in each horizontal bar from left to right) matrix, crystalline clasts, sedimentary clasts, and melt (the rest being mineral clasts and unidentified lithic clasts) in 28 suevite samples from Eyreville B drill core (based on modal point counting; see also Table 3). In the right part, stratigraphic columns are shown for comparison: left column—subunits (this study), right column—geologic column from Horton et al. (this volume; see Fig. 4 for general information and more details).

schist/gneiss), and clasts are commonly larger than ~10 cm. Sedimentary clasts are more abundant than crystalline clasts. Only melt particles of type 2 occur in this subunit. Our lowermost sample CB6-115 (depth = 1473.5 m) is somewhat different from the other samples of this subunit, showing a low proportion of matrix and a high abundance of melt particles. A sample from subunit U4 (CB6-114; depth = 1467.4 m) with large, mostly sedimentary clasts, and melt particles is shown in Figure 5E.

Subunit 5 (U5, 1474.1–1486.1 m)

Subunit U5 is similar to subunit U2. The proportion of melt is very low (<2 vol% in our samples). The suevite is porous and clast-rich; crystalline clasts (i.e., schist/gneiss) are dominant. All melt particles (type 2) are altered. A sample from subunit U5, highly porous suevite with mostly crystalline clasts (CB6-117; depth = 1481.7 m) is shown in Figure 5F.

Subunit 6 (U6, 1486.1–1551.2 m)

The lowermost subunit, ~65 m in thickness, is very heterogeneous. The suevite contains large blocks of cataclastic gneiss/schist. Otherwise, sedimentary clasts (e.g., siltstone, shale, sandstone, conglomerate) are generally more abundant than crystalline clasts (schist/gneiss and granite), but some crystalline clast–rich parts have been noted (e.g., between 1510.8 and 1512.0 m). Melt particles are relatively abundant in the upper part of the subunit (~12 vol% of melt in samples CB6-120 and CB6-121; depth = 1504.3 and 1508.5 m, respectively), but they are rare in the lower polymict intervals (P1 and P2 according to Horton et al., this volume). Melt particles were also observed macroscopically in the core in interval P2 (1521.6–1537.8 m) but not in interval P1 (1547.5–1551.2 m). Melt particles are strongly altered; some samples contain abundant smectite (e.g., sample CB6-121, depth = 1508.5 m). A sample from subunit U6 with rare melt particles and large, mostly sedimentary clasts (CB6-126; depth = 1529.3 m) is shown in Figure 5G. Figure 5H shows a sample (CB6-124; depth = 1516.2 m) from a cataclastic gneiss block.

Petrography of Suevite and Impact Melt Rock

Characteristics of the Matrix

The color of the suevite matrix varies from light to dark gray throughout the impact breccia section. The matrix is mostly fragmental; the suevite grades into impact melt rock with a melt matrix only in two intervals (1402.0–1407.5 m and 1450.2–1451.2 m; Fig. 4). In the lower impact melt rock interval, the melt rock contains microlites of plagioclase (sample CB6-108; depth = 1451.0 m). In the upper impact melt rock interval, tiny pyroxene microlites occur in the melt matrix; (e.g., sample KB-2; depth = 1402.9 m). The proportion of matrix in the suevite is, on average, ~34 vol% (based on our modal point counting). Matrix is most abundant in the upper part (maximum value of 67 vol% observed in sample CB6-094, depth = 1399.7 m; Table 3), but no simple trend was observed

TABLE 3. MODAL COMPOSITION (VOL%) OF 28 SUEVITE SAMPLES FROM DEPTH INTERVAL 1399.2–1529.3 m

Sample:	CB6-093	CB6-094	CB6-095	CB6-096	CB6-097	CB6-098	CB6-099	CB6-100	CB6-101	CB6-102	CB6-103	CB6-104	CB6-105	CB6-106
Depth (m):	1399.2	1399.7	1401.3	1409.3	1412.8	1418.8	1421.7	1427.0	1431.1	1436.6	1440.0	1443.7	1445.8	1447.0
Matrix	53.4	66.7	45.7	39.4	48.1	33.9	32.0	41.5	42.9	25.8	27.0	32.4	54.9	44.3
Mineral clasts														
Quartz clasts	2.3	3.2	3.9	1.7	2.2	1.1	2.3	n.d.*	1.8	1.5	9.0	0.7	2.0	0.7
Other mineral clasts	0.5	n.d.	n.d.	0.6	n.d.	n.d.	0.6	0.7	0.6	1.0	0.9	n.d.	n.d.	n.d.
Melt														
Melt particles	20.4	7.7	n.d.	12.0	14.6	31.7	17.4	5.6	0.6	1.0	n.d.	n.d.	n.d.	1.4
Partially melted clasts	2.4	3.8	6.2	9.1	2.7	2.2	2.3	1.4	n.d.	0.5	1.8	0.7	2.9	n.d.
Lithic clasts														
Schist/gneiss	0.3	n.d.	1.6	n.d.	0.5	2.2	12.2	6.3	4.7	12.4	0.9	10.8	n.d.	6.4
Phyllite	0.3	n.d.	n.d.	n.d.	6.5	n.d.	n.d.	n.d.	n.d.	1.0	1.8	0.7	5.9	n.d.
Other crystalline clasts	1.0	5.1	5.4	0.6	2.2	n.d.	7.0	35.2	40.0	24.7	49.5	38.8	2.9	8.6
Fine-grained sediments	5.7	7.7	3.1	4.6	2.2	1.6	11.0	0.7	0.6	2.6	n.d.	0.7	3.9	2.1
Siltstone	2.6	2.6	1.6	1.1	5.4	2.2	9.3	n.d.	4.1	n.d.	1.8	1.4	2.9	35.0
Sandstone	1.6	2.6	n.d.	17.1	4.9	21.5	0.6	0.7	n.d.	0.5	2.7	n.d.	20.6	n.d.
Graywacke	4.4	n.d.	n.d.	8.6	1.6	n.d.	n.d.	2.8	n.d.	n.d.	n.d.	n.d.	n.d.	n.d.
Other sedimentary	1.5	n.d.	32.6	2.3	1.1	0.5	1.2	3.5	1.2	0.5	n.d.	n.d.	n.d.	1.4
Polycrystalline quartz	2.3	n.d.	n.d.	1.1	4.3	1.6	2.9	n.d.	2.9	1.5	3.6	12.9	n.d.	n.d.
Other/unidentified	1.3	0.6	n.d.	1.7	3.8	1.6	1.2	1.4	0.6	26.8	0.9	0.7	3.9	n.d.

Sample	CB6-107	CB6-108	CB6-109	CB6-110	CB6-111	CB6-113	CB6-114	CB6-115	CB6-116	CB6-117	CB6-118	CB6-120	CB6-121	CB6-126
Depth (m)	1449.8	1451.0	1452.3	1455.2	1458.2	1464.0	1467.4	1473.5	1480.8	1481.7	1484.1	1504.3	1508.5	1529.3
Matrix	22.2	10.8	14.0	24.5	36.5	28.0	33.3	1.9	23.0	44.5	7.3	36.7	26.9	37.9
Mineral clasts														
Quartz clasts	5.0	0.5	3.4	2.1	2.9	n.d.*	2.8	0.6	n.d.	3.7	1.1	3.6	2.8	1.1
Other mineral clasts	0.6	n.d.	n.d.	n.d.	1.9	n.d.	n.d.	1.3	n.d.	0.6	n.d.	0.7	n.d.	n.d.
Melt														
Melt particles	18.9	16.9	54.2	8.9	n.d.	19.0	n.d.	n.d.	n.d.	n.d.	n.d.	4.3	2.8	1.1
Partially melted clasts	19.4	56.8	12.8	14.1	2.9	4.0	2.8	35.4	1.8	0.6	0.6	7.9	9.7	1.1
Lithic clasts														
Schist/gneiss	1.1	4.0	3.9	1.0	n.d.	7.0	n.d.	1.9	63.7	23.8	n.d.	n.d.	n.d.	3.4
Phyllite	n.d.	n.d.	n.d.	n.d.	n.d.	n.d.	n.d.	n.d.	n.d.	n.d.	n.d.	n.d.	n.d.	n.d.
Other crystalline clasts	0.6	1.7	2.2	5.7	22.1	5.0	11.1	n.d.	n.d.	17.1	15.8	5.0	2.1	8.0
Fine-grained sediments	16.1	3.2	3.4	19.8	4.8	9.0	14.6	8.2	11.5	2.4	0.6	28.1	21.4	29.9
Siltstone	4.4	n.d.	3.4	3.1	7.7	5.0	31.3	13.9	n.d.	n.d.	n.d.	6.5	6.2	4.6
Sandstone	n.d.	0.3	n.d.	n.d.	n.d.	2.0	0.7	n.d.	n.d.	1.2	58.8	n.d.	n.d.	2.3
Graywacke	1.7	1.3	1.1	7.8	n.d.	11.0	2.1	35.4	n.d.	n.d.	n.d.	n.d.	27.6	6.9
Other sedimentary	7.2	3.0	n.d.	n.d.	19.2	n.d.	n.d.	n.d.	n.d.	n.d.	11.9	4.3	n.d.	2.3
Polycrystalline quartz	n.d.	n.d.	0.6	3.1	n.d.	7.0	1.4	n.d.	n.d.	5.5	1.7	n.d.	0.7	n.d.
Other/unidentified	2.8	1.4	1.1	9.9	1.9	3.0	n.d.	1.3	n.d.	0.6	2.3	2.9	n.d.	1.1

Note: Clasts and grains smaller than 0.2 mm were counted as matrix. Totals are 100 vol%.
*Not detected.

with regard to matrix abundance with depth (Fig. 6). Matrix consists mainly of mineral and rock clasts similar to the larger clasts (abundant quartz and mica).

Mineral Composition

Mineral clasts include (in order of estimated decreasing abundance) quartz, K-feldspar, plagioclase, muscovite, biotite, chlorite, and opaque minerals (mostly pyrite). Accessory minerals, present either as single grains in matrix or within rock clasts, include epidote (frequently observed in graywacke clasts), zircon, garnet (in crystalline clasts), apatite, and tourmaline. Calcite rarely forms patches in matrix and fills cracks in the suevite. Calcite is more common in lithic clasts, mostly filling fractures. Some amygdules in melt-rich samples are filled with zeolites. X-ray diffraction analysis was performed on six representative suevite samples and confirmed the occurrence of the rock-forming minerals identified optically (quartz, K-feldspar, plagioclase, muscovite, chlorite, calcite, and pyrite). Two samples, CB6-115 and CB6-121 (depth = 1473.5 and 1508.5 m, respectively), very rich in phyllosilicate minerals, were also analyzed before and after treatment with ethylene glycol. The diffractograms show a d-spacing that increases from 12 Å to 17 Å, which denotes the occurrence of smectite (see Fig. 7).

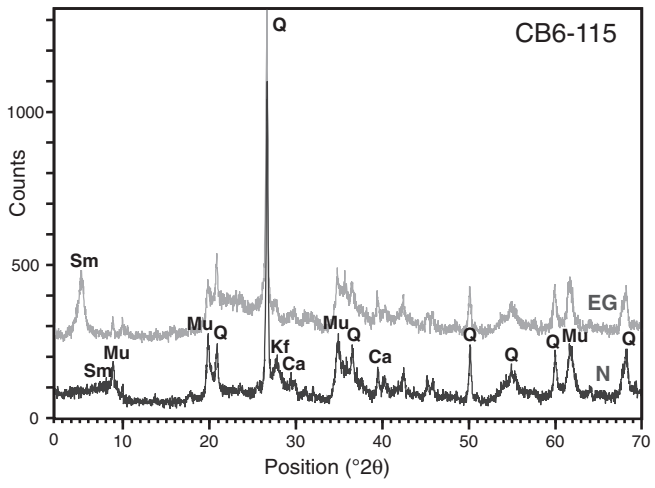

Figure 7. X-ray diffraction spectra for suevite sample CB6-115 (depth = 1473.5 m) particularly rich in phyllosilicate minerals. N—normal spectrum, EG—spectrum (shifted up the *y*-axis by 200 counts for easier comparison) obtained from the same sample after treatment with ethylene glycol, where the first peak belongs to the expanded smectite (in which the crystal lattice is expanded as a result of the glycol treatment). Q—quartz, Sm—smectite, Mu—muscovite, Kf—K-feldspar, Ca—calcite. Minerals were identified using the Joint Committee on Powder Diffraction Standards database (JCPDS, 1980). Identification of smectite is according to Moore and Reynolds (1997).

Lithic Clast Populations

Lithic fragments include sedimentary (siltstone, mudstone, shale, sandstone, graywacke, and conglomerate), metamorphic (schist, phyllite, gneiss, and quartzite), and igneous (granite, pegmatite, and dolerite) lithologies. Clasts are angular to subrounded, and sizes range from less than a millimeter, through centimeter sizes, to meter-sized cataclastic blocks occurring especially in the bottom part of the impact breccia section. The proportions of the different types of clasts and of melt particles in the size range from 0.2 to ~10 mm, as estimated from point counting analysis, are reported in Table 3 and Figure 6. On average, sedimentary clasts are slightly more abundant (~26 vol%) than crystalline clasts (~18 vol%). Within the sedimentary clast population, fine-grained sediments, such as siltstone and mudstone, are most abundant, representing ~13 vol%, on average; graywacke (~4 vol%, on average) and sandstone (~5 vol%, on average) are also represented. Conglomerate clasts in suevite are comparatively rarer at thin-section scale, but they occur as relatively large clasts in the core (~40 cm in size; e.g., samples CB6-112, CB6-125, and KB-6; depth = 1459.2 m, 1522.7 m, and 1468.7 m, respectively). The crystalline-clast population includes gneiss and schist (~6 vol%); the gneiss clasts have similar lithology to that of the cataclastic gneiss blocks and boulders that occur in the impact breccia section. In addition, the crystalline-clast population includes granite and pegmatite clasts. Clasts of dolerite are extremely rare and somewhat difficult to distinguish from impact melt with microlites.

Melt Particles and Melt Matrix

The term "melt particle" is used for all forms of melt, of different types and shapes, as described in detail later herein, and sizes range from a few hundred micrometers to a few centimeters. Macrophotographs, microphotographs, and scanning electron microscope (SEM) images of melt particles are shown in Figures 8, 9, and 10, respectively. Melt particles are most abundant near the top of the impact breccia section, between 1397 and ~1430 m (subunit U1), where the suevite contains 6–34 vol% of melt particles (see Fig. 6) and grades into impact melt rock between 1402 and 1407.5 m (Horton et al., this volume; Wittmann et al., this volume, Chapter 16). Between ~1430 and 1448.4 m (subunit U2), the melt particles are rare and make up less than 3 vol% (i.e., in samples CB6-101 to CB6-106; depth = 1431.1 and 1447.0 m, respectively). The suevite becomes melt-rich again in the interval 1448.4–1457 m (subunit U3), where it grades into impact melt rock between 1450.2 and 1451.2 m (Horton et al., this volume; Wittmann et al., this volume, Chapter 16). Our sample CB6-108 (depth = 1451.0 m), from this interval, contains ~74 vol% of melt and partly melted clasts, but still has some clastic groundmass. Below 1457 m, the melt abundance is very variable, from <0.6 to 35 vol%. The percentage of melt particles in this lower part is typically below 13 vol%, but some samples with higher melt abundances occur as well, e.g., ~35 vol% in sample CB6-115 (depth = 1473.5 m).

Millimeter- to centimeter-sized melt particles (up to 5 cm in size; Figs. 8A and 8B) are mostly ovoid to amoeboid in shape (Fig. 8B) and commonly show flow structures (Figs. 9A, 9C, and 9D). Several major types of melt particles have been distinguished, on the basis of color, microtexture, and chemical composition: (1) clear, brownish, or greenish, unaltered glass with high silica content, often with flow texture (dark- and light-colored schlieren; Figs. 9A, 9B, 9C, and 10A); (2) brown melt, entirely altered to fine-grained phyllosilicate minerals, often with undigested clasts (Fig. 9D); (3) recrystallized silica melt (Figs. 9E and 9F); (4) melt with feldspar (Fig. 9G) and/or pyroxene microlites (Fig. 9H); and (5) dark brown melt (melted shale or carbon-rich clasts?; Fig. 9I). The most important features of the different types of melt particles are summarized in Table 2.

Most of the melt fragments are devitrified and altered; fragments of unaltered, colorless to brownish glass (type 1) were observed mainly in subunit U1, at depths around 1415 m. This type of glass shows abundant schlieren, and some particles display shard-like (Fig. 9C) and "flame" shapes (Fig. 9B). The melt type 2 is the most abundant type and is present in all subunits. The silica melt particles (type 3, with ~98 wt% of SiO_2) are often recrystallized to microcrystalline quartz. Most microclasts in the melt particles are quartz. In some melt particles, grains of calcite (e.g., in sample CB6-110; depth = 1455.2 m; Fig. 10B) were observed; rarely, secondary carbonate partially replaces altered melt particles (e.g., in sample CB6-109; depth = 1452.3 m; Fig. 9J). Small grains of pyrite and marcasite, as well as anatase and rutile (identified by microRaman spectrometry), occur in melt particles of types 1 and 2 (Figs. 10A and 10B). The melt with microlites (type 4) occurs mostly as melt matrix in impact melt rock and only rarely as melt particles. The crystallites in melt particles of type 4 were studied by optical microscopy and SEM-EDX, and they were identified as Al-rich pyroxenes (also Wittmann et al., this volume, Chapter 16) in the impact melt rock samples from the M2 interval. In the sample CB6-108 from the M1 section, melt with crystallites of plagioclase (labradorite) occurs. The dark-brown melt (type 5) occurs in amoeboid shapes and is probably a melt of shale or other fine-grained sediment. The different types of melt particles have been characterized by SEM-EDX, and details on the chemical composition of these melt particles are reported in the companion paper by Bartosova et al. (this volume).

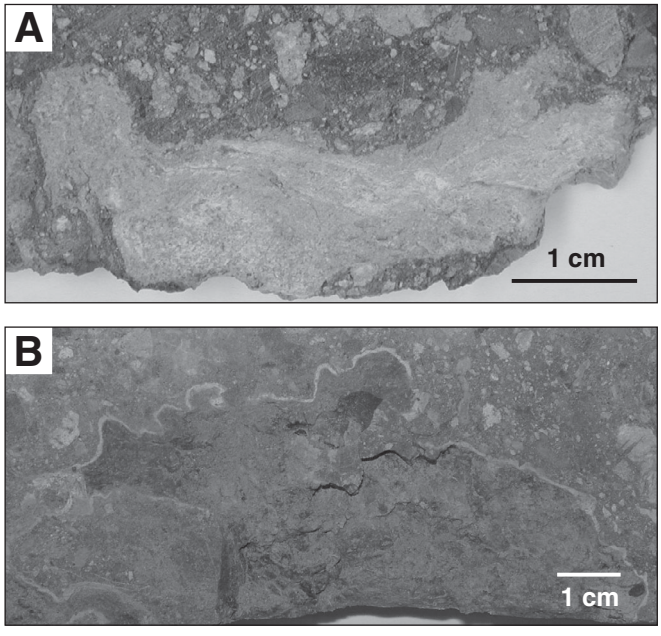

Figure 8. Macrophotographs of melt particles in suevite from the Eyreville B drill core, Chesapeake Bay impact structure. (A) Melt particle (type 2) altered to phyllosilicate minerals and partially replaced by carbonate (sample CB6-109; depth = 1452.3 m). (B) Altered melt particle with amoeboid shape (depth = 1399.4 m).

Shock Metamorphic Features in Minerals

Shock metamorphic effects in minerals represent the most important evidence for the recognition of an impact origin of a geological structure (e.g., Stöffler and Langenhorst, 1994). Shock metamorphic and shock-related features (such as ballen quartz and quartz toasting) observed in the impact breccia section are illustrated in Figures 11 and 12. A great diversity of shock effects in minerals is known, and these have been abundantly described, mostly for quartz, in the literature over the last 40 years (see, e.g., Stöffler and Langenhorst, 1994; Huffman and Reimold, 1996; French, 1998; Reimold and Koeberl, 2008, and references therein). Upon shock compression, quartz develops irregular fractures (which are not diagnostic shock effects) at very low shock pressures (<5 GPa), and planar fractures (PFs) and planar deformation features (PDFs) at higher pressures. Both PFs and PDFs have orientations that are crystallographically controlled, parallel to rational crystallographic planes (e.g., Stöffler and Langenhorst, 1994, and references therein).

Quartz grains in Chesapeake Bay impact breccia samples, occurring either as single grains in the matrices or as grains within rock clasts, show a variety of shock effects. Planar fractures are less common than PDFs; mostly one set and rarely two sets of PFs were noted. The PFs generally cross the entire quartz grains and are spaced more than 15 μm apart. Occasionally, PFs and PDFs occur together in the same quartz grain. Quartz grains with PDFs have been noted in all investigated suevite samples. Mostly one or two sets of PDFs in quartz (Fig. 11A) occur, and rarely three or four sets were observed. Frequently, PDFs are decorated with tiny fluid inclusions. Individual PDF sets mostly cross the whole host grain, but there are also sets occurring only in a part of a quartz grain. The PDFs are <2 μm wide, and parallel sets are spaced ~2–7 μm apart. The PDFs are best developed in polycrystalline quartz clasts (Fig. 11B), where decorated PDFs penetrating entire grains are common. In some quartz grains, the PDFs are difficult to resolve, for example, in clasts of fine-grained gneiss. Most of the sedimentary clasts are too fine-grained (siltstone, mudstone)

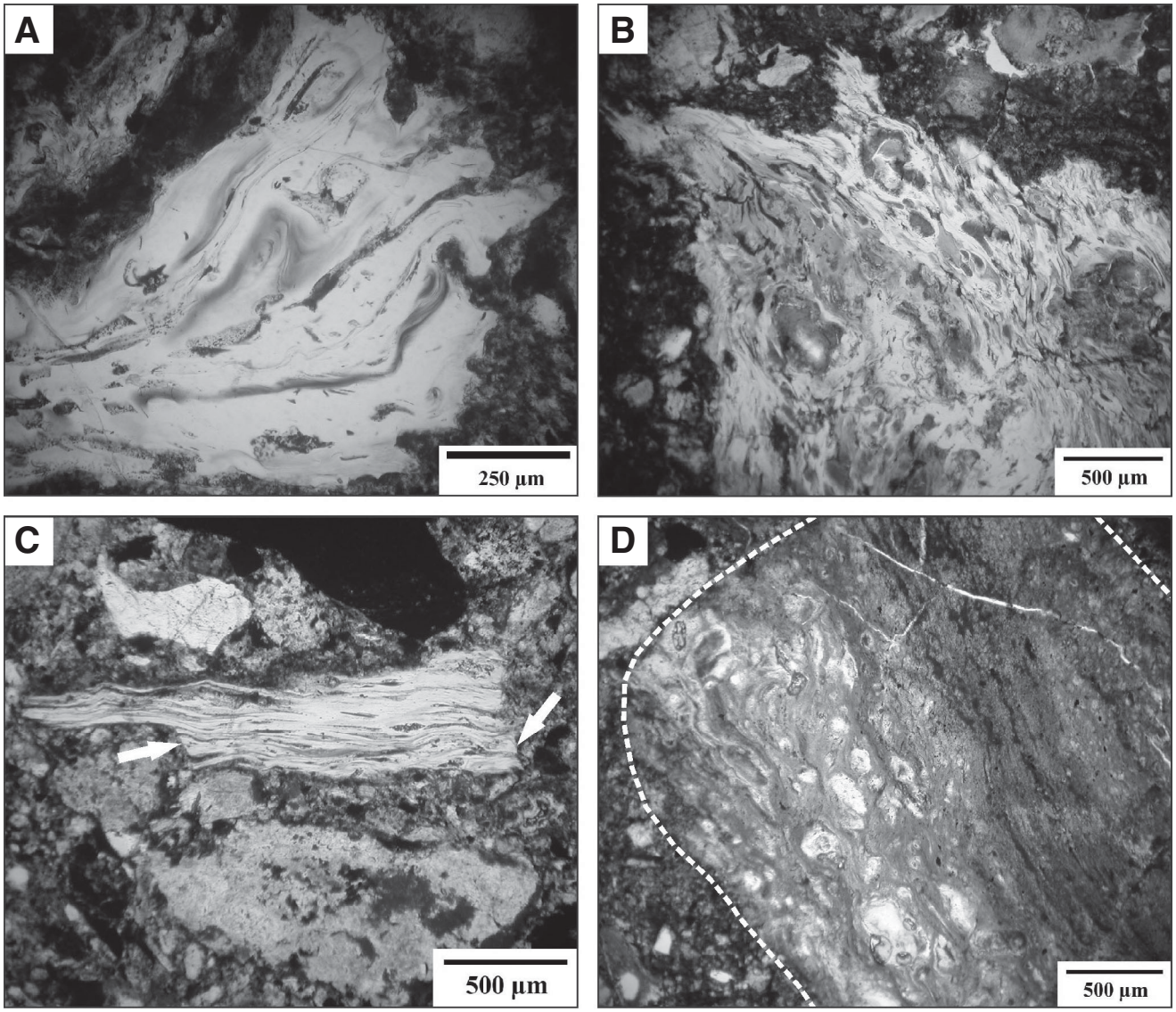

Figure 9 (*continued on following page*). Microphotographs of the different types of melt particles in the suevite and impact melt rock of the Eyreville B drill core. (A) Clear glass particle (type 1), colorless with brown schlieren, amoeboid (sample CB6-098; depth = 1418.8 m), plane-polarized light. (B) Clear glass particle (type 1), light brownish with brown schlieren and "flame-shaped" structures (sample CB6-098; depth = 1418.8 m), plane-polarized light. (C) Clear glass particle (type 1), colorless with brown schlieren, shard-like; the arrows mark sharp edges, which suggest that the particle had been broken before or during deposition (sample CB6-098; depth = 1418.8 m), plane-polarized light. (D) Altered melt particle (type 2) recrystallized to phyllosilicate minerals and with abundant undigested grains (sample CB6-093; depth = 1399.2 m), plane-polarized light. The outline of the melt particle is marked with a dashed line. (E) Recrystallized silica melt (type 3), clear with some brownish parts, botryoidal shape (sample KB-2; depth = 1402.87 m), plane-polarized light. (F) Recrystallized silica melt (type 3) with botryoidal shape (sample KB-2; depth = 1402.87 m); the same particle as in Figure 9E, but in cross-polarized light. (G) Impact melt with intersertal texture, with crystallites of plagioclase (type 4; sample CB6-108; depth = 1451.0 m), cross-polarized light. (H) Impact melt with microporphyritic texture, with crystallites of pyroxene (type 4; sample KB-2; depth = 1402.9 m), plane-polarized light. (I) Dark brown, altered melt particle (type 5), probably derived from shale or a fine-grained sediment, with abundant tiny undigested grains (sample CB6-107; depth = 1449.8 m), plane-polarized light. (J) Melt particle altered to phyllosilicate minerals and partially replaced with secondary carbonate (sample CB6-109; depth = 1452.3 m), cross-polarized light.

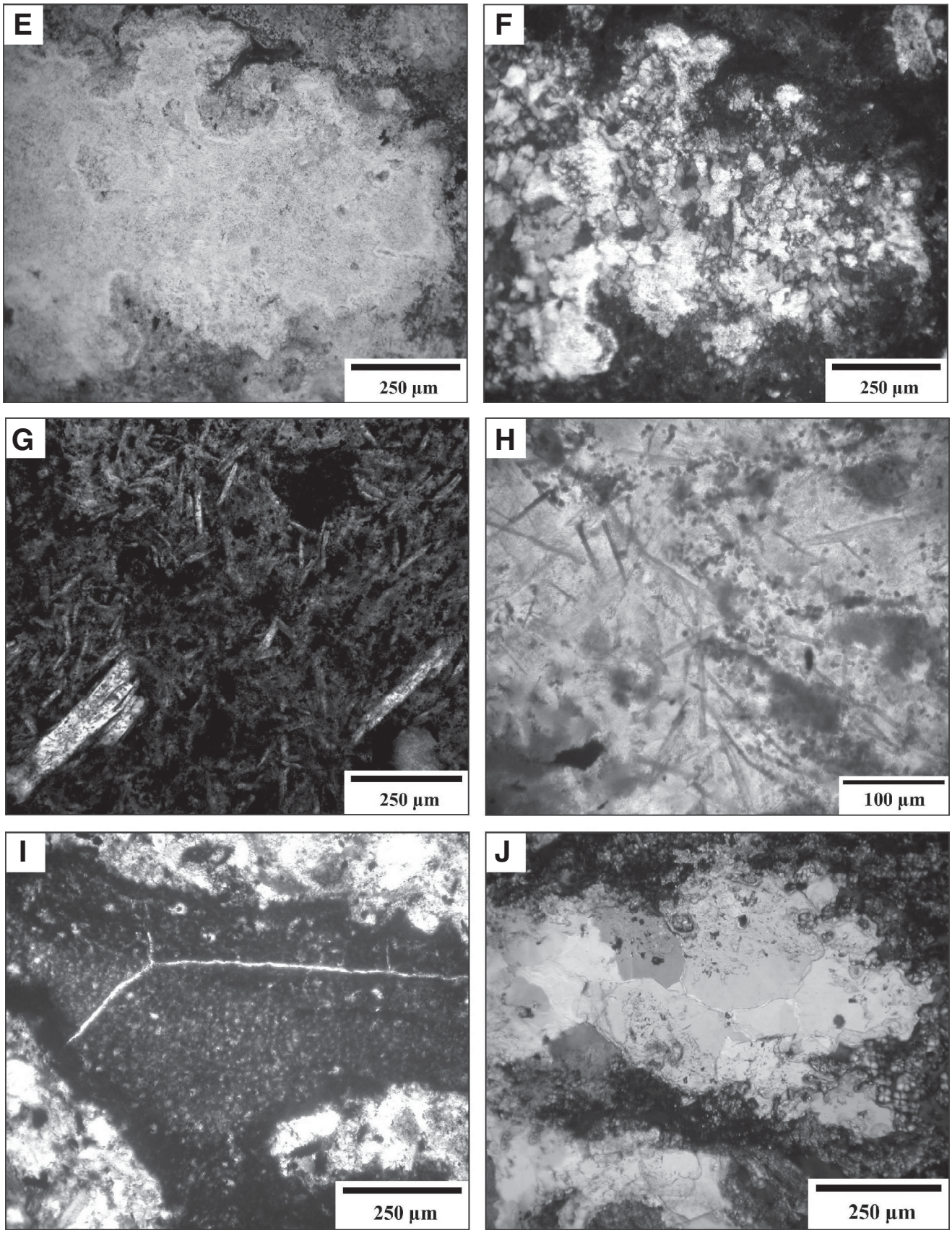

Figure 9 (*continued*).

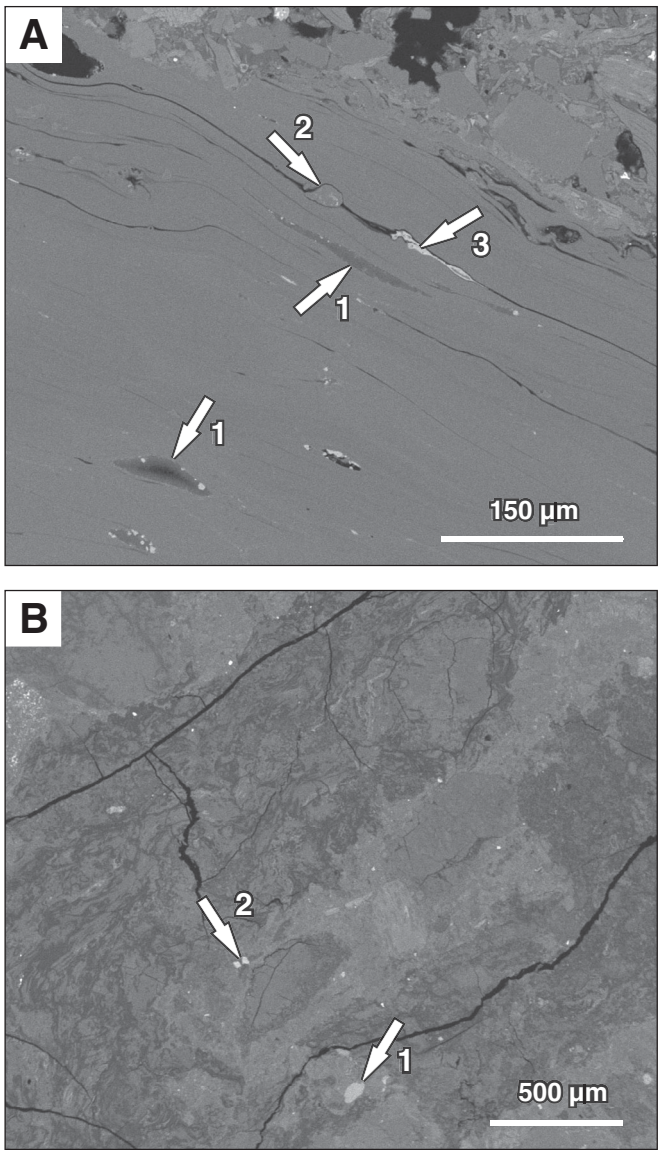

Figure 10. Backscattered electron images of melt particles in suevite. (A) Microtexture of a clear glass particle (type 1). The glass obviously has a fluidal texture. The particle is mostly composed of silica (>95% of SiO_2). Microfractures are filled with phyllosilicate minerals (1). An undigested quartz grain is visible in the upper part of the image (2). In addition, there is a small elongate grain of rutile (3). Sample CB6-098; depth = 1418.81 m. (B) Melt particle partially altered to phyllosilicate minerals (intermediate type, between type 1 and 2, according to our classification). The lighter areas are silica-rich (up to 98 wt% of SiO_2), whereas the darker areas are altered to phyllosilicate minerals. A small grain of calcite (1) and two tiny grains of rutile (2) occur. Sample CB6-110, depth = 1455.22 m.

to determine whether quartz grains have been affected by shock metamorphic transformation.

Because PDFs cannot be clearly resolved under the optical microscope, the TEM was used for characterization of their microstructure. Observations were made on a FIB foil cut across a quartz grain with one PDF set (sample CB6-097; depth = 1412.8 m). The PDFs are represented by planes of high dislocation density and are decorated with tiny fluid inclusions (Fig. 12). The inclusions typically display negative crystal shapes with a maximum size of ~0.5 µm. The PDFs in the investigated quartz grain did not show any amorphous silica phase along the rhombohedral planes; the original amorphous phase is totally recrystallized.

Shock effects are rarely observed in minerals other than quartz in our Eyreville core samples. Rare K-feldspar grains with PDFs were noted, e.g., in a granite-derived clast in sample CB6-099 (depth = 1421.7 m). Overall, PDFs are difficult to resolve in feldspar, possibly because of postimpact alteration.

Results of our systematic analysis of the shock metamorphic effects in quartz grains, carried out on 14 suevite samples, are reported in Table 4. The investigated samples cover nearly the entire depth interval of the impact breccia section. Shock effects were evaluated separately for single quartz grains and for each type of rock clasts; however, the results could be statistically evaluated only for the most abundant clast types. In each thin section, quartz grains in one type of rock clast (e.g., graywacke) were counted together, not separately in each individual clast. Next, an average value from all the investigated thin sections was calculated for a particular clast type. Generally, the clasts of the same lithology have similar proportions of shocked clasts. On average, ~16 rel% of all the quartz grains are shocked (i.e., show PFs and/or PDFs). Single grains in the matrix, which represent a substantial part of all the grains counted, are shocked to a similar percentage (~15 rel%, on average). The proportion of shocked quartz grains in sedimentary clasts is higher than the average proportion of shocked grains from all analyzed quartz grains. Graywacke clasts contain ~19 rel% of shocked quartz grains, and sandstone clasts contain ~47 rel% of shocked quartz grains, on average. However, the sandstone clasts were not abundant enough to provide reliable statistics. About 21.5 rel%, on average, of the quartz grains in polycrystalline quartz clasts are shocked. PFs and PDFs are rarely observed in gneiss/schist clasts (~1 rel% of the quartz grains are shocked).

No obvious trend in the distribution of shocked quartz grains with depth through the impactite sequence is observed (Fig. 13). When only single quartz grains in matrix are taken into account, the results for individual samples are slightly different (Fig. 13), but they do not show any trend with depth either. We also compared the proportion of shocked quartz grains with the abundance of matrix, melt, crystalline clasts, and sedimentary clasts, but no correlation was observed. The only observed, though weak, trend is the increase in abundance of single shocked quartz grains in matrix with the

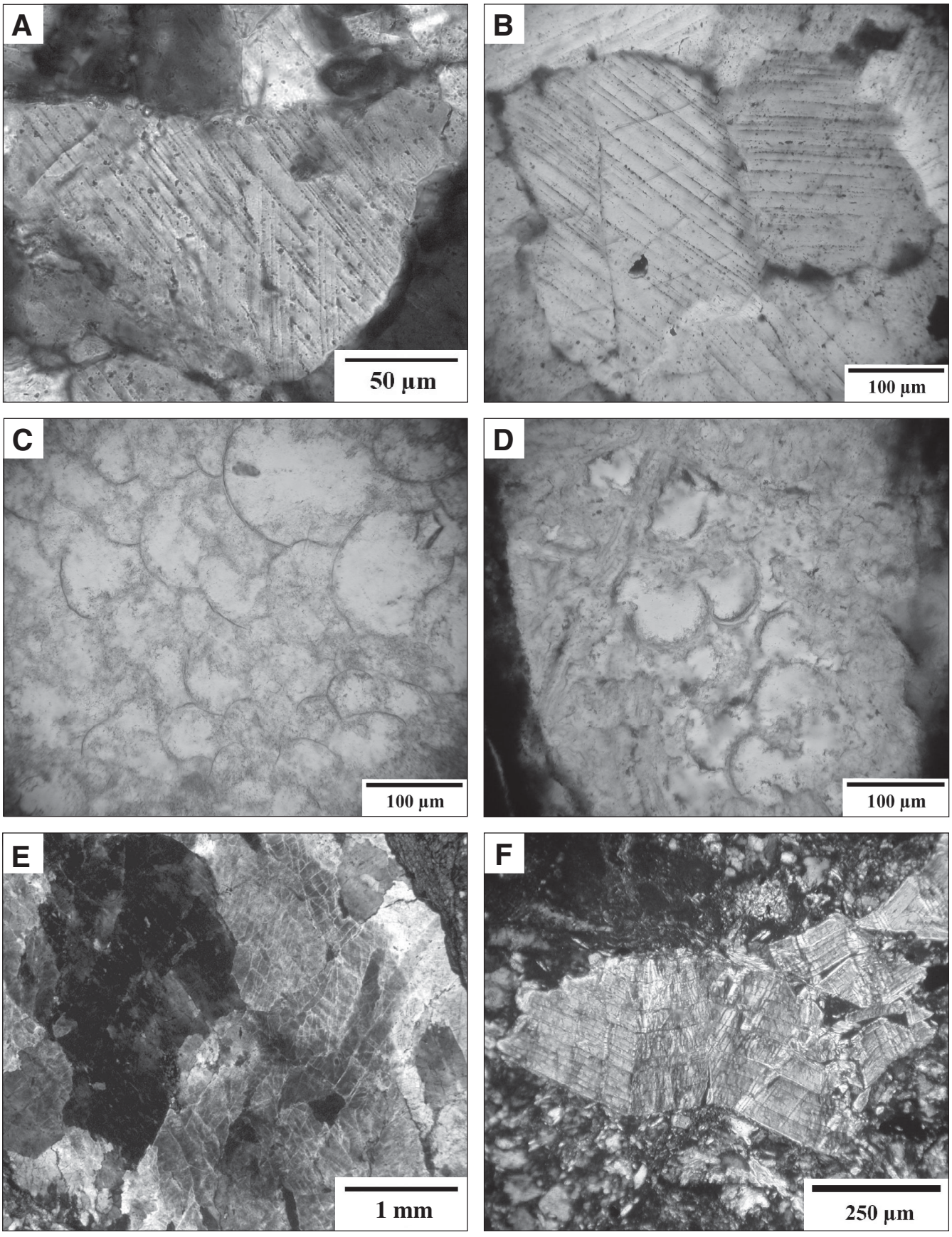
A
50 µm
B
100 µm
C
100 µm
D
100 µm
E
1 mm
F
250 µm

increasing proportion of sedimentary clasts (correlation coefficient $r = 0.69$).

Impact-Diagnostic Features and Other Microscopic Features in Minerals

Besides PFs and PDFs in quartz and in feldspars, ballen quartz, toasting of quartz grains, undulose extinction in quartz, and kink-banding of mica were observed. Ballen quartz was identified exclusively in melt-rich suevites and in impact melt rocks (e.g., KB-4, CB6-107, CB6-108; depth = 1405.7 m, 1449.8 m, and 1451.0 m, respectively; Figs. 11C and 11D). Ballen with a mean size of ~80–100 µm occur in silica clasts, generally within melt particles (melt type 3). Ballen quartz with heterogeneous extinction (type III), ballen quartz with intraballen polycrystallinity (type IV), and rare ballen quartz with homogeneous extinction (type II) were noted, according to the classification by Ferrière et al. (2009b). No ballen cristobalite (type I) and ballen quartz of type V (according to Ferrière et al., 2009b) were observed in our samples. Ballen quartz and ballen cristobalite are considered to be impact-diagnostic features (Ferrière et al., 2009b); however, it is not clear yet if the different types of ballen are the result of postimpact alteration processes and/or due to the pressure-temperature (*P-T*) conditions during the back-transformation of cristobalite to α-quartz.

Quartz grains in the suevite from the Eyreville B drill core commonly have toasted appearance (Fig. 11E). About 8 rel% of all quartz grains in suevite display a toasted appearance; the toasted quartz grains do not necessarily show PDFs. The quartz grains in the impact melt rock from the depth interval 1402–1407.5 m (M2) show only slight toasting together with PDFs. The sample of suevite/impact melt rock (CB6-108; depth = 1451.0 m) from the lower impact melt rock interval (M1, 1450.2–1451.2 m) shows quartz grains with very strong toasting and decorated PDFs.

Undulose extinction, which is by itself not of impact-diagnostic value, is observed for the majority of the quartz grains, including grains without PFs or PDFs. Kink bands occasionally occur in mica (mostly in muscovite; e.g., in sample CB6-100; depth = 1427.01 m; Fig. 11F); however, since kink-banding is also observed in mica from nonimpact settings, such as in tectonically deformed rocks, it cannot be considered to be a diagnostic shock effect (e.g., French, 1998, p. 33).

Alteration of the Impactites

The impact breccia section shows a large variety of alteration effects that have significantly modified the mineralogy and affected the chemical composition of the rocks (see Bartosova et al., this volume); some minerals are partially or totally replaced by secondary minerals, such as biotite by chlorite or feldspar by sericite. Especially in the rock clasts, this alteration can be pre-impact because the same alteration effects are noted in the lower basement-derived section (Townsend et al., this volume). In suevite and cataclasite, veins or patches of carbonate occur, mostly in the lower part of the impact breccia section (below 1500 m). However, in cataclasite blocks, some of the veins might be of pre-impact age. Secondary opaque minerals (e.g., pyrite) occur in clusters and patches, many at the boundaries between clasts and matrix. Commonly, melt particles (especially type 2) are altered to phyllosilicate minerals. Phyllosilicate minerals are also abundant in matrix. The occurrence of smectite was

Figure 11. Microphotographs of typical shock metamorphic or shock-induced features observed in samples from the Eyreville B drill core, Chesapeake Bay impact structure. (A) Quartz grain with two sets of decorated planar deformation features (PDFs; sample CB6-100, depth = 1427.0 m), cross-polarized light. (B) Polycrystalline quartz grains with one set of decorated PDFs each and some irregular (i.e., nonplanar) fractures (sample CB6-104; depth = 1443.7 m), cross-polarized light. (C) Ballen quartz (alpha-quartz, type IV) clast in a sample of impact melt rock (sample KB-4; depth = 1405.7 m), plane-polarized light. (D) Ballen quartz (alpha-quartz, type II) in suevite (sample CB6-107; depth = 1449.8 m), plane-polarized light. (E) Quartz grains with toasted appearance in suevite (sample CB6-113; depth = 1464.0 m), cross-polarized light. (F) Kink banding in a muscovite clast in suevite (sample CB6-100; depth = 1427.0 m), cross-polarized light.

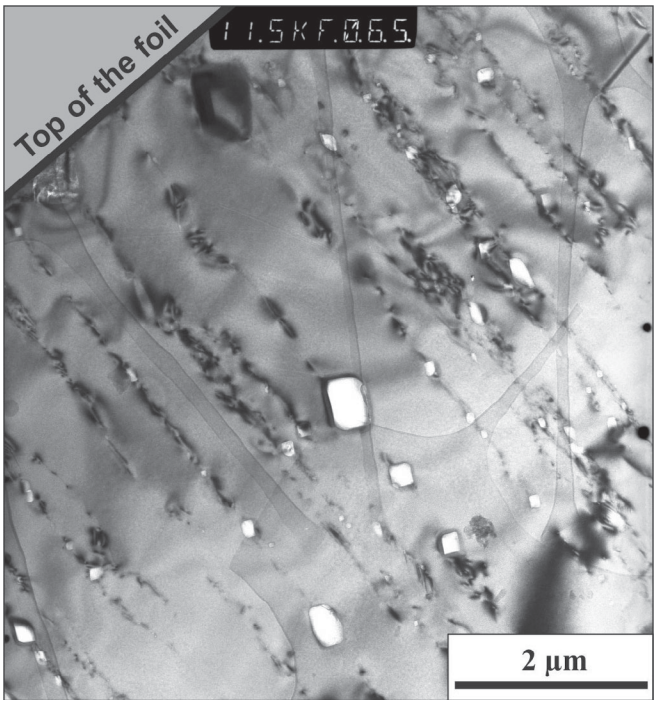

Figure 12. Transmission electron microscope (TEM) bright field photomicrograph of one planar deformation feature (PDF) set in a quartz grain from suevite (sample CB6-097; depth = 1412.8 m). PDF planes show a high dislocation density and are decorated with numerous tiny fluid inclusions (white in the figure). Note that no amorphous phase occurs along the rhombohedral planes. The light-gray network shown in the background corresponds to the carbon net supporting the specimen.

TABLE 4. CHARACTERISTICS OF QUARTZ GRAINS IN SUEVITE FROM THE EYREVILLE B DRILL CORE (VALUES IN REL%)

Sample:	CB6-093	CB6-094	CB6-096	CB6-099	CB6-101	CB6-105	CB6-107	CB6-108	CB6-110	CB6-114	CB6-117	CB6-120	CB6-121	CB6-126
Depth (m):	1399.2	1399.7	1409.3	1421.7	1431.1	1445.8	1449.8	1451.0	1455.2	1467.4	1481.7	1504.3	1508.5	1529.3
Undeformed	2.2	n.d.*	n.d.	0.3	0.2	n.d.	n.d.	n.d.	n.d.	n.d.	n.d.	n.d.	n.d.	5.4
Undulose extinction	45.5	37.7	53.1	35.5	38.7	36.3	27.9	43.9	46.3	57.3	48.3	58.6	76.4	47.3
Fluid inclusions	23.6	44.6	27.2	48.5	43.1	40.5	32.6	32.8	15.4	14.2	33.2	12.4	12.1	22.8
Subplanar fluid inclusion trails	4.2	3.0	2.9	0.9	4.0	1.3	1.4	0.5	0.3	0.3	4.3	1.1	0.9	1.8
Toasted appearance	12.6	4.8	4.5	0.6	2.2	3.1	25.1	14.1	11.7	n.d.	0.3	7.1	0.3	1.2
PFs	2.2	2.2	1.8	0.9	2.2	1.3	0.5	1.0	0.3	0.5	2.4	1.5	n.d.	3.6
PDFs 1 set	5.6	4.8	8.3	9.9	7.0	14.4	5.1	3.0	12.9	20.7	8.7	12.0	7.3	12.6
PDFs 2 or more sets	1.0	2.2	1.3	2.3	2.0	1.1	n.d.	n.d.	6.0	7.0	2.4	2.6	2.4	5.4
PDFs 1 set + toasted	1.9	n.d.	0.8	0.9	0.4	1.6	5.1	3.0	4.3	n.d.	n.d.	2.3	n.d.	n.d.
PDFs 2 and more sets + toasted	1.3	0.9	0.2	0.3	n.d.	0.3	2.3	1.5	2.9	n.d.	0.3	2.3	0.6	n.d.
Shocked (PFs and/or PDFs)	11.9	10.0	12.3	14.2	11.7	18.7	13.0	8.6	26.3	28.2	13.9	20.7	10.3	21.6

Note: On average, 360 grains were investigated per thin section. Totals are 100% (excluding the last line, which summarizes the percentage of shocked quartz grains). PF—planar fracture; PDF—planar deformation feature.
*Not detected.

confirmed by XRD analyses in suevite samples from the lower parts of the impact breccia section (in samples CB6-115 and CB6-121; depth = 1473.5 and 1508.5 m, respectively). Chamosite, an alteration mineral of the chlorite group, was identified in suevite and cataclastic gneiss by microRaman spectroscopy; chamosite occurs abundantly in the form of patches and fracture fillings, mostly in the lower part of the impact breccia section (typically around 1500 m depth). Amygdules filled with zeolites (faujasite and phillipsite) were noted in the melt-rich parts of the suevite (e.g., sample CB6-108; depth = 1451.0 m).

DISCUSSION AND INTERPRETATION

Implications for the Formation of the Impact Breccia

Generally, clast size increases with increasing depth in the impact breccia section; additionally, matrix proportions are much higher in the uppermost part of the section. In the lower part of the impact breccia section, clasts are more abundant and large blocks of cataclastic gneiss occur. Large clasts and blocks, similar to cataclastic gneiss blocks that occur in the lower part of the impact breccia (below 1474 m), were also observed in the STP test hole (e.g., Horton et al., 2005b). Some blocks of cataclastic gneiss may have been incorporated into the suevite during the collapse of the central uplift, as previously suggested by Horton et al. (2005b) for the STP test hole. The lowermost parts of the impact breccia section (subunits U5 and U6), which contain large blocks of cataclastic gneiss, are relatively melt-poor. These two subunits probably represent ground-surge material. A ground-surge origin for the lower part of the impact breccia section (1468–1551 m) was also suggested by Wittmann et al. (2008), based on the scarcity of melt fragments and clast-size distribution. The presence of large gneiss blocks and the overall increasing proportion of crystalline basement-derived rock suggest a more autochthonous character of the materials in these lower parts of the impact breccia section (Jolly et al., 2008). In our point counting, we observed abundant sedimentary clasts in subunit U6 (1486.1–1551.2 m). However, we counted proportions of relatively small clasts (<~1 cm); the observations by Jolly et al. (2008) suggest that in the smaller clasts, the proportion of sedimentary clasts is higher than in larger clasts (clasts >4 cm).

Regarding shape and texture of the different melt particles, it seems that the shard-like melt particles (clear glass, type 1; Fig. 9C), which have sharp edges and sharp contacts to matrix, were solidified before incorporation into the impact breccia. In addition, this type of melt fragment (type 1) was found only in the upper part of the suevite sequence (above 1430 m). These observations suggest that subunit U1 (1397.2–1430 m) represents fallback impact breccia. Further, the upper part of the impact breccia section contains more matrix and small clasts derived from different types of target rocks (see also Jolly et al., 2008). The melt rock intervals (M1 and M2) are very clast-rich and heterogeneous. The melt rocks included in the suevite clearly

do not represent a coherent melt sheet, but rather individual melt bodies incorporated into the fallback material.

Below 1430 m, some parts of the investigated section (i.e., U3; 1448.4–1457 m) contain abundant melt particles and small clasts, and these probably also represent fallback material. The melt-poor, crystalline clast–rich subunit (U2; 1430–1448.4 m) might represent ground-surge material or material slumped either from the central uplift or from the margin of the transient crater. Wittmann et al. (2008, this volume, Chapter 17) have observed some shard-like particles also in the lower parts of the section (e.g., in the interval 1451–1468 m), and they interpret the impactites above 1468 m as a mixture of fallback and ground-surge material, with fallback material becoming more important toward the top of the section. Shard-like melt particles were also found in Exmore breccia from the Eyreville drill core and are interpreted as fallout from the ejecta plume (Reimold et al., this volume).

The petrographic and geochemical diversity of the melt particles from the impact breccia section suggests that the particles were derived from different precursors. More information about chemical composition of the different types of melt particles from the impact breccia, including discussion about possible precursors, can be found in Bartosova et al. (this volume).

Comparison with Suevite from the STP Test Hole

Before the drilling at Eyreville, suevite was cored at Chesapeake Bay only in the STP test hole, but, unfortunately, only limited observations of the suevite from this test hole are reported in the literature (Horton et al., 2005b, 2006, 2008; Lee et al., 2005, 2006; Gohn et al., 2007). In Gohn et al. (2007), the suevite from the STP test hole is described as part of a crystalline-clast breccia, where clasts of gneiss and chloritized mafic rock dominate. In the Eyreville drill core, a mafic lithology containing abundant amphibole and chlorite occurs (e.g., sample CB6-123; depth = 1514.3 m), but it is not among the most abundant components of the suevite, according to our petrographic observations and further confirmation from our chemistry-based HMX (Harmonic least-squares MiXing) mixing calculations (Bartosova et al., this volume). According to Horton et al. (2005b), the suevite from the STP test hole is crumbly to moderately cohesive and contains metamorphic and igneous rock fragments and less abundant particles of impact melt rock. Only rare sedimentary clasts occur in the suevite from the STP test hole (Horton et al., 2008), whereas sedimentary clasts constitute an important component of suevite from the Eyreville B core. This implies that the suevite from the STP test hole is similar to the lower part of the impact breccia section from the Eyreville B core. However, insufficient core recovery at the STP test hole makes further comparison of the two cores difficult (J.W. Horton Jr., 2008, personal commun.). Suevite from the STP test hole (polymict, poorly sorted, and not bedded) was first interpreted as fallback material (Horton et al., 2005b), but later, an origin similar to that of the "crater suevite" in the Ries crater, i.e., suevite that never left the crater cavity (von Engelhardt and Graup, 1984), was proposed by Horton et al. (2008). The crater suevite from the Ries crater has a relatively higher clast/melt ratio compared to the Ries fallout suevite, contains clasts that are on average shocked to a lower stage, and lacks aerodynamically shaped glass bodies (von Engelhardt, 1997). The melt particles in the suevite from the STP test hole are glassy or partly aphanitic, with some flow lamination (Horton et al., 2005b). Our observations of melt particles are somewhat comparable to the descriptions by these authors,

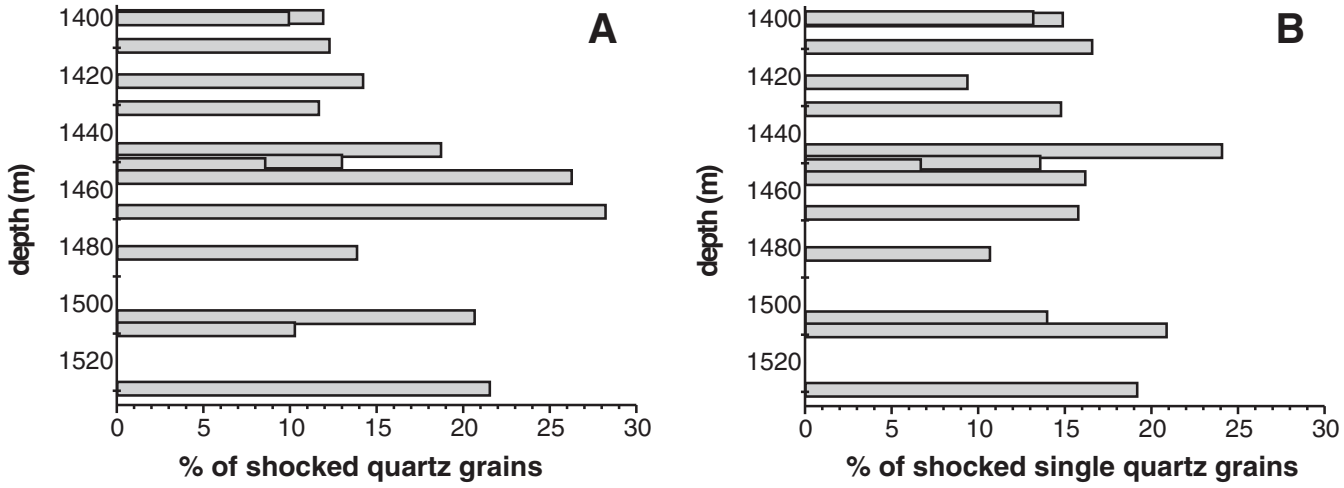

Figure 13. Bar diagrams showing changes in the relative proportion of shocked quartz grains (i.e., grains with planar fractures [PFs] and/or planar deformation features [PDFs]) with depth in the suevite samples from the Eyreville B drill core. (A) Relative percent of total shocked quartz (i.e., single quartz grains in matrix and quartz grains in lithic clasts). (B) Relative percent of shocked quartz, single quartz grains in matrix only. No obvious trend with depth is observed.

with the notable exception that still other melt types (i.e., types 3, 4, and 5) were distinguished during our study (see Table 2). Horton et al. (2005b) described quartz grains with multiple sets of decorated PDFs within the suevite breccia from the STP test hole, which is in agreement with our own observations on samples from the Eyreville B core. Similarly, we also observed large blocks of cataclasite (some >10 m thick; Horton et al., 2005b) in the Eyreville B core.

Comparison with Exmore Breccia

The Exmore beds represent washback material deposited by a collapsing marine water column and associated tsunami waves (e.g., Poag et al., 2004, p. 185). It has also been proposed that the lower parts of this sequence, which contain abundant and partly very large blocks (Gohn et al., this volume), represent avalanche deposits. The finer-grained materials are generally described as "Exmore breccia" (cf. Reimold et al., this volume). The unit consists of a fine matrix containing millimeter-sized mineral clasts, millimeter- to centimeter-sized lithic clasts, and generally rare melt particles. However, melt particles are enriched in some depth intervals in the upper parts of the Exmore breccia (Reimold et al., this volume). In contrast to suevite, Exmore breccia contains abundant glauconite and microfossils, and evidence of shock metamorphism is rare in the microclasts (Reimold et al., this volume).

The Exmore breccia has been cored in several drill holes in the Chesapeake Bay impact structure, and PDFs in quartz in some clasts of crystalline basement rocks have been observed (e.g., Koeberl et al., 1996; Poag et al., 2004, p. 217). More rarely, PDFs have been reported in single quartz grains within Exmore breccia (Poag et al., 2004, p. 217; Horton et al. 2005a). In contrast, in suevite, the shock metamorphic effects are more abundant in single quartz grains and sedimentary clasts than in crystalline clasts. The occurrence of melt particles mostly in the uppermost part of the Exmore beds suggests that fallback material similar to that incorporated into the uppermost suevite of the impact breccia section continued to settle down during the subsequent deposition of the Exmore breccia. Most melt particles that occur in the Exmore breccia are completely altered to secondary phyllosilicate minerals and, in rare cases, replaced by carbonate (Reimold et al., this volume; also see Ferrell and Dypvik, this volume), as are some melt particles in suevite from the Eyreville B drill core (e.g., in sample CB6-109; depth = 1452.3 m).

Shock Petrographic Characteristics

Investigated suevite samples show a large variety of shock metamorphic effects, particularly PDFs in quartz and melt particles, which attest to the mixing of different target rocks that were previously shocked at different pressures according to their original position (i.e., depth) in the stratigraphic column. There is a weak trend ($r = 0.69$) of increasing proportion of shocked single grains with increasing sedimentary component. This could mean that in the samples with predominantly sedimentary clasts, the single quartz grains in the matrix also originated mostly from sediments. This means that the single quartz grains would be relatively more shocked, as are their parent sediments (e.g., relatively larger proportions of shocked grains in graywacke and sandstone than in the other lithologies). Our observation, that PDFs are more abundant in the sedimentary clasts than in the crystalline basement clasts, is in agreement with the fact that the target sediments were overlying the crystalline basement before the impact and would have been subjected to higher shock pressures because they were located closer to the point of impact. It is well established that the shock wave attenuates rapidly with increasing distance from the point of impact (e.g., Stöffler, 1971; Robertson and Grieve, 1977; Melosh, 1989, p. 60–66; French, 1998, p. 18).

In previous studies of Exmore breccia that involved descriptions of shock metamorphism in clasts, shock effects were observed only in single quartz grains or clasts derived from the crystalline basement (e.g., Koeberl et al., 1996; Poag et al., 2004, p. 217; Horton and Izett, 2005), but no shock metamorphic effects in sedimentary clasts were reported. In contrast, we found abundant PDFs in sedimentary clasts in suevite, e.g., in graywacke and sandstone.

As documented by optical microscopy and supported by TEM work, most of the PDFs in quartz are decorated with tiny fluid inclusions (Fig. 12). No amorphous phase (i.e., glass) was observed along the rhombohedral planes. Initially, PDFs are amorphous lamellae formed during shock compression (e.g., Stöffler and Langenhorst, 1994; Grieve et al., 1996). The occurrence of fluid inclusions and of dislocations, in place of an amorphous phase, indicates that primary PDFs were altered (e.g., Leroux et al., 1994; Stöffler and Langenhorst, 1994; Grieve et al., 1996; Leroux, 2005). The amorphous phase was probably recrystallized due to the hydrothermal alteration of the impact breccia and thermal overprint from the hot suevite host package.

The full range of progressive stages of shock metamorphism (e.g., Stöffler and Langenhorst 1994) has been observed in most of the investigated suevite samples, including PDFs in quartz grains (rarely observed in feldspar), silica glass (rare ballen quartz observed), and more or less abundant melt particles. The quartz grains in the samples from the impactite section commonly show one or two sets, rarely more sets, of PDFs. The formation of PDFs requires pressures of at least 8–10 GPa (e.g., Stöffler and Langenhorst, 1994; Huffman and Reimold, 1996; French, 1998, p. 33). A detailed study of PDFs in some quartz grains from Exmore breccia, including universal stage measurements of PDF orientations, was reported by Koeberl et al. (1996). The occurrence of silica glass, as well as of melt particles, is consistent with shock pressures of at least 50 GPa (e.g., Stöffler and Langenhorst, 1994). The presence of impact melt rocks indicates that at least some target rocks experienced extremely high pressures and temperatures (more than 60 GPa and 1500 °C, respectively; French, 1998, p. 33).

Hydrothermal Alteration

Evidence for postimpact hydrothermal alteration is known for more than 60 impact structures (for reviews, see Naumov, 2002, 2005). Hydrothermal mineral associations in the majority of the terrestrial craters are very similar, and the dominant assemblage consists of phyllosilicate minerals (smectite, chlorite, and mixed-layered smectite-chlorite), various zeolites, calcite, and pyrite. For impact structures in which the target rocks contained significant amount of carbonate, the carbonate-quartz-sulfide association is also widespread (Naumov, 2002, 2005).

In suevite from the Chesapeake Bay impact structure, the original glassy groundmass of most of the melt particles has been altered to secondary minerals, such as smectite (cf. Fig. 7). The presence of smectite is in good agreement with the findings by Dypvik and Jansa (2003), who reported that in a Na-rich marine or brackish environment, impact glass should alter to smectitic clays (also see Ferrell and Dypvik, this volume). The zeolites (phillipsite and faujasite) occurring in the melt-rich suevite indicate low-temperature (<300 °C; Chipera and Apps, 2001) hydrothermal alteration, probably at ~100 °C (cf. Chipera and Apps, 2001; Osinski, 2005).

Additionally, veins and patches of carbonate, as well as secondary pyrite, occur within suevite and cataclastic gneiss samples from the Eyreville B drill core and are interpreted to be of postimpact hydrothermal origin. Horton et al. (2005b) have also suggested that the decoration of PDFs in quartz may be a consequence of the hydrothermal alteration. Our initial TEM observations seem to support this hypothesis of fluid circulation in rocks and minerals. Based on analyses of fluid inclusions, Horton et al. (2006) have shown that hydrothermal fluids associated with sparry calcite veins from the deeper crystalline-clast breccia reached temperatures up to the boiling point of seawater (~220 °C at 300 m water depth). The notable alteration of feldspars, as well as the chloritization of mica observed in our samples, is interpreted to be possibly—at least in part—of preimpact age because similar alteration has been observed in granitoids and schists in the basement rocks (e.g., Townsend et al., this volume).

Comparison with Other Impact Structures

The Chesapeake Bay impact structure was formed in a layered submarine terrain composed of a sedimentary sequence and underlying crystalline basement, similar to that at many other craters, including, e.g., Ries and Chicxulub (Kring, 2005). The location in a shallow-water marine environment makes the Chesapeake Bay impact structure comparable with, e.g., the Montagnais, Mjølnir, and Lockne impact structures (Dypvik and Jansa, 2003; Lindström et al., 2005).

Studies of submarine impact craters have demonstrated that the presence of water and the physical properties of target rocks have a major influence on the formation of the impact structure and on the associated sedimentary processes (Dypvik and Jansa, 2003). The shape of the Chesapeake Bay impact structure is similar to the shape of the Mjølnir impact structure (40 km in diameter), both of which have been described as having an "inverted sombrero" geometry (Dypvik and Jansa, 2003; Gohn et al., 2006a). The deposition of the suevite in the case of the Chesapeake Bay structure was probably somewhat similar to that described from the Yaxcopoil-1 drill core (located ~62 km from the crater center) at the Chicxulub impact structure (~180 km in diameter). At Yaxcopoil-1, according to Stöffler et al. (2004), after the ground surge and the formation of the ejecta curtain, the main fallback phase occurred, followed by the late fallback phase, which was modified by atmospheric interaction. In the central moat of the Chesapeake Bay impact structure, the deposition of fallback material was disturbed by slumping of material off the central uplift (Horton et al., 2005b) and interrupted by the return of fluidized sediments into the central cavity about 10 min after the impact (according to numerical modeling results discussed by Kenkmann et al., this volume). At Chicxulub, in the Yucatán-6 (Y6) drill core (located in the inner part of the ring depression surrounding the peak ring structure), the clasts in suevite increase in size, and crystalline basement clasts become more abundant with increasing depth (Claeys et al., 2003), similar to what we observed in the impact breccia section from the Eyreville B drill core. However, at Y6, silicate melt fragments become more abundant with increasing depth, and a layer of impact melt underlies the suevite section, which is the reverse of our observations from the Eyreville B drill core. Furthermore, the abundance of carbonates in the upper target sediments from Chicxulub had a large influence on the distribution of the impactites and makes some features of Chicxulub difficult to compare with the Chesapeake Bay structure.

In the Eyreville drill core, only two impact melt rock intervals were cored (5.5 m and 1 m in thickness, depth intervals 1402.0–1407.5 and 1450.2–1451.2 m, respectively; Horton et al., this volume; Wittmann et al., this volume, Chapters 16 and 17), whereas a continuous melt sheet is expected in an impact structure of this size (Shah et al., 2005, this volume). However, the lower amount of melt, as observed during our investigations, corresponds to what is expected for an impact structure with a diameter of ~20–40 km (i.e., the estimated size of the transient crater) and for an impact into a target made up of weak, wet sediments and water (Shah et al., 2005). Nevertheless, because the impact melt can be distributed unevenly within the impact structure, it is then difficult to estimate the amount of melt for the full Chesapeake Bay structure only based on information obtained from drilling. An ~3-km-thick impact melt sheet is believed to occur inside of the peak ring at Chicxulub (Kring, 2005). In the Montagnais structure (45 km in diameter), the impact breccia on the central uplift contains two layers of recrystallized melt (71 and 35 m thick; Dypvik and Jansa, 2003). At the Lockne structure (only 7 km in diameter), impact melt occurs as sand-sized particles in the arenites that formed in the final stages of the resurge deposits, but there is no information about the presence of melt bodies in the central part of the crater (Lindström

et al., 2005). For the Chesapeake Bay impact structure, Shah et al. (2005) suggested—from investigation of the magnetic anomalies—that the volume of melt surrounding the central peak is 0.4–7 km^3. Clearly, the total amount of impact melt at the Chesapeake Bay impact structure remains unresolved. The impact melt rock at the Chesapeake Bay impact structure contains microlites of feldspars and pyroxenes, probably formed by quenching of the impact melt; feldspar and pyroxene microlites have also been described in the impact melt from, e.g., Ries and Chicxulub (von Engelhardt, 1972; Osinski, 2003; Kring et al., 2004). Shard-like melt particles were observed in the upper part of impact breccia at the Chesapeake Bay impact structure. Similarly, angular shards of holohyaline glass have been described from surficial suevites from the Ries crater (e.g., Osinski et al., 2004). In the Ries crater, melt particles are preserved in a vitreous state in the chilled bottom and top layers of the suevite, whereas devitrified melt particles in the interior section of the suevite are altered (von Engelhardt, 1972). Melt particles of type 1 in the upper part of the impact breccia in the Eyreville B core could similarly have been preserved in the glassy state due to rapid cooling, compared to the slower cooling of melt in the deeper parts of the impact breccia section.

SUMMARY AND CONCLUSIONS

Forty-three samples from the impact breccia section at the Chesapeake Bay impact structure were subjected to detailed petrographic analysis. The suevite from the Eyreville B drill core is characterized by a grayish, fine-grained, clastic matrix that contains a variety of rock and mineral clasts, melt particles, and secondary minerals. The melt particles in the suevite are small (not larger than a few centimeters) and mostly elongated or amoeboid. The relative abundance of melt particles varies significantly through the suevite section: melt is most enriched near the top, where the suevite locally grades into impact melt rock. Five different types of melt particles have been distinguished, and the diversity of the melt particles suggests that they were formed from different precursors. The impactites from the Eyreville B drill core show evidence of hydrothermal alteration. Most of the melt particles (except for those at depths around 1415 m, where clear glass occurs) are altered to secondary minerals, such as smectite. Microcrystalline carbonates fill fractures and occur as irregular patches in suevite, but they occur more commonly in lithic clasts. Rarely, carbonates replace melt particles. The impactites contain a large variety of clasts with shock metamorphic indicators, such as PDFs in quartz, and melt particles, together with low-shocked material. This implies mixing of the different target rocks that were previously shocked at different pressures according to their original positions. The presence of impact melt rocks indicates that at least some target rocks experienced pressures of >60 GPa and temperatures >1500 °C.

Six different subunits of suevite have been recognized based mostly on the abundance and characteristics of lithic clasts and melt particles. The clast size generally increases with depth. Sedimentary clasts are dominant in most subunits (especially in U1, also in U3, U4, and in some parts of U6). There are melt-rich subunits (U1 and U3) and some melt-poor subunits with predominantly crystalline clasts (such as U2 and U5). The lower subunits (U5 and U6; below 1474 m) have larger clasts and large blocks of cataclastic gneiss, and mostly rare melt particles, that show no evidence of aerial transport, and they probably represent ground-surge material. Subunit U1, with shard-like melt particles and relatively small clasts originating from all different target lithologies, probably represents fallback material. Due to the origin of the core from the central crater moat, near the central uplift, deposition of the impact breccia sequence could have been disturbed by slumping of material from the central uplift and/or from the margin of the central crater. Consequently, we propose that the melt-poor subunit (U2) might represent "slump" breccia. The deposition of the impact breccia section was terminated by the ocean resurge that deposited the sedimentary sequence of the Exmore beds above the impactite sequence.

ACKNOWLEDGMENTS

The drilling at Eyreville was supported by the International Continental Scientific Drilling Program (ICDP), U.S. Geological Survey (USGS), and National Aeronautics and Space Administration (NASA). The present work was supported by the Austrian Science Foundation FWF, project P18862-N10 (to Koeberl). We thank J.W. Horton Jr. and A. Wittmann for valuable discussions. We are very grateful to A. Schreiber and R. Wirth (GeoForschungsZentrum [GFZ], Potsdam, Germany) for the FIB preparation, A. Greshake (Museum of Natural History, Humboldt University, Berlin, Germany) for assistance with the transmission electron microscope (TEM), E. Libowitzky (University of Vienna) for assistance with the microRaman measurements, as well as F. Koller (University of Vienna) for help with optical microscopy. W. Füzi and L. Slawek (both University of Vienna) are thanked for expert thin-section preparation. We thank Bevan French and Gordon Osinski for careful reviews that substantially improved this paper.

APPENDIX. DETAILED PETROGRAPHIC DESCRIPTIONS OF SAMPLES FROM THE IMPACT BRECCIA SECTION

Sample and rock type*	Midpoint depth† (m)	Description based on macroscopic and microscopic observations	Mineral composition§	Shock metamorphism	Melt types present
CB6-093 S	1399.2	Suevite with clastic gray matrix; angular to subangular gray clasts <1 cm (sandstone, siltstone, mudstone, graywacke); yellowish to beige melt particles up to 1.8 cm angular to amoeboid; olive green elongated melt particles with flow structures, altered and crumbly	Qtz, feldspar, Ms, Bt, opaque minerals	PDFs not easy to resolve, many single Qtz grains with PDFs, some decorated, most shocked grains toasted	2, interm.#, 3
CB6-094 S	1399.7	Suevite with gray fine-grained matrix; subangular to rounded clasts of siltstone <2 cm, large amoeboid melt particles up to 4 cm, dark olive green, crumbly, with white rim; subangular clasts of sandstone and polycrystalline quartz <0.5 cm; clasts of crystalline basement rocks, beige clasts with gray bands <2 cm; small clasts of shale	Qtz, Kfs, Ms, Bt, Chl, opaque minerals	Qtz grains with PDFs, commonly decorated, at least 2 sets, some PFs, many Qtz grains toasted	3
CB6-095 S	1401.3	Suevite with greenish gray clastic matrix, angular to subangular clasts of siltstone <1 cm, rounded clasts of crystalline basement <1 cm, minor dark purple melt particles <0.8 cm, yellowish weathered clasts or melt particles <2 cm, large clast (3 cm) of arkose (rounded gray and white grains)	Qtz, Kfs, Ms, Bt, Pl, opaque minerals, Ap	Toasted Qtz grains, PDFs in Qtz, especially in clasts of polycrystalline Qtz	2 (5?)
CB6-096 S	1409.3	Suevite with gray matrix, some parts of matrix melted, very rich in clasts; subangular clasts of mudstone <2 cm; subrounded clasts of schist <2 cm; subangular clasts of siltstone <1 cm; yellowish subrounded clasts of sandstone <1.5 cm; white subangular to rounded clasts <0.6 cm; amoeboid purple brown melt particles with flow structures; beige melt particle with rounded shape; yellowish melt particle with irregular shape	Qtz, feldspar, Bt, opaque minerals	PDFs in some clasts and single Qtz grains, toasted Qtz	2
CB6-097 S	1412.8	Suevite with light-gray matrix, very rich in clasts, dark-gray subangular clasts <2.5 cm, some with beige bands; angular beige clasts <1 cm; rounded clasts of granite <1.5 cm, fractured; white clasts of polycrystalline quartz; yellowish subangular soft clay clasts <1.5 cm; small clasts of graywacke; recrystallized greenish to yellowish melt particles <2.5 cm with schlieren	Qtz, Pl, Kfs, Ms, Bt, opaque minerals	PDFs especially in polycrystalline Qtz, at least two sets, some toasted Qtz grains	1, rare 2
CB6-098 S	1418.8	Suevite with gray matrix, very rich in clasts, angular to subrounded gray clasts of siltstone <2 cm; yellowish amoeboid altered clasts; reddish subangular clast of granite 0.5 cm; large (5 cm) yellowish clast of sandstone, partly melted and altered; white elongated melt clasts 1 cm long; melt particle 2 cm long with olive green altered core	Qtz, Bt, Ms, feldspar, opaque minerals, carbonate	Abundant PDFs especially in polycrystalline Qtz clasts	1, rare 2
CB6-099 S	1421.7	Altered suevite with gray matrix; rich in clasts; subangular clasts of mudstone <1 cm, part of one mudstone clast melted; clasts of siltstone <2 cm; large yellowish fractured subangular clast of sandstone (4 cm) plus a few smaller clasts; beige crumbly clasts of altered melt <2 cm; olive melt particles, rounded or elongated with white crystals in the middle, amoeboid shape, <4 cm long, mostly altered to clay minerals	Qtz, Ms, Bt, Kfs, Pl, opaque minerals, Chl, Tur, Ep	Abundant PDFs especially in polycrystalline Qtz clasts, at least two sets, toasted Qtz grains, PDFs in feldspar	1, interm.
CB6-100 S	1427.0	Suevite with gray matrix, crystalline clasts very abundant, subangular fractured white to gray crystalline clasts <2.5 cm, one pinkish subangular clast of granite; minor angular to subangular dark-gray clasts of siltstone <0.5 cm; a few shale clasts <3 mm	Qtz, Pl, Kfs, Ms, Bt, Chl, opaque minerals, carbonate, garnet, amphibole, Ep	Abundant well-developed PDFs in Qtz, some with 2 sets, toasted Qtz grains, kink banding in Ms	2, rare 1
CB6-101 S	1431.1	Suevite with gray matrix rich in clasts; angular to subangular clasts of siltstone <0.7 cm; white to gray subangular clasts of schist <2 cm; large yellowish melt particle with partly melted crystalline clast, some dark olive crystals and green pigment, amoeboid, 4.5 cm; abundant small vesicles; altered melt on the bottom edge of the sample	Qtz, Kfs, Pl, Ms, Bt, Chl, opaque minerals, Ttn, Ep	Most Qtz grains show PDFs, some at least two sets, decorated, some Qtz grains toasted	2, 4

(*Continued*)

APPENDIX. DETAILED PETROGRAPHIC DESCRIPTIONS OF SAMPLES FROM THE IMPACT BRECCIA SECTION (*Continued*)

Sample and rock type*	Midpoint depth† (m)	Description based on macroscopic and microscopic observations	Mineral composition§	Shock metamorphism	Melt types present
CB6-102 S	1436.6	Suevite with light-gray matrix, small angular clasts of mudstone <0.5 cm, clasts of siltstone <0.5 cm; large clasts of schist up to 5 cm; large clast through all core diameter with light-gray grains, coarse-grained, very fractured, meta-arkose or crystalline rock?; sulfide minerals with ochre pigment rim; dark olive green melt particles ~1 cm; abundant vesicles	Qtz, Kfs, Ms, Bt, Pl, opaque minerals, Gr	PDFs in Qtz, some decorated especially in polycrystalline Qtz, some at least 3 sets, some Qtz grains toasted	2
CB6-103 S	1440.0	Suevite, very light gray, large clasts with light pinkish and greenish crystals form majority of the sample, one clast of granite along all sample (12 cm), angular to subangular clasts of siltstone <0.1 cm; cavities after altered melt, dark beige, elongated <3.5 cm; angular beige clast of sandstone 2.5 cm; pyrite grains occur	Qtz, Kfs, Pl, Ms, Chl, Ep, carbonate, opaque minerals	PFs and PDFs (up to 4 sets) in Qtz	2
CB6-104 S	1443.75	Suevite with light-gray matrix, angular to subangular clasts of siltstone and mudstone to 1 cm, one large clast through all diameter of the core plus a few smaller clasts <1 cm of schist; clasts of polycrystalline quartz with light-gray crystals <2.5 cm; cavities <1 cm; olive green crumbly weathered melt particles <2 cm	Qtz, Kfs, Pl, Ms, Chl, graphite, opaque minerals	Abundant PDFs, up to 3 sets, especially in polycrystalline Qtz, PDFs also in schist, some Qtz grains very toasted and fractured	2, 5
CB6-105 S	1445.8	Suevite with light-gray matrix, angular dark-gray clasts of siltstone to 0.5 cm; large olive green amoeboid melt particle 3.5 cm; light-gray clasts of sandstone <0.7 cm; sample is fractured on the bottom edge	Qtz, feldspar, Ms, Chl, opaque minerals	Decorated PDFs in Qtz, toasted Qtz in single grains or clasts	2
CB6-106 S	1447.0	Suevite with light-gray matrix, subangular clasts of siltstone <2 cm, somewhere with filled parallel cracks, light-gray subangular crystalline clasts <3 cm; subrounded to subangular greenish-gray metasedimentary clasts <1.5 cm; vesicles <1 cm	Qtz, Kfs, Pl, Chl, Ms, Bt, opaque minerals, Ep	PDFs in Qtz, at least 2 sets, toasted Qtz grains	2, 5?
CB6-107 S	1449.8	Suevite with gray matrix, rich in clasts; angular to, subangular, often irregularly shaped clasts of mudstone <2 cm; angular brown clasts, amoeboid <3 cm, sometimes with bands; subrounded clasts of polycrystalline quartz <2 cm; rounded silica-melt clast with clear core and light rim, 2 cm in size	Qtz, feldspar, Ms, Bt, opaque minerals	Toasted Qtz grains, PDFs, ballen Qtz	2, 3, 5
CB6-108 S/I	1451.0	Suevite; very fractured; altered; minor matrix, most clasts deformed; clasts of mudstone <3 cm; dark beige to gray clast (5 cm) with lighter and darker bands; olive green crystals; light-gray to yellowish amoeboid melt particles to 1.5 cm; deformed purple-colored melt particles with residual quartz grains inside; matrix also melted	Qtz, Pl, Bt, opaque minerals	Some very toasted Qtz clasts, ballen Qtz, some decorated PDFs, abundant ballen Qtz	3, 4, all partly melted
CB6-109 S	1452.3	Minor matrix, dark-gray subangular clasts of mudstone to 2 cm, large beige to gray amoeboid clast 4 cm; amoeboid melt particles, elongated to 4 cm with schlieren, yellowish with ochre rim; gray subangular clasts of siltstone up to 0.5 cm in size	Qtz, Kfs, Pl, carbonate, Ms, Bt, opaque minerals, Zrn	Up to 3 sets of PDFs in Qtz, toasted Qtz grains, rare ballen Qtz	2, 3, 5, (1)
CB6-110 S	1455.2	Suevite; minor dark-gray matrix, abundant angular dark-gray clasts of mudstone <2.5 cm, some partly melted; angular beige clasts <1.7 cm; small white clasts <4 mm, white clasts with gray bands <1.5 cm; large clast of graywacke ~6 cm with white, greenish, and gray crystals	Qtz, Pl, Kfs, mica, carbonate, opaque minerals	Qtz with PDFs in graywacke, granite, sandstone clasts, at least 2 sets; toasted Qtz grains	5, 4, 2, interm.#
CB6-111 S	1458.2	Minor matrix, angular to subangular dark-gray clasts of siltstone <3.5 cm; greenish beige clasts of mudstone <1.5 cm, crumbly; light-gray subangular to rounded clasts of granite <3 cm; light-gray clasts of sandstone, subrounded, <1.2 cm; small white subangular clasts of polycrystalline quartz up to 0.4 cm in size	Qtz, Kfs, Pl, carbonate, mica, opaque minerals, Ap, Tur	Abundant PDFs in polycrystalline Qtz, some toasted Qtz grains	2

(*Continued*)

APPENDIX. DETAILED PETROGRAPHIC DESCRIPTIONS OF SAMPLES FROM THE IMPACT BRECCIA SECTION (*Continued*)

Sample and rock type*	Midpoint depth† (m)	Description based on macroscopic and microscopic observations	Mineral composition§	Shock metamorphism	Melt types present
CB6-112 M	1459.2	Clast of conglomerate, 40 cm; white subangular grains <0.5 cm; light-gray subrounded clasts of siltstone <2 cm; dark-gray subrounded clasts of mudstone <1 cm; gray rounded clasts of sandstone; subrounded clast of polycrystalline quartz ~2.5 cm plus similar smaller finer-grained clasts	Qtz, Kfs, Pl, Ms, opaque minerals, carbonate, Ap	Strongly toasted Qtz grains, abundant PDFs, often 2 sets	
CB6-113 S	1464.0	Suevite with gray matrix; dark-gray subangular clasts of mudstone and siltstone <3.5 cm; white to gray subangular clasts of sandstone <1 cm; clasts of graywacke, crystalline clasts; yellowish amoeboid melt particles <1.5 cm; parts of core are fractured	Qtz, Kfs, Ms, Bt, Chl, carbonate, opaque minerals, Tur	PDFs and PF in Qtz, kink banding in mica	2
CB6-114 S	1467.4	Suevite with gray matrix; angular dark-gray clasts of siltstone <3.5 cm with bands; light-gray clasts of graywacke with white sub-mm crystals 5 cm; weathered clayish clasts of various colors (light yellowish, dark gray, dark beige) <0.5 cm; minor subrounded white clasts <3 mm; minor subrounded light-gray clasts <0.5 cm; crystalline clasts occur	Qtz, Kfs, Bt, Ms, carbonate, opaque minerals	PDFs, not decorated	2
CB6-115 S	1473.5	Suevite with greenish gray matrix, upper part fractured beige to gray siltstone; dark-gray subangular clasts of mudstone <2 cm; light-beige clayish clasts <1.5 cm; light-gray clast of graywacke 3 cm	Qtz, Kfs, Ms, Bt, opaque minerals	Kink banding in mica, PDFs not decorated, up to 3 sets	2, melted matrix?
CB6-116 S	1480.8	Suevite with gray matrix; one part consists of gray clasts of schist subangular <2 cm in lighter gray matrix; black angular clast of mudstone 1.2 cm; part weathered, porous, with ochre-colored pigment in abundant vesicles, boundaries of different parts are inclined from horizontal level (about 80 degrees)	Qtz, feldspar, Ms, Chl, opaque minerals	Rare PDFs mostly in larger grains of polycrystalline Qtz	2?
CB6-117 S	1481.7	Suevite with light-gray matrix, fractured and altered; small subangular clasts of mudstone <4 mm; dark-beige to gray angular clasts <1.2 cm; gray subrounded clasts of schist <0.5 cm; amoeboid polycrystalline quartz <2 cm; porous and weathered parts, parts with ochre pigment	Qtz, Kfs, Ms, Chl, Bt, carbonate, Ep, Tur	Abundant PDFs especially in polycrystalline Qtz, at least 2 sets, toasted Qtz grains	2?
CB6-118 S	1484.1	Suevite; angular clasts of sandstone, white with minor gray minerals <2 cm; large light-gray yellowish clasts with tiny fractures filled with darker material <1 cm; darker beige subangular clasts of mudstone <1 cm; large clast of graywacke 5 cm; white greenish crumbly clast 2 cm; weathered cavities, parts with ochre pigment	Qtz, Kfs, mica, carbonate, opaque minerals	Some PDFs (not decorated) in arkose and sandstone clasts	2?
CB6-119 C	1494.0	Cataclasite of gneiss; matrix poor; light-gray matrix, subangular gray clasts <3 cm, fractured; minor white clasts; cavities; minor subangular darker gray clasts, minor ochre spots; white veinlets of carbonate	Qtz, Ms, Chl, opaque minerals, Bt, carbonate	Toasted large single grains of Qtz (with tiny PDFs), some PDFs in large Qtz crystals	
CB6-120 S	1504.3	Suevite with gray matrix; white to gray angular clasts <1 cm; large light-beige clast 4 cm with light rim, weathered; minor angular clasts of mudstone <0.5 cm; clast with white and greenish crystals 1.5 cm; subangular to subrounded clasts of siltstone <2 cm; two dark reddish and beige clasts of mudstone 0.6 and 2.5 cm	Qtz, Ms, Pl, Kfs, Chl, carbonate, opaque minerals, Bt	Toasted Qtz grains with tiny PDFs, PDFs and PFs in Qtz	2
CB6-121 S	1508.5	Suevite, matrix with white and greenish crystals; large beige to yellowish to gray clasts of supposedly siltstone <3.5 cm; gray subangular clasts of siltstone <1.2 cm; clasts of graywacke; crumbly, abundant vesicles	Qtz, Ms, Kfs, Chl, opaque minerals, Tur, Zrn	PDFs in Qtz, toasted Qtz grains	2
CB6-122 C	1511.9	Cataclasite of gneiss, light-gray with darker-gray to greenish fractured clasts; parts with polycrystalline quartz; small fractures filled with carbonate; tiny sulfides in a cavity	Qtz, Chl, carbonate, Ms, Kfs, opaque minerals	Many Qtz grains with PDFs, some PFs	

(*Continued*)

APPENDIX. DETAILED PETROGRAPHIC DESCRIPTIONS OF SAMPLES FROM THE IMPACT BRECCIA SECTION (*Continued*)

Sample and rock type*	Midpoint depth† (m)	Description based on macroscopic and microscopic observations	Mineral composition§	Shock metamorphism	Melt types present
CB6-123 C	1514.3	Cataclasite of mafic rock; greenish gray clasts <5 cm, very fractured; fractures filled with dark greenish minerals; carbonate in form of small white crystals or filling of fractures	Qtz, Kfs, Pl, amphibole (Tr), Chl, Ms, opaque minerals, carbonate	Rare PDFs, Qtz too fine-grained and rare	
CB6-124 C	1516.2	Cataclasite of gneiss; gray clasts up to 3 cm, very fractured; fractures filled with light-gray to greenish minerals	Qtz, Chl, Ms, carbonate, Kfs, opaque minerals	Many Qtz grains with PDFs, some PFs	
CB6-125 M	1522.7	Clast of conglomerate (about 40 cm long in the core); subrounded to rounded clasts of siltstone <4 cm; subrounded white clasts of sandstone <0.5 cm; inclined white vein (about 70 degrees); minor clasts of mudstone to 3 mm	Qtz, Pl, Kfs, Ms, calcite, opaque minerals, Zrn	Most of the Qtz grains shocked, toasted, abundant PDFs, at least 2 sets, some PFs	
CB6-126 S	1529.3	Suevite with gray matrix; large angular clast of sandstone 10 cm, light-gray with white minerals in tiny fractures plus smaller sandstone clasts; angular clasts of mudstone <1.5 cm; subangular white clasts <4 mm; greenish gray crumbly weathered clasts, altered melt particles	Qtz, Kfs, Bt, Ms, Chl, carbonate, Pl, opaque minerals	Tiny PDFs in sandstone and in single Qtz grains	5
CB6-127 S	1535.4	Suevite; gray matrix; subangular darker-gray clasts of siltstone <3 cm; angular to subangular light-gray to white clasts <1.5 cm; large clasts of arkose <5 cm with white and light-gray grains <3 mm; clasts of graywacke	Qtz, Kfs, Ms, Bt, carbonate, opaque minerals, Zrn	Many grains slightly toasted, especially in conglomerate clast, some PDFs	5
CB6-128 L	1536.5	Polymict lithic impact breccia; upper part—massive white and gray quartz, fractured and altered along fractures; middle part—beige clayish material; bottom part—gray matrix, angular gray clasts <1.5 cm, deformed white clasts <0.5 cm	Qtz, Kfs, Pl, Ms, Bt, Chl, carbonate, opaque minerals, Tur	PDFs in Qtz	
CB6-129 C	1542.7	Cataclastic schist/gneiss, gray clasts <0.8 cm, deformed, mylonitic structure, narrow white bands, inclined layering (about 45 degrees), graphitic	Qtz, Chl, Ms, Bt, opaque minerals, garnet	No shock effects, Qtz too fine-grained and not abundant	
CB6-130 C	1547.4	Cataclastic schist/gneiss, light greenish gray schist, highly deformed, with white quartz veins; minor sulfides (ochre rim) in veins, in upper part inclined layering (45 degrees); small bottom part—gray matrix with angular white and gray clasts to 0.5 cm	Qtz, Ms, Chl, carbonate, Ep, opaque minerals	Some PFs and PDFs in veins, decorated, some toasted Qtz grains	
KB-2 I	1402.9	Impact melt rock, clast-rich with dark-gray melt matrix; some larger clasts of sandstone; small quartz clasts; other small partly melted clasts; abundant flow textures	Qtz, feldspar, opaque minerals, laths of pyroxene	PDFs in Qtz, at least 2 sets, but generally not much shocked and only slightly toasted	4,3, rare 2
KB-3 I	1404.4	Impact melt rock, dark-gray melt matrix, some larger clasts—schist, sandstone, quartz; small clasts of fine-grained sediments; most clasts partly melted; some small (mm-sized) altered olive-green melt particles; abundant flow structures	Qtz, Bt, feldspar, clay minerals, opaque minerals	PDFs in Qtz, at least 2 sets, Qtz slightly toasted, similar to KB2, but more shocked	4/2 transitions between, 3

(*Continued*)

APPENDIX. DETAILED PETROGRAPHIC DESCRIPTIONS OF SAMPLES FROM THE IMPACT BRECCIA SECTION (*Continued*)

Sample and rock type*	Midpoint depth† (m)	Description based on macroscopic and microscopic observations	Mineral composition§	Shock metamorphism	Melt types present
KB-4 I	1405.7	Impact melt rock, dark-gray melt matrix, clasts are only small and all are partly melted, some clasts of dark-gray fine sediments; sandstone clasts; abundant flow textures in melt matrix	Qtz, feldspar, Bt, opaque minerals, laths of pyroxene	PDFs in Qtz, slightly toasted, ballen Qtz	4, 3, 5?
KB-5 S	1412.9	Suevite with light-gray particulate matrix, clasts are small (<2 cm), abundant dark-gray sedimentary clasts—siltstone, mudstone; clasts of schist, clast of granite, very abundant small (~0.5 cm) yellowish melt particles, similar to sample CB6-097	Qtz, Ms, Bt, Kfs, Pl, Chl, opaque minerals	PDFs in Qtz, some slightly toasted, abundant in polycrystalline Qtz	1, 2
KB-6 M	1468.7	Conglomerate clast (40 cm), large clasts (5 cm) of mostly sandstone, some crosscutting quartz veins, opaque minerals (rutile, ilmenite) in veins and fractures, clasts of granite, all fractured (possibly pre-impact fracturing)	Qtz, Pl, Kfs, opaque minerals (rutile, ilmenite), Chl	Qtz grains very toasted, abundant PDFs in Qtz	

*S—suevite, I—impact melt rock, L—polymict lithic impact breccia, C—cataclasite, M—conglomerate.
†Depths are corrected values (L. Edwards, U.S. Geological Survey, 2007, personal commun.).
§Qtz—quartz, Kfs—K-feldspar, Pl—plagioclase, Ms—muscovite, Bt—biotite, Chl—chlorite, Tur—tourmaline, Tr—tremolite, Zrn—zircon, Ep—epidote (Kretz, 1983). Minerals are listed in order of abundance, which is only estimated from the microscopic observations.
#interm.—melt type intermediate between type 1 and 2.

REFERENCES CITED

Bartosova, K., Ferrière, L., Koeberl, C., Reimold, W.U., Gibson, R., and Schmitt, R.T., 2007a, Lithological, petrographical, and geochemical investigations of suevite from the Eyreville core, Chesapeake Bay impact structure: Geological Society of America Abstracts with Programs, v. 39, no. 6, p. 451.

Bartosova, K., Ferrière, L., Koeberl, C., and Reimold, W.U., 2007b, Investigations of melt particles in suevite from the Eyreville B core, Chesapeake Bay impact structure: Geological Society of America Abstracts with Programs, v. 39, no. 6, p. 314.

Bartosova, K., Koeberl, C., Schmitt, R.T., Reimold, W.U., and Ferrière, L., 2008, A petrographical, geochemical, and shock metamorphic study of suevite from the Eyreville drill core, Chesapeake Bay impact structure, USA: Houston, Texas, Lunar and Planetary Science, v. 39, abstract no. 1065 (CD-ROM).

Bartosova, K., Mader, D., Schmitt., R.T., Ferrière L., Koeberl, C., Reimold, W.U., and Brandstaetter, F., 2009, this volume, Geochemistry of the impact breccia section of the Eyreville drill core, Chesapeake Bay impact structure, USA, *in* Gohn, G.S., Koeberl, C., Miller, K.G., and Reimold, W.U., eds., The ICDP-USGS Deep Drilling Project in the Chesapeake Bay Impact Structure: Results from the Eyreville Core Holes: Geological Society of America Special Paper 458, doi: 10.1130/2009.2458(18).

Brodie, K., Fettes, D., and Harte, B., 2007, Structural terms including fault rock terms, Chapter 2.3, *in* Fettes, D., and Desmons, J., eds., Metamorphic Rocks: A Classification and Glossary of Terms; Recommendations of the International Union of Geological Sciences: Cambridge, UK, Cambridge University Press, p. 24–31, 111–125, and 126–242.

Chipera, S.J., and Apps, J.A., 2001, Geochemical stability of natural zeolites, *in* Bish, D.L., and Ming, D.W., eds., Natural Zeolites: Occurrence, Properties, Applications: Reviews in Mineralogy and Geochemistry, v. 45, p. 117–161.

Claeys, P., Heuschkel, S., Lounejeva-Baturina, E., Sanchez-Rubio, G., and Stöffler, D., 2003, The suevite of drill hole Yucatàn 6 in the Chicxulub impact crater: Meteoritics & Planetary Science, v. 38, p. 1299–1317.

Collins, G.S., and Wünnemann, K., 2005, How big was the Chesapeake Bay impact?: Insight from numerical modeling: Geology, v. 33, p. 925–928, doi: 10.1130/G21854.1.

Deutsch, A., and Koeberl, C., 2006, Establishing the link between the Chesapeake Bay impact structure and the North American tektite strewn field: The Sr-Nd isotopic evidence: Meteoritics & Planetary Science, v. 41, p. 689–703.

Dypvik, H., and Jansa, J.F., 2003, Sedimentary signatures and processes during marine bolide impacts: A review: Sedimentary Geology, v. 161, p. 309–337, doi: 10.1016/S0037-0738(03)00135-0.

Edwards, L.E., Powars, D.S., Gohn, G.S., and Dypvik, H., 2009, this volume, Chapter 3, Geologic columns for the ICDP-USGS Eyreville A and B cores, Chesapeake Bay impact structure: Sediment breccias, 444 to 1096 m depth, *in* Gohn, G.S., Koeberl, C., Miller, K.G., and Reimold, W.U., eds., The ICDP-USGS Deep Drilling Project in the Chesapeake Bay Impact Structure: Results from the Eyreville Core Holes: Geological Society of America Special Paper 458, doi: 10.1130/2009.2458(03).

Edwards, L.E., Powars, D.S., Browning, J.V., McLaughlin, P.P., Jr., Miller, K.G., Self-Trail, J.M., Kulpecz, A.A., and Elbra, T., 2009, this volume, Chapter 4, Geologic columns for the ICDP-USGS Eyreville A and C core holes, Chesapeake Bay impact structure: Postimpact sediments, 0 to 444 m depth, *in* Gohn, G.S., Koeberl, C., Miller, K.G., and Reimold, W.U., eds., The ICDP-USGS Deep Drilling Project in the Chesapeake Bay Impact Structure: Results from the Eyreville Core Holes: Geological Society of America Special Paper 458, doi: 10.1130/2009.2458(04).

Ferrell, R.E., Jr., and Dypvik, H., 2009, this volume, The mineralogy of the Exmore–Chickahominy boundary section of the Chesapeake Bay impact structure—The Eyreville core, *in* Gohn, G.S., Koeberl, C., Miller, K.G., and Reimold, W.U., eds., The ICDP-USGS Deep Drilling Project in the Chesapeake Bay Impact Structure: Results from the Eyreville Core Holes: Geological Society of America Special Paper 458, doi: 10.1130/2009.2458(31).

Ferrière, L., Koeberl, C., Reimold, W.U., Hecht, L., and Bartosova K., 2009a, The origin of "toasted" quartz in impactites revisited: Lunar and Planetary Science, v. 40, abstract no. 1751 (CD-ROM).

Ferrière, L., Koeberl, C., and Reimold, W.U., 2009b, Characterization of ballen quartz and cristobalite in impact breccias: New observations and constraints on ballen formation: European Journal of Mineralogy, v. 21, p. 203–217, doi: 10.1127/0935-1221/2009/0021-1898.

French, B.M., 1998, Traces of Catastrophe: A Handbook of Shock-Metamorphic Effects in Terrestrial Meteorite Impact Structures: Lunar and Planetary Institute Contribution 954, 120 p.

Gohn, G.S., Clark, A.C., Queen, D.G., Levine, J.S., McFarland, E.R., and Powars, D.S., 2001, Operational and Geological Summary for the USGS-NASA Langley Corehole, Hampton, Virginia: U.S. Geological Survey Open-File Report 01-87, 19 p.

Gohn, G.S., Powars, D.S., Bruce, T.S., and Self-Trail, J.M., 2005, Physical geology of the impact-modified and impact-generated sediments in the USGS-NASA Langley core, Hampton, Virginia, *in* Horton, J.W., Jr., Powars, D.S., and Gohn, G.S., eds., Studies of the Chesapeake Bay Impact Structure—The USGS-NASA Langley Corehole, Hampton, Virginia, and Related Coreholes and Geophysical Surveys: U.S. Geological Survey Professional Paper 1688, p. C1–C38.

Gohn, G.S., Koeberl, C., Miller, K.G., Reimold, W.U., Browning, J.V., Cockell, C.S., Dypvik, H., Edwards, L.E., Horton, J.W., Jr., McLaughlin, P.P., Jr., Ormö, J., Plescia, J.B., Powars, D.S., Sanford, W.E., Self-Trail, J.M., and Voytek, M.A., 2006a, Preliminary site report for the 2005 ICDP-USGS deep corehole in the Chesapeake Bay impact crater: Houston, Texas, Lunar and Planetary Science, v. 37, abstract no. 1713 (CD-ROM).

Gohn, G.S., Koeberl, C., Miller, K.G., Reimold, W.U., Cockell, C.S., Horton, J.W., Jr., Sanford, W.E., and Voytek, M.A., 2006b, Chesapeake Bay impact structure drilled: Eos (Transactions, American Geophysical Union), v. 87, no. 35, p. 349–355, doi: 10.1029/2006EO350001.

Gohn, G.S., Koeberl, C., Miller, K.G., Reimold, W.U., and the Scientific Staff of the Chesapeake Bay Impact Structure Drilling Project, 2006c, Chesapeake Bay impact structure deep drilling project completes coring: Scientific Drilling, no. 3, p. 34–37.

Gohn, G.S., Sanford, W.E., Powars, D.S., Horton, J.W., Jr., Edwards, L.E., Morin, R.H., and Self-Trail, J.M., 2007, Site Report for USGS Test Holes Drilled at Cape Charles, Northampton County, Virginia, in 2004: U.S. Geological Survey Open-File Report 2007-1094, 22 p.

Gohn, G.S., Powars, D.S., Dypvik, H., and Edwards, L.E., 2009, this volume, Rock-avalanche and ocean-resurge deposits in the late Eocene Chesapeake Bay impact structure: Evidence from the ICDP-USGS Eyreville cores, Virginia, USA, *in* Gohn, G.S., Koeberl, C., Miller, K.G., and Reimold, W.U., eds., The ICDP-USGS Deep Drilling Project in the Chesapeake Bay Impact Structure: Results from the Eyreville Core Holes: Geological Society of America Special Paper 458, doi: 10.1130/2009.2458(26).

Grieve, R.A.F., Langenhorst, F., and Stöffler, D., 1996, Shock metamorphism of quartz in nature and experiment: II. Significance in geoscience: Meteoritics & Planetary Science, v. 31, p. 6–35.

Horton, J.W., Jr., and Izett, G.A., 2005, Crystalline-rock ejecta and shocked minerals of the Chesapeake Bay impact structure, USGS-NASA Langley core, Hampton, Virginia, with supplemental constraints on the age of impact, *in* Horton, J.W., Jr., Powars, D.S., and Gohn, G.S., eds., Studies of the Chesapeake Bay Impact Structure–The USGS-NASA Langley Corehole, Hampton, Virginia, and Related Coreholes and Geophysical Surveys: U.S. Geological Survey Professional Paper 1688, p. E1–E30.

Horton, J.W., Jr., Aleinikoff, J.N., Kunk, M.J., Gohn, G.S., Edwards, L.E., Self-Trail, J.M., Powars, D.S., and Izett, G.A., 2005a, Recent research on the Chesapeake Bay impact structure, USA—Impact debris and reworked ejecta, *in* Kenkmann, T., Hörz, F., and Deutsch, A., eds., Large Meteorite Impacts III: Geological Society of America Special Paper 384, p. 147–170.

Horton, J.W., Jr., Gohn, G.S., Jackson, J.C., Aleinikoff, J.N., Sanford, W.E., Edwards, L.E., and Powars, D.S., 2005b, Results from a scientific test hole in the central uplift, Chesapeake Bay impact structure, Virginia, USA: Houston, Texas, Lunar and Planetary Science, v. 36, abstract no. 2003 (CD-ROM).

Horton, J.W., Jr., Powars, D.S., and Gohn, G.S., 2005c, Studies of the Chesapeake Bay Impact Structure—Introduction and discussion, *in* Horton, J.W., Jr., Powars, D.S., and Gohn, G.S., eds., Studies of the Chesapeake Bay Impact Structure–The USGS-NASA Langley Corehole, Hampton, Virginia, and Related Coreholes and Geophysical Surveys: U.S. Geological Survey Professional Paper 1688, p. A1–A24.

Horton, J.W., Jr., Vanko, D.A., Naeser, C.W., Naeser, N.D., Larsen, D., Jackson, J.C., and Belkin, H.E., 2006, Postimpact hydrothermal conditions at the central uplift, Chesapeake Bay impact structure, Virginia, USA: Lunar and Planetary Science, v. 37, abstract no. 1842 (CD-ROM).

Horton, J.W., Jr., Gohn, G.S., Powars, D.S., and Edwards, L.E., 2008, Origin and emplacement of impactites in the Chesapeake Bay impactite structure, Virginia, USA, *in* Evans, K.R., Horton, J.W., Jr., King, D.T., Jr., and Morrow, J.R., eds., The Sedimentary Record of Meteorite Impacts: Geological Society of America Special Paper 437, p. 73–97.

Horton, J.W., Jr., Gibson, R.L., Reimold, W.U., Wittmann, A., Gohn, G.S., and Edwards, L.E., 2009, this volume, Geologic column for the ICDP-USGS Eyreville B core, Chesapeake Bay impact structure: Impactites and crystalline rocks, 1096–1766 m, *in* Gohn, G.S., Koeberl, C., Miller, K.G., and Reimold, W.U., eds., The ICDP-USGS Deep Drilling Project in the Chesapeake Bay Impact Structure: Results from the Eyreville Core Holes: Geological Society of America Special Paper 458, doi: 10.1130/2009.2458(02).

Huffman, A.R., and Reimold, W.U., 1996, Experimental constraints on shock-induced microstructures in naturally deformed silicates: Tectonophysics, v. 256, p. 165–217, doi: 10.1016/0040-1951(95)00162-X.

JCPDS (Joint Committee on Powder Diffraction Standards), 1980, Mineral Powder Diffraction File-Data Book: Joint Committee on Powder Diffraction Standards, International Centre for Diffraction Data.

Jolly, L.C., Gibson, R.L., Reimold, W.U., and Horton, J.W., Jr., 2008, Clast characteristics in the suevitic and lithic breccias from the ICDP-USGS Eyreville B drill core, Chesapeake Bay impact structure, Virginia, USA, *in* Large Meteorite Impacts and Planetary Evolution IV, Conference program & abstract volume: Houston, Texas, Lunar and Planetary Institute Contribution no. 1423, p. 105–106.

Kenkmann, T., Collins, G.S., Wittmann, A., Wünnemann, K., Reimold, W.U., and Melosh, J.H., 2009, this volume, A model for the formation of the Chesapeake Bay impact crater as revealed by drilling and numerical simulation, *in* Gohn, G.S., Koeberl, C., Miller, K.G., and Reimold, W.U., eds., The ICDP-USGS Deep Drilling Project in the Chesapeake Bay Impact Structure: Results from the Eyreville Core Holes: Geological Society of America Special Paper 458, doi: 10.1130/2009.2458(25).

Koeberl, C., 1989, New estimates of area and mass for the North American tektite strewn field, *in* Proceedings of the 19th Lunar and Planetary Science Conference: New York, Cambridge University Press, p. 745–751.

Koeberl, C., Poag, C.W., Reimold, W.U., and Brandt, D., 1996, Impact origin of the Chesapeake Bay structure and the source of the North American tektites: Science, v. 271, p. 1263–1266, doi: 10.1126/science.271.5253.1263.

Koeberl, C., Reimold, W.U., Gohn, G.S., and Miller, K.G., 2007, The 2005/2006 ICDP-USGS deep drilling project near the center of the Chesapeake Bay impact structure, Virginia, USA: A 2007 update: Houston, Texas, Lunar and Planetary Science, v. 38, abstract no. 1206 (CD-ROM).

Kretz, R., 1983, Symbols for rock-forming minerals: The American Mineralogist, v. 68, p. 277–279.

Kring, D.A., 2005, Hypervelocity collisions into continental crust composed of sediments and an underlying crystalline basement: Comparing the Ries (~24 km) and Chicxulub (~180 km) impact craters: Chemie der Erde, v. 65, p. 1–46, doi: 10.1016/j.chemer.2004.10.003.

Kring, D.A., Hörz, F., Zurcher, L., and Urrutia Fucugauchi, J., 2004, Impact lithologies and their emplacement in the Chicxulub impact crater: Initial results from the Chicxulub Scientific Drilling Project, Yaxcopoil, Mexico: Meteoritics & Planetary Science, v. 39, p. 879–897.

Lee, S.R., Horton, J.W., Jr., and Walker, R.J., 2005, Osmium-isotope and platinum-group-element systematics of impact-melt rocks, Chesapeake Bay impact structure, Virginia, USA: Houston, Texas, Lunar and Planetary Science, v. 36, abstract no. 1700 (CD-ROM).

Lee, S.R., Horton, J.W., Jr., and Walker, R.J., 2006, Confirmation of a meteoritic component in impact-melt rocks of the Chesapeake Bay impact structure, Virginia, USA—Evidence from osmium isotopic and PGE systematics: Meteoritics & Planetary Science, v. 41, p. 819–833.

Leroux, H., 2005, Weathering features in shocked quartz from the Ries impact crater, Germany: Meteoritics & Planetary Science, v. 40, p. 1347–1352.

Leroux, H., Reimold, W.U., and Doukhan, J.-C., 1994, A TEM investigation of shock metamorphism in quartz from the Vredefort Dome, South Africa: Tectonophysics, v. 230, p. 223–239, doi: 10.1016/0040-1951(94)90137-6.

Lindström, M., Shuvalov, V., and Ivanov, B., 2005, Lockne crater as a result of marine-target oblique impact: Planetary and Space Science, v. 53, p. 803–815, doi: 10.1016/j.pss.2005.02.005.

McDonald, I., Bartosova, K., and Koeberl, C., 2009, this volume, Search for a meteoritic component in impact breccia from the Eyreville core, Chesapeake Bay impact structure: Considerations from platinum group element contents, *in* Gohn, G.S., Koeberl, C., Miller, K.G., and Reimold, W.U., eds., The ICDP-USGS Deep Drilling Project in the Chesapeake Bay Impact Structure: Results from the Eyreville Core Holes: Geological Society of America Special Paper 458, doi: 10.1130/2009.2458(21).

Melosh, H.J., 1989, Impact Cratering—A Geological Process: New York, Oxford University Press, 245 p.

Moore, D.M., and Reynolds, R.C., Jr., 1997, X-Ray Diffraction and the Identification and Analysis of Clay Minerals: Oxford, UK, Oxford University Press, 378 p.

Naumov, M.V., 2002, Impact-generated hydrothermal systems: Data from Popigai, Kara, and Puchezh-Katunki impact structures in meteorite impacts *in* Plado, J., and Pesonen, L., eds., Precambrian Shields, Impact Studies Volume 2: Heidelberg-Berlin, Springer, p. 117–172.

Naumov, M.V., 2005, Principal features of impact-generated hydrothermal circulation systems: Mineralogical and geochemical evidence: Geofluids, v. 5, p. 165–184, doi: 10.1111/j.1468-8123.2005.00092.x.

Osinski, G.R., 2003, Impact glasses in fallout suevites from the Ries impact structure, Germany: An analytical SEM study: Meteoritics & Planetary Science, v. 38, p. 1641–1667.

Osinski, G.R., 2005, Hydrothermal activity associated with the Ries impact event, Germany: Geofluids, v. 5, p. 202–220, doi: 10.1111/j.1468-8123.2005.00119.x.

Osinski, G.R., Grieve, R.A.F., and Spray, J.G., 2004, The nature of the groundmass of surficial suevite from the Ries impact structure, Germany, and constraints on its origin: Meteoritics & Planetary Science, v. 39, p. 1655–1683.

Poag, C.W., 1997, The Chesapeake Bay bolide impact: A convulsive event in Atlantic Coastal Plain evolution: Sedimentary Geology, v. 108, p. 45–90, doi: 10.1016/S0037-0738(96)00048-6.

Poag, C.W., Powars, D.S., Poppe, L.J., Mixon, R.B., Edwards, L.E., Folger, D.W., and Bruce, S., 1992, Deep Sea Drilling Project Site 612 bolide event: New evidence of a late Eocene impact-wave deposit and a possible impact site, U.S. east coast: Geology, v. 20, p. 771–774, doi: 10.1130/0091-7613(1992)020<0771:DSDPSB>2.3.CO;2.

Poag, C.W., Powars, D.S., Poppe, L.J., and Mixon, R.B., 1994, Meteoroid mayhem in Ole Virginny—Source of the North American tektite strewn field: Geology, v. 22, p. 691–694, doi: 10.1130/0091-7613(1994)022<0691:MMIOVS>2.3.CO;2.

Poag, C.W., Hutchinson, D.R., Colman, S.M., and Lee, M.W., 1999, Seismic expression of the Chesapeake Bay impact crater: Structural and morphologic refinements based on new seismic data, *in* Dressler, B.O., and Sharpton, V.L., eds., Large Meteorite Impacts and Planetary Evolution II: Geological Society of America Special Paper 339, p. 149–164.

Poag, C.W., Plecsia, J.B., and Molzer, P.C., 2002, Ancient impact structures on modern continental shelves: The Chesapeake Bay, Montagnais, and Toms Canyon craters, Atlantic margin of North America: Deep-Sea Research–Part II. Topical Studies in Oceanography, v. 49, p. 1081–1102, doi: 10.1016/S0967-0645(01)00144-8.

Poag, C.W., Koeberl, C., and Reimold, W.U., 2004, The Chesapeake Bay Crater: Geology and Geophysics of a Late Eocene Submarine Impact Structure; Impact Studies: Heidelberg, Springer, 522 p.

Reimold, W.U., and Koeberl, C., 2008, Catastrophes, extinctions and evolution: 50 years of impact cratering studies, *in* Gupta, H., and Fareeduddin, F., eds., Recent Advances in Earth System Sciences: Geological Society of India Memoir 66, p. 69–110.

Reimold, W.U., Kenkmann, T., Gibson, R.L., Bartosova, K., Schmitt, R.T., Hecht, L., Koeberl, C., and Horton, J.W., Jr., 2007, Dike breccias in the deep basement-derived section of the Eyreville B core, Chesapeake Bay impact structure: Geological Society of America Abstracts with Programs, v. 39, no. 6, p. 451.

Reimold, W.U., Bartosova, K., Schmitt, R.T., Hansen, B., Crasselt, C., Koeberl, C., Wittmann, A., and Powars, D., 2009, this volume, Petrographic observations on the Exmore breccia, ICDP-USGS drilling at Eyreville, Chesapeake Bay impact structure, USA, *in* Gohn, G.S., Koeberl, C., Miller, K.G., and Reimold, W.U., eds., The ICDP-USGS Deep Drilling Project in the Chesapeake Bay Impact Structure: Results from the Eyreville Core Holes: Geological Society of America Special Paper 458, doi: 10.1130/2009.2458(29).

Robertson, P.B., and Grieve, R.A.F., 1977, Shock attenuation at terrestrial impact structures, *in* Roddy, D.J., Pepin, R.O., and Merrill, R.B, eds., Impact and Explosion Cratering: New York, Pergamon Press, p. 687–702.

Shah, A.K., Brozena, J., Vogt, P., Daniels, D., and Plescia, J., 2005, New surveys of the Chesapeake Bay impact structure suggest melt pockets and target-structure effect: Geology, v. 33, p. 417–420, doi: 10.1130/G21213.1.

Shah, A.K., Daniels, D.L., Kontny, A., and Brozena, J.M., 2009, this volume, Megablocks and melt pockets in the Chesapeake Bay impact structure constrained using magnetic field measurements and properties of the Eyreville and Cape Charles cores, *in* Gohn, G.S., Koeberl, C., Miller, K.G., and Reimold, W.U., eds., The ICDP-USGS Deep Drilling Project in the Chesapeake Bay Impact Structure: Results from the Eyreville Core Holes: Geological Society of America Special Paper 458, doi: 10.1130/2009.2458(10).

Short, N.M., and Gold, D.P., 1996, Petrography of shocked rocks from the central peak at the Manson impact structure, *in* Koeberl, C., and Anderson, R.R., eds., The Manson Impact Structure, Iowa; Anatomy of an Impact Crater: Geological Society of America Special Paper 302, p. 245–265.

Stöffler, D., 1971, Progressive metamorphism and classification of shocked and brecciated crystalline rocks at impact craters: Journal of Geophysical Research, v. 76, p. 5541–5551, doi: 10.1029/JB076i023p05541.

Stöffler, D., and Grieve, R.A.F., 2007, Impactites, Chapter 2.11, *in* Fettes, D., and Desmons, J., eds., Metamorphic Rocks: A Classification and Glossary of Terms; Recommendations of the International Union of Geological Sciences: Cambridge, UK, Cambridge University Press, p. 82–92, 111–125, and 126–242.

Stöffler, D., and Langenhorst, F., 1994, Shock metamorphism of quartz in nature and experiment: I. Basic observation and theory: Meteoritics, v. 29, p. 155–181.

Stöffler, D., Artemieva, N.A., Ivanov, B., Hecht, L., Kenkmann, T., Schmitt, R.T., Tagle, R.A., and Wittmann, A., 2004, Origin and emplacement of the impact formations at Chicxulub, Mexico, as revealed by the ICDP deep drilling at Yaxcopoil-1 and by numerical modeling: Meteoritics & Planetary Science, v. 39, p. 1035–1067.

Thein, J., 1987, A tektite layer in Upper Eocene sediments of the New Jersey continental slope (Site 612, Leg 95), *in* Poag, C.W., Watts, A.B., et al., Initial Reports of the Deep Sea Drilling Project, Leg 95: Washington, D.C., U.S. Government Printing Office, p. 565–579.

Thomas, W.A., Chowns, T.M., Daniels, D.L., Neathery, T.L., Glower, L., III, and Gleason, R.J., 1989, The subsurface Appalachians beneath the Atlantic and Gulf coastal plains, *in* Hatcher, R.D., Jr., Thomas, W.A., and Viele, G.W., eds., The Appalachian-Ouachita Orogen in the United States: Boulder, Colorado, Geological Society of America, Geology of North America, v. F2, p. 445–458.

Townsend, G.N., Gibson, R.L., Horton, J.W., Jr., Reimold, W.U., Schmitt, R.-T., and Bartosova, K., 2009, this volume, Petrographic and geochemical comparisons between the lower crystalline basement-derived section and the granite megablock and amphibolite megablock of the Eyreville B core, Chesapeake Bay impact structure, USA, *in* Gohn, G.S., Koeberl, C., Miller, K.G., and Reimold, W.U., eds., The ICDP-USGS Deep Drilling Project in the Chesapeake Bay Impact Structure: Results from the Eyreville Core Holes: Geological Society of America Special Paper 458, doi: 10.1130/2009.2458(13).

von Engelhardt, W., 1972, Shock produced rock glasses from the Ries crater: Contributions to Mineralogy and Petrology, v. 36, p. 265–292, doi: 10.1007/BF00444336.

von Engelhardt, W., 1997, Suevite breccia of the Ries impact crater, Germany: Petrography, chemistry and shock metamorphism of crystalline rock clasts: Meteoritics & Planetary Science, v. 32, p. 545–554.

von Engelhardt, W., and Graup, G., 1984, Suevite of the Ries crater, Germany: Source rocks and implications for cratering mechanics: Geologische Rundschau, v. 73, p. 447–481.

Whitehead, J., Spray, J.G., and Grieve, R.A.F., 2002, Origin of "toasted" quartz in terrestrial impact structures: Geology, v. 30, p. 431–434, doi: 10.1130/0091-7613(2002)030<0431:OOTQIT>2.0.CO;2.

Wirth, R., 2004, Focused ion beam (FIB): A novel technology for advanced application of micro- and nanoanalysis in geosciences and applied mineralogy: European Journal of Mineralogy, v. 16, p. 863–876, doi: 10.1127/0935-1221/2004/0016-0863.

Wittmann, A., Reimold, W.U., Hansen, B., and Kenkmann, T., 2008, Petrography of the suevite-like depth interval (1397–1550 m) in drill core Eyreville-B, Chesapeake Bay impact structure, USA: Houston, Texas, Lunar and Planetary Science, v. 39, abstract no. 2435 (CD-ROM).

Wittmann, A., Schmitt, R.T., Hecht, L., Kring, D.A., and Povenmire, H., 2009a, this volume, Chapter 16, Petrology of impact melt rocks from the Chesapeake Bay crater, USA, *in* Gohn, G.S., Koeberl, C., Miller, K.G., and Reimold, W.U., eds., The ICDP-USGS Deep Drilling Project in the Chesapeake Bay Impact Structure: Results from the Eyreville Core Holes: Geological Society of America Special Paper 458, doi: 10.1130/2009.2458(16).

Wittmann, A., Reimold, W.U., Schmitt, R.T., Hecht, L., and Kenkmann, T., 2009, this volume, Chapter 17, The record of ground zero in the Chesapeake Bay impact crater—Suevites and related rocks, *in* Gohn, G.S., Koeberl, C., Miller, K.G., and Reimold, W.U., eds., The ICDP-USGS Deep Drilling Project in the Chesapeake Bay Impact Structure: Results from the Eyreville Core Holes: Geological Society of America Special Paper 458, doi: 10.1130/2009.2458(17).

Manuscript Accepted by the Society 3 March 2009

Printed in the USA

The Geological Society of America
Special Paper 458
2009

Geochemistry of the impact breccia section (1397–1551 m depth) of the Eyreville drill core, Chesapeake Bay impact structure, USA

Katerina Bartosova*
Dieter Mader
Department of Lithospheric Research, University of Vienna, Althanstrasse 14, A-1090 Vienna, Austria

Ralf Thomas Schmitt
Museum für Naturkunde–Leibniz Institute at Humboldt University Berlin, Invalidenstrasse 43, 10115 Berlin, Germany

Ludovic Ferrière
Department of Lithospheric Research, University of Vienna, Althanstrasse 14, A-1090 Vienna, Austria, and
Department of Earth Science, University of Western Ontario, 1151 Richmond Street, London, ON, N6A 5B7, Canada

Christian Koeberl
Department of Lithospheric Research, University of Vienna, Althanstrasse 14, A-1090 Vienna, Austria

Wolf Uwe Reimold
Museum für Naturkunde–Leibniz Institute at Humboldt University Berlin, Invalidenstrasse 43, 10115 Berlin, Germany

Franz Brandstätter
Natural History Museum, Burgring 7, A-1010 Vienna, Austria

ABSTRACT

The Chesapeake Bay impact structure, which is 85 km in diameter and 35.5 Ma old, was drilled and cored in a joint International Continental Scientific Drilling Program (ICDP) and U.S. Geological Survey (USGS) drilling project at Eyreville Farm, Virginia, U.S.A. In the Eyreville drill core, 154 m of impact breccia were recovered from the depth interval 1397–1551 m. Major- and trace-element concentrations were determined in 75 polymict impactite samples, 10 samples of cataclastic gneiss blocks, and 24 clasts from impactites. The chemical composition of the polymict impactites does not vary much in the upper part of the section (above ~1450 m), whereas in the lower part, larger differences occur. Polymict impactites show a decrease of SiO_2 content, and slight increases of TiO_2, Al_2O_3, and Fe_2O_3 abundances, with depth. This is in agreement with an increase of the schist/gneiss component with depth. Concentrations of siderophile elements (Co, Ni) are lower in the polymict impactites than in the

*katerina.bartosova@univie.ac.at

Bartosova, K., Mader, D., Schmitt, R.T., Ferrière, L., Koeberl, C., Reimold, W.U., and Brandstätter, F., 2009, Geochemistry of the impact breccia section (1397–1551 m depth) of the Eyreville drill core, Chesapeake Bay impact structure, USA, *in* Gohn, G.S., Koeberl, C., Miller, K.G., and Reimold, W.U., eds., The ICDP-USGS Deep Drilling Project in the Chesapeake Bay Impact Structure: Results from the Eyreville Core Holes: Geological Society of America Special Paper 458, p. 397–433, doi: 10.1130/2009.2458(18).

basement-derived schists and do not indicate the presence of an extraterrestrial component. The five petrographically determined types of melt particles, i.e., clear glass, altered melt, recrystallized silica melt, melt with microlites, and dark-brown melt, have distinct chemical compositions. Mixing calculations of the proportions of rocks involved in the formation of various polymict impactites and melt particles were carried out using the Harmonic least-squares MiXing (HMX) calculation program. The calculations suggest that the metamorphic basement rocks (i.e., gneiss and schist) constitute the main component of the polymict impactites, together with significant sedimentary and possible minor pegmatite/granite and amphibolite components. The sedimentary component is derived mostly from a sediment characterized by a composition similar to that of the Cretaceous Potomac Formation. Compositions of the melt particles were modeled as mixtures of target rocks or major rock-forming minerals. However, the results of the mixing calculations for the melt particles are not satisfactory, and the composition of the particles could have been modified by hydrothermal alteration. Carbon isotope ratios were determined for 18 samples. The results imply a hydrothermal origin for the carbonate veins from the basement-derived core section; carbon-rich sedimentary clasts from the Exmore breccia and suevite have a $\delta^{13}C$ range typical for organic matter in sediments.

INTRODUCTION

The late Eocene Chesapeake Bay impact structure, with a diameter of 85 km, is one of the largest and best-preserved impact structures on Earth (e.g., Poag et al., 1994, 2004; Koeberl et al., 1996; Gohn et al., 2006a). The structure was discovered by analyses of seismic profiles, followed by studies of core samples of the informally named Exmore breccia (Poag et al., 1994). The formation of this structure as a consequence of an impact event was confirmed by Koeberl et al. (1996) from the presence of shocked minerals within the crater fill. Based on geographic position, age, and chemical and isotopic data, previous studies led to the conclusion that the Chesapeake Bay impact structure is the likely source of the North American tektites (Koeberl et al., 1996; Deutsch and Koeberl, 2006).

Suevite was first found in the Chesapeake Bay impact structure at the bottom of the 2004 Sustainable Technology Park (STP) test hole (Gohn et al., 2007; Fig. 1), located at Cape Charles near the center of the impact structure. In 2005, ~154 m of impact breccia were recovered in the International Continental Scientific Drilling Program (ICDP)–U.S. Geological Survey (USGS) Eyreville drill core in the 1397.2–1551.2 m depth interval (Figs. 1 and 2A), within the deep crater moat, a few kilometers to the north of the Cape Charles drill site. At Eyreville, the downhole crater fill consists of postimpact sediments, clastic breccias and sedimentary megablocks (i.e., Exmore beds, interpreted as resurge breccia [Poag et al., 1992; Reimold et al., this volume], and avalanche deposits [Gohn et al., this volume]), a large granitic megablock and a smaller amphibolitic block intercalated with gravelly sand, polymict impact breccia with cataclastic gneiss blocks, and pegmatite/granite and mica schist derived from the crystalline basement (Fig. 2A; Gohn et al., 2006a, 2006b, 2008, this volume).

Previous Geochemical Studies and Dating of the Chesapeake Bay Impact Structure

Samples of impactites from the Chesapeake Bay impact structure are available from various drill cores. Poag et al. (2004) published major- and trace-element contents for a large suite

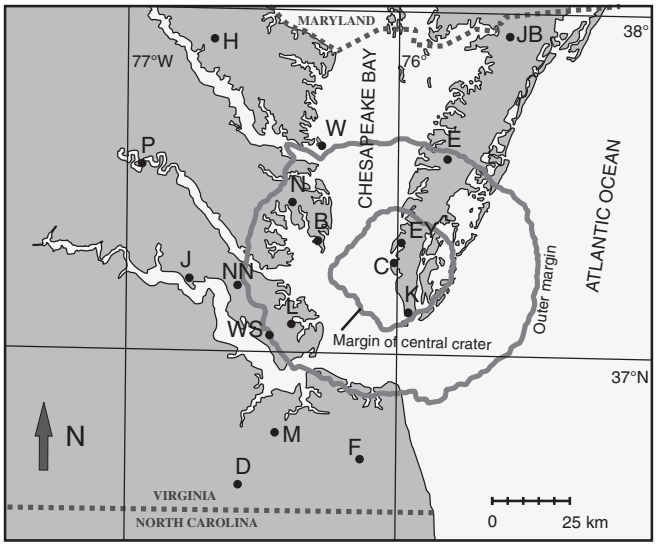

Figure 1. Map of Chesapeake Bay (modified from Horton et al., 2005b), showing the location of the Chesapeake Bay impact structure and major core holes. B—Bayside, C—Cape Charles U.S. Geological Survey (USGS) Sustainable Technology Park (STP), D—Dismal Swamp, E—Exmore, EY—Eyreville, F—Fentress, H—Haynesville, J—Jamestown, JB—Jenkins Bridge, K—Kiptopeke, L—USGS-NASA Langley, M—MW4, N—North, NN—Newport News Park 2, P—Putneys Mill, W—Windmill Point, and WS—Watkins School.

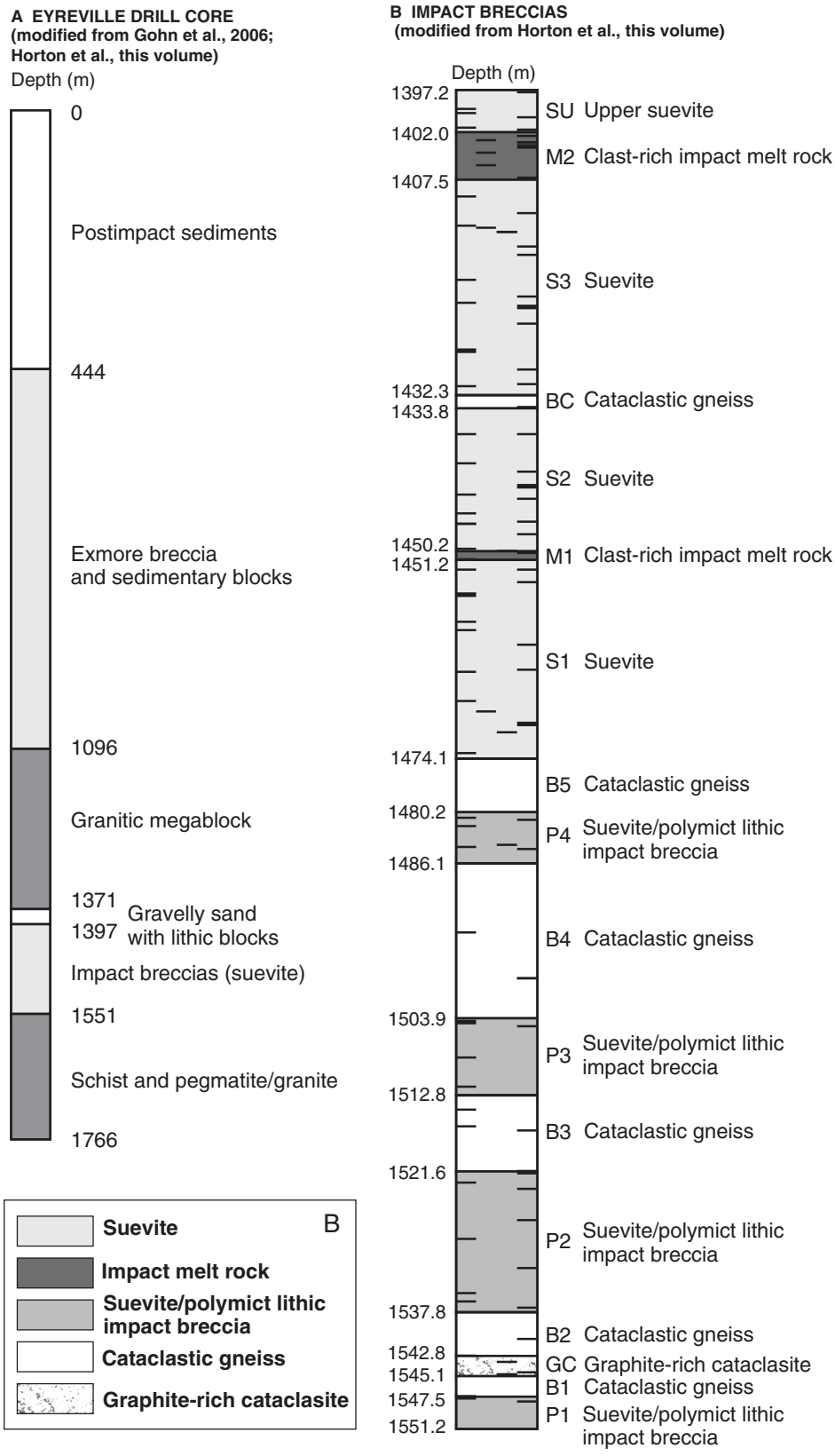

Figure 2. (A) Simplified geologic column showing the Eyreville drill core and the main lithologies present (modified from Gohn et al., 2006a, 2008; Horton et al., this volume). Depths are below surface in meters. (B) Detailed geologic column of the impact breccia section modified from Horton et al. (this volume). The tick marks inside the column show the stratigraphic position of the samples, from left to right: samples CB6-X (samples 100, 110, 120, and 130 marked with a thick line); sample KB-X; samples W2-X and RG-X; samples W-X (samples 60, 70, 80, 90, and 100 marked with a thick line). Depths are below surface in meters.

of clasts of different lithic types (quartz sand, glauconitic sand, clayey sand, silt, clay, cherty breccia) that had been extracted from Exmore breccia samples from the Exmore, Newport News, and Windmill Point cores (Fig. 1). The samples analyzed by Poag et al. (2004) show large variations in both major- and trace-element contents. An extensive study of the chemical composition of the main target sediments was also performed by Deutsch and Koeberl (2006). Their study presents geochemical data of samples from drill cores and outcrops, including several pre-impact sedimentary formations (Potomac, Aquia, Piney Point, and Nanjemoy Formations; Fig. 3), as well as the first postimpact unit—the Chickahominy Formation.

Horton and Izett (2005) carried out chemical analyses of a single rhyolite clast from the Exmore breccia and one monzogranite sample, both taken from the Langley core. The granite, assumed to be part of the crater basement, was cored at a depth of 626.3 m in the Langley core and was dated as being of Neoproterozoic age, 612 ± 10 Ma ($^{206}Pb/^{238}U$ weighted average age of igneous zircons; Horton et al., 2005a). Horton and Izett (2005) also interpreted the age of the impact to be 35.3 ± 0.1 Ma (±1σ), based on $^{40}Ar/^{39}Ar$ dating of North American tektites. Ages of 35.7–35.8 Ma were obtained using the occurrence of calcareous nannofossils by Frederiksen et al. (2005) and based on sediment accumulation rates (Edwards et al., 2005).

Lee et al. (2006) analyzed samples from the STP test hole and found that the rhenium and platinum group element (PGE) concentrations of the impact melt rock are 30–270 times higher than those of basement gneiss. This, together with osmium isotopic data, indicated the presence of a very small, but discernible meteoritic component (see also discussion in McDonald et al., this volume), which could be 0.01%–0.1% by mass, according to mixing calculations (Lee et al., 2006). The type of the projectile has not yet been constrained.

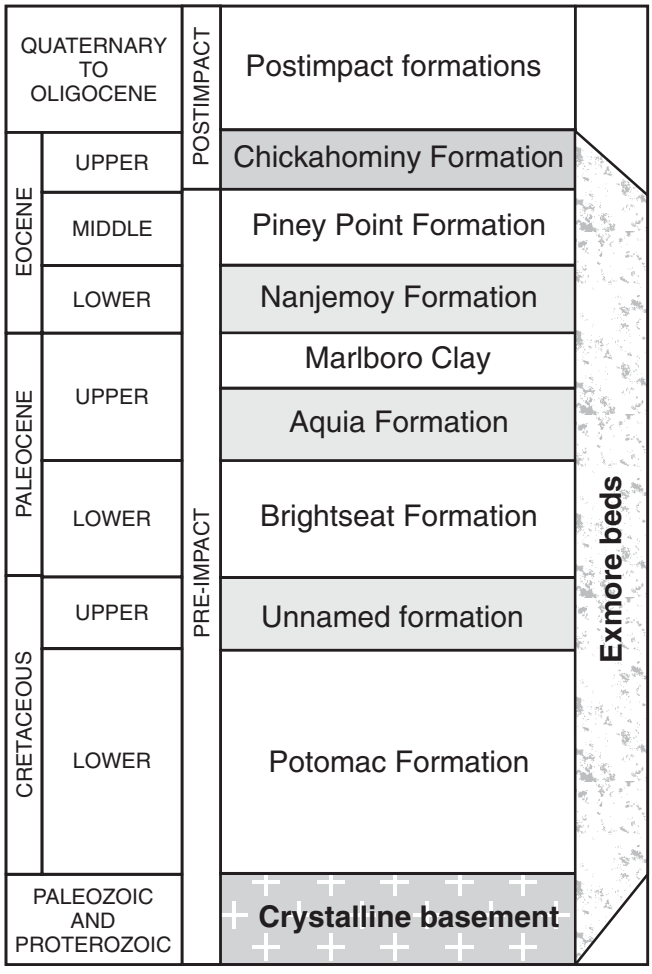

Figure 3. Schematic stratigraphic succession of pre-impact sedimentary formations overlying the crystalline basement in southeastern Virginia (modified from Poag et al., 2004). The terminal Eocene Chickahominy Formation represents the first postimpact sedimentary formation. Impact-generated Exmore breccia is filling the impact crater.

North American Tektites

Initial evidence of an impact in the region along the eastern United States seaboard came from distal ejecta, which are part of the North American tektite strewn field. The North American strewn field contains tektites, microtektites, shocked minerals, and high-pressure minerals (e.g., reidite, coesite, and stishovite; Glass, 1989, 2002). The general location of the source crater of the North American tektites along the east coast of the United States was suggested on the basis of the abundance and composition of distal ejecta (e.g., Thein, 1987; Koeberl, 1989). Poag et al. (1994) excluded the possibility that the North American tektites originated from the Toms Canyon underwater structure, a crater-like feature that has, to date, not been confirmed as being of impact origin. Koeberl et al. (1996) found good agreement in chemical composition between the North American tektites and breccia fragments from the Chesapeake Bay impact structure. The source of the tektites was further linked to the Chesapeake Bay impact structure by Deutsch and Koeberl (2006). These authors showed a correlation of Sr-Nd data and a great similarity in refractory and lithophile element contents, including the rare earth elements (REEs), between the tektites and the target sediments, one Exmore breccia sample, and one granite sample from the Bayside core from the Chesapeake Bay impact structure. These isotope and compositional data by Deutsch and Koeberl (2006), as well as others by Whitehead et al. (2000), excluded the nearly coeval Popigai impact structure in Russia as a possible source crater for the North American tektites.

Eyreville Drill Core

In 2005–2006, three boreholes were drilled at Eyreville Farm in Northampton County, Virginia, USA, as part of the ICDP-USGS Chesapeake Bay Impact Structure Drilling Project. Eyreville hole A was cored in 2005 between 125 and 941 m depth. Eyreville hole B was cored in 2005 from 738 m to a final

depth of 1766 m. In Eyreville hole C, postimpact sediments were cored in 2006 from the land surface to a depth of 140 m (Gohn et al., 2006a, 2008). The uppermost section of the composite Eyreville drilling consists of 444 m of postimpact sediments that overlie 652 m of Exmore breccia and sedimentary blocks. A granitic megablock and a smaller amphibolitic block occur below the Exmore breccia, embedded in gravelly sand. A section of impact breccia was cored in the depth interval from 1397 to 1551 m. The crystalline basement-derived rocks below that consist of granites and pegmatites alternating with mica schists (Gohn et al., 2006a, 2008; Horton et al., this volume; Fig. 2A). Kenkmann et al. (this volume) consider it unlikely that these crystalline rocks represent in situ crater floor and suggest that they probably represent parautochthonous blocks derived from the unshocked material originally at the edge of the transient cavity.

Petrography of the Impact Breccia Section

The detailed petrography of the Eyreville impact breccia is discussed by Bartosova et al. (this volume) and by Wittmann et al. (this volume, Chapters 16 and 17); here, we provide a brief summary of these observations. The nomenclature used for the impactites follows the definitions by Stöffler and Grieve (2007). In the Eyreville B drill core, the impact breccia between 1397 and 1551 m depth is composed mostly of suevite (Figs. 2A and 2B; Horton et al., this volume; Bartosova et al., this volume). Suevite is present also in the form of several dikes in the crystalline basement (Reimold et al., 2007a).

The suevite of the Eyreville B drill core has a grayish, fine-grained, clastic matrix and contains a variety of rock and mineral clasts, melt particles, and secondary minerals. Mineral clasts include quartz, K-feldspar, plagioclase, muscovite, biotite, chlorite, opaque minerals, and other accessory minerals. Rock clasts include sedimentary, metamorphic, and igneous lithologies. Sizes and proportions of different lithic clast types vary significantly throughout the core. However, the clasts become larger and more abundant with increasing depth (Bartosova et al., this volume). In the upper part of the section, the suevite is mostly melt-rich (melt constitutes more than ~20 vol%) and intercalated with impact melt rock (Wittmann et al., 2008, this volume, Chapters 16 and 17) in the intervals 1402.2–1407.5 m and 1450.2–1451.2 m. In the deeper part of the section, below 1474 m, the suevite and rare polymict lithic impact breccia contain large blocks (Horton et al., this volume) consisting mostly of cataclastic, monomict breccia of fine-grained gneiss and minor schist. The main minerals in the cataclastic gneiss are quartz, chlorite, muscovite, biotite, K-feldspar, and plagioclase, as well as secondary carbonate, and opaque and other accessory minerals. Many quartz grains in the impactites exhibit shock deformation in the form of planar fractures (PFs; per se not shock diagnostic) and/or planar deformation features (PDFs); some PDF sets are decorated. Ballen quartz was noted in melt-rich suevite and impact melt rock samples from depths around 1405 and 1450 m. Rare feldspar grains with PDFs and mica with kink banding are also present (Bartosova et al., this volume).

Preliminary results of analyses of the Eyreville core were reported by Bartosova et al. (2007a, 2007b, 2008), Gibson et al. (2007), Jolly et al. (2007), Mader et al. (2007), Reimold et al. (2007a, 2007b), Schmitt et al. (2007), Townsend et al. (2007), Fernandes et al. (2008), and Wittmann et al. (2008). More details about the petrography of the impact breccia section can be found in Bartosova et al. (this volume), Horton et al. (this volume), and Wittmann et al. (this volume, Chapters 16 and 17). Chemical compositions of the main lithologies from the Eyreville drill core are reported and discussed in Schmitt et al. (this volume).

In this study, we present chemical data for 85 impactites and 24 clasts of target rock components separated from impactite samples. In addition, carbon isotopic data are reported for 18 samples of Exmore breccia (444–1096 m), impact breccia (1397–1551 m), and samples from the basal crystalline section (1551–1766 m; Fig. 2A), as the Eyreville drill core provides the unique opportunity to investigate carbon concentrations and C isotopic systematics throughout the complete fill of a large impact structure. This detailed study allowed us to constrain the chemical composition of the impactites and to compare it with the compositions of both the target lithologies and with the North American tektites. Compositions of melt particles within the impactite sequence were also analyzed. The proportions of various target lithologies involved in formation of the polymict impactites and of melt particles therein are estimated by mixing calculations.

SAMPLES AND ANALYTICAL METHODS

Eighty-five samples from the 1397–1551 m depth interval of the Eyreville B drill core were subjected to whole-rock chemical analysis. This suite of samples from the impact breccia sequence consists of 64 suevites, 9 impact melt rocks, 2 polymict lithic impact breccias, and 10 cataclastic gneisses. More detail about the petrography of these samples is presented in Bartosova et al. (this volume) and Wittmann et al. (this volume, Chapters 16 and 17). In addition, 24 large rock clasts from the polymict impactite section were analyzed. The Berlin suite of samples has the designation W-X (plus a few additional W2-X). The Vienna sample suite has the numbers CB6-X, which correspond to samples CK-X from the original sampling, and there are also a few additional samples KB-X. There are also two samples (RG-X) from the Johannesburg sample suite.

Representative aliquots of ~60 g were cut, crushed to smaller pieces, and powdered in an agate mill. In the polymict impactites, we tried to avoid clasts larger than ~1.5 cm. Abundances of major and some trace elements (Ba, Ce, Co, Cr, Cu, Mo, Nb, Ni, Pb, Rb, Sr, Th, U, V, Y, Zn, and Zr) were determined by X-ray fluorescence (XRF) spectrometry at the Museum of Natural History, Berlin, Germany, with a SIEMENS SRS 3000 instrument. Glass tablets were prepared from the sample powders and used for the XRF analyses. For more details on this method, see Schmitt et al. (2004). Additional XRF analyses (samples W2-X and KB-X) were carried out at the University of Witwatersrand, Johannes-

burg, South Africa. Details of the analytical procedures and accuracies are given in Reimold et al. (1994). The contents of some major (Na, K, and Fe) and most trace elements, including rare earth elements (REEs), were determined by instrumental neutron activation analysis (INAA) at the Department of Lithospheric Research, University of Vienna, Austria. About 130 mg of each sample powder were sealed in polyethylene capsules. Three international rock standards were used for reference: the carbonaceous chondrite Allende (Smithsonian Institution, Washington, D.C., USA; Jarosewich et al., 1987), granite AC-E (Centre de Recherche Pétrographique et Géochimique, Nancy, France; Govindaraju, 1989), and Devonian Ohio shale SDO-1 (U.S. Geological Survey; Govindaraju, 1989). All standards and samples were irradiated in the 250 kW Triga reactor of the Atomic Institute of the Austrian Universities for 8 h at a neutron flux of 2.10^{12} n cm^{-2} s^{-1}. More detail about the instrumentation and method is given by Koeberl (1993) and Son and Koeberl (2005). For those elements for which contents were determined by both methods (XRF and INAA), the results were generally in good agreement. For major elements, XRF data are reported; whereas for trace elements, those data that were acquired by the more precise method are presented.

Microchemical analysis of melt particles was carried out at the Natural History Museum in Vienna on a JEOL JSM 6400 scanning electron microscope with an energy-dispersive X-ray analyzer (SEM-EDX). Polished thin sections were examined in secondary electron and backscattered electron modes. The compositions of different types of melt were analyzed using a KEVEX SuperDry Si(Li) detector linked to a VANTAGE EDS system (operating conditions 15 kV acceleration potential and ~1–2 nA sample current). The following elements were analyzed and results recalculated to oxide contents: Si, Al, Ca, Fe, Mg, K, Na, Ti, Mn, and Cr. The analytical results were automatically normalized to 100 wt%. The standardless EDX analyses have a precision of ~3 rel% and accuracies of 10 rel%. Detection limits are ~0.2–0.5 wt% for major elements. A beam with a diameter of ~2 µm was used for detailed analyses. Defocused beam was used for determining the average composition of the melt particles; areas of ~50 × 50 µm to 200 × 200 µm were analyzed.

Carbon isotopic compositions and carbon contents of 18 samples, including several clasts and veins from three of the five major lithological units (Exmore breccia, impact breccia, and basal crystalline section; Fig. 2A), were determined. From the Exmore breccia, some clasts of fine-grained carbon-bearing sediments (arkose, mudstone, siltstone, and shale) and a piece of vitrinitic wood (CB6-059; M. Malinconico, 2007, personal commun.) were selected for analysis. In suevite, clasts of fine-grained sediments (siltstone, mudstone, shale), together with some secondary carbonate in a melt particle (CB6-109) and one carbonate vein (CB6-122), were analyzed. From below the impact breccia section, two samples (CB6-131 and CB6-132) from a graphitic breccia (1551–1560 m), and narrow (<1-mm-wide) carbonate veins in graphitic breccia (CB6-132) and in schist (CB6-145) were selected for carbon isotope analysis. From each sample, 0.2–5 mg powder of sufficiently large clasts were drilled out and weighed into tin capsules. The carbon content and isotopic composition of carbon were measured in the Stable Isotope Laboratory at the Department of Lithospheric Research, University of Vienna, using a Carlo Erba Element Analyzer coupled to a Micromass Optima stable isotope ratio mass spectrometer. Each powder sample was analyzed at least three times with a precision between 0.13‰ and 1.33‰. As laboratory standards, replicate analyses of a graphite (USGS-24, Coplen et al., 2006) and of a carbonatite (NBS-18; Verkouteren and Klinedinst, 2004) were used; accuracy was better than 0.6‰ for USGS-24 and better than 0.48‰ for NBS-18.

RESULTS

The major- and trace-element contents of 85 samples of the polymict impactites and cataclastic gneiss are presented in Appendix 1. Chemical compositions of 24 lithic clasts from the same section are shown in Appendix 2. Average compositions of the impactites are summarized in Table 1, and average compositions of major lithologies from the Eyreville drill core are reported in Table 2 (data from Schmitt et al., this volume). The average compositions of the subunits of the impact breccia section, as well as correlation coefficients for the average polymict impactites and the cataclastic gneiss, are presented in Schmitt et al. (this volume). The paper by Schmitt et al. discusses the geochemistry of all impactite and basement units in the Eyreville core, whereas the present paper is focused on the impact breccia.

The impact melt rock and polymict lithic impact breccia (only 9 and 2 samples, respectively) have compositions similar to those of the suevite from similar depths; thus, we discuss all these samples mostly together as one group of polymict impactites. The only major difference is a depletion of MgO in the impact melt rock from the interval M2 (Fig. 2B, as defined by Horton et al., this volume) when compared to the MgO content of the suevite. Also most of the cataclastic gneiss samples have a composition similar to that of the suevite, and significant differences occur only with regard to the relatively lower contents of Ba and Rb in the gneiss compared to suevite from a similar depth. When we compare the average chemical composition of the different types of impactites (Table 1), the contents of most elements in the gneiss are comparable with the polymict impactites. The gneiss has slightly higher MgO, Cr, Ni, Ba, Hf, Ta, and Th contents and a lower Cs content than the polymict impactites.

Major-Element Contents

The suevites can be divided into two groups: upper suevites (above 1474 m depth, mostly melt-rich) and lower suevites (below 1474 m depth), where further subdivision of the large suite of suevite samples is appropriate.

Figure 4 shows bivariate plots of the variation of major-element oxide contents with depth in the 75 samples of polymict impactites (suevite, impact melt rock, and polymict lithic impact

TABLE 1. AVERAGE COMPOSITION OF IMPACTITES FROM THE IMPACT BRECCIA SECTION, EYREVILLE B DRILL CORE

Rock type	Average polymict impactites*		Upper suevites S1–S3, SU		Lower suevites P1–P4		Impact melt rock M1–M2		Polymict lithic impact breccia		Cataclastic gneiss B1–B4	
Depth range (m)	1397.2–1551.2		1397.2–1474.1		1486.1–1551.2		1407.5–1451.2		1536.5–1537.5		1474.1–1547.5	
Number of samples	*n* = 73/75†		*n* = 47/48		*n* = 15/16		*n* = 9/9		*n* = 2/2		*n* = 9/10	
	Average	Stdev.§	Average	Stdev.	Average	Stdev.	Average	Stdev.	Average	Stdev.	Average	Stdev.
(wt%)												
SiO_2	66.2	2.8	66.7	2.6	64.1	2.5	68.2	2.4	63.5	0.2	66.3	3.5
TiO_2	0.89	0.14	0.87	0.12	1.00	0.18	0.80	0.07	0.94	0.04	0.89	0.07
Al_2O_3	14.8	1.1	14.7	1.0	15.6	1.1	13.9	0.8	15.5	0.1	14.8	1.4
Fe_2O_3#	5.63	0.87	5.45	0.87	6.26	0.77	5.35	0.62	6.17	0.11	5.57	0.67
MnO	0.08	0.02	0.08	0.02	0.08	0.01	0.06	0.01	0.09	<0.01	0.08	0.02
MgO	1.78	0.48	1.79	0.40	2.10	0.47	1.17	0.41	1.86	0.02	2.34	0.74
CaO	1.50	0.47	1.60	0.48	1.13	0.40	1.59	0.19	1.62	0.14	1.35	0.96
Na_2O	1.54	0.72	1.78	0.78	1.04	0.29	1.29	0.20	1.04	0.01	1.50	0.71
K_2O	3.21	0.82	3.10	0.71	3.59	1.12	3.02	0.66	3.67	0.10	3.19	0.71
P_2O_5	0.14	0.03	0.13	0.03	0.15	0.04	0.13	0.02	0.15	<0.01	0.13	0.03
SO_3	0.1	0.1	0.1	0.1	0.1	0.1	<0.1	n.a.**	0.3	0.1	<0.1	n.a.
LOI	3.6	1.4	3.4	1.4	4.5	1.1	3.3	1.7	4.7	0.1	3.5	0.8
Total	99.5	n.a.	99.6	n.a.	99.6	n.a.	98.9	n.a.	99.5	n.a.	99.7	n.a.
(ppm)												
Sc	13.3	1.9	13.0	1.8	14.5	2.0	12.2	1.3	14.6	1.2	14.1	1.7
V	104	14	103	12	114	14	89	11	117	13	102	10
Cr	67.8	15.4	64.1	12.7	77.9	17.8	68.1	18.5	77.6	11.7	94.3	21.9
Co	15.4	2.6	15.1	2.6	17.3	1.9	13.9	2.0	16.8	1.4	15.7	2.3
Ni	34	6	33	3	38	9	32	8	36	2	40	11
Zn	112	50	108	59	126	26	108	33	128	35	93	10
Rb	140	40	132	32	174	47	117	32	184	18	131	30
Sr	210	81	217	71	209	121	195	20	110	1	126	57
Y	44	8	42	7	50	10	38	6	56	1	47	8
Zr	248	34	246	33	258	44	241	12	261	45	298	43
Cs	9.94	3.91	9.19	3.86	12.6	3.8	8.59	1.87	13.9	0.2	5.90	4.29
Ba	465	125	468	132	464	126	451	108	491	47	555	100
La	36.6	6.0	35.3	5.2	41.1	6.6	33.7	3.7	46.0	1.2	42.7	7.4
Ce	76.0	18.3	72.4	10.3	90.4	31.6	67.6	7.4	90.8	4.7	86.4	12.8
Nd	32.1	5.3	30.8	4.67	36.9	5.76	29.5	2.8	36.4	0.6	36.7	5.2
Sm	6.76	1.24	6.45	1.16	7.53	1.30	6.78	0.89	8.29	0.96	7.48	0.91
Eu	1.55	0.23	1.52	0.19	1.71	0.29	1.43	0.15	1.80	<0.01	1.68	0.21
Gd	6.22	1.73	5.83	1.89	6.97	1.33	6.66	0.75	7.56	0.77	6.95	1.00
Tb	1.03	0.16	1.00	0.14	1.15	0.18	0.95	0.12	1.25	0.01	1.22	0.15
Tm	0.51	0.09	0.49	0.08	0.56	0.12	0.50	0.09	0.61	0.00	0.61	0.07
Yb	3.14	0.41	3.07	0.35	3.39	0.49	2.96	0.34	3.58	0.54	3.81	0.57
Lu	0.47	0.07	0.45	0.06	0.52	0.08	0.44	0.03	0.51	0.14	0.57	0.07
Hf	6.36	0.84	6.17	0.72	7.04	0.91	6.08	0.44	7.23	1.64	7.98	1.35
Ta	1.28	0.18	1.24	0.16	1.42	0.18	1.17	0.13	1.44	0.34	1.50	0.45
Th	11.7	2.0	11.3	1.6	13.5	2.2	10.8	1.5	13.1	1.6	14.8	6.0
U	2.96	0.72	2.83	0.69	3.51	0.66	2.65	0.40	3.34	1.11	3.23	1.14
Eu/Eu^* ††	0.72	0.07	0.74	0.07	0.72	0.05	0.63	0.04	0.70	0.08	0.71	0.06
La_N/Yb_N §§	7.89	0.66	7.77	0.62	8.19	0.70	7.79	0.23	8.82	1.56	7.55	0.36

Note: All major element contents and V, Ni, Sr, Y, Zr, and Ba contents were analyzed by X-ray fluorescence (XRF); all other element contents were determined by instrumental neutron activation analysis (INAA). LOI—loss on ignition. Abbreviations M1–M2, P1–P2, S1–S3, and SU (see Fig. 2) refer to subunits as defined by Horton et al. (this volume).

*Average polymict impactites—suevite, impact melt rock, and polymict lithic impact breccias.

†*n*—number of samples averaged for trace elements analyzed by INAA/number of samples averaged for major elements and trace elements analyzed by XRF.

§Standard deviation.

#Total Fe as Fe_2O_3.

**Not applicable.

††$Eu/Eu^* = Eu_N/(Sm_N \times Gd_N)^{0.5}$; subscript N denotes chondrite-normalized values (Taylor and McLennan, 1985).

§§Subscript N denotes chondrite-normalized values (Taylor and McLennan, 1985).

TABLE 2. AVERAGE COMPOSITION OF MAJOR LITHOLOGIES FROM THE EYREVILLE DRILL CORE (DATA FROM SCHMITT ET AL., THIS VOLUME)

Rock type	Schist of the basal crystalline section		Pegmatite/granite of the basal crystalline section		Amphibolite		Granitic rocks of the megablock		Exmore breccia	
Depth range (m)	1554.1–1689.0		1592.3–1766.1		1376.4–1389.7		1096.8–1369.0		444.4–864.3	
Number of samples	*n* = 28/37*		*n* = 23/25		*n* = 3/6		*n* = 30/30		*n* = 73/73	
	Average	Stdev.†	Average	Stdev.	Average	Stdev.	Average	Stdev.	Average	Stdev.
(wt%)										
SiO_2	56.6	7.9	73.7	4.5	45.5	1.1	72.5	1.7	75.6	4.3
TiO_2	0.91	0.22	0.04	0.05	1.40	0.52	0.27	0.14	0.52	0.11
Al_2O_3	18.6	3.4	14.5	2.4	18.4	0.6	14.1	0.8	10.3	1.7
Fe_2O_3§	7.87	3.41	0.58	0.53	11.8	1.1	1.96	1.02	3.10	1.03
MnO	0.07	0.03	0.05	0.04	0.22	0.09	0.04	0.05	0.04	0.02
MgO	2.06	1.53	0.13	0.10	5.89	0.53	0.38	0.17	0.80	0.32
CaO	1.89	1.34	1.23	1.06	8.49	1.15	1.64	0.60	1.47	0.99
Na_2O	1.66	0.99	4.15	1.59	2.63	0.51	3.15	0.66	1.39	0.18
K_2O	3.56	1.16	3.41	2.07	0.83	1.11	4.88	1.73	2.54	0.31
P_2O_5	0.08	0.06	0.05	0.06	0.20	0.08	0.06	0.04	0.12	0.07
SO_3	0.3	0.3	<0.1	n.a.#	0.3	0.3	<0.1	n.a.	0.2	0.1
LOI	6.1	2.0	1.7	1.4	4.0	1.3	0.6	0.4	3.7	1.2
Total	99.7	n.a.	99.5	n.a.	99.7	n.a.	99.6	n.a.	99.8	n.a.
(ppm)										
Sc	19	6	3.3	4.0	26	1	5.1	3.1	7.4	2.2
V	168	54	<15	n.a.	181	6	28	12	63	16
Cr	104	50	21	20	153	6	9.4	1.5	46	13
Co	21	12	0.5	0.3	52	5	2.4	1.5	9.0	2.4
Ni	54	33	37	45	70	31	26	4	22	6
Zn	133	69	37	26	92	13	52	22	46	20
Rb	209	90	280	169	19	6	234	70	72	10
Sr	136	64	44	22	315	65	200	78	180	17
Y	53	17	59	31	41	28	57	24	22	5
Zr	173	40	44	25	98	61	243	112	200	34
Cs	20	21	5.3	4.7	2.0	0.3	3.5	1.0	2.1	0.6
Ba	449	174	<30	n.a.	249	391	801	246	503	79
La	39	13	6.6	7.9	4.9	0.3	71	35	22	4
Ce	78	25	16	16	12	1	132	60	47	8
Nd	34	11	10	9	7.0	1	46	17	20	4
Sm	7.2	2.5	3.2	2.6	2.0	0.1	7.3	2.2	4.0	0.8
Eu	1.6	0.5	0.2	0.1	0.9	0.1	1.2	0.3	1.0	0.2
Gd	6.5	1.8	3.3	2.6	n.d.**	n.a.	6.2	2.7	3.9	0.7
Tb	1.1	0.3	0.6	0.5	0.5	0.1	0.9	0.5	0.6	0.1
Tm	0.5	0.2	0.5	0.3	0.2	0.1	0.5	0.3	0.3	0.1
Yb	3.3	1.2	2.2	1.8	1.3	0.1	2.6	2.1	1.9	0.4
Lu	0.5	0.2	0.3	0.2	0.2	<0.1	0.4	0.4	0.3	0.1
Hf	4.9	1.1	1.5	1.2	1.9	0.1	6.5	3.0	4.9	0.8
Ta	2.5	3.7	7.9	6.8	0.6	0.1	2.0	1.5	0.7	0.2
Th	12	4	6.3	8.2	0.8	<0.1	32	15	6.4	1.9
U	5.4	3.3	14	13	n.d.	n.a.	6.0	5.8	1.8	0.4

Note: All major-element contents and V, Ni, Sr, Y, Zr, and Ba contents were analyzed by X-ray fluorescence (XRF); all other element contents were determined by instrumental neutron activation analysis (INAA). LOI—loss on ignition. Abbreviations M1–M2, P1–P2, S1–S3, and SU (see Fig. 2) refer to subunits as defined by Horton et al. (this volume).

**n*—number of samples averaged for trace elements analyzed by INAA/number of samples averaged for major elements and trace elements analyzed by XRF.

†Standard deviation.

§Total Fe as Fe_2O_3.

#Not applicable.

**Not determined.

breccia) and 10 samples of cataclastic gneiss. The contents of SiO_2 and CaO in polymict impactites decrease with depth, and there is a slight increase of TiO_2, Al_2O_3, and Fe_2O_3 abundances with depth. The average Na_2O content in polymict impactites above ~1450 m (of ~2 wt%) is about two times higher than the average Na_2O content in the polymict impactites from below ~1450 m (~1 wt%). Contents of the other major oxides do not show any significant trends with depth. In the polymict impactites, there is an elevated K_2O content to >4 wt% in the depth interval 1480.2–1486.1 m (designated P4 by Horton et al., this volume; see Fig. 2B), whereas most of the other impactites have K_2O contents <4 wt%. Loss on ignition (LOI) values also increase with depth in the polymict impactites.

Harker diagrams (Fig. 5) show the variability in major-element contents within the impactites. An inverse correlation between SiO_2 and Al_2O_3, Fe_2O_3, and MgO is observed. There is no significant correlation between SiO_2 and CaO, Na_2O, and K_2O contents. In the SiO_2-Na_2O diagram, the Na-rich suevite samples from above ~1450 m and the Na-poor suevite samples from the lower parts of the investigated section are well distinguished; the impact melt rock and cataclastic gneiss mostly fall between these two groups.

The ternary diagram CaO–K_2O + Na_2O–Fe_2O_3 + MgO (Fig. 6) shows the average and range of compositions of the investigated impactites compared with average compositions of other main lithologies from the Eyreville drill core, including pegmatite/granite and schist of the basal crystalline section, amphibolite, granitic rocks of the megablock, gravelly sand, and Exmore breccia. The suevite, impact melt rock, and cataclastic gneiss have similar proportions of CaO, K_2O + Na_2O, and Fe_2O_3 + MgO; suevite displays the largest range of proportions. Average schist has proportions of the plotted oxides very similar to the average impactites, whereas gravelly sand, Exmore breccia, granitic megablock samples, and especially pegmatites/granites of the basal crystalline section have comparatively elevated K_2O + Na_2O contents. The contents of CaO and LOI values are not correlated with each other in the impactites (Fig. 7).

Trace-Element Contents

Variations of some trace-element contents with depth are shown in Figure 8. The trace-element contents mostly do not show obvious trends with depth.

Lithophile Elements

The abundances of the lithophile elements Ba, Rb, and Sr show minor variations in the upper part of the impact breccia section (above ~1430 m, Fig. 8); larger variations appear in the lower part. The Ba contents vary between 400 and 600 ppm in most of the polymict impactites (Fig. 8). There are a few outliers among the upper suevites (above 1474 m), with higher values, up to 1041 ppm. Barium contents are relatively constant within each subsection of the impact breccia (as designated by Horton et al., this volume; see Fig. 2). The Ba contents of the cataclastic gneiss, with values between 381 and 736 ppm, are slightly higher than those for the polymict impactites from similar depth. The Rb contents of the polymict impactites show a slightly decreasing trend from the top of the section to ~1417 m depth; between 1417 m and 1474 m, the contents vary from 28 to 223 ppm. Below 1474 m, the polymict impactites have generally slightly higher Rb contents (141–228 ppm) than the intercalated cataclastic gneiss blocks (88–168 ppm; Fig. 8). The Sr content mostly varies only between 160 and 250 ppm in the upper part of the polymict impactites, above ~1430 m, but the variations become larger down to 1474 m depth, ranging from 140 to 360 ppm in most samples. Below 1474 m, the Sr content is highly variable. There is a low Sr content (below 150 ppm) in the polymict impactites of the interval between 1480.2 and 1486.1 m (P4) and in the lowest part, below 1530 m; significantly higher Sr contents (265–474 ppm) were determined for the depth interval at 1500–1528 m. The cataclastic gneiss samples show relatively low Sr contents (<232 ppm). In the lowermost cataclastic gneiss blocks (below 1537.7 m), the Sr contents are <104 ppm (Fig. 8). The Zr contents vary mostly between 200 and 300 ppm in the polymict impactites and are most variable in the P4 interval at 1480.2–1486.1 m.

The Cs, Rb, Sr, Ba, and U contents are not correlated with Al_2O_3, but there is a slight positive correlation between the Th and Al_2O_3 abundances observed for the suevite samples (correlation coefficient r = 0.63). Correlations of some lithophile elements (Rb-K_2O and Sr-CaO) are displayed in Figures 9A and 9B. There is clearly an increase of Rb content with increasing K_2O contents (r = 0.87 for suevite, and r = 0.87 for cataclastic gneiss). Strontium data show significant correlation with CaO contents only for cataclastic gneiss (r = 0.80).

Chalcophile Elements

The Cu contents in the impactite samples rarely exceed 40 ppm, and in about half of the samples, the Cu values are below the detection limit. There are some higher Cu values, up to 57 ppm, in the polymict impactites at the depth interval of 1451.2–1474.1 m (S1) and up to 55 ppm in the interval 1521.6–1537.8 m (P2). An exceptionally high Cu content is observed in the lowermost sample of cataclastic gneiss (161 ppm, CB6-130, depth = 1547.4 m). The Cr contents vary between 24 and 124 ppm in the impact breccia section (Fig. 8). The Cr content varies from 24 to 102 ppm in the polymict impactites from above 1474 m, from 40 to 112 ppm in the polymict impactites below 1474 m, and from 68 to 124 ppm in the cataclastic gneiss. Zinc contents vary between 40 and 170 ppm in the impact breccia section and do not show any specific trend with depth (Fig. 8). The samples of cataclastic gneiss have Zn abundances similar to those of the upper suevites above 1474 m, but their values are lower than the values for the lower suevites. An exceptionally high value (455 ppm) was found in suevite sample W-088a (depth = 1461.3 m).

Siderophile Elements

The average contents of Cr and the siderophile elements Co and Ni in suevite, impact melt rock, polymict lithic impact

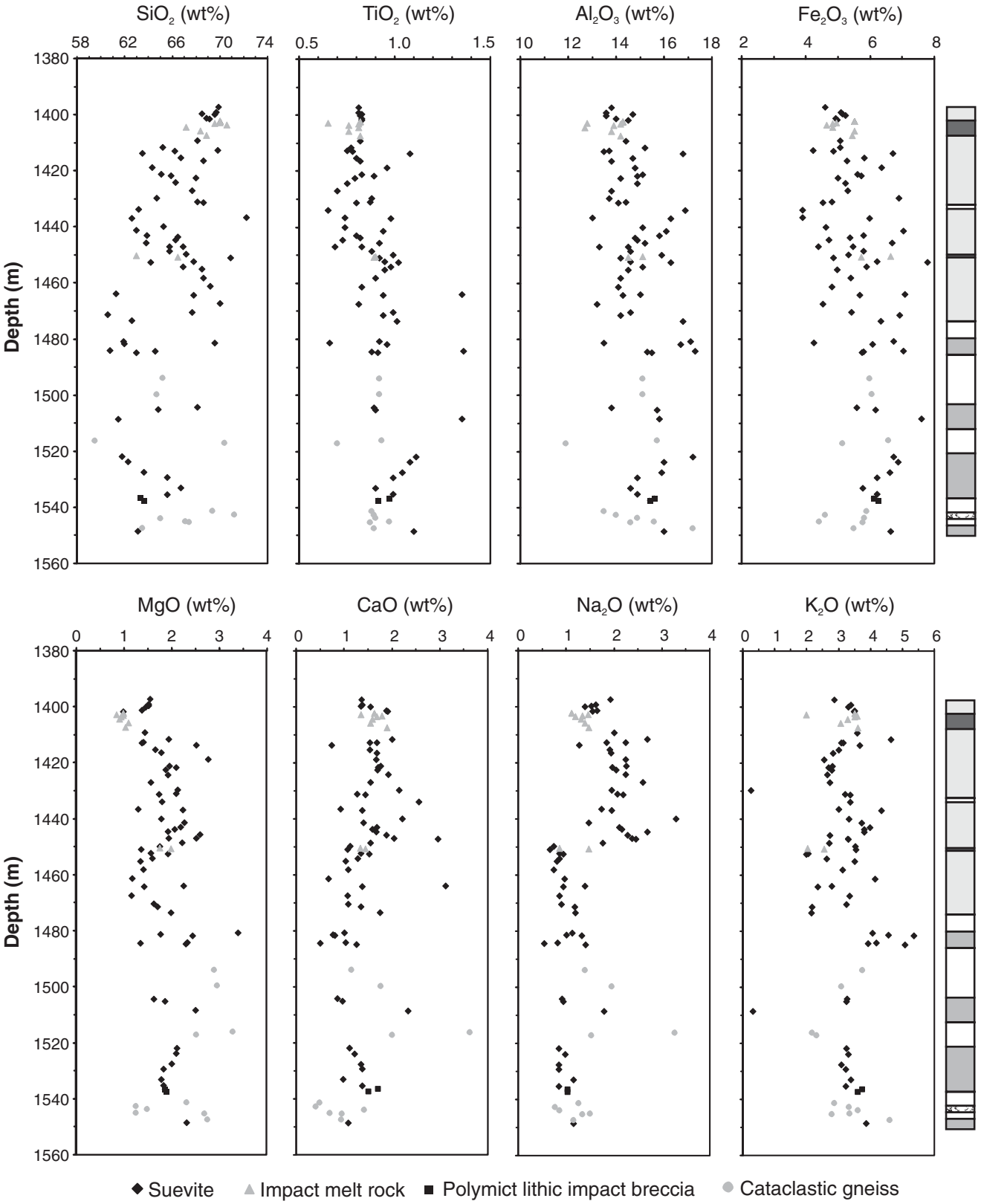

Figure 4. Variations of concentrations (in wt%) of some major oxides with depth (SiO_2, TiO_2, Fe_2O_3, MgO, Al_2O_3, CaO, Na_2O, and K_2O). Samples of suevite, impact melt rock, polymict lithic impact breccia, and cataclastic gneiss are plotted. Contents of SiO_2 and CaO show a slight decrease, whereas TiO_2, Fe_2O_3, and Al_2O_3 contents increase with increasing depth. Content of Na_2O is much higher above ~1450 m than in the lower part of the studied section. The geologic column according to Horton et al. (this volume) is shown on the right side (see Fig. 2 for legend and more details).

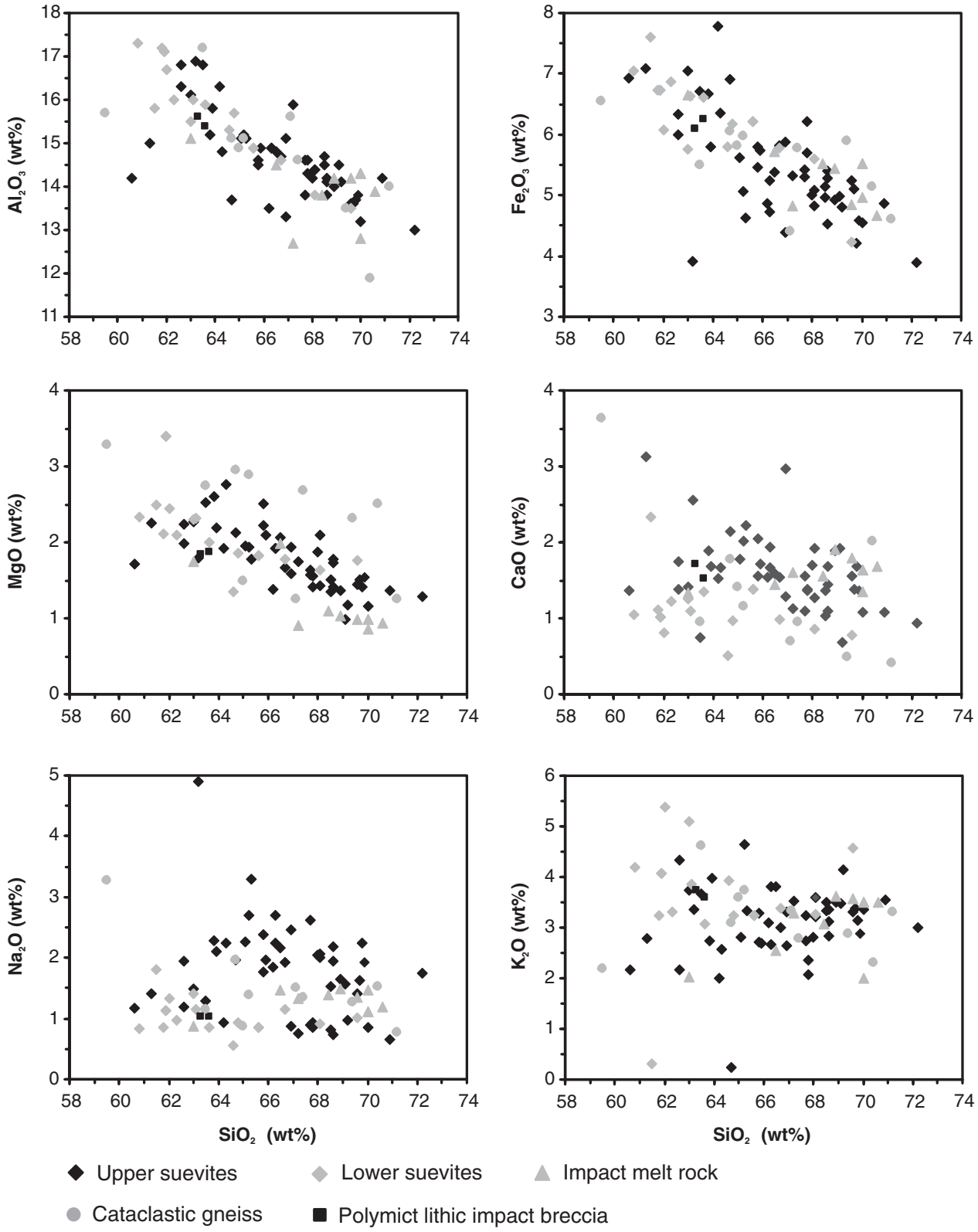

Figure 5. Harker diagrams of the contents of the major oxides Al_2O_3, Fe_2O_3, MgO, CaO, Na_2O, and K_2O plotted versus SiO_2 for upper suevite (above 1474 m), lower suevite (below 1474 m), impact melt rock, polymict lithic impact breccia, and cataclastic gneiss. The diagrams show a negative linear correlation of Al_2O_3, Fe_2O_3, and MgO content with the SiO_2 content. In the diagram of Na_2O, two groups of suevites can be distinguished—Na-rich suevites from the upper part of the unit (above ~1450 m) and Na-poor suevites from the lower part.

breccia, and cataclastic gneiss are presented in Table 3. Cobalt and Ni show only minor variation for most of the impactite samples (Fig. 8). Cobalt content varies between 10 and 23 ppm in the upper suevites, and within the other impactites, the variation is even smaller. The Ni content varies between 24 and 40 ppm in the majority of the impactite samples. Higher Ni contents (above 45 ppm) were observed in two samples of the lower suevites, in two samples of cataclastic gneiss, and in one impact melt rock (49 ppm in sample KB-4, depth = 1405.7 m). Contents of Au in the impactites are low, mostly below 1 ppb or below detection limit; an exceptionally high value of 7.3 ppb was found in a sample of impact melt rock (KB-2, depth = 1042.9 m). The Ir contents are below the detection limit (of ~2 ppb) in the majority of the investigated samples, with a maximum measured value of 0.76 ppb (sample CB6-126, depth = 1529.3 m).

Rare Earth Elements (REEs)

All analyzed samples are enriched in REEs relative to chondritic values. Chondrite-normalized REE patterns for the different impactites are shown in Figure 10. All impactite samples show very similar REE patterns, with normalized abundances decreasing toward the heavy REEs (HREEs), and a negative Eu anomaly. Also, the average REE patterns of all subunits of the impact breccia section, as defined by Horton et al. (this volume), are all very similar. The average values of La_N/Yb_N and Eu/Eu* (as defined by Taylor and McLennan, 1985) for the impactites are shown in Table 1.

The sum of the REE abundances slightly decreases with increasing SiO_2 content ($r = -0.52$) and increases with increasing Al_2O_3 content ($r = 0.69$) in the polymict impactites. No significant correlation between the sum of the REEs and the content of other major oxides was observed. The sum of the HREEs does not correlate with the Zr or P content, but it increases slightly with increasing Y content in the polymict impactites ($r = 0.58$).

Chemical Composition of Clasts in Polymict Impact Breccia

The polymict impact breccia contains clasts of various target rock types. Here, we present chemical analyses of 24 different clasts, the sizes of which range from a few centimeters to ~0.5 m. The clasts include schist, gneiss, amphibolite, granite, sedimentary rocks (graywacke, arkose, conglomerate), and other clasts (Appendix 2). The clasts have quite variable chemical compositions, according to their petrographic characteristics. The sedimentary clasts are mostly silica-rich (up to 80 wt% SiO_2), whereas the amphibolite clasts contain only ~42 wt% SiO_2. Harker diagrams (Fig. 11) show a decrease of Al_2O_3, Fe_2O_3, and MgO with increasing SiO_2 content for the different clasts. There is a slight decrease in CaO with increasing SiO_2 content, but no obvious trend was observed for Na_2O and K_2O versus SiO_2.

The ternary diagram CaO–K_2O + Na_2O–Fe_2O_3 + MgO (Fig. 12) shows the relative composition of the different clasts investigated. Most clasts have a relatively low CaO content (<3 wt%, rarely up to 9.4 wt%). Gneiss clasts have quite variable compositions; some clasts are richer in alkali oxides, whereas

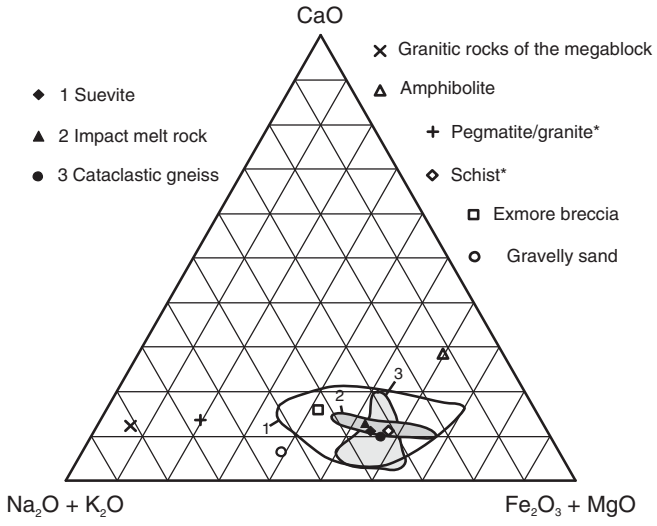

Figure 6. Ternary diagram CaO–K_2O + Na_2O–Fe_2O_3 + MgO shows the relative composition of the studied impactites (averages and ranges; this study) and the main lithologies (averages; Schmitt et al., this volume) from the Eyreville drill core. All the impactites have similar relative composition; average composition of the impactites is very close to the average composition of schist. Compositions of basement granites and pegmatites and granite/granitic gneiss block are shifted toward Na_2O + K_2O; amphibolite block is enriched in Fe_2O_3 + MgO and CaO. "*" denotes lithologies of the basal crystalline section.

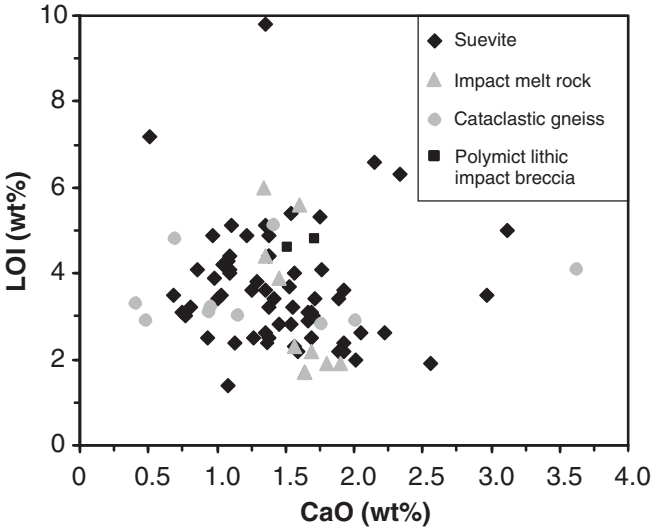

Figure 7. Bivariate plot showing that there is no correlation between CaO and loss on ignition (LOI) contents. This means that the LOI is not caused predominantly by the presence of carbonate, but it is probably related to the content of organic matter and/or structural water in secondary phyllosilicate minerals.

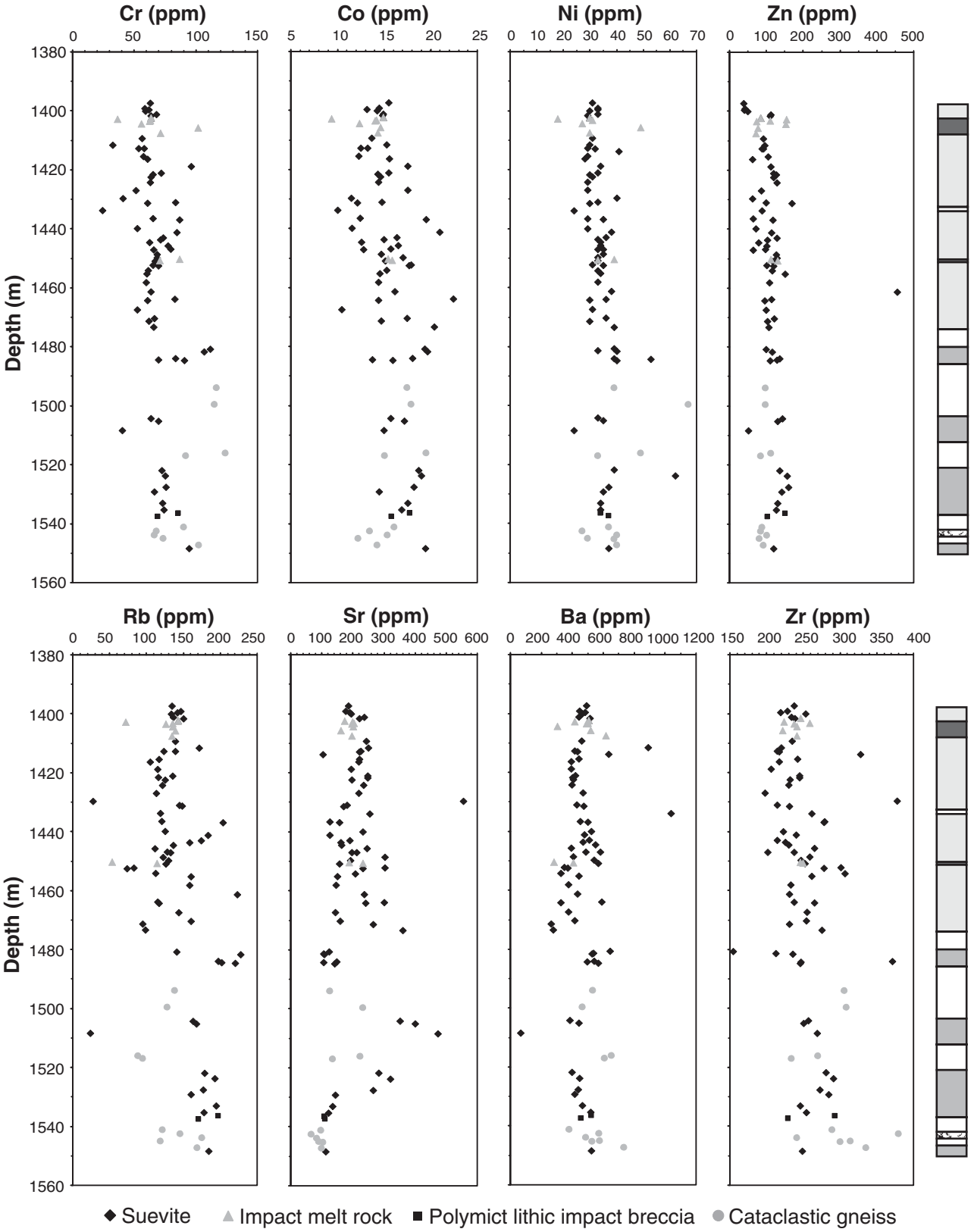

Figure 8. Variations of contents (in ppm) of selected trace elements with depth (Cr, Co, Ni, Zn, Rb, Sr, Ba, and Zr). Samples of suevite, impact melt rock, polymict lithic impact breccia, and cataclastic gneiss are plotted. Generally, the trace-element contents are less variable in the uppermost part of the section. The geologic column according to Horton et al. (this volume) is shown on the right side (see Fig. 2 for legend and more details).

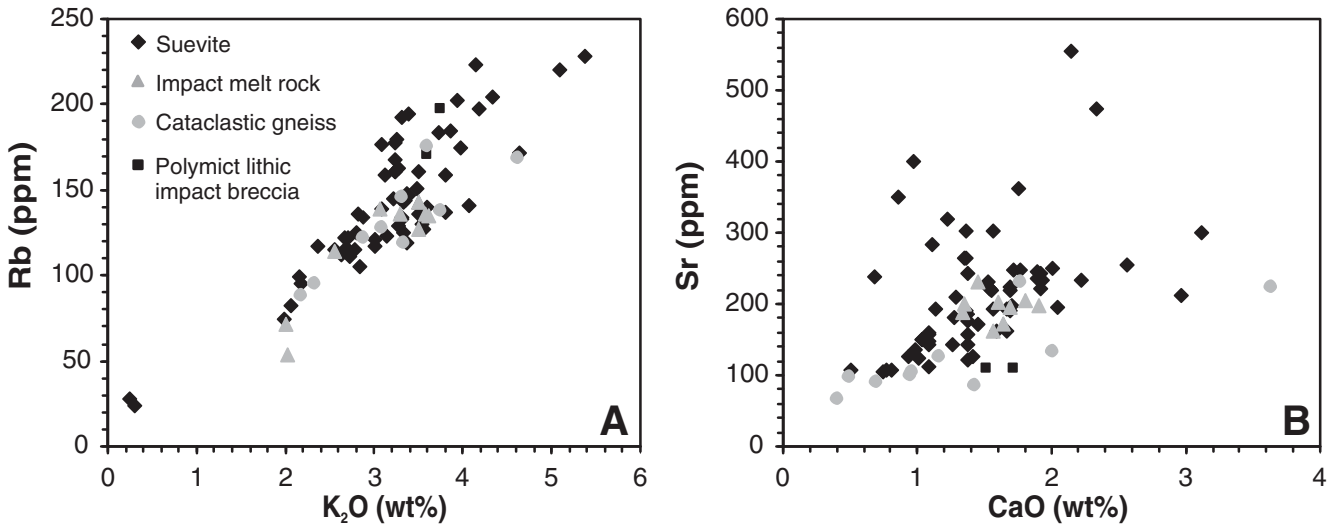

Figure 9. Binary diagram for (A) K_2O versus Rb and (B) CaO versus Sr contents in samples from the impact breccia section. There is a positive correlation between Rb and K_2O in the impactites (e.g., $r = 0.87$ for suevite). The Sr contents are reasonably well correlated with CaO content only for the cataclastic gneiss ($r = 0.80$).

TABLE 3. ABUNDANCES OF SIDEROPHILE AND RELATED ELEMENTS IN THE IMPACTITES FROM THE EYREVILLE B DRILL CORE

Rock type	Upper suevites S1–S3, SU		Lower suevites P1–P4		Impact melt rock M1–M2		Polymict lithic impact breccia		Cataclastic gneiss B1–B4	
Depth range (m)	1397.2–1474.1		1486.1–1551.2		1407.5–1451.2		1536.5–1537.5		1474.1–1547.5	
Number of samples	Average (*n* = 47/48)*	Stdev.†	Average (*n* = 15/16)	Stdev.	Average (*n* = 9/9)	Stdev.	Average (*n* = 2/2)	Stdev.	Average (*n* = 9/10)	Stdev.
Cr	64.1	12.7	77.9	17.8	68.1	18.5	77.6	11.7	94.3	21.9
Co	15.1	2.6	17.3	1.9	13.9	2.0	16.8	1.4	15.7	2.3
Ni	32.6	3.4	38.4	8.6	31.9	8.5	35.5	2.1	40.0	11.4

Note: Values are in ppm. Abbreviations M1–M2, P1–P2, S1–S3, and SU (see Fig. 2) refer to subunits as defined by Horton et al. (this volume).
**n*—number of samples averaged for Cr and Co/number of samples averaged for Ni.
†Standard deviation.

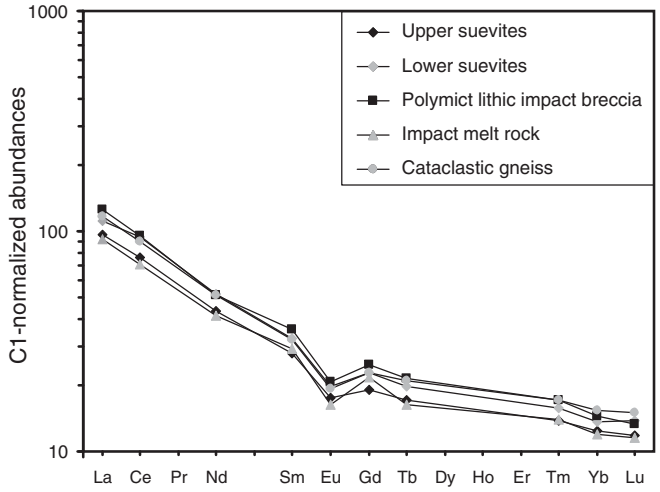

Figure 10. Chondrite (C1)–normalized rare earth element (REE) distribution patterns for the averages of different impactite groups, all of which have very similar REE patterns. Normalization factors are from Taylor and McLennan (1985).

others gneiss clasts are Fe- and Mg-rich. The amphibolite clasts are Fe- and Mg-rich. The average composition of the polymict impactites falls between the compositions of the clasts (Fig. 12).

Contents of lithophile and chalcophile trace elements are quite variable within each lithological clast group, and the different groups do not show distinct clustering of values. Contents of siderophile elements are highest in the mafic rock clast (sample CB6-123), and in amphibolite and schist clasts.

Rare earth element patterns of most of the clasts are very similar, with negative Eu anomalies, but there are a few samples with different patterns. These include two gneiss samples (W-064 and CB6-122, Eu/Eu* = ~1), as well as a pyrite-rich schist (sample W-098) and a mafic rock (sample CB6-123) that have the most pronounced positive Eu anomalies (Eu/Eu* = 1.16 and 1.24, respectively) and the lowest contents of the light REEs (LREEs).

Chemical Composition of Melt Particles

Five types of melt particles were distinguished in the suevite from the Eyreville B drill core (Bartosova et al., 2008),

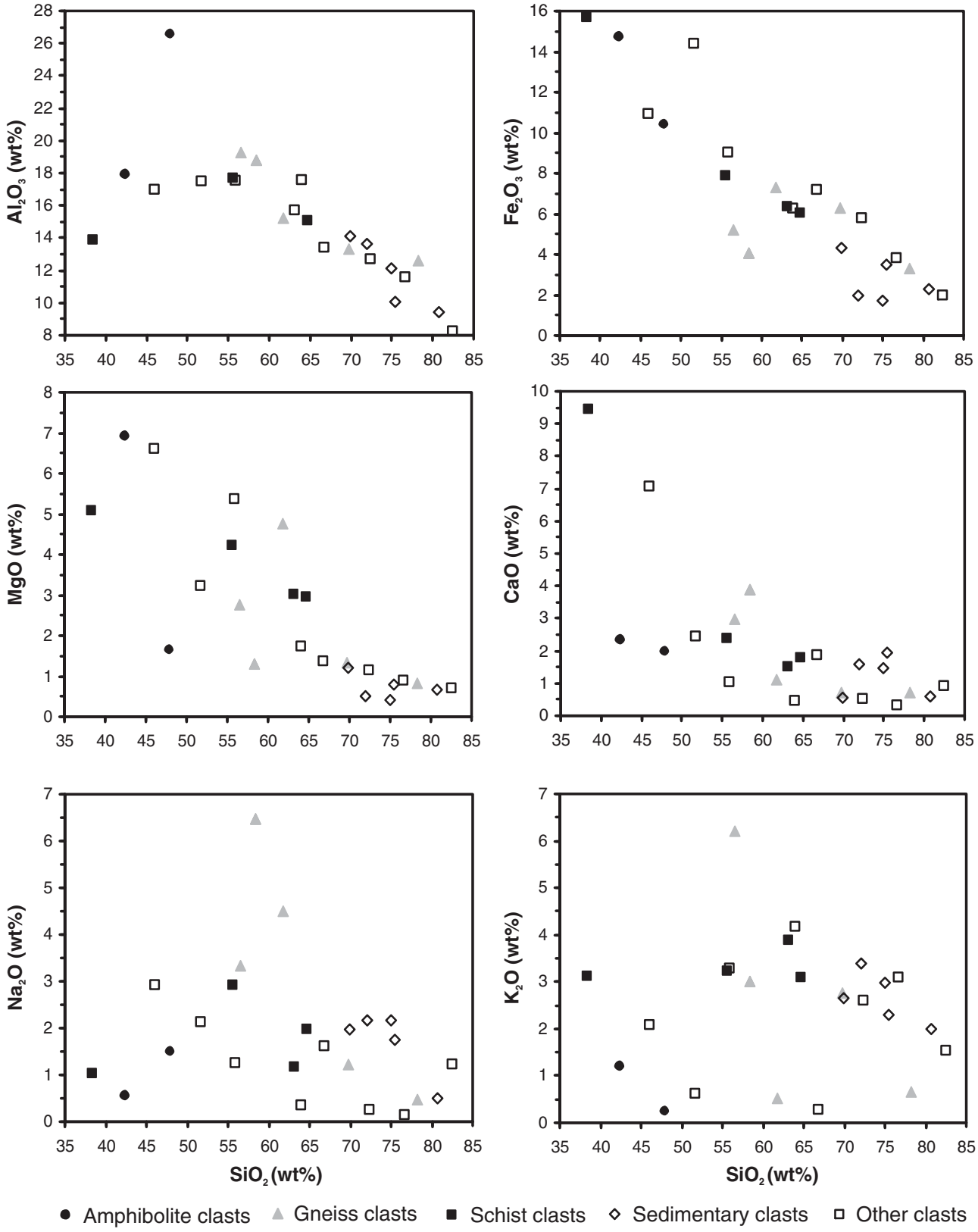

Figure 11. Harker diagrams for the contents of Al_2O_3, Fe_2O_3, MgO, CaO, Na_2O, and K_2O versus SiO_2 content for clasts in the polymict impact breccia. The diagrams show a negative correlation of Al_2O_3, Fe_2O_3, and MgO with SiO_2. There is a slight decrease in CaO with increasing SiO_2 content, but no obvious trend was observed for Na_2O and K_2O versus SiO_2 content.

mostly based on color, microtexture, and chemical composition: (1) clear, brownish, or greenish glass, often with flow texture (dark schlieren); (2) brown melt, completely altered to very fine–grained phyllosilicate minerals; (3) recrystallized silica melt; (4) melt with microlites; and (5) dark-brown melt with abundant undigested grains. Table 4 displays the average chemical compositions of the five different types of melt particles. Melt particles have quite distinct compositions. The altered glass (type 2) has a lower content of SiO_2 (<70 wt%, ~64 wt% on average) compared to type 1. Other abundant oxides detected in melt particles of type 2 are Al_2O_3 (~21 wt%), Fe_2O_3 (~5.6 wt%), and MgO (2.4 wt% on average). The glass of type 1 has more than 70 wt% SiO_2 (~81 wt%, on average) and contains proportionally lower amounts of other oxides in comparison to type 2. The silica melt (type 3) consists of nearly pure SiO_2 (>97.8 wt% SiO_2 on average) with some minor Al_2O_3 and Fe_2O_3, probably in some inclusions or alteration minerals. The melt with pyroxene microlites (type 4) is composed of SiO_2 (~76 wt% on average), Al_2O_3 (~14 wt%), Fe_2O_3 (~4.2 wt%), and low proportions of other oxides. The dark-brown melt (type 5) has SiO_2 content similar to melt type 2 (~63 wt% on average), but slightly higher Al_2O_3 (~25 wt%) and Fe_2O_3 (~6.6 wt%) contents.

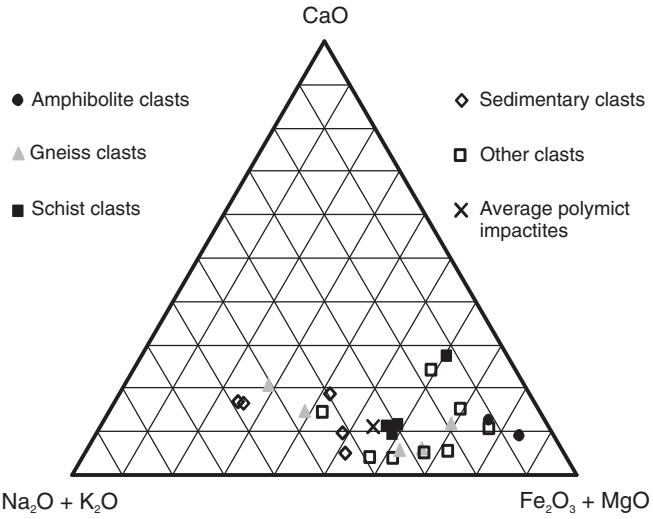

Figure 12. Ternary diagram showing relative contents of major elements in clasts from the polymict impact breccia. Clasts of amphibolite and schist are relatively rich in Fe_2O_3 + MgO. Compositions of gneiss and sedimentary rock clasts are rather variable, and some of these clasts are rich in alkali oxides.

Compositions of individual melt particles were compared with compositions of major rock-forming minerals (e.g., quartz, feldspars, mica), but it appears that none of the melt particles, except for the silica melt (type 3), has a monomineral composition. Furthermore, the individual melt particles were compared with compositions of the different target lithologies. Ternary diagrams comparing contents of some major oxides in individual melt particles and main target lithologies are reported in Figure 13. The SiO_2-rich melt particles—the particles of type 3—are not shown in the ternary diagrams because many major element contents are below the detection limit in these particles. The melt particles do not have the same composition as any of the major target lithologies, which is especially apparent when the particles and target lithologies are compared in various ternary diagrams (Figs. 13A, 13B, and 13C). Melt type 1 has similar composition to graywacke clasts, and melt type 5 is similar to fine-grained sedimentary clasts in the suevite, which were analyzed by SEM-EDX. Proportions of CIPW normative minerals (see Cross et al., 1902) were calculated for individual melt particles and compared with different target lithologies in various ternary diagrams (Figs. 13D and 13E), and it appears that melt particles do not have a monolithological composition. In the diagram SiO_2–CaO + Na_2O + K_2O–Fe_2O_3 + MgO (Fig. 13C), all of the melt particles cluster toward the SiO_2 corner. The different melt types can be better distinguished in this plot than in those of Figures 13A and 13B. Similar behavior is observed when the CIPW-normative mineral abundances for individual melt particles are plotted in ternary diagrams (Figs. 13A and 13B). In the diagram showing proportions of quartz, orthoclase, and plagioclase (Fig. 13B), the different types of melt can be distinguished better than in

TABLE 4. COMPOSITION OF MELT PARTICLES FROM SUEVITE FROM THE EYREVILLE B DRILL CORE

Melt type	Type 1 clear glass		Type 2 altered melt		Type 3 recrystallized silica melt		Type 4 melt with microlites		Type 5 dark-brown melt	
	Average (*n* = 7)	Stdev.*	Average (*n* = 8)	Stdev.	Average (*n* = 6)	Stdev.	Average (*n* = 5)	Stdev.	Average (*n* = 12)	Stdev.
SiO_2	81.3	7.9	64.4	3.9	97.8	1.8	76.3	2.4	63.1	4.2
TiO_2	0.8	0.4	1.3	0.6	b.d.†	n.a.§	0.6	0.1	0.7	0.1
Al_2O_3	11.6	4.9	21.0	2.0	1.1	1.1	13.8	1.8	24.7	4.6
Fe_2O_3#	3.6	1.9	5.6	1.4	0.4	0.3	4.2	0.4	6.6	1.6
MnO	b.d.	n.a.	b.d.	n.a.	b.d.	n.a.	b.d.	n.a.	b.d.	n.a.
MgO	1.0	0.6	2.4	1.3	b.d.	n.a.	0.7	0.2	2.2	0.4
CaO	0.5	0.3	1.5	0.6	b.d.	n.a.	1.3	0.4	0.8	0.3
Na_2O	0.5	0.1	1.8	0.9	b.d.	n.a.	0.9	0.3	b.d.	n.a.
K_2O	0.6	0.3	1.8	1.3	b.d.	n.a.	2.1	0.7	1.6	1.0
Cr_2O_3	b.d.	n.a.	b.d.	n.a.	b.d.	n.a.	b.d.	n.a.	b.d.	n.a.

Note: Values are in wt%. Totals are normalized to 100 wt%.
*Standard deviation.
†Below detection limit.
§Not applicable.
#Total Fe as Fe_2O_3.

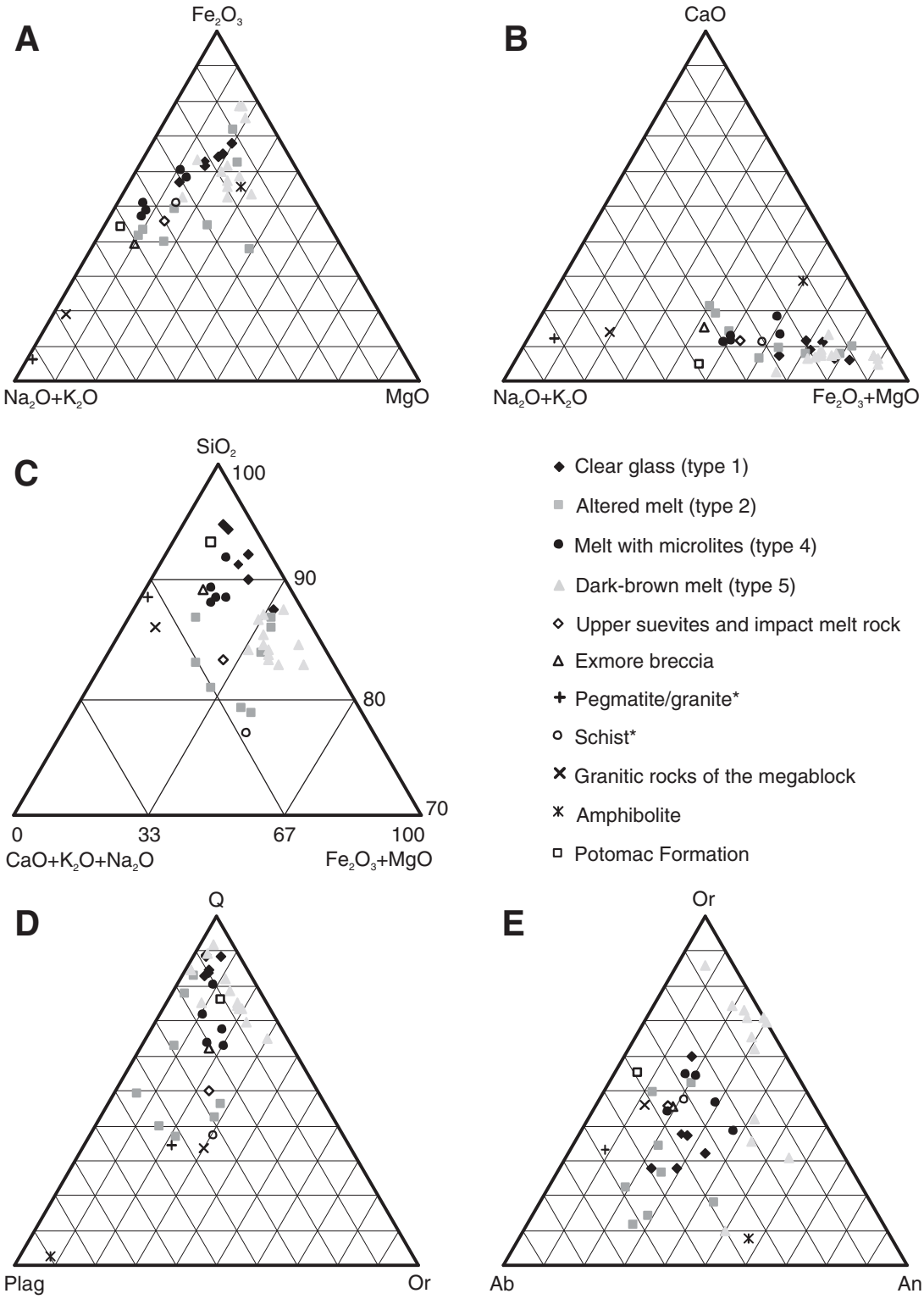

Figure 13. Ternary diagrams (A, B, and C) comparing contents of some major oxides in individual melt particles (this study) and main lithologies from the Eyreville drill core (compositions are from Schmitt et al., this volume). Each composition of a melt particle shown in the figures represents an average value of several analyses by scanning electron microscope with an energy-dispersive X-ray analyzer (SEM-EDX). Composition of the Potomac Formation (Table 5) is based on data from Deutsch and Koeberl (2006). An average composition of the melt-rich impactites (i.e., upper suevites and impact melt rock) is plotted for comparison. Proportions of normative minerals were calculated for individual melt particles and target lithologies according to the CIPW norm (Cross et al., 1902). (D–E) Ternary diagrams of the relative abundance of normative minerals. Q—quartz, Plag—plagioclase, Or—orthoclase, Ab—albite, An—anorthite. "*" denotes lithologies of the basal crystalline section.

the orthoclase-albite-anorthite diagram (Fig. 13A; the particles of type 3 plot into the quartz corner).

Mixing Calculations

In order to model the compositions of the polymict impactites (i.e., average polymict impactites, upper suevites, lower suevites, and impact melt rock) and of the melt particles, we performed mixing calculations using the Harmonic least-squares MiXing (HMX) calculation program (Stöckelmann and Reimold, 1989), similar to work done by, e.g., French et al. (1997) or Koeberl and Reimold (2003) for other impact structures. The compositions of the impactites and some target lithologies are shown in Tables 1 and 2, compositions of the melt particles are shown in Table 4, and composition of the target sedimentary formations is shown in Table 5. Eight components were used: schist and pegmatite/granite of the basement crystalline section, amphibolite, and cataclastic gneiss (Table 2), and four sedimentary target formations (Table 5). The composition of crystalline basement-derived components was determined as an average composition of samples of each lithology from the Eyreville drill core (Table 2; data from Schmitt et al., this volume). As sedimentary components (Table 5), average compositions of the lower Cretaceous Potomac Formation, the upper Paleocene Aquia Formation, the lower Eocene Nanjemoy Formation, and the middle Eocene Piney Formation were calculated based on data from Deutsch and Koeberl (2006). Relative component proportions were calculated using eight major oxide (SiO_2, TiO_2, Al_2O_3, Fe_2O_3, MgO, CaO, Na_2O, and K_2O) abundances, six major oxide abundances (Na_2O and K_2O excluded), and two sets of calculations with the six major oxide plus two trace-element abundances (Y, Th, or La, Hf). The alkali oxides were excluded from some runs because Na and K are mobile and volatile elements, and their content could be influenced by volatilization at high temperature (which would have influenced especially the impact melt rock and melt particles) and by postimpact alteration (see also French et al., 1997). The trace elements Y, Th, La, and Hf were used in the calculations because they are refractory, relatively immobile, and show large enough variations between the different component rocks.

The results of the mixing calculations for the impactites are summarized in Tables 6 and 7. According to our calculations, the main components of the average polymict impactites are gneiss (>40%), schist (>30%), and sediments (~20%, mainly from the Cretaceous Potomac Formation), and possibly minor proportions of other lithologies (pegmatite/granite and amphibolite; Table 6). Impact melt rock is composed mainly of schist (>40%), sediment (~40%, probably mostly Potomac Formation), and possibly minor gneiss and granite/pegmatite components. The upper suevites consist mainly of gneiss (nearly 50%), schist (>25%), and sediments (~20%, mostly Potomac Formation). The proportion of granite/pegmatite reaches >5% only in the calculations with Na and K involved. This is because the granite/pegmatite has high content of Na_2O (4.2 wt% on average) compared to the other components, which is significant in the calculations. The results of the mixing calculations for these impactites have low discrepancy factors (<1). Lower suevites have an even higher metamorphic rock component (>70% of gneiss and schist), besides sedimentary target rocks (~20%, mostly Nanjemoy Formation), but there are quite variable results and large discrepancies (>3.3) for the lower suevites. The discrepancy factors are a measure of the validity of the results: the lower the factor, the better and more statistically valid the result (Stöckelmann and Reimold, 1989). The data shown in Table 7 indicate that some of the calculations reproduce the observed compositions fairly well, lending credibility to the results.

TABLE 5. COMPOSITION OF PRE-IMPACT SEDIMENTARY FORMATIONS USED FOR MIXING CALCULATIONS

Formation	Potomac	Aquia	Nanjemoy	Piney
Age	Lower Cretaceous	Upper Paleocene	Lower Eocene	Middle Eocene
Number of samples	*n* = 3*	*n* = 2	*n* = 2	*n* = 1
(wt%)				
SiO_2	79.5	59.8	69.7	55.8
TiO_2	0.66	1.01	1.04	0.50
Al_2O_3	8.98	6.24	7.52	3.75
Fe_2O_3†	2.45	6.19	7.41	4.04
MnO	0.02	0.09	0.08	0.07
MgO	0.25	0.87	1.25	0.88
CaO	0.28	8.34	0.81	17.3
Na_2O	0.95	0.22	0.19	0.16
K_2O	1.93	1.89	2.51	1.38
P_2O_5	0.03	0.07	0.10	0.13
LOI	4.18	14.9	8.82	15.5
Total	99.23	99.63	99.38	99.53
(ppm)				
Sc	4.18	7.13	8.72	4.49
V	54	122	99	73
Cr	14.6	88.6	104	56.6
Co	2.75	3.43	4.96	3.70
Ni	10	19	21	13
Zn	22	50	81	55
Rb	46.2	73.3	104	58.8
Sr	112	375	97	692
Y	13	24	33	14
Zr	123	805	853	320
Cs	0.99	2.90	3.84	2.29
Ba	422	173	205	75
La	9.71	65.2	41.4	33.5
Ce	20.3	141	96.9	85.5
Nd	10.0	71.9	49.0	42.5
Sm	1.66	13.1	8.98	6.37
Eu	0.45	1.46	1.42	1.03
Gd	1.48	10.3	7.48	4.64
Tb	0.22	1.24	1.23	0.71
Tm	0.14	0.65	0.66	0.35
Yb	0.98	3.85	4.58	2.25
Lu	0.14	0.64	0.65	0.33
Hf	2.34	27.4	27.0	11.9
Ta	0.36	1.65	1.80	0.87
Th	3.78	25.8	14.6	9.07
U	0.93	7.20	6.95	3.95

Note: The values are averages calculated from data published by Deutsch and Koeberl (2006). LOI—loss on ignition.
**n*—number of samples averaged.
†Total Fe as Fe_2O_3.

TABLE 6. RESULTS OF HMX CALCULATIONS FOR AVERAGE POLYMICT IMPACTITES, UPPER SUEVITES, LOWER SUEVITES, AND IMPACT MELT ROCK

	Forcing to 100%	Pegmatite/ granite*	Cataclastic gneiss	Schist*	Amphibolite	Potomac Formation	Aquia Formation	Nanjemoy Formation	Piney Formation	Discre-pancy
Average polymict impactites										
8major	yes/no†	0.2 ± 2.0	49.7 ± 3.9	30.1 ± 1.8	0 ± 1.5	17.9 ± 2.5	2.0 ± 2.3	0 ± 1.6	0 ± 1.1	0.8
6major	yes/no	0 ± 3.7	34.3 ± 10.1	34.5 ± 3.0	3.6 ± 2.9	27.6 ± 9.3	0 ± 3.6	0.1 ± 2.3	0 ± 1.8	0.3
Y Th	yes/no	0 ± 0.8	49.1 ± 2.5	31.4 ± 1.9	0 ± 0.6	18.6 ± 0.9	0 ± 0.9	0 ± 0.9	0.9 ± 0.5	0.8
La Hf	yes/no	0 ± 2.0	47.0 ± 2.2	31.9 ± 1.7	0 ± 0.8	19.4 ± 0.9	1.8 ± 1.1	0 ± 1.5	0 ± 0.8	0.5
Average polymict impactites—volatile free										
8major	yes/no	2.4 ± 1.1	45.4 ± 3.1	30.9 ± 1.8	0 ± 1.1	16.4 ± 2.6	2.1 ± 2.4	2.8 ± 1.8	0 ± 1.0	0.4
6major	yes/no	0 ± 7.1	44.0 ± 16.3	32.3 ± 3.5	0 ± 5.4	21.0 ± 14.9	2.5 ± 6.6	0 ± 2.2	0 ± 2.2	0.1
Y Th	yes/no	0 ± 1.3	20.4 ± 2.9	46.5 ± 2.4	0 ± 1.2	28.6 ± 1.6	4.5 ± 1.4	0 ± 1.4	0 ± 0.8	1.1
La Hf	yes	0 ± 1.0	46.1 ± 1.7	31.9 ± 1.3	0 ± 0.4	20.2 ± 0.9	1.3 ± 0.7	0 ± 0.8	0.4 ± 0.5	0.3
	no	0 ± 1.0	46.2 ± 1.6	31.8 ± 1.3	0 ± 0.4	20.2 ± 0.9	1.3 ± 0.7	0 ± 0.7	0.4 ± 0.5	0.3
Impact melt rock										
	Forcing to 100%	Pegmatite/ granite*	Cataclastic gneiss	Schist*	Amphibolite	Potomac Formation	Aquia Formation	Nanjemoy Formation	Piney Formation	Discre-pancy
8major	yes/no	0 ± 1.1	0 ± 1.9	52.2 ± 1.9	0 ± 0.9	44.2 ± 2.1	0 ± 1.6	1.1 ± 1.5	2.5 ± 0.8	0.9
6major	yes/no	0 ± 1.8	0 ± 2.0	49.5 ± 1.8	0.7 ± 1.7	46.5 ± 1.9	0 ± 1.7	0.8 ± 1.5	2.5 ± 1.3	0.3
Y Th	yes/no	6.9 ± 1.2	9.6 ± 2.7	40.5 ± 2.2	0 ± 0.9	31.2 ± 1.5	5.4 ± 1.3	6.4 ± 1.6	0 ± 1.0	0.8
La Hf	yes/no	0 ± 1.0	9.2 ± 3.1	47.7 ± 3.4	0 ± 0.9	37.9 ± 2.1	5.1 ± 1.4	0 ± 1.2	0 ± 1.0	6.3
Impact melt rock—volatile free										
8major	yes	1.7 ± 2.0	0 ± 3.0	49.0 ± 1.7	0 ± 0.9	41.7 ± 1.9	0 ± 2.7	5.3 ± 2.3	2.3 ± 1.0	0.4
	no	2.1 ± 2.3	0 ± 3.3	48.5 ± 1.8	0 ± 1.0	40.9 ± 2.0	0 ± 3.0	5.9 ± 2.6	2.3 ± 1.2	0.4
6major	yes	6.8 ± 1.7	0 ± 2.2	46.1 ± 1.3	0 ± 1.2	36.9 ± 2.4	5.0 ± 2.2	5.2 ± 1.1	0 ± 0.9	0.1
	no	4.7 ± 4.0	0 ± 7.0	46.4 ± 2.2	0 ± 3.1	39.9 ± 6.9	5.2 ± 5.4	3.2 ± 1.0	0 ± 1.4	0.01
Y Th	yes	0 ± 2.7	11.2 ± 3.0	41.6 ± 2.5	0 ± 1.1	40.9 ± 1.6	6.4 ± 2.2	0 ± 2.3	0 ± 1.5	0.6
	no	0 ± 2.8	12.3 ± 2.9	40.1 ± 2.5	0 ± 1.0	40.4 ± 1.6	6.5 ± 2.3	0 ± 2.3	0 ± 1.5	0.5
La Hf	yes/no	2.1 ± 1.7	11.3 ± 2.9	43.3 ± 2.6	0 ± 0.7	37.2 ± 1.5	6.2 ± 1.5	0 ± 1.3	0 ± 0.8	1.3
Upper suevites (1397–1474 m)										
	Forcing to 100%	Pegmatite/ granite*	Cataclastic gneiss	Schist*	Amphibolite	Potomac Formation	Aquia Formation	Nanjemoy Formation	Piney Formation	Discre-pancy
8major	yes/no	4.4 ± 2.3	48.8 ± 4.3	24.5 ± 2.0	2.4 ± 1.6	18.4 ± 2.7	1.6 ± 2.5	0 ± 1.8	0 ± 1.3	1.2
6major	yes/no	0 ± 2.7	31.5 ± 7.8	31.3 ± 2.3	5.5 ± 2.1	31.6 ± 7.2	0 ± 2.6	0 ± 1.9	0.1 ± 1.5	0.3
Y Th	yes/no	1.1 ± 0.9	46.8 ± 2.1	27.7 ± 1.5	1.7 ± 0.6	21.6 ± 0.8	0 ± 1.0	0 ± 0.9	1.0 ± 0.5	0.5
La Hf	yes/no	0 ± 0.9	50.0 ± 1.8	27.9 ± 1.4	0 ± 0.6	20.4 ± 0.9	0 ± 1.3	0 ± 1.0	1.7 ± 0.7	0.4
Upper suevites—volatile free										
8major	yes/no	5.8 ± 1.5	46.4 ± 3.6	25.6 ± 2.2	1.5 ± 1.5	16.4 ± 3.1	2.3 ± 2.9	2.0 ± 2.2	0 ± 1.2	0.7
6major	yes	1.4 ± 2.9	47.7 ± 7.2	27.6 ± 1.8	0 ± 2.3	19.7 ± 6.6	3.6 ± 2.4	0 ± 1.4	0 ± 1.2	0.2
	no	0.9 ± 4.2	47.4 ± 9.8	27.6 ± 2.1	0 ± 3.3	20.2 ± 8.9	3.5 ± 3.8	0 ± 1.5	0 ± 1.5	0.1
Y Th	yes/no	0 ± 1.6	16.0 ± 3.1	47.4 ± 2.5	0 ± 1.2	31.3 ± 1.7	5.0 ± 1.7	0 ± 1.8	0 ± 1.0	1.1
La Hf	yes	0 ± 0.6	47.9 ± 1.3	28.9 ± 1.0	0 ± 0.5	21.6 ± 0.7	0 ± 1.2	0 ± 0.9	1.6 ± 0.7	0.2
	no	0 ± 0.6	48.1 ± 1.2	28.5 ± 1.0	0 ± 0.5	21.5 ± 0.7	0.1 ± 1.2	0 ± 0.9	1.6 ± 0.7	0.2
Lower suevites (1474–1551 m)										
	Forcing to 100%	Pegmatite/ granite*	Cataclastic gneiss	Schist*	Amphibolite	Potomac Formation	Aquia Formation	Nanjemoy Formation	Piney Formation	Discre-pancy
8major	yes/no	0 ± 3.8	47.1 ± 9.5	36.9 ± 5.1	0 ± 3.4	0 ± 4.3	0 ± 4.5	16.0 ± 4.0	0 ± 2.1	6.8
6major	yes/no	0 ± 9.6	63.4 ± 14.7	28.9 ± 7.6	0 ± 8.4	0 ± 11.4	0 ± 7.5	7.7 ± 5.3	0 ± 6.9	3.4
Y Th	yes/no	0 ± 1.5	63.0 ± 5.2	29.9 ± 3.7	0 ± 1.4	0 ± 1.8	0 ± 1.7	7.1 ± 2.5	0 ± 1.2	3.5
La Hf	yes/no	0 ± 3.5	61.5 ± 6.0	32.6 ± 4.6	0 ± 3.7	4.7 ± 5.2	0 ± 2.9	1.2 ± 2.9	0 ± 2.0	3.8
Lower suevites—volatile free										
8major	yes	0 ± 3.9	37.9 ± 9.0	42.7 ± 5.0	0 ± 3.3	0 ± 4.4	0 ± 4.6	19.4 ± 4.0	0 ± 2.0	5.9
	no	0 ± 3.1	1.8 ± 3.3	65.5 ± 4.1	0 ± 1.9	0 ± 3.0	0 ± 3.2	32.7 ± 3.9	0 ± 1.6	5.5
6major	yes/no	0 ± 10.3	48.9 ± 14.7	37.2 ± 7.6	0 ± 8.5	3.2 ± 11.5	0 ± 7.1	10.7 ± 5.0	0 ± 6.7	3.3
Y Th	yes/no	0 ± 2.3	19.4 ± 5.8	54.4 ± 4.1	0 ± 2.3	6.8 ± 2.9	0 ± 2.2	19.4 ± 3.5	0 ± 1.4	3.7
La Hf	yes/no	0 ± 3.5	72.2 ± 5.7	27.8 ± 4.5	0 ± 1.5	0 ± 2.3	0 ± 2.3	0 ± 2.3	0 ± 1.3	4.7

Note: Values are in %. All calculations were made with normal values and with volatile-free values, where all components and mixtures were recalculated on volatile-free basis; all calculations were made with and without forcing to 100%, the results of which are mostly similar. 8major—calculations with oxides of eight major elements (Si, Ti, Al, Mg, Fe, Ca, Na, and K); 6major—calculations with oxides of six major elements (Si, Ti, Al, Mg, Fe, and Ca); Y Th—calculations with six major oxides and Y and Th; La Hf—calculations with six major oxides and La and Hf. The compositions of all components and mixtures are shown in Tables 1, 2, and 5. Harmonic least-squares MiXing (HMX) calculations are after Stöckelmann and Reimold (1989).

*From the basal crystalline section.

†Yes/no means that results with and without forcing to 100% are the same.

TABLE 7. CALCULATED COMPOSITIONS OF CHESAPEAKE BAY IMPACTITES (HMX CALCULATIONS) COMPARED WITH OBSERVED COMPOSITIONS

	Polymict impactites				Impact melt rock				Upper suevites				Lower suevites			
	8major	$\Delta_{obs-calc}$*	La Hf	$\Delta_{obs-calc}$	8major	$\Delta_{obs-calc}$	Y Th	$\Delta_{obs-calc}$	8major	$\Delta_{obs-calc}$	La Hf	$\Delta_{obs-calc}$	8major	$\Delta_{obs-calc}$	Y Th	$\Delta_{obs-calc}$
Forcing to 100%	yes/no†		yes/no		yes/no		yes/no		yes/no		yes/no		yes/no		yes/no	
SiO_2	66.0	0.21	66.0	0.19	68.1	0.14	68.0	0.24	66.5	0.21	66.5	0.17	63.8	0.26	63.9	0.14
TiO_2	0.87	0.02	0.87	0.02	0.80	0.001	0.80	0.002	0.85	0.02	0.86	0.01	0.94	0.06	0.92	0.08
Al_2O_3	14.8	0.01	14.8	0.01	13.9	0.002	13.9	0.03	14.7	0.009	14.6	0.03	15.4	0.21	15.6	0.08
Fe_2O_3	5.63	–0.003	5.63	–0.003	5.34	0.008	5.33	0.02	5.45	0.004	5.46	–0.02	6.36	–0.10	6.28	–0.02
MgO	1.81	–0.03	1.80	–0.02	1.18	–0.01	1.20	–0.032	1.81	–0.024	1.8	–0.009	2.09	0.01	2.13	–0.03
CaO	1.49	0.01	1.48	–0.02	1.59	0.002	1.59	0.001	1.59	0.015	1.58	0.02	1.22	–0.09	1.21	–0.08
Na_2O	1.47	0.07	n.a.§	n.a.	1.29	–0.002	n.a.	n.a.	1.62	0.16	n.a.	n.a.	1.12	–0.08	n.a.	n.a.
K_2O	3.10	0.11	n.a.	n.a.	2.91	0.11	n.a.	n.a.	3.02	0.08	n.a.	n.a.	3.30	0.29	n.a.	n.a.
La	n.a.	n.a.	36.2	0.46	n.a.	n.a.	n.a.	n.a.	n.a.	n.a.	35.3	0.18	n.a.	n.a.	n.a.	n.a.
Hf	n.a.	n.a.	6.40	–0.03	n.a.	n.a.	n.a.	n.a.	n.a.	n.a.	6.19	–0.01	n.a.	n.a.	n.a.	n.a.
Y	n.a.	n.a.	n.a.	n.a.	n.a.	n.a.	37.8	0.21	n.a.	n.a.	n.a.	n.a.	n.a.	n.a.	48.6	1.42
Th	n.a.	n.a.	n.a.	n.a.	n.a.	n.a.	10.4	0.08	n.a.	n.a.	n.a.	n.a.	n.a.	n.a.	13.7	–0.17
Calculations with volatile-free compositions																
	Polymict impactites				Impact melt rock				Upper suevites				Lower suevites			
	8major	$\Delta_{obs-calc}$	La Hf	$\Delta_{obs-calc}$	8major	$\Delta_{obs-calc}$	Y Th	$\Delta_{obs-calc}$	8major	$\Delta_{obs-calc}$	La Hf	$\Delta_{obs-calc}$	8major	$\Delta_{obs-calc}$	Y Th	$\Delta_{obs-calc}$
Forcing to 100%	yes/no		no		yes/no		no		yes/no		no		no		yes/no	
SiO_2	68.8	–0.04	68.8	–0.03	70.6	–0.01	70.6	–0.001	69.1	–0.04	69.1	–0.03	66.9	0.21	67.0	0.10
TiO_2	0.9	0.02	0.91	0.02	0.83	–0.001	0.83	–0.003	0.88	0.02	0.89	0.009	1.04	0.01	1.01	0.05
Al_2O_3	15.4	–0.02	15.4	–0.03	14.4	–0.002	14.4	0.013	15.2	–0.02	15.2	–0.002	16.3	0.07	16.3	0.08
Fe_2O_3	5.89	–0.05	5.86	–0.02	5.54	–0.009	5.53	0.002	5.68	–0.05	5.68	–0.04	6.7	–0.16	6.66	–0.11
MgO	1.87	–0.02	1.87	–0.02	1.23	–0.018	1.25	–0.43	1.86	–0.01	1.86	–0.009	2.14	0.04	2.14	0.05
CaO	1.56	–0.002	1.56	0.002	1.65	0	1.65	–0.003	1.65	–0.005	1.65	0.002	1.26	–0.08	1.26	–0.08
Na_2O	1.55	0.45	n.a.	n.a.	1.35	–0.006	n.a.	n.a.	1.69	0.15	n.a.	n.a.	1.12	–0.03	n.a.	n.a.
K_2O	3.25	0.08	n.a.	n.a.	3.04	0.08	n.a.	n.a.	3.18	0.03	n.a.	n.a.	3.57	0.19	n.a.	n.a.
La	n.a.	n.a.	37.6	0.49	n.a.	n.a.	n.a.	n.a.	n.a.	n.a.	36.5	0.19	n.a.	n.a.	n.a.	n.a.
Hf	n.a.	n.a.	6.63	–0.03	n.a.	n.a.	n.a.	n.a.	n.a.	n.a.	6.41	–0.01	n.a.	n.a.	n.a.	n.a.
Y	n.a.	n.a.	n.a.	n.a.	n.a.	n.a.	39.6	0.07	n.a.	n.a.	n.a.	n.a.	n.a.	n.a.	53.0	–0.84
Th	n.a.	n.a.	n.a.	n.a.	n.a.	n.a.	10.8	0.11	n.a.	n.a.	n.a.	n.a.	n.a.	n.a.	13.8	0.32

Note: Compositions of the impactites as obtained from the HMX calculations are shown for selected runs presented in Table 6. 8major—calculations with oxides of eight major elements (Si, Ti, Al, Mg, Fe, Ca, Na, and K); Y Th—calculations with oxides of six major elements (Si, Ti, Al, Mg, Fe, and Ca) and Y and Th; La Hf—calculations with six major oxides and La and Hf.

*$\Delta_{obs-calc}$ = difference between observed and calculated value.

†Yes/no means that results with and without forcing to 100% are the same.

§Not applicable.

The same eight target rocks were used to model the composition of the different types of melt particles (Tables 8 and 9). The components of the SiO_2-rich melt (type 3) were not calculated because many major oxides were below detection limit, and the composition suggests a single silica-rich precursor. The mixing calculations with eight major elements for the clear glass and altered melt particles yielded very large discrepancy factors (>18) for most melt types, and a lower discrepancy (5.3) was obtained only for melt type 4. According to the calculations with six major elements, particles of type 1 could have had mostly sedimentary precursors (mostly from Potomac Formation) and ~27% of a gneiss component, whereas the melt particles of type 2 could be mixtures of schist with a minor pegmatite/granite component. Calculations for melt type 4 result in a mixture of Potomac Formation (~77% or 49% calculated with eight or six major elements, respectively), schist (20% or 27%), pegmatite (0% or 21%), and minor contributions of other components. Melt type 5 could not be modeled as a mixture of the major lithologies with reasonable discrepancy values. The melt particles were also modeled as mixtures of common rock-forming minerals. The main components of the clear glass particles would be quartz (~70%), plagioclase, muscovite, biotite, and chlorite. However, some calculated abundances show fairly large deviations from the observed compositions of the melt particles, casting doubt on the validity of the mixing calculation results. The altered melt particles can be modeled with a somewhat better discrepancy factor as mixtures of quartz (~30%), muscovite (~30%), biotite, plagioclase, and chlorite. Melt type 4 could not be modeled as mixtures of the minerals with reasonable discrepancy values (discrepancy factors are >23). Components of melt type 5 could be muscovite (~44%), quartz (~31%), biotite (20%), and anorthite (~4%), but the discrepancy obtained is relatively high (>4). Mixing calculations do

TABLE 8. RESULTS OF HMX MIXING CALCULATIONS FOR DIFFERENT MELT TYPES

Clear glass (type 1), reproduced from target lithologies										
	Forcing to 100%	Pegmatite/ granite*	Cataclastic gneiss	Schist*	Amphibolite	Potomac Formation	Aquia Formation	Nanjemoy Formation	Piney Formation	Discre-pancy
6major	yes/no†	0 ± 2.4	27.9 ± 6.7	0 ± 2.2	0 ± 1.6	72.1 ± 5.0	0 ± 2.3	0 ± 2.2	0 ± 1.2	1.1
Clear melt (type 1), reproduced from rock-forming minerals										
		Qtz	Kfs	Alb	An	Bt	Ms	Chl#		
8major	yes	76.9 ± 2.9	0 ± 1.6	4.5 ± 1.0	3.4 ± 0.8	5.0 ± 1.8	3.7 ± 1.9	6.6 ± 1.8		14.6
	no	72.5 ± 2.6	0 ± 1.6	4.4 ± 0.9	3.2 ± 0.7	6.4 ± 1.7	1.9 ± 1.8	4.8 ± 1.6		13.3
6major	yes	64.5 ± 7.2	0 ± 9.1	0 ± 9.1	2.8 ± 0.6	12.2 ± 2.1	20.5 ± 6.6	0 ± 5.1		4.3
	no	64.6 ± 7.2	0 ± 9.1	0 ± 9.1	2.8 ± 0.6	12.2 ± 2.1	20.5 ± 6.6	0 ± 5.1		4.3
Altered melt (type 2), reproduced from target lithologies										
	Forcing to 100%	Pegmatite/ granite*	Cataclastic gneiss	Schist*	Amphibolite	Potomac Formation	Aquia Formation	Nanjemoy Formation	Piney Formation	Discre-pancy
6major	yes	5.3 ± 4.9	0 ± 6.0	94.7 ± 9.0	0 ± 3.9	0 ± 6.6	0 ± 5.5	0 ± 5.0	0 ± 3.3	8.6
	no	9.2 ± 5.9	0 ± 7.1	81.0 ± 9.7	0 ± 4.4	0 ± 7.4	0 ± 6.2	0 ± 5.5	0 ± 3.8	8.7
Altered melt (type 2), reproduced from rock-forming minerals										
		Qtz	Kfs	Alb	An	Bt	Ms	Chl#		
8major	yes	30.5 ± 1.9	0 ± 5.2	16.1 ± 2.3	8.8 ± 1.3	8.5 ± 4.1	25.0 ± 3.2	11.1 ± 2.2		11.4
	no	30.5 ± 1.9	0 ± 5.2	16.2 ± 2.3	8.8 ± 1.3	8.5 ± 4.1	25.0 ± 3.2	11.1 ± 2.2		11.4
6major	yes	33.4 ± 3.0	0 ± 9.0	0 ± 9.0	8.1 ± 2.1	22.8 ± 2.5	35.7 ± 6.0	0 ± 2.4		2.3
	no	33.4 ± 3.0	0 ± 9.0	0 ± 9.0	8.1 ± 2.1	22.8 ± 2.5	35.7 ± 6.0	0 ± 2.4		2.3
Melt with microlites (type 4), reproduced from target lithologies										
	Forcing to 100%	Pegmatite/ granite*	Cataclastic gneiss	Schist*	Amphibolite	Potomac Formation	Aquia Formation	Nanjemoy Formation	Piney Formation	Discre-pancy
8major	yes	0 ± 1.2	0 ± 2.2	20.0 ± 4.3	0 ± 1.0	76.7 ± 3.0	0 ± 2.0	0 ± 2.1	3.3 ± 1.2	5.9
	no	0 ± 1.2	0 ± 2.4	20.2 ± 4.1	0 ± 1.1	73.5 ± 3.4	0 ± 2.2	0 ± 2.2	3.3 ± 1.2	5.3
6major	yes/no	21.1 ± 3.6	0 ± 3.4	26.7 ± 3.5	0 ± 1.1	48.8 ± 5.0	3.4 ± 3.1	0 ± 2.8	0 ± 1.7	1.2
Dark-brown melt (type 5), reproduced from rock-forming minerals										
		Qtz	Kfs	Alb	An	Bt	Ms	Chl#		
6major	yes/no	30.5 ± 2.6	0 ± 1.9	0 ± 1.9	4.4 ± 1.0	19.8 ± 1.4	44.4 ± 3.1	0 ± 1.3	0.9 ± 1.3	4.5

Note: Values are in %. All compositions of the components were recalculated to the same format as data obtained for the melt particles by scanning electron microscope with an energy-dispersive X-ray analyzer (SEM-EDX): 100% of SiO_2, TiO_2, Al_2O_3, Fe_2O_3, MgO, CaO, Na_2O, K_2O, and Cr_2O_3. All calculations were made with and without forcing to 100%, and the results are mostly similar. 8major—calculations with oxides of eight major elements (Si, Ti, Al, Mg, Fe, Ca, Na, and K); 6major—calculations with oxides of six major elements (Si, Ti, Al, Mg, Fe, and Ca). The compositions of all components are shown in Tables 1, 2, and 5, and compositions of the melt particles are given in Table 4. Symbols of rock-forming minerals are after Kretz (1983). Compositions of the rock-forming minerals from Anthony et al. (1995) were used. Harmonic least-squares MiXing (HMX) calculations are after Stöckelmann and Reimold (1989). Only results yielding discrepancies lower than 15 are shown.

*From the basal crystalline section.

†Yes/no means that results with and without forcing to 100% are the same.

#Chamosite.

TABLE 9. CALCULATED COMPOSITIONS OF THE MELT PARTICLES (HMX CALCULATIONS) COMPARED WITH OBSERVED COMPOSITIONS

Melt type	Clear glass (type 1)			Altered melt (type 2)				Melt with microlites (type 4)				Dark-brown melt (type 5)	
	6major	$\Delta_{obs-calc}$*	6major	$\Delta_{obs-calc}$	6major	$\Delta_{obs-calc}$	6major	$\Delta_{obs-calc}$	8major	$\Delta_{obs-calc}$	6major	$\Delta_{obs-calc}$	6major	$\Delta_{obs-calc}$
Reproduced from	Target rocks		Minerals		Target rocks		Minerals		Target rocks		Target rocks		Minerals	
Forcing to 100%	yes/no†		no		yes		no		no		yes/no		yes/no	
SiO_2	80.6	0.70	80.3	0.98	63.9	0.54	63.0	1.41	76.3	0.02	76.2	0.10	61.7	1.43
TiO_2	0.78	0.02	0.42	0.38	0.97	0.33	0.79	0.51	0.61	–0.007	0.61	–0.006	0.68	0.02
Al_2O_3	11.4	0.25	11.0	0.61	20.7	0.31	20.5	0.48	13.5	0.33	13.7	0.10	22.6	2.13
Fe_2O_3	3.54	0.06	2.91	0.69	5.95	–0.35	5.45	0.15	4.18	0.02	4.18	0.02	5.08	1.52
MgO	0.90	0.10	1.36	–0.36	2.29	0.11	2.75	–0.35	0.70	0.003	0.71	–0.01	2.41	–0.21
CaO	0.55	–0.05	0.50	–0.001	1.58	–0.08	1.48	0.02	1.30	–0.002	1.30	0.005	0.80	0.002
Na_2O	n.a.§	n.a.	n.a.	n.a.	n.a.	n.a.	n.a.	n.a.	1.01	–0.11	n.a.	n.a.	n.a.	n.a.
K_2O	n.a.	n.a.	n.a.	n.a.	n.a.	n.a.	n.a.	n.a.	2.21	–0.11	n.a.	n.a.	n.a.	n.a.

Note: Compositions of the melt particles as obtained from the HMX mixing calculations are shown for selected runs presented in Table 8. 8major—calculations with oxides of eight major elements (Si, Ti, Al, Mg, Fe, Ca, Na, and K); 6major—calculation with oxides of six major elements (Si, Ti, Al, Mg, Fe, and Ca).

*$\Delta_{obs-calc}$ = difference between observed and calculated value.

†Yes/no means that results with and without forcing to 100% are the same.

§Not applicable.

not suggest an appreciable content of other mafic minerals (such as amphibole or pyroxene) in the melt particles. Results of these calculations are not shown, since they do not provide any additional information and some of them have high discrepancies.

Carbon Isotopes

The $\delta^{13}C$ values reported in ‰ relative to the Vienna Peedee belemnite (VPDB) standard are shown in Figure 14 and listed in Table 10. The sedimentary clasts contain <3 wt% carbon and have $\delta^{13}C$ values between −29‰ and −21‰. The vitrinite and the graphitic gneiss samples have values of −20‰ and −21‰, respectively. The $\delta^{13}C$ values of the carbonate material are about −7‰ and −14‰, and the melt particle from suevite at 1452.2 m depth yielded a value of −8‰. The different types of samples analyzed can be clearly distinguished according to their C content and isotopic composition (Fig. 14).

DISCUSSION

Composition of the Impactites and Melt Particles

The composition of the polymict impactites varies mostly due to the variable contents of clasts of different target lithologies. The decreasing trend of SiO_2 content with depth can be explained by a decrease of the relatively SiO_2-rich sedimentary component, whereas Al_2O_3, Fe_2O_3, and TiO_2 increase with depth (Fig. 4), probably due to an enhancement in gneiss and schist components, which are relatively rich in these oxides (Tables 1

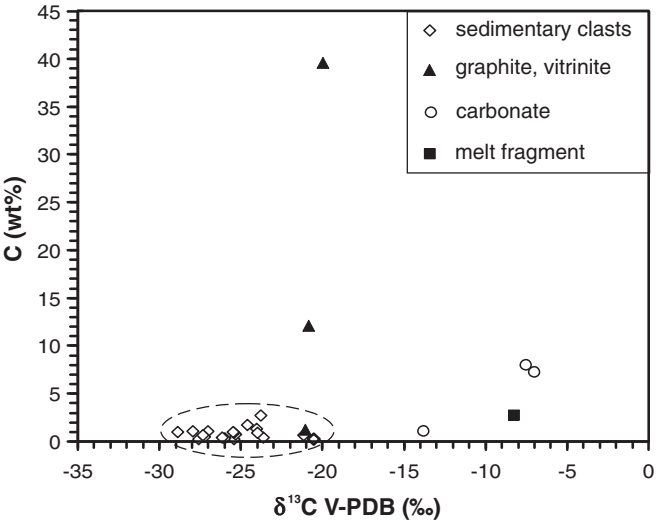

Figure 14. Carbon content against $\delta^{13}C$ values of the analyzed samples of sedimentary clasts, graphite-rich breccia, carbonate veins, carbonate in a melt fragment, and vitrinite from the Eyreville drill core. The sedimentary clasts (marked with dashed line) contain <3 wt% carbon and have $\delta^{13}C$ values from −29‰ to −21‰. V-PDB—Vienna Peedee belemnite.

and 2). This interpretation is in agreement with petrographic observations (Bartosova et al., this volume), as in the lower part of the impact breccia section, clasts of gneiss and schist are more abundant than in the upper part. However, in some of the polymict impactites from ~1520 m depth, the sedimentary clast component seems to be dominant (Bartosova et al., this volume). The lower SiO_2 and higher Al_2O_3 and Fe_2O_3 contents in these samples could be caused by an increased proportion of fine-grained sediments (e.g., mudstones and shales) in the sedimentary component.

The upper part of the impact breccia section (above 1450 m) shows an enrichment of Na that might be a result of an enhanced granitic component (Schmitt et al., this volume) or of a seawater component. However, if the enhanced Na content originated from a granitic component, then enrichment in other elements abundant in granite (e.g., K and Rb) should also be observed, which is not the case (see Figs. 4 and 8). On the other hand, the samples with high Na contents are also relatively enriched in Mg, which has very low concentrations in granite, but is the second most abundant cation in seawater. Sanford (2005) suggested that the Exmore breccia may still contain the original seawater from the time of breccia deposition. Brines sampled from the Exmore breccia in the Kiptopeke drill core (Sanford, 2005) and from the impact breccia section of the Eyreville core (Gohn et al., 2008) both have high salinities.

The ternary diagram $CaO–K_2O + Na_2O–FeO + MgO$ (Fig. 6) shows that the relative abundances of these oxides in suevite, impact melt rock, and cataclastic gneiss are very similar. The suevite shows the largest range in the ternary diagram, in accordance with its larger petrographic heterogeneity compared to the impact melt rock and gneiss. For most elements, variations in the concentrations are much smaller in the upper part of the impact breccia than in the lower part (Figs. 4 and 8). This is in agreement with petrographic observations—the upper parts of the impact breccia section are more homogeneous (contain more matrix and millimeter-sized clasts are dominant above 1430 m), whereas the clasts become larger in the lower parts (Bartosova et al., this volume).

Elevated siderophile element contents can be significant indicators of a meteoritic component (e.g., Koeberl, 1998). The contents of Co, Ni, and Cr in the polymict impactites are generally low (Tables 1 and 3). The highest values of siderophile elements were observed in cataclastic, monomict breccia of gneiss, but this is due to the original mineral composition of the gneiss (e.g., local sulfide provenance). The highest meteoritic component would be expected to be present in the melt-rich rocks (e.g., Montanari and Koeberl, 2000), but no significant enrichment of siderophile elements was detected in the analyzed impact melt rock samples. The exceptionally high Au content in sample KB-2 (7.3 ppb) is not correlated with an enrichment in other siderophile elements. The highest content of Ir found by Lee et al. (2006) in a clast of impact melt rock from the STP test hole was 0.466 ppb. However, this value is still below the limit of detection of our INAA measurements. Because the contribution of material from the impactor is usually very small within the impactites and because the contents of Cr, Co, and Ni can be high in the target rocks, detailed platinum group element analyses are more suitable for identifying a meteoritic component (Koeberl, 1998). For further discussion, see McDonald et al. (this volume).

TABLE 10. RESULTS OF THE CARBON STABLE ISOTOPE ANALYSES OF THE SAMPLES FROM EYREVILLE DRILL CORE

Sample	Lithological unit	Depth (m)	Type of clast	$\delta^{13}C$ (‰, VPDB)		Carbon content (wt%)		Weight (µg)
CB6-027	E	508.59	Arkose	–20.5	± 0.39	0.23	± 0.02	1935
CB6-034-1	E	521.74	Mudstone	–23.8	± 0.84	2.75	± 0.25	4225
CB6-034-2	E	521.74	Arkose	–27.6	± 1.33	0.22	± 0.04	2461
CB6-036-1	E	523.28	Black shale	–24.6	± 0.45	1.76	± 0.35	2298
CB6-036-2	E	523.28	Siltstone	–28.9	± 0.45	1.02	± 0.12	2692
CB6-059	E	761.79	Vitrinite	–20.0	± 0.43	39.6	± 1.78	165
CB6-094	S	1399.73	Siltstone	–25.5	± 0.73	0.21	± 0.01	4493
CB6-096	S	1409.30	Mudstone	–23.6	± 0.17	0.45	± 0.26	2610
CB6-099	S	1421.65	Mudstone	–27.0	± 0.72	1.03	± 0.15	3139
CB6-107-1	S	1449.81	Mudstone	–25.3	± 0.17	0.77	± 0.04	3777
CB6-107-2	S	1449.81	Mudstone	–24.0	± 0.72	1.35	± 0.05	2643
CB6-109-1	S	1452.33	Melt particle	–8.25	± 0.89	2.70	± 0.26	3688
CB6-109-2	S	1452.33	Shale	–26.0	± 0.83	0.29	± 0.03	4756
CB6-110-1	S	1455.22	Shale	–25.5	± 0.43	0.90	± 0.13	2648
CB6-110-2	S	1455.22	Siltstone	–26.1	± 0.71	0.45	± 0.01	3487
CB6-113	S	1463.98	Siltstone/shale	–21.1	± 1.07	0.64	± 0.06	3534
CB6-114	S	1467.37	Siltstone	–27.2	± 0.55	0.51	± 0.03	3383
CB6-120-1	S	1504.25	Shale	–25.5	± 0.13	1.00	± 0.02	3377
CB6-120-2	S	1504.25	Siltstone	–24.0	± 0.71	0.88	± 0.08	2907
CB6-122	S	1511.86	Carbonate vein	–7.53	± 0.84	7.98	± 0.38	824
CB6-126	S	1529.27	Siltstone	–27.4	± 0.77	0.63	± 0.05	4552
CB6-131	GB	1551.48	Graphite	–20.8	± 0.28	12.1	± 1.55	363
CB6-132-1	GB	1559.51	Graphite-rich breccia	–21.1	± 0.71	1.26	± 0.71	3134
CB6-132-2	GB	1559.51	Carbonate vein	–13.8	± 1.27	1.07	± 0.24	2674
CB6-145	SC	1667.80	Carbonate vein	–7.01	± 1.07	7.28	± 0.89	496

Note: Lithological units: E—Exmore, S—suevite, GB—graphitic breccia, SC—schist.

Some of our results of the mixing calculations for the impactites are constrained by rather low discrepancy factors (<1). However, the discrepancy values of the calculations for lower suevites are overall larger (>3), which suggests that these results should be considered with caution. The mixing calculations suggest that the polymict impactites were derived mostly from the metamorphic rocks of the crystalline basement. Other important target components were sediments, mostly from the lowermost and thickest sedimentary unit, i.e., the Cretaceous Potomac Formation (~600–1300 m thick; Poag et al., 2004; Fig. 3). The impact melt rock is composed mainly of schist and sedimentary target rocks (Potomac Formation). The lower suevites (below 1474 m) are relatively enriched in the metamorphic rock (gneiss, schist) component compared to the upper suevites, according to the mixing calculations; this would be in agreement also with the trends of major-element contents with depth, discussed already.

The granite/pegmatite component is nearly absent in the lower suevites but can constitute more than 5% in the upper suevites (only in the calculations where Na_2O and K_2O are included). This would be in agreement with the suggestion by Schmitt et al. (this volume) that the enrichment of Na in the upper suevites is due to an enhanced granitic component; however, as discussed already, the enhanced Na content can be a result of a seawater component. We have observed granitic clasts in most parts of the core, but they are relatively rare.

Mixing calculations suggest that the sedimentary component of the upper suevites originates mostly from the lower Cretaceous Potomac Formation. The sedimentary component in the lower suevites is seemingly derived mostly from the lower Eocene Nanjemoy Formation; however, this result should be considered with caution due to the high discrepancy values of the calculations for lower suevites.

Results of the mixing calculations are generally in agreement with petrographical observations (i.e., clast populations present) as reported by Bartosova et al. (this volume). The petrographic observations confirm the abundance of gneiss/schist, especially in some melt-poor intervals of the polymict impactites (i.e., 1430–1448 m and 1474–1486 m; Bartosova et al., this volume). For the sedimentary component, it is not possible to distinguish, based on our petrographic observations, from which sedimentary formation the clasts originated due to the absence of microfossil constraints. In the results of our mixing calculations, the metamorphic rock component is higher, and sedimentary component is lower, than expected from the point counting data for suevite (i.e., the estimated proportion of sedimentary clasts is higher than of crystalline clasts; Bartosova et al., this volume). However, the clasts constitute only ~45 vol% of the suevite, on average, and the rest of the analyzed material is present as matrix and melt (Bartosova et al., this volume), which can have different compositions from the population of larger clasts.

The melt particles of type 1 and 4 were best modeled as mixtures of target lithologies (Potomac Formation and crystalline basement lithologies), whereas for melt types 2 and 5, mixtures of rock-forming minerals (quartz, anorthite, and mica) have relatively lower discrepancy factors than calculations with rock-type components and would, thus, appear to be more reliable. However, the results of mixing calculations for the melt particles are not satisfactory, as shown by deviations between observed and calculated values given in Table 9. The calculations with eight major elements gave mostly high discrepancies; relatively lower discrepancies were obtained only in the calculations with six major elements. The silica melt (type 3) is probably a melt of quartz or a silica-rich rock. The dark-brown melt could be a melt of a shale or a fine-grained sediment; also the composition is very similar to the composition of fine-grained sedimentary clasts (mudstones) in the suevite (as analyzed by SEM-EDX). The original composition, especially of the type 2 melt particles, could have been modified significantly by hydrothermal alteration. Changes of composition due to hydrothermal alteration have been described, for example, in melt particles from the Yaxcopoil-1 drill core within the Chicxulub impact structure (Hecht et al., 2004; Tuchscherer et al., 2004). At Chicxulub, Claeys et al. (2003) observed silicate melt phases with different composition and degree of alteration at the thin section scale and, thus, concluded that no widespread homogenization of the melt took place. This is similar to our observations and conclusions for melt particles from the Chesapeake Bay impact structure (Bartosova et al., this volume; Reimold et al., this volume).

Comparison of the Melt-Rich Impactites and the North American Tektites

The average chemical composition of melt-rich impactites (i.e., upper suevites [from above 1474 m depth] and impact melt rock; average of 57 samples) was compared with the composition of bediasites (Deutsch and Koeberl, 2006) and georgiaites (Albin et al., 2000), and the results are shown in Figure 15. The composition of the melt-rich impactites was recalculated on a volatile-free basis. When compared with melt-rich impactites, the georgiaites are enriched in Si and Ba. All other elements are depleted in the georgiaites—most depleted are Mn, Mg, and Ca, and Ni, Y, and Cs. All trace elements are depleted by a factor of ~0.6 in georgiaites as compared to melt-rich impactites. The bediasites are enriched in Si and Hf when compared with the average melt-rich impactites. The REE contents are very similar in bediasites and melt-rich impactites. Most LREEs are slightly enriched in bediasites, whereas the HREEs are slightly depleted. Bediasites are also depleted in Mn, Mg, Ca, Ni, and Cs compared to melt-rich impactites. Both types of tektites are depleted in Ta, Th, and U in comparison with the melt-rich impactites.

For many elements, the similarities between the melt-rich impactites (upper suevites and impact melt rock) and tektites are greater than between the Exmore breccia and tektites or average target sediments and tektites, when our results are compared to the study by Deutsch and Koeberl (2006). The tektites show the largest depletion in Mn, Mg, Ca, Ni, and Cs in comparison with the melt-rich impactites. Similar depletion was observed by Deutsch and Koeberl (2006) when tektites were compared with

target sediments and Exmore breccia. The tektites are enriched in Na compared to target sediments (Deutsch and Koeberl, 2006), but there is no such enrichment when comparisons are made against the composition of upper suevites and impact melt rock. The enhanced Na content in the Exmore breccia and upper suevites is probably due to the granitic clast content and/or seawater component. However, both the melt-rich impactites and the Exmore breccia are not real pre-impact target rocks. They are only models for mixtures of pre-impact target rocks that could be involved in the formation of the tektites.

Hydrothermal Alteration

Evidence of hydrothermal alteration of the impactites is described in Bartosova et al. (this volume) and Wittmann et al. (this volume, Chapters 16 and 17). The hydrothermal alteration has been studied also in the samples from the STP test hole, and details of hydrothermal changes and conditions have been presented by, e.g., Horton et al. (2006a, 2006b) and Larsen et al. (2006). Figure 7 shows that there is no correlation between the CaO content and the LOI for the studied impactites. This means that the LOI is not caused predominantly by the presence of carbonate, but there are probably other effects, such as content of organic matter or/and structural water in phyllosilicate minerals. A positive correlation of CaO and LOI was observed, for example, in the Yaxcopoil-1 impactites at Chicxulub (Tuchscherer et al., 2004), but the contents of carbonate in these impactites were one order of magnitude higher than in the Chesapeake Bay impactites. The occurrence of secondary phyllosilicate minerals (such as smectite), a typical product of alteration, was identified in Chesapeake Bay suevite samples (Bartosova et al., this volume; Wittmann et al., this volume, Chapters 16 and 17). Organic matter is present mostly in fine-grained sediments (i.e., siltstones, mudstones, and shales). Graphite, likely derived from graphitic schist, also occurs in the impactites. The LOI increases with increasing depth in the impactites, suggesting higher alteration in the lower parts of the section. This is also in agreement with petrographic observations because the evidence of hydrothermal alteration (e.g., the presence of smectite or secondary carbonate) is more pronounced in the lower part of the impact breccia section (Bartosova et al., this volume).

Carbon Isotopes

The vitrinite in the Exmore breccia (CB6-059, depth = 761.8 m) has a $\delta^{13}C$ value of −20‰, which is at the higher end of the typical C-isotopic composition of coal (e.g., Coplen et al., 2002). Modern C3 plants have no $\delta^{13}C$ values higher than −23‰ (Bocherens et al., 1993; Gröcke, 1998), but there are some Cretaceous plants with values around −20‰ (Bocherens et al., 1993) or −21‰ (van Bergen and Poole, 2002). Furthermore, this could be an indication of saline conditions, which can cause a positive

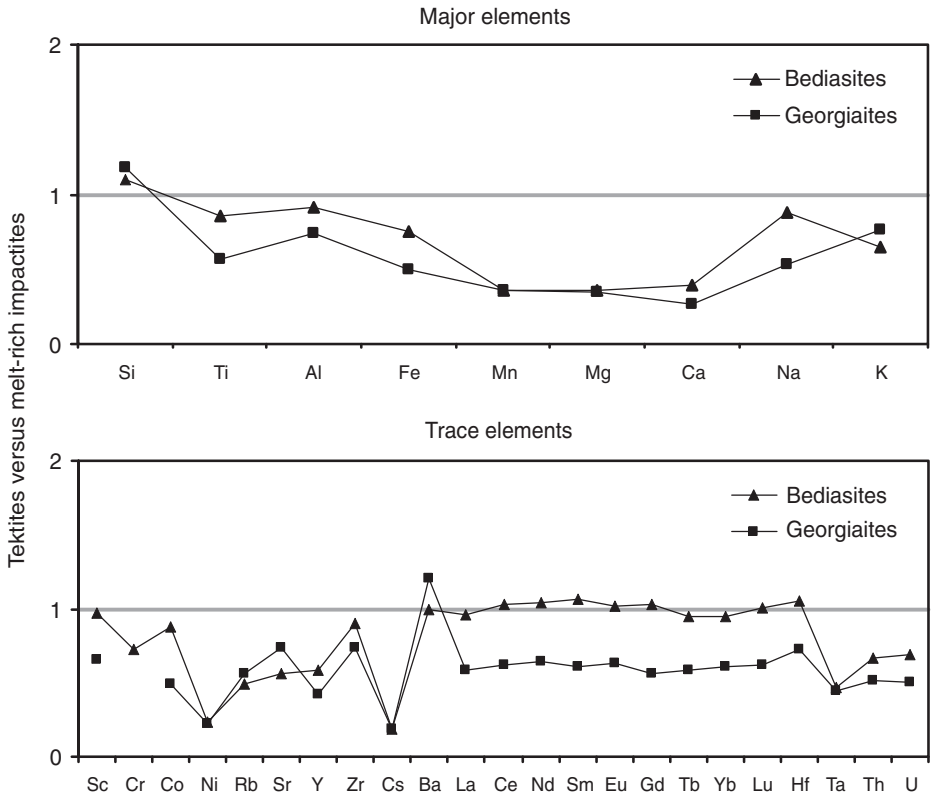

Figure 15. The elemental ratios of the average compositions of tektites, i.e., bediasites (from Deutsch and Koeberl, 2006) and georgiaites (from Albin et al., 2000), versus the average composition of the melt-rich impactites (i.e., upper suevites and impact melt rock) from the Eyreville drill core (average of 57 samples, this work). The composition of the melt-rich impactites was recalculated on a volatile-free basis. Compared to Chesapeake Bay melt-rich impactites, bediasites are depleted in most of elements but enriched in Si and slightly enriched in some light rare earth elements (LREEs). Most of the REEs have very similar abundances to those of bediasites and melt-rich impactites. Compared to the melt-rich impactites, georgiaites are enriched in Si and Hf but depleted in all other elements, especially in Mn, Mg, and Ca in terms of major elements and in Ni and Cs in terms of trace elements.

shift to −21‰ for plant material in sediments (Gröcke, 1998). The graphitic gneiss samples CB6-131 (depth = 1551.5 m) and CB6-132 (depth = 1559.5 m) have $\delta^{13}C$ values of −21‰, which is in the typical range of elemental carbon. The carbonate veins (CB6-122, depth = 1511.9 m; CB6-132, depth = 1559.5 m; CB6-145, depth = 1667.8 m) and the carbonate in one melt fragment in suevite (CB6-109, depth = 1452.3 m) show $\delta^{13}C$ values of −7.5‰, −7.0‰, −13.8‰, and −8.3‰, respectively. These lower values compared to marine carbonate (e.g., Coplen et al., 2002) suggest a hydrothermal origin of the veins; the lower value of −14‰ might also be due to a mixture with carbon of organic matter.

The $\delta^{13}C$ values of sedimentary clasts in suevite and in Exmore breccia range from −21.1‰ to −27.4‰ (average: −25.8‰), and from −23.8‰ to −28.9‰ (average: −25.2‰), respectively. This is the typical range for organic matter in sediments (e.g., Coplen et al., 2002). Previous carbon isotope studies of organic matter in mudstones of the Arundel Formation (Potomac Formation) yielded $\delta^{13}C$ values from −22‰ to −23‰ (Mora and Jahren, 2001). Elliott and Mora (2004) reported $\delta^{13}C$ values in the range from −18.9‰ to −25.4‰ (average: −22.1‰) for bulk terrestrial organic matter in mudstones of the Potomac Formation. No trend in the stable carbon isotope data with depth and within the different impact lithologies was observed. The slightly lower $\delta^{13}C$ values of our samples compared to the previously published data of the target rocks can be interpreted as the result of postimpact hydrothermal alteration. No evidence for isotope fractionation due to impact was found. However, carbon isotope data of unshocked target sediments are necessary for comparison with the results of this preliminary investigation.

SUMMARY AND CONCLUSIONS

Major- and trace-element contents were analyzed in 85 samples from the impactite section in the Eyreville B drill core. Furthermore, 24 clasts of different target lithologies were analyzed from the polymict impactite sequence. The main conclusions are:

(1) Chemical compositions of the polymict impactites are primarily the result of the mixing of the different target rocks, i.e., crystalline rocks and overlying sedimentary rocks of Cretaceous to Eocene age.

(2) Major- and trace-element contents show only limited variations in polymict impactites from the upper part of the section, and larger variations are observed in the lower part. The larger heterogeneity of the lower part was also documented by the petrographic observations (Bartosova et al., this volume). Some trends in major-element contents with depth (e.g., increase of the Fe_2O_3 and TiO_2 contents) suggest that the schist component in suevite increases with increasing depth, in agreement with our petrographic observations.

(3) Mixing calculations of proportions of components involved in formation of the polymict impactites show that the rocks derived from the metamorphic basement rocks (gneiss and schist) constitute the main components of the polymict impactites (more than ~75%), together with a sedimentary component (~20%), and a possible minor component of other lithologies (pegmatite/granite and amphibolite). The sedimentary component is represented mostly by the lowermost and thickest Potomac Formation. However, the proportion of the metamorphic basement-derived rocks is higher than expected from the petrographic observations (Bartosova et al., this volume).

(4) The polymict impactites are not enriched in siderophile elements compared to the schist/gneiss of the basal crystalline section. The highest siderophile element contents were found in cataclastic gneiss. No enrichment of the siderophile elements was found in the impact melt rock.

(5) The melt particles were modeled by mixing calculations as mixtures of target lithologies and of common rock-forming minerals (quartz, feldspars, and mica). However, the mixing calculations for melt particles do not give satisfactory results, and the original composition of some melt particles has been modified by alteration. More analyses of melt particles are necessary to better constrain their source lithologies.

(6) The presence of some secondary minerals (e.g., secondary pyrite, carbonate veins, and smectite; Bartosova et al., this volume) and the carbon isotopic values of the carbonate veins imply postimpact hydrothermal alteration.

(7) The carbon isotopic ratios show typical values for the various types of samples analyzed.

ACKNOWLEDGMENTS

The drilling at Eyreville was supported by the International Continental Scientific Drilling Program (ICDP), U.S. Geological Survey (USGS), and the National Aeronautics and Space Administration (NASA). We appreciate the work of general contractor Drilling, Observation and Sampling of the Earth's Continental Crust and drilling operator Major Drilling, USA. The help of J.W. Horton Jr. and the staff at the USGS National Center, Reston, during the sampling process is appreciated. The present work was supported by the Austrian Science Foundation FWF, project P18862-N10 (to Koeberl). We appreciate the help of H. Böck, M. Villa, M. Bichler, and G. Steinhauser (Atominstitut Vienna) with the irradiations. We thank K. Krahn and H.R. Knöfler for extensive technical support in sample preparation and X-ray fluorescence (XRF) analysis. For additional XRF analyses, we thank Sharon Farrell-Turner (University of the Witwatersrand, Johannesburg). We thank P. Claeys and J. Morrow for careful reviews, which helped to substantially improve the paper.

APPENDIX 1. WHOLE-ROCK CHEMICAL COMPOSITIONS OF SAMPLES FROM THE EYREVILLE B DRILL CORE

Sample	W	CB6	CB6	W	CB6	W	W	KB	W	W	KB	KB	W	CB6
	055	093	094	056a	095	057	058	2	059	060	3	4	062	096
Depth (m)	1397.4	1399.2	1399.7	1400.1	1401.3	1401.7	1402.3	1402.9	1403.2	1403.6	1404.4	1405.7	1407.5	1409.3
Rock type	sv	sv	sv	sv	sv	sv	imr	imr	imr	imr	imr	imr	imr	sv
(wt%)														
SiO_2	69.9	69.7	68.5	69.6	68.9	69.1	70.0	70.0	69.6	70.6	67.2	68.4	68.9	68.1
TiO_2	0.81	0.81	0.83	0.82	0.83	0.83	0.82	0.65	0.81	0.76	0.81	0.76	0.82	0.82
Al_2O_3	13.8	13.6	14.7	13.6	14.0	14.5	14.3	12.8	14.2	13.9	12.7	13.8	14.2	14.4
Fe_2O_3*	4.59	5.10	5.15	5.24	4.93	4.98	5.51	4.96	4.84	4.66	4.83	5.51	5.44	5.08
MnO	0.05	0.05	0.05	0.06	0.07	0.05	0.07	0.05	0.05	0.04	0.05	0.08	0.06	0.08
MgO	1.54	1.51	1.51	1.45	1.37	0.99	0.99	0.85	0.98	0.94	0.90	1.10	1.03	1.43
CaO	1.37	1.38	1.36	1.56	1.89	1.92	1.64	1.35	1.80	1.69	1.60	1.56	1.9	1.92
Na_2O	1.93	1.62	1.53	1.40	1.65	1.56	1.12	1.46	1.34	1.20	1.32	1.39	1.48	2.00
K_2O	2.88	3.39	3.33	3.31	3.50	3.48	3.50	2.00	3.58	3.51	3.29	3.07	3.61	3.59
P_2O_5	0.13	0.13	0.13	0.13	0.12	0.12	0.12	0.11	0.12	0.12	0.11	0.13	0.13	0.12
SO_3	<0.1	<0.1	<0.1	<0.1	<0.1	<0.1	<0.1	n.d.†	<0.1	<0.1	n.d.	n.d.	<0.1	<0.1
LOI	2.4	2.5	2.6	2.3	2.2	2.2	1.7	4.4	1.9	2.2	5.6	2.3	1.9	2.4
Total	99.40	99.79	99.69	99.47	99.46	99.73	99.77	98.63	99.22	99.62	98.41	98.10	99.47	99.94
(ppm)														
Sc	12.6	11.9	12.2	12.0	12.9	12.5	12.8	9.31	12.7	11.9	10.7	13.0	13.0	12.2
V	97	99	101	90	109	94	94	77	86	87	77	78	101	105
Cr	63.1	58.8	61.9	59.0	68.3	63.6	63.6	36.4	63.0	62.7	55.8	102	71.6	56.4
Co	15.5	14.5	13.2	14.3	14.9	14.9	14.9	9.36	14.2	14.0	12.4	14.6	14.3	13.7
Ni	31	33	33	30	33	29	30	18	31	30	27	49	30	31
Cu	32	36	31	33	30	32	<30	<30	<30	<30	<30	<30	34	31
Zn	39	42	40	49	113	111	84	155	111	73	154	78	73	92
As	12.1	18.4	11.8	11.5	6.83	8.61	26.0	8.33	22.4	31.0	10.6	15.6	15.0	5.52
Se	<1.9	<1.6	<1.7	0.46	<2.0	<1.4	<1.5	<1.0	<1.4	<1.4	<1.1	<1.5	<1.5	<1.7
Br	3.3	10	4.1	1.3	7.5	0.7	0.5	1.4	0.9	0.7	1.1	<0.7	0.7	7.5
Rb	134	147	142	134	136	150	143	71.7	136	127	71.7	139	135	140
Sr	185	177	191	194	236	221	172	199	204	196	202	161	198	243
Y	45	45	42	45	45	42	46	29	42	40	33	32	44	41
Zr	238	228	219	253	234	239	247	224	259	238	241	222	241	235
Nb	<10	11	10	<10	10	<10	<10	11	<10	<10	13	14	<10	<10
Mo	<10	<10	<10	<10	<10	<10	<10	n.d.	<10	<10	n.d.	n.d.	<10	<10
Sb	2.27	2.59	1.28	2.41	1.06	2.32	2.99	3.00	3.44	2.14	2.98	2.85	3.06	1.29
Cs	9.27	9.13	8.28	6.04	3.70	5.84	10.8	6.88	7.00	7.47	7.11	9.83	6.75	3.28
Ba	492	448	482	465	444	516	508	418	503	491	306	521	620	462
La	38.3	32.2	33.7	33.1	32.8	35.5	33.9	30.3	33.0	30.2	35.3	32.5	29.3	31.6
Ce	75.9	66.2	68.8	67.5	67.6	70.7	68.1	57.1	66.5	63.7	69.7	66.3	59.9	65.1
Nd	31.0	29.6	30.2	28.4	29.6	33.4	30.9	26.2	30.6	29.0	31.0	27.5	24.8	26.0
Sm	6.50	5.76	5.49	5.56	5.60	6.18	7.47	6.53	6.17	5.73	7.51	6.15	5.75	5.29
Eu	1.60	1.43	1.42	1.42	1.42	1.48	1.41	1.26	1.37	1.35	1.36	1.42	1.32	1.39
Gd	n.d.	5.86	5.33	n.d.	5.15	n.d.	6.83	5.84	7.28	6.73	6.72	5.23	6.41	5.34
Tb	1.03	1.02	0.91	0.90	0.91	0.99	0.96	0.81	0.88	0.88	0.94	0.93	0.84	0.86
Tm	0.48	0.46	0.43	0.40	0.50	0.46	0.48	0.42	0.44	0.43	0.49	0.55	0.42	0.43
Yb	3.11	2.95	3.03	3.15	3.07	2.95	3.08	2.67	2.78	2.63	2.98	3.05	2.53	2.98
Lu	0.50	0.46	0.47	0.49	0.47	0.45	0.47	0.41	0.43	0.42	0.46	0.48	0.41	0.47
Hf	6.29	5.89	5.80	6.47	5.62	6.34	5.86	5.69	6.29	5.52	6.53	6.03	5.65	5.67
Ta	1.29	1.23	1.09	1.11	1.06	1.31	1.14	1.07	1.11	1.06	1.22	1.24	0.99	1.13
W	3.9	n.d.	2.1	3.7	1.7	3.7	1.8	<3.1	1.8	1.5	1.8	3.0	1.7	1.5
Ir (ppb)	<1.9	<1.4	<1.7	<1.8	<2.0	<1.4	<1.7	<1.1	<1.6	<1.6	<1.2	<1.8	<1.7	<1.7
Au (ppb)	<1.2	0.70	<1.1	<0.8	0.4	0.6	0.8	7.3	0.8	0.6	1.1	2.5	1.4	0.7
Pb	<15	<15	17	16	18	16	<15	n.d.	16	<15	n.d.	n.d.	15	<15
Th	11.2	10.9	11.0	10.4	10.1	11.2	11.1	8.02	11.2	11.6	9.48	10.7	9.50	10.2
U	2.76	2.93	2.49	2.43	2.27	2.84	2.8	2.45	2.63	2.5	2.55	2.22	2.18	2.63

(*Continued*)

APPENDIX 1. WHOLE-ROCK CHEMICAL COMPOSITIONS OF SAMPLES FROM THE EYREVILLE B DRILL CORE (*Continued*)

Sample	W	CB6	KB	RG	W	W	CB6	W	CB6	W	W	CB6	W	CB6
	065a	097	5	018	066	067	098	069	099	070	071a	100	073	101
Depth (m)	1411.7	1412.8	1412.9	1413.8	1415.4	1416.4	1418.8	1421.2	1421.7	1422.5	1424.3	1427	1429.7	1431.1
Rock type	sv	sv	sv	sv	sv	sv	sv	sv	sv	sv	sv	sv	sv	sv
(wt%)														
SiO_2	65.2	69.8	66.2	63.5	66.7	68.6	64.3	65.1	65.9	68.0	66.3	67.7	64.7	68.1
TiO_2	0.77	0.75	0.78	1.08	0.80	0.82	0.96	0.83	0.89	0.79	0.75	0.70	0.88	0.87
Al_2O_3	15.2	13.7	13.5	16.8	14.7	13.8	14.8	15.1	14.9	14.2	14.9	13.8	13.7	14.4
$Fe_2O_3^*$	5.07	4.22	4.86	6.71	5.81	5.28	6.35	5.62	5.73	5.00	5.24	5.30	6.91	4.82
MnO	0.11	0.06	0.07	0.08	0.08	0.07	0.10	0.08	0.08	0.08	0.08	0.07	0.06	0.08
MgO	1.94	1.41	1.38	2.52	1.66	1.78	2.76	1.96	2.09	1.88	1.92	1.57	2.13	2.10
CaO	2.01	1.69	1.54	0.75	1.54	1.69	1.67	1.77	1.72	1.70	1.93	1.55	2.15	1.27
Na_2O	2.70	2.24	1.85	1.28	1.92	1.94	2.24	2.26	1.97	2.04	2.24	2.61	1.96	2.07
K_2O	4.64	3.15	3.09	3.66	3.00	2.83	2.56	2.82	2.69	2.80	2.66	2.73	0.25	3.21
P_2O_5	0.15	0.12	0.13	0.17	0.11	0.11	0.14	0.12	0.12	0.12	0.12	0.12	0.11	0.14
SO_3	<0.1	<0.1	n.d.†	<0.1	0.1	<0.1	0.4	0.1	<0.1	<0.1	0.1	0.4	0.2	0.1
LOI	2.0	2.5	5.4	3.1	2.8	3.0	3.1	4.1	3.4	3.0	3.6	3.2	6.6	2.5
Total	99.79	99.64	98.80	99.65	99.22	99.92	99.38	99.86	99.49	99.61	99.84	99.75	99.65	99.66
(ppm)														
Sc	15.3	10.9	11.9	n.d.	12.0	12.7	18.6	13.9	13.2	12.4	12.4	11.4	8.71	14.8
V	99	96	88	113	95	101	134	102	108	100	106	91	79	105
Cr	32.9	53.8	57.9	n.d.	57.7	61.1	96.1	72.2	65.4	63.6	62.9	51.2	41.1	83.8
Co	15.3	12.5	13.3	n.d.	12.3	15.6	17.6	15.5	14.3	14.6	14.4	17.6	11.5	14.8
Ni	30	29	32	41	29	28	34	33	30	31	29	29	40	33
Cu	<30	<30	<30	31	36	<30	<30	32	33	32	<30	<30	31	<30
Zn	96	89	93	n.d.	104	63	113	120	127	120	130	86	63	100
As	24.1	9.81	8.74	n.d.	11.6	18.7	13.5	5.52	6.21	5.51	5.35	31.2	39.1	5.75
Se	<1.5	<1.9	<1.3	n.d.	<1.5	<2.0	<2.8	<1.3	<1.7	<1.2	<1.3	<2.2	<1.2	<2.4
Br	1.2	6.7	5.2	n.d.	1.3	1.6	5.5	2.8	8.8	1.7	1.7	7.7	2.9	4.9
Rb	171	123	139	n.d.	118	105	115	136	116	125	122	113	27.0	145
Sr	251	225	221	105	221	220	194	248	247	198	234	219	555	181
Y	47	36	28	54	41	37	42	42	37	41	34	34	22	38
Zr	220	215	217	328	242	217	206	245	245	232	230	198	378	215
Nb	<10	<10	14	17	<10	<10	<10	<10	11	<10	<10	<10	<10	11
Mo	<10	<10	n.d.	<10	<10	<10	<10	<10	<10	<10	<10	<10	<10	<10
Sb	1.97	1.12	1.66	n.d.	1.32	1.63	1.43	1.19	0.78	1.14	0.91	3.61	8.46	0.57
Cs	4.72	5.18	7.08	n.d.	10.1	8.21	11.5	12.1	9.66	10.3	11.3	8.14	12.9	6.67
Ba	893	417	434	635	444	394	396	421	403	409	398	469	<30	429
La	34.2	27.4	29.4	n.d.	31.9	28.3	31.9	38.8	31.8	33.6	31.0	29.0	24.1	30.2
Ce	70.2	57.3	63.2	n.d.	65.7	56.6	66.6	82.3	65.7	71.8	64.9	60.8	50.3	64.3
Nd	34.0	23.1	27.4	n.d.	28.1	24.0	29.4	34.5	28.7	30.7	28.1	25.2	22.1	26.7
Sm	7.06	4.33	5.46	n.d.	6.45	5.25	5.98	7.99	5.21	7.05	6.69	5.01	5.88	5.21
Eu	1.52	1.24	1.30	n.d.	1.31	1.19	1.66	1.59	1.39	1.52	1.42	1.33	1.24	1.41
Gd	6.32	4.39	4.78	n.d.	6.00	5.12	6.03	8.33	5.48	6.75	6.69	5.16	6.25	5.09
Tb	0.95	0.77	0.83	n.d.	0.83	0.75	1.03	1.11	0.87	1.00	0.97	0.84	0.90	0.91
Tm	0.51	0.39	0.38	n.d.	0.43	0.38	0.52	0.62	0.46	0.56	0.54	0.42	0.49	0.46
Yb	3.19	2.55	2.63	n.d.	2.59	2.34	3.32	3.28	2.78	3.06	2.90	2.80	2.30	2.89
Lu	0.51	0.41	0.44	n.d.	0.42	0.37	0.52	0.42	0.46	0.39	0.36	0.43	0.29	0.45
Hf	5.82	5.14	5.67	n.d.	5.61	4.84	5.26	6.23	6.08	5.69	5.44	4.97	7.63	5.66
Ta	1.15	1.00	1.19	n.d.	1.20	0.99	1.20	1.40	1.25	1.29	1.33	1.03	1.23	1.25
W	1.6	<1.7	3.0	n.d.	1.5	2.1	4.3	3.1	2.2	1.9	2.1	2.2	2.6	<1.7
Ir (ppb)	<1.6	<1.9	<1.4	n.d.	<1.7	0.43	<2.9	<1.5	<1.7	<1.4	<1.5	<2.2	<1.3	<2.4
Au (ppb)	0.7	<1.3	3.2	n.d.	0.5	0.4	0.5	0.8	0.4	0.3	<0.8	<1.2	1.7	<1.5
Pb	43	28	n.d.	<15	27	<15	27	26	51	16	26	18	<15	19
Th	9.84	8.8	10.5	n.d.	10.6	8.9	11.3	13.2	10.5	11.3	10.4	10.2	11.8	9.9
U	2.05	1.68	2.09	n.d.	2.51	2.05	2.70	3.00	2.72	2.76	2.88	2.55	2.65	2.21

(*Continued*)

APPENDIX 1. WHOLE-ROCK CHEMICAL COMPOSITIONS OF SAMPLES FROM THE EYREVILLE B DRILL CORE (*Continued*)

Sample	W	W	CB6	W	CB6	W	W	CB6	W	CB6	CB6	W	W	CB6
	074	076	102	077	103	079	080a	104	081a	105	106	082	083	107
Depth (m)	1431.4	1433.9	1436.6	1437	1440	1441.3	1443.1	1443.7	1444.6	1445.8	1447	1447.1	1448.7	1449.8
Rock type	sv	sv	sv	sv	sv	sv	sv	sv	sv	sv	sv	sv	sv	sv
(wt%)														
SiO_2	68.6	63.2	72.2	62.6	65.3	63.0	63.9	66.5	66.3	63.8	65.8	66.9	65.8	67.2
TiO_2	0.80	0.65	0.74	0.98	0.74	0.94	0.80	0.82	0.73	0.92	0.83	0.69	0.88	0.99
Al_2O_3	14.1	16.9	13.0	16.3	15.1	16.1	15.8	14.8	14.9	15.2	14.5	13.3	14.6	15.9
$Fe_2O_3^*$	4.52	3.91	3.90	5.99	4.62	7.04	5.80	5.38	4.72	6.68	5.47	4.39	5.79	5.32
MnO	0.07	0.12	0.06	0.10	0.11	0.12	0.10	0.10	0.09	0.10	0.11	0.11	0.08	0.07
MgO	1.73	1.79	1.29	2.24	1.78	2.27	2.19	2.07	1.92	2.6	2.51	1.94	2.22	1.75
CaO	1.45	2.56	0.93	1.38	2.22	1.41	1.69	1.59	1.67	1.89	2.05	2.97	1.56	1.13
Na_2O	2.19	4.91	1.74	1.95	3.29	1.48	2.11	2.16	2.70	2.28	2.38	2.46	1.77	0.75
K_2O	3.36	3.36	3.00	4.34	3.33	3.73	3.98	3.8	3.81	2.73	3.28	3.31	2.71	3.53
P_2O_5	0.13	0.13	0.08	0.14	0.12	0.11	0.12	0.13	0.13	0.13	0.12	0.12	0.14	0.16
SO_3	<0.1	<0.1	<0.1	0.1	<0.1	0.2	0.1	0.2	0.1	0.1	<0.1	0.1	<0.1	<0.1
LOI	2.8	1.9	2.5	3.2	2.6	3.4	3.1	2.2	2.9	3.4	2.6	3.5	4.0	2.4
Total	99.75	99.43	99.44	99.32	99.21	99.80	99.69	99.75	99.97	99.83	99.65	99.79	99.55	99.20
(ppm)														
Sc	13.0	11.5	10.8	17.3	11.2	16.8	14.3	13.8	11.0	14.7	14.0	12.8	13.3	15.5
V	101	74	87	122	111	117	106	102	95	115	113	95	103	116
Cr	60.7	24.1	65.2	86.7	52.4	84.9	73.8	71.2	62.7	77.7	80.0	65.6	68.5	68.6
Co	12.2	10.0	12.5	19.5	11.6	21.0	16.4	15.0	12.6	16.6	15.8	12.8	14.7	17.1
Ni	30	24	29	35	29	38	36	33	34	34	35	33	35	33
Cu	<30	<30	<30	33	35	<30	36	<30	31	32	30	<30	30	31
Zn	169	89	65	119	71	115	129	103	80	102	97	65	127	129
As	3.86	1.87	3.11	4.61	2.12	4.40	3.27	3.27	2.35	4.00	1.88	3.35	4.27	34.5
Se	<0.9	<1.2	<2.2	<1.4	<2.1	<1.5	<1.3	<2.4	<2.4	<2.5	<2.3	<1.2	<1.3	<2.5
Br	2.7	0.8	8.0	2.7	13	2.0	1.5	6.9	2.7	20	9.3	2.1	3.8	1.9
Rb	148	119	121	204	125	184	174	159	n.d.[†]	111	129	133	123	130
Sr	171	254	127	157	233	127	190	162	163	246	196	212	303	193
Y	40	43	39	53	38	51	46	45	44	39	45	38	44	51
Zr	231	262	279	278	223	240	215	226	230	265	238	202	259	247
Nb	<10	<10	10	<10	<10	17	17	11	<10	10	11	<10	12	11
Mo	<10	<10	<10	<10	<10	<10	<10	<10	<10	<10	<10	<10	<10	<10
Sb	0.73	0.35	0.37	1.02	0.22	0.29	0.72	0.28	0.41	0.53	0.18	0.34	1.29	2.26
Cs	6.28	2.48	11.3	15.6	7.49	8.66	8.50	5.40	4.29	5.43	3.66	3.46	9.41	10.2
Ba	473	1041	450	503	523	478	512	471	549	395	581	486	406	541
La	33.7	38.6	34.5	45.1	32.2	42.8	41.6	34.3	33.0	37.2	34.5	29.0	42.0	45.9
Ce	68.5	80.2	70.4	92.9	65.1	88.0	85.4	70.9	64.4	76.4	70.3	60.5	85.4	93.3
Nd	29.7	32.9	28.5	38.1	26.5	36.3	34.8	29.0	26.2	30.9	28.7	25.6	36.4	40.4
Sm	6.82	7.43	5.2	9.30	4.79	8.32	7.83	5.76	5.63	6.23	5.72	5.83	8.02	7.76
Eu	1.45	1.66	1.46	2.01	1.44	1.84	1.71	1.53	1.34	1.56	1.47	1.35	1.74	1.84
Gd	6.11	7.04	5.28	8.20	4.78	8.40	6.89	5.57	5.60	5.54	6.15	4.95	7.90	7.37
Tb	0.92	1.06	0.91	1.28	0.83	1.20	1.08	0.97	0.81	0.98	0.99	0.81	1.11	1.25
Tm	0.51	0.58	0.43	0.71	0.41	0.66	0.57	0.47	0.37	0.50	0.50	0.45	0.60	0.56
Yb	2.99	3.36	2.97	3.82	2.80	3.61	3.11	3.13	2.60	3.17	3.40	2.62	3.41	3.81
Lu	0.37	0.44	0.47	0.48	0.42	0.44	0.40	0.50	0.33	0.50	0.52	0.34	0.44	0.58
Hf	5.85	6.46	7.37	7.47	5.72	6.56	5.67	6.12	5.51	6.92	6.13	4.87	6.58	6.52
Ta	1.24	1.35	1.14	1.64	1.03	1.60	1.25	1.17	0.99	1.28	1.18	0.91	1.25	1.46
W	1.6	<1.9	1.7	2.4	3.7	<2.9	2.2	1.0	<4.0	1.9	1.4	0.7	2.1	<2.4
Ir (ppb)	<1.0	<1.3	<2.3	<1.6	<2.1	<1.7	<1.5	<2.4	<1.3	<2.7	<2.4	<1.4	<1.4	<2.6
Au (ppb)	<0.9	0.7	<1.3	1.1	<1.3	0.8	<0.9	0.9	0.8	<1.3	<1.3	0.6	1.2	0.5
Pb	<15	<15	<15	<15	<15	16	22	<15	<15	<15	<15	<15	21	25
Th	10.7	14.0	9.60	15.3	9.10	14.3	11.4	10.7	9.52	11.1	10.7	9.41	11.8	15.2
U	2.62	2.84	2.03	4.01	2.08	3.20	2.50	2.37	1.73	2.50	2.14	1.93	2.98	4.58

(*Continued*)

APPENDIX 1. WHOLE-ROCK CHEMICAL COMPOSITIONS OF SAMPLES FROM THE EYREVILLE B DRILL CORE (*Continued*)

Sample	W	W	CB6	CB6	W	W	CB6	CB6	W	CB6	W	CB6	W	W
	2-18	084	108	109	085a	086a	110	111	088a	113	089a	114	090a	2-19
Depth (m)	1450.4	1450.7	1451	1452.3	1452.6	1454.2	1455.2	1458.2	1461.3	1464	1464.3	1467.4	1470.4	1471.4
Rock type	imr	imr	sv	sv	sv	sv	sv	sv	sv	sv	sv	sv	sv	sv
(wt%)														
SiO_2	63.0	66.5	70.9	67.8	64.2	66.9	68.5	68.6	69.2	61.3	67.8	70.0	67.7	60.6
TiO_2	0.90	0.89	0.92	0.95	1.02	0.98	0.95	0.90	0.83	1.35	0.94	0.81	0.99	0.94
Al_2O_3	15.1	14.5	14.2	14.6	16.3	15.1	14.5	14.2	14.1	15.0	14.3	13.2	14.6	14.2
$Fe_2O_3^*$	6.65	5.72	4.86	6.21	7.78	5.88	4.97	5.40	4.81	7.08	5.69	4.54	5.42	6.92
MnO	0.06	0.08	0.07	0.08	0.09	0.06	0.06	0.08	0.08	0.13	0.06	0.07	0.08	0.06
MgO	1.75	1.99	1.36	1.56	1.92	1.59	1.35	1.41	1.17	2.25	1.42	1.16	1.63	1.71
CaO	1.34	1.45	1.08	1.36	1.53	1.29	1.03	1.09	0.68	3.12	1.38	1.08	1.09	1.36
Na_2O	0.87	1.47	0.66	0.86	0.94	0.87	0.81	0.74	0.97	1.40	0.94	0.86	0.90	1.18
K_2O	2.03	2.55	3.55	2.06	1.99	2.64	3.50	3.12	4.15	2.79	2.36	3.35	3.24	2.17
P_2O_5	0.16	0.13	0.13	0.13	0.16	0.15	0.15	0.14	0.11	0.34	0.13	0.12	0.15	0.15
SO_3	n.d.†	<0.1	0.1	0.1	<0.1	<0.1	0.1	0.1	<0.1	<0.1	<0.1	0.1	<0.1	n.d.
LOI	6.0	3.9	1.4	3.6	3.7	3.8	3.5	4.0	3.5	5.0	4.9	4.3	4.1	9.8
Total	97.86	99.18	99.23	99.31	99.63	99.26	99.42	99.78	99.60	99.76	99.92	99.59	99.91	99.09
(ppm)														
Sc	12.7	13.4	12.9	12.3	14.4	12.5	12.4	12.8	12.4	15.8	12.2	10.7	13.1	12.5
V	98	105	102	98	110	109	109	101	90	131	97	93	120	107
Cr	87.0	70.8	66.9	65.3	69.7	61.4	60.5	59.7	63.5	82.8	61.1	52.5	66.6	61.9
Co	15.5	15.8	15.1	17.9	17.7	15.3	14.6	14.4	16.2	22.4	14.4	10.5	17.5	14.7
Ni	39	33	33	31	35	33	34	33	38	36	30	31	36	30
Cu	<30	30	<30	<30	30	<30	32	<30	<30	39	<30	<30	57	<30
Zn	112	130	118	102	120	116	151	109	455	114	95	99	122	103
As	47.3	12.4	35.8	44.6	24.5	23.1	23.1	22.7	28.1	26.0	18.7	14.0	21.4	12.5
Se	<1.4	<1.3	<2.3	<2.3	<1.4	<1.3	<2.4	<1.7	<1.7	<2.3	<1.6	<1.9	<1.6	<1.4
Br	2.2	3.2	1.2	3.2	1.0	1.5	5.3	8.0	2.0	2.7	3.4	2.8	2.4	4.3
Rb	53.7	115	127	83.0	74.0	112	161	159	223	115	117	144	161	95.2
Sr	188	232	158	303	232	209	151	147	237	300	242	143	160	265
Y	38	41	41	33	44	43	51	46	57	40	37	44	52	35
Zr	246	250	252	301	278	307	262	233	231	238	265	255	254	231
Nb	15	15	13	11	16	13	11	11	<10	13	11	11	11	14
Mo	n.d.	<10	<10	<10	<10	<10	<10	<10	<10	<10	<10	<10	<10	n.d.
Sb	4.85	2.84	3.41	3.80	4.96	4.18	3.1	2.44	6.09	2.27	2.23	2.19	2.67	1.90
Cs	10.6	10.9	7.82	3.80	13.6	14.1	19.7	14.3	15.7	13.5	12.3	10.7	14.3	9.52
Ba	283	408	570	350	371	329	444	374	434	590	325	377	416	264
La	39.0	39.7	40.0	37.6	47.5	37.9	39.5	36.3	38.1	38.9	31.3	30.6	38.7	35.5
Ce	76.3	80.6	83.0	75.1	97.2	78.1	80.9	74.4	77.2	78.8	65.4	60.8	78.6	71.3
Nd	31.4	33.7	35.8	30.6	42.6	35.3	36.1	32.6	28.4	38.7	28.6	27.1	31.5	29.5
Sm	7.79	7.91	6.70	6.32	9.69	7.53	6.56	6.36	7.28	7.28	6.25	5.04	7.29	6.78
Eu	1.63	1.72	1.68	1.58	1.95	1.53	1.61	1.48	1.56	1.83	1.41	1.23	1.65	1.46
Gd	7.52	7.41	6.28	6.56	9.56	6.80	6.97	6.26	6.9	6.77	4.90	4.92	7.10	6.02
Tb	1.16	1.13	1.08	1.07	1.36	1.20	1.11	1.04	1.15	1.14	0.92	0.82	1.14	1.00
Tm	0.67	0.59	0.51	0.47	0.68	0.49	0.50	0.54	0.49	0.53	0.50	0.42	0.49	0.45
Yb	3.53	3.36	3.29	3.16	3.94	3.47	3.21	3.17	3.39	3.06	2.92	2.67	3.28	3.01
Lu	0.44	0.42	0.50	0.50	0.48	0.53	0.49	0.49	0.5	0.47	0.45	0.42	0.52	0.38
Hf	6.79	6.36	6.67	7.55	7.29	7.75	6.17	6.05	6.07	6.03	6.93	6.03	6.53	6.11
Ta	1.36	1.35	1.39	1.34	1.42	1.40	1.35	1.41	1.35	1.36	1.30	1.02	1.29	1.19
W	2.2	2.4	2.4	2.8	2.5	4.5	2.0	2.8	4.4	n.d.	4.5	n.d.	4.5	12.5
Ir (ppb)	<1.5	<1.5	<2.4	<2.5	<1.6	<1.6	<2.6	0.49	<2.2	<2.3	<1.9	<1.7	<1.9	<1.4
Au (ppb)	1.0	0.7	<1.1	0.9	0.5	<1.0	0.8	1.3	<1.1	0.6	<1.1	0.7	1.5	1.3
Pb	n.d.	32	27	25	28	31	74	40	75	19	24	41	37	n.d.
Th	12.5	12.7	12.0	13.1	14.0	12.9	12.4	12.5	12.5	8.90	12.7	9.80	12.2	11.9
U	3.37	3.15	3.39	3.68	3.66	4.21	3.16	3.89	4.16	2.75	3.74	2.59	3.56	2.71

(*Continued*)

APPENDIX 1. WHOLE-ROCK CHEMICAL COMPOSITIONS OF SAMPLES FROM THE EYREVILLE B DRILL CORE (*Continued*)

Sample	CB6	CB6	CB6	W	CB6	W	W	CB6	W	CB6	W	CB6	CB6	W
	115	116	117	092	118	2-21	093	119	095	120	096a	121	124	099
Depth (m)	1473.5	1480.8	1481.7	1481.4	1484.1	1484.4	1484.8	1494	1499.7	1504.3	1505.2	1508.5	1516.2	1517.1
Rock type	sv	sv	sv	sv	sv	sv	sv	cg	cg	sv	sv	sv	cg	cg
(wt%)														
SiO_2	62.6	61.9	62	69.6	60.8	64.6	63.0	65.2	64.7	68.1	64.8	61.5	59.5	70.4
TiO_2	1.01	0.92	0.96	0.66	1.36	0.88	0.91	0.92	0.92	0.89	0.90	1.35	0.93	0.70
Al_2O_3	16.8	17.1	16.7	13.5	17.3	15.3	15.5	15.1	15.1	13.8	15.7	15.8	15.7	11.9
$Fe_2O_3^*$	6.34	6.74	6.07	4.24	7.04	5.80	5.76	5.98	6.06	5.59	6.18	7.61	6.56	5.14
MnO	0.06	0.09	0.07	0.06	0.09	0.06	0.10	0.08	0.09	0.08	0.07	0.07	0.13	0.08
MgO	1.98	3.39	2.44	1.76	2.33	1.35	2.30	2.89	2.95	1.63	1.86	2.50	3.28	2.51
CaO	1.75	1.01	0.81	0.77	1.04	0.51	1.26	1.16	1.77	0.86	0.97	2.34	3.63	2.01
Na_2O	1.19	1.13	1.33	1.01	0.83	0.55	1.41	1.39	1.96	0.92	0.94	1.80	3.27	1.53
K_2O	2.16	4.07	5.37	4.56	4.19	3.93	5.09	3.75	3.09	3.27	3.24	0.31	2.18	2.32
P_2O_5	0.14	0.10	0.12	0.12	0.20	0.14	0.14	0.16	0.18	0.13	0.12	0.15	0.11	0.13
SO_3	<0.1	<0.1	0.1	0.1	0.3	n.d.[†]	0.1	<0.1	<0.1	0.1	<0.1	<0.1	0.1	<0.1
LOI	5.3	3.4	3.2	3.0	4.2	7.2	3.6	3.0	2.8	4.1	4.9	6.3	4.1	2.9
Total	99.33	99.85	99.17	99.38	99.68	100.32	99.17	99.63	99.62	99.47	99.68	99.73	99.49	99.62
(ppm)														
Sc	14.1	14.9	16.1	n.d.	16.7	13.4	13.5	14.9	14.6	12.1	13.5	9.8	17.1	11.7
V	105	120	120	84	138	106	114	109	115	92	122	108	113	79
Cr	65.7	112	107	n.d.	83.5	69.8	91	117	115	63.8	69.8	40.3	124	91.6
Co	20.4	19.4	19.7	n.d.	18.1	13.7	16	17.5	17.9	15.7	17.2	15	19.6	15.1
Ni	39	39	40	33	39	53	40	39	67	33	35	24	49	33
Cu	44	<30	<30	<30	37	<30	<30	<30	<30	30	<30	<30	32	<30
Zn	107	99	116	n.d.	136	130	110	97	98	144	131	52	112	85
As	33.4	7.7	11.3	n.d.	21.9	29.7	13.4	3.91	4.19	27.1	21.6	7.86	1.6	0.95
Se	<1.7	<2.1	<1.6	n.d.	<2.4	<1.5	<1.7	<2.2	<1.3	<2.0	<1.8	<1.9	<2.3	<1.6
Br	<1.1	0.9	1.7	n.d.	4.9	8.3	3.4	0.8	0.4	3.3	3.5	8.7	1.0	0.8
Rb	99.1	141	228	n.d.	197	202	220	138	128	163	168	23.6	88.3	95.0
Sr	361	124	108	106	149	106	142	126	232	351	400	474	223	134
Y	41	45	61	48	59	35	63	56	50	47	52	22	40	37
Zr	275	255	236	213	371	247	246	306	309	257	251	269	270	234
Nb	10	13	13	<10	16	16	12	15	<10	10	11	11	12	10
Mo	<10	<10	<10	<10	<10	n.d.	<10	<10	<10	<10	<10	<10	<10	<10
Sb	1.77	0.33	1.47	n.d.	2.32	3.69	1.21	0.33	0.18	2.77	2.26	2.24	0.11	0.05
Cs	8.09	4.01	13.9	n.d.	15.3	15.0	9.16	3.96	3.42	10.7	14.4	4.62	2.52	2.39
Ba	278	646	528	536	543	495	568	533	467	386	442	68	654	610
La	46.2	42.6	48.4	n.d.	53.4	42.0	42.8	45.9	48.1	39.2	39.3	20.1	45.2	37.6
Ce	89.0	81.1	93.4	n.d.	104	83.8	86.8	90.2	100	75.8	79.3	42.8	87.2	83.2
Nd	38.9	33.2	42.2	n.d.	44.2	35.0	36.7	41.5	41.5	32.2	36.0	21.5	38.7	36.1
Sm	7.28	6.33	7.74	n.d.	8.19	7.30	7.86	8.00	9.33	6.02	7.31	4.70	7.29	7.36
Eu	1.73	1.30	1.89	n.d.	1.98	1.73	1.68	1.70	1.92	1.57	1.68	1.04	1.81	1.62
Gd	7.34	5.25	6.48	n.d.	6.95	7.30	5.80	7.03	8.10	6.03	6.80	4.84	7.12	6.93
Tb	1.17	0.91	1.16	n.d.	1.25	1.03	1.03	1.26	1.44	1.00	1.07	0.86	1.26	1.15
Tm	0.50	0.48	0.58	n.d.	0.58	0.60	0.44	0.61	0.58	0.50	0.46	0.31	0.61	0.60
Yb	3.11	3.11	3.66	n.d.	3.97	3.17	3.30	3.98	4.24	3.24	3.43	1.96	3.92	3.19
Lu	0.49	0.47	0.55	n.d.	0.63	0.51	0.50	0.59	0.61	0.49	0.51	0.29	0.60	0.50
Hf	6.75	6.32	6.67	n.d.	9.84	6.73	6.52	7.97	8.04	7.03	6.55	5.85	7.42	6.27
Ta	1.43	1.23	1.37	n.d.	1.53	1.49	1.22	1.34	1.42	1.23	1.23	1.26	1.50	1.15
W	2.2	n.d.	n.d.	n.d.	n.d.	3.6	<5.6	n.d.	<6.0	n.d.	5.2	n.d.	n.d.	2.1
Ir (ppb)	<1.8	<2.1	<1.6	n.d.	<2.4	<1.6	<2.2	<2.3	<1.7	<1.9	<2.2	<1.8	<2.3	<1.6
Au (ppb)	<1.3	<1.4	<1.5	n.d.	0.8	<1.2	<1.2	<1.5	<1.2	<1.4	<1.1	0.1	0.6	0.3
Pb	28	<15	<15	23	17	n.d.	26	<15	17	43	24	<15	<15	<15
Th	13.0	12.2	13.4	n.d.	15.1	12.9	12.3	13.3	14.7	11.7	12.6	10.4	13.4	12.1
U	3.64	2.65	3.20	n.d.	4.17	3.24	3.10	3.13	3.41	3.22	3.67	2.22	2.87	2.44

(*Continued*)

APPENDIX 1.WHOLE-ROCK CHEMICAL COMPOSITIONS OF SAMPLES FROM THE EYREVILLE B DRILL CORE (*Continued*)

Sample	W	W	W	CB6	W	CB6	CB6	W	W	CB6	W	W	RG	CB6	W
	100a	101	102a	126	104a	127	128	105a	106	129	2-29	107	076	130	109
Depth (m)	1521.9	1523.9	1527.6	1529.3	1533.1	1535.4	1536.5	1537.5	1541.3	1542.7	1543.9	1545	1545.3	1547.4	1548.5
Rock type	sv	sv	sv	sv	sv	sv	plib	plib	cg	cg	cg	cg	cg	cg	sv
(wt%)															
SiO_2	61.8	62.3	63.6	65.6	66.7	63.3	64.7	63.6	69.4	71.2	65.0	67.1	67.4	63.5	63.1
TiO_2	1.11	1.08	1.04	0.99	0.90	0.97	1.05	0.91	0.88	0.89	0.90	0.97	0.87	0.89	1.10
Al_2O_3	17.2	16.0	15.9	14.9	14.6	15.6	15.8	15.4	13.5	14	14.9	15.6	14.6	17.2	16.0
Fe_2O_3*	6.74	6.87	6.62	6.22	5.78	6.09	6.04	6.25	5.89	4.61	5.81	4.41	5.78	5.50	6.64
MnO	0.08	0.08	0.08	0.08	0.08	0.09	0.08	0.09	0.06	0.05	0.10	0.05	0.07	0.08	0.09
MgO	2.11	2.09	2.00	1.83	1.78	1.84	1.80	1.87	2.32	1.25	1.49	1.25	2.69	2.75	2.32
CaO	1.11	1.22	1.35	1.38	0.98	1.72	1.00	1.52	0.49	0.41	1.42	0.70	0.96	0.95	1.09
Na_2O	0.85	0.98	0.85	0.85	1.15	1.04	1.02	1.03	1.26	0.77	0.87	1.50	1.34	1.15	1.15
K_2O	3.25	3.31	3.08	3.23	3.39	3.74	3.86	3.60	2.87	3.32	3.60	3.34	2.79	4.61	3.86
P_2O_5	0.17	0.27	0.15	0.16	0.16	0.15	0.16	0.15	0.11	0.06	0.16	0.11	0.14	0.11	0.14
SO_3	0.2	0.2	<0.1	0.1	<0.1	0.2	<0.1	0.4	<0.1	<0.1	n.d.†	<0.1	<0.1	<0.1	<0.1
LOI	5.1	4.9	5.1	4.4	3.9	4.8	4.4	4.6	2.9	3.3	5.1	4.8	3.2	3.1	4.4
Total	99.72	99.30	99.77	99.74	99.42	99.54	99.91	99.42	99.68	99.86	99.35	99.83	99.84	99.84	99.89
(ppm)															
Sc	15.8	16.0	15.8	13.4	14.4	14.6	15.5	13.7	12.5	13.2	13.6	15.5	n.d.	13.7	17.9
V	116	111	119	121	104	112	126	107	93	98	105	102	103	98	137
Cr	72.6	75.3	75.9	66.3	73.2	74.1	85.9	69.3	90.4	67.9	66.4	73.4	n.d.	102	94.4
Co	18.7	19.0	18.2	14.5	17.6	16.9	17.8	15.8	16.1	13.5	15.4	12.2	n.d.	14.3	19.5
Ni	39	62	37	35	34	34	34	37	37	27	40	29	39	40	37
Cu	55	42	<30	<30	<30	31	<30	<30	<30	<30	<30	<30	<30	161	32
Zn	136	156	160	142	131	127	152	103	89	85	101	81	n.d.	93	120
As	34.3	29.5	20.5	25.8	24.1	35.0	31.6	28.5	42.3	0.69	18.5	2.60	n.d.	<1.4	17.0
Se	<1.8	<2.1	<1.7	<2.1	<1.6	<2.2	<2.2	<2.6	<1.6	<2.0	<1.5	<1.7	n.d.	<2.1	0.18
Br	3.6	6.3	3.2	5.7	2.5	5.0	3.2	6.2	0.7	1.0	6.1	0.9	n.d.	1.1	2.2
Rb	179	193	177	161	195	178	197	171	122	146	175	119	n.d.	168	185
Sr	284	320	265	143	136	122	109	110	97	66	85	90	104	99	112
Y	56	57	50	47	48	53	56	55	52	44	38	44	47	62	55
Zr	281	291	273	285	246	254	293	229	289	380	241	314	300	335	249
Nb	12	<10	13	12	12	13	13	12	15	14	15	12	13	22	12
Mo	10	<10	<10	<10	<10	<10	<10	<10	<10	<10	n.d.	<10	<10	<10	<10
Sb	3.85	1.47	1.77	2.89	2.30	2.32	2.74	3.08	0.22	0.18	2.27	0.58	n.d.	0.11	1.33
Cs	16.0	15.8	15.4	13.7	14.9	12.5	13.7	14.0	7.45	7.21	16.2	5.54	n.d.	4.33	13.6
Ba	400	446	438	416	465	521	524	457	381	575	489	578	529	736	523
La	42.9	46.9	48.0	42.3	38.6	39.5	45.2	46.9	37.0	38.0	37.2	36.9	n.d.	58.6	40.4
Ce	92.2	98.9	102	79.7	84.4	77.3	87.4	94.1	79.4	72.6	75.7	77.3	n.d.	112	85.1
Nd	39.7	44.4	42.9	36.5	37.6	34.7	36.8	36.0	32.5	30.3	33	31.3	n.d.	45.0	37.0
Sm	8.33	10.4	8.62	7.13	8.18	6.86	7.61	8.97	7.08	6.03	7.08	7.07	n.d.	8.05	8.01
Eu	1.83	2.31	1.88	1.58	1.85	1.62	1.80	1.80	1.52	1.28	1.82	1.50	n.d.	1.91	1.76
Gd	8.50	9.79	8.06	6.45	8.60	6.71	7.01	8.10	6.20	5.64	6.03	6.70	n.d.	8.81	6.9
Tb	1.29	1.58	1.29	1.06	1.33	1.15	1.26	1.24	1.12	1.03	1.11	1.17	n.d.	1.46	1.21
Tm	0.56	0.80	0.70	0.49	0.72	0.53	0.61	0.61	0.58	0.54	0.61	0.61	n.d.	0.77	0.65
Yb	3.46	4.08	3.78	3.36	3.64	3.46	3.96	3.19	3.30	3.56	3.63	3.47	n.d.	5.03	3.18
Lu	0.58	0.61	0.58	0.51	0.54	0.53	0.61	0.41	0.51	0.55	0.54	0.54	n.d.	0.73	0.55
Hf	7.46	7.20	7.78	7.17	7.20	6.52	8.39	6.08	7.29	10.4	6.40	8.51	n.d.	9.51	6.81
Ta	1.61	1.81	1.55	1.31	1.56	1.31	1.68	1.20	1.21	1.51	1.28	1.42	n.d.	2.66	1.54
W	4.5	4.1	3.9	n.d.	3.1	n.d.	n.d.	<2.9	3.1	n.d.	4.0	6.3	n.d.	n.d.	3.2
Ir (ppb)	<1.6	<1.9	<1.6	0.76	<1.4	<2.1	<2.2	<1.4	<2.1	<1.9	<1.7	<2.2	n.d.	<2.1	<2.4
Au (ppb)	1.2	1.1	1.2	<1.5	0.8	0.9	0.8	1.0	<0.8	<1.3	1.1	0.4	n.d.	0.6	0.8
Pb	33	36	40	42	18	16	29	23	<15	<15	n.d.	<15	<15	<15	25
Th	15.7	19.5	15.1	12.7	14.2	11.7	14.2	12.0	11.3	13.2	11.7	12.9	n.d.	30.4	12.3
U	4.46	4.66	4.19	3.58	3.59	3.17	4.12	2.55	2.30	3.28	2.67	2.89	n.d.	6.11	3.59

Note: All major-element contents and V, Ni, Sr, Y, Zr, and Ba contents were analyzed by X-ray fluorescence (XRF); all other element contents were determined by instrumental neutron activation analysis (INAA). LOI—loss on ignition. Rock types: sv—suevite, imr—impact melt rock, plib—polymict lithic impact breccia, cg—cataclastic gneiss.

*Total Fe as Fe_2O_3.

†Not determined.

APPENDIX 2. CHEMICAL COMPOSITIONS OF CLASTS IN IMPACT BRECCIA OF THE EYREVILLE B DRILL CORE

Sample	W 56b	W 63	W 64	W 65b	W 78	W 80b	W 81b	W 85c	W 87	CB6 112	W 88b	W 89b
Depth (m)	1400.1	1408.3	1410.3	1411.7	1439.8	1443.1	1444.6	1452.6	1459.1	1459.2	1461.3	1464.3
Rock type	amph	Ms-Qtz schist	amphibolitic gneiss	granite	gneiss	clast*	sed (gw)	gneiss	arkose	cong	clast*	clast*
(wt%)												
SiO_2	47.9	63.2	56.5	82.5	58.4	51.6	69.9	78.3	72.0	75.0	72.4	66.8
TiO_2	1.40	0.89	0.70	0.49	0.53	1.24	0.64	0.71	0.90	0.79	1.24	1.00
Al_2O_3	26.6	15.7	19.3	8.20	18.8	17.5	14.1	12.6	13.6	12.1	12.7	13.4
Fe_2O_3 †	10.4	6.32	5.22	2.00	4.07	14.4	4.31	3.33	1.94	1.71	5.79	7.17
MnO	0.07	0.08	0.35	0.02	0.09	0.20	0.06	0.03	0.07	0.07	0.07	0.05
MgO	1.65	3.01	2.75	0.71	1.31	3.24	1.21	0.81	0.52	0.42	1.15	1.38
CaO	2.00	1.50	2.99	0.92	3.87	2.48	0.54	0.71	1.58	1.46	0.52	1.87
Na_2O	1.50	1.17	3.34	1.21	6.48	2.14	1.97	0.47	2.16	2.16	0.26	1.62
K_2O	0.24	3.87	6.20	1.54	3.01	0.64	2.66	0.66	3.40	2.98	2.60	0.27
P_2O_5	0.05	0.13	0.16	0.04	0.12	0.03	0.12	0.10	0.18	0.21	0.20	0.06
SO_3	<0.1	<0.1	<0.1	<0.1	0.7	0.2	<0.1	<0.1	<0.1	<0.1	0.1	0.2
LOI	7.8	3.3	2.1	2.1	1.9	5.7	4.0	2.0	2.8	2.6	2.9	5.7
Total	99.61	99.17	99.61	99.73	99.28	99.37	99.51	99.72	99.15	99.50	99.93	99.52
(ppm)												
Sc	25.1	15.6	13.2	5.02	8.10	16.5	n.d.§	8.14	9.42	8.38	11.0	9.64
V	186	111	158	54	98	136	72	65	90	79	95	84
Cr	126	123	26.4	24.6	13.3	78.1	n.d.	35.4	37.7	34.8	46.6	45.9
Co	24.4	18.8	15.4	5.72	8.07	12.8	n.d.	10.0	8.43	10.5	11.9	16.2
Ni	33	38	30	21	22	<15	32	24	33	30	36	31
Cu	38	32	<30	<30	<30	37	<30	<30	72	33	30	<30
Zn	174	123	373	147	43	61	n.d.	56	46	48	174	46
As	2.57	1.65	10.6	5.74	12.4	2.87	n.d.	21.4	21.8	25.6	16.1	22.1
Se	<2.6	<1.6	<1.4	<0.9	<1.0	<1.4	n.d.	<1.1	<1.4	<1.8	<1.6	<1.5
Br	1.0	0.4	0.8	1.9	1.6	9.0	n.d.	1.0	0.9	1.4	1.3	4.3
Rb	31.7	153	246	56.3	97.6	34.7	n.d.	32.9	158	119	160	27.8
Sr	342	132	380	143	376	403	114	127	84	85	78	408
Y	26	51	42	15	40	<10	39	21	48	46	51	12
Zr	270	237	185	134	262	317	231	208	280	229	460	313
Nb	<10	<10	<10	<10	<10	15	10	<10	<10	<10	14	<10
Mo	<10	<10	<10	<10	<10	<10	<10	<10	<10	<10	<10	<10
Sb	5.05	0.14	1.83	2.83	1.31	0.43	n.d.	3.30	4.32	3.17	2.35	4.20
Cs	22.6	3.82	4.32	2.42	1.18	5.39	n.d.	7.00	7.87	5.76	16.5	9.84
Ba	61	658	987	164	521	105	323	237	558	547	313	49
La	37.7	40.5	21.1	19.9	36.1	23.9	n.d.	49.2	29.1	36.3	42.1	11.2
Ce	80.4	80.0	40.9	40.1	76.5	48.4	n.d.	94.6	60.6	72.1	84.9	25.6
Nd	34.3	34.4	17.6	16.8	33.6	22.7	n.d.	31.6	28.3	30.7	38.5	11.1
Sm	6.83	7.14	3.28	3.43	7.22	4.70	n.d.	6.92	6.34	5.76	8.64	3.20
Eu	1.38	1.66	0.98	0.70	1.52	0.69	n.d.	1.40	1.38	1.50	1.52	0.78
Gd	n.d.	7.00	3.15	3.42	7.51	5.02	n.d.	5.92	5.90	5.47	7.90	3.60
Tb	1.13	1.01	0.42	0.48	1.03	0.61	n.d.	0.93	1.00	0.91	1.34	0.62
Tm	0.60	0.54	0.25	0.24	0.61	0.27	n.d.	0.45	0.40	0.41	0.58	0.30
Yb	3.29	3.30	1.31	1.47	3.69	1.57	n.d.	2.39	3.00	2.56	4.55	1.55
Lu	0.52	0.53	0.23	0.23	0.48	0.26	n.d.	0.30	0.46	0.40	0.68	0.24
Hf	7.06	5.82	4.37	3.12	6.29	8.61	n.d.	5.23	7.05	5.25	13.5	8.42
Ta	2.09	1.25	0.66	0.65	1.28	1.70	n.d.	0.99	1.33	0.83	1.69	<0.05
W	2.9	2.2	1.8	0.7	<2.5	1.9	n.d.	1.1	<5.3	n.d.	5.4	<5.0
Ir (ppb)	<2.6	<1.9	<1.4	<0.9	<1.2	<1.6	n.d.	<1.2	0.53	<1.7	<1.9	<1.9
Au (ppb)	0.8	<0.7	<0.8	<0.6	0.5	<0.9	n.d.	0.4	<1.2	<1.5	1.1	0.9
Pb	<15	<15	50	<15	<15	18	<15	<15	<15	<15	21	<15
Th	20.6	13.6	11.9	5.75	16.6	16.8	n.d.	8.86	10.6	10.3	15.1	12.4
U	6.46	2.62	1.83	1.25	3.53	4.69	n.d.	1.85	2.78	1.72	4.33	3.24

Note: All major-element contents and V, Ni, Sr, Y, Zr, and Ba contents were analyzed by X-ray fluorescence (XRF); all other element contents were determined by instrumental neutron activation analysis (INAA). LOI—loss on ignition. Rock types: amph—amphibolite, cong—conglomerate, sed—sedimentary clast, pb—polymict breccia, gw—graywacke. Minerals: Ms—muscovite, Bt—biotite, Qtz—quartz (Kretz, 1983).

*Gray-green, extremely fine-grained, crumbly to powdery clasts, presumably fine-grained sedimentary clasts or highly altered clasts/melt.

†Total Fe as Fe_2O_3.

§Not determined.

(*Continued*)

APPENDIX 2. CHEMICAL COMPOSITIONS OF CLASTS IN IMPACT BRECCIA OF THE EYREVILLE B DRILL CORE (*Continued*)

Sample	W 90b	W 95	W 96b	W 97	CB6 122	W 98	CB6 123	CB6 125	W 102b	W 103	W 104b	W 105b
Depth (m)	1470.4	1499.7	1505.2	1510.8	1511.9	1513.6	1514.3	1522.7	1527.6	1530.8	1533.1	1537.5
Rock type	clast*	Bt-Ms-Qtz schist	pb†	pb†	gneiss	mica schist§	mafic rock	cong	gw?	mica schist§	gneiss	amph
(wt%)												
SiO_2	63.9	64.7	76.7	55.9	61.8	38.4	46.0	75.4	80.7	55.6	69.7	42.4
TiO_2	1.05	0.92	0.61	0.98	0.89	0.73	1.44	1.12	0.57	0.92	1.02	2.61
Al_2O_3	17.6	15.1	11.6	17.5	15.2	13.9	17.0	10.1	9.40	17.7	13.3	17.9
Fe_2O_3#	6.31	6.06	3.83	8.99	7.33	15.7	10.9	3.47	2.26	7.90	6.29	14.70
MnO	0.07	0.09	0.04	0.11	0.11	0.35	0.27	0.07	0.03	0.11	0.12	0.23
MgO	1.76	2.95	0.88	5.38	4.77	5.07	6.59	0.79	0.68	4.22	1.33	6.93
CaO	0.49	1.77	0.33	1.05	1.13	9.43	7.06	1.93	0.59	2.39	0.72	2.34
Na_2O	0.36	1.96	0.13	1.25	4.50	1.03	2.91	1.75	0.51	2.91	1.21	0.56
K_2O	4.19	3.09	3.08	3.28	0.52	3.13	2.09	2.30	2.00	3.22	2.75	1.20
P_2O_5	0.09	0.18	0.11	0.08	0.06	0.16	0.15	0.16	0.04	0.03	0.23	0.59
SO_3	<0.1	<0.1	<0.1	0.2	0.1	2.5	0.2	<0.1	<0.1	<0.1	<0.1	0.6
LOI	4.1	2.8	2.6	4.8	2.9	8.9	5.1	2.9	2.6	4.5	2.8	9.2
Total	99.92	99.62	99.91	99.52	99.31	99.30	99.71	99.99	99.38	99.50	99.47	99.26
(ppm)												
Sc	16.0	14.6	7.57	19.0	20.5	18.5	36.0	8.52	6.28	20.9	10.7	26.2
V	127	115	71	180	161	148	223	85	62	131	85	246
Cr	85.5	115	44.4	252	168	102	262	35.9	28.6	151	41.3	129
Co	17.0	17.9	9.55	20.9	23.0	91.5	44.5	10.2	4.32	22.9	11.5	63.2
Ni	40	67	29	64	58	42	123	25	23	42	30	164
Cu	43	<30	35	<30	72	270	54	<30	<30	<30	<30	43
Zn	96	98	60	105	113	118	130	69	40	122	98	146
As	0.81	4.19	79.0	7.76	11.7	57.1	15.2	16.9	7.39	9.16	5.01	28.2
Se	<1.8	<1.3	<1.0	<1.9	<2.3	<2.1	<3.0	0.42	<1.4	<2.0	<1.6	<3.5
Br	0.2	0.4	1.3	0.7	0.8	1.2	1.1	1.4	1.7	1.7	1.4	15.8
Rb	209	128	159	171	22.5	142	86.0	107	103	139	144	52.8
Sr	110	232	55	72	176	222	447	99	96	378	75	151
Y	66	50	39	50	20	22	21	29	25	39	54	41
Zr	235	309	192	170	163	55	110	195	212	207	453	189
Nb	14	<10	<10	11	<10	<10	<10	<10	<10	12	10	16
Mo	<10	<10	<10	<10	<10	11.00	<10	<10	<10	<10	<10	<10
Sb	0.65	0.18	4.34	0.50	0.26	2.40	0.37	2.17	1.47	0.25	0.86	5.14
Cs	20.5	3.42	10.1	8.94	0.93	3.65	3.67	6.01	6.69	6.64	8.11	23.6
Ba	613	467	393	455	70	172	244	391	317	1708	339	378
La	28.0	48.1	23.9	30.7	18.9	6.47	8.97	28.9	24.4	42.2	37.1	36.8
Ce	102	100	47.3	63.9	38.0	14.0	19.5	55.5	52.1	89.7	79.6	77.0
Nd	38.9	41.5	21.1	23.5	17.5	7.68	10.8	26.5	22.0	37.4	37.2	42.5
Sm	6.17	9.33	4.64	5.83	3.86	1.99	2.84	5.18	4.05	7.89	8.11	9.84
Eu	1.78	1.92	1.30	1.51	1.48	0.91	1.31	1.42	1.29	1.60	1.81	1.96
Gd	6.80	8.10	4.20	4.90	4.77	2.90	3.63	4.45	3.65	8.09	7.42	12.1
Tb	1.22	1.44	0.63	0.91	0.78	0.47	0.63	0.80	0.56	1.14	1.26	1.75
Tm	0.60	0.58	0.29	0.39	0.42	0.21	0.31	0.39	0.28	0.55	0.65	0.69
Yb	3.41	4.24	2.15	3.08	2.73	1.72	2.19	2.31	2.01	3.44	3.72	3.78
Lu	0.64	0.61	0.33	0.47	0.43	0.27	0.34	0.35	0.32	0.53	0.58	0.45
Hf	6.23	8.04	4.83	4.33	4.05	1.34	2.52	4.96	4.86	5.95	12.6	4.77
Ta	1.63	1.42	0.73	1.11	0.95	0.23	0.40	0.87	0.83	1.95	1.35	1.22
W	0.1	<6.0	<3.5	2.3	n.d.**	<4.9	n.d.	n.d.	1.1	<3.1	3.0	4.3
Ir (ppb)	<2.2	<1.7	<1.2	<2.3	<2.4	<2.5	<3.1	<1.6	<1.2	<1.8	<1.4	<1.8
Au (ppb)	0.1	<1.2	0.7	<1.1	<1.8	<1.2	<1.9	<1.3	0.4	0.4	<0.7	0.6
Pb	<15	17	<15	<15	<15	<15	<15	<15	<15	71	43	<15
Th	15.4	14.7	7.69	11.0	9.85	0.85	0.91	6.46	7.74	18.6	13.2	2.04
U	1.03	3.41	1.88	3.32	2.74	<0.4	<0.6	1.53	1.73	3.58	3.24	0.33

Note: All major-element contents and V, Ni, Sr, Y, Zr, and Ba contents were analyzed by X-ray fluorescence (XRF); all other element contents were determined by instrumental neutron activation analysis (INAA). LOI—loss on ignition. Rock types: amph—amphibolite, cong—conglomerate, sed—sedimentary clast, pb—polymict breccia, gw—graywacke.

*Gray-green, extremely fine-grained, crumbly to powdery clasts, presumably fine-grained sedimentary clasts or highly altered clasts/melt.

†With mica schist, phyllite, meta-siltstone clasts.

§Carbonatized, with ore mineralization.

#Total Fe as Fe_2O_3.

**Not determined.

REFERENCES CITED

Albin, E.F., Norman, M.D., and Roden, M., 2000, Major and trace element compositions of georgiaites: Clues to the source of North American tektites: Meteoritics & Planetary Science, v. 35, p. 795–806.

Anthony, J.E., Bideaux, R.A., Bladh, K.W., and Nichols, M.C., 1995, Handbook of Mineralogy: Volume II. Silica, Silicates: Tucson, Arizona, Mineral Data Publishing, 904 p.

Bartosova, K., Ferrière, L., Koeberl, C., Reimold, W.U., Gibson, R., and Schmitt, R.T., 2007a, Lithological, petrographical, and geochemical investigations of suevite from the Eyreville core, Chesapeake Bay impact structure: Geological Society of America Abstracts with Programs, v. 39, no. 6, p. 451.

Bartosova, K., Ferrière, L., Koeberl, C., and Reimold, W.U., 2007b, Investigations of melt particles in suevite from the Eyreville B core, Chesapeake Bay impact structure: Geological Society of America Abstracts with Programs, v. 39, no. 6, p. 314.

Bartosova, K., Koeberl, C., Schmitt, R.T., Reimold, W.U., and Ferrière, L., 2008, A petrographical, geochemical, and shock metamorphic study of suevite from the Eyreville drillcore, Chesapeake Bay impact structure, USA: Houston, Texas, Lunar and Planetary Science, v. 39, abstract no. 1065 (CD-ROM).

Bartosova, K., Ferrière, L., Koeberl, C., Reimold, W.U., and Gier, S., 2009, this volume, Petrographic and shock metamorphic studies of the impact breccia section (1397–1551 m depth) of the Eyreville drill core, Chesapeake Bay impact structure, USA, *in* Gohn, G.S., Koeberl, C., Miller, K.G., and Reimold, W.U., eds., The ICDP-USGS Deep Drilling Project in the Chesapeake Bay Impact Structure: Results from the Eyreville Core Holes: Geological Society of America Special Paper 458, doi: 10.1130/2009.2458(15).

Bocherens, H., Friis, E.M., Mariotti, A., and Pedersen, K.R., 1993, Carbon isotopic abundances in Mesozoic and Cenozoic fossil plants: Palaeoecological implications: Lethaia, v. 26, p. 347–358, doi: 10.1111/j.1502-3931.1993.tb01541.x.

Claeys, P., Heuschkel, S., Lounejeva-Baturina, E., Sanchez-Rubio, G., and Stöffler, D., 2003, The suevite of drill hole Yucatàn 6 in the Chicxulub impact crater: Meteoritics & Planetary Science, v. 38, p. 1299–1317.

Coplen, T.B., Böhlke, J.K., De Bievre, P., Ding, T., Holden, N.E., Hopple, J.A., Krouse, R., Lamberty, A., Peiser, H.S., Revesz, K.M., Rieder, S.E., Rosman, K.J.R., Roth, E., Taylor, P.D.P., Vocke, R.D., Jr., and Xiao, Y.K., 2002, Isotopic abundance variations of selected elements: Pure and Applied Chemistry, v. 74, p. 1987–2017, doi: 10.1351/pac200274101987.

Coplen, T.B., Brand, W.A., Gehre, M., Gröning, M., Meijer, H.A.J., Toman, B., and Verkouteren, R.M., 2006, New guidelines for $\delta^{13}C$ measurements: Analytical Chemistry, v. 78, no. 7, p. 2439–2441, doi: 10.1021/ac052027c.

Cross, W., Iddings, J.P., Pirrson, L.V., and Washington, H.S., 1902, A quantitative chemico-mineralogical classification and nomenclature of igneous rocks: The Journal of Geology, v. 10, p. 555–690.

Deutsch, A., and Koeberl, C., 2006, Establishing the link between the Chesapeake Bay impact structure and the North American tektite strewn field: The Sr-Nd isotopic evidence: Meteoritics & Planetary Science, v. 41, p. 689–703.

Edwards, L.E., Barron, J.A., Bukry, D., Bybell, L.M., Cronin, T.M., Poag, C.W., Weems, R.E., and Wingard, G.L., 2005, Paleontology of the Upper Eocene to Quaternary postimpact section in the USGS-NASA Langley core, Hampton, Virginia, *in* Horton, J.W., Jr., Powars, D.S., and Gohn, G.S., eds., Studies of the Chesapeake Bay Impact Structure—The USGS-NASA Langley Corehole, Hampton, Virginia, and Related Coreholes and Geophysical Surveys: U.S. Geological Survey Professional Paper 1688, p. H1–H47.

Elliott, W.S., Jr., and Mora, G., 2004, Stable isotopic composition of terrestrial organic matter from continental sediments of the mid-Cretaceous Potomac Group, Chesapeake Bay, Maryland: Geological Society of America Abstracts with Programs, v. 36, no. 5, p. 292.

Fernandes, V.A., Wittmann, A., Schmitt, R.T., Reimold, W.U., Hecht, L., and Povenmire, H., 2008, Petrography, geochemistry, and radiometric dating of impact melts from the Chesapeake Bay impact structure, USA: Houston, Texas, Lunar and Planetary Science, v. 39, abstract no. 2383 (CD-ROM).

Frederiksen, O., Edwards, L.E., Self-Trail, J.M., Bybell, L.M., and Cronin, T.M., 2005, Paleontology of the impact-modified and impact-generated sediments in the USGS-NASA Langley core, Hampton, Virginia, *in* Horton, J.W., Jr., Powars, D.S., and Gohn, G.S., eds., Studies of the Chesapeake Bay Impact Structure—The USGS-NASA Langley Corehole, Hampton, Virginia, and Related Coreholes and Geophysical Surveys: U.S. Geological Survey Professional Paper 1688, p. D1–D37.

French, B.M., Koeberl, C., Gilmour, I., Shirey, S.B., Dons, J.A., and Naterstad, J., 1997, The Gardnos impact structure, Norway: Petrology and chemistry of target rocks and impactites: Geochimica et Cosmochimica Acta, v. 61, p. 873–904, doi: 10.1016/S0016-7037(96)00382-1.

Gibson, R.L., Townsend, G.N., Horton, J.W., Jr., and Reimold, W.U., 2007, Pre-impact tectonothermal evolution of the crystalline target in the ICDP-USGS Eyreville-B core, Chesapeake Bay impact structure: Geological Society of America Abstracts with Programs, v. 39, no. 6, p. 451.

Glass, B.P., 1989, North American tektite debris and impact ejecta from DSDP Site 612: Meteoritics, v. 24, p. 209–218.

Glass, B.P., 2002, Upper Eocene impact ejecta/spherule layers in marine sediments: Chemie der Erde, v. 62, p. 173–196, doi: 10.1078/0009-2819-00017.

Gohn, G.S., Koeberl, C., Miller, K.G., Reimold, W.U., Cockell, C.S., Horton, J.W., Jr., Sanford, W.E., and Voytek, M.A., 2006a, Chesapeake Bay impact structure drilled: Eos (Transactions, American Geophysical Union), v. 87, p. 349–355, doi: 10.1029/2006EO350001.

Gohn, G.S., Koeberl, C., Miller, K.G., Reimold, W.U., Browning, J.V., Cockell, C.S., Dypvik, H., Edwards, L.E., Horton, J.W., Jr., McLaughlin, P.P., Ormö, J., Plescia, J.B., Powars, D.S., Sanford, W.E., Self-Trail, J.M., and Voytek, M.A., 2006b, Preliminary site report for the 2005 ICDP-USGS deep corehole in the Chesapeake Bay impact crater: Houston, Texas, Lunar and Planetary Science, v. 37, abstract no. 1713 (CD-ROM).

Gohn, G.S., Sanford, W.E., Powars, D.S., Horton, J.W., Jr., Edwards, L.E., Morin, R.H., and Self-Trail, J.M., 2007, Site Report for USGS Test Holes Drilled at Cape Charles, Northampton County, Virginia, in 2004: U.S. Geological Survey Open-File Report 2007-1094, 22 p.

Gohn, G.S., Koeberl, C., Miller, K.G., Reimold, W.U., Browning, J.V., Cockell, C.S., Horton, J.W., Jr., Kenkmann, T., Kulpecz, A.A., Powars, D.S., Sandford, W.E., and Voytek, M.A., 2008, Deep drilling into the Chesapeake Bay impact structure: Science, v. 320, doi: 10.1126/science.1158708, p. 1740–1745.

Gohn, G.S., Koeberl, C., Miller, K.G., and Reimold, W.U., 2009, this volume, Deep drilling in the Chesapeake Bay impact structure—An overview, *in* Gohn, G.S., Koeberl, C., Miller, K.G., and Reimold, W.U., eds., The ICDP-USGS Deep Drilling Project in the Chesapeake Bay Impact Structure: Results from the Eyreville Core Holes: Geological Society of America Special Paper 458, doi: 10.1130/2009.2458(01).

Govindaraju, K., 1989, 1989 compilation of working values and sample description for 272 geostandards: Geostandards Newsletter, v. 13, p. 1–113, doi: 10.1111/j.1751-908X.1989.tb00476.x.

Gröcke, D.R., 1998, Carbon-isotope analyses of fossil plants as a chemostratigraphic and palaeoenvironmental tool: Lethaia, v. 31, p. 1–13.

Hecht, L., Wittmann, A., Schmitt, R.T., and Stöffler, D., 2004, Composition of impact melt particles and the effects of post-impact alteration in suevitic rocks at the Yaxcopoil-1 drill core, Chicxulub crater, Mexico: Meteoritics & Planetary Science, v. 39, p. 1169–1186.

Horton, J.W., Jr., and Izett, G.A., 2005, Crystalline-rock ejecta and shocked minerals of the Chesapeake Bay impact structure, USGS-NASA Langley core, Hampton, Virginia, with supplemental constraints on the age of impact, *in* Horton, J.W., Jr., Powars, D.S., and Gohn, G.S., eds., Studies of the Chesapeake Bay Impact Structure—The USGS-NASA Langley Corehole, Hampton, Virginia, and Related Coreholes and Geophysical Surveys: U.S. Geological Survey Professional Paper 1688, p. E1–E30.

Horton, J.W., Jr., Aleinikoff, J.N., Kunk, M.J., Naeser, C.W., and Naeser, N.D., 2005a, Petrography, structure, age, and thermal history of granitic coastal plain basement in the Chesapeake Bay impact structure, USGS-NASA Langley core, Hampton, Virginia, *in* Horton, J.W., Jr., Powars, D.S., and Gohn, G.S., eds., Studies of the Chesapeake Bay Impact Structure—The USGS-NASA Langley Corehole, Hampton, Virginia, and Related Coreholes and Geophysical Surveys: U.S. Geological Survey Professional Paper 1688, p. B1–B29.

Horton, J.W., Jr., Powars, D.S., and Gohn, G.S., 2005b, Studies of the Chesapeake Bay Impact Structure—Introduction and discussion, *in* Horton, J.W., Jr., Powars, D.S., and Gohn, G.S., eds., Studies of the Chesapeake Bay Impact Structure—The USGS-NASA Langley Corehole, Hampton, Virginia, and Related Coreholes and Geophysical Surveys: U.S. Geological Survey Professional Paper 1688, p. A1–A24.

Horton, J.W., Jr., Vanko, D.A., Naeser, C.W., Naeser, N.D., Larsen, D., Jackson, J.C., and Belkin, H.E., 2006a, Postimpact hydrothermal conditions at the central uplift, Chesapeake Bay impact structure, Virginia, USA: Houston, Texas, Lunar and Planetary Science, v. 37, abstract no. 1842 (CD-ROM).

Horton, J.W., Jr., Vanko, D.A., Naeser, C.W., Naeser, N.D., Larsen, D., Jackson, J.C., and Belkin, H.E., 2006b, Hydrothermal alteration of breccias at the central uplift, Chesapeake Bay impact structure: Geological Society of America Abstracts with Programs, v. 38, no. 7, p. 59.

Horton, J.W., Jr., Gibson, R.L., Reimold, W.U., Wittmann, A., Gohn, G.S., and Edwards, L.E., 2009, this volume, Geologic columns for the ICDP-USGS Eyreville B core, Chesapeake Bay impact structure: Impactites and crystalline rocks, 1766 to 1096 m depth, *in* Gohn, G.S., Koeberl, C., Miller, K.G., and Reimold, W.U., eds., The ICDP-USGS Deep Drilling Project in the Chesapeake Bay Impact Structure: Results from the Eyreville Core Holes: Geological Society of America Special Paper 458, doi: 10.1130/2009.2458(02).

Jarosewich, E., Clarke, R.S.J., and Barrows, J.N., 1987, The Allende meteorite reference sample: Smithsonian Contributions to the Earth Sciences, v. 27, p. 1–49.

Jolly, L.C., Gibson, R.L., Horton, J.W., Jr., Reimold, W.U., Hecht, L., and Czaja, P., 2007, Petrography and chemistry of suevites in the impactites sequence, Eyreville B core, Chesapeake Bay impact structure: Geological Society of America Abstracts with Programs, v. 39, no. 6, p. 315.

Kenkmann, T., Collins, G.S., Wittmann, A., Wünnemann, K., Reimold, W.U., and Melosh, H.J., 2009, this volume, A model for the formation of the Chesapeake Bay impact crater as revealed by drilling and numerical simulation, *in* Gohn, G.S., Koeberl, C., Miller, K.G., and Reimold, W.U., eds., The ICDP-USGS Deep Drilling Project in the Chesapeake Bay Impact Structure: Results from the Eyreville Core Holes: Geological Society of America Special Paper 458, doi: 10.1130/2009.2458(25).

Koeberl, C., 1989, New estimates of area and mass for the North American tektite strewn field, *in* Proceedings of the 19th Lunar and Planetary Science Conference: New York, Cambridge University Press, p. 745–751.

Koeberl, C., 1993, Instrumental neutron activation analysis of geochemical and cosmochemical samples: A fast and reliable method for small sample analysis: Journal of Radioanalytical and Nuclear Chemistry, v. 168, p. 47–60, doi: 10.1007/BF02040877.

Koeberl, C., 1998, Identification of meteoritic components in impactites, *in* Grady, M.M., Hutchinson, R., McCall, G.J.H., and Rothery, D.A., eds., Meteorites: Flux with Time and Impact Effects: Geological Society of London Special Publication 140, p. 133–153.

Koeberl, C., and Reimold, W.U., 2003, Geochemistry and petrography of impact breccias and target rocks from the 145 Ma Morokweng impact structure, South Africa: Geochimica et Cosmochimica Acta, v. 67, p. 1837–1862, doi: 10.1016/S0016-7037(02)00994-8.

Koeberl, C., Poag, C.W., Reimold, W.U., and Brandt, D., 1996, Impact origin of the Chesapeake Bay structure and the source of the North American tektites: Science, v. 271, p. 1263–1266, doi: 10.1126/science.271.5253.1263.

Kretz, R., 1983, Symbols for rock-forming minerals: The American Mineralogist, v. 68, p. 277–279.

Larsen, D., Smith, J., Zivkovic, V., Horton, J.W., Jr., and Vanko, D.A., 2006, Authigenic-mineral evidence for post-impact diagenesis and alteration in the Chesapeake Bay impact structure: A progress report: Geological Society of America Abstracts with Programs, v. 38, no. 3, p. 82.

Lee, S.R., Horton, J.W., Jr., and Walker, R.J., 2006, Confirmation of a meteoritic component in impact-melt rocks of the Chesapeake Bay impact structure, Virginia, USA—Evidence from osmium isotopic and PGE systematics: Meteoritics & Planetary Science, v. 41, p. 819–833.

Mader, D., Bartosova, K., Koeberl, C., and Reimold, W.U., 2007, Stable carbon isotope studies of impact breccia clasts from the Eyreville core, Chesapeake Bay impact structure, Virginia, USA: Geological Society of America Abstracts with Programs, v. 39, no. 6, p. 314.

McDonald, I., Bartosova, K., and Koeberl, C., 2009, this volume, Search for a meteoritic component in impact breccia from the Eyreville core, Chesapeake Bay impact structure: Considerations from platinum-group element contents, *in* Gohn, G.S., Koeberl, C., Miller, K.G., and Reimold, W.U., eds., The ICDP-USGS Deep Drilling Project in the Chesapeake Bay Impact Structure: Results from the Eyreville Core Holes: Geological Society of America Special Paper 458, doi: 10.1130/2009.2458(21).

Montanari, A., and Koeberl, C., 2000, Impact Stratigraphy; The Italian Record: Berlin, Springer-Verlag, 364 p.

Mora, G., and Jahren, A.H., 2001, Stable-carbon isotope composition of organic matter from early angiosperms present in the Arundel Formation (Potomac Group), Maryland, USA: Geological Society of America Abstracts with Programs, v. 33, no. 6, p. 236.

Poag, C.W., Powars, D.S., Poppe, L.J., Mixon, R.B., Edwards, L.E., Folger, D.W., and Bruce, S., 1992, Deep Sea Drilling Project Site 612 bolide event: New evidence of a late Eocene impact-wave deposit and a possible impact site, U.S. East Coast: Geology, v. 20, p. 771–774, doi: 10.1130/0091-7613(1992)020<0771:DSDPSB>2.3.CO;2.

Poag, C.W., Powars, D.S., Poppe, L.J., and Mixon, R.B., 1994, Meteoroid mayhem in Ole Virginny: Source of the North American tektite strewn field: Geology, v. 22, p. 691–694, doi: 10.1130/0091-7613(1994)022<0691:MMIOVS>2.3.CO;2.

Poag, C.W., Koeberl, C., and Reimold, W.U., 2004, The Chesapeake Bay Crater: Geology and Geophysics of a Late Eocene Submarine Impact Structure: Impact Studies: Heidelberg, Springer, 522 p.

Reimold, W.U., Koeberl, C., and Bishop, J., 1994, Roter Kamm impact crater, Namibia: Geochemistry of basement rocks and breccias: Geochimica et Cosmochimica Acta, v. 58, p. 2689–2710, doi: 10.1016/0016-7037(94)90138-4.

Reimold, W.U., Kenkmann, T., Gibson, R.L., Bartosova, K., Schmitt, R.T., Hecht, L., Koeberl, C., and Horton, J.W., Jr., 2007a, Dike breccias in the deep basement-derived section of the Eyreville B core, Chesapeake Bay impact structure: Geological Society of America Abstracts with Programs, v. 39, no. 6, p. 451.

Reimold, W.U., Bartosova, K., Schmitt, R.T., Wittek, A., and Koeberl, C., 2007b, First observations on Exmore breccia from the ICDP-USGS Eyreville core, Chesapeake Bay impact structure: Geological Society of America Abstracts with Programs, v. 39, no. 6, p. 314.

Reimold, W.U., Bartosova, K., Schmitt, R.T., Hansen, B., Crasselt, C., Koeberl, C., Wittmann, A., and Powars, D.S., 2009, this volume, Petrographic observations on the Exmore breccia, ICDP-USGS Drilling at Eyreville, Chesapeake Bay impact structure, USA, *in* Gohn, G.S., Koeberl, C., Miller, K.G., and Reimold, W.U., eds., The ICDP-USGS Deep Drilling Project in the Chesapeake Bay Impact Structure: Results from the Eyreville Core Holes: Geological Society of America Special Paper 458, doi: 10.1130/2009.2458(29).

Sanford, W.E., 2005, A simulation of the hydrothermal response to the Chesapeake Bay bolide impact: Geofluids, v. 5, p. 185–201, doi: 10.1111/j.1468-8123.2005.00110.x.

Schmitt, R.T., Wittmann, A., and Stöffler, D., 2004, Geochemistry of drill core samples from Yaxcopoil-1, Chicxulub impact crater, Mexico: Meteoritics & Planetary Science, v. 39, p. 979–1001.

Schmitt, R.T., Reimold, W.U., Bartosova, K., and Koeberl, C., 2007, Chemical composition of rock types from the Eyreville A and B drill cores, Chesapeake Bay impact structure, Virginia/USA: Geological Society of America Abstracts with Programs, v. 39, no. 6, p. 315.

Schmitt, R.T., Bartosova, K., Reimold, W.U., Mader, D., Wittmann, A., Koeberl, C., and Gibson, R.L., 2009, this volume, Geochemistry of impactites and crystalline basement-derived lithologies from the ICDP-USGS Eyreville A and B drill cores, Chesapeake Bay impact structure, Virginia, USA, *in* Gohn, G.S., Koeberl, C., Miller, K.G., and Reimold, W.U., eds., The ICDP-USGS Deep Drilling Project in the Chesapeake Bay Impact Structure: Results from the Eyreville Core Holes: Geological Society of America Special Paper 458, doi: 10.1130/2009.2458(22).

Son, T.H., and Koeberl, C., 2005, Chemical variation within fragments of Australasian tektites: Meteoritics & Planetary Science, v. 40, p. 805–815.

Stöckelmann, D., and Reimold, W.U., 1989, The HMX mixing calculation program: Mathematical Geology, v. 21, p. 853–860, doi: 10.1007/BF00894452.

Stöffler, D., and Grieve, R.A.F., 2007, Impactites, Chapter 2.11, *in* Fettes, D., and Desmons, J., eds., Metamorphic Rocks: A Classification and Glossary of Terms, Recommendations of the International Union of Geological Sciences: Cambridge, UK, Cambridge University Press, p. 82–92, 111–125, and 126–242.

Taylor, S.R., and McLennan, S.M., 1985, The Continental Crust: Its Composition and Evolution: An Examination of the Geochemical Record Preserved in Sedimentary Rocks: Oxford, Blackwell, 312 p.

Thein, J., 1987, A tektite layer in Upper Eocene sediments of the New Jersey continental slope (Site 612, Leg 95), *in* Poag, C.W., Watts, A.B., et al., eds., Initial Reports of the Deep Sea Drilling Project, Leg 95: Washington, D.C., U.S. Government Printing Office, p. 565–579.

Townsend, G.N., Gibson, R.L., Horton, J.W., Jr., Reimold, W.U., Schmitt, R.T., Hecht, L., and Czaja, P., 2007, Petrographic and chemical analysis of the lower crystalline basement-derived section, and the upper granite and amphibolite megablocks, Eyreville-B core, Chesapeake Bay impact structure: Geological Society of America Abstracts with Programs, v. 39, no. 6, p. 314.

Tuchscherer, M.G., Reimold, W.U., Koeberl, C., and Gibson, R.L., 2004, Major and trace element characteristics of impactites from the Yaxcopoil-1 borehole, Chicxulub structure, Mexico: Meteoritics & Planetary Science, v. 39, p. 955–978.

Van Bergen, P.F., and Poole, I., 2002, Stable carbon isotopes of wood: A clue to palaeoclimate?: Palaeogeography, Palaeoclimatology, Palaeoecology, v. 182, p. 31–45, doi: 10.1016/S0031-0182(01)00451-5.

Verkouteren, M.R., and Klinedinst, D.B., 2004, Value Assignment and Uncertainty Estimation of Selected Light Stable Isotope Reference Materials: RMs 8543–8545, RMs 8562–8564, and RM 8566: Gaithersburg, Maryland, National Institute of Standards and Technology (NIST) Special Publication 260-149, 59 p.

Whitehead, J., Papanastassiou, D.A., Spray, J.G., Grieve, R.A.F., and Wasserburg, G.J., 2000, Late Eocene impact ejecta: Geochemical and isotopic connections with the Popigai impact structure: Earth and Planetary Science Letters, v. 181, p. 473–487, doi: 10.1016/S0012-821X(00)00225-9.

Wittmann, A., Reimold, W.U., Hansen, B., and Kenkmann, T., 2008, Petrography of the suevite-like depth interval (1397–1550 m) in drill core Eyreville-B, Chesapeake Bay impact structure, USA: Houston, Texas, Lunar and Planetary Science, v. 39, abstract no. 2435 (CD-ROM).

Wittmann, A., Reimold, W.U., Schmitt, R.T., Hecht, L., and Kenkmann, T., 2009, this volume, Chapter 16, The record of ground zero in the Chesapeake Bay impact crater—Suevites and related rocks, *in* Gohn, G.S., Koeberl, C., Miller, K.G., and Reimold, W.U., eds., The ICDP-USGS Deep Drilling Project in the Chesapeake Bay Impact Structure: Results from the Eyreville Core Holes: Geological Society of America Special Paper 458, doi: 10.1130/2009.2458(16).

Wittmann, A., Schmitt, R.T., Hecht, L., Kring, D.A., Reimold, W.U., and Povenmire, H., 2009, this volume, Chapter 17, Petrology of impact melt rocks from the Chesapeake Bay crater, USA, *in* Gohn, G.S., Koeberl, C., Miller, K.G., and Reimold, W.U., eds., The ICDP-USGS Deep Drilling Project in the Chesapeake Bay Impact Structure: Results from the Eyreville Core Holes: Geological Society of America Special Paper 458, doi: 10.1130/2009.2458(17).

Manuscript Accepted by the Society 3 March 2009

Printed in the USA

CHAPTER 8: MELT IN THE IMPACT BRECCIAS FROM THE EYREVILLE DRILL CORE, CHESAPEAKE BAY IMPACT STRUCTURE, USA

Katerina Bartosova[1*], Lutz Hecht[2], Christian Koeberl[1], Eugen Libowitzky[3], and Wolf Uwe Reimold[2].

[1]*Department of Lithospheric Research, University of Vienna, Althanstrasse 14, A-1090 Vienna, Austria.*
[2]*Museum für Naturkunde, Leibniz-Institute at Humboldt University Berlin, Invalidenstrasse 43, 10115 Berlin, Germany.*
[3]*Institute of Mineralogy and Crystallography, University of Vienna, Althanstrasse 14, A-1090 Vienna, Austria.*

*Corresponding author: *E-mail: katerina.bartosova@univie.ac.at*

submitted to *Meteoritics and Planetary Science,* accepted with major revision

ABSTRACT

The Chesapeake Bay impact structure, located at the east coast of the USA, has a diameter of 85 km and is 35.3 Myr old. The structure has been drilled to about 1.8 km depth in the central part, at Eyreville farm, in an ICDP-USGS drilling project. The drill core has recovered about 154 m of impact breccias (1397-1551 m depth), including about 104 m of suevite and 6 m of impact melt rock. In a detailed study of melt in the impactites, tens of melt particles were studied by optical microscope, electron microprobe and microRaman spectroscopy. The melt particles were grouped into six different melt types (m1-m6), which were characterized in detail by microscopic observations. Compositions of several melt particles of each type were analyzed. The particles of different melt types have also somewhat distinct compositions; however the compositions of the different groups are overlapping. Furthermore, the compositional variations within each melt type and also within some melt particles are quite large, which is result of features like heterogeneity of the main melt phase, schlieren, presence of more melt phases, variable amount of crystallites and undigested clast, and alteration. The different melt types vary also in their abundance and intervals of occurrence. The most common melt types occur over a wide depth range, whereas other types are found only in the impact melt rock intervals. Based on microscopic studies, chemical analyses, and Harmonic least-squares MiXing (HMX) calculations, possible precursors of the melt were estimated. The melt type m3 is a melt of nearly pure quartz, but except for this melt type, no mono-mineral melts were noted. The melt type m5 is a melt of shale or fine-grained sediment. The main precursor mineral component of the other melt types is quartz and the melt was formed probably from the pre-impact sediments (mainly the Potomac Formation, melt types m1, m4, and m6) or possibly schist/gneiss (m2). However, the composition of the melt particles is a result of

the precursors, the process of melting and solidification, but also the post-impact alteration. Element maps revealed compositional variations of different phases and schlieren in melt. The melt particles contain some mineral phases – e.g., undigested clasts of quartz, feldspar, and opaque minerals – pyrite, marcasite, rutile, and graphite. Tiny anatase crystals are abundant. In the melt-rich suevites, zeolites and ballen quartz and rare ballen cristobalite are present.

Keywords: Chesapeake Bay impact structure, suevite, impact melt rock, melt particles, electron microprobe

INTRODUCTION

Chesapeake Bay impact structure, Eyreville drill core

The Chesapeake Bay impact structure is located at the east coast of the United States (Poag et al., 1994; Koeberl et al., 1996; Fig. 8-1). The 85-km-diameter (Poag et al., 2004), 35.3-Myr-old (Horton and Izett, 2005) impact structure is one of the largest and best preserved ones on Earth. Today, the crater is buried beneath about 200 – 550 m of post-impact sediments (Poag et al., 2004, p. 51). Several drill cores have been obtained in the crater area (Fig. 8-1) and sampled the Exmore breccia, where shocked quartz grains and parts of impact melt were found, especially in the crystalline basement clasts (Poag et al., 2004, p. 217, 224). But only the two most recent and deepest cores, the Sustainable Technology Park (STP) test hole (2004) and the Eyreville drill core (2005-2006), reached the impact breccia, including suevites with melt particles and shock metamorphic features (Horton et al., 2008; Horton et al., 2009a). The Eyreville drill core comprises (from top to bottom) post-impact sediments, sediment clast breccias and sedimentary megablocks (the so-called Exmore breccia beds), a large granitic and a small amphibolitic megablock, gravelly sand, impact breccia (including suevite and impact melt rock), and granites/pegmatites and mica schists (Fig. 8-2; Gohn et al., 2006).

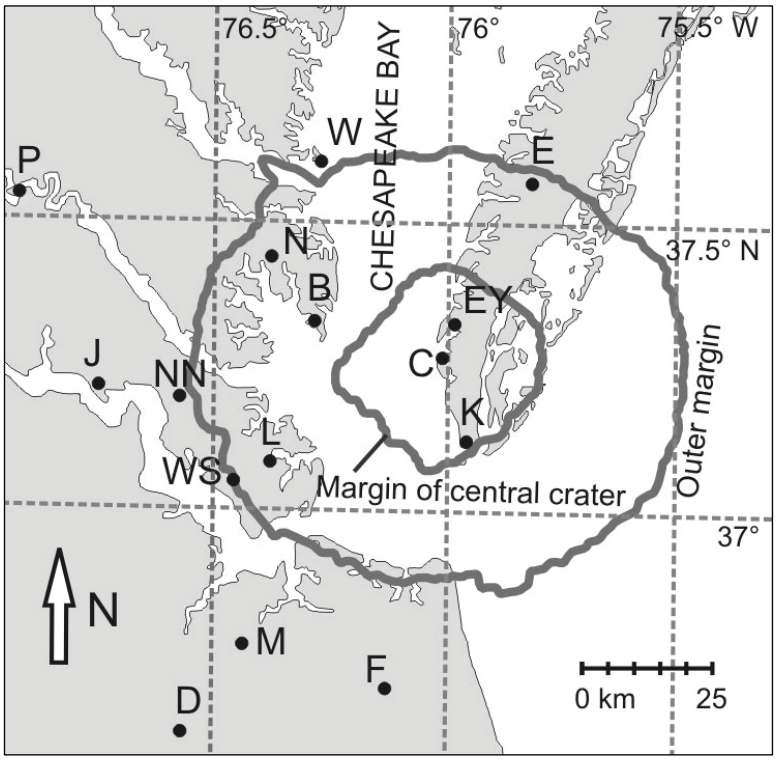

Fig. 8-1. Map of Chesapeake Bay (modified from Horton et al. 2005). Locations of the Chesapeake Bay impact structure and major core holes are shown. B-Bayside, C-Cape Charles USGS Sustainable Technology Park (STP), D-Dismal Swamp, E-Exmore, EY-Eyreville, F-Fentress, J-Jamestown, K-Kiptopeke, L-USGS-NASA Langley, M-MW4, N-North, NN-Newport News Park 2, P-Putneys Mill, W-Windmill Point, and WS-Watkins School.

Petrography of the impact breccia section

The impact breccia section (1397.2 – 1551.2 m depth) of the Eyreville drill core consists mostly of suevite and large blocks of gneiss (Horton et al., 2009a, 2009b; Bartosova et al., 2009a; Fig. 8-3). In the upper part (above ~1474 m) the suevite is melt-rich and contains two intervals (5.5 and 1 m thick) of impact melt rock (Wittmann et al., 2009a, 2009b). In the deeper part of the impact breccia section (below 1474 m) melt-poor suevite and polymict lithic impact breccia alternate with large blocks of cataclastic gneiss (Horton et al., 2009a; Bartosova et al., 2009a). The suevite has a grayish clastic matrix and contains a variety of rock and mineral clasts, melt particles, as well as secondary minerals. The lithic clasts in suevite comprise abundant clasts of pre-impact sediments of the Atlantic coastal plain (e.g., sandstones, siltstones, and mudstones), as well as clasts of the crystalline basement (e.g., granite, gneiss, and schist; Bartosova et al., 2009a), which is a distal part of the Appalachian orogen (Thomas et al., 1989). The melt-poor bottom part of the impact breccias with larger clasts and gneiss blocks and scarce melt particles, with no hint of air transport, is probably of ground-surge origin (Bartosova et al., 2009a). Near the top of the impact breccia section the proportion of fallback material increases. The uppermost section, with small clasts of all different types and abundant melt particles, some of which are shard-like, represents the fallback material.

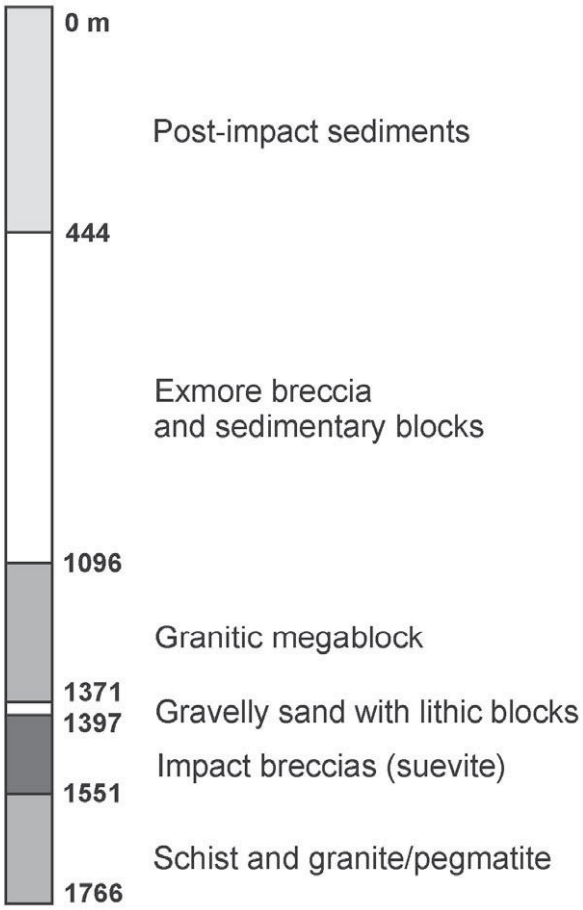

Fig. 8-2. Simplified stratigraphic column of the Eyreville drill core showing the main lithologies. Modified from Gohn et al. (2006) and Horton et al. (2009a). Depth below surface in meters.

Generally, the abundance of melt particles decreases and the clasts become larger with depth. Various shock metamorphic and related effects have been observed in the impact breccia (Bartosova et al., 2009a). Rare planar fractures and abundant planar deformation features occur in quartz. Quartz grains have commonly toasted appearance and ballen quartz was occasionally noted (Bartosova et al., 2009a). The presence of some secondary minerals (e.g., secondary pyrite, carbonate veins, and smectite), as well as the carbon isotopic composition of the carbonate veins, imply post-impact hydrothermal alteration of the impact breccia section (Bartosova et al., 2009a, 2009b). Horton et al. (2006) estimated the conditions of the hydrothermal alteration in the STP testhole to ~100 °C in the upper sedimentary-clast breccia and to ~220°C in the deeper crystalline-clast breccia.

Geochemical analyses of the Eyreville core samples and previous geochemical studies

All samples described in this paper were subjected to bulk chemical analyses (Bartosova et al., 2009a; Schmitt et al., 2009). Average compositions of the main lithological units of the Eyreville drill core are presented in Schmitt et al. (2009). Chemical composition of the impact breccias is primarily the result of the mixing of the different target rocks, i.e., rocks of the crystalline basement and overlying sedimentary rocks (Bartosova et al., 2009b). Mixing calculations suggest that the polymict parts of the impact breccia section consist mostly of metamorphic basement rocks (i.e., gneiss and schist) together with significant sedimentary and possible minor pegmatite/granite and amphibolite components (Bartosova et al., 2009b). No significant enrichment in siderophile elements was found in the suevites and impact melt rocks from the Eyreville drill core (Bartosova et al., 2009a).

Also the abundance of platinum group elements in the suevites is very low and the type of the Chesapeake Bay projectile has not yet been identified (McDonald et al., 2009; Goderis et al., 2009). The presence of a meteoritic component has so far been reported only in the impact melt rocks from the STP test hole (Lee et al., 2006).

A large suite of analyses of the Exmore breccia samples is presented in Poag et al. (2004). Deutsch and Koeberl (2006) analyzed several samples of the target lithologies and confirmed that the Chesapeake Bay impact structure is the source of the North American tektites

Melt in the Chesapeake Bay impact structure

In the Eyreville drill core, melt is most abundant in the upper part of the impact breccia section (above ~1474 m; Bartosova et al., 2009a; Wittmann et al., 2009a). Melt represents commonly more than 20 vol% of the impact breccias in the upper part and around ~1450 m and even >70 vol% of melt in the samples transitional between suevite and impact melt rock (Bartosova et al., 2009a). However, there are only two thin layers of impact melt rock (Wittmann et al., 2009b), which are probably just small melt pockets, rather than wide-spread melt sheets. So far, no large bodies of impact melt have been found in the Chesapeake Bay impact structure. Shah et al. (2005) estimated that the volume of impact melt distributed around the central peak is 0.4–7.5 km^3. Magnetic field measurements in combination with recent magnetic investigations of the Eyreville drill core suggest that some melt bodies might be present in the western part of the inner basin (Shah et al., 2009). Wittmann et al. (2009a) estimated the total volume of melt in the crater to be 6-10.5 km^3.

Five different melt types have been identified based on the microscopic studies of the impact breccia samples from the Eyreville drill core (Bartosova et al., 2009a). Preliminary compositional analyses by scanning electron microscope with an energy-dispersive X-ray analyzer were performed. However, these were only standardless analyses with results automatically recalculated to 100% (Bartosova et al., 2009b). Thus it was necessary to analyze the composition of the melt particles by electron microprobe. The melt particles and the impact melt rocks have been studied also by Wittmann et al. (2009b). Here we present microprobe analyses of melt in the impact melt rocks and melt particles in suevite, with a focus on the characteristics of the different melt types.

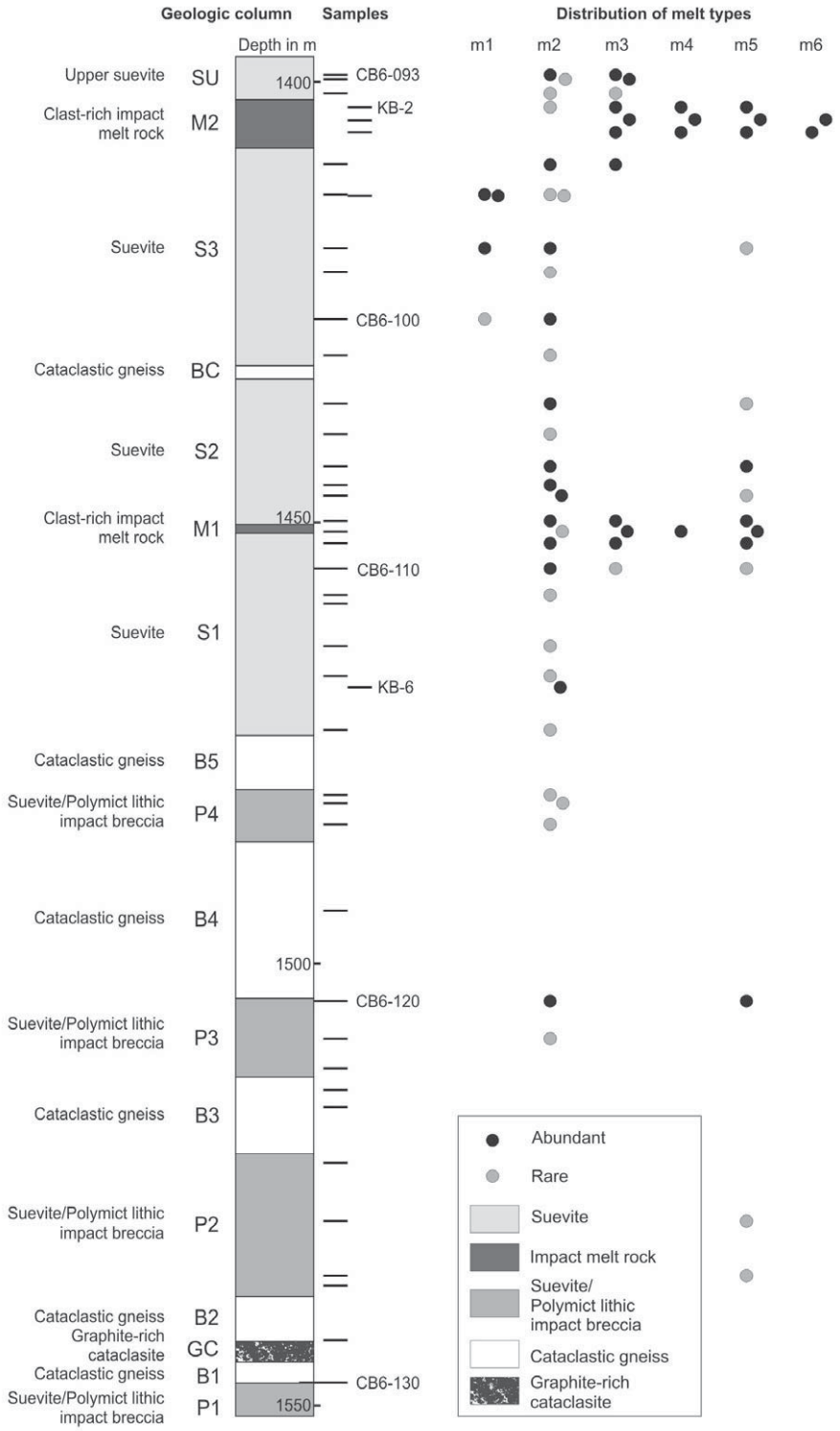

Fig. 8-3. Geologic column of the impact breccia section of the Eyreville-B drill core, modified from Horton et al. (2009a). Positions of the samples are indicated by lines on the right side of the column. The occurrence of the different melt types in the sample is indicated by the dots. Black dots – abundant occurrence of typical examples of the melt type. Gray dots – rare and /or not typical examples of the melt type.

SAMPLES AND ANALYTICAL METHODS

From the Eyreville drill core, 43 impact breccia samples from the interval 1397.2 – 1551.2 m depth were studied; their positions in the core are shown in Fig 8-3. The samples include 30 suevite and three impact melt rock samples, i.e., 33 samples containing impact melt; the remaining ten samples being polymict lithic impact breccia and cataclastic gneiss. All samples were subjected to detailed petrographic and geochemical studies (Bartosova et al., 2009a, 2009b).

Thin sections of all samples were studied by optical microscope. Melt particles were described in detail and the different melt types were identified. Polished thin sections of the impact melt rocks and melt-rich suevite were used for additional instrumental analyses. Thin sections with most abundant melt, i.e., with many melt particles of many different melt types, were selected.

Electron microprobe analyses were performed on a JEOL JXA 8500F at the Museum of Natural History, Berlin. The microprobe was calibrated using Smithsonian international mineral standards. Counting times were 40 s on the peak and 20 s on background. The analyses were performed in two different modes. Defocused beam with a diameter of 20 μm was used to obtain the average composition of each melt particle and for analyses of larger homogeneous phases. The acceleration voltage was 20 kV and probe current 20 nA. Focused beam with a diameter of 1-3 μm was used to identify small phases, clasts, and crystals, operating at 15 kV and 15 nA. Following elements were analyzed: S, Na, Fe, K, Ti, Al, Mg, Cr, Ca, Mn, and P. Further, several element maps and profiles were obtained in the most interesting parts of the melt particles, for better understanding of the relations of the different melt phases. In addition, photographs in back-scattered electron (BSE) mode were taken.

Raman microspectroscopy was used to identify mineral phases with high spatial resolution (l-2 μm lateral, 2-3 μm depth, using a 50x/0.75 objective). The measurements were performed on a Renishaw RM1000 confocal edge filter-based microRaman spectrometer with a 17 mW, 632.8 nm HeNe laser and a 20 mW 488 nm Ar ion laser excitation system with a thermoelectrically cooled charge-coupled device (CCD) array detector, at the Institute of Mineralogy and Crystallography, University of Vienna. A 1200 lines/mm grating monochromator provided a spectral resolution (apparatus function) of 3-4 cm-1 (red) and 5-6 cm-1 (blue). Spectra were calibrated with the Rayleigh line and the 520.5 cm-1 line of a Si standard. The spectra were compared with those from libraries from Renishaw and from the RRUFF data-base (Downs, 2006) using Grams/32 software.

Table 8-1. Studied melt-bearing samples of the impact breccia section of the Eyreville drill core, Chesapeake Bay impact structure.

Sample*	Midpoint depth† (m)	Rock type§	Melt types present#	Method**
CB6-093	1399.2	Melt-rich suevite	2, 3, 1/2?, 2/3	M, E, R
CB6-094	1399.7	Melt-rich suevite	2, 3	M
CB6-095	1401.3	Suevite	2, 3, 2/3	M
CB6-096	1409.3	Melt-rich suevite	2, 3, 2/3	M
CB6-097	1412.7	Melt-rich suevite	1, rare 2, 1/2, 2/3	M, E, R
CB6-098	1418.8	Melt-rich suevite	1, rare 2, rare 5, 1/2, 2/3	M, E, R
CB6-099	1421.6	Melt-rich suevite	2, 1/2, 2/3	M, E, R
CB6-100	1427.0	Suevite	2, rare 1	M
CB6-101	1431.1	Melt-poor suevite	2, 4pl††?	M
CB6-102	1436.6	Melt-poor suevite	2, rare 5	M
CB6-103	1440.0	Melt-poor suevite	2	M
CB6-104	1443.7	Melt-poor suevite	2, 5	M
CB6-105	1445.8	Melt-poor suevite	2	M, R
CB6-106	1446.9	Melt-poor suevite	2, 5	M
CB6-107	1449.8	Melt-rich suevite	2, 3, 5	M, E, R
CB6-108	1451.0	Suevite / Impact melt rock	rare 2, 3, 4, 5, 2/3, all partly melted	M, E, R
CB6-109	1452.3	Melt-rich suevite	2, 3, 5, 2/3	M, E, R
CB6-110	1455.2	Melt-rich suevite	2, 3, 5, 4pl?	M
CB6-111	1458.2	Melt-poor suevite	2	M
CB6-113	1464.0	Melt-rich suevite	2	M, R
CB6-114	1467.4	Melt-poor suevite	2	M
CB6-115	1473.5	Melt-rich suevite	2, parts with melt matrix?	M, R
CB6-116	1480.8	Melt-poor suevite	2	M
CB6-117	1481.7	Melt-poor suevite	2	M
CB6-118	1484.1	Melt-poor suevite	2	M
CB6-120	1504.2	Melt-rich suevite	2, 5	M, R
CB6-121	1508.5	Melt-rich suevite	2, 2/3	M, R
CB6-126	1529.3	Melt-poor suevite	5	M
CB6-127	1535.4	Melt-poor suevite	5	M
KB-2	1402.9	Impact melt rock	rare 2, 3, 4, 5, rare 2/3	M, E, R
KB-3	1404.4	Impact melt rock	3, 5, 6, 2/4, 3/4	M, E. R
KB-4	1405.7	Impact melt rock	3, 4, 5, 6, 3/4	M, E, R
KB-5	1412.9	Suevite	1, 2, 1/2	M

* CB6-X and KB-X are unique numbers of the samples. Samples CB6-X are marked as CK-X in the original drill core stored at the USGS in Reston, Washington.

† Depths are corrected values (L. Edwards, USGS, pers. comm., 2008)

§ Melt-rich suevite means >10 vol% of melt; Melt-poor suevite means <5 vol% of melt

Types x/y are mixed or transitional melts of the two types listed

** Methods used to investigate the sample: M - optical microscopy, R - microRaman spectroscopy, E - electron microprobe

†† 4pl - subtype of melt type m4 with only plagioclase crystallites

RESULTS

Melt types

With this work we continue our previous studies of melt particles from the impact breccia of the Eyreville drill core (Bartosova et al., 2009a, 2009b). All analyzed samples are listed in Table 8-1. Additional thin sections were prepared so that more melt particles could be studied; two to four thin sections of each sample were investigated. We grouped the melt particles into the melt types, which have been recognized based primarily on microscopic appearance (color, texture) in our previous studies (Bartosova et al., 2009a). Additionally, a new melt type was identified in the impact melt rock.

Table 8-2. Characteristic features of melt types identified in the impact breccia section of the Eyreville drill core, Chesapeake Bay impact structure.

Type	m1	m2	m3	m4	m5	m6
Color*	Light brown, rarely colorless or greenish	Beige to dark brown	Colorless, some brownish stains	Brownish to dark gray	Dark brown to black	Beige to brown
Shape	Amoeboid, "flame" shaped, many are shard-like	Oval to amoeboid	Amoeboid, some preserve shapes of original clasts	Amoeboid, irregular shapes, forms matrix in impact melt rock intervals or rare single particles	Oval to amoeboid	Oval to amoeboid
Texture, vesicles, inclusions, clasts	Schlieren are common, some particles have vesicles. Undigested clasts are rare.	Commonly fluidal texture, many cracks and undigested grains	Some parts recrystallized into cherty texture or to ballen quartz, globular textures near the rims	Laths of feldspars and/or pyroxenes, intersertal or microporphyritic texture. Dark brown globules occur.	Commonly contains undigested clasts, some fluidal textures	Typical globular or worm-like textures, some undigested clasts
Chemical composition	Totals ~80 wt%, relatively silica rich (~ 67 wt%)	Totals ~80 wt%, lower in Si and higher in Al compared to m1	High totals, more than 95 wt% of SiO_2	High totals, high Si content (~76 wt% of SiO_2)	Totals about 92 wt%, melt type lowest in Si and highest in Al and Fe	High totals, high Si content (~75 wt% of SiO_2); similar composition to m4
Interval of occurrence† (m)	1412.7–1427 (CB6-097:CB6-100)	1399.2–1508.5 (CB6-093:CB6-121)	1399.7–1455.2 (CB6-094:CB6-110)	1402.9–1451 (KB-2:CB6-108)	1418.8–1535.40 (CB6-098:CB6-127)	1404.4–1405.7 (KB-3:KB-4)
Notes	Only in the upper part, shard shapes suggest solidification before incorporation	Most abundant melt type, large depth interval of occurrence	Abundant in the melt-rich parts	Only in the impact melt rock intervals	Abundant in lower parts of impact breccia section	Only in the upper impact melt rock interval

* color in plane-polarized light under optical microscope

† in our samples

About 20 melt particles of each melt type, occurring in suevite (melt types m1, m2, m3, and m5) samples, were analyzed by electron microprobe. The melt types typical for the impact melt rocks (m4 and m6) are less abundant, occur in a limited depth-range (i.e., only in a small number of samples), thus only a smaller number of analyses could be measured. The characteristic appearance and features of the different melt particles are summarized in Table 8-2 and shown on optical microphotographs (Fig. 8-4) and on BSE images (Fig. 8-5).

Composition of the analyzed melt particles is presented in Table 8-3. The composition of each particle reported is an average of several microprobe analyses of the individual particle measured with defocused beam. Between 3 and 46 measurements were done on each melt particle, depending on its size and homogeneity. Table 8-4 summarizes average compositions of the different melt types. Some analyses of different melt and mineral phases, mostly obtained using focused electron beam, are presented in Table 8-5.

The distribution of the melt types with depth is shown in Table 8-1 and Fig. 8-3. It is apparent that the melt type m2 is most abundant and also the melt type m5 is present in many samples over a wide depth range. On the other hand, particles of type m3 are present only in the melt-rich parts of the impact breccia and the melt types m4 and m6 occur exclusively in the impact melt rocks. The particles of melt type m1 are present only in a certain depth interval, in the suevite unit S3 (as defined by Horton et al., 2009a; Fig. 8-3).

To better illustrate the chemical composition of the melt particles and its variation, several diagrams are used. Figure 8-6 shows the variation in content of the main oxides for the different melt types. Harker diagrams show the relations of selected oxides and SiO_2 and the compositional differences between the melt types (Fig. 8-7). To better describe the heterogeneous melt particles, we also use several ternary diagrams (Fig. 8-8, similar to e.g., Coney et al., 2009). Unlike in other diagrams, not the average compositions of the melt particles, but all single spots analyzed in the particles are plotted. There are also a ternary diagrams (Fig. 8-8a and 8-8b) showing positions of the target lithologies and common rock-forming and clay minerals for comparison.

Melt type m1

The melt of type m1 is clear, brownish, or rarely greenish melt phase. In optical microscope melt type m1 is relatively homogeneous, with some slight schlieren, without crystallites (Figs. 8-4a-c, 8-5a-d). It contains only rare undigested clasts and is isotropic in cross-polarized light. The particles have amoeboid or "flame" shapes, and some of them are shard-like. The melt type m1 occurs only in the upper part of the impact breccia section (typically in the samples CB6-097, 1412.8m; KB-5, 1412.9; and CB6-098, 1418.8 m). Rare particles of type m1, mostly transitional to type m2, occur also in the deeper parts of the impact breccia section (down to 1427 m). The particles of type m1 seem to be most pristine, but the SEM and microprobe analyses revealed, that this melt type has been highly altered. The melt appears only slightly altered in the optical microscope view, however, detailed photographs in back-scattered electron mode show alteration texture and porosity (Fig. 8-5b). Some of the particles have also very low totals, probably due to water content, alteration, and porosity. There are also some parts clearly formed by alteration minerals, typically in vesicles, but we tried to avoid these parts during the microprobe measurements. Based on differences in chemical composition, including

totals, two subtypes of the melt type m1 have been distinguished: m1a corresponding to the melt particles from sample CB6-098 and m1b corresponding to particles from sample CB6-097, with very low totals ~72 wt%, lower SiO_2, and higher Al_2O_3 contents compared to m1a (Table 8-3). All m1 type melt particles have relatively high silica contents, when the composition is recalculated to 100 wt%. The subtype m1b is closer to melt type m2 in chemical composition. However, melt particles of subtype m1b are slightly enriched in SiO_2 and depleted in FeO, MgO, and K_2O compared to melt particles of type m2 (in composition recalculated to 100 wt%). Although the composition of the melt type m1 is heterogeneous (see Fig. 8-7), in most cases there are no distinct phases. The phases of different composition appear mostly as faint schlieren. Only rarely there are undigested clasts and also rare secondary alteration phases appear. In many particles, there are abundant tiny (a few micrometers in size) anatase crystals (Figs. 8-4c, 8-5c). Irregular distribution of these crystals is probably the main reason of TiO_2 content variations.

Especially in larger particles, mixing of phases/schlieren with different composition was observed and documented on element maps (see the part "Relations between phases and alteration"). Spot analyses of some m1 particles are shown in Table 8-5. The ternary diagram Al_2O_3-MgO+FeO-SiO_2 (Fig. 8-8c) shows that there is a trend from the SiO_2 apex towards Al_2O_3 plus some FeO+MgO. There are a few spots (analyses of type m1b) plotting closer to the amphibolite composition. The K_2O-Na_2O-CaO plot shows one trend from the center of the triangle towards CaO and a second trend from relatively CaO-rich to K_2O-rich compositions. In the diagram Al_2O_3-K_2O-FeO+MgO there is a trend between the Al_2O_3 and FeO+MgO component. One melt particle (of type m1b) shows a different trend – variable proportions of K_2O and FeO+MgO with relatively constant Al_2O_3 content. In diagram CaO-Na_2O+K_2O-FeO+MgO most analyses form a homogeneous group, but again analyses of one particle scatter towards the Na_2O+K_2O apex. The microprobe data suggest that at least in some of the m1 particles, the alteration zones have relatively higher contents of Al_2O_3, FeO, MgO, and K_2O - oxides that are common in clay minerals. However, this is not a general rule, as there are many other features influencing the compositional variations. The compositions suggest that quartz, feldspars, muscovite, but also biotite or chlorite could be precursors of the melt. In some ternary diagrams the melt particles plot also close to illite or vermiculite, which could form by alteration of the melt. Also most of the target lithologies plot into similar areas in the ternary diagrams, except for the amphibolite and rocks from the Piney Point and Aquia Formations.

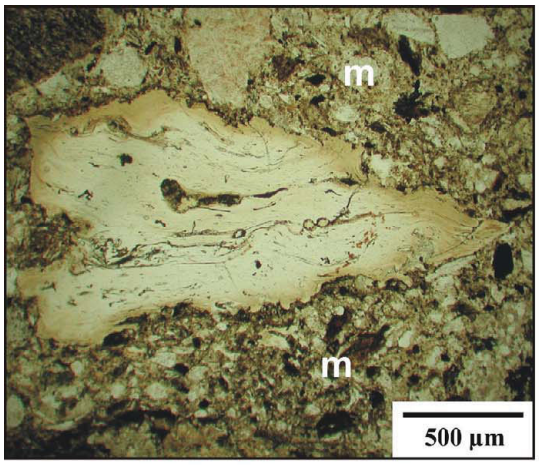

A m1, CB6-098, 1418.8 m

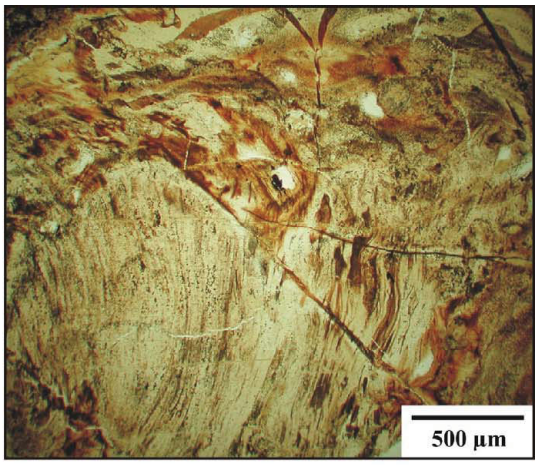

B m1, CB6-097, 1418.8 m

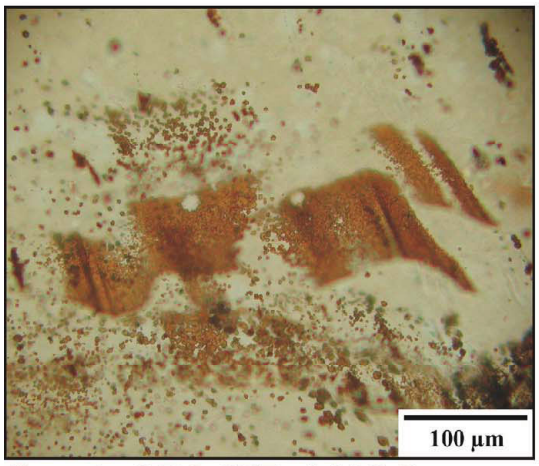

C m1, CB6-097, 1418.8 m

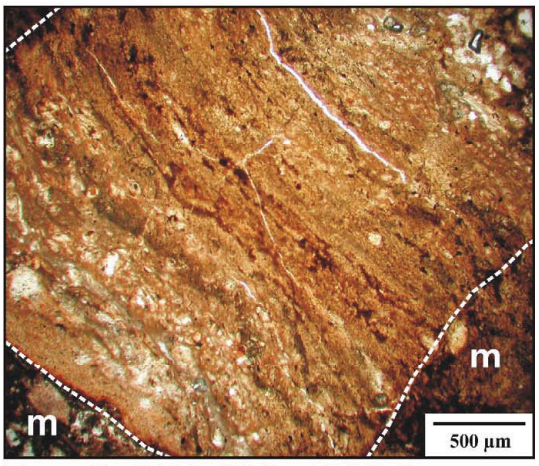

D m2, CB6-093, 1399.2 m

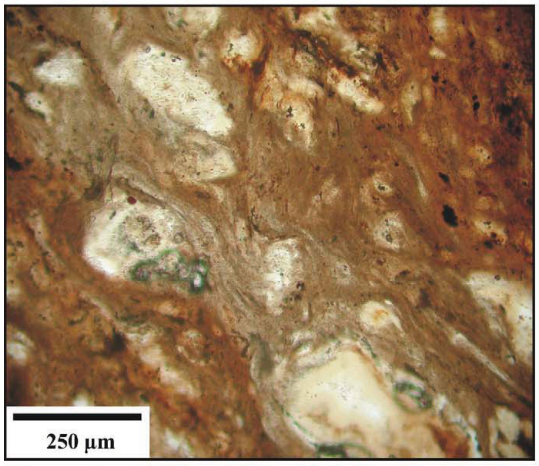

E m2, CB6-093, 1399.2 m

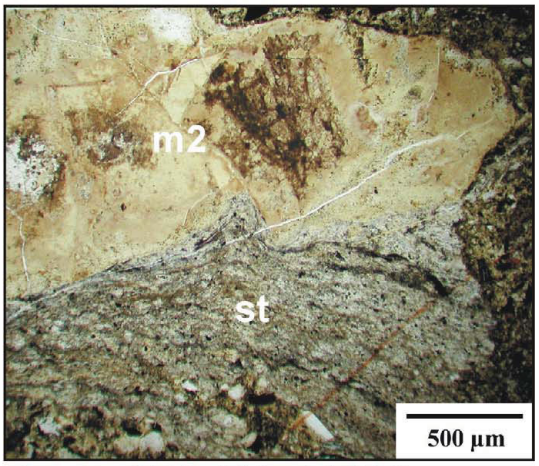

F m2, CB6-110, 1455.2 m

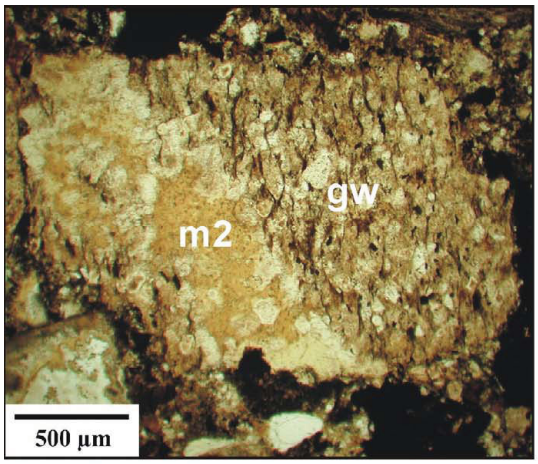

G m2, CB6-107, 1449.8 m

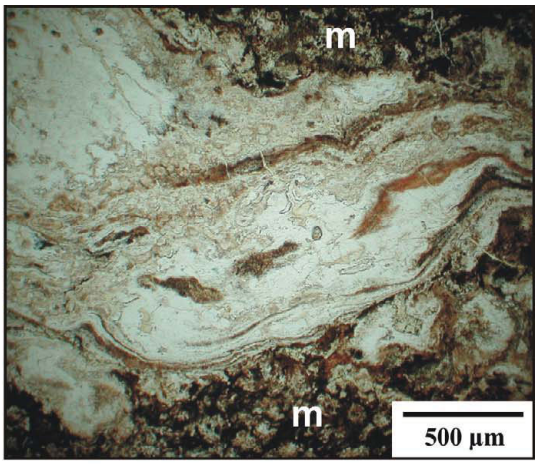

H m3, CB6-108, 1451.0 m

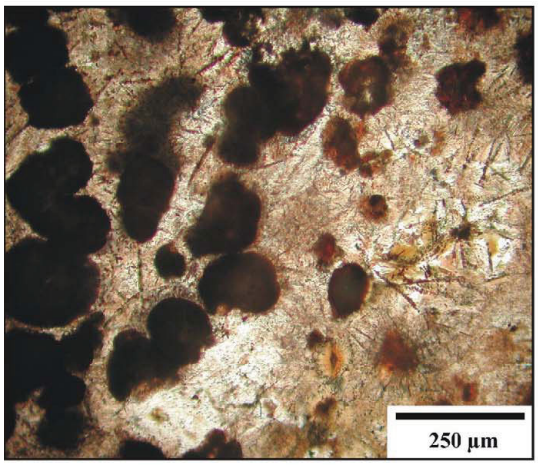

I m4, KB-4, 1405.7 m

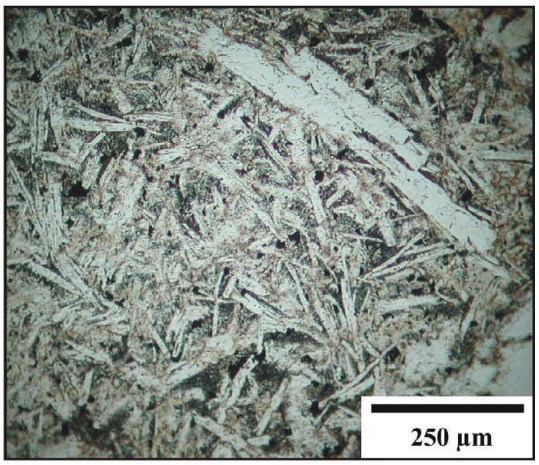

J m4pl, CB6-108, 1451.0 m

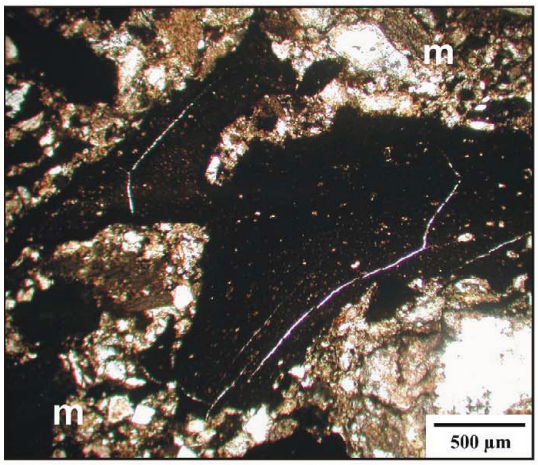

K m5, CB6-107, 1449.1 m

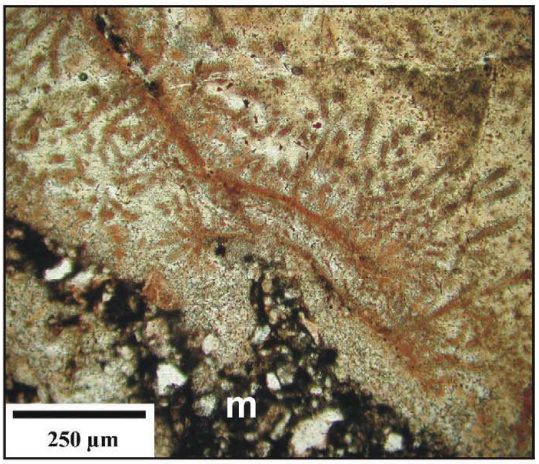

L m6, KB-3, 1404.4 m

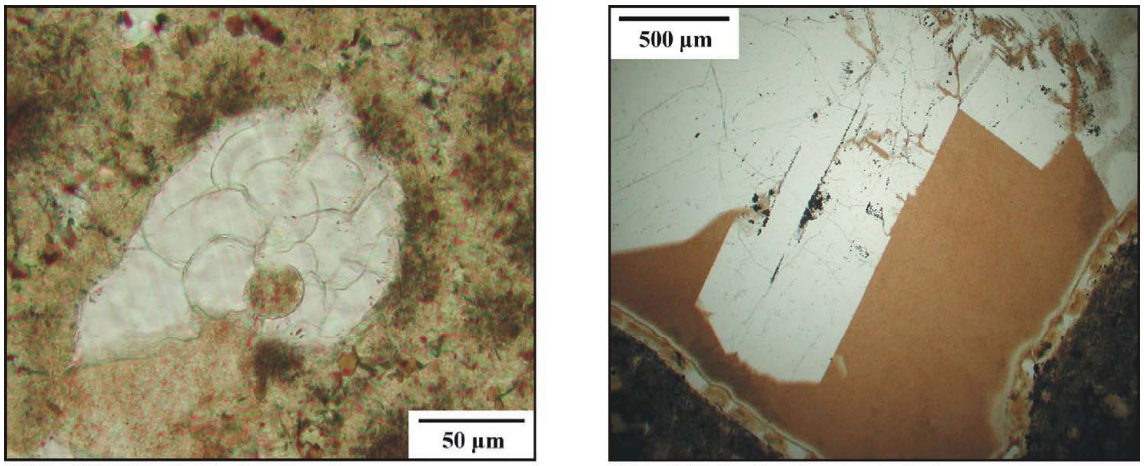

Figure 8-4: Optical microphotographs of the melt types and mineral phases, plane-polarized light. a) Melt type m1, relatively homogeneous melt; m – matrix. b) Melt type m1 with abundant schlieren. c) Detail of melt type m1 with abundant, tiny, brown disseminated anatase crystals. d) Melt type m2; m – matrix. e) detail of melt type m2 with undigested quartz clasts (the lighter spots). f) Melt type m2 in partly melted siltstone clast; st – siltstone. g) Melt type m2 in partly melted graywacke clast; gw – graywacke. h) Melt type m3 with some darker (brownish) stains (probably alteration minerals); m - matrix. i) Melt type m4 with dark brown globules and pyroxene crystallites (dark, tiny, elongated crystallites mainly in the right part). j) subtype m4pl with only plagioclase crystallites. k) Melt type m4, dark with amoeboid shape; m - matrix. l) Melt type m6 with typical structure; m - matrix. m) Small ballen cristobalite incorporated in melt type m6. n) Zeolites filling a vug; dark part (beige) – mordenite, clear part – paulingite, tiny opaque crystals in the clear part – pyrite.

Melt type m2

Melt type m2, a brownish melt, entirely altered to fine-grained phyllosilicate minerals, with undigested clasts, is the most common melt type (Figs. 8-4d-e, 8-5f-h). The particles have an amoeboid shape; commonly, soft material was lost during the thin section preparation. This melt type occurs in most samples (from the uppermost sample CB6-093, 1399.2 m to sample CB6-121, 1508.5 m). Melt type m2 is very variable in composition. Compared to melt type m1a, type m2 has generally lower SiO_2 and higher Al_2O_3 values (Fig. 8-6). Contents of Na_2O and K_2O are similar, but more variable than in type m1. Values of CaO, FeO, and MgO are higher than in m1. This is probably due to the high content of phyllosilicate minerals. Rarely, the type m2 melt particles contain secondary carbonate (an example from sample CB6-109 is shown in Fig. 8-5h). Some particles are transitional between the melt type m1 and m2 (Fig. 8-5e), i.e., with homogeneous parts similar to the melt phase of m1 and parts altered. In a few cases, melt type m2 was found in partly melted sedimentary clasts, i.e., part of the clast is melted and part of it is still preserved (Figs. 8-4g-h).

Melt type m2 is very heterogeneous and consists of many different phases. There are parts of brownish homogeneous melt, parts with high silica content, altered parts, undigested clasts, and pores, cracks, and vesicles. Composition of some phases is shown

in Table 8-5. The ternary diagram Al_2O_3-MgO+FeO-SiO_2 shows a similar trend like m1, but the points are more scattered compared to m1 particles (Fig. 8-8d). In the diagram K_2O-Na_2O-CaO most of the analyses scatter from the CaO apex, with trend towards K_2O, and in some cases Na_2O components. In the diagrams Al_2O_3-K_2O-FeO+MgO and CaO-Na_2O+K_2O-FeO+MgO most of the analyses form a homogeneous group, but some scatter again towards the K_2O- and Na_2O-rich composition. The diagrams suggest that the precursors could be the main rock-forming minerals – quartz, feldspars, and micas. In terms of clay minerals, in ternary diagrams this melt type plots closest to illite, montmorillonite, or vermiculite. The composition plots also close to the basement schist and gneiss and the particles rich in Na and K could possibly have some granitic component.

Melt type m3

Melt type m3, a recrystallized silica melt, is relatively common. The melt particles are colorless, with some brownish patches (Fig. 8-4h). Some altered parts occur mostly at the rims of the melt particles (Figs. 8-5i-j). This melt type is common in the melt-rich parts of the suevite, as well as in the impact melt rocks. The shapes are amoeboid, but in some cases the original clast shapes are only slightly deformed. This type is also the most homogeneous melt type, consisting of more than 93 wt% of SiO_2 and a low amount of other oxides. Totals are high, about 100 wt%. The melt particles have commonly a cherty texture and some parts show ballen silica.

Typical compositions of the silica melt and the associated altered parts are given in Table 8-5. Ternary diagrams are not shown for melt type m3, because contents of many major oxides are commonly very low, close to or below detection limit. Main component of this melt type is SiO_2; all melt particles of melt type m3 plot into the SiO_2 apex in the ternary diagram Al_2O_3-MgO+FeO-SiO_2. The melt precursor is quartz with possible small contributions of alkali feldspar or muscovite.

Melt type m4

Melt type m4 (Figs. 8-4i, 8-5k-n), which contains feldspar and/or pyroxene microlites, occurs typically as melt matrix in the impact melt rock. This melt consists of small pyroxene crystallites, larger plagioclase crystallites, and a Si-rich matrix. In some places dark brown and Si- and Fe-rich globules occur within the melt (Figs. 8-4i, 8-5m-n). There is a subtype, i.e., particles of impact melt with larger intersertal plagioclase crystallites (and no pyroxene crystals; Fig. 8-4j), but this melt was not distinguished as a separate type. This melt type is very rare; only one particle was found and analyzed (Tables 8-3 and 5, type m4pl). The problem is that these melt particles may look similar to dolerite clasts. Thus, only one of these particles was clearly recognized as melt (due to its

amoeboid shape), while many of other similar particles are probably dolerite clasts (have rounded shapes and some are affected by shock metamorphism).

The melt of type m4 consists of several melt phases, some of them silica-rich, plus crystallites of pyroxenes and plagioclase, globules, and small opaque minerals (see Table 8-5). Melt type m4 is relatively enriched in Na and K compared to other melt types. The individual analyses in ternary diagram K_2O-Na_2O-CaO in the Figure 8-8e show variable proportions of CaO and K_2O with a relatively constant Na_2O proportion. In the diagram Al_2O_3-K_2O-FeO+MgO the analyses scatter near the Al_2O_3 apex and also in the diagram CaO-Na_2O+K_2O-FeO+MgO the composition ranges over a wide area. The ternary diagrams suggest a SiO_2-rich precursor with some feldspar component (probably basic plagioclase), but also some biotite or other mafic or opaque minerals. The relative composition plots close to e.g., the Potomac Formation or the basement schist and gneiss, some points also close to granite.

Melt type m5

Melt type m5, a dark brown melt, is also wide-spread through the impact breccia. M5 occurs in our samples from sample KB-2 (1402.9 m) to the lowermost suevite sample CB6-127 (1535.4 m). The melt particles have oval to amoeboid shapes (Fig. 8-4k). The melt type m5 does not show any distinct phases. It consists of very fine-grained phyllosilicate minerals, but also some small undigested clasts are present (Figs. 8-5o-p). A brown-colored secondary phase, rich in Fe and Mg, probably phyllosilicate or altered glass resembling palagonite, appears in the vesicles of these particles (see analyses in Table 8-5). Melt type m5 is rich in FeO, MgO, and poor in SiO_2.

In the ternary diagrams Al_2O_3-MgO+FeO-SiO_2 the melt type m5 is most scattered from the SiO_2 apex compared to all other melt types (Fig. 8-8f). In the diagram K_2O-Na_2O-CaO nearly all the analyses show variable proportions of CaO and K_2O, with low Na_2O. Data in Table 8-3 show that CaO content is around 1 wt% in most m5 particles, but the K_2O content is quite variable. As is illustrated in the K_2O-Na_2O-CaO diagram, the proportion (and also absolute content, especially K_2O content, according to the microprobe data) of these oxides is variable between the different m5 particles, but is mostly relatively constant within one particle. Thus, these differences are probably due to primary different composition of the melt clasts. In the other ternary diagrams the analyses suggest high proportions of FeO and MgO, and only some particles show higher Na_2O and K_2O proportions. The precursors implied by ternary diagrams are quartz and feldspars with substantial mica (biotite) and possibly some amphibole components. The possible alteration minerals are illite, montmorillonite, or vermiculite. In terms of target lithologies, the composition of gneiss and schist, for example, plot in similar areas of the ternary diagrams.

Melt type m6

Melt type m6, a brownish altered melt with globular and worm-like texture (Figs. 8-4l, 5q-r), is a new melt type that was not described in Bartosova et al. (2009a, 2009b). Characteristic micro-textures in forms of globules, stars and structures with shapes similar to bark-beetle holes occur. This melt type occurs only in the thicker impact melt rock interval, in samples KB-3, 1404.4 m and KB-4, 1405.7 m. The variations of the composition are relatively small, but this is probably also because melt particles from only one sample were analyzed. This melt type is relatively rich in Na_2O and CaO. Chemical composition of melt type m6 is close to the melt type m4, but melt type m6 has slightly lower totals and lower contents of the alkali elements.

The melt of type m6 is also not homogeneous and contains many different phases, globules, and small crystallites (see spot analyses in Table 8-5). In the ternary diagrams (Fig. 8-8g) the analyses plot similar as the melt of type m4, but with less scatter. The diagram K_2O-Na_2O-CaO shows a very clear trend from CaO to K_2O, with relatively low Na_2O proportion, slightly increasing towards the CaO apex. This trend is probably mostly due to variable amounts of a K-rich phase, probably K-feldspar (see Table 8-5). The data in the diagram CaO-Na_2O+K_2O-FeO+MgO display two trends – variations between MgO+FeO and Na_2O+K_2O and between MgO+FeO and CaO. The ternary diagrams show that there is a variable composition commonly within a single melt particle. Possible minerals involved in the formation of the melt type m6 are, according to the ternary diagrams, quartz, plagioclase (probably basic), K-feldspar, and mica. Concerning the target lithologies, the ternary diagrams suggest a component of the different sedimentary rocks and, possibly, some granitic component.

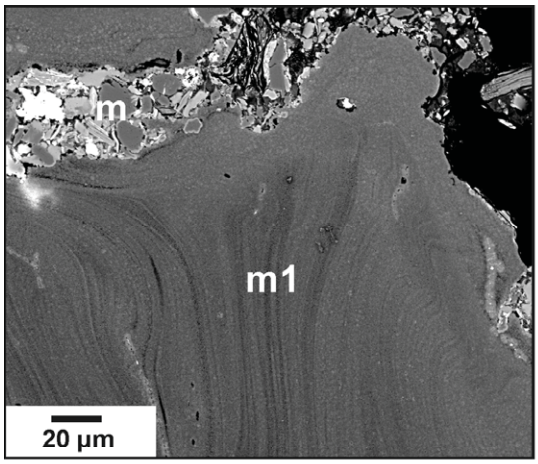

A m1, CB6-098, 1418.8 m

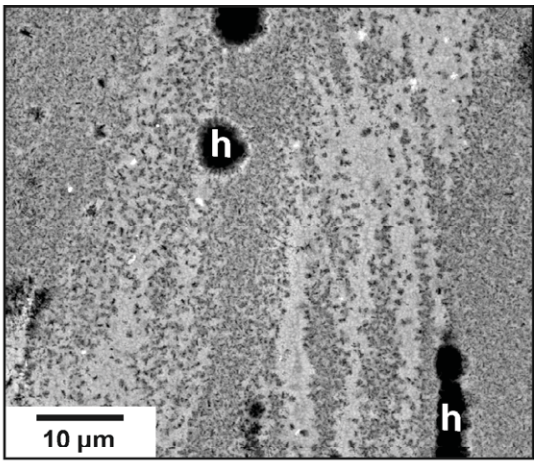

B m1, CB6-098, 1418.8 m

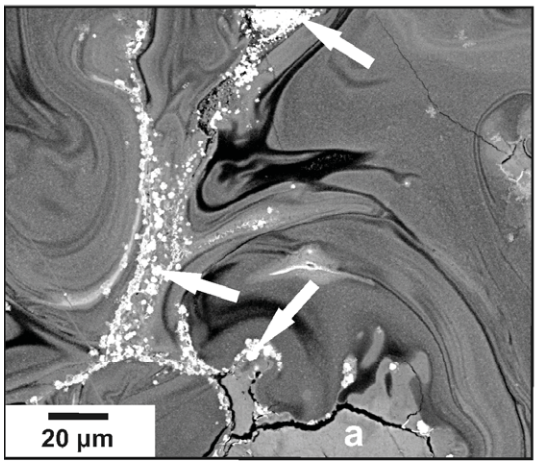

C m1, CB6-098, 1418.8 m

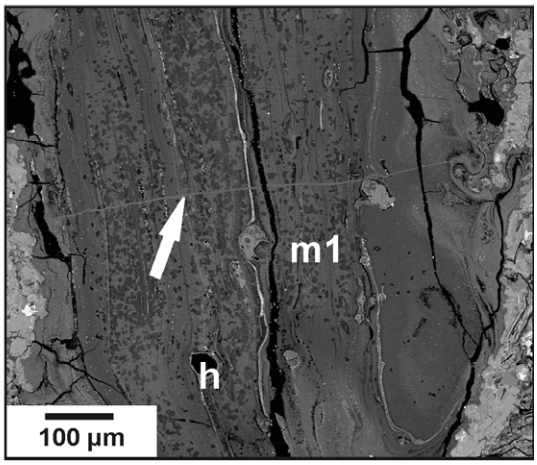

D m1, CB6-097, 1412.8 m

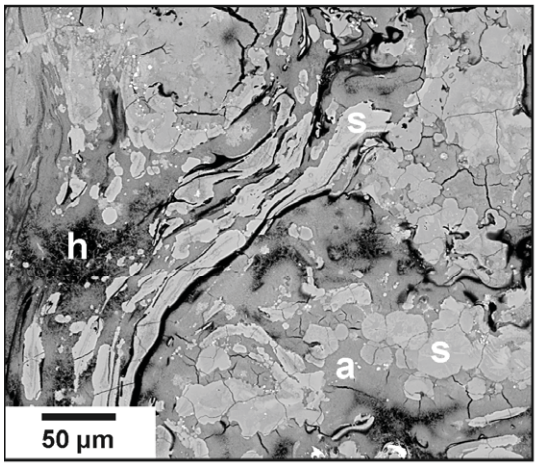

E m1/m2, CB6-098, 1418.8 m

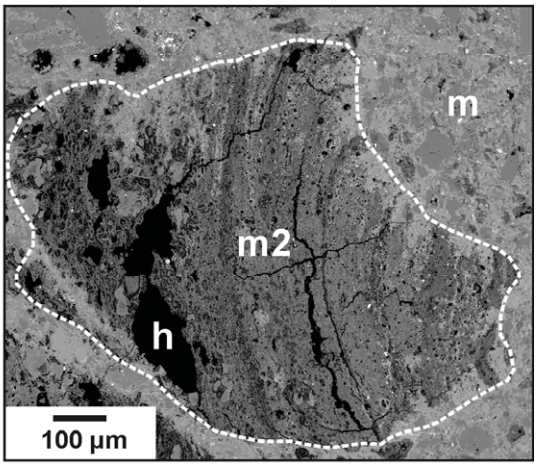

F m2, CB6-093, 1399.2 m

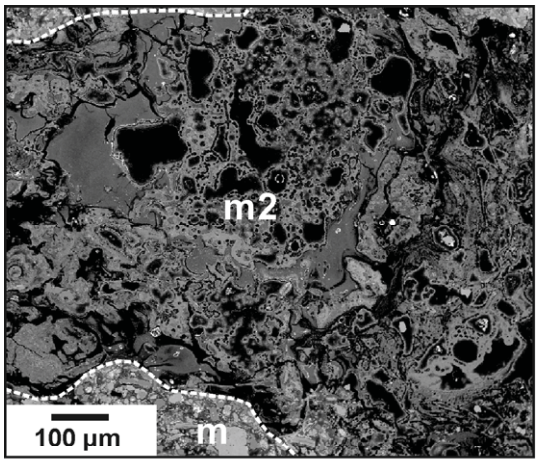

G m2, CB6-097, 1412.8 m

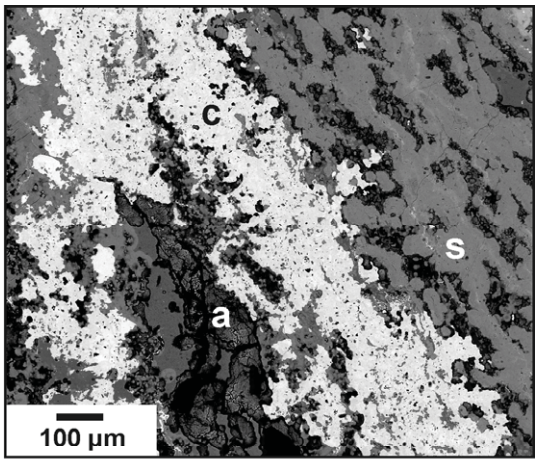

H m2, CB6-109, 1452.3 m

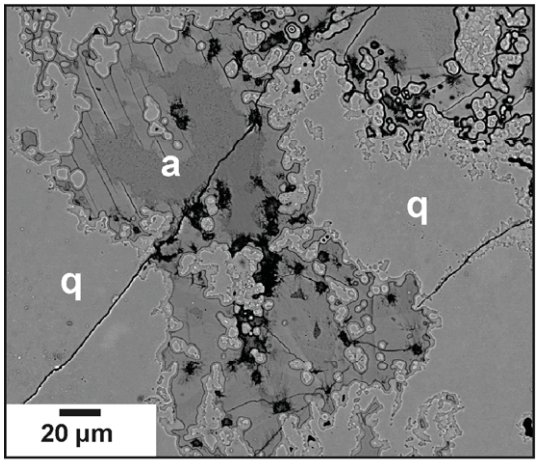

I m3, CB6-107, 1449.8 m

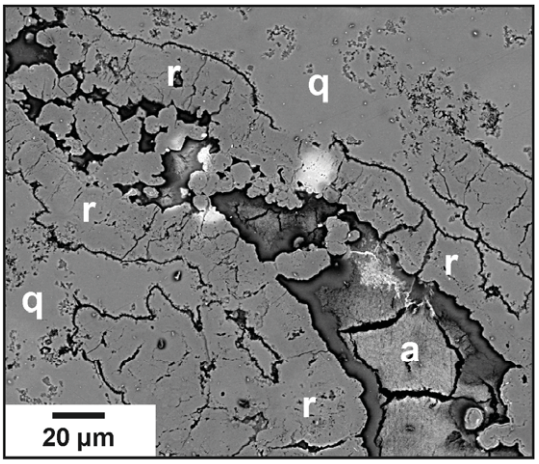

J m3, CB6-109, 1452.3 m

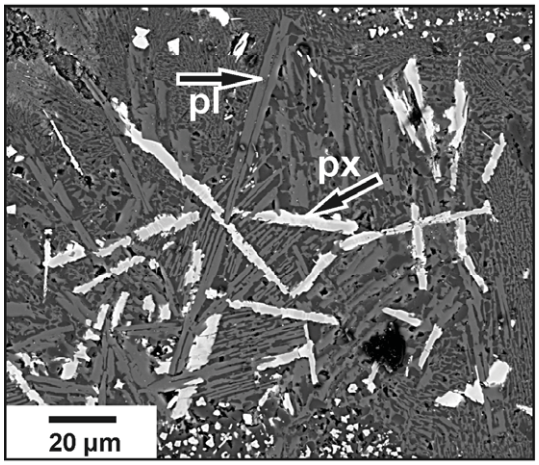

K m4, KB-2, 1402.9 m

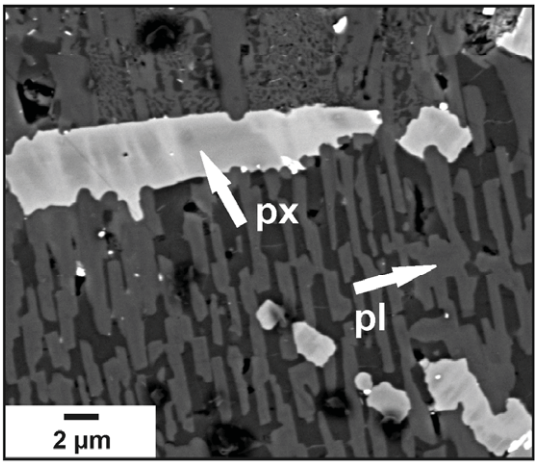

L m4, KB-2, 1402.9 m

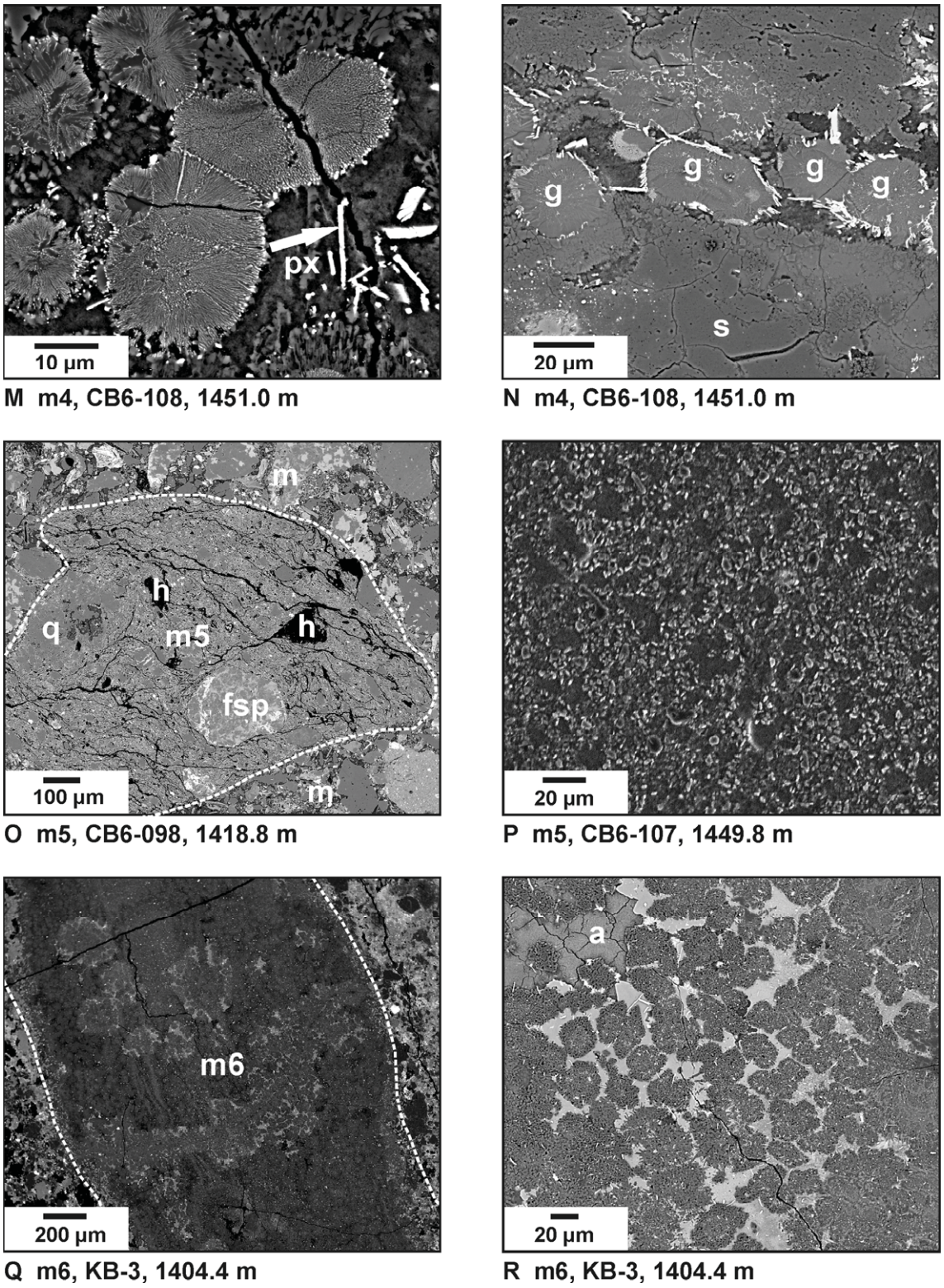

Fig. 8-5. Back-scattered electron images showing examples of melt particles of different types and their important features. a) Melt type m1, relatively homogeneous, with faint schlieren; m1 – melt particle, m – matrix. b) Melt type m1 in closer view, showing that also this melt type has undergone alteration; h – hole in the melt particle. c) Melt type m1, with faint schlieren; the arrows mark abundant tiny white grains of anatase; a – altered part. d) melt type m1. There are some altered parts (the darker spots) and tiny white anatase crystals, mostly arranged into bands. The arrow marks a later alteration veinlet. Note the complicated rims of the melt particle, including abundant cracks; h – hole in the particle. e)

Complicated structure of a melt particle intermediate between melt type m1 and m2; s – SiO_2-rich parts; a – altered parts; h – hole in the melt particle. f) Melt type m2; h – hole in the melt particle, m - matrix. g) Complicated structure of a melt particle of type m2 with different alteration phases and many pores and holes. h) Melt type m2 with secondary carbonate; s – SiO_2-rich phase, c – carbonate, a – alteration, m - matrix. i) Typical shapes of melt type m3, a part near the rim of the particle with some alteration; q – the silica melt, a – alteration. j) Melt type m3. In the center is a fracture filled with alteration minerals; there are quartz rims on both sides of the fracture, possibly formed during the hydrothermal alteration; q – silica melt, r – silica rim, a – alteration. k),l) – Melt type m4, typical texture of melt type 4 with crystallites; px – white pyroxene crystallites, pl – gray plagioclase crystallites; see also Fig. 8-10d. m) Globules formed in the melt of type m4; px – pyroxene crystallites. n) Globules formed in the melt of type m4; g – globules, s – SiO_2-rich phase. o) Melt type m5 with some undigested clasts; fsp – feldspar clast, q – quartz clast, h – hole in the melt particle, m – matrix. p) Close view of the structure of melt type m5. q) Melt type m6, picture shows typical texture of this melt. r) Melt type m6 with typical texture; a – alteration; see also Fig 8-10e.

Compositional differences and variations of the melt types

As is shown in the variation diagrams in Fig. 8-7, the data for each melt type shows some scatter, but still form distinct groups, with some overlap. The differences in composition of the different types can be well distinguished e.g., in the SiO_2 versus Al_2O_3 diagram with the original microprobe data (Fig. 8-7). When the melt particles are compared to the target lithologies in the Harker diagrams with values recalculated to 100 wt% (Fig. 8-7), the melt types m2, m5, and m1b are similar to the basement-derived gneiss or schist. Melt of type m1a is closest to the composition of the Potomac Formation rocks, whereas melts of types m4 and m6 are somewhere between Potomac Formation and schist and closest to the Exmore breccia, which is itself a mixture and not a specific target lithology. Silica-rich melt type m3 is not comparable with any target lithology.

Compositions of the melt particles of one melt type can be quite variable. The average contents of some major elements together with the variations for the different melt types are shown in Table 8-4 and Fig. 8-6. The totals and SiO_2 contents are very variable in melt types m1a and m2. Melt type m1 has relatively low contents of Na_2O and thus low absolute values of standard deviations of this oxide. Melt type m3 shows little compositional variation. The melt types m4 and m6 have relatively low standard deviations of some elements, but high variations of CaO and Na_2O. Melt type m5 shows a significant variation in the contents of Al_2O_3 and FeO.

Table 8-3. Electron microprobe analyses of melt particles from the Eyreville drill core, Chesapeake Bay impact structure. Values in wt%.

Sample*	No. of analyses		SiO_2	TiO_2	Al_2O_3	FeO	MnO	MgO	CaO	Na_2O	K_2O	Cr_2O_3	P_2O_5	Total
Melt type m1a														
CB6-098c	30	mean	74.46	1.08	7.69	2.79	0.03	0.86	0.52	0.33	1.40	<0.05	0.03	89.19
		σ	6.79	1.24	1.44	0.86	0.01	0.25	0.25	0.07	0.77	-	0.04	6.09
CB6-098c	13	mean	76.57	0.54	5.64	1.66	<0.03	0.50	0.58	0.27	0.64	<0.05	<0.03	86.44
		σ	2.95	0.07	0.31	0.49	-	0.17	0.06	0.01	0.17	-	-	2.33
CB6-098c	20	mean	68.78	0.63	6.83	3.39	0.03	1.09	0.44	0.29	1.30	<0.05	<0.03	82.80
		σ	4.31	0.06	0.66	0.90	0.01	0.30	0.04	0.03	0.27	-	-	3.57
CB6-098c	10	mean	80.67	0.35	4.26	0.66	<0.03	0.14	0.22	0.31	0.16	<0.05	<0.03	86.80
		σ	3.38	0.02	0.16	0.07	-	0.02	0.01	0.01	0.02	-	-	3.60
CB6-098c	18	mean	73.90	0.61	6.58	2.99	0.03	0.95	0.51	0.29	1.15	<0.05	<0.03	87.06
		σ	5.13	0.07	0.60	1.00	0.01	0.34	0.08	0.02	0.33	-	-	3.82
CB6-098a	25	mean	67.55	0.39	5.54	1.87	<0.03	0.49	0.61	0.29	0.19	<0.05	<0.03	76.95
		σ	5.31	0.26	2.14	1.29	-	0.41	0.52	0.07	0.05	-	-	4.08
CB6-098a	21	mean	76.88	1.31	7.61	2.93	0.03	0.87	0.46	0.25	1.73	<0.05	<0.03	92.10
		σ	4.40	1.89	1.98	1.24	0.02	0.44	0.21	0.04	1.06	-	-	3.69
CB6-098a	18	mean	78.82	0.38	4.56	1.01	<0.03	0.24	0.24	0.29	0.22	<0.05	<0.03	85.78
		σ	2.57	0.10	0.84	0.50	-	0.19	0.06	0.06	0.04	-	-	2.35
CB6-098a	10	mean	85.26	0.39	4.67	0.70	<0.03	0.14	0.27	0.25	0.21	<0.05	<0.03	91.93
		σ	2.26	0.03	0.34	0.11	-	0.04	0.09	0.04	0.02	-	-	2.67
CB6-098a	9	mean	86.09	0.44	5.41	0.87	<0.03	0.16	0.33	0.25	0.20	<0.05	0.03	93.79
		σ	1.33	0.02	0.26	0.13	-	0.02	0.05	0.02	0.02	-	0.01	1.66
Melt type m1b														
CB6-097a	46	mean	57.96	0.75	7.75	2.02	<0.03	0.66	0.71	0.50	0.93	<0.05	<0.03	71.32
		σ	6.00	0.95	2.65	1.04	-	0.40	0.45	0.45	0.87	-	-	4.43
CB6-097a	35	mean	54.32	0.69	9.77	3.25	0.03	1.10	1.02	0.42	0.42	<0.05	<0.03	71.04
		σ	5.73	0.88	2.68	0.94	0.01	0.34	0.39	0.16	0.29	-	-	3.37
CB6-097a	24	mean	49.87	0.99	12.20	4.41	0.05	1.67	0.80	0.36	0.49	<0.05	<0.03	70.84
		σ	6.98	0.76	2.48	1.39	0.03	0.57	0.20	0.09	0.18	-	-	3.84
CB6-097a	15	mean	50.80	0.91	13.22	5.24	0.06	1.86	0.97	0.30	0.60	<0.05	<0.03	73.97
		σ	2.75	0.70	1.42	1.36	0.06	0.51	0.34	0.08	0.09	-	-	2.32
CB6-097a	14	mean	52.68	1.00	11.36	3.54	0.03	1.37	0.77	0.31	0.48	<0.05	<0.03	71.54
		σ	7.52	1.55	3.77	1.19	0.02	0.46	0.33	0.08	0.22	-	-	3.86
Melt type m2														
CB6-099a	10	mean	48.01	0.04	13.05	6.67	0.05	2.76	1.05	0.34	0.81	<0.05	<0.03	72.79
		σ	2.66	0.01	1.30	0.70	0.02	0.53	0.41	0.27	0.11	-	-	3.07
CB6-099a	8	mean	49.91	0.88	11.77	7.22	0.06	2.71	0.88	0.29	0.81	<0.05	<0.03	74.54
		σ	3.32	0.94	1.13	0.98	0.02	0.31	0.11	0.04	0.21	-	-	2.58
CB6-099a	9	mean	51.48	0.07	12.16	6.31	0.05	2.72	0.97	0.29	0.89	<0.05	<0.03	74.95
		σ	3.19	0.05	1.30	0.81	0.02	0.43	0.19	0.12	0.68	-	-	3.79
CB6-099a	9	mean	61.34	0.33	10.45	5.18	0.03	2.04	1.07	0.22	0.53	<0.05	0.07	81.26
		σ	15.93	0.88	4.86	2.49	0.02	1.03	0.62	0.10	0.25	-	0.15	7.45
CB6-107a	7	mean	57.78	1.49	16.91	7.43	0.09	2.93	1.46	0.27	0.58	<0.05	<0.03	88.96
		σ	3.64	0.70	2.34	0.57	0.01	0.63	0.27	0.06	0.21	-	-	1.57
CB6-107a	4	mean	59.18	1.20	16.58	9.28	0.14	3.39	1.25	0.22	0.32	<0.05	<0.03	91.59
		σ	2.30	0.17	0.73	0.55	0.01	0.28	0.27	0.05	0.05	-	-	1.11
CB6-093a	11	mean	50.12	0.85	17.88	5.41	0.04	2.19	1.00	1.58	4.71	<0.05	0.05	83.84
		σ	11.75	0.73	3.08	1.88	0.01	0.97	0.36	1.19	2.50	-	0.03	9.46
CB6-093a	33	mean	45.16	0.95	16.78	5.45	0.05	2.05	1.22	2.18	4.09	<0.05	0.13	78.07
		σ	8.15	0.54	2.07	1.93	0.02	0.86	0.92	1.88	1.39	-	0.11	9.20
CB6-093a	8	mean	42.61	0.74	17.15	4.54	0.05	1.56	1.73	2.70	4.24	<0.05	0.16	75.51
		σ	3.19	0.31	1.53	1.71	0.02	0.61	0.56	0.89	1.80	-	0.07	5.05
CB6-109b	14	mean	62.87	0.06	14.53	5.18	0.06	1.97	1.84	0.40	0.26	<0.05	<0.03	87.18
		σ	6.39	0.04	5.29	1.25	0.02	0.48	0.78	0.06	0.07	-	-	1.91
CB6-109a	13	mean	66.55	0.95	10.79	4.38	0.04	1.16	1.14	0.28	0.41	<0.05	<0.03	85.72
		σ	5.60	0.89	2.74	1.63	0.02	0.47	0.15	0.10	0.12	-	-	3.10
CB6-109a	12	mean	66.75	0.76	9.88	3.68	0.04	1.01	1.20	0.27	0.35	<0.05	0.04	84.00
		σ	4.40	0.58	2.44	1.31	0.02	0.37	0.11	0.05	0.10	-	0.08	3.84
CB6-109a	8	mean	58.60	0.06	13.29	5.05	0.05	1.83	1.21	0.31	0.66	<0.05	<0.03	81.08
		σ	3.95	0.03	2.25	1.46	0.02	0.49	0.28	0.09	0.13	-	-	2.99
CB6-098c	20	mean	64.85	0.36	10.67	4.97	0.04	1.79	1.06	0.79	0.47	<0.05	<0.03	85.01
		σ	10.23	0.94	4.42	2.11	0.02	0.78	0.65	0.36	0.22	-	-	3.35
CB6-098a	8	mean	67.63	0.29	4.48	1.66	<0.03	0.41	0.25	0.17	0.20	<0.05	<0.03	75.13

		σ	9.09	0.12	1.77	0.70	-	0.17	0.08	0.04	0.07	-	-	11.01
CB6-097a	18	mean	61.33	0.67	7.84	2.82	0.04	1.11	0.63	0.42	0.92	<0.05	<0.03	75.80
		σ	9.67	1.13	4.37	1.63	0.02	0.69	0.34	0.34	1.40	-	-	8.80
CB6-097a	21	mean	56.69	0.32	12.08	5.55	0.08	2.24	1.02	0.30	0.67	<0.05	0.12	79.07
		σ	8.73	0.56	2.88	1.56	0.04	0.64	0.60	0.12	0.23	-	0.39	4.72
CB6-097a	16	mean	45.15	1.24	14.22	6.56	0.06	2.55	0.96	0.21	1.32	<0.05	0.03	72.29
		σ	8.42	0.74	3.53	2.44	0.02	0.87	0.53	0.15	0.54	-	0.05	5.86
Melt type m3														
CB6-152a	6	mean	93.54	<0.03	2.61	1.04	<0.03	0.16	0.26	0.22	0.52	<0.05	<0.03	98.38
		σ	4.15	-	1.73	0.69	-	0.12	0.19	0.12	0.56	-	-	1.14
CB6-152a	6	mean	94.51	0.04	1.60	0.88	<0.03	0.13	0.20	0.15	0.08	<0.05	<0.03	97.60
		σ	2.01	0.08	0.76	0.56	-	0.09	0.12	0.04	0.03	-	-	0.61
CB6-152a	7	mean	94.63	<0.03	1.41	0.67	<0.03	0.11	0.16	0.11	0.07	<0.05	<0.03	97.18
		σ	1.56	-	0.50	0.24	-	0.04	0.06	0.04	0.04	-	-	0.92
CB6-152a	6	mean	95.60	0.04	1.16	0.58	<0.03	0.07	0.09	0.10	0.05	<0.05	<0.03	97.70
		σ	1.48	0.03	0.58	0.29	-	0.04	0.05	0.06	0.02	-	-	0.51
CB6-152a	5	mean	97.94	<0.03	0.45	0.24	<0.03	0.03	0.05	0.06	0.02	<0.05	<0.03	98.83
		σ	1.43	-	0.29	0.15	-	0.03	0.03	0.04	0.01	-	-	0.93
CB6-152a	6	mean	96.70	<0.03	0.92	0.55	<0.03	0.06	0.08	0.13	0.05	<0.05	<0.03	98.49
		σ	0.88	-	0.13	0.09	-	0.02	0.01	0.02	0.02	-	-	0.74
CB6-093a	6	mean	96.98	<0.03	0.75	0.28	<0.03	0.08	0.11	0.14	0.06	<0.05	<0.03	98.45
		σ	1.25	-	0.32	0.19	-	0.07	0.07	0.05	0.02	-	-	0.80
CB6-108a	8	mean	93.81	0.16	2.68	0.48	<0.03	0.23	0.32	0.16	0.32	<0.05	0.19	98.37
		σ	2.51	0.27	1.15	0.24	-	0.13	0.38	0.06	0.33	-	0.30	1.02
CB6-108d	9	mean	93.78	0.15	2.56	0.47	<0.03	0.22	0.40	0.16	0.31	<0.05	0.24	98.30
		σ	2.32	0.26	1.12	0.23	-	0.12	0.42	0.06	0.31	-	0.30	0.97
CB6-108d	8	mean	95.22	0.13	2.23	0.53	<0.03	0.22	0.30	0.10	0.56	<0.05	0.15	97.98
		σ	2.55	0.14	1.10	0.22	-	0.07	0.11	0.06	0.47	-	0.09	0.82
CB6-108d	20	mean	95.92	0.04	0.75	0.06	<0.03	0.02	0.05	0.13	0.12	<0.05	<0.03	97.11
		σ	1.62	0.06	0.47	0.08	-	0.02	0.02	0.05	0.06	-	-	1.74
CB6-108d	15	mean	98.73	<0.03	0.36	<0.04	<0.03	<0.02	0.05	0.09	0.06	<0.05	<0.03	99.33
		σ	0.79	-	0.16	-	-	-	0.02	0.03	0.02	-	-	0.62
CB6-109b	5	mean	98.98	<0.03	0.33	0.04	<0.03	<0.02	0.06	0.12	0.03	<0.05	<0.03	99.59
		σ	1.11	-	0.10	0.03	-	-	0.03	0.03	<0.01	-	-	1.11
CB6-154a	4	mean	96.21	0.06	1.54	0.52	<0.03	0.15	0.33	0.16	0.19	<0.05	0.03	99.20
		σ	1.60	0.03	0.59	0.27	-	0.07	0.19	0.06	0.17	-	-	0.74
CB6-153a	15	mean	92.77	0.22	4.71	1.46	<0.03	0.26	0.24	0.14	0.19	<0.05	<0.03	100.03
		σ	3.53	0.22	2.22	0.77	-	0.11	0.10	0.03	0.06	-	-	0.85
CB6-153d	8	mean	94.50	<0.03	2.15	0.87	<0.03	0.20	0.15	0.17	0.49	<0.05	<0.03	98.56
		σ	2.50	-	1.17	0.95	-	0.32	0.06	0.08	0.81	-	-	1.06
CB6-153d	9	mean	93.24	<0.03	1.95	1.08	<0.03	0.14	0.25	0.19	0.09	<0.05	<0.03	96.98
		σ	1.03	-	0.51	0.29	-	0.05	0.13	0.06	0.09	-	-	0.57
Melt type m4														
CB6-108d - m4 pl	28	mean	52.41	1.74	21.98	2.42	0.12	0.79	8.23	2.61	2.39	<0.05	0.92	93.62
		σ	4.41	2.01	3.64	1.29	0.09	0.59	1.65	0.76	1.57	-	0.75	4.87
CB6-108d	35	mean	78.82	0.71	9.22	3.24	0.06	1.03	1.21	0.64	1.01	<0.05	0.23	96.19
		σ	10.22	0.41	5.00	2.30	0.05	0.74	1.10	0.43	1.60	-	0.47	4.77
CB6-154a	17	mean	75.29	0.83	12.22	4.17	0.05	0.88	2.42	1.24	3.16	<0.05	0.11	100.38
		σ	6.67	0.54	3.41	2.12	0.02	0.53	2.19	0.44	2.72	-	0.09	1.23
CB6-154a	20	mean	78.17	0.51	10.96	3.26	0.05	0.63	1.74	1.08	2.33	<0.05	0.10	98.83
		σ	7.65	0.29	4.10	1.30	0.03	0.27	1.51	0.59	2.14	-	0.09	1.03
CB6-154a	30	mean	71.37	0.77	14.91	4.70	0.08	1.19	1.97	1.39	2.45	<0.05	0.12	98.96
		σ	3.16	0.45	1.57	1.40	0.03	0.44	1.27	0.49	2.04	-	0.06	1.47
CB6-154a	34	mean	77.91	0.67	11.71	3.79	0.05	0.78	1.37	0.94	2.72	<0.05	0.09	100.06
		σ	6.20	0.34	3.24	2.31	0.03	0.61	1.55	0.52	2.63	-	0.10	1.90
CB6-152a	31	mean	73.71	0.67	13.75	3.41	0.05	0.60	1.55	1.85	3.17	<0.05	0.13	98.90
		σ	7.49	0.26	4.20	2.17	0.03	0.62	1.39	0.95	2.82	-	0.07	1.39
CB6-153a	39	mean	71.89	0.76	14.54	4.81	0.09	1.11	1.25	0.93	4.01	<0.05	0.11	99.51
		σ	4.66	0.24	2.35	1.64	0.03	0.48	1.01	0.40	2.20	-	0.04	2.28
Melt type m5														
CB6-152a	7	mean	64.07	0.49	17.27	7.81	0.06	2.07	1.13	0.40	0.26	<0.05	<0.03	93.56
		σ	4.94	0.19	2.65	1.79	0.02	0.32	0.39	0.12	0.09	-	-	3.73
CB6-107a	10	mean	52.90	0.76	25.14	4.73	0.04	2.44	1.01	0.18	3.09	<0.05	0.03	90.33
		σ	3.74	0.24	2.36	0.65	0.01	0.22	0.14	0.02	0.61	-	0.02	1.97
CB6-107a	4	mean	53.82	0.95	23.53	8.91	0.06	3.25	1.13	0.25	0.79	<0.05	<0.03	92.71

		σ	6.83	0.37	3.18	2.38	0.02	0.55	0.31	0.03	0.03	-	-	1.33
CB6-107a	4	mean	53.20	0.92	22.67	5.63	0.06	3.09	1.54	0.29	1.26	<0.05	0.04	88.72
		σ	3.59	0.18	2.02	1.36	0.04	0.61	0.24	0.07	0.26	-	0.02	1.09
CB6-107a	5	mean	53.79	0.87	22.55	5.61	0.06	2.56	1.32	0.24	1.50	<0.05	<0.03	88.52
		σ	5.51	0.20	2.27	2.06	0.04	0.85	0.24	0.07	0.30	-	-	1.84
CB6-107a	9	mean	55.78	0.83	19.59	10.83	0.14	3.22	1.02	0.25	0.87	<0.05	<0.03	92.60
		σ	7.14	0.54	3.90	2.91	0.10	0.67	0.26	0.04	0.35	-	-	3.30
CB6-107a	5	mean	50.58	0.67	25.22	5.75	0.06	3.41	1.46	0.33	1.15	<0.05	<0.03	88.66
		σ	1.61	0.15	2.00	0.34	0.01	0.18	0.17	0.03	0.07	-	-	1.01
CB6-107a	5	mean	52.79	1.32	18.00	6.44	0.10	2.81	1.56	0.35	1.01	<0.05	<0.03	84.41
		σ	4.20	0.81	3.50	2.01	0.05	0.72	0.38	0.06	0.34	-	-	2.74
CB6-107a	5	mean	50.62	0.93	26.62	5.57	0.05	3.22	1.16	0.22	1.75	<0.05	<0.03	90.17
		σ	0.69	0.26	1.87	0.56	0.02	0.22	0.19	0.05	0.21	-	-	0.92
CB6-107a	5	mean	46.39	0.83	29.63	5.78	0.07	2.99	0.96	0.26	2.57	<0.05	<0.03	89.50
		σ	1.35	0.11	1.51	0.72	0.02	0.15	0.09	0.02	0.28	-	-	0.71
CB6-107a	5	mean	50.82	1.02	26.08	5.03	0.06	2.75	1.27	0.26	1.77	<0.05	<0.03	89.08
		σ	3.15	0.27	3.17	0.74	0.02	0.24	0.06	0.05	0.28	-	-	0.76
CB6-107a	5	mean	46.84	1.14	30.48	5.83	0.05	3.11	1.13	0.20	2.64	<0.05	<0.03	91.44
		σ	1.20	0.41	1.03	0.29	0.02	0.20	0.12	0.02	0.33	-	-	0.39
CB6-107a	5	mean	51.59	0.70	23.58	5.26	0.06	2.89	1.35	0.22	2.24	<0.05	<0.03	87.90
		σ	1.88	0.31	2.74	1.02	0.02	0.50	0.33	0.02	0.51	-	-	1.08
CB6-108a	9	mean	61.48	0.99	17.35	8.22	0.16	2.95	1.13	0.20	0.40	<0.05	<0.03	92.91
		σ	8.03	0.39	4.06	2.14	0.04	0.84	0.30	0.02	0.09	-	-	2.24
CB6-109b	14	mean	64.76	0.49	17.17	6.46	0.14	1.95	1.52	0.32	0.58	<0.05	0.07	93.47
		σ	12.31	0.32	7.05	3.43	0.10	1.12	0.37	0.07	0.57	-	0.18	2.27
CB6-109b	14	mean	55.26	1.22	26.26	6.98	0.10	2.31	1.24	0.23	1.07	<0.05	<0.03	94.71
		σ	6.67	0.54	4.59	2.32	0.07	0.43	0.29	0.03	0.39	-	-	1.22
CB6-109a	8	mean	58.88	0.61	19.47	9.40	0.10	2.68	1.22	0.19	0.48	<0.05	0.06	93.11
		σ	9.57	0.33	5.69	3.18	0.05	0.76	0.38	0.03	0.16	-	0.13	1.31
CB6-109a	6	mean	55.52	1.12	15.37	8.81	0.13	3.29	1.54	0.20	1.60	<0.05	0.50	88.11
		σ	2.83	0.16	1.32	1.07	0.05	0.38	0.39	0.02	0.17	-	0.36	1.50
CB6-109b	15	mean	51.43	0.86	23.38	9.44	0.07	3.21	1.56	0.27	0.52	<0.05	0.04	90.80
		σ	3.03	0.25	2.06	1.17	0.02	0.38	0.61	0.03	0.06	-	0.02	1.01
CB9-098c	12	mean	49.07	0.70	22.31	6.84	0.15	2.53	0.72	0.85	5.52	<0.05	0.10	88.80
		σ	5.08	0.41	1.29	1.56	0.04	0.69	0.18	0.82	1.34	-	0.09	3.56
CB6-154a	6	mean	57.71	1.07	25.59	4.07	0.05	0.96	0.55	1.36	5.87	<0.05	<0.03	97.26
		σ	11.71	0.73	7.44	2.53	0.02	0.66	0.45	0.88	4.19	-	-	7.48
CB6-154a	7	mean	44.06	1.11	30.14	10.74	0.08	2.45	2.17	0.23	0.36	<0.05	<0.03	91.38
		σ	0.87	0.07	1.42	0.65	0.01	0.45	0.11	0.05	0.07	-	-	0.77
CB6-153d	17	mean	58.49	1.10	23.42	4.83	0.04	1.45	0.49	1.03	6.45	<0.05	0.13	97.44
		σ	7.30	0.73	4.78	2.31	0.02	0.66	0.32	0.28	2.70	-	0.22	2.15
Melt type m6														
CB6-153d	38	mean	73.74	0.75	11.84	5.32	0.07	0.70	1.34	0.48	0.45	<0.05	0.11	94.79
		σ	6.25	0.29	3.04	1.52	0.02	0.32	0.37	0.10	0.51	-	0.06	2.06
CB6-153d	8	mean	74.67	1.24	11.04	3.90	0.04	0.64	1.41	0.64	1.44	<0.05	0.07	95.12
		σ	2.26	1.09	0.90	1.26	0.02	0.27	0.76	0.22	1.31	-	0.06	1.21
CB6-153d	18	mean	73.10	0.90	12.55	3.85	0.04	0.55	1.65	0.74	2.65	<0.05	0.15	96.19
		σ	2.49	0.19	1.52	0.77	0.01	0.20	1.35	0.33	1.79	-	0.17	1.11
CB6-153d	17	mean	73.35	0.80	12.95	4.08	0.05	0.51	2.61	0.90	1.45	<0.05	0.09	96.82
		σ	2.42	0.17	1.96	0.80	0.01	0.24	1.81	0.42	1.76	-	0.09	1.42
CB6-153d	13	mean	75.03	0.84	12.29	3.69	0.05	0.51	2.51	0.87	1.02	<0.05	0.08	96.89
		σ	2.86	0.22	1.83	0.91	0.01	0.20	1.54	0.38	0.77	-	0.03	1.29
CB6-153a	45	mean	78.46	0.68	10.64	3.75	0.05	0.60	1.27	0.41	1.97	<0.05	0.08	97.92
		σ	5.40	0.28	2.58	1.27	0.02	0.39	0.93	0.20	2.42	-	0.05	2.03

Note: Mean composition and standard deviation are shown for each single melt particle analyzed.
* unique sample number, letters a, b, c, d mark the unique thin section

Table 8-4. Average composition of melt types from the Eyreville drill core, Chesapeake Bay impact structure. Composition of the averaged single melt particles was measured by electron microprobe (Table 8-3). Values in wt%.

Melt type	No. of particles analyzed		SiO_2	TiO_2	Al_2O_3	FeO	MnO	MgO	CaO	Na_2O	K_2O	Cr_2O_3	P_2O_5	Total
m1a	10	mean	76.90	0.61	5.88	1.89	<0.03	0.55	0.42	0.28	0.72	<0.05	<0.03	87.28
		σ	6.15	0.33	1.24	1.06	-	0.37	0.14	0.03	0.61	-	-	
m1b	5	mean	53.13	0.87	10.86	3.69	0.04	1.33	0.86	0.37	0.58	<0.05	<0.03	71.74
		σ	3.20	0.14	2.15	1.22	0.02	0.47	0.14	0.08	0.20	-	-	
m2	18	mean	56.44	0.63	12.81	5.41	0.05	2.02	1.11	0.62	1.23	<0.05	0.04	80.38
		σ	8.16	0.45	3.56	1.75	0.03	0.77	0.36	0.74	1.46	-	0.05	
m3	17	mean	95.76	0.05	1.58	0.57	<0.03	0.12	0.17	0.13	0.18	<0.05	<0.03	98.51
		σ	2.00	0.06	1.10	0.40	-	0.08	0.10	0.04	0.18	-	-	
m4	7	mean	75.31	0.70	12.47	3.91	0.06	0.89	1.65	1.15	2.69	<0.05	0.13	98.98
		σ	3.08	0.10	2.06	0.66	0.02	0.23	0.44	0.39	0.93	-	0.05	
m5	23	mean	53.91	0.90	23.08	6.91	0.08	2.68	1.22	0.36	1.90	<0.05	0.05	91.11
		σ	5.30	0.23	4.31	1.97	0.04	0.62	0.37	0.30	1.78	-	0.10	
m6	6	mean	74.72	0.87	11.89	4.10	0.05	0.59	1.80	0.67	1.49	<0.05	0.10	96.29
		σ	1.98	0.20	0.90	0.61	0.01	0.08	0.60	0.20	0.76	-	0.03	

Note: Mean composition, obtained by averaging mean composition for several single melt particles, and standard deviation are shown for each melt type.

Mineral phases in the melt particles

Mineral phases in the melt particles were identified by optical microscopy, microRaman spectroscopy, and electron microprobe. The most abundant mineral phase in the melt particles is quartz. Quartz appears commonly in a form of undigested clasts (typically in particles of type m2 and m5, rarely in other melt types). The undigested clasts are usually small (< 0.5 mm) and rounded. The melt type m3 is almost completely recrystallized to quartz, maybe some chalcedony is present. Undigested feldspar clasts were noted in melt types m2 and m5, but are much less common. There are abundant opaque grains, especially in the melt type m2. The opaque phases include common pyrite, marcasite, rutile, and also ilmenite and graphite occur. In the melt types m1 and m2, there are very abundant, tiny anatase grains (Figs. 8-4c, 8-5c, 8-9a). Anatase can be irregularly disseminated in the melt, but commonly is concentrated in small veinlets or along schlieren. Rarely the melt particles of type m2 contain secondary carbonate (Fig, 8-5h), which was found to be calcite with only traces of MgO, but with a substantial Mn content (MnO/CaO up to 0.13). In the melt particles with carbonate in sample CB6-109 (depth 1452.3 m), also tiny greenish apatite crystals occur.

The melt-rich parts of the suevite occasionally contain ballen silica, commonly crystallized from the silica melt type m3. The ballen silica in the Chesapeake Bay impactites were characterized according to categories defined by Ferrière et al. (2009). Ballen quartz with heterogeneous extinction (type III), and ballen quartz with intraballen polycrystallinity (type IV) are most common. Also rare occurrence of ballen quartz with homogeneous extinction (type II) and ballen cristobalite (type I) was noted (Figs. 8-4m, 8-9b). Ballen cristobalite occurs as rare small clasts within the melt type m6 (in sample KB-3, 1404.4 m).

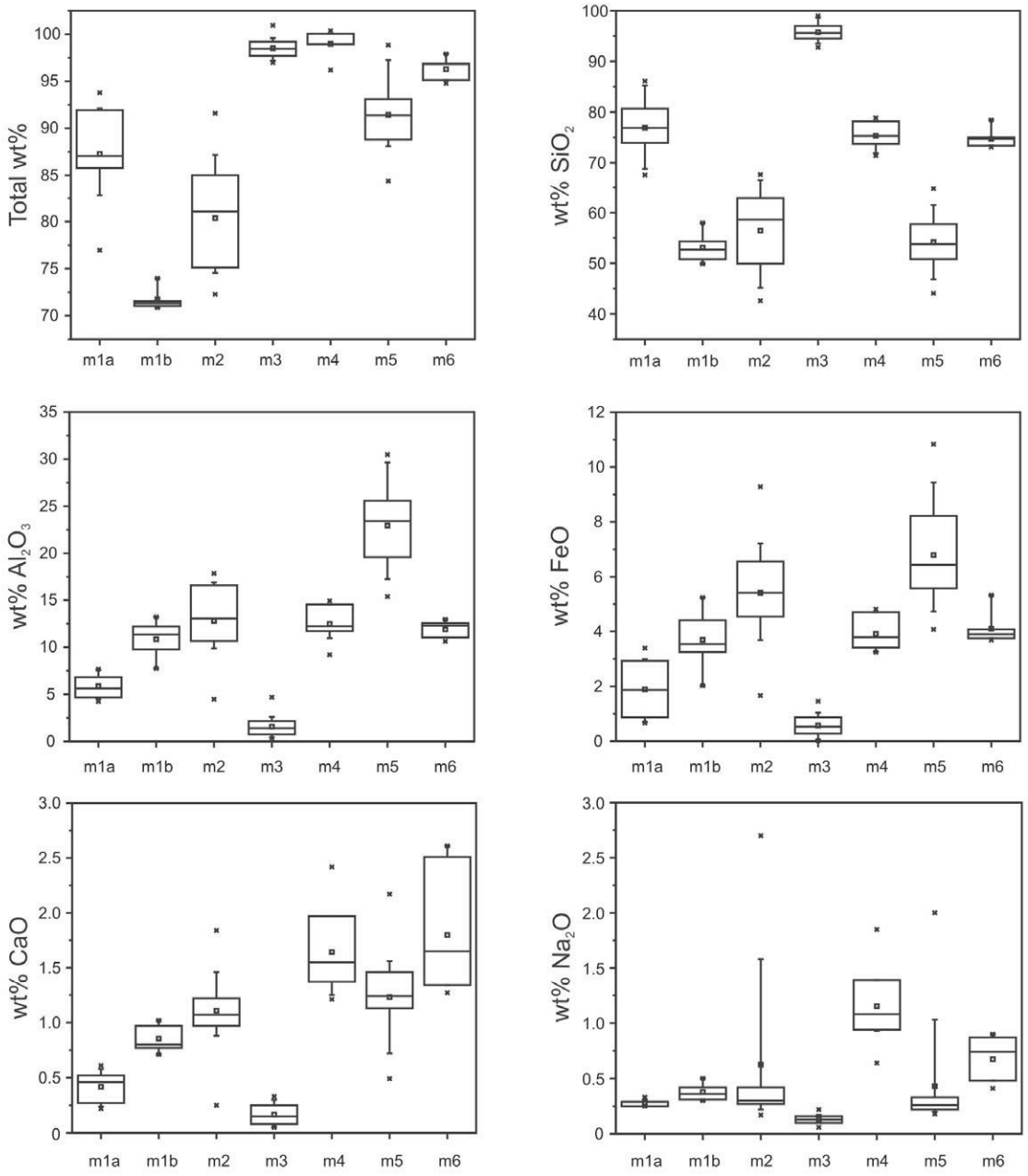

Fig. 8-6. Box diagrams showing average compositions and variations of the most important oxides in the different melt types. Average values and variations in composition are shown. The horizontal lines in the box denote the 25th, 50th, and 75th percentile values. The error bars denote the 5th and 95th percentile values. The symbols below the 5th percentile and above the 95th percentile error bar denote the 1st and 99th percentile value, respectively. The square symbol in the box denotes the mean of the data. Original electron microprobe data, not normalized to 100%, were used for plotting.

Table 8-5. Single spot electron microprobe analyses of some phases in the melt particles. Most of the spots were analyzed with focused beam (1-3 μm in diameter), unless defocused (20 μm in diameter) analyses is noted.

SiO_2	TiO_2	Al_2O_3	FeO	MgO	MnO	CaO	Na_2O	K_2O	Cr_2O_3	P_2O_5	Total	note
CB6-097a m1												
54.11	0.06	19.74	0.63	0.13	<0.01	5.20	3.50	4.83	0.03	0.03	88.27	alteration phase, schlieren
54.02	0.10	20.21	0.58	0.06	<0.01	5.55	3.39	4.89	0.04	0.03	88.89	
54.90	0.07	20.59	0.36	0.03	<0.01	5.80	3.52	4.70	<0.01	0.03	89.99	
58.60	0.36	8.78	3.23	0.90	0.02	0.74	0.56	0.25	<0.01	0.02	73.44	melt, gray phase
57.72	0.58	7.89	3.13	0.87	0.01	0.60	0.58	0.21	0.03	<0.01	71.61	
45.55	5.11	5.85	1.07	0.20	<0.01	0.31	0.23	3.22	<0.01	0.01	61.53	darker spot
42.24	0.25	8.30	0.62	0.11	<0.01	0.13	0.19	5.71	0.01	0.08	57.65	
51.53	<0.01	17.60	6.94	2.18	0.03	1.51	0.54	0.47	0.01	<0.01	80.81	rim of a vug, alteration minerals
54.11	0.05	18.19	7.93	2.26	0.05	1.59	0.50	0.50	<0.01	<0.01	85.19	
49.45	0.04	15.98	7.77	1.65	0.06	1.49	0.41	0.57	<0.01	<0.01	77.42	
CB6-098c m1/m2												
54.54	0.16	15.59	8.72	2.42	0.07	1.22	1.21	0.44	0.03	<0.01	84.40	alteration rim of a hole
55.44	0.07	16.02	7.84	2.43	0.06	1.04	0.95	0.45	<0.01	<0.01	84.31	
54.37	0.06	15.61	7.74	2.32	0.05	1.32	1.36	0.48	0.02	0.02	83.35	
90.42	0.44	5.24	1.79	0.31	0.04	0.08	0.29	0.25	<0.01	<0.01	98.86	light part
94.68	0.11	1.71	0.54	0.06	<0.01	0.07	0.32	0.14	<0.01	<0.01	97.62	
90.27	0.24	4.55	2.21	0.36	0.05	0.06	0.24	0.36	0.04	<0.01	98.38	
85.29	0.27	4.44	1.08	0.18	0.03	0.22	0.31	0.14	0.05	0.02	92.02	lighter phase
86.41	0.23	3.20	1.00	0.22	<0.01	0.22	0.31	0.13	<0.01	<0.01	91.72	
82.36	0.68	11.59	3.77	0.59	0.06	0.17	0.28	0.39	0.03	0.06	99.98	
83.40	0.78	10.12	3.63	0.56	0.05	0.21	0.31	0.41	0.01	0.06	99.54	
53.92	0.12	14.58	7.65	2.14	0.04	0.87	1.21	0.33	0.04	<0.01	80.88	darker phase
51.89	0.11	14.55	7.64	2.12	0.06	0.76	1.21	0.32	<0.01	<0.01	78.65	
56.15	0.10	15.74	9.02	2.56	0.10	0.67	0.86	0.62	0.02	<0.01	85.84	
56.20	0.06	16.16	8.72	2.45	0.02	0.64	0.88	0.60	<0.01	<0.01	85.72	
81.75	0.78	11.37	3.82	0.72	0.06	0.27	0.30	0.33	0.01	0.12	99.51	lighter globules
85.64	0.60	7.47	3.06	0.81	0.02	0.20	0.28	0.69	<0.01	0.03	98.79	
CB6-109a particle of type m2, very heterogeneous and with secondary carbonate												
100.45	0.02	0.16	0.01	<0.01	0.01	0.02	0.08	0.04	<0.01	<0.01	100.79	gray phase, homogeneous
99.92	0.01	0.35	0.02	0.01	<0.01	0.04	0.15	0.05	0.01	<0.01	100.56	
0.09	<0.01	0.04	0.12	0.02	2.98	49.39	0.03	<0.01	<0.01	0.06	52.73	carbonate
0.88	0.04	0.35	0.20	0.06	3.71	48.26	<0.01	0.01	<0.01	0.05	53.55	
0.00	<0.01	0.09	0.32	0.05	5.92	46.95	0.03	<0.01	<0.01	0.07	53.42	
94.37	0.18	3.58	0.41	0.15	0.01	0.21	0.15	0.16	0.01	0.01	99.23	two gray phases
93.99	0.08	2.28	0.49	0.22	<0.01	0.56	0.31	0.22	<0.01	0.03	98.16	
55.27	0.13	16.27	7.67	2.77	0.08	1.10	0.25	0.47	<0.01	<0.01	83.99	alteration minerals
53.42	0.12	15.36	7.18	3.05	0.08	1.13	0.25	0.48	0.04	<0.01	81.11	
CB6-109b m3												
61.93	0.05	17.47	8.62	2.75	0.02	1.58	0.26	0.92	<0.01	0.02	93.61	alteration minerals
62.08	0.04	17.69	8.74	2.48	0.05	1.39	0.32	0.84	0.01	0.01	93.64	
62.00	0.03	17.67	8.58	2.53	0.06	1.34	0.38	1.03	<0.01	<0.01	93.62	
98.98	<0.01	0.09	0.03	<0.01	<0.01	0.02	0.05	0.02	0.01	<0.01	99.20	quartz phase
99.42	0.02	0.04	0.04	<0.01	0.01	0.02	0.07	0.01	0.01	<0.01	99.63	
99.16	<0.01	0.07	0.05	<0.01	0.02	0.02	0.05	0.02	<0.01	<0.01	99.38	
KB-2a m4												
73.07	1.11	12.23	3.77	0.43	0.05	0.85	1.30	2.72	<0.01	0.11	95.62	dark crystals
62.88	0.19	16.40	7.57	0.69	0.10	1.02	0.78	2.50	<0.01	0.05	92.17	
44.42	1.45	12.78	25.62	15.34	0.41	0.34	0.06	0.03	0.04	0.04	100.52	pyroxene crystallites
44.87	0.95	13.42	23.71	16.61	0.47	0.32	0.05	0.01	<0.01	0.03	100.44	
44.49	0.93	15.12	21.37	17.52	0.37	0.28	0.08	0.02	0.05	0.03	100.24	
44.26	1.11	13.93	25.63	14.92	0.50	0.29	0.10	0.09	<0.01	0.05	100.87	
47.90	0.91	11.25	29.34	11.72	0.51	0.31	0.22	0.47	0.02	0.04	102.69	
45.59	0.93	15.23	21.05	17.37	0.36	0.29	0.07	0.04	0.14	0.07	101.11	
43.70	1.17	13.09	28.18	12.86	0.64	0.27	0.07	0.17	<0.01	0.03	100.18	
54.28	0.06	28.29	0.35	0.03	0.06	11.74	4.37	0.32	<0.01	0.02	99.52	feldspar laths
66.97	0.20	20.46	0.32	0.03	0.03	8.14	3.15	0.22	0.02	0.02	99.57	
65.43	0.14	20.48	0.33	0.02	0.03	7.67	4.01	0.28	<0.01	0.02	98.41	
55.61	0.25	27.23	0.35	0.01	0.01	10.86	4.50	0.39	0.03	0.02	99.27	
90.59	0.22	4.20	0.35	0.04	<0.01	0.20	0.76	1.88	<0.01	0.03	98.27	dark matrix phase
92.06	0.11	1.89	2.76	1.18	0.05	0.20	0.09	0.09	0.04	<0.01	98.47	
97.63	0.06	1.18	1.68	0.51	0.05	0.06	0.14	0.17	<0.01	<0.01	101.47	
CB6-108d m4pl												
52.75	0.06	30.83	0.17	0.05	0.01	13.37	4.39	0.38	<0.01	<0.01	102.01	feldspar laths particle
52.02	0.10	30.99	0.34	0.08	0.04	13.80	4.06	0.42	0.01	<0.01	101.86	
53.07	0.11	30.34	0.37	0.07	0.02	12.95	4.56	0.46	0.02	<0.01	101.97	
52.85	0.14	30.08	0.54	0.14	0.01	13.18	4.49	0.38	0.05	<0.01	101.85	
53.17	0.10	28.83	0.48	0.09	<0.01	11.99	4.98	0.50	0.02	0.01	100.18	
52.60	0.08	29.49	0.42	0.05	0.03	12.51	4.46	0.51	0.01	<0.01	100.15	
53.31	0.08	29.02	0.45	0.10	0.03	12.05	4.90	0.58	<0.01	0.03	100.55	
52.30	0.11	29.86	0.42	0.06	0.06	12.81	4.71	0.50	0.05	0.05	100.93	
CB6-108d m4												

75.24	0.92	14.83	6.85	2.17	0.09	0.24	0.25	0.10	<0.01	0.06	100.75	globules
76.24	0.87	13.87	6.64	1.81	0.09	0.21	0.26	0.08	<0.01	0.07	100.14	
74.08	0.96	15.12	7.22	1.99	0.12	0.24	0.24	0.08	0.01	0.07	100.14	
76.27	0.84	14.06	7.06	1.81	0.08	0.21	0.20	0.07	0.06	0.03	100.68	
KB-2a m4 defocused analyses												
73.50	0.93	15.03	6.72	2.26	0.06	0.07	0.34	0.04	<0.01	<0.01	98.94	globules
75.07	0.83	15.02	7.04	2.15	0.07	0.11	0.34	0.04	<0.01	0.04	100.70	
73.49	0.91	14.90	7.55	2.13	0.09	0.12	0.26	0.06	<0.01	0.03	99.52	
KB-3d m5												
46.09	0.81	25.44	4.77	2.44	0.04	1.19	0.77	0.88	0.04	0.01	82.49	brownish melt or secondary minerals in vesicles
49.98	0.81	26.12	3.78	2.35	0.02	1.58	1.11	0.91	<0.01	0.03	86.67	
51.30	0.06	22.27	3.22	2.45	0.03	1.22	1.21	1.10	0.08	<0.01	82.95	
49.67	0.08	22.75	5.14	2.63	0.05	1.40	1.02	0.76	<0.01	0.02	83.51	
KB-2a m5												
47.47	0.25	18.23	5.97	3.76	0.07	3.68	0.36	0.76	<0.01	1.59	82.13	brownish melt or minerals
43.37	1.80	14.58	6.40	3.49	0.05	3.52	0.38	0.91	<0.01	0.74	75.25	
KB-3d m6												
96.85	0.05	1.05	0.12	<0.01	<0.01	0.03	0.25	0.36	0.01	0.02	98.75	darker phase
93.66	0.02	2.51	0.38	0.02	<0.01	0.08	0.35	1.26	<0.01	<0.01	98.29	
68.75	0.04	15.70	1.37	0.09	<0.01	0.30	1.51	11.59	0.02	<0.01	99.37	lighter phase
74.92	0.19	12.01	0.59	0.08	<0.01	0.26	1.15	8.86	0.02	<0.01	98.07	
KB-3d m6												
82.63	0.26	8.05	3.55	0.42	0.03	0.91	0.49	0.30	0.02	0.09	96.74	dark phase
81.90	0.34	8.83	3.89	0.46	0.08	1.02	0.39	0.23	<0.01	0.10	97.23	
81.21	0.40	9.92	3.41	0.49	0.05	1.00	0.39	0.55	0.07	0.15	97.64	
KB-3d m6												
65.42	0.03	17.60	0.42	0.09	0.01	0.13	0.15	15.35	<0.01	<0.01	99.19	lighter phase
65.80	0.06	17.53	0.11	0.02	<0.01	0.05	0.16	16.20	<0.01	<0.01	99.92	
CB6-108d zeolites defocused analyses												
70.35	<0.01	10.94	<0.01	<0.01	<0.01	2.34	2.47	0.28	<0.01	<0.01	86.38	beige part
69.90	<0.01	10.85	0.02	<0.01	<0.01	2.32	2.80	0.28	0.01	<0.01	86.18	
69.67	0.02	10.81	0.01	<0.01	<0.01	2.34	2.48	0.22	0.01	<0.01	85.56	
71.41	0.01	10.89	<0.01	<0.01	<0.01	2.39	2.51	0.29	0.02	<0.01	87.53	
71.23	<0.01	10.92	0.01	<0.01	<0.01	2.40	2.46	0.23	<0.01	<0.01	87.24	
71.25	0.01	11.01	0.02	<0.01	<0.01	2.41	2.46	0.23	<0.01	<0.01	87.38	
73.87	0.01	11.50	0.01	<0.01	0.01	2.52	2.11	0.48	0.03	<0.01	90.54	
74.08	<0.01	11.37	0.01	<0.01	<0.01	2.47	2.18	0.39	<0.01	<0.01	90.50	
58.88	0.01	15.75	0.05	<0.01	<0.01	0.42	4.75	4.83	<0.01	<0.01	84.69	colorless part
58.94	<0.01	15.76	0.07	0.01	<0.01	0.40	4.27	4.65	<0.01	<0.01	84.10	
64.48	<0.01	17.35	0.05	<0.01	<0.01	0.46	4.61	5.33	<0.01	0.01	92.29	
68.48	<0.01	18.52	0.03	<0.01	<0.01	0.51	3.65	5.70	<0.01	<0.01	96.88	
68.23	0.01	18.16	0.04	<0.01	<0.01	0.47	3.81	5.36	<0.01	<0.01	96.08	
68.56	<0.01	17.66	0.06	<0.01	<0.01	0.41	3.87	5.67	<0.01	<0.01	96.23	
68.19	<0.01	17.43	0.03	0.01	<0.01	0.43	3.74	5.47	<0.01	<0.01	95.30	
68.84	0.03	17.74	0.10	<0.01	0.01	0.42	3.39	5.96	<0.01	0.01	96.50	
CB6-108a zeolites defocused analyses												
67.02	0.01	17.37	0.08	0.01	0.01	0.44	6.51	3.70	<0.01	<0.01	95.14	colorless part
66.67	0.02	17.08	0.03	<0.01	<0.01	0.43	6.49	3.56	0.01	<0.01	94.29	
67.49	0.01	17.22	<0.01	<0.01	<0.01	0.43	6.59	3.36	<0.01	<0.01	95.11	
65.94	0.01	16.73	0.05	<0.01	<0.01	0.43	6.76	3.13	0.02	<0.01	93.06	
67.35	<0.01	16.52	0.06	<0.01	<0.01	0.39	6.77	3.51	0.01	<0.01	94.60	
71.12	<0.01	10.65	0.02	0.01	0.01	2.36	2.66	0.24	0.01	<0.01	87.06	beige part
70.66	<0.01	10.68	<0.01	<0.01	0.01	2.40	2.64	0.24	<0.01	<0.01	86.64	
73.04	<0.01	11.04	<0.01	<0.01	<0.01	2.43	2.69	0.24	<0.01	<0.01	89.44	

Note: Each part is marked by a heading with the unique sample number and the melt type analyzed. In the last column there is description of the phases analyzed. The shades of gray are described as seen in the back-scattered electron mode, except for the zeolites and brownish minerals in m5, where colors under optical microscope are described.

Rare zircon grains have been noted in the melt particles and in impact melt rocks. In the melt-rich parts, zeolites are occasionally found filling the cavities or possibly altering the impact melt. In the optical microscope, a colorless, isotropic phase and a beige phase were recognized (Fig. 8-4n). The beige phase was identified by electron microprobe and microRaman spectroscopy as mordenite and the colorless phase as paulingite or possibly faujasite (see analyses in Table 8-5).

In the melt of type m4, pyroxene and plagioclase crystallites were identified (Fig. 8-5k-n). The pyroxenes are Al-rich. The plagioclase laths have composition of andesine. The

plagioclase crystals of the subtype m4pl (Fig. 8-4h; without pyroxene crystallites) have labradorite composition. No high-pressure polymorphs, such as coesite or stishovite, were found.

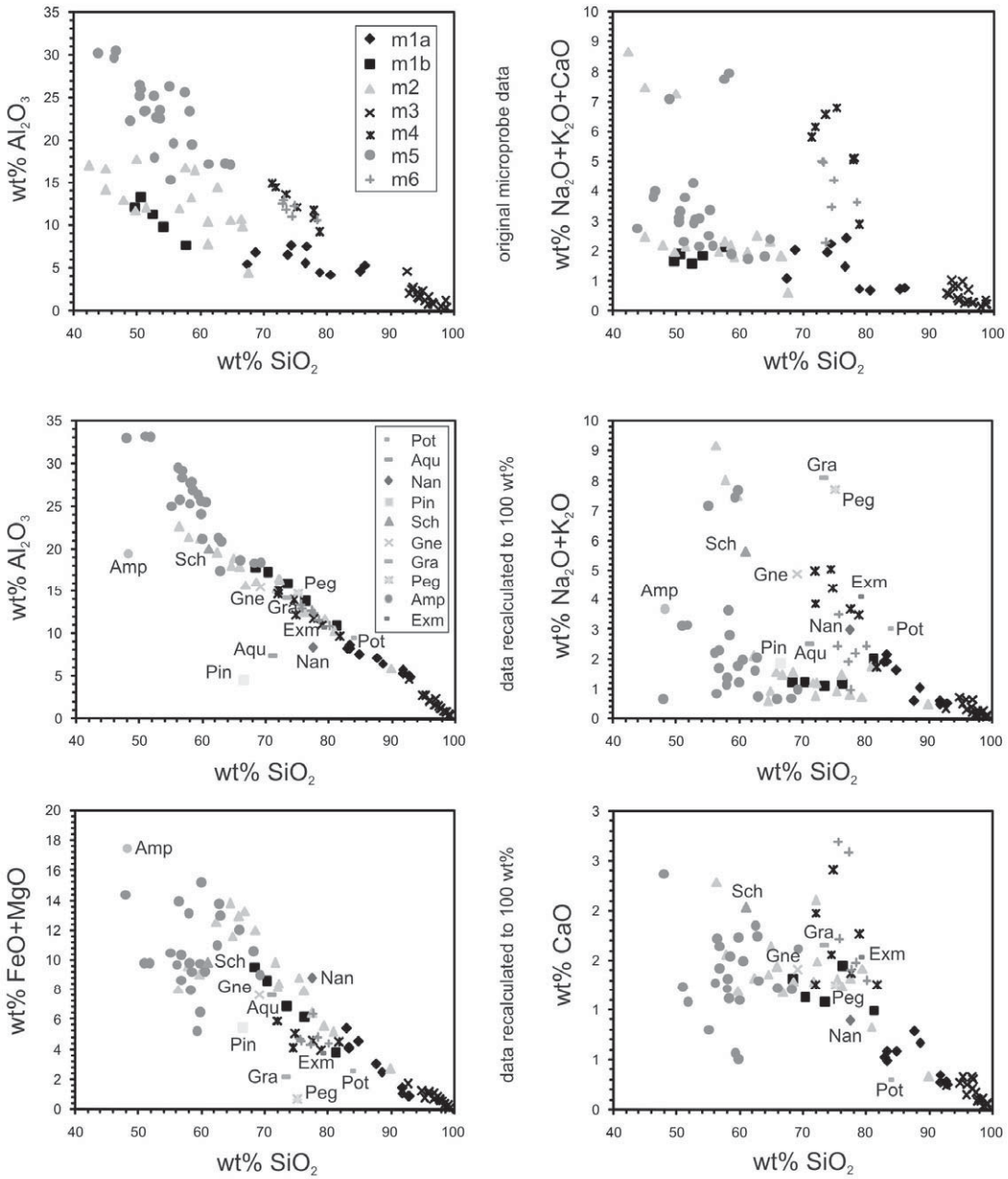

Figure 8-7: Variation diagrams showing the differences in composition of melt particles of the different melt types. First two diagrams (Al_2O_3 versus SiO_2 and Na_2O+K_2O+CaO versus SiO_2) use the original microprobe data. Especially the first diagram (SiO_2 versus Al_2O_3) shows that the compositions of the different melt types differ, although some of the melt types overlap. The next four diagrams, where also compositions of the main target lithologies and Exmore breccia are plotted, use data recalculated to 100 wt%. The compositions of melt type m4 and m6 are very similar. In the last diagram, CaO versus SiO_2, the lithologies very rich in CaO (Aquia Formation, Piney Point Formation and amphibolite are not plotted. Pot – Potomac Formation, Aqu – Aquia Formation, Nan – Nanjemoy Formation, Pin – Piney Point Formation, Peg – pegmatite and granite of the basement crystalline section, Gra – granitic rocks of the megablock, Amp – amphibolitic block, Sch – schist of the basement crystalline section, Gne – cataclastic gneiss, Exm – Exmore breccia.

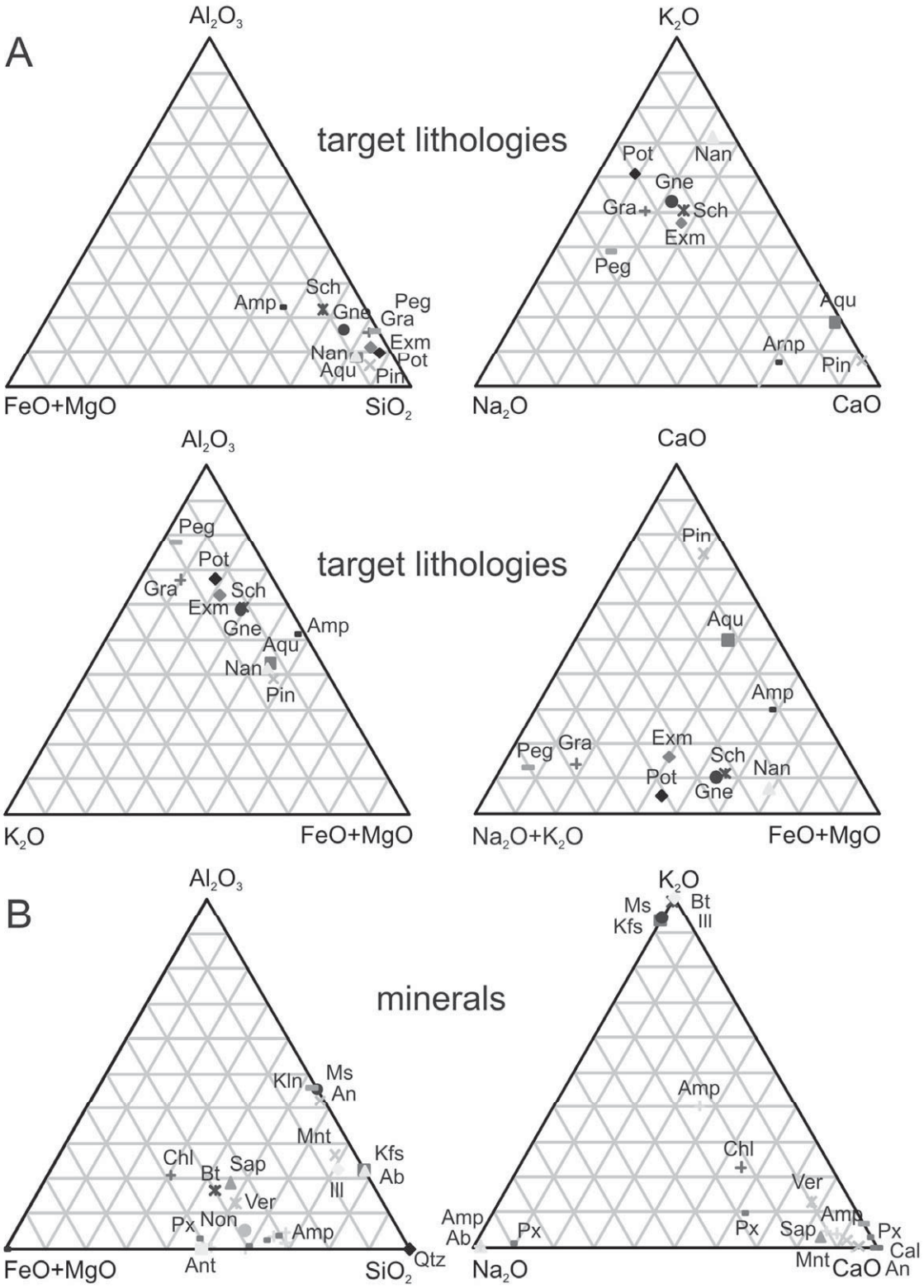
A
target lithologies
Al2O3
FeO+MgO
SiO2
Amp
Sch
Gne
Peg
Gra
Exm
Nan
Aqu
Pot
Pin
K2O
Na2O
CaO
Pot
Nan
Gne
Gra
Sch
Exm
Peg
Aqu
Amp
Pin
target lithologies
Al2O3
K2O
FeO+MgO
Peg
Pot
Gra
Sch
Exm
Gne
Amp
Aqu
Nan
Pin
CaO
Na2O+K2O
FeO+MgO
Pin
Aqu
Amp
Peg
Gra
Exm
Sch
Nan
Pot
Gne
B
minerals
Al2O3
FeO+MgO
SiO2
Kln
Ms
An
Mnt
Chl
Sap
Kfs
Ab
Bt
Ill
Ver
Px
Non
Amp
Ant
Qtz
K2O
Na2O
CaO
Ms
Bt
Kfs
Ill
Amp
Chl
Ver
Amp
Ab
Px
Px
Sap
Amp
Px
Mnt
Cal
An

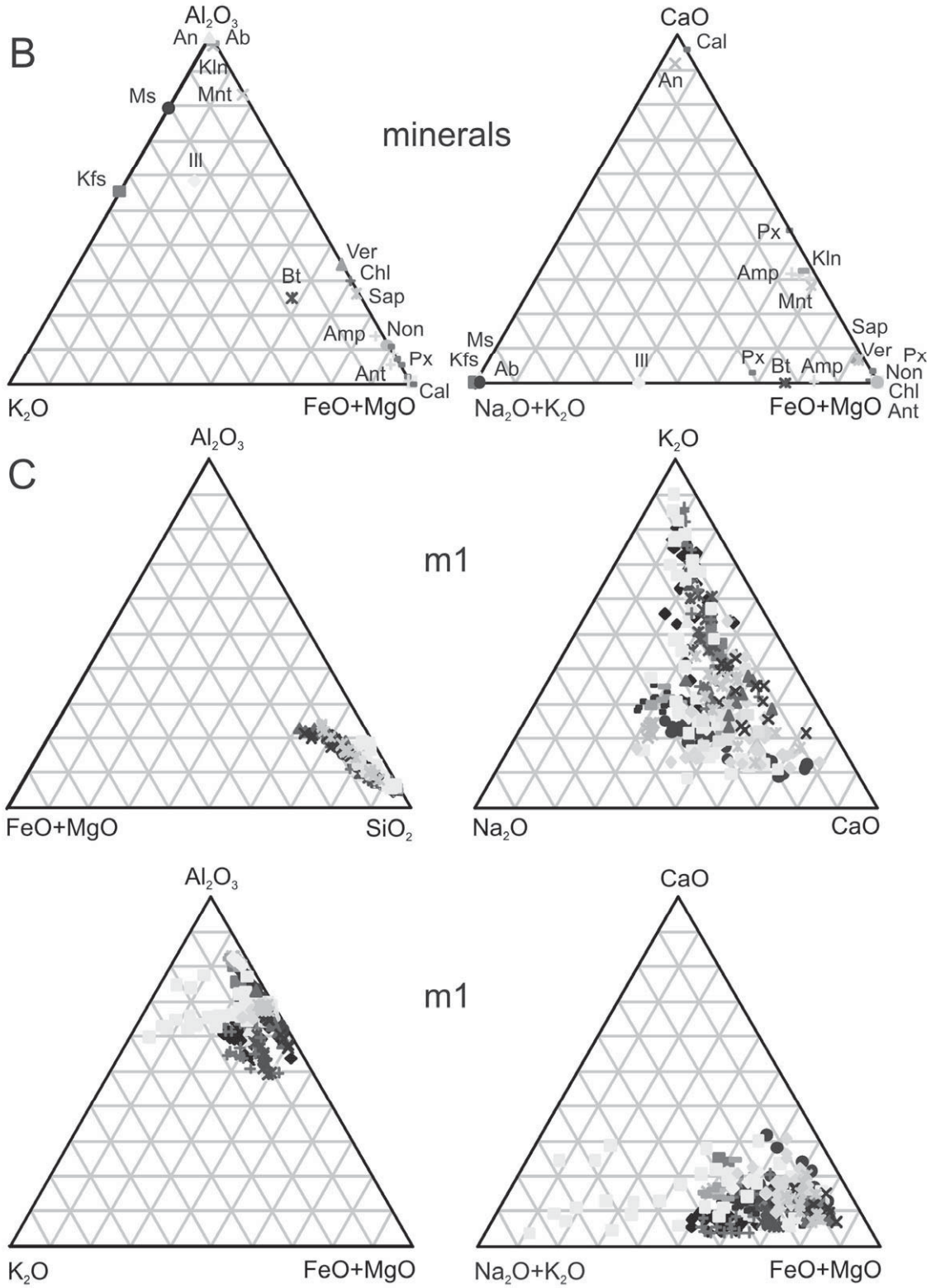
B
minerals
Al2O3
An
Ab
Kln
Ms
Mnt
Ill
Kfs
Ver
Chl
Bt
Sap
Amp
Non
Px
Ant
Cal
K2O
FeO+MgO
CaO
Cal
An
Px
Kln
Amp
Mnt
Sap
Ver
Px
Ms
Kfs
Ab
Ill
Px
Bt
Amp
Non
Chl
Ant
Na2O+K2O
FeO+MgO
C
m1
Al2O3
FeO+MgO
SiO2
K2O
Na2O
CaO
m1
Al2O3
K2O
FeO+MgO
CaO
Na2O+K2O
FeO+MgO

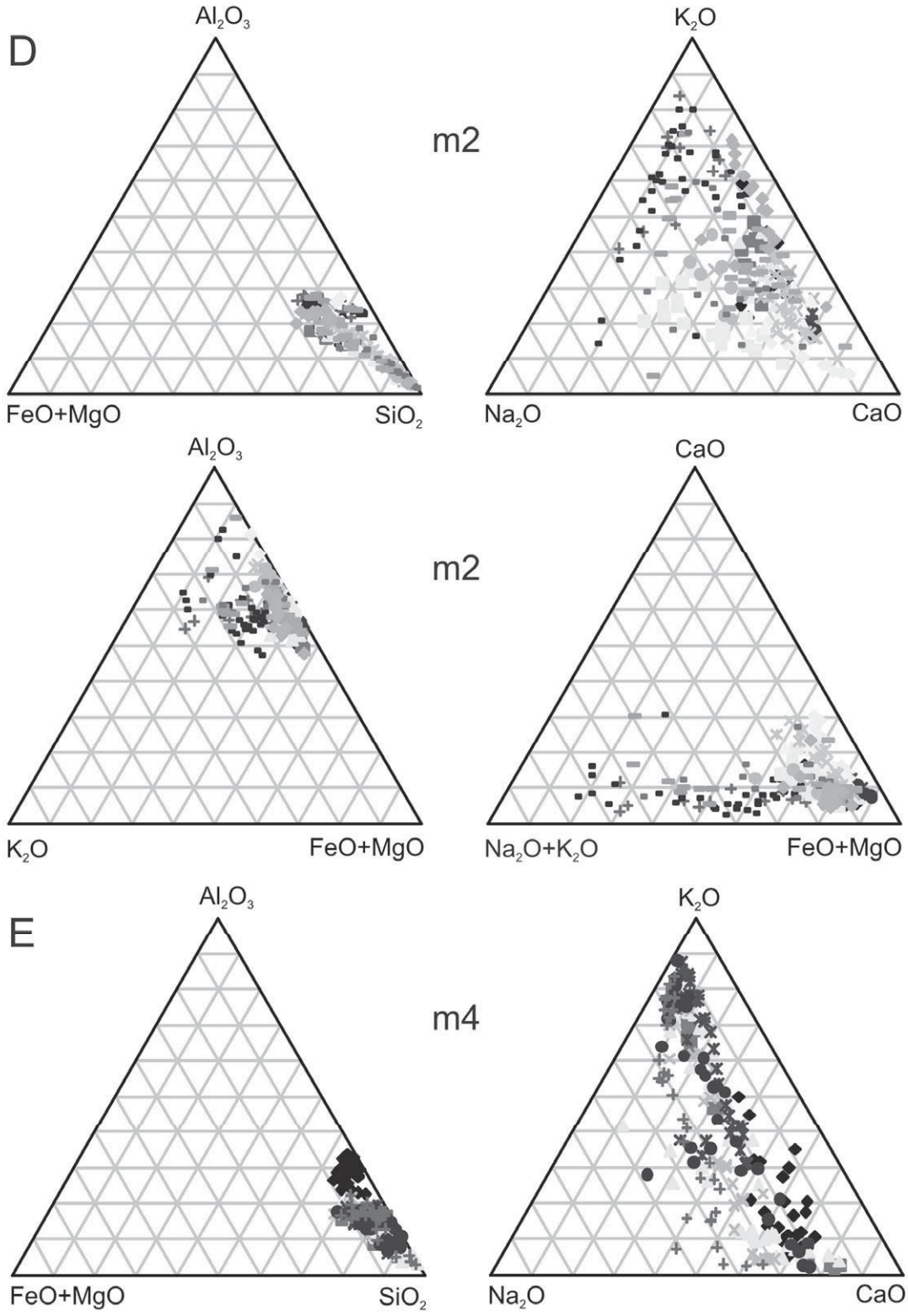
D
Al_2O_3
FeO+MgO
SiO_2
m2
K_2O
Na_2O
CaO
Al_2O_3
K_2O
FeO+MgO
m2
CaO
Na_2O+K_2O
FeO+MgO
E
Al_2O_3
FeO+MgO
SiO_2
m4
K_2O
Na_2O
CaO

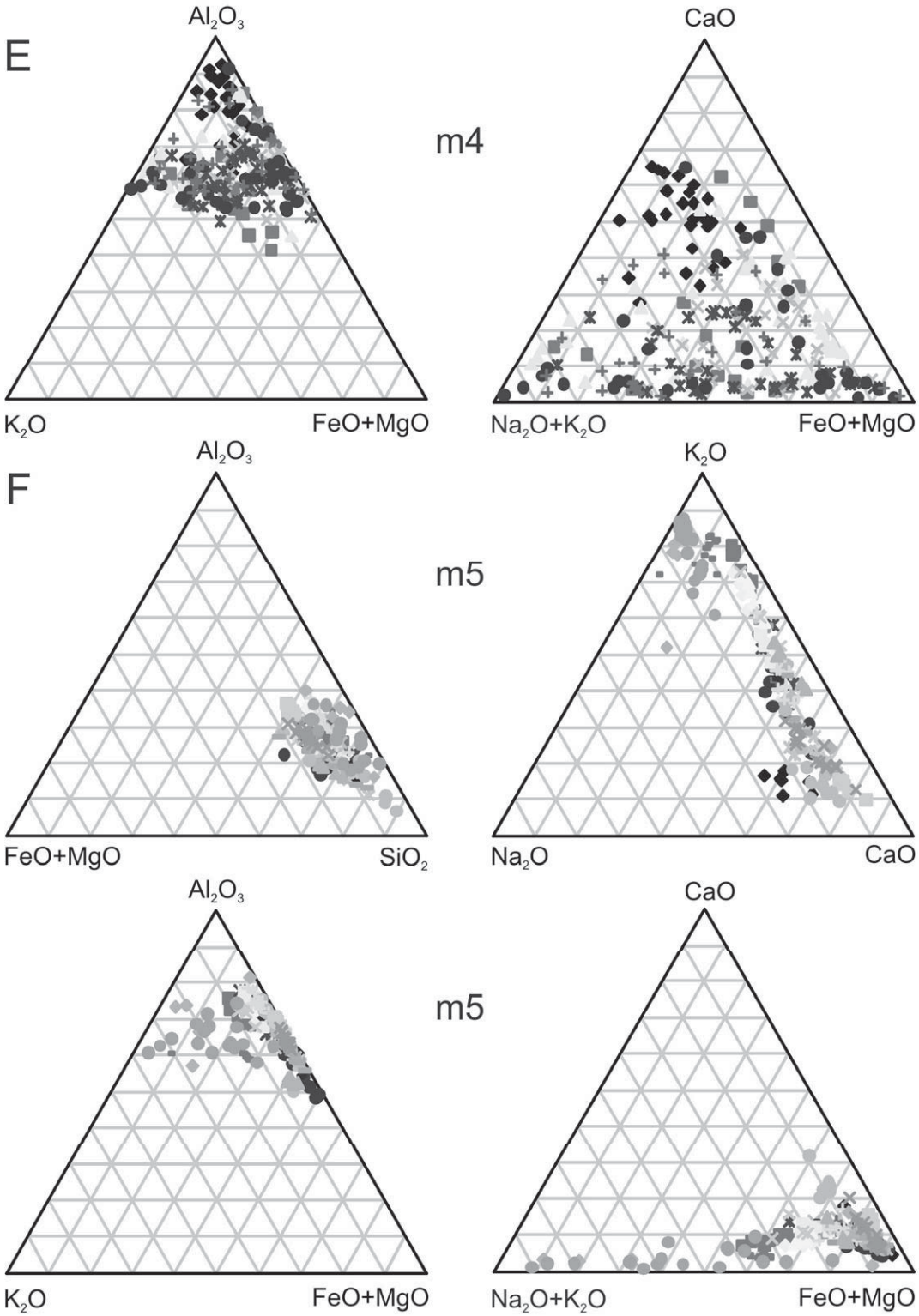
E
Al_2O_3
K_2O
FeO+MgO
m4
CaO
Na_2O+K_2O
FeO+MgO
F
Al_2O_3
FeO+MgO
SiO_2
m5
K_2O
Na_2O
CaO
Al_2O_3
K_2O
FeO+MgO
m5
CaO
Na_2O+K_2O
FeO+MgO

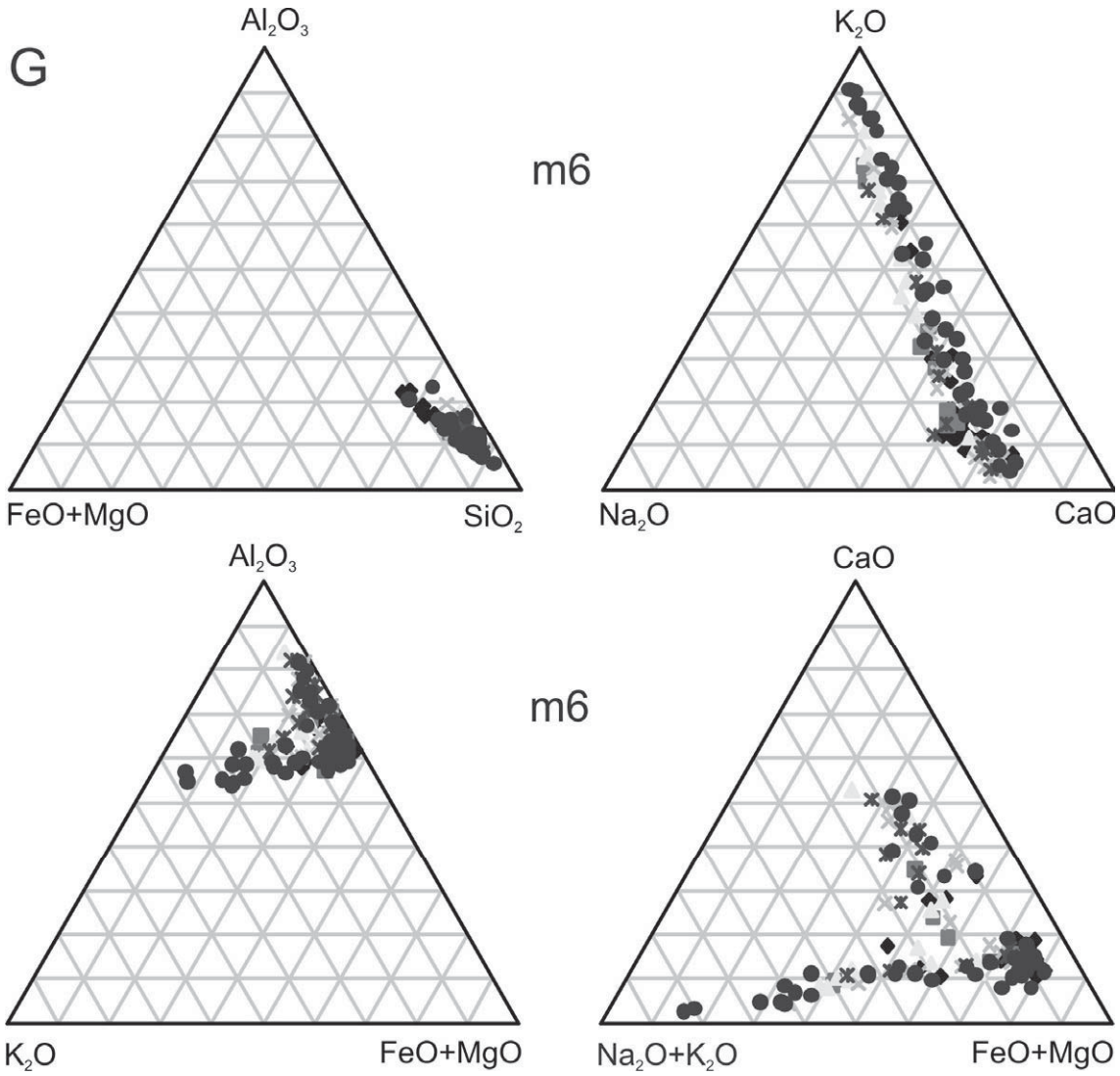

Fig. 8-8: Ternary diagrams showing compositions of single spots analyzed in the melt particles. a) Composition of the target lithologies and Exmore breccia. Pot – Potomac Formation, Aqu – Aquia Formation, Nan – Nanjemoy Formation, Pin – Piney Point Formation, Peg – pegmaite and granite of the basement crystalline section, Gra – granitic rocks of the megablock, Amp – amphibolitic block, Sch – schist of the basement crystalline section, Gne – cataclastic geniss, Exm – Exmore breccia. Data from Deutsch and Koeberl (2006) and Schmitt et al. (2009). b) Composition of important rock-forming and clay minerals. Qtz – quartz, Kfs- K-feldspar. Ab – albite, An – anorthite, Bt – biotite, Ms – muscovite, Chl – chlorite (chamosite), Cal – calcite, Amp – amphiboles, Px – pyroxenes, Kln – kaolinite, Ill – illite, Mnt – montmorillonite, Sap – saponite, Non – nontronite, Ver – vermiculite, Ant – antigorite.. Data from Anthony et al. (1995). c) Compositions of melt particles of type m1. Analyses of all single spots are plotted, each data series corresponds to one particle. d) Compositions of melt particles of type m2. e) Compositions of melt particles of type m4. f) Compositions of melt particles of type m5. g) Compositions of melt particles of type m6. Note: Melt particles of type m3 plot all in the SiO_2 apex. Contents of other major oxides are commonly close to or below detection limit, thus ternary diagrams are not shown for this melt type.

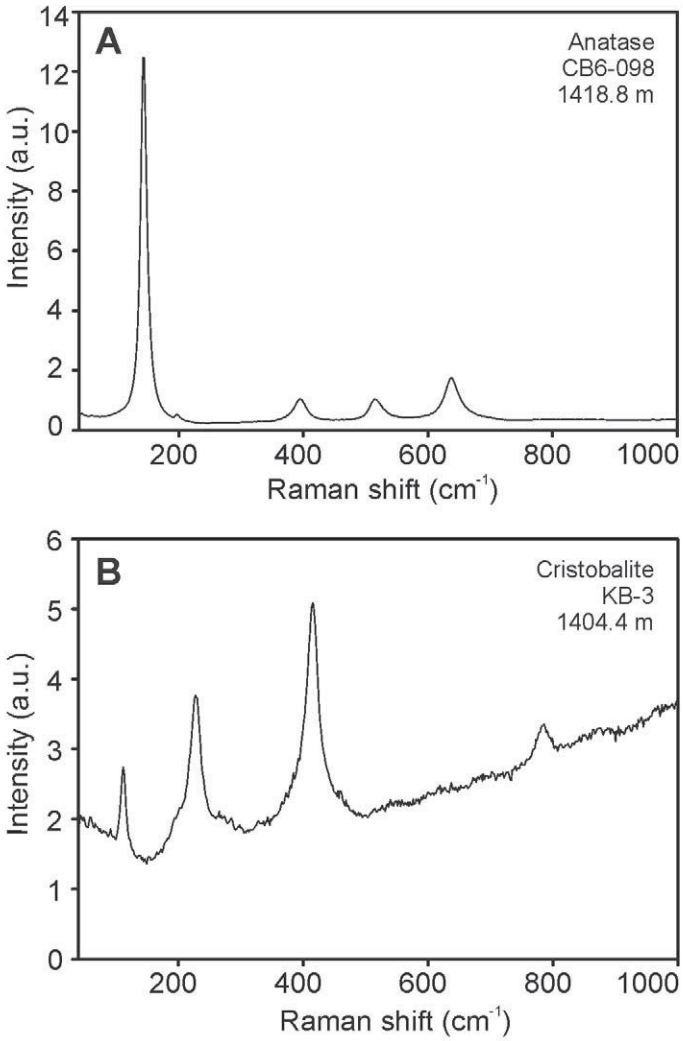

Fig. 8-9: Raman spectra for anatase and cristobalite. a) Raman spectrum of a tiny (~8 µm) anatase crystal, example from a melt particle of type m1. b) Raman spectrum of rare ballen cristobalite from a silica clast incorporated in a melt particle of type m6.

Relations between phases and alteration of the melt

For a better understanding of the relations of the different melt phases and possible influence of alteration, some element maps and profiles were obtained (Figs. 8-10 and 8-11). These analyses were performed mostly on melt type m1, where many interesting features, such as mixing and schlieren of slightly different melts, appear. The occurrence and composition of lighter and darker schlieren is illustrated in, e.g., several BSE photographs and element maps of particles from sample CB6-098 (depth 1418.8 m; Figs. 8-10a-b). Figure 8-10a illustrates mixing of "lighter" and "darker" melt, where the lighter parts are enriched in Al and K and possibly slightly enriched in Fe and Na. In the right part of the image is also a quartz rim that probably formed during post-impact hydrothermal alteration. Figure 8-10b also shows schlieren with slightly less compositional differences. The lighter parts are slightly enriched in Al, Si, and slightly enriched in Mg. The probably alteration phases at the bottom of the area shown in Figure 8-10b are depleted in Si, and enriched in Al, Mg, Fe, and Ca. Other element maps documenting the alteration of melt type m1 are presented in Fig. 8-10c, showing an

alteration vein transecting the melt particle, in horizontal direction in the BSE photograph. The vein contains abundant anatase, as is apparent from the Ti element map. In the BSE picture, there is also apparent slight change in composition of the melt near the vein. This area around the vein is slightly enriched in Si. Aside from Ti, the vein is also enriched in Ca, Fe, and Mg. Compositional variations of melt type m1 are documented on two line-scans of melt particles from sample CB6-097 (depth = 1412.8 m). In Fig. 8-11a, there are two thin schlieren rich in anatase, as is documented by the two Ti peaks. The larger light schlieren in the right part of the profile is enriched in Si, and K and depleted in Fe, Mg, and Al. In Fig. 8-11b a light gray schlieren is visible in the center of the particle; this schlieren is enriched in Al, Na, K, and Ca and depleted in Si, Fe, and Mg, with zonation in Ca and K. This compositional difference is primary, but could have been further modified by hydrothermal alteration. The precursor of the schlieren might be a plagioclase with K-feldspar rim.

Element maps are also very useful for studying the phases in melt type m4 with microlites. The maps in Fig. 8-10d (KB-2, depth = 1402.9 m) clearly show the compositional differences of the different phases. The pyroxene crystallites (white in the BSE image) concentrate Fe, Mg and Mn. The gray laths rich in Ca, Na, and Al are plagioclases. The matrix contains a dark gray phase, very Si-rich (probably nearly pure SiO_2) and another a bit lighter phase containing Si, Al, K, and some Na.

Relations of the different phases were documented also in the melt type m6. In Fig. 8-10e there are globules enriched in Si, Fe, Mg, and Ca. It is probably spherulitic quartz with tiny inclusions of other minerals. The light “background” phase on the left is enriched in K, while the dark phase on the right is Mg-rich.

Mixing calculations

We tried to reproduce the average compositions of the melt particles as mixtures of different target lithologies and rock-forming minerals. Preliminary mixing calculations for the melt particles were presented in Bartosova et al. (2009b); however, only the approximate compositions of the melt particles, measured by SEM-EDX, were used in that study. Here we present mixing calculations for the average composition of each melt type, obtained by electron microprobe analyses of several melt particles of each type.

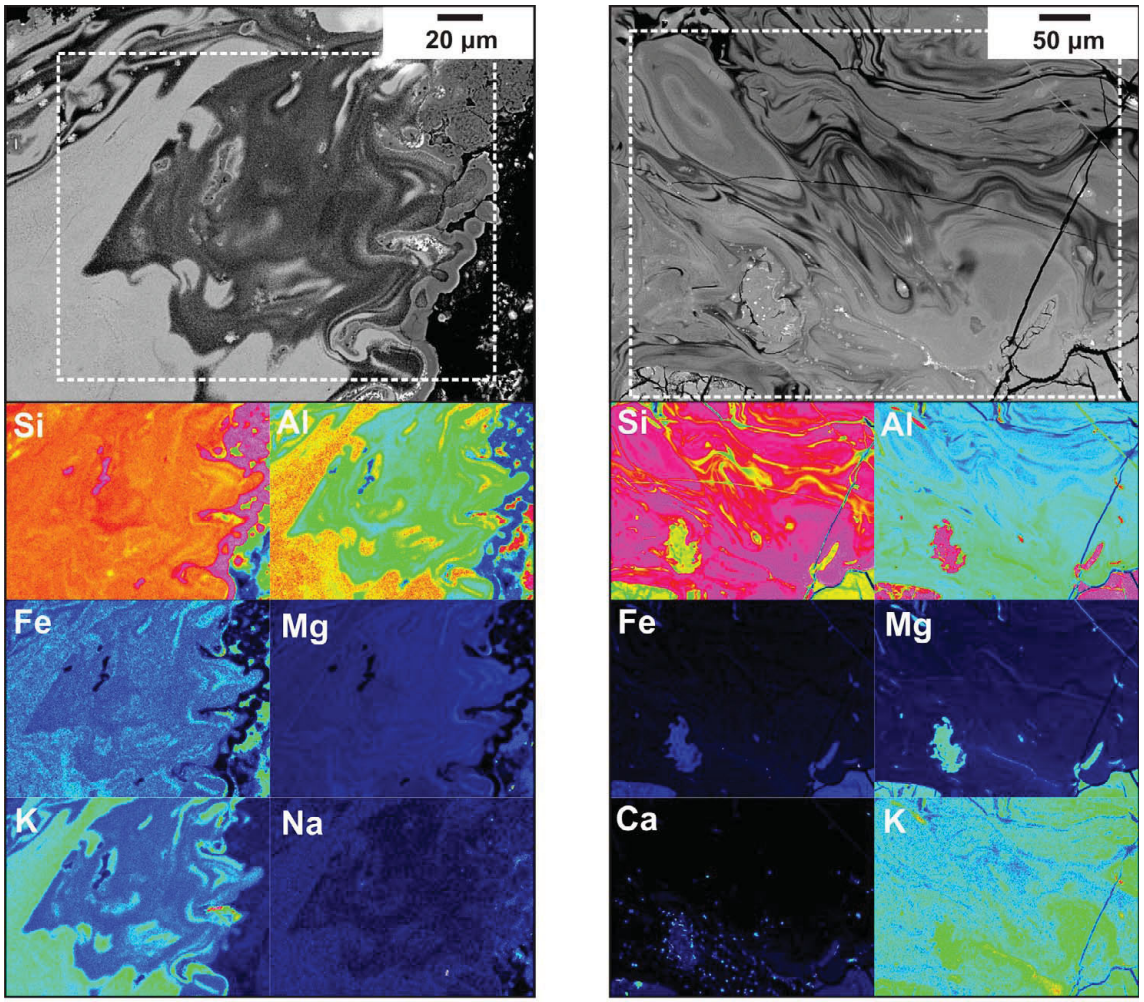

A m1, CB6-098, 1418.8 m

B m1, CB6-098, 1418.8 m

Results of the mixing calculations are summarized in Tables 8-6-9. For the mixing calculations, compositions of all components and mixtures were recalculated to 100% of 10 major oxides. For each melt type results of runs with all the major oxides are shown (SiO_2, TiO_2, Al_2O_3, FeO, MnO, MgO, CaO, Na_2O, K_2O; and also P_2O_5 for the runs with target lithologies). Because the runs with all the major oxides yield mostly high discrepancies, more runs were calculated for each melt type and selected runs, where the oxides with largest discrepancies were excluded, are shown in the tables. The excluded elements were mostly Ti, Mn, and P, which have low concentrations. Further it has been suggested by Wittmann et al. (2009a) that Ti could be redistributed during alteration. Other elements excluded in some runs were Na and K, which are relatively mobile and volatile.

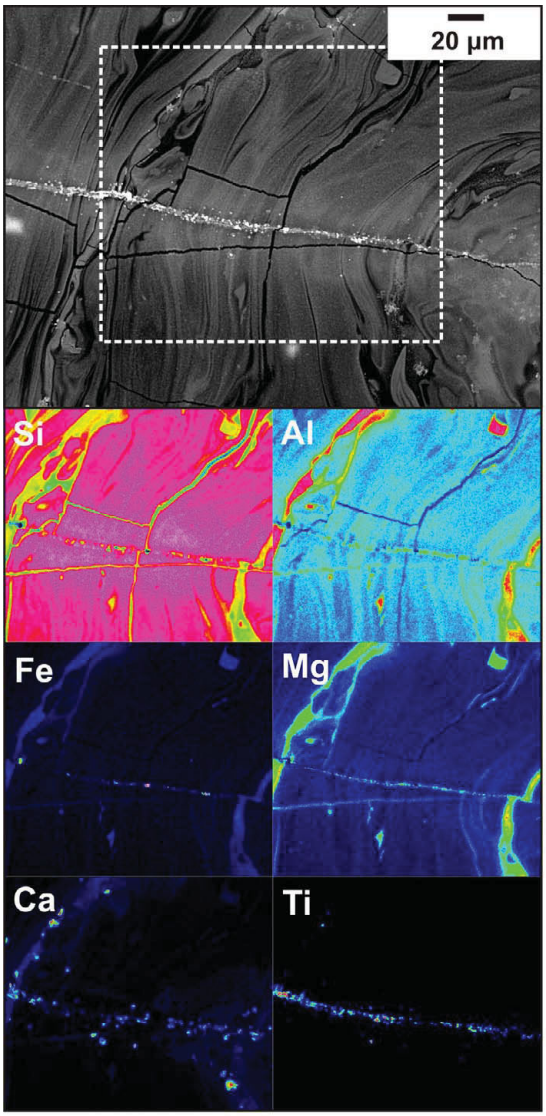

C m1, CB6-098, 1418.8 m

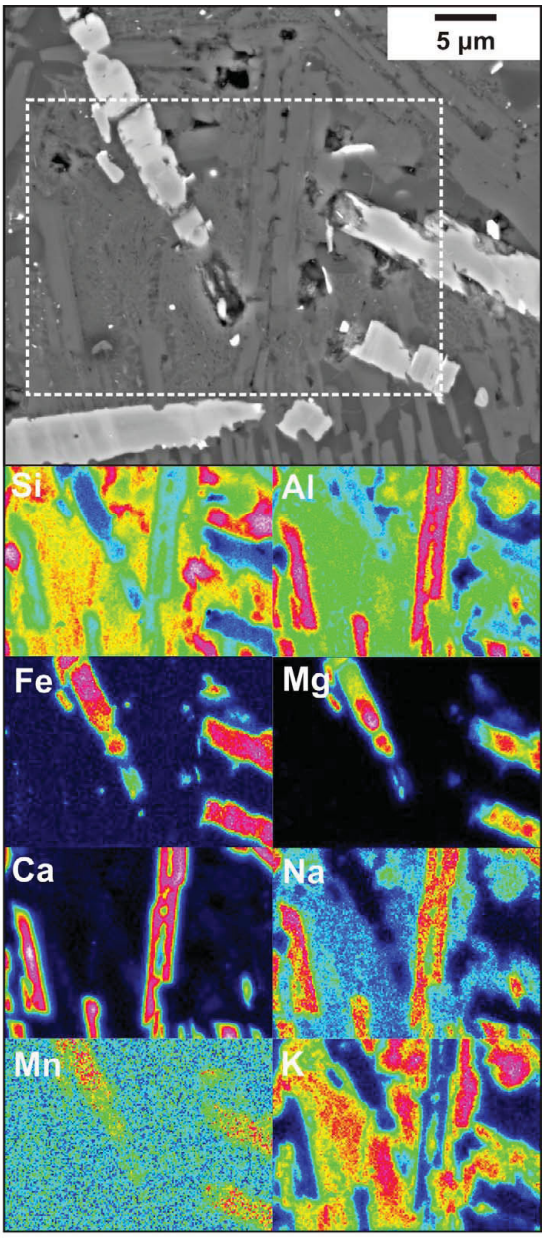

D m4, KB-2, 1402.9 m

For the calculations with target lithologies, the following rock types were used: pre-impact sedimentary formations - Potomac, Aquia, Nanjemoy, and Piney Point (data from Deutsch and Koeberl, 2006), and rocks of the crystalline basement - schist, gneiss, pegmatite/granite, and amphibolite (data from Schmitt et al., 2009). In some calculations, pegmatite/granite component was replaced by the composition of the granitic rocks of the megablock (Schmitt et al., 2009), but the results were very similar, thus are not presented here. For each run the discrepancy value is shown. This value indicates how well can be the melt modeled from the components – the lower the discrepancy, the smaller the difference between the modeled and observed compositions. In the calculations using the target lithologies, discrepancies <2 were obtained for some melt types, but only when

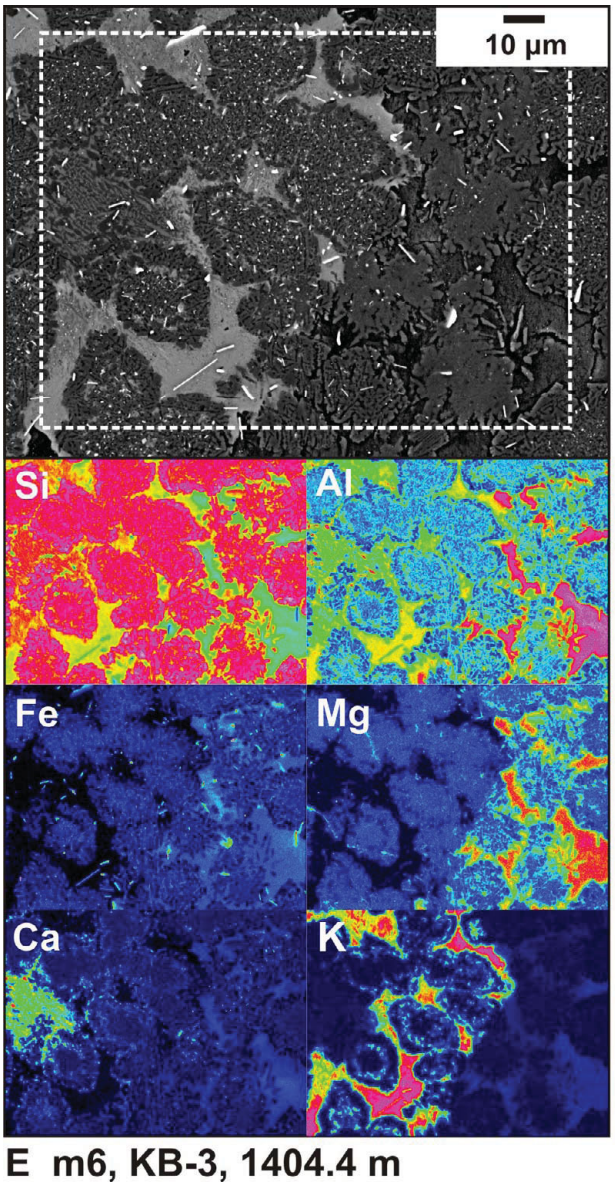

Figure 8-10: Element maps showing composition detail of interesting features in some melt particles from the Eyreville drill core. a) Melt particle of type m1 with schlieren of different composition and a Si-rich rim. b) Melt particle of type m1 with schlieren of different composition and some probably altered parts (the Al-rich areas at the bottom). c) Melt particle of type m1 with an alteration veinlet. Note the slight change in composition around the veinlet. d) Element map of melt type m4 enables to clearly distinguish the pyroxene crystals (Fe and Mg-rich), plagioclase crystals (Ca and Na-rich) and two Si-rich matrix phases. e) Detail of the structure of melt type m6. The globular structures are Si-rich, but also enriched in Fe, Mg, and Ca. The "background" phase is Al- and K-rich in the left part and Al- and Mg-rich in the right part.

some of the oxides were excluded from the calculations (Table 8-6 and 8-7). The composition of melt type m2 is closest to the gneiss and schist (probably >70 wt%), the rest being formed of the sedimentary formations (Nanjemoy and/or Potomac). Melt type m4 was calculated to be composed mostly of the sediments (mainly Potomac Formation), with more than 20% of schist or gneiss and possible minor pegmatite. The melt particles of type m6 were probably formed also mostly from sedimentary formations, mainly from the lowermost Potomac Formation, and <20% of schist. The results for the melt types m1 have higher discrepancies. The melt type m1a consists only form the Potomac Formation (~90 wt%) and some low amounts of Nanjemoy Formation. Precursor for the melt type m1b was probably a mixture of the Potomac Formation and schist or gneiss. The mixing calculations for melt type m3 and m5 have very high discrepancies and can not be modeled from the used target lithologies.

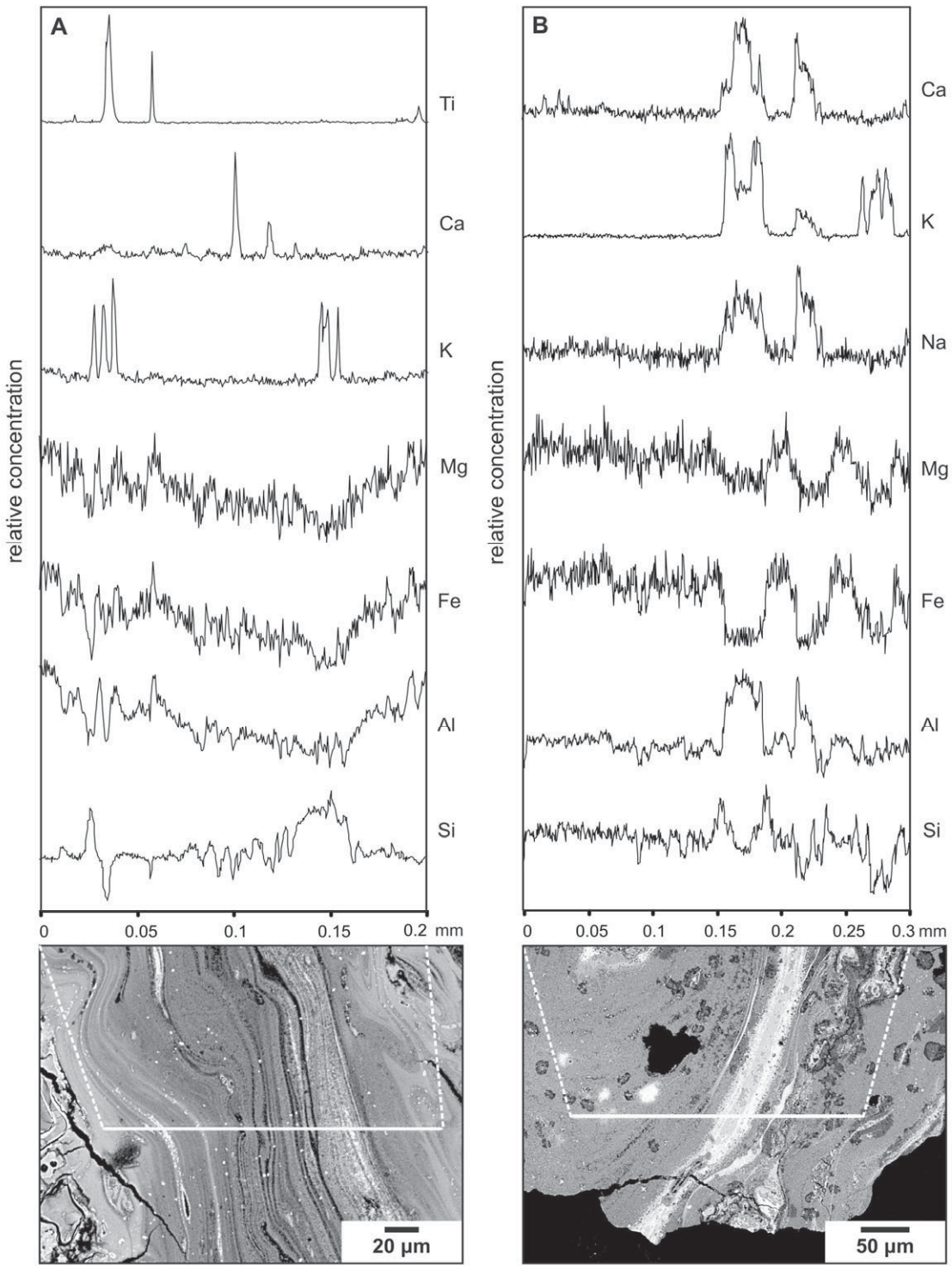

Fig. 8-11: Profiles showing variation of abundances of some elements in the melt particles from the Eyreville drill core. a) Profile through a part of a melt particle of type m1, rich in schlieren of different composition. Note the Ti-peaks associated with the stripes rich in tiny white anatase. b) Profile through a part of melt particle of type m1. Note the different composition of the light-gray layer in the middle. The black parts are vugs in the melt particle.

To better understand the composition and precursors of the melt types, the melt particles compositions were modeled as mixtures of rock forming minerals (Tables 8-8 and 9). The following minerals were used: quartz, K-feldspar, albite, anorthite, muscovite, biotite, chlorite (chamosite), hornblende, riebekite, and grunerite. Results of mixing calculations with all nine major oxides (excluding P2O5), and runs excluding oxides, for which the errors were largest – TiO2 and K2O, are shown.

Melt type m3 can be well modeled, even with all 9 oxides, as a mixture of quartz, <3 wt% of muscovite, and small amounts of other minerals. Calculations for other melt types have high discrepancies in the calculations with all nine major oxides, but reasonable discrepancies for the runs without TiO_2 and very low discrepancies for the runs without TiO_2 and K_2O. For most of the melt types, quartz is the main component. Melt type m1a contains ~78 wt% of quartz, <10 wt% of mica (mainly muscovite), low amounts of plagioclase and possibly amphibole. The components of melt type m1b are quartz (<50 wt%), mica (>20 wt%) and again low possible amounts of feldspars and amphiboles. Melt type m2 consists of >40 wt% of quartz, >30 wt% of mica (mainly muscovite), ~ 10 wt% plagioclase and <10 wt% of amphiboles. Melt type m4 contains ~50 wt% of quartz, the rest comprising mica ~ 20 wt%, feldspars >13 wt%, and >6 wt% of amphiboles. Calculated components of the melt type m5 (melt type with the lowest SiO_2 content) are mica ~50 wt%, quartz >20 wt%, >6 wt% of amphiboles, and a low amount of feldspars. Composition of melt type m6 is similar to m4; it is composed of >55 wt% of quartz, ~19 wt% of muscovite, ~10 wt% of feldspars and ~10 wt% of amphiboles.

For some runs (not shown here), also other amphibole compositions were used; the results were similar. From the composition of the melt and from the calculations it is evident that the possible amphiboles mixed into the impact melt would have to be high-Fe low-Ca amphiboles. Pyroxenes were not used for the calculations, because most of the melt types have a quartz-rich precursor, thus presence of pyroxenes is not probable. Furthermore, pyroxenes are not abundant in the target lithologies.

Table 8-6. Precursors of melt particles from the Eyreville drill core, Chesapeake Bay impact structure. Results based on HMX mixing calculations modeling composition of the melt types from the target lithologies. Values in %.

	Potomac Formation	Aquia Formation	Nanjemoy Formation	Piney Formation	Schist*	Cataclastic gneiss	Pegmatite/ granite*	Amphibolite	Discrepancy[#]
Melt type m1a									
10 major	99.16 ± 1.32	0 ± 0.27	0 ± 0.22	0.84 ± 0.29	0 ± 0.22	0 ± 0.22	0 ± 0.22	0 ± 0.21	68
- Ti, Mn, Na, K, P	88.86 ± 4.86	0 ± 1.03	10.57 ± 4.28	0.57 ± 1.68	0 ± 1.14	0 ± 1.12	0 ± 1.07	0 ± 0.96	5.7
- Na, K, P	94.59 ± 1.64	0 ± 0.13	4.67 ± 1.47	0.74 ± 0.61	0 ± 0.13	0 ± 0.13	0 ± 0.13	0 ± 0.13	5.5
Melt type m1b									
10 major	85.99 ± 2.28	7.31 ± 2.03	0 ± 0.14	0 ± 0.05	0 ± 0.05	0 ± 0.05	0 ± 0.05	0 ± 0.05	102
- Ti, Mn, Na, K, P	26.95 ± 4.96	0 ± 3.86	3.52 ± 3.50	0 ± 3.67	15.27 ± 4.87	54.26 ± 10.69	0 ± 8.06	0 ± 2.59	1.4
- Na, K, P	44.92 ± 3.29	0 ± 0.50	0.46 ± 0.71	0 ± 0.60	53.33 ± 3.29	1.30 ± 1.48	0 ± 0.53	0 ± 0.53	11
Melt type m2									
10 major	23.00 ± 3.54	0 ± 0.47	17.84 ± 4.06	0 ± 0.57	56.05 ± 3.69	0 ± 0.47	0 ± 0.46	1.54 ± 0.64	14
- Ti, Mn, Na, K, P	0 ± 5.91	0 ± 5.84	17.00 ± 6.65	0 ± 4.40	28.33 ± 5.21	54.67 ± 12.33	0 ± 8.10	0 ± 3.18	1.6
- Na, K, P	7.22 ± 1.98	0 ± 0.38	8.73 ± 2.67	0 ± 1.37	35.14 ± 5.06	48.91 ± 7.03	0 ± 0.38	0 ± 0.56	3.2
Melt type m3									
10 major	100 ± 2.74	0 ± 0.23	0 ± 0.18	0 ± 0.34	0 ± 0.18	0 ± 0.18	0 ± 0.18	0 ± 0.18	149
- Ti, Mn, Na, K, P	100 ± 6.25	0 ± 0.71	0 ± 0.75	0 ± 2.08	0 ± 0.75	0 ± 0.75	0 ± 0.75	0 ± 1.15	37
Melt type m4									
10 major	32.82 ± 3.27	0 ± 0.45	27.01 ± 3.61	4.13 ± 0.44	0 ± 0.44	20.57 ± 3.34	14.59 ± 2.09	0 ± 0.67	9.9
- Ti, Mn, Na, K, P	61.56 ± 0.03	0 ± 0.03	1.21 ± 0.02	3.72 ± 0.01	28.34 ± 0.03	0 ± 0.05	4.53 ± 0.02	0.64 ± 0.003	<0.01
-Ti, Mn, P	65.30 ± 1.96	0 ± 6.87	0 ± 5.91	4.05 ± 2.58	30.65 ± 1.63	0 ± 3.49	0 ± 1.10	0 ± 1.59	0.19
Melt type m5									
10 major	0 ± 0.47	0 ± 0.46	0 ± 0.46	0 ± 0.46	100 ± 2.26	0 ± 0.46	0 ± 0.46	0 ± 0.46	26
- Ti, Mn, Na, K, P	0 ± 8.23	0 ± 8.81	0 ± 8.09	0 ± 7.91	100 ± 16.65	0 ± 9.60	0 ± 7.69	0 ± 5.31	11
- Al, Na, K, P	0 ± 0.71	0 ± 0.62	0 ± 0.63	0 ± 0.62	100 ± 2.07	0 ± 0.69	0 ± 0.70	0 ± 0.62	3.9
Melt type m6									
10 major	57.11 ± 2.27	0 ± 0.16	34.75 ± 2.30	6.57 ± 0.54	1.58 ± 0.63	0 ± 0.16	0 ± 0.17	0 ± 0.16	16
- Ti, Mn, Na, K, P	67.70 ± 8.95	12.04 ± 6.78	0 ± 6.12	0 ± 2.30	18.50 ± 5.70	0 ± 6.33	1.76 ± 5.43	0 ± 2.46	1.7
- Al, Mg, K, P	55.74 ± 0.36	14.15 ± 0.46	24.81 ± 0.56	0.16 ± 0.18	3.13 ± 0.48	0 ± 0.17	0 ± 0.12	0 ± 0.14	0.07

Note: Values in %. All compositions of the components were recalculated to 100% of the major oxides (SiO_2, TiO_2, Al_2O_3, FeO, MnO, MgO, CaO, Na_2O, K_2O, and P_2O_5). Calculations with all 10 major oxides (first row for each melt type), and with only some oxides (the excluded elements are listed in the first column) are shown. Harmonic least-squares mixing calculations are after Stöckelmann and Reimold (1989). Chemical composition of target lithologies - data by Deutsch and Koeberl (2006) - the pre-impact sedimentary formations (first four columns) and Schmitt et al. (2009) - the other target lithologies sampled in the Eyreville drill core.

* from the basal crystalline section of the Eyreville drill core

[#] Discrepancy characterizes how well can be the mixture modeled from the components. The lower the discrepancy, the smaller the difference between the composition of the modeled and the real melt.

Table 8-7. Comparison of observed composition (Table 8-4) of the melt types from the Eyreville drill core with compositions modeled from target lithologies with HMX mixing calculations (presented in this table). Values in wt%.

	Melt type m1a		Melt type m1b		Melt type m2		Melt type m3		Melt type m4		Melt type m5		Melt type m6	
	calculated	$\Delta_{obs-calc}$*	calculated	$\Delta_{obs-calc}$*	calculated	$\Delta_{obs-calc}$*	calculated	$\Delta_{obs-calc}$*	calculated	$\Delta_{obs-calc}$*	calculated	$\Delta_{obs-calc}$*	calculated	$\Delta_{obs-calc}$*
SiO_2	87.13	0.97	74.52	-0.42	68.65	1.55	97.2	0.3	76.21	-0.12	59.83	-0.63	77.77	-0.17
TiO_2	0.70	<0.01	1.14	0.07	0.92	-0.14	0.58	<0.01	0.72	<0.01	0.99	<0.01	0.90	0.01
Al_2O_3	6.86	-0.13	13.71	1.43	15.9	0.49	1.82	-0.23	11.83	0.77	22.08	3.22	12.30	0.18
FeO	2.20	-0.04	4.03	1.11	6.51	0.22	0.63	-0.05	4.00	-0.04	7.61	-0.02	4.27	<0.01
MnO	0.02	<0.01	0.04	0.01	0.07	<0.01	0.01	<0.01	0.06	<0.01	0.08	<0.01	0.05	<0.01
MgO	0.38	0.25	0.49	1.36	2.08	0.44	0.13	-0.01	0.90	-0.05	2.84	0.10	0.62	<0.01
CaO	0.74	<0.01	1.18	<0.01	1.41	-0.03	0.26	-0.09	1.67	<0.01	1.39	-0.05	1.88	<0.01
Na_2O	0.33	<0.01	0.60	-0.08	1.15	-0.37	0.15	-0.02	1.28	-0.10	0.52	-0.12	0.69	0.01
K_2O	1.26	-0.44	0.93	-0.12	2.89	-1.35	0.25	-0.07	2.69	0.03	3.34	-1.25	1.97	-0.42
P_2O_5	0.03	<0.01	0.02	<0.01	0.07	-0.02	0.03	<0.01	0.09	0.04	0.08	-0.03	0.08	0.02

Note: Resulting compositions of the melt particles as obtained from the HMX mixing calculations are shown for runs with all 10 major oxides presented in Table 8-6.

* Δobs-calc = difference between observed and calculated value

Table 8-8. Precursors of melt types from the Eyreville drill core, Chesapeake Bay impact structure. Results based on HMX mixing calculations modeling composition of the melt types from rock forming minerals. Values in %.

	Qtz	Kfs	Alb	An	Bt	Ms	Chl	Hbl	Rbk	Gru	Discrepancy[#]
Melt type m1a											
9 major	78.92 ± 1.38	0 ± 1.46	1.17 ± 0.80	2.33 ± 0.69	2.67 ± 1.30	10.13 ± 1.54	2.73 ± 1.68	0 ± 1.21	1.49 ± 1.23	0 ± 1.14	10
- Ti	78.92 ± 0.51	0 ± 0.84	1.97 ± 0.47	2.26 ± 0.44	0 ± 1.00	10.38 ± 1.24	4.66 ± 1.07	0 ± 0.81	0 ± 0.78	1.07 ± 0.52	0.8
- Ti, K	77.46 ± 0	0.36 ± 0	0 ± 0	1.56 ± 0	0 ± 0	13.67 ± 0	2.34 ± 0	1.22 ± 0	2.82 ± 0	0.57 ± 0	<0.01
Melt type m1b											
9 major	61.97 ± 2.62	0 ± 0.64	4.22 ± 0.72	6.08 ± 0.98	13.08 ± 1.47	0 ± 0.65	6.39 ± 1.93	0 ± 0.75	0.18 ± 0.67	0 ± 0.73	76
- Ti	59.99 ± 1.19	0 ± 0.42	3.71 ± 0.71	5.72 ± 0.63	0 ± 0.50	9.08 ± 1.04	15.16 ± 1.10	0 ± 0.46	0 ± 0.50	0.88 ± 0.47	13
- Ti, K	50.90 ± 0.31	0 ± 0.35	2.40 ± 0.16	4.08 ± 0.18	0 ± 0.34	27.04 ± 0.41	8.66 ± 0.25	2.69 ± 0.17	0 ± 0.33	4.24 ± 0.41	0.07
Melt type m2											
9 major	47.61 ± 1.29	0 ± 0.62	5.80 ± 0.95	6.74 ± 0.58	10.93 ± 1.00	16.13 ± 1.33	10.51 ± 0.98	0 ± 0.54	1.34 ± 0.69	0 ± 0.59	5.6
- Ti	45.07 ± 0.82	0 ± 0.62	5,55 ± 0.62	4.45 ± 0.37	0 ± 0.76	22.56 ± 1.00	11.84 ± 0.64	3.77 ± 0.58	0 ± 0.55	5.80 ± 0.61	1.7
- Ti, K	43.03 ± 0.16	0 ± 0.18	4.34 ± 0.15	3.80 ± 0.09	0 ± 0.18	27.45 ± 0.21	10.64 ± 0.12	4.72 ± 0.11	0 ± 0.18	6.02 ± 0.16	<0.01
Melt type m3											
9 major	95.06 ± 0.22	0 ± 0.42	0.39 ± 0.40	0.82 ± 0.19	0.29 ± 0.20	1.72 ± 0.86	0.38 ± 0.46	0 ± 0.12	1.04 ± 0.68	0 ± 0.45	0.7
- Ti	95.01 ± 0.34	0 ± 0.38	0 ± 0.66	0.81 ± 0.38	0 ± 1.17	2.04 ± 1.00	0.41 ± 0.83	0 ± 0.57	1.51 ± 0.81	0 ± 0.92	0.6
- Ti, K	94.55 ± 0.19	0 ± 0.37	0.31 ± 0.19	0.78 ± 0.13	0 ± 0.31	2.73 ± 0.33	0.59 ± 0.19	0 ± 0.12	1.05 ± 0.26	0 ± 0.24	<0.01
Melt type m4											
9 major	54.23 ± 2.27	0 ± 3.67	6.26 ± 2.01	8.23 ± 1.55	10.55 ± 2.02	16.38 ± 4.42	0 ± 4.95	0 ± 2.21	4.35 ± 3.44	0 ± 2.70	33
- Ti	51.73 ± 0.26	3.61 ± 0.50	7.33 ± 0.30	8.17 ± 0.11	3.27 ± 0.63	17.77 ± 0.54	0 ± 0.46	0 ± 0.52	1.92 ± 0.45	6.22 ± 0.40	<0.01
- Ti, K	47.15 ± 0	12.15 ± 0	6.36 ± 0	6.88 ± 0	0 ± 0	15.97 ± 0	0 ± 0	2.17 ± 0	2.04 ± 0	7.29 ± 0	<0.01
Melt type m5											
9 major	29.65 ± 1.90	0 ± 0.61	0 ± 0.63	6.82 ± 0.60	19.70 ± 1.28	36.44 ± 2.60	5.26 ± 1.29	0 ± 0.60	2.89 ± 0.87	0 ± 0.62	20
- Ti	27.05 ± 1.28	0 ± 0.61	0.56 ± 0.60	4.02 ± 0.74	0 ± 0.80	41.85 ± 1.95	13.93 ± 1.30	4.28 ± 0.90	0 ± 0.59	6.64 ± 1.31	7.6
- Ti, K	20.13 ± 0.47	0 ± 0.53	0 ± 0.41	3.29 ± 0.30	2.35 ± 0.94	49.86 ± 0.92	10.38 ± 0.41	5.25 ± 0.42	0 ± 0.32	6.73 ± 0.60	<0.01
Melt type m6											
9 major	57.86 ± 2.21	0 ± 2.81	0.004 ± 1.54	10.48 ± 1.24	2.47 ± 2.26	19.02 ± 3.00	0 ± 2.35	0 ± 1.67	9.39 ± 2.29	0.18 ± 2.71	37
- Ti	56.64 ± 0.62	0 ± 1.00	2.82 ± 0.65	9.96 ± 0.37	0 ± 1.15	19.36 ± 1.01	0 ± 0.61	0 ± 0.71	3.37 ± 0.93	7.24 ± 0.67	1.4
- Ti, K	55.03 ± 3.26	3.58 ± 3.81	2.03 ± 1.09	9.16 ± 2.67	0 ± 3.93	19.36 ± 4.65	0 ± 1.86	0 ± 6.39	3.93 ± 3.20	6.92 ± 6.14	0.02

Note: Values in %. All compositions of the components were recalculated to 100% of the major oxides (SiO_2, TiO_2, Al_2O_3, FeO, MnO, MgO, CaO, Na_2O, K_2O, and P_2O_5). Calculations with all 9 major oxides (without P_2O_5), without TiO_2, and without TiO_2 and K_2O are shown. Symbols of rock forming minerals are after Kretz (1983); Qtz - quartz, Kfs - K-feldspar, Alb - albite, An - anorthite, Bt - biotite, Ms - muscovite, Chl - chlorite (chamosite), Hbl - hornblende, Rbk - riebeckite, Gru - grunerite. Compositions of the rock forming minerals are from Anthony et al. (1995) were used. Harmonic least-squares mixing calculations are after Stöckelmann and Reimold (1989).

[#] Discrepancy characterizes how well can be the mixture modeled from the components. The lower the discrepancy, the smaller the difference between the composition of the modeled and the real melt.

Table 8-9. Comparison of observed compositions (Table 8-4) of the melt types from the Eyreville drill core with compositions modeled from rock forming minerals with HMX mixing calculations (presented in this table). Values in wt%.

	Melt type m1a		Melt type m1b		Melt type m2		Melt type m3		Melt type m4		Melt type m5		Melt type m6	
	calculated	$\Delta_{obs-calc}$*	calculated	$\Delta_{obs-calc}$*	calculated	$\Delta_{obs-calc}$*	calculated	$\Delta_{obs-calc}$*	calculated	$\Delta_{obs-calc}$*	calculated	$\Delta_{obs-calc}$*	calculated	$\Delta_{obs-calc}$*
SiO_2	88.13	-0.03	74.33	-0.23	70.21	-0.02	97.20	<0.01	76.21	-0.11	59.20	<0.01	77.67	-0.07
TiO_2	0.12	0.58	0.50	0.71	0.40	0.38	0.04	0.01	0.44	0.27	0.72	0.27	0.17	0.72
Al_2O_3	6.15	0.58	6.29	8.85	13.91	1.99	1.20	0.40	12.41	0.19	20.11	5.19	12.02	0.28
FeO	2.07	0.09	5.16	-0.02	6.55	0.18	0.56	0.02	3.80	0.15	7.14	0.45	3.94	0.32
MnO	0.02	<0.01	0.06	<0.01	0.07	<0.01	0.01	<0.01	0.06	<0.01	0.11	-0.02	0.05	<0.01
MgO	0.74	-0.11	2.43	-0.58	2.76	-0.24	0.13	<0.01	1.40	-0.50	3.21	-0.26	0.65	-0.04
CaO	0.49	-0.01	1.26	-0.07	1.42	-0.04	0.18	<0.01	1.67	-0.01	1.41	-0.07	2.12	-0.25
Na_2O	0.32	<0.01	0.54	-0.02	0.92	-0.14	0.14	<0.01	1.17	<0.01	0.46	-0.06	0.80	-0.10
K_2O	1.34	-0.52	1.29	-0.48	2.81	-1.27	0.22	-0.04	2.78	-0.06	5.46	-3.37	2.28	-0.73

Note: Resulting compositions of the melt particles as obtained from the HMX mixing calculations are shown for runs with all 9 major oxides (without P_2O_5) presented in Table 8-8.

* Δobs-calc = difference between observed and calculated value

Comparison with sedimentary target rocks from Eyreville drill core

We have compared the average compositions of the melt types with target rocks and rock fragments drilled in the Eyreville drill core. The melt compositions normalized to 100% were compared with the crystalline basement lithologies, but especially with the different sedimentary clasts occurring in the Exmore breccia. Bulk analyses of all our Eyreville core samples are published in Schmitt et al. (2009).

The comparison shows that melt type m1a is closest to the composition of the gravelly sand or graywacke (e.g., sample CB6-089 or CB6-064, respectively). Melt type m1b is closest to a siltstone or graywacke (e.g., sample CB6-058, or CB6-060 and CB6-067), although the composition does not match so well. Melt type m2 has the major oxide values similar to siltstone or clay (e.g., samples CB6-058 and CB6-041). No bulk sample from the Eyreville drill core is Si-rich enough to give the composition of melt type m3; closest is the composition of gravelly sand (sample CB6-091). Melt type m4 can be best compared with the composition of the Exmore breccia. From the target lithologies, sandstone or graywacke clasts are closest (e.g., samples CB6-045 or CB6-060). Melt type m5 could be a melt of clay (compare samples CB6-053 and CB6-056). Melt type m6 has a similar composition and similar possible precursors as melt type m4. Melt type m6 is close to the Exmore breccia composition and from the target lithologies to a sandstone or graywacke (e.g., sample CB6-045 or CB6-060).

DISCUSSION

Compositional variations of the melt

As there are significant compositional variations in the melt type m1, we have separated the m1 melt particles into two distinctly different groups, m1a and m1b, corresponding to the two analyzed samples containing m1 (CB6-098 and CB6-097, respectively). We suggest that the different compositions of the m1 particles from the two samples can be explained by different degree of alteration of the two samples, besides possible different composition of the original melt particles. Melt type m1 seems to be one of the most pristine melt type under optical microscope, however, the detailed SEM study revealed some alteration (see Fig. 8-5b), which is further supported by the low totals. Melt type m2 is a very variable melt type. This is probably because it is a large category, where altered particles, some with larger differences in appearance, are grouped. This melt type has also a very large depth-range. The melt of type m3 has a relatively uniform composition, with high proportions of SiO_2 and only slight variations in composition. Variations in most oxides of melt type m4 are relatively low compared to the other melt types, but higher in CaO and Na_2O. The low variations can be due to a limited depth range of occurrence of

melt type m4. In melt type m5 there are high variations of FeO and also K_2O. These variations are probably primary, i.e., can not be explained only by different degree of alteration, because there are high variations even among particles from one sample. Variations of melt type m6 are low for most oxides, this is probably because this melt type is not abundant and thus only a few particles from only one sample were analyzed. There are high variations in CaO content, which could result from secondary hydrothermal alteration.

Precursors of the melt particles

In our earlier work we tried to use the HMX mixing calculations for determining the precursors of the melt particles. However, although the mixing calculations worked well for the modeling of the components of bulk suevite, the modeling of formation of melt particles yielded high discrepancies (Bartosova et al., 2009b). This might have had several possible reasons, including hydrothermal alteration of the melt particles, but also analytical limitations, as the earlier data were just EDX analyses.

Here we use precise microprobe data, but even so, melt types m3 and m5 could not be modeled as mixtures of target rocks, with reasonable discrepancies. In the mixing calculation using rock-forming minerals, melt type m3 was modeled as a mixture of quartz and a low amount of other minerals with very low discrepancies. The precursor of melt type m3 was probably quartz, quartzite, or a quartz arenite. Melt type m5 is a melt of a black shale, mudstone, or clay. These particles were partly melted or completely melted and are now recrystallized to fine-grained phyllosilicate minerals. Previous analyses have shown that the composition is similar to fine-grained sedimentary clasts from the suevite from the Eyreville drill core (Bartosova et al., 2009b). Composition of melt type m5 is also similar to some clay clasts from the Exmore breccia (see Schmitt et al., 2009, Appendix, e.g., sample CB6-053). Melt type m1a was formed form a SiO2 rich precursor, according to the mixing calculations probably the Potomac Formation, while melt type m1b has probably besides Potomac Formation a substantial amount of schist or gneiss. The melt type m2 could have been formed mainly from the basement gneiss and schist according to the mixing calculations. However, this melt type is strongly altered and the composition probably has been substantially changed during alteration. The calculations suggest that the melt type m4 precursors are sediments (mainly similar to Potomac Formation), plus schist and/or gneiss. Melt of type m6 was probably formed only from the lowermost sedimentary formations (also mainly the thickest Potomac Formation), but a schist component is also possible. These results are in agreement with the comparison of melt particles and target lithologies in Harker diagrams (Fig. 8-7).

The results of the mixing calculations are also generally in agreement with what can be derived from the ternary diagrams (Fig. 8-8). The diagrams further confirm that nearly

no mono-mineral melt was noted, even when single spot analyses were examined. Silica melt forms the melt type m3 (although in parts small amounts of other components and alteration phases occur) and rarely occurs as small parts in other melt types. The few other exceptions already mentioned are the undigested clasts, crystallites in m4, K-feldspar phase in m6 (Tab. 8-5), and a possible feldspar schlieren in m1 (Fig. 8-11b).
The mixing calculations model only the average composition of each melt type. In reality, each melt type is represented by individual melt particles, which have similar composition, but the range of the compositions is relatively wide and compositions of some melt types are overlapping (see Figs. 8-7 and 8-8). Thus, the mixing calculations should be considered with caution. We suggest that the mixing calculations can give a good estimate of the main component of the melt particles. However, especially for the minor contributions of different rock types (< 5 %), it is not very probable that these were really mixed in the melt, because no large homogenized melt source is expected. These chemical differences from the main component can be easier explained by inhomogeneities in target rocks or by later modification of the melt particles by alteration.

The comparison with the samples from the Eyreville drill core shows that the melt types are mostly comparable to some of the target sediments. The composition does not fit perfectly, but the suite of core samples does not cover all the pre-impact sedimentary lithologies. The target sediments contain a wide range of possible precursors, from clay to sandstone. Most of the mixing calculations show that the melts are formed mostly from the sedimentary formations. Only the melt types m2 and m5 seem to be mixtures of mainly the basement schist and/or gneiss according to the mixing calculations. But also for these melts, a possible sedimentary precursor can be found in the Eyreville samples. Furthermore, especially for these two melt types, the texture of the particles suggests rather a sedimentary precursor. Melt type m5 looks like melted or in some cases only partly melted shale or mudstone clast. For melt type m2, several cases have been noted where this melt type occurs together or as partial melt of a siltstone or graywacke (Figs. 8-4f-g). We suggest that most of the melt types could be derived from the different target sediments or their mixtures (compare also with analyses of clasts from Exmore breccia by Poag et al., 2004, p.235-239).

The impact breccias have been affected by hydrothermal alteration (e.g., Bartosova et al., 2009a; Horton et al., 2006), which influenced also the melt particles compositions, complicating the determination of the precursors. The melt composition can, for example, appear more silica-rich compared to the original melt composition, because the alkali and alkaline earth elements are more easily leached from the crystal or glass structure than Si and are replaced by H^+ or H_3O^+ (hydrolysis reactions; e.g., Righi and Meunier, 1995).

Comparison with previous studies of the Chesapeake Bay impact melt

In general, our present data are in good agreement with the preliminary analyses of (Bartosova et al., 2009). Important data were presented by Wittmann et al. (2009a, 2009b). In the study of Wittmann et al. (2009a), many of the melt particles analyzed by these authors have low totals (as low as ~ 70 wt%), similarly to our melt types m1b and m2. Wittmann et al. (2009a) sorted the melt particles in suevites mostly based on their shape and texture; no correlation between the shape and chemical composition or color and composition was noted. Our groups of melt particles based on the appearance show overlapping, but slightly different compositions. At least in some diagrams showing the relations of the chemical composition, the particles cluster into groups (Fig. 8-7). The triangular plot SiO_2-Al_2O_3-FeO+MgO by Wittmann et al. (2009a, Fig. 15) shows a trend similar to our melt particle analyses – there are particles with very high SiO_2 proportion, but then other with various amount of Al_2O_3 and FeO+MgO.

In our optical microscopy studies, complemented by microRaman spectroscopy, we did not found any high pressure polymorphs. First observations of coesite in the Chesapeake Bay impact structure were presented by Horton et al. (2009b), based on XRD and Raman studies of selected grains from the suevite from Eyreville drill core. These authors further reported occurrence of monoclinic tridymite, reidite (high-pressure $ZrSiO_4$); and baddeleyite (ZrO_2). Most of the melt particles from the Eyreville drill core have been changed by alteration. According to XRD analyses by Horton et al. (2009b), melt particles have been altered mostly to smectite.

Important phases and features of the melt

The compositional variations in the melt type m1 are probably partly primary (i.e., there are schlieren of different composition in the melt). But these differences could have been enhanced during the post-impact alteration, because the parts with different composition probably react differently with the alteration fluids. The changes by alteration have been observed e.g., near veinlets crosscutting the melt particles. The element map (Fig. 8-10c) shows that the melt particle is enriched in Si near the alteration vein. Silica could have been enriched by Si-rich fluids from the veinlet. Presence of Si-rich alteration fluids is documented also by the Si-rich rim in some melt particles (Fig. 8-10a). Also some secondary quartz filling vugs occurs in the melt-rich parts of the impact breccia (Bartosova et al., 2009a).

Other mineral phases also formed in the melt particles during post-impact alteration. Very abundant are tiny grains of anatase, which occur typically in the melt type m1 and m2. They are irregularly disseminated or concentrated along fractures and veinlets. Wittmann et al. (2009a) suggest that the low-temperature TiO_2 polymorph, anatase, which is disseminated in the form of small crystals in melt particles, was redistributed during the

post-impact hydrothermal alteration. Our observations are in agreement with this hypothesis, as the anatase crystals are abundant in tiny post impact veins intersecting the melt particles (see e.g., Fig. 8-10c).

Undigested clasts in melt include mostly quartz, feldspar, or rare zircon. The undigested clasts are most abundant in melt type m2 and m5. For these clasts the temperature was probably too low or the time was too short to dissolve the grains in the melt. In some cases the material of the original clast was not entirely melted or some clasts were incorporated into the melt particle later after its formation.

In the melt type m4, in the impact melt rock, crystallites of pyroxene and feldspar were noted. The occurrence of these crystallites is typical for the impact melt; they probably crystallized during the quenching of the impact melt. Feldspar and pyroxene microlites were described also in the impact melt from, e.g., Ries (Engelhardt, 1972, Osinski, 2003) or Chicxulub (Kring et al., 2004; Hecht et al., 2004).

In the melt-rich suevites and impact melt rocks, in SiO_2 clasts and also commonly in the melt type m3, ballen silica was found. Three different types of ballen quartz (according to Ferrière et al., 2009) were recognized. Additionally, rare ballen cristobalite was noted. Ballen quartz has been observed in about one fifth of the known impact craters, mostly from clasts in impact melt rocks, but also from suevites (Ferrière et al., 2009). The ballen silica forms by transformation from diaplectic quartz glass or by nucleation from lechatelierite. However, the exact process of formation of the different ballen types is not clear (Ferrière et al., 2009).

The zeolites, occurring in the melt-rich parts, are typical products of low-temperature hydrothermal alteration, and are known as typical hydrothermal association in terrestrial impact craters (Naumov, 2005). The zeolites (mordenite and paulingite) identified in the melt-rich parts indicate low-temperature hydrothermal alteration probably at ~100 °C (Chipera and Apps, 2001; Osinski, 2005).

Comparison with melt particles from Chicxulub and other craters

When we compare the melt particles from the Chesapeake Bay impact structure and from Chicxulub impact structure, the Chesapeake Bay melt particles are much more variable. In the plot Na_2O+K_2O versus SiO_2 by Hecht et al. (2004; Fig. 11) most of the particles from the Chicxulub drill core Yaxcopoil-1 plot into the field of andesite and trachyandesite. The Chesapeake Bay particles (Fig. 8-7) show much more scattered distribution and many of the melt particles have higher SiO_2 contents (commonly SiO_2 content >75 wt%, when renormalized to 100%). The analyzed melt particles from the Chesapeake bay impact seem to have much more variable composition than the melt particles from Chicxulub analyzed by Hecht et al. (2004); both the compositional range within each melt type and the composition range of the entire group of all melt particles are much larger. Melt type 3

from Chicxulub (Hecht et al., 2004) with pyroxene and feldspar crystallites could be compared to our melt type 4 – with pyroxene and feldspar. But the melt with crystallites from the Chesapeake Bay impact breccia (melt type m4) is different in composition, e.g., lower in MgO and CaO and more silica rich; Si is enriched in the "matrix" between the crystallites (Fig. 8-10d). Some of the melt particles from the Chicxulub impact structure have also relatively high CaO content (up to ~9 wt%), which is probably derived from the carbonate target rocks (Hecht et al., 2004). The Chicxulub target rocks were 2-3 km of carbonates and evaporites overlying a Pan-African basemen (Claeys et al., 2003, and references therein). The variability in composition of the melt particles from the Chesapeake Bay impact structure reflects the variability of the target rocks and suggests that there was no widespread homogenization of the melt, as was similarly suggested also for Chicxulub melt particles from the Yucatàn 6 well by Claeys et al. (2003). However, different degrees of alteration also could have enhanced the compositional variability.

In the upper part of the Eyreville core, mostly around 1415 m, melt type m1 occurs, with clear to brownish particles. Many of them are shard like and were probably solidified before and broken during deposition. Angular shards of holohyaline glass have been observed also in surficial suevites from the Ries Crater (e.g., Osinski et al., 2004). In the Ries crater, melt particles are preserved in the vitreous state in the bottom and top layers of the suevite, probably because these parts chilled faster than the interior section of the suevite (Engelhardt, 1972). In the Eyreville drill core from Chesapeake Bay, very altered melt particles occur also in the uppermost layer of the impact breccia (e.g., in sample CB6-093, depth =1399.2 m). While cooling rate and then hydrothermal alteration had substantial influence on the final appearance and composition of the melt particles, the primary compositional differences must have played also a significant role, because different melt types (e.g., m1 and m2) can be found within one sample.

When the analyses and ternary plots (Fig. 8-8) are compared with the ternary diagrams for melt particles from the Bosumtwi impact structure in Coney et al. (2009), the Chesapeake particles are closer to the within crater and south-of-crater suevite, but different from the north-of crater suevite. Most of the Bosumtwi melt particles plot closer to the Na_2O apex in the K_2O-Na_2O-CaO diagram compared to the Chesapeake Bay particles. Some of the melt analyses from south-of-crater Bosumtwi suevite plot into the SiO_2 apex, but have lower SiO_2 content then our melt type m3. Melt particles from within-crater and north-of-crater Bosumtwi suevite are generally less silica-rich, then the Chesapeake particles. However, the differences are of course primarily based on different target rocks, which are mostly metasedimentary rocks, meta-graywacke and phyllite-slate, together with some metavolcanic rocks and granitoids, in the case of Bosumtwi crater (Coney et al., 2009; Ferrière et al., 2007). Many particles from the within-crater Bosumtwi

impactites yielded very low totals (~ 70 wt%), similar to our observations for melt types m1b and m2.

Amount of melt in the Chesapeake Bay impact structure – comparison with other impact craters

The melt in the Chesapeake Bay impact structure is present mostly in the form of small melt particles, mm- to cm-sized. The maximum size of the particles observed in our samples is ~5 cm (sample CB6-109, depth = 1452.3 m) and ~6 cm in the core (Bartosova et al., 2009a).

The melt particles are most abundant in the upper part of the impact breccia, around 1405 and 1450 m (Bartosova et al., 2009a). There are only two thin intervals of the impact melt rock in the Eyreville drill core, 5.5 m and 1 m thick (depth intervals 1402.0–1407.5 and 1450.2–1451.2 m, respectively; Wittmann et al., 2009a, 2009b; Horton et al., 2009a). However, although most of the material in these intervals is partly or entirely melted, and the impact melt rocks are very clast-rich. In parts, especially in the boundaries to suevite, the rocks are transitional between impact melt rock and suevite. These impact melt intervals seem to accumulation of melted and partly melted material rather than a typical impact melt rock with clasts in melt matrix. In the upper part of the suevite, there are mostly the melt particles of type m1 and m2. In the impact melt rocks, the melt types m4 (in form of melt matrix) and m3 are typical and abundant. In the lower part of the impact breccias of the Eyreville drill core, the melt is much less abundant (Bartosova et al., 2009a) and only melt particles of type m2 and m5 occur. In the overlying Exmore breccia, the melt particles are rare but ubiquitous (Reimold et al., 2009). These particles probably originate from the ejecta plume and were incorporated into the surge-back sediments. There are some intervals in which the melt particles are enriched – these were probably deposited in a later stage of the surge-back process, when the ocean started to calm down (Reimold et al., 2009).

In such a large structure as the Chesapeake Bay impact structure, a continuous melt sheet is expected (Shah et al., 2005, 2009). Wittmann et al. (2009a) estimated the total mass of melt retained within the crater to be about 6 – 10.5 km^3. In the Chesapeake Bay impact structure, so far no large volumes of melt rock have been discovered. Shah et al. (2009) suggest that melt bodies might be present in the western part of the inner basin. Wittmann et al. (2009a) also mention the possibility that the melt rocks could have been reworked during the ocean resurge (maybe dispersed in reaction between the hot melt and seawater) or that an impact sheet is buried at depth. This would be similar to the Chicxulub impact structure, where a layer of impact melt underlies the suevite section (studies of Yucatán-6 drill core; Claeys et al., 2003). Osinski et al. (2008) suggested that

especially in the craters formed in sedimentary targets, a large amount of melt could be part of the groundmass. However, according to our microscopic and SEM observations, the groundmass of the suevites is clastic. Melt matrix occurs only in the impact melt rock intervals and some amount of melt can be present in the groundmass of the very melt-rich suevites near the impact melt rock intervals.

At many impact structures, even in those with smaller diameters, large continuous melt sheets have been observed. The Chicxulub impact structure (~180 km in diameter) probably contains a ~3 km thick impact melt sheet (Kring, 2005). In the Popigai impact structure (100 km in diameter), the sheet of impact melt rock (called tagamite) is hundreds of meters thick (Grieve and Cintala, 1992). In the Montagnais structure (45 km in diameter), the impact breccia on the central uplift contains two layers of recrystallized melt (71 and 35 m thick; Dypvik and Jansa, 2003). At the Manson impact structure (~36 km in diameter), which has the same size-range as the Chesapeake Bay impact structure (Wittmann et al., 2009a) a sheet of impact melt breccia, ~50 m thick, occurs in the central peak area (Koeberl, 1996b). Melt sheets also exist in some small craters formed in the crystalline rocks; at the Brent crater (originally ~3.8 km in diameter) there is 34-m-thick melt zone (Grieve and Cintala, 1992).

On the other hand, the volume of melt can be much smaller than expected from the crater size. A similar problem was encountered at the Bosumtwi impact structure, where the amount of melt in the drill cores (LB-07A and LB-08A) was much smaller than predicted (Koeberl et al., 2007; Artemieva, 2007). One possible reason could be an oblique impact, which would produce less melt (Wittmann et al., 2009a, and references therein). Also, the target rocks rich in volatiles can increase the excavation efficiency and thus the volume of excavated melt can be much larger than the volume preserved in the crater (Wittmann et al., 2009a; Kieffer and Simonds, 1980). This scenario – dispersion of impactites driven by the vaporization of water in the target rocks - has been proposed e.g., for the Bosumtwi impact structure (Artemieva, 2007). Also in some other impact structures, where the target rock included a thick sedimentary cover, the melt volume is relatively low, e.g., in Ries or Logoisk crater (Grieve and Cintala, 1992). Furthermore, Collins and Wünemann (2005) proposed that the Chesapeake Bay impact structure is so large mostly because of the special target properties – up to 1000 m of unconsolidated sediments and their high strength contrast to the basement rocks. These authors suggest that the diameter of the structure could have been as small as only 40 km if it had hit a more strong and homogeneous (terrestrial) target.

CONCLUSIONS

Tens of melt particles from the Chesapeake Bay impact structure have been studied by optical microscope, electron microprobe, and microRaman spectroscopy. Six different melt types have been recognized in the suevite and melt rock from the impact breccia section of the Eyreville drill core based on their appearance under the optical microscope and their chemical composition was measured.

Type m1 is a clear brownish melt, relatively homogeneous, slightly altered, with two subtypes – m1a with totals ~87 wt% and ~77 wt% SiO_2 and m1b with totals ~72 wt% and ~53 wt% SiO_2. Type m2 is a brownish melt, totally altered to phyllosilicate minerals, inhomogeneous, with abundant undigested clasts, and with low totals of ~80 wt% and ~56 wt% SiO_2. Type m3 is a colorless melt with some brownish stains, with >95 wt% of SiO_2 and totals close to 100 wt%. Melt type m4, with pyroxene and plagioclase crystallites forms matrix in the impact melt rocks, has ~75 wt% of SiO_2 and totals close to 100 wt%. Dark brown melt particles of type m5 have commonly undigested clasts, only 54 wt% of SiO_2, and the highest contents of Al_2O_3 and FeO; totals are ~91 wt%. The last melt type, m6, brownish melt with typical globular texture, occurs exclusively in the upper impact melt rock interval; it has 75 wt% of SiO_2 and the totals are ~96 wt%.

The different groups of melt particles have also different, but overlapping chemical compositions. However, chemical variations within one type of the melt particles, but also within some of the melt particles, are large. Particles display primary compositional differences due to schlieren and mixing of melt phases with different composition, and irregular distribution of crystallites and undigested clasts. There are also secondary changes due to the hydrothermal alteration – the melt particles were recrystallized to phyllosilicate minerals, and secondary minerals, such as zeolites or anatase, formed. Parts of the silica melt recrystallized to ballen quartz, and rare ballen cristobalite was also noted. Except for the nearly pure silica melt (melt type m3), no mono-mineralic melts were found. The chemical analyses and mixing calculations show that most of the melt particles are relatively silica-rich and probably originate from quartz-rich target rocks. We suggest that the pre-impact sediments could be precursors for all of the melt types. The pre-impact sedimentary formations (e.g., those similar to rocks from the Cretaceous age Potomac Formation) are main components for the melt types m1, m4, and m6. The melt types m2 and m5 most likely formed from a fine-grained, clay-rich sediment. The basement-derived schist or gneiss could also be involved in the formation of for some melt types (namely m2). The melt type m3 is melted quartz, quartzite, or quartz arenite. However, alteration could have substantially changed the composition of most melt types and makes the estimation of the melt precursors difficult.

Acknowledgments: The drilling at Eyreville was supported by ICDP, USGS, and NASA. We appreciate the professional work of general contractor DOSECC and drilling operator Major Drilling, USA. Peter Czaja is especially thanked for the electron microprobe measurements. The help of J. W. Horton Jr. and the staff at the USGS National Center, Reston, during the sampling process is highly appreciated. The present work was supported by the Austrian Science Foundation FWF, project P18862-N10 (to C.K.). The stay of K.B. in Berlin was supported by European Commission's Research Infrastructure Action via the SYNTHESYS Project. Ludovic Ferrière and Axel Wittmann are thanked for helpful and inspiring discussions and Dieter Mader for analytical support.

References:

Anthony J. E., Bideaux R. A., Bladh K. W., and Nichols M. C. 1995. *Handbook of Mineralogy, Volume II, Silica, Silicates*. Tucson: Mineral Data Publishing. 904 p.

Artemieva N. 2007. Possible reasons of shock melt deficiency in the Bosumtwi drill cores. *Meteoritics and Planetary Science* 42: 883–894.

Bartosova K., Ferrière L., Koeberl C., Reimold W. U., and Gier S. 2009a. Petrographic and shock metamorphic studies of the impact breccia section (1397 – 1551 m depth) of the Eyreville drill core, Chesapeake Bay impact structure, USA. In *The ICDP-USGS deep drilling project in the Chesapeake Bay impact structure: Results from the Eyreville core holes,* edited by Gohn G. S., Koeberl C., Miller K. G., and Reimold W. U. *Geological Society of America Special Paper* 458: 317-348.

Bartosova K., Mader D., Schmitt R. T., Ferrière L., Koeberl C., Reimold W. U., and Brandstaetter F. 2009b. Geochemistry of the impact breccia section of the Eyreville drill core, Chesapeake Bay impact structure, USA. In *The ICDP-USGS deep drilling project in the Chesapeake Bay impact structure: Results from the Eyreville core holes,* edited by Gohn G. S., Koeberl C., Miller K. G., and Reimold W. U. *Geological Society of America Special Paper* 458: 397-433.

Chipera S. J. and Apps J. A. 2001. Geochemical stability of natural zeolites. In *Natural zeolites: Occurrence, Properties, Applications,* edited by Bish D. L. and Ming D. W. *Reviews in Mineralogy and Geochemistry* 45: 117–161.

Claeys P., Heuschkel S., Lounejeva-Baturina E., Sanchez-Rubio G., and Stöffler D. 2003. The suevite of drill hole Yucatàn 6 in the Chicxulub impact crater. *Meteoritics and Planetary Science* 38: 1299–1317.

Collins G. S. and Wünnemann K. 2005. How big was the Chesapeake Bay impact? Insight from numerical modeling. *Geology* 33: 925–928.

Coney L., Reimold W. U., Gibson R. L., Koeberl C., and Ogilvie P. 2009. Melt particle characteristics of the within- and out-of-crater suevites from the Bosumtwi impact structure, Ghana: Implications for crater formation. In *Large Meteorite Impacts and Planetary Evolution IV,* edited by Gibson R.L. and Reimold W.U., *Geological Society of America Special Paper*. In press.

Deutsch A. and Koeberl C. 2006. Establishing the link between the Chesapeake Bay impact structure and the North American tektite strewn field: The Sr-Nd isotopic evidence. *Meteoritics and Planetary Science* 41: 689–703.

Downs R. T. 2006. The RRUFF Project: an integrated study of the chemistry, crystallography, Raman and infrared spectroscopy of minerals. Program and Abstracts of the 19th General Meeting of the International Mineralogical Association in Kobe, Japan. O03-13.

Dypvik H. and Jansa J. F. 2003. Sedimentary signatures and processes during marine bolide impacts: a review. *Sedimentary Geology* 161: 309–337.

Engelhardt W. von. 1972. Shock produced rock glasses from the Ries crater. *Contributions to Mineralogy and Petrology* 36: 265–292.

Ferrière L., Koeberl C., Reimold W. U., and Mader D. 2007. Drill core LB-08A, Bosumtwi impact structure, Ghana: Geochemistry of fallback breccia and basement samples from the central uplift. *Meteoritics and Planetary Science* 42: 689–708.

Ferrière L., Koeberl C., and Reimold W. U. 2009. Characterization of ballen quartz and cristobalite in impact breccias: new observations and constraints on ballen formation. *European Journal of Mineralogy* 1: 203-217.

Goderis S., Hertogen J., Vanhaecke F., and Claeys P. 2009. Siderophile elements from the Eyreville drill cores of the Chesapeake Bay impact structure do not constrain the nature of the projectile. In *Large Meteorite Impacts and Planetary Evolution IV,* edited by Gibson R.L. and Reimold W.U., *Geological Society of America Special Paper*. In press.

Gohn G. S., Koeberl C., Miller K. G., Reimold W. U., Cockell C. S., Horton J. W. Jr., Sanford W.E., and Voytek M.A. 2006. Chesapeake Bay impact structure drilled: *EOS, Transactions American Geophysical Union* 87: 349 & 355.

Grieve R. A. F. and Cintala M. J. 1992. An analysis of differential impact melt-crater scaling and implication for the terrestrial impact record. *Meteoritics* 27: 526-538.

Hecht L., Wittmann A., Schmitt R-T., and Stöffler D. 2004. Composition of impact melt particles and the effects of post-impact alteration in suevitic rocks at the Yaxcopoil-1 drill core, Chicxulub crater, Mexico. *Meteoritics and Planetary Science* 39: 1169-1186.

Horton J. W. Jr. and Izett G. A. 2005. Crystalline-rock ejecta and shocked minerals of the Chesapeake Bay impact structure, USGS-NASA Langley core, Hampton, Virginia, with supplemental constraints on the age of impact. *US Geological Survey Professional Paper* 1688: E1–E30.

Horton J. W. Jr., Powars D. S., and Gohn G. S. 2005. Studies of the Chesapeake Bay Impact Structure – Introduction and discussion: *US Geological Survey Professional Paper* 1688: A1–A24.

Horton J. W. Jr., Vanko D. A., Naeser C. W., Naeser N. D., Larsen D., Jackson J. C., and Belkin H. E. 2006. Postimpact hydrothermal conditions at the central uplift, Chesapeake Bay impact structure, Virginia, USA (abstract #1842). 37th Lunar and Planetary Science Conference. CD-ROM.

Horton J. W. Jr., Gohn G. S., Powars D. S., and Edwards L. E. 2008. Origin and emplacement of impactites in the Chesapeake Bay impact structure, Virginia, USA. In *The sedimentary record of meteorite impacts*, edited by Evans K. R., Horton J. W. Jr., King D. T. Jr., and Morrow J. R. *Geological Society of America Special Paper* 437: 73–97.

Horton J. W. Jr., Gibson R. L., Reimold W. U., Wittmann A., Gohn G. S., and Edwards L. E. 2009a. Geologic column for the ICDP-USGS Eyreville B core, Chesapeake Bay impact structure: Impactites and crystalline rocks, 1,096-1,766 m. In *The ICDP-USGS deep drilling project in the Chesapeake Bay impact structure: Results from the Eyreville core holes,* edited by Gohn G. S., Koeberl C., Miller K. G., and Reimold W. U. *Geological Society of America Special Paper* 458: 21-49.

Horton J. W. Jr., Kunk M. J., Belkin H. E., Aleinikoff J. N., Jackson J. C., and Chou I-M. 2009b. Evolution of crystalline target rocks and impactites in the Chesapeake Bay impact structure, ICDP-USGS Eyreville B core. In *The ICDP-USGS deep drilling project in the Chesapeake Bay impact structure: Results from the Eyreville core holes,* edited by Gohn G. S., Koeberl C., Miller K. G., and Reimold W. U. *Geological Society of America Special Paper* 458: 277-316.

Kieffer S. W. and Simonds C. H. 1980. The role of volatiles and lithology in the impact cratering process. *Review of Geophysics and Space Physics* 18: 143-181.

Koeberl C., Poag C. W., Reimold W. U., and Brandt D. 1996. Impact origin of the Chesapeake Bay structure and the source of the North American tektites. *Science* 271: 1263–1266.

Koeberl C., Reimold W. U., Kracher A., Träxler B., Vormaier A., and Körner W. 1996b. Mineralogical, petrological, and geochemical studies of drill core samples from the Manson impact structure, Iowa. In *The Manson Impact Structure, Iowa: Anatomy of an Impact Crater* edited by Koeberl C. and Anderson R.R. *Geological Society of America Special Paper* 302: 145–219.

Koeberl C., Milkereit B., Overpeck J. T., Scholz C.A., Amoako P. Y. O., Boamah D., Danuor S., Karp T., Kueck J., Hecky R. E., King J. W., and Peck J. A. 2007. An international and multidisciplinary drilling project into a young complex impact structure: The 2004 ICDP Bosumtwi Crater Drilling Project – An overview. *Meteoritics and Planetary Science* 42: 483–511.

Kretz R. 1983. Symbols for rock-forming minerals. *American Mineralogist*. 68: 277-279.

Kring D. A. 2005. Hypervelocity collisions into continental crust composed of sediments and an underlying crystalline basement: comparing the Ries (~24 km) and Chicxulub (~180 km) impact craters. *Chemie der Erde* 65: 1–46.

Kring D. A., Hörz F., Zurcher L., and Urrutia Fucugauchi J. 2004. Impact lithologies and their emplacement in the Chicxulub impact crater: Initial results from the Chicxulub Scientific Drilling Project, Yaxcopoil, Mexico. *Meteoritics and Planetary Science* 39: 879–897.

Lee S. R., Horton J. W. Jr., and Walker R. J. 2006. Confirmation of a meteoritic component in impact-melt rocks of the Chesapeake Bay impact structure, Virginia, USA - Evidence from osmium isotopic and PGE systematics. *Meteoritics and Planetary Science* 41: 819–833.

McDonald I., Bartosova K., and Koeberl C. 2009. Search for a meteoritic component in impact breccia from the Eyreville core, Chesapeake Bay impact structure: Considerations from platinum-group element contents. In *The ICDP-USGS deep drilling project in the Chesapeake Bay impact structure: Results from the Eyreville core holes,* edited by Gohn G.S., Koeberl C., Miller K.G., and Reimold W.U. *Geological Society of America Special Paper* 458: 469-479.

Naumov M.V. 2005. Principal features of impact-generated hydrothermal circulation systems: mineralogical and geochemical evidence. *Geofluids* 5: 165–184.

Osinski G. R. 2003. Impact glasses in fallout suevites from the Ries impact structure, Germany: An analytical SEM study. *Meteoritics and Planetary Science* 38: 1641–1667.

Osinski G. R. 2005. Hydrothermal activity associated with the Ries impact event, Germany. *Geofluids* 5: 202–220.

Osinski G. R., Grieve R. A. F., and Spray J. G. 2004. The nature of the groundmass of surficial 1040 suevite from the Ries impact structure, Germany, and constraints on its origin. *Meteoritics and Planetary Science* 39: 1655–1683.

Osinski G. R., Grieve R. A. F, Collins G. S., Marion C., and Sylvester P. 2008. The effect of target lithology on the products of impact melting. *Meteoritics and Planetary Science* 43: 1939–1954.

Poag C. W., Powars D.S., Poppe L. J., and Mixon R. B. 1994. Meteoroid mayhem in Ole Virginny: source of the North American tektite strewn field. *Geology* 22: 691–694.

Poag C. W., Koeberl C., and Reimold W. U. 2004. *The Chesapeake Bay Crater: Geology and Geophysics of a late Eocene Submarine Impact Structure, Impact Studies series.* Heidelberg: Springer. 522 p.

Reimold W. U., Bartosova K., Schmitt R. T., Hansen B., Crasselt C., Koeberl C., Wittmann A., and Powars D. 2009. Petrographic observations on the Exmore Breccia, ICDP-USGS Drilling at Eyreville, Chesapeake Bay impact Structure, USA. In *The ICDP-USGS deep drilling project in the Chesapeake Bay impact structure: Results from the Eyreville core holes,* edited by Gohn G. S., Koeberl C., Miller K. G., and Reimold W. U. *Geological Society of America Special Paper* 458: 655-698.

Righi D. and Meunier A. 1995. Origin of clays by rock weathering and soil formation. In *Origin and mineralogy of clays,* edited by Velde B., Berlin: Springer. 334 p.

Schmitt R. T., Bartosova K., Reimold W. U., Mader D., Wittmann A., Koeberl C., and Gibson R. L. 2009. Geochemistry of impactites and crystalline basement-derived lithologies from the ICDP-USGS Eyreville A and B drill cores, Chesapeake Bay impact structure, Virginia/USA. In *The ICDP-USGS deep drilling project in the Chesapeake Bay impact structure: Results from the Eyreville core holes,* edited by Gohn G. S., Koeberl C., Miller K. G., and Reimold W. U. *Geological Society of America Special Paper* 458: 481-541.

Shah A. K., Brozena J., Vogt P., Daniels D., and Plescia J. 2005. New surveys of the Chesapeake Bay impact structure suggest melt pockets and target-structure effect. *Geology* 33: 417–420.

Shah A. K., Daniels D. L., Kontny A., and Brozena J. 2009. Megablocks and melt pockets in the Chesapeake Bay impact structure constrained by magnetic field measurements and properties of the Eyreville and Cape Charles cores. In *Deep drilling in the Chesapeake Bay impact structure,* edited by Gohn G. S., Koeberl C., Miller K. G., and Reimold W. U. *Geological Society of America Special Paper* 458: 195-208.

Stöckelmann D. and Reimold W. U. 1989. The HMX mixing calculation program. *Mathematical Geology* 21: 853–860.

Thomas W. A., Chowns T. M., Daniels D. L., Neathery T. L., Glower. L. III., Gleason. R. J. 1989. The subsurface Appalachians beneath the Atlantic and Gulf coastal plains. In *Geology of North America: The Appalachian-Ouachita Orogen in the United States,* edited by Hatcher. R. D. Jr., Thomas W.A., and Viele, G.W. Boulder: Geological Society of America. F2: 445–458.

Wittmann A., Reimold W. U., Schmitt R. T., Hecht L., and Kenkmann T. 2009a. The record of ground zero in the Chesapeake Bay impact crater – suevites and related rocks. In *Deep drilling in the Chesapeake Bay impact structure,* edited by Gohn G. S., Koeberl C., Miller K. G., and Reimold W. U. *Geological Society of America Special Paper* 458: 349-376.

Wittmann A., Schmitt R.-T., Hecht L., Kring D. A., and Povenmire H. 2009b. Petrology of impact melt rocks from the Chesapeake Bay crater, USA. In *Deep drilling in the Chesapeake Bay impact structure,* edited by Gohn G. S., Koeberl C., Miller K. G., and Reimold W. U. *Geological Society of America Special Paper* 458: 377-396.

CHAPTER 9: SHOCK-METAMORPHISM INVESTIGATIONS OF QUARTZ GRAINS IN CLASTS FROM IMPACT BRECCIA OF THE EYREVILLE DRILL CORE, CHESAPEAKE BAY IMPACT STRUCTURE, USA

Katerina Bartosova* and Christian Koeberl

Department of Lithospheric Research, University of Vienna, Althanstrasse 14, A-1090 Vienna, Austria.

*Corresponding author: *E-mail: katerina.bartosova@univie.ac.at*

submitted to *Meteoritics and Planetary Science*, under review

ABSTRACT

The Chesapeake Bay impact structure, ~85 km-in-diameter, has been drilled in years 2005–2006 at Eyreville, Virginia, USA to a total depth of 1766 m. In the drill core, the abundance of shock-metamorphosed material is very variable with depth. Most abundant shocked mineral and lithic clasts, as well as melt particles, occur in suevite samples from the impact breccia section (1397–1451 m depth). Shocked quartz (i.e., quartz grains with planar fractures (PF) and/or planar deformation features [PDFs]) and melt particles, though rare, are also dispersed in the Exmore Formation unit (444–867 m depth). Other lithologies occurring in the Eyreville drill core show no clear evidence of shock-metamorphism (such as presence of PDFs); namely, the sedimentary lithic blocks in the basal part of the Exmore beds, the granitic megablock and the gravelly sand interval below, and the basement-derived schists and pegmatites.

In this study we report on the investigation of 40 samples from the impact breccia section. The proportion of shocked quartz grains was investigated in clasts of different lithologies; no linear trends with depth were noted. However, generally, the highly shocked clasts tend to become less abundant with increasing depth, and some differences between clasts of distinct lithologies were noted. Crystalline clasts (i.e., granitoids and schists/gneisses; derived from the crystalline basement) are commonly only slightly shocked (contain generally less than 10 rel% of shocked quartz grains). The clasts of metamorphosed sediments (mostly metasandstones) show a low proportion of shocked quartz grains (mostly <10 rel%). Sedimentary clasts (i.e., sandstone, wacke, and conglomerate) show a wide range of proportions of shocked quartz grains, with several of them being highly shocked clasts (most values between 0 and 40 rel%). Conglomerates show the highest proportion of shocked quartz grains of all types of clasts (up to 83 rel%). Polycrystalline quartz clasts, which could have been derived from various lithologies, are also commonly highly shocked (contain mostly between 10 and 40 rel% of shocked quartz grains). These hard non-porous clasts are possibly more liable to be shocked.

Universal-stage investigations of the crystallographic orientations of PDFs in quartz grains of several clasts show that the dominant PDF orientations are $\{10\bar{1}3\}$, $\{10\bar{1}2\}$, and also $\{10\bar{1}4\}$. Our results suggest that the investigated clasts were shocked at pressures of up to ~20 GPa. However, the impact breccia section is a mixture of target rocks shocked at different stages of shock metamorphism, including unshocked clasts, clasts with PFs and/or PDFs, partly melted clasts, melt particles, and impact melt rocks (suggesting shock pressures of up to ~60 GPa).

Keywords: Chesapeake Bay impact structure, shock-metamorphism, planar deformation features, universal stage

INTRODUCTION

Chesapeake Bay impact structure and the Eyreville drill core

Chesapeake Bay impact structure is one of the largest impact structures on Earth (Poag et al., 1994; Earth Impact Database). The structure is 35.3 Myr old (Horton and Izett, 2005) and ~85 km in diameter (Poag et al., 2004). The structure is located along the east coast of the United States, (see the map in, e.g., Horton et al. (2009a). However, it has been suggested that the large diameter is partly a result of the specific target properties – rheologic contrast between unconsolidated sediments and crystalline basement on the continental shelf – and consequent resurge and sliding processes during the impact formation (Collins and Wünnemann, 2005). These authors estimate that the transient crater diameter was only about 28 km. The structure has a specific complex crater shape described as “inverted sombrero” (Gohn et al., 2006a), with a deep inner crater that contains a small central uplift structure (Poag et al., 1999) surrounded by a shallower outer basin. Sedimentation resumed shortly after the impact, and today 200–550 m of postimpact sediments cover the impact structure (Poag et al., 2004), which is thus very well preserved.

Relatively abundant, but mostly shallow cores have been drilled in the Chesapeake Bay structure area (Poag et al., 2004). To better understand the complicated structure of the crater, it was decided to drill a deep core in the central part of the Chesapeake Bay impact structure. Before drilling the main core, a test hole – Sustainable Technology Park (STP) testhole – was drilled in 2004. Subsequently, three stacked drill cores, Eyreville A, B, and C, were recovered in years 2005–2006 at Eyreville farm, in Northampton County, Virginia. The Eyreville core was drilled to a total depth of 1766 m and recovered (from top to bottom) post-impact sediments, Exmore Formation, sediment boulders and sand, granitic megablock, gravelly sand, impact breccias (suevites and cataclastic gneiss

blocks), and basement-derived pegmatites and schists (Fig. 9-1a; Gohn et al., 2006a, 2006b; Edwards et al., 2009; Horton et al., 2009a).

Previous shock-metamorphism studies of impactites from the Chesapeake Bay impact structure

Prior to the drilling of the two deep cores – the STP testhole and the Eyreville core – in the center of the Chesapeake Bay impact structure, shocked clasts and grains were reported from the Exmore breccia, but also from ejecta recovered in deep sea cores (see Koeberl et al., 1996; Glass, 1989, 2002). Koeberl et al. (1996) reported abundant shocked quartz grains (i.e., quartz grains with planar fractures (PF) and/or planar deformation features (PDFs) and shocked granitic clasts in samples from the Exmore breccia recovered from four drill cores; namely Exmore, Windmill Point, Kiptopeke, and Newport News. Shock-metamorphism effects were found by these authors in quartz and feldspar grains. In addition, partly or nearly totally melted granitoid-derived clasts, commonly containing shocked quartz and feldspar grains, were noted by Koeberl et al. (1996). Shocked and melted clasts of sedimentary origin were very rare in the Exmore breccia samples investigated by Koeberl et al. (1996). In the Exmore breccia, PDFs were found to be much more common in quartz from crystalline basement fragments than in individual quartz grains (Koeberl et al., 1996; Poag et al., 2004). PDFs in quartz-bearing clasts from the Exmore breccia have orientations characteristic for shock-metamorphism and provided further evidence of an impact origin of the Chesapeake Bay structure (Koeberl et al., 1996). Koeberl et al. (1996) determined PDFs orientations in 24 quartz grains and the following orientations were reported by the authors of this study: (0001), $\{10\bar{1}3\}$, $\{10\bar{1}2\}$, $\{11\bar{2}2\}$, $\{10\bar{1}1\}$, $\{11\bar{2}1\}$, and $\{51\bar{6}1\}$. Further universal-stage (U-stage) determination of the crystallographic orientations of PDFs in 22 quartz grains from Exmore breccia samples (from the Exmore corehole) were performed by Poag et al. (2004). The most abundant PDF orientation reported by these authors was the $\{10\bar{1}3\}$ orientation, similarly to the measurements reported by Koeberl et al. (1996). Other PDF orientations noted by Poag et al. (2004) include the $\{10\bar{1}2\}$, $\{10\bar{1}1\}$, and $\{21\bar{3}1\}$ orientations.

In the Eyreville drill core (Fig. 9-1a), extremely rare shocked clasts were found in the Exmore breccia samples (Reimold et al., 2009; Glidewell et al., 2008). Shock-metamorphism effects in the impact breccia section have been qualitatively investigated (Bartosova et al., 2009; Wittmann et al., 2009a; Horton et al., 2009b), but only scarce quantitative studies and/or U-stage measurements were performed (see below).

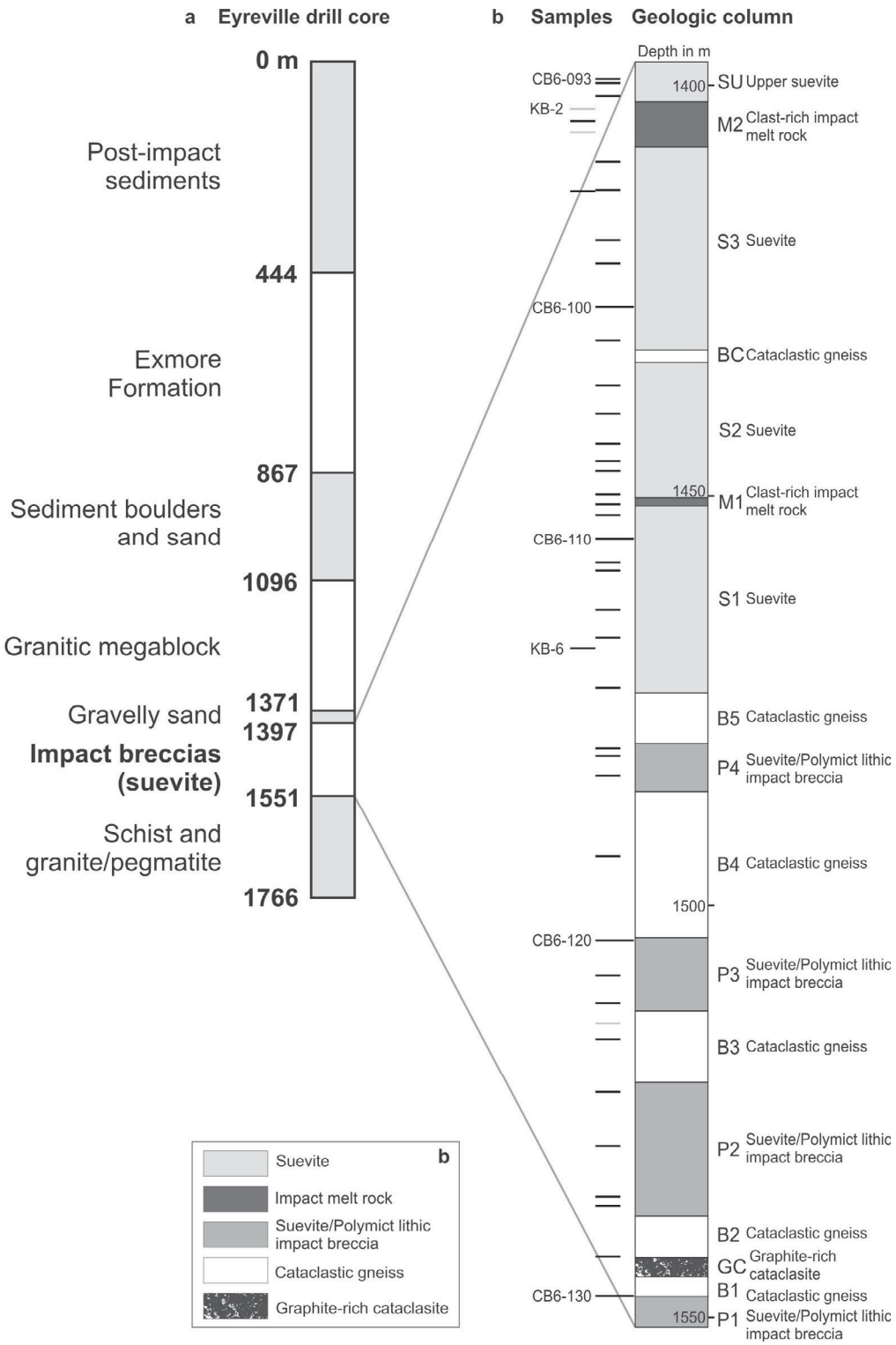

Fig. 9-1. Simplified stratigraphic column of the Eyreville drill core (a) showing the main lithologies and detailed geologic column of the impact breccia interval (b). Modified from Gohn et al. (2006a) and Horton et al. (2009a). Depth below surface in meters. Position of all samples is marked; samples investigated in this study are marked with black lines, three samples not used in this study with gray lines.

Bartosova et al. (2009) noted that PFs are much less common than PDFs in quartz grains from impact breccia samples. Mostly one or two sets of PDFs in quartz grains occur, and rarely three or four sets were observed by these authors (under the flat-stage optical microscope). In some quartz grains, the PDFs are difficult to resolve, such as in clasts of fine-grained gneiss. Frequently, PDFs are decorated with tiny fluid inclusions. Using transmitted electron microscopy (TEM), Bartosova et al. (2009) showed that PDFs are represented by planes of high dislocation density and that inclusions typically display negative crystal shapes with a maximum size of ~0.5 μm. Interestingly, no amorphous silica phase was observed by the authors along the PDF planes, showing that the original amorphous phase was totally recrystallized. Bartosova et al. (2009) also used a similar point counting method as the one used for the current study and reported on quartz grain characteristics (such as undulose extinction, toasted appearance, presence of PFs, PDFs, etc.) for 14 thin sections of suevite samples. The authors of this study noted if the investigated grains were single quartz grain in the matrix or part of a clast. No trends with increasing depth were found in the proportion of shocked grains for either all quartz grains or only the single grains in the matrix (Bartosova et al., 2009).

Glidewell et al. (2008) reported on shock-metamorphism effects from other units of the Eyreville drill core. Some weak shock-metamorphism effects, like mosaicism in quartz, were reported from gravelly sand samples. Weak shock-metamorphism effects were found also in the upper part of the granite megablock and features suggesting higher shock-metamorphism, including PFs and possible PDFs, were reported in quartz grains from the basement-derived schists and pegmatite section (Glidewell et al.; 2008). However, these observations have not been confirmed by other studies (e.g., Horton et al., 2009b; Townsend et al., 2009). Glidewell et al. (2008) performed also some U-stage measurements of PDFs in quartz grains from the Eyreville drill core. In the lower suevite (in the impact breccia section, below 1474 m depth), PDFs with orientations parallel to $\{10\bar{1}3\}$ were found to be dominant, but PDFs with $\{21\bar{3}1\}$ and $\{51\bar{6}1\}$ orientations were also noted. Rare PFs and PDFs were also found in quartz grains of the basement granite, in association with suevite dikes (Horton et al., 2009a).

Some high-pressure polymorphs of different minerals have also been described in impactite samples from the Chesapeake Bay impact structure. Jackson et al. (2006) reported on a shock-induced polymorph (TiO_2II) of anatase and rutile in suevitic impact breccias from the STP testhole. Wittmann et al. (2009a, 2009b) identified reidite – the high-pressure polymorph of $ZrSiO_4$ – in intergrowths with zircon in lithic clasts with metamorphic fabric in suevite samples from the Eyreville drill core. Coesite was reported for the first time in the Chesapeake Bay impact structure by Horton et al. (2009b), in mineral concentrates from the upper suevite unit from the Eyreville drill core.

SAMPLES AND METHODS

All samples investigated in this study were collected from the impact breccia interval of the Eyreville B drill core (1397–1551 m; Fig. 9-1b). It comprises 30 samples of suevite, one sample of polymict impact breccia, one sample of impact melt rock, five samples of cataclastic gneiss, and three samples of a conglomerate clast from suevite; the position of the investigated samples is reported in Fig. 9-1b.

One to four thin sections of each of the samples were prepared. The thin sections were carefully examined under the optical microscope and the ones that were deemed suitable for further shock-metamorphism investigations were selected.

The main part of this study is based on a systematic analysis of the relative proportion of shocked quartz grains (i.e., quartz grains with PFs and/or PDFs). Only quartz grains with sizes larger than 50 μm within a given lithic clast were examined and data were collected separately for each different type of rock clast. Only clasts with quartz grains generally larger than 50 μm in diameter were considered. Thus, no siltstone, mudstone, and shale clasts were studied. Furthermore, only large enough clasts containing more than 20 quartz grains were counted. In respect to evaluate the statistical significance of our results, three categories of clasts were distinguished: clasts with 20–49 quartz grains, with 50–99, and with 100 and more quartz grains. Counting through each clast was done along traverses spaced usually at 0.2–0.3 mm, depending on the size of the clast and of the grains within the clast considered. Properties of quartz grains; e.g., undulose extinction, presence of fluid inclusions, toasted appearance, PFs, and PDFs (and number of sets) was noted.

The second part of this study consists of U-stage investigations of the crystallographic orientations of PDFs in quartz grains. A four-axis U-stage mounted on an optical microscope was used (see, e.g., Reinhard, 1931 and Emmons, 1943 for general information). The conventional method, as reported in Engelhardt and Bertsch (1969), was used for the indexing of the planes measured. However, the new version of the stereographic projection template reported in Ferrière et al. (2009) was preferred because it allows the indexing of five more characteristic crystallographic orientations of PDFs in quartz than the template reported in Engelhardt and Bertsch (1969). Due to the U-stage layout, only clasts in the central part of the thin sections were investigated. In accordance with recommendations by Ferrière et al. (2009), a large number of PDF sets were measured in each individual clast. Thus only clasts with enough quartz grains showing PDFs were investigated. For each clast, the number of investigated quartz grains and of PDF sets was noted. Only absolute frequency (see, e.g., Engelhardt and Bertsch 1969; Ferrière et al., 2009), with unindexed PDF sets excluded, are presented here. The PDF sets that plot into the overlapping zone between $\{10\bar{1}3\}$ and $\{10\bar{1}4\}$ crystallographic orientations were counted as a separate category.

RESULTS

Shock-metamorphism effects in the impact breccia section of the Eyreville drill core

In the Eyreville drill core, most abundant effects of shock-metamorphism can be found in the impact breccia section (1397-1551 m). Clasts of all stages of shock-metamorphism, including unshocked clasts, rare PFs and common PDFs in quartz grains (Figs. 9-2a-c), partly melted clasts, as well as melt particles, occur in suevite samples (e.g., Bartosova et al., 2009; Wittmann et al., 2009a). Quartz grains with toasted appearance are also common (Figs. 9-2c, d). The proportion of melt particles in suevite has been already the subject of detailed investigations by Bartosova et al. (2009) and Wittmann et al. (2009a).

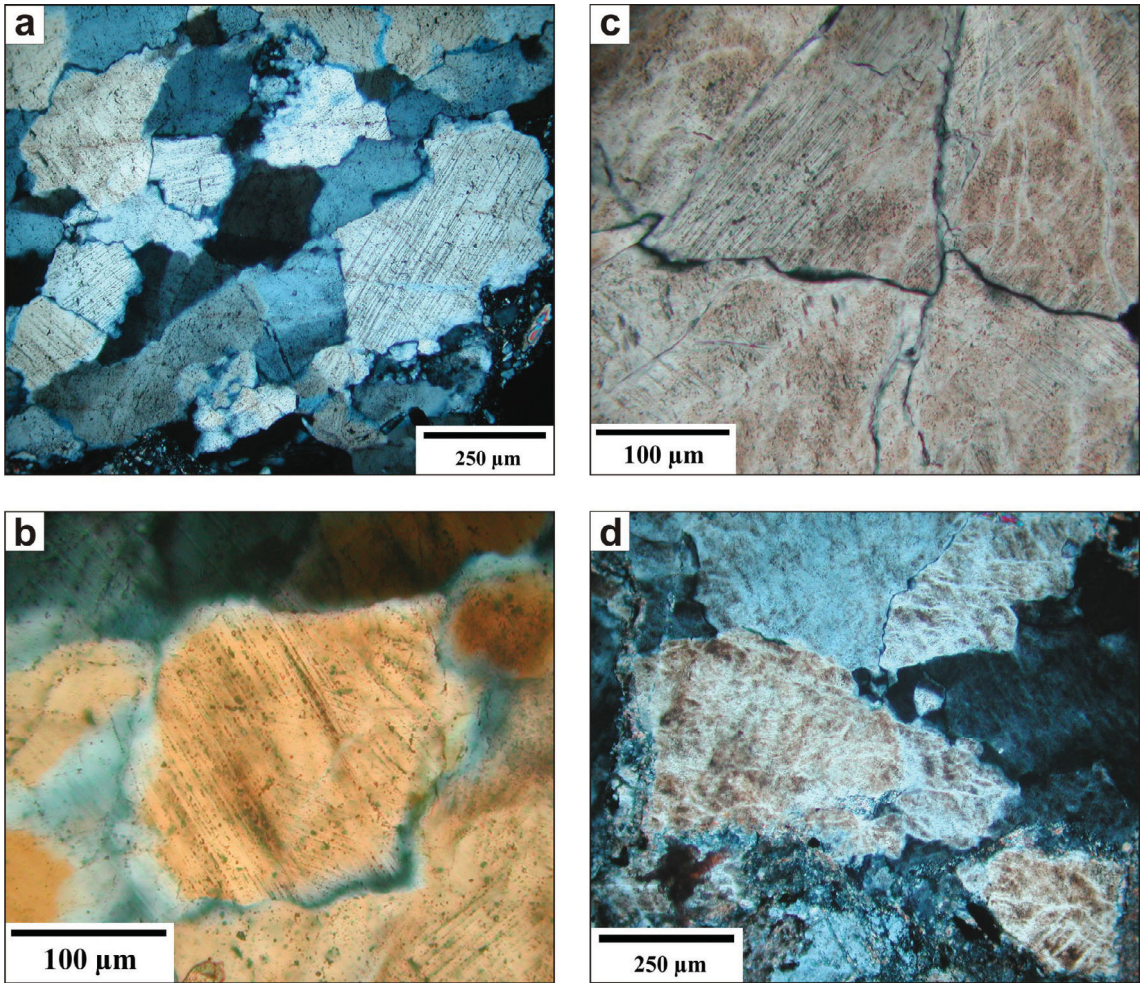

Fig 9-2. Microphotographs (in cross-polarized light) of shock-metamorphism effects in quartz grains. a) Quartz grains with one prominent set of PDF in a polycrystalline quartz clast from sample CB6-105, 1445.76 m depth. b) Quartz grain with two sets of decorated PDF in a polycrystalline quartz clast from sample CB6-102, 1436.56 m depth. c) Toasted quartz grains with PDFs in a granitoid clast from sample CB6-100, 1427.01 m depth. d) Toasted quartz grains in a conglomerate clast, sample CB6-112, 1459.20 m depth.

Table 9-1. Proportions of shocked quartz grains (in rel%) in investigated clasts of different lithologies occurring in samples from in the impact breccia section of the Eyreville drill core.

Sample	Depth (m)	Lithology*	Average	Median	Polycrystalline quartz (pq)								Pq of sedimentary origin		Fine-grained pq	Pq with fine-grained parts		Sandstone				Conglomerate
					Clast 1	2	3	4	5	6	7	8	1	2	1	1	2	1	2	3	4	1
CB6-093	1399.22	sv	21	27	29													27				
CB6-094	1399.73	sv	16	13																		
CB6-095	1401.31	sv	42	42																		83
KB-3	1404.35	imr	4.5	4.5																		
CB6-096	1409.30	sv	8.9	7.9	25																	
CB6-097	1412.75	sv	19	21	20	4.3	22	39										35	22			
KB-5	1412.87	sv	16	19	22	16	25											31				
CB6-098	1418.81	sv	15	19	19	27	26											0.3				
CB6-099	1421.65	sv	11	4.0	41	9.1	17	36							9.1							
CB6-100	1427.01	sv	23	19												39						
CB6-101	1431.10	sv	14	11	43	25	33	21							4.9							
CB6-102	1436.56	sv	7.9	4.5												8.3	n.d.†					
CB6-103	1440.00	sv	19	22	13	22										22						
CB6-104	1443.65	sv	20	23	7.7	41	32	32	22	27	30	24										
CB6-105	1445.76	sv	14	14	16													20	21	21	8.5	
CB6-106	1446.95	sv	10	8.1																		
CB6-107	1449.81	sv	13	12																		
CB6-108	1451.01	sv	2.9	3.6	n.d.																	
CB6-109	1452.33	sv	6.3	1.8																		
CB6-110	1455.22	sv	5.3	2.3														2.3				
CB6-111	1458.22	sv	65	77									77	92								
CB6-112	1459.20	cg	56	56																		56
CB6-113	1463.98	sv	14	8.3									36					4.7				
CB6-114	1467.37	sv	14	13														21				
KB-6	1468.65	cg	53	53																		53
CB6-115	1473.46	sv	11	11																		
CB6-116	1480.81	sv	3.4	2.0	n.d.	9.1												7.3				
CB6-117	1481.74	sv	12	7.1	9.5	17												38	20			
CB6-118	1484.13	sv	6.5	5.2														6.1	4.3	1.6		
CB6-119	1494.04	gn	6.0	6.0																		
CB6-120	1504.25	sv	4.0	2.1									5.1					0.9	1.8	n.d.		
CB6-121	1508.49	sv	10	13														23				
CB6-122	1511.86	gn	4.5	4.5																		
CB6-124	1516.23	gn	4.0	4.0																		
CB6-125	1522.72	cg	70	70																		70
CB6-126	1529.27	sv	28	27														28				
CB6-127	1535.40	sv	13	4.2	n.d.													0.8				53
CB6-128	1536.51	plb	0.5	0.2	2.0	0.5																
CB6-129	1542.65	gn	n.d.	n.d.																		
CB6-130	1547.41	gn	5.4	5.4																		

Note: Color highlights of the results depend of the number of quartz grains counted per investigated clast; dark gray - 20 to 49 quartz grains counted, light gray - 50 to 99 quartz grains counted, no color - 100 and more grains counted.

* Lithology: cg - conglomerate, gn - cataclastic gneiss, imr - impact melt rock, plb - polymict lithic breccia, sv - suevite

† Not detected

Table 9-1. *Continued* Proportions of shocked quartz grains (in rel%) in investigated clasts of different lithologies occurring samples from in the impact breccia section of the Eyreville drill core.

Sample	Depth (m)	Wacke					Slightly metamorphosed sediments			Metamorphosed sediments		Granitoid		Gneiss/Schist				Other				
		Clast 1	2	3	4	5	1	2	3	1	2	1	2	1	2	3	4	1	2	3	4	5
CB6-093	1399.22	29	26	28			4.5	n.d.†														
CB6-094	1399.73	12	15				27	8.7														
CB6-095	1401.31											0.8										
KB-3	1404.35													7.7				1.3				
CB6-096	1409.30	7.9					n.d.	8.3	3.3													
CB6-097	1412.75									23								4.5	33	3.8	14	0.9
KB-5	1412.87	2.0												5.6	0.6			23				
CB6-098	1418.81									n.d.								19				
CB6-099	1421.65						n.d.	n.d.		2.0				3.6	2.1			4.0				
CB6-100	1427.01						n.d.					15	58					n.d.	22			
CB6-101	1431.10						n.d.	2.4						4.0				n.d.	16	17	4.9	
CB6-102	1436.56									7.0	4.5			10	3.1	3.1		n.d.	35			
CB6-103	1440.00																					
CB6-104	1443.65													2.7	15	4.9	2.8					
CB6-105	1445.76	2.0					13	13														
CB6-106	1446.95						8.1			16		29		3.6	n.d.	n.d.		14				
CB6-107	1449.81	12																24	1.9			
CB6-108	1451.01													3.4				3.8	4.3			
CB6-109	1452.33	17					n.d.							1.8								
CB6-110	1455.22																	14	n.d.			
CB6-111	1458.22																	24				
CB6-112	1459.20																					
CB6-113	1463.98	11								5.3												
CB6-114	1467.37	5.1	4.3															25				
KB-6	1468.65																					
CB6-115	1473.46													11								
CB6-116	1480.81													2	n.d.	3.8	1.4					
CB6-117	1481.74	33					n.d.	2.0	0.4	4.8								n.d.				
CB6-118	1484.13																	14				
CB6-119	1494.04													6.0								
CB6-120	1504.25	n.d.	14	3.8	8.6	12	3.4	0.4		2.1				n.d.								
CB6-121	1508.49	n.d.	13	n.d.	n.d.	22												14				
CB6-122	1511.86													4.5								
CB6-124	1516.23													4.0								
CB6-125	1522.72																					
CB6-126	1529.27	44	14	26																		
CB6-127	1535.40	6.2												4.2								
CB6-128	1536.51											0.3		n.d.				n.d.	n.d.			
CB6-129	1542.65													n.d.								
CB6-130	1547.41													5.4								

Note: Color highlights of the results depend of the number of quartz grains counted per investigated clast; dark gray - 20 to 49 quartz grains counted, light gray - 50 to 99 quartz grains counted, no color - 100 and more grains counted.

* Lithology: cg - conglomerate, gn - cataclastic gneiss, imr - impact melt rock, plb - polymict lithic breccia, sv - suevite

† Not detected

In our study, only unmelted clasts, preserved well enough to recognize their nature (lithology) and shock-metamorphism effects in quartz grains, were investigated. In the impact melt rock samples, only rare unmelted clasts are present, and, thus, our investigations were somewhat limited for these samples. Shock-metamorphism effects are ubiquitous in the suevite samples. In samples of cataclastic gneiss blocks, shock-metamorphism effects are also present. In the lowermost samples (e.g., in the polymict breccia sample CB6-128 and in the cataclastic gneiss sample CB6-130) only rare PDFs were noted. In cataclastic gneiss sample recovered at 1542.7 m (sample CB6-129) no shock-metamorphism effects were found.

Point counting of shock metamorphism-effects

Point counting of shock-metamorphism effects in quartz grains was performed for all 40 samples. For some samples, more than one thin section was investigated. A total of more than 27,000 quartz grains were examined in about 200 clasts.

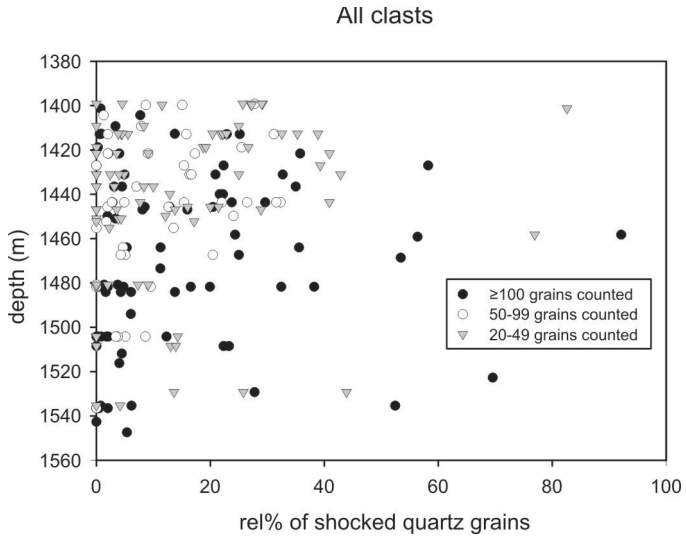

Fig. 9-3. Diagram showing results of special point counting of shock-metamorphism effects in quartz grains. Samples of the impact breccia interval were investigated. All studied clasts are shown in this diagram. Three groups differing in number of grains investigated are plotted with different symbols.

The proportion of shocked quartz grains was calculated for each clast (Table 9-1, Figs. 9-3-5). Because the number of counted grains, i.e., the statistical value of the measurement, differs for each clast, the clasts were grouped into three categories in Fig. 9-3. Also average and median values of the relative proportion of shocked quartz grains for each sample were calculated (Fig. 9-4). For further evaluation of the results, the clasts were sorted according to their lithologies and grouped into several categories: polycrystalline quartz clasts, sedimentary clasts (sandstone, wacke, and conglomerate), metamorphosed sedimentary clasts, and crystalline rock clasts (Fig. 9-5). However, several clasts that could not be definitely grouped into one of these categories are shown only in Fig. 9-3.

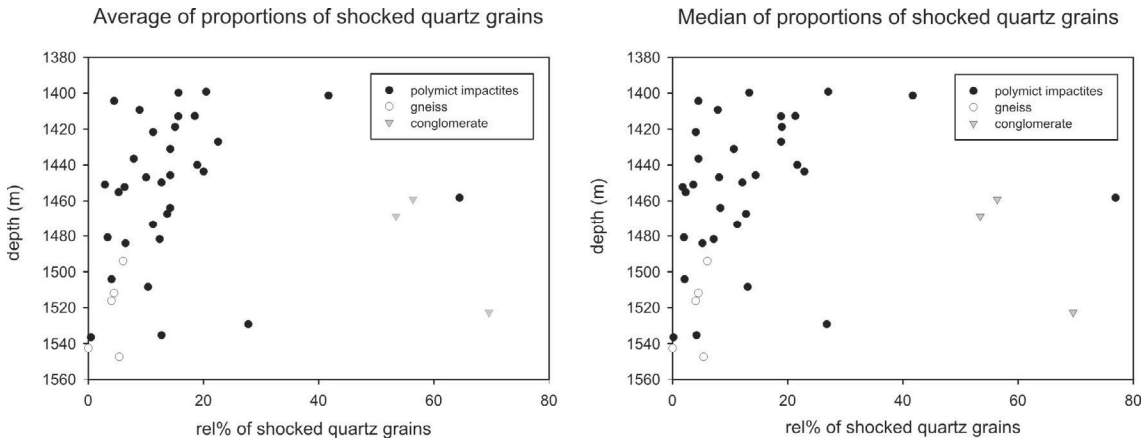

Fig. 9-4. Diagram showing results of point counting of shock-metamorphism effects in quartz grains. Average (a) and median (b) values of proportions of shocked quartz grains of all clasts in one sample are shown. Note the slight decreasing trend with increasing depth.

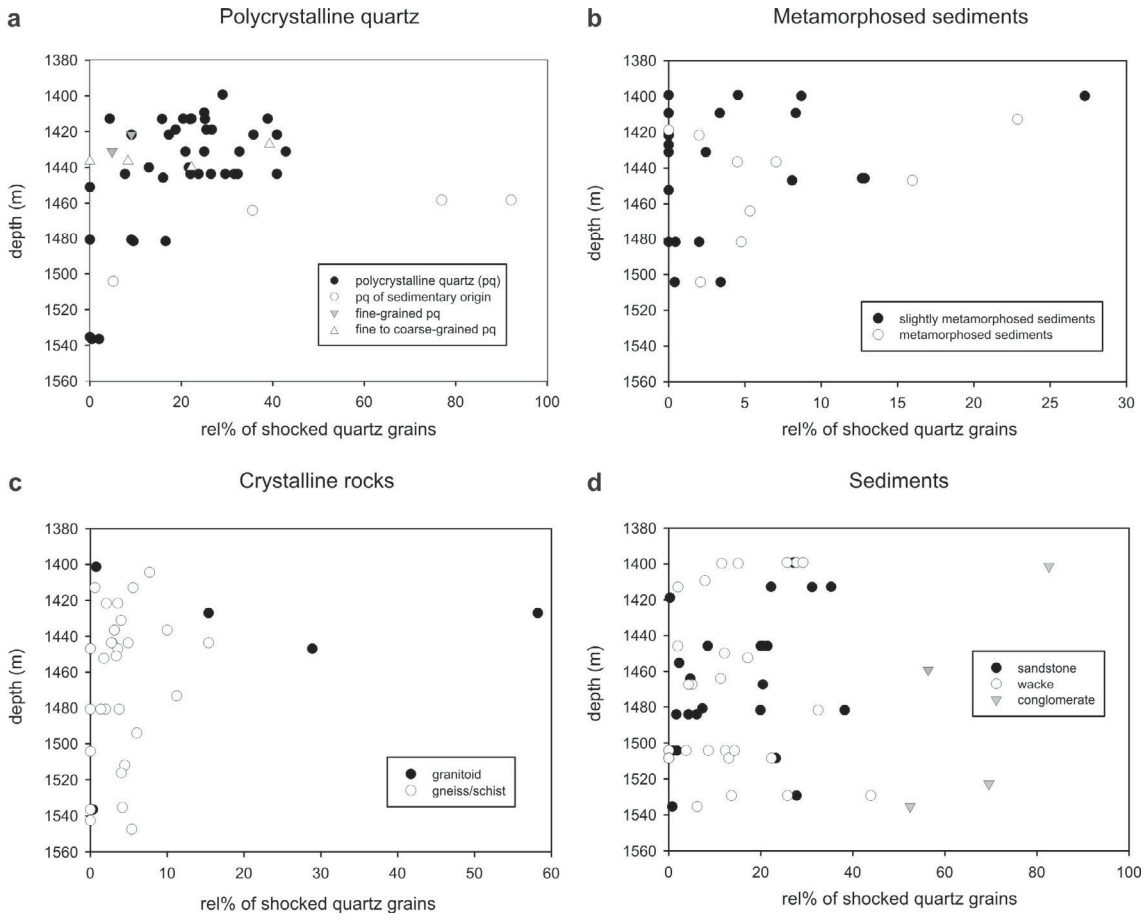

Fig. 9-5. Diagram showing results of special point counting of shock-metamorphism effects in quartz grains. The investigated clasts are sorted into categories according to their lithology.

Clast lithologies

The different clast lithologies are described here to provide some information on the texture, mineralogy, and grain-sizes of the clasts. Microphotographs of typical clasts of the investigated lithologies are shown in Fig. 9-6. The polycrystalline quartz clasts are composed only of quartz, with quartz grains of different shapes and sizes; typically the grains have irregular shapes, with no interstitial matrix, and grain size between ~0.1–0.5 mm (Fig. 9-6a). A few polycrystalline quartz clasts are probably of sedimentary origin, as the original texture with rounded quartz grains is apparent. Polycrystalline quartz clats with smaller grain size (<0.1 mm) were grouped into the category "fine-grained polycrystalline quartz" (Fig. 9-6b). The granitoid category includes typically granite, with quartz, feldspar, and mica, mostly medium-grained, with quartz grain sizes commonly ~0.2–0.3 mm (Fig. 9-6c). Gneiss clasts are mostly fine-grained (grain size around 0.05 mm), with aligned grains of especially mica. The gneiss consists mainly of quartz, mica, and feldspar. It can also contain parts of polycrystalline quartz with usually coarser grains (~0.2 mm; Fig. 9-6d). Schist clasts are less abundant than gneiss clasts. The schists have more mica and better aligned grains (Fig. 9-6e). They consist of mainly mica and quartz, and can contain also feldspar and graphite. The quartz grains have sizes ~0.05-0.1 mm. The conglomerate clasts are not so common, but occur as relatively large clasts in the suevite (of typically tens of cm in diameter). The subangular to rounded clasts within the conglomerates are embedded in fine-grained matrix and are 0.2–4 mm in size (Fig. 9-6f). The clasts within conglomerate comprise quartz and feldspar, as well as lithic clasts such as siltstone, sandstone, graywacke, and rarely also granite. Sandstone clasts consist typically only of quartz, but rare other minerals occur (Fig. 9-6g). There is only small amount of matrix in between the subangular to rounded grains; the grain size is typically 0.1–0.15 mm. Graywacke clasts have higher amount of matrix compared to sandstone clasts (Fig. 9-6h) and contain mostly quartz grains, but also feldspar grains with grain sizes between 0.05–0.3 mm. Opaque minerals are common in some graywacke clasts. The metamorphosed sediments are mostly sandstones, in which some metamorphic overprint is apparent, typically in the presence of aligned mica grains (Fig 9-6i). Two categories – slightly metamorphosed and metamorphosed (with higher proportion of aligned grains) were distinguished. The grain sizes of these clasts, consisting mostly of quartz, with some mica, are typically 0.05–0.1 mm.

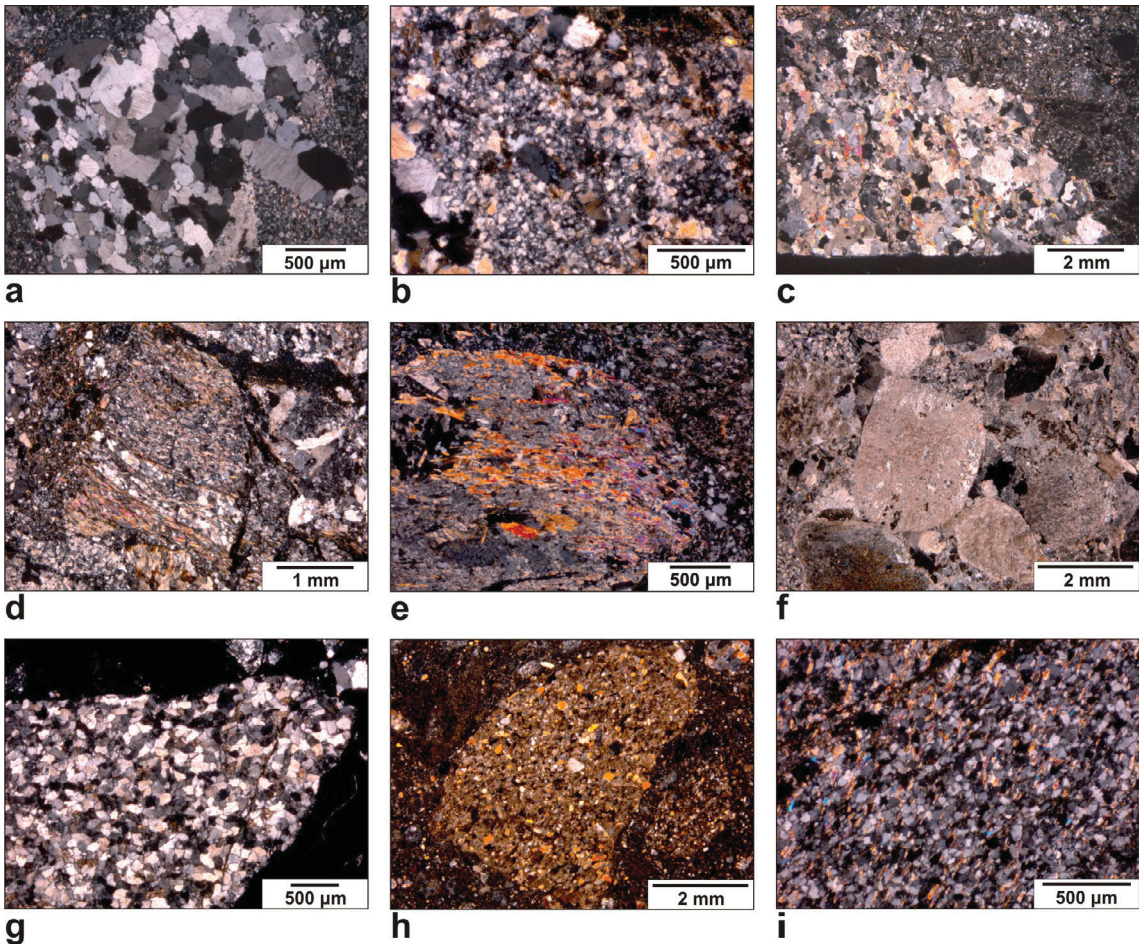

Fig. 9-6: Microphotographs of clasts of different lithologies in cross polarized light. a) Polycrystalline quartz clast from sample CB6-101. b) Fine-grained polycrystalline quartz clast from sample CB6-099. c) Granitoid clast from sample CB6-100. d) Gneiss clast from sample CB6-104. e) Schist clast from sample CB6-106. f) Conglomerate clast from sample CB6-112. g) Sandstone clast from sample CB6-117. h) Graywacke clast from sample CB6-093. i) Metamorphosed sandstone clast from sample CB6-109.

Trends in distribution of the shock-metamorphism effects

According to our shock counting results (Table 9-1, Figs. 9-3 and 9-4), there is no clear linear trend of proportion of shocked quartz grains with increasing depth. The results suggest however that highly shocked clasts become generally less abundant with increasing depth. Nevertheless, there are some exceptions to this trend, e.g., the highly shocked conglomerate samples or relatively highly shocked clasts in the suevite samples CB6-111 and CB6-126.

Our investigations seem to indicate that the proportion of shocked quartz grains in the different clasts investigated is rather dependent on the lithology of clast (i.e., also on the original position of the clasts in the target; Fig. 9-5) than on the present depth of the clasts in the core. The polycrystalline quartz clasts are commonly highly shocked (Fig 9-5a). Values between 20 and 40 rel% of shocked quartz grains are common, although some polycrystalline quartz clasts have lower proportion of shocked quartz. In the lower parts of

the impact breccia section (below ~1470 m) only relatively less shocked polycrystalline quartz clasts (with <17 rel% of shocked quartz grains) occur. The metamorphosed sedimentary clasts are much less shocked (Fig. 9-5b) and have mostly less than ~10 rel% of shocked quartz grains, with only a few clasts being more shocked. Somewhat similar proportions were found for crystalline clasts – mostly gneiss/schist and some granitoid clasts (Fig 9-5c). Only few crystalline clasts have more than 10 rel% of shocked quartz grains. However, there are some outliers – e.g., a granitic clasts with very high proportion of shocked quartz grains, discussed below. The sedimentary clasts (sandstones, wackes, and conglomerates; Fig. 9-5d) show very variable values of rel% of shocked quartz grains from 0 to ~40 rel%. Conglomerate clasts are clearly the most shocked clasts with up to ~83 rel% of shocked quartz grains.

In the conglomerates, only the single quartz grains, commonly coarse sand to pebble sized, were counted. The conglomerates also include clasts of other lithologies, such as pebbles of sandstone with small sand-sized quartz grains. These sandstone clasts within conglomerate clasts, investigated in samples CB6-095 and CB6-127, are also highly shocked, but have a lower proportion of shocked quartz grains than the single quartz grains in the host conglomerate clast. Some granitic pebbles were also noted as component of the conglomerate clasts. It is possible that the highly shocked granitic clast from sample CB6-100 could have originated from a conglomerate.

In samples of the cataclastic gneiss blocks, the shock-metamorphism effects seem to be distributed rather heterogeneously. The gneiss clasts are generally not much shocked and contain generally less than 10 rel% of shocked quartz grains. In cataclastic gneiss sample CB6-122 quartz grains from all the thin section were studied, but in addition, polycrystalline quartz parts occurring in the gneiss were studied separately. Some of these parts of polycrystalline quartz appear to be more shocked (have up to 20 rel% of shocked quartz grains) than the finer-grained parts containing also other minerals (mostly mica). These observations suggest that the coarser-grained polycrystalline quartz parts of gneiss are more liable to develop PDFs than the finer grained parts with abundant mica. It is probable that some of the polycrystalline quartz clasts that we investigated were originally part of a gneissic unit and now occur as clasts in the matrix of suevite samples.

Universal-stage investigations

Six suitable lithic clasts were selected for detailed U-stage investigations. Clasts of different lithologies were selected in order to compare possible differences between clasts of different origin. Three of the investigated clasts are polycrystalline quartz clasts, which are abundant in the investigated thin sections and commonly contain nicely developed decorated PDFs. Two clasts of sandstone and one granitoid clast were also investigated with the U-stage. The results are presented in Table 9-2 and in Figures 9-7 and 9-8.

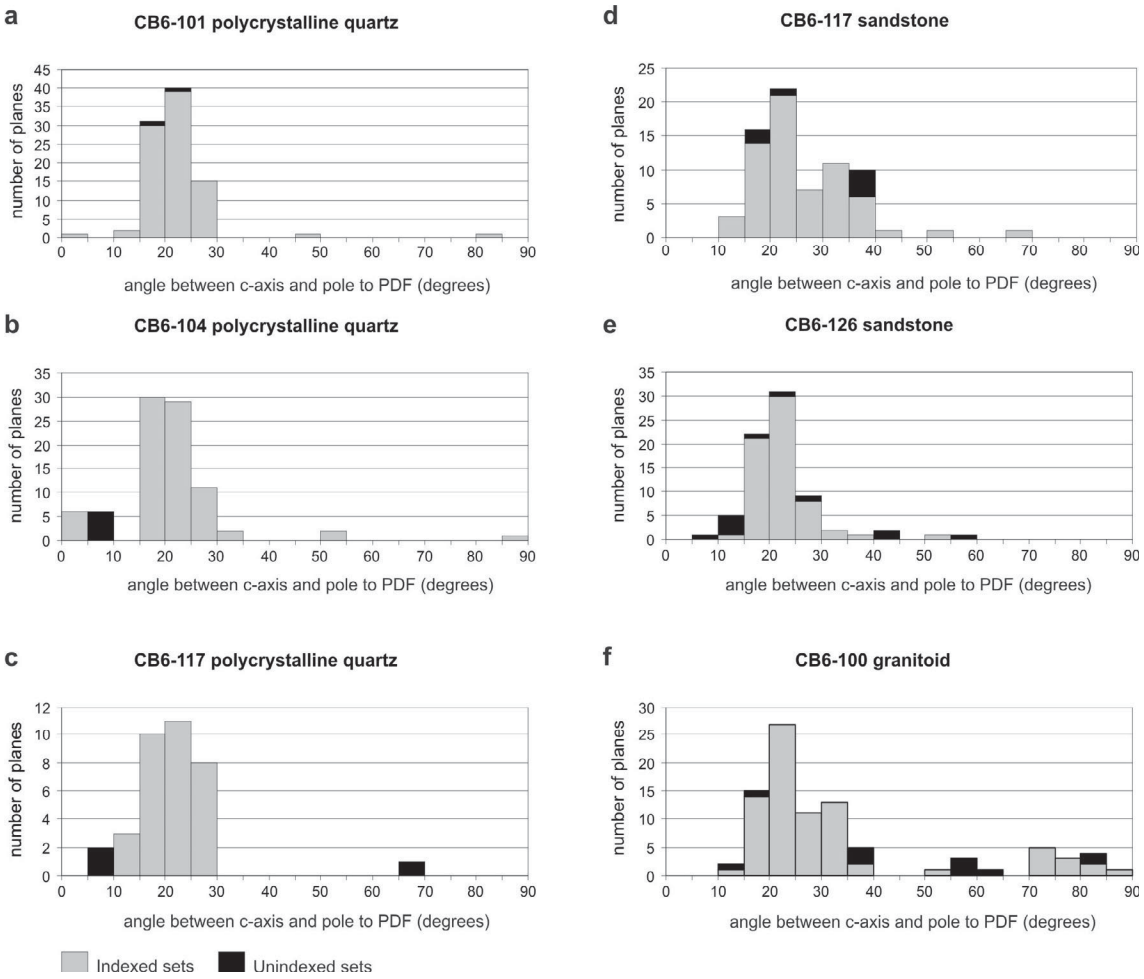

Fig. 9-7: Histograms of angles between c-axis and pole to PDF, binned by 5°, in quartz grains from six clasts from suevite samples. Both indexed (gray) and unindexed (black) PDF sets are plotted. a) Polycrystalline quartz clast from sample CB6-101, 1431.10 m depth. b) Polycrystalline quartz clast from sample CB6-104, 1443.65 m depth. c) Polycrystalline quartz clast from sample CB6-117, 1481.74 m depth. d) Sandstone clast from sample CB6-117, 1481.74 m depth. e) Sandstone clast from sample CB6-126, 1529.27 m depth. f) Granitoid clast from sample CB6-100, 1427.01 m depth.

It should be noted that the clasts investigated by U-stage are not fully representative of the respective clast lithology, as only clasts with a relatively high proportion of shocked quartz grains (based on the results of our point counting study) were selected in order to reach a good precision of the U-stage investigations. For each clast the crystallographic orientation of more than 70 PDF sets were measured, except for a polycrystalline quartz clast in sample CB6-117, where only 35 PDF sets were observed. A large proportion, from ~38 to 82 rel% (for the various thin sections; see Table 9-2), of all the poles to the PDF planes measured are oriented at ~23° to the c-axis, corresponding to the $\{10\bar{1}3\}$ orientation. Other PDFs are commonly orientated parallel to $\{10\bar{1}2\}$ and $\{10\bar{1}4\}$ orientations (Table 9-2). Basal PDFs [parallel to (0001)] are common only in the polycrystalline quartz clast from sample CB6-104, representing 7.4 rel%. Other measured PDF orientations, accounting for less than a few rel% per section, include $\{10\bar{1}1\}$, $\{10\bar{1}0\}$,

$\{11\bar{2}2\}$, $\{11\bar{2}1\}$, $\{21\bar{3}1\}$, $\{51\bar{6}1\}$, $\{22\bar{4}1\}$, and $\{31\bar{4}1\}$. In most investigated clasts, quartz grains display commonly only one set of PDFs, and, thus, the number of indexed PDF sets per grain is low (~1.3; see Table 9-2). Only in the granitoid clast from sample CB6-100 grains with two PDF sets are most abundant and the number of PDF sets per grain is higher (2.0).

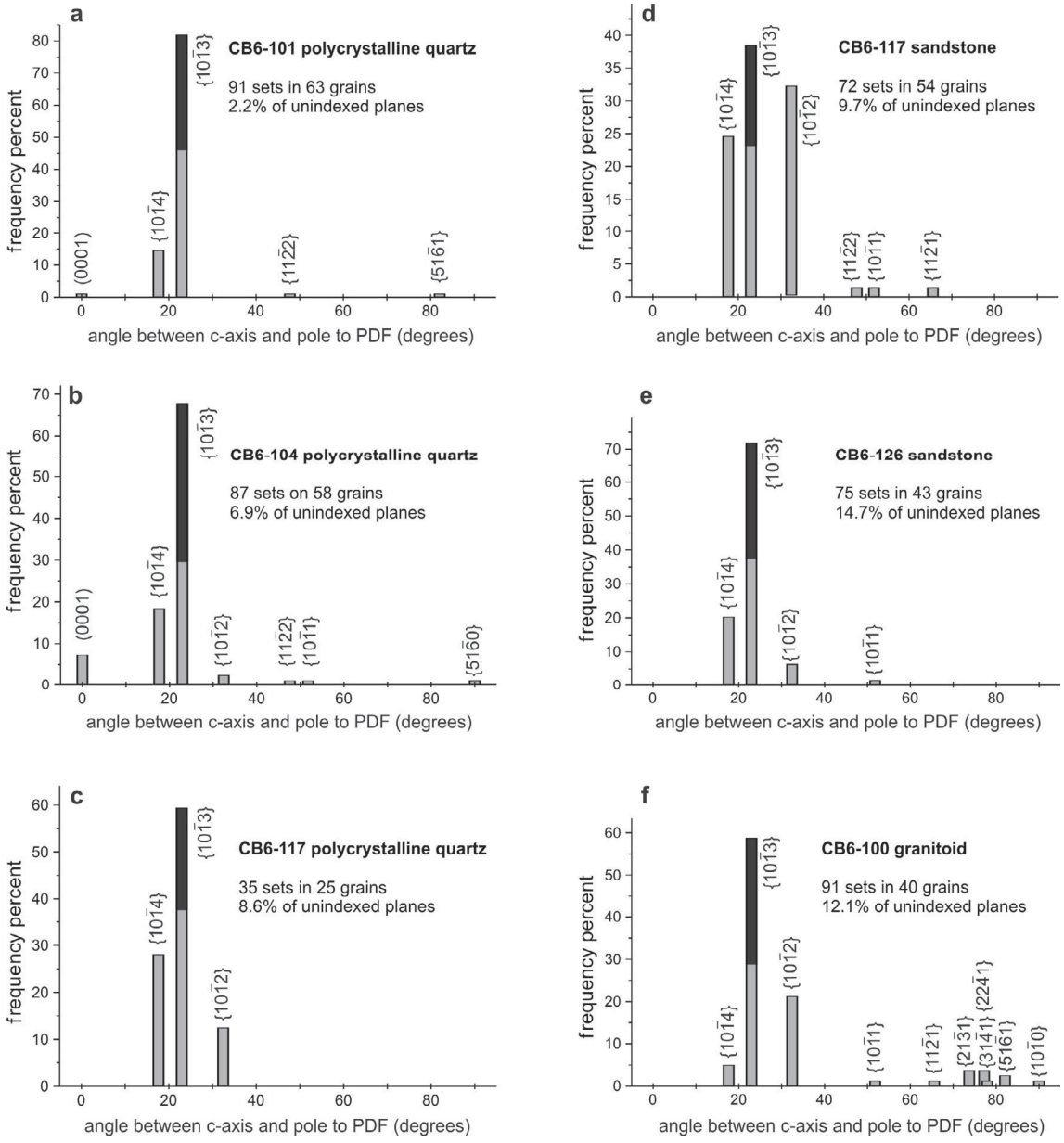

Fig. 9-8: Histograms of absolute frequency percent of PDF orientations in quartz grains from six clasts from suevite samples. Only indexed PDF sets (recalculated to 100%) are plotted. The PDF planes that fall into the overlapping area of the orientations $\{10\bar{1}3\}$ and $\{10\bar{1}4\}$ are plotted as $\{10\bar{1}3\}$, but marked black in the histogram column. a) Polycrystalline quartz clast from sample CB6-101, 1431.10 m depth. b) Polycrystalline quartz clast from sample CB6-104, 1443.65 m depth. c) Polycrystalline quartz clast from sample CB6-117, 1481.74 m depth. d) Sandstone clast from sample CB6-117, 1481.74 m depth. e) Sandstone clast from sample CB6-126, 1529.27 m depth. f) Granitoid clast from sample CB6-100, 1427.01 m depth.

Table 9-2. Results of petrographic examination of quartz grains and universal-stage determination of PDF crystallographic orientations in quartz grains from clasts of different lithologies in samples from the impact breccia interval from the Eyreville drill core.

Sample	CB6-100	CB6-101	CB6-104	CB6-117	CB6-117	CB6-126
Lithology*	granitoid	pq	pq	pq	sst	sst
Rel% of shocked quartz grains[§]	58	33	34	9.5	28	32
No. of investigated grains	40	63	43	25	54	58
No. of measured PDF sets	91	91	75	35	72	87
No. of indexed PDF sets	80	89	64	32	65	81
Absolute frequency of unindexed PDF sets	12	2.2	15	8.6	9.7	6.9
No. of indexed PDF sets per grain	2.0	1.4	1.5	1.2	1.1	1.4

PDF crystallographic orientations	Polar angle (°)	Absolute frequency (%) of indexed PDF crystallographic orientations[#]					
(0001)	0	n.d.[†]	1.1	7.4	n.d.	n.d.	n.d.
$\{10\bar{1}3\}$	22.95	29	46	30	38	23	38
$\{10\bar{1}3\}/\{10\bar{1}4\}$**	overlap	30	36	38	22	15	34
$\{10\bar{1}2\}$	32.42	21	n.d.	2.5	13	32	6.3
$\{10\bar{1}1\}$	51.79	1.3	n.d.	1.2	n.d.	1.5	1.6
$\{10\bar{1}0\}$	90	1.3	n.d.	n.d.	n.d.	n.d.	n.d.
$\{11\bar{2}2\}$	47.73	n.d.	1.1	1.2	n.d.	1.5	n.d.
$\{11\bar{2}1\}$	65.56	1.3	n.d.	n.d.	n.d.	1.5	n.d.
$\{21\bar{3}1\}$	73.71	3.8	n.d.	n.d.	n.d.	n.d.	n.d.
$\{51\bar{6}1\}$	82.07	2.5	1.1	n.d.	n.d.	n.d.	n.d.
$\{11\bar{2}0\}$	90	n.d.	n.d.	n.d.	n.d.	n.d.	n.d.
$\{22\bar{4}1\}$	77.2	3.8	n.d.	n.d.	n.d.	n.d.	n.d.
$\{31\bar{4}1\}$	77.91	1.3	n.d.	n.d.	n.d.	n.d.	n.d.
$\{40\bar{4}1\}$	78.87	n.d.	n.d.	n.d.	n.d.	n.d.	n.d.
$\{51\bar{6}0\}$	90	n.d.	n.d.	1.2	n.d.	n.d.	n.d.
$\{10\bar{1}4\}$	17.62	5.0	15	19	28	25	20

* Lithology: pq - polycrystalline quartz, sst - sandstone.

[§] Based on point counting of shock-metamorphism effects under petrographic microscope (without U-stage).

[#] Recalculated to 100% without unindexed PDF sets were excluded.

[†] Not detected.

**PDF planes which plot in the overlapping zone between $\{10\bar{1}3\}$ and $\{10\bar{1}4\}$ crystallographic orientations.

DISCUSSION

Trends in proportions of shocked quartz grains

In the results of the special point counting of shocked quartz grains no linear trend with depth was observed. This is in agreement with the previous results by Bartosova et al. (2009), where all quartz grains in a thin section (both in matrix and in clasts) were investigated. The proportion of shocked quartz grains was counted both for all grains investigated in the thin section and also for only single grains in matrix and no trends with depth were observed (Bartosova et al., 2009).

The present study reveals that there are some differences in term of recorded shock-deformation between the clasts of different lithologies. The crystalline rocks, mostly the gneisses, which represent the deeper part of the target (e.g., Poag et al, 2004) display relatively low proportions of shocked quartz grains (<10 rel%). Similarly, in metamorphosed sediments the proportion of shocked quartz grains rarely exceeds 10 rel%. On the other hand, some of the sedimentary clasts (sandstones and wackes) have up to 40 rel% (and rarely more) of shocked quartz grains. These observations indicate that the investigated sediment clasts, representing the upper part of the target, were shocked to the highest degree. The differences in the proportions of shocked quartz grains observed in the sediment clasts, i.e., the wide range of values from 0 to about 40 rel% of shocked quartz grains, could be explained by the difference in the original position of the clasts in the target (i.e., depth but also distance from the impact center). The sediments that were originally at higher distance from the impact center would be less shocked due to the attenuation of the spherical shock wave with increasing distance (Melosh, 1989). Furthermore, the shock wave energy can be deposited heterogeneously even at the microscopic scale in porous sedimentary targets (Grieve et al., 1996). Several conglomerate clasts show the highest proportion of shocked quartz grains from all investigated lithologies, thus were probably derived from a highly shocked part of the target. It has been also noted, that larger proportion of shocked quartz grains occurs among the large single grains in a conglomerate compared to small quartz grains within e.g., sandstone pebbles in the conglomerate. Similar observations regarding grain size (larger quartz grains having higher abundances of PDFs) have been noted in samples from, e.g., the Ries crater (Walzebuck and Engelhardt, 1979).

Concerning the polycrystalline quartz clasts, they could have been derived from e.g., gneiss, granite, quartzite or quartz veins. They are also relatively highly shocked, commonly contain between 20 and 40 rel% of shocked quartz grains. It is thus not excluded that at least some of them originated from the higher parts of the target. However, some polycrystalline quartz parts investigated in the cataclastic gneiss block sample CB6-122 from 1511.86 m depth in the core have also relatively high proportion of shocked quartz grains (up to 20 rel%). Thus, it seems that the polycrystalline quartz is more liable to be shocked. In the Gosses Bluff impact structure it has been observed that PDFs are more common in silicified sandstone than in adjacent porous sandstone (Milton et al., 1972). These observations suggest that development of PDFs is favored in hard non-porous rocks with lower compressibility. This could be the reason of relatively high proportion of shocked quartz grains in the polycrystalline quartz clasts from the Eyreville drill core. The porosity and/or volatile content, as well as some lithological contrasts, texture, fabric, grain size, and/or pre-shock orientation of grains can be also in part

responsible of the observed differences since all this parameters can significantly influence the development of PDFs in quartz.

There are some differences in the PDF orientation distribution between the investigated clasts. The granitoid clast (from sample CB6-100) with no basal orientations and with relatively common $\{10\bar{1}2\}$ orientations is probably more shocked. This would be in agreement with the high proportion of shocked quartz grains in the granitoid clast (58.2 rel%). The sandstone clast from sample CB6-117 has also abundant orientations $\{10\bar{1}2\}$, which might suggest a higher shock level. On the other hand, the polycrystalline quartz clast from sample CB6-104 with 7.4 % of basal planes is probably less shocked than the other investigated clasts. No obvious trends in the PDF orientations distinct for the clasts of the same lithology were noted.

The shock-metamorphism studies were performed on suevite and associated lithologies in the interval of impact breccias, which is a mixture of different target rocks shocked to different stages, from unshocked to melted clasts. Thus, no thermobarometry is possible to perform for the suevite as a whole (Grieve et al., 1996), although we can conclude, that at least some parts of the target rocks have been shocked at more than 60 GPa and 1500 °C (French et al., 1998).

In some impact craters the PDF orientations in the target rocks change according to shock wave attenuation with depth (Grieve et al., 1996). This is the case of for example the Brent crater, formed in crystalline target, where PDF orientations in parautochtonous rocks in the center of the crater were studied (Robertson and Grieve, 1977). In the complex structure Puchesz-Katunki a study estimated the shock pressures from ~40 GPa at the top of the central uplift to ~10 GPa at 5 km depth based largely on variations of PDF orientations (Ivanov, 1994). Another study of shock attenuation with depth has been performed recently by Ferrière et al. (2008) on nearly autochtonous monomict impact breccia from the Bosumtwi impact crater. In the Eyreville drill core, there is unfortunately not possible to perform such studies, because the larger monomict parts (i.e., the granitic block and crystalline-basement derived schists and pegmatites), are generally unshocked (e.g., Horton et al., 2009a, 2009b; Townsend et al., 2009).

There are some differences in distribution of PDF orientations between the impact craters formed in crystalline and sedimentary target rocks. In some impact structures in sedimentary targets, e.g., B.P. and Oasis structures, the orientations $\{10\bar{1}3\}$ and $\{10\bar{1}2\}$ are subordinate to higher angle orientations (Grieve et al., 1996). This is not the case for the studied sandstone clasts from Eyreville drill core where only rare PDF orientations with higher angles were noted. In some other craters formed in sedimentary targets the PDF orientations distribution is more similar to crystalline targets, e.g., in Sierra Madera structure (Grieve et al., 1996).

Comparison with previous shock-metamorphism studies of the Chesapeake Bay impactites

In the Eyreville drill core samples, but also in the impactites of the Chesapeake Bay impact structure in general, only scarce statistical studies and U-stage measurements of PDFs in quartz grains have been performed (e.g., Koeberl et al., 1996, Poag et al., 2004, Glidewell et al., 2008). We found that in the impact breccia interval of the Eyreville drill core the amount of highly shocked clasts and average of proportion of shocked quartz grains of the samples generally slightly decreases with depth (Fig. 9-3). This is in agreement with previous studies in which the overall amount of shocked material, e.g., of melt particles, was found to generally decrease with depth in the impact breccia interval (Bartosova et al., 2009). In agreement with the works by Glidewell et al. (2008), we found that most of the PDFs are orientated parallel the $\{10\bar{1}3\}$ orientation. The other PDF orientations reported by Glidewell et al. (2008) – $\{21\bar{3}1\}$ and $\{51\bar{6}1\}$ – were found only in the granitoid clast in sample CB6-100, where they represent less than 4 rel% of the measured PDF sets.

Koeberl et al. (1996) reported that typical crystallographic orientations of PDFs in quartz grains derived from samples of the Exmore Formation are, in order of decreasing abundance, $\{10\bar{1}3\}$, $\{10\bar{1}2\}$, $\{51\bar{6}1\}$, $\{10\bar{1}1\}$, (0001), and $\{11\bar{2}2\}$, with only minor proportions other orientations. Other U-stage measurements by Poag et al. (2004) yielded the same dominant orientations $\{10\bar{1}3\}$, $\{10\bar{1}2\}$, and also relatively common high-index PDF orientations. Some planes with the $\{10\bar{1}4\}$ orientation could also be present in the data presented by the authors of these two studies, but because the $\{10\bar{1}4\}$ PDF pole orientation was only added recently by Ferrière et al. (2009) to the template used for indexing, it is not possible to back-estimate their proportion. However, interestingly, the distribution of the PDF orientations reported by Koeberl et al. (1996) is not similar to any of the clasts measured in the present study. Some of the orientations reported by these authors ($\{51\bar{6}1\}$, (0001), and $\{10\bar{1}1\}$) are rather rare in our samples, where the orientations $\{10\bar{1}3\}$ and $\{10\bar{1}4\}$ are dominant. Also the orientation $\{10\bar{1}2\}$ is less abundant in our samples compared to the study by Koeberl et al. (1996). The additional measurements by Poag et al. (2004) are comparable to our results for granitoid clast from sample CB6-100. In these two previous studies only quartz grains from the Exmore breccia, and not from suevite samples, were investigated. Other important difference is that in the previous U-stage studies PDF orientations determined in several different single grains and clasts were combined, while in our study only grains within one clast were investigated.

Based on our U-stage examination, we estimate that the investigated clasts were moderately to highly shocked, probably up to ~20 GPa (Stöffler and Langenhorst, 1994; Grieve et al., 1996; Huffman and Reimold, 1996).

Discussion of indexing the U-stage measurements

As already mentioned, the new indexing template (including five additional and previously not reported characteristic crystallographic orientations of PDFs in quartz) and recommendations formulated by Ferrière et al. (2009) were used for the indexing of our U-stage measurements. Interestingly, a large proportion (up to 28 rel%; see Table 9-2) of the poles to the PDF planes seems to correspond to the recently added $\{10\bar{1}4\}$ orientation. PDF planes parallel to the $\{10\bar{1}4\}$ orientation have also been recently reported by Gurov et al. (2009) in a suevite sample from the Obolon impact structure (in Ukraine), representing about 14 % of all measured PDFs. This PDF orientation is also somewhat common in quartz grains in breccia samples from the Tabun Khara Obo impact structure (in Mongolia; Amgaa, pers.com.).

Based on our investigations on samples from Chesapeake Bay, in which PDF planes parallel to the $\{10\bar{1}4\}$ orientation represent an abundant population, it seems that TEM investigations are necessary to precisely estimate the real proportion of $\{10\bar{1}3\}$ and $\{10\bar{1}4\}$ orientations, because, as already suggested by Ferrière et al. (2009), it is impossible to uniquely distinguish between this two orientations using U-stage when the angle between c-axis and poles to the PDF is comprised between ~18 and 23°.

CONSLUSIONS

The investigated samples from the impact breccia section show a variety of shock metamorphism effects, including abundant PDFs in quartz grains. The presence of highly shocked, as well as unshocked rocks, implies mixing of different target rocks, previously shocked at different pressure (and temperature) according to their original position in the target. The presence of impact melt rocks within the impact breccia section indicates that at least some target rocks experienced pressures in excess of 60 GPa and temperatures >1500 °C (French, 1998). Clasts with the highest proportion of shocked quartz grains become generally less abundant with increasing depth. Clasts derived from the deeper part of the target (i.e., the crystalline basement rocks) show generally low proportions of shocked quartz grains. Clasts derived from the upper part of the target (i.e., the pre-impact sediments) show a wide range of proportions of shocked quartz grains, including many highly shocked clasts. The large differences among sediments (values from 0 to 40 rel% of shocked quartz grains) are possibly related to the original position in the target (i.e., different distance from the impact center), but a lithology effect (i.e., differences in porosity, granulometry, etc.) could also be responsible for some of the observed variations in apparent recorded shock deformation. Clasts of polycrystalline quartz are generally highly shocked, suggesting that the polycrystalline quartz is liable to be shocked.

The crystallographic orientations of PDFs in quartz grains of clasts in suevite are dominated by $\{10\bar{1}3\}$ and $\{10\bar{1}2\}$ orientations, plus the $\{10\bar{1}4\}$ orientation. Based on our U-stage results, we can estimate that the investigated clasts were moderately to highly shocked, probably up to ~20 GPa.

Acknowledgments: The drilling at Eyreville was supported by ICDP, USGS, and NASA. We appreciate the work of general contractor DOSECC and drilling operator Major Drilling, USA. The present work was supported by the Austrian Science Foundation FWF, project P18862-N10 (to C.K.). The help of the staff at the USGS National Center, Reston, during the sampling process is appreciated. Special thanks belong to L. Ferrière for introduction into the methodology, valuable discussions and suggestions, as well as improvement of the manuscript text.

References:

Bartosova K., Ferrière L., Koeberl C., Reimold W. U., and Gier S. 2009. Petrographic and shock metamorphic studies of the impact breccia section (1397–1551 m depth) of the Eyreville drill core, Chesapeake Bay impact structure, USA. In *The ICDP-USGS deep drilling project in the Chesapeake Bay impact structure: Results from the Eyreville core holes,* edited by Gohn G. S., Koeberl C., Miller K. G., and Reimold W. U. *Geological Society of America Special Paper* 458: 317–348.

Collins G. S. and Wünnemann K. 2005. How big was the Chesapeake Bay impact? Insight from numerical modeling. *Geology* 33: 925–928.

Earth Impact Database 2009. http://www.unb.ca/passc/ImpactDatabase/ (accessed 1st December 2009).

Edwards L. E., Powars D. S., Gohn G. S., and Dypvik H. 2009. Geologic columns for the ICDP-USGS Eyreville A and B cores, Chesapeake Bay impact structure: Sediment breccias, 444 to 1,096 m depth. In *The ICDP-USGS deep drilling project in the Chesapeake Bay impact structure: Results from the Eyreville core holes,* edited by Gohn G. S., Koeberl C., Miller K. G., and Reimold W. U. *Geological Society of America Special Paper* 458: 51–90.

Emmons R. C. 1943. The universal stage (with five axes of rotation). Geological Society of America Memoir 8, 205 p.

Engelhardt W.v. and Bertsch W. 1969. Shock-induced planar deformation structures in quartz from the Ries crater, Germany. *Contributions to Mineralogy and Petrology* 20: 203–234.

Ferrière L., Koeberl C., Ivanov B., and Reimold W. U. 2008. Shock metamorphism of Bosumtwi impact crater rocks, shock attenuation, and uplift formation. *Science* 322: 1678–1681.

Ferrière L., Morrow J. R., Amgaa T., and Koeberl C. 2009. Systematic study of universal-stage measurements of planar deformation features in shocked quartz: Implications for statistical significance and representation of results. *Meteoritics and Planetary Science* 44: 925–940.

French B. M. 1998. *Traces of catastrophe: A handbook of shock-metamorphic effects in terrestrial meteorite impact structures.* LPI contribution No. 954, Lunar and Planetary Institute, Houston, 120 p.

Glass B. P. 1989. North American tektite debris and impact ejecta from DSDP Site 612. *Meteoritics* 24: 209–218.

Glass B. P. 2002. Upper Eocene impact ejecta/spherule layers in marine sediments. *Chemie der Erde* 62: 173–196.

Glidewell J., Harris R. S., King, D. T., Jr., and Petruny L. W. 2008. Stratigraphy, petrology, and shock petrography based on well logs and selected samples from the Eyreville drill core: Chesapeake Bay impact structure, Virginia (abstract #2438). 39th Lunar and Planetary Science Conference. CD-ROM.

Gohn G. S., Koeberl C., Miller K. G., Reimold W. U., Cockell C. S., Horton J. W. Jr., Sanford W.E., and Voytek M.A. 2006a. Chesapeake Bay impact structure drilled: *EOS, Transactions American Geophysical Union* 87: 349 & 355.

Gohn G. S., Koeberl C., Miller K. G., Reimold W. U., and the scientific staff of the Chesapeake Bay impact structure drilling project. 2006b. Chesapeake Bay impact structure deep drilling project completes coring. *Scientific Drilling* 2006/3: 34–37.

Grieve R. A. F., Langenhorst F., and Stöffler D. 1996. Shock metamorphism of quartz in nature and experiment: II. Significance in geoscience. *Meteoritics and Planetary Science* 31: 6–35.

Gurov E., Gurova E., Chernenko Y., and Yamnichenko A. 2009. The Obolon impact structure, Ukraine, and its ejecta deposits. *Meteoritics and Planetary Science* 44: 389–405.

Horton J. W. Jr. and Izett G. A. 2005. Crystalline-rock ejecta and shocked minerals of the Chesapeake Bay impact structure, USGS-NASA Langley core, Hampton, Virginia, with supplemental constraints on the age of impact. *US Geological Survey Professional Paper* 1688: E1–E30.

Horton J. W. Jr., Gibson R. L., Reimold W. U., Wittmann A., Gohn G. S., and Edwards L. E. 2009a. Geologic column for the ICDP-USGS Eyreville B core, Chesapeake Bay impact structure: Impactites and crystalline rocks, 1,096-1,766 m. In *The ICDP-USGS deep drilling project in the Chesapeake Bay impact structure: Results from the Eyreville core holes,* edited by Gohn G. S., Koeberl C., Miller K. G., and Reimold W. U. *Geological Society of America Special Paper* 458: 21–49.

Horton J. W. Jr., Kunk M. J., Belkin H. E., Aleinikoff J. N., Jackson J. C., and Chou I-M. 2009b. Evolution of crystalline target rocks and impactites in the Chesapeake Bay impact structure, ICDP-USGS Eyreville B core. In *The ICDP-USGS deep drilling project in the Chesapeake Bay impact structure: Results from the Eyreville core holes,* edited by Gohn G. S., Koeberl C., Miller K. G., and Reimold W. U. *Geological Society of America Special Paper* 458: 277–316.

Huffman A. R. and Reimold W. U. 1996. Experimental constraints on shock-induced microstructures in naturally deformed silicates. *Tectonophysics* 256: 165–217.

Ivanov B. A. 1994. Geochemical models of impact cratering: Puchezh-Katunki structure. *Geological Society of America Special Paper* 293: 81–91.

Jackson J. C., Horton J. W. Jr., Chou I.-M., and Belkin H. E. 2006. A shock-induced polymorph of anatase and rutile from the Chesapeake Bay impact structure, Virginia, U.S.A. *American Mineralogist* 91: 604–608.

Koeberl C., Poag C. W., Reimold W. U., and Brandt D. 1996. Impact origin of the Chesapeake Bay structure and the source of the North American tektites. *Science* 271: 1263–1266.

Melosh H. J. 1989. *Impact cratering—A geological process.* New York: Oxford University Press. 245 p.

Milton D. J., Barlow B. C., Brett R., Brown A. R., Glikson A. Y., Manwaring E. A., Moss F. J., Sedmik E. C. E., Son J. V., and Young G. A. 1972. Gosses Bluff impact structure, Australia. *Science* 175: 1199-1207.

Poag C. W., Powars D. S., Poppe L. J., and Mixon R. B. 1994. Meteoroid mayhem in Ole Virginny: source of the North American tektite strewn field. *Geology* 22: 691–694.

Poag C. W., Hutchinson D. R., Colman S. M., and Lee M. W. 1999. Seismic expression of the Chesapeake Bay impact crater: Structural and morphologic refinements based on new seismic data. In *Large meteorite impacts and planetary evolution II*, edited by Dressler B. O. and Sharpton V. L. *Geological Society of America Special Paper* 339: 149–164.

Poag C. W., Koeberl C., and Reimold W. U. 2004. *The Chesapeake Bay Crater: Geology and Geophysics of a late Eocene Submarine Impact Structure, Impact Studies series.* Heidelberg: Springer. 522 p.

Reimold W. U., Bartosova K., Schmitt R. T., Hansen B., Crasselt C., Koeberl C., Wittmann A., and Powars D. 2009. Petrographic observations on the Exmore Breccia, ICDP-USGS Drilling at Eyreville, Chesapeake Bay impact structure, USA. In *The ICDP-USGS deep drilling project in the Chesapeake Bay impact structure: Results from the Eyreville core holes,* edited by Gohn G. S., Koeberl C., Miller K. G., and Reimold W. U. *Geological Society of America Special Paper* 458: 655–698.

Reinhard M. 1931. *Universaldrehtischmethoden*. Basel, Switzerland: Birkhäuser. 118 p.

Robertson P. B. and Grieve R. A. F. 1977. Shock attenuation at terrestrial impact structures. In *Impact and Explosion Cratering,* edited by Roddy D. J., Pepin R. O., and Merrill R. B. Pergamon Press, New York. p. 687–702.

Stöffler D. and Langenhorst F. 1994. Shock metamorphism of quartz in nature and experiment: I. Basic observation and theory. *Meteoritics* 29: 155–181.

Townsend G. N., Gibson R. L., Horton J. W. Jr., Reimold W. U., Schmitt R. T., and Bartosova K. 2009. Petrographic and geochemical comparisons between the crystalline basement-derived section and the granite and amphibolite megablocks of the Eyreville-B core, Chesapeake Bay impact structure, USA. In *The ICDP-USGS deep drilling project in the Chesapeake Bay impact structure: Results from the Eyreville core holes,* edited by Gohn G. S., Koeberl C., Miller K. G., and Reimold W. U. *Geological Society of America Special Paper* 458: 255–276.

Walzebuck J. P. and Engelhardt W. v. 1979. Shock deformation of quartz influenced by grain size and shock direction: Observations on quartz-plagioclase rocks from the basement of the Ries Crater, Germany. *Contributions to Mineralogy and Petrology* 70: 267-271.

Wittmann A., Reimold W. U., Schmitt R. T., Hecht L., and Kenkmann T. 2009a. The record of ground zero in the Chesapeake Bay impact crater – suevites and related rocks. In *The ICDP-USGS deep drilling project in the Chesapeake Bay impact structure: Results from the Eyreville core holes,* edited by Gohn G. S., Koeberl C., Miller K. G., and Reimold W. U. *Geological Society of America Special Paper* 458: 349–376.

Wittmann A., Schmitt R.-T., Hecht L., Kring D. A., and Povenmire H. 2009b. Petrology of impact melt rocks from the Chesapeake Bay crater, USA. In *The ICDP-USGS deep drilling project in the Chesapeake Bay impact structure: Results from the Eyreville core holes,* edited by Gohn G. S., Koeberl C., Miller K. G., and Reimold W. U. *Geological Society of America Special Paper* 458: 377–396.

CHAPTER 10: PETROGRAPHY, MINERALOGY, AND GEOCHEMISTRY OF DEEP GRAVELLY SAND IN THE EYREVILLE B CORE, CHESAPEAKE BAY IMPACT STRUCUTRE

Katerina Bartosova[1*], Susanne Gier[2], J. Wright Horton Jr.[3], Christian Koeberl[1], Dieter Mader[1], and Henning Dypvik[4]

[1]*Department of Lithospheric Research, University of Vienna, Althanstrasse 14, A–1090 Vienna, Austria. E-mail: katerina.bartosova@univie.ac.at.*
[2]*Department of Geodynamics and Sedimentology, University of Vienna, Althanstrasse 14, A–1090 Vienna, Austria*
[3]*U.S. Geological Survey, 926A National Center, Reston, Virginia 20192, USA*
[4]*Department of Geosciences, University of Oslo, P.O. Box 1047, Blindern, NO–0316 Oslo, Norway*

*Corresponding author: *E-mail: katerina.bartosova@univie.ac.at*

submitted to *Meteoritics and Planetary Science,*
accepted with major revision, revised version

ABSTRACT: The ICDP-USGS Eyreville drill cores in the Chesapeake Bay impact structure reached a total depth of 1766 m and comprise (from the bottom upwards) basement-derived schists and granites/pegmatites, impact breccias, gravelly sand and crystalline blocks, a granitic slab, sedimentary breccias, and post-impact sediments. The gravelly sand and crystalline block section forms a ~26-m-thick interval that includes an amphibolite block and boulders of cataclastic gneiss and suevite. New petrographic, mineralogical, and geochemical analyses of samples from this interval are interpreted in the context of previous work. The gravelly sand is poorly sorted and generally massive, but crude size-sorting and subtle, discontinuous layers occur locally. The sand is clast supported. It consists mainly of quartz (mono- and polycrystalline) and K-feldspar (mostly microcline) sand grains with silt-clay matrix (typically 30–40 vol%) and dispersed gravel-sized clasts. Other mineral grains occur only in accessory amounts. Lithic clasts are sparse (only a few vol%). The sub-mm clasts are angular to subangular and rarely subrounded; larger clasts are subrounded and rarely rounded. Quartz and K-feldspar are the main sand-size mineral constituents and smectite and kaolinite are the principal clay minerals, according to X-ray diffraction analyses. Geochemical analyses show that the gravelly sand is silica-rich (mostly >80 wt% SiO_2). Trends with depth include a slight decrease in SiO_2 and slight increase in Fe_2O_3. Middle gravelly sand (below the amphibolite block) is finer-grained, contains more abundant clay minerals, and displays more variable chemical compositions than upper gravelly sand above the block. The basal gravelly sand (below the cataclasite boulder) has a lower SiO_2 content (<80 wt%), less K-feldspar, and more

mica. The basal gravelly sand samples are more diverse in composition, and they contain more lithic clasts and melt particles that are probably reworked from the underlying suevite. Our mineralogical and geochemical results agree with previous interpretations that the gravelly sand is an avalanche deposit derived probably from the non-marine Potomac Formation from the lower part of the target sediment, in contrast to polymict diamictons higher in the core that have been interpreted as ocean-resurge debris flows. The mineralogy and geochemistry of the gravelly sand are typical for a passive continental margin source. There is no discernible mixing with marine sediments (no glauconite or marine microfossils noted) during the impact remobilization and redeposition. Reworked melt particles and rip-up clasts derived from the suevites are found only in the basal gravelly sand. The unshocked amphibolite block and cataclasite boulder might have originated from the outer parts of the transient crater.

Keywords: Chesapeake Bay impact structure, gravelly sand, modal point counting, X-ray diffraction

INTRODUCTION

Chesapeake Bay impact structure

The Chesapeake Bay impact structure is ~35.3 Myr old and 85 km in diameter (Horton and Izett, 2005; Poag et al., 2004). The structure is located along the east coast of the United States (Fig. 10-1). It is the largest impact structure in the United States and one of the largest and best preserved impact structures on Earth (e.g., Poag et al., 1992, 1994; Gohn et al., 2006a; http://www.unb.ca/passc/ImpactDatabase/index.html). The impact origin of the Chesapeake Bay structure was suggested by Poag et al. (1992, 1994), based on structural and sedimentary characteristics (including finding of shocked quartz). Later this was confirmed by universal stage investigations of shocked quartz from the Exmore breccia by Koeberl et al. (1996). The Chesapeake Bay impact structure is a complex crater, with a shape described as an “inverted sombrero” (Horton et al., 2005) – a deep inner crater with a small central uplift structure is surrounded by a shallower outer basin (Poag et al., 1999; Powars and Bruce, 1999).

Today, the crater is covered by 200–550 m of sediments (Poag et al., 2004). Although the area has been subjected to extensive drilling, only a few drill cores have been drilled in the central part of the impact structure. The Kiptopeke drill core (drilled in 1989 to a depth of 607.5 m, Powars and Bruce, 1999, Plate 5 therein) did not penetrate the full crater fill, and core recovery was poor in the breccia interval (Powars and Bruce, 1999; Poag et al., 2004). In 2004, the U.S. Geological Survey drilled and partially cored

an 823-m deep test hole near Cape Charles (Gohn et al., 2007), which was used in site characterization for the ICDP-USGS deep drilling described below.

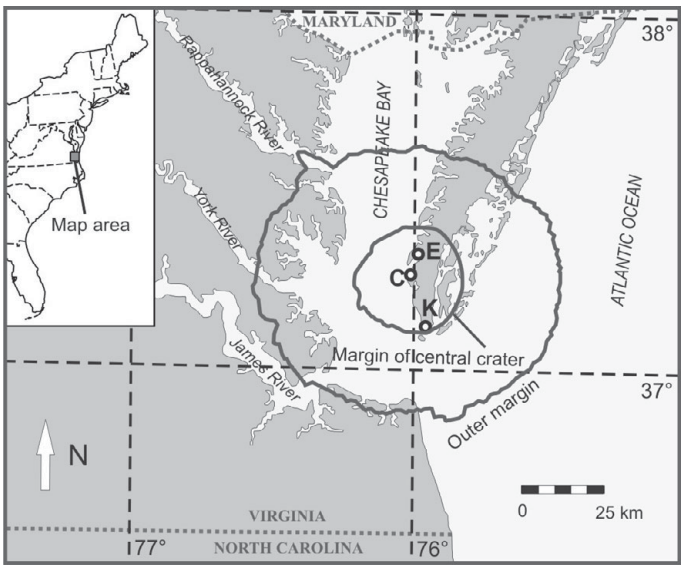

Fig. 10-1. Map of the southern part of Chesapeake Bay modified from Horton et al. (2009a). Locations of the Chesapeake Bay impact structure and core holes in the central part of the structure are shown. E-Eyreville, C-Cape Charles, K-Kiptopeke.

Eyreville drill cores

The Eyreville core holes were drilled as part of the International Continental Drilling Program–U.S. Geological Survey (ICDP–USGS) Chesapeake Bay impact structure drilling project, at Eyreville Farm, in Northampton County, Virginia. In 2005–2006, three cores, Eyreville A, B, and C were recovered. Eyreville A was cored between 125 and 941 m depths, Eyreville B was drilled from 738 m to a final depth of 1766 m, and Eyreville C sampled the post-impact sediments from the land surface to a depth of 140 m (Gohn et al., 2006a, 2006b, 2008).

The Eyreville drill cores include (from the bottom upwards) granites/pegmatites and mica schists, impact breccias, the gravelly sand and crystalline block section, a large granitic slab, sediment-clast breccias and sediment blocks (including the Exmore Formation), and post-impact sediments (Fig. 10-2; Gohn et al., 2006a, 2008). After extensive studies of the Eyreville drill cores, detailed geologic logs were published for the depth intervals 1766–1096 m (Horton et al., 2009a), 1096–444 m (Edwards et al., 2009a), and 444–0 m (post-impact sediments; Edwards et al., 2009b).

The deepest rocks of the core, schist intercalated with granites and pegmatites (see e.g., Townsend et al., 2009; Horton et al., 2009b) probably do not represent the real bottom of the crater, but rather blocks originating from the outer parts of the crater (Horton et al., 2009b; Kenkmann et al., 2009). The impact breccia interval contains mostly suevite that is melt rich in the upper part and melt poor in the lower part, two thin intervals of impact melt rock and large blocks of cataclastic gneiss occur (more details in e.g., Bartosova et al., 2009a, 2009b; Wittmann et al., 2009a, 2009b; Horton et al., 2009b). A thin gravelly sand and crystalline block section, which is the subject of this study, occurs

above the impact breccias (Fig. 10-2). A large granitic slab above consists of fine- to coarse-grained locally gneissic granite (Townsend et al., 2009; Horton et al., 2009a, 2009b). The thickest section of the Eyreville drill cores consists of sedimentary breccias and sediment blocks. This section includes an informal lower unit of "sediment boulders and sand" (*SBS*, 1095.7–867.4 m) overlain by a recently formalized Exmore Formation (Edwards et al., 2009a). Edwards et al. (2009a) subdivide the Exmore Formation into four informal units (from base to top): a lower diamicton member (*Edl*, 867.4–856.6 m), block-dominated member (*Eb*, 856.6–618.2 m), upper diamicton member (*Edu*, 618.2–451.0 m), and stratified member (*Es*, 451.0–443.9 m). The diamicton members (interpreted as resurge debris flows; Gohn et al., 2009; Ormö et al., 2009), consist of polymict sediment clasts and fewer crystalline rock clasts in a muddy glauconitic quartz sand matrix with mixed-age microfossils (Edwards et al., 2009a; Self-Trail et al., 2009), as well as melt particles and rare shocked quartz grains (Reimold et al., 2009). Chemical analyses of the Eyreville samples and geochemical characteristics of the main units sampled in the Eyreville drill cores are presented in Schmitt et al. (2009).

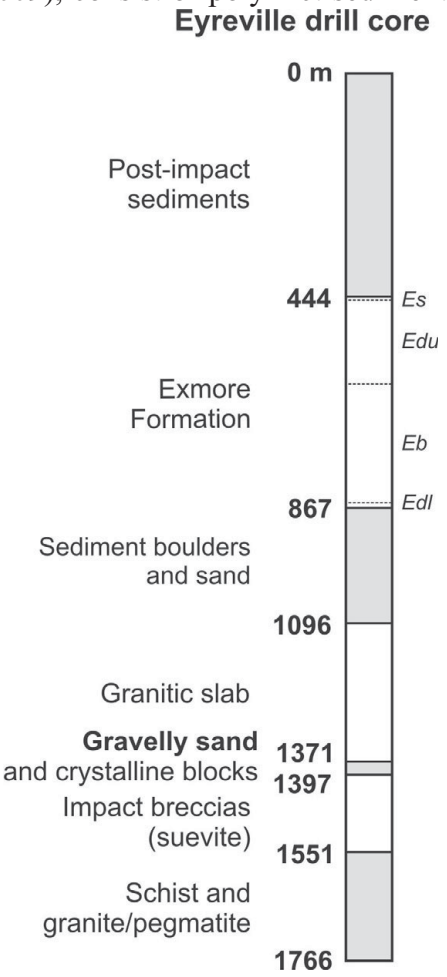

Fig. 10-2. Simplified stratigraphic column of the Eyreville drill core showing the main lithologies. Modified from Gohn et al. (2008) and Horton et al. (2009a). The Exmore beds are subdivided according to Edwards et al. (2009a). On the right side of the column, the members of the Exmore Formation – lower diamicton member (*Edl*), block-dominated member (*Eb*), upper diamicton member (*Edu*), and stratified member (*Es*) are indicated (Edwards et al., 2009a). Depth is below surface in meters.

Previous studies of the gravelly sand and crystalline block section

The term "gravelly sand and crystalline block section" is used in the text of the paper for the whole studied interval (1371.11–1397.16 m depth). The term "gravelly sand" is used only for the sand intervals of the section. The gravelly sand is further subdivided into "basal gravelly sand" (between suevite and cataclastic gneiss boulder, 1396.44–1397.16 m depth), "middle gravelly sand" (between suevite boulder and amphibolite block, 1389.71–

1393.00 m depth), and "upper gravelly sand" (between amphibolite block and granitic slab, 1371.11–1376.39 m depth).

The gravelly sand and crystalline block section has been described in broader studies of the Eyreville drill cores as discussed below. The earlier data and annotations provide a context for interpreting the new data in this report.

General petrography

The gravelly sand and crystalline block section (Fig. 10-3) is about 26 m thick and contains a large amphibolite block, about 13 m in size (1389.71–1376.39 m). Further a boulder of cataclastic gneiss (1396.44–1393.42 m), a suevite boulder (1393.42–1393.00 m), and smaller lithic clasts are present (Horton et al., 2009a).

The gravelly sand consists of fine- to very coarse-grained quartz sand with minor amounts of silt and clay, granules of quartz and feldspar, and sparse well rounded to subangular quartz pebbles; the sand is unlithified except near the base (Horton et al., 2009a). There is no distinct bedding. There are recycled, rounded quartz and chert pebbles dispersed in the gravelly sand, but no coherent clasts of Cretaceous and Paleogene target sediments Gohn et al. (2009). In contrast to the Exmore Formation diamicton members, there is generally no glauconite except for possible rare grains reported from the basal part (1396.77 m depth, Horton et al., 2009a, Reimold et al., 2009). No diagnostic shock effects in minerals were noted; only one quartz grain, possibly reworked, with planar fractures was reported by Reimold et al. (2009).

The suevite boulder consists of clasts of granitic gneiss, black shale, flow-laminated melt clasts are elongate and subhorizontally aligned, and black matrix (Horton et al., 2009a). It is probably a rip-up clast from the underlying suevite section (Horton et al., 2007a).

The amphibolite block is dark gray to green, relatively homogeneous, and foliated (Townsend et al., 2009). The rock consists of plagioclase, amphibole (pargasite to hornblende, Townsend et al., 2009), biotite, accessory quartz and epidote, and traces of secondary minerals (Horton et al., 2009a, 2009b). The block is most likely of igneous origin and has been metamorphosed in mid- to upper-amphibolite facies (Townsend et al., 2009).

Source and formation

The basal and middle gravelly sand contains sparse, poorly preserved, likely thermally altered, pollen (found at 1392.6 and 1396.5 m) and is barren of calcareous nannofossils and dinocysts (Self-Trail et al., 2009). The pollen and spore assemblages are Early Cretaceous in age and representative of a basal non-marine, pre-Zone I Potomac Formation source (Self-Trail et al., 2009), indicating that these sediments originated from

the basal part of the Potomac Formation or an older sediment source. This assemblage may represent mass wasting of an unnamed formation only slightly younger than the Waste Gate Formation (Self-Trail et al., 2009). These are the oldest pollen and spore assemblages found to date in the crater fill (Self-Trail et al., 2009). Sands above the granitic slab contain younger Early Cretaceous (Aptian-Albian) pollen and spores. This implies that sands below the granite slab were derived from a unit older than the sands above the granitic slab (Self-Trail et al., 2009).

Depositional mechanisms of the upper impactites (above suevite) of the Eyreville drill core have been studied by Gohn et al. (2009) and Horton et al. (2009b). These authors suggested that water saturated Cretaceous sand below the granitic slab could have lowered the friction so that the granite slab slid (hydroplaned?) a considerable distance from around the transient crater rim, possibly over a distance of at least 5 km (Horton et al., 2009a; Horton et al 2007a; Collins and Wünnemann, 2005). This would also explain the out-of-sequence stratigraphy in the Eyreville cores – pre-Mesozoic granite slab above Lower Cretaceous sediments (Gohn et al., 2009; Horton et al., 2009). This sliding, as well as the deposition of the non-marine sediment blocks from 1095.7 to 866.7 m, most likely occurred before the first arrival of resurge material, as indicated by the absence of glauconite and the total absence of marine microfossils (Self-Trail et al., 2009).

$^{40}Ar/^{39}Ar$ thermochronology of detrital microclines from the gravelly sand gives a wide range of pre-impact ages, from 218 to 328 Ma; the age spectra do not show any discernible disturbance by the impact event (Horton et al., 2009b).

Basal gravelly sand with melt particles

The basal gravelly sand has been described as "gravelly sand with melt particles" (Horton et al., 2009a) and interpreted as "reworked suevite" (Horton et al., 2007b). The basal gravelly sand interval is also darker and more consolidated than the upper parts, probably as a result of its location within a thermal aureole above the suevites (Horton et al., 2009b; Malinconico et al., 2009). The basal 0.7 m of the basal gravelly sand contains up to 3.2 vol% of melt fragments (Reimold et al., 2009). Impact melt clasts were altered to clay phyllosilicates (Horton et al. 2007b, 2009a), but some of the particles may contain remnants of glass (Reimold et al., 2009). The particles do not exhibit broken vesicle rims and may originate from reworking of suevite (Horton et al., 2009a). The melt particles from 1396.7 m depth have been analyzed by electron microprobe by Reimold et al. (2009).

Alteration

The post-impact alteration of the Eyreville sedimentary breccias has been studied by Larsen et al. (2009). One sample from the upper gravelly sand (1375 m depth) is described

as sandstone that includes mono- and polycrystalline quartz and microcline as well as rock fragments and "microtektites". The feldspars show dissolution, albitization, and replacement by clay minerals; in addition, some early stage quartz cementation was noted (Larsen et al., 2009). Bulk and clay-mineral X-ray diffraction (XRD) analyses indicate that most abundant minerals of the upper gravelly sand are quartz and K-feldspar; the clay fraction consists mainly of expandable clays and kaolinite (Larsen et al., 2009). Ferrell and Dypvik (2009) analyzed clay minerals in one sample from the matrix of the middle gravelly sand from 1390 m depth, and found smectite and kaolinite to be the main components of the clay fraction. Bulk XRD analyses of several gravelly sand samples by Horton et al. (2009b) identified quartz, K-feldspar, muscovite, kaolinite, and smectite to be the main components of the gravelly sand. Also chlorite, plagioclase, and amphibole were noted in some samples (Horton et al., 2009b). Vitrinite reflectance data have been used to model the post-impact thermal history (Malinconico et al., 2009). Vitrinite from 1398 m showed an increased reflectance (0.47–0.91 % R), probably due to conductive heat from the underlying suevite (Malinconico et al., 2009). Thermal alteration index of spores and pollen showed also increased values (Self-Trail et al., 2009).

SAMPLES AND ANALYTICAL METHODS

Seventeen samples were collected from the gravelly sand and crystalline block section (samples CB6-087 to CB6-092, KB-1, and KB1-09 to KB10-09), and three more thin sections from the sample suite of the Natural History Museum in Berlin (W-50, W-53, and W-54) were studied. All samples are listed in Table 10-1 and their stratigraphic positions in the core are shown in Fig. 10-3. The samples were collected to cover the whole gravelly sand and crystalline block section (1371.1–1397.2 m), except for the large amphibolite block and cataclasite boulder, as these lithologies are not the subject of the present study. The gravelly sand without any large clasts was sampled. Clasts >0.5 cm were excluded from the samples used for powder preparation.

Thin sections were prepared for all samples (typically two for each sample, Table 10-1). Samples were impregnated with epoxy resin in vacuum before the thin section preparation. Main mineral components, sizes and shapes of grains, and other important features were described under petrographic microscope. Sedimentary grain size terms used are based on the classification by Blair and McPherson (1999). Modal analyses by point counting were performed on one thin section of each gravelly sand sample (on 17 thin sections in total; Table 10-2). About 800 points were counted per thin section. The counted components were matrix, mineral grains (single grains in matrix), rock clasts (without counting individual minerals within rock clasts), as well as reworked melt

particles. Grains and clasts with apparent diameter less than 0.05 mm were counted as matrix.

Table 10-1. List of samples of gravelly sand and associated rocks used in this study of the Eyreville B drill core.

sample	box	slot	midpoint (m)	rock type	sampled*	no. of thin sections
CB6-087	221	1	1371.13	gravelly sand	a	1
CB6-088	221	2	1371.37	gravelly sand	a	2
W-50	221	2	1371.78	gravelly sand	b	1
KB9-09	221	3	1372.29	gravelly sand	c	2
KB10-09	221	5	1373.27	gravelly sand	c	2
KB1-09	222	1	1373.75	gravelly sand	c	2
KB2-09	222	2	1374.54	gravelly sand	c	2
KB3-09	222	4	1375.46	gravelly sand	c	2
CB6-089	222	4	1375.61	gravelly sand	a	2
CB6-090	225	1	1382.53	amphibolite block	a	1
KB4-09	227	4	1389.84	gravelly sand	c	2
CB6-091	227	5	1390.35	gravelly sand	a	2
W-53	227	5	1390.53	gravelly sand	b	1
KB5-09	227	5	1390.88	gravelly sand	c	2
KB6-09	228	1	1391.40	gravelly sand	c	2
KB7-09	228	3	1392.23	gravelly sand	c	2
KB-1	228	4	1393.12	suevite boulder	d	1
KB8-09	228	4	1393.48	cataclasite boulder	c	1
CB6-092	230	1	1396.54	gravelly sand with reworked suevite	a	3
W-54	230	2	1396.72	gravelly sand with reworked suevite	b	1

Note: Samples CB6- were originally marked as CK- in the core boxes.

* Sampling details: a – sampled by Christian Koeberl, March 2006; b – sampled by Uwe Reimold, March 2006; c – sampled by Wright Horton, February 2009; d – sampled by Katerina Bartosova, November 2007.

A part of each sample (~60 g) was separated, powdered in an agate mill, and analyzed for chemical composition. Abundances of major and some trace elements were determined by X-ray fluorescence (XRF). Most samples were analyzed at the Museum of Natural History, Berlin on the SIEMENS SRS 3000 instrument (see Schmitt et al., 2004, for more details on the method). Ten additional samples KB1-09 to KB10-09 were analyzed at the University of Vienna on a Philips PW2400 sequential spectrometer. The detection limit is about 0.02 wt% for major element oxides and about 1 ppm for trace elements. Loss on ignition (LOI) was determined for all samples.

The contents of trace elements including rare earth elements and some major elements (Na, K, and Fe) were determined by instrumental neutron activation analysis (INAA) at the University of Vienna, Austria. Three international rock standards were used for reference. All samples and standards were irradiated in the 250 kW Triga reactor of the Atomic Institute of the Austrian Universities for about 8 hours at a neutron flux of $2x10^{12}$ $n.cm^{-2}.s^{-1}$. The method has been described in detail by Koeberl (1993), Son and Koeberl (2005), and Mader and Koeberl (2009). Contents of some elements were determined by both methods (XRF and INAA). For major elements XRF data are reported. For the trace elements, data acquired with the most precise method for the respective elements are presented (Table 10-3).

Eleven gravelly sand samples were further characterized by the X-ray diffraction (XRD) analyses at the University of Vienna on Philips diffractometer (PW 3710, goniometer PW 1820), CuK_{α} radiation (45 kV, 35 mA), step size of 0.02 degree, and a counting time of 1s per step. Minerals were identified using the Joint Committee on Powder Diffraction Standards database (JCPDS, 1980). Selected samples (CB6-089, KB4-09, KB6-09, and KB9-09) were used for further studies of the clay fraction (<2 μm). Clay fraction was separated by a standard sedimentological method and oriented XRD mounts were prepared. The samples were analyzed after air-drying, after saturation with Mg-ions, K-ions, ethylene glycol and glycerol, and after heating to 550 °C. A PANalytical X´Pert Pro diffractometer (CuK_{α}- radiation, 40 kV, 40 mA, step size 0.0167, 5 s per step) was used for the analyses. All the procedures used for XRD identification of clay minerals are described in detail in Moore and Reynolds (1997). Clay fraction analyses were complemented by simultaneous thermal analysis (STA) of sample KB9-09 at the University of Natural Resources and Applied Life Sciences in Vienna on a NETZSCH STA 409 instrument in the temperature range 25–1000 °C.

Raman microspectroscopy was used to identify accessory minerals. The measurements were performed on a Renishaw RM1000 confocal edge filter-based microRaman spectrometer with a 17 mW, 632.8 nm HeNe laser excitation system with a thermoelectrically cooled charge-coupled device (CCD) array detector, at the Institute of Mineralogy and Crystallography, University of Vienna. The spectra were compared with libraries from Renishaw and RRUFF data-base (Downs, 2006) using Grams/32 software.

Polished thin sections were examined in secondary electron and backscattered electron modes on a JEOL JSM 6400 scanning electron microscope with an energy-dispersive X-ray analyzer (SEM-EDX) at the Natural History Museum in Vienna. For compositional analyses defocused beam operating at 15 kV acceleration potential and ~1–2 nA sample current, was used. The following elements were analyzed and results were recalculated to oxide contents (automatically normalized to 100 wt%): Si, Al, Ca, Fe, Mg, K, Na, Ti, Mn, and Cr. The standardless EDX analyses have a precision of ~3 rel% and accuracies of 10 rel%. Detection limits are ~0.2–0.5 wt% for major elements.

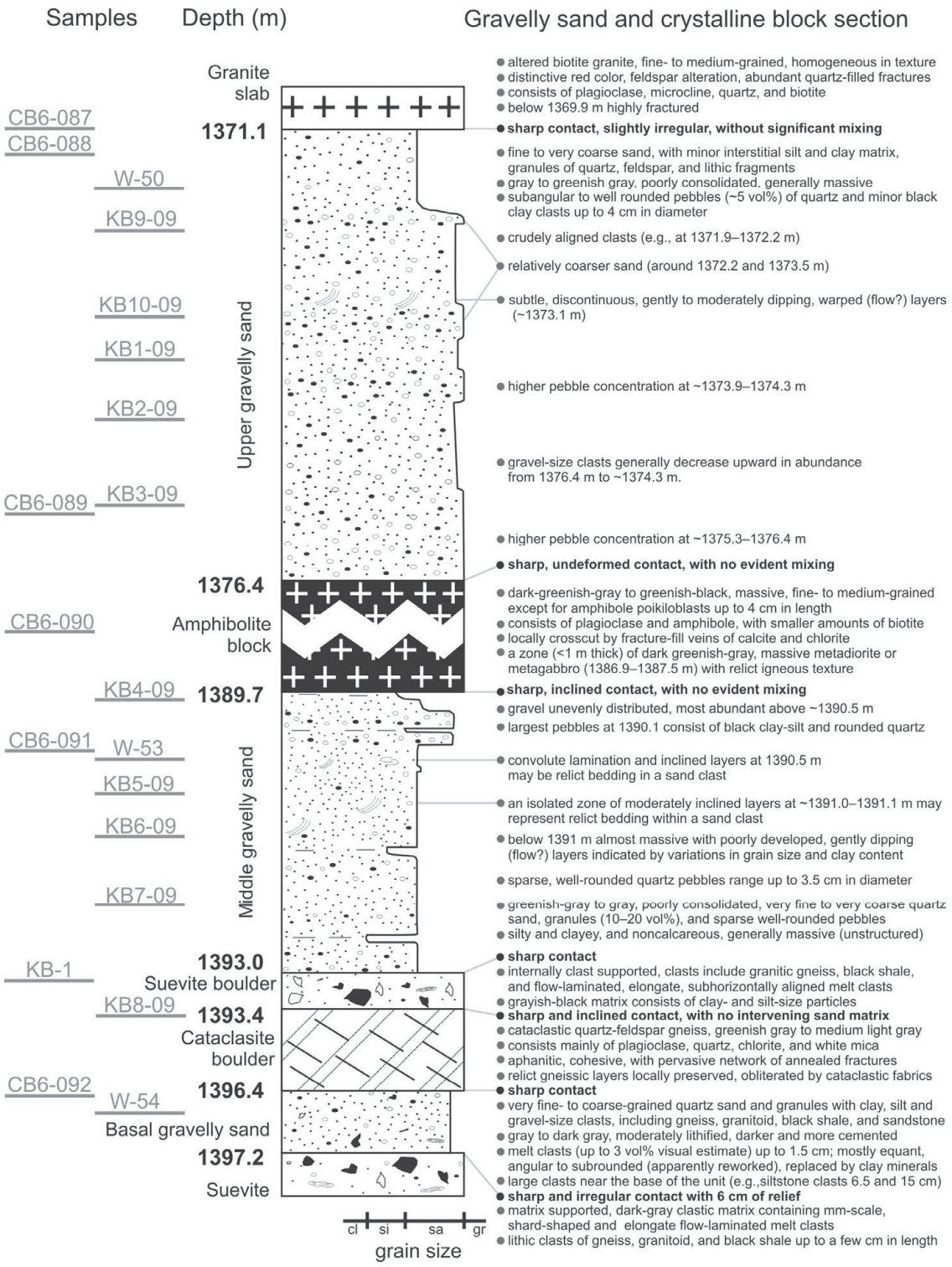

Fig. 10-3. Detailed stratigraphic column of the gravelly sand and crystalline block section of the Eyreville-B drill core, modified from Horton et al. (2009a), showing important features and changes in gravelly sand. Depth below surface in meters. Positions of the samples are indicated on the left side of the column. Detailed core descriptions are included.

RESULTS

Macroscopic observation of the samples

Detailed macroscopic observations of the samples are listed in Appendix. Cut core pieces of the gravelly sand samples are shown in Fig. 10-4. The gravelly sand is gray to greenish in color. It is well cemented only in the basal part (between upper suevite and cataclasite boulder); most of the unit is poorly lithified. The gravelly sand was very poorly consolidated when the core came out of the ground, but became more firm after drying. The samples are crumbly and can be even more easily disaggregated in water. The gravelly sand is mostly homogeneous, with no bedding. Rare bands that are finer in grain-size and different in color, slightly inclined from horizontal in the core, occur. The grains are mostly sand-sized or granule-sized (<3 mm), but rarely some larger rounded quartz pebbles occur (up to 1.5 cm observed in our samples and generally <3 cm observed in the core). The macroscopically visible larger quartz grains (>1 mm in size) are subangular to rounded. Other larger clasts consist of subangular feldspar. Lithic clasts are mostly subangular and relatively rare (compared to polymict diamictons of the Exmore Formation); more abundant lithic clasts occur in the basal gravelly sand, where also altered melt particles were noted. The lithic clasts are typically small pebbles (<1cm), difficult to classify macroscopically, and include mudstone, siltstone, and granite. Larger rock clasts (up to 15 cm) are present in the basal gravelly sand (see Fig. 10-3). The coarsest samples (KB10-09, KB2-09, KB3-09, and CB6-089) are from a coarser-grained part of the upper gravelly sand (Fig. 10-3). The uppermost part (~1.5 cm) of the gravelly sand sample CB6-087, just below the granitic slab, is darker gray and contains some mm-sized granitic clasts.

Core description

Core descriptions (that include data from Horton et al., 2009a, Appendix 3 therein) are summarized in Fig. 10-3. The basal gravelly sand is distinctly darker and more consolidated than the middle and upper gravelly sands. It is generally fine-grained, but on the other hand contains abundant larger clasts. The basal gravelly sand includes melt particles probably reworked from the suevite below. The suevite boulder above the basal gravelly sand is interpreted as a rip-up clast derived from the underlying suevite section, but differs from the uppermost suevite in being clast supported (Horton et al., 2009a). The middle gravelly sand is generally finer-grained than the upper gravelly sand. There are rare finer beds and some inclined layers, which may be only relict bedding within sandstone clasts in the core. Rare warped (flow?) layers occur also in the upper gravelly sand. Well developed dewatering structures, such as those documented in sediment boulders and sand above the granite slab (Gohn et al., 2009) were not observed in the gravelly sand.

The amphibolite and cataclastic gneiss show no evidence of shock metamorphism, which suggests their origin from the outer parts of the transient crater.

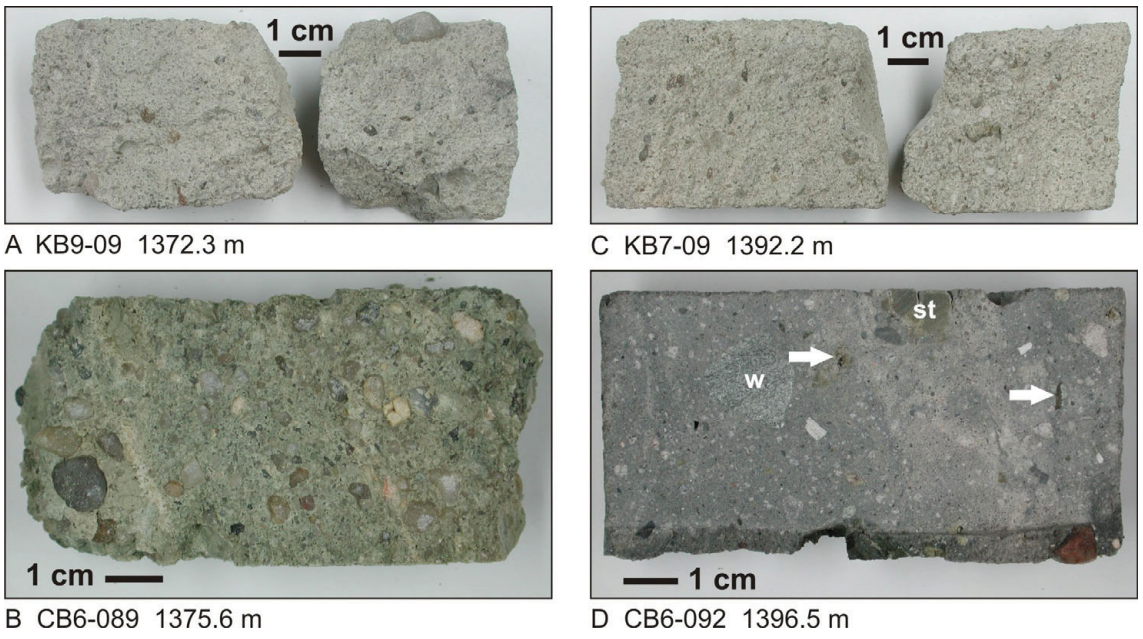

Fig. 10-4. Macroscopic photographs of gravelly sand samples. a) Sample KB9-09, 1372.3 m. A typical example of grayish upper gravelly sand with small quartz grains and some larger pebbles (e.g., top right) in clayey matrix. b) Sample CB6-089, 1375.6 m. This upper gravelly sand sample is coarser than other gravelly sand samples, and the color also is different, with a greenish hue. c) Sample KB7-09, 1392.2 m. A typical sample of the middle gravelly sand; light gray with small quartz grains and no larger rock clasts. d) Sample CB6-092, 1396.5 m. Sample of the basal gravelly sand. There are abundant rock clasts (including w – wacke, st – siltstone) and small melt particles (marked with arrows).

Microscopic observation of the samples

Petrographic descriptions of all samples are presented in the Appendix. Figure 10-5 shows some photomicrographs of the gravelly sand. The sand is poorly sorted and clast supported. The matrix is brownish, fine-grained, and clayey. The sub-mm sand grains are angular to subangular or rarely subrounded. Very coarse sand to pebble-sized grains (up to several mm in diameter) are commonly subrounded to rarely rounded. The fine-grained samples contain commonly ~5, the coarser-grained samples up to ~20 gravel-sized particles (granules or rarely pebbles) per thin section. The most abundant clasts are monocrystalline quartz, and polycrystalline quartz (mostly larger clasts) is less abundant. Polycrystalline quartz clasts range from fine- to coarse-grained. Some polycrystalline quartz grains have sutured boundaries; some are aligned and elongated typical of a metamorphic origin. The second most abundant mineral is feldspar. Among the feldspar grains, K-feldspars (mostly microcline with tartan twinning) are dominant. Plagioclase is rare; more abundant only in the basal part (sample CB6-092). Rare detrital micas occur only as silt-size and rarely larger particles in the matrix. Muscovite is most abundant, but biotite and chlorite also occur. Mica is also present in some rock clasts. Rare carbonate

patches were noted in samples CB6-088 and KB10-09. There are small, disseminated common opaque minerals, e.g., pyrite, marcasite, and rutile. Accessory minerals include garnet, poikilitic staurolite, titanite, tourmaline, zircon, and possibly kyanite. The quartz and feldspar grains do not show any zones of overgrowth in the optical microscope. Many of the grains in the gravelly sand are fractured (Fig. 10-5c), commonly along the rims, but also fractures through complete grains occur. Rock clasts recognized in the thin sections include sandstone/wacke, siltstone, schist, gneiss, and granite.

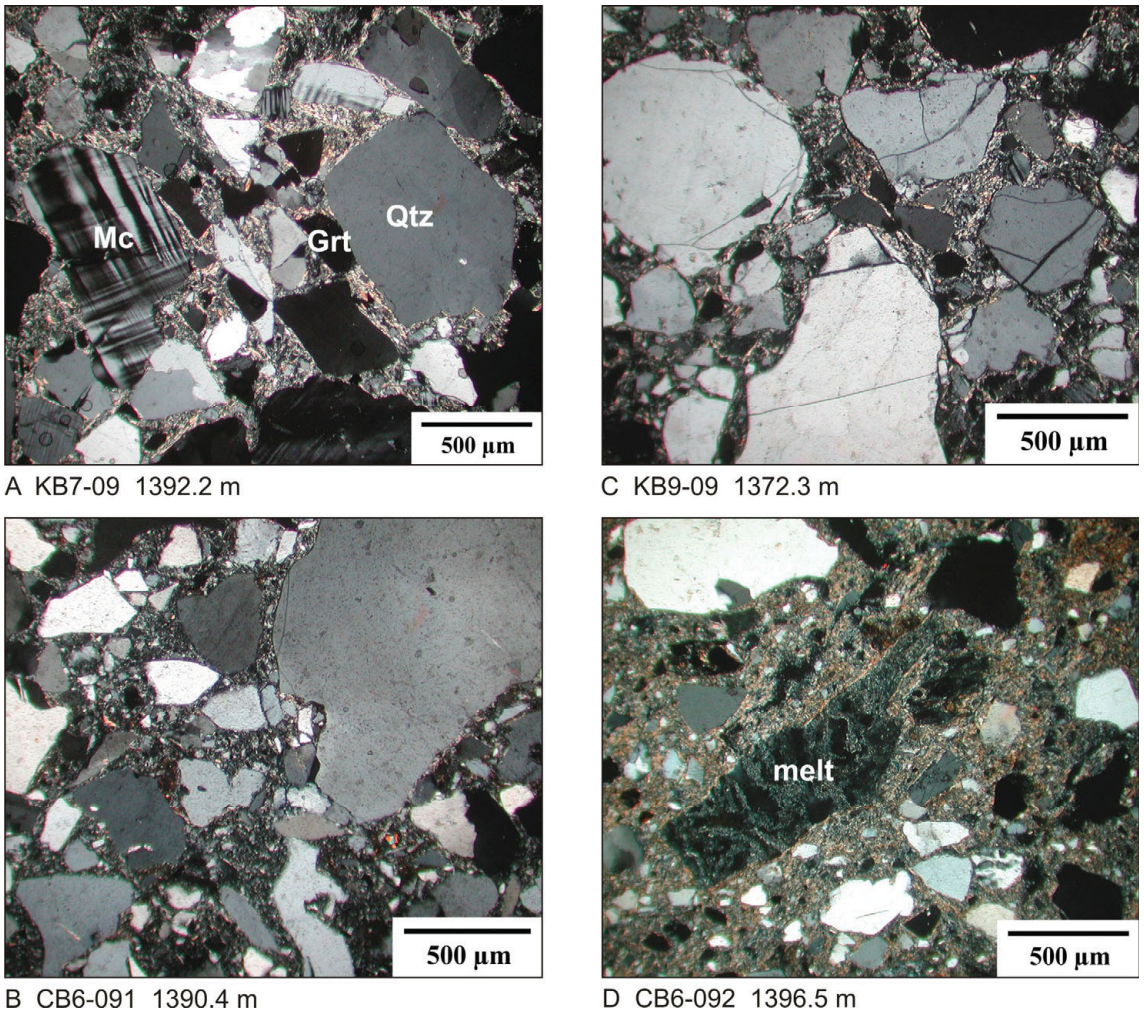

Fig. 10-5. Photomicrographs of the gravelly sand samples, cross-polarized light. a) Sample KB7-09, 1392.2 m. Typical gravelly sand with the main components Qtz – quartz and Mc – microcline, and a garnet grain (Grt) grain. b) Sample CB6-091, 1390.4 m. A typical gravelly sand sample, note the poor sorting and subangular to subrounded shapes of the clasts. c) Sample KB9-09, 1372.3 m. Fractured grains in the gravelly sand. d) CB6-092, 1396.5 m. Sample of the basal gravelly sand. There is an altered melt particle in the middle. Note the higher proportion of matrix compared to the other samples.

Melt particles were observed in the basal gravelly sand in samples CB6-092 and W-54. The melt particles are brownish and altered to clay minerals. Commonly, parts of the soft material have been removed during the thin section preparation. Particles have subangular to amoeboid shapes. The melt particles are similar to particles of melt type m2 defined in the suevite by Bartosova et al. (2009a). This type of melt particle is brown, very soft, altered to phyllosilicate minerals, and commonly contains undigested clasts (Bartosova et al., 2009a). There are rare tiny (<0.2 mm) greenish grains resembling glauconite in the two samples from the basal part (CB6-092 and W-54), but detailed analyses revealed that all these grains are formed by chlorite (see below).

We did not observe any microtektites as described by Larsen et al. (2009). A single particle resembling a tektite, 0.15 mm long, brownish and isotropic, was observed in sample CB6-089, but the particle is elongated rather than spherical. No distinct features were observed in the samples from just below the granitic block and the amphibolite block (samples CB6-087 and KB-4).

Modal point counting results

Modal point counting was performed on thin sections of all gravelly sand samples to determine the proportions of matrix and different clast types, and to study possible changes with depth (Table 10-2 and Fig. 10-6).

Because the gravelly sand samples are soft and crumbly, reflecting poor cementation, thin section preparation was very difficult and in some thin sections holes occur. Consequently, only the good quality thin sections were used for further discussion. Thin sections with large proportion of holes (> ~5 vol%, marked in Table 10-2) were excluded from this discussion and classification.

The point-count results show that matrix in the thin sections represents a substantial part of the unit. In most samples, the matrix forms between 30 and 40 vol%. In the basal gravelly sand samples, the matrix proportion exceeds 40 vol% and forms nearly 60 vol% in the lowermost sample W-54 (Fig. 10-6a). Lithic and melt clasts can be relatively large at the thin section scale and influence the vol% of other components. To show the changes in the proportion of matrix, the larger clasts (lithic and melt clasts) were excluded, and the rel% of matrix and mineral clasts were calculated. The results are shown in Fig. 10-6b. The proportion of matrix is slightly higher in the samples from below the amphibolite block compared to the samples above the block. Below the amphibolite block the proportion of matrix slightly increases with depth and is highest in the samples from below the cataclasite boulder (CB6-092 and W-54). The most abundant clasts are monocrystalline quartz clasts that comprise commonly more than 30 rel%, and more than 40 rel% in the four uppermost samples (Fig. 10-6b). In some samples the proportion is lower, but is compensated by higher proportion of polycrystalline quartz clasts. This is the

case of the most coarse-grained samples KB10-09 and CB6-089. It has been noted by Lewis and McConchie (1994) that the proportion of polycrystalline quartz is often a function of grain size. Quartz and polycrystalline quartz together form more than 50 rel% of most samples, except for samples from the basal gravelly sand and lowermost samples of the middle gravelly sand. The second most important detrital mineral component are K-feldspar clasts; their proportion varies around 7 rel% in most samples. Only in the two lowermost samples (CB6-092 and W-54) is the proportion of K-feldspar much lower, ≤2 rel%. In these two samples, slightly more abundant plagioclase was noted, but only in accessory amounts. Other mineral clasts, including mica, opaque minerals, and accessory minerals, are very rare. These mineral clasts together comprise less than 0.6 rel%, except for one sample from below the amphibolitic block, where up to 1.1 rel% were noted (sample KB6-09).

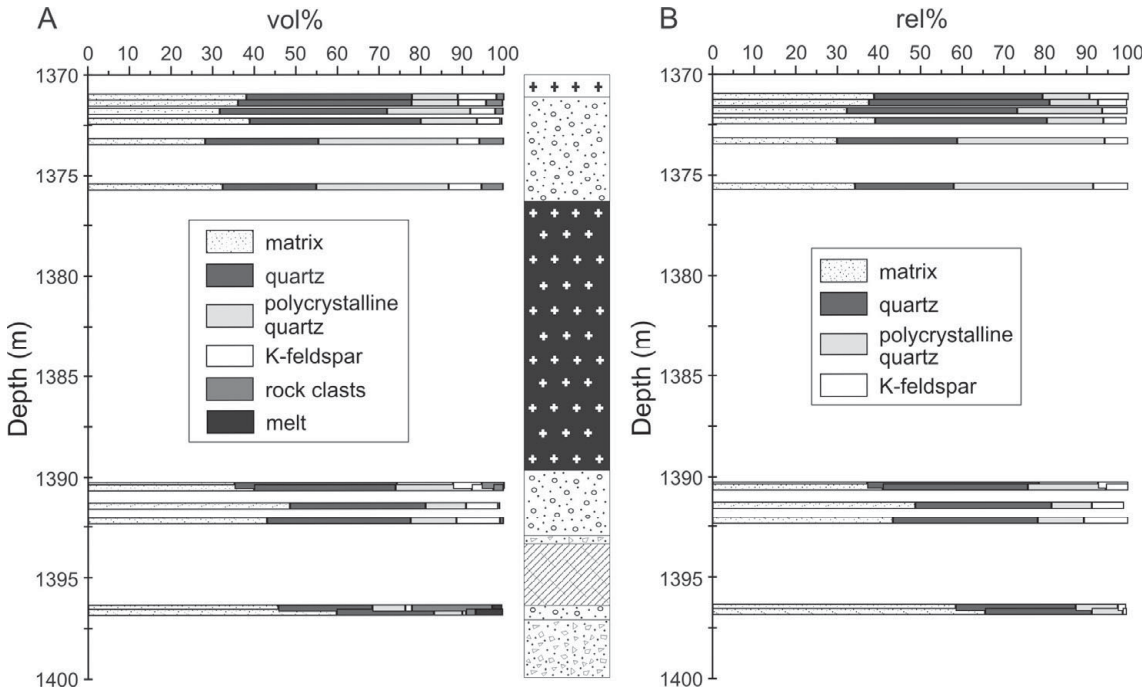

Fig. 10-6. Stack column diagrams showing the results of modal point counting (data from Table 10-2). Only results for samples with good quality thin sections are shown. Geologic column of the gravelly sand interval is displayed for comparison (more details in the geologic column in Fig. 10-3). a) The diagram shows volume percent of the components – from left to right in each bar – matrix, quartz, polycrystalline quartz, K-feldspar, rock clasts, melt particles. The remainder comprises other mineral clasts (mica, opaque minerals, and accessories including plagioclase). b) The diagram shows relative percent of the components – from left to right in each bar – matrix, quartz, polycrystalline quartz, and K-feldspar. Lithic clasts and melt particles are excluded. The remainder comprises other mineral clasts (mica, opaque minerals, and accessories including plagioclase).

Detailed study of the basal gravelly sand samples

The two samples from the basal part, CB6-092 and W-54, were studied in more detail by microRaman spectroscopy and SEM-EDX. To test the possible glauconite presence, several greenish grains, which could not be definitely identified by optical microscopy, were analyzed. The microRaman spectroscopy provided similar spectra (more resembling chlorite) for all grains, but did not provide unambiguous results. According to SEM-EDX analyses, all greenish grains in sample CB6-092 and some grains in sample W-54 are iron-rich chlorite (Table 10-3). Some greenish grains in sample W-54 contain, in addition to main chlorite phase, other different phases, as revealed by back scattered electron (BSE) images. This is the case of for example one grain (Figs. 10-7a and 10-7b) previously described as glauconite based on optical microscopic observation (Reimold et al., 2009). Here the iron-rich chlorite (light in BSE image; Tab. 10-3) is associated with another phase (dark in BSE image, Fig. 10-7b, bleached in optical microscope image, Fig. 10-7a) that contains 7.5 wt% of K_2O, and otherwise nearly only SiO_2 and Al_2O_3. This phase could be a remnant of an altered K-feldspar. Some grains contain a phase (dark in BSE) very rich in SiO_2 (>70 wt%), some Al_2O_3 (15-20 wt%), and only small amounts of other oxides (Table 10-3). Some grains also contain rutile (Fig. 10-7c, the white phase in the grain). No phase with a composition similar to glauconite was noted.

Melt particles from the basal gravelly sand were studied by SEM-EDX. In the BSE images the porous, altered texture was obvious for all particles (Fig. 10-7d). No particles with preserved fresh glass phase were noted. The texture of the melt particles resembles the particles of type m2 as described in the suevite from the Eyreville B drill core by Bartosova et al. (2009a). Also, the composition (Table 10-3) of the melt particles from the basal gravelly sand is closest to the melt type m2 (or also m5) from suevite analyzed with the same instrument by Bartosova et al. (2009b).

Table 10-2. Modal composition (vol%) of 17 gravelly sand samples from the Eyreville B drill core. Based on point counting of one thin section per sample.

samples	CB6-087	CB6-088	W-50	KB9-09	KB10-09	KB1-09*	KB2-09*	KB3-09*	CB6-089	KB4-09*	CB6-091	W-53	KB5-09*	KB6-09	KB7-09	CB6-092	W-54
depth (m)	1371.1	1371.4	1371.8	1372.3	1373.3	1373.8	1374.5	1375.5	1375.6	1389.8	1390.4	1390.5	1390.9	1391.4	1392.2	1396.5	1396.7
MATRIX	38.1	36.1	31.7	38.9	28.2	28.3	34.5	19.7	32.4	38.5	35.2	39.9	29.0	48.5	43.0	45.7	59.7
MINERAL CLASTS																	
monocrystalline quartz	39.8	41.7	40.2	41.1	27.2	42.0	34.1	40.1	22.5	45.5	39.0	34.0	45.7	32.6	34.5	22.6	23.4
polycrystalline quartz	11.0	11.2	20.0	13.5	33.4	16.2	20.4	31.0	31.8	9.4	13.5	18.3	16.1	9.7	11.0	7.9	6.8
K-feldspar	9.3	6.7	6.0	5.6	5.3	9.7	8.9	6.9	7.9	6.1	6.9	5.2	7.2	7.7	10.5	1.6	0.9
mica	n.d.[†]	n.d.	n.d.	0.1	n.d.	0.2	0.2	0.2	n.d.	n.d.	n.d.	n.d.	0.2	0.6	n.d.	0.5	0.1
opaque minerals	n.d.	0.2	0.1	0.2	n.d.	0.2	0.4	n.d.	n.d.	n.d.	0.1	n.d.	n.d.	0.6	0.1	n.d.	0.2
accessory minerals[#]	n.d.	0.2	0.2	0.1	0.1	0.2	n.d.	n.d.	0.1	0.2	n.d.	0.1	n.d.	n.d.	n.d.	n.d.	0.1
LITHIC CLASTS																	
chert	1.2	0.2	0.1	n.d.	0.1	0.5	n.d.	n.d.	1.7	0.2	1.4	n.d.	0.2	n.d.	0.2	n.d.	n.d.
K-feldspar+quartz+mica[$]	0.4	1.9	0.7	0.2	2.5	1.7	1.6	0.7	3.0	n.d.	3.9	1.4	1.0	n.d.	0.3	1.9	0.2
metamorphic clasts**	n.d.	1.9	n.d.	n.d.	2.0	n.d.	n.d.	n.d.	n.d.	n.d.	n.d.	n.d.	n.d.	n.d.	n.d.	n.d.	0.2
fine-grained sediments	n.d.	n.d.	n.d.	0.1	0.1	0.2	n.d.	n.d.	n.d.	n.d.	n.d.	n.d.	n.d.	0.1	0.1	1.7	1.3
sandstone/wacke	n.d.	n.d.	0.6	n.d.	1.1	0.3	n.d.	1.3	n.d.	n.d.	n.d.	0.3	0.5	n.d.	n.d.	12.8	0.2
other clasts[††]	0.1	n.d.	0.6	n.d.	n.d.	0.6	n.d.	n.d.	0.5	n.d.	n.d.	0.6	n.d.	0.3	0.1	2.9	0.4
MELT	n.d.	n.d.	n.d.	n.d.	n.d.	n.d.	n.d.	n.d.	n.d.	n.d.	n.d.	n.d.	n.d.	n.d.	n.d.	2.4	6.6
points counted	679	1003	1073	827	809	636	496	538	743	426	1120	1184	403	715	863	833	1002

Note: Totals are 100 vol%. Clasts smaller than 0.05 mm were counted as matrix.

*lower-quality thin sections, with large proportion of holes in the thin section (>5 vol%). The results have only limited use in the discussion

[†] not detected

[#] including plagioclase

[§] clasts of metamorphic or igneous origin

** schist, gneiss and phyllite

[††] mostly unidentified clasts

Table 10-3. Results of SEM-EDX analyses of samples from the basal gravelly sand, Eyreville B drill core.

sample	CB6-092 grain 1		W-54 grain 1			W-54 grain 3		W-54 grain 4		CB6-092 melt		W-54 melt particles	
details	light*	light	dark	light	light	dark	light	dark	light	average (n=7)[#]	stdev[†]	average (n=16)	stdev
SiO_2	30.0	25.1	45.9	29.6	31.6	76.4	20.8	79.9	18.2	56.9	2.2	58.1	4.2
TiO_2	b.d.[§]	b.d.	b.d.	b.d.	b.d.	1.3	b.d.	0.6	0.6	b.d.		b.d.	
Al_2O_3	21.7	27.6	42.5	26.1	27.0	20.1	33.2	17.3	23.9	31.8	3.0	28.2	4.4
FeO**	34.2	37.7	1.0	37.8	31.9	0.6	35.3	0.9	32.0	5.5	2.4	6.3	2.2
MnO	b.d.	0.8	b.d.	b.d.	b.d.	b.d.	b.d.	b.d.	b.d.	b.d.		b.d.	
MgO	12.4	7.5	2.1	6.2	7.9	b.d.	8.2	b.d.	20.0	2.5	0.6	3.7	0.7
CaO	b.d.	b.d.	b.d.	b.d.	b.d.	b.d.	b.d.	b.d.	b.d.	0.6	0.2	1.2	0.5
Na_2O	1.0	0.8	0.6	b.d.	0.9	0.5	2.0	b.d.	4.9	0.7	0.4	1.5	0.7
K_2O	b.d.	b.d.	7.5	b.d.	0.6	0.6	b.d.	0.8	b.d.	1.5	1.0	0.5	0.2
Cr_2O_3	b.d.	b.d.	b.d.	b.d.	b.d.	b.d.	b.d.	b.d.	b.d.	b.d.		b.d.	

Note: Values are in wt%. Totals are normalized to 100%. Representative analyses of different phases of greenish grains from the basal gravelly sand are presented. In last columns, an average composition of melt particles of each sample is shown.

* in BSE image

[#] number of analyses of melt particles averaged

[†] standard deviation

[§] below detection limit

** total Fe as FeO

Bulk XRD analyses

The eleven selected samples of gravelly sand generally show very similar XRD patterns, but there are some slight differences. Examples of some typical XRD patterns are shown in Fig. 10-8. In all samples, quartz is the main component. Other identified minerals are K-feldspar (likely mostly microcline), clay minerals, and rare mica and possibly plagioclase. The results are summarized in Table 10-4.

The basal gravelly sand sample (Fig. 10-7a) differs from the other samples in a higher content of mica (muscovite and chlorite), which is present in the matrix and also in rock clasts, as observed in the microscopic studies. No clay mineral peaks were detected. In general, the middle gravelly sand (Fig. 10-7b) is much richer in expandable clay mineral components (with a distinct smectite peak) than the upper gravelly sand (Figs. 10-7c and d, with a barely recognizable smectite peak). Expandable clay minerals are most abundant in the middle of the middle gravelly sand interval, in samples KB5-09 and KB6-09. Kaolinite is most abundant in the middle gravelly sand and in the upper part of the upper gravelly sand. Small mica peaks occur in most samples. Generally, the XRD results are in good agreement with the microscopy observations. The slight differences are likely due to the minerals included in matrix, which naturally bears also the clay minerals.

There are probably small amounts of plagioclase (e.g., in samples KB4-09 and CB6-092) and possible trace amounts of calcite. However, these minerals are not easily discernible due to peak coincidence. The addition of 1 molar hydrochloric acid to the sample powder did not indicate the presence of carbonate. Only rare carbonate patches and clasts and accessory amounts of plagioclase were observed in some samples under the microscope.

Table 10-4. Results of bulk rock XRD for gravelly sand samples of the Eyreville B drill core.

sample	depth (m)	quartz	K-feldspar	kaolinite	smectite	mica	plagioclase
CB6-088	1371.37	x	x	x	x	x	-
KB9-09	1372.29	x	x	x	x	x	-
KB10-09	1373.27	x	x	?	?	?	-
KB2-09	1374.54	x	x	?	?	?	-
KB3-09	1375.46	x	x	?	?	?	-
CB6-089	1375.61	x	x	x	x	x	-
KB4-09	1389.84	x	x	x	x	x	?
KB5-09	1390.88	x	x	x	x	x	-
KB6-09	1391.40	x	x	x	x	x	-
KB7-09	1392.23	x	x	x	x	x	-
CB6-092	1396.54	x	x	-	?	x*	?

Note: x = present, ? = possibly present, - = absent
* much more abundant compared to other samples; muscovite and chlorite

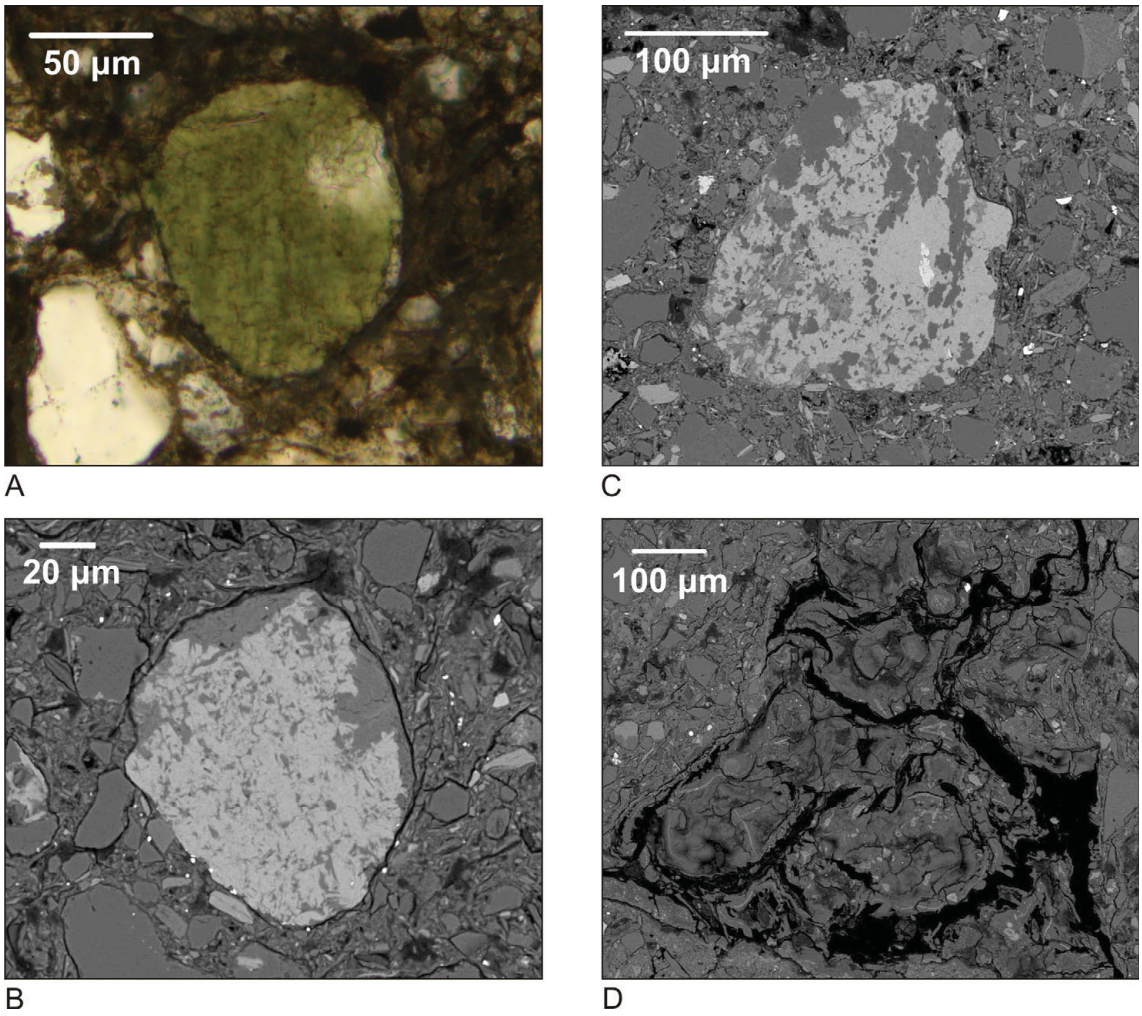

Fig. 10-7. Images of sample W-54 (1396.72 m depth). a) Green chlorite grain, resembling glauconite, microphotograph in plane-polarized light. b) The same chlorite grain in BSE image. c) Another chlorite grain, with dark SiO_2-rich phase and rutile (white phase in the middle of the grain). BSE image. d) Altered melt particle in BSE image.

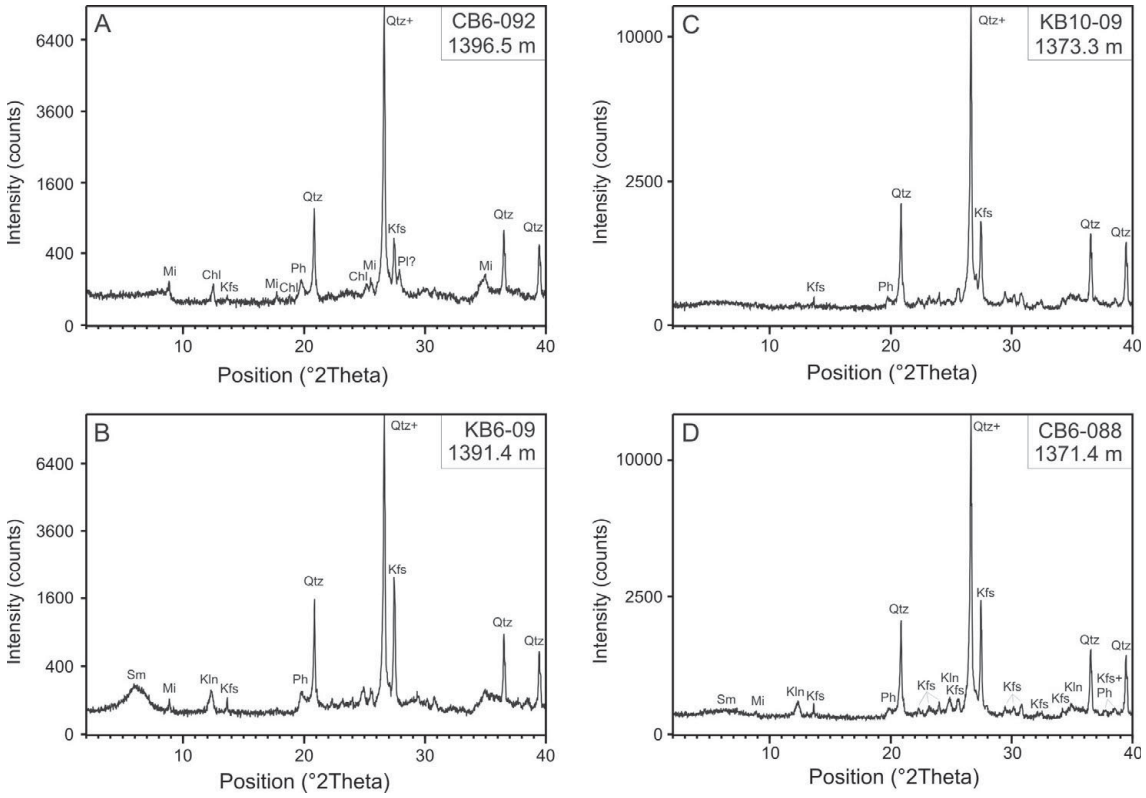

Fig. 10-8. X-ray diffraction spectra of selected bulk gravelly sand samples. Qtz – quartz, Kfs – K-feldspar, Kln – kaolinite, Sm – smectite, Chl – chlorite, Mi – mica, Ph – peak of various phyllosilicates, here probably kaolinite plus mica. Other small peaks of K-feldspar and of phyllosilicates, commonly coinciding with each other, are labeled only in Fig 10-8d. Note that some peaks may be overlapping, e.g., main quartz peak at 3.34 Å (Qtz+) contains a mica and a K-feldspar peak. Minerals were identified using the Joint Committee on Powder Diffraction Standards database (JCPDS, 1980). Note the square root vertical scale. a) Sample CB6-092, 1396.5 m. b) KB6-09, 1391.4 m. c) Sample KB10-09, 1373.3 m. d) Sample CB6-088, 1371.4 m.

Clay-fraction XRD analyses

Clay minerals (fraction <2 μm) were studied in detail in four of the gravelly sand samples from different depths (two from upper and two from middle gravelly sand). The samples have comparable assemblages of clay minerals; only the intensities of peaks in diffractograms are slightly different. XRD analyses of air-dried samples and specially treated samples (see Samples and analytical methods) were performed (Fig. 10-9) and complemented with simultaneous thermal analysis (STA).

The main components of the clay fraction are expandable clays (identified as smectite) and kaolinite, with traces of mica. Traces of the main sand components, K-feldspar and possibly quartz, also occur as clay-size particles. The diffraction pattern of an air-dried sample (Fig. 10-9a) shows typical peaks of smectite (main peak at 12.62 Å), kaolinite (main peak at 7.15 Å), minor mica (main peak at 9.98 Å), K-feldspar (main peak at 3.24 Å), and possibly quartz (main peak at 3.33 Å). In some samples probable traces of halite were noted (main peak at 2.81 Å), which might have crystallized from the salty pore

water. After saturation with ethylene glycol, smectite expanded to 16.68 Å. The spectrum of an ethylene glycol saturated sample was also used to check, whether the clay fraction contains a mixed-layered illite/smectite. The °Δ2θ value (difference in 2θ between the second and third smectite peak) is ≤5.31 suggesting that there is no significant illite component (<10 %). After heating to 550 °C, smectite collapsed to a 9.59 Å and kaolinite peaks disappeared (Fig. 10-9a), which confirmed that there is no chlorite (in the four studied samples from above the cataclasite boulder). The K-saturated samples (Fig. 10-9b) show typical peaks of kaolinite (7.14 Å). There are some traces of mica (9.90 Å), K-feldspar (3.23 Å), and possibly quartz (3.33 Å). The 12.23 Å smectite peak expanded to 16.43 Å after saturation with ethylene glycol. After saturation with Mg ions (Fig. 10-9c), there are again typical peaks of smectite (15.06 Å), kaolinite (7.07 Å) and traces of mica, K-feldspar, and quartz. The smectite peak expanded to 17.84 Å after saturation with glycerol in sample CB6-089. However, other samples did not expand fully during the usual time (Fig. 10-9d) and expanded only after a different glycerol saturation method on a ceramic plate was used. This suggests that some high-charged smectite is present.

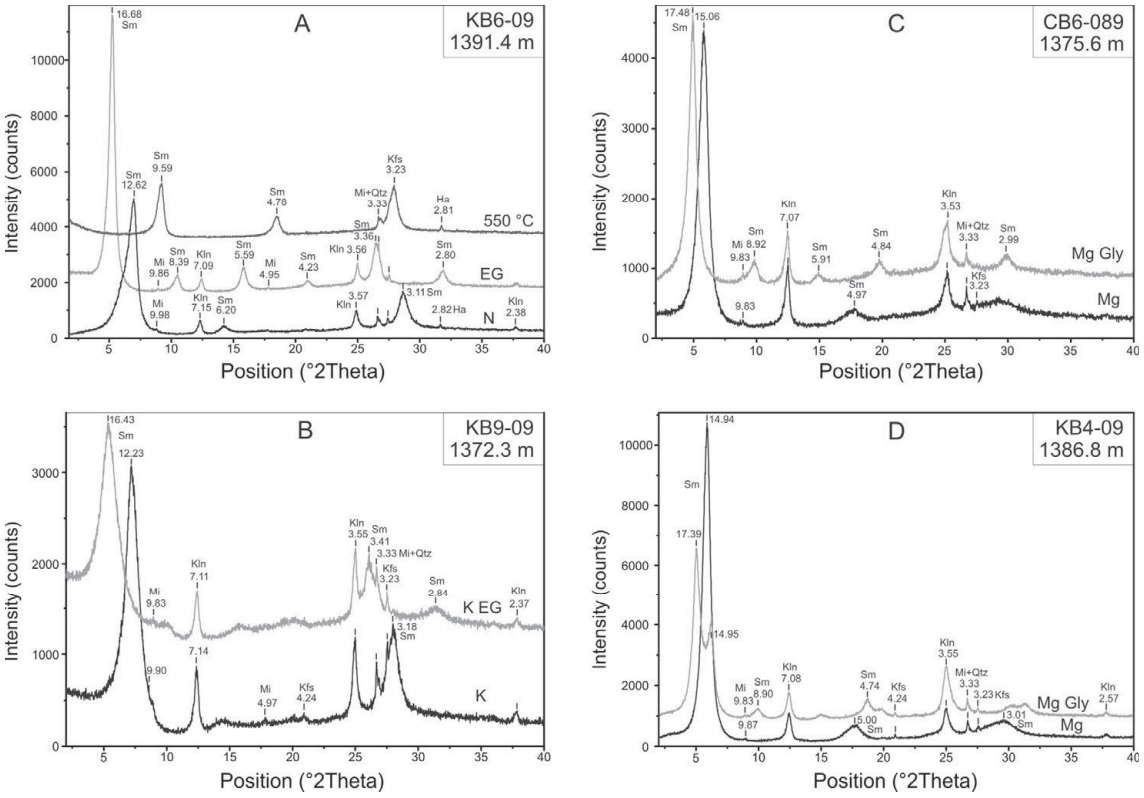

Fig. 10-9. X-ray diffraction spectra of the clay fraction (<2 µm). The d-spacing values in Å are marked in the diagrams. Qtz – quartz, Kfs – K-feldspar, Kln – kaolinite, Sm – smectite, Mi – mica, Ha – halite. a) Sample KB6-09 air-dried (N), saturated with ethylene glycol (EG) and after heating to 550 °C (second spectrum shifted by 1500 and third spectrum by 3500 counts). b) Sample KB9-09 saturated with K and with K and ethylene glycol (second spectrum shifted by 1000 counts). c) Sample CB6-089 saturated with Mg and Mg and glycerol (second spectrum shifted by 600 counts). d) Sample KB4-09 saturated with Mg and Mg and glycerol (second spectrum shifted by 600 counts).

The STA further confirms the presence of smectite and kaolinite. There are characteristic endothermic peaks of smectite at 104 °C (loss of interlayer water) and 674 °C (loss of OH groups) and an endothermic peak typical for kaolinite at 518 °C (loss of OH groups). The residual mass after heating to 1000 °C was 89.67 % of the original mass.

Geochemical analyses

All samples were analyzed for major and trace elements. The results are shown in Table 10-5 and Fig. 10-10. Analyses published in Schmitt et al. (2009) are included to complete the data and discuss possible trends. Chemical analyses are shown for a sample from the amphibolite block and cataclastic gneiss boulder, but only the gravelly sand samples are displayed in Fig. 10-10 and discussed and compared in following text.

The gravelly sand samples are silica-rich. Except for three samples in the lower part, all samples have >80 wt% of SiO_2. Towards the base of the interval, the gravelly sand shows a slight decrease in the SiO_2 content. The lowest SiO_2 values were measured in basal gravelly sand samples CB6-092 and W-54, which have high matrix proportions and contain material reworked from the suevite. Sample KB6-09 also has lower SiO_2 content. The Al_2O_3 content shows a slightly decreasing trend in the upper gravelly sand. In the middle gravelly sand the values are relatively steeply increasing. The Al_2O_3 content correlates negatively with the SiO_2 content ($R^2 = 0.92$). Values of Fe_2O_3 content do not show any clear trend with depth. MgO abundance shows some increase and then decrease in the upper gravelly sand; in the middle gravelly sand the MgO contents are more variable. The highest Fe_2O_3 and MgO contents correspond with the lowest SiO_2 content in the lowermost samples (KB6-09, CB6-092, and W-54). Contents of Na_2O, K_2O, and CaO do not show any particular trends. Sodium is most abundant in the two basal gravelly sand samples (CB6-092 and W-54). The CaO content correlates well with MgO abundance. Generally, the chemical composition is relatively constant in the analyzed upper gravelly sand samples, whereas larger variations occur in the middle gravelly sand samples.

Siderophile element contents and Cr concentrations are low in the analyzed samples (compared to sedimentary breccias above or suevite below the gravelly sand and crystalline block section; Schmitt et al., 2009); the average values are 21 ppm of Cr, 4 ppm of Co, and 15 ppm of Ni. The highest, but still rather low contents occur in the samples from the basal gravelly sand (maximum values 41 ppm of Cr, 10 ppm of Co, and 42 ppm of Ni). The Th and U concentrations are relatively high in the two lowermost samples. Highest Th and U values occur in the uppermost sample CB6-087. These elements (and Rb) probably originated from granite clasts in the gravelly sand or possibly could have been mobilized from the granite slab above.

The chondrite-normalized rare earth element patterns are very similar for all the gravelly sand samples. There is a slight decreasing trend towards enrichment in the heavy

rare earth elements with no or a slightly negative Eu anomaly (average Eu/Eu* = 0.84; as defined by Taylor and McLennan, 1985).

Schmitt et al. (2009) suggested that the composition of the basal gravelly sand samples can be modeled as a mixture of the gravelly sand above (upper and middle gravelly sand) and the suevite below. Harmonic least-squares mixing (HMX) calculations were performed (Stöckelmann and Reimold, 1989) to test this hypothesis and to obtain an estimate of the proportion of the two components. For the gravelly sand component average composition of studied samples of upper and middle gravelly sand (excluding KB6-09 with slightly outlying composition; see Fig. 10-11e) were used. For the suevite component, an average composition of upper suevite (1397–1402 m) from Schmitt et al. (2009) was used. The composition of the sand below the cataclasite boulder was calculated as an average composition of the samples CB6-092 and W-54. Mixing calculations using nine major oxides yielded results with a very low discrepancy (0.27). Discrepancy indicates how well the mixture can be modeled – the lower the discrepancy, the smaller the difference between the modeled and observed compositions. The calculated proportions are 60.7 (±1.7) % of gravelly sand and 39.3 (±1.7) % of upper suevite. More detailed results are shown in Table 10-6. Other runs of mixing calculations (not shown here), using some trace elements, gave similar results but with higher discrepancies (0.4–1.8). It should be noted that the grain size distribution of the two components might play a role in the mixing process.

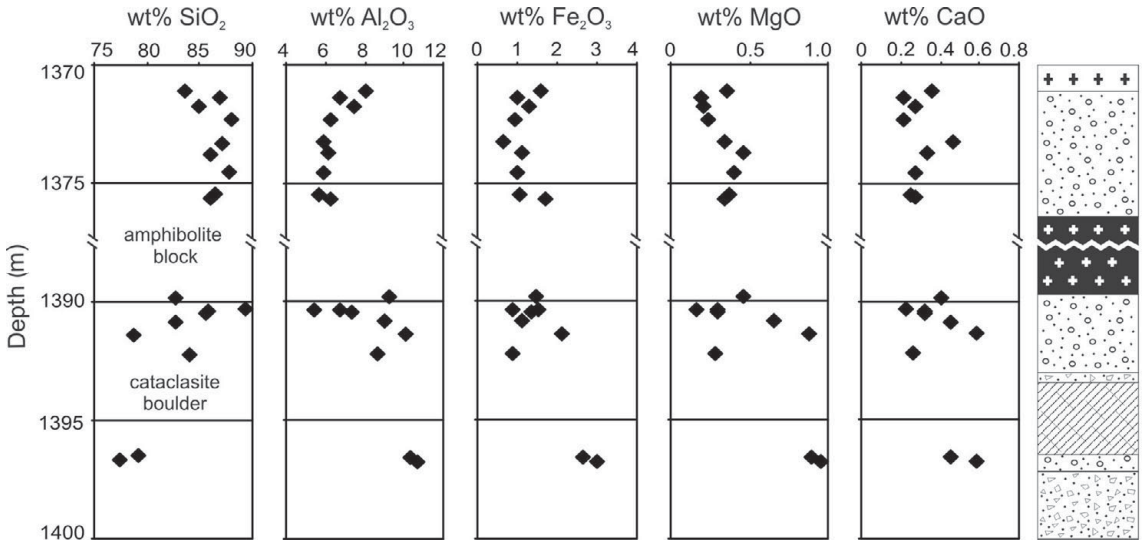

Fig. 10-10. Variations of concentrations (in wt%) of some major oxides with depth below surface in meters. All gravelly sand samples are plotted, blocks and boulders of other lithologies of the interval (amphibolite, cataclastic gneiss, and suevite) are excluded. Geologic column of the gravelly sand interval is shown for comparison (more details in the geologic column in Fig. 10-3). There is slight decrease of SiO_2 content and slight increase of Al_2O_3 and Fe_2O_3 content with depth. Variations in CaO and MgO are very similar to each other. The chemical composition of the samples is relatively constant in the upper gravelly sand, but much more variable in the middle gravelly sand. The basal gravelly sand samples (CB6-092 and W-54) with reworked suevite material show significant differences in composition.

Table 10-5. Whole rock chemical composition of samples from the gravelly sand interval, Eyreville B core, Chesapeake Bay impact structure.

sample	CB6-087*	CB6-088*	W-50*	KB9-09	KB10-09	KB1-09	KB2-09	KB3-09	CB6-089*	CB6-090*
depth (m)	1371.1	1371.4	1371.8	1372.3	1373.3	1373.7	1374.5	1375.5	1375.6	1382.5
lithology	gravelly sand	gravelly sand	gravelly sand	gravelly sand	gravelly sand	gravelly sand	gravelly sand	gravelly sand	gravelly sand	amphibolite
wt%										
SiO_2	83.6	86.9	84.9	88.0	87.2	86.1	87.7	86.5	86.0	47.0
TiO_2	0.30	0.20	0.19	0.21	0.09	0.15	0.10	0.08	0.13	1.20
Al_2O_3	8.10	6.80	7.50	6.22	5.89	6.09	5.89	5.63	6.30	19.10
Fe_2O_3[§]	1.56	1.01	1.29	0.97	0.67	1.12	0.98	1.08	1.72	11.90
MnO	0.02	0.01	0.02	0.01	0.02	0.02	0.01	0.01	0.01	0.14
MgO	0.36	0.20	0.21	0.24	0.34	0.47	0.40	0.37	0.34	6.18
CaO	0.36	0.21	0.28	0.21	0.47	0.33	0.27	0.25	0.28	8.23
Na_2O	0.57	0.26	0.25	0.36	0.36	0.43	0.37	0.39	0.32	2.58
K_2O	2.27	2.09	2.64	1.95	2.69	2.39	2.54	2.55	2.72	0.21
P_2O_5	0.05	0.01	0.01	0.03	0.02	0.02	0.02	0.02	<0.01	0.14
SO_3	<0.1	<0.1	<0.1	n.d.[#]	n.d.	n.d.	n.d.	n.d.	<0.1	0.2
LOI	2.4	1.6	1.9	1.6	1.4	1.7	1.4	1.3	1.4	3.0
Total	99.59	99.29	99.19	99.8	99.23	98.83	99.73	98.16	99.22	99.88
ppm										
Sc	4.37	3.05	2.83	2.84	1.91	2.28	1.67	1.59	3.52	27.1
V	36	23	28	13	13	8	9	14	33	186
Cr	17.8	14.1	16.4	18.5	15.4	18.8	16.8	15.3	16.9	160
Co	5.80	3.80	3.45	3.83	1.34	1.02	2.27	0.82	1.37	56.3
Ni	21	11	8	16	4	<11	7	10	10	154
Zn	42	17	14	19	14	10	8	9	14	102
Rb	104	60.1	71.9	59.1	78.7	63.0	70.4	58.5	80.6	12.6
Sr	88	96	144	92	146	143	133	134	137	328
Y	25	10	<10	12	7	7	5	6	15	<10
Zr	160	108	481	86	32	37	31	21	67	82
Sb	0.13	0.12	0.10	0.12	0.09	0.09	0.09	0.07	0.07	0.08
Cs	3.20	1.39	1.43	1.28	1.28	1.24	1.23	0.99	1.70	2.11
Ba	408	422	631	448	509	603	662	689	601	76
La	36.9	12.6	9.81	15.6	16.1	5.76	7.23	6.55	8.70	4.97
Ce	72.7	26.5	20.1	31.3	19.7	9.88	10.6	13.7	19.0	12.4
Nd	27.0	11.3	7.75	12.4	6.57	4.12	3.61	6.39	8.38	8.06
Sm	4.36	1.92	1.79	2.99	1.26	0.92	0.91	1.52	1.67	2.05
Eu	0.85	0.55	0.49	0.64	0.37	0.26	0.3	0.44	0.59	0.98
Gd	3.89	1.99	1.28	2.77	1.16	0.88	0.78	1.13	1.67	<1.42
Tb	0.66	0.36	0.23	0.39	0.17	0.17	0.11	0.18	0.30	0.52
Tm	0.30	0.22	0.16	0.2	0.12	0.15	0.07	0.09	0.21	0.28
Yb	1.98	1.45	0.90	1.16	0.79	1.03	0.49	0.51	1.44	1.46
Lu	0.32	0.23	0.15	0.18	0.13	0.17	0.08	0.08	0.24	0.22
Hf	4.19	2.69	2.59	2.61	1.75	1.41	1.95	1.09	1.33	1.94
Ta	0.98	0.45	0.31	0.47	0.31	0.23	0.21	0.16	0.24	0.69
Ir (ppb)	<1	<0.8	<0.8	<0.9	<0.8	<0.8	<0.6	<0.6	<0.8	<2.1
Au (ppb)	0.2	<0.4	0.4	<0.6	<0.8	<1.5	<1.5	<0.5	0.1	<1
Th	14.0	3.22	2.92	3.69	2.63	2.16	2.03	1.74	3.03	0.79
U	2.75	1.22	1.12	1.45	1.43	0.66	1.25	0.73	0.95	0.25

Note: All major oxides contents and V, Sr, Y, Zr, and Ba contents were analyzed by XRF, all other element contents determined by INAA.

* data from Schmitt et al. (2009)

[§] total Fe as Fe_2O_3

[#] not determined

Table 10-5. *Continued* Whole rock chemical composition of samples from the gravelly sand interval, Eyrevile B core, Chesapeake Bay impact structure.

sample	KB4-09	CB6-091*	W-53a*	W-53b*	KB5-09	KB6-09	KB7-09	KB8-09	CB6-092*†	W-54*†
depth (m)	1389.8	1390.3	1390.4	1390.5	1390.9	1391.4	1392.2	1393.5	1396.5	1396.7
lithology	gravelly sand	gravelly sand	gravelly sand	gravelly sand	gravelly sand	gravelly sand	gravelly sand	cataclastic gneiss	gravelly sand	gravelly sand
wt%										
SiO_2	82.6	89.4	85.7	85.6	82.7	78.8	84.09	61.8	79.1	77.4
TiO_2	0.39	0.20	0.25	0.18	0.5	0.83	0.18	0.98	0.52	0.55
Al_2O_3	9.21	5.40	6.80	7.40	9.01	10.1	8.63	16.3	10.3	10.7
Fe_2O_3§	1.49	0.91	1.54	1.33	1.11	2.14	0.88	6.97	2.64	3.01
MnO	0.03	0.01	0.01	0.02	0.02	0.04	0.02	0.13	0.02	0.03
MgO	0.46	0.17	0.30	0.30	0.66	0.88	0.28	3.33	0.89	0.95
CaO	0.4	0.23	0.32	0.32	0.45	0.59	0.26	1.11	0.45	0.58
Na_2O	0.54	0.18	0.41	0.29	0.48	0.53	0.47	2.09	0.74	0.74
K_2O	2.47	1.67	2.45	2.72	2.61	2.40	2.77	3.36	2.75	2.53
P_2O_5	0.05	0.02	<0.01	0.01	0.03	0.09	0.04	0.19	0.05	0.06
SO_3	n.d.#	<0.1	<0.1	<0.1	n.d.	n.d.	n.d.	n.d.	<0.1	0.1
LOI	2.3	1.3	1.5	1.6	2.3	2.8	2.1	3.1	2.4	2.6
Total	99.95	99.49	99.28	99.77	99.93	99.1	99.71	99.37	99.86	99.25
ppm										
Sc	4.62	2.40	2.39	2.59	4.65	7.01	2.72	16.2	7.37	8.06
V	29	25	46	32	28	34	25	115	71	61
Cr	24.1	16.4	14.2	14.5	30.7	40.9	15.4	151	36.1	39.1
Co	4.00	4.56	2.90	2.74	2.09	3.80	2.89	18.5	9.57	10.4
Ni	16	16	<19	6	12	19	11	111	42	28
Zn	17	20	12	10	16	22	10	121	29	31
Rb	69.4	57.6	65.6	70.3	73.7	63.5	74.9	125	125	114
Sr	128	68	127	155	168	171	122	145	118	134
Y	11	15	<10	<10	11	22	9	35	40	38
Zr	119	109	142	114	181	284	57	245	218	256
Sb	0.14	0.16	0.12	0.13	0.12	0.20	0.24	0.13	0.88	1.03
Cs	1.59	1.19	1.22	1.31	1.64	2.12	1.23	2.97	11.8	11.6
Ba	467	280	490	603	557	466	525	440	413	405
La	15.0	16.3	8.84	9.21	15.7	22.8	11.7	28.8	43.5	33.3
Ce	30.8	34.3	17.4	17.7	29.6	43.4	21.5	61.9	83.0	67.1
Nd	12.4	15.2	7.06	8.28	12.8	20.2	9.77	19.7	35.7	28.3
Sm	2.88	2.74	1.56	1.45	2.67	4.34	2.17	7.09	7.01	5.49
Eu	0.66	0.64	0.44	0.46	0.73	1.13	0.55	1.33	1.51	1.27
Gd	2.27	3.17	n.d.	n.d.	2.8	3.93	1.73	8.10	7.15	n.d.
Tb	0.37	0.48	0.27	0.23	0.41	0.61	0.30	1.11	1.10	0.94
Tm	0.17	0.24	0.16	0.14	0.28	0.37	0.17	0.57	0.43	0.41
Yb	1.19	1.55	1.07	1.18	1.85	2.26	1.05	2.96	2.91	2.86
Lu	0.19	0.24	0.16	0.18	0.30	0.35	0.17	0.45	0.44	0.42
Hf	3.24	2.42	3.74	2.35	6.65	7.36	1.66	6.05	5.34	6.07
Ta	0.66	0.59	0.38	0.30	0.77	1.00	0.29	1.41	1.03	1.14
Ir (ppb)	<1	<0.8	<1	<0.8	<1.1	<1.2	<0.8	<1.4	<1.1	<1.7
Au (ppb)	<0.7	<0.4	0.2	0.2	<0.7	0.6	<0.6	<1.1	0.5	<0.9
Th	4.71	4.44	3.11	2.60	3.97	4.78	2.95	14.0	8.68	9.20
U	2.10	1.46	1.18	1.07	1.92	2.16	2.25	2.57	2.65	2.51

Note: All major oxides contents and V, Sr, Y, Zr, and Ba contents were analyzed by XRF, all other element contents determined by INAA.

* data from Schmitt et al. (2009)

† with reworked suevite

§ total Fe as Fe_2O_3

not determined

Table 10-6. Details of HMX mixing calculations modeling the composition of the gravelly sand from the basal part (from ~1396 m) of the Eyreville B drill core.

	Gravelly sand (1371.1–1392.2 m)		Upper suevite (1397–1402 m)		Basal gravelly sand (1396.5–1396.7 m)		Basal gravelly sand (1396.5–1396.7 m)	
	average	standard deviation	average	standard deviation	average	standard deviation	calculated	$\Delta_{obs-calc}$*
SiO_2	85.8	2.0	69.3	0.5	78.3	1.2	78.8	-0.5
TiO_2	0.21	0.11	0.82	0.01	0.54	0.02	0.45	0.09
Al_2O_3	6.99	1.26	14.0	0.5	10.5	0.3	10.4	0.1
FeO	1.18	0.30	5.00	0.23	2.83	0.26	2.73	0.09
MnO	0.02	0.01	0.06	0.01	0.03	0.01	0.03	<0.01
MgO	0.34	0.13	1.40	0.21	0.92	0.04	0.76	0.16
CaO	0.31	0.08	1.58	0.26	0.52	0.09	0.52	<0.01
Na_2O	0.38	0.11	1.62	0.18	0.74	<0.01	0.74	<0.01
K_2O	2.44	0.32	3.32	0.23	2.64	0.16	2.69	-0.05
P_2O_5	0.03	0.01	0.13	0.01	0.06	0.01	n.a.	n.a.
SO_3	<0.1	n.d. †	<0.1	n.d.	<0.1	n.d.	n.a.	n.a.
LOI	1.73	0.38	2.4	0.2	2.50	0.14	n.a.	n.a.
Total	99.41	n.a. §	99.63	n.a.	99.56	n.a.	n.a.	n.a.

Note: Average compositions the components (gravelly sand [average of middle and upper gravelly sand samples from this study excluding samples KB6-09, CB6-092, and W-54] and Upper suevite [data from Schmitt et al., 2009]) as well as the resulting mixture (basal gravelly sand [samples CB6-092 and W-54]) are shown. The last two columns show composition of the calculated mixture and its difference from the real basal gravelly sand. HMX mixing calculations are after Stöckelmann and Reimold (1989).

* Δobs–calc = difference between observed and calculated value
† not determined
§ not applicable

Sedimentological classification

According to the modal point counting analyses the gravelly sand could be classified as a wacke (Boggs, 2006; Williams et al., 1982; Dott, 1964), because matrix forms more than 30 vol% in the studied samples. It should be noted that the point counting limit for matrix size was set at 0.05 mm (as smaller clasts are difficult to identify), while in the sedimentary classifications the limit is typically lower, mostly 0.03 mm (Dott, 1964). However, this difference probably would not significantly change the point counting results and certainly would not change the classification of the samples as wackes. Clasts larger than sand size (>2 mm) are present, but they are not a major part of the samples. Modal composition of the gravelly sand samples was plotted into the ternary classification diagram; see Fig. 10-11a. Most of the samples are classified as feldspathic wackes according to this classification, although they are very close to quartz wackes. The two lowermost samples of the gravelly sand interval fall into the category of lithic wackes, due to incorporation of lithic clasts from the underlying suevite. Sample CB6-092 is anomalous due to a large lithic clast present in the thin section. Two samples containing material from the underlying suevite (CB6-089 and W-54) were excluded from the provenance discrimination diagrams described below.

To determine the provenance of the gravelly sand, ternary diagrams after Dickinson et al. (1983) were used. These diagrams were primarily established for sandstones with a lower proportion of matrix and constructed based on analyses of North American Phanerozoic sandstones. Although not every sandstone sample plots correctly in these provenance diagrams, they have a good general validity (Boggs, 2006). Most of our samples plot into the field of continental block – craton interior (Fig. 10-11b). It should be

noted here that we did not use the Gazzi-Dickinson method (e.g., Ingersoll, 1984) for the point counting. If the points were counted with the Gazzi-Dickinson method, a large part of the points counted as lithic clasts would fall into category of quartz or feldspar, thus moving all the points towards the continental block composition in diagram 11b.

The detrital mode of the gravelly sand is closest to the "quartzose mode" defined by Dickinson (1988): dominantly monocrystalline quartz with minor polycrystalline quartz and feldspars (K-feldspar>plagioclase), which is characteristic for weathered cratonic landmasses or recycled sediments. However, polycrystalline quartz is also relatively abundant, or even more abundant than monocrystalline quartz in some samples. The accessory minerals garnet, staurolite, and tourmaline suggest metamorphic source rocks (e.g., Tucker, 1991; Pettijohn, 1975; McLane, 1995).

Geochemical tools for assigning tectonic settings to sandstones were used. The chemical compositions of the gravelly sand are consistent with the characteristics of passive continental margin sandstone as described by Bhatia (1983): enriched in SiO_2 and depleted in Na_2O, CaO, and TiO_2. The ternary diagram for tectonic settings discrimination – Fig. 10-11c (after Toulkeridis et al., 1999 and Bhatia, 1983) shows that the gravelly sand has a composition that is typical for sandstones of passive continental margin. Figure 10-11d shows a bivariate plot of K_2O/Na_2O versus SiO_2. According to this tectonic discrimination diagram for sandstone-mudstone suites by Roser and Korsch (1986) all our samples fall into the passive margin field. Another index of geochemical tectonic setting discrimination – TiO_2 versus (Fe_2O_3+MgO) (Fig. 10-11e; after Bhatia, 1983) provides further evidence that the gravelly sand composition is typical for passive margin sandstones.

DISCUSSION

General petrography, trends with depth, and classification

The gravelly sand is petrographically classified as feldspathic wacke according to its modal composition (e.g., Boggs, 2006; see Fig. 10-11a). The sand has been named gravelly (e.g. Horton et al., 2009a), because also grains larger than the sand size limit (2 mm) occur. These coarser grains do not form a major component of the unit, however, in some samples they are abundant (e.g., KB10-09 and CB6-089; see Appendix).

Some general differences between the basal, middle, and upper gravelly sand samples have been noted in this study. The samples from the middle gravelly sand are richer in the expandable clay minerals, compared to the upper gravelly sand samples, as revealed by the bulk XRD analyses. This is in agreement with the fact that the middle gravelly sand samples have higher proportion of matrix according to the modal point

counting analysis. The samples from the basal gravelly sand have slightly different mineralogical composition, contain more matrix, more abundant lithic clasts, and melt particles.

K-feldspar grains are much more abundant than plagioclase grains in the gravelly sand, as common in sandstones (Tucker, 1991). This reflects the greater chemical stability of K-feldspars and its much more common appearance in continental basement rocks, which are the provenance of many sandstones. Probably for the same reasons, K-feldspars are more abundant in the gravelly sand, although being reworked from an older sediment.

Most analyzed samples are very silica rich (contain >80 wt% SiO_2). There is a slight decrease in SiO_2 content with depth (Fig. 10-10). The samples with lowest silica content represent the basal part of the interval; the lowest SiO_2 content and also the highest Fe_2O_3 content correspond to samples with the highest matrix content. The content of K_2O is much higher than Na_2O and CaO (Fig. 10-11d), which is in agreement with the significant dominance of K-feldspar among the feldspars. There are some slight differences in chemical composition between the middle and upper gravelly sand. The middle gravelly sand samples have more variable composition and generally lower SiO_2 contents. Major differences can be found in the samples from the basal gravelly sand (CB6-092 and W-54). These samples have lower SiO_2 content and higher content of Al_2O_3, Fe_2O_3, and Na_2O. As noted by Schmitt et al. (2009), and further confirmed by HMX mixing calculations, the basal gravelly sand is most likely a mixture of gravelly sand similar to the sand above (middle and upper gravelly sand) and of the suevite below.

The discrimination diagrams (Fig. 10-11), based on modal and chemical composition of the gravelly sand, indicate that the tectonic setting of the gravelly sand was a passive continental margin and the source of the sand was a continental block. This is in accordance with the position of the Chesapeake Bay impact structure (or more precisely of the source sedimentary formations of the gravelly sand) on the passive Atlantic continental margin in the Virginia Coastal Plain. The most probable precursor of the gravelly sand, the fluvial-deltaic deposits of the Potomac Formation (or an older unknown formation), were derived from the Appalachian Mountains, as were also the other younger formations of marine origin. Although these provenance and tectonic setting results were expected, they further indicate that the gravelly sand was derived from the local continental shelf sediments and no discernible exotic material was mixed into the gravelly sand.

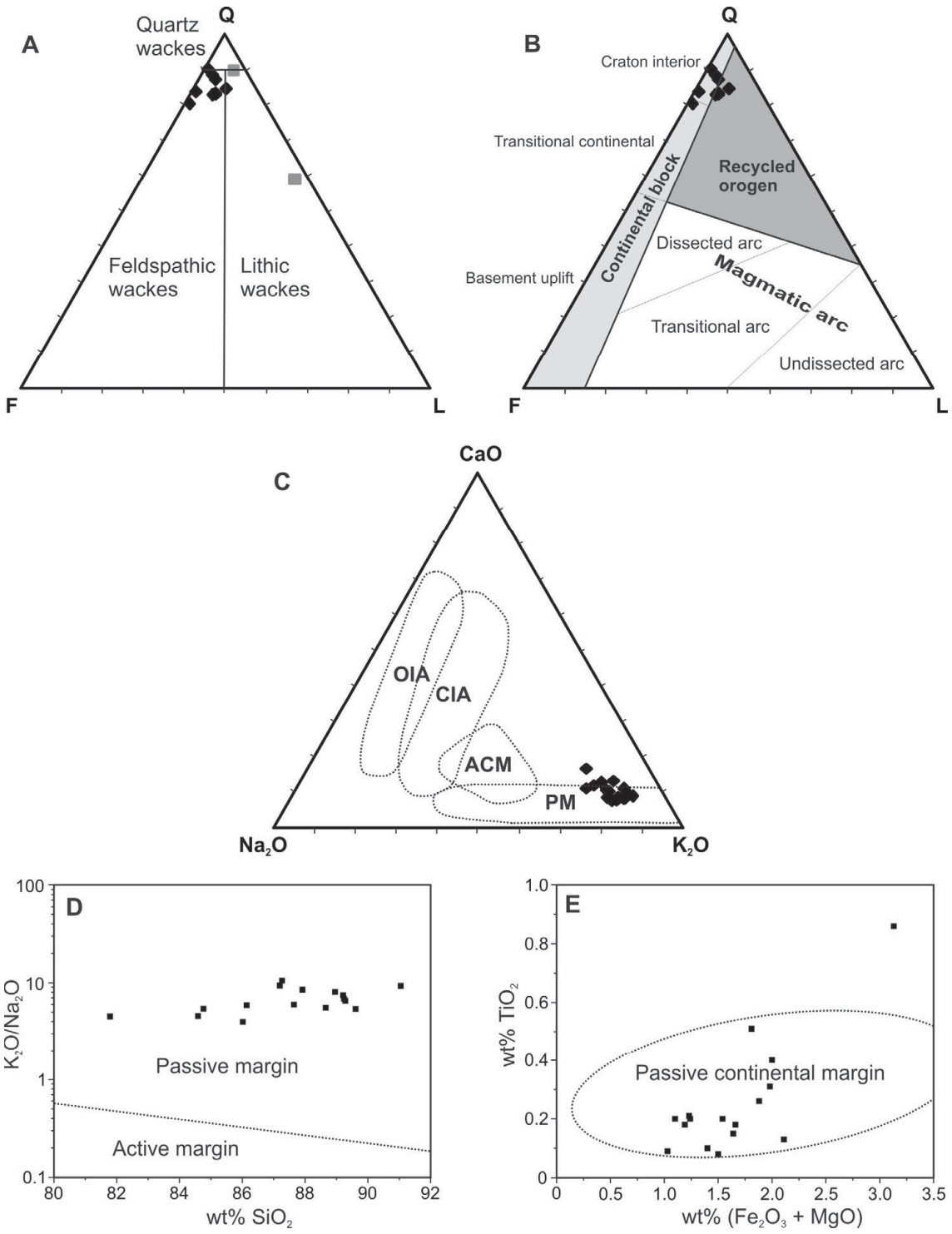

Fig. 10-11. Classification and provenance diagrams for sandstones in general. Point counting data (only the good quality thin sections) from Table 10-2 and geochemical data from Table 10-5 were used for plotting. The two basal gravelly sand samples with incorporated suevite material are plotted only in the A diagram, but are excluded from other diagrams. a) classification ternary diagram for wackes after Boggs (2006) and Willimans et al. (1982), modified from Dott (1964). The corners of the diagram are Q – siliceous resistates (mono- and polycrystalline quartz and chert), F – feldspars (feldspars), and L – labile fragments (lithic clasts). The two samples from the basal part (below cataclasite boulder) are marked with gray squares. b) Provenance diagram after Dickinson et al. (1983). The corners of the ternary diagram Q – quartzose grains, F – monocrystalline feldspar grains, and L – unstable polycrystalline lithic fragments contain the same components as in A. c) Ternary diagram

CaO-Na_2O-K_2O after Toulkeridis (1999) and Bhatia (1983). OIA – Oceanic island arch, CIA – Continental island arch, ACM – Active continental margin, PM – Passive margin. d) Cut-out of a bivariate diagram after Roser and Korsch (1986). Ratio K_2O/Na_2O versus SiO_2 abundance is plotted and tectonic setting is characterized. Only part of the original diagram showing our samples is plotted. Note the logarithmic vertical scale. The values are recalculated to 100% volatile free. e) Bivariate diagram after Bhatia (1983). TiO_2 content is plotted versus (Fe_2O_3+MgO) content to discriminate tectonic setting. The values are recalculated to 100% volatile free. All samples (except sample KB6-09) fall into the area typical for passive continental margin. Fields of other tectonic settings would plot out of the diagram area.

Comparison with previous studies

Our observations of the gravelly sand and crystalline block section of the Eyreville B drill core are in generally good agreement with previous studies. Macroscopic observations are similar to those of Gohn et al. (2009) and Horton et al. (2009a, 2009b). The main mineral components of the gravelly sand are quartz and K-feldspar grains, which is in accordance with the observations by, e.g., Reimold et al. (2009). These authors interpret the polycrystalline quartz to be derived from granitic and gneissic rocks, matching the microscopic observations.

Bulk XRD analyses of the gravelly sand have been performed by Horton et al. (2009b). The mineral identified assemblage is very similar to the results of our study: quartz, K-feldspar (microcline), kaolinite, smectite, and mica (muscovite). In the lowermost sample (at 1396.9 m), Horton et al. (2009b) noted the presence of amphibole. Amphibole was not found in our samples; the mineral could be part of some rock clasts not present in our samples. Chlorite is not a significant component of our samples, except for sample CB6-092, based on the XRD and microscopic studies. Results of bulk XRD analyses by Larsen et al. (2009) identified quartz and K-feldspar as the main components of a gravelly sand sample from 1375.2 m depth, which is similar to the results of this study. In the clay fraction of the gravelly sand, Larsen et al. (2009) also detected expandable clays, kaolinite, and traces of illite. Related, but more detailed clay mineralogy results for a sample from the gravelly sand interval (1390 m depth) are presented by Ferrell and Dypvik (2009), who, in addition, detected traces of serpentine.

In previous studies of the basal gravelly sand interval, small supposedly glauconite grains (Reimold et al., 2009, Fig. 5I) were noted, based only on optical microscopy studies. We also observed green grains resembling glauconite in samples CB6-092 and W-54, and all the grains (including the grain presented in Fig. 5I in Reimold et al., 2009) are composed of the same mineral, which has a composition of iron-rich chlorite. No glauconite was detected in our microRaman and SEM-EDX analyses.

Comparison with sedimentary breccias above the granite slab

We compared our data for the gravelly sand below the granite to data from the sedimentary breccias above the granite slab. We consider the five main subdivisions of the sediment section above the granite by Edwards et al. (2009a). The distinction between monomict sedimentary breccias (*SBS* and *Eb*) derived entirely from nonmarine sediments of the Cretaceous Potomac Formation and interpreted as avalanche deposits and polymict diamictons (*Edl* and *Edu*) interpreted as ocean-resurge debris flows (Edwards et al., 2009a; Gohn et al. 2009; Self-Trail et al., 2009), is particularly important. Polymict diamictons (*Edl* and *Edu*) and stratified member (*Es*) are called "higher Exmore members" further in the text.

When the modal composition of the gravelly sand and the higher Exmore members is compared (Reimold et al., 2009), it is obvious that the higher Exmore members contain more matrix. In the higher Exmore members, matrix commonly forms >40 vol%, or even >50 vol%, whereas in the gravelly sand the proportion of matrix is higher than 40 vol% only in the four lowermost samples. Glauconite is relatively abundant in the higher Exmore members (Edwards et al., 2009a), where it forms commonly about 2 vol% (Reimold et al., 2009), but is absent in the gravelly sand. In addition the abundance of feldspars is different, further suggesting a different source. K-feldspar (mostly microcline) forms more than 5 vol% in all samples of the gravelly sand (except for the two different basal samples CB6-092 and W-54), while in the higher Exmore members, K-feldspar is less common at <5 vol% in most samples (Reimold et al., 2009). On the other hand, plagioclase is rare (absent or accessory) in the gravelly sand, but more abundant ubiquitous in higher Exmore members, where it forms ~3 vol%. Mica is rare in both Exmore higher members and gravelly sand, contributing <1 vol%. The rock clast (both sedimentary and crystalline) content is variable, but similar in both gravelly sand and higher Exmore members, typically a few vol%. Carbonate was noted only in some samples, as rare clasts or patches in both gravelly sand and Exmore Formation; its content is very variable. Gravelly sand has not been found to contain carbonate fossils, as noted by Self-Trail et al. (2009). This indicates rather non-marine origin, although marine microfossils can be absent even in marine sediments under poor environmental conditions. Melt particles were detected only in the basal part of the gravelly sand and are probably reworked from the underlying suevite (e.g., Horton et al., 2009b). In the Exmore upper diamicton member, there are some layers with abundant melt particles, probably fallback particles incorporated from the ejecta plume that form up to tens of vol% (Reimold, 2009).

The XRD analyses confirm differences in mineral composition between the gravelly sand and the polymict diamictons (*Edl* and *Edu*) in the Exmore Formation. In bulk XRD analyses of the polymict diamictons, less K-feldspar, but more abundant muscovite and some albite were detected by Larsen et al. (2009). In the clay fraction of the *Edu* member,

in addition to the same minerals as in the gravelly sand, minor illite and glauconite were detected (Larsen et al., 2009). The expandable clays were found to be smectite, vermiculite, and smectite-vermiculite intergrade varieties (Larsen et al., 2009). However, Larsen et al. (2009) suggested that high-charge smectite instead of vermiculite might be present in the Exmore diamictons and sediment boulders and sand. Larsen et al. (2009) noted that the existence of vermiculite is puzzling, as it is a typical weathering product of mafic rocks. In our analyses of the gravelly sand, smectite in some samples did not expand fully after the usual time saturated with Mg ions and glycerol (Fig. 10-9d). However, after more efficient saturation on a ceramic plate, all of the samples expanded. This suggests that some high-charged smectite, but no vermiculite, is present. Larsen et al. (2009) further noted that the abundance of smectite (and vermiculite) indicates an authigenic origin rather than simply reworking of detrital clay from the pre-impact sediments. Ferrell and Dypvik (2009) found smectites, relatively high amounts of mica, and chlorite in all Exmore members (except for the uppermost stratified member). The same clay minerals were found also in the block-dominated Exmore member and in the unit of sediment boulders and sand above the granite (Ferrell and Dypvik, 2009). Kaolinite is rare in the polymict diamictons and nearly absent in the uppermost samples (above 450 m depth). Higher amounts of kaolinite were detected only in some samples from the *Eb* member and from the *SBS* unit below 1000 m depth (Ferrell and Dypvik, 2009). In contrast, kaolinite is abundant in the gravelly sand samples. The kaolinite might have been derived from the relatively abundant feldspars of the gravelly sand.

The chemical composition of the gravelly sand is compared with the analyses of samples of sedimentary breccias from above the granitic slab (data from Schmitt et al., 2009). The stratified member of the Exmore Formation is less silica rich in the uppermost part (above ~444 m). Samples from ~446 m depth are similar in composition to the gravelly sand, have ~80 wt% of SiO_2, but higher Fe_2O_3, Na_2O, and CaO contents. Upper diamicton member samples have generally lower SiO_2 content and higher content of most other major oxides (Al_2O_3, Fe_2O_3, Na_2O, and CaO) compared to gravelly sand. The same difference in chemical composition can be found in the *Eb* member (in both matrix and larger clasts and blocks) and *Edl* member. In part of the *SBS* section (below 867.4 m), the samples are also generally much lower in SiO_2 and higher in other major oxides than the gravelly sand, but some boulders with composition similar to gravelly sand were observed (further discussed below).

Comparison with suevite

The suevite is clearly different in texture and composition from the gravelly sand. It contains melt particles and has much a higher proportion and variety of rock clasts. Material derived from the Potomac Formation, which is the likely source material for the

gravelly sand, may be a minor component of the upper suevite (about 20 %), while basement-derived schist and gneiss may have been the main components of the suevite (based on mixing calculations; see Bartosova et al., 2009b).

The melt particles from the basal part of the gravelly sand (samples CB6-092 and W-54) are (under petrographic microscope) similar to melt type m2 (brownish melt altered to phyllosilicates) in the suevite, as defined by Bartosova et al. (2009a). In addition, the chemical composition of the melt particles (Table 10-3) is comparable to the composition of type m2 or m5 melt particles (Bartosova et al., 2009b). Reimold et al. (2009) reported some glassy melt particles from the basal gravelly sand. We observed some parts of melt particles that appeared to be glassy under the optical microscope, but SEM revealed alteration texture in all melt particles.

Suevite contains in contrast to the gravelly sand other abundant components as plagioclase, muscovite, chlorite, and in some cases calcite, according to the results of bulk XRD analyses (Bartosova et al., 2009a, and unpublished data). These minerals occur as mineral clasts in the suevite matrix but also in rock clasts in the suevite. In the gravelly sand these components are minor and were not detected by XRD. Horton et al. (2009b) also detected rutile, andalusite, and tourmaline in the upper suevite samples using XRD.

The suevites are rich in shocked and melted clasts, which have not been detected in the gravelly sand, except for the reworked melt particles along the base. These observations confirm that gravelly sand was deposited after suevite formation and from a different, relatively homogeneous source material.

Source and emplacement

The gravelly sand originated from the lowermost part of the Potomac Formation according to its pollen flora (Self-Trail et al., 2009). The gravelly sand samples are the most silica-rich samples from the Eyreville drill cores, containing >80 wt% of SiO_2. The Potomac Formation probably was the most silica-rich target material (quartz sand with dispersed silt and clay beds; Powars and Bruce, 1999; Poag et al., 2004). Potomac Formation samples from the Jamestown drill core have also SiO_2 contents above 80 wt% (Deutsch and Koeberl, 2006). In addition, contents of other major oxides are comparable in the gravelly sand and the Potomac Formation samples. Some SiO_2-rich samples with compositions similar to the gravelly sand occur in the gravelly sand and sedimentary blocks above the granitic block Schmitt et al. (2009). For example, sample CB6-071 (unit *SBS*, 1073.4 m depth) and sample CB6-064 (unit *SBS*, 904.6 m depth) are similar in composition to the gravelly sand. Also their appearance in thin section is similar to the gravelly sand and might suggest a similar source of these samples and the gravelly sand below the granitic slab. Sample CB6-049 (unit *Eb*, 622.1 m depth) is the uppermost

chemically similar sample. However, it is more fine-grained and mineralogically different from the gravelly sand, containing more plagioclase and accessory minerals.

The Lower Cretaceous Potomac Formation is the oldest and thickest pre-impact sedimentary unit in the Chesapeake Bay region, deposited during fluvial-deltaic regime (Powars and Bruce, 1999). Most of the younger (Upper Cretaceous and lower Tertiary) glauconite carrying formations were deposited during marine sedimentation that dominated after general transgression (Poag et al., 2004). These formations were the main glauconite source in the polymict diamictons (*Edl* and *Edu*) interpreted as so-called resurge debris flows above 867.4 m (Self-Trail et al., 2009). The absence of glauconite in the gravelly sand indicates that the source material was probably non-marine, and for sure different than for the polymict diamictons. No melt particles were observed in the middle and upper gravelly sand. Melt particles occur only in the basal part of the gravelly sand and their abundance is highest in the lowermost gravelly sand sample. The melt particles are probably reworked from the underlying suevite (Horton et al., 2009a, Gohn et al., 2009). The chemical composition also indicates that the sand below the cataclasite boulder is a mixture of the gravelly sand and suevite (what was further verified by mixing calculations in the present study). Lithic clasts are relatively rare and small in the studied samples. Modal and chemical composition displays values typical of sandstones deposited on passive continental margin. This is in agreement with the hypothesis that the gravelly sand interval was deposited by an avalanche of the pre-impact sediments (Gohn et al., 2009; Horton et al., 2009b), with probably no exotic material (e.g., from the ejecta plume) included. The sole of the granite slab is fractured, which may be related to its origin and emplacement during the crater collapse (Gohn et al., 2009; Horton et al., 2009a, 2009b). The fractured grains of gravelly sand (Fig. 10-6c) could be a result of the impact and of violent deposition of the gravelly sand and sliding of the granitic slab on top of it, however, the fractures might have different origin (including possible fracturing during thin section preparation). The amphibolite block and cataclasite boulder show no evidence of shock metamorphism, which might suggest their origin in the outer parts of the transient crater (as was suggested from the other crystalline blocks from the Eyreville core, e.g., Kenkmann et al., 2009). “Microtektites” reported from the gravelly sand above the amphibolite block (1375.2 m depth) by Larsen et al. (2009) were not confirmed in our study. No features like dewatering structures, such as those documented above the granite slab (Gohn et al., 2009), were observed either.

CONCLUSIONS

Twenty samples from the gravelly sand interval have been subjected to petrographic, mineralogical, and geochemical analyses. The gravelly sand is a poorly consolidated sediment consisting of sand to gravel-sized grains embedded in a fine-grained, clayey matrix. The main components, as detected by optical microscopy and XRD analyses, are quartz (mono- and polycrystalline) and K-feldspar (microcline). Other mineral grains constitute <1 vol%. Further, there are relatively rare lithic clasts that comprise mostly <5 vol%. The samples are silica-rich, with more than 80 wt% of SiO_2; Al_2O_3 (~7 wt%), K_2O (~2.5 wt%), and Fe_2O_3 (~1.5 wt%) are other abundant components. There are no enrichments in siderophile elements.

The relatively thin gravelly sand and crystalline block section (~26 m; 1397.16-1371.1 m) contains a large amphibolite block (~10 m) and two boulders of respectively cataclasite and suevite. These blocks divide the gravelly sand into three intervals that have slightly different compositional characteristics.

The upper gravelly sand is generally coarser-grained, has a lower amount of matrix, and a slightly different chemical composition (e.g., higher SiO_2 content) compared to the middle gravelly sand. The bulk XRD analyses also suggest less abundant clay minerals in the upper gravelly sand. There is no compositional difference between the clay fraction in the upper and middle gravelly sand, which in both cases consists of smectite and kaolinite with traces of mica.

The basal gravelly sand (1397.16–1396.44 m) contains more matrix, less K-feldspar, and more mica compared to the sands above. In terms of chemical composition the basal part differs in lower SiO_2 content and higher content of Al_2O_3 and Fe_2O_3. There are more lithic clasts and a few vol% of melt particles, likely reworked from the suevite. Mixing calculations suggest that the samples of the basal gravelly sand are a mixture of about 60 % of (middle and upper) gravelly sand and 40 % of suevite. No glauconite was observed.

The results of this study are in agreement with previous interpretations that the gravelly sand formed by an avalanche during the impact event (Gohn et al., 2009; Horton et al., 2009b), and that the source material is probably the lowermost Potomac Formation or similar material (Self-Trail et al, 2009). Fractured grains within the sand could have been formed by the impact or during the violent and rapid transport and sliding of the granitic slab on top of the sand. The chemical composition of the gravelly sand is similar to the compositions of previously analyzed samples of non-marine sediments from the Potomac Formation (e.g., Deutsch and Koeberl, 2006). The absence of marine microfossils (Self-Trail et al., 2009) and absence of glauconite indicate a non-marine source material. The provenance and tectonic setting discrimination diagrams show values

that are typical for passive continental margin sandstone. The amphibolite block and cataclasite boulder are clearly exotic and might have originated from the outer parts of the transient crater.

Acknowledgments: The drilling at Eyreville was supported by ICDP, USGS, and NASA. We appreciate the work of general contractor DOSECC and drilling operator Major Drilling, USA. The present work was supported by the Austrian Science Foundation FWF, project P18862-N10 (to C.K.). The help of the staff at the USGS National Center, Reston, during the sampling process is appreciated. We appreciate the help of E. Klapfer and J. Sterba (Atominstitut Vienna) with the irradiations. We thank R-T. Schmitt, K. Krahn and H.R. Knöfler (Museum of Natural History, Humboldt-University, Berlin, Germany) and P. Nagl and P. McDonald (Univ. Vienna) for the XRF analysis. The assistance of E. Libowitzky (Univ. Vienna) with the microRaman spectroscopy and of F. Brandstaetter (Natural History Museum, Vienna) with the SEM-EDX analyses is highly appreciated. We thank F. Ottner (Univ. of Natural Resources and Applied Life Sciences, Vienna) for performing simultaneous thermal analysis. W.U. Reimold (Museum of Natural History, Humboldt-University, Berlin, Germany) is thanked for providing thin sections of the gravelly sand samples from the Berlin sample suite. We thank C. W. Poag and an anonymous reviewer, as well as the internal USGS reviewers G.S. Gohn and L.E. Edwards, for constructive comments that helped to substantially improve the manuscript.

References:

Bartosova K., Ferrière L., Koeberl C., Reimold W. U., and Gier S. 2009a. Petrographic and shock metamorphic studies of the impact breccia section (1397 – 1551 m depth) of the Eyreville drill core, Chesapeake Bay impact structure, USA. In *Deep drilling in the Chesapeake Bay impact structure,* edited by Gohn G. S., Koeberl C., Miller K. G., and Reimold W. U. *Geological Society of America Special Paper* 458: 317–348.

Bartosova K., Mader D., Schmitt R. T., Ferrière L., Koeberl C., Reimold W. U., and Brandstaetter F. 2009b. Geochemistry of the impact breccia section of the Eyreville drill core, Chesapeake Bay impact structure, USA. In *Deep drilling in the Chesapeake Bay impact structure,* edited by Gohn G. S., Koeberl C., Miller K. G., and Reimold W. U. *Geological Society of America Special Paper* 458: 397–433.

Bhatia M. R. 1983. Plate tectonics and geochemical composition of sandstones. *Journal of Geology* 91: 611-627.

Blair T. C. and McPherson J. G. 1999. Grain size and textural classification of coarse sedimentary particles. *Journal of Sedimentary Research* 69: 6–19.

Boggs S. Jr. 2006. Principles of sedimentology and stratigraphy. Fourth edition, Pearson education, Inc., Upper Saddle River, New Jersey, 662 p.

Collins G. S. and Wünnemann K. 2005. How big was the Chesapeake Bay impact? Insight from numerical modeling. *Geology* 33: 925–928.

Deutsch A. and Koeberl C. 2006. Establishing the link between the Chesapeake Bay impact structure and the North American tektite strewn field: The Sr-Nd isotopic evidence. *Meteoritics and Planetary Science* 41: 689–703.

Dickinson W. R. 1970. Interpreting detrital modes of graywacke and arkose. *Journal of Sedimentary Petrology* 40: 695–707.

Dickinson W. R., Beard L. S., Brakenridge G. R., Erjavec J. L., Ferguson R. C., Inman K. F., Knepp R. A., Lindberg F. A., and Ryberg P. T. 1983. Provenance of North American Phanerozoic sandstones in relation to tectonic setting. *Geological Society of America Bulletin* 94: 222–235.

Dickinson W. R. 1988. Provenance and sediment dispersal in relation to paleotectonics and paleogeography of sedimentary basins. In *New Perspectives in basin analysis*, edited by Kleinspehn K. L. and Paola C., Springer, p. 3–25.

Dott R. H. Jr. 1964. Wacke, graywacke and matrix – what approach to immature sandstone classification? *Journal of Sedimentary Petrology* 34: 625–632.

Downs R. T. 2006. The RRUFF Project: an integrated study of the chemistry, crystallography, Raman and infrared spectroscopy of minerals. Program and Abstracts of the 19th General Meeting of the International Mineralogical Association in Kobe, Japan. O03-13.

Edwards L. E., Powars D. S., Gohn G. S., and Dypvik H. 2009a. Geologic columns for the ICDP-USGS Eyreville A and B cores, Chesapeake Bay impact structure: Sediment breccias, 444 to 1,096 m depth. In *Deep drilling in the Chesapeake Bay impact structure,* edited by Gohn G. S., Koeberl C., Miller K. G., and Reimold W. U. *Geological Society of America Special Paper* 458: 51–90.

Edwards L. E., Powars D. S., Browning J. V., McLaughlin P. P., Miller K. G., Self-Trail J. M., Kulpecz A. A., and Elbra T. 2009b. Geologic columns for the ICDP-USGS Eyreville A and C coreholes, Chesapeake Bay impact structure: Post-impact sediments, 0 to 444 m depth. In *Deep drilling in the Chesapeake Bay impact structure,* edited by Gohn G. S., Koeberl C., Miller K. G., and Reimold W. U. *Geological Society of America Special Paper* 458: 91–114.

Ferrell R. E. Jr. and Dypvik H. 2009. The mineralogy of the Exmore – Chickahominy boundary section of the Chesapeake Bay Impact structure – the Eyreville core. In *Deep drilling in the Chesapeake Bay impact structure,* edited by Gohn G. S., Koeberl C., Miller K. G., and Reimold W. U. *Geological Society of America Special Paper* 458: 723–746.

Gohn G. S., Koeberl C., Miller K. G., Reimold W. U., Cockell C. S., Horton J. W. Jr., Sanford W.E., and Voytek M.A. 2006a. Chesapeake Bay impact structure drilled: *EOS, Transactions American Geophysical Union* 87: 349 & 355.

Gohn G. S., Koeberl C., Miller K. G., Reimold W. U., and the scientific staff of the Chesapeake Bay impact structure drilling project. 2006b. Chesapeake Bay impact structure deep drilling project completes coring. *Scientific Drilling* 2006: 34–37.

Gohn G. S., Sanford W. E., Powars D. S., Horton J. W. Jr., Edwards L. E., Morin R. H., and Self-Trail J. M. 2007. Site report for USGS test holes drilled at Cape Charles, Northampton County, Virginia, in 2004: *U.S. Geological Survey Open-File Report* 2007–1094, 22 p.

Gohn G. S., Koeberl C., Miller K. G., Reimold W. U., Browning J. V., Cockell C. S., Horton J. W. Jr., Kenkmann T., Kulpecz A.A., Powars D. S., Sanford W.E., and Voytek M. A. 2008. Deep drilling into the Chesapeake Bay impact structure. *Science* 320: 1740–1745.

Gohn G. S., Powars D. S., Dypvik H., and Edwards L. E. 2009. Rock-avalanche and ocean-resurge deposits in the late Eocene Chesapeake Bay impact structure: Evidence from the ICDP-USGS Eyreville cores, Virginia, USA. In *Deep drilling in the Chesapeake Bay impact structure,* edited by Gohn G. S., Koeberl C., Miller K. G., and Reimold W. U. *Geological Society of America Special Paper* 458: 587–616.

Horton J. W. Jr. and Izett G. A. 2005. Crystalline-rock ejecta and shocked minerals of the Chesapeake Bay impact structure, USGS-NASA Langley core, Hampton, Virginia, with supplemental constraints on the age of impact. In *Studies of the Chesapeake Bay impact structure—The USGS-NASA Langley corehole, Hampton, Virginia, and related coreholes and geophysical surveys*, edited by Horton J. W. Jr., Powars D. S., and Gohn G. S. *US Geological Survey Professional Paper* 1688: E1–E30.

Horton J. W. Jr., Powars D. S., and Gohn G. S. 2005. Studies of the Chesapeake Bay impact structure—Introduction and discussion. In *Studies of the Chesapeake Bay impact structure—The USGS-NASA Langley corehole, Hampton, Virginia, and related coreholes and geophysical surveys*, edited by Horton J. W. Jr., Powars D. S., and Gohn G. S. *US Geological Survey Professional Paper* 1688: A1–A24.

Horton J. W. Jr., Aleinikoff J. N., Kunk M. J., Jackson J. C., Belkin H., and Chou I.-M. 2007a. Initial studies of breccias, blocks, and crystalline rocks in the ICDP-USGS Eyreville-B core, Chesapeake Bay impact structure, 1095–1766 m depth. *Geological Society of America Abstracts with Programs*, 39, no. 6, 451.

Horton J. W. Jr., Gohn G. S., Gibson R. L., Reimold W. U., and Edwards L. E. 2007b. Geologic column of the ICDP-USGS Eyreville-B core, Chesapeake Bay impact structure: Breccias, blocks, and crystalline rocks, 1095–1766 m depth. *Geological Society of America Abstracts with Programs*, 39, no. 6, 314.

Horton J. W. Jr., Gohn G. S., Powars D. S., and Edwards L. E. 2008. Origin and emplacement of impactites in the Chesapeake Bay impact structure, Virginia, USA. In *The sedimentary record of meteorite impacts*, edited by Evans K., Horton J. W. Jr., King D. T. Jr., and Morrow J. R. *Geological Society of America Special Paper 437*: 73–97.

Horton J. W. Jr., Gibson R. L., Reimold W. U., Wittmann A., Gohn G. S., and Edwards L. E. 2009a. Geologic column for the ICDP-USGS Eyreville B core, Chesapeake Bay impact structure: Impactites and crystalline rocks, 1,096–1,766 m. In *Deep drilling in the Chesapeake Bay impact structure,* edited by Gohn G. S., Koeberl C., Miller K. G., and Reimold W. U. *Geological Society of America Special Paper* 458: 21–49.

Horton J. W. Jr., Kunk M. J., Belkin H. E., Aleinikoff J. N., Jackson J. C., and Chou I-M. 2009b, Evolution of crystalline target rocks and impactites in the Chesapeake Bay impact structure, ICDP-USGS Eyreville B core. In *Deep drilling in the Chesapeake Bay impact structure,* edited by Gohn G. S., Koeberl C., Miller K. G., and Reimold W. U. *Geological Society of America Special Paper* 458: 277–316.

Ingersoll R. V., Bullard T. F., Ford R. L., Grimm J. P., Pickle J. D., and Sares S. W. 1984. The effect of grain size on detrital modes: a test of Gazzi-Dickinson point-counting method. *Journal of Sedimentary Petrology* 54: 103–116.

JCPDS, 1980, Mineral powder diffraction file-Data book, Joint Committee on Powder Diffraction Standards, International Centre for Diffraction Data, USA.

Kenkmann T., Collins G. S., Wittmann A., Wünnemann K., Reimold W. U., and Melosh J. H. 2009. A model for the formation of the Chesapeake Bay impact crater as revealed by drilling and numerical simulation. In *Deep drilling in the Chesapeake Bay impact structure,* edited by Gohn G. S., Koeberl C., Miller K. G., and Reimold W. U. *Geological Society of America Special Paper* 458: 571–586.

Koeberl C. 1993. Instrumental neutron activation analysis of geochemical and cosmochemical samples: A fast and reliable method for small sample analysis. *Journal of Radioanalytical and Nuclear Chemistry* 168: 47–60.

Koeberl C., Poag C. W., Reimold W. U., and Brandt D. 1996. Impact origin of the Chesapeake Bay structure and the source of the North American tektites. *Science* 271: 1263–1266.

Larsen D., Stephens E. C., and ZivkovicV.B., 2009, Postimpact alteration of sedimentary breccias in the ICDP-USGS Eyreville A and B cores with comparison to the Cape Charles core, Chesapeake Bay impact structure, Virginia, USA. In *Deep drilling in the Chesapeake Bay impact structure,* edited by Gohn G. S., Koeberl C., Miller K. G., and Reimold W. U. *Geological Society of America Special Paper* 458: 699–722.

Lewis D.W. and McConchie D. 1994. Practical Sedimentology, Springer, 213 p.

Mader D. and Koeberl C. 2009. Using Instrumental Neutron Activation Analysis for geochemical analyses of terrestrial impact structures: Current analytical procedures at the University of Vienna Geochemistry Activation Analysis Laboratory. Applied Radiation and Isotopes 67: 2100–2103.

Malinconico M. L., Sanford W. E., and Horton J.W. Jr. 2009. Post-impact thermal history of the Chesapeake Bay impact structure, based on downhole vitrinite reflectance data, ICDP-USGS Eyreville deep core holes and Cape Charles test holes. In *Deep drilling in the Chesapeake Bay impact structure,* edited by Gohn G. S., Koeberl C., Miller K. G., and Reimold W. U. *Geological Society of America Special Paper* 458: 905–931.

McLane M. 1995. Sedimentology. Oxford University Press, New York, 423 p.

Moore D. M. and Reynolds R. C. Jr. 1997. X-ray diffraction and the identification and analysis of clay minerals: Oxford University Press, Oxford (U.K.), 378 p.

Ormö J., Sturkell E., Horton J. W. Jr., Powars D. S., and Edwards L. E. 2009. Comparison of clast frequency and size in the resurge deposits at the Chesapeake Bay impact structure (Eyreville A and Langley cores): Clues to the resurge process. In *Deep drilling in the Chesapeake Bay impact structure,* edited by Gohn G. S., Koeberl C., Miller K. G., and Reimold W. U. *Geological Society of America Special Paper* 458: 617–632.

Pettijohn F. J. 1975. Sedimentary rocks. Third edition, Harper & Row Publishers, New York, 628 p.

Poag C. W., Powars D. S., Poppe L. J., Mixon R. B., Edwards L. E., Folger D. W., and Bruce S. 1992. Deep Sea Drilling Project Site 612 bolide event: New evidence of a late Eocene impact-wave deposit and a possible impact site, U.S. east coast. *Geology* 20: 771–774.

Poag C. W., Powars D. S., Poppe L. J., and Mixon R. B. 1994. Meteoroid mayhem in Ole Virginny: source of the North American tektite strewn field. *Geology* 22: 691–694.

Poag C. W., Hutchinson D. R., Colman S. M., and Lee M. W. 1999. Seismic expression of the Chesapeake Bay impact crater: Structural and morphologic refinements based on new seismic data. In *Large meteorite impacts and planetary evolution II*, edited by Dressler B. O. and Sharpton, V. L. *Geological Society of America Special Paper* 339: 149–164.

Poag C. W., Koeberl C., and Reimold W. U. 2004. *The Chesapeake Bay Crater: Geology and Geophysics of a late Eocene Submarine Impact Structure, Impact Studies series.* Heidelberg, Springer. 522 p.

Powars D. S. and Bruce T. S. 1999. The effects of the Chesapeake Bay impact crater on the geological framework and correlation of hydrogeologic units of the lower York-James Peninsula, Virginia. *US Geological Survey Professional Paper* 1612: 1–82.

Reimold W. U., Bartosova K., Schmitt R. T., Hansen B., Crasselt C., Koeberl C., Wittmann A., and Powars D. 2009. Petrographic observations on the Exmore Breccia, ICDP-USGS Drilling at Eyreville, Chesapeake Bay impact Structure, USA. In *Deep drilling in the Chesapeake Bay impact structure,* edited by Gohn G. S., Koeberl C., Miller K. G., and Reimold W. U. *Geological Society of America Special Paper* 458: 655–698.

Roser B. P. and Korsch J. 1986. Determination of tectonic setting of sandstone-mudstone suites using SiO_2 content and K_2O/Na_2O ratio. *Journal of Geology* 94: 635–650.

Self-Trail J. M., Edwards L. E., and Litwin R.J. 2009. Paleontological interpretations of crater processes and infilling of syn-impact sediments from the Chesapeake Bay impact structure. In *Deep drilling in the Chesapeake Bay impact structure,* edited by Gohn G. S., Koeberl C., Miller K. G., and Reimold W. U. *Geological Society of America Special Paper* 458: 633–654.

Son T. H. and Koeberl C. 2005. Chemical variation within fragments of Australasian tektites. *Meteoritics and Planetary Science* 40: 805–815.

Schmitt R. T., Wittmann A., and Stöffler D. 2004. Geochemistry of drill core samples from Yaxcopoil-1, Chicxulub impact crater, Mexico. *Meteoritics and Planetary Science* 39: 979–1001.

Schmitt R. T., Bartosova K., Reimold W. U., Mader D., Wittmann A., Koeberl C., and Gibson R. L. 2009. Geochemistry of impactites and crystalline basement-derived lithologies from the ICDP-USGS Eyreville A and B drill cores, Chesapeake Bay impact structure, Virginia/USA. In *Deep drilling in the Chesapeake Bay impact structure,* edited by Gohn G. S., Koeberl C., Miller K. G., and Reimold W. U. *Geological Society of America Special Paper* 458: 481–541.

Stöckelmann D. and Reimold W. U. 1989. The HMX mixing calculation program. *Mathematical Geology* 21: 853–860.

Taylor S. R. and McLennan S. M. 1985. The Continental Crust: its Composition and Evolution. An Examination of the Geochemical Record Preserved in Sedimentary Rocks. Oxford, Blackwell, 312 p.

Townsend G. N., Gibson R. L., Horton J. W. Jr., Reimold W. U., Schmitt R. T., and Bartosova K. 2009. Petrographic and geochemical comparisons between the crystalline basement-derived section and the granite and amphibolite megablocks of the Eyreville-B core, Chesapeake bay impact structure, USA. In *Deep drilling in the Chesapeake Bay impact structure,* edited by Gohn G. S., Koeberl C., Miller K. G., and Reimold W. U. *Geological Society of America Special Paper* 458: 255–276.

Toulkeridis T., Clauer N., Kröner A., Reimer T., and Todt W. 1999. Characterization, provenance, and tectonic setting of Fig Tree greywackes from the Archaean Barberton Greenstone Belt, South Africa. *Sedimentary Geology* 124: 113–129.

Tucker M. E. 1991. Sedimentary Petrology. Wiley, John & Sons, 260 p.

Williams H. F., Turner F. J., and Gilbert C. M. 1982. Petrography, second edition, W. H. Freeman and Co., San Francisco, 626 p.

Wittmann A., Reimold W. U., Schmitt R. T., Hecht L., and Kenkmann T. 2009a. The record of ground zero in the Chesapeake Bay impact crater – suevites and related rocks. In *Deep drilling in the Chesapeake Bay impact structure,* edited by Gohn G. S., Koeberl C., Miller K. G., and Reimold W. U. *Geological Society of America Special Paper* 458: 349–376.

Wittmann A., Schmitt R.-T., Hecht L., Kring D. A., and Povenmire H. 2009b. Petrology of impact melt rocks from the Chesapeake Bay crater, USA. In *Deep drilling in the Chesapeake Bay impact structure,* edited by Gohn G. S., Koeberl C., Miller K. G., and Reimold W. U. *Geological Society of America Special Paper* 458: 377–396.

APPENDIX

Macroscopic and microscopic description of samples from the gravelly sand interval, 1371-1397 m.

CB6-087 1371.1 m
Macro: Gravelly sand with light gray matrix, subangular sand to granule-sized quartz grains (up to 3 mm), and pinkish white angular clasts, probably feldspar. The sand is massive, but one finer-grained part occurs. There is one pink and greenish gray granule-sized clast (3 mm) of altered granite plus some smaller similar clasts.
Micro: The sand is grain supported. The grains are sand-sized, most smaller than 1 mm, but some grains up to 2 mm occur. The grains are angular to subangular. The most abundant mineral is quartz, including polycrystalline quartz grains - both coarse and fine-grained. The grains are slightly fractured. Feldspar grains are mostly microcline. Mica is rare. Accessory minerals include garnet, titanite, epidote, and opaque minerals (up to 0.8 mm). The matrix is light brown, fine-grained, and clay-rich.

CB6-088 1371.4 m
Macro: Gravelly sand with gray matrix, massive, with subangular quartz sand grains (to 2 mm) plus a few larger pebbles up to 15 mm. Lithic clasts include white gravel-sized clasts (some with greenish alteration) up to 25 mm and a gray pebble, amoeboid, 20 mm.
Micro: The sand is grain supported. Most of the grains are sand sized - smaller than 2 mm, but there are some gravel-sized grains up to 5 mm. The sediment is very poorly sorted. The small (sub mm) grains are angular to subangular, some of the larger grains are subrounded. The grains are slightly fractured. Quartz is the most abundant mineral grain. There are also some larger grains (very coarse sand- to rarely granule-sized) of polycrystalline quartz, some coarse-grained and some cherty. There is some feldspar, mostly microcline. Mica is rare, occurs only as very fine sand-sized grains in matrix and in the schist clasts (muscovite and chlorite, rare biotite). Some carbonate patches occur. Accessory garnet, fractured (up to 0.7 mm), poikilitic staurolite (up to 0.4 mm), titanite, zircon, and epidote were noted. There is one large opaque grain, ~2.5 mm and other smaller sand-sized grains, up to 0.8 mm, subrounded to rounded grains, or aggregates of small grains. One large pebble (~10 mm), composed of fine-grained quartz, with metamorphosed, aligned grains is present. There are some large grains (up to 0.6 mm) inside the clast that resemble augen within layers of fine elongated, folded, quartz grains. Other larger clasts are a feldspar granule (4 mm), a polycrystalline quartz granule (4 mm) and a schist sand-sized clast (0.5 mm). Some clasts (quartz + K-feldspar) are probably granite-derived. A sandstone clast, about 1 mm in size, is also present. The matrix is light brown, fine-grained, and clay-rich.

W-50 1371.8 m
Macro: **No** macroscopic sample was available for this study.
Micro: The sand is grain supported. The grain size ranges through all sand-sizes (from sub mm to about 2 mm), but rare granule-sized grains up to 4 mm occur. The sediment is very poorly sorted. Grains are angular to subangular; some of the larger grains are subrounded. The grains are only slightly fractured. Mineral grains include abundant quartz with undulose extinction, some with fluid inclusions. Also feldspar, mostly microcline with tartan twinning, is abundant. Mica is extremely rare, only very fine sand-sized grains (<0.1 mm) of muscovite and chlorite occur in the matrix. There are opaque minerals, <0.2 mm, commonly with irregular shapes, and some accessory minerals, mostly garnet. The larger,

very coarse sand to granule sized, grains are mostly polycrystalline quartz. Polycrystalline quartz is coarse- to fine-grained, some with sutured boundaries. There are also a few chert sand-sized clasts (<1 mm). The matrix is brownish in plane-polarized light, fine-grained, and clay-rich.

KB9-09 1372.3 m

Macro: Gravelly sand, massive, relatively coarse, with abundant grayish or greenish subangular to rounded quartz grains up to 15 mm, but mostly sand-sized (about 1-2 mm). The matrix is light gray to greenish. Rock clasts (possibly only polycrystalline quartz) are rounded pebbles, grayish to pinkish, up to 12 mm.

Micro: The sand is grain supported. Grains are sand-sized, mostly smaller than 1 mm, but there are some granule-sized grains, some more than 3 mm – these are mostly the polycrystalline quartz grains or rarely monocrystalline quartz grains. The grains are angular to subangular or nearly subrounded in case of the larger (~2 mm) grains. The polycrystalline quartz grains are mostly coarse-grained, some with sutured crystal boundaries, but also fine-grained polycrystalline quartz grains occur. The grains are fractured. The clasts are mostly quartz, but also feldspar, some microcline, altered, with tartan twinning, was noted. Mica is extremely rare, mostly very fine sand-sized (<0.15 mm), occurs as part of the matrix or rare grains enclosed in quartz and feldspar. There is accessory poikilitic staurolite (one grain, 1 mm), garnet (up to 0.5 mm), and titanite. Rare small (<0.3 mm) opaque grains or clusters occur as well. The matrix is light brown in plane-polarized light, fine-grained, and clay-rich.

KB10-09 1373.3 m

Macro: Gravelly sand, massive, relatively coarse, similar to KB2-09, with abundant grayish to greenish subangular to rounded quartz grains up to 20 mm, commonly granule-sized (>2 mm). The matrix is light gray to yellowish. Only polycrystalline quartz pebbles (up to 20 mm) and no other rock clasts were identified macroscopically.

Micro: The sand is grain supported. The grains are substantially larger than in other samples. Granule-sized grains (~3 mm) are common. The sediment is very poorly sorted. Smaller grains are subangular and larger grains are subrounded. Some of the grains are fractured. There are abundant monocrystalline quartz grains and also abundant polycrystalline quartz of many different types – coarse-grained, fine-grained, cherty, with sutured boundaries, or metamorphosed with elongated crystals. There is altered feldspar, commonly microcline, and some carbonate clasts or patches. Mica clasts are rare, fine to very fine sand-sized (<0.3 mm) in matrix or in clasts, mostly muscovite and some altered biotite. Rare small (<0.2 mm) opaque minerals and rare accessory garnet and staurolite are present.

One large subrounded to rounded rock pebble, probably gneiss or schist (>5 mm), and another very coarse sand-sized clast of schist (~1.5 mm), were noted. An elongated sandstone clast, larger than 5 mm, is present. The matrix is light brown in plane-polarized light, fine-grained, and clay-rich.

KB1-09 1373.8 m

Macro: Gravelly sand, massive, with abundant grayish subrounded quartz grains up to 4 mm, but mostly sand-sized (about 1 mm). The matrix is light greenish to gray. There are some gravel-sized white to light gray rock or quartz clasts, up to 5 mm in size.

Micro: The sand is grain supported. Grains are sand-sized, only rarely granule-sized. Most of the clasts are about 1 mm in size, but many are smaller. Also some larger grains of polycrystalline quartz (coarse sand to rarely granule-sized) occur (including one large

subrounded grain, ~6 mm). The sediment is poorly sorted. The grains are angular to subangular, rarely subrounded, and the grains are slightly fractured. Most grains are quartz, single crystals or polycrystalline quartz – with larger crystals or microcrystalline. Some polycrystalline quartz grains are of metamorphic origin, with grains elongated in one direction. Some quartz grains have fluid inclusions. There also are abundant feldspar grains, K-feldspar, mostly microcline with tartan twinning. Some mica grains are larger, to about 0.3 mm, but most are just very fine sand-sized elongated grains; muscovite and altered biotite. The elongated mica grains are commonly folded around the larger quartz clasts. Accessory minerals include staurolite with typical poikilitic texture (up to 0.3 mm), small garnet clasts (about 0.15 mm), and tiny zircons. Rounded opaque grains, probably sulfides or organic carbon, were noted. There is a rounded elongated clast of very fine-grained sediment. The matrix is light brown in plane-polarized light, fine-grained, and clay-rich.

KB2-09 1374.5 m

Macro: Gravelly sand, massive, a bit coarser than KB1-09, with abundant grayish or greenish subangular to subrounded quartz grains up to 10 mm, but mostly sand-sized (about 1-2 mm). The matrix is light greenish to gray. There are some white to light gray rock or quartz granules and pebbles, up to 5 mm.

Micro: The sand is grain supported. Grains are sand-sized in one of the thin sections (up to 2 mm), but in the other thin section there are some granules larger than 3 mm. The sediment is poorly sorted. Grains are angular to subangular. Many of the grains are fractured. The clasts are mostly quartz, both monocrystalline and polycrystalline. There are feldspar grains, some microcline with tartan twinning. Other small grains are muscovite and altered biotite. Opaque minerals, probably sulfides, are rare; one larger opaque grain (0.4 mm) occurs. The accessories include a large tourmaline grain (0.45 mm) incorporated in a clast with quartz, originally probably a schist clast; zircon and titanite also occur. There are some subrounded sediment clasts (sandstone, siltstone). The matrix is light brown in plane-polarized light, fine-grained, and clay-rich.

KB3-09 1375.5 m

Macro: Gravelly sand, massive, a bit coarser than KB1-09, with abundant grayish to greenish subangular to subrounded quartz grains up to 15 mm, but mostly sand-sized (1-2 mm). The matrix is light greenish to gray. There are some gravel-sized white lo light gray or pinkish quartz or rock clasts, up to 10 mm.

Micro: The sand is grain supported. In one thin section, the grains are mostly sand-sized (<2 mm), but in the other one there are some granule-sized grains up to 3 mm in size. Also several pebbles (~5 mm) occur. Grains are very poorly sorted. These larger grains are polycrystalline quartz (some with fine quartz crystals, some with larger crystals with sutured boundaries) and are subangular to subrounded. The smaller grains are angular to subangular. Some of the grains are fractured. The mineral grains are mostly quartz. Some grains are single crystals, but there is also polycrystalline quartz, coarse- to very fine-grained. Some of the quartz grains contain fluid inclusions. Feldspar grains, mostly microcline with tartan twinning, are common. Mica grains are rare and small, muscovite and altered biotite, some mica is also incorporated in quartz clasts. Accessories are rare and include poikilitic staurolite (up to 0.6 mm) and garnet. Opaque minerals (probably some rutile) are rare. A fine-grained rock clast with quartz and a yellow to brownish mineral – probably amphibole and opaque minerals – was noted. The matrix is light brown in plane-polarized light, fine-grained, and clay-rich.

CB6-089 1375.6 m

Macro: Gravelly sand, coarser, massive, with greenish-gray matrix. Some lighter yellowish bands inclined about 20° from horizontal level occur. Rounded gravel-sized quartz grains have up to 10 mm, on average about 4 mm.

Micro: The sand is grain supported. There are many sand-sized grains around 1 mm, some smaller, but also many granule- to gravel-sized grains (>3 mm). The sediment is very poorly sorted. The grains are angular to subangular, larger grains also subrounded. Some grains are fractured. Quartz grains are most abundant, both monocrystalline and polycrystalline, fine-grained and coarse-grained. Further there is feldspar, altered, mostly microcline. Mica is rare, mostly fine sand-sized grains in matrix or in clasts, up to 0.3 mm. The accessories include poikilitic staurolite up to 0.8 mm, few tourmaline clasts, and probably titanite. There are some small patches/aggregates of opaque minerals, but no larger grains (all <0.3 mm). The granule-sized clasts are mostly polycrystalline quartz grains and some granules possibly originate from granite (quartz + feldspar or quartz + muscovite). There are also rare wacke/siltstone granules (up to 3 mm). The matrix is light brown, fine-grained, and clay-rich.

CB6-090 1382.5 m

Macro: Very fractured, massive, dark green amphibolite. There are fractures with dark filling, light olive-green minerals, probably amphibole; minor white minerals, feldspar(?), and small sub-mm sulfides.

Micro: The rock consists mainly of amphibole crystals (greenish in plane-polarized light) and feldspars. The feldspars (mostly plagioclase) are fractured but not significantly altered. Amphibole compositions in the amphibolite block, although not determined for this sample, range from pargasite to hornblende (Townsend et al., 2009). Accessory quartz and rare mica are present. There are large grains and aggregates of opaque minerals, commonly in veins. The veins, probably filling fractures, are formed of a clayey material and there are probably rare carbonate patches in the veins.

KB4-09 1389.8 m

Macro: Gravelly sand, finer than samples KB1-09 to KB3-09, with abundant grayish to greenish subangular to subrounded quartz grains, sand- to granule-sized up to 3 mm, but mostly <1 mm. The sample is massive, but a finer-grained lens occurs. The matrix is light gray. There are rare white or gray rock or quartz pebbles, to 10 mm.

Micro: The sand is grain supported. The grain size is smaller than in the samples KB1-09 to KB3-09. The grains are sand-sized, vast majority smaller than 1 mm, but there are rare grains up to 2 mm. Most grains are monocrystals. There is only one larger quartz granule, 3 mm in size. The grains are angular to subangular. Some of the grains are fractured. Most of the grains are quartz, mostly monocrystalline, but also some polycrystalline. Further there are abundant feldspar grains, mostly microcline with tartan twinning. Mica grains are elongated, small, probably only muscovite. There is accessory plagioclase, staurolite with poikilitic structure (up to 0.6 mm), tourmaline, titanite, zircon, and some subrounded opaque minerals. The matrix is light brown in plane-polarized light, fine-grained, and clay-rich.

CB6-091 1390.4 m

Macro: Gravelly sand with light gray matrix, with one lighter finer-grained band – nearly horizontal in the core. There are minor sand-sized gray grains (up to 2 mm); sand-sized angular to granule-sized rounded quartz grains; a large rounded clast with greenish core and pinkish rim with a few small dark red crystals.

Micro: The sand is grain supported. Most of the grains are sand-sized, smaller than 1 mm, but there are also some larger grains, granule-sized (up to 3 mm) in one and gravel-sized (up to 6 mm) in the second thin section. The sediment is poorly sorted. Grains are angular to subangular, some large grains rarely subrounded. Some of the grains are fractured. Most of the grains consist of quartz, mainly monocrystalline, but also polycrystalline quartz, which is mostly coarse but ranges to fine-grained in some cases. Feldspar grains are mostly microcline. Mica occurs only as part of the matrix. There is accessory garnet, poikilitic staurolite, and possibly kyanite. Relatively abundant, but still accessory and small opaque minerals, <0.3 mm, subrounded grains, or aggregates, occur. Some opaque minerals, with reddish hue and strange skeletal textures, ~0.8 mm, are possibly of organic origin. The large grains are quartz, polycrystalline quartz, and microcline. Some altered sand-sized clasts of probably sedimentary origin, occur. The matrix is light brown in plane-polarized light, fine-grained, and clay-rich.

W-53 1390.5 m

Macro: The macroscopic sample was not available for this study.

Micro: The sand is grain supported. Most grains are sand-sized, smaller than 2 mm, but some larger grains occur. The grains are very poorly sorted. Sand-sized grains are angular to subangular, some larger clasts are subrounded. Some grains are fractured.

Most of the grains are quartz. There is also abundant feldspar, mostly microcline. Mica is extremely rare, only very fine sand-sized grains in the matrix. Accessory minerals include tourmaline, staurolite, and opaque minerals (<0.2 mm). The larger clasts include polycrystalline quartz, which is of average grain size, in some cases coarse-grained with sutured boundaries, and rarely fine-grained. Some granule-sized, probably granite-derived, clasts (quartz + K-feldspar and quartz + muscovite) and small (sub-mm) chert clasts were noted. The matrix is brownish in plane-polarized light, and fine-grained.

KB5-09 1390.9 m

Macro: Gravelly sand, massive, coarser than KB4-09, with abundant grayish (greenish) subangular to subrounded quartz grains up to 5 mm, but mostly sand-sized, about 1 mm. The matrix is light gray. No rock clasts were noted. Some grains are fractured.

Micro: The sand is matrix supported. Most of the grains are sand-sized, smaller than 1 mm, none exceed 2 mm in one thin section, but in the other thin section there are rare granules of polycrystalline quartz more than 3 mm in size. The grains are angular to subangular. The sediment is very poorly sorted. The grains are only slightly fractured. There are mostly quartz grains, most monocrystalline, some polycrystalline – also one larger subrounded grain with very finely crystallized quartz occurs. In addition, abundant feldspars are present, some very altered, abundant microcline with tartan twinning. Elongated mica grains (mostly muscovite) are small, rarely larger than 1 mm, commonly folded around the quartz grains. Rare biotite occurs. There are some opaque minerals, larger oval grains or some small disseminated grains, probably some rutile. Accessory minerals (e.g., tourmaline) are rare. The matrix is light brown in plane-polarized light, fine-grained, and clay-rich.

KB6-09 1391.4 m

Macro: Gravelly sand, massive, similar to KB5-09, with abundant grayish or greenish subangular to subrounded quartz grains up to 4 mm, but mostly sand-sized, about 1 mm. The matrix is light gray to greenish. There are no rock clasts.

Micro: The sand is grain supported. Grains are sand-sized, mostly smaller than 1 mm, but very coarse sand-sized grains (about 1.5 mm) are also common. Grains are angular to

subangular. The grains are slightly fractured. The most abundant grains are quartz, mostly monocrystalline, only rarely polycrystalline. Feldspar grains are common, some very altered, abundant microcline with tartan twinning. There are some muscovite grains up to ~0.5 mm. Accessory minerals include tourmaline, poikilitic staurolite (about 0.5 mm), and small garnet. Opaque minerals occur as grains or irregular patches. The matrix is light brown in plane-polarized light, fine-grained, and clay-rich.

KB7-09 1392.2 m

Macro: Gravelly sand, similar to KB6-09, with abundant grayish or greenish subangular to rounded quartz pebbles up to 7 mm, but mostly sand-sized grains, about 1 mm. The matrix is light gray to greenish. Litho- or quartz pebbles are rounded and up to 13 mm in size.

Micro: The sand is grain supported. Most of the grains are sand-sized, smaller than 1 mm, but some are around 2 mm and rare granule-sized clasts also occur. The grains are angular to subangular. Some grains are fractured. There are mostly quartz grains, single crystals and some polycrystalline quartz, and altered feldspar grains, mostly microcline with tartan twinning. Mica grains are rare, mostly muscovite and rare altered biotite, only small grains in matrix or enclosed in quartz, about 0.05 mm. There is accessory garnet, tourmaline, staurolite, and possibly kyanite. Opaque minerals have rounded or rectangular shapes, and sizes up to 0.5 mm. The largest clasts are polycrystalline quartz grains (both with coarse to fine grains, subangular to subrounded, mostly larger, up to 3 mm). Rare altered rock clasts, probably sandstone/wacke, were noted as well. The matrix is light brown in plane-polarized light, fine-grained, and clay-rich.

KB-1 1393.1 m

Macro: Suevite boulder. Lithic pebbles up to 10 mm occur. There are white clasts, beige mudstone clasts, dark gray clasts, and some small olive-green melt particles.

Micro: The sample is similar to suevite samples below, with fine-grained, dark brown, clay-rich matrix. It is matrix supported, matrix proportion is higher than in the gravelly sand. The matrix contains abundant very fine to medium sand-sized grains, ~0.1 mm. Further there are coarse to very coarse sand-sized grains (~1 mm). The minerals include quartz (angular grains, mono- and polycrystalline) and feldspar. Mica is commonly present in clasts and in matrix; muscovite (<0.3 mm) and biotite (<0.2 mm). Some chloritized biotite is present in clasts. Lithic granules and pebbles (up to 5 mm in length) are abundant and include schist, siltstone, sandstone with altered feldspars, black shale, and probably amphibolite. Brown altered melt particles (similar to melt type m2 of Bartosova et al., 2009a) are present, but not well preserved.

KB8-09 1393.5 m

Macro: Light gray cataclastic gneiss, with clasts of fine-grained dark gray rock, and some light-colored veins or alteration zones in fractures.

Micro: Very fine-grained cataclastic gneiss. The sample is similar to the cataclastic gneiss in blocks from the underlying impact breccia section (Horton et al., 2009a). The sample contains quartz grains and less abundant feldspar grains, altered, probably K-feldspar. There are aligned micas – muscovite and chlorite, but some mica grows in other directions – probably later mica generation. Carbonate is present as clasts and patches. Epidote occurs in some parts. Opaque minerals form grains of irregular shapes or clusters of small grains. There are some coarser-grained parts. Rare larger grains include quartz grains of ~0.3 mm and one feldspar grain ~1 mm in length.

CB6-092 1396.5 m

Macro: Gravelly sand with reworked suevite in a fine-grained gray matrix. Lithic clasts include angular white gravel-sized clasts up to 4 mm, fractured beige mudstone or siltstone pebbles up to 10 mm, minor gray granules and pebbles (up to 5 mm), and an angular banded white and gray pebble (15 mm). Matrix is not homogeneous, there are some light-colored parts.

Micro: Matrix supported, matrix forms higher proportion of the sample than in the upper samples. The matrix is brown in plane-polarized light, fine-grained, and clay-rich. There are many small grains ~0.1 mm, but also many very coarse sand-sized (1-2 mm) or rarely granule-sized grains, including rock clasts. The grains are angular to subangular. Grains are not significantly fractured. The most common mineral is quartz. Polycrystalline quartz is common, mostly coarse-grained. In addition, there are feldspars, mostly microcline, but also rare plagioclase in clasts and as single grains in matrix. Chlorite and muscovite occur mostly as part of larger clasts (e.g., in wacke), but also as small grains in matrix. Opaque minerals have sizes up to 1 mm and are oval or angular. Accessory minerals include garnet, tourmaline, and titanite. There are clasts of polycrystalline quartz (~2 mm), fine-grained sediment granules (siltstone, 4 mm and some smaller), wacke pebbles (~10 mm), a sandstone granule (~4 mm), and a metasandstone clast (~2 mm). Further there is an unidentified pebble, with star-like crystals and opaque minerals, ~5 mm. Brown melt particles (up to 2 mm, similar to melt type m2 of Bartosova et al., 2009a) are completely altered to phyllosilicates and contain sparse undigested quartz grains.

W-54 1396.7 m

Macro: The macroscopic sample was not available for this study.

Micro: Gravelly sand with reworked suevite, matrix supported. The grains are sand-sized, with sizes commonly around 0.1 mm. Most of the grains are smaller than 1 mm. A few larger grains occur. The grains are very poorly sorted. The grains are angular to subangular, and slightly fractured. Mostly quartz grains, but feldspar grains also occur. There are rare small fine to medium sand-sized (<0.4 mm) mica grains in the matrix; muscovite and biotite. Mica occurs also in some rock clasts. There are some opaque minerals, <0.2 mm, and accessory tourmaline. Rare tiny greenish grains (~0.1 mm) in this sample are possibly glauconite. Polycrystalline quartz grains as well as lithic clasts of mudstone, siltstone, sandstone, and crystalline rock (probably schist) occur, commonly 1-2 mm in size. There is a relatively higher proportion of matrix compared to other samples. There are abundant melt particles, altered, parts of the particles were removed during the thin section preparation. The particles are most similar to our melt type m2 (Bartosova et al., 2009a).The melt clasts have subangular to amoeboid shapes and are larger than other clasts, up to 6 mm.

CHAPTER 11: CONCLUSIONS

The International Continental Drilling Program (ICDP) and U.S. Geological Survey (USGS) Deep Drilling Project provided new insights into the structure and formation of the Chesapeake Bay impact structure. The Eyreville drill core has been studied from many aspects by several scientific teams and a wide range of data, from general (e.g., geologic column) to detailed observations (on, e.g., mineralogy, shock metamorphism, and paleontology) was obtained. New important information regarding, e.g., overall shape and structure, formation mechanisms, shock metamorphic effects, and nature and volume of melt, were gained.

The impact breccia interval consists mainly of suevites that contain abundant clasts showing shock metamorphic effects. Other parts of the Eyreville drill core show only rare shock metamorphic effects, e.g., in the form of rare shocked quartz grains in the Exmore breccia. Other lithologies, such as crystalline basement-derived rocks at the bottom of the core or the granitic megablock, are unshocked. In the impact breccias, shock metamorphic effects such as planar fractures and planar deformation features were observed. Related features, such as toasted quartz, ballen silica, or kink-banding in mica, were noted. Systematic investigations of the proportions of shocked quartz grains in clasts showed that the highly shocked clasts are generally less abundant with increasing depth. Also differences between lithologies were noted. The crystalline rock clasts (from the lower parts of the target) have mostly low proportions of shocked quartz grains, whereas sedimentary clasts (supposedly from the upper layers of the target) include many highly shocked clasts, which is in agreement with the shock attenuation with depth.

Melt particles are present throughout the impact breccia interval, though very rare in the lowermost part. Most abundant melt particles occur near the top of the impact breccia section, especially in the areas around the two thin intervals of impact melt rocks. The melt particles probably originate from the ejecta plume; many were still hot and plastic at the time of deposition, whereas some (shard-like) fragments were apparently already solidified. Microscopic observations, as well as geochemical data, suggest mainly sedimentary precursors of the melt particles. The impact melt rock intervals include some melt matrix sections, but most parts are just an accumulation of partly melted material, rather than impact melt rocks *sensu stricto*. The melt rock intervals do not seem to represent large melt sheets, but only isolated pods.

Geochemical mixing calculations showed that the polymict impactites (excluding the large gneiss blocks) of the impact breccias were probably formed mainly from the basement crystalline rocks (gneiss and schist, >75%) with a significant sedimentary component (mostly Potomac Formation, ~20%). In the impact breccia interval, both types of subintervals, rich in sedimentary clasts and with dominant crystalline clasts (including

m-sized blocks), occur. Generally, the crystalline clasts (mainly gneisses) become more abundant with depth, as is suggested also by the geochemical data (e.g., decrease of SiO_2 content and increase of FeO content with depth). The lower parts of the impact breccia intervals were formed by ground-surge and slumping. The uppermost part consists mainly of fallback material from the ejecta plume (including abundant melt particles).

The impact breccia formation was interrupted by a rock avalanche that formed the overlying gravelly sand interval. The gravelly sand incorporated some melt particles from suevite in the bottom part, but the rest of the interval lacks shocked clasts and melt particles. It consists of relatively homogeneous, poorly consolidated quartz sand with rare lithic clasts. The material probably originated from the Cretaceous Potomac Formation. No hints of a marine origin (e.g., microfossils or glauconite pellets) were noted.

The crater modification continued by slumping of large lithic blocks, generally unshocked, thus probably originating from the outer parts of the transient crater. These include an amphibolitic block within the gravelly sand interval, a huge granitic slab above the gravelly sand, and sedimentary blocks in the interval of sediment boulders and sand. The thickest and uppermost impactite unit is the Exmore Formation, which was formed mainly by resurge of ocean water with sediments. It contains abundant glauconite and marine microfossils. In the upper part, intervals with enhanced melt particle content occur. The particles were probably accumulated from the ejecta plume after diminishing of the resurge process, during relatively calm intervals between the waves.

The Geological Society of America
Special Paper 458
2009

Petrographic observations on the Exmore breccia, ICDP-USGS drilling at Eyreville, Chesapeake Bay impact structure, USA

W.U. Reimold*
Museum für Naturkunde–Leibniz Institute at Humboldt University Berlin, Invalidenstrasse 43, D-10115 Berlin, Germany

K. Bartosova
Department of Lithospheric Research, University of Vienna, Althanstrasse 14, A-1090 Vienna, Austria

R.T. Schmitt
B. Hansen
C. Crasselt
Museum für Naturkunde–Leibniz Institute at Humboldt University Berlin, Invalidenstrasse 43, D-10115 Berlin, Germany

C. Koeberl
Department of Lithospheric Research, University of Vienna, Althanstrasse 14, A-1090 Vienna, Austria

A. Wittmann
Museum für Naturkunde–Leibniz Institute at Humboldt University Berlin, Invalidenstrasse 43, D-10115 Berlin, Germany,
and *Lunar and Planetary Institute, 3600 Bay Area Boulevard, Houston, Texas 77058, USA*

D.S. Powars
U.S. Geological Survey, MS 926A, 12201 Sunrise Valley Drive, Reston, Virginia 20192, USA

ABSTRACT

The International Continental Scientific Drilling Program (ICDP)–U.S. Geological Survey (USGS) Eyreville A and B drill cores sampled crater fill in the region of the crater moat, ~9 km to the NE of the center of the Chesapeake Bay impact structure, Virginia, USA. They provide a 953 m section (444–1397 m depth) of sedimentary clast breccia and intercalated sedimentary and crystalline megablocks known as Exmore beds, deposited on top of the impactite sequence between 1397 and 1551 m depth. We petrographically investigated the sandy-clayey groundmass-dominated breccia, which resembles a diamictite ("Exmore breccia"), and which, in its lower parts, carries sedimentary and crystalline blocks. The entire breccia interval is characterized by the presence of glauconite and bioclastic carbonate, which distinguishes the Exmore breccia from other sandy facies above and below in the stratigraphy. The

*uwe.reimold@museum.hu-berlin.de

Reimold, W.U., Bartosova, K., Schmitt, R.T., Hansen, B., Crasselt, C., Koeberl, C., Wittmann, A., and Powars, D.S., 2009, Petrographic observations on the Exmore breccia, ICDP-USGS drilling at Eyreville, Chesapeake Bay impact structure, USA, *in* Gohn, G.S., Koeberl, C., Miller, K.G., and Reimold, W.U., eds., The ICDP-USGS Deep Drilling Project in the Chesapeake Bay Impact Structure: Results from the Eyreville Core Holes: Geological Society of America Special Paper 458, p. 655–698, doi: 10.1130/2009.2458(29).

sediment-clast breccia exhibits strong heterogeneity from sample to sample with respect to groundmass nature, e.g., clay versus sand content, as well as clast content, in general, and shocked clast content, in particular. There is a consistently significantly larger macroscopic sedimentary to crystalline clast content. On the microscopic scale, the intersample sediment to crystalline clast ratios are quite variable. A very small component of shocked material, in the form of shock-deformed quartz, and to an even lesser degree feldspar, and somewhat more abundant but still relatively scarce shard-shaped, altered melt particles, is present throughout the section. However, between ~458 and 469 m, and between 514 and 527 m depths, the abundance of such melt particles is notably enhanced. These sections are also chemically distinct and relatively more mafic than the other parts of the Exmore breccia. It appears that from the time of deposition of the 527 m material, calming of the ocean occurred over the crater area as a result of abatement of resurge activity, so that ejecta from the plume above the crater could accumulate within the crater area to a larger degree. Deposition of ejecta fallout from the collapsing ejecta plume was terminated by the time of deposition of the 458 m material. This raises questions about the positioning of the exact upper contact of Exmore breccia to post-Exmore sediment (Chickahominy Formation), which is currently placed at 444 m depth and which possibly should be revised to 458 m depth. Based on a significant record of granite-derived material with shocked minerals, the shocked debris component seems to be largely derived from crystalline target rocks. This provides further evidence that the basement-derived material of the basal section of the Eyreville drill cores, which is essentially unshocked, is likely of an allochthonous nature and that the drilling did not intersect the actual crater floor.

INTRODUCTION

The 85-km-diameter Chesapeake Bay impact structure in Virginia, USA, is the seventh largest known impact structure on Earth (Earth Impact Database, 2008; www.unb.ca/passc/ImpactDatabase/) and the largest known in the United States. Its existence at the eastern coast of the United States (Fig. 1) was first proposed by Poag et al. (1992, 1994) and Powars et al. (1992, 1993) on the basis of a seemingly anomalous breccia layer that was then correlated with the North American tektite strewn field (Poag et al., 1994, 2004, and references therein). The impact origin of this structure was confirmed by the recognition of shock metamorphic indicators (e.g., Poag et al., 1992, 1994, 2004; Koeberl et al., 1996; Glass and Liu, 2001). The structure is ca. 35.5 Ma old (late Eocene), based on micropaleontological evidence and the assumption that the Chesapeake Bay impact structure is the source of the North American tektites (e.g., Poag and Aubry, 1995; Poag, 1996, 1997). A weighted mean $^{40}Ar/^{39}Ar$ age of 35.3 ± 0.1 Ma (±1σ) was obtained by Horton and Izett (2005) for bediasite and georgiaite tektites; see also a review of chronological information in Poag et al. (2004) and Horton et al. (2005a, 2005b). The entire impact structure is preserved below a blanket of postimpact late Eocene to Quaternary sediments (Gohn et al., 2008; Browning et al., this volume; Edwards et al., this volume, Chapter 4; Kulpecz et al., this volume). The Chesapeake Bay structure is one of only a few impact structures known that were formed in marine settings. It must be considered one of the best studied impact structures in the world, since extensive geophysical data acquisition and earlier

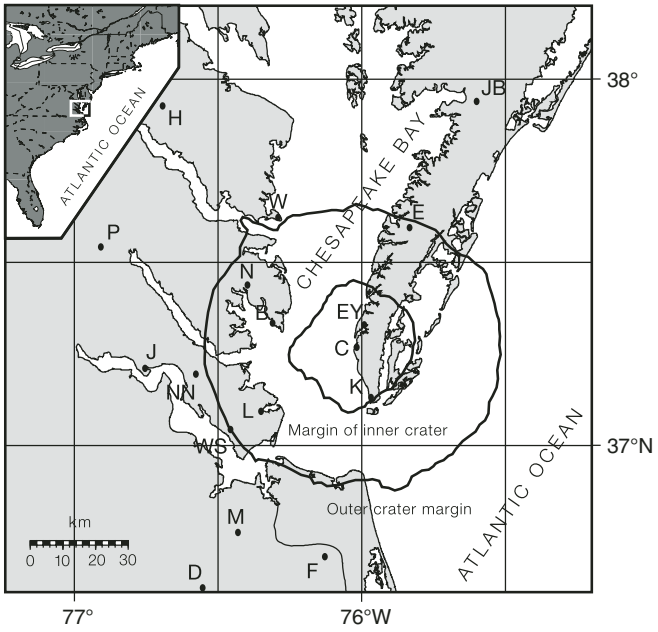

Figure 1. Location map for the Chesapeake Bay impact structure (inset: location of map area on U.S. East Coast), modified from Horton et al. (2005a). Also shown are the locations in the impact structure of important core drillings: B—Bayside, C—Cape Charles U.S Geological Survey (USGS) Sustainable Technology Park (STP), D—Dismal Swamp, E—Exmore, EY—Eyreville, F—Fentress, H—Haynesville, J—Jamestown, JB—Jenkins Bridge, K—Kiptopeke, L—USGS-NASA Langley, M—MW4, N—North, NN—Newport News Park 2, P—Putneys Mill, W—Windmill Point, and WS—Watkins School.

shallow drilling have contributed to a rather detailed knowledge about the geometry and general lithology of this impact structure (reviewed in great detail by Poag et al., 2004; see also review by Horton et al., 2008; Catchings et al., 2008).

The geometry of the structure has been extensively investigated with geophysical methods, including the acquisition of many kilometers of seismic profiles (Poag et al., 2004; Catchings et al., 2008). The structure is characterized by a geometry that resembles an inverted sombrero, with a deep inner crater of 30–40 km diameter surrounded by a more shallow outer annulus of 24 km width. A steep fault scarp marks the outer diameter of ~85 km (Poag et al., 2004). It is also thought that the floor of the transient crater penetrated crystalline basement to a depth of ~1.6 km below sea level (Poag et al., 2004; Horton et al., 2005b, 2005c, 2005d; and as modeled by Collins and Wünnemann, 2005). Poag et al. (2004) also made a case for a small central peak (central uplift) of perhaps 15–20 km diameter and maybe 900 m elevation occurring in the central part of the structure. The peculiar "inverted-sombrero" geometry is thought to be related to the strong rheological contrasts between target layers (due to the contrasting material strengths of the crystalline rocks of the basement on the one hand, and the overlying unconsolidated sediments and water column on the other). Collins and Wünnemann (2005) generated a numerical model that is generally consistent with the observed geometry and crater-fill stratigraphy. New modeling results for the Chesapeake Bay impact are discussed by Kenkmann et al. (this volume). A detailed potential field study (gravity and magnetics) by Shah et al. (2005) suggested that kilometer-sized melt "pockets" occur in the vicinity of the central peak, and gravity data were used by these authors to further delineate, and investigate the shape of, the central uplift. The possible occurrence of large basement-derived blocks and impact melt volumes in the impact structure was investigated by Shah et al. (this volume) with magnetic modeling.

According to Poag et al. (2004), the Chesapeake Bay impact structure is unique because (1) it was formed on a passive continental margin, which ensured that postimpact deformation, if any, was minimal; (2) it was formed in a relatively deep continental shelf setting, and so marine deposition could resume immediately after the catastrophic effects of the impact event had abated; thus, the structure was completely preserved and permits the investigation of not only the full rock record related to the immediate postimpact environmental effects but also of the final transition to renewed sedimentation and biocolonization of the impact crater area; (3) it could be expected that the interior of this structure would reveal a complete record of impact breccia accumulation and subsequent resurge deposition of washback sediment; and (4) the hydrological situation, with a large quantity of brine occurring in the breccia body of the crater interior, could be investigated (Sanford, 2005; Sanford et al., 2004, this volume).

Further reasons for drilling include: benefits from recovering continuous cores from a complete section of late Eocene and younger sediments for comparison with the tectonostratigraphic results of the New Jersey transect (Browning et al., this volume; Kulpecz et al., this volume), and improved understanding of large-scale impact into marine targets from shock petrographic studies of basement-derived rocks and detailed analysis of the crater-fill deposits, as well as investigation of groundwater quality with regard to regional water supplies, and even deep biosphere investigations (various papers in this volume). Therefore, the International Continental Scientific Drilling Program (ICDP) and the U.S. Geological Survey (USGS) combined forces to lead a drilling project into the deep crater interior, aiming at comprehensive recovery of the entire crater fill and basement below the crater (e.g., Gohn et al., 2006a, 2006b, 2008). Despite technical difficulties (Gohn et al., this volume, Chapter 1), a nearly complete drill core section covering pre-impact basement rocks, impactites, resurge and avalanche deposits, and postimpact sediment was recovered, with excellent core recovery, in the form of three stacked drill cores (Eyreville A–C). First reports on drilling operations and outcomes were published by Gohn et al. (2006a, 2006b, 2008).

The three core holes were drilled at Eyreville Farm on the southern end of the Delmarva Peninsula (Fig. 1) between July 2005 and May 2006. The drill site is located some 9 km from the center of the impact structure, off the central uplift and above the inner crater moat. Eyreville A was drilled between 125 and 941 m depths. Due to coring deviation in the lower section of Eyreville A, a new core hole, Eyreville B, was cored between 737.6 m and 1766 m (final) depth. Finally, in a separate project, the uppermost postimpact sediments were drilled in Eyreville C to a depth of 140.2 m. On aggregate, this provided a 1766-m-deep core section composed of the following intervals: postimpact sediments to a depth of 444 m, sediment-clast breccia and sediment megablocks to 1096 m, a granite megablock between 1096 and 1371 m, sedimentary and crystalline blocks from 1371 to 1397 m, impact breccias (suevites, impact melt rock, and polymict lithic impact breccia, as well as intercalated crystalline blocks) to 1551 m, and finally schist, granite, and pegmatites to the final coring depth of 1766 m. Detailed lithological information based on Eyreville A–C drill core examinations is provided by Browning et al. (this volume), Kulpecz et al. (this volume), Edwards et al. (this volume, Chapters 3 and 4), and Horton et al. (this volume). Our own macroscopic observations regarding the Exmore bed interval in Eyreville A and B are listed in Table A1 here.

A geochemical consortium study with contributions from the Museum for Natural History Berlin, the University of Vienna, and the University of Witwatersrand in Johannesburg provided major- and trace-element data for all major lithological packages in the Eyreville cores (Schmitt et al., this volume), and several contributions of our group are focused on the crystalline rocks (Gibson et al., this volume; Townsend et al., this volume) and the impactite section (Bartosova et al., this volume, Chapters 15 and 18; Wittmann et al., this volume, Chapters 16 and 17).

Here, we focus on the petrographic analysis of the section between 444 and 1397 m depths, which has been traditionally but informally known as the "Exmore beds." Generally, the Exmore beds are distinguished as lithic, mostly but not exclusively

sedimentary blocks and a diamictite-like breccia facies. The latter has been informally termed "Exmore breccia" and is the focus of this investigation. This sequence has been considered to be a sedimentary succession formed from crater-derived debris mixed with target source material in the course of immediate-postimpact tsunami surge and resurge, as well as avalanche, flow (e.g., Horton et al., 2008, and references therein; Gohn et al., this volume, Chapters 1 and 26). Poag et al. (2004) proposed that this breccia sequence would provide a good approximation of the mixture of target rocks impacted at Chesapeake Bay. It is our aim to provide a first record of modal compositional change along this Exmore bed profile in the drill cores Eyreville A and B, as well as shock petrographic information, especially with regard to accumulation of shocked debris with depth.

PREVIOUS WORK ON EXMORE BEDS

Poag et al. (2004) provided a comprehensive review of the geophysical, lithostratigraphic, petrographic, and chemical data available to that time. Horton et al. (2008) provide the most up-to-date (pre-Eyreville drilling) and detailed account of the nature and origin of the Exmore beds. Here, only the most important results that are pertinent for further discussion are summarized.

Informal Naming

Powars et al. (1992) and Poag (1997) informally named a thick breccia package that completely covers the entire complex impact structure from central peak to outer rim "Exmore breccia" after the town of Exmore, Virginia, where (Fig. 1) the first drill core of this material was recovered. Another informal term that has been applied widely in the Chesapeake Bay literature is "Exmore beds." These strata consist of a mélange of sand-sized material to kilometer-sized blocks from a wide range of sediment and crystalline rocks. Because of the chaotic lithological mixtures observed, Gohn et al. (2005) introduced the term "diamicton" for these breccias. D.T. King (Auburn University, 2008, personal commun.) recommends replacing the term "diamicton" with "impactoclastic deposit," a term also given in the glossary to the impactite nomenclature recommendation by Stöffler and Grieve (2007). We do not use this term because it has been applied in the past to impact ejecta such as the Cretaceous-Paleogene (K-P) boundary deposits. As will be discussed later in this paper, the Exmore breccia facies are made up of a mixture of reworked impactite plus sedimentary material from both within and outside of the crater structure. This mixture cannot be regarded as an equivalent to primary impact ejecta. Since the work of Koeberl et al. (1996), it has been known that impact-generated materials, such as impact glass particles and shock-deformed fragments of mineral and lithic clasts, are part of these beds. Consequently, the genesis of this breccia has been discussed in terms of impact-disruption and subsequent turbulent mixing of impact debris with material from outside the transient cavity due to water-column collapse, resurge and backsurge interaction, and runup and wash-back related to postimpact tsunami (Poag et al., 2004; Gohn et al., 2005, this volume, Chapter 26; Horton et al., 2005c; Powars et al., this volume).

It must be clarified what is meant in this paper by the term "Exmore breccia." In our view, this unit constitutes the actual bulk breccia facies, what has been termed by the USGS Reston group the "diamicton," whereas diamicton plus lithic block intersections constitute the entire "Exmore beds" package.

Occasionally, and also in this volume, the term "sedimentary clast breccia" has been applied to describe the Exmore breccia facies. We must emphasize that the Exmore breccia has indeed been found to be dominated by a sediment clast component, also in this study (see following). However, crystalline clasts and crystalline rock–derived mineral clasts are ubiquitous in this sequence (e.g., Poag et al., 2004; this work). For this reason, we caution against the use of the term "sedimentary clast breccia."

Edwards et al. (this volume, Chapter 3) propose a so-called Exmore Formation. They reserve this name for the depth interval between ~867 and 443.9 m depth. They furthermore subdivide this section into four members: a lower diamicton member from ~867 to ~855 m, a block-dominated member from ~856 to 618.2 m, an upper diamicton member from 618.2 to 450.95 m, and a stratified member from 450.95 to 443.90 m. We trust that this division will be debated in the coming years; until it has been formally accepted, we will adhere to the all-inclusive Exmore beds and Exmore breccia terminology, as defined in this section.

Distribution and Thickness

The regional thickness of the Exmore beds as determined from drilling and seismic interpretation is highly variable, between ~1200 m in the inner basin and 200 m in the outer reaches of the impact structure (Poag et al., 2004, their figure 6.12). The upper limit may still be too small, as the deep seismic data of Catchings et al. (2008) suggest that the Exmore Beds may extend to 1.75 km depth in the deepest part of the crater moat. Just outside the outer rim on the western side of the Chesapeake Bay impact structure, but still within the outer fracture zone, Exmore beds thin to ~8 m thickness (Horton et al., 2008). According to Powars and Bruce (1999), the Exmore beds may extend in this region as far as 4–12.8 km from the outer crater rim.

Exmore breccia has been intersected in many core holes in the interior of the Chesapeake Bay impact structure (see Poag et al., 2004, their figure 6.2), which provide a composite stratigraphic section across the impact structure that shows the relatively thin (~20 m) package at the edge of the impact structure thickening dramatically in the crater moat region to more than 250 m, and thinning again over the central uplift. Several specific drilling ventures of recent years have provided important insights in this regard (e.g., Horton et al., 2008).

In the National Aeronautics and Space Administration (NASA) Langley drill core (Horton et al., 2005a, 2005b), located above the southwestern annular trough of the impact structure, Exmore breccia was recovered between 183.3 m and 269.4 m

depth. The clast population was sediment dominated, with sparse crystalline clasts. In the USGS Cape Charles STP-2 (Sustainable Technology Park) borehole (Gohn et al., 2007), Exmore breccia was intersected approximately (only cuttings were recovered) between 353.6 and 356.6 m depth. Chips recovered from crystalline rocks intersected in this drilling included granitic rocks and chert. Silty clays and clayey silts are important sedimentary components. Interestingly, the recovery of phosphate minerals is mentioned, besides many of the minerals normally associated with this breccia. This is potentially significant with regard to the observation by Schmitt et al. (this volume) that the uppermost part of the Exmore breccia investigated here is enriched in phosphate relative to the lower sections. With regard to regional significance, Gohn et al. (2007, p. 16) stated that "regionally within the structure the lower part of the sediment-clast breccia consists of blocks and mega-blocks of pre-impact sediment within a matrix of exotic or locally derived sediments" (Powars and Bruce, 1999; Poag et al., 2004; Gohn et al., 2005). In contrast, in the outer parts of the structure sediment blocks were apparently found to be more of a local significance (autochthonous to parautochthonous). With respect to the Eyreville drilling, which is the focus of this work, it is important to note that Gohn et al. (2007) considered the sediment blocks of the inner crater to be allochthonous, having been emplaced after slumping into the central part of the crater in the course of late-stage gravitational collapse. In summary, these authors defined the Exmore beds as consisting of abundant pebbles, cobbles, and small boulders of pre-impact Cretaceous and early Paleogene sediments, as well as sparse pebbles and cobbles of pre-impact crystalline rocks. The matrix to these clast components is composed of calcareous, muddy, quartz-glauconite sand and granules.

The Sustainable Technology Park hole, drilled to 823 m depth on the northeast flank of the central uplift (Horton et al., 2005d), included 300 m of "sediment-clast breccia" with clayey or sandy groundmass. Interestingly, Horton et al. (2005d) referred to progressive lithification of the core with depth, which they interpreted as indicative of possible hydrothermal alteration of the sediments on top of the central uplift.

The lithology of the breccia (as summarized by Poag et al., 2004) is highly complex. Sediments, based on micropaleontological evidence, are Cretaceous (Albian) to late Eocene strata, including 11 pre-impact sedimentary formations present in the target area (Potomac to Piney Point Formations; Poag et al., 2004, their figure 2.4). Apparently large clasts from these formations represent the bulk of the clast component in the Exmore beds. The groundmass of the breccia is generally formed from glauconite-quartz sand, with varied proportions of silty and clay-sized material.

Detailed sedimentological analysis has been performed by various groups; Poag et al. (2004) also reviewed this work. However, Gohn et al. (this volume, Chapter 26) and Edwards et al. (this volume, Chapter 4) focus on these aspects of the Exmore beds and their meaning for the interpretation of breccia-generating processes.

Petrography

Shock metamorphosed clasts in Exmore breccia have been reported by Poag et al. (1992), Koeberl et al. (1996), Powars et al. (2001), Reimold et al. (2002), and Horton et al. (2001, 2002, 2005a, 2005b, 2005c, 2005d). Shock deformation includes so-called shock-extension fractures (which are regarded as nondiagnostic but are frequently observed in impact breccias, and which have been produced at <10 GPa shock pressures in experiments with quartzite and granite; Huffman and Reimold, 1996), planar fractures, planar deformation features (PDF) in single or multiple sets per host grain, impact melt, and very rare impact glass fragments or spherules (Koeberl et al., 1996; Reimold et al., 2002; Poag et al., 2004).

Poag (2000, 2002) and Poag et al. (2001) reported that millimeter-sized framboidal pyrite aggregates with spherical, hollow shapes had been found in an ~3-cm-thick laminated silt-rich interval at the top of the Exmore breccia in the NASA Langley core. They concluded that these aggregates represented sites where impact debris fallout—likely glass spherules ejected from the Chesapeake Bay crater—originally had been deposited. Accordingly, they termed this uppermost part of the Exmore breccia the "fallout layer" (see also Poag et al., 2004, their figures 6.22 and 6.24).

Poag et al. (2004) also presented other petrographic findings on their selected particulate samples: (1) Besides sedimentary lithologies, granitoids constituted a significant proportion of clasts. (2) They identified irregular variation between core holes, some of which were found to be sedimentary clast dominated, others of which were dominated by granitoid fractions. The subcentimeter particulate fractions analyzed by Poag et al. (2004) mostly contained significant siltstone/mudstone clast proportions. (3) They found that the proportion of shock-deformed clasts was consistently very much smaller than 1% of the investigated sample materials, and that most was derived from granitoid precursors. Furthermore, clasts with low shock and high shock degrees were found well-mixed, and neither type was concentrated in particular stratigraphic sections. (4) Only minor amounts of mafic clast material was noted, and no volcanic component was observed. (5) Impact glass spherules were found in lower parts of the Exmore breccia stratigraphy.

Horton et al. (2005a, 2005b) described the matrix of the Exmore breccia as "unsorted and unstratified and muddy, fossiliferous, quartz-glauconite sand." These authors found that the majority of clasts were sediment derived and that crystalline clasts were sparse. They also reported some large sediment clasts with irregular shapes and centimeter-thick rinds and took this as suggestive of fallback ejecta origin. Horton et al. (2005a, 2005b) noted that "in the western annular trough materials interpreted as fallback ejecta occur only as reworked clasts in sedimentary deposits"; i.e., only in the Exmore beds. These particles included shocked quartz and feldspar, cataclastically deformed crystalline rock fragments, possible impact melt, and damaged microfossils. They concluded that the lack of rounded shapes of

shock-deformed felsic clasts could indicate that these clasts were derived from crystalline basement in the target. Consistent with previous work (Koeberl et al., 1996; Reimold et al., 2002; Horton et al., 2004; Poag et al., 2004), it appeared that most shocked particles with PDFs were derived from the 10–20 GPa zone of the transient crater. Horton et al. (2005a, 2005b) referred to the presence of limited amounts of ejecta material in the Exmore beds but failed to find a distinct fallout layer, and they cited scouring and removal of proximal ejecta due to resurge erosion.

Horton and Izett (2005) reported on Exmore breccia occurring in the USGS-NASA Langley core hole. They distinguished clasts of Paleogene and Cretaceous sediment up to boulder size and only sparse pebbles of crystalline rock. They identified rare quartz grains in the sandy matrix that contain multiple (up to 5) sets of PDF, as well as PDF-bearing quartz grains in reworked crystalline rock clasts. They took this as evidence indicating a "hybrid impact origin" for the Exmore breccia. As previously presented by Horton et al. (2005a, 2005b), they reported findings of angular felsite clasts with PDF-bearing quartz crystals, as well as spherulitic felsite clasts, and they concluded that both these types could represent rare impact melt rock clasts.

Just recently, a detailed account of the nature and origin of the Exmore beds was published by Horton et al. (2008). They summarized this sequence as an 8–200-m-thick sequence from outside of the impact structure to its central parts. They distinguished a thin upper part of some 1–2-m-thick "stratified silts and sands" (fine to locally medium sands and laminated clayey silts) overlying a "diamicton." The stratified (informal) member is considered equivalent to a "fallout layer," and comparable to the "Dead Zone" of Poag (2002), Poag et al. (2004), and Poag and Norris (2005). Other detail relevant to this work includes: occurrence of sparse clasts of shocked crystalline rocks, which they regarded as ejecta. They included monomict and polymict cataclastic breccias. They did report finding sparse individual shocked quartz grains in the sand fraction of the groundmass. Horton et al. (2008) noted that the matrix between clasts in the Exmore breccia is characteristically microfossiliferous and contains shell fragments.

Geochemical Work with Reference to Exmore Breccia

Poag et al. (2004) reported a large number of analyses of Exmore breccia and various sediment components from the Exmore core hole carried out in an attempt to discriminate the lithological components that constitute the Exmore breccia, to characterize the indigenous component of siderophile elements in the breccia, and to investigate the presence of a meteoritic component. They did not find a systematic chemical change with depth. The rare earth element (REE) abundances and patterns determined were typical for post-Archean upper continental crustal rocks (sedimentary rocks). Attempts using absolute major- and trace-element abundances or CIPW normative values to unambiguously discriminate between the sedimentary components that contributed to Exmore breccia failed. Consequently, it also was not possible to calculate a proper indigenous component for siderophile elements in Exmore breccia. No clear-cut indication for the presence of a meteoritic component was observed in siderophile element data, including data for Ir. Based on original work by Koeberl et al. (1996), Poag et al. (2004) compared the average chemical compositions for their Exmore breccia sample suite and for North American tektites. Besides some general similarities for selected elements, they noted significant differences between the compositions of Exmore breccia and tektite averages.

An extensive study of the chemical and Sr and Nd isotopic compositions of the most important target sediments was reported by Deutsch and Koeberl (2006). They discussed chemical data for samples from drill cores and outcrops, including the preimpact sedimentary formations (Potomac Formation, Aquia Formation, Piney Point Formation, Nanjemoy Formation), as well as the first postimpact formation—the Chickahominy Formation—and one clast of crystalline basement. These authors concluded that the Exmore breccia could have been produced as a mixture of target sediments plus granite, but that this mixture required an additional, as yet undetermined component. They found that neither the average Exmore breccia chemical composition nor an average target sediment composition could adequately reproduce the composition of the two different types of North American tektites (bediasites and georgiaites). In terms of rare earth elements (REEs), the Exmore breccia does, however, seem to lie in the middle of the spread of chondrite (CI)-normalized abundance patterns for the respective target sediments. Obviously, it is not possible to judge from these elemental abundances alone what the crystalline rock component would have been. Nd and Sr isotopes also did not provide additional information, since data for Exmore breccia, target sediments, and target crystalline rocks are not very well discriminated.

Transition to Postimpact Sediments

Poag et al. (2004, p. 255) declared that "because the impact took place in moderately deep water (~300 m) on the middle continental shelf, normal marine sedimentation resumed immediately after the bolide-generated atmospheric and oceanic perturbations ceased." Following Poag (2002), they recognized immediately above the Exmore beds a so-called "dead zone," which they described as a 19–49-cm-thick layer dominated by clayey silt where indigenous microfossils appeared to be absent. It is composed of fine, horizontal, parallel laminae of fine to very fine sand, silt, and clay. This narrow zone was covered by the clay-dominated Chickahominy Formation of up to 200 m thickness.

The fine, horizontal clay and silt laminae of the dead zone were described by Poag et al. (2004) as disturbed by horizontal, vertical, and inclined burrows filled with medium- to coarse-grained sand and reworked microfossils derived from the groundmass of Exmore breccia underneath. In the NASA Langley core, the dead zone does not contain pyrite

aggregates like the so-called "fallback layer" below; instead, pyrite occurs "stratiform" within laminae. Contrary to the NASA Langley observations, in the Bayside core, these pyrite lattices were not observed.

Chickahominy clay was described as typically gray-green clay that weathers to olive-brown and contains variable amounts of fine-grained, comminuted glauconite and muscovite. The clay may be silty or sandy, is rich in fossils, and shows a fine to coarse, although sometimes faint, lamination. Moderate burrowing was also reported by Poag et al. (2004) from the lower boundary of the Chickahominy Formation, and the smallest and most abundant burrows are filled with framboidal pyrite.

Horton et al. (2005a, 2005b) reported that the transition from Exmore beds to postimpact deposition was gradational. In particular, they concluded that "impact-related debris was still settling out of the water column and washing into the partially filled crater while normal sedimentation resumed." However, they noted reworking of microfossils, some of pre-impact and some of postimpact age.

OBJECTIVES FOR THIS STUDY

We carried out a preliminary stratigraphic assessment of the entire Exmore breccia interval recovered from the Eyreville A and B core holes (Table A1). In addition, an extensive sample suite was collected for petrographic and chemical characterization. This included selected clasts (mainly sampled by staff of the University of Vienna) and Exmore groundmass-dominated samples (the Museum for Natural History Berlin suite). In particular, the nature of groundmass along the Exmore section, the statistics of clasts on the microscopic scale, and the chemical variations throughout this package were investigated. In addition and for comparison with the breccia lithologies, samples from the immediate post-Exmore deposition, the so-called transition zone or dead zone, and from sands occurring just below the megablocks and above the uppermost impactite deposit were analyzed. This work does not focus on the sedimentological character of the Exmore beds and associated lithologies, which is discussed in detail in other contributions to this volume (Gohn et al., this volume, Chapter 26; Edwards et al., this volume, Chapter 4; Powars et al., this volume), or the general stratigraphy of the Eyreville cores, which is covered by Horton et al. (this volume). Instead, we have focused on the shock petrographic characterization of microclasts, and our main purpose for this work was to unravel whether any fallback material could be part of the Exmore breccia composition.

Sample Depths

All sample depths reported herein are so-called "revised meters composite depth" values, i.e., computationally adjusted original "feet as boxed" values converted to meters that can be regarded as the best estimate of *true depth.* Details of the conversion procedure are given in Horton et al. (this volume).

RESULTS

The Exmore bed interval at Eyreville occurs between 444 and 1397 m depth. Horton et al. (this volume) describe the upper limit as the contact to "postimpact sediment," the lowermost section of which (so-called post–Exmore breccia transition zone) was also sampled by us. Below 1397 m, lithologies that have been termed "pre-resurge impact breccias and melt rocks" or "polymict impact breccias and associated rocks" occur. According to Horton et al. (this volume), the interval just above that depth contains reworked material from the underlying impact breccias; for example, a suevite boulder has been located there. We took several samples of sandy facies from this transitional interval to compare its clast content with that of the average Exmore breccia above.

Stratigraphic Observations

During the first sampling party in March 2006, the entire Eyreville A–C cores were recorded in some detail. A few examples of typical Exmore breccia appearance, in terms of more or less dense, sandy groundmass facies, and variable density and character of clasts of sand, pebble, cobble, and boulder size, are illustrated in Figure 2. Figure 3 represents a schematic stratigraphic column of the Exmore bed study interval (composite for Eyreville A and B sections), based on the stratigraphic column of Edwards et al. (this volume, Chapter 4). Also indicated are the sampling locations of the Berlin sample suite (marked W- or W2-), as well as several specific samples from the Vienna suite (labeled CB6-) that were subject to detailed analysis. Besides a number of samples from the bottommost section of the post-Exmore bed transition zone (i.e., the basal section of the post-Exmore Chickahominy Formation), which is of particular interest as a record for the recolonization of the crater area after termination of the impact and subsequent environmental perturbations, relatively dense sampling was done in the upper part of the breccia package. Further samples were collected by the Vienna group, some from this uppermost part, but particularly covering also the sedimentary blocks in the Exmore beds. The purpose for these dual sampling strategies was (1) to collect petrographic information about the breccia (groundmass and coarse- to fine-grained clast populations) that would provide statistically relevant data on provenance of shocked particles and mixture of crystalline and sedimentary clasts derived from the various target rocks; and (2) to chemically analyze all available sedimentary and crystalline lithologies for detailed characterization of components possibly involved in the mixing process responsible for the production of North American tektite compositions. Our macroscopic core descriptions are summarized in Table A1.

In Table A2, detailed microscopic observations on all Berlin and Vienna Exmore bed samples are presented, including much information on the lithic blocks and boulders that were sampled by K. Bartosova and C. Koeberl but that are not directly the

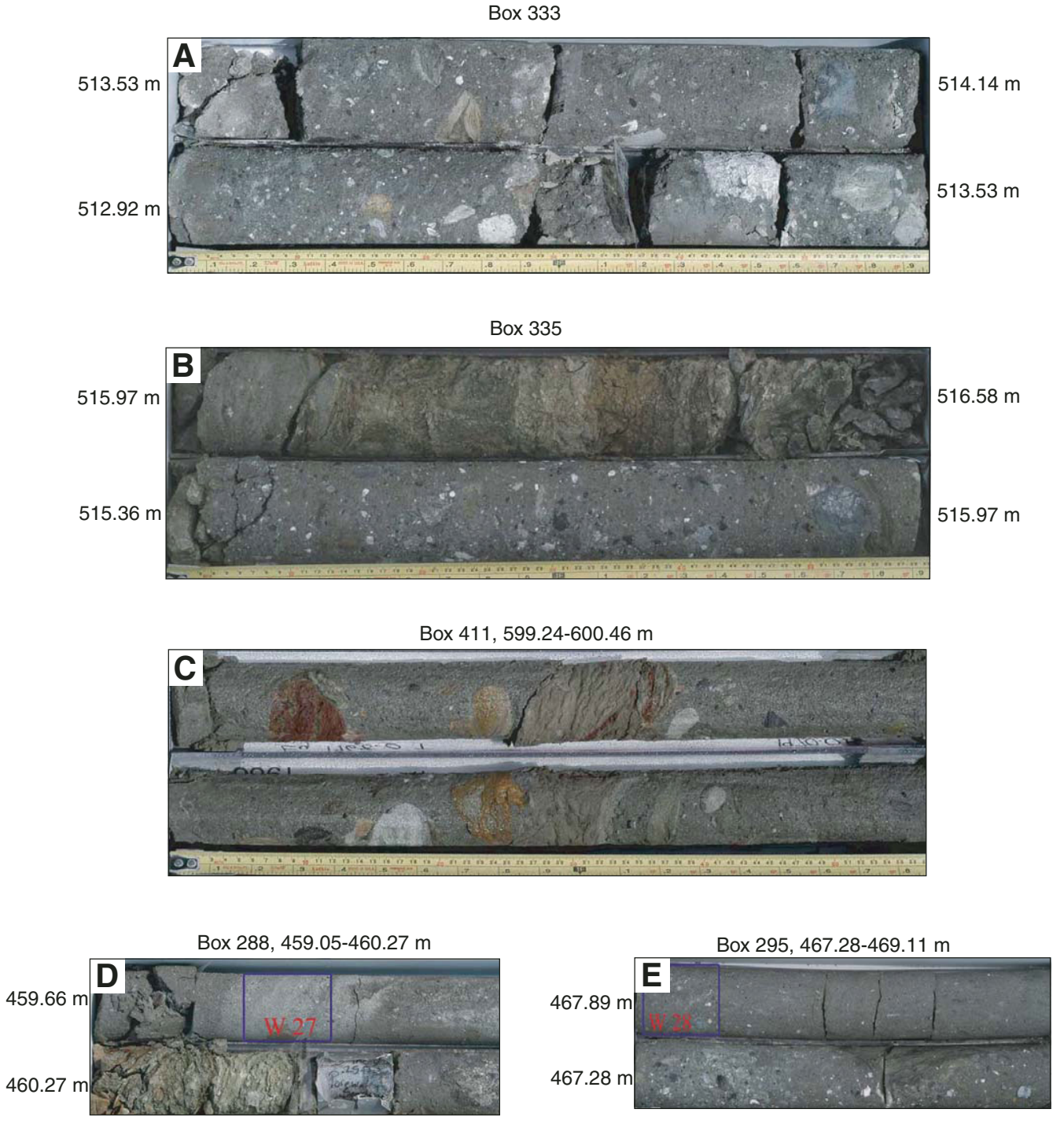

Figure 2. Several core-box images depicting the lithological variation of what has been informally termed "Exmore beds" or "Exmore breccia." Note the variable appearance in terms of both clast- and groundmass-dominated varieties, groundmass character (sandy or seemingly finer-grained, greenish, yellowish, or gray in color), and clast content (clast size ranging from blocks of sedimentary lithologies to moderately sized granitoid-derived clast populations, and pebble- to sand-size dominated fractions). In general, the appearance and local population of larger clasts are not representative of the overall composition of the clast fraction, as individual large pebbles or blocks do not represent the entire population. For a further selection of Exmore breccia core images, see Poag et al. (2004, p. 177–183). The two images in D represent core boxes from the altered melt shard-enriched zone between 458 and 469 m depth (see section on Petrographic Description). Clearly, this zone is highly heterogeneous with large sediment and crystalline clasts, and different clast sizes, abundances, and grain-size ranges from section to section (see Figs. 4G and 4H).

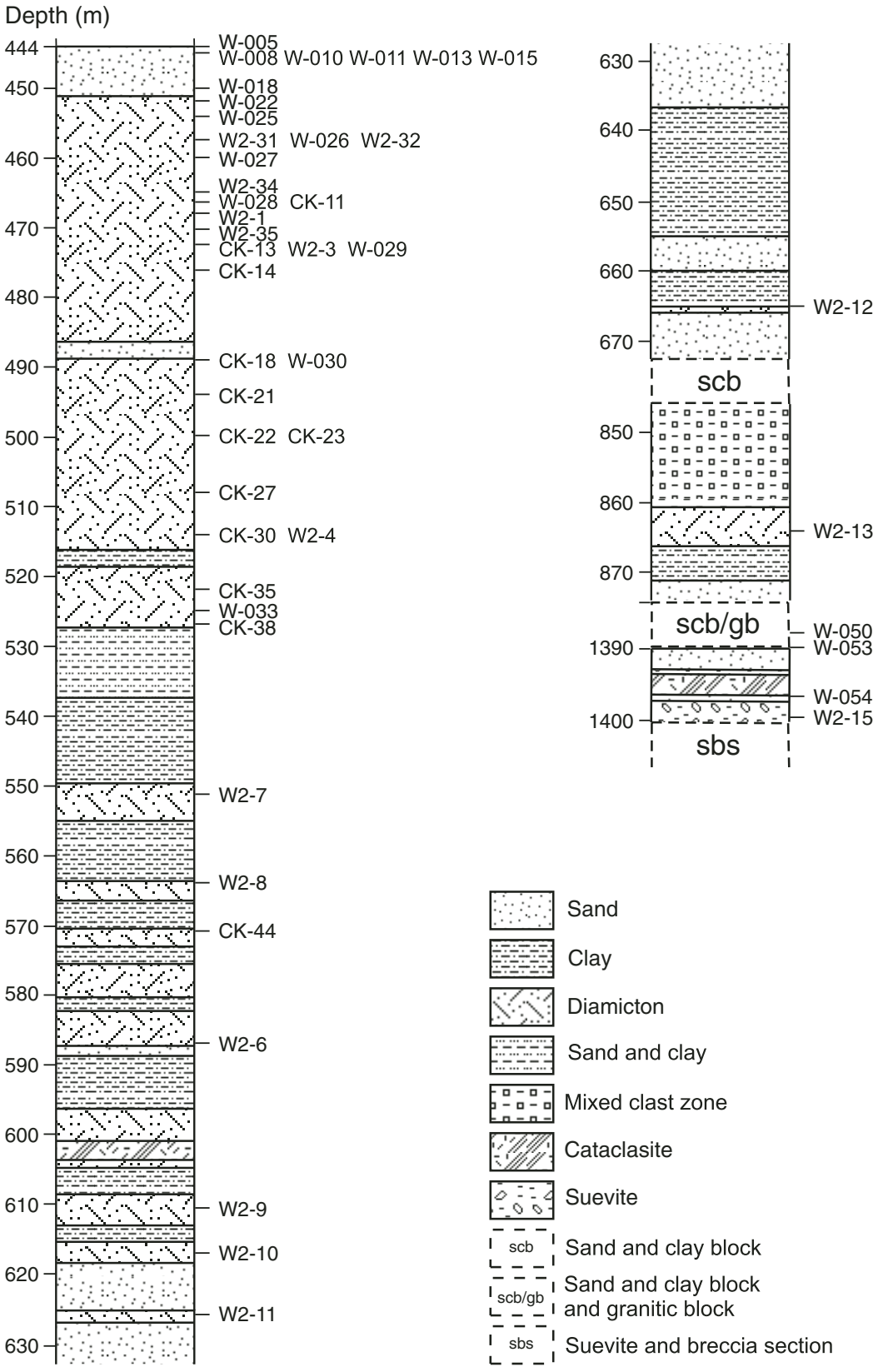

Figure 3. Lithostratigraphy of the Exmore breccia interval in drill cores Eyreville A and B composite (see also Edwards et al., this volume, Chapter 4; Powars et al., this volume). Please note that sample prefixes "CK-" and "CB6-" have been used interchangeably throughout the text.

subject of the present report. The stratigraphic profile of Figure 3 demonstrates that Exmore breccia is mostly contained in the cores above 527 m depth, and a series of narrow intersections alternating with extensive blocks of clayey or sandy lithologies derived from Cretaceous and Paleogene pre-impact sediment units (Edwards et al., this volume, Chapter 4) makes up the bulk of the lower succession. The lowermost part of the section has been drawn discontinuous, as the sedimentary, granitic, and amphibolitic megablocks (marked scb/gb) are not subject of this investigation.

Petrography of the Postimpact Sediments

Samples W-001–W-010 from the so-called transition zone are characterized by tightly laminated claystone and silt. Where claystone is prevalent, silt occurs as lenses or <1-mm-wide bands, and further silty to sandy facies are contained in abundant burrows that cut across bedding (at all possible angles) or that are arranged subparallel to laminae. A number of up to several millimeter wide, generally <0.3-mm-thick lenses of pyrite crystals and crystal aggregates with euhedral cubic crystal habits or framboidal texture occur. Occasionally, the framboidal aggregates enclose clasts and therefore must postdate the deposition of these sediments. Contrary to the underlying Exmore breccia, glauconite pellets and fragments of pellets are very rare, and they are significantly finer-grained as well. The matrix of these clays and silts is too fine-grained to be resolved by the optical microscope. It is variably light-gray to beige or brownish, depending on the respective phyllosilicate/quartz ratios and nature of the locally dominant phyllosilicates. The clasts are also rather fine-grained and dominated by quartz and feldspar (mostly microcline). Traces of muscovite occur, and minor carbonate in the form of fossil-derived, fine-grained debris (very little). Clay pellets, small (mostly <1–2 mm) sandstone clasts, and accessory bioclastic carbonate (very rare microfossils, some traces of shells) occur here and there. Other carbonate (e.g., as another clast or a groundmass component) could not be observed optically. This is consistent with the generally low CaO contents of these samples (see section on Chemical Character). Small (sand-sized) clasts of crystalline rocks are rare. In W-004, from 444.30 m depth, a clast of fine-grained felsic granophyre and a single, altered impact melt fragment were observed. In W-007 (444.57 m depth), a single particle of diaplectic quartz glass was noted, and in W-009 (444.75 m depth), a single droplet-shaped, devitrified and altered impact melt fragment was observed. No other impact-deformed or melted debris can be reported from our samples of post–Exmore breccia sediment, which is—even in comparison to the scarce occurrences throughout the Exmore breccia (see following discussion)—very rare indeed, and this constitutes a significant difference to the uppermost Exmore breccia section. Clay and mudstone clasts, most of subrounded to ovoid shape, are quite prominent, especially in the lowermost samples from our transition zone sample suite.

General Petrographic Description of Exmore Breccia

Figure 4 shows a series of hand specimens and core images that emphasize the variety of lithologies summarily known as Exmore breccia. Figures 4A and 4G are of clast-poor (groundmass-supported) varieties, in contrast to Figures 3B–3E which are characterized by equal clast and groundmass proportions (variably clast- or groundmass-supported). Also, the nature of clasts is very heterogeneous, and sedimentary lithic clasts in the larger size fraction are dominant, but at least in Figures 4B–4E, crystalline rock–derived clasts are also recognizable. Figures 4E and 4F illustrate the variegated nature of sedimentary clasts, in this case, through the different colors of various sandstone and mudstone (yellowish, reddish) varieties. Finally, Figure 4G emphasizes the rarity of macroscopically recognizable impact melt clasts throughout the Exmore breccia sequence.

Typical low-magnification textural overviews (optical microscopy) of postimpact sediment (Figs. 5A–5C) and Exmore breccia (Figs. 5D–5H) are presented in Figure 5. The postimpact sediment examples are characterized by a significantly finer-grained groundmass in comparison to that of Exmore breccia, and clast content is also, in general, finer-grained. It is furthermore obvious that, on average, glauconite content is reduced or even absent in postimpact sediment samples (see Figs. 5A–5C and 5I). In terms of clast sizes, both lithologies display mostly angular to

Figure 4. A selection of hand specimens of Exmore breccia. (A) Sandy groundmass with relatively small clast content composed of both sedimentary rocks (the dark clast upper right is shale-derived) and granitoid/pegmatite-derived clasts (light colored). Sample CB6-015 is from ~478.7 m depth. Beige to gray, silty to sandy groundmass is siliciclastic. Rare melt particles in this sample are consistently smaller than 2 mm. (B) Brownish groundmass with sand-sized particles. The optically identifiable clast content is much enhanced compared to the core section shown in A, and both sedimentary lithologies (dark-gray shale and yellowish-greenish sandstone) as well as granitoid-derived clasts are recognizable. Sample W-032 is from ~515.5 m depth (width of image = 14 cm). (C) Sample CB6-034 from 521.74 m depth is a clast-dominated section with a large fluidal-textured melt particle in upper midsection of this image. Groundmass in this case is beige to light-gray colored. The clast content includes meta-arkose, graywacke, and dark-gray, fine-grained (shaley) sedimentary rocks, besides some granitoid-derived material. (D) Another clast-dominated example, sample CB6-036 from 523.3 m depth. Note the seemingly dense nature of the groundmass, which does not display recognizable sand-sized particles. Pink clasts are K-feldspar. Section of core is 11.5 cm long. (E–F) Drill core sections from 599.30 to 599.51 m, and from 599.91 to 600.12 m depths, with sand-sized groundmass and several prominent sediment-derived clasts (siltstone varieties). Note that these large clasts, in comparison to most of the larger clasts shown in A–D, are strongly rounded. (G) Short section of melt fragment rich–Exmore breccia (box 288, ~459.87 m). All melt is completely altered to pistachio-green secondary phyllosilicate (smectite). (H) Small (9-cm-wide) section of drill core from 861 m depth showing a prominent impact melt particle with reddish schlieren of partially melted crystalline precursor material. Widths of core segments shown in E and F are 63.5 mm, H is 9 cm wide.

CB6-015, depth 478.7 m

depth 515.56 m; 14 cm

CB6-034, depth 521.74 m

depth 523.28 m; 11.5 cm

599.30-599.51 m

599.91-600.12 m

W-027, depth 861.29 m; 9 cm

W-027, depth 459.87 m

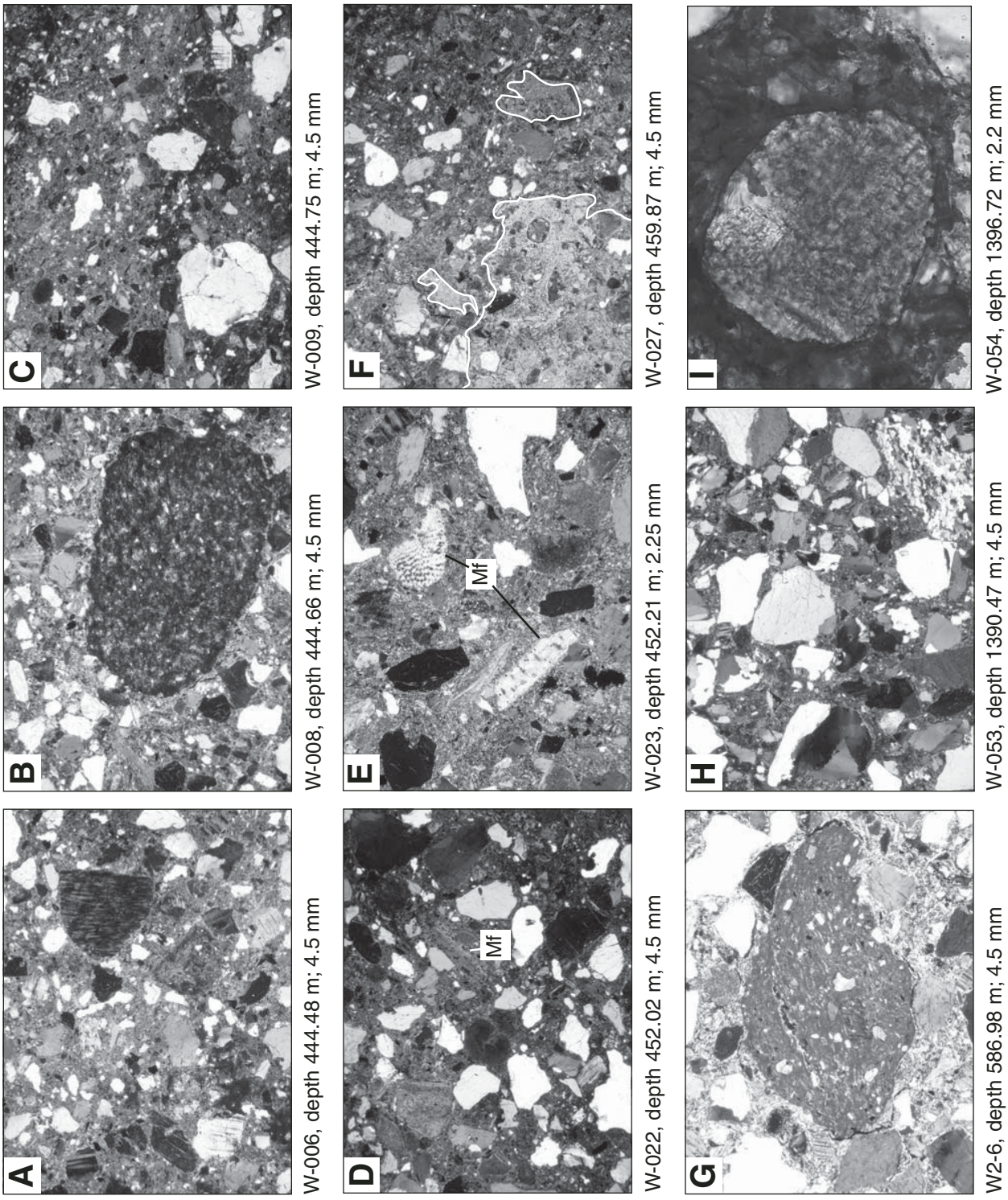

Figure 5. Low magnification imagery of the different sedimentary breccia types investigated in this project. (A–C) Examples of the groundmass and fine-grained clast content in post–Exmore breccia transition zone samples. Note the significant proportion of microcline clasts in the sand-sized fraction in A, which is not typical for the Exmore breccia below this interval. Large shale and siltstone clasts in these transition zone samples are quite rare. (B) Groundmasses are dominated by finest-grained dark-brown phyllosilicate, besides a very fine-grained quartz fraction. Carbonate abundance is very limited. The groundmass does, however, present a mottled (or streaky) appearance due to the local occurrence of dark-brown clay bands between slightly "coarser"-grained silty bands, laminae, and lenses. This variation is, for example, shown in the sequence of laminae from lower left to upper right in C. (D) An example of Exmore breccia groundmass, which is matrix dominated with relatively widely spaced clasts derived from both sedimentary and crystalline precursors. As in E and F, the glauconite fraction is prominent, whereas it is basically absent in the samples from the post–Exmore breccia transition zone. A long sliver of bioclastic carbonate (Mf) extends from the center of image D toward its upper right corner. Note the highly diverse clast shapes. (E) Exmore breccia with a larger clast proportion (more densely spaced than in the previous image), with a number of fossil fragments in the central part of the image, glauconite pellets, several dense, dark shale particles, and otherwise quartz and alkali feldspar fragments. Note that this image (width 2.25 mm) is enlarged compared to the previous selection, and that therefore the grain-size distribution shown in E is actually much smaller. (F) A large melt shard (left side) and several other impact melt shards in the heterogranular clast population of W-027 from 459.87 m depth. These shard shapes are characterized by highly variable boundaries involving both sharp, angular edges indicative of brittle disruption and globular and even vesicular shapes and textures that demonstrate the originally molten state. Clasts in the larger melt shard are essentially quartz particles (light) and oxidized remnants of mafic precursor minerals. Note the small, glauconite particle seemingly enclosed in a slightly ovoid vesicle at right side of this melt shard—this is caused by coincidental presence of this little glauconite pellet in the groundmass directly below this particle and accessed by the grinding of the thin section. (G) A large shale particle in Exmore breccia groundmass of sample W2-6 from 586.98 m depth, showing the extremely fine-grained clayey matrix, and tiny, i.e., silt-sized, quartz fragments. Light-colored breccia groundmass is dominated by phyllosilicate, minor carbonate, and silica. (H) A typical example of sandstone from the sedimentary block zone just above the impactite section in drill core Eyreville B. Note the absence of glauconite, and the overall more angular nature of the clast population, which is dominated by particles derived from the crystalline basement (granitic >> schistose lithologies). Width of field of view for A–D and F–H = 4.5 mm; width of field of view for E = 2.25 mm. All images were taken with crossed polarizers. (I) Glauconite pellet, diameter ~1250 µm, in sample W-054, 1396.72 m depth. Plane polarized light. Mf—microfossil.

subrounded clasts of quartz and feldspar, whereas in both lithologies, the soft mudstone/clay particles are well rounded. Bioclastic carbonate is prominent in Exmore breccia (see Figs. 5D and 5E) as sampled throughout the Exmore beds, but it is scarce in postimpact sediment. It is also our observation that crystalline rock clasts occur comparatively less in the postimpact sediment. In Figure 5F, a microphotograph of impact melt accumulation, typical for this upper section of Exmore breccia, is shown. Note the bleached, altered appearance of these particles that often display angular, shard-like shapes. Like the large particle in this image, they may also display ample ovoid openings filled with breccia groundmass (note the glauconite pellet in an opening in this large particle), and these are interpreted to represent vesicles. Many of these particles are highly vesicular. The maximum size of these melt clasts observed macroscopically is ~5 cm, whereas in thin section, the largest particles observed are mostly smaller than 1 cm, and only rarely up to 2 cm, in size. In terms of frequency, the majority of melt particles are, however, smaller than 1 mm and grade down to tens of micrometers. Besides angular, shard-shaped melt particles, we also observed perfectly round particles, as well as droplet-shaped particles. It is the abundant roundish/ovoid vesicles that impart the shard shapes to fragments of melt.

In general, the groundmass of Exmore breccia can be described as either distinctly sandy or denser, clayey, and then obviously finer-grained. Locally, clayey lamina alternate with silty or sandy bands and lenses. At the thin-section scale, these alternations do not signify sorting. Groundmass colors vary from light gray, via greenish, to dark gray and brownish, where the amount of phyllosilicate exceeds that of quartz significantly. In our sample suite, grain-size variation in groundmass is significant, but we did not observe a distinct change with depth. Locally, groundmass contains micritic carbonate, and individual samples may have a sericite component as well. Distinct phosphate as reported by Gohn et al. (2007) was not observed here.

The average size of microclasts, which may vary from sample to sample or even indicate some kind of sorting over three or four sample intervals, is very heterogeneous. There is no distinct trend recorded by our samples. Most of the Berlin samples were collected by avoiding macroscopically visible clasts in order to sample preferably the groundmass fractions. Microclasts are generally in the <1–3 mm size range. Glauconite pellets and fragments thereof are a consistent feature of the Exmore breccia. The sizes of these pellets vary—in some samples, they are consistently smaller than 1 mm; in other samples, there are more heterogranular fractions, with size ranges from <1 to 3 mm. Microclasts are usually dominated by quartz, and feldspar clasts form the secondmost abundant mineral clast type. Microcline with tartan extinction and perthitic alkali feldspar is most prominent, and plagioclase is comparatively rare. Other minerals represented are muscovite, which is only rarely noted to be kink-banded, biotite laths, chlorite (likely both primary chlorite and a secondary phase after biotite), rare amphibole, and very rare pyroxene. Pyrite has been observed only locally, both as cubic and framboidal crystals/aggregates. Certainly, pyrite observations are not concentrated in

the uppermost Exmore breccia, as proposed by Poag et al. (2004). Trace minerals furthermore include zircon, tourmaline, tiny apatite crystals in quartz (although no concentration of this mineral in the uppermost breccia has been noted, as advocated by the chemical data presented by Schmitt et al., this volume), epidote, rutile/anatase, staurolite, and a few optically unidentified accessory phases. It is obviously not possible to distinguish between quartz derived from crystalline and sedimentary precursors, but there are a small number of observations of shocked quartz with single sets of PDFs, which demonstrate that at least part of this microquartz population is likely from the deep (crystalline) target. The feldspathic clasts also resemble feldspar from the deeper basement-derived drill core section, and these most likely are at least in part derived from there. Felsic mineral clasts occur in both angular and subrounded, rarely rounded, shapes, indicating that both sediment-derived material and clasts from the impact-disrupted basement occur together in the Exmore breccia.

Lithic clasts range in size (at the thin-section scale) from several centimeters to <1 mm. As with the microclast population and clast-size statistics, these larger clasts do not allow—at least for our sample suite and at the thin section scale—a conclusion about a distinct sorting/grading situation. Some samples contain a distinctly equigranular lithic clast fraction, and others are very heterogranular in this respect. Sediment-derived clasts are the dominant clast type. They represent a range of clay/claystone, mudstone, siltstone, sandstone, quartzite, chert, and even conglomerate clast types. Many of the softer lithologies are well rounded, and angular sandstone and quartzite clasts are rather rare. Some of the quartzite fragments may be of crystalline target origin, although it is possible that these particles were part of the pre-impact sediment sequence as well. These quartzite particles have a slightly banded and mylonitic texture and clearly have been recrystallized under dynamic conditions. Other crystalline clasts are either granitoid derived (granites and felsic gneiss) or had schist precursors. Both felsic and mafic schists are represented, as well as the graphitic schist drilled in the basement section of Eyreville B core (Horton et al., this volume). K-feldspar–rich granitoid is rather rare. Several well-rounded granitoid-derived clasts were seen, some of which are encapsulated into clay rims.

Mafic crystalline clasts are rare. Amphibolite is noted only in traces, and a distinct fine-grained, mafic extrusive lithology occurs again and again as a rare component throughout the Exmore bed sequence. It is composed of altered feldspar laths in a dark mesostasis (as shown in the example of Fig. 6F). Likely, this lithology represents the dolerite dikes that apparently could have occurred throughout the target volume as part of a regional set of dikes.

Carbonate clasts are very rare. Sometimes larger carbonate crystals occur as part of mineral aggregates that could represent particles from the crystalline target. Also, secondary carbonate occurs in granitoid-derived clasts, as carbonate-rich bands are known from the basement-derived lower sequence of Eyreville B. In addition, local patches of micritic to microsparitic secondary carbonate occur in groundmass. Carbonate is prominent and obvious in many samples as microscopic bioclastic matter, including shell fragments and microfossils (Figs. 6A–6E). The microfossil content of the Exmore beds is the subject of other publications in this volume (e.g., Self-Trail et al., this volume), but we identified bryozoa and planktonic foraminifera. As with other microclast types, these manifestations of organic debris are irregularly distributed throughout our sample suite.

Several varieties of alteration occur. There is pre-Exmore breccia alteration of clast constituents, such as chloritization of mafic minerals in clasts and sericitization of feldspar, and, locally, Exmore breccia groundmass is impregnated with secondary carbonate or sericite. Also, there are local occurrences of carbonate- or quartz-filled veinlets cutting across breccia and signifying a postimpact brittle deformation event and subsequent infill. This late-stage tectonism may have been related to subsidence of the crater fill and adjustment of the disrupted and deformed rocks of the central uplift and crater floor.

Several larger (>0.5 cm) granitoid clasts are deformed cataclastically, either in the form of an intricate network of fine fractures, or, in a few clasts, involving additional grain rotation to result in a proper cataclasite. Similar material has been reported by Horton et al. (2005a, 2005b) and Horton and Izett (2005).

Shock Metamorphism

A central factor to this investigation was the search for shock-deformed/melted material in the Exmore breccia. In the past (and as summarized previously), rare impact spherules and very rare impact melt particles, as well as some shock-deformed quartz and feldspar clasts, had been observed in Exmore breccia. Figure 7A shows a particle from sample W-011 (444.99 m depth), right from the top of the Exmore breccia sequence, which had originally been thought to represent an impact glass particle. However, subsequent electron microprobe analysis left no doubt that this is actually an altered (bleached) glauconite micropellet. Nevertheless, shock metamorphosed quartz was found throughout the Exmore breccia sequence, although at a very low quantity. Shock deformation of quartz includes very rare clasts of microscopic quartz and quartz in crystalline clasts with undulatory extinction, shock extension fractures (cf. Figs. 7B and 7C), planar fractures (very rare), and planar deformation features (PDFs). Overwhelmingly, only a single set of PDFs per host crystal has been observed, and only a handful of grains display two sets, as in the example shown in Figure 7E. Figure 7F shows a particle with reduced birefringence, irregularly shaped shock extension fractures, and very short remnants of PDFs. In addition, a significant number of samples contains rare to locally abundant (see next section) melt fragments. In Figure 7D, one of the rare partially melted crystalline clasts is shown, where schlieren of remnant crystalline fragments are embedded in shock melt. This image also shows examples (at smaller grain sizes) of altered, frequently angular particles that are also frequently characterized by high concentrations of vesicles. In Figure 8, other examples of these altered melt particles are shown. These

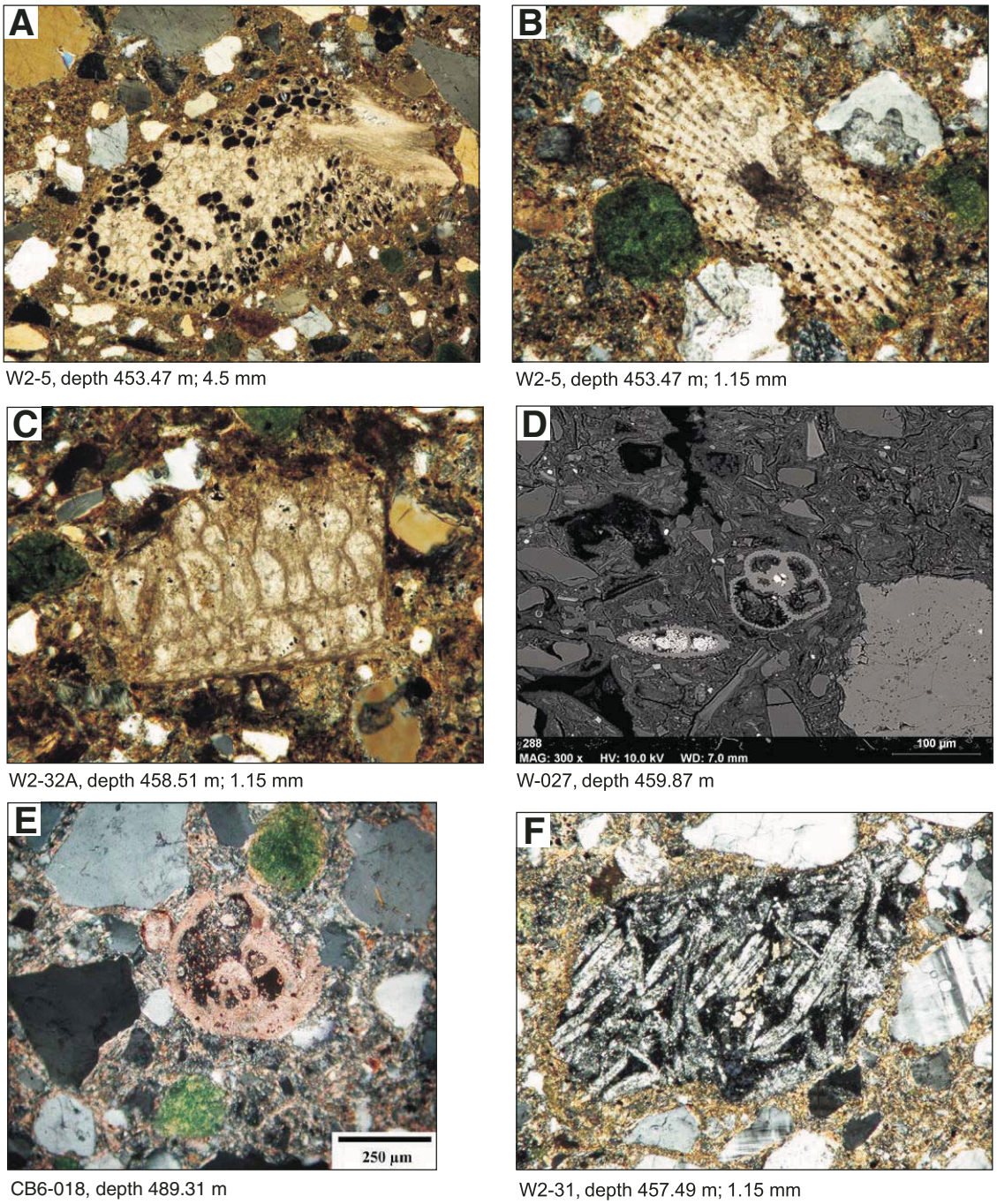

W2-5, depth 453.47 m; 4.5 mm

W2-5, depth 453.47 m; 1.15 mm

W2-32A, depth 458.51 m; 1.15 mm

W-027, depth 459.87 m

CB6-018, depth 489.31 m

W2-31, depth 457.49 m; 1.15 mm

Figure 6. Examples of bioclastic carbonate "debris" observed in Exmore breccia, as well as a typical dolerite clast. (A) Exmore breccia W2-5 from 453.47 m depth: example of a bryozoan. The microfossil is surrounded by typical Exmore breccia groundmass with sand-sized, quartz-dominated clast content and relatively fine-grained glauconite pellets. Width of field of view = 4.5 mm. (B) W2-5: Spine of a sea-urchin; width of field of view = 1.15 mm. (C) Sample W2-32A: another example of a bryozoan from 458.51 m depth; width of field of view = 1.15 mm. (D) Backscattered electron image of two examples of planktonic foraminifera. Dark clasts are quartz; slightly lighter clasts are feldspathic or granitoid derived. Width of image = 475 µm. (E) Another case of planktonic foraminifera, from sample CB6-018, depth 489.31 m. Scale bar length = 250 µm. (F) Clasts derived from volcanic precursors are relatively rare in Exmore breccia. This example of a dolerite clast is subrounded. It consists of laths of altered plagioclase set between dark, altered pyroxene and mesostasis. Other clasts in this image are composed of microcline (right, middle), quartzite (upper right), a quartzo-feldspathic granitoid (upper edge), and much quartz. Sample W2-31, 457.49 m depth; width of field of view = 1.15 mm. Images A–C, E, and F were taken with crossed polarizers.

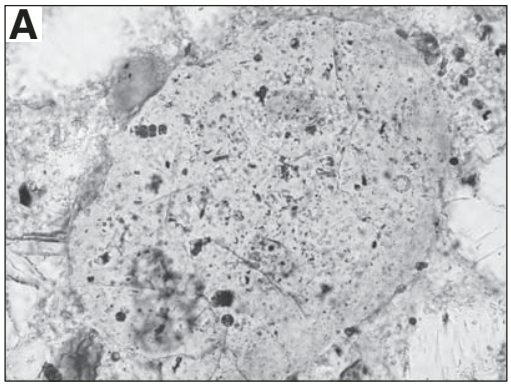

W-011, depth 444.99 m; 1.15 mm

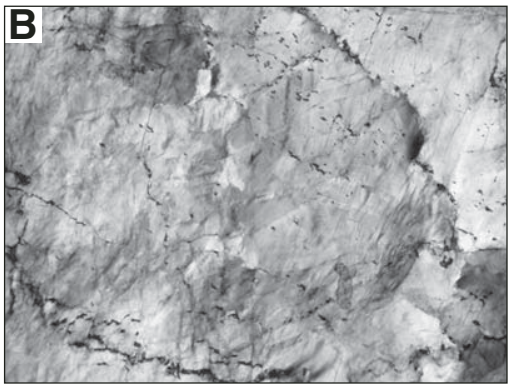

W-026A, depth 457.72 m; 2.25 mm

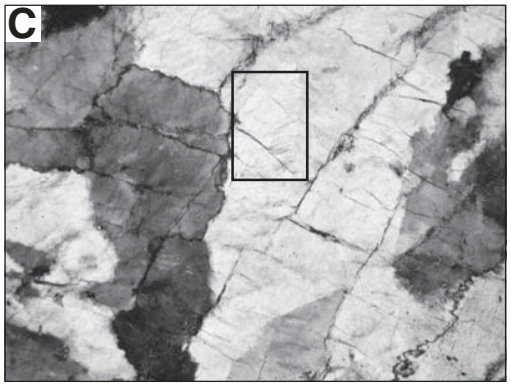

W-026A, depth 457.72 m; 1.15 mm

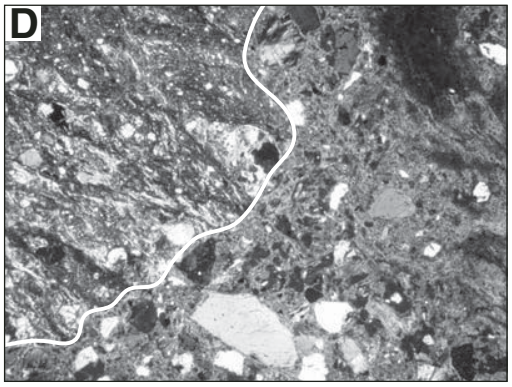

W2-32A, depth 458.51 m; 4.5 mm

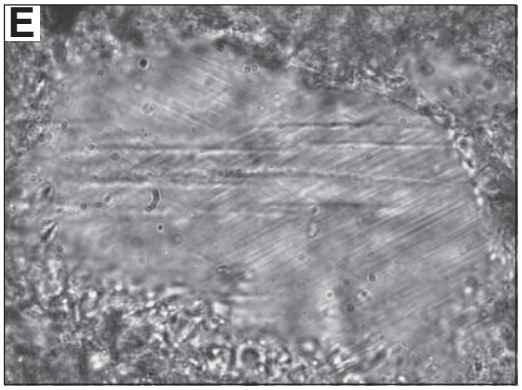

W-027, depth 459.87 m; 90 µm

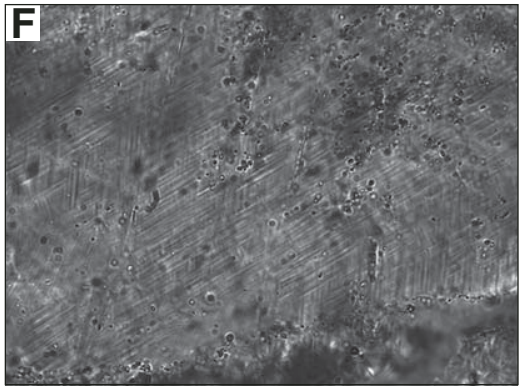

W-027, depth 459.87 m; 90 µm

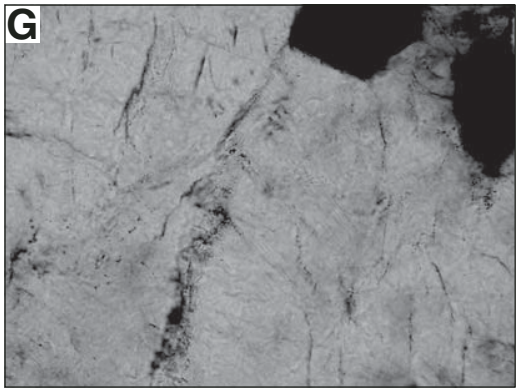

W-033, depth 525.70 m; 1.15 mm

melts all have one factor in common: they have been extensively altered to either finest-grained silica, as in Figure 8C, or to phyllosilicate (smectites), as in the cases of the apparently bleached particles (compare alteration textures in Fig. 9). Carbonate as an alteration product in groundmass is relatively rare and confined to seemingly irregularly distributed patches. Vesicles are either filled by breccia groundmass, which is explained as the result of thin-section cutting through highly porous melt particles having opened windows into underlying groundmass, or by secondary phyllosilicate, sometimes deposited as single or double linings on the inside of vesicles (Fig. 8D), or filling entire vesicle spaces. As shown in some examples of Figure 8, these melt particles are frequently devoid of large concentrations of microclasts. When they occur, however, they are mostly composed of silica. The tiny quartz particles reveal shock deformation in the form of one set of PDFs only in exceptional cases. In Figure 9, a series of backscattered electron images shows altered melt particles and their vesicles and vesicle fillings. Both intact and collapsed vesicle linings are seen, and the latter are indicative of disruption after deposition of the sedimentary breccia. Such melt particles do occur throughout the Exmore beds, but they are indeed enriched in the uppermost parts (as discussed further below). In sample W-027 (459.83 m depth; see Table 1), a granular-textured zircon crystal was observed (Fig. 9G). The amoeboid vesicles visible in this image testify to the once-melted state of this grain. Zeolites as possible alteration products of impact melt were not observed in this Exmore breccia sample suite.

Throughout the sequence (see Table A2), occasional microclasts of partially melted granitoid are present, as well as rare clasts of breccia ("breccia-in-breccia" occurrences)—both in the form of a melt breccia likely representing impact melt, and also polymict lithic breccia or suevite.

Figure 7. Evidence for shock metamorphism and impact melting. (A) A well-rounded particle in Exmore breccia sample W-011 (uppermost Exmore breccia sample available to us) from 444.99 m depth. This particle was originally thought to represent an impact glass particle but was subsequently revealed by electron microprobe analysis to be an altered glauconite micropellet. Plane polarized light; width of field of view = 1.15 mm. (B) Sample W-026A, 457.72 m depth. Strongly strained quartz-pegmatite clast with strong undulatory extinction. This kind of deformation is not impact-diagnostic and could also have been caused in the crystalline basement by pre-impact tectonic deformation. As with true impact-diagnostic deformation, this kind of high-strain deformation is also quite rarely observed in Exmore breccia clasts. Crossed polarizers; width of field of view = 2.25 mm. (C) Another quartz-pegmatite clast with similar high-strain deformation of quartz (undulatory extinction), but this time a rather dense network of short extension fractures is also seen. These curved or somewhat irregular microfractures are typical for shock deformation between ~5 and 10 GPa. However, as it is not clear whether similar patterns of microfractures could not also be the result of other (nonshock) deformation processes, this deformation effect does not represent impact-diagnostic evidence. In the framed area, a set of here essentially invisible planar deformation features (PDFs) occurs. One set of these deformation features per host grain is indicative of ~10 GPa shock pressure. The dark grain in the mid-left area of the image also has a set of nearly straight and parallel fractures, which could be shock-induced planar fractures. Sample W-026A, 457.72 m depth; crossed polarizers; width of field of view = 1.15 mm. (D) Several irregularly shaped impact melt shards, with a larger impact melt clast in the left half of the image. This particle is approximately three-quarters isotropic melt; the remainder is composed of a dense suite of schlieren of partially melted, otherwise plastically deformed, but still crystalline remnants of the precursor material. The particle is subrounded to angular in shape. Such impact melt particles are very rare compared to the strongly altered, bleached-looking shards. Sample W2-32A from 458.51 m depth; crossed polarizers; width of field of view = 4.5 mm. (E) One of only a few felsic mineral clasts with PDFs (planar deformation features) observed in Exmore breccia, indicative of a shock metamorphism regime between ~10 and 25 GPa. This quartz crystal contains two sets of PDFs oriented NW-SE and NE-SW, as well as a set of distinctly wider spaced planar fractures (PF) of subhorizontal orientation. Sample W-027, 459.87 m depth; plane polarized light; width of field of view = 90 µm. (F) Another quartz grain in sample W-027 with dense array of PDFs. Crossed polarizers; width of field of view = 90 µm. (G) Sample W-033, 525.70 m depth; crossed polarized light; width of field of view = 1.15 mm. Quartz clast with dense array of shock extension fractures indicative of shock deformation at 5–10 GPa.

Sedimentary Lithologies from below the Megablock Zone

At 1371.83 m depth, a graywacke (W-050) clast was sampled. It is composed of a 5-mm-wide band with brownish, phyllosilicate-dominated groundmass (matrix dominated) between two wider bands of felsic clast-dominated (clast-supported) groundmass. This graywacke resembles the Exmore breccia in its groundmass appearance and clast population, grain-size distribution, and grain-shape variation, but it entirely lacks glauconite and fossil carbonate components. The clast population is quartz and feldspar dominated, but the phyllosilicate-rich lithic clasts and fine-grained quartzitic clast types that are normally observed in Exmore breccia are lacking. Shock deformation was not noted in the clasts.

Two other samples (W-053 and -054 from 1390.53 and 1396.76 m depth, respectively) represent a gritty sandstone occurring between the amphibolitic block (Horton et al., this volume; Townsend et al., this volume) and the impactite succession below. Main clast components are granitoid-derived quartz and feldspar, a few granitic clasts, and a quartzitic lithology with well-sutured grain boundaries that is thought to be derived from felsic basement gneiss. Also, minor chert, siltstone, carbonate-cemented siltstone, and fossil carbonate occur. There are a number of altered (bleached) melt particles and, in addition, three still glassy ones. Overall, glassy melt clasts are extremely rare in our samples over the entire cored Exmore sequence. This is in accordance with observations reported by Poag et al. (2004), who reported very rare impact melt particles in their numerous samples from a number of drill cores. In aggregate, only five such particles were noted. The total melt component in W-054 is estimated at 2–3 vol%. Groundmass of W-54 is more sericitic than that of W-53 and also contains traces of secondary carbonate.

A sample (W2-15, 1399.50 m depth) of the upper suevite unit (as defined by Horton et al., this volume; see also Wittmann

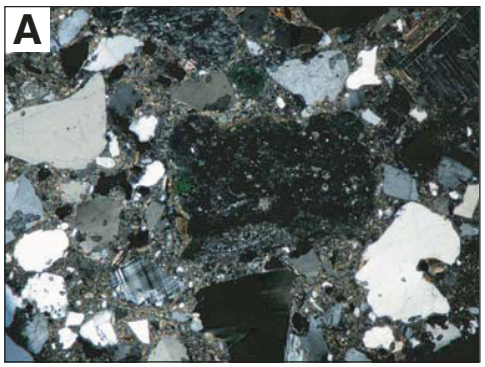

W-014, depth 445.65 m; 2.25 mm

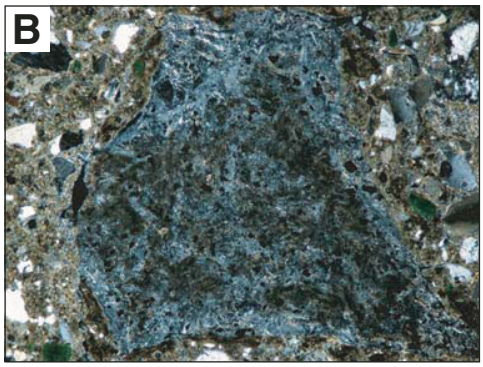

W-024, depth 454.10 m; 4.5 mm

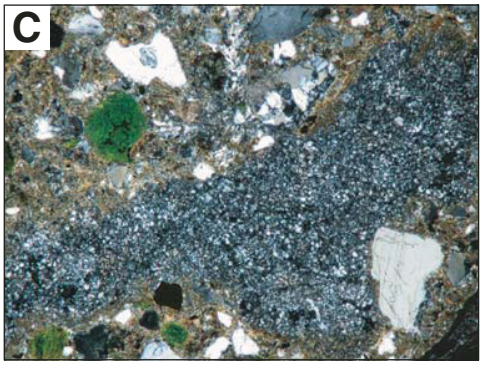

W-024, depth 454.10 m; 2.25 mm

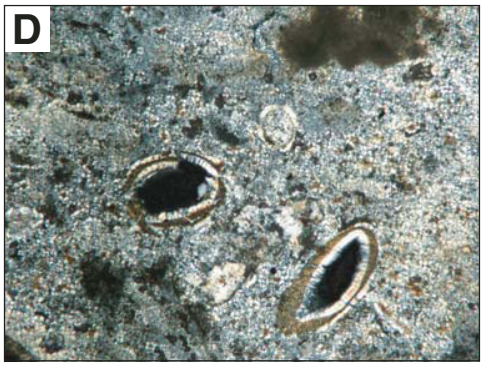

W2-32A, depth 458.51 m; 1.15 mm

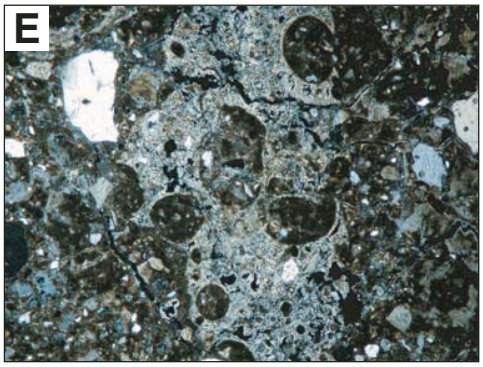

W-027, depth 459.87 m; 4.5 mm

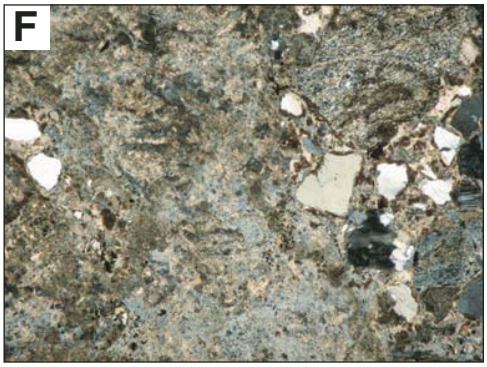

W-026B, depth 458.51 m; 2.25 mm

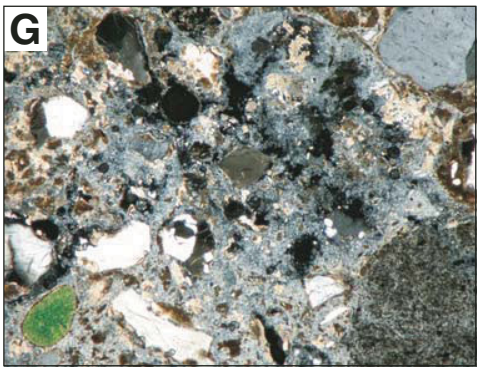

W-026B, depth 458.51 m; 2.25 mm

et al., this volume, Chapter 16; Bartosova et al., this volume, Chapters 15 and 18) was also analyzed and is characterized by a huge proportion—in comparison to Exmore breccia—of impact melt fragments (compare Table 1).

Modal Analyses

In Table 1, the results are compiled for a large number of modal analyses by point counting of entire thin sections (~800–1000 spots per thin section) of Exmore breccia and other lithologies. These point-counting analyses, however, covered only the <4 mm fraction of thin sections, which were selected in order to obtain a true statistical picture, as it was a priori known and already macroscopically evident in the thin sections that larger clasts are heterogeneously distributed throughout the diamictite. Clearly, there are several consistent features in these modal data. First, the abundances of lithic clasts are rather small compared to the overall clast contents. As explained already, this is due to the analysis having been restricted to a limited size fraction only. Matrix proportions are higher for post–Exmore breccia sediment than for Exmore breccia and underlying sediment. Matrix content is highly variable, from <30 vol% to ~57 vol% in Exmore breccia, and also in sediments from below the Exmore breccia (32–62 vol%). One exception is sample W-026B (458.09 m depth; see Table 1), which yielded only 2.7 vol% matrix. The reason for this is that the total amount of altered melt and other clasts, as well as a significant amount of secondary carbonate (rarely observed at all in the other samples), is overwhelming. Figures 8F and 8G show two typical impressions of the densely packed melt fragments in sample W-026B. Note the significant amount of secondary carbonate. Sediment clasts amount to <11 vol% and in most cases <5 vol%, but they frequently exceed the proportions of crystalline rock clasts (also mostly <5 vol%, with some samples between 5 and 11 vol%, and the remainder <1 vol%). Unshocked quartz is the major clast component, followed by glauconite, alkali feldspar, and plagioclase. Finally, carbonate clasts, mostly of bioclastic origin, are a significant clast component. Essentially all other minerals counted are minor and even trace components.

Shocked quartz and feldspar are rare. They are so rare indeed that, even if they were noted and recorded in the general descriptions in Table A2, they may not have been identified by stepwise point counting. Slightly elevated abundance is noted for a few samples that are also relatively enriched in the altered melt component. This occurs essentially between the depths of 457 and 468 m, where altered melt abundances up to 62.5 vol% were recorded. Several other melt-rich samples were found between 499.6 and 526.7 m depth. However, none of these samples reaches figures such as those determined for the upper melt-rich zone. Statistically, traces of melt occur throughout the Exmore package. An attempt to compare the main lithic clast component of Exmore breccia samples by plotting sedimentary, crystalline, and other lithic clast proportions as determined from point counting the <4 mm size fraction resulted in a huge spread of data points in a ternary diagram, failing to indicate any trend or cluster of data.

In Figure 10, various petrographic data are plotted versus depth, from post–Exmore breccia sediment at the top to the onset of the impactite section below the Exmore beds (represented in the depth profiles by data for suevite sample W2-15, 1399.50 m depth; see Table 1). A number of observations can be made on these profiles: the Exmore breccia is highly heterogeneous, but much of the action takes place in its upper part (incidentally an observation that also holds for the chemical systematics; cf. section on chemical character of Exmore breccia below and especially Fig. 15; also see Schmitt et al., this volume). The ratio of crystalline to sedimentary clast proportions fluctuates significantly above ~540 m depth, and it shows a strong decline in the uppermost breccia and into the post–Exmore breccia sediment zone. The sum of crystalline clasts and feldspar over sum of sediment clasts is also highly variable compared to depth, and it is not comparable with the former profile. This could be taken as an indication that quartz and feldspar are derived from both crystalline and sedimentary precursors. The gravelly sand at the base of the Exmore sequence contains up to several volume percent shocked clasts and melt fragments.

The concentrations of carbonate (combined microfossil and secondary carbonate) are also highly variable with depth. In particular, the uppermost Exmore breccia and a narrow zone at ~520 m depth show prominent carbonate components. Notably, matrix of Exmore breccia does not feature a prominent secondary carbonate

Figure 8. Examples of altered impact melt shards (all images taken with crossed polarizers). (A) Sample W-014 from 445.65 m depth. The particle in the center is largely isotropic with remnant clastic material only visible in its lowermost area. The particle has a typical somewhat angular shape kept by many of the melt clasts observed. Width of field of view = 2.25 mm. (B) Completely altered (to montmorillonite-smectite), vesicle-poor impact melt particle with angular to slightly curved margins typical for many of the shard shapes in Exmore breccia. Clast remnants in this particle are also altered to phyllosilicate, so that it is likely that they were remnants of originally mafic minerals. Sample W-024, 454.10 m depth; width = 4.5 mm. (C) A somewhat extended, also completely altered melt particle from the same sample. This time, however, the alteration minerals are phyllosilicate and chert-like silica. The particle is surrounded by a seam of relatively darker-brown groundmass, which resembles a reaction rim. Such rims are quite regularly observed and are likely the result of chemical exchange as part of postdepositional alteration. Width of field of view = 2.25 mm. (D) Part of a large, completely altered melt particle with several preserved vesicles that show the same dual alteration filling also discussed in Figure 9. Brownish patches are oxidic/phyllosilicate remnants of mafic precursor minerals. Sample W2-32A, 458.51 m depth; width of field of view = 1.15 mm. (E) Highly vesicular, 3-mm-long, irregularly formed melt fragment. Also, this fragment is completely altered to secondary phyllosilicates. Its irregular outline is due to the intersection of many globular vesicle segments. Note the presence of many small melt particles in the groundmass. Sample W-027, 459.87 m depth; width of field of view = 4.5 mm. (F) Sample W-026B: a melt shard–rich specimen. Note the dense packing of mottled melt particles that also contain a significant amount of secondary carbonate in the form of local replacement of melt. Width of field of view = 2.25 mm. (G) Another example of altered melt in W-026B. Width = 2.25 mm.

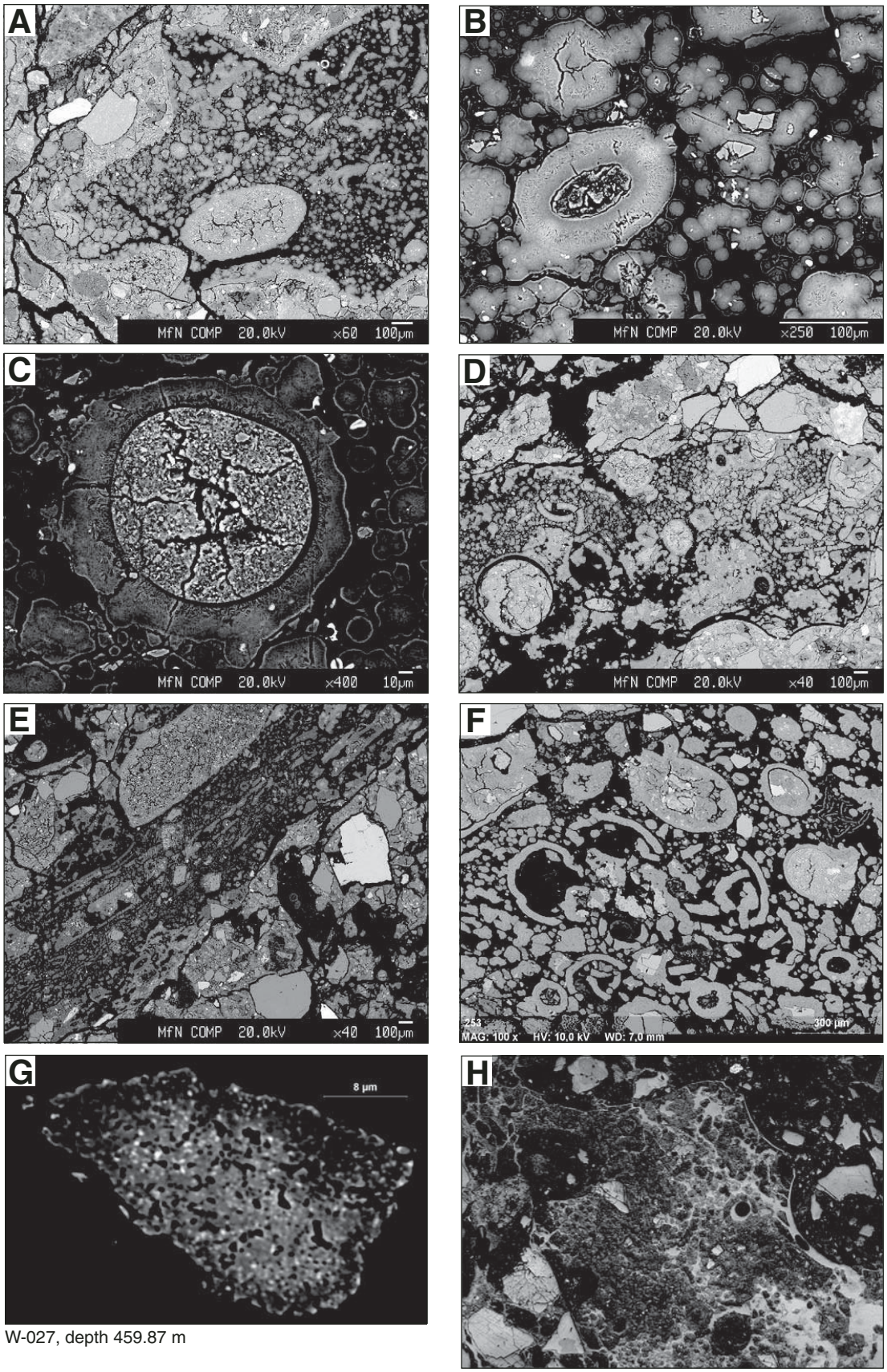

W-027, depth 459.87 m

W-027, depth 459.87 m; 2.2 mm

component, although in thin sections, centimeter-sized patches of mixed carbonate-phyllosilicate matrix do occur. The relative concentration of shocked clasts shows spikes in the uppermost Exmore breccia, as already discussed. Melt fragments are strongly enriched in the upper part of the Exmore breccia, above 520 m. Glauconite is prominent throughout the profile, with a possibly significant maximum in the uppermost Exmore breccia. Finally the clast-matrix profile shows some significant variation, but this variation does not indicate any trends with depth.

Electron-Microprobe Analysis of Altered Melt Particles

The chemical compositions of four altered, shard-shaped melt particles, one claystone particle, one glauconite pellet, and two matrix domains in Exmore breccia sample W-027 from 459.81 m depth, and three altered, angular melt particles and two claystone particles in gravelly sand sample W-054 from 1396.86 m depth were analyzed with the field-emission cathode (JEOL 8500F) electron microprobe (EMP) at the Museum of Natural History in Berlin. Analyses were obtained with a defocused electron beam (diameter 20 µm), according to the measurement parameters and procedures given in Wittmann et al. (this volume, Chapter 17). Means of the analyses on the respective particles and domains are listed in Table 2. All measurements and the averages of measurements on individual particles are presented in Figures 11 and 12, respectively, together with typical phyllosilicate compositions after Deer et al. (1992).

Figure 9. Backscattered electron images (A–G) of impact melt fragments in impact melt shard–rich Exmore breccia sample W-027 from 459.87 m depth. Pervasively altered (to montmorillonite) impact melt particle with ovoid vesicles and, for such particles, typical alteration texture. Vesicles are generally filled with material optically resembling Exmore breccia groundmass material. Scale bar length in A = 100 µm. (B) Higher-magnification view of some ovoid vesicles in another melt particle. Here, the vesicles are internally zoned and fillings consist of an outer zone of montmorillonite and an inner area of typical breccia groundmass type. All material exterior to the vesicles is smectite. Scale bar length = 100 µm. (C) Another vesicle with an outer layer composed of smectite and an inner fill of breccia groundmass material. Scale bar length = 10 µm. (D) Another, somewhat extended melt shard with intact as well as collapsed vesicles. Angular gray particles are quartz fragments. Note the appearance of the typical breccia groundmass exterior to the shard. White particle at upper right is a pyrite fragment. Scale bar length = 100 µm. (E) Strongly extended melt particle with a number of gray quartz clasts. Also visible are strongly extended fragments of vesicle linings that also testify to the plastic deformation of the entire shard. Scale bar length = 100 µm. (F) Portion of another melt shard that is vesicle rich (note the intact vesicles and the numerous remnants of collapsed vesicle rims that are also altered to smectite) and strongly altered. Alteration products have been determined as smectite and carbonate. Scale bar length = 300 µm. (G) Granular-textured zircon crystal. Note the amoeboid vesicles (dark) testifying to the stage of complete melting of this grain. (H) Microphotograph of a completely altered (to smectite and local patches/veinlets of carbonate) melt particle in sample W-027. Crossed polarizers; width of field of view = 2.2 mm.

The ACF diagram of Figure 11 (abbreviations ACF and AFK are explained in the figure caption) demonstrates that our glauconite analyses match the reference composition of this mineral very well. The claystone clasts analyzed have a wide range of compositions that overlap with those of melt particles but extend strongly toward the F apex. Melt particle compositions cluster for individual particles, but overall they scatter around the montmorillonite reference composition. The corresponding AFK plot essentially shows the same, but in this presentation, the illite reference composition is distinctly different from the main data cluster because of the high K content of this mineral, which does not correspond to the compositions of the analyzed melt particles.

Figure 12 represents a ternary plot involving the concentrations of the main major-element components of the phases of interest. Again, the average compositions of melt particles and claystones cluster tightly in the vicinity of the montmorillonite/illite reference points. It is also interesting to note that Exmore breccia matrix is relatively similar in composition to the claystone and melt shard particles. However, in Table 2, it is obvious that matrix is comparatively enriched in TiO_2.

Chemical Character of the Exmore Breccia

A detailed discussion of the chemical variations within the Exmore breccia sequence is provided by Schmitt et al. (this volume). The Exmore breccia displays a substantial variation in chemical compositions, on a sample to sample scale, which does not correspond to a systematic variation with depth. The SiO_2, Al_2O_3, and Fe_2O_3 contents of the Exmore breccia cover wide ranges of 60.9–84.9, 6.5–16.5, and 1.42–6.58 wt%, respectively, with averages of 75.6, 10.3, and 3.10 wt%, respectively. SiO_2 content is negatively correlated with the contents of TiO_2, Al_2O_3, Fe_2O_3, MgO, CaO, P_2O_5, loss on ignition (LOI), V, and Cr. A significant carbonate component in the Exmore breccia, based on a possible positive correlation of CaO and LOI contents, is not recognizable. In contrast, the CaO content is enriched in some parts of the sequence, compared to the remainder of the data suite, and it is strongly positively correlated with the P_2O_5 content (Schmitt et al., this volume; Fig. 1).

A plot of chemical composition versus depth for the entire sequence provides a surprising result initially recognized by Reimold et al. (2007). The Exmore breccia sequence can be divided into separate units with strongly different chemical signatures. Table 3 shows the average chemical compositions (and standard deviations) for these five different depth zones: (1) 444.9–450.7 m, (2) 450.7–468 m, (3) 468–518 m, (4) 518–528 m, and (5) below 528 m. According to Schmitt et al. (this volume), units 2 and 4 display distinctly lower $SiO_2/(Al_2O_3 + Fe_2O_3 + MgO)$ ratios compared to the other units. Both units show an enrichment of TiO_2, Sc, V, Cr, and Rb compared to the other units. At the top of unit 2, a distinct enrichment in P_2O_5 is noted that is strongly positively correlated with CaO abundance and is most likely due to the formation of apatite, the presence of which, however, has not been confirmed yet in the Eyreville core, but

TABLE 1. MODAL ANALYSES BY POINT COUNTING OF ENTIRE THIN SECTIONS (EXCLUDING CLASTS >4 mm; SEE TEXT FOR DISCUSSION)

Sample	W-005	W-008	W-010	W-011	W-013	W-015	W-018	W-022	W2-5	W-025	W2-31	W-026B	W2-32	W2-32B	W-027	W2-34	W-028	CK-11	W2-1A	W2-1B
Depth (m)	444.4	444.6	444.9	444.92	445.26	446.17	450.53	452.30	453.44	454.55	457.49	458.09	458.51	458.51	459.83	465.17	467.29	467.33	468.85	468.85
Type	PEBS†	PEBS†	PEBS†	EB§	EB	EB	EB	EB	EB	EB	EB	EB	EB	EB	EB	EB	EB	EB	EB	EB
Matrix	63.5	57.5	74.2	52.0	44.6	42.7	44.6	46.0	55.8	46.4	53.2	2.7	27.0	33.5	21.5	57.6	50.1	45.1	48.3	53.4
Clasts																				
Sediment clasts	4.2	5.6	0.7	3.4	1.1	1.6	1.1	3.5	1.1	2.5	1.4	3.3	1.7	0.5	1.5	0.7	5.0	1.1	2.5	1.3
Crystalline clasts	0.0	0.1	0.0	0.0	0.7	1.4	0.4	0.3	0.4	1.0	0.8	1.3	2.2	0.0	0.7	0.2	4.2	10.9	0.1	1.4
Calcite	0.0	0.0	0.0	0.1	0.0	0.0	0.0	0.0	0.0	0.0	0.0	0.0	0.0	0.1	0.1	0.1	0.2	0.0	0.3	0.0
Muscovite	0.0	0.0	0.0	0.1	0.2	0.1	0.0	0.0	0.0	0.0	0.0	0.1	0.0	0.0	0.0	0.2	0.5	0.2	0.1	0.1
Biotite	0.2	0.0	0.0	0.2	0.0	0.1	0.0	0.0	0.0	0.0	0.0	0.0	0.0	0.1	0.0	0.0	0.0	0.1	0.0	0.1
Chlorite	0.0	0.0	0.0	0.0	0.0	0.0	0.5	0.0	0.0	0.2	0.2	0.2	0.3	0.2	0.0	0.1	0.0	0.1	0.3	0.0
Amphibole	0.0	0.0	0.0	0.0	0.0	0.0	0.0	0.0	0.0	0.0	0.0	0.0	0.0	0.0	0.0	0.0	0.0	0.0	0.0	0.0
Zircon	0.0	0.0	0.1	0.0	0.0	0.0	0.1	0.1	0.0	0.0	0.0	0.0	0.0	0.1	0.0	0.3	0.0	0.0	0.5	0.0
Rutile/anatase	0.1	0.1	0.0	0.1	0.0	0.1	0.0	0.0	0.0	0.0	0.0	0.1	0.0	0.0	0.0	0.0	0.0	0.0	0.0	0.0
Pyrite	1.6	0.0	0.0	0.1	0.1	0.1	0.0	0.0	0.0	0.0	0.0	0.3	0.0	0.0	0.0	0.0	0.4	0.0	0.7	0.1
Other opaque minerals	0.3	0.0	0.1	0.0	0.0	0.0	0.0	0.1	0.3	0.0	0.3	0.0	0.1	0.4	0.0	0.2	0.2	0.1	0.0	0.4
Plagioclase	0.3	0.7	0.9	0.1	2.2	1.0	1.0	0.7	1.7	0.7	2.7	0.4	1.9	3.8	0.1	1.5	0.5	0.4	1.1	1.8
Epidote	0.0	0.0	0.0	0.0	0.0	0.0	0.0	0.0	0.1	0.0	0.0	0.0	0.0	0.0	0.0	0.0	0.0	0.0	0.0	0.0
Zeolite	0.0	0.0	0.0	0.0	0.0	0.0	0.0	0.0	0.0	0.0	0.0	0.0	0.0	0.0	0.0	0.0	0.0	0.0	0.0	0.0
Garnet	0.0	0.0	0.0	0.0	0.0	0.0	0.0	0.0	0.0	0.0	0.0	0.0	0.0	0.0	0.0	0.0	0.0	0.0	0.0	0.0
Quartz unshocked	27.9	31.9	21.1	32.1	41.4	46.2	45.0	32.7	29.5	33.4	37.3	35.8	23.7	46.1	9.3	34.7	28.6	27.5	17.3	36.3
Quartz with PF	0.0	0.0	0.0	0.0	0.0	0.3	0.0	0.0	0.0	0.0	0.0	1.0	0.4	0.2	0.0	0.0	0.1	0.0	0.0	0.0
Quartz with PDF	0.0	0.0	0.0	0.1	0.0	0.0	0.0	0.0	0.0	0.0	0.0	1.0	0.2	0.1	0.0	0.0	0.0	0.0	0.0	0.0
Ballenquartz	0.0	0.0	0.0	0.0	0.0	0.0	0.0	0.0	0.0	0.0	0.0	0.0	0.4	0.0	0.0	0.0	0.0	0.0	0.0	0.2
K-feldspar unshocked	1.5	3.2	1.8	8.0	6.5	3.4	4.4	4.5	2.7	4.5	0.5	0.3	1.5	4.3	0.7	2.4	2.4	5.1	1.7	2.0
K-Fsp with PF#	0.0	0.0	0.0	0.0	0.0	0.0	0.0	0.0	0.0	0.0	0.0	0.0	0.0	0.1	0.0	0.0	0.0	0.0	0.0	0.0
K-Fsp with PDF#	0.0	0.0	0.0	0.0	0.0	0.0	0.0	0.0	0.0	0.0	0.0	0.0	0.0	0.1	0.0	0.0	0.0	0.0	0.0	0.0
Checkerboard Fsp	0.0	0.0	0.0	0.0	0.0	0.0	0.0	0.0	0.0	0.0	0.0	0.0	0.7	0.0	0.0	0.0	0.0	0.0	0.0	0.2
Carbonate clasts/fossils	0.3	0.6	0.6	1.3	1.8	0.8	0.8	2.8	1.6	4.2	0.7	2.4	0.4	1.0	2.3	0.2	3.4	0.1	0.6	0.5
Glauconite	0.1	0.2	0.4	2.3	1.3	2.2	1.9	9.3	6.8	7.0	2.9	0.0	1.6	0.2	1.3	1.5	0.9	1.3	0.1	2.2
Melt clasts	0.0	0.0	0.0	0.0	0.0	0.0	0.2	0.0	0.0	0.0	0.0	36.2	37.8	9.3	62.5	0.2	3.6	7.9	26.3	0.0
Second. carb.	0.0	0.0	0.0	0.0	0.0	0.0	0.0	0.0	0.0	0.0	0.0	15.0	0.0	0.0	0.0	0.0	0.0	0.0	0.0	0.0
Total	100	100	100	100	100	100	100	100	100	100	100	100	100	100	100	100	100	100	100	100

(*Continued*)

TABLE 1. MODAL ANALYSES BY POINT COUNTING OF ENTIRE THIN SECTIONS (EXCLUDING CLASTS >4 mm; SEE TEXT FOR DISCUSSION) (*Continued*)

Sample	CK-13	W2-3	W-029	CK-14	CK-18	W-030	CK-21	CK-22	CK-23	CK-27	CK-30	W2-4	CK-35	W-033	CK-38	W2-7	W2-8	CK-44	W2-6	W2-9
Depth (m)	472.65	472.91	473.63	476.14	489.31	490.12	494.96	499.61	500.66	508.59	514.17	514.37	522.02	525.66	526.69	551.2	564.3	571.31	586.98	610.67
Type	EB	EB	EB	EB	EB	EB	EB	EB	EB	EB	EB	EB	EB	EB	EB	EB	EB	EB	EB	EB
Matrix	57.2	49.3	46.5	51.8	51.5	56.8	53.5	47.9	56.8	56.3	42.2	36.1	35.9	51.6	40.1	55.9	51.3	50.6	49.2	51.7
Clasts																				
Sediment clasts	0.8	1.5	2.1	0.4	5.3	1.1	0.5	1.3	0.8	1.2	4.7	1.7	10.7	2.1	3.4	2.4	1.5	2.3	0.8	1.0
Crystalline clasts	1.0	0.2	0.3	2.8	1.3	0.3	1.2	1.0	1.3	0.7	7.1	2.6	5.1	0.2	6.9	0.2	0.5	0.9	0.9	0.9
Calcite	0.0	0.0	0.0	0.0	0.0	0.0	0.0	0.0	0.0	0.0	0.0	0.1	0.0	0.0	0.0	0.0	0.0	0.0	0.0	0.0
Muscovite	0.2	0.0	0.0	0.2	0.2	0.0	0.3	0.3	0.1	0.2	0.4	0.0	1.3	0.0	0.3	0.0	0.0	0.0	0.0	0.0
Biotite	0.1	0.0	0.0	0.1	0.1	0.0	0.0	0.2	0.1	0.1	0.0	0.2	0.0	0.0	0.1	0.0	0.0	0.0	0.0	0.0
Chlorite	0.0	0.0	0.0	0.1	0.0	0.0	0.0	0.0	0.0	0.0	0.0	0.3	0.0	0.0	0.1	0.0	0.3	0.0	0.2	0.1
Amphibole	0.0	0.0	0.0	0.0	0.0	0.0	0.0	0.0	0.0	0.0	0.0	0.0	0.0	0.0	0.0	0.1	0.0	0.0	0.1	0.0
Zircon	0.0	0.0	0.0	0.0	0.0	0.0	0.0	0.0	0.0	0.0	0.0	0.2	0.0	0.0	0.0	0.3	0.1	0.0	0.1	0.0
Rutile/anatase	0.0	0.0	0.0	0.0	0.0	0.1	0.0	0.0	0.0	0.0	0.0	0.0	0.0	0.1	0.0	0.2	0.2	0.0	0.0	0.1
Pyrite	0.0	0.0	0.1	0.0	0.0	0.0	0.0	0.0	0.0	0.0	0.0	0.0	0.0	0.1	0.0	0.0	0.0	0.0	0.0	0.2
Other opaque minerals	0.1	0.2	0.0	0.3	0.2	0.1	0.1	0.6	0.2	0.1	0.4	0.2	0.0	0.2	0.2	0.3	0.1	0.0	0.3	0.4
Plagioclase	0.1	2.3	0.5	0.4	0.3	0.3	0.4	0.5	0.3	0.6	0.3	1.3	0.7	0.7	0.2	2.6	2.5	0.6	2.9	1.6
Epidote	0.0	0.0	0.0	0.0	0.0	0.0	0.0	0.0	0.0	0.0	0.0	0.0	0.0	0.0	0.0	0.0	0.0	0.0	0.0	0.0
Zeolite	0.0	0.0	0.0	0.0	0.0	0.0	0.0	0.0	0.0	0.0	0.0	0.0	0.0	0.0	0.0	0.0	0.0	0.0	0.0	0.0
Garnet	0.0	0.0	0.0	0.0	0.0	0.0	0.0	0.0	0.0	0.0	0.0	0.0	0.0	0.0	0.0	0.0	0.1	0.1	0.1	0.2
Quartz unshocked	30.6	40.3	41.5	33.1	29.9	34.4	33.8	32.6	31.0	32.1	26.0	34.1	25.9	38.2	21.2	34.0	38.5	37.0	40.8	39.9
Quartz with PF	0.0	0.0	0.0	0.0	0.0	0.0	0.0	0.0	0.0	0.0	0.0	0.0	0.0	0.0	0.0	0.0	0.0	0.0	0.0	0.0
Quartz with PDF	0.0	0.0	0.0	0.0	0.0	0.0	0.0	0.0	0.0	0.0	0.0	0.0	0.0	0.0	0.0	0.0	0.0	0.0	0.0	0.0
Ballenquartz	0.0	0.0	0.0	0.0	0.0	0.0	0.0	0.0	0.0	0.0	0.0	0.1	0.0	0.0	0.0	0.0	0.0	0.0	0.0	0.0
K-feldspar unshocked	7.0	1.5	4.2	5.9	6.4	3.1	6.9	6.9	6.1	6.3	3.8	2.7	4.6	2.8	4.2	1.6	2.4	6.3	2.9	1.8
K-Fsp with PF	0.0	0.0	0.0	0.0	0.0	0.0	0.0	0.0	0.0	0.0	0.0	0.0	0.0	0.0	0.0	0.0	0.0	0.0	0.0	0.0
K-Fsp with PDF	0.0	0.0	0.0	0.0	0.0	0.0	0.0	0.0	0.0	0.0	0.0	0.0	0.0	0.0	0.0	0.0	0.0	0.0	0.0	0.0
Checkerboard Fsp	0.0	0.2	0.0	0.0	0.0	0.0	0.0	0.0	0.0	0.0	0.0	0.3	0.0	0.0	0.0	0.0	0.0	0.0	0.1	0.0
Carbonate clasts/fossils	0.0	2.0	2.0	2.1	0.1	1.7	0.3	0.3	0.1	0.1	1.1	0.3	7.6	1.4	1.9	0.5	1.0	0.1	0.4	0.3
Glauconite	1.8	2.1	2.8	1.8	1.9	2.0	2.0	1.1	2.6	1.9	1.2	1.2	1.5	1.6	0.9	1.8	1.5	1.3	1.3	1.7
Melt clasts	1.0	0.1	0.0	1.0	2.5	0.0	0.7	7.2	0.4	0.0	12.7	18.7	6.6	0.9	20.3	0.0	0.0	0.7	0.0	0.0
Second. carb.	0.0	0.0	0.0	0.0	0.0	0.0	0.0	0.0	0.0	0.0	0.0	0.0	0.0	0.0	0.0	0.0	0.0	0.0	0.0	0.0
Total	100	100	100	100	100	100	100	100	100	100	100	100	100	100	100	100	100	100	100	100

(*Continued*)

TABLE 1. MODAL ANALYSES BY POINT COUNTING OF ENTIRE THIN SECTIONS (EXCLUDING CLASTS >4 mm), COMPARE TEXT FOR DISCUSSION (*Continued*)

Sample	W2-10	W2-11	W2-12	W2-13	W-050	W-053	W-054	W2-15
Depth (m)	616.80	626.27	665.17	864.29	1371.7	1390.42	1396.70	1399.50
Type	EB	EB	EB	EB	Sand	Sand	Sand	U.S.**
Matrix	46.2	41.0	48.8	50.6	45.8	31.8	62.8	17.7
Clasts								
Sediment clasts	1.2	0.7	1.0	1.1	0.9	5.3	3.8	5.9
Crystalline clasts	0.8	0.0	0.1	0.8	0.2	0.4	0.7	8.4
Calcite	0.0	0.0	0.0	0.0	0.0	0.0	0.0	0.0
Muscovite	0.0	0.0	0.0	0.0	0.1	0.0	0.0	0.0
Biotite	0.1	0.0	0.0	0.0	0.0	0.0	0.0	1.1
Chlorite	0.0	0.0	0.0	0.0	0.0	0.0	0.1	0.0
Amphibole	0.0	0.0	0.0	0.0	0.0	0.0	0.0	0.0
Zircon	0.0	0.0	0.0	0.0	0.1	0.0	0.0	0.1
Rutile/anatase	0.0	0.0	0.0	0.0	0.0	0.0	0.0	0.0
Pyrite	0.0	0.0	0.0	0.0	0.1	0.0	0.1	0.0
Other opaque minerals	0.0	0.3	0.0	0.2	0.1	0.0	0.2	0.2
Plagioclase	3.0	3.2	2.7	3.7	0.7	0.1	0.0	0.2
Epidote	0.0	0.2	0.0	0.0	0.0	0.0	0.0	0.0
Zeolite	0.0	0.0	0.0	0.0	0.0	0.0	0.0	0.0
Garnet	0.0	0.0	0.0	0.0	0.0	0.0	0.0	0.0
Quartz unshocked	43.4	49.9	45.1	40.5	44.6	57.3	28.4	7.1
Quartz with PF	0.0	0.0	0.0	0.0	0.0	0.0	0.1	0.1
Quartz with PDF*	0.0	0.0	0.0	0.0	0.0	0.0	0.0	0.7
Ballenquartz	0.0	0.0	0.0	0.0	0.0	0.0	0.0	1.0
K-feldspar unshocked	2.0	2.8	1.7	1.0	7.4	4.9	1.1	0.9
K-Fsp with PF	0.0	0.0	0.0	0.0	0.0	0.0	0.0	0.0
K-Fsp with PDF	0.0	0.0	0.0	0.0	0.0	0.0	0.0	0.0
Checkerboard Fsp	0.0	0.0	0.0	0.0	0.0	0.0	0.0	0.3
Carbonate clasts/fossils	0.2	0.9	0.1	0.1	0.0	0.1	0.1	0.8
Glauconite	3.1	0.9	0.6	1.9	0.0	0.0	0.0	0.0
Melt clasts	0.0	0.0	0.0	0.0	0.0	0.1	3.2	55.3
Second. Carb.	0.0	0.0	0.0	0.0	0.0	0.0	0.0	0.0
Total	100	100	100	100	100	100	100	100

**Note:* Where significant "Quartz with PDF" has been counted, this does not include shocked quartz in crystalline rock clasts (category "Crystalline clasts" includes both shocked and unshocked clasts). Sample prefixes "CK-" and "CB6-" have been used interchangeably throughout the text.
†PEBS—post–Exmore Bed sediments.
§EB—Exmore breccias.
#PF—planar fractures; PDF—planar deformation features.
**U.S.—Upper Suevite.

which has been detected in Exmore breccia in the Cape Charles drill core (Gohn et al., 2007). The chemical data for our sample suite, as discussed by Schmitt et al. (this volume), demonstrate that the Exmore breccia is likely a mixture of all sedimentary and crystalline target components analyzed to date.

Comparison of Exmore breccia and post–Exmore breccia sediment is possible with Figures 1 and 12 of Schmitt et al. (this volume). The chemical compositions of the post–Exmore breccia samples are quite variable and, in the case of several elements (e.g., SiO_2, Al_2O_3, Fe_2O_3, MgO), values are on the same magnitude as those for Exmore breccia samples (cf. Table 3). It is interesting to note that Figure 1 of Schmitt et al. (this volume) shows that the CaO content of post–Exmore breccia samples is significantly lower than the values for a considerable number of samples of Exmore breccia from the 444–470 m interval. This indicates that the carbonate content of the post–Exmore breccia samples is similar to that of upper Exmore breccia. Interestingly, several trace elements seem to be partially enriched in post–Exmore breccia samples, including V, Sc, Cr, and Co. For V, the relatively large range for Exmore subunits 2 and 4 is even exceeded in post–Exmore breccia samples.

Major-element ranges and means for the five subunits of Exmore breccia, in comparison to values for the post–Exmore breccia sample suite, are plotted in Figure 13 (cf. Table 3). It is obvious that Exmore units 2 and 4 are significantly more mafic than the others, with regard to MgO, Fe_2O_3, and TiO_2 abundances, and that they are also enriched in CaO. Notably, units 2 and 4 roughly correspond to the altered melt-enriched sections of Exmore breccia. Relatively high TiO_2 contents were also determined by electron-microprobe analysis of breccia groundmass (see previous section). However, our petrographic observations do not allow us to conclude that these two sections contain a comparatively enriched mafic component. It is clear, though, that our chemical data do not exclude this possibility either. This would have to be extended to the post–Exmore breccia interval as well, since these samples have similar "mafic" character.

K_2O and Al_2O_3 abundances show wide variability between the different units, which is tentatively related to alteration and clay mineral contents. As discussed by Schmitt et al. (this volume), P_2O_5 is enriched in some samples of units 2 and 4, and it is distinctly enriched at the top of unit 2 (Fig. 14). However, the spread of values within these units is very large. It follows

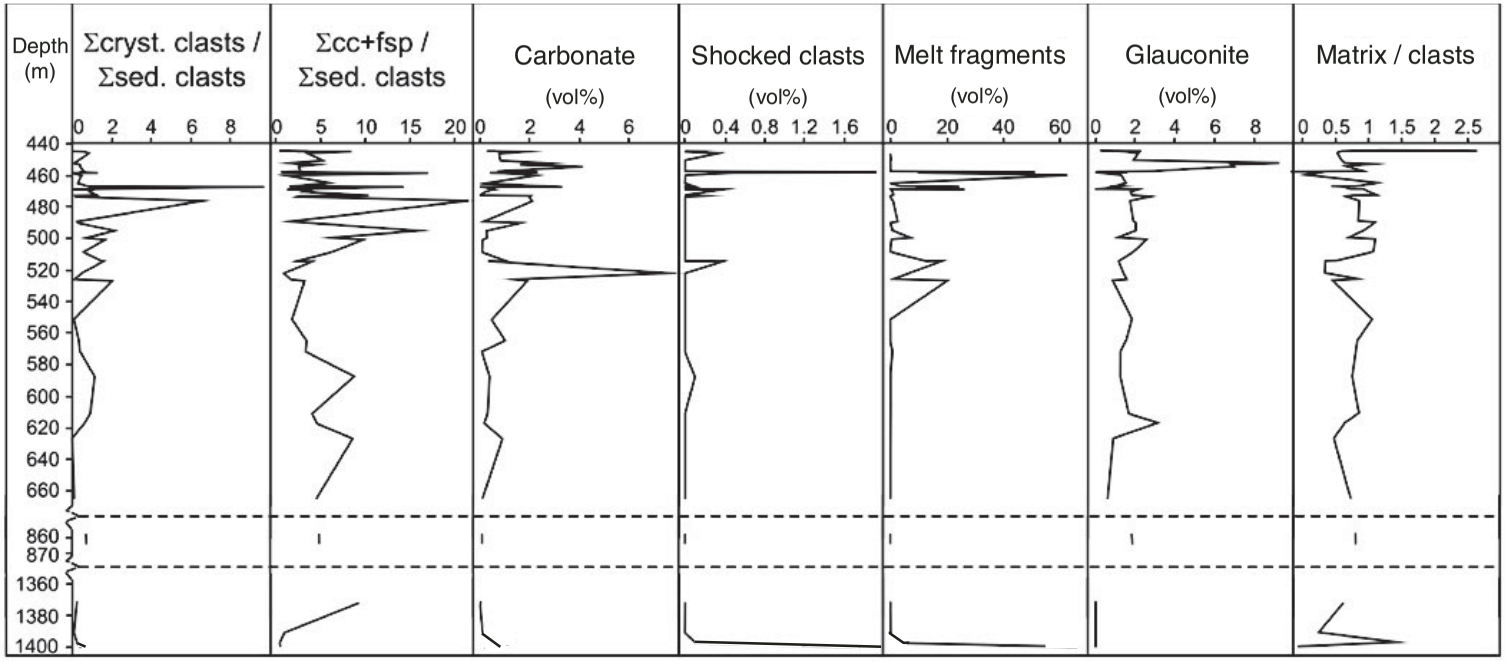

Figure 10. Modal composition data for selected Exmore breccia samples plotted versus depth (see raw data of Table 1). Note that the depth axis is discontinuous because of intercalations of various large megablocks. Sample W2-15 is our uppermost specimen of the impactite sequence drilled below the Exmore beds. Only shocked quartz mineral clasts were recorded, not shocked quartz contained in lithic clasts (especially relevant to sample W2-15). Cc—crystalline clasts; fsp—feldspar.

TABLE 2. SELECTED ELECTRON-MICROPROBE DATA FOR ALTERED MELT PARTICLES IN EXMORE AND GRAVELLY SAND SAMPLES, AS WELL AS FOR GLAUCONITE, CLAYSTONE PELLETS, AND PHYLLOSILICATE MINERAL–RICH MATRIX TO EXMORE BRECCIA

Sample name	Component type	*n**	SiO_2		TiO_2		Al_2O_3		MnO		FeO†		MgO		CaO		Na_2O		K_2O		SO_3		Total§	
			mean (wt%)	σ	mean (wt%)	σ	mean (wt%)	σ	mean (wt%)	σ	mean (wt%)	σ	mean (wt%)	σ	mean (wt%)	σ	mean (wt%)	σ	mean (wt%)	σ	mean (wt%)	σ	mean (wt%)	σ
W-027	Melt shards	10	64.0	0.4	0.34	0.10	26.20	0.37	n.d.	n.a.	4.08	0.12	2.30	0.13	0.60	0.19	2.02	0.31	0.41	0.09	n.d.	n.a.	82.6	1.6
W-027	Melt shards	9	65.1	0.5	0.36	0.06	24.31	0.39	n.d.	n.a.	4.37	0.14	2.48	0.10	0.74	0.17	2.01	0.33	0.51	0.28	n.d.	n.a.	83.3	1.8
W-027	Melt shards	7	64.2	0.2	0.41	0.04	25.76	0.29	n.d.	n.a.	4.35	0.14	2.22	0.13	0.96	0.18	1.67	0.26	0.38	0.11	n.d.	n.a.	83.6	2.6
W-027	Melt shards	10	63.0	0.4	0.26	0.05	28.27	0.53	n.d.	n.a.	3.53	0.12	2.14	0.11	0.81	0.24	1.49	0.34	0.47	0.21	n.d.	n.a.	84.2	1.9
W-054	Melt particle	8	61.5	0.5	0.24	0.25	22.77	0.27	n.d.	n.a.	9.15	0.18	2.78	0.20	1.37	0.37	1.03	0.09	0.79	0.07	n.d.	n.a.	87.0	1.8
W-054	Melt particle	9	61.6	0.4	0.37	0.07	22.08	0.31	n.d.	n.a.	9.08	0.12	3.18	0.12	1.66	0.45	0.93	0.08	0.77	0.08	n.d.	n.a.	85.6	1.3
W-054	Melt particle	10	61.7	0.8	0.70	0.80	21.58	0.27	n.d.	n.a.	8.21	0.41	3.19	0.21	2.60	0.46	0.94	0.07	0.61	0.10	n.d.	n.a.	85.4	1.4
W-027	Claystone	7	60.8	2.1	0.16	0.02	23.05	0.55	0.22	0.14	7.59	1.76	4.40	0.74	0.55	0.14	1.49	0.28	1.69	0.41	0.05	0.03	86.2	3.4
W-054	Claystone	11	57.4	6.5	1.19	1.16	23.43	1.38	n.d.	n.a.	9.63	5.26	3.49	1.19	1.84	0.63	1.35	0.24	1.39	1.23	0.19	0.10	76.4	3.9
W-054	Claystone	8	59.9	3.9	2.34	2.88	22.90	1.55	n.d.	n.a.	7.68	1.28	2.87	0.46	1.98	0.95	1.14	0.18	0.82	0.46	0.38	0.15	80.8	5.1
W-027	Glauconite	9	54.4	0.9	n.d.	n.a.	7.51	0.89	n.d.	n.a.	24.15	1.24	4.90	0.20	n.d.	n.a.	0.33	0.14	8.56	0.66	0.10	0.06	93.0	0.9
W-027	Matrix	5	66.6	6.8	1.94	1.09	21.14	4.64	n.d.	n.a.	3.70	0.85	2.25	0.62	1.01	0.25	2.03	0.73	1.19	0.56	0.15	0.06	89.3	2.9
W-027	Matrix	5	61.9	0.5	4.45	0.88	21.57	0.53	n.d.	n.a.	3.61	0.10	2.18	0.03	1.70	0.33	2.09	0.24	1.74	0.16	0.72	0.21	88.4	1.0

Note: Eyreville A sample W-027 is from 459.81 m depth; Eyreville B sample W-054 is from 1396.86 m depth. n.a.—not applicable; n.d.—not determined.
*n—number of analyses per particle.
†All iron as FeO.
§Totals as measured; all other data were normalized to 100 wt%.

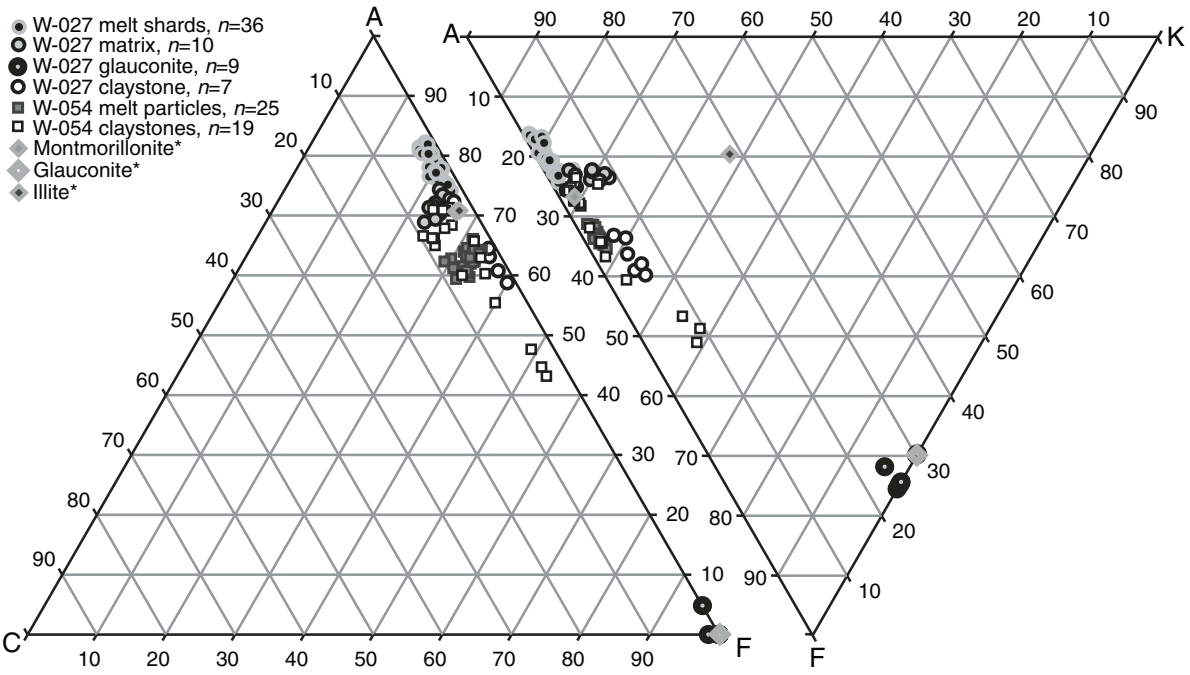

Figure 11. ACF and AFK diagrams for electron-microprobe data for melt particles, glauconite, claystone clasts, and Exmore breccia matrix (diagrams after Eskola, 1939). Asterisks signify reference compositions for selected phyllosilicate minerals are after Deer et al. (1992). Molecular proportions were calculated from electron microprobe data, which are expressed as Al = Al – (Na + K), F = Fe + Mg + Mn, and C = Ca, and K = K.

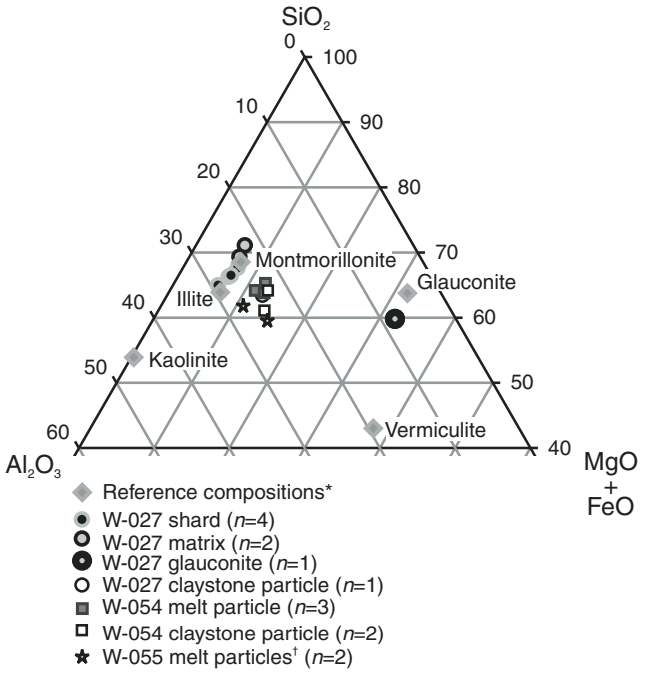

Figure 12. Comparison of the mean compositions of altered melt particles from Exmore breccia, as well as glauconite, claystone, and Exmore breccia matrix compositions, with reference mineral compositions (after Deer et al., 1992) in terms of the SiO_2-Al_2O_3-(MgO + FeO) ternary diagram. *After Deer et al. (1992). †From the uppermost suevite for comparison.

that a phosphate component likely occurs locally in the sequence. However, X-ray diffraction analysis of a P_2O_5-enriched sample did not confirm the presence of crystalline apatite (at least not in excess of the detection limit of around 5 vol%). Besides P_2O_5, a number of trace elements, including Sc, V, Cr, and Zn, also show a particular behavior for samples of units 2 and 4. Data spreads for these sample subsets are very large, and exceptionally high values are noted for samples from these two units. It is tempting to relate this to the specific alteration of melt fragments that characterizes these units (see, e.g., Figs. 8F and 8G, which show elevated secondary carbonate content in sample W-026B [458.51 m depth; see Table 1] from unit 4).

Figures 15A–15C illustrate the rare earth element (REE) chemistry of the Exmore breccia as a function of depth of the analyzed samples. All three diagrams (representing variation of ΣREE, the La/Lu ratios, and the magnitude of the Eu* anomalies) are characterized by very strong scatter in the upper part of the respective profiles. Post–Exmore breccia sediment samples display strong scatter as well, and they do not indicate a change at the Exmore–post-Exmore interface. Individual samples form outliers in these plots, but it has been ascertained (and illustrated by selected sample numbers plotted into the diagrams) that this erratic behavior is not related to a few specific samples. It is likely that much—if not all—of this REE variability must be related to the individual abundances of REE-bearing trace minerals. It also stands to reason that analysis of further samples

TABLE 3. AVERAGE CHEMICAL COMPOSITION, STANDARD DEVIATION, AND RANGE OF ROCK COMPOSITIONS FOR THE POST–EXMORE BRECCIA TRANSITION ZONE AND THE DIFFERENT UNITS OF THE EXMORE BRECCIA (BASED ON DATA OF SCHMITT ET AL., THIS VOLUME)

Unit	Post–Exmore breccia transition zone				Exmore breccia unit 1				Exmore breccia unit 2				Exmore breccia unit 3				Exmore breccia unit 4				Exmore breccia unit 5			
Depth range	443.9–444.9 m				444.9–450.7 m				450.7–468 m				468–518 m				518–528 m				below 528 m			
*n**	10				8				19				26				8				12			
	Mean	Dev†	Min	Max	Mean	Dev	Min	Max	Mean	Dev	Min	Max	Mean	Dev	Min	Max	Mean	Dev	Min	Max	Mean	Dev	Min	Max
(wt%)																								
SiO_2	70.5	9.2	56.3	81.0	81.2	2.2	78.4	84.9	71.6	4.2	60.9	78.5	76.6	1.3	74.1	78.9	71.5	3.6	66.4	77.8	78.7	1.2	76.4	80.6
TiO_2	0.56	0.11	0.41	0.77	0.37	0.07	0.28	0.49	0.55	0.15	0.35	0.91	0.51	0.04	0.45	0.63	0.75	0.08	0.51	0.72	0.49	0.05	0.44	0.62
Al_2O_3	13.1	3.4	8.7	18.6	8.1	1.2	6.5	10.2	11.1	2.4	7.6	16.5	10.2	0.5	9.1	11.2	12.0	1.1	10.0	13.5	9.4	0.5	8.6	10.3
Fe_2O_3§	4.15	3.19	1.68	12.0	1.94	0.35	1.45	2.59	4.06	1.15	2.49	6.58	2.86	0.32	2.27	3.48	3.96	0.67	2.77	4.55	2.28	0.48	1.42	3.12
MnO	0.02	0.00	0.02	0.02	0.03	0.01	0.02	0.04	0.04	0.03	0.01	0.16	0.04	0.01	0.03	0.10	0.05	0.02	0.03	0.08	0.04	0.01	0.02	0.06
MgO	1.13	0.54	0.52	2.03	0.53	0.08	0.41	0.66	1.00	0.34	0.47	1.72	0.74	0.14	0.42	1.04	1.24	0.27	0.80	1.53	0.49	0.09	0.26	0.60
CaO	1.04	0.39	0.55	1.61	0.91	0.08	0.83	1.05	2.29	1.48	0.78	7.40	1.13	0.30	0.90	2.32	1.99	0.87	1.08	3.73	0.94	0.18	0.60	1.24
Na_2O	1.70	0.20	1.38	2.00	1.31	0.22	0.94	1.59	1.31	0.19	1.06	1.88	1.44	0.14	1.26	1.85	1.49	0.06	1.41	1.58	1.38	0.22	1.10	2.85
K_2O	2.36	0.27	1.91	2.66	2.57	0.13	2.34	2.81	2.45	0.56	0.82	3.20	2.57	0.11	2.35	2.88	2.44	0.11	2.27	2.63	2.66	0.16	2.50	3.11
P_2O_5	0.05	0.01	0.03	0.07	0.08	0.02	0.05	0.09	0.19	0.10	0.03	0.41	0.11	0.02	0.08	0.15	0.12	0.01	0.09	0.13	0.09	0.02	0.05	0.12
LOI#	4.7	2.5	2.6	9.7	2.5	0.3	1.9	2.8	4.9	1.5	2.8	9.4	3.4	0.6	2.6	5.0	4.1	0.9	2.8	5.7	3.3	0.7	1.8	4.1
(ppm)																								
Sc	9.7	4.1	5.3	17	4.8	0.8	3.6	6.1	8.7	2.9	5.9	15	7.3	0.6	6.1	8.4	9.6	1.8	6.4	12	6.0	0.5	5.2	6.7
V	79	30	38	129	43	11	28	61	76	15	55	107	61	7	42	73	80	12	61	99	51	7	39	64
Cr	45	16	31	76	30	4	24	37	57	13	31	82	43	4	36	52	59	14	39	82	39	6	27	46
Co	16	9	7.5	40	8.3	4.5	5.1	16	9.0	2.9	5.4	19	9.0	1.5	6.6	12	12	2	8.5	16	8.0	0.6	7.3	9.2
Ni	26	5	16	35	25	7	18	39	22	6	12	36	23	4	14	32	28	3	24	32	16	5	10	24
Zn	48	21	27	89	24	8	16	39	53	22	29	123	43	9	30	73	74	26	38	115	35	7	26	51
Rb	71	8	62	89	65	8	49	73	75	16	40	100	72	3	64	80	80	8	66	90	69	4	63	77
Sr	222	17	195	250	208	23	184	251	183	19	126	219	175	10	161	195	173	8	158	182	171	8	158	183
Y	23	6	15	35	15	3	12	19	24	7	14	44	22	3	18	28	26	5	19	34	19	2	16	23
Zr	191	39	134	250	178	28	137	219	207	51	126	332	207	19	172	243	214	19	193	248	179	23	128	221
Cs	2.6	1.2	1.7	5.4	1.6	0.2	1.2	1.9	2.5	0.8	1.3	4.1	2.2	0.2	1.8	2.7	2.7	0.4	2.0	3.3	1.6	0.2	1.3	2.1
Ba	554	84	405	686	619	63	565	763	449	98	164	586	513	34	446	598	450	42	393	514	524	32	451	563
La	27	8	17	43	16	3	13	20	24	4	18	31	22	2	18	26	25	2	23	29	19	2	16	21
Ce	54	16	37	86	34	5	28	42	52	9	37	66	47	4	38	55	53	6	45	62	41	3	32	43
Nd	23	7	17	36	15	3	12	19	22	4	16	30	20	2	16	26	22	3	18	27	18	2	13	20
Sm	4.8	1.6	2.9	8.1	2.8	0.4	2.3	3.2	4.5	0.7	3.2	5.8	4.2	0.7	3.3	5.9	4.4	0.6	3.3	5.1	3.5	0.3	3.1	3.9
Eu	1.2	0.4	0.9	1.9	0.8	0.1	0.7	0.9	1.2	0.2	0.8	1.5	1.1	0.1	0.9	1.2	1.2	0.1	0.9	1.3	0.9	0.1	0.8	1.0
Gd	4.3	1.3	3.1	6.7	n.d.**				4.0	0.8	2.6	5.3	3.9	0.4	3.1	4.9	4.6	0.8	3.0	5.4	3.3	0.3	2.4	3.6
Tb	0.7	0.2	0.5	1.1	0.4	0.1	0.4	0.5	0.7	0.1	0.4	0.9	0.6	0.1	0.5	0.8	0.8	0.1	0.5	0.9	0.5	0.1	0.4	0.6
Tm	0.3	0.1	0.2	0.5	0.2	0.1	0.2	0.2	0.3	0.1	0.2	0.5	0.3	0.1	0.3	0.4	0.4	0.1	0.3	0.5	0.3	0.1	0.2	0.3
Yb	2.0	0.5	1.4	2.9	1.5	0.2	1.2	1.8	2.0	0.4	1.4	4.7	1.9	0.2	1.6	2.5	2.3	0.3	1.9	2.9	1.6	0.1	1.4	1.9
Lu	0.3	0.1	0.2	0.5	0.2	0.1	0.2	0.3	0.3	0.1	0.2	0.4	0.3	0.1	0.2	0.4	0.4	0.1	0.3	0.5	0.2	0.1	0.2	0.3
Hf	4.7	0.9	3.6	6.5	4.2	0.5	3.2	4.9	4.8	1.0	3.4	7.3	5.2	0.7	4.2	7.0	5.2	0.4	4.7	6.2	4.8	0.6	3.6	5.6
Ta	0.7	0.1	0.5	1.0	0.6	0.2	0.4	1.2	0.7	0.2	0.5	1.1	0.7	0.1	0.5	0.9	0.9	0.2	0.6	1.0	0.6	0.1	0.5	0.7
Th	6.2	1.5	5.2	9.9	4.3	0.9	3.0	5.6	7.4	2.3	5.0	13	6.2	0.9	4.3	8.2	8.1	2.2	5.7	13	5.5	0.7	4.6	7.5
U	1.8	0.6	1.2	3.0	1.3	0.1	1.1	1.5	2.0	0.4	1.4	2.8	1.8	0.3	1.4	2.5	2.4	0.5	1.5	3.0	1.5	0.2	1.3	1.9

*n—number of samples.
†Dev—standard deviation.
§Total Fe as Fe_2O_3.
#LOI—loss on ignition.
**n.d.—not determined.

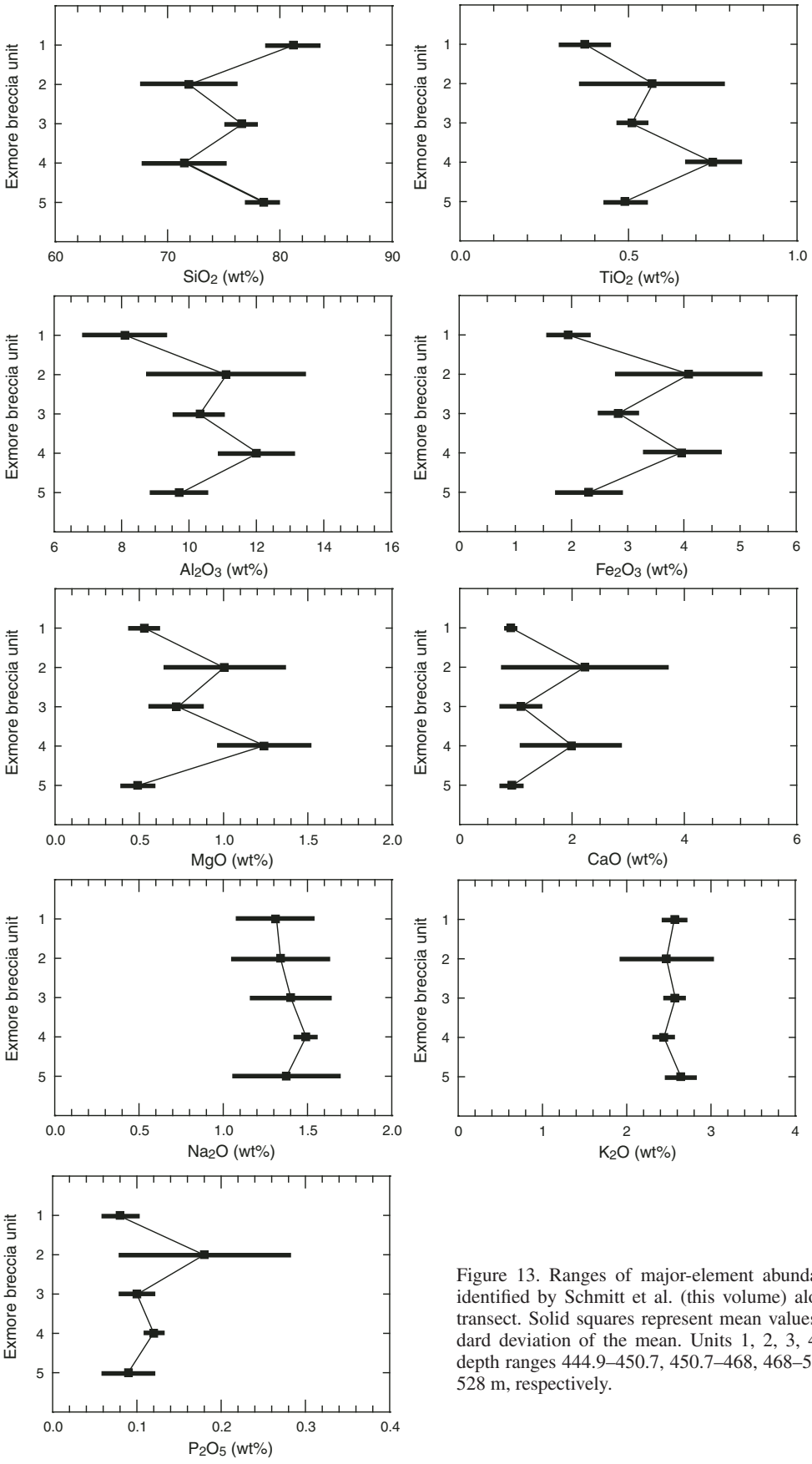

Figure 13. Ranges of major-element abundances for the five units identified by Schmitt et al. (this volume) along the Exmore breccia transect. Solid squares represent mean values, and bars are the standard deviation of the mean. Units 1, 2, 3, 4, and 5 occur over the depth ranges 444.9–450.7, 450.7–468, 468–518, 518–528, and below 528 m, respectively.

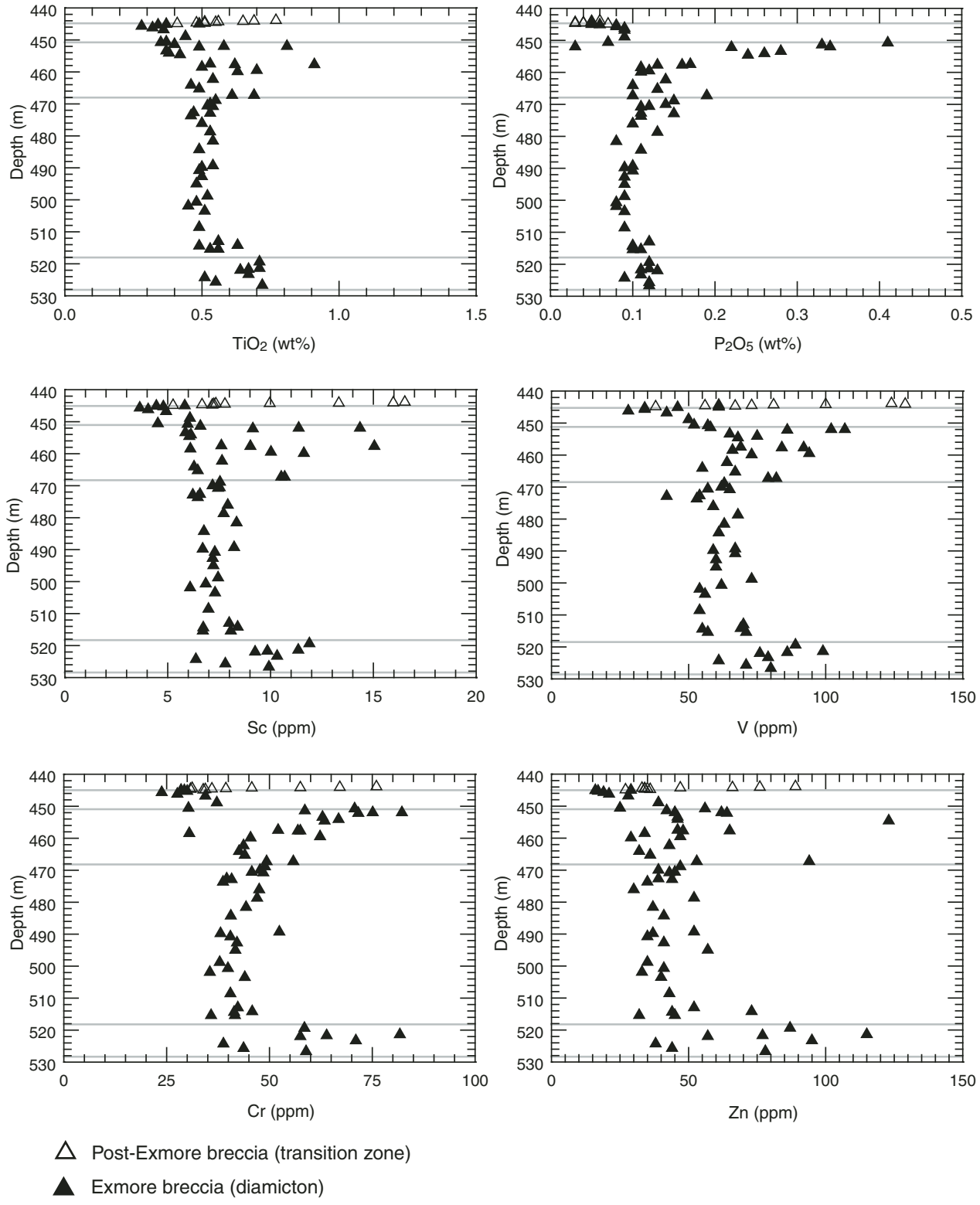

Figure 14. Oxide or trace-element abundance versus depth profiles for the data of Exmore breccia units 1–4. Note the significant data spread and exceptionally high concentration values for selected samples and for all six elements in units 2 and 4. Unit boundaries are, from top to base, at 444.9, 450.7, 468, 518, and 528 m, respectively.

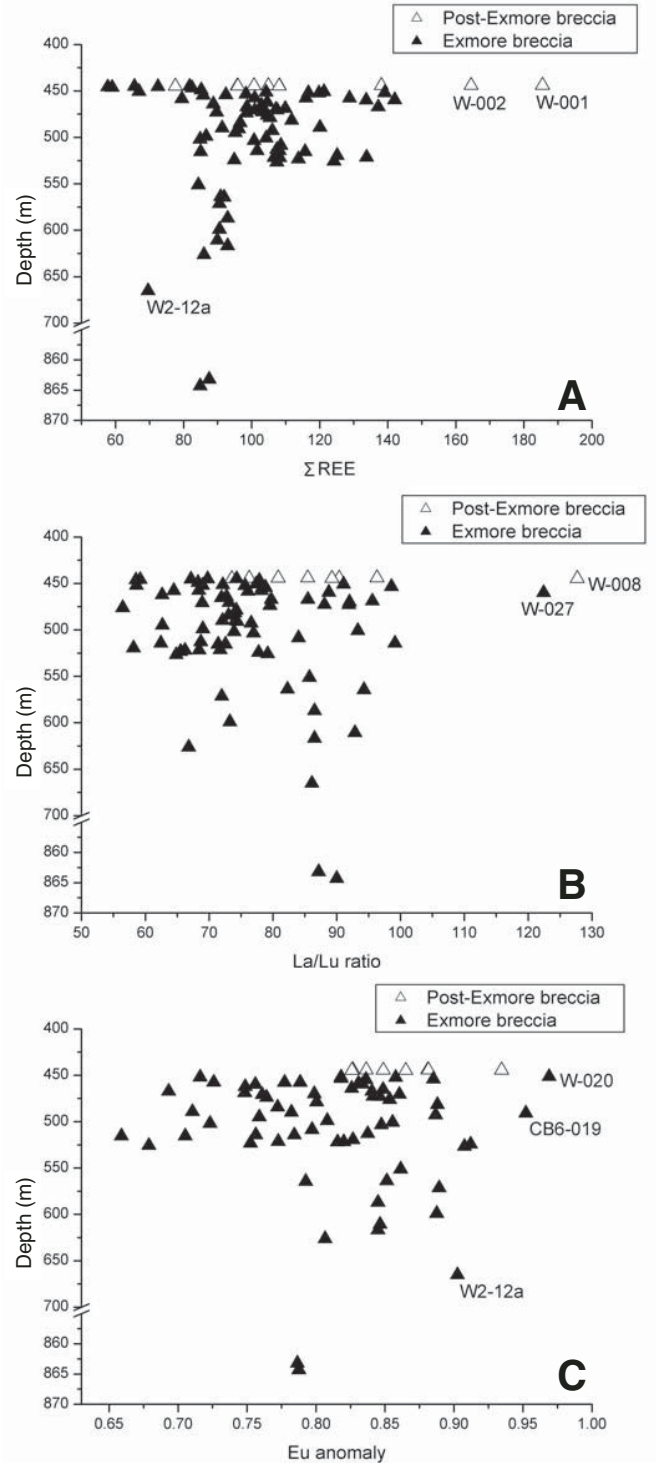

Figure 15. Rare earth element (REE) systematics for post–Exmore breccia and Exmore breccia samples, plotted versus depth: (A) ΣREE (data in ppm); (B) La/Lu ratios; and (C) Eu anomalies, calculated as $Eu/Eu^* = Eu_N/([Sm_N \times Gd_N]^{0.5})$. For selected samples that form outliers in these diagrams, the sample ID's have been given. Clearly, outliers in the different diagrams are not consistently the same samples. Note that the depth scale is discontinuous to allow the presentation of all data from the Exmore sequence at a reasonable resolution.

from the lower part of the Exmore interval will not result in greater scatter there as well.

DISCUSSION

General features of the Exmore breccia, in part known from previous drillings, include:

(1) a distinct intersample heterogeneity with respect to clast content and groundmass nature, e.g., regarding clay versus sand content;

(2) a significantly larger sedimentary than crystalline clast content;

(3) variable, from sample to sample, sediment versus crystalline clast content;

(4) distinct glauconite and fossil carbonate components that distinguish the Exmore breccia from other sandy facies above and below in the stratigraphic column;

(5) presence of a very small component of shocked material, in the form of shock-deformed quartz (and to a lesser degree feldspar); and

(6) notably, these shocked particles are mostly derived from crystalline target rocks, essentially the crystalline basement below the sedimentary cover strata. Evidence for this includes the observation that all lithic clasts with shocked minerals represent crystalline granitoid basement-derived material.

In addition, it is recognized in this study, for the first time, that there are two units in the Exmore breccia sequence within the central crater that are strongly enriched in altered melt particles. The diamicton between 458 and 469 m depth carries an especially significant component of altered impact glass and impact melt. In individual thin sections, this component can be as high as >50 vol% (Table 1). Traces of melt and shocked particles (not statistically recorded in our point-counting modal analyses) have been observed to continue through into the lowermost post–Exmore breccia sediment. However, these are extremely rare, and they are likely fallout particles derived from the collapsing ejecta plume. They are most likely a signature of reworking of the last Exmore breccia deposit.

With regard to impact processes, the lowermost Exmore breccia–related sand and boulder unit below the megablock section does contain an ~30 cm suevite boulder, likely attesting to reworking of the uppermost impact breccia deposit. In addition, a significant component of altered melt clasts is recorded in sample W-054, which may indicate that fallout from the ejecta plume was in full swing during the emplacement of the basal Exmore breccia. The sedimentary and unshocked clast material that forms the bulk of the Exmore breccia sequence, much of which is characterized by rounded grain shapes, is likely derived from the wider crater region and even beyond, as a result of ocean water resurge into the crater cavity. However, the fact that an upper section of Exmore breccia contains significantly more shocked material and especially shard-shaped impact melt particles forces the conclusion that upon deposition of this section, resurge had strongly abated, and comparatively less distal sediment was washed into

the crater at that time (or, vice versa, a higher proportion of ejecta fallout was incorporated into the sediment). It appears, however, that the lack of strong melt abundance in the uppermost part of the Exmore breccia (444–458 m) is due to the fact that major fallout from the ejecta plume had abated before these sediments were deposited.

Kenkmann et al. (this volume) applied the combined knowledge of this observation, the modeling results by Collins and Wünnemann (2005; see also Collins et al., 2008), and new modeling outcomes, and they provide a first approximation of the time frame during which postimpact resurge processes could have taken place. Kenkmann et al. (this volume) conclude that it took some 20 min for turbulent resurge to abate, but that resurge at a scale (tens of meters) not resolvable by the modeling procedure could have continued for some more time. Against these findings, it does appear reasonable to assume that the entire Exmore breccia deposit, in places up to 1200 m thick, was deposited in just slightly longer than 20 min.

The exceedingly rare melt breccia or polymict impact breccia microclasts found scattered throughout the Exmore breccia were likely ripped off the uppermost impact breccia deposit just at the onset of the avalanche/resurge phase. It is also possible that some of this material could have been introduced into the Exmore package as part of air-fall debris.

The different compositions of melt particles from an Exmore breccia sample toward the top and a sample from the basal part of the resurge deposit could be interpreted to suggest different alteration conditions, as indicated by the pervasive replacement of originally likely glassy melt with phyllosilicates. The melt shards from the top of the resurge section may indicate a stronger, yet different alteration trend in that they contain a higher concentration of Al_2O_3 compared to the altered melt particles from the basal portion of the resurge deposits, which apparently retained more MgO and FeO. Calcium does not indicate a reliable trend, likely due to the easy mobilization of this component during hydrous alteration. The similar contents of TiO_2 (Table 3) in the analyzed melt particles suggest that this element was not mobilized during alteration. In summary, this would suggest different alteration trends of glassy melt particles with depth in the resurge deposits.

Alternatively, different original compositions of melt particles could be reflected by the different Fe and Mg contents determined now in altered melt particles. Such different compositions are suggested by the results on impact melt particles in impact breccias by Wittmann et al. (this volume, Chapter 16). However, the widely differing SiO_2 contents in melt particles found by these authors in the suevites below the resurge deposits are not indicated in the currently available data for samples W-054 and W-027. Data by Wittmann et al. (this volume, Chapter 16) for melt particles from the upper suevite unit suggest an even higher concentration of FeO in these particles. This trend of increasing FeO contents with depth may suggest the formation of a chamosite-chlorite component together with smectites at depth. Formation of a chlorite component at a depth of 1400 m is in accordance with the relative stability of smectites between ~300 and 800 m and formation of mixed-layer smectite-chlorites at depth (Viereck et al., 1982). This could likely also be due to different alteration conditions close to the contact between resurge material and suevites, which differed in composition and heat capacity compared to the upper resurge deposits.

The near complete lack of ejecta fallout in the Exmore breccia between 444 and 458 m depth raises the question: should the Exmore breccia be restricted to an upper limit at 458 m depth, where essentially, on the basis of this petrographic study, deposition of impact ejecta was terminated? However, Schmitt et al. (this volume) found a boundary between their units 1 and 2 at 450.7 m depth, which is not directly consistent with our petrographic findings.

Finally, the observation that significant amounts of shocked clasts derived from granitic basement occur scattered throughout the Exmore breccia has implications for the interpretation of the lower section of the Eyreville B core, namely, the basement-derived material (Horton et al., this volume). This section is nearly entirely devoid of shock deformation (also Gibson et al., this volume), with the exception of locally injected impact breccia (Reimold et al., 2007) and the immediate host rock to one cataclastic dike breccia (sample W2-26, 1663.7 m depth; this work), which displays a few quartz grains with one or two sets of PDFs and several grains with PFs. In contrast, granitoid-derived shocked material is found throughout the Exmore breccia and is likely fallout from the impact ejecta plume. Consequently, it must be concluded that the drilled basement-derived rocks represent allochthonous material from an original location that must have been far removed from the impact site. This conclusion is also in agreement with Catchings et al. (2008), whose interpretation of deep seismic data suggests that the floor of the impact structure is at least 2.6 km and perhaps as much as 3.5 km deep.

CONCLUSIONS

The Eyreville ICDP-USGS drill core has provided a complete and—in comparison with previously available sections—much expanded record of the early postimpact deposition of Exmore breccia–type diamictite and intercalated sedimentary and crystalline rock blocks. The sandy-clayey groundmass-dominated breccia that resembles a diamictite (termed "Exmore breccia") was comprehensively sampled for this petrographic investigation throughout the Exmore beds. Micropetrographic analysis led to the recognition of strong heterogeneity from sample to sample with respect to groundmass nature, e.g., regarding clay versus sand content, as well as clast content in general and shocked clast content in particular.

Macroscopically, we observe that the sedimentary clast proportion is consistently larger than the amount of crystalline clasts. On the microscopic scale, the sediment versus crystalline clast ratios are highly variable from sample to sample. The entire breccia interval is characterized by the presence of glauconite and bioclastic carbonate components; this distinguishes

the Exmore breccia from other sandy facies above (very rare and small glauconite pellets) and below (no glauconite observed) in the Eyreville stratigraphic column.

A very small component of shocked material, in the form of shock-deformed quartz (and, to an even lesser degree, feldspar), as well as somewhat more abundant but still overall scarce shard-shaped, and comprehensively altered melt particles, is present throughout the entire sequence of breccia. Optical and scanning electron microscope (SEM) observations as well as first electron-microprobe results suggest that the alteration product is montmorillonite dominated. Carbonate alteration is rare. The abundance of melt particles is particularly high between ~458 and 469 m depth, and between 514 and 527 m depth. The results of the petrographic study are in accord with the chemical definition of unit 2, which places a significant boundary at ~469 m depth, below which only very little impact melt and shocked debris are encountered. Chemically defined unit 4 (Schmitt et al., this volume) is also rich in altered melt fragments, but not to the same extent as unit 2. Nevertheless, chemical and petrographic analyses concur with regard to the delimitation of these two units, as does the lithic and seismic analysis by Powars et al. (this volume).

Seemingly from the time of deposition of the material recorded at ~527 m depth, calming of the ocean occurred over the impact crater area, so that ejecta from the plume above the crater could accumulate to a larger degree than earlier. It appears that deposition of ejecta fallout from the collapsing ejecta plume was terminated by the time of deposition of the 458-m-depth material. Above this level, only very rare shocked particles and impact melt clasts could be observed.

This raises questions about the positioning of the exact upper contact of the Exmore breccia to post-Exmore sediment (Chickahominy Formation), which is currently placed at 444 m depth. It should possibly be revised to 458 m depth.

Based on a significant record of granite-derived material with shocked minerals, the shocked debris component seems to be largely derived from crystalline target rocks. This provides further (see, e.g., Kenkmann et al., this volume) evidence that the basement-derived material of the basal section of the Eyreville drilling, which is essentially unshocked, is likely allochthonous, and it seems that drilling did not intersect the actual crater floor.

ACKNOWLEDGMENTS

The Eyreville drilling project was made possible with the generous support of the International Continental Scientific Drilling Project (ICDP) and the U.S. Geological Survey (USGS) and additional financial support from the National Science Foundation of the United States. The Buyrn family is thanked for access to their property and their interest in the drilling venture. Koeberl acknowledges funding from the Austrian Science Foundation FWF, grant P-18862-N10, and Reimold acknowledges research support from the German Science Foundation (grant RE 528/4-1). We are grateful for technical support from Antje Dittmann, Hans-Rudolf Knöfler, and Uli Raschke (all Museum of Natural History Berlin). Reviewers Henning Dypvik and David King provided valuable input. Any use of trade, product, or firm names is for descriptive purposes only and does not imply endorsement by the U.S. government.

TABLE A1. MACROSCOPIC DESCRIPTION OF THE EYREVILLE A AND B EXMORE BED SECTIONS, LISTING THE VARIOUS CONTACTS THAT WERE DETERMINED AT THE FIRST SAMPLING PARTY AT THE U.S. GEOLOGICAL SURVEY IN RESTON, VIRGINIA

(*N.B.: The sediment terminology applied refers to loose though rather coherent [sand, mud] or consolidated [clay, mudstone, siltstone, sandstone] lithologies. In particular, where consolidated sedimentary clasts in the Exmore Breccia are cited, they are considered "stone" rather than unconsolidated sediment. Where no color is given for sedimentary units, they are generally of beige to light greenish colors. Please note that the prefixes "CK-" and "CB6-" are used interchangeably throughout the text.)*

Core Eyreville A (all depths in meters)

Base of postimpact sediments–top Exmore breccia at 445.28
To 446.90 coarse grit alternating with sands
To 451.04 coarse grit alternating with sands
At 467.89 a 25-cm-large shale clast
476.25 to 478.60 laminated red sand
485.15 to 489.51 sand, followed by alternating medium-grained, clast-rich sandy breccia and large clasts of mostly sandstone
Scattered granitoid clasts but sediment clast–dominated; some granitoid clasts could be highly shocked (or strongly altered)
Apparent increase of 1–2-cm-sized clasts at 520.45
Sandstone megaclast from ~527.30 to 535.84
Laminated and folded, 30-cm-long breccia, then the next megaclast to 549.55
Breccia with decimeter-sized clasts to 563.58
Breccia to 565.40
Folded sand and mud, then gritty breccia from 570.34 to 572.05
Mudstone clast to 575.40
Breccia alternating with decimeter-sized sediment clasts to 580.22
Large sediment clast to 584.15

Breccia to 586.28
Sandstone megaclast to 596.49
Breccia to 600.46
Graphitic schist (pebbly, muddy material protected in Plexiglas holder)—presumably a large clast—to 603.47
Sandy breccia with scattered, up to 7 cm granitoid clasts to 604.63
Laminated mud and banded sand (megaclast) to 616.61
Cataclasis and faulting of sand at 639.68
Gritty sandstone (clast or breccia) from 616.00 (discordant contact) to 618.13 (contact bleached)
Sand to 625.18
Gritty sand to 626.51
Sand with decimeter-wide intercalations of grit to 636.76
Red clay to 654.89
Sand to 660.99
Mud to 664.98
Grit to 665.74
Partially well-laminated sandstone to 674.57
1-dm-wide conglomerate to 674.71
….core loss….
Folded sandstone from 676.96 to 678.45
Laminated mudstone to 678.79
Clay from 695.25 to 685.80
Sand to 698.24
Grit to 698.54
Sand to 703.51
Mud to 704.64
Sand to 707.93
Mud to 708.17
Beige sand to 711.46
Sand and mud (intercalated) to 711.95
Sand to 713.35
Red clay to 741.43
Beige clay to 742.58
Gritty sand to 743.59
Sand with clay nodules to 745.02
Sand with up to 20-cm-wide grit stringers to 748.25
Clay to 749.14
Sand to 759.07
Sand (locally laminated) with reddish stringers to 762.52
Around 761.70, a 33-cm-long laminated black sand and shale section
Black shale from 762.52 to 762.85
Laminated sand to 763.83
Black shale with sand stringers to 763.92
Sand, in places distinctly gritty, with shale nodules, to 802.11
Gritty clay with >1-cm-wide sandstone nodules to 802.78
Gray sand to 821.02
Whitish, well-banded sand to 824.65
Gray, gritty sand to 825.54
White, laminated sand to 826.34
Gray, mottled sand with 1–2-cm-wide shale clasts to 829.97
Beige sand to 830.43
Sharp, at 45 degree inclined contact to clay/sandy clay that extends up to 832.53
Alternating reddish and greenish clay with isolated sand lenses to 842.99
Sand to 848.26 (locally medium grained, gritty and containing a few small [<0.5 cm] shale clasts; only at 844.24, a larger, 5 cm shale clast)
A faulted (stepped), 2.5-cm-wide shale band at ~848.56
Beige sand to 854.31
A concordant, 3.5-cm-wide grit band at 849.66 (also a few subangular to rounded shale clasts < 6 cm wide)
Clay to 854.75
Beige sand, with nodules and pebbles of quartz >2 cm wide, as well as black sand clasts, to 862.28
More varied, brecciated (higher-energy currents?) sediment to 866.76
Strongly disrupted clay to 871.33
Sand-dominated interval to 897.61 (some decimeter-sized clasts of clay at 890.02–890.56, shale 884.86–884.96, shale 874.17–874.26, mottled medium-grained sand at 873.94–874.06)
Clay interval from 897.61 to 899.07
Sand to 909.83

…core loss…
Clay (and some sand) to 913.97
Sand to end of core Eyreville A at 940.37, with a few, short clay intersections and minor grit

Core Eyreville B (all depths in meters)

Sand from 938.6 to 942.49
Clay to 944.27
Beige sand with a few centimeter-sized, dark-gray sand bands to 954.27
Folded and shale nodule bearing sand to 955.52
Quartz nodule–rich sand to 971.09, with shale from 962.1 to 962.25
Sand, in places gritty, to 975.36
Fine-grained, beige, clean sand to 988.22
Laminated, in places shale nodular sand to 992.49
Silty sand to 993.28
Sand to 997.73, then more clayey material to 999.74
Well-banded sand to 1006.45, then gradual contact (over 5 cm) to black shale, which is found until 1016.33 (some well laminated, on the millimeter scale, sandy to shaley alternations)
Beige clay from 1014.92 to 1016.02
Sand to 1023.67
Clay to 1024.59
Sand to 1035.04, with a few shale bands
Black, laminated shale to 1039.95
Shale nodular sand from 1049.61 to 1051.35
Sand to 1062.32 (includes a few decimeters of shaley bands)
Shale to 1062.93
Sand to 1063.23
Clay to 1063.45
Sand to 1068.75 (well-banded shale from 1066.89 to 1067.29)
Shale nodular clay to sand to 1069.73
Well-banded sand to 1072.68
Gritty sand to 1073.6
Sand with isolated 1–3 cm clasts to 1082.98
Coherent shale to 1083.14
Medium-grained sand, then sharp and 40 degree inclined contact to black shale to 1086.7
Well-laminated sand with narrow clay band to 1086.84
Sand to 1095.45 (a 5 cm, well-rounded sandstone pebble at 1095.33)
At 1095.24, pebbly, light-gray siltstone, with a sharp, 20 degree contact to *granite megablock*

Megablock zone to contact to sand and lithic block unit at 1368.4
Gritty sand with well-rounded sandstone, mudstone, and shale clasts at the centimeter scale, changing in grain size to 1375.87 where it is nearly a true grit, extending to 1376.39
To 1389.67—mafic, amphibole-rich intrusion
To 1393.12—gritty sand with up to 5-cm-long shale clasts: *Contact to impactite sequence.*

TABLE A2. PETROGRAPHIC OBSERVATIONS ON EXMORE BED SAMPLES OF THE BERLIN AND VIENNA EYREVILLE SAMPLE SUITES

(N.B.: These descriptions pertain to the samples also discussed by Schmitt et al. [this volume].)

Post–Exmore breccia transition zone

W-001 Claystone/Siltstone, 443.91 m depth: Tightly (<1 mm) laminated claystone with microbands or lenses of fine-grained silt. Laminae are, depending on phyllosilicate to quartz microcrystal ratio, either beige or light brown. Locally, up to several-millimeter-wide, but <0.3-mm-thick lenses of pyrite crystals (euhedral cubic or framboidal) occur. Traces of muscovite and a single glauconite micropellet were noted. No shocked or impact-generated particles.

W-002 Siltstone/Claystone, 444.09 m depth: Very similar to W-001, but specimen is suggestive of cross-bedding. Even less silt fraction than in W-001. Even these rare occurrences of silt are finer grained than in the sample above. Besides scarce quartz microcrystals, no other mineral phases can be resolved with the optical microscope. No shocked or impact-generated particles.

W-003 Siltstone, 444.18 m depth: Fine-grained silt (phyllosilicate-dominated matrix) with very fine-grained clasts, many of which are seemingly elongate parallel to the lamination of the sediment. Larger muscovite flakes are often distinctly discordant to the bedding. Clast

population: qz > fsp (Kfs > pl), some biotite and muscovite, some granite-derived intergrowths of quartz + muscovite or quartz + microcline, traces of glauconite (very small pellets), <0.5 vol% carbonate (some of which is intergrown with granite-derived silicates), a few sandstone clasts (1 with some glauconite), <1 vol% opaques (mostly massive or porous pyrites), several clay pellets, a trace (tiny grains) of fossil carbonate. No shocked particles or impact-generated material.

W-004 Siltstone, 444.30 m depth: Similar to W-003, but 1 fragment of quenched granophyre, and 1 possible altered impact melt fragment.

W-005 Sandstone, 444.43 m depth: Clay-cemented. Similar to W-003/W-004 but slightly coarser-grained clast population. Generally similar clast components to these samples, but also a small component of sandstone/siltstone pellets. A lot of framboid pyrite enclosing clasts, i.e., of clear postdepositional origin. Very little glauconite. No shocked clasts, but 1 grain of altered impact glass. No bioclastic carbonate.

W-006 Sandstone, 444.48 m depth: Like W-005 but slightly more glauconite and more clay/siltstone pellets. Has a slightly more heterogranular clast population. A few clasts of typical but extremely fine-grained quartz-sericite schist. A handful of "stick-like," very thin fossil remnants; no bioclastic carbonate. No shock-deformed clasts.

W-007 Sandstone, 444.57 m depth: Similar to W-006, with a heterogranular grain-size distribution of clasts. Significant amount of mudstone pellets, one with fossil carbonate (shell fragments), very little glauconite. One fragment of diaplectic quartz glass.

W-008 Sandstone, 444.66 m depth: Similar to W-006/-007 but a few 3–4-mm-sized mudstone pellets. Slightly larger overall grain sizes, on average. Several well-rounded bioclastic carbonate clasts. No shock-deformed clasts or impact debris.

W-009 Sandstone, 444.75 m depth: A further slight increase of average grain size. Lots of mudstone pellets, also a few graphitic schist clasts. More glauconite than samples above (there seems to be an indication of regular increase of glauconite content from W-003 to W-009). Traces of bioclastic carbonate. One droplet-shaped devitrified impact melt fragment. No shock-deformed clasts.

W-010 Sandstone, 444.87 m depth: Slightly finer-grained clast population than above. Contains a 1 cm mudstone patch (angular outline, therefore likely a clast). No shock-deformed clasts.

All the above samples are rich in very fine-grained (clay-type) groundmass.

Exmore breccia

(Exmore breccia denotes the clast-rich material in this volume referred to as "diamicton.")

W-011 Exmore breccia, 444.99 m depth: Typical though glauconite-poor Exmore breccia. Fine-grained (clasts are generally <1 mm in size, and there are only rare 1–2-mm-size siltstone ovoids). A small bioclastic carbonate clast component (fossil remnants). The clast population is dominated by quartz and alkali feldspar. The groundmass has some carbonate. One quartz clast with 1 set of planar fractures (PFs). No other shocked material observed. In contrast to the material below, the clast population is dominated by angular fragments (~70%).

W-012 Exmore breccia, 445.08 m depth: Contains fragments of graywacke (with ~30 vol% phyllosilicate-rich and extremely fine-grained groundmass) with angular to subrounded clasts of quartz > feldspar (K-fs >> plag) > siltstone and mudstone > glauconite (well-rounded pellets), traces of calcareous fossils, a single clast of carbonate-cemented sandstone, and one of mylonitic quartzitic schist. No significant mineral deformation (only some irregular fracturing mostly in feldspar clasts). Generally fine-grained clasts (<1 mm).

W-013 Exmore breccia, 445.28 m depth: Similar to W-012 in terms of groundmass proportion and clast population, but there is a significant change in clast sorting (more size variation). Glauconite pellets are generally larger than in W-012 and are relatively more abundant. Sample contains a well-rounded clast of altered, fine-grained, granitic gneiss.

W-014 Exmore breccia, 445.65 m depth: Similar to W-013 but somewhat more siltstone and micrite clasts (generally well rounded). A new clast variety is represented by a very fine-grained microquartzite (not chert grain size yet!). Clast grain-size distribution is variable but skewed toward smaller sizes. This also leads to a somewhat denser packing of clasts and a slight reduction of groundmass proportion in comparison to samples above. Some metaquartzite clasts have a mylonitic texture with well-sutured grains, and with a subparallel and locally even folded fabric. A relatively large mollusk fragment. No significant deformation.

W-015 Exmore breccia, 446.21 m depth: Similar to W-014, with a large grain-size variation. A new clast type is seen in the form of a sandstone that is matrix supported with a sericite-dominated groundmass. The quartz clasts commonly have strong mosaicism and even a few subplanar fractures—clear evidence of low-shock deformation (<15 GPa). Many angular quartz clasts with undulatory extinction. Relatively little and rather fine-grained glauconite pellets. Several clasts of mica-schist.

W-016 Exmore breccia, 446.79 m depth: Like W-015, but also containing a few large clasts of graphitic schist, and 1 granite-gneiss clast with severely altered feldspar. Comparatively little glauconite and relatively small glauconite grain size.

W-017 Exmore breccia, 448.88 m depth: Relatively finer-grained (<1 mm) clasts are dominant, but there are also several large (up to 7 mm wide) siltstone clasts. Carbonate clasts (most of them of bioclastic origin) are prominent. Sample contains more granitic gneiss clasts than seen in all samples from above together. There is a large, moderately shocked, medium-grained granite clast (probably derived from vein quartz) with rare planar deformation features (PDFs), reduced birefringence, and mosaicism. Also one 2-mm-sized mica schist clast with nice crenulation.

W-018 Exmore breccia, 450.57 m depth: This breccia sample has a much finer-grained clast population than seen in the samples above. Some quartz clasts have undulatory extinction. Several very fine-grained chert particles. Some medium-grained clasts of either framboid pyrite or pyrite-cemented quartz grains. No shock-deformed clasts.

W-019 Exmore breccia, 450.78 m depth: Much finer-grained clast population than samples above; also a few >1 cm clasts. Significantly more glauconite as well as carbonate clasts. The latter amount to ~25 vol% and include a large number of fossil fragments. No shocked clasts.

W-020 Exmore breccia, 451.38 m depth: Carbonate fossil (shell fragments)–rich and glauconite-rich sample. Several large ovoid clasts of carbonate and siltstone, besides mostly <1 mm clasts. The sample is, at 40 vol%, groundmass supported. Contains a 1-cm-sized clast of partially melted (presumably shock melted; appearing bleached due to alteration of the melt) granite.

W-021 Contact Exmore breccia–claystone clast, 451.84 m depth: The sample is—in comparison to the other Exmore breccia samples above—extremely fine grained (not just the claystone clast part). This breccia sequence is graded and only has narrow lamina between clay material that actually carries glauconite and fine-grained quartz and feldspar particles, together with a trace of bioclastic carbonate. The clay

section is entirely devoid of glauconite. A single clast of silica-cemented sandstone and a few quartzitic clasts occur. No shocked particles in this sample. The groundmass is sericite dominated.

W-023 Bedded Exmore breccia, 452.02 m depth: A large (7 mm) unshocked and rather fresh granite clast. Groundmass amounts to 45 vol%; clast population is skewed to smaller grain sizes in comparison to above samples. The glauconite content is comparatively moderate. Very little carbonate compared to the previous samples. All carbonate is bioclastic.

W-022 (Wedge of Exmore breccia between claystone clasts), 452.21 m depth: Glauconite-rich, but less carbonate clast proportion than in W-020. A >1 cm siltstone clast and several unshocked vein quartz clasts. A well-rounded granite clast is encapsulated in a mud-shell.

W2-5 Exmore breccia, 453.44 m depth: Typical Exmore breccia, but somewhat heterogeneous. Dominated by a <1 to 2 mm sand fraction. Several nice microfossil fragments, and, if any, very little shocked debris.

W-24 Exmore breccia, 454.10 m depth: Medium- to fine-grained clast population. All clasts are <3 mm in size. Quartz and K-feldspar are dominant, but one also sees a lot of granitic (qz-fsp) and vein quartz fragments. Glauconite is abundant as in W13, but the carbonate content is reduced compared to above.

W-025 Graded Exmore breccia, 454.59 m depth: One large (>12 mm) fragment of fine-grained mica schist that is largely melted (presumably shock melted). The melt portion is rather altered (bleached). A second, only 3-mm-wide particle like this occurs as well. Less glauconite than above and only a few calcareous fossil fragments. Several apparent vugs with fillings with schlieric appearance. A single, possibly volcanic particle with subophitic texture (pyroxene altered to greenish phyllosilicate).

W2-31 Exmore breccia, 457.49 m depth: One large brown mudstone clast, 1 fragment of chloritized igneous rock. Heterogranular sandy breccia with a lot of basement-derived microcline, several well-rounded granitoid-derived clasts. No shocked material.

CB6-006 Exmore breccia, 457.72 m depth: Typical Exmore breccia with glauconite pellets up to 1 mm. There are some clasts of fine-grained sediments, granite, and other target rocks. No thin section.

W-026A Coarse clast-rich Exmore breccia, 457.72 m depth: Fine-grained (<1 mm) breccia with many large (up to 1.5 cm) clasts. Most large ones are fossiliferous carbonate, but very fine-grained mica schist and siltstone are prominent as well. A nearly opaque graphitic schist fragment occurs. About 25 vol% of this sample consists of partially carbonate-altered melt fragments of often schlieric, fluidal-textured appearance. Very little glauconite. A single low-shock (rare PDFs, but numerous shock extension fractures, reduced birefringence) quartzitic clast. Note that the so-called medium-grained quartzitic component is likely derived from the aplitic to quartz-pegmatitic phase drilled in the crater floor.

W-026B (2nd section) Exmore breccia, 458.09 m depth: Breccia groundmass comparable to W-026A, but this segment has an even higher (60 vol%) proportion of melt fragments. Contains a 4-mm-wide, medium-grained quartzitic clast, all quartz grains of which are shocked with 1 set of PDFs. Melt fragments are strongly carbonate-altered. Several small shocked quartz/quartzite clasts that contain 1 set of PDFs. There are also numerous quartz clasts with shock extension fractures and reduced birefringence (<8 GPa shock). One large (>3 cm) breccia clast where essentially every quartz grain is shocked to ≤8–10 GPa (some with 1 set of PDFs, others with reduced birefringence and shock extension fractures). Melt shards have highly angular shapes with often lobate and even round surfaces. There are also melt fragments with dense arrays of vesicles.

W-027 Layered Exmore breccia, 457.87 m depth: Contains ~60 vol% of altered (carbonatized, bleached) melt shards. Some breccia clasts of the same breccia type (breccia-in-breccia), and some of these show folding at amplitudes of 100–300 µm. Vesicles and angular or lobate shard forms are displayed. The typical clast population of the upper Exmore breccia samples is present, but the bioclastic carbonate component is very small, and hardly any glauconite occurs. This leads to the assumption that this section of the Exmore package contains a lot of air-fall debris and far less resurge sediment than the overlying section.

W2-32 Exmore breccia, 458.51 m depth: Highly enriched in altered melt fragments, with some of them being vesicular. This melt fraction extends into the finer-grained size range. Lithic clasts are derived from graphitic schist, shale, phyllite, mudstone, and there is a distinct, 0.5-cm-sized clay nodule. No shocked clasts.

W2-32B Exmore breccia, 458.51 m depth: Gradational contact between typical unsorted Exmore breccia material and an ~1-cm-wide, well-sorted sand band. This sand does not, in contrast to Exmore breccia, contain glauconite, is less heterogranular, and has an overall clast population that is skewed to a lower size value than that of the typical breccia.

CB6-007 Exmore breccia plus sedimentary clast, 459.49 m depth: There is a small part of Exmore breccia with glauconite. Larger part is formed by a sedimentary clast. The clast is formed by siltstone in one part, but in another part, the grains become larger and merge into graywacke. In the clast population, there is abundant quartz and feldspar; rare biotite; rare muscovite; and abundant clusters of opaque minerals up to 0.6 mm in size.

CB6-008 Exmore breccia, 460.39 m depth: Matrix supported; fine-grained brownish matrix with subangular to subrounded clasts mostly to 0.5 mm, rarely to 2 mm. The mineral clasts include quartz; K-feldspar—commonly microcline with tartan twinning, some altered; plagioclase; abundant glauconite pellets to 1.2 mm; carbonate—some larger fossils; rare muscovite; rare altered biotite to 0.3 mm; and isometric opaques. Rock clasts include a large clast of siltstone, schist, and other sedimentary clasts.

CB6-009 Sandstone clast, 460.74 m depth: Clast supported; only a small proportion of light matrix, angular to more rarely subrounded grains. Minerals present are most abundant quartz; K-feldspar; abundant muscovite; biotite/chlorite; plagioclase; opaque minerals—very small, some aggregates; accessory brown and green tourmaline; and trace of staurolite. There is a small part of typical Exmore breccia with glauconite.

W2-33 Exmore breccia, 462.27 m depth. No thin section.

CB6-010 Exmore breccia, 464.09 m depth: Matrix supported; brownish fine-grained matrix contains subangular mineral clasts to 2.5 mm and rock clasts to 5 mm. Minerals present are quartz—subangular grains to 1.5 mm; K-feldspar—abundant grains to 2 mm, some tartan twinning, cleavage; plagioclase; muscovite, small elongated clasts to 0.8 mm; not abundant glauconite pellets to 1.5 mm; very rare biotite; some bioclastic carbonate; opaque minerals, rarely larger aggregates to 0.8 mm, some opaque minerals also around "bleached" accessory garnet; other accessories are staurolite, and green/brown tourmaline; chlorite only in rock clasts. Rock clasts include siltstone, schist, graywacke, chert, and polycrystalline quartz.

W2-34 Exmore breccia, 465.17 m depth: Dominated by <1 to 3 mm clasts—heterogranular. No apparent preferred fabric. Glauconite in the form of mostly very fine-grained particles. Several sizable wedge-shaped slivers of bioclastic carbonate. No melt, no shocked particles noted.

W-028 Gritty Exmore breccia, 467.33 m depth: Typical Exmore breccia and clast population, but there are relatively many coarse (>3 mm) clasts. Still a significant (10 vol%) component of large (several mm to >1 cm) altered melt clasts but significantly more marine debris (glauconite, bioclastic carbonate) than in W-027. A large number of phyllite (some with kink folds) and mica schist clasts (well rounded). Matrix and melt clasts are rather carbonate altered. *NB: It is evident that the melt fragment–rich zone of the Exmore sequence is enriched in felsic clasts in comparison with the Exmore samples above, which also have a significant mafic clast (phyllite, mica schist, siltstone, graphitic schist) component.*

CB6-011 Exmore breccia, 467.33 m depth: Matrix supported; fine-grained brownish matrix with sericite, contains angular to subangular mineral clasts, many different rock clasts, and melt particles. The minerals present are quartz; K-feldspar—commonly microcline with tartan twinning; plagioclase; glauconite; rare muscovite to 0.6 mm; rare biotite to 1 mm; rare biogenic carbonate; and irregularly disseminated opaque minerals. There is an elongated melt particle, 7 mm, very altered, plus another similar smaller melt particle. Lithic clasts include fine-grained sedimentary clasts (e.g., siltstone), unrecognized crystalline clasts, phyllite, schist, polycrystalline quartz. There is one quartz grain with toasted appearance.

W2-01A Exmore breccia, 468.85 m depth: Relatively glauconite poor. Heterogranular clast content (clasts between 0.7 cm and <1 mm, dominated by sand size fraction). Clast shapes are angular to well-rounded (as usual for Exmore Breccia). An 0.8 cm clam-shell fragment. Several clasts of meta-quartzite (presumably derived from quartzitic schist band). No shocked fragments. Matrix is phyllosilicate dominated and seemingly has bimodal grain size population (<1 mm and >2 mm).

W2-01B Clast in Exmore breccia, 468.85 m depth: Fine-grained sand facies (groundmass) containing a lot of small fragments of bioclastic carbonate. Little glauconite; rare biotite and muscovite grains of nice, elongated flake shapes. Throughout the section, clay laminae occur, but they do not define a proper lamination and rather occur in a way consistent with bioturbation.

W2-02 Exmore breccia, 469.97 m depth: Rare up to 1-cm-sized clasts in a sand-size–dominated matrix. A large roundish clast is schist. The sample is matrix supported. A single, brown-rimmed and finest-grained recrystallized clast is interpreted as impact melt on the basis of it containing a vesicle.

W2-35 Exmore breccia, 470.63 m depth: A large Fe-chloritized clast of igneous rock. Altered brown shale fragments. Reasonable glauconite content. Several glauconitic sandstone clasts. Heterogranular breccia, with clasts ranging in size from 0.6 cm to <1 mm. Dominated by sand-size clasts. Several large schist, dolerite, and shale clasts. Weak preferred orientation of clasts. No shocked particles seen.

CB6-012 Exmore breccia, 470.76 m depth: Brownish fine-grained matrix contains various angular to subrounded mineral clasts up to 1.5 mm. Minerals present are quartz; K-feldspar—cleavage, commonly microcline; glauconite pellets to 1.5 mm; muscovite; rare altered biotite; rare plagioclase; carbonate—one large 1.5 mm mollusk shell fragment, other bioclastic carbonate; isometric grains of opaque minerals to 0.3 mm; and traces of staurolite, zircon, garnet, and titanite. Rock clasts include schist, fine-grained sediments, granite, and polycrystalline quartz. There are rare melt particles.

CB6-013 Exmore breccia, 472.65 m depth: Matrix-supported breccia; fine-grained brownish matrix contains angular to subrounded clasts, mostly less than 1 mm, but sizes of clasts are not uniform. Minerals present are quartz; K-feldspar—some microcline with tartan twinning; plagioclase; glauconite pellets up to 0.2 mm; elongated biotite up to 0.5 mm; elongated muscovite up to 0.5 mm; opaque minerals; carbonate—some bioclastic, mollusk shells, foraminifers; accessory titanite. Lithic clasts include large clast of altered granite/pegmatite (>2 cm), clast of siltstone, subrounded clast of chert, other small rock clasts. There are rare melt particles.

W2-03 Exmore breccia, 472.91 m depth: Several sizable altered, brown (in schlieren dark-gray) nodules with red-brown altered rims are shale fragments. Contains a 7-mm-size, gray particle that might represent lithic impact breccia. Groundmass dominated by < 1 mm particles; glauconite poor, hardly any shale/mudstone.

W-029 Exmore breccia, 473.67 m depth: Back to normal fine-grained (mostly <1 mm) breccia, with several millimeter-sized siltstone and quartzitic clasts and entirely lacking melt fragments. Also, in comparison to above, a distinct increase in glauconite abundance, but only minor bioclastic carbonate. No shocked particles.

CB6-014 Exmore breccia, 476.14 m depth: Brownish fine-grained matrix with sericite contains angular to subangular clasts mostly to 1 mm, size of clasts is variable. Mineral clasts include quartz; K-feldspar—some microcline; glauconite pellets to 1.5 mm; bioclastic carbonate—mollusk shells, foraminifers; biotite in clasts; not abundant disseminated isometric opaque minerals to 0.2 mm; accessory zircon. Rock clasts include schist, phyllite, mudstone, chert, and polycrystalline quartz. There are rare altered melt particles.

CB6-015 Exmore breccia, 478.70 m depth: Matrix supported; fine-grained brownish matrix contains subangular mineral clasts, relatively abundant rock clasts—mostly fine-grained sediments. Minerals present are quartz; K-feldspar—abundant, commonly microcline; glauconite; muscovite rarely to 0.6 mm; biotite—rare single clasts; plagioclase; opaque minerals—small isometric grains or rare larger aggregates. Accessories are staurolite, garnet. Rock clasts include siltstone, phyllite, schist, rare chert, and polycrystalline quartz. There are possibly some altered melt particles.

CB6-016 Exmore breccia, 481.60 m depth: Fine-grained brownish matrix contains various angular to subangular mineral clasts, up to 2 cm, but mostly to 0.7 cm. Minerals present are quartz; K-feldspar—commonly altered, some microcline with tartan twinning; glauconite pellets up to 1.2 mm; plagioclase; muscovite; isometric grains of opaque minerals to 0.3 mm; biogenic carbonate; accessory staurolite, titanite, and zircon. Rock clasts include schist, polycrystalline quartz, and other rocks. There are possibly some altered melt particles.

CB6-017 Exmore breccia, 484.30 m depth: Matrix supported; brownish, fine-grained matrix contains subangular mineral clasts up to 1.8 mm, mostly about 0.5 mm. Minerals present are quartz—clasts to 1.5 mm; K-feldspar—rarely up to 1.8 mm, cleavage, commonly microcline with tartan twinning; glauconite pellets up to 2 mm; plagioclase; rare muscovite and biotite; rare chlorite—mostly in clasts; bioclastic carbonate—shells, foraminifers; not abundant opaque minerals; accessory garnet and staurolite. Rare rock clasts include crystalline rocks, fine-grained sediments, and chert. There are rare altered melt particles.

CB6-018 Exmore breccia, 489.31 m depth: Matrix supported; brownish matrix with sericite contains angular to subangular mineral clasts and rock clasts. Minerals present are quartz; K-feldspar—some microcline with tartan twinning; plagioclase; glauconite pellets up to 1 mm; rare muscovite to 1.3 mm; not abundant allotriomorph opaque minerals up to 0.4 mm; rare bioclastic carbonate; accessory zircon and tourmaline; chlorite only in clasts. Lithic clasts include polycrystalline quartz, siltstone, and other rocks. There is an altered melt particle, 3 mm.

W-030 Exmore breccia, 489.80 m depth: Typical fine-grained Exmore breccia with <3 vol% glauconite. A 1.5 cm angular siltstone clast contains some carbonate clasts itself. A second clast of this nature is rimmed by authigenic pyrite. A 0.5 cm, considerably altered (sericitized) clast is likely derived from a granitoid or medium-grained volcanic precursor, as angular relics of plagioclase are still discernible. Several particles of muscovite-quartz schist are well-rounded. Glauconite is also well rounded, but the felsic clast assemblage is variably angular to well rounded. No shocked particles noted. The groundmass is argillitic/sericitic and at best contains traces of carbonate.

CB6-019 Exmore breccia, 490.83 m depth: Brownish fine-grained matrix contains various mineral clasts up to 3.5 mm, but mostly to 0.8 mm. Minerals present are quartz to 3 mm; K-feldspar up to 3.5 mm, commonly with cleavage, commonly microcline; plagioclase; glauconite pellets to 1 mm; not abundant muscovite to 0.6 mm, mostly small clasts in matrix; isometric grains of opaque minerals to 0.2 mm; accessory garnet and staurolite. Small rock clasts include schist, other crystalline clasts, graywacke, and polycrystalline quartz. There is an amoeboidal altered melt particle, 1 cm.

CB6-020 Exmore breccia, 492.68 m depth: Matrix supported; fine-grained brownish matrix contains abundant mineral subangular clasts to 2 mm. Minerals present are quartz; K-feldspar—cleavage, some microcline; glauconite pellets to 1.2 mm; rare muscovite and biotite; plagioclase; opaque minerals; accessory titanite, staurolite, and tourmaline; rare chlorite in clasts. Rare millimeter-sized rock clasts include fine-grained sediments, schist, and polycrystalline quartz.

CB6-021 Exmore breccia, 494.96 m depth: Brownish matrix with sericite contains angular to subangular clasts rarely up to 3 mm, mostly to 1 mm. Minerals present are quartz; K-feldspar—commonly microcline, some altered; abundant glauconite pellets to 2 mm; rare muscovite and biotite to 0.6 mm; rare plagioclase; very rare chlorite; biogenic carbonate; not very abundant isometric grains of opaque minerals to 0.2 mm; accessory tourmaline and titanite. Lithic clasts include siltstone, shale, granite, and polycrystalline quartz. There are some altered melt particles and one clast of polycrystalline quartz with toasted appearance.

CB6-022 Exmore breccia, 499.61 m depth: Matrix supported; fine-grained brownish matrix contains angular to subangular clasts, most less than 1 mm, rarely up to 2 mm. Minerals present are quartz—angular to subrounded grains; K-feldspar—subangular to subrounded, altered, fractured, some microcline with tartan twinning; glauconite pellets to 1 mm; rare plagioclase; muscovite; opaque minerals—clusters, allotriomorph grains, disseminated; chlorite and carbonate only in clasts. There is a melt particle with amoeboidal shape, 2 mm, clear with dark patches and brown rim, altered. Lithic clasts include a large clast (at least 2 cm) of partly melted granite, cataclastic, very altered–bleached, with chlorite and carbonate; siltstone, and shale.

CB6-023 Exmore breccia, 500.66 m depth: Brownish matrix with sericite contains subangular to subrounded mineral clasts, mostly to 0.5 mm, rarely up to 2 mm. Minerals present are quartz; K-feldspar—abundant, commonly microcline with tartan twinning, some very altered; rare plagioclase; glauconite pellets to 1 mm, one 2.5 mm; rare muscovite to 1 mm; not abundant biogenic carbonate; irregularly disseminated opaque minerals to 0.2 mm; accessory zircon, garnet and staurolite; biotite and chlorite only in clasts. Lithic clasts include siltstone and other fine-grained sedimentary clasts, granite. There are altered melt particles.

CB6-024 Exmore breccia, 501.87 m depth: Fine-grained brownish matrix contains various angular to subangular mineral clasts up to 2.2 mm, mostly to 0.7 mm. Minerals present are quartz; K feldspar—altered, cleavage, some microcline; glauconite pellets to 1.5 mm; not abundant muscovite to 0.2 mm; plagioclase; rare altered biotite; carbonate—some bioclastic, and in some other clasts; opaque minerals—isometric grains or clusters; accessory garnet, staurolite, and titanite; chlorite only in clasts. Lithic clasts include fine-grained sediments, polycrystalline quartz, and granite. There are possibly some altered melt particles.

CB6-025 Exmore breccia, 503.45 m depth: May contain some parts of a large clast of altered schist. White and greenish gray, horizontal metamorphic layering, probably altered schist, plus part of gray matrix with 1 cm rounded quartz grain. No thin section.

CB6-026 Exmore breccia plus clay clast, 507.14 m: Macroscopic description—beige to gray matrix; dark-gray angular clasts to 0.5 cm; there is a large clast with white to light-gray matrix, in some parts reddish or yellowish, with quartz grains up to 3 mm; minor angular gray clasts to 1 cm. No thin section.

CB6-027 Exmore breccia, 508.59 m depth: Matrix supported; fine-grained brownish matrix contains angular to subrounded mineral clasts, mostly to 1 mm, rarely up to 3 mm, not uniform in size. Minerals present are quartz; K-feldspar—subangular to subrounded, up to 4 mm, some microcline with tartan twinning; not abundant plagioclase; glauconite pellets to 1.5 mm; biogenic carbonate; rare muscovite to 1 mm; opaque minerals; very rare biotite to 0.5 mm; accessory garnet; chlorite only in clasts. Lithic clasts include mylonitic siltstone, schist, and polycrystalline quartz. There is one possibly bioclastic nodule of fine grained carbonate with glauconite pellets.

CB6-029 Exmore breccia, 513.02 m depth: Fine-grained brownish matrix contains lot of different mineral clasts up to 2.2 mm, mostly to 0.5 mm. Minerals present are quartz; K feldspar—abundant, subangular; some patches of secondary carbonate; glauconite—relatively less abundant pellets to 0.5 mm; rare plagioclase; opaque minerals—not very abundant, isometric grains or irregular clusters; accessory zircon to 0.1 mm, garnet, staurolite, tourmaline; chlorite only in clasts.

CB6-030 Exmore breccia, 514.17 m depth: Brownish fine-grained matrix contains angular to subangular mineral clasts to 1.5 mm, mostly to 0.5 mm. Minerals present are quartz; K feldspar—some microcline with tartan twinning; plagioclase; relatively less abundant glauconite; rare muscovite to 1 mm; very rare biotite to 0.5 mm; chlorite—rare single grains, but common in clasts; not abundant opaque minerals—disseminated, isometric, exceptionally to 0.6 mm; carbonate—some clasts to 3 mm; accessory zircon and garnet. Lithic clasts include siltstone and other fine-grained sediments, schist, and chert. There are altered melt particles, some replaced by carbonate, one particle with shale precursor. There is possibly one quartz grain with toasted appearance.

W2-04 Exmore breccia, 514.37 m depth: Abundant, up to >0.5 cm altered melt clasts, and many, mostly 3–5-mm-large schist clasts. Also weakly shocked K-feldspar and quartz-pegmatite clasts with reduced birefringence and local mosaicism in quartz.

CB6-031 Exmore breccia, 515.41 m depth: Brownish fine-grained matrix contains a lot of mineral clasts, some up to 3 mm but mostly smaller. The minerals present are quartz; K-feldspar—some microcline; glauconite—abundant pellets to 1 mm; not abundant muscovite; not abundant altered biotite; rare plagioclase; some bioclastic carbonate, some patches of secondary carbonate; accessory garnet, staurolite, and tourmaline. Lithic clasts include siltstone, mudstone, shale, polycrystalline quartz, and chert. There are large clayish parts, probably altered melt.

W-032 Exmore breccia, 515.44 m depth: Typical sedimentary clast breccia, with relatively little glauconite and hardly any bioclastic carbonate clasts. About 3 vol% of mostly small (<2.5 mm) melt fragments. The groundmass, however, does seem to contain a large number of very small altered melt particles. A zircon crystal without shock fracturing.

CB6-032 Clast of schist/gneiss mylonite, 519.38 m depth: Typical mylonite, banding plus crenulation, tiny microfaults, ribbons, particles partially rotated, recrystallization, lenses of feldspar or quartz—augen, D1 + D2 + impact. Minerals present are quartz; very abundant sericite; K-feldspar—large augen; plagioclase—large augen; some aggregates of muscovite; opaque minerals—some large grains, isometric, hypidiomorph, commonly with new recrystallized quartz around and also abundant skeletal crystals.

CB6-033 Clast of impact melt breccia, 521.38 m depth: All the rock is fused, matrix is melt. Some recrystallized or locally melted inclusions, clasts partially melted, most clasts less than 0.5 mm. Minerals present are fractured quartz; feldspar; opaque minerals—clusters, irregular shapes. The minerals are difficult to resolve due to partial melting. There is one larger clast of meta-arkose, also partially melted, granite, small clasts of chert.

CB6-034 Exmore breccia, 521.74 m depth: Brownish, fine-grained matrix contains subangular to subrounded mineral clasts up to 2 mm, mostly to 0.5 mm. Minerals present are quartz; K-feldspar—commonly microcline, tartan twinning; patches of secondary carbonate, also carbonate clasts; glauconite pellets to 1 mm; plagioclase; not abundant muscovite to 0.5 mm; rare biotite; opaque minerals—isometric to 0.2 mm, abundant in some clasts; accessory staurolite; chlorite only in clasts. Lithic clasts include large clast of graywacke, siltstone, and other fine-grained sediments, unrecognized crystalline clasts. There is a large altered melt particle.

CB6-035 Exmore breccia, 522.02 m depth: A minor part of this sample is typical Exmore breccia with very fine-grained altered matrix, subangular to subrounded mineral clasts mostly to 1 mm, commonly altered and fractured. Minerals present are quartz; carbonate—some clasts of carbonate, including some bioclastic carbonate, also patches of secondary allotriomorph carbonate, some carbonate filling the factures in clast; K-feldspar; small glauconite pellets to 1 mm; rare altered plagioclase; rare muscovite; very rare biotite; rare chlorite; opaque minerals—clusters of allotriomorph grains. The larger part of the thin section represents an altered graywacke clast that consists mostly of quartz and feldspar. Other lithic clasts include siltstone, sandstone with carbonate veins, mica schist, and chert. There is an altered melt particle, 2 mm. There is one quartz grain with toasted appearance and subplanar open fractures.

CB6-036 Exmore breccia, 523.28 m depth: Brownish, fine-grained matrix contains mostly subangular mineral clasts to 0.5 mm, rarely to 2 mm. Minerals present are quartz; K-feldspar; glauconite pellets to 1 mm; carbonate, patches of secondary carbonate, some carbonate clasts, also bioclastic carbonate; plagioclase; muscovite rare to 0.5 mm; rare altered biotite; opaque minerals in clusters; accessory staurolite and garnet; chlorite only in rock clasts. Lithic clasts include siltstone, fine-grained sedimentary clasts, graywacke, schist, unresolved crystalline clasts, and polycrystalline quartz. There is one large melt particle (1 cm) plus other smaller, altered, partially replaced by carbonate.

CB6-037 Exmore breccia, 524.33 m depth: Matrix supported; brownish fine-grained matrix contains subangular to subrounded mineral clasts to 2 mm. Minerals present are quartz; K-feldspar—abundant, with cleavage, common microcline; abundant glauconite pellets to 0.6 mm, also some pale green—altered?—glauconite; plagioclase; muscovite—rarely longer than 1 mm; rare biotite; rare chlorite—altering biotite or in clasts; opaque minerals—mostly isometric grains, irregularly distributed; accessory garnet, titanite, greenish/brownish tourmaline, and staurolite. Rare rock clasts include siltstone, polycrystalline quartz, chert, sandstone, shale, and crystalline clasts.

W-033 Exmore breccia, 525.70 m depth: Relatively little glauconite and carbonate fragments. A large zircon crystal. Two largely recrystallized quartzitic clasts, the texture of which seemingly suggests that they could have been ballen quartz. The breccia groundmass is somewhat carbonatized. Comparatively few large ovoid clasts of metapelite or quartzitic lithologies. One 6-mm-wide angular clast of graphitic schist. A handful of altered and relatively small melt fragments. One 3-mm-wide, moderately shocked (2 or 3 sets of PDFs per quartz grain) quartz-aplite clast.

CB6-038 Exmore breccia, 526.69 m depth: Matrix supported; fine-grained matrix contains angular to subrounded clasts. Minerals present are quartz—rarely to 4 mm; K-feldspar—subangular to subrounded, altered, fractured, some microcline with tartan twinning; plagioclase; primary carbonate clasts to 1.5 mm, secondary allotriomorph grains, carbonate as alteration product after melt particles, also some bioclastic carbonate; glauconite pellets to 1 mm, relatively less abundant; rare biotite; muscovite—rare, but abundant in some clasts; chlorite—rare clasts, mostly altering mica in lithic clasts; opaque minerals—clusters of allotriomorph grains; accessory tourmaline in a clast. Lithic clasts include fine-grained sediments, schist. There is a partly melted clast of phyllite. Further, there are altered melt particles (0.6 and 1 cm) replaced by carbonate.

CB6-039 Graywacke, 527.81 m depth: Clast supported; fine-grained brownish matrix contains small subangular to subrounded mineral clasts to 0.6 mm, mostly less than 0.4 mm, there is some lamination, parallel orientation of mica. Minerals present are quartz—subangular to subrounded grains; K-feldspar—subangular to subrounded, altered, some microcline with tartan twinning; not abundant plagioclase; muscovite to 2 mm; biotite; chlorite—altering other mica; opaque minerals—irregular isometric grains; accessory epidote and titanite.

CB6-040 Graywacke, 537.27 m depth: Clast supported; similar to CB6-039, but contains more matrix, small clasts up to 0.6 mm, but nearly all to 0.4 mm, densely packed, mica aligned but not so evident like in sample CB6-039. There is ocher pigment in one part. Minerals present are quartz; K-feldspar—subangular to subrounded, altered, some microcline with tartan twinning; not much plagioclase; muscovite; rare biotite; chlorite—altering other mica; opaque minerals—single grains to 0.6 mm; very rare glauconite; accessory zircon.

CB6-041 Clay, 542.32 m depth: Claystone or mudstone, beige with reddish-ocher pigment. No thin section.

W2-07 Exmore breccia, 551.20 m depth: Significant glauconite content of variable but <2 mm grain size; minor shale clast component. Clasts are generally <3 mm in size, with individual clasts up to 0.8 cm. No melt fragments, no shocked particles.

CB6-042 Exmore breccia, 563.83 m depth: Matrix supported; fine-grained brownish matrix with sericite contains angular to subangular mineral clasts to 3 mm, but mostly less than 1 mm, and rare rock clasts. Minerals present are quartz; K-feldspar—some microcline; plagioclase; abundant glauconite, some elongated pellets more than 2 mm; rare muscovite to 0.5 mm; carbonate—one larger bioclast plus some foraminifers; very rare biotite and chlorite; opaque minerals—isometric to irregular shapes; accessory zircon and tourmaline. Lithic clasts include polycrystalline quartz, chert, mudstone, and altered schist.

W2-08 Exmore breccia, 564.37 m depth: Typical Exmore breccia; relatively fine-grained with clasts generally smaller than 2 mm and only a handful of fine-grained schist clasts <3 mm. A lot of very fine-grained quartz debris. Contains rare, well-rounded, and in 1 case mantled (although grain was partially destroyed in sectioning) impact melt fragments.

CB6-043 Claystone, 567.51 m depth: Beige to yellowish clay or mudstone, fractured. No thin section.

CB6-044 Exmore breccia, 571.36 depth: Brownish fine-grained matrix with sericite contains subangular to subrounded clasts mostly to 0.5 mm, rarely to 2 mm. The mineral clasts are quartz; K-feldspar—some microcline, some altered, cleavage; plagioclase; glauconite—abundant pellets to 1.5 mm; rare muscovite to 0.6 mm, very rare biotite; bioclastic carbonate; accessory titanite; small irregularly disseminated

opaque minerals, isometric to 0.2 mm; chlorite only in clasts. The lithic clasts include siltstone and other fine-grained sediments, schist, chert, and other rocks. There is one altered amoeboidal melt particle.

CB6-045 Exmore breccia plus clast of sandstone, 583.14 m depth: Typical Exmore breccia, matrix supported; clasts less abundant but larger than in sandstone, angular to subrounded. Minerals present are quartz; K-feldspar; glauconite pellets up to 1 mm; carbonate nodule 0.3 mm wide, also bioclastic carbonate; muscovite; plagioclase; biotite, chlorite; opaque minerals—isometric, irregular shapes; accessory garnet and epidote. Lithic clasts include chert, polycrystalline quartz, and fine-grained metasedimentary clast. There is a melt fragment (7 mm), brownish with dark grains, isotropic.

Large sandstone clast: Clast supported; subangular to subrounded clasts, average clast size about 0.2 mm, but all less than 0.3 mm. Minerals present are subangular to subrounded quartz; K-feldspar—subangular to subrounded, some microcline with tartan twinning, some perthite, some grains are fresh, some altered; plagioclase; muscovite—elongated grains to 1 mm; biotite—elongated crystals to 7 mm, altered, oxidized; rare chlorite; opaque minerals—isometric or irregular grains.

W2-06 Exmore breccia, 586.98 m depth: Sample cut by a number of <1-mm-wide calcite veinlets. Contains a large (1 cm) carbonate-cemented nodule. Several large (0.5 cm) quartz and feldspar crystals derived from granite-pegmatite. No shocked clasts or melt clasts.

CB6-046 Red claystone, 591.56 m depth: Very fine clay, finer than CB6-056, but contains also some larger clasts. Minerals present are quartz, K-feldspar, muscovite, and accessory staurolite.

CB6-047 Exmore breccia, 599 m depth: Fine-grained brownish matrix contains small subangular clasts, variable sizes up to 1.2 mm. Minerals present are quartz—subangular grains to 2 mm; K-feldspar—grains to 2 mm, commonly microcline with tartan twinning; rare plagioclase; abundant glauconite pellets to 1.5 mm; not abundant muscovite to 1 mm; carbonate—large carbonate nodule, some smaller bioclasts; opaque minerals—in matrix not very abundant to 0.3 mm; in clasts—abundant, to 2 mm, also impregnation; accessory titanite and allanite, chlorite and biotite only in clasts. Lithic clasts include polycrystalline quartz, mylonitic siltstone, fine-grained sediments, granite, volcanic rock, schist, and chert. There is one rounded nodule (3 mm) of fine-grained carbonate with abundant rounded glauconite pellets. There is one quartz grain with toasted appearance.

CB6-048 Graywacke, 601.61 m depth: Clast supported; matrix is brownish with sericite, mica clasts and other elongated clasts are aligned, clasts mostly to 0.3 mm, rarely up to 1 mm. Minerals present are quartz; K-feldspar—some perthite, some microcline with tartan twinning, altered; not abundant plagioclase; muscovite—quite abundant, to 1 mm; rare altered biotite; rare chlorite; rare disseminated opaque minerals to 0.2 mm; accessory epidote.

W2-09 Exmore breccia, 610.67 m depth: Only a few sizable clasts (up to 0.5 cm). No melt particles. Several elongated slivers of schist. Glauconite-poor and fine-grained groundmass (<1.5 mm). A single 0.6 mm metagraywacke clast with incipient quartz-ribbon formation that designates this particle as derived from the metamorphosed basement. Contains a large number of subrounded to angular biotite clasts.

W2-10 Exmore breccia, 616.80 m depth: Contains several prominent mudstone pellets. A subrounded garnet clast, 1 altered melt fragment (partially melted schist), micropegmatitic (granophyric-textured) clasts. Sample has a distinct sedimentary structure, with glauconite occurring mainly in up to several-millimeter-wide bands. Rather fine-grained sample with majority of clasts <1.5 mm.

CB6-049 Sandstone, 622.14 m depth: Clast supported; clasts up to 2 mm, mostly to 0.5 mm. Minerals present are subangular quartz grains; K-feldspar—abundant, commonly microcline, cleavage; plagioclase; rare muscovite; opaque minerals—not very abundant, single grains to 0.2 mm; accessory staurolite, garnet, green tourmaline, and zircon. There are rare clasts of polycrystalline quartz and chert.

W2-11 Exmore breccia, 626.27 m depth: Contains several high-interference color epidote clasts and a large shale nodule.

CB6-050 Red clay, 644.55 m depth: Red mudstone, with beige parts, crumbly. No thin section.

CB6-051 Arkose, 655.12 m depth: Very light-brownish matrix with sericite contains angular to rarely subrounded clasts, mostly to 0.3 mm, rarely up to 1 mm. Minerals present are quartz; K-feldspar—abundant, fractured, some perthite, some microcline with tartan twinning; some altered plagioclase; muscovite; very rare biotite; opaque minerals—not abundant irregularly disseminated, to 0.2 mm; accessory very small clasts of titanite. There are some small clasts of chert.

W2-12 Exmore breccia, 665.17 m depth: Contains one 1-cm-sized, round and another 2-cm-sized mudstone pellet, as well as a quartz-rich mudstone clast. No shocked clasts. Glauconite poor (only a handful of very fine-grained particles <1 mm). Mostly heterogranular sand (<2.5 mm) but skewed to <1 mm.

CB6-052 Siltstone, 678.68 m depth: Very fine-grained laminated sediment, brownish matrix with phyllosilicates, some opaque layers, most grains to 0.05 mm, mica only slightly aligned. Minerals present are quartz—small grains rarely to 0.3 mm; K-feldspar—rarely up to 0.3 mm; muscovite—abundant small grains; not abundant biotite; opaque minerals in some layers, small bands, some microfossil clasts; accessory staurolite.

CB6-053 Clay, 680.31 m depth: Greenish gray mudstones, angular clasts. No thin section.

CB6-054 Graywacke, 688.23 m depth: Fine-grained brownish matrix contains small clasts to 1.5 mm. Minerals present are angular to subrounded quartz grains; K-feldspar—subangular to subrounded, fractured, altered, some microcline with tartan twinning, also perthite; plagioclase; muscovite—elongated grains to 1 mm, not very abundant; rare biotite and chlorite; opaque minerals, not very abundant, commonly rounded single grains sized to 0.6 mm.

CB6-055 Graywacke, 710.24 m depth: Fine-grained brownish matrix contains clasts to 1.5 mm, mostly to 0.5 mm. Minerals present are angular to subangular quartz grains; K-feldspar—abundant, some microcline, some altered; muscovite—abundant elongated grains; plagioclase; rare altered biotite; accessory staurolite, titanite, garnet, and zircon.

CB6-056 Mudstone, 721.40 m depth: Very fine-grained material, grains to 0.06 mm, no larger clasts. Minerals present are quartz, muscovite, and biotite.

CB6-057 Graywacke, 743.39 m depth: Matrix supported; fine-grained brownish matrix with sericite contains subangular to subrounded mineral clasts, mostly to 1 mm, rarely up to 2.5 mm. The minerals present are quartz; K-feldspar—common microcline with tartan twinning; not abundant plagioclase; very rare muscovite; very rare altered biotite; accessory titanite, garnet, and zircon. There are some clasts of polycrystalline quartz.

CB6-058 Siltstone, 760.23 m depth: Very fine-grained siltstone, small clasts mostly to 0.15 mm. The minerals present are quartz—subangular to subrounded grains, to 0.15 mm; K-feldspar; muscovite—elongated grains to 0.3 mm; chlorite—after mica; opaque minerals—not very abundant, subangular to rounded; rare biotite and glauconite.

CB6-059 Vitrinite, 761.79 m depth: Black, crumbly, small clasts. No thin section.

CB6-060 Graywacke, 802.97 m depth: Matrix supported; very fine-grained brownish matrix contains not abundant large subangular to subrounded mineral clasts to 1.5 mm, but also some small clasts to 0.1 mm. There are clasts of quartz; K-feldspar; not very much muscovite to 0.6 mm; rare altered biotite; irregular clusters of opaque minerals; accessory staurolite. There are rare clasts of polycrystalline quartz and chert.

CB6-061 Graywacke, 822.28 m depth: Clast supported; fine-grained light brownish matrix with sericite contains subangular to subrounded mineral clasts to 0.5 mm, very rarely up to 2 mm. Minerals present are quartz; K-feldspar—some microcline with tartan twinning; not abundant plagioclase; muscovite—not abundant to 1.5 mm; rare altered biotite; rare chlorite; opaque minerals—rare isometric to 0.2 mm; accessory epidote and zircon.

CB6-062 Mudstone, 841.61 m depth: Greenish-gray mud, crumbly. No thin section.

CB6-063 Exmore breccia, 863.15 m depth: Matrix with sericite contains subangular to subrounded clasts mostly to 1 mm, some up to 3 mm. The minerals present are quartz; K-feldspar—some fractured, microcline with tartan twinning; plagioclase; glauconite pellets to more than 1 mm; rare muscovite to 0.7 mm; isometric opaque minerals to 1 mm; accessory zircon and blue/green tourmaline. There is a large clast and other smaller clasts of polycrystalline quartz and a small clast of schist. There is an altered melt particle. There are some quartz clasts with toasted appearance.

W2-13 Exmore breccia, 864.29 m depth: Fine-grained, rather equigranular, <1.5 mm clast content, with larger clasts all <4 mm. Very fine-grained glauconite fraction but a large number of grains. Rare calcareous microfossil fragments, a single shocked quartz-microcline clast, and a single altered, possible melt fragment.

CB6-064 Graywacke, 904.59 m depth: Brownish fine-grained matrix contains clasts that are mostly to 2 mm in size. Minerals present are quartz—subangular clasts to 2 m; K-feldspar—common microcline; rare muscovite; opaque minerals—irregular shapes, to 0.3 mm; rare plagioclase; accessory staurolite and garnet. There are some clasts of polycrystalline quartz and sandstone.

CB6-065 Graywacke, 915.80 m depth: Fine-grained brownish matrix contains small subangular to subrounded mineral clasts to 1.5 mm. The minerals present are quartz—subangular to subrounded grains, to 1.5 mm; K-feldspar—subangular to subrounded grains, some with fractures or cleavage, altered, some microcline with tartan twinning, also perthite; muscovite; rare chlorite and biotite; opaque minerals—single grains or clusters, grains to 0.6 mm.

CB6-066 Graywacke, 940.34 m depth: Matrix supported; fine-grained brownish matrix contains subangular to subrounded grains mostly to 0.2 mm. Minerals present are quartz—subangular to rounded grains, also rare polycrystalline quartz grains; K-feldspar—some microcline with tartan twinning; plagioclase; muscovite—elongated grains to 1.5 cm; chlorite—altering mica; opaque minerals—irregular shapes, small clusters; accessory epidote, titanite, and tourmaline.

CB6-067 Graywacke, 989.18 m depth: Very fine-grained brown matrix, layers and parts of siltstone and graywacke, mica is aligned in part. Minerals present are subangular to subrounded quartz grains to 0.6 mm; K-feldspar—altered, some microcline; very abundant muscovite to 0.6 mm; very abundant biotite; opaque minerals—some layers, some calcareous biogenic microclasts; accessory staurolite, garnet, zircon, titanite, and tourmaline.

CB6-068 Mudstone, 1007.30 m depth: Dark-gray mud, crumbly. No thin section.

CB6-069 Mudstone, 1036.76 m depth: Dark siltstone, homogeneous, no larger grains. No thin section.

CB6-070 Siltstone, 1065.72 m depth: Very fine-grained brown matrix contains small grains around 0.06 mm, weak foliation. Minerals present are quartz—small grains to 0.25 mm; K-feldspar—altered, fractured, some microcline; muscovite—abundant, mostly aligned elongated grains to 0.6 mm, one large grain 1.5 mm; biotite—altered, to 0.6 mm, not abundant opaque minerals to 0.2 mm; accessory zircon, titanite, and staurolite.

CB6-071 Gravelly sand, 1073.40 m depth: Fine-grained brown matrix contains mineral clasts to 1 mm. Minerals present are quartz; K-feldspar—some microcline; rare plagioclase; very rare opaque minerals in matrix to 0.2 mm; accessory garnet, titanite, and zircon; muscovite—abundant small grains in granite clast. There are two large rounded clasts—polycrystalline quartz (1 cm) and large clast of fine-grained granite (2 cm)—plus other smaller clasts of these lithologies.

W-034B Contact between Exmore breccia and large melt fragment, 1095.76 m depth: Two large (>3 mm; >1 cm long and up to 6 mm wide), fluidal-textured, altered melt fragments, with a green alteration product (nontronite?). The larger particle has a sperm-like shape. The breccia lacks glauconite and does not have carbonate fossil clasts either. Secondary carbonate does, however, occur in the groundmass. Several inclusions of quartz-pegmatite in the melt clasts are suggestive of low shock degree (<10 GPa). A mafic clast component (<0.1 vol%) consists of amphibolite and metabasalt; the latter is olivine-bearing.

W-034C Clast in Exmore Breccia, 1095.76 m depth: Mylonitic quartz–mica schist with very nice S-C fabric and felsic delta clasts between ropes of biotite. Partially annealed (fine-grained recrystallized); minor carbonate alteration. If shocked, then no higher than 8 GPa.

Samples W-35 to W-049 are from the granitic megablock and have been studied by the Johannesburg Group (Gibson et al., this volume; Townsend et al., this volume).

CB6-087 Gravelly sand, 1371.13 m depth: Fine-grained brownish matrix contains subangular to subrounded clasts to 3 mm, densely packed, high clast to groundmass ratio. Minerals present are quartz—subangular to subrounded; K-feldspar—subangular to subrounded, some with fractures or cleavage, altered, some microcline with tartan twinning, also perthite; plagioclase; rare muscovite, biotite, and chlorite; opaque minerals—rare single grains; accessory apatite, epidote, and garnet. There are some clasts of polycrystalline quartz and fine-grained sandstone. There are some quartz grains with toasted appearance.

CB6-088 Gravelly sand, 1371.37 m depth: Matrix supported; fine-grained brownish matrix contains subangular to subrounded clasts to 4 mm. The minerals present are quartz; K-feldspar—subangular to subrounded, some with factures or cleavage, altered, some microcline with tartan twinning, perthite; rare biotite; opaque minerals—rare, one large clast 2.5 mm, fractured; accessory epidote. Contains some clasts of polycrystalline quartz and a granitic clast.

W-050 Graywacke, 1371.78 m depth: Contains a 5-mm-wide band with brownish, phyllosilicate-dominated groundmass between two wider layers with a grayish, felsic clast–dominated groundmass. The former layer is matrix supported (~50 vol%), the latter is clast supported

(only 35 vol% matrix). One of the two gray layers contains a round pellet of quartz-diorite. The graywacke resembles the Exmore breccia in its clast-groundmass appearance and clast population, but it lacks entirely the glauconite and bioclastic carbonate components. Grain-size distribution and grain shapes are essentially comparable with Exmore breccia as well. The clast populations of all three layers are dominated by quartz and K-feldspar. Also the phyllosilicate-rich metapelite lithologies and the fine-grained quartzitic clast types are lacking. No evidence of shock deformation noted.

CB6-089 Gravelly sand, 1375.16 m depth: Matrix supported; fine-grained brownish matrix contains subangular to subrounded clasts to 6 mm, Minerals present are quartz—some polycrystalline clasts, fluid inclusions, subplanar subparallel fractures—decorated; K feldspar—subangular to subrounded, some with factures or cleavage, altered, some microcline with tartan twinning, perthite; altered plagioclase; rare muscovite and chlorite; rare altered biotite; rare opaque minerals. There are some clasts of polycrystalline quartz.

W-051 Amphibolite, 1377.38 m depth: Fine- to medium-grained, greenish amphibole with prominent subparallel alignment (foliation). Additional phases are plagioclase and biotite, as well as ilmenite and traces of pyrite. Amphibole has a well-developed cleavage (stronger than normal, it seems), and biotite is in small part kink banded. Thus, if any shock at all, then only of very low degree (<5 GPa).

W-052 Amphibolite, 1383.05 m depth: Coarse-grained amphibole, locally poikilitic (quartz and plagioclase poikiloblasts). This sample does not show a foliation, but shows local shearing, whereby amphibole has been locally folded.

CB6-091 Gravelly sand, 1390.35 m depth: Matrix supported; fine-grained brownish matrix contains angular to subrounded clasts to 3 mm. The minerals present are quartz—angular to subangular; K-feldspar—subangular to subrounded, some with fractures or cleavage, altered, some microcline with tartan twinning, perthite; opaque minerals—rare single grains. There are some clasts of polycrystalline quartz.

W-053 Gritty sandstone (between amphibolite block and impact breccia succession), 1390.47 m depth: Main clast components are granitoid-derived quartz and feldspar; also a few granitic clasts; as well as a quartzitic component with well-sutured quartz crystals—likely basement derived. Minor chert.

CB6-092 Gravelly sand with reworked melt particles, 1396.54 m depth: Very fine-grained brownish matrix contains angular to subrounded mineral clasts, mostly to 2 mm, rarely larger, all different sizes in very fine-grained matrix. The minerals present are quartz—angular to subrounded, rarely larger than 2 mm; K-feldspar—with cleavage, some microcline; rare clasts of muscovite and biotite; rare chlorite—altering biotite; opaque minerals—not abundant, irregularly disseminated, one 0.6 mm but other smaller, high clast content; accessory garnet; plagioclase in crystalline clasts. Lithic clasts include polycrystalline quartz, rare fine-grained sediments, rare crystalline clasts, and a clast of graywacke. There are some altered melt particles, apparently reworked from underlying suevite.

W-054 Gritty sandstone (between amphibolite block and suevite succession), 1396.72 m depth: The maximum clast size in this sample is smaller than that of W-053. The clast-matrix ratio is also smaller in W-054. Dominated by clasts derived from granitoid precursors, but also metasedimentary material (siltstone, carbonate-cemented siltstone, fossil carbonate, chert). No bioclastic carbonate and only two tiny glauconite grains. There are also quite a number of altered melt particles, some quite bleached, and 3 still glassy. The total melt component is of the order of 2–3 vol%. The groundmass is largely sericite (argillitic), with traces of carbonate.

W2-15 Upper Suevite, 1399.50 m depth: Strongly altered, extremely fine matrix contains numerous up to >1-cm-sized melt fragments. Clasts are mostly granitoid derived but a sandstone clast facies is also present. Largest basement derived clast in thin section is 0.4 cm wide.

REFERENCES CITED

Bartosova, K., Ferrière, L., Koeberl, C., Reimold, W.U., and Gier, S., 2009, this volume, Chapter 15, Petrographic and shock metamorphic studies of the impact breccia section (1397–1551 m depth) of the Eyreville drill core, Chesapeake Bay impact structure, USA, *in* Gohn, G.S., Koeberl, C., Miller, K.G., and Reimold, W.U., eds., The ICDP-USGS Deep Drilling Project in the Chesapeake Bay Impact Structure: Results from the Eyreville Core Holes: Geological Society of America Special Paper 458, doi: 10.1130/2009.2458(15).

Bartosova, K., Mader, D., Schmitt, R.T., Ferrière, L., Koeberl, C., Reimold, W.U., and Brandstätter, F., 2009, this volume, Chapter 18, Geochemistry of the impact breccia section (1397–1551 m depth) of the Eyreville drill core, Chesapeake Bay impact structure, USA, *in* Gohn, G.S., Koeberl, C., Miller, K.G., and Reimold, W.U., eds., The ICDP-USGS Deep Drilling Project in the Chesapeake Bay Impact Structure: Results from the Eyreville Core Holes: Geological Society of America Special Paper 458, doi: 10.1130/2009.2458(18).

Browning, J.V., Miller, K.G., McLaughlin, P.P., Jr., Edwards, L.E., Kulpecz, A.A., Powars, D.S., Wade, B.S., Feigenson, M.D., and Wright, J.D., 2009, this volume, Integrated sequence stratigraphy of the postimpact sediments from the Eyreville core holes, Chesapeake Bay impact structure inner basin, *in* Gohn, G.S., Koeberl, C., Miller, K.G., and Reimold, W.U., eds., The ICDP-USGS Deep Drilling Project in the Chesapeake Bay Impact Structure: Results from the Eyreville Core Holes: Geological Society of America Special Paper 458, doi: 10.1130/2009.2458(33).

Catchings, R.D., Powars, D.S., Gohn, G.S., Horton, J.W., Jr., Goldman, M.R., and Hole, J.A., 2008, Anatomy of the Chesapeake Bay impact structure by seismic imaging, Delmarva Peninsula, Virginia, USA: Journal of Geophysical Research–Solid Earth, v. 113, p. B08413, doi: 10.1029/2007JB005421.

Collins, G.S., and Wünnemann, K., 2005, How big was the Chesapeake Bay impact?: Insight from numerical modeling: Geology, v. 33, p. 925–928, doi: 10.1130/G21854.1.

Collins, G.S., Kenkmann, T., Wünnemann, K., Wittmann, A., Reimold, W.U., and Melosh, H.J., 2008, A model for the formation of the Chesapeake Bay impact crater as revealed by drilling and numerical simulation [abs.], *in* Gibson, R.L., and Reimold, W.U., eds., Large Meteorite Impacts and Planetary Evolution IV, Vredefort, South Africa, 17–21 August 2008: Lunar and Planetary Institute Contribution 1432, 2 p.

Deer, W.A., Howie, R.A., and Zussman, J., 1992, An Introduction to the Rock-Forming Minerals (2nd edition): Harlow, UK, Pearson, Prentice Hall, 696 p.

Deutsch, A., and Koeberl, C., 2006, Establishing the link between the Chesapeake Bay impact structure and the North American tektite strewn field: The Sr-Nd isotopic evidence: Meteoritics & Planetary Science, v. 41, p. 689–703.

Earth Impact Database, 2008, Earth Impact Database: http://www.unb.ca/passc/ImpactDatabase (accessed June 2008).

Edwards, L.E., Powars, D.S., Gohn, G.S., and Dypvik, H., 2009, this volume, Chapter 3, Geologic columns for the ICDP-USGS Eyreville A and B cores, Chesapeake Bay impact structure: Sediment-clast breccias, 1096 to 444 m depth, *in* Gohn, G.S., Koeberl, C., Miller, K.G., and Reimold, W.U., eds., The ICDP-USGS Deep Drilling Project in the Chesapeake Bay Impact Structure: Results from the Eyreville Core Holes: Geological Society of America Special Paper 458, doi: 10.1130/2009.2458(03).

Edwards, L.E., Powars, D.S., Browning, J.V., McLaughlin, P.P., Jr., Miller, K.G., Self-Trail, J.M., Kulpecz, A.A., and Elbra, T., 2009, this volume, Chapter 4, Geologic columns for the ICDP-USGS Eyreville A and C cores, Chesapeake Bay impact structure: Postimpact sediments, 444 to 0 m depth, *in* Gohn, G.S., Koeberl, C., Miller, K.G., and Reimold, W.U., eds., The ICDP-USGS Deep Drilling Project in the Chesapeake Bay Impact Structure: Results from the Eyreville Core Holes: Geological Society of America Special Paper 458, doi: 10.1130/2009.2458(04).

Eskola, P., 1939, Die Metamorphen Gesteine, *in* Barth, T.M., Correns, C.W., and Eskola, P., eds., Die Entstehung der Gesteine: Ein Lehrbuch der Petrogenese: Berlin, Springer-Verlag, p. 263–404.

Gibson, R.L., Townsend, G.N., Horton, J.W., Jr., and Reimold, W.U., 2009, this volume, Pre-impact tectonothermal evolution of the crystalline basement-derived rocks in the ICDP-USGS Eyreville B core, Chesapeake Bay impact structure, *in* Gohn, G.S., Koeberl, C., Miller, K.G., and Reimold, W.U., eds., The ICDP-USGS Deep Drilling Project in the Chesapeake Bay Impact Structure: Results from the Eyreville Core Holes: Geological Society of America Special Paper 458, doi: 10.1130/2009.2458(12).

Glass, B.P., and Liu, S., 2001, Discovery of high-pressure $ZrSiO_4$ polymorph in naturally occurring shock-metamorphosed zircons: Geology, v. 29, p. 371–373, doi: 10.1130/0091-7613(2001)029<0371:DOHPZP>2.0.CO;2.

Gohn, G.S., Powars, D.S., Bruce, T.S., and Self-Trail, J.M., 2005, Physical geology of the impact-modified and impact-generated sediments in the USGS-NASA Langley core, Hampton, Virginia, *in* Horton, J.W., Jr., Powars, D.S., and Gohn, G.S., eds., Studies of the Chesapeake Bay Impact Structure—The USGS-NASA Langley Corehole, Hampton, Virginia, and Related Coreholes and Geophysical Surveys: U.S. Geological Survey Professional Paper 1688, p. C1–C38.

Gohn, G.S., Koeberl, C., Miller, K.G., Reimold, W.U., Cockell, C.S., Horton, J.W., Jr., Sanford, W.E., and Voytek, M.A., 2006a, Chesapeake Bay impact structure drilled: Eos (Transactions, American Geophysical Union), v. 87, no. 35, p. 349, 355, 360, doi: 10.1029/2006EO350001.

Gohn, G.S., Koeberl, C., Miller, K.G., and Reimold, W.U., 2006b, Chesapeake Bay impact structure deep drilling project completes coring: Scientific Drilling, v. 3, p. 34–37.

Gohn, G.S., Sanford, W.E., Powars, D.S., Horton, J.W., Jr., Edwards, L.E., Morin, R.H., and Self-Trail, J.M., 2007, Site Report for USGS Test Holes Drilled at Cape Charles, Northampton County, Virginia, in 2004: U.S. Geological Survey Open-File Report 2007-1094, 22 p.

Gohn, G.S., Koeberl, C., Miller, K.G., Reimold, W.U., Browning, J.V., Cockell, C.S., Horton, J.W., Jr., Kenkmann, T., Kulpecz, A.A., Powars, D.S., Sanford, W.E., and Voytek, M.A., 2008, Deep drilling into the Chesapeake Bay impact structure: Science, v. 320, p. 1740–1745, doi: 10.1126/science.1158708.

Gohn, G.S., Koeberl, C., Miller, K.G., and Reimold, W.U., 2009, this volume, Chapter 1, Deep drilling in the Chesapeake Bay impact structure—An overview, *in* Gohn, G.S., Koeberl, C., Miller, K.G., and Reimold, W.U., eds., The ICDP-USGS Deep Drilling Project in the Chesapeake Bay Impact Structure: Results from the Eyreville Core Holes: Geological Society of America Special Paper 458, doi: 10.1130/2009.2458(01).

Gohn, G.S., Powars, D.S., Dypvik, H., and Edwards, L.E., 2009, this volume, Chapter 26, Rock-avalanche and ocean-resurge deposits in the late Eocene Chesapeake Bay impact structure: Evidence from the ICDP-USGS Eyreville cores, Virginia, USA, *in* Gohn, G.S., Koeberl, C., Miller, K.G., and Reimold, W.U., eds., The ICDP-USGS Deep Drilling Project in the Chesapeake Bay Impact Structure: Results from the Eyreville Core Holes: Geological Society of America Special Paper 458, doi: 10.1130/2009.2458(26).

Horton, J.W., Jr., and Izett, G.A., 2005, Crystalline-rock ejecta and shocked minerals of the Chesapeake Bay impact structure, USGS-NASA Langley core, Hampton, Virginia, with supplemental constraints on the age of impact, *in* Horton, J.W., Jr., Powars, D.S., and Gohn, G.S., eds., Studies of the Chesapeake Bay Impact Structure—The USGS-NASA Langley Corehole, Hampton, Virginia, and Related Coreholes and Geophysical Surveys: U.S. Geological Survey Professional Paper 1688, p. E1–E30.

Horton, J.W., Jr., Aleinikoff, J.N., Izett, G.A., Naeser, C.W., and Naeser, N.D., 2001, Crystalline rocks from the first corehole to basement in the Chesapeake Bay impact structure, Hampton, Virginia: Geological Society of America Abstracts with Programs, v. 33, no. 6, p. A-446.

Horton, J.W., Jr., Kunk, M.J., Naeser, C.W., Naeser, N.D., Aleinikoff, J.N., and Izett, G.A., 2002, Petrography, geochronology, and significance of crystalline basement rocks and impact-derived clasts in the Chesapeake Bay impact structure, southeastern Virginia: Geological Society of America Abstracts with Programs, v. 34, no. 6, p. 466.

Horton, J.W., Jr., Koeberl, C., Reimold, W.U., Aleinikoff, J.N., Gohn, G.S., Izett, G.A., Kunk, M.J., Naeser, C.W., Naeser, N.D., Poag, C.W., and Powars, D.S., 2004, Review of petrography, geochemistry, and geochronology, Chesapeake Bay crater, *in* Edwards, L.E., Horton, J.W., Jr., and Gohn, G.S., compilers, ICDP-USGS Workshop on Deep Drilling in the Central Crater of the Chesapeake Bay Impact Structure, Virginia, USA: Proceedings Volume: U.S. Geological Survey Open-File Report 2004-1016, CD-ROM version, 33 slides with explanatory notes (PowerPoint, 3 Mb).

Horton, J.W., Jr., Powars, D.S., and Gohn, G.S., 2005a, Studies of the Chesapeake Bay impact structure—Introduction and discussion, *in* Horton, J.W., Jr., Powars, D.S., and Gohn, G.S., eds., Studies of the Chesapeake Bay Impact Structure—The USGS-NASA Langley Corehole, Hampton, Virginia, and Related Coreholes and Geophysical Surveys: U.S. Geological Survey Professional Paper 1688, p. A1–A24.

Horton, J.W., Jr., Aleinikoff, J.N., Kunk, M.J., Gohn, G.S., Edwards, L.E., Self-Trail, J.M., Powars, D.S., and Izett, G.A., 2005b, Recent research on the Chesapeake Bay impact structure, USA—Impact debris and reworked ejecta, *in* Kenkmann, T., Hörz, F., and Deutsch, A., eds., Large Meteorite Impacts III: Geological Society of America Special Paper 384, p. 147–170.

Horton, J.W., Jr., Gohn, G.S., Powars, D.S., and Edwards, L.E., 2005c, Origin and emplacement of breccias in the Chesapeake Bay impact structure, Virginia, USA [abs.], *in* Evans, K.R., et al., eds., SEPM Research Conference: The Sedimentary Record of Meteorite Impacts, Springfield, Missouri, 21–23 May 2005, Abstracts with Program: SEPM, p. 19–20.

Horton, J.W., Jr., Gohn, G.S., Jackson, J.C., Aleinikoff, J.N., Sanford, W.E., Edwards, L.E., and Powars, D.S., 2005d, Results from a scientific test hole in the central uplift, Chesapeake Bay impact structure, Virginia, USA: Houston, Texas, Lunar and Planetary Science Contribution No. 1234, v. 26, abstract 2003 (CD-ROM).

Horton, J.W., Jr., Gohn, G.S., Powars, D.S., and Edwards, L.E., 2008, Origin and emplacement of impactites in the Chesapeake Bay impact structure, Virginia, USA, *in* Evans, K.R., Horton, J.W., Jr., King, D.T., Jr., and Morrow, J.R., eds., The Sedimentary Record of Meteorite Impacts: Geological Society of America Special Paper 437, p. 73–97.

Horton, J.W., Jr., Gibson, R.L., Reimold, W.U., Wittmann, A., Gohn, G.S., and Edwards, L.E., 2009, this volume, Geologic columns for the ICDP-USGS Eyreville B core, Chesapeake Bay impact structure: Impactites and crystalline rocks, 1766 to 1096 m depth, *in* Gohn, G.S., Koeberl, C., Miller, K.G., and Reimold, W.U., eds., The ICDP-USGS Deep Drilling Project in the Chesapeake Bay Impact Structure: Results from the Eyreville Core Holes: Geological Society of America Special Paper 458, doi: 10.1130/2009.2458(02).

Huffman, A.R., and Reimold, W.U., 1996, Experimental constraints on shock-induced microstructures in naturally deformed silicates: Tectonophysics, v. 256, p. 165–217, doi: 10.1016/0040-1951(95)00162-X.

Kenkmann, T., Collins, G.S., Wittmann, A., Wünnemann, K., Reimold, W.U., and Melosh, H.J., 2009, this volume, A model for the formation of the Chesapeake Bay impact crater as revealed by drilling and numerical simulation, *in* Gohn, G.S., Koeberl, C., Miller, K.G., and Reimold, W.U., eds., The ICDP-USGS Deep Drilling Project in the Chesapeake Bay Impact Structure: Results from the Eyreville Core Holes: Geological Society of America Special Paper 458, doi: 10.1130/2009.2458(25).

Koeberl, C., Poag, C.W., Reimold, W.U., and Brandt, D., 1996, Impact origin of the Chesapeake Bay structure, and source of the North American tektites: Science, v. 271, p. 1263–1266, doi: 10.1126/science.271.5253.1263.

Kulpecz, A.A., Miller, K.G., Browning, J.V., Edwards, L.E., Powars, D.S., McLaughlin, P.P., Jr., Harris, A.D., and Feigenson, M.D., 2009, this volume, Postimpact deposition in the Chesapeake Bay impact structure: Variations in eustasy, compaction, sediment supply, and passive-aggressive tectonism, *in* Gohn, G.S., Koeberl, C., Miller, K.G., and Reimold, W.U., eds., The ICDP-USGS Deep Drilling Project in the Chesapeake Bay Impact Structure: Results from the Eyreville Core Holes: Geological Society of America Special Paper 458, doi: 10.1130/2009.2458(34).

Poag, C.W., 1996, Structural outer rim of Chesapeake Bay impact crater—Seismic and borehole evidence: Meteoritics & Planetary Science, v. 31, p. 218–226.

Poag, C.W., 1997, The Chesapeake Bay bolide impact: A convulsive event in Atlantic Coastal Plain evolution: Sedimentary Geology, v. 108, p. 45–90, doi: 10.1016/S0037-0738(96)00048-6.

Poag, C.W., 2000, Nature and distribution of deposits derived from the Chesapeake Bay submarine impact: Geological Society of America Abstracts with Programs, v. 32, no. 7, p. A-163.

Poag, C.W., 2002, Tsunamis and hypercanes: Late-stage impact depositional systems at Chesapeake Bay crater [abs.]: Eos (Transactions, American Geophysical Union), Spring Meeting, abstract T21A-06, p. S352.

Poag, C.W., and Aubry, M.-P., 1995, Upper Eocene impactites of the U.S. East Coast: Depositional origins, biostratigraphic framework, and correlation: Palaios, v. 10, no. 1, p. 16–43, doi: 10.2307/3515005.

Poag, C.W., and Norris, R.D., 2005, Stratigraphy and paleoenvironments of early postimpact deposits—USGS-NASA Langley core, Chesapeake Bay impact crater, *in* Horton, J.W., Jr., Powars, D.S., and Gohn, G.S., eds., Studies of the Chesapeake Bay Impact Structure—The USGS-NASA Langley Corehole, Hampton, Virginia, and Related Coreholes and Geophysical Surveys: U.S. Geological Survey Professional Paper 1688, p. F1–F52.

Poag, C.W., Powars, D.S., Poppe, L.J., Mixon, R.B., Edwards, L.E., Folger, D.W., and Bruce, S., 1992, Deep Sea Drilling Project Site 612 bolide event—New evidence of a late Eocene impact-wave deposit and a possible impact site, U.S. East Coast: Geology, v. 20, p. 771–774.

Poag, C.W., Powars, D.S., Poppe, D.S., and Mixon, R.B., 1994, Meteoroid mayhem in Ole Virginny—Source of the North American tektite strewn field: Geology, v. 22, p. 691–694, doi: 10.1130/0091-7613(1994)022<0691:MMIOVS>2.3.CO;2.

Poag, C.W., Gohn, G.S., and Powars, D.S., 2001, From shocked basement to fallout spherules: The coring record at the Chesapeake Bay crater: Geological Society of America Abstracts with Programs, v. 33, no. 7, p. 433.

Poag, W.C., Koeberl, C., and Reimold, W.U., 2004, The Chesapeake Bay Crater: Impact Studies: Berlin, Springer, 522 p.

Powars, D.S., and Bruce, T.S., 1999, The Effects of the Chesapeake Bay Impact Crater on the Geological Framework and Correlation of Hydrogeologic Units of the Lower York–James Peninsula, Virginia: U.S. Geological Survey Professional Paper 1612, p. 1–82.

Powars, D.S., Mixon, R.B., and Bruce, S., 1992, Uppermost Mesozoic and Cenozoic geologic cross section, outer coastal plain of Virginia, *in* Gohn, G.S., ed., Proceedings of the 1988 U.S. Geological Survey Workshop on the Geology and Geohydrology of the Atlantic Coastal Plain: U.S. Geological Survey Circular 1059, p. 85–101.

Powars, D.S., Poag, C.W., and Mixon, R.B., 1993, The Chesapeake Bay "impact crater": Seismic and stratigraphic evidence: Geological Society of America Abstracts with Programs, v. 25, no. 7, p. A378.

Powars, D.S., Bruce, T.S., Bybell, L.M., Cronin, T.M., Edwards, L.E., Frederiksen, N.O., Gohn, G.S., Horton, J.W., Jr., Izett, G.A., Johnson, G.H., Levine, J.S., McFarland, E.R., Poag, C.W., Quick, J.E., Schindler, J.S., Self-Trail, J.M., Smith, M.J., Stamm, R.G., and Weems, R.E., 2001, Preliminary geologic summary of the USGS-NASA Langley corehole, Hampton, Virginia: U.S. Geological Survey Open-File Report 01-87-B, 20 p., http://pubs.usgs.gov/of/2001/0f01-087/.

Powars, D.S., Catchings, R.D., Goldman, M.R., Gohn, G.S., Horton, J.W., Jr., Edwards, L.E., Rymer, M.J., and Gandhok, G., 2009, this volume, High-resolution seismic-reflection images across the ICDP-USGS Eyreville deep drilling site, Chesapeake Bay impact structure, *in* Gohn, G.S., Koeberl, C., Miller, K.G., and Reimold, W.U., eds., The ICDP-USGS Deep Drilling Project in the Chesapeake Bay Impact Structure: Results from the Eyreville Core Holes: Geological Society of America Special Paper 458, doi: 10.1130/2009.2458(11).

Reimold, W.U., Koeberl, C., and Poag, C.W., 2002, Chesapeake Bay impact crater: Petrographic and geochemical investigations of the impact breccia fill: Geological Society of America Abstracts with Programs, v. 34, no. 6, p. 466.

Reimold, W.U., Bartosova, K., Schmitt, R.T., Wittek, A., and Koeberl, C., 2007, First observations on Exmore breccia from the ICDP-USGS Eyreville core, Chesapeake Bay impact structure: Geological Society of America Abstracts with Programs, v. 39, no. 6, p. 314.

Sanford, W.E., 2005, A simulation of the hydrothermal response to the Chesapeake Bay bolide impact: Geofluids, v. 5, p. 185–201, doi: 10.1111/j.1468-8123.2005.00110.x.

Sanford, W.E., Gohn, G.S., Powars, D.S., Horton, J.W., Jr., Edwards, L.E., Self-Trail, J.M., and Morin, R.H., 2004, Drilling the central crater of the Chesapeake Bay impact structure: A first look: Eos (Transactions, American Geophysical Union), v. 85, p. 369–377, doi: 10.1029/2004EO390001.

Sanford, W.E., Voytek, M.A., Powars, D.S., Jones, B.F., Cozzarelli, I.M., Cockell, C.S., and Eganhouse, R.P., 2009, this volume, Pore-water chemistry from the ICDP-USGS core hole in the Chesapeake Bay impact structure—Implications for paleohydrology, microbial habitat, and water resources, *in* Gohn, G.S., Koeberl, C., Miller, K.G., and Reimold, W.U., eds., The ICDP-USGS Deep Drilling Project in the Chesapeake Bay Impact Structure: Results from the Eyreville Core Holes: Geological Society of America Special Paper 458, doi: 10.1130/2009.2458(36).

Schmitt, R.T., Bartosova, K., Reimold, W.U., Mader, D., Wittmann, A., Koeberl, C., and Gibson, R.L., 2009, this volume, Geochemistry of impactites and crystalline basement-derived lithologies from the ICDP-USGS Eyreville A and B drill cores, Chesapeake Bay impact structure, Virginia, USA, *in* Gohn, G.S., Koeberl, C., Miller, K.G., and Reimold, W.U., eds., The ICDP-USGS Deep Drilling Project in the Chesapeake Bay Impact Structure: Results from the Eyreville Core Holes: Geological Society of America Special Paper 458, doi: 10.1130/2009.2458(22).

Self-Trail, J.M., Edwards, L.E., and Litwin, R.J., 2009, this volume, Paleontological interpretations of crater processes and infilling of synimpact sediments from the Chesapeake Bay impact structure, *in* Gohn, G.S., Koeberl, C., Miller, K.G., and Reimold, W.U., eds., The ICDP-USGS Deep Drilling Project in the Chesapeake Bay Impact Structure: Results from the Eyreville Core Holes: Geological Society of America Special Paper 458, doi: 10.1130/2009.2458(28).

Shah, A.K., Brozena, J.P.V., Daniels, D., and Plescia, J., 2005, New surveys of the Chesapeake Bay impact structure suggest melt pockets and target-structure effect: Geology, v. 33, p. 417–420.

Shah, A.K., Daniels, D.L., Kontny, A., and Brozena, J., 2009, this volume, Megablocks and melt pockets in the Chesapeake Bay impact structure constrained by magnetic field measurements and properties of the Eyreville and Cape Charles cores, *in* Gohn, G.S., Koeberl, C., Miller, K.G., and Reimold, W.U., eds., The ICDP-USGS Deep Drilling Project in the Chesapeake Bay Impact Structure: Results from the Eyreville Core Holes: Geological Society of America Special Paper 458, doi: 10.1130/2009.2458(10).

Stöffler, D., and Grieve, R.A.F., 2007, Impactites, Chapter 2.11, *in* Fettes, D., and Desmons, J., eds., Metamorphic Rocks: A Classification and Glossary of Terms; Recommendations of the International Union of Geological Sciences Subcommission on the Systematics of Metamorphic Rocks: Cambridge, UK, Cambridge University Press, p. 82–92, 111–125, and 126–242.

Townsend, G.N., Gibson, R.L., Horton, J.W., Jr., Reimold, W.U., Schmitt, R.T., and Bartosova, K., 2009, this volume, Petrographic and geochemical comparisons between the lower crystalline basement-derived section and the granite megablock and amphibolite megablock of the Eyreville B core, Chesapeake Bay impact structure, USA, *in* Gohn, G.S., Koeberl, C., Miller, K.G., and Reimold, W.U., eds., The ICDP-USGS Deep Drilling Project in the Chesapeake Bay Impact Structure: Results from the Eyreville Core Holes: Geological Society of America Special Paper 458, doi: 10.1130/2009.2458(13).

Viereck, L.G., Griffin, B.J., Schmincke, H.-U., and Pritchard, R.G., 1982, Volcaniclastic rocks of the Reydarfjordur drill hole, Eastern Iceland: 2. Alteration: Journal of Geophysical Research, v. 87, p. 6459–6476, doi: 10.1029/JB087iB08p06459.

Wittmann, A., Reimold, W.U., Schmitt, R.T., Hecht, L., and Kenkmann, T., 2009, this volume, Chapter 16, The record of ground zero in the Chesapeake Bay impact crater—Suevites and related rocks, *in* Gohn, G.S., Koeberl, C., Miller, K.G., and Reimold, W.U., eds., The ICDP-USGS Deep Drilling Project in the Chesapeake Bay Impact Structure: Results from the Eyreville Core Holes: Geological Society of America Special Paper 458, doi: 10.1130/2009.2458(16).

Wittmann, A., Schmitt, R.T., Hecht, L., Kring, D.A., Reimold, W.U., and Povenmire, H., 2009, this volume, Chapter 17, Petrology of impact melt rocks from the Chesapeake Bay crater, USA, *in* Gohn, G.S., Koeberl, C., Miller, K.G., and Reimold, W.U., eds., The ICDP-USGS Deep Drilling Project in the Chesapeake Bay Impact Structure: Results from the Eyreville Core Holes: Geological Society of America Special Paper 458, doi: 10.1130/2009.2458(17).

Manuscript Accepted by the Society 3 March 2009

Printed in the USA

The Geological Society of America
Special Paper 458
2009

Geochemistry of impactites and crystalline basement-derived lithologies from the ICDP-USGS Eyreville A and B drill cores, Chesapeake Bay impact structure, Virginia, USA

Ralf T. Schmitt*
Museum für Naturkunde–Leibniz Institute at Humboldt University Berlin, Invalidenstrasse 43, 10115 Berlin, Germany

Katerina Bartosova
Department of Lithospheric Research, Center for Earth Sciences, University of Vienna, Althanstrasse 14, A-1090 Vienna, Austria

Wolf Uwe Reimold
Museum für Naturkunde–Leibniz Institute at Humboldt University Berlin, Invalidenstrasse 43, 10115 Berlin, Germany, and *Impact Cratering Research Group, School of Geosciences, University of the Witwatersrand, Private Bag 3, PO Wits, Johannesburg, 2050, South Africa*

Dieter Mader
Department of Lithospheric Research, Center for Earth Sciences, University of Vienna, Althanstrasse 14, A-1090 Vienna, Austria

Axel Wittmann
Museum für Naturkunde–Leibniz Institute at Humboldt University Berlin, Invalidenstrasse 43, 10115 Berlin, Germany, and *Lunar and Planetary Institute, 3600 Bay Area Boulevard, Houston, Texas 77058, USA*

Christian Koeberl
Department of Lithospheric Research, Center for Earth Sciences, University of Vienna, Althanstrasse 14, A-1090 Vienna, Austria

Roger L. Gibson
Impact Cratering Research Group, School of Geosciences, University of the Witwatersrand, Private Bag 3, PO Wits, Johannesburg, 2050, South Africa

ABSTRACT

We investigated whole-rock chemical compositions of 318 samples of Exmore breccia (diamicton), impactite (suevite, impact melt rock, polymict lithic impact breccia), and crystalline basement-derived rocks from 444 to 1766 m depth in the International Continental Scientific Drilling Program (ICDP)–U.S. Geological Survey (USGS) Eyreville A and B drill cores (Chesapeake Bay impact structure, Virginia, USA). Here, we compare the average chemical compositions for the Exmore breccia

*ralf-thomas.schmitt@mfn-berlin.de

Schmitt, R.T., Bartosova, K., Reimold, W.U., Mader, D., Wittmann, A., Koeberl, C., and Gibson, R.L., 2009, Geochemistry of impactites and crystalline basement-derived lithologies from the ICDP-USGS Eyreville A and B drill cores, Chesapeake Bay impact structure, Virginia, USA, *in* Gohn, G.S., Koeberl, C., Miller, K.G., and Reimold, W.U., eds., The ICDP-USGS Deep Drilling Project in the Chesapeake Bay Impact Structure: Results from the Eyreville Core Holes: Geological Society of America Special Paper 458, p. 481–541, doi: 10.1130/2009.2458(22).

(diamicton), the impactites and their subunits, sandstone, granite, granitic gneiss, and amphibolite of the lithic block section (1095.7–1397.2 m depth), cataclastic gneiss of the impact breccia section, and schist and pegmatite/granite of the basal crystalline section (1551.2–1766.3 m depth). The granite of the megablock (1097.7–1371.1 m depth) is of I-type and is seemingly related to a syncollisional setting. The amphibolite (1377.4–1387.5 m depth) of the lithic block section is of igneous origin and has a tholeiitic character. Based on chemical composition, the Exmore breccia (diamicton) can be subdivided into five units (444.9–450.7, 450.7–468, 468–518, 518–528, and 528–~865 m depth). The units in the depth intervals of 450.7–468 and 518–528 m are enriched in TiO_2, MgO, Sc, V, Cr, and Zn contents compared to the other Exmore breccia units. In some samples, especially at ~451–455 m depth, the Exmore breccia contains significant amounts of P_2O_5. The Exmore breccia is recognized as a mixture of all sedimentary and crystalline target components, and, when compared to the impactites, it contains a significant amount of a SiO_2-rich target component of sedimentary origin. The chemical composition of the impactites overlaps the compositional range for the Exmore breccia. The impactites generally display a negative correlation of SiO_2 and CaO, and a positive correlation of TiO_2, Al_2O_3, Fe_2O_3, and MgO with depth. This is the result of an increasing basement schist component, and a decreasing sedimentary and/or granitic component with depth. Suevite units S2 and S3 display distinct enrichment of Na_2O by a factor of ~2 compared to all other impactite units, which is interpreted to reflect a higher granitic component in these units.

INTRODUCTION

General Overview

With a diameter of ~85 km, the Chesapeake Bay impact structure in Virginia, USA, is the largest known impact structure in the United States, and it counts among the largest known on Earth (e.g., Poag et al., 1994, 2002, 2004; Koeberl et al., 1996; Horton et al., 2004, 2005a, 2005b, 2005c, 2008a; Gohn et al., 2006a, 2006b). Proof of its impact origin was established by Koeberl et al. (1996) in the form of impact melt particles and shock metamorphosed quartz and feldspar detected in the Exmore breccia. The crater structure was formed in the late Eocene, and it has been dated by paleontological methods to 35.5–35.8 Ma (Poag and Aubry, 1995; Frederiksen et al., 2005; Edwards et al., 2005; Horton et al., 2005a). The Chesapeake Bay impact structure is completely preserved below a cover of Upper Eocene to Pleistocene sedimentary rocks (Poag et al., 2004). Based on distribution and chemical and isotopic studies of tektites in comparison with crater-fill rocks, the Chesapeake Bay impact structure has been identified as the probable source crater for the North American tektite strewn field (e.g., Poag et al., 1994; Koeberl et al., 1996; Glass et al., 1998; Deutsch and Koeberl, 2006). Therefore, the radiometric age of these tektites, ranging from 35.2 to 35.5 Ma (Glass et al., 1986; Obradovich et al., 1989; Horton and Izett, 2005), is probably the age of this impact event.

The Chesapeake Bay impact occurred in a shelf environment at the passive continental margin of North America (e.g., Powars and Bruce, 1999). Beneath a column of seawater 0–340 m deep (e.g., Horton et al., 2005a), a Lower Cretaceous to Eocene sedimentary sequence of 400 to >750 m thickness occurred that consisted mainly of unconsolidated, siliciclastic, and water-saturated sediments, e.g., sand, silts, and clays (e.g., Poag et al., 2004; Horton et al., 2005a). The underlying crystalline basement consisted of metamorphic rocks of Proterozoic age intruded by igneous rocks ranging in age from Neoproterozoic to Permian (Horton et al., 2004, 2005c, 2008b; Horton and Izett, 2005; Gibson et al., 2007).

A special feature of the Chesapeake Bay impact structure is its inverted sombrero-like crater geometry, which was visualized by geophysical investigations (Poag et al., 2004; Collins and Wünnemann, 2005; Horton et al., 2005a; Shah et al., 2005). This involves a shallower outer zone of ~85 km diameter formed in the sedimentary sequence, and an inner zone (diameter ~35 km) extending deeper into the crystalline basement to a depth of ~1 km. This complex crater geometry is thought to be the result of a large competence contrast in the target volume between, on the one hand, the water column and the mainly unconsolidated sediments and, on the other hand, the crystalline basement (Poag et al., 2004; Collins and Wünnemann, 2005; Horton et al., 2005a; Shah et al., 2005). Geophysical signatures are suggestive of the presence of a rather small, irregularly shaped central uplift structure (diameter ~12 km, 500–800 m high) in the inner zone, which is surrounded by an annular moat (Horton et al., 2005a, 2005c; Shah et al., 2005). Although the outer parts of the Chesapeake Bay impact structure have been extensively drilled in the past (e.g., Horton et al., 2008a), the Sustainable Technology Park (STP) drill hole (Horton et al., 2005b, 2008a; Gohn et al., 2007a) at Cape Charles near the center of the structure and the International Continental Scientific Drilling Program (ICDP)–U.S. Geological Survey (USGS) Eyreville drill hole (see next section) are the first deep drillings into the inner zone of the structure.

The cores from the Eyreville drill holes form the basis for this investigation.

Previous geochemical studies of the rocks of the Chesapeake Bay impact structure have been limited by the available samples, which mostly consisted of pre- and postimpact sedimentary rocks (e.g., Poag et al., 2004; Deutsch and Koeberl, 2006), and some drill cores of Exmore beds and their sedimentary blocks and crystalline clasts (e.g., felsite clasts; Koeberl et al., 1996; Poag et al., 2004; Horton et al., 2004; Horton and Izett, 2005). Nevertheless, most of the crystalline clasts of previous drillings were too small for whole-rock analysis. Crystalline basement rocks of monzogranite type drilled in the USGS-NASA Langley borehole were chemically investigated by Horton et al. (2004) and Horton and Izett (2005).

The Eyreville drill core provides an unprecedented variety of samples from a complete section through postimpact sediments, crater-fill deposits, and crystalline basement-derived rocks. We focus in our study on whole-rock chemistry of Eyreville A and B drill core samples in the depth range from 444 to 1766 m, and we provide a first summary report on the characteristics of the different lithological units and rock types. The extensive database presented here will hopefully serve as a useful resource for further studies. Further results of detailed geochemical studies of the Exmore breccia, the granitic megablock, the basal crystalline section, and the impact breccia section are reported in the companion papers by Reimold et al. (this volume), Townsend et al. (this volume), and Bartosova et al. (this volume), and Wittmann et al. (this volume, Chapters 16 and 17), respectively.

The Eyreville Drill Holes

The Chesapeake Bay Impact Structure Deep Drilling Project is a joint venture by the International Continental Scientific Drilling Program (ICDP), the U.S. Geological Survey (USGS), and the National Aeronautics and Space Administration (NASA) (see introductory paper by Gohn et al., this volume). In 2005–2006, three boreholes were drilled at Eyreville Farm in Northampton County, Virginia, USA (Gohn et al., 2006a, 2006b, 2008, this volume). This location, at a radial distance of ~9 km from the center of the crater structure within the annular moat of the inner crater basin, was selected to obtain a complete section through the crater-fill deposits and to reach the crystalline basement of the crater. Eyreville drill hole A reached a final depth of 941 m and was cored between 125 and 941 m. Eyreville drill hole B was cored from 738 m to a final depth of 1766 m. In the Eyreville drill hole C, postimpact sediments were cored to a depth of 140 m (Gohn et al. 2006a, 2006b, 2008, this volume). The principal lithologies, as revealed in the combined Eyreville drill cores, are—from top to bottom—444 m of postimpact sediment (depth range 0–443.9 m), 652 m of Exmore bed lithologies (depth range 443.9–1095.7 m), 302 m of lithic blocks (depth range 1095.7–1397.2 m), including a 274 m intersection of a granitic megablock, 154 m of impact breccia (depth range 1397.2–1551.2 m), and 215 m of crystalline basement-derived rock (depth range 1551.2–1766.3 m). The latter either represent(s) (an) allochthonous megablocks or the autochthonous crater floor (Gohn et al., 2006a, 2006b, 2008; Edwards et al., this volume; Horton et al., this volume; Kenkmann et al., this volume).

Lithologies of the Eyreville A and B Drill Holes

Postimpact Section (Depth Range 0–443.9 m)

The upper part of the postimpact section consists of nonmarine sediments of Pleistocene age, whereas in the lower part, marine sediments of Pliocene to late Eocene age occur (Gohn et al., 2006a).

Exmore Bed Section (Depth Range 443.9–1095.7 m)

The 652-m-thick Exmore bed section is composed of an intercalation of a diamicton and sedimentary blocks (Edwards et al., this volume; Reimold et al., this volume). These sediments have been interpreted as avalanche and resurge deposits of mainly sedimentary impact breccias (Poag et al., 2004, and references therein; Gohn et al., 2007b, this volume; Powars et al., 2008). In this paper, the diamicton is termed Exmore breccia in conjunction with Reimold et al. (this volume).

The uppermost part of the Exmore bed section (443.9–445.0 m depth), the so-called post-Exmore breccia transition zone (Gohn et al., 2005; Horton et al., 2008a; Reimold et al., this volume), consists of laminated siltstones and claystones from 443.9 to 444.3 m, and a sandstone unit from 444.3 to 445.0 m depth (Edwards et al., this volume; Reimold et al., this volume).

The middle part of this section (445.0–527.1 m depth) consists mainly of Exmore breccia, a glauconite-bearing sedimentary and crystalline clast breccia, descriptively termed a diamicton, with a fine-grained, phyllosilicate-rich groundmass and a predominantly sand-size clast component, including some larger sedimentary and crystalline (mainly granitoid-derived) rock clasts. The Exmore breccia also contains rare, altered, mostly shard-shaped impact melt particles, and shocked rock and mineral clasts, which are most common in the depth intervals 458–469 and 514–527 m (Reimold et al., this volume).

The lower part of this section (527.1–1095.7 m depth) consists mainly of blocks of various sedimentary rocks, such as claystone, siltstone, mudstone, sandstone, and greywacke, and several thin intercalations of Exmore breccia with a thicknesses up to 6 m (Edwards et al., this volume). The core intersections of sedimentary blocks measure between ~2 and ~30 m in length. The blocks, in many cases, occur in direct contact to each other, without Exmore breccia matrix buffers.

Lithic Block Section (Depth Range 1095.7–1397.2 m)

The lithic block section is dominated by a 274-m-thick granitic megablock from 1097.7 to 1371.1 m depth (Horton et al., this volume; Townsend et al., this volume). This megablock consists of a fine- to coarse-grained biotite-granite, which in its upper part contains several intervals of granitic gneiss. The granites and granitic gneisses have distinctly different ages of 254 ± 3

and 615 ± 7 Ma, respectively (Horton et al., 2007, this volume). The granitic rocks contain several biotite-plagioclase-amphibole schist xenoliths (Townsend et al., this volume), are cut by granite-pegmatites, and show some fracture zones. No shock metamorphic overprint was confirmed by Townsend et al. (this volume), nor can it be supported here; although Glidewell et al. (2008) reported possible shock effects.

The basal portion of the lithic block section (Horton et al., 2008b, this volume; Reimold et al., this volume; Townsend et al., this volume) consists of three clastic sediment layers, mainly sandstones, with partially larger grain sizes ("gravelly sand" of Horton et al., this volume; depth ranges of 1371.1–1376.4, 1389.7–1393.0, and 1396.4–1397.2 m, respectively), with intercalations of an unshocked amphibolite block (1376.4–1389.7 m depth), a suevite boulder (1393.1–1393.4 m depth), and a cataclastic schist block (1393.4–1396.4 m depth). The lowermost layer shows admixture of suevite components, which is indicative of reworking of the underlying suevite (Glidewell et al., 2008; Horton et al., 2008b, this volume).

Impact Breccia Section (Depth Range 1397.2–1551.2 m)

The impact breccia section (Bartosova et al., this volume; Horton et al., this volume; Wittmann et al., this volume, Chapters 16 and 17) can be subdivided based on petrographic observations from top to bottom into: (1) the upper suevite (SU, 1397.2–1402.0 m depth); (2) a clast-rich impact melt rock (M2, 1402.2–1407.5 m depth); (3–4) two suevite units (S3 and S2, 1407.5–1432.3 m, and 1433.8–1450.2 m depth, respectively), which are separated by a cataclastic boulder of quartz-feldspar schist; (5) a clast-rich impact melt rock (M1, 1450.2–1451.2 m depth); (6) a further suevite unit (S1, 1451.2–1474.1 m depth); and (7) a complex intercalation (1474.1–1551.2 m) of several blocks of cataclastic gneiss (B5 to B1) with core length intervals of 2.4–17.8 m and polymict impact breccias (P4 to P1) with core length intervals of 3.7–16.2 m, as well as a 2.3-m-thick graphite-rich brecciated gneiss from 1542.8 to 1545.1 m depth.

The suevites consist of lithic clasts of sedimentary, metamorphic, and igneous origin, displaying all stages of shock metamorphism, and melt particles embedded in a fine-grained lithic matrix (Bartosova et al., this volume; Wittmann et al., this volume, Chapter 16). The abundance of matrix and melt particles decreases with depth (Bartosova et al., this volume; Wittmann et al., this volume, Chapter 16). Sizes of lithic clasts are quite variable, generally increase with depth, and reach up to 50 cm at the base of this section (Wittmann et al., this volume, Chapter 16). Within the suevites, two small layers at 1402.0–1407.5 m and around 1450 m depth represent clast-rich impact melt rocks (Fernandes et al., 2008; Wittmann et al., this volume, Chapters 16 and 17).

The cataclastic, coarse-grained quartz-plagioclase gneisses (B5 to B1) were strongly deformed and metamorphosed prior to the impact under amphibolite-facies and retrograde greenschist-facies conditions. They are believed to have been brecciated as a result of the impact (Gibson et al., this volume; Horton et al., 2008b, this volume; Townsend et al., this volume). The polymict impact breccias (P4 to P1) of the basal 77 m of the impact breccia section contain angular to subrounded, unshocked and shocked clasts, mainly of metamorphic origin, which range in size from centimeters to decimeters but can locally be up to several meters. Many samples of the polymict impact breccia contain highly altered microscopic melt particles (Bartosova et al., this volume), which classify them as suevite (Stöffler and Grieve, 2007), although the melt component of the polymict impact breccias is generally very low. Samples without melt particles are also present, and they have been classified as polymict lithic impact breccia in accordance with the recommended impactite nomenclature of Stöffler and Grieve (2007).

Basal Crystalline Section (Depth Range 1551.2–1766.3 m)

The basal crystalline section of the drill core consists of a 215-m-thick sequence of metamorphic and igneous rocks (Gibson et al., 2007, this volume; Horton et al., this volume; Townsend et al., this volume). Rocks of this section do not display shock-metamorphic features (Townsend et al., 2007, this volume), which may be an indication that this section does not represent the autochthonous crater floor but is more likely (an) allochthonous megablock(s) slumped into the crater (Horton et al., this volume; Kenkmann et al., this volume). In the upper part of this section (1551.2–~1690 m depth; based on the geologic column of Horton et al., this volume), muscovite-plagioclase-biotite-quartz-sillimanite schists with locally abundant graphite are the most common lithology (Townsend et al., this volume). These schists are intercalated with thin granites or pegmatites. In contrast, mainly coarse-grained quartz- and quartz-feldspar (±mica) pegmatites (Townsend et al., this volume) are observed in the lower part (~1690–1766.3 m depth; Horton et al., this volume). These rocks exhibit thin intercalations of schists, which are completely missing below 1717.7 m. The schists were metamorphosed under mid- to upper-amphibolite-facies conditions and underwent plastic and brittle deformation prior to the impact (Gibson et al., 2007, this volume; Townsend et al., 2007, this volume; Horton et al., 2008b, this volume). A hydrothermally altered mylonite zone with local occurrences of cataclasite, epidosite, and tourmalinite occurs in the depth range between 1643.9 and 1655.1 m (Gibson et al., this volume; Townsend et al., this volume; Horton et al., this volume). The lithologies of the basal crystalline section are crosscut by cataclastic breccia, polymict lithic breccia, and suevitic dikes (e.g., at depths of ~1611, ~1555.6, and 1607–1609.5 m, respectively). While not all cataclasites can be identified as impact-related, some of them—as well as the polymict lithic breccia and suevitic dikes—were clearly formed during the impact event (Reimold et al., 2007).

SAMPLES AND ANALYTICAL METHODS

During the sampling event at USGS National Center, Reston, Virginia, USA, in March 2006, samples of the Chesapeake Bay drill cores Eyreville A and B were taken by W.U. Reimold

(code W) and C. Koeberl (CB6). During later visits to the drill core repository, additional samples were taken by R.L. Gibson (code RG), W.U. Reimold (W2), and K. Bartosova (KB). Altogether, 318 samples were selected for whole-rock chemical analysis. The petrographic classification of these samples is based on macroscopic and thin-section studies; partial descriptions are contained in the companion papers by Bartosova et al. (this volume), Reimold et al. (this volume), and Townsend et al. (this volume). For easier handling of this data set, it has been organized into simplified lithological groups. Sample statistics according to lithostratigraphy are compiled in Table 1.

The analyzed masses were 20–80 g per sample, depending on available sample size, grain size, and density. Exmore breccia and impact breccia samples were prepared for analysis by avoiding lithic clasts with diameters larger than ~1–2 cm. If necessary, large visible lithic clasts were separated. Samples were ground using agate grinding devices.

Whole-rock chemical analysis was carried out by X-ray fluorescence spectroscopy (XRF) with a SIEMENS SRS 3000 at the Museum of Natural History, Berlin, Germany, on glass tablets (samples W- and CB6-). Major and trace elements were measured on glass tablets (0.600 g of pulverized sample material, dried at 105 °C, 3.600 g of di-lithiumtetraborate, and, depending on the oxidation grade of the sample, ~0.5–2.0 g NH_4NO_3). Details of the analytical procedures were described by Schmitt et al. (2004). The detection limits were 1.0 wt% for SiO_2, 0.5 wt% for Al_2O_3, 0.1 wt% for SO_3, 0.05 wt% for Fe_2O_3, 0.01 wt% for TiO_2, MnO, MgO, CaO, Na_2O, K_2O, and P_2O_5, 30 ppm for Cu and Ba, 15 ppm for V, Sr, Zr, and Pb, and 10 ppm for Ni, Y, Nb, and Mo. The standard errors are 0.5 wt% for SiO_2, 0.1 wt% for Al_2O_3 and SO_3, 0.05 wt% for Fe_2O_3, MgO, CaO, Na_2O, and K_2O, 0.01 wt% for TiO_2, MnO, and P_2O_5, 30 ppm for Ba, 25 ppm for Cu, 20 ppm for Pb, 10 ppm for Mo, and 5 ppm for V, Ni, Sr, Y, Zr, and Nb. Additional XRF analyses (samples W2- and KB-) were carried out at the University of Witwatersrand, Johannesburg, South Africa. Details of the analytical procedures and accuracies for these samples were reported in Reimold et al. (1994).

For determination of loss on ignition (LOI), ~1 g of pulverized sample material, dried at 105 °C, was heated in a porcelain crucible for 4 h at 1000 °C. LOI was calculated using the weight difference before and after heating. Detection limit and standard error for LOI are ~0.1 wt%.

Trace-element contents (Sc, Cr, Co, Zn, As, Se, Br, Rb, Sb, Cs, La, Ce, Nd, Sm, Eu, Gd, Tb, Tm, Yb, Lu, Hf, Ta, W, Ir, Au, Th, and U) were determined by instrumental neutron activation analysis (INAA) at the Department of Lithospheric Research, Center for Earth Sciences, University of Vienna, Austria. Analytical techniques, standards, instrumentation, data correction, and information on accuracy and precision were described in detail by Koeberl (1993) and Son and Koeberl (2005). For the elements measured by both XRF and INAA, the results are generally in good agreement. For trace elements, data acquired by the more precise method were selected for this study.

RESULTS

The 318 individual whole-rock analyses of the rocks from the Eyreville A and B drill cores are compiled, according to increasing sample depths, in Table A1.

Major elements SiO_2, TiO_2, Al_2O_3, Fe_2O_3, MgO, CaO, Na_2O, and K_2O are plotted against depth for each drill core section to display general chemical patterns. These plots are shown for the Exmore bed, lithic block, impact breccia, and basal crystalline sections in Figures 1, 2, 3, and 4, respectively. In addition, we present Harker diagrams for sedimentary rocks (Fig. 5), impactites (Fig. 6), and crystalline rocks (Fig. 7). C1 chondrite-normalized

TABLE 1. SAMPLE STATISTICS FOR WHOLE-ROCK CHEMICAL ANALYSIS

Section of Eyreville A and B drill core	Depth range (m)	Rock type	Number of samples
Exmore bed section	443.9–1095.7	Post-Exmore breccia transition zone	10
		Exmore breccia (diamicton)	73
		Sediments of sedimentary blocks	27
Lithic block section	1095.7–1397.2	Granite of the megablock	18
		Granitic gneiss of the megablock	8
		Pegmatite of the megablock	4
		Xenoliths in rocks of the megablock	3
		Sandstone	9
		Amphibolite	6
		Cataclastic schist	1
Impact breccia section	1397.2–1551.2	Suevite	64
		Clast-rich impact melt rock	9
		Polymict lithic impact breccia	2
		Cataclastic/felsic gneiss	10
Basal crystalline section	1551.2–1766.3	Schist of the basal crystalline section	37
		Epidosite of the basal crystalline section	3
		Pegmatite/granite of the basal crystalline section	25
		Dike breccias of the basal crystalline section	9

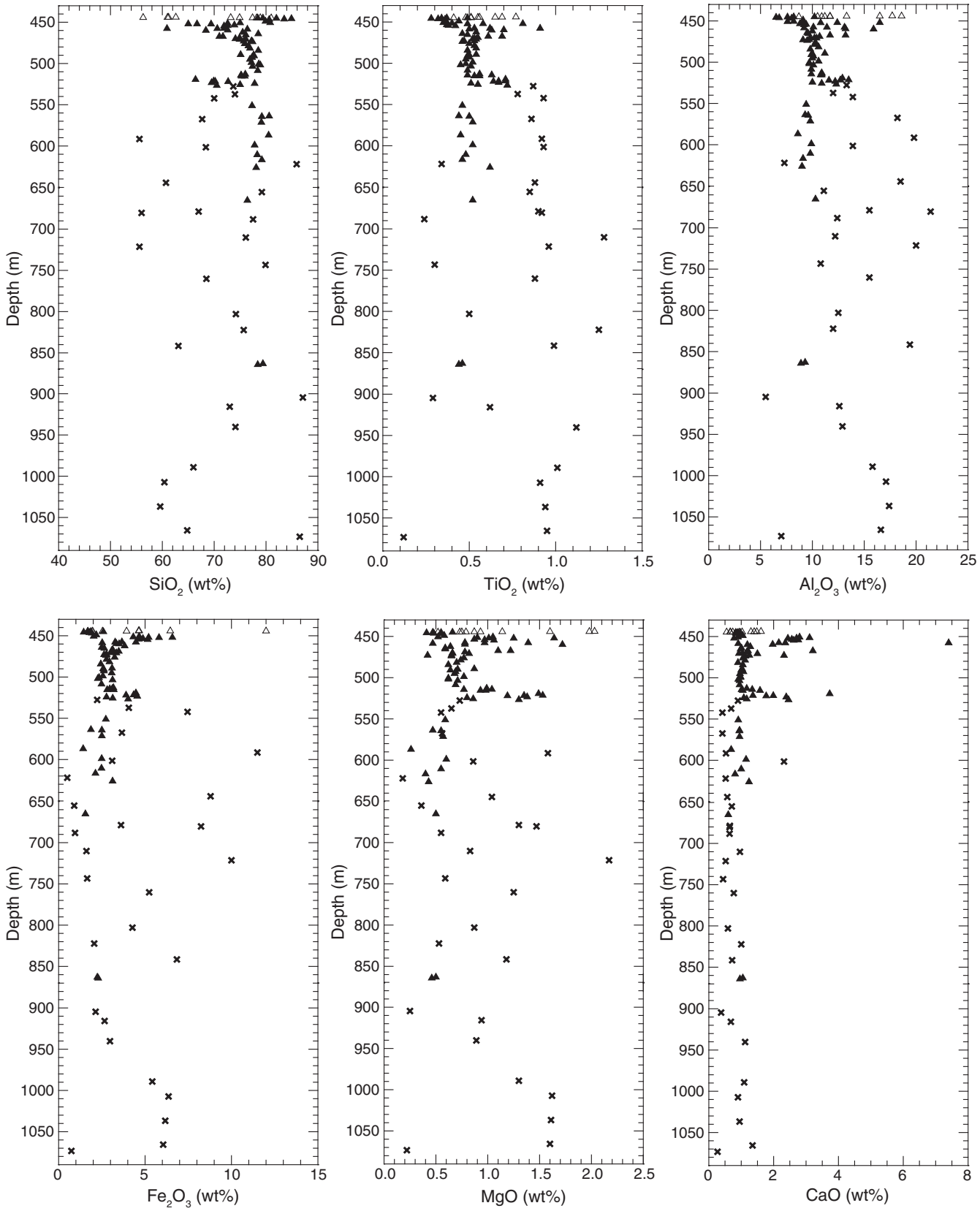

Figure 1 (*continued on following page*). Variations of major-element (SiO_2, TiO_2, Al_2O_3, Fe_2O_3, MgO, CaO, Na_2O, K_2O, and P_2O_5) abundances with depth for the Exmore bed section (443.9–1095.7 m) of the Eyreville A and B drill cores.

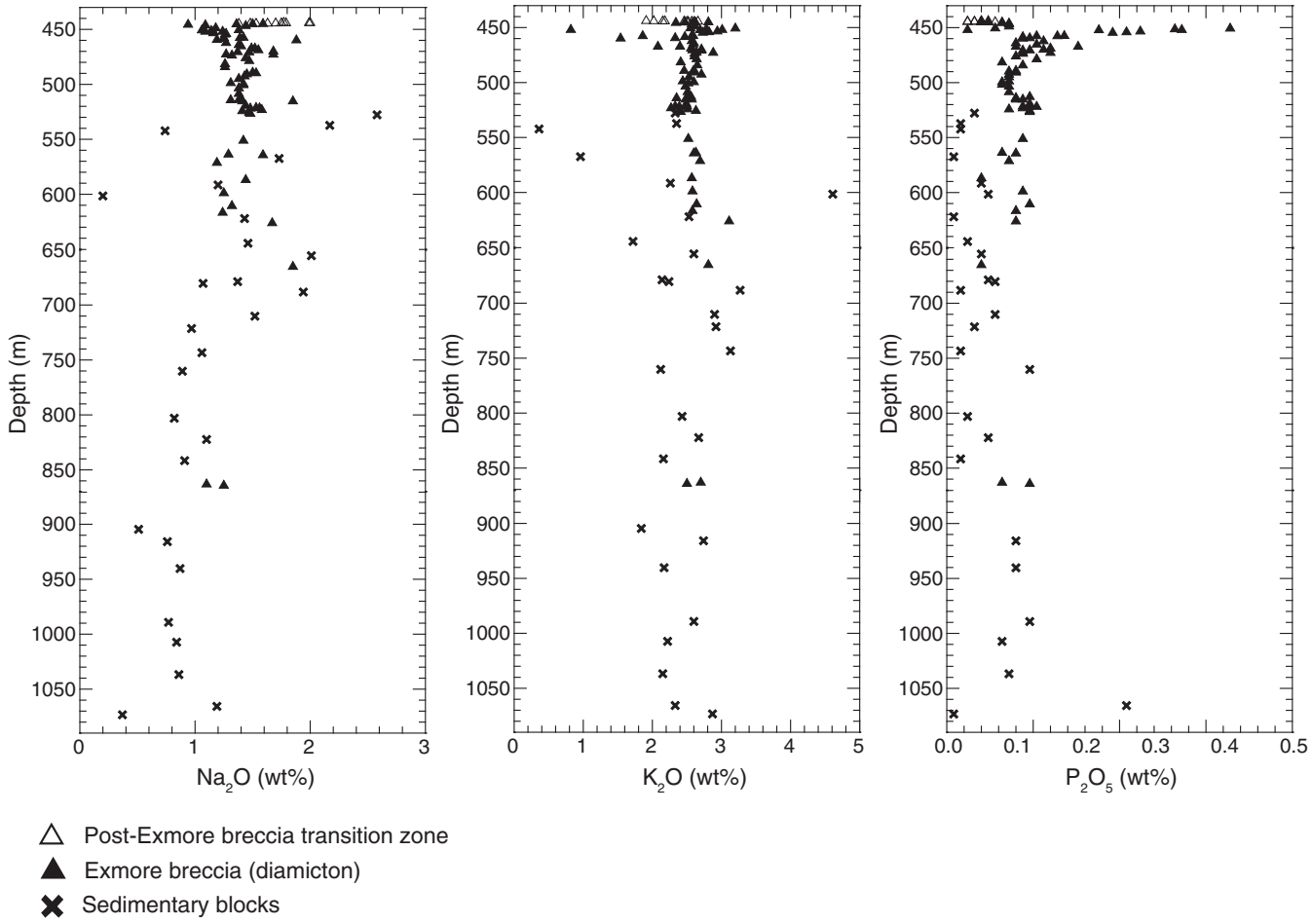

Figure 1 (*continued*).

(Taylor and McLennan, 1985) rare earth element (REE) patterns for major rock types are shown in Figure 8.

Average chemical compositions and ranges of rock composition are given for the major rock types in Tables 2–6. The average composition and ranges of composition are given for the Exmore breccia (diamicton) and the sandstone of the lithic block section in Table 2, for the crystalline rocks of the lithic block section in Table 3, for the impactite average calculated from all suevite, impact melt rock, and polymict lithic impact breccia samples in Table 4, for the different units of the impact breccia section in Table 5, and for the schist, pegmatite/granite, and epidosite of the basal crystalline section in Table 6.

To investigate possible correlations between elemental abundances, correlation matrices containing correlation coefficients for pairs of major and selected trace elements were calculated for the Exmore breccia, the granite and granitic gneiss of the megablock, the impactite (suevite, impact melt rock, and polymict lithic impact breccia), the cataclastic gneiss of the impact breccia section, and the schist of the basal crystalline section; all these are compiled in appendix Table A2.

DISCUSSION

Chemical Characterization of the Eyreville Drill Core Lithologies

Exmore Bed Section (443.9–1095.7 m)

Post-Exmore breccia transition zone. Post-Exmore breccia transition zone samples from 443.9 to 444.9 m depth were analyzed (Table A1). Based on chemical composition, this interval could be subdivided into an upper part (443.9–444.3 m depth) and a lower part (444.4–444.9 m depth). The upper part is characterized by ranges of SiO_2, Al_2O_3, and Fe_2O_3 of 56.3–62.6, 13.3–18.6, and 4.6–12.0 wt%, respectively (Fig. 1). The lowest SiO_2 and Al_2O_3, and the highest Fe_2O_3 contents were observed in the lowermost sample of this upper part of the transition zone at 444.3 m depth. In the SiO_2/Al_2O_3 versus Fe_2O_3/K_2O discrimination diagram of Herron (1988), these samples plot into the fields of shale and Fe-shale (Fig. 9). In the Harker diagrams, these samples do not fall into the range for the Exmore breccia and display different correlations between the major elements in comparison

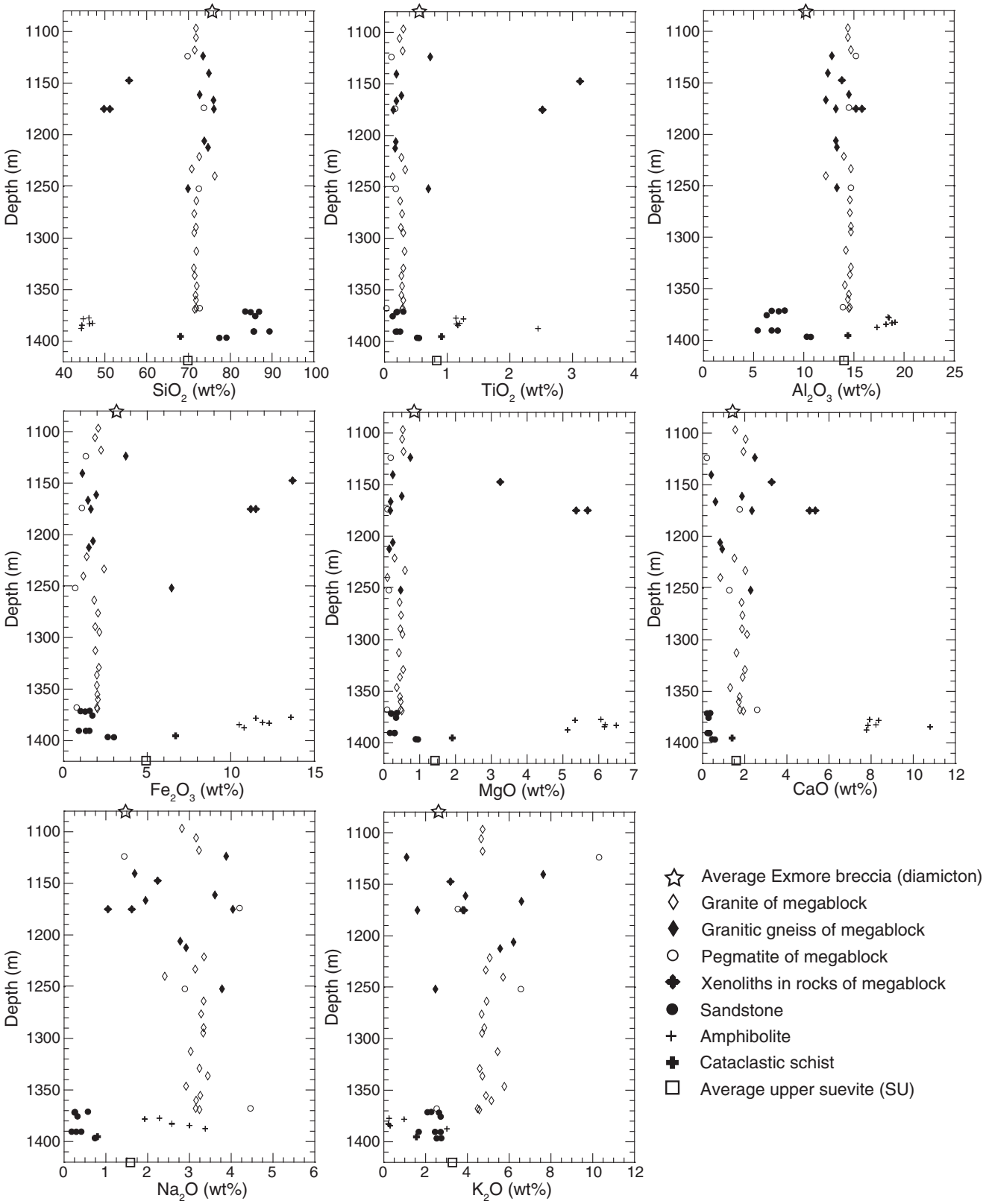

Figure 2. Variations of major-element (SiO_2, TiO_2, Al_2O_3, Fe_2O_3, MgO, CaO, Na_2O, and K_2O) abundances with depth for the lithic block section (1095.7–1397.2 m) of the Eyreville B drill core. For comparison, average Exmore breccia (Table 2) and average upper suevite (Table 5) compositions are shown at the top and bottom of the diagrams, respectively.

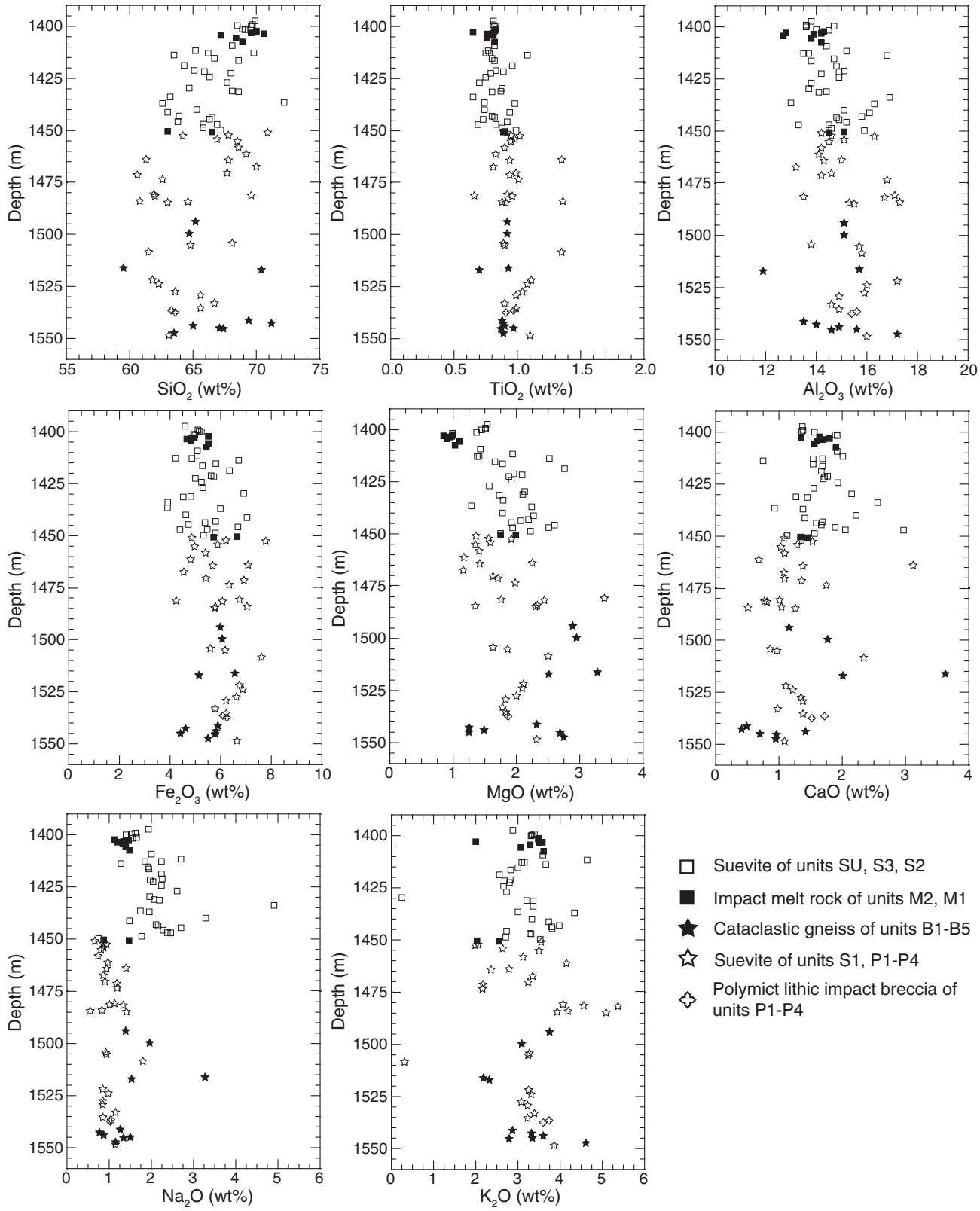

Figure 3. Variations of major-element (SiO_2, TiO_2, Al_2O_3, Fe_2O_3, MgO, CaO, Na_2O, and K_2O) abundances with depth for the impact breccia section (1397.2–1551.2 m) of the Eyreville B drill core. Note that the suevite is subdivided into two groups composed of samples from the SU to S2 units, and from S1 to P (P1–P4), respectively (unit names after Horton et al., this volume).

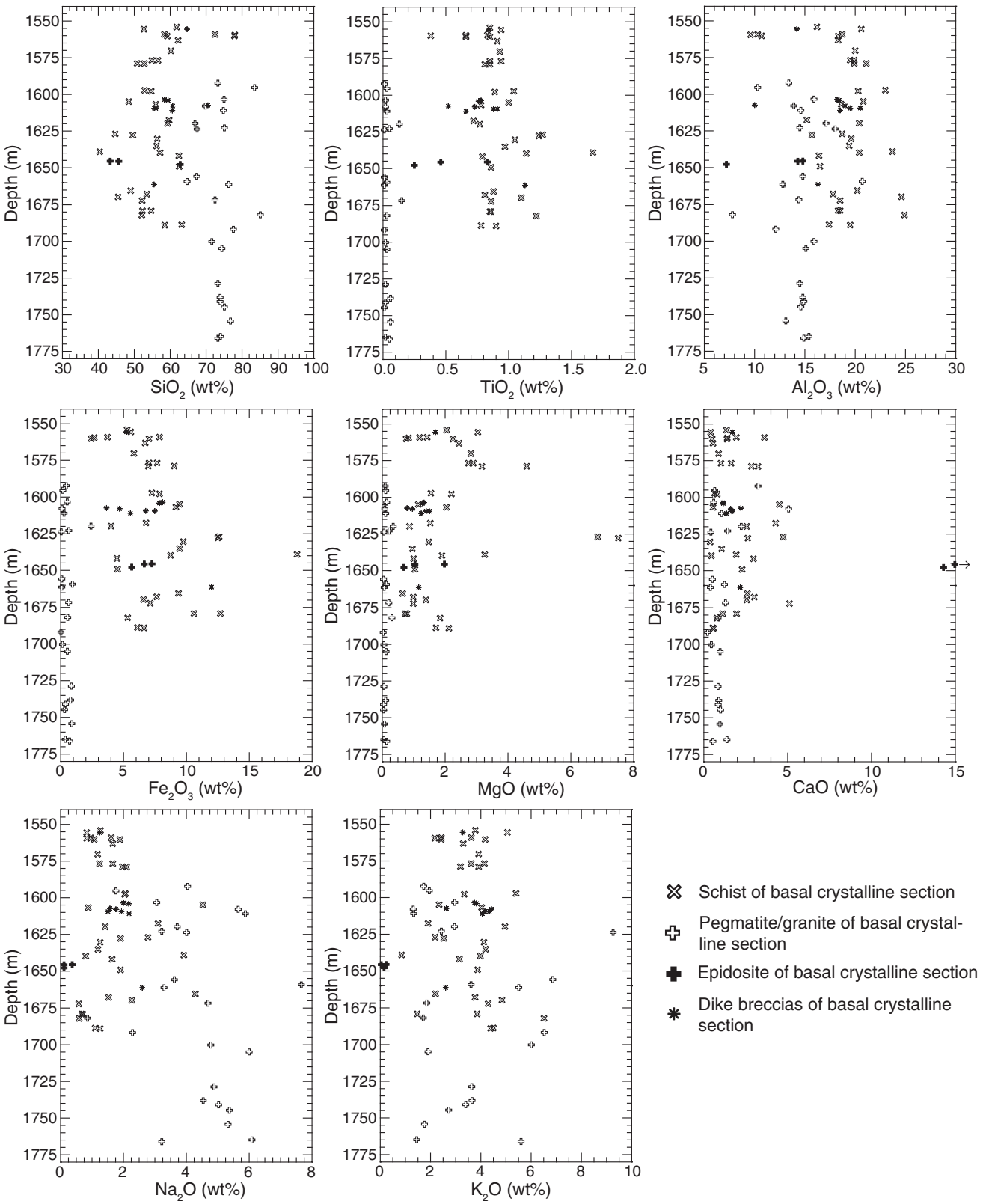

Figure 4. Variations of major-element (SiO_2, TiO_2, Al_2O_3, Fe_2O_3, MgO, CaO, Na_2O, and K_2O) abundances with depth for the basal crystalline section (1551.2–1766.3 m) of the Eyreville B drill core.

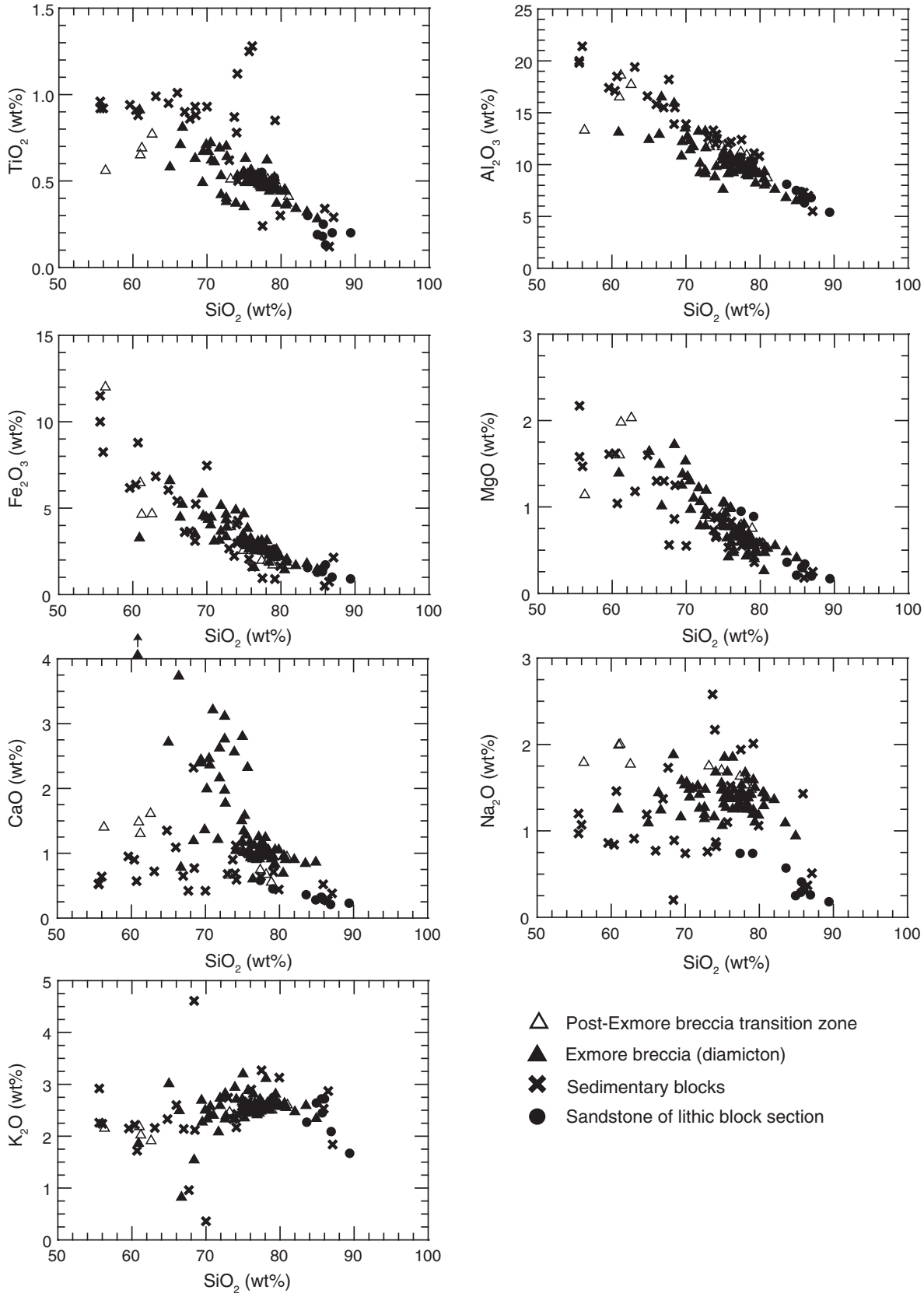

Figure 5. Harker diagrams (SiO_2 versus TiO_2, Al_2O_3, Fe_2O_3, MgO, CaO, Na_2O, and K_2O) for sedimentary lithologies of the Eyreville A and B drill cores.

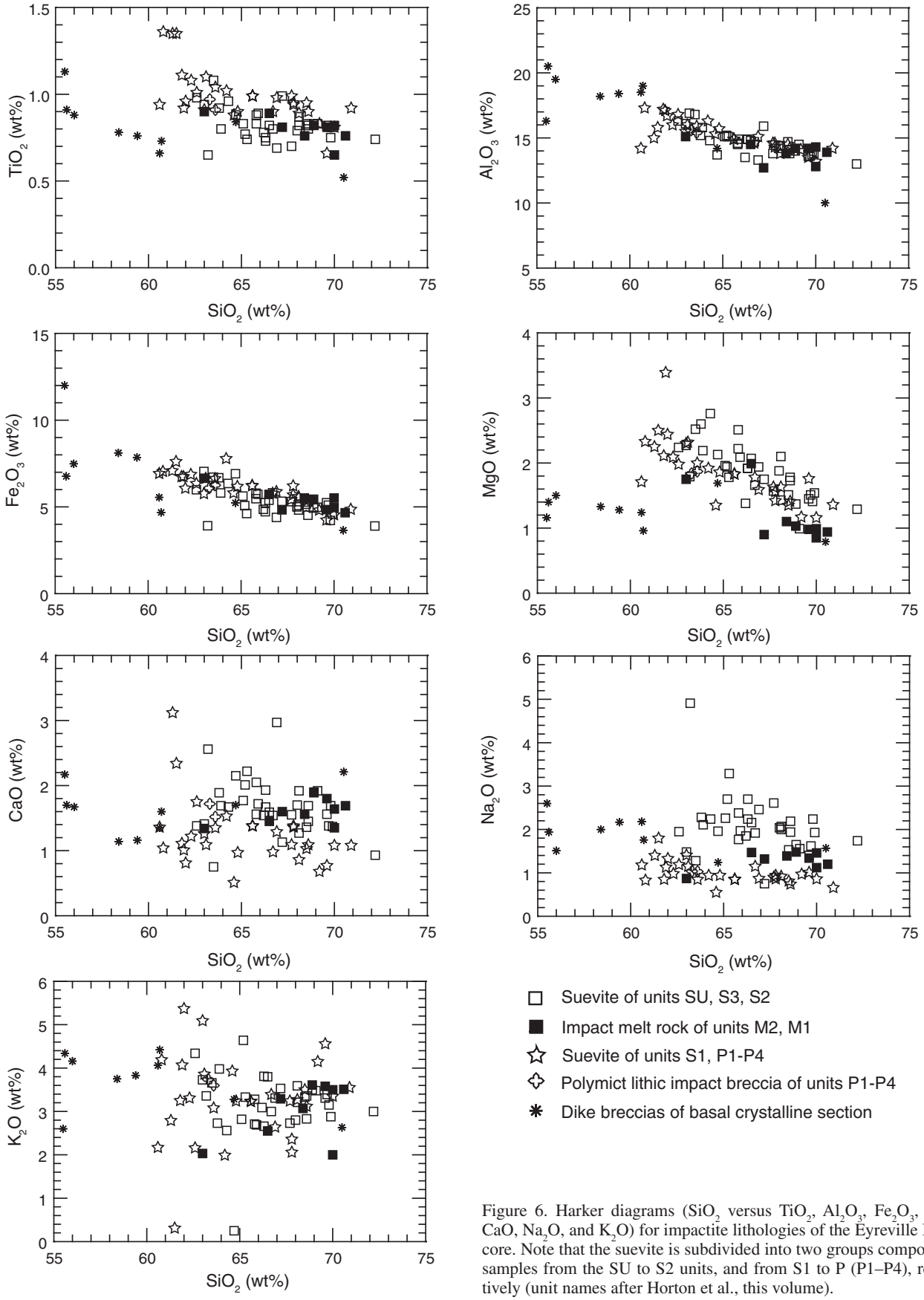

Figure 6. Harker diagrams (SiO_2 versus TiO_2, Al_2O_3, Fe_2O_3, MgO, CaO, Na_2O, and K_2O) for impactite lithologies of the Eyreville B drill core. Note that the suevite is subdivided into two groups composed of samples from the SU to S2 units, and from S1 to P (P1–P4), respectively (unit names after Horton et al., this volume).

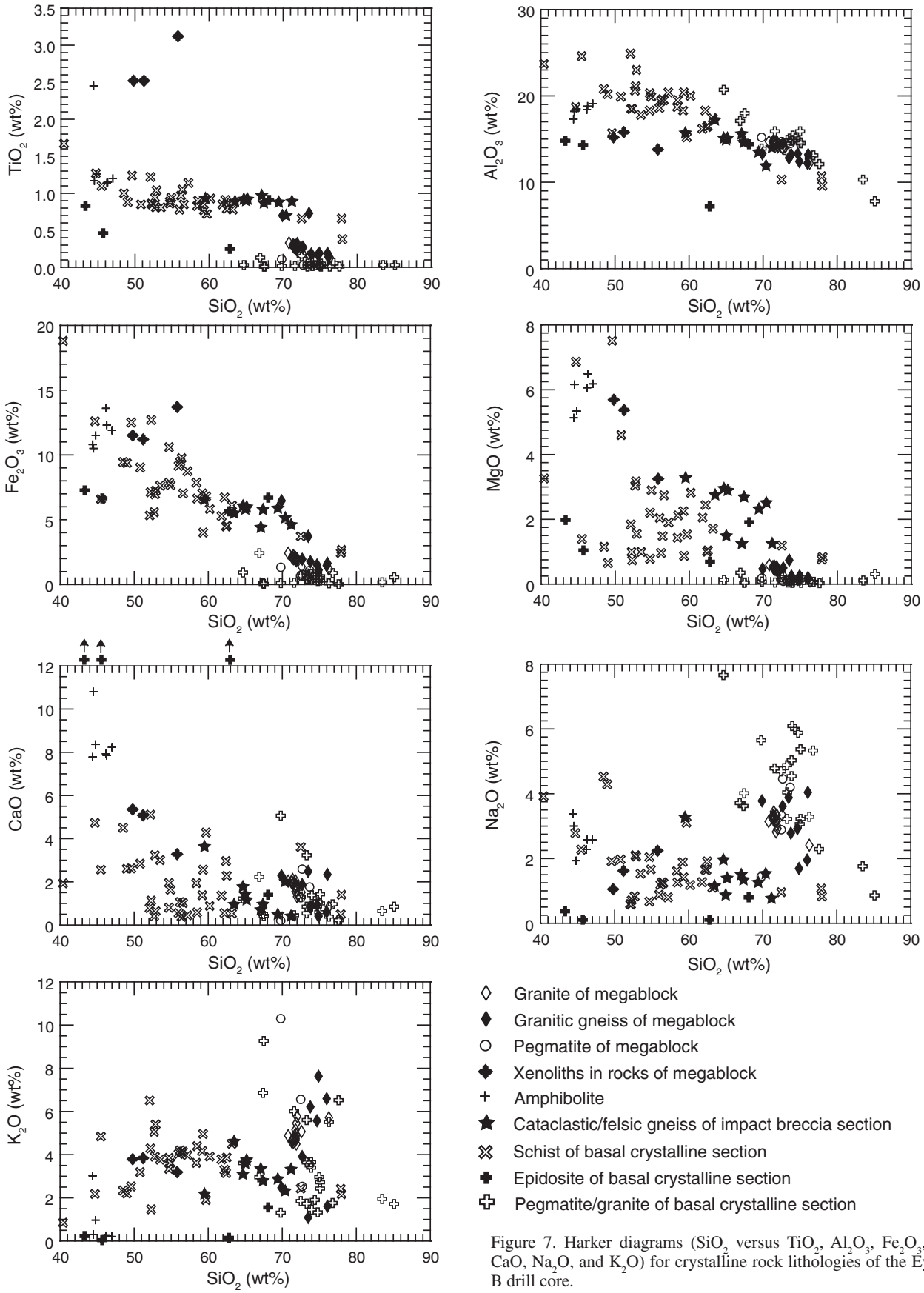

Figure 7. Harker diagrams (SiO_2 versus TiO_2, Al_2O_3, Fe_2O_3, MgO, CaO, Na_2O, and K_2O) for crystalline rock lithologies of the Eyreville B drill core.

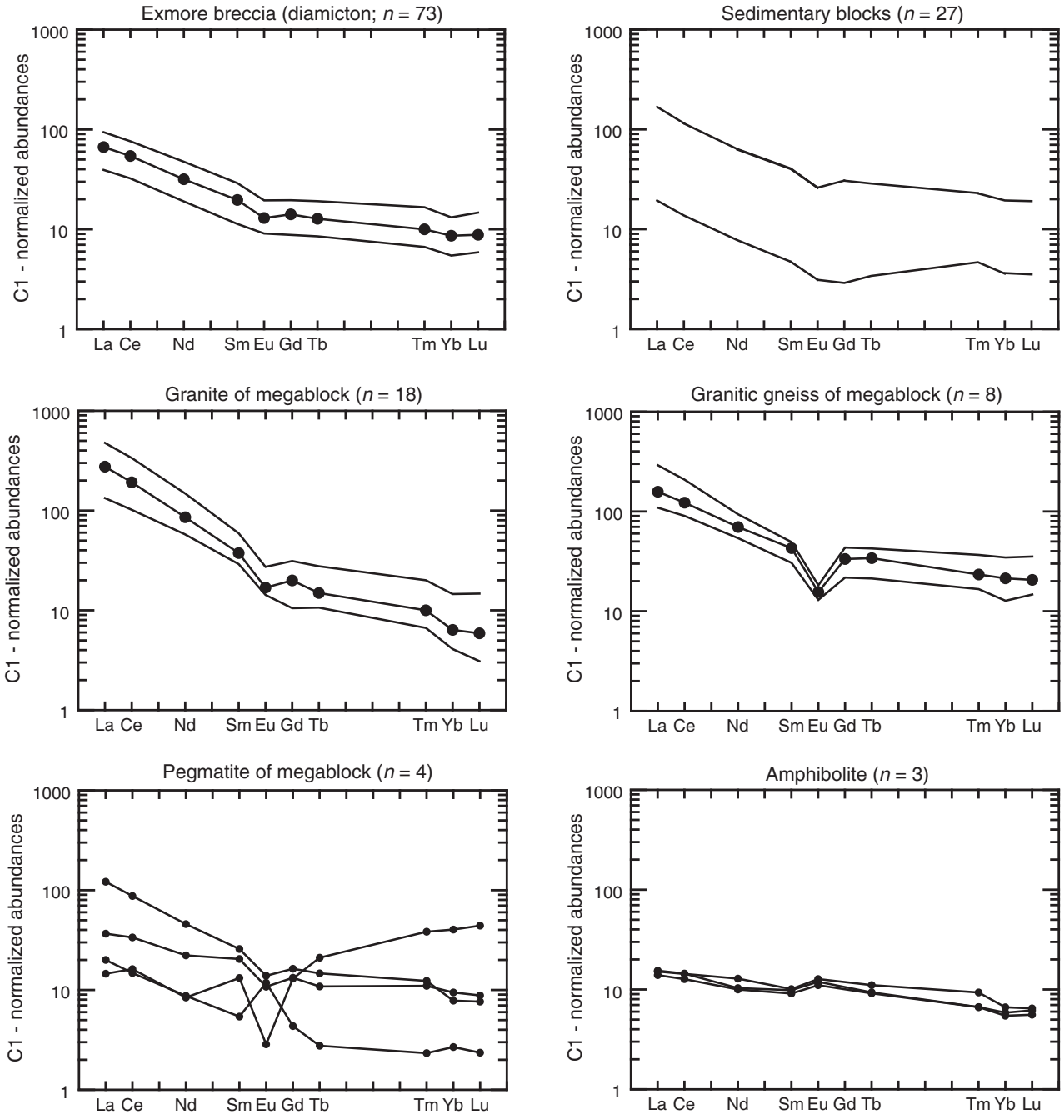

Figure 8 (*continued on following page*). C1 chondrite–normalized rare earth element (REE) patterns for major rock types of the Eyreville A and B drill cores. Normalization factors are from Taylor and McLennan (1985). For most rock types, the minimum (lower line), average (middle dotted line), and maximum (upper line) C1 chondrite–normalized REE patterns are shown. For the sedimentary blocks of the Exmore bed section, only the minimum (lower line) and maximum (upper line) patterns are plotted. The patterns for the pegmatite of the megablock and the amphibolite display individual samples; *n* = number of analyses.

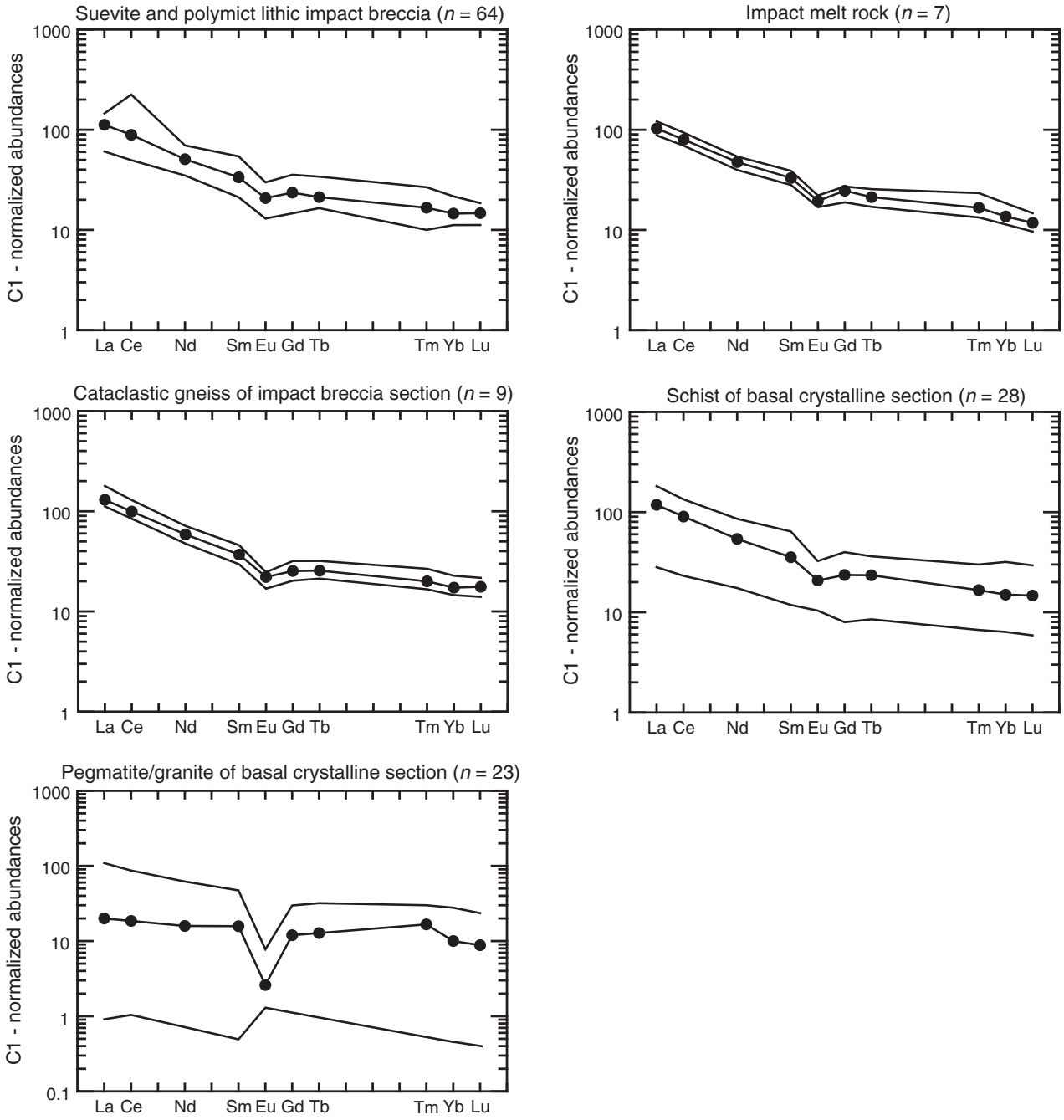

Figure 8 (*continued*).

TABLE 2. AVERAGE CHEMICAL COMPOSITION, STANDARD DEVIATION, AND RANGE OF ROCK COMPOSITIONS FOR THE EXMORE BRECCIA AND SANDSTONE OF CLASTIC LAYERS IN THE LITHIC BLOCK SECTION OF THE EYREVILLE B DRILL CORE

Rock type	Exmore breccia (diamicton)					Sandstone above/below amphibolite block					Sandstone below cataclastic schist block					Average Exmore breccia from Poag et al. (2004)			
Depth range (m)	445.0–864.3					1371.1–1376.4 /1389.7–1393.0 m					1396.4–1397.2 m								
	Mean	Dev*	Min	Max	n§	Mean	Dev*	Min	Max	n§	Mean	Dev*	Min	Max	n§	Mean	Dev*	Min	Max
(wt%)																			
SiO_2	75.6	4.3	60.9	84.9	73	86.0	1.8	83.6	89.4	7	78.3	1.2	77.4	79.1	2	64.5	10.1	32.7	85.3
TiO_2	0.52	0.11	0.28	0.91	73	0.21	0.05	0.13	0.30	7	0.54	0.02	0.52	0.55	2	0.58	0.22	0.02	0.92
Al_2O_3	10.3	1.7	6.5	16.5	73	6.9	0.9	6.3	8.1	7	10.5	0.3	10.3	10.7	2	9.4	2.9	3.1	16.1
Fe_2O_3†	3.10	1.03	1.42	6.58	73	1.34	0.30	0.91	1.72	7	2.83	0.26	2.64	3.01	2	5.92	2.73	0.76	18.6
MnO	0.04	0.02	0.01	0.16	73	0.01	0.01	0.01	0.02	7	0.03	0.01	0.02	0.03	2	0.04	0.02	0.01	0.09
MgO	0.80	0.32	0.26	1.72	73	0.27	0.07	0.17	0.36	7	0.92	0.04	0.89	0.95	2	1.25	0.62	0.06	3.82
CaO	1.47	0.99	0.60	7.40	73	0.29	0.05	0.21	0.36	7	0.52	0.09	0.45	0.58	2	4.91	5.33	0.34	26.8
Na_2O	1.39	0.18	0.94	1.88	73	0.33	0.13	0.18	0.57	7	0.74	0.00	0.74	0.74	2	1.28	0.41	0.12	2.14
K_2O	2.54	0.31	0.82	3.20	73	2.37	0.39	1.67	2.72	7	2.64	0.15	2.53	2.75	2	2.92	0.90	1.65	7.24
P_2O_5	0.12	0.07	0.03	0.41	73	0.02	0.01	<0.01	0.05	5	0.06	0.01	0.05	0.06	2	0.37	0.56	0.04	2.93
SO_3	0.2	0.1	<0.1	0.5	25	<0.1		<0.1	0.2	7	<0.1		<0.1	0.1	2	n.a.#		n.a.#	n.a.#
LOI	3.7	1.2	1.8	9.4	73	1.7	0.4	1.3	2.4	7	2.5	0.1	2.4	2.6	2	8.0	4.7	0.4	22.8
(ppm)																			
Sc	7.4	2.2	3.6	15	73	3.0	0.7	2.4	4.4	7	7.7	0.5	7.4	8.1	2	8.76	3.54	2.02	17.3
V	63	16	28	107	73	32	8	23	46	7	66	7	61	71	2	105	28	20	138
Cr	46	13	24	82	73	16	1	14	18	7	38	2	36	39	2	89	32	11	180
Co	9.0	2.4	5.1	19	73	3.5	1.4	1.4	5.8	7	10	1	9.6	10	2	10	5	2	23
Ni	22	6	10	39	73	20	2	18	23	7	28	0	28	28	2	22	9	8	56
Zn	46	20	16	123	73	18	11	10	42	7	30	1	29	31	2	144	136	11	510
Rb	72	10	40	100	73	73	16	58	104	7	119	8	114	125	2	93	26	58	207
Sr	180	17	126	251	73	116	33	68	155	7	126	11	118	134	2	233	94	104	513
Y	22	5	12	44	73	16	6	<10	25	6	39	1	30	40	2	19	5	5	24
Zr	200	34	126	332	73	169	141	67	481	7	237	27	218	256	2	244	148	80	776
Cs	2.1	0.6	1.2	4.1	73	1.6	0.7	1.2	3.2	7	12	0	12	12	2	3.0	1.3	0.8	7.8
Ba	503	79	164	763	73	491	129	280	631	7	409	6	413	405	2	291	94	51	554
La	22	4	13	31	73	15	10	8.7	37	7	38	7	33	44	2	33	29	11	173
Ce	47	8	28	66	73	30	20	17	73	7	75	11	67	83	2	78	89	20	527
Nd	20	4	12	30	73	12	7	7.1	27	7	32	5	28	36	2	35	35	10	212
Sm	4.0	0.8	2.3	5.9	73	2.2	1.0	1.5	4.4	7	6.3	1.1	5.5	7.0	2	6.5	5.7	1.8	34
Eu	1.0	0.2	0.7	1.5	73	0.6	0.1	0.4	0.9	7	1.4	0.2	1.3	1.5	2	1.4	1.4	0.3	8.2
Gd	3.9	0.7	<2.0	5.4	64	2.4	1.1	1.3	3.9	5	7.2				1	6.1	4.7	1.9	28
Tb	0.6	0.1	0.4	0.9	73	0.4	0.2	0.2	0.7	7	1.0	0.1	0.9	1.1	2	0.9	0.7	0.3	3.9
Tm	0.3	0.1	0.2	0.5	73	0.2	0.1	0.1	0.3	7	0.4	0.1	0.4	0.4	2	0.4	0.1	0.2	0.8
Yb	1.9	0.4	1.2	2.9	73	1.4	0.4	0.9	2.0	7	2.9	0.1	2.9	2.9	2	2.5	1.0	1.0	5.2
Lu	0.3	0.1	0.2	0.5	73	0.2	0.1	0.2	0.3	7	0.4	0.1	0.4	0.4	2	0.3	0.1	0.1	0.6
Hf	4.9	0.8	3.2	7.3	73	2.8	0.9	1.3	4.2	7	5.7	0.5	5.3	6.1	2	5.5	2.2	0.9	12
Ta	0.7	0.2	0.4	1.2	73	0.5	0.3	0.2	1.0	7	1.1	0.1	1.0	1.1	2	0.7	0.2	0.1	1.1
Th	6.4	1.9	3.0	13	73	4.7	4.1	2.6	14	7	9.0	0.4	8.7	9.2	2	7.2	3.7	2.6	22
U	1.8	0.4	1.1	3.0	73	1.4	0.6	1.0	2.8	7	2.6	0.1	2.5	2.7	2	2.2	0.9	0.9	5.0

Note: For comparison the average Exmore breccia composition from Poag et al. (2004) is listed. LOI—loss on ignition.

*Dev—standard deviation.

†Total Fe as Fe_2O_3.

§*n*—number of analyses.

TABLE 3. AVERAGE CHEMICAL COMPOSITION, STANDARD DEVIATION, AND RANGE OF ROCK COMPOSITIONS FOR THE CRYSTALLINE ROCKS OF THE LITHIC BLOCK SECTION OF THE EYREVILLE B DRILL CORE

Rock type	Granite of the megablock					Granitic gneiss of the megablock					Xenoliths in rocks of the megablock					Amphibolite				
Depth range (m)	1096.8–1118.0/1221.3–1240.1/1263.8–1369.0					1123.8–1212.4/1252.0					1147.5/1175.1–1175.2					1376.4–1389.7				
	Mean	Dev*	Min	Max	n§	Mean	Dev*	Min	Max	n§	Mean	Dev*	Min	Max	n§	Mean	Dev*	Min	Max	n§
(wt%)																				
SiO_2	71.9	1.1	70.8	76.3	18	74.0	2.0	69.9	76.1	8	52.3	3.1	49.8	55.8	3	45.5	1.1	44.4	47.0	6
TiO_2	0.28	0.04	0.13	0.33	18	0.32	0.25	0.14	0.73	8	2.72	0.35	2.52	3.12	3	1.40	0.52	1.14	2.45	6
Al_2O_3	14.4	0.6	12.2	14.7	18	13.1	0.7	12.2	14.5	8	14.9	1.0	13.8	15.8	3	18.4	0.6	17.3	19.1	6
Fe_2O_3†	1.95	0.28	1.18	2.42	18	2.45	1.80	1.12	6.46	8	12.1	1.4	11.2	13.7	3	11.8	1.1	10.5	13.6	6
MnO	0.04	0.01	0.02	0.04	18	0.04	0.02	0.02	0.08	8	0.18	0.03	0.16	0.22	3	0.22	0.09	0.14	0.32	6
MgO	0.45	0.11	0.10	0.59	18	0.34	0.21	0.15	0.74	8	4.77	1.33	3.25	5.69	3	5.89	0.53	5.13	6.49	6
CaO	1.76	0.31	0.84	2.11	18	1.47	0.86	0.41	2.48	8	4.57	1.33	3.28	5.35	3	8.49	1.15	7.78	10.8	6
Na_2O	3.16	0.24	2.41	3.44	18	3.08	0.90	1.69	4.04	8	1.64	0.60	1.05	2.24	3	2.63	0.51	1.93	3.38	6
K_2O	4.92	0.38	4.49	5.77	18	4.39	2.47	1.09	7.63	8	3.61	0.36	3.19	3.84	3	0.83	1.11	0.21	3.02	6
P_2O_5	0.08	0.03	0.01	0.17	18	0.04	0.06	0.01	0.17	8	0.94	0.38	0.50	1.16	3	0.20	0.08	0.14	0.34	6
SO_3	<0.1		<0.1	<0.1	18	<0.1		<0.1	<0.1	8	<0.1		<0.1	<0.1	3	0.3	0.3	0.1	0.8	6
LOI	0.6	0.2	0.3	1.1	18	0.5	0.2	0.2	0.7	8	1.6	1.3	0.4	3.0	3	4.0	1.3	3.0	6.6	6
(ppm)																				
Sc	4.0	1.6	1.6	8.8	18	7.8	3.4	2.8	12	8	22	11	15	35	3	26	1	25	27	3
V	28	5	<15	35	17	31	23	<10	76	7	214	47	177	267	3	181	6	173	190	6
Cr	9.8	1.4	8.3	14	18	9.4	1.1	7.9	11	8	45	23	19	61	3	153	6	148	160	3
Co	2.4	0.6	0.7	3.3	18	1.9	1.6	0.6	5.0	8	34	4	30	36	3	52	5	46	56	3
Ni	24	2	21	29	18	30	4	24	34	8	69	25	40	85	3	70	31	39	105	6
Zn	54	11	31	73	18	59	35	23	132	8	258	112	185	387	3	92	13	77	102	3
Rb	232	17	207	273	18	208	94	63	347	8	369	74	321	454	3	19	6	13	26	3
Sr	235	28	151	290	18	154	113	73	420	8	511	412	48	838	3	315	65	210	406	6
Y	45	10	35	72	18	81	25	39	111	8	80	31	61	116	3	41	28	<10	61	2
Zr	262	41	168	341	18	277	158	195	666	8	311	38	282	354	3	98	61	50	218	6
Cs	3.3	0.9	1.6	5.0	18	3.6	1.2	1.4	5.1	8	22	5	18	27	3	2.0	0.3	1.6	2.1	3
Ba	925	118	643	1173	18	558	269	109	786	8	1049	511	465	1409	3	249	391	50	1042	6
La	91	23	44	157	18	52	20	36	96	8	76	43	26	104	3	4.9	0.3	4.6	5.1	3
Ce	166	42	88	291	18	106	34	78	180	8	154	81	60	205	3	12	1	11	13	3
Nd	54	12	48	60	18	44	9	34	59	8	69	30	35	87	3	7.0	1.0	6.3	8.1	3
Sm	7.6	1.5	5.9	12	18	8.7	1.4	6.2	10	8	12	3	8.0	14	3	2.0	0.1	1.9	2.1	3
Eu	1.3	0.2	1.1	2.1	18	1.2	0.2	1.0	1.4	8	3.3	1.4	2.3	4.9	3	0.9	0.1	0.9	1.0	3
Gd	5.5	1.8	2.9	8.6	18	9.2	2.4	6.0	12	8	9.5	0.6	8.8	10	3	n.d.#				
Tb	0.7	0.2	0.5	1.3	18	1.6	0.4	1.0	2.0	8	1.6	0.3	1.4	1.9	3	0.5	0.1	0.4	0.5	3
Tm	0.3	0.1	0.2	0.6	18	0.7	0.2	0.5	1.1	8	0.8	0.4	0.5	1.2	3	0.2	0.1	0.2	0.3	3
Yb	1.4	0.5	0.9	3.2	18	4.7	1.8	2.8	7.6	8	4.2	2.8	2.3	7.4	3	1.3	0.1	1.2	1.5	3
Lu	0.2	0.1	0.1	0.5	18	0.7	0.3	0.5	1.2	8	0.6	0.4	0.3	1.1	3	0.2	0.0	0.2	0.2	3
Hf	6.9	0.8	5.5	8.5	18	8.2	3.9	6.0	18	8	7.9	0.9	7.1	9.0	3	1.9	0.1	1.8	1.9	3
Ta	1.7	0.7	0.4	3.2	18	2.0	1.2	0.9	4.5	8	2.3	0.8	1.9	3.2	3	0.6	0.1	0.5	0.7	3
Th	40	9	18	51	18	25	14	16	57	8	7.8	0.9	6.9	8.4	3	0.8	0.0	0.8	0.8	3
U	4.9	2.3	2.2	10	18	5.2	1.9	2.7	7.9	8	3.0	0.3	2.7	3.3	3	n.d.#				

Note: LOI—loss on ignition.

*Dev—standard deviation.

†Total Fe as Fe_2O_3.

§*n*—number of analyses.

TABLE 4. CHEMICAL COMPOSITION, STANDARD DEVIATION, AND RANGE OF COMPOSITION OF AVERAGE IMPACTITE OF THE IMPACT BRECCIA SECTION OF THE EYREVILLE B DRILL CORE

Rock type	Average impactite (suevite, impact melt rock, and polymict lithic impact breccia)				
Depth range (m)	1397–1549				
	Mean	Dev*	Min	Max	$n^{\S}$
(wt%)					
SiO_2	66.2	2.8	60.6	72.2	75
TiO_2	0.89	0.14	0.65	1.36	75
Al_2O_3	14.8	1.1	12.7	17.3	75
Fe_2O_3†	5.63	0.87	3.90	7.78	75
MnO	0.08	0.02	0.04	0.13	75
MgO	1.78	0.48	0.85	3.39	75
CaO	1.50	0.47	0.51	3.12	75
Na_2O	1.54	0.72	0.55	4.91	75
K_2O	3.21	0.82	0.25	5.37	75
P_2O_5	0.14	0.03	0.08	0.34	75
SO_3	0.2	0.1	<0.1	0.4	30
LOI	3.6	1.4	1.4	9.8	75
(ppm)					
Sc	13	2	8.7	19	71
V	104	14	74	138	75
Cr	68	15	24	112	71
Co	16	2	10	22	71
Ni	34	6	18	62	75
Zn	111	51	39	455	71
Rb	141	40	24	228	71
Sr	210	81	105	555	75
Y	44	8	22	63	75
Zr	248	34	155	378	75
Cs	10	4	2.5	20	71
Ba	465	125	<30	1041	74
La	37	6	20	48	71
Ce	76	18	43	194	71
Nd	32	5	22	44	71
Sm	6.8	1.3	4.3	10	71
Eu	1.6	0.2	1.0	2.3	71
Gd	6.5	1.2	<4.0	9.8	68
Tb	1.0	0.2	0.8	1.6	71
Tm	0.5	0.1	0.3	0.8	71
Yb	3.1	0.4	2.0	4.1	71
Lu	0.5	0.1	0.3	0.6	71
Hf	6.4	0.8	4.8	9.8	71
Ta	1.3	0.2	0.9	1.8	71
Th	12	2	8.8	20	71
U	3.0	0.7	1.7	4.7	71

Note: LOI—loss on ignition.
*Dev—standard deviation.
†Total Fe as Fe_2O_3.
§*n*—number of analyses.

to those for the Exmore breccia (Fig. 5). The V/Cr ratios for these samples are 1.7–1.9, which are supposed to be indicative of slightly anoxic conditions at sediment deposition (Ernst, 1970). This is also indicated by elevated SO_3 contents (0.8–0.9 wt%) in the samples of this depth interval compared to samples of the lower part of the transition zone (Table A1).

Samples of the lower part of the transition zone (444.4–444.9 m depth) have distinctly different composition and are characterized by SiO_2, Al_2O_3 and Fe_2O_3 contents of 73.2–81.0, 8.7–11.7, and 1.7–3.9 wt%, respectively. The average SiO_2 content is 77.3 wt%, and the $SiO_2/(Al_2O_3 + Fe_2O_3 + MgO)$ ratios for samples from this part range from 4.4 to 7.4 (average 5.7). In this part, the SiO_2 content and the $SiO_2/(Al_2O_3 + Fe_2O_3 + MgO)$ ratio increase, whereas Al_2O_3 and Fe_2O_3 contents decrease with depth. The uppermost sample (W-005; 444.4 m depth) of this lower unit has a remarkable SO_3 content of 1.2 wt% compared to all other samples of the transition zone, which is consistent with a centimeter-sized pocket of framboidal to cubic textured pyrite observed in the drill core (see Reimold et al., this volume). In the Harker diagrams, the samples of this lower unit plot into the field of the Exmore breccia (Fig. 5), and they are similar to the Exmore breccia in chemical composition. These samples can be classified as arkoses and litharenites (Fig. 9) based on the classification of Herron (1988).

These observations are consistent with petrographic observations showing an upper part with laminated siltstone and claystone, and a lower part of slightly glauconitic sandstone (Edwards et al., this volume; Reimold et al., this volume). Based on petrographic observations by Reimold et al. (this volume), the transition between the post-Exmore breccia transition zone and the top of the Exmore breccia should be placed between samples W-010 and W-011 at a depth of ~444.96 m. There are no significant chemical differences between the lower unit of the post-Exmore breccia transition zone and the upper unit of the Exmore breccia (Fig. 1). This is also confirmed by petrographic observations of Edwards et al. (this volume), which show a continuous glauconitic sandstone unit from 444.37 to 450.95 m depth.

The lower part of the post-Exmore breccia transition zone does not show distinct enrichments in Cr, Co, Ni, and Ir abundances in comparison to other Exmore breccia samples (Table A1). Therefore, no chondritic impactor component is indicated by the data for the samples of these sediments.

Exmore breccia. The Exmore breccia (diamicton) displays substantial variation in chemical composition and SiO_2, Al_2O_3, and Fe_2O_3 contents of 60.9–84.9, 6.5–16.5, and 1.4–6.6 wt%, respectively (Fig. 1; Table 2). Exmore breccia major and trace elements do not show a distinct correlation with depth (Fig. 1), with the exception of Sr, which displays generally an exponential decrease from top to bottom (r = –0.55, Table A2). In contrast, TiO_2, Al_2O_3, Fe_2O_3, MgO, CaO, P_2O_5, LOI, V, Cr, and the total REE abundances display negative correlations with the SiO_2 content (e.g., Fig. 5; Table A2). A significant carbonate component in the Exmore breccia, based on a positive correlation of CaO and LOI, is not recognizable. Only the sample W-026 (457.7 m depth) contains significant amounts of carbonate, which is also confirmed by petrographic observations (Reimold et al., this volume). On the other hand, the CaO content is strongly positively correlated with P_2O_5 abundance (r = 0.78; Table A2), likely due to the presence of apatite. The wide range of chemical compositions leads, in the classification of Herron (1988), to a trend from Fe-shale over shale–graywacke–litharenite/arkose to subarkose (Fig. 9).

TABLE 5. AVERAGE CHEMICAL COMPOSITION, STANDARD DEVIATION, AND RANGE OF ROCK COMPOSITIONS OF THE DIFFERENT SUBUNITS OF THE IMPACT BRECCIA SECTION OF THE EYREVILLE B DRILL CORE

Unit[#]	Upper Suevite SU					Upper impact melt rock M2					Suevite S3					Suevite S2				
Depth range (m)	1397–1402					1402–1408					1409–1431					1434–1450				
	Mean	Dev*	Min	Max	n[§]	Mean	Dev*	Min	Max	n[§]	Mean	Dev*	Min	Max	n[§]	Mean	Dev*	Min	Max	n[§]
(wt%)																				
SiO_2	69.3	0.5	68.5	69.9	6	69.2	1.2	67.2	70.6	7	66.7	1.8	63.5	69.8	16	65.6	2.5	62.6	72.2	13
TiO_2	0.82	0.01	0.81	0.83	6	0.78	0.06	0.65	0.82	7	0.83	0.09	0.70	1.08	16	0.82	0.11	0.65	0.99	13
Al_2O_3	14.0	0.5	13.6	14.7	6	13.7	0.7	12.7	14.3	7	14.5	0.8	13.5	16.8	16	15.1	1.1	13.0	16.9	13
Fe_2O_3[†]	5.00	0.23	4.59	5.24	6	5.11	0.37	4.66	5.51	7	5.41	0.75	4.22	6.91	16	5.31	0.98	3.90	7.04	13
MnO	0.06	0.01	0.05	0.07	6	0.06	0.01	0.04	0.08	7	0.08	0.01	0.06	0.11	16	0.09	0.02	0.06	0.12	13
MgO	1.40	0.21	0.99	1.54	6	0.97	0.08	0.85	1.10	7	1.89	0.38	1.38	2.76	16	2.04	0.35	1.29	2.60	13
CaO	1.58	0.26	1.36	1.92	6	1.65	0.18	1.35	1.90	7	1.65	0.33	0.75	2.15	16	1.77	0.57	0.93	2.97	13
Na_2O	1.62	0.18	1.40	1.93	6	1.33	0.13	1.12	1.48	7	2.09	0.32	1.28	2.70	16	2.31	0.99	0.75	4.91	13
K_2O	3.32	0.23	2.88	3.50	6	3.22	0.57	2.00	3.61	7	2.94	0.89	0.25	4.64	16	3.45	0.48	2.71	4.34	13
P_2O_5	0.13	0.01	0.12	0.13	6	0.12	0.01	0.11	0.13	7	0.13	0.02	0.11	0.17	16	0.13	0.02	0.08	0.16	13
SO_3	<0.1		<0.1	<0.1	6	<0.1		<0.1	<0.1	4	0.2	0.1	<0.1	0.4	7	0.1	0.1	<0.1	0.2	7
LOI	2.4	0.2	2.2	2.6	6	2.9	1.5	1.7	5.6	7	3.3	1.2	2.0	6.6	16	2.9	0.6	1.9	4.0	13
(ppm)																				
Sc	12	1	12	13	6	13	1	12	13	5	13	2	8.7	19	15	14	2	11	17	13
V	98	7	90	109	6	86	9	77	101	7	101	12	79	134	16	104	14	74	122	13
Cr	62	4	59	68	6	73	17	63	102	5	61	15	33	96	15	68	16	24	87	13
Co	15	1	13	16	6	14	1	14	15	5	14	2	12	18	15	15	3	10	21	13
Ni	32	2	29	33	6	31	9	18	49	7	32	4	28	41	16	33	4	24	38	13
Zn	66	36	39	113	6	84	16	73	111	5	104	27	63	169	15	99	24	65	129	13
Rb	141	7	134	150	6	136	6	127	143	5	123	31	28	171	15	142	29	111	204	13
Sr	201	23	177	236	6	190	17	161	204	7	233	93	105	555	16	197	52	127	303	13
Y	44	2	42	45	6	38	7	29	46	7	38	7	22	54	16	44	5	38	53	13
Zr	235	11	219	253	6	239	13	222	259	7	241	47	198	378	16	243	24	202	279	13
Cs	7.0	2.2	3.7	9.3	6	8.4	1.8	6.8	11	5	8.5	2.9	3.3	13	15	7.4	3.7	2.5	16	13
Ba	475	28	444	516	6	481	97	306	620	7	472	131	<30	893	15	534	162	395	1041	13
La	34	2	32	38	6	32	2	29	34	5	31	3	24	39	15	38	5	29	46	13
Ce	69	4	66	76	6	65	3	60	68	5	65	7	50	82	15	77	11	61	93	13
Nd	30	2	28	33	6	29	3	25	31	5	28	4	22	35	15	32	5	26	40	13
Sm	5.8	0.4	5.5	6.5	6	6.3	0.7	5.7	7.5	5	6.0	1.0	4.3	8.0	15	6.8	1.4	4.8	9.3	13
Eu	1.5	0.1	1.4	1.6	6	1.4	0.1	1.3	1.4	5	1.4	0.1	1.2	1.7	15	1.6	0.2	1.3	2.0	13
Gd	5.4	0.4	<5.0	5.9	3	6.5	0.8	5.2	7.3	5	5.9	1.0	4.4	8.3	15	6.4	1.3	4.8	8.4	13
Tb	1.0	0.1	0.9	1.0	6	0.9	0.1	0.8	1.0	5	0.9	0.1	0.8	1.1	15	1.0	0.2	0.8	1.3	13
Tm	0.5	0.1	0.4	0.5	6	0.5	0.1	0.4	0.6	5	0.5	0.1	0.4	0.6	15	0.5	0.1	0.4	0.7	13
Yb	3.0	0.1	3.0	3.2	6	2.8	0.2	2.5	3.1	5	2.8	0.3	2.3	3.3	15	3.2	0.4	2.6	3.8	13
Lu	0.5	0.1	0.5	0.5	6	0.4	0.1	0.4	0.5	5	0.4	0.1	0.3	0.5	15	0.5	0.1	0.3	0.6	13
Hf	6.1	0.3	5.6	6.5	6	5.9	0.3	5.5	6.3	5	5.7	0.7	4.8	7.6	15	6.3	0.7	4.9	7.5	13
Ta	1.2	0.1	1.1	1.3	6	1.1	0.1	1.0	1.2	5	1.2	0.1	1.0	1.4	15	1.3	0.2	0.9	1.6	13
Th	11	1	10	11	6	11	1	9.5	12	5	11	1	8.8	13	15	12	2	9.1	15	13
U	2.6	0.3	2.3	2.9	6	2.5	0.3	2.2	2.8	5	2.5	0.4	1.7	3.0	15	2.7	0.8	1.7	4.6	13

(*Continued*)

TABLE 5. AVERAGE CHEMICAL COMPOSITION, STANDARD DEVIATION, AND RANGE OF ROCK COMPOSITIONS OF THE DIFFERENT SUBUNITS OF THE IMPACT BRECCIA SECTION OF THE EYREVILLE B DRILL CORE (*Continued*)

Unit#	Lower impact melt rock M1					Suevite S1					Polymict impact breccia (suevite/polymict lithic impact breccia) P4 + P3 + P2 + P1					Cataclastic/felsic gneiss B4 + B3 + B2 + B1				
Depth range (m)	1450–1451					1451–1474					1481–1549					1494–1547				
	Mean	Dev*	Min	Max	n§	Mean	Dev*	Min	Max	n§	Mean	Dev*	Min	Max	n§	Mean	Dev*	Min	Max	n§
(wt%)																				
SiO_2	64.8	2.5	63.0	66.5	2	66.6	3.3	60.6	70.9	13	64.0	2.4	60.8	69.6	18	66.3	3.5	59.5	71.2	10
TiO_2	0.90	0.07	0.89	0.90	2	0.97	0.13	0.81	1.35	13	1.00	0.17	0.66	1.36	18	0.89	0.07	0.70	0.97	10
Al_2O_3	14.8	0.4	14.5	15.1	2	14.7	0.9	13.2	16.8	13	15.6	1.1	13.5	17.3	18	14.8	1.4	11.9	17.2	10
Fe_2O_3†	6.19	0.66	5.72	6.65	2	5.84	0.99	4.54	7.78	13	6.25	0.72	4.24	7.61	18	5.57	0.67	4.41	6.56	10
MnO	0.07	0.01	0.06	0.08	2	0.08	0.02	0.06	0.13	13	0.08	0.01	0.06	0.10	18	0.08	0.02	0.05	0.13	10
MgO	1.87	0.17	1.75	1.99	2	1.58	0.32	1.16	2.25	13	2.07	0.45	1.35	3.39	18	2.34	0.74	1.25	3.28	10
CaO	1.40	0.08	1.34	1.45	2	1.37	0.59	0.68	3.12	13	1.18	0.41	0.51	2.34	18	1.35	0.96	0.41	3.63	10
Na_2O	1.17	0.42	0.87	1.47	2	0.95	0.20	0.66	1.40	13	1.04	0.28	0.55	1.80	18	1.50	0.71	0.77	3.27	10
K_2O	2.29	0.37	2.03	2.55	2	2.85	0.69	1.99	4.15	13	3.60	1.05	0.31	5.37	18	3.19	0.71	2.18	4.61	10
P_2O_5	0.15	0.02	0.13	0.16	2	0.15	0.06	0.11	0.34	13	0.15	0.04	0.10	0.27	18	0.13	0.03	0.06	0.18	10
SO_3	<0.1				1	0.1	0.1	<0.1	0.1	5	0.2	0.1	<0.1	0.4	11	<0.1		<0.1	0.1	10
LOI	5.0	1.5	3.9	6.0	2	4.4	1.9	1.4	9.8	13	4.5	1.0	3.0	7.2	18	3.5	0.8	2.8	5.1	10
(ppm)																				
Sc	13	1	13	13	2	13	1	11	16	13	15	2	9.8	18	17	14	2	12	17	9
V	102	5	98	105	2	106	11	90	131	13	114	14	84	138	18	102	10	79	115	10
Cr	79	11	71	87	2	64	7	53	83	13	78	17	40	112	17	94	22	66	124	9
Co	16	1	16	16	2	16	3	11	22	13	17	2	14	20	17	16	2	12	20	9
Ni	36	4	33	39	2	34	3	30	39	13	38	8	24	62	18	40	11	27	67	10
Zn	121	13	112	130	2	139	96	95	455	13	126	26	52	160	17	93	10	81	112	9
Rb	84	43	54	115	2	128	41	74	223	13	175	45	24	228	17	131	29	88	175	9
Sr	210	31	188	232	2	224	70	143	361	13	198	119	106	474	18	126	57	66	232	10
Y	40	2	38	41	2	43	7	33	57	13	51	10	22	63	18	47	8	37	62	10
Zr	248	3	246	250	2	260	25	231	307	13	258	43	155	371	18	298	43	234	380	10
Cs	11	1	11	11	2	13	3	7.8	20	13	13	4	4.0	16	17	5.9	4.3	2.4	16	9
Ba	346	88	283	408	2	394	99	264	590	13	467	119	68	646	18	555	100	381	736	10
La	39	1	39	40	2	38	5	31	48	13	42	6	20	48	17	43	7	37	59	9
Ce	78	3	76	81	2	78	9	61	97	13	90	30	43	194	17	86	13	73	112	9
Nd	33	2	31	34	2	34	5	27	43	13	37	5	22	44	17	37	5	30	45	9
Sm	7.9	0.1	7.8	7.9	2	7.0	1.1	5.0	9.7	13	7.6	1.3	4.7	10	17	7.5	0.9	6.0	9.3	9
Eu	1.7	0.1	1.6	1.7	2	1.6	0.2	1.2	2.0	13	1.7	0.3	1.0	2.3	17	1.7	0.2	1.3	1.9	9
Gd	7.5	0.1	7.4	7.5	2	6.6	1.2	4.9	9.6	13	7.0	1.3	4.8	9.8	17	7.0	1.0	5.6	8.8	9
Tb	1.1	0.1	1.2	1.2	2	1.1	0.1	0.8	1.4	13	1.2	0.2	0.9	1.6	17	1.2	0.1	1.0	1.5	9
Tm	0.6	0.1	0.6	0.7	2	0.5	0.1	0.4	0.7	13	0.6	0.1	0.3	0.8	17	0.6	0.1	0.5	0.8	9
Yb	3.4	0.1	3.4	3.5	2	3.2	0.3	2.7	3.9	13	3.4	0.5	2.0	4.1	17	3.8	0.6	3.2	5.0	9
Lu	0.4	0.1	0.4	0.4	2	0.5	0.1	0.4	0.5	13	0.5	0.1	0.3	0.6	17	0.6	0.1	0.5	0.7	9
Hf	6.6	0.3	6.4	6.8	2	6.6	0.6	6.0	7.8	13	7.1	0.9	5.9	9.8	17	8.0	1.3	6.3	10	9
Ta	1.4	0.1	1.4	1.4	2	1.3	0.1	1.0	1.4	13	1.4	0.2	1.2	1.8	17	1.5	0.5	1.2	2.7	9
Th	13	1	13	13	2	12	1	8.9	14	13	13	2	10	20	17	15	6	11	30	9
U	3.3	0.2	3.2	3.4	2	3.5	0.5	2.6	4.2	13	3.5	0.7	2.2	4.7	17	3.2	1.1	2.3	6.1	9

*dev—standard deviation.

†total Fe as Fe_2O_3.

§n—number of analyses.

#Subdivision after Horton et al. (this volume).

The REE patterns for the samples of the Exmore breccia are generally similar (Fig. 8). They indicate enrichments by 40–100 for La, and 5–15 for Yb, respectively, compared to C1 chondrite composition (Fig. 8). The light REEs are enriched compared to the heavy REEs (average $La_N/Yb_N = 7.8$), and a negative Eu anomaly (average Eu/Eu* = 0.77; $Eu/Eu^* = Eu_N/[Sm_N \times Gd_N]^{0.5}$) is visible in essentially all these patterns (Fig. 8). The REE patterns of the Exmore breccia are similar in shape to the REE patterns of the schist of the crystalline block section, cataclastic gneiss of the impact breccia section, suevite/polymict lithic impact breccia, and impact melt rock. The REE abundances of the Exmore breccia are slightly lower in comparison to these lithologies. This is interpreted as the result of admixture of a sedimentary component to the Exmore breccia. Many of the analyzed sedimentary block samples show low REE concentrations in comparison to the other major lithologies (Fig. 8; Table A1).

Based on chemical observations (Fig. 1, 11, and 12), the Exmore breccia can be subdivided into five units with the following depth ranges: (1) 444.9–450.7 m, (2) 450.7–468 m, (3) 468–518 m, (4) 518–528 m, and (5) 528–~865 m.

(1) The uppermost unit (444.9–450.7 m depth) is characterized by the highest average SiO_2 content of 81.2 wt% (78.4–84.9 wt%)

TABLE 6. AVERAGE CHEMICAL COMPOSITION, STANDARD DEVIATION, AND RANGE OF ROCK COMPOSITIONS FOR THE MAJOR CRYSTALLINE ROCK GROUPS OF THE BASAL CRYSTALLINE SECTION OF THE EYREVILLE B DRILL CORE

Rock type	Schist					Pegmatite and granite					Epidosite				
Depth (m)	1554.1–1689.0					1592.3–1766.1					1645.6–1647.8				
	Mean	Dev*	Min	Max	*n*§	Mean	Dev*	Min	Max	*n*§	Mean	Dev*	Min	Max	*n*§
(wt%)															
SiO_2	56.6	7.9	40.4	78.0	37	73.7	4.5	64.7	85.1	25	50.6	10.6	43.3	62.8	3
TiO_2	0.91	0.22	0.38	1.67	37	0.04	0.05	0.01	0.15	25	0.51	0.29	0.25	0.83	3
Al_2O_3	18.6	3.4	9.6	24.9	37	14.5	2.4	7.8	20.7	25	12.1	4.3	7.2	14.8	3
Fe_2O_3†	7.87	3.41	2.43	18.8	37	0.58	0.53	0.02	2.41	25	6.52	0.81	5.65	7.26	3
MnO	0.07	0.03	0.02	0.17	37	0.05	0.04	0.01	0.15	25	0.30	0.11	0.19	0.41	3
MgO	2.06	1.53	0.65	7.51	37	0.13	0.10	0.03	0.35	25	1.24	0.67	0.69	1.98	3
CaO	1.89	1.34	0.38	5.11	37	1.23	1.06	0.22	5.06	25	21.5	6.3	14.3	25.6	3
Na_2O	1.66	0.99	0.58	4.53	37	4.15	1.59	0.86	7.66	25	0.20	0.15	0.11	0.37	3
K_2O	3.56	1.16	0.85	6.51	37	3.41	2.07	1.31	9.26	25	0.14	0.10	0.04	0.23	3
P_2O_5	0.08	0.06	0.02	0.36	37	0.05	0.06	<0.01	0.30	20	0.42	0.58	0.07	1.09	3
SO_3	0.3	0.3	<0.1	1.2	22	<0.1		<0.1	0.3	25	<0.1		<0.1	<0.1	3
LOI	6.1	2.0	2.7	10.7	37	1.7	1.4	0.3	5.9	25	5.8	1.3	4.6	7.2	3
(ppm)															
Sc	19	6	6.8	37	28	3.3	4.0	0.1	17	23	9.1	1.4	8.2	11	3
V	168	54	54	280	37	<15		<15	100	25	67	26	42	93	3
Cr	104	50	44	305	28	21	20	5.2	77	23	76	6	71	83	3
Co	21	12	3.4	60	28	0.5	0.3	0.2	1.4	23	16	8	9.4	26	3
Ni	54	33	23	160	37	37	45	19	253	23	27	3	24	30	3
Zn	133	69	33	320	28	37	26	9	112	23	327	128	219	468	3
Rb	209	90	83	493	28	280	169	82	772	23	15	8	<5	21	2
Sr	136	64	60	386	37	44	22	<15	99	24	147	73	107	231	3
Y	53	17	24	97	37	59	31	12	148	25	15	6	<10	26	2
Zr	173	40	98	251	37	44	25	<15	110	20	138	43	90	173	3
Cs	20	21	5.9	98	28	5.3	4.7	1.2	25	23	2.4	2.4	0.2	4.9	3
Ba	449	174	108	742	37	<30		<30	205	25	<30		<30	32	3
La	39	13	9.3	60	28	6.6	7.9	0.3	36	23	28	7	20	35	3
Ce	78	25	20	116	28	16	16	0.9	75	23	59	19	41	79	3
Nd	34	11	11	54	28	10	9	<0.8	39	22	32	11	23	45	3
Sm	7.2	2.5	2.4	13	28	3.2	2.6	0.1	9.6	23	7.3	0.9	6.5	8.3	3
Eu	1.6	0.5	0.8	2.5	28	0.2	0.1	0.1	0.6	23	1.4	0.2	1.3	1.6	3
Gd	6.5	1.8	2.2	11	28	3.3	2.6	<0.2	8.2	19	5.1	0.8	4.3	5.8	3
Tb	1.1	0.3	0.4	1.7	28	0.6	0.5	0.0	1.5	23	0.9	0.3	0.6	1.2	3
Tm	0.5	0.2	0.2	0.9	28	0.5	0.3	<0.1	0.9	13	0.4	0.2	0.3	0.6	3
Yb	3.3	1.2	1.4	7.0	28	2.2	1.8	0.1	6.1	23	2.5	1.0	1.8	3.6	3
Lu	0.5	0.2	0.2	1.0	28	0.3	0.2	<0.1	0.8	21	0.4	0.1	0.3	0.5	3
Hf	4.9	1.1	2.7	6.8	28	1.5	1.2	0.1	4.8	23	3.9	0.4	3.4	4.1	3
Ta	2.5	3.7	0.4	19	28	7.9	6.8	0.7	25	23	1.2	0.6	0.7	1.9	3
Th	12	4	1.3	20	28	6.3	8.2	0.1	34	23	9.4	6.2	4.9	16	3
U	5.4	3.3	0.4	12	28	14	13	<1	43	22	4.5	1.8	2.5	5.9	3

Note: LOI—loss on ignition.

*Dev—standard deviation.

†Total Fe as Fe_2O_3.

§*n*—number of analyses.

compared to all other units of the Exmore breccia. The $SiO_2/(Al_2O_3 + Fe_2O_3 + MgO)$ ratios for samples from this unit range from 6.2 to 10.2 (average 7.9; Fig. 11).

(2) The unit from 450.7 to 468 m depth displays a much lower average SiO_2 content of 71.9 wt% (60.9–78.5 wt%). The $SiO_2/(Al_2O_3 + Fe_2O_3 + MgO)$ ratios for these samples vary from 3.0 to 6.3 (average 4.6; Fig. 11). This unit displays characteristic element enrichments, e.g., of the TiO_2, Al_2O_3, Fe_2O_3, MgO, CaO, Sc, V, Cr, Zn, and Rb contents (Fig. 12), in comparison to units 1, 3, and 5, and it has the highest content of P_2O_5 within the Exmore breccia (Figs. 1 and 12). The P_2O_5 content is especially enriched at the top of this unit (Figs. 1 and 12), and it is strongly positively correlated with the CaO content (Fig. 10).

(3) The underlying unit (468–518 m depth) has a higher average SiO_2 content of 76.6 wt% (74.1–78.9 wt%) compared to unit 2, but it has a lower SiO_2 content compared to unit 1. Unit 3 samples have $SiO_2/(Al_2O_3 + Fe_2O_3 + MgO)$ ratios of 5.0–6.1 (average 5.6; Fig. 11). No characteristic enrichments compared to the overlying unit 2 were observed for unit 3 (Fig. 12).

(4) The unit from 518 to 528 m depth has a chemical signature that is very similar to that of unit 2. The average SiO_2 content is 71.5 wt% (66.4–77.8 wt%). The $SiO_2/(Al_2O_3 + Fe_2O_3 + MgO)$ ratios are in the range from 3.5 to 5.7 (average 4.2; Fig. 11). Distinct element enrichments similar to those of unit 2 are typical for this unit (see Fig. 12). In contrast to unit 2, the P_2O_5 content is only slightly higher than the average content of this oxide in the Exmore breccia (Figs. 1 and 12).

(5) The few and relatively thin Exmore breccia layers between 528 and ~865 m depth are intercalated with sedimentary blocks. Here, Exmore breccia is chemically relatively homogeneous, with an average SiO_2 content of 78.7 wt% (76.4–80.6 wt%, Fig. 1). The $SiO_2/(Al_2O_3 + Fe_2O_3 + MgO)$ ratios vary from 6.1 to 7.8 (average 6.5; Fig. 11). A correlation of major elements with depth could not be observed for this unit, with the exception of Na_2O, which generally decreases with depth (Fig. 1).

Sedimentary blocks. The chemical compositions of the sedimentary blocks within the Exmore bed section (443.9–1095.7 m depth) are quite diverse (Table A1), and they correspond to their petrographic variability. For example, SiO_2, Al_2O_3, and Fe_2O_3 contents vary from 55.6 to 87.1, 5.5 to 21.4, and 0.5 to 11.5 wt%, respectively (Fig. 1). Only limited petrographic investigation of these sediments was carried out by our group, since our work is mainly focused on the Exmore breccia, impactites, and crystalline target rocks. Therefore, it is not yet clear whether or not the available sedimentary block analyses can be considered representative of the sedimentary target. Consequently, we do not give an average composition for the sedimentary blocks here.

Lithic Block Section (1095.7–1397.2 m)

Granitic megablock. Petrographic investigation of the granitic megablock (1097.7–1371.1 m depth) has identified granite, granitic gneiss, pegmatite, and xenoliths (Horton et al., this volume; Townsend et al., this volume). In the total alkali-silica (TAS) diagram (Cox et al., 1979), our samples of granite, granitic gneiss, and pegmatite all plot into the granite field (Fig. 13).

In contrast to granite and granitic gneiss, the xenoliths have much lower SiO_2 (49.8–55.8 wt%) and Na_2O (1.05–2.24 wt%),

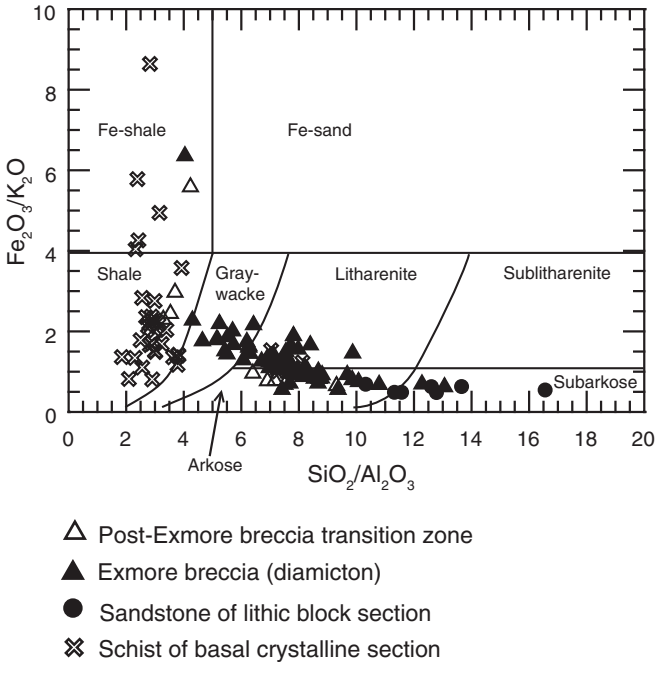

Figure 9. SiO_2/Al_2O_3 versus Fe_2O_3/K_2O discrimination diagram for sedimentary rocks, modified after Herron (1988). The samples of the post-Exmore breccia transition zone, Exmore breccia, and sandstone of the lithic block section are plotted for chemical rock classification. The schist compositions of the basal crystalline section are shown for comparison and possible determination of the protoliths of these rocks.

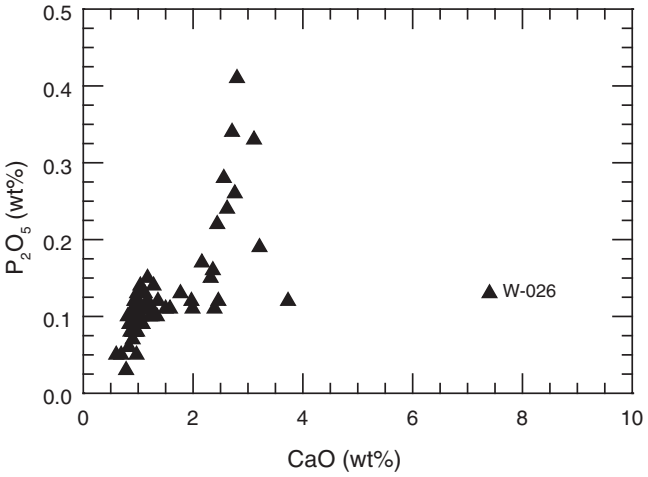

Figure 10. CaO versus P_2O_5 variation diagram for Exmore breccia (diamicton) samples. Note the strong positive correlation for these oxides. Sample W-026 does not follow this correlation due to a significant amount of carbonate, which is also confirmed by petrographic observations (Reimold et al., this volume).

and higher TiO_2 (2.52–3.12 wt%), Fe_2O_3 (11.2–13.7 wt%), and MgO (3.25–5.69 wt%) contents (Table 3). Based on their compositions and metamorphic assemblages, these rocks can be classified chemically as mafic schists. Owing to their comparatively high TiO_2, Fe_2O_3, and MgO abundances, these schists are different from the schists of the basal crystalline section (Fig. 7; Table 6). They have distinctly higher SiO_2, TiO_2, K_2O, P_2O_5, Zr, Rb, Sr, Y, and REE abundances, and lower Al_2O_3, CaO, Na_2O, Cr, and Co abundances in comparison to the amphibolite of the lithic block section (Table 3). Therefore, these mafic schists constitute a separate suite of target rocks.

Granite and granitic gneiss are relatively similar in terms of average chemical composition, but the granitic gneiss displays larger variability of major- and trace-element composition compared to the granite, which leads to greater standard deviations on the average composition (Fig. 2; Table 3). Distinct correlations of major- or trace-element contents with depth were not observed for the granite or granitic gneiss, with the exception of the total REE abundances, which increase with depth in the granite (Table A2). Granite, granitic gneiss, and pegmatite display considerable variability of CaO, Na_2O, and K_2O contents (Table 3). For the granitic gneiss, strongly positive correlations were observed between the CaO and Na_2O abundances, whereas the CaO and Na_2O contents are strongly and negatively correlated to the K_2O content (Table A2). This indicates a negative correlation between plagioclase and alkali feldspar contents of this gneiss.

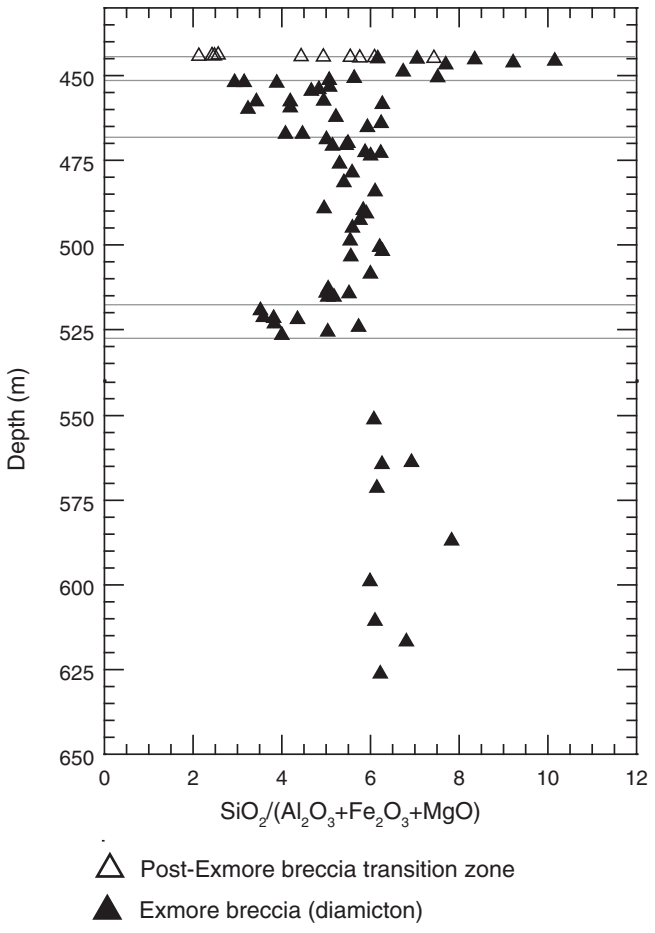

Figure 11. Variations of the $SiO_2/(Al_2O_3 + Fe_2O_3 + MgO)$ ratio with depth for the post-Exmore breccia transition zone and samples from the upper part of the Exmore breccia (diamicton), to a depth of 650 m. Note that this diagram does not contain analyses of sedimentary blocks from the Exmore beds. Boundaries between the post-Exmore breccia transition zone and the Exmore breccia units 1 to 5 (from top to bottom) are marked at 444.9, 450.7, 468, 518, and 528 m depths.

The alumina saturation indices ($A/CNK = Al_2O_3/[CaO + Na_2O + K_2O]$, mole proportions) for the granite and granitic gneiss are <1.1 for most of the analyzed samples. The average A/CNK is 1.05 for both average granite and average granitic gneiss. This indicates that the granite and the protoliths of the granitic gneiss are of the I-type (Chappell and White, 1974). Based on the Rb versus Yb + Ta discrimination diagram (Pearce et al., 1984), the granite of the megablock relates to a syncollisional setting, whereas the samples of the granitic gneiss and pegmatite display substantial variation and plot into the fields for syncollisional, within-plate, and volcanic-arc granites (Fig. 14A). In the Ta versus Yb discrimination diagram, the granite of the megablock plots into the fields for syncollisional and volcanic-arc settings (Fig. 14B).

The REE patterns (Fig. 8) show enrichments in REEs for the granite and granitic gneiss by factors of 105–500, and 100–200, respectively, for La, and 3–15, and 15–35, respectively, for Yb, compared to the C1 chondrite composition. All REE patterns display a distinct enrichment of light REEs over heavy REEs. For the average granite and average granitic gneiss, the La_N/Yb_N ratio is 43.7 and 7.5, respectively. Granite and granitic gneiss display negative Eu anomalies with average Eu/Eu* of 0.61 and 0.40, respectively. The REE patterns of the pegmatite display weak enrichment in REEs compared to those of the granite and granitic gneiss and a great variability in the REE patterns that exhibit both negative and positive Eu anomalies (Fig. 8).

Amphibolite block. Analyses of amphibolite samples (depth range 1377.4–1387.5 m) display some variations in the major-element contents, especially with respect to Fe_2O_3, MgO, CaO, Na_2O, K_2O, and P_2O_5 abundances (Fig. 2). Only the Na_2O content increases slightly with depth. The other major-element abundances are not correlated with depth. Sample RG-003 from 1387.5 m depth displays significantly higher TiO_2, K_2O, and Ba contents compared to all other amphibolite samples.

In the TAS diagram (Cox et al., 1979), the amphibolite samples plot into the fields of gabbro and foid gabbro (sample RG-003) (Fig. 13). Based on the discrimination diagram CaO-MgO-FeO after Walker et al. (1960), the amphibolites are of igneous origin; only one sample (RG-003) plots into the overlapping field of igneous and sedimentary precursors (Fig. 15A). In the Ni versus Zr/Ti discrimination diagram of Winchester and Max (1982), all amphibolite samples plot into the field of igneous precursors (Fig. 15B). The TiO_2 contents of the amphibolites

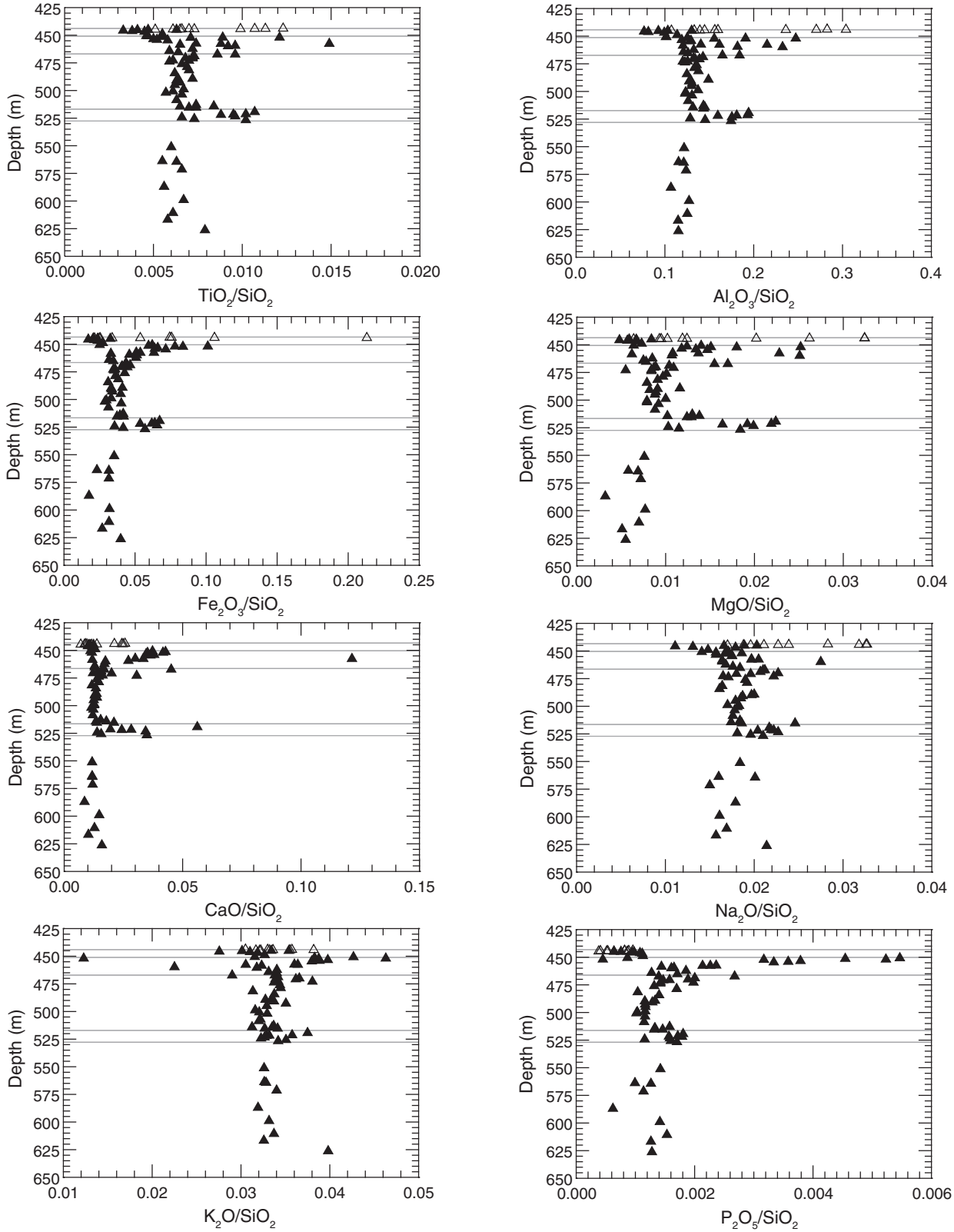

Figure 12 (*continued on following page*). Variation diagrams of SiO_2-normalized abundances of major and selected trace elements (TiO_2, Al_2O_3, Fe_2O_3, MgO, CaO, Na_2O, K_2O, P_2O_5, Sc, V, Cr, Co, Zn, Rb, and Zr) with depth for the post-Exmore breccia transition zone and samples from the upper part of the Exmore breccia (diamicton), to a depth of 650 m. Note that this diagram does not contain analyses of sedimentary blocks from the Exmore beds. Boundaries between the post-Exmore breccia transition zone and the Exmore breccia units 1 to 5 (from top to bottom) are marked at 444.9, 450.7, 468, 518, and 528 m depths.

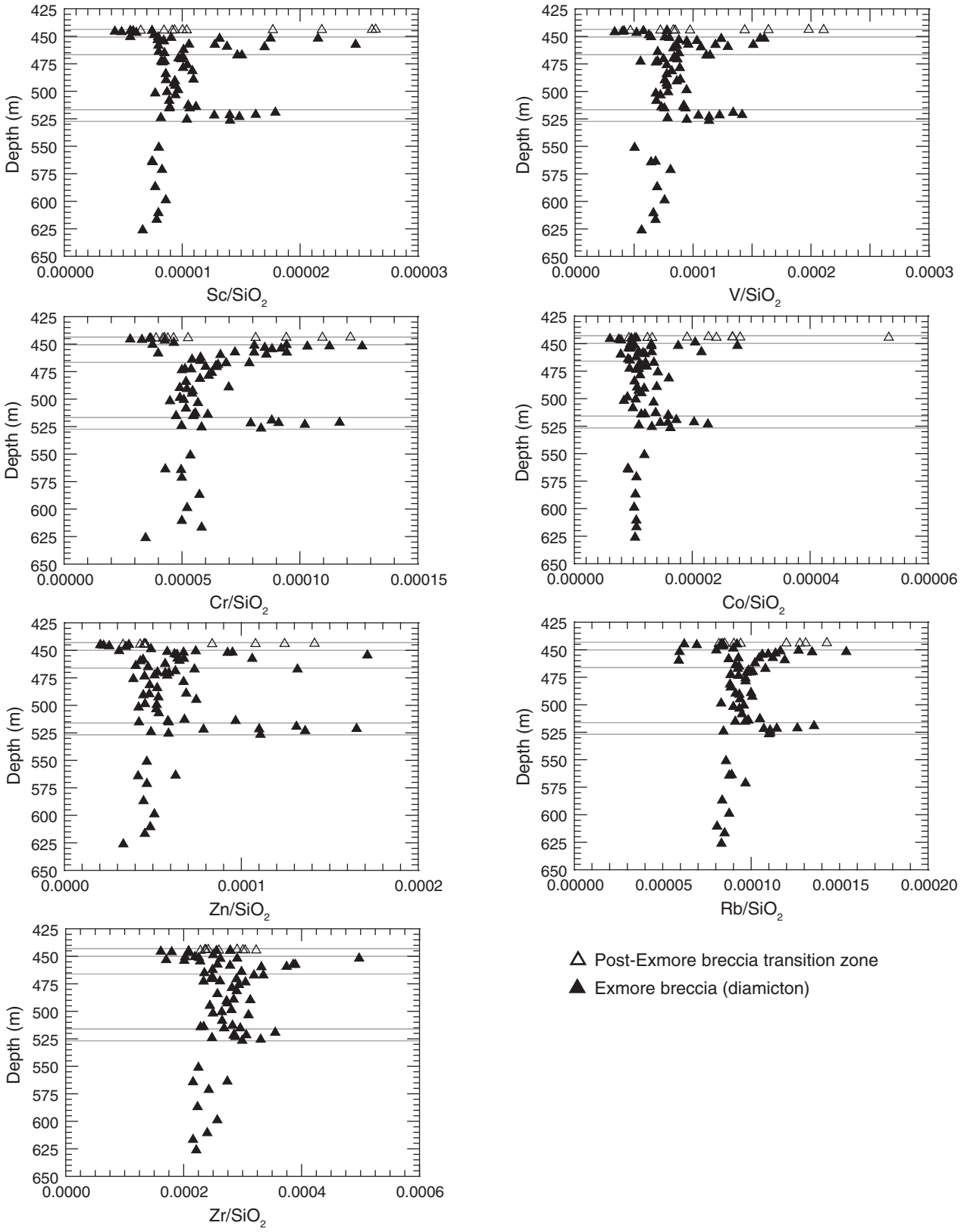

Figure 12 (*continued*).

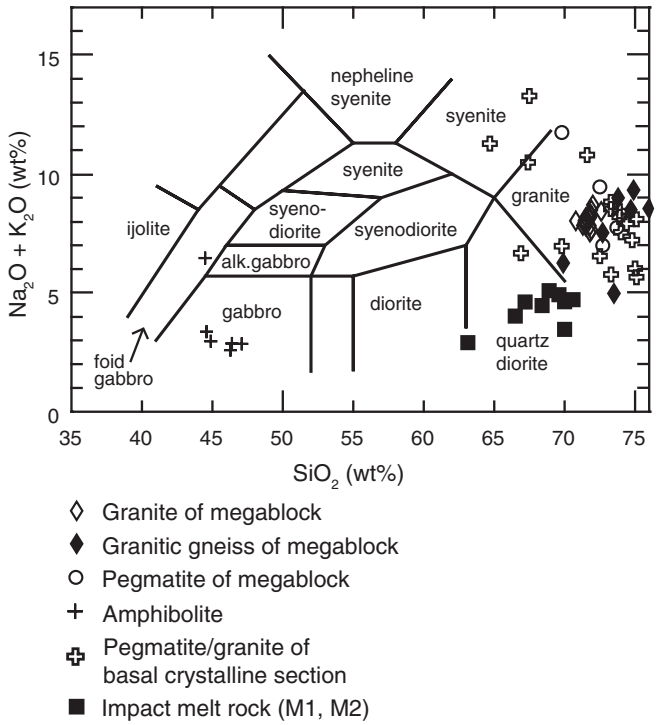

Figure 13. Total alkali-silica (TAS) plot after Cox et al. (1979). Most granite, granitic gneiss, and pegmatite samples from the megablock, and pegmatite and granite samples of the basal crystalline section plot into the granite field. Impact melt rocks generally have a quartz dioritic composition. The amphibolite data plot into the fields of gabbro and foid gabbro.

(1.14–2.45 wt%) are much higher than those for average pelites (0.6–0.7 wt%; Taylor and McLennan, 1985), also indicating an igneous precursor. In the Na_2O/K_2O versus Na_2O+K_2O discrimination diagram after Miyashiro (1975), the samples plot into the field of fresh basalt precursors (Fig. 15C). Based on the P_2O_5 versus Zr discrimination diagram (Winchester and Floyd, 1976), most amphibolite samples (except sample W-051) have tholeiitic character (Fig. 15D).

The REE patterns (Fig. 8) for the amphibolite samples are quite different from all other REE patterns of this sample suite. Compared to C1 chondrite composition, the REEs display only a slight enrichment by factors of ~15 for La and 5–7 for Yb. In contrast to all other investigated rocks, the amphibolites display only a minimal enrichment of light REEs compared to heavy REEs (average $La_N/Yb_N = 2.5$), and they show slightly positive Eu anomalies (average Eu/Eu* = 1.20) (Fig. 8).

Sandstone above and below the Amphibolite block. Three clastic sediment layers ("gravelly sand" of Horton et al., this volume; 1371.1–1376.4, 1389.7–1393.0, and 1396.4–1397.2 m depths, respectively) occur above and below the amphibolite block (1376.4–1389.7 m depth). All nine analyzed samples (Table A1) contain sand-sized particles and are, thus, classified as sandstone. Compositionally, the three layers can be grouped—based on these samples—into two different units. The two upper layers (1371.1–1376.4, 1389.7–1393.0 m depths, respectively) display similar chemical composition, suggesting that they represent the same unit. In contrast, the lower layer (1396.4–1397.2 m depth) is significantly different, displaying lower SiO_2 and higher

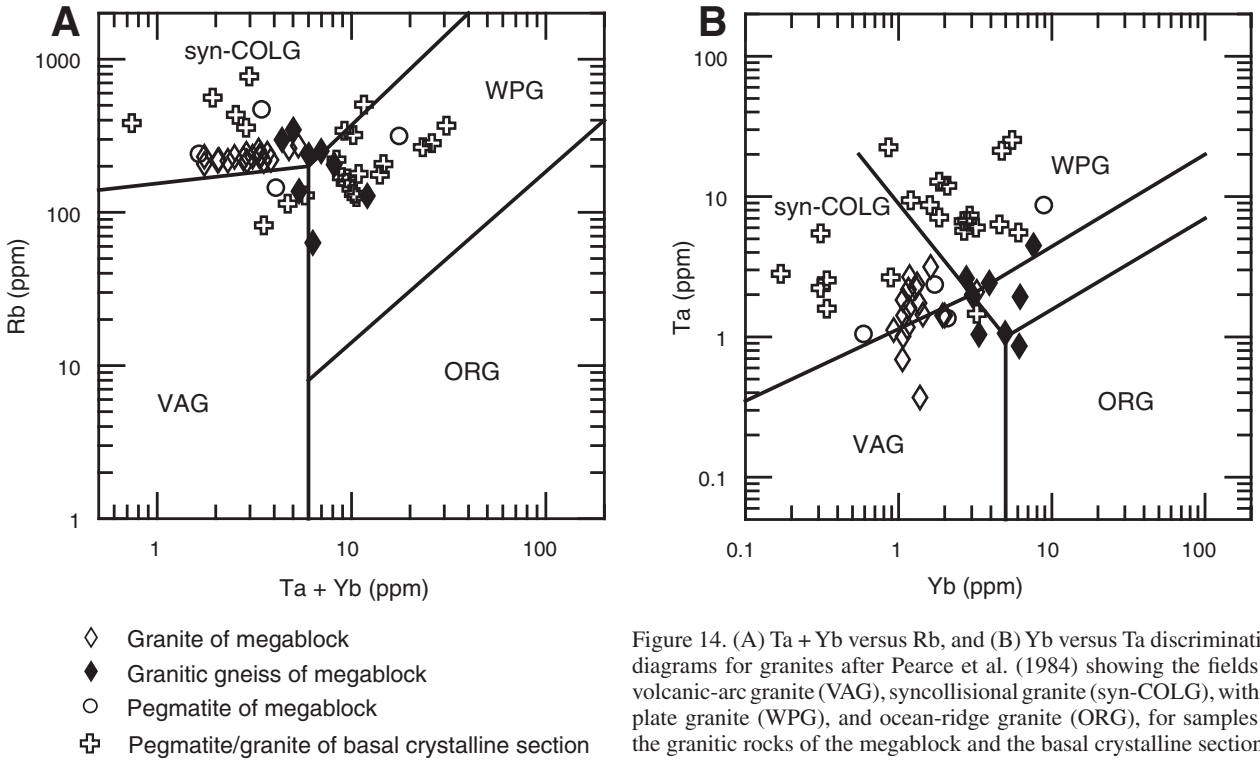

Figure 14. (A) Ta + Yb versus Rb, and (B) Yb versus Ta discrimination diagrams for granites after Pearce et al. (1984) showing the fields of volcanic-arc granite (VAG), syncollisional granite (syn-COLG), within-plate granite (WPG), and ocean-ridge granite (ORG), for samples of the granitic rocks of the megablock and the basal crystalline sections.

TiO_2, Al_2O_3, Fe_2O_3, MgO, Na_2O, P_2O_5, and Zr contents. The composition of the lower layer is relatively similar to the average chemical composition of Exmore breccia (Fig. 2; Table 2). The chemical composition of this lower layer can be modeled as a mixture of the average composition of the two upper layers and the upper suevite composition (Fig. 2; Tables 2 and 5). This is in agreement with petrographic observations that indicate an admixture of altered impact melt particles within this layer (Horton et al., 2008b, this volume; Reimold et al., this volume). In the classification diagram of Herron (1988), the samples from the upper layers (1371.1–1376.4 and 1389.7–1393.0 m depths, respectively) plot into the subarkose field, whereas the samples of the lowermost layer fall into the arkose field (Fig. 9). The two upper layers have a different chemical composition from that of the average Exmore breccia, with, for example, higher SiO_2, and lower TiO_2, Al_2O_3, Fe_2O_3, MgO, CaO, Na_2O, P_2O_5, V, Cr, Co, Sr, Zr, and REE contents (Figs. 2 and 5; Table 2). This composition corresponds well with that of sedimentary sandstone block samples from 622.1 (sample CB6-049), 904.6 (CB6-064), and 1073.4 m depths (CB6-071) (Fig. 5).

Impact Breccia Section (1397.2–1551.2 m)

Impactites (suevite, impact melt rock, polymict lithic impact breccia). Major- and trace-element contents in the suevite, impact melt rock, and polymict lithic impact breccia samples display substantial variation from sample to sample,

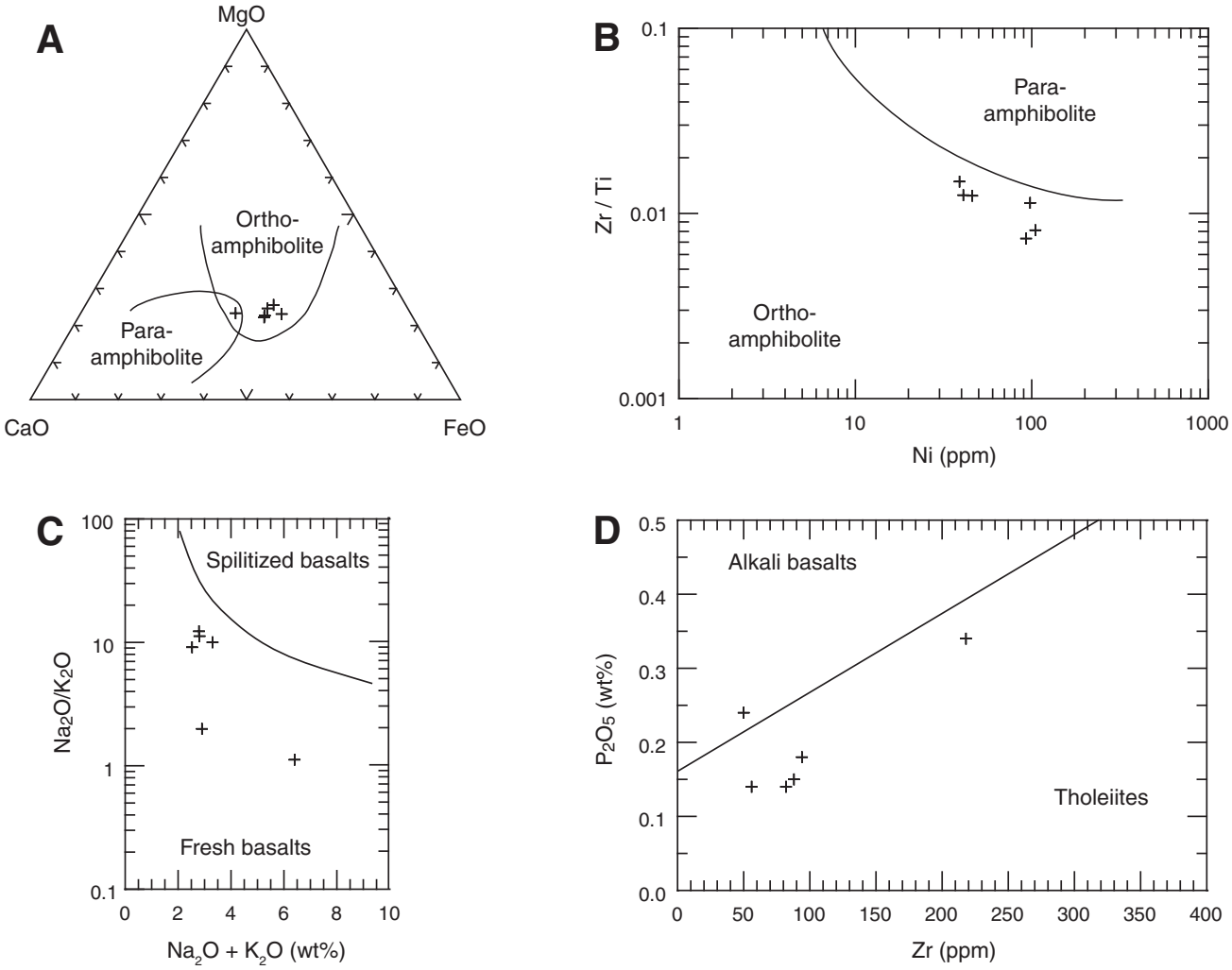

Figure 15. Discrimination diagrams for amphibolite. (A) Ternary CaO-MgO-FeO diagram (total Fe as FeO) after Walker et al. (1960) for the discrimination of ortho- and para-amphibolite precursors. Sample RG-003 plots into the field of ortho- *and* para-amphibolite precursors. (B) Ni versus Zr/Ti discrimination diagram after Winchester and Max (1982) for the discrimination of ortho- and para-amphibolite precursors using immobile elements. (C) Na_2O/K_2O versus $Na_2O + K_2O$ discrimination diagram after Miyashiro (1975) to discriminate between fresh and spilitized basalt precursors. Sample W-051 plots into the field of alkali basalts. (D) Zr versus P_2O_5 variation diagram after Winchester and Floyd (1976) for the discrimination between precursors of alkali basalt and tholeiite character.

but there are no significant differences in general composition between these three rock types (Figs. 3 and 6). Exceptions are Na_2O, which displays a slight enrichment at the top of this section (unit SU) and a distinct enrichment by a factor of ~2 between 1408 and 1450 m depth (units S3 and S2), in comparison to all other impactite samples, and K_2O, which shows an enrichment in the polymict lithic impact breccia unit P4 from 1480 to 1486 m (Figs. 3 and 6). The suevite samples were subdivided on the basis of their different Na_2O contents into two groups composed of the samples from the suevite units SU to S2, and from S1 to P (P1 to P4), respectively (unit names after Horton et al., this volume). The samples of polymict lithic impact breccia in units P1–P4 do not show differences in element abundances and chemical behavior in comparison to the suevite samples of this interval.

Negative correlations between SiO_2 and TiO_2, Al_2O_3, Fe_2O_3, MgO, P_2O_5, LOI, V, Cr, Co, Ni, and the total REE abundances are observed in the impactite samples; however, no correlations exist between SiO_2 and CaO, Na_2O, and K_2O (Fig. 6; Table A2). A significant carbonate content of the impactites based on a positive correlation of CaO and LOI is not recognized. Correlations between CaO, Na_2O, and K_2O were not observed for suevites of the units S1 to P (Fig. 16), whereas the suevites of units SU to S2 displayed a weak positive correlation of CaO and Na_2O contents (r = 0.62, Fig. 16). The average K_2O content of the impactites is 3.21 wt% (Table 4). This abundance is higher than the K_2O content of the average continental crust of 2.6 wt% (Wedepohl, 1995). This enrichment is believed not to be the result of postimpact hydrothermal alteration as observed in many impact craters (e.g., French et al., 1997; Reimold et al., 1994), but instead to be related to the generally high K_2O contents of the target rocks.

The Cr, Co, and Ni contents of the impactites are generally low and do not exceed the ranges for Cr, Co, and Ni contents in the crystalline rocks of the Chesapeake Bay target. The Cr/Co, Ni/Co and Ni/Cr ratios of the average impactite are 4.25, 2.13, and 0.50, respectively, and they are distinctly different from the respective chondritic ratios of 4.5–7.6, 19.4–21.1, and 4.5–7.6 (Wasson and Kallemeyn, 1988). While Lee et al. (2006) reported Ir concentrations below 0.5 ppb as a possible meteoritic

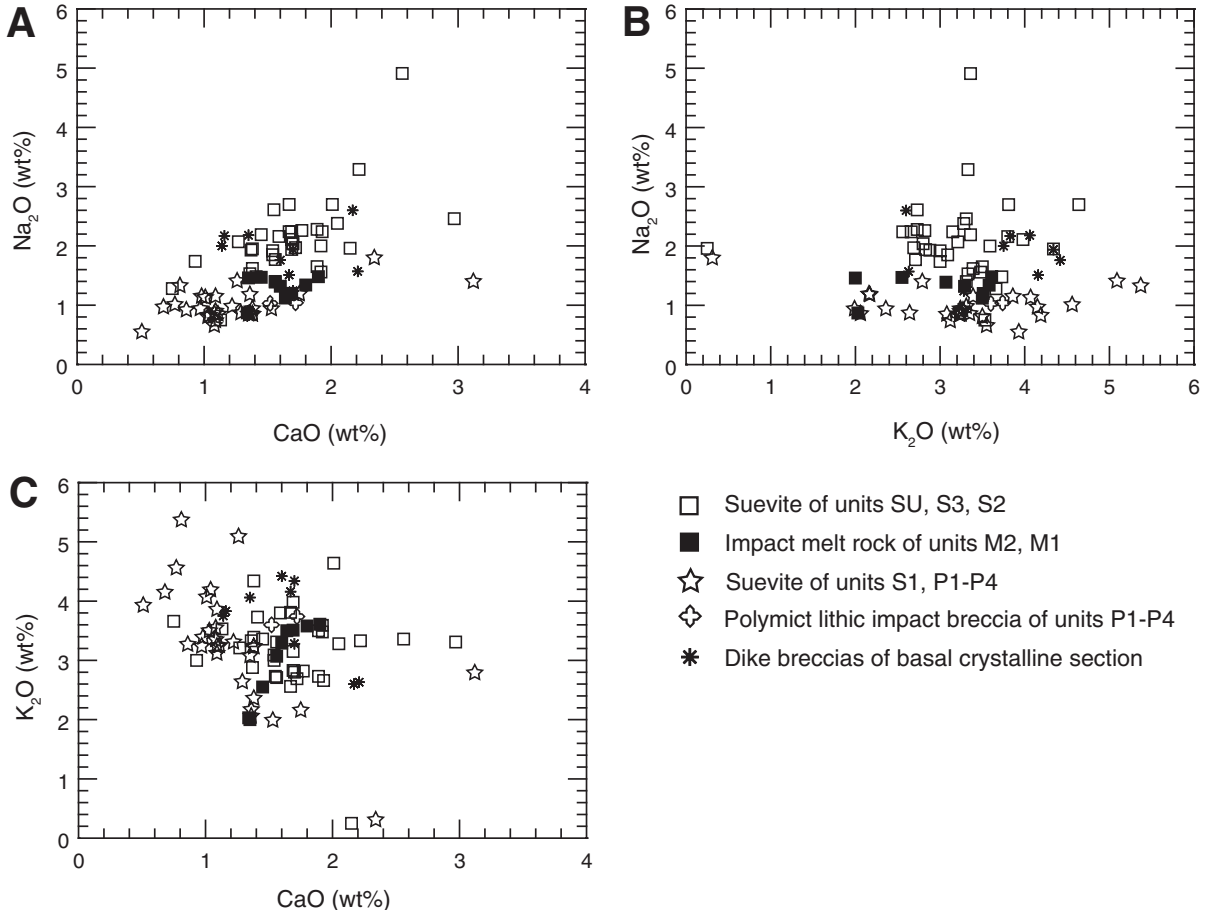

Figure 16. (A) CaO versus Na_2O, (B) K_2O versus Na_2O, and (C) CaO versus K_2O variation diagrams for the Eyreville impactites. Suevite is subdivided into two groups composed of samples from SU to S2 units, and from S1 to P (P1–P4), respectively (unit names after Horton et al., this volume). Note the positive correlation of CaO versus Na_2O, especially for suevite samples of the SU to S2 units, whereas K_2O versus Na_2O, and CaO versus K_2O do not show distinct correlations.

component in samples from the Sustainable Technology Park (STP) drill hole at Cape Charles, all Ir analyses by INAA for the Eyreville drill core samples were below the detection limit of ~2 ppb. Therefore, the presence of a chondritic component in these impactites is not indicated. This observation has been confirmed by high-resolution platinum group element analyses (McDonald et al., this volume).

The C1 chondrite-normalized REE distribution patterns for suevite/polymict lithic impact breccia and impact melt rock are shown in Figure 8. All three rock types have similar REE patterns, with a larger variability especially for the suevite/polymict lithic impact breccia. The REE data for suevite/polymict lithic impact breccia and impact melt rock indicate enrichment by factors of 60–160 and 90–140, respectively, for La, and 10–20 and 10–16, respectively, for Yb compared to the C1 chondrite composition. Light REEs are enriched over heavy REEs (La_N/Yb_N = 8.1, for average impactite). Both rock types display negative Eu anomalies (Eu/Eu* = 0.74 for average impactite). REE patterns for these impactites do not indicate significant differences relative to the REE patterns for schist of the basal crystalline section, cataclastic gneiss of the impact breccia section, and granitic gneiss of the megablock (Fig. 8). In comparison to the REE patterns of the Exmore breccia, the REE patterns of suevite/polymict lithic impact breccia and impact melt rock are similar in shape, but the samples have slightly higher REE abundances than those of the Exmore breccia.

The complete set of analyses for suevite, polymict lithic impact breccia, and impact melt rock does not display clear trends with depth (Fig. 3). However, the average compositions of the various impactite units (Table 5) indicate some distinct trends with depth (Fig. 17). The SiO_2 and CaO contents display a negative correlation with depth, whereas the TiO_2, Al_2O_3, Fe_2O_3, and MgO contents are positively correlated with depth (Fig. 16). The K_2O and P_2O_5 abundances do not show any correlation with depth, whereas the Na_2O content suggests a generally negative trend with depth, except for suevite units S3 and S2, which are relatively enriched by a factor of ~2 in Na_2O compared to suevite units S1 and P (Fig. 16). The chemical data indicate more of a gradual change of whole-rock composition with depth for the impact breccia section than any evidence for chemically distinguishable units. Petrographic observations on the impactites indicate a decrease of melt and matrix abundances with depth as well as changes in the clast population (Bartosova et al., this volume; Wittmann et al., this volume, Chapter 16). In the SU unit, the lithic clast components are mainly sedimentary and igneous rocks, in S3 and S2, they are metamorphic rocks, and in S1, they are sedimentary rocks, whereas in the polymict impact breccia unit P, metamorphic clasts dominate again. The chemical trends are the result of an increase with depth of a component that is characterized by significant TiO_2, Al_2O_3, Fe_2O_3, and MgO contents, and relatively lower values of SiO_2, CaO, and possibly Na_2O. This is most likely the result of an increasing proportion of basement schist, and a decrease of the abundances of sedimentary and/or granite/granitic gneiss components. The enrichment of Na_2O in suevite units S2 and S3, positively correlated with CaO (Fig. 15A), is most likely due a higher amount of a granitic component represented by granitic gneiss, granite, and/or pegmatite in these units.

The two impact melt rocks, M2 and M1 (Fernandes et al., 2008; Horton et al., this volume; Wittmann et al., this volume, Chapters 16 and 17), are significantly different from each other for the major elements, especially SiO_2, TiO_2, Al_2O_3, Fe_2O_3, MgO, and K_2O (Fig. 17; Table 6). In the TAS diagram (Cox et al., 1979), the impact melt rock samples generally have a quartz dioritic composition (Fig. 13).

Cataclastic gneiss. The cataclastic gneiss blocks (units B1 to B5; after Horton et al., this volume) in the impact breccia section are impactites (monomict impact breccia) per definition (Stöffler and Grieve, 2007). These rocks are discussed in this paper as a specific crystalline basement-derived lithology (see also Townsend et al., this volume). The cataclastic gneiss displays a wide range of chemical compositions (Figs. 3 and 7; Table 5). This gneiss has an average SiO_2 content of 66.3 wt% (59.5–71.2 wt%), which is intermediate to the schists of the basal crystalline section (average 56.7 wt%, 40.4–78.0 wt%) and the granitic gneiss of the megablock (average 74.0 wt%, 69.9–76.1 wt%).

The Harker diagrams (Fig. 7) display some chemical similarities between this cataclastic gneiss and the schists of the basal crystalline section; however, the chemical signature of this gneiss differs from that of the schists in its distinctly higher SiO_2 content, and it is completely different from that of the granitic gneiss of the megablock in terms of the relationship between SiO_2 and TiO_2, Fe_2O_3, MgO, Na_2O, and K_2O contents (Fig. 7). The protolith (magmatic or sedimentary) of this gneiss has yet to be resolved. In the TAS diagram (Cox et al., 1979), these gneiss samples plot into the quartz diorite field, whereas in the discrimination diagram of Herron (1988) for sedimentary precursors, these samples plot into the fields of Fe-shale, shale, and—mainly—graywacke. According to its SiO_2 content, the cataclastic gneiss could be classified as felsic gneiss. The chemical composition of this gneiss is similar to that of the average impactite (Tables 4 and 5), with the exception of the MgO and CaO contents, which are distinctly higher and lower in the cataclastic gneiss, respectively.

The C1 chondrite-normalized REE distribution patterns of the cataclastic gneiss samples are similar to those of the schists of the basal crystalline section (Fig. 8). The REEs show enrichment factors of 110–200 for La, and 15–21 for Yb compared to C1 chondrite composition. Light REEs are enriched over heavy REEs (average La_N/Yb_N = 7.6), and a negative Eu anomaly (average Eu/Eu* = 0.72) is present (Fig. 8).

Basal Crystalline Section (1551.2–1766.3 m)

Schist of the basal crystalline section. The schist samples of the basal crystalline section are chemically highly variable (Figs. 4 and 7; Table 6), corresponding to their great petrographic variability (see Townsend et al., this volume). Average SiO_2, Al_2O_3, and Fe_2O_3 contents are 56.7 wt% (40.4–78.0 wt%), 18.7 wt% (9.6–24.9 wt%), and 7.7 wt% (2.4–18.8 wt%),

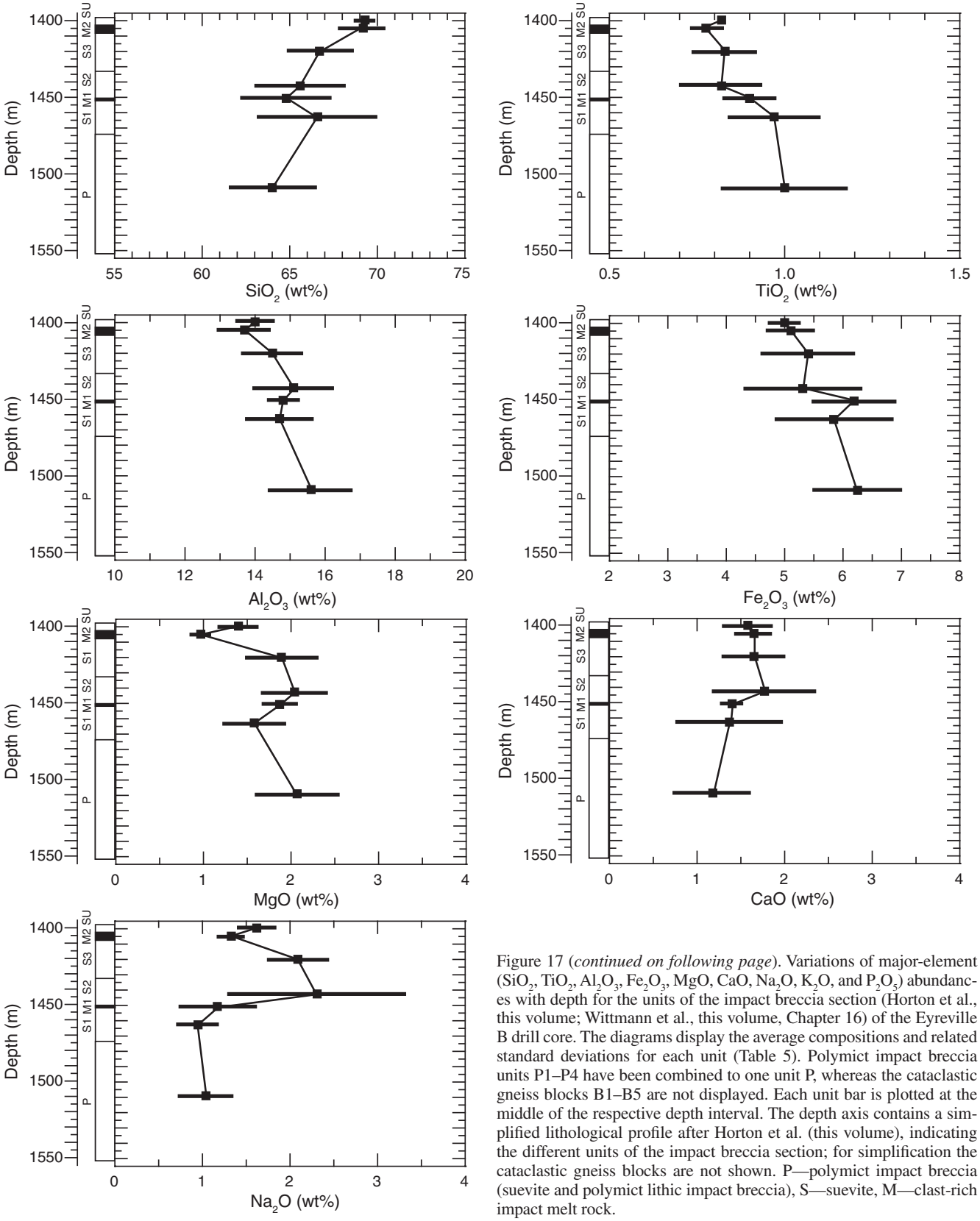

Figure 17 (*continued on following page*). Variations of major-element (SiO_2, TiO_2, Al_2O_3, Fe_2O_3, MgO, CaO, Na_2O, K_2O, and P_2O_5) abundances with depth for the units of the impact breccia section (Horton et al., this volume; Wittmann et al., this volume, Chapter 16) of the Eyreville B drill core. The diagrams display the average compositions and related standard deviations for each unit (Table 5). Polymict impact breccia units P1–P4 have been combined to one unit P, whereas the cataclastic gneiss blocks B1–B5 are not displayed. Each unit bar is plotted at the middle of the respective depth interval. The depth axis contains a simplified lithological profile after Horton et al. (this volume), indicating the different units of the impact breccia section; for simplification the cataclastic gneiss blocks are not shown. P—polymict impact breccia (suevite and polymict lithic impact breccia), S—suevite, M—clast-rich impact melt rock.

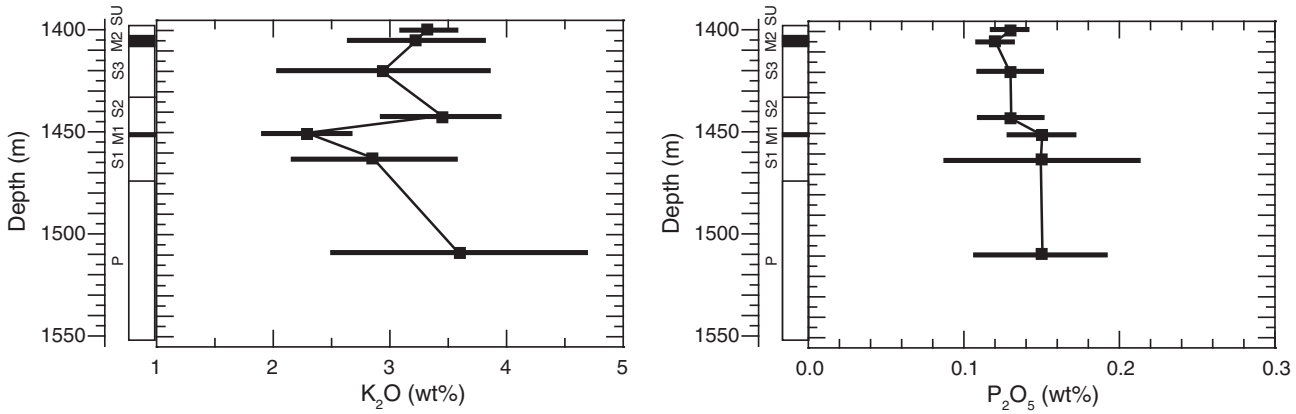

Figure 17 (*continued*).

respectively. The low SiO_2 contents of most schist samples indicate chemically a mafic to intermediate character, but there are a few samples (~8% of the samples) with a felsic character and high SiO_2 contents up to 78 wt%, which indicates the local presence of quartz-rich layers, which were also observed macroscopically. High LOI values (up to 10.7 wt%) are characteristic for graphite-rich schists. In the Harker diagrams (Fig. 7), the schists of the basal crystalline section show some similarity to the cataclastic gneiss of the impact breccia section; generally, they have lower SiO_2 and MgO, and higher Al_2O_3 and Fe_2O_3 contents in comparison to the cataclastic gneiss. Major and trace elements are not correlated with depth. Negative correlation trends are observed between the SiO_2 content and the contents of TiO_2, Al_2O_3, Fe_2O_3, Cr, Co, and Rb (Fig. 7; Table A2). In contrast, the abundances of MgO, CaO, Na_2O, K_2O, and P_2O_5 are not significantly correlated with SiO_2, or with each other (Fig. 7; Table A2). The schists of the basal crystalline section are most likely of the para type (pelitic protolith); the samples plot in the discrimination diagram for sedimentary precursors (Herron, 1988) into the fields for shale and Fe-shale (Fig. 9).

C1 chondrite-normalized REE distribution patterns for schist samples from the basal crystalline section display enrichment factors of 30–200 for La, and 6–30 for Yb compared to C1 chondrite composition (Fig. 8). The light REEs are enriched over heavy REEs (average $La_N/Yb_N = 8.0$), and a negative Eu anomaly (average Eu/Eu* = 0.71) occurs for all samples (Fig. 8). The REE patterns of the cataclastic gneiss samples of the impact breccia section plot within the range of REE patterns for the schist of the basal crystalline section (Fig. 8).

Pegmatite and granite of the basal crystalline section. Pegmatite and granite samples of the basal crystalline section plot in the TAS diagram (Cox et al., 1979) mainly into the granite field (Fig. 13). Samples plotting into the syenite or quartz diorite fields are coarse-grained, petrographically inhomogeneous pegmatites. In contrast to granite and granitic gneiss of the megablock, pegmatite and granite of the basal crystalline section include many samples with Na_2O contents that are higher than the respective K_2O contents. With the exception of Rb, the trace-element abundances are generally low in comparison with the granite and granitic gneiss of the megablock (Tables 3 and 6).

Alumina saturation index (A/CNK = Al_2O_3/[CaO +Na_2O + K_2O], mole proportions) values for the pegmatites and granites of the basal crystalline section are highly variable (average 1.1, 0.7–1.8). Based on the Rb versus Yb + Ta and Yb versus Ta discrimination diagrams (Pearce et al., 1984), the pegmatites and granites from the basal crystalline section plot into the fields for syncollisional, within-plate and volcanic-arc granites, similar to the granitic gneiss and pegmatites of the megablock (Fig. 14). However, most of the analyzed samples are pegmatites, and, therefore, these discrimination diagrams may not be directly applicable owing to the possibility of inhomogeneous whole-rock compositions or differentiation processes during pegmatite formation.

The REE patterns of the pegmatite and granite samples of the basal crystalline section are also very variable, similar to those for the pegmatites of the megablock (Fig. 8). Most of the samples show REE enrichment by factors up to 100 for La, and up to 20 for Yb, compared to C1 chondrite composition, and they display distinct negative Eu anomalies. Enrichment of light REEs over heavy REEs is much less than for granite and granitic gneiss of the megablock, cataclastic gneiss of the impact breccia section, and schist of the basal crystalline section. Eight samples (CB6-136, W-123a, W-127a, W-128, CB6-144, W-136a, CB6-148, W-142) display different patterns with only slight enrichments of REE or depletion of some REE elements in comparison with C1 chondrite composition (factor 0.9–4 for La, and 0.4–1.5 for Yb). These samples display only very slight enrichment of light REEs over heavy REEs and are characterized by slightly positive Eu anomalies.

Epidosite of the basal crystalline section. The occurrence of epidosite is limited to a hydrothermally altered zone of the basal crystalline section between 1643.9 and 1655.1 m depth (Fig. 4; Horton et al., this volume; Townsend et al., this volume). The epidosite, not surprisingly, shows the highest CaO (average 21.5 wt%, 14.3–25.6 wt%) and the lowest Na_2O (average 0.20, 0.11–0.37 wt%) and K_2O (average 0.14 wt%, 0.04–0.23 wt%) contents of all analyzed crystalline basement-derived

rocks. Townsend et al. (this volume) relate this rock to metamorphism of an original marl protolith, but involving a hydrothermal component.

Impact-related dikes of the basal crystalline section. Impact-related breccia dikes occur locally within the basal crystalline section (Reimold et al., 2007; Horton et al., this volume). Most of these dikes are too thin for whole-rock chemical analysis. We analyzed a polymict lithic breccia dike (depth ~1555.6 m, W-113a), suevitic dikes (1603.3–1604.3 m, CB6-138, W-121; and 1607.0–1609.5 m, W2-24), and cataclastic breccia dikes (~1607.9 m, W-123b; ~1609.5 m, CB6-139, W-124; ~1611.0 m, W-125b; and 1661.2 m, W-136b). In the Harker diagrams, the samples W-113a (polymict lithic breccia dike) and W2-24 (suevitic dike) are similar to suevite, impact melt rock, and polymict lithic impact breccia (Fig. 6). In contrast, the other seven samples from suevitic and cataclastic dikes show distinctly different behavior, especially with regard to SiO_2 and MgO contents, in comparison to the suevite, impact melt rock, and polymict lithic impact breccia (Fig. 6). In the SiO_2 versus $Al_2O_3 + Fe_2O_3 +$ MgO diagram (Fig. 18A), the dike breccia samples are arranged, together with the impactite (suevite, impact melt rock, and polymict lithic impact breccia) data, on a mixing line between SiO_2-rich and Al_2O_3+Fe_2O_3+MgO–rich end members, but they show larger variability with respect to both end members than the impactites. Although in the ternary Fe_2O_3 + MgO–CaO + Na_2O–K_2O diagram (Fig. 18B) most of the dike breccias plot into the field of the impactites, mixing trends between schist/felsic gneiss and granite/granitic gneiss/pegmatite components for the dike breccias are obvious. The dike breccia samples analyzed here occur mainly in pegmatite or at pegmatite-schist interfaces. Therefore, the individual dike breccia compositions are seemingly influenced, or in some samples dominated, by locally derived material from the host rock(s). This conclusion is strongly supported by our petrographic observations, which show a large proportion of locally derived clastic material within impact breccia dikes (Reimold et al., 2007).

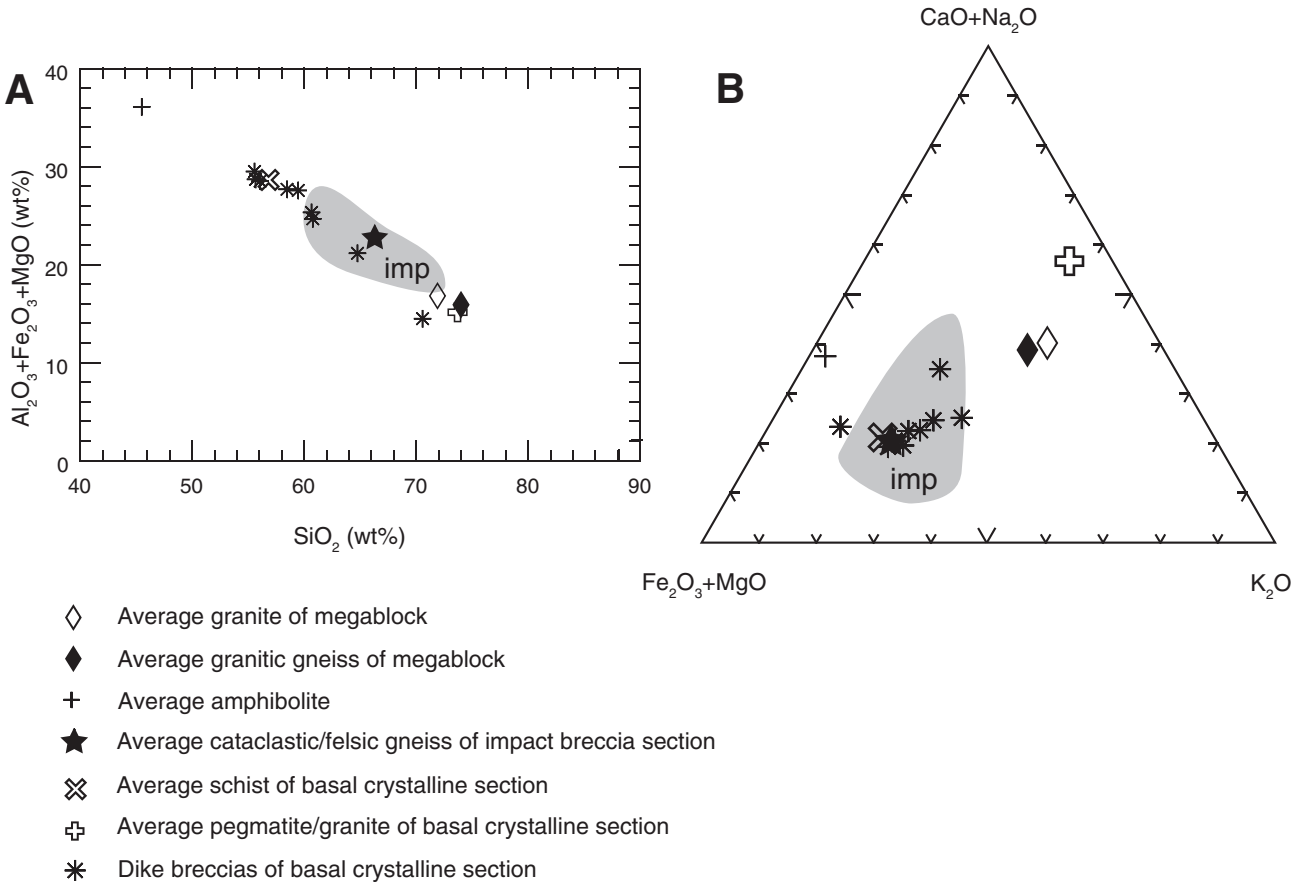

Figure 18. (A) SiO_2 versus $Al_2O_3 + Fe_2O_3 +$ MgO variation diagram and (B) ternary Fe_2O_3 + MgO–CaO + Na_2O–K_2O plot for the impact-related dike breccias of the basal crystalline section. For comparison, both diagrams show the field of impactites (suevite, impact melt rock, polymict lithic impact breccia; imp—dark gray), and the average contents of the major crystalline target components, namely, granite and granitic gneiss of the megablock (Table 3), amphibolite (Table 3), cataclastic/felsic gneiss (Table 5), and schist and pegmatite/granite of the basal crystalline section (Table 6). Samples W-073 and CB6-121 were not used in the Fe_2O_3 + MgO–CaO + Na_2O–K_2O ternary plot for the field of impactites due to their extremely low K_2O contents in comparison to all other impactite samples.

Comparison of Eyreville Drill Core Results with Previously Studied Crystalline Basement Rocks

In the past, a felsite clast from the Exmore breccia and a monzogranite from the crystalline basement of the USGS-NASA Langley drill core were chemically investigated (Horton et al., 2004; Horton and Izett, 2005). Equivalent samples are not contained in our suite of crystalline rocks from the Eyreville cores.

Monzogranite NL2083.1 ("Langley Granite") from the USGS-NASA Langley drill core (Horton et al., 2004; Horton and Izett, 2005) displays a chemical composition similar to those of the granite and granitic gneiss of the megablock of the Eyreville drill core. Based on the Rb versus Yb + Ta and Ta versus Yb discrimination diagrams (Pearce et al., 1984), and the REE patterns, this monzogranite shows more similarities to the granitic gneiss than to the granite of the Eyreville megablock. The radiometric age of this monzogranite is 612 ± 10 Ma (Horton et al., 2004), which corresponds well to the radiometric age of the granitic gneiss of the Eyreville megablock of 615 ± 7 Ma (Horton et al., 2007, this volume). Although the monzogranite is not foliated, the chemical and radiometric data indicate that the Langley monzogranite and the granitic gneiss of the Eyreville megablock could represent a specific component of the crystalline target of the Chesapeake Bay crater.

Components of the Chesapeake Bay Target

Crystalline Basement-Derived Components of the Chesapeake Bay Target

The lithological profile of the Eyreville drill cores (Horton et al., this volume) is made up of ~540 m of crystalline rocks in the lithic block (granite, granitic gneiss, amphibolite), impact breccia (cataclastic gneiss), and basal crystalline (schist, pegmatite/granite) sections. The mafic schist (xenoliths in the megablock) and epidosite portions were not considered for this estimation of the Chesapeake Bay target composition because their proportions in the target cannot be estimated from a single drill core intersection. Calculated on the basis of integrated drill core segments, the crystalline target rocks at Eyreville consist of 34.8 vol% granite (megablock; average composition in Table 3), 21.3 vol% basement schist (basal crystalline section; average composition in Table 6), 17.3 vol% granitic gneiss (megablock; average composition in Table 3), 16.5 vol% pegmatite/granite (basal crystalline section; average composition in Table 6), 7.6 vol% felsic gneiss (impact breccia section; average composition in Table 5), and 2.5 vol% amphibolite (average composition in Table 3). The granitic component of ~69 vol% based on the integrated crystalline drill core segments is thus the dominant part of the basement in the Chesapeake Bay area. An average chemical composition of the crystalline basement based on the proportions of crystalline target rocks in the Eyreville drill core was not calculated here, as the clast population of the impactites displays completely different proportions of metamorphic and igneous rocks (Bartosova et al., this volume; Wittmann et al., this volume, Chapter 16). This indicates that the distribution of the crystalline rocks as observed in the Eyreville drilling may not be representative for the whole Chesapeake Bay basement, and the crystalline rocks in the basement may be strongly variable in terms of lateral and vertical extension.

Sedimentary Components of the Chesapeake Bay Target

Sedimentary target rocks occur in the Eyreville cores mainly as sedimentary blocks in the Exmore bed section. Since this work is mainly focused on the impactites and crystalline target rocks, only very limited petrographic and chemical investigation of these sediments has been carried out. The lack of detail (e.g., micropaleontological information) does not allow us to identify from which of the many different pre-impact sedimentary formations (e.g., Poag et al., 2004) the blocks are derived. The small number of available chemical analyses may not be representative for the various pre-impact sedimentary rocks. Therefore, we have not calculated an average composition for them. Chemical compositions of several clearly identified sedimentary target rocks (from cores adjacent to the crater) have been presented in the past, e.g., by Poag et al. (2004) and Deutsch and Koeberl (2006). In order to be able to compare the full range of compositions of sedimentary target rocks, we plotted a field of their respective analytical data, with which the ranges of compositions of impact-generated rocks are compared (Figs. 19–21). The sedimentary target rocks are characterized by great petrographic variability (Edwards et al., this volume), and, accordingly, their chemical compositions are highly diverse (e.g., Figs. 1 and 5). Therefore, there is a wide overlap of the chemical compositions of the pre-impact sedimentary rocks and granitic and metamorphic rocks, with the exception of the pegmatite/granite of the basal crystalline section, and the amphibolite, which is, however, only a minor crystalline target component in the Eyreville core (Figs. 19–21). These diagrams also illustrate that the sedimentary target includes—in addition to the already mentioned crystalline basement components—at least two more important components that must be taken into consideration for further studies. One of these components is rich in SiO_2, most likely of quartz sandstone origin, whereas the other component is rich in Al_2O_3, Fe_2O_3, and MgO, which is most likely indicative of a clay/claystone component (see Figs. 19–21).

Composition of Exmore Breccia

Poag et al. (2004) calculated an average composition for the Exmore breccia based on ~40 samples from three drill cores. In this study, we calculated an average composition of the Exmore breccia based on the Eyreville drill core samples (Table 2). We used only the samples designated diamicton, and we excluded all clay-rich fragments and larger clasts within individual samples, and sedimentary blocks of the Exmore bed section. Our average Exmore breccia is distinctly different from that of Poag et al. (2004), which was much lower in SiO_2 and Na_2O, and higher in Fe_2O_3, MgO, CaO, K_2O, P_2O_5, and LOI contents (Table 2). The

average Exmore breccia of Poag et al. (2004) contains most likely carbonate and clay components, which are not apparent in the average Exmore breccia composition calculated here. This finding is indicative of regional variations in the composition of the Exmore breccia. Nevertheless, an unambiguous definition of the Exmore breccia sensu stricto (see discussion about nomenclature in, e.g., Horton et al., 2008a; Reimold et al., this volume) is necessary to avoid differences, which are only the result of variable sample sets used in calculation, e.g., diamicton samples without clay and/or clast components, diamicton samples with clay and/or clast components, and Exmore bed samples composed of diamicton and all sedimentary clasts and blocks, respectively.

The variation diagrams (Figs. 19A, 20A, and 21A) show that the Eyreville core–based composition of Exmore breccia is presumably a mixture of all major crystalline and sedimentary target components as expected for an avalanche and resurge deposit of impact breccias (Poag et al., 2004, and references therein; Powars et al., 2008). There is only a partial overlap between the composition of Exmore breccia and sedimentary target rocks (Figs. 19A, 20A, and 21A). In the SiO_2 versus Al_2O_3 + Fe_2O_3 + MgO diagram (Fig. 19A), the Exmore breccia data are—in the range from ~66 to 85 wt% SiO_2—negatively correlated, which is matched well by the data for the sedimentary and crystalline target rocks. At lower SiO_2 contents—in the range from 60 to 66 wt% SiO_2—Exmore breccia shows a positive correlation, which is opposite to the trend for the sedimentary and crystalline target rocks. This is caused by the presence of a CaO- and P_2O_5-rich component, most likely apatite, in the Exmore breccia samples (Figs. 1, 10, and 12). This is also illustrated in the ternary Fe_2O_3 + MgO–CaO + Na_2O–K_2O plot (Fig. 20A), which shows an extension of the Exmore breccia field in the direction of the CaO + Na_2O end member. In the analyzed crystalline target rocks of the Eyreville drilling, only the xenoliths of the megablock and the epidosite of the basal crystalline section

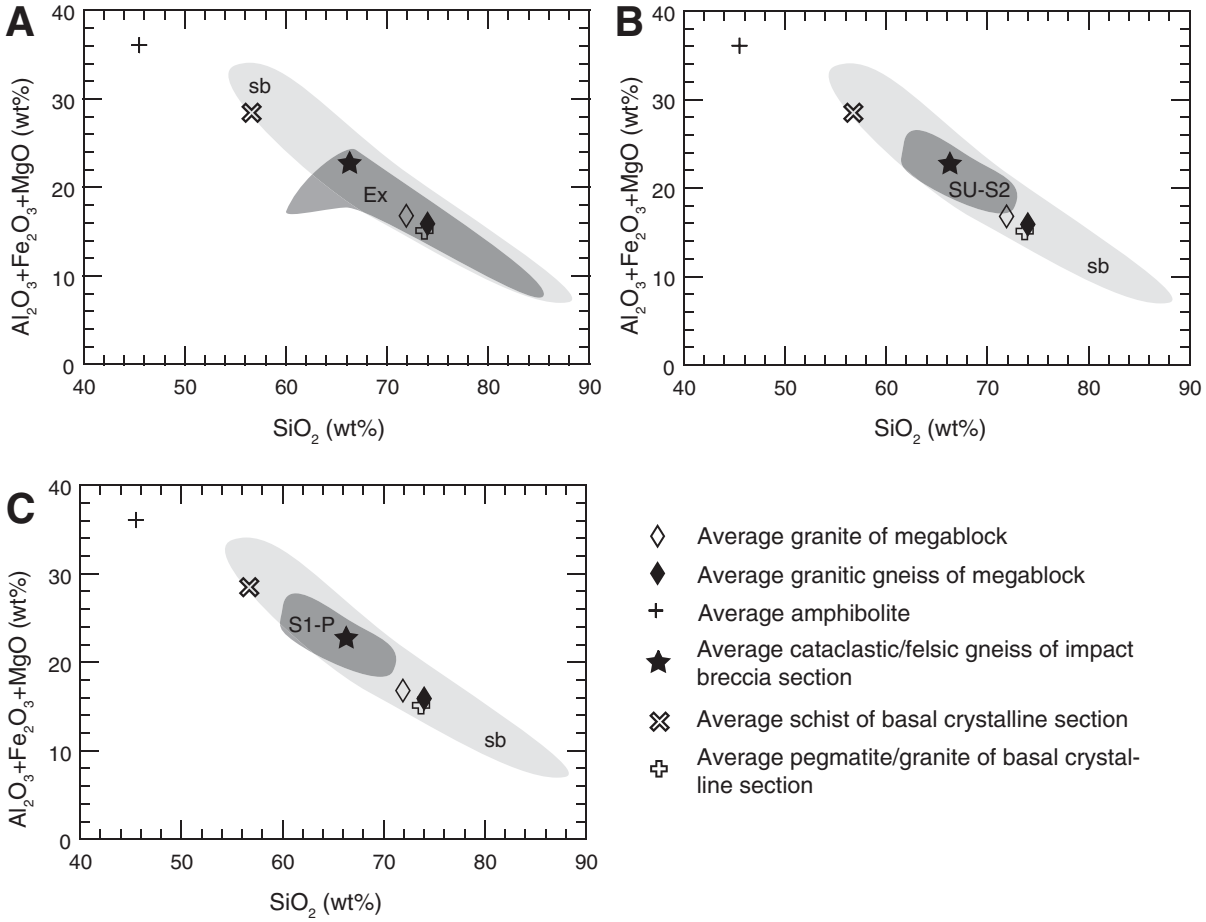

Figure 19. SiO_2 versus Al_2O_3 + Fe_2O_3 + MgO variation diagrams for (A) Exmore breccia (diamicton, Ex—dark gray), (B) suevite and impact melt rock from the SU to S2 units (SU-S2—dark gray), and (C) suevite and polymict lithic impact breccia from the S1 to P units (S1-P—dark gray). For comparison, the diagrams also show the compositional field for sedimentary blocks in the Exmore beds (sb—light gray), and the average contents of the major crystalline target components—granite and granitic gneiss of the megablock (Table 3), amphibolite (Table 3), cataclastic/felsic gneiss (Table 5), and schist and pegmatite/granite of the basal crystalline section (Table 6). Unit names for the impact breccia section are after Horton et al. (this volume).

have such high P_2O_5 contents, which are necessary for this CaO- and P_2O_5-rich component. Nevertheless, a postimpact sedimentary origin of this CaO- and P_2O_5-rich component must be considered. In comparison to the impactites, the Exmore breccia has a distinctly higher content of granite and/or granitic gneiss components and additionally a SiO_2-rich component (Fig. 19A), most likely of sedimentary origin. The importance of these SiO_2-rich components is also clearly visible in the Sc–Co–Zr/10 plot, which shows an extension of the Exmore breccia field in the direction of granite and granitic gneiss (Fig. 21A).

Composition of Impactites

Suevite and impact melt rock of the SU to S2 units and suevite and polymict lithic impact breccia from the S1 to P (P1 to P4) units display nearly identical fields in the SiO_2 versus Al_2O_3

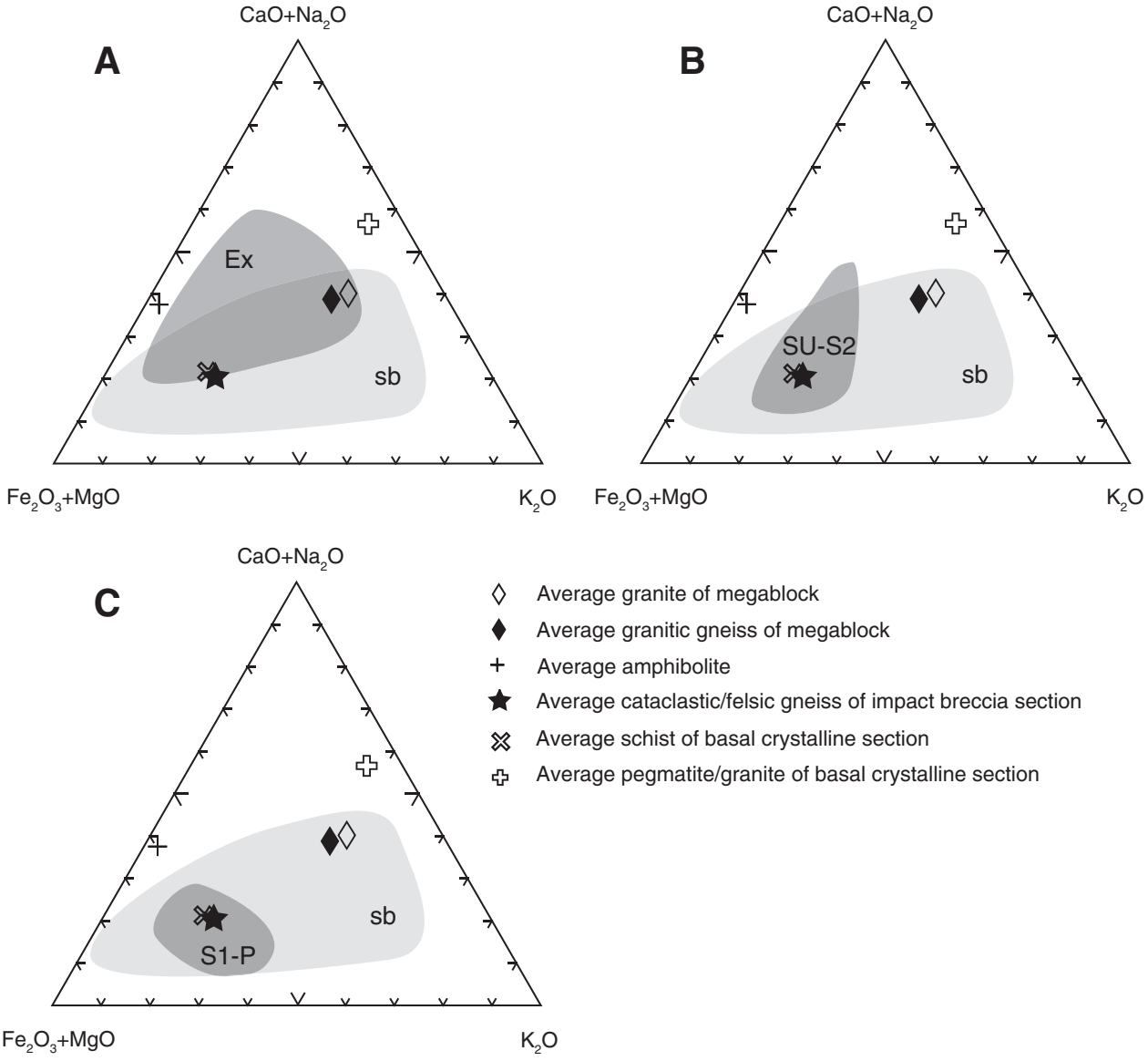

Figure 20. Fe_2O_3 + MgO–CaO + Na_2O–K_2O ternary plots for (A) Exmore breccia (diamicton, Ex—dark gray), (B) suevite and impact melt rock from the SU to S2 units (SU-S2—dark gray), and (C) suevite and polymict lithic impact breccia from the S1 to P units (S1-P—dark gray). Samples W-073 and CB6-121 were not used in these plots for the fields of SU-S2 and S1-P, respectively, due to their extremely low K_2O contents in comparison to all other impactite samples. For comparison, the ternary plots also show the compositional field for sedimentary blocks from the Exmore beds (sb—light gray), and the average contents of the major crystalline target components—granite and granitic gneiss of the megablock (Table 3), amphibolite (Table 3), cataclastic/felsic gneiss (Table 5), and schist and pegmatite/granite of the basal crystalline section (Table 6). Unit names for the impact breccia section are after Horton et al. (this volume).

+ Fe_2O_3 + MgO variation diagram (Figs. 19B and 19C) and in the ternary Sc–Co–Zr/10 plot (Figs. 21B and 21C). However, in the Fe_2O_3 + MgO–CaO + Na_2O–K_2O ternary plot (Figs. 20B and 20C), the field for suevite and impact melt rock from SU to S2 units is significantly extended in the direction of the CaO + Na_2O end member. This gives a first indication for admixture of a granite, granitic gneiss, or pegmatite component to these suevites and impact melt rocks. The fields for both impactite groups are centered in all these diagrams on the field for sedimentary target rocks (Figs. 19–21). This is solely a result of the wide range of chemical composition of the sedimentary target rocks. In contrast, the petrographic investigation of the impactites shows that most clasts in the cores were derived from the crystalline target (Bartosova et al., this volume; Wittmann et al., this volume, Chapter 16). This observation must be taken into consideration for the interpretation of the chemical data. Based on the SiO_2 versus Al_2O_3 + Fe_2O_3 + MgO variation diagram and the Fe_2O_3 + MgO–CaO + Na_2O–K_2O and Sc–Co–Zr/10 ternary plots (Figs. 19B, 19C, 20B, 20C, 21B, and 21C), the composition of both impactite groups (SU to S1, and S1 to P, respectively)

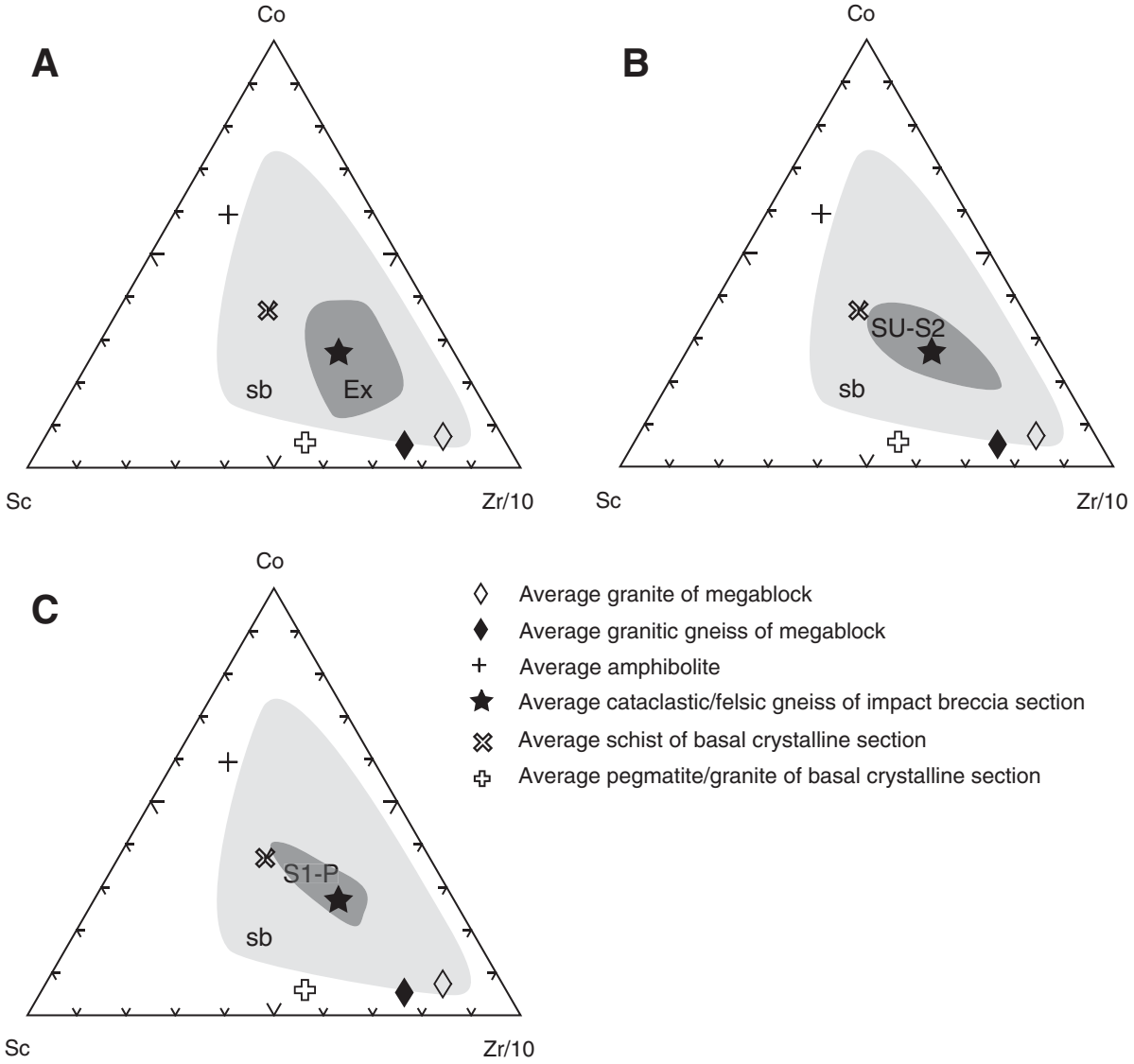

Figure 21. Sc-Co-Zr/10 ternary plots for (A) Exmore breccia (diamicton, Ex—dark gray), (B) suevite and impact melt rock from the SU to S2 units (SU-S2—dark gray), and (C) suevite and polymict lithic impact breccia from the S1 to P units (S1-P—dark gray). For comparison, the ternary plots also show the compositional field for sedimentary blocks from the Exmore beds (sb—light gray), and the average contents of the major crystalline target components—granite and granitic gneiss of the megablock (Table 3), amphibolite (Table 3), cataclastic/felsic gneiss (Table 5), and schist and pegmatite/granite of the basal crystalline section (Table 6). Unit names for the impact breccia section are after Horton et al. (this volume).

is very similar to that of the felsic gneiss occurring within the impact breccia section. The Sc–Co–Zr/10 trace-element ternary plot (Figs. 21B and 21C) shows that both impactite groups can be regarded as a mixture of basement schist with granite and/or granitic gneiss components. The proportion of the granite and/or granitic gneiss component is much higher for the suevite and impact melt rock of the SU to S2 units than for the suevite and polymict lithic impact breccia of the S1 to P units. This is in good agreement with the petrographic observations, which show a dominant metamorphic rock (schist) component in the lower part of the impact breccia section (Bartosova et al., this volume; Wittmann et al., this volume, Chapter 16).

CONCLUSIONS

This work presents chemical analyses of 318 samples from the Eyreville A and B drill cores, with a focus on the Exmore breccia (diamicton), impactites (suevite, impact melt rock, polymict lithic impact breccia), and crystalline basement-derived lithologies. Average chemical compositions were calculated for the first time for six major crystalline target components: granite (Table 3), pegmatite (Table 6), granitic gneiss (Table 3), felsic gneiss (Table 5), basement schist (Table 6), and amphibolite (Table 3). Averages are also given for the impactite calculated from all suevite, polymict lithic impact breccia, and impact melt rock samples (Table 4), and the subunits of the impact breccia section (Table 5), and the diamicton-type Exmore breccia (Table 2).

The Exmore breccia is subdivided, based on chemical observations, into five units: (1) 444.9–450.7 m, (2) 450.7–468 m, (3) 468–518 m, (4) 518–528 m, and (5) 528–864 m depth. Units 2 and 4 display distinctly lower $SiO_2/(Al_2O_3 + Fe_2O_3 + MgO)$ ratios compared to the other units. Both units show a characteristic enrichment in the TiO_2, MgO, Sc, V, Cr, and Zn contents compared to the other units, whereas P_2O_5 is distinctly enriched and strongly correlated with the CaO content at the top of unit 2, possibly due to the presence of apatite. Variation diagrams (Figs. 19–21) indicate that the Exmore breccia is most likely a mixture of all sedimentary and crystalline target components. Besides basement schist, granite, and/or granitic gneiss components, the Exmore breccia contains a significant amount of a SiO_2-rich target component of possibly sedimentary origin (e.g., quartz sandstone), which is not recognized in the compositions of the impactites.

The clastic sediment layers ("gravelly sand" of Horton et al., this volume; 1371.1–1376.4, 1389.7–1393.0 m depth) in the lithic block section have a different chemical composition from that of the average Exmore breccia (Table 2), and they correspond chemically to distinct sedimentary sandstone blocks analyzed at depths of 622.1, 904.6, and 1073.4 m, respectively.

The chemical compositions of suevite, impact melt rock, and polymict lithic impact breccia are similar and overlap with the field of Exmore breccia compositions (cf., e.g., Figs. 6 and 19–21). All impactites are mixtures of the different sedimentary and crystalline target rocks. The impactites of the impact breccia section display a generally negative correlation of the contents of SiO_2 and CaO with depth, whereas TiO_2, Al_2O_3, Fe_2O_3, and MgO abundances are positively correlated with depth (Fig. 17). This could well be a result of increasing basement schist and decreasing sedimentary and granite/granitic gneiss components with depth. The Na_2O content shows a distinct enrichment in the S3 and S2 suevite units (1407.5–1450.2 m, Figs. 3 and 17) compared to the other suevite units, which could be caused by a higher granitic component within these units (see Figs. 20B, 20C, 21B, and 21C).

Further studies are necessary to comprehensively determine the chemical compositions of all sedimentary and crystalline components of the Chesapeake Bay target, as a proper basis for mixing calculations to further constrain the generation of the impactites and the Exmore breccia. Especially representative average chemical compositions of sedimentary target rocks are still missing, which should come preferably from drill cores from outside of the crater. These data are also necessary to investigate the source rocks of the North American tektites (bediasites and georgiaites), and to determine the precursors of variable impact melt compositions (e.g., Wittmann et al., this volume, Chapter 17) observed in the melt-bearing impactites of the Chesapeake Bay crater.

ACKNOWLEDGMENTS

The drilling at Eyreville was supported by the International Continental Scientific Drilling Program (ICDP), the U.S. Geological Survey (USGS), and the National Aeronautics and Space Administration (NASA). The help of J.W. Horton Jr. and the staff at the USGS National Center, Reston, during the sampling process is much appreciated. We thank Kathrin Krahn and Hans-Rudolf Knöfler (Museum of Natural History, Berlin) for extensive technical support. We appreciate the help of H. Böck, M. Villa, and M. Bichler (Atominstitut Vienna) with the irradiations. We thank Sharon Farrell-Turner (University of the Witwatersrand, Johannesburg) for additional X-ray fluorescence (XRF) analyses, and B. Dressler and I. McDonald for constructive reviews that significantly improved this paper. This work was supported by the Austrian Science Foundation FWF, project P18862-N10 (to Koeberl), and a South African National Research Foundation grant (GUN2074407, to Gibson and Reimold). This is Lunar and Planetary Institute contribution 1414.

REFERENCES CITED

Bartosova, K., Mader, D., Schmitt, R.T., Ferrière, L., Koeberl, C., Reimold, W.U., and Brandstätter, F., 2009, this volume, Geochemistry of the impact breccia section (1397–1551 m depth) of the Eyreville drill core, Chesapeake Bay impact structure, USA, *in* Gohn, G.S., Koeberl, C., Miller, K.G., and Reimold, W.U., eds., The ICDP-USGS Deep Drilling Project in the Chesapeake Bay Impact Structure: Results from the Eyreville Core Holes: Geological Society of America Special Paper 458, doi: 10.1130/2009.2458(18).

Chappell, B.W., and White, A.J.R., 1974, Two contrasting granite types: Pacific Geology, v. 8, p. 173–174.

Collins, G.S., and Wünnemann, K., 2005, How big was the Chesapeake Bay impact?: Insights from numerical modeling: Geology, v. 33, p. 925–928, doi: 10.1130/G21854.1.

Cox, K.G., Bell, J.D., and Pankhurst, R.J., 1979, The Interpretation of Igneous Rocks: London, Allen and Unwin, 450 p.

Deutsch, A., and Koeberl, C., 2006, Establishing the link between the Chesapeake Bay impact structure and the North American tektite strewn field: The Sr-Nd isotopic evidence: Meteoritics & Planetary Science, v. 41, p. 689–703.

Edwards, L.E., Barron, J.A., Bukry, D., Bybell, L.M., Cronin, T.M., Poag, C.W., Weems, R.E., and Wingard, G.L., 2005, Paleontology of the Upper Eocene to Quaternary postimpact section in the USGS-NASA Langley core, Hampton Virginia, *in* Horton, J.W., Jr., Powars, D.S., and Gohn, G.S., eds., Studies of the Chesapeake Bay Impact Structure—The USGS-NASA Langley Corehole, Hampton, Virginia, and Related Coreholes and Geophysical Surveys: U.S. Geological Survey Professional Paper 1688, p. H1–H47.

Edwards, L.E., Powars, D.S., Gohn, G.S., and Dypvik, H., 2009, this volume, Geologic columns for the ICDP-USGS Eyreville A and B cores, Chesapeake Bay impact structure: Sediment-clast breccias, 1096 to 444 m depth, *in* Gohn, G.S., Koeberl, C., Miller, K.G., and Reimold, W.U., eds., The ICDP-USGS Deep Drilling Project in the Chesapeake Bay Impact Structure: Results from the Eyreville Core Holes: Geological Society of America Special Paper 458, doi: 10.1130/2009.2458(03).

Ernst, W., 1970, Methods in Geochemistry and Geophysics: Amsterdam, Elsevier, 152 p.

Fernandes, V.A., Wittmann, A., Schmitt, R.T., Reimold, U., Hecht, L., and Povenmire, H., 2008, Petrography, geochemistry, and radiometric dating of impact melts from the Chesapeake Bay impact structure, USA: Lunar and Planetary Science Conference, v. 39, abstract 2383 (CD-ROM).

Frederiksen, O., Edwards, L.E., Self-Trail, J.M., Bybell, L.M., and Cronin, T.M., 2005, Paleontology of the impact-modified and impact-generated sediments in the USGS-NASA Langley core, Hampton, Virginia, *in* Horton, J.W., Jr., Powars, D.S., and Gohn, G.S., eds., Studies of the Chesapeake Bay Impact Structure—The USGS-NASA Langley Corehole, Hampton, Virginia, and Related Coreholes and Geophysical Surveys: U.S. Geological Survey Professional Paper 1688, p. D1–D37.

French, B.M., Koeberl, C., Gilmour, I., Shirey, S.B., Dons, J.A., and Naterstad, J., 1997, The Gardnos impact structure, Norway: Petrology and geochemistry of target rocks and impactites: Geochimica et Cosmochimica Acta, v. 61, p. 873–904, doi: 10.1016/S0016-7037(96)00382-1.

Gibson, R.L., Townsend, G.N., Horton, J.W., Jr., and Reimold, W.U., 2007, Pre-impact tectonothermal evolution of the crystalline target in the ICDP-USGS Eyreville-B core, Chesapeake Bay impact structure: Geological Society of America Abstracts with Programs, v. 39, no. 6, p. 451 (abs. 167-6).

Gibson, R.L., Townsend, G.N., Horton, J.W., Jr., and Reimold, W.U., 2009, this volume, Pre-impact tectonothermal evolution of the crystalline basement-derived rocks in the ICDP-USGS Eyreville B core, Chesapeake Bay impact structure, *in* Gohn, G.S., Koeberl, C., Miller, K.G., and Reimold, W.U., eds., The ICDP-USGS Deep Drilling Project in the Chesapeake Bay Impact Structure: Results from the Eyreville Core Holes: Geological Society of America Special Paper 458, doi: 10.1130/2009.2458(12).

Glidewell, J., Harris, R.S., King, D.T., Jr., and Petruny, L.W., 2008, Stratigraphy, petrology, and shock petrography based on well logs and selected samples from the Eyreville drill core: Chesapeake Bay impact structure, Virginia: Lunar and Planetary Science, v. 39, abstract 2438 (CD-ROM).

Glass, B.P., Hall, C.M., and York, D., 1986, $^{40}Ar/^{39}Ar$ laser-probe dating of North American tektite fragments from Barbados and the age of the Eocene-Oligocene boundary: Chemical Geology, v. 59, p. 181–186.

Glass, B.P., Koeberl, C., Blum, J.D., and McHugh, C.M.G., 1998, Upper Eocene tektite and impact ejecta layer on the continental slope off New Jersey: Meteoritics & Planetary Science, v. 33, p. 229–241.

Gohn, G.S., Powars, D.S., Bruce, T.S., and Self-Trail, J.M., 2005, Physical geology of the impact-modified and impact-generated sediments in the USGS-NASA Langley core, Hampton, Virginia, *in* Horton, J.W., Jr., Powars, D.S., and Gohn, G.S., eds., Studies of the Chesapeake Bay Impact Structure—The USGS-NASA Langley Corehole, Hampton, Virginia, and Related Coreholes and Geophysical Surveys: U.S. Geological Survey Professional Paper 1688, p. C1–C38.

Gohn, G.S., Koeberl, C., Miller, K.G., Reimold, W.U., Cockell, C.S., Horton, J.W.J., Sanford, W.E., and Voytek, M.A., 2006a, Chesapeake Bay impact structure drilled: Eos (Transactions, American Geophysical Union), v. 87, p. 349–355, doi: 10.1029/2006EO350001.

Gohn, G.S., Koeberl, C., Miller, K.G., Reimold, W.U., and the Scientific Staff of the Chesapeake Bay Impact Structure Drilling Project, 2006b, Chesapeake Bay impact structure deep drilling project completes coring: Scientific Drilling, v. 3, p. 34–37.

Gohn, G.S., Sanford, W.E., Powars, D.S., Horton, J.W., Jr., Edwards, L.E., Morin, R.H., and Self-Trail, J.M., 2007a, Site Report for USGS Test Holes Drilled at Cape Charles, Northampton County, Virginia: U.S. Geological Survey Open-File Report 2007-1094, 22 p.

Gohn, G.S., Powars, D.S., Edwards, L.E., Durand, C.T., and Seefelt, E.L., 2007b, Sediment-avalanche deposits in the late Eocene Chesapeake Bay impact structure: Evidence from the ICDP-USGS Eyreville cores, Virginia, USA: Geological Society of America Abstracts with Programs, v. 39, no. 6, p. 532 (abs. 199-1).

Gohn, G.S., Koeberl, C., Miller, K.G., Reimold, W.U., Browning, J.V., Cockell, C.S., Horton, J.W., Jr., Kenkmann, T., Kulpecz, A.A., Powars, D.S., Sanford, W.E., and Voytek, M.A., 2008, Deep drilling into the Chesapeake Bay impact structure: Science, v. 320, p. 1740–1745, doi: 10.1126/science.1158708.

Gohn, G.S., Koeberl, C., Miller, K.G., and Reimold, W.U., 2009, this volume, Deep drilling in the Chesapeake Bay impact structure—An overview, *in* Gohn, G.S., Koeberl, C., Miller, K.G., and Reimold, W.U., eds., The ICDP-USGS Deep Drilling Project in the Chesapeake Bay Impact Structure: Results from the Eyreville Core Holes: Geological Society of America Special Paper 458, doi: 10.1130/2009.2458(01).

Herron, M.M., 1988, Geochemical classification of terrigenous sands and shales from core or log data: Journal of Sedimentary Petrology, v. 58, p. 820–829.

Horton, J.W., Jr., and Izett, G.A., 2005, Crystalline-rock ejecta and shocked minerals of the Chesapeake Bay impact structure, USGS-NASA Langley core, Hampton, Virginia, with supplemental constraints on the age of impact, *in* Horton, J.W., Jr., Powars, D.S., and Gohn, G.S., eds., Studies of the Chesapeake Bay Impact Structure—The USGS-NASA Langley Corehole, Hampton, Virginia, and Related Coreholes and Geophysical Surveys: U.S. Geological Survey Professional Paper 1688, p. E1–E30.

Horton, J.W., Jr., Kunk, M.J., Naeser, C.W., Naeser, N.D., Aleinikoff, J.N., and Izett, G.A., 2004, Petrography, geochemistry, and geochronology of crystalline basement and impact-derived clasts from coreholes in the western annular trough, Chesapeake Bay impact structure, Virginia, USA, *in* Edwards, L.E., Horton, J.W., Jr., and, Gohn, G.S., eds., ICDP-USGS Workshop on Deep Drilling in the Central Crater of the Chesapeake Bay Impact Structure, Virginia, USA: U.S. Geological Survey Open-File Report 2004-1016, p. 28–29.

Horton, J.W., Jr., Aleinikoff, J.N., Kunk, M.J., Gohn, G.S., Edwards, L.E., Self-Trail, J.M., Powars, D.S., and Izett, G.A., 2005a, Recent research on the Chesapeake Bay impact structure, USA—Impact debris and reworked ejecta, *in* Kenkmann, T., Hörz, F., and Deutsch, A., eds., Large Meteorite Impacts III: Geological Society of America Special Paper 384, p. 147–170.

Horton, J.W., Jr., Gohn, G.S., Jackson, J.C., Aleinikoff, J.N., Sanford, W.E., Edwards, L.E., and Powers, D.S., 2005b, Results from a scientific test hole in the central uplift, Chesapeake Bay impact structure, Virginia, USA: Lunar and Planetary Science, v. 36, abstract 2003 (CD-ROM).

Horton, J.W., Jr., Powars, D.S., and Gohn, G.S., 2005c, Studies of the Chesapeake Bay Impact Structure—The USGS-NASA Langley Corehole, Hampton, Virginia, and Related Coreholes and Geophysical Surveys: U.S. Geological Survey Professional Paper 1688, chapters paginated separately.

Horton, J.W., Jr., Aleinikoff, J.N., Kunk, M.J., Jackson, J.C., Belkin, H., and Chou, I-M., 2007, Initial studies of breccias, blocks, and crystalline rocks in the ICDP-USGS Eyreville-B core, Chesapeake Bay impact structure 1095–1766 m depth: Geological Society of America Abstracts with Programs, v. 39, no. 6, p. 451 (abs. 167-5).

Horton, J.W., Jr., Gohn, G.S., Powars, D.S., and Edwards, L.E., 2008a, Origin and emplacement of impactites in the Chesapeake Bay impact structure, Virginia, USA, *in* Evans, K.R., Horton, J.W., Jr., King, D.T., Jr., and Morrow, J.R., eds., The Sedimentary Record of Meteorite Impacts: Geological Society of America Special Paper 437, p. 73–97.

Horton, J.W., Jr., Kunk, M.J., Belkin, H.E., Aleinikoff, J.N., Jackson, J.C., and Chou, I-M., 2008b, Evolution of crystalline target rocks and impactites in the Chesapeake Bay impact structure, ICDP-USGS Eyreville B core: Lunar and Planetary Science, v. 39, abstract 1196 (CD-ROM).

Horton, J.W., Jr., Gibson, R.L., Reimold, W.U., Wittmann, A., Gohn, G.S., and Edwards, L.E., 2009, this volume, Geologic columns for the ICDP-USGS Eyreville B core, Chesapeake Bay impact structure: Impactites

and crystalline rocks, 1766 to 1096 m depth, *in* Gohn, G.S., Koeberl, C., Miller, K.G., and Reimold, W.U., eds., The ICDP-USGS Deep Drilling Project in the Chesapeake Bay Impact Structure: Results from the Eyreville Core Holes: Geological Society of America Special Paper 458, doi: 10.1130/2009.2458(02).

Kenkmann, T., Collins, G.S., Wittmann, A., Wünnemann, K., Reimold, W.U., and Melosh, H.J., 2009, this volume, A model for the formation of the Chesapeake Bay impact crater as revealed by drilling and numerical simulation, *in* Gohn, G.S., Koeberl, C., Miller, K.G., and Reimold, W.U., eds., The ICDP-USGS Deep Drilling Project in the Chesapeake Bay Impact Structure: Results from the Eyreville Core Holes: Geological Society of America Special Paper 458, doi: 10.1130/2009.2458(25).

Koeberl, C., 1993, Instrumental neutron activation analysis of geochemical and cosmochemical samples: A fast and proven method for small samples analysis: Journal of Radioanalytical and Nuclear Chemistry, v. 168, p. 47–60, doi: 10.1007/BF02040877.

Koeberl, C., Poag, C.W., Reimold, W.U., and Brandt, D., 1996, Impact origin of the Chesapeake Bay structure and the source of the North American tektites: Science, v. 271, p. 1263–1266, doi: 10.1126/science.271.5253.1263.

Lee, S.R., Horton, J.W., Jr., and Walker, R.J., 2006, Confirmation of a meteoritic component in impact-melt rocks of the Chesapeake Bay impact structure, Virginia, USA—Evidence from osmium isotopic and PGE systematics: Meteoritics & Planetary Science, v. 41, no. 6, p. 819–833.

McDonald, I., Bartosova, K., and Koeberl, C., 2009, this volume, Search for a meteoritic component in impact breccia from the Eyreville core, Chesapeake Bay impact structure: Considerations from platinum group element contents, *in* Gohn, G.S., Koeberl, C., Miller, K.G., and Reimold, W.U., eds., The ICDP-USGS Deep Drilling Project in the Chesapeake Bay Impact Structure: Results from the Eyreville Core Holes: Geological Society of America Special Paper 458, doi: 10.1130/2009.2458(21).

Miyashiro, A., 1975, Classification, characteristics, and origin of ophiolites: The Journal of Geology, v. 83, p. 249–281.

Obradovich, J., Snee, L.W., and Izett, G.A., 1989, Is there more than one glassy impact layer in the late Eocene?: Geological Society of America Abstracts with Programs, v. 21, no. 6, p. 134.

Pearce, J.A., Harris, N.B.W., and Tindle, A.G., 1984, Trace element discrimination diagrams for the tectonic interpretation of granitic rocks: Journal of Petrology, v. 25, p. 956–983.

Poag, C.W., and Aubry, M.-P., 1995, Upper Eocene impactites of the U.S. East Coast: Depositional origins, biostratigraphic framework, and correlation: Palaios, v. 10, p. 16–43, doi: 10.2307/3515005.

Poag, C.W., Powars, D.S., Poppe, L.J., and Mixon, R.B., 1994, Meteoroid mayhem in Ole Virginny: Source of the North American tektite strewn field: Geology, v. 22, p. 691–694, doi: 10.1130/0091-7613(1994)022<0691:MMIOVS>2.3.CO;2.

Poag, C.W., Plescia, J.B., and Molzer, P.C., 2002, Ancient impact structures on modern continental shelves: The Chesapeake Bay, Montagnais, and Toms Canyon craters, Atlantic Margin of North America: Deep-Sea Research: Part II. Topical Studies in Oceanography, v. 49, p. 1081–1102, doi: 10.1016/S0967-0645(01)00144-8.

Poag, C.W., Koeberl, C., and Reimold, W.U., 2004, The Chesapeake Bay Crater: Geology and Geophysics of a Late Eocene Submarine Impact Structure: New York, Springer, 522 p.

Powars, D.S., and Bruce, T.S., 1999, The Effects of the Chesapeake Bay Impact Crater on the Geological Framework and Correlation of Hydrogeologic Units of the Lower York–James Peninsula, Virginia: U.S. Geological Survey Professional Paper 1612, 82 p.

Powars, D.S., Catchings, R.D., Gohn, G.S., and Horton, J.W., Jr., 2008, High-resolution seismic reflection images spanning the 1.76-km-deep ICDP-USGS Eyreville coreholes within the moat of the Chesapeake impact structure: Lunar and Planetary Science, v. 39, abstract 1391 (CD-ROM).

Reimold, W.U., Koeberl, C., and Bishop, J., 1994, Roter Kamm impact crater, Namibia: Geochemistry of basement rocks and breccias: Geochimica et Cosmochimica Acta, v. 58, p. 2689–2710, doi: 10.1016/0016-7037(94)90138-4.

Reimold, W.U., Kenkmann, T., Gibson, R., Bartosova, K., Schmitt, R.T., Hecht, L., Koeberl, C., and Horton, J.W., Jr., 2007, Dike breccias in the deep basement-derived section of the Eyreville B core, Chesapeake Bay impact structure: Geological Society of America Abstracts with Programs, v. 39, no. 6, p. 451 (abs. 167-7).

Reimold, W.U., Bartosova, K., Schmitt, R.T., Hansen, B., Crasselt, C., Koeberl, C., Wittmann, A., and Powars, D.S., 2009, this volume, Petrographic observations on the Exmore breccia, ICDP-USGS Drilling at Eyreville, Chesapeake Bay impact structure, USA, *in* Gohn, G.S., Koeberl, C., Miller, K.G., and Reimold, W.U., eds., The ICDP-USGS Deep Drilling Project in the Chesapeake Bay Impact Structure: Results from the Eyreville Core Holes: Geological Society of America Special Paper 458, doi: 10.1130/2009.2458(29).

Schmitt, R.T., Wittmann, A., and Stöffler, D., 2004, Geochemistry of drill core samples from Yaxcopoil-1, Chicxulub impact crater, Mexico: Meteoritics & Planetary Science, v. 39, p. 979–1001.

Shah, A.K., Brozena, J., Vogt, P., Daniels, D., and Plescia, J., 2005, New surveys of the Chesapeake Bay impact structure suggest melt pockets and target-structure effect: Geology, v. 33, p. 417–420, doi: 10.1130/G21213.1.

Son, T.H., and Koeberl, C., 2005, Chemical variation within fragments of Australasian tektites: Meteoritics & Planetary Science, v. 40, p. 805–815.

Stöffler, D., and Grieve, R.A.F., 2007, Towards a unified nomenclature of metamorphic petrology: Impactites—A proposal on behalf of the IUGS Subcommission on the Systematics of Metamorphic Rocks: International Union of Geological Sciences (IUGS) Subcommission on the Systematics of Metamorphic Rocks: http://www.bgs.ac.uk/SCMR/docs/papers/paper_11.pdf, 15 p. (accessed 2 January 2007).

Taylor, S.R., and McLennan, S.M., 1985, The Continental Crust: Its Composition and Evolution: Oxford, Blackwell Scientific, 312 p.

Townsend, G., Gibson, R.L., Horton, J.W., Jr., Reimold, W.U., Schmitt, R.T., Hecht, L., and Czaja, P., 2007, Petrographic and chemical analysis of the lower crystalline basement-derived section, and the upper granite and amphibolite megablocks, Eyreville-B core, Chesapeake Bay impact structure: Geological Society of America Abstracts with Programs, v. 39, no. 6, p. 314 (#abs. 116-9).

Townsend, G.N., Gibson, R.L., Horton, J.W., Jr., Reimold, W.U., Schmitt, R.T., and Bartosova, K., 2009, this volume, Petrographic and geochemical comparisons between the lower crystalline basement-derived section and the granite megablock and amphibolite megablock of the Eyreville B core, Chesapeake Bay impact structure, USA, *in* Gohn, G.S., Koeberl, C., Miller, K.G., and Reimold, W.U., eds., The ICDP-USGS Deep Drilling Project in the Chesapeake Bay Impact Structure: Results from the Eyreville Core Holes: Geological Society of America Special Paper 458, doi: 10.1130/2009.2458(13).

Walker, K.R., Joplin, G.A., Lovering, J.F., and Green, R., 1960, Metamorphic and metasomatic convergence of basic rocks and lime-magnesia sediments of the Precambrian of North-West Queensland: Journal of the Geological Society of Australia, v. 6, p. 149–177.

Wasson, J.T., and Kallemeyn, G.W., 1988, Composition of chondrites: Philosophical Transactions of the Royal Society of London, v. A325, p. 535–544.

Wedepohl, K.H., 1995, The composition of the continental crust: Geochimica et Cosmochimica Acta, v. 59, p. 1217–1232, doi: 10.1016/0016-7037(95)00038-2.

Winchester, J.A., and Floyd, P.A., 1976, Geochemical magma type discrimination: Application to altered and metamorphosed basic igneous rocks: Earth and Planetary Science Letters, v. 28, p. 459–469, doi: 10.1016/0012-821X(76)90207-7.

Winchester, J.A., and Max, M.D., 1982, The geochemistry and origins of the Precambrian rocks of the Rosslare Complex, SE Ireland: Journal of the Geological Society of London, v. 139, p. 309–319, doi: 10.1144/gsjgs.139.3.0309.

Wittmann, A., Reimold, W.U., Schmitt, R.T., Hecht, L., and Kenkmann, T., 2009, this volume, Chapter 16, The record of ground zero in the Chesapeake Bay impact crater—Suevites and related rocks, *in* Gohn, G.S., Koeberl, C., Miller, K.G., and Reimold, W.U., eds., The ICDP-USGS Deep Drilling Project in the Chesapeake Bay Impact Structure: Results from the Eyreville Core Holes: Geological Society of America Special Paper 458, doi: 10.1130/2009.2458(16).

Wittmann, A., Schmitt, R.T., Hecht, L., Kring, D.A., Reimold, W.U., and Povenmire, H., 2009, this volume, Chapter 17, Petrology of impact melt rocks from the Chesapeake Bay crater, USA, *in* Gohn, G.S., Koeberl, C., Miller, K.G., and Reimold, W.U., eds., The ICDP-USGS Deep Drilling Project in the Chesapeake Bay Impact Structure: Results from the Eyreville Core Holes: Geological Society of America Special Paper 458, doi: 10.1130/2009.2458(17).

Manuscript Accepted by the Society 3 March 2009

Printed in the USA

TABLE A1. WHOLE-ROCK CHEMICAL COMPOSITIONS OF SAMPLES FROM THE EYREVILLE A AND B DRILL CORES

Sample		W 001	W 002	W 003	W 004	W 005	W 006	W 007	W 008	W 009	W 010	W 011	W 012	W 013	W 014	W 015	W 016	W 017
Core		A	A	A	A	A	A	A	A	A	A	A	A	A	A	A	A	A
Depth (m)		443.9	444.1	444.2	444.3	444.4	444.5	444.6	444.7	444.8	444.9	445.0	445.1	445.3	445.7	446.2	446.8	448.9
Type*		post-Ex br	post-Ex br	post-Ex br	post-Ex br	post-Ex br	post-Ex br	post-Ex br	post-Ex br	post-Ex br	post-Ex br	Ex br	Ex br	Ex br	Ex br	Ex br	Ex br	Ex br
(wt%)																		
SiO_2		62.6	61.2	61.0	56.3	73.2	74.9	77.4	78.9	78.2	81.0	78.4	79.4	82.0	84.9	83.5	80.6	79.9
TiO_2		0.77	0.69	0.65	0.56	0.51	0.55	0.51	0.48	0.51	0.41	0.49	0.37	0.34	0.28	0.32	0.36	0.44
Al_2O_3		17.7	18.6	16.5	13.3	11.7	11.7	11.2	10.5	10.9	8.7	10.2	8.2	7.6	6.5	6.8	8.0	9.1
Fe_2O_3†		4.66	4.63	6.46	12.0	3.93	2.54	1.97	1.70	1.95	1.68	1.86	2.59	1.67	1.45	1.78	1.92	2.18
MnO		0.02	0.02	0.02	0.02	0.02	0.02	0.02	0.02	0.02	0.02	0.02	0.02	0.02	0.04	0.03	0.03	0.02
MgO		2.03	1.98	1.60	1.14	0.87	0.93	0.79	0.75	0.73	0.52	0.66	0.47	0.55	0.41	0.48	0.55	0.58
CaO		1.61	1.30	1.48	1.40	0.66	1.03	0.74	0.55	0.67	0.94	0.97	0.83	0.90	0.86	0.84	0.96	1.05
Na_2O		1.77	2.00	1.99	1.79	1.75	1.70	1.63	1.48	1.53	1.38	1.59	1.50	1.36	0.94	1.09	1.44	1.18
K_2O		1.91	2.02	2.18	2.15	2.46	2.66	2.57	2.50	2.52	2.60	2.62	2.81	2.47	2.34	2.59	2.57	2.61
P_2O_5		0.06	0.05	0.05	0.05	0.03	0.04	0.04	0.03	0.05	0.07	0.05	0.06	0.08	0.08	0.09	0.09	0.09
SO_3		<0.1	0.8	0.8	0.9	1.2	<0.1	<0.1	<0.1	<0.1	<0.1	<0.1	0.3	0.2	<0.1	<0.1	<0.1	<0.1
LOI		6.7	6.4	6.5	9.7	3.8	3.2	3.0	2.6	2.6	2.6	2.7	2.6	2.7	2.1	1.9	2.7	2.8
Total		99.83	99.69	99.23	99.31	100.13	99.27	99.87	99.51	99.68	99.92	99.56	99.15	99.89	99.90	99.42	99.22	99.95
(ppm)	m#																	
Sc	(1)	16.5	16.0	13.3	9.96	7.34	7.78	7.24	6.67	7.17	5.26	5.83	4.45	4.79	3.64	4.05	4.92	6.08
V	(2)	124	129	100	81	61	73	56	67	61	38	61	46	34	34	28	42	50
Cr	(1)	76.0	67.1	57.5	45.7	31.2	39.4	36	30.8	34.4	33.9	28.5	29.3	30.0	23.8	27.6	34.4	37.2
Co	(1)	14.3	16.4	16.4	15.9	14.0	40	18.7	9.80	10.3	7.51	8.25	8.14	7.95	5.14	6.31	6.37	16.4
Ni	(2)	31	35	26	16	28	28	25	25	24	22	19	23	31	18	39	27	21
Cu	(2)	35	33	<30	<30	<30	32	<30	<30	<30	<30	<30	<30	31	<30	36	<30	<30
Zn	(1)	89	76	66	47	33	35	34	36	27	29	34	16	17	19	21	28	39
As	(1)	3.86	4.20	6.31	7.06	1.90	34	35	34	36	27	29	7.06	6.83	2.61	3.70	3.48	4.3
Se	(1)	<1.7	<1.6	<1.9	<1.8	<2.0	2.54	2.76	3.23	3.28	3.07	3.66	<1.3	<1.2	<0.7	<1.2	<1.3	<1.4
Br	(1)	8.3	7.6	3.8	3.0	8.2	<1.2	<1.3	<1.2	<1.2	<1.3	<1.2	3.8	5.2	2.0	3.2	5.2	1.6
Rb	(1)	89	80	73.2	71.8	62.3	5.1	5.3	13	5.0	2.2	2.5	73.1	68.3	58.8	70.4	67.5	71.8
Sr	(2)	225	232	230	225	196	237	215	195	212	250	224	251	219	194	209	197	184
Y	(2)	35	30	27	17	20	21	24	20	24	15	19	16	15	13	12	16	17
Zr	(2)	182	148	144	134	220	228	250	205	218	185	219	203	171	137	150	168	200
Nb	(2)	<10	<10	<10	<10	<10	<10	<10	<10	<10	<10	<10	<10	<10	<10	<10	<10	<10
Mo	(2)	<10	<10	<10	<10	<10	<10	<10	<10	<10	<10	<10	<10	<10	<10	<10	<10	<10
Sb	(1)	0.31	0.24	0.31	0.28	0.14	0.15	0.18	0.23	0.20	0.21	0.16	0.37	0.51	0.20	0.22	0.23	0.28
Cs	(1)	5.37	3.83	3.15	2.59	1.67	1.99	1.91	1.66	1.97	1.72	1.79	1.56	1.59	1.24	1.44	1.59	1.89
Ba	(2)	405	467	493	520	545	610	626	585	603	686	627	763	624	599	617	573	585
La	(1)	42.8	37.5	29.6	23.1	23.5	20.9	25.2	33.2	21.8	17.1	19.9	14.6	17.0	13.1	13.1	18.7	19.2
Ce	(1)	85.5	75.6	63.7	49.6	47.3	45.9	49.3	44.7	44.0	37.3	35.8	32.1	36.1	28.0	28.3	40.5	42.1
Nd	(1)	35.6	32.3	29.2	19.5	18.4	18.5	21.4	19.1	18.5	17.2	19.4	13.2	13.1	11.5	12.2	17.1	17.1
Sm	(1)	8.13	7.09	5.36	4.46	4.18	3.52	4.43	4.37	4.01	2.89	3.18	2.72	2.99	2.27	2.46	3.10	3.13
Eu	(1)	1.90	1.76	1.51	1.19	1.05	1.04	1.11	0.99	1.07	0.86	0.94	0.83	0.77	0.67	0.73	0.84	0.94
Gd	(1)	6.67	6.00	5.12	4.20	3.17	3.29	3.62	3.05	3.55	n.d.§	n.d.§	n.d.§	n.d.§	n.d.§	n.d.§	n.d.§	n.d.§
Tb	(1)	1.12	0.94	0.76	0.65	0.57	0.55	0.59	0.52	0.58	0.51	0.42	0.45	0.49	0.39	0.41	0.46	0.52
Tm	(1)	0.46	0.41	0.36	0.27	0.28	0.25	0.31	0.25	0.25	0.20	0.21	0.2	0.23	0.18	0.22	0.19	0.24
Yb	(1)	2.89	2.52	2.22	1.67	1.96	1.67	1.81	1.64	1.88	1.36	1.63	1.21	1.56	1.35	1.39	1.41	1.75
Lu	(1)	0.45	0.39	0.35	0.29	0.26	0.27	0.28	0.26	0.30	0.24	0.27	0.21	0.25	0.22	0.22	0.24	0.28
Hf	(1)	4.64	3.56	3.81	3.70	4.83	6.46	6.00	4.85	4.94	4.35	4.38	4.40	4.03	3.16	3.79	4.44	4.94
Ta	(1)	0.97	0.81	0.78	0.72	0.52	0.61	0.58	0.58	0.57	0.54	0.55	0.52	0.53	0.41	1.19	0.49	0.59
W	(1)	1.1	<6.9	<4.7	<4.7	0.6	0.3	2.9	<5.3	<2.3	8.0	<2.5	<2.4	1.5	<2.0	<2.2	<3.2	1.4
Pb	(2)	<15	<15	<15	<15	<15	<15	<15	<15	<15	<15	<15	<15	<15	<15	<15	<15	<15
Th	(1)	9.86	7.61	6.31	5.26	5.34	5.86	6.21	5.19	5.22	5.27	4.34	3.57	5.14	3.52	2.99	5.29	5.62
U	(1)	2.55	2.05	1.86	1.59	1.48	1.29	1.58	3.04	1.19	1.27	1.28	1.29	1.53	1.08	1.23	1.37	1.27
(ppb)																		
Ir	(1)	<1.4	<1.4	<1.5	<1.4	<1.0	<1.2	<1.1	<1.0	<1.0	<1.4	<1.2	<1.3	<1.2	<0.7	<1.3	<1.4	<1.4
Au	(1)	1.1	<1.8	<2.0	<2.2	0.4	<1.1	<1.1	1.1	<1.6	<1.1	<1.1	<1.0	<1.0	<0.9	<1.0	<0.9	<1.1

(*Continued*)

TABLE A1. WHOLE-ROCK CHEMICAL COMPOSITIONS OF SAMPLES FROM THE EYREVILLE A AND B DRILL CORES (*Continued*)

Sample		W 018	W 019	W 020	W 021	W 023	W 022	W 2-05	W 024	W 025	W 2-31	W 026	CB6 006	W 2-32	CB6 007m	W 027	W 2-33	CB6 010
Core		A	A	A	A	A	A	A	A	A	A	A	A	A	A	A	A	A
Depth (m)		450.6	450.8	451.4	451.8	452.0	452.2	453.4	454.1	454.6	457.4	457.7	457.7	458.5	459.5	459.9	462.3	464.1
Type*		Ex br	Ex br	Ex br	Ex br	Ex br	Ex br	Ex br	Ex br	Ex br	Ex br	Ex br	Ex br	Ex br	Ex br	Ex br	Ex br	Ex br
(wt%)																		
SiO_2		80.8	75.0	72.6	66.7	65.0	69.4	73.9	72.6	71.9	71.9	60.9	70.6	76.4	72.6	68.4	75.5	78.5
TiO_2		0.37	0.35	0.40	0.81	0.58	0.49	0.37	0.38	0.42	0.53	0.91	0.62	0.50	0.70	0.63	0.54	0.46
Al_2O_3		8.2	7.6	9.1	16.5	12.4	10.8	8.8	9.4	9.2	10.1	13.1	11.4	9.2	13.2	15.9	10.0	9.5
Fe_2O_3†		2.03	4.66	4.32	5.21	6.58	5.81	4.88	4.64	5.15	3.66	3.27	4.47	2.52	3.34	3.50	3.82	2.49
MnO		0.03	0.02	0.03	0.01	0.03	0.03	0.04	0.03	0.04	0.05	0.09	0.05	0.04	0.04	0.02	0.16	0.04
MgO		0.52	1.05	0.90	1.01	1.64	1.25	0.87	0.97	1.06	0.78	1.39	0.97	0.47	0.78	1.72	0.64	0.59
CaO		0.90	2.80	3.11	0.78	2.71	2.44	2.56	2.76	2.62	2.16	7.40	2.36	0.91	1.97	1.19	1.28	1.01
Na_2O		1.38	1.06	1.14	1.24	1.09	1.16	1.16	1.27	1.26	1.42	1.25	1.39	1.25	1.19	1.88	1.27	1.38
K_2O		2.55	3.20	2.78	0.82	3.01	2.69	2.94	2.82	2.73	2.59	1.86	2.57	2.47	2.33	1.54	2.57	2.60
P_2O_5		0.07	0.41	0.33	0.03	0.34	0.22	0.28	0.26	0.24	0.17	0.13	0.16	0.11	0.12	0.11	0.14	0.10
SO_3		<0.1	0.2	0.1	<0.1	0.3	0.2	n.d.§	0.1	0.3	n.d.§	0.1	0.2	n.d.§	<0.1	<0.1	n.d.§	<0.1
LOI		2.7	3.6	4.9	6.1	5.5	5.3	5.8	4.6	4.6	6.4	9.4	5.1	5.3	3.2	4.4	2.8	2.8
Total		99.55	99.95	99.71	99.21	99.18	99.79	100.60	99.83	99.52	99.76	99.80	99.89	99.17	99.47	99.29	98.72	99.47
(ppm)	m#																	
Sc	(1)	4.52	5.97	6.59	14.4	11.4	9.14	5.86	6.13	6.05	7.61	15.0	9.02	6.10	10.0	11.6	7.64	6.28
V	(2)	52	57	58	107	102	86	65	75	68	69	92	84	66	94	73	64	55
Cr	(1)	30.3	70.7	58.6	75.1	82.2	71.6	62.9	66.8	63.4	52.1	57.5	56.9	30.5	62.3	45.4	43.7	42.6
Co	(1)	7.65	9.80	7.41	18.5	11.5	9.07	7.20	6.68	6.82	7.85	13.1	9.29	8.89	8.70	5.39	7.93	7.17
Ni	(2)	19	23	22	26	36	25	16	21	21	13	29	27	14	27	23	13	23
Cu	(2)	<30	<30	<30	<30	<30	<30	<30	<30	<30	<30	38	<30	<30	<30	110	<30	<30
Zn	(1)	25	56	42	45	62	64	46	46	123	46	65	48	34	47	29	43	32
As	(1)	4.97	6.62	8.50	1.80	6.71	5.44	8.02	6.11	7.22	5.48	13.0	5.57	2.14	4.06	2.39	4.00	4.21
Se	(1)	<1.3	<1.5	<1.0	<1.4	<1.6	<1.2	<1.0	<1.3	<1.2	<1.0	<1.6	<1.3	<0.9	<1.8	<1.4	<1.1	<1.1
Br	(1)	4.6	2.8	2.7	4.5	2.3	3.2	9.0	3.4	3.6	7.2	1.6	1.7	6.2	2.1	3.2	5.2	2.2
Rb	(1)	64.9	95.1	84.6	39.7	100	93.3	84.1	80.0	76.0	80.7	56.5	73.8	66.7	86.4	40.4	77.1	71.5
Sr	(2)	185	206	219	126	187	179	183	186	188	197	169	205	187	175	187	183	171
Y	(2)	12	28	22	21	44	29	21	21	24	22	27	33	14	29	14	22	20
Zr	(2)	177	152	164	332	189	182	126	146	164	185	235	275	213	272	227	188	234
Nb	(2)	<10	<10	<10	<10	<10	<10	<10	<10	<10	<10	<10	<10	<10	<10	<10	<10	<10
Mo	(2)	<10	<10	<10	<10	<10	<10	n.d.§	<10	<10	n.d.§	<10	<10	n.d.§	<10	<10	n.d.§	<10
Sb	(1)	0.23	0.37	0.28	0.19	0.41	0.30	0.36	0.29	0.37	0.38	0.65	0.34	0.21	0.49	0.38	0.36	0.19
Cs	(1)	1.38	2.19	2.50	3.60	4.12	3.61	1.96	2.06	1.98	2.74	2.34	2.73	1.32	3.72	1.26	2.35	1.88
Ba	(2)	565	473	522	164	404	434	479	485	464	473	355	501	586	464	264	527	525
La	(1)	15.7	27.5	21.8	24.6	30.3	26.7	20.7	19.7	18.6	21.2	28.2	25.7	17.5	31.3	29.6	21.3	19.5
Ce	(1)	32.6	61.7	50.1	55.3	64.9	57.6	45.5	44.6	40.1	47.3	59.8	52.4	37.3	65.5	63.1	48.2	41.0
Nd	(1)	13.3	22.5	20.9	22.1	27.4	22.9	20.6	17.8	16.9	18.7	25.0	24.0	15.9	30.3	26.7	21.5	17.8
Sm	(1)	2.50	4.85	4.01	4.46	5.75	4.29	4.18	3.77	3.79	4.36	5.28	4.64	3.19	5.48	5.46	4.38	3.60
Eu	(1)	0.74	1.30	1.15	1.11	1.42	1.12	1.03	0.97	0.91	1.09	1.28	1.18	0.78	1.35	1.25	1.09	0.92
Gd	(1)	n.d.§	n.d.§	3.26	4.99	4.90	3.73	3.54	3.00	2.90	4.83	4.70	4.64	2.58	4.50	4.70	4.52	3.22
Tb	(1)	0.39	0.80	0.62	0.76	0.80	0.66	0.58	0.50	0.50	0.68	0.90	0.69	0.42	0.77	0.66	0.67	0.52
Tm	(1)	0.19	0.29	0.28	0.38	0.49	0.31	0.29	0.27	0.26	0.38	0.50	0.33	0.21	0.37	0.31	0.38	0.27
Yb	(1)	1.30	1.96	1.78	2.52	2.73	2.12	1.68	1.56	1.56	2.02	2.73	2.07	1.37	2.24	1.59	2.19	1.67
Lu	(1)	0.20	0.30	0.30	0.42	0.44	0.35	0.21	0.25	0.24	0.31	0.44	0.33	0.23	0.35	0.24	0.34	0.27
Hf	(1)	4.15	3.58	4.41	7.34	4.68	3.94	3.42	3.36	4.05	4.88	5.25	4.78	6.46	5.10	5.28	5.22	4.65
Ta	(1)	0.50	0.55	0.55	1.02	0.61	0.61	0.47	0.47	0.57	0.78	0.93	0.76	0.77	0.88	1.05	0.75	0.65
W	(1)	<2.8	0.1	<1.5	1.9	1.9	1.6	0.6	1.2	0.7	1.2	2.6	0.9	1.7	1.6	1.0	1.2	0.7
Pb	(2)	<15	<15	<15	<15	<15	<15	n.d.§	<15	<15	n.d.§	<15	<15	n.d.§	<15	<15	n.d.§	<15
Th	(1)	4.12	7.10	5.23	9.91	6.41	8.81	5.12	5.20	4.97	6.15	7.58	6.42	6.01	10.4	13.1	6.21	5.45
U	(1)	1.25	2.26	2.20	1.78	2.09	1.81	1.67	1.59	1.91	1.85	2.15	2.26	1.42	2.52	2.45	1.65	1.62
(ppb)																		
Ir	(1)	<1.3	<1.8	<1.1	<1.4	<2.0	<1.3	<1.0	<1.7	<1.6	<1.2	<2.0	<1.5	<1.0	<2.0	<2.0	0.4	<1.3
Au	(1)	0.1	0.3	<1.1	<1.3	0.7	<1.2	1.5	0.5	<0.7	1.5	0.6	0.5	0.6	0.5	<0.9	1.2	<0.6

(*Continued*)

TABLE A1. WHOLE-ROCK CHEMICAL COMPOSITIONS OF SAMPLES FROM THE EYREVILLE A AND B DRILL CORES (*Continued*)

Sample		W 2-34	W 028	CB6 011	W 2-01a	W 2-02a	W 2-35	CB6 012	CB6 013	W 2-03	W 029	CB6 014	CB6 015	CB6 016	CB6 017	CB6 018	W 030	CB6 019
Core		A	A	A	A	A	A	A	A	A	A	A	A	A	A	A	A	A
Depth (m)		465.2	467.3	467.3	468.9	470.0	470.6	470.8	472.7	472.9	473.7	476.1	478.7	481.6	484.3	489.3	489.8	490.8
Type*		Ex br	Ex br	Ex br	Ex br	Ex br	Ex br	Ex br	Ex br	Ex br	Ex br	Ex br	Ex br	Ex br	Ex br	Ex br	Ex br	Ex br
(wt%)																		
SiO_2		76.1	71.7	71.0	74.9	74.1	76.1	74.9	77.2	75.7	77.4	75.9	76.6	76.9	78.5	75.1	77.6	77.7
TiO_2		0.49	0.69	0.61	0.55	0.53	0.52	0.54	0.47	0.53	0.46	0.50	0.53	0.54	0.49	0.54	0.50	0.49
Al_2O_3		9.6	13.2	11.7	10.7	9.8	10.2	10.4	9.7	9.1	9.5	10.3	10.2	10.6	9.8	11.2	10.0	9.9
Fe_2O_3 †		2.64	3.14	3.09	3.48	3.03	3.09	3.34	2.78	2.63	2.74	3.24	2.77	2.94	2.44	3.09	2.58	2.61
MnO		0.04	0.03	0.05	0.10	0.05	0.05	0.06	0.04	0.04	0.05	0.04	0.04	0.05	0.03	0.03	0.04	0.04
MgO		0.59	1.22	1.10	0.78	0.66	0.66	0.82	0.65	0.42	0.65	0.77	0.74	0.70	0.62	0.87	0.71	0.64
CaO		0.98	1.21	3.21	1.17	1.04	0.93	1.50	1.25	2.32	1.13	1.05	1.12	0.90	1.05	1.03	1.02	1.00
Na_2O		1.40	1.52	1.49	1.55	1.68	1.37	1.47	1.27	1.68	1.32	1.44	1.47	1.26	1.26	1.50	1.53	1.45
K_2O		2.59	2.08	2.40	2.56	2.71	2.58	2.71	2.64	2.88	2.61	2.61	2.64	2.41	2.65	2.46	2.59	2.62
P_2O_5		0.13	0.10	0.19	0.15	0.14	0.12	0.11	0.11	0.15	0.11	0.10	0.13	0.08	0.11	0.10	0.09	0.10
SO_3		n.d.§	<0.1	<0.1	n.d.§	n.d.§	n.d.§	<0.1	<0.1	n.d.§	0.1	0.1	0.1	<0.1	<0.1	0.5	<0.1	<0.1
LOI		5.0	4.2	5.0	5.0	4.3	4.5	3.5	3.1	4.3	3.3	3.7	3.2	3.1	2.6	3.5	2.9	3.0
Total		99.56	99.09	99.84	100.94	98.04	100.12	99.35	99.21	99.75	99.37	99.75	99.54	99.48	99.55	99.92	99.56	99.55
(ppm)	m#																	
Sc	(1)	6.46	10.5	10.7	7.54	7.18	7.53	7.45	6.57	6.23	6.46	7.92	7.72	8.35	6.76	8.23	6.70	7.29
V	(2)	67	82	79	63	62	57	65	54	42	53	59	68	63	61	67	59	67
Cr	(1)	44.0	49.3	55.8	48.9	47.7	45.7	48.5	39.6	39.9	38.7	47.5	47.0	44.3	40.6	52.4	38.1	40.5
Co	(1)	7.18	8.67	9.59	8.26	8.49	8.60	9.19	7.24	7.23	8.13	10.8	8.56	12.3	8.02	10.5	8.25	9.21
Ni	(2)	12	19	29	14	19	14	27	22	15	22	26	27	25	26	25	21	25
Cu	(2)	<30	39	97	<30	<30	<30	59	<30	<30	<30	48	48	<30	39	32	33	<30
Zn	(1)	36	53	94	47	39	45	43	39	46	35	30	52	37	41	52	37	35
As	(1)	2.68	5.63	6.91	4.88	4.44	4.36	3.92	3.68	4.72	3.37	11.5	3.65	12.5	3.61	5.28	4.13	4.24
Se	(1)	<1.0	<1.4	<1.3	0.01	<1.0	1.1	<1.6	<1.4	<0.9	0.3	<1.4	<1.5	<1.6	<1.4	<1.6	<1.1	<1.5
Br	(1)	n.d.	3.7	3.4	6.5	6.1	7.1	5.3	2.0	7.6	4.5	2.8	5.6	1.3	3.1	5.6	3.9	2.4
Rb	(1)	70.9	66.3	76.7	73.8	74.8	76.0	73.1	68.3	68.3	71.9	73.5	74.2	67.7	69.4	75.1	70.8	72.5
Sr	(2)	174	169	180	187	166	165	192	195	162	172	195	182	167	171	174	174	167
Y	(2)	21	17	30	25	23	22	27	22	20	23	23	25	24	22	24	22	20
Zr	(2)	179	229	238	186	185	188	217	202	177	236	223	216	223	202	214	243	212
Nb	(2)	<10	<10	<10	<10	<10	<10	<10	<10	<10	<10	<10	<10	<10	<10	<10	<10	<10
Mo	(2)	n.d.§	<10	<10	n.d.§	n.d.§	n.d.§	<10	<10	n.d.§	<10	<10	<10	<10	<10	<10	<10	<10
Sb	(1)	0.24	0.56	0.53	0.37	0.33	0.49	0.36	0.42	0.34	0.26	0.35	0.42	0.35	0.27	0.58	0.37	0.30
Cs	(1)	1.95	2.22	2.57	2.31	2.26	2.71	2.13	1.93	1.98	1.99	2.15	2.15	2.34	1.97	2.37	2.05	2.05
Ba	(2)	523	438	447	534	520	530	574	598	550	507	569	529	485	505	494	520	548
La	(1)	22.3	21.9	30.5	23.9	23.0	23.4	21.2	22.8	20.6	21.4	22.9	22.9	24.7	20.1	25.5	19.4	21.2
Ce	(1)	47.6	46.7	62.9	49.9	48.8	51.6	45.9	48.5	43.8	46.0	48.6	49.2	52.3	43.7	54.6	42.9	45.2
Nd	(1)	21.2	17.1	27.3	22.0	22.8	20.3	20.9	20.3	19.6	18.9	20.1	21.4	22.0	20.2	25.5	17.5	18.9
Sm	(1)	4.15	4.41	5.71	4.72	4.40	4.36	4.83	3.59	4.00	4.23	3.65	3.93	3.87	4.78	5.66	3.88	3.25
Eu	(1)	1.04	0.99	1.51	1.18	1.08	1.10	1.06	1.04	0.99	1.02	1.09	1.02	1.15	1.07	1.13	0.98	1.07
Gd	(1)	3.38	4.30	5.28	4.92	3.88	3.50	3.73	3.97	3.69	3.9	4.21	3.85	4.08	3.72	4.20	3.8	3.66
Tb	(1)	0.62	0.75	0.88	0.69	0.62	0.62	0.58	0.59	0.55	0.67	0.64	0.56	0.66	0.56	0.66	0.66	0.58
Tm	(1)	0.27	0.36	0.41	0.29	0.34	0.36	0.34	0.28	0.28	0.29	0.41	0.31	0.38	0.27	0.34	0.29	0.29
Yb	(1)	2.05	1.77	2.35	2.01	1.95	1.90	2.00	1.68	1.73	1.74	2.50	1.94	2.14	1.79	2.16	1.72	1.78
Lu	(1)	0.31	0.28	0.36	0.25	0.25	0.32	0.31	0.26	0.23	0.27	0.41	0.31	0.33	0.28	0.34	0.27	0.28
Hf	(1)	5.25	5.40	4.55	4.65	4.98	5.32	4.75	4.22	4.92	4.87	5.26	5.78	5.85	4.21	6.13	5.29	4.70
Ta	(1)	0.63	1.13	0.93	0.66	0.69	0.69	0.59	0.57	0.54	0.53	0.65	0.60	0.61	0.58	0.73	0.61	0.64
W	(1)	n.d.§	1.1	1.6	0.6	0.5	0.9	0.6	<5.6	0.5	0.7	<5.7	0.7	<6.4	0.9	0.9	0.7	<5.9
Pb	(2)	n.d.§	<15	<15	n.d.§	n.d.§	n.d.§	<15	<15	n.d.§	<15	<15	<15	<15	<15	17	<15	<15
Th	(1)	6.26	9.65	10.5	6.07	6.25	7.18	6.62	5.87	5.19	5.85	6.36	6.27	6.15	4.65	8.22	5.60	4.91
U	(1)	1.42	2.15	2.83	1.69	1.62	1.64	1.71	1.62	1.43	1.74	1.88	2.14	1.83	1.60	2.21	1.58	1.72
(ppb)																		
Ir	(1)	<1.1	<1.8	<1.5	<0.8	<1.1	<1.2	<1.5	<1.3	<0.9	<1.5	<1.3	<1.4	<1.6	<1.3	<1.5	<1.5	<1.4
Au	(1)	<0.1	<0.8	0.4	1.8	0.9	3.1	<1.9	0.9	0.7	<0.8	1.0	<1.8	0.8	0.7	<1.8	<0.8	0.6

(*Continued*)

TABLE A1. WHOLE-ROCK CHEMICAL COMPOSITIONS OF SAMPLES FROM THE EYREVILLE A AND B DRILL CORES (*Continued*)

Sample		CB6 020	CB6 021	W 031	CB6 023	CB6 024	CB6 025	CB6 027	CB6 029	CB6 030	W 2-04	W 032	CB6 031	CB6 032m	CB6 033m	CB6 034	CB6 035	CB6 036
Core		A	A	A	A	A	A	A	A	A	A	A	A	A	A	A	A	A
Depth (m)		492.7	495.0	498.8	500.7	501.9	503.5	508.6	513.0	514.2	514.4	515.4	515.4	519.4	521.4	521.7	522.0	523.3
Type*		Ex br	Ex br	Ex br	Ex br	Ex br	Ex br	Ex br	Ex br	Ex br	Ex br	Ex br	Ex br	Ex br	Ex br	Ex br	Ex br	Ex br
(wt%)																		
SiO_2		77.3	76.9	77.2	78.6	78.9	77.4	78.4	76.0	75.2	75.2	75.3	75.9	66.4	69.9	70.2	72.7	69.5
TiO_2		0.50	0.48	0.52	0.48	0.45	0.51	0.49	0.56	0.63	0.49	0.53	0.56	0.71	0.71	0.67	0.64	0.67
Al_2O_3		10.1	10.0	10.6	9.7	9.7	10.1	9.9	10.9	10.9	9.9	10.8	10.9	12.9	13.5	12.7	11.6	12.2
Fe_2O_3†		2.62	3.07	2.56	2.34	2.27	3.12	2.48	3.17	3.10	2.96	2.81	3.19	4.47	4.47	4.34	3.90	4.55
MnO		0.04	0.03	0.03	0.03	0.03	0.03	0.03	0.03	0.04	0.03	0.04	0.03	0.08	0.04	0.05	0.05	0.07
MgO		0.69	0.68	0.77	0.62	0.62	0.71	0.69	0.99	1.04	0.77	0.93	0.98	1.49	1.53	1.35	1.19	1.38
CaO		1.07	0.96	0.98	0.95	0.91	0.95	0.95	1.17	1.34	1.01	1.58	1.05	3.73	1.36	1.99	1.77	2.39
Na_2O		1.43	1.38	1.31	1.42	1.42	1.38	1.38	1.40	1.38	1.31	1.85	1.41	1.44	1.53	1.56	1.48	1.58
K_2O		2.71	2.53	2.44	2.52	2.60	2.48	2.51	2.56	2.35	2.52	2.57	2.48	2.49	2.50	2.33	2.39	2.27
P_2O_5		0.09	0.09	0.09	0.08	0.08	0.09	0.09	0.12	0.10	0.10	0.11	0.10	0.12	0.12	0.11	0.13	0.11
SO_3		<0.1	0.1	<0.1	0.1	<0.1	0.1	<0.1	<0.1	<0.1	n.d.§	0.1	<0.1	0.2	<0.1	0.2	0.1	0.2
LOI		2.9	3.2	2.8	2.9	2.6	3.2	2.8	3.1	3.3	4.6	3.2	3.1	5.7	4.2	4.2	3.8	4.4
Total		99.45	99.42	99.30	99.74	99.58	100.07	99.72	100.00	99.38	98.89	99.82	99.70	99.73	99.86	99.70	99.75	99.32
(ppm)	m#																	
Sc	(1)	7.19	7.22	7.45	6.85	6.09	7.30	6.98	7.99	8.40	6.73	6.71	8.07	11.9	11.4	9.85	9.25	10.3
V	(2)	60	60	73	62	54	56	54	70	69	55	57	71	89	99	86	76	79
Cr	(1)	42.1	41.7	37.9	39.9	35.5	44.0	40.5	42.3	45.8	41.4	35.8	41.6	58.5	81.7	63.9	57.5	71.0
Co	(1)	8.45	8.75	6.96	8.19	6.65	10.4	7.79	10.5	9.0	8.54	12.0	12.1	11.5	14.2	11.1	10.6	15.7
Ni	(2)	23	25	22	22	23	25	22	26	25	32	22	29	31	29	26	27	32
Cu	(2)	50	52	<30	<30	30	32	<30	35	33	<30	37	<30	59	<30	51	33	<30
Zn	(1)	41	57	35	41	33	40	43	52	73	44	32	45	87	115	77	57	95
As	(1)	3.51	4.94	3.18	4.43	3.27	4.41	6.47	5.04	5.00	3.88	4.39	4.91	48.9	10.4	9.33	10.3	15.8
Se	(1)	<1.5	<1.5	<1.2	<1.2	<1.3	<1.5	<1.4	<1.5	<1.8	<1.0	<0.9	<1.6	<1.4	<1.5	<1.5	<1.4	<1.5
Br	(1)	3.4	7.2	2.2	2.8	6.0	1.9	2.6	2.0	5.9	5.8	3.1	6.2	2.5	2.6	2.2	2.9	2.5
Rb	(1)	77.8	72.1	64.1	75.4	71.0	72.3	74.3	79.7	74.0	73.9	68.5	73.3	90.0	88.2	80.4	77.9	76.9
Sr	(2)	185	176	170	171	176	173	171	168	176	161	191	175	173	178	178	170	158
Y	(2)	22	19	18	21	18	20	23	24	26	21	18	28	34	28	24	25	25
Zr	(2)	212	188	217	208	197	240	208	215	176	172	223	204	236	200	215	207	200
Nb	(2)	<10	<10	<10	<10	<10	<10	<10	<10	<10	<10	<10	<10	<10	<10	<10	<10	<10
Mo	(2)	<10	<10	<10	<10	<10	<10	<10	<10	<10	n.d.§	<10	<10	<10	<10	<10	<10	<10
Sb	(1)	0.29	0.47	0.29	0.40	0.32	0.40	0.31	0.56	0.70	0.50	0.52	0.63	0.75	0.66	0.69	0.47	0.79
Cs	(1)	2.17	2.05	1.82	2.01	2.07	2.01	2.14	2.58	2.39	2.23	1.91	2.54	3.25	3.13	2.71	2.63	2.46
Ba	(2)	519	474	483	470	524	498	496	498	446	484	499	492	466	458	436	402	393
La	(1)	23.2	19.8	18.3	23.2	17.7	22.4	23.9	23.8	22.5	22.8	18.6	25.7	27.3	29.1	23.1	23.7	24.9
Ce	(1)	48.8	43.5	40.4	48.4	38.1	46.6	50.0	49.7	48.0	48.2	39.2	51.7	57.5	61.7	49.4	50.2	52.0
Nd	(1)	22.2	19.4	17.3	21.4	18.1	20.2	23.1	20.6	23.5	18.2	15.5	22.8	24.8	27.1	20.9	20.6	21.9
Sm	(1)	3.79	4.75	3.73	3.68	4.19	3.71	3.75	3.92	5.49	4.32	3.88	5.93	4.74	5.02	4.12	4.18	4.45
Eu	(1)	1.11	1.02	0.91	1.04	0.87	1.02	1.00	1.15	1.13	1.08	0.91	1.12	1.28	1.31	1.15	1.19	1.20
Gd	(1)	3.86	3.52	3.20	3.75	3.25	3.68	3.95	4.50	3.78	4.10	4.0	4.56	4.73	5.33	4.44	4.73	5.36
Tb	(1)	0.62	0.59	0.57	0.58	0.48	0.58	0.62	0.72	0.70	0.63	0.67	0.75	0.85	0.83	0.71	0.69	0.77
Tm	(1)	0.30	0.31	0.26	0.28	0.25	0.31	0.30	0.42	0.41	0.28	0.31	0.43	0.51	0.42	0.31	0.37	0.37
Yb	(1)	1.93	1.96	1.62	1.63	1.55	1.90	1.75	2.21	2.29	1.77	1.65	2.26	2.93	2.64	2.11	2.27	2.41
Lu	(1)	0.30	0.32	0.27	0.25	0.24	0.29	0.28	0.35	0.36	0.23	0.26	0.35	0.47	0.41	0.34	0.36	0.38
Hf	(1)	6.96	6.72	5.88	4.66	5.06	5.69	5.58	4.81	4.35	4.85	5.50	5.35	6.17	5.39	5.40	4.96	4.98
Ta	(1)	0.66	0.65	0.68	0.68	0.56	0.85	0.71	0.84	0.88	0.67	0.89	0.79	1.01	1.03	0.99	0.82	0.97
W	(1)	<6.7	<1.1	1.2	<6.2	0.7	<6.2	<6.5	3.2	<1.0	0.6	0.9	<1.0	n.d.§	n.d.§	n.d.§	n.d.§	n.d.§
Pb	(2)	<15	<15	<15	<15	26	<15	<15	<15	<15	n.d.§	<15	<15	17	<15	<15	<15	30
Th	(1)	5.86	5.28	6.06	7.04	4.28	6.31	8.13	6.06	6.50	5.99	7.70	6.81	8.58	8.38	7.92	6.47	6.97
U	(1)	1.79	1.78	1.67	1.95	1.56	1.92	2.40	2.26	2.53	1.69	1.90	2.09	2.47	3.01	2.50	2.07	2.55
(ppb)																		
Ir	(1)	<1.4	<1.4	<1.5	<1.2	<1.2	<1.5	<1.4	<1.4	<1.7	<1.0	<1.2	<1.5	<1.2	<1.3	<1.2	<1.2	<1.3
Au	(1)	1.1	<1.7	0.6	0.8	<1.6	1.0	0.7	1.1	1.2	3.7	<0.8	0.9	<2.2	<1.5	0.5	<2.1	<2.6

(*Continued*)

TABLE A1. WHOLE-ROCK CHEMICAL COMPOSITIONS OF SAMPLES FROM THE EYREVILLE A AND B DRILL CORES (*Continued*)

Sample		CB6 037	W 033	CB6 038	CB6 039	CB6 040	CB6 041	W 2-07	CB6 042	W 2-08	CB6 043	CB6 044	W 2-06	CB6 046	CB6 047	CB6 048	W 2-09	W 2-10
Core		A	A	A	A	A	A	A	A	A	A	A	A	A	A	A	A	A
Depth (m)		524.3	525.7	526.7	527.8	537.3	542.3	551.2	563.8	564.4	567.5	571.4	587.0	591.6	599.0	601.6	610.7	616.8
Type*		Ex br	Ex br	Ex br	sb/ gray-wacke	sb/ gray-wacke	sb/ clay	Ex br	Ex br	Ex br	sb/ clay	Ex br	Ex br	sb/ clay	Ex br	sb/ gray-wacke	Ex br	Ex br
(wt%)																		
SiO_2		77.8	75.0	70.5	73.7	74.0	70.0	77.3	80.6	79.2	67.7	79.1	80.5	55.6	77.8	68.4	78.3	79.2
TiO_2		0.51	0.55	0.72	0.87	0.78	0.93	0.46	0.44	0.50	0.86	0.52	0.45	0.92	0.52	0.93	0.48	0.46
Al_2O_3		10.0	10.9	12.3	13.3	12.0	13.9	9.4	9.3	9.6	18.2	9.8	8.6	19.8	9.9	13.9	9.8	9.1
Fe_2O_3†		2.77	3.13	4.02	2.23	4.06	7.46	2.73	1.87	2.50	3.66	2.50	1.42	11.5	2.49	3.10	2.48	2.13
MnO		0.03	0.04	0.07	0.03	0.02	0.02	0.04	0.03	0.04	0.02	0.04	0.04	0.04	0.04	0.14	0.04	0.04
MgO		0.80	0.86	1.30	0.73	0.65	0.55	0.59	0.47	0.55	0.56	0.57	0.26	1.58	0.60	0.86	0.55	0.40
CaO		1.08	1.17	2.46	0.90	0.69	0.42	0.91	0.95	0.94	0.42	0.95	0.69	0.53	1.15	2.32	1.00	0.81
Na_2O		1.41	1.47	1.48	2.58	2.17	0.74	1.42	1.29	1.59	1.73	1.19	1.44	1.20	1.25	0.20	1.32	1.24
K_2O		2.51	2.63	2.41	2.33	2.35	0.36	2.52	2.63	2.60	0.96	2.69	2.57	2.26	2.58	4.61	2.64	2.58
P_2O_5		0.09	0.12	0.12	0.04	0.02	0.02	0.11	0.08	0.10	0.01	0.09	0.05	0.05	0.11	0.06	0.12	0.10
SO_3		<0.1	0.2	<0.1	<0.1	<0.1	<0.1	n.d.§	<0.1	n.d.§	<0.1	0.1	n.d.§	<0.1	0.1	<0.1	n.d.§	n.d.§
LOI		2.8	3.2	4.3	2.7	2.6	5.5	4.0	1.8	3.3	5.5	2.5	4.1	6.2	2.9	5.1	4.0	3.9
Total		99.80	99.27	99.68	99.41	99.34	99.90	99.48	99.46	100.92	99.62	100.05	100.12	99.68	99.44	99.62	100.73	99.96
(ppm)	m#																	
Sc	(1)	6.37	7.80	9.92	11.3	9.11	15.0	6.22	6.01	5.94	21.3	6.56	6.20	20.4	6.70	15.8	6.25	6.21
V	(2)	61	71	80	92	86	121	39	55	51	139	64	56	147	59	99	52	54
Cr	(1)	38.8	43.7	58.9	44.7	37.0	61.9	40.8	34.6	39.3	65.6	39.5	41.4	78.1	40.6	69.5	39.1	46.2
Co	(1)	8.53	9.87	11.5	21.6	17.3	7.53	8.28	7.33	7.29	25.4	8.33	9.19	20.8	7.90	16.8	8.24	8.35
Ni	(2)	24	24	29	24	30	24	12	22	14	28	24	12	35	23	33	15	16
Cu	(2)	<30	<30	<30	<30	<30	<30	<30	31	<30	<30	<30	<30	<30	<30	<30	<30	<30
Zn	(1)	38	44	78	63	38	42	44	51	33	58	37	36	117	40	100	38	36
As	(1)	4.55	5.03	6.33	1.50	0.67	1.11	4.35	2.78	4.76	5.53	7.12	4.19	1.28	5.40	4.85	3.61	3.43
Se	(1)	<1.4	<1.3	<1.0	<2.1	<1.8	<2.6	<1.0	<1.3	<1.0	<2.4	<1.6	<1.0	<3.2	<1.4	<2.8	<1.0	<1.1
Br	(1)	12	4.6	139	23	18	7.9	12	14	9.0	12	15	14	12	14	6.3	8.8	11
Rb	(1)	65.6	83.1	77.7	70.8	58.7	18.2	67.0	71.7	69.4	42.3	76.6	66.3	119	68.1	195	63.2	67.3
Sr	(2)	182	180	168	217	109	96	169	180	161	124	166	178	155	183	119	166	174
Y	(2)	19	23	30	21	27	<10	19	17	17	36	18	20	34	23	69	20	19
Zr	(2)	193	248	211	412	391	398	174	221	171	278	192	180	157	200	342	188	171
Nb	(2)	<10	<10	<10	<10	<10	<10	<10	<10	<10	<10	<10	<10	10	<10	11	<10	<10
Mo	(2)	<10	<10	<10	<10	<10	<10	n.d.§	<10	n.d.§	<10	<10	n.d.§	<10	<10	<10	n.d.§	n.d.§
Sb	(1)	0.40	0.42	0.55	0.32	0.24	0.30	0.26	0.20	0.25	0.37	0.64	0.22	0.35	0.27	0.20	0.22	0.22
Cs	(1)	1.96	2.47	2.96	1.86	1.43	1.40	1.80	1.63	1.67	2.30	2.08	1.64	6.23	1.80	6.68	1.59	1.55
Ba	(2)	514	494	433	558	573	121	451	521	521	223	488	503	401	518	743	551	518
La	(1)	22.5	26.7	24.0	26.5	28.4	8.21	19.3	20.5	19.8	25.6	20.0	18.0	38.4	19.8	45.7	19.5	19.9
Ce	(1)	44.6	56.7	49.7	57.0	58.1	14.6	41.2	41.7	42.6	45.1	42.0	38.6	70.9	42.8	62.5	42.1	42.4
Nd	(1)	17.6	25.7	20.6	24.3	25.3	5.56	18.7	18.2	18.7	21.5	18.0	17.3	29.2	17.2	32.6	17.5	19.6
Sm	(1)	3.31	5.11	4.03	4.47	4.50	1.17	3.76	3.31	3.83	4.10	3.35	3.58	5.52	3.38	7.25	3.80	3.87
Eu	(1)	0.94	1.15	1.21	1.28	1.42	0.24	0.95	0.95	0.94	0.99	0.96	0.96	1.60	0.99	0.87	1.00	1.00
Gd	(1)	3.03	5.22	4.09	4.10	4.82	2.10	3.13	3.55	3.43	3.66	3.24	3.24	5.76	3.46	4.60	3.43	3.38
Tb	(1)	0.52	0.94	0.69	0.64	0.69	0.26	0.53	0.52	0.54	0.73	0.52	0.54	0.82	0.56	0.82	0.53	0.55
Tm	(1)	0.29	0.34	0.39	0.33	0.41	0.24	0.27	0.30	0.25	0.45	0.33	0.28	0.47	0.32	0.59	0.24	0.28
Yb	(1)	1.86	2.09	2.34	2.17	2.17	1.57	1.66	1.63	1.59	3.32	1.82	1.61	2.75	1.77	4.27	1.62	1.71
Lu	(1)	0.29	0.34	0.37	0.34	0.33	0.28	0.21	0.25	0.21	0.56	0.28	0.21	0.42	0.27	0.65	0.21	0.23
Hf	(1)	4.68	5.07	5.11	8.93	9.98	10.8	4.70	4.72	4.99	6.91	5.60	5.11	4.27	4.26	8.07	4.97	5.27
Ta	(1)	0.60	0.75	0.84	0.85	0.70	1.08	0.56	0.53	0.53	0.96	0.69	0.56	0.89	0.61	0.95	0.51	0.54
W	(1)	1.7	<1.7	<4.1	1.6	<4.4	1.6	<0.8	<3.7	0.8	0.7	2.5	0.7	5.1	1.9	14	1.4	3.0
Pb	(2)	15	<15	<15	<15	15	<15	n.d.§	<15	n.d.§	<15	<15	n.d.§	19	<15	<15	n.d.§	n.d.§
Th	(1)	5.70	13.1	7.54	7.54	5.15	8.37	5.30	5.10	5.62	9.05	5.14	5.40	10.5	6.34	11.8	5.23	5.38
U	(1)	1.48	2.64	2.09	1.79	1.21	1.76	1.36	1.68	1.51	10.7	1.57	1.46	1.34	1.94	3.76	1.41	1.37
(ppb)																		
Ir	(1)	<1.2	<1.7	<1.3	<1.8	<1.5	<2.2	<1.0	<1.1	<1.0	<2.1	<1.4	<1.0	<2.6	<1.2	<2.4	<1.1	<1.1
Au	(1)	<1.0	<1.0	<1.1	<1.2	0.3	<0.9	2.7	<1.0	1.4	<1.2	<1.0	0.5	0.6	<1.0	<1.1	1.2	6

(*Continued*)

TABLE A1. WHOLE-ROCK CHEMICAL COMPOSITIONS OF SAMPLES FROM THE EYREVILLE A AND B DRILL CORES (*Continued*)

Sample		CB6 049	W 2-11	CB6 050	CB6 051	W 2-12A	CB6 052	CB6 053	CB6 054	CB6 055	CB6 056	CB6 057	CB6 058	CB6 060	CB6 061	CB6 062	CB6 063	W 2-13
Core		A	A	A	A	A	A	A	A	A	A	A	A	A	A	A	A	A
Depth (m)		622.1	626.3	644.6	655.1	665.2	678.7	680.3	688.2	710.2	721.4	743.4	760.2	803.0	822.3	841.6	863.2	864.3
Type*		sb/ sand-stone	Ex br	sb/ clay	sb/ arkose	Ex br	sb/ silt-stone	sb/ clay	sb/ gray-wacke	sb/ gray-wacke	sb/ clay	sb/ gray-wacke	sb/ silt-stone	sb/ gray-wacke	sb/ gray-wacke	sb/ mud-stone	Ex br	Ex br
(wt%)																		
SiO_2		85.9	78.1	60.7	79.2	76.4	67.0	56.0	77.5	76.1	55.6	79.9	68.5	74.2	75.7	63.1	79.4	78.4
TiO_2		0.34	0.62	0.88	0.85	0.52	0.90	0.92	0.24	1.28	0.96	0.30	0.88	0.50	1.25	0.99	0.46	0.44
Al_2O_3		7.3	9.0	18.5	11.1	10.3	15.5	21.4	12.4	12.2	20.0	10.8	15.5	12.5	12.0	19.4	9.3	8.9
Fe_2O_3	†	0.50	3.12	8.79	0.90	1.55	3.61	8.24	0.95	1.61	10.0	1.65	5.24	4.27	2.06	6.84	2.24	2.29
MnO		0.02	0.06	0.04	0.02	0.02	0.04	0.03	0.01	0.05	0.07	0.01	0.03	0.02	0.08	0.03	0.04	0.04
MgO		0.18	0.43	1.04	0.36	0.50	1.30	1.47	0.55	0.83	2.17	0.59	1.25	0.87	0.53	1.18	0.50	0.46
CaO		0.52	1.24	0.57	0.71	0.60	0.65	0.64	0.64	0.96	0.52	0.44	0.77	0.59	1.00	0.72	1.05	0.96
Na_2O		1.43	1.67	1.46	2.01	1.85	1.37	1.07	1.94	1.52	0.97	1.06	0.89	0.82	1.10	0.91	1.10	1.25
K_2O		2.53	3.11	1.72	2.60	2.81	2.14	2.24	3.27	2.90	2.92	3.13	2.12	2.43	2.67	2.16	2.70	2.50
P_2O_5		0.01	0.10	0.03	0.05	0.05	0.06	0.07	0.02	0.07	0.04	0.02	0.12	0.03	0.06	0.02	0.08	0.12
SO_3		<0.1	n.d.§	<0.1	<0.1	n.d.§	<0.1	<0.1	<0.1	<0.1	<0.1	<0.1	<0.1	0.1	0.1	<0.1	<0.1	n.d.§
LOI		1.2	3.0	5.8	2.0	3.6	7.4	7.6	1.8	2.1	6.3	2.1	4.6	3.5	2.8	3.9	2.4	3.6
Total		99.93	100.45	99.53	99.80	98.20	99.97	99.68	99.32	99.62	99.55	100.00	99.90	99.83	99.35	99.25	99.27	98.96
(ppm)	m#																	
Sc	(1)	2.35	5.19	18.4	6.09	5.36	15.9	22.2	3.04	7.62	22.9	4.67	16.5	11.7	7.02	21.0	5.77	5.51
V	(2)	27	44	130	55	42	123	186	29	71	150	45	96	90	61	139	55	45
Cr	(1)	12.7	27.0	75.9	27.4	29.0	61.3	87.4	18.9	28.2	81.3	22.5	55.0	50.9	29.8	73.8	37.6	43.6
Co	(1)	9.25	8.05	18.7	7.63	7.67	15.3	6.85	2.67	3.78	27.5	6.20	15.4	9.57	5.56	108	7.32	7.46
Ni	(2)	18	13	36	21	13	28	25	20	21	37	21	29	27	23	51	22	10
Cu	(2)	<30	<30	45	<30	<30	34	50	<30	<30	41	<30	30	<30	<30	36	<30	<30
Zn	(1)	13	26	102	23	26	107	68	12	28	102	24	62	45	20	85	26	31
As	(1)	2.41	3.26	7.41	0.76	1.80	2.93	0.47	<0.8	0.35	2.72	1.15	0.67	4.43	3.03	15.2	5.61	3.34
Se	(1)	<0.9	<1.1	<2.3	<1.9	<1.0	<1.9	<2.9	<1.1	<1.6	<3.0	<1.1	<2.3	<1.8	<1.4	<2.6	<1.2	<0.9
Br	(1)	23	5.7	7.8	14	8.9	9.9	9.9	13	8.0	6.5	6.6	5.8	8.5	10	6.8	10	8.8
Rb	(1)	56.9	65.0	110	70.0	66.4	88.8	113	66.9	61.0	133	64.3	90.6	91.8	66.6	106	70.5	72.7
Sr	(2)	193	158	157	202	165	153	340	230	241	149	212	182	180	185	197	181	174
Y	(2)	<10	21	55	24	16	39	21	12	27	39	14	45	26	30	35	21	18
Zr	(2)	204	173	213	517	128	293	156	116	399	162	118	335	124	617	227	193	155
Nb	(2)	<10	<10	12	<10	<10	11	10	<10	10	<10	<10	10	<10	13	<10	<10	<10
Mo	(2)	<10	n.d.§	<10	<10	n.d.§	<10	<10	<10	<10	<10	<10	<10	<10	<10	<10	<10	n.d.§
Sb	(1)	0.08	0.18	0.41	0.15	0.14	0.50	0.29	<0.1	0.14	0.45	0.09	0.30	0.25	0.13	0.51	0.19	0.21
Cs	(1)	0.75	1.26	7.02	1.00	1.42	3.69	6.45	0.82	0.80	6.46	1.16	3.32	3.11	0.87	5.57	1.55	1.55
Ba	(2)	619	550	339	618	563	465	479	765	718	553	734	449	493	649	417	553	548
La	(1)	15.7	16.7	19.9	34.7	15.5	37.1	55.4	12.5	25.8	33.1	12.8	39.8	26.3	30.6	39.0	19.2	18.0
Ce	(1)	31.2	41.2	40.1	69.9	32.4	78.1	99.7	26.5	54.7	66.5	27.2	83.1	52.5	62.6	78.4	40.7	39.0
Nd	(1)	10.9	17.4	15.9	27.8	13.2	34.3	29.2	10.9	24.9	28.7	10.8	36.1	23.9	27.6	34.6	17.7	17.0
Sm	(1)	1.96	3.39	2.98	5.21	3.07	6.69	4.23	2.04	4.70	5.56	2.07	7.52	4.40	5.02	6.65	3.28	3.78
Eu	(1)	0.57	0.90	0.91	1.18	0.80	1.87	0.98	0.72	1.34	1.41	0.65	2.02	1.19	1.06	1.74	0.85	0.94
Gd	(1)	2.22	3.43	4.49	4.97	2.39	7.35	3.74	1.53	4.21	5.26	2.10	6.93	4.23	4.14	5.99	3.31	3.52
Tb	(1)	0.27	0.56	0.86	0.73	0.43	1.07	0.53	0.30	0.72	0.86	0.31	1.16	0.66	0.68	0.97	0.50	0.55
Tm	(1)	0.17	0.29	0.60	0.38	0.21	0.53	0.31	0.16	0.39	0.53	0.19	0.62	0.34	0.45	0.50	0.25	0.28
Yb	(1)	0.80	1.87	3.91	2.20	1.40	3.22	1.81	1.01	2.60	3.40	1.05	3.83	2.14	2.61	2.84	1.43	1.60
Lu	(1)	0.12	0.25	0.62	0.35	0.18	0.51	0.32	0.15	0.40	0.54	0.16	0.59	0.33	0.42	0.45	0.22	0.20
Hf	(1)	2.72	4.94	5.81	11.9	3.92	7.14	4.05	4.09	11.34	4.47	2.44	7.99	3.38	15.8	5.94	3.55	4.67
Ta	(1)	0.41	0.57	1.05	1.03	0.48	1.03	1.04	0.26	1.19	0.89	0.29	1.04	0.62	1.34	1.04	0.52	0.57
W	(1)	4.3	1.2	2.0	0.7	1.9	0.5	5.4	<2.3	1.6	1.4	<1.0	1.1	1.5	1.2	1.4	0.8	<0.8
Pb	(2)	<15	n.d.§	<15	15	n.d.§	<15	<15	<15	15	<15	<15	<15	<15	<15	<15	<15	n.d.§
Th	(1)	5.31	5.64	10.3	12.0	4.63	9.69	12.9	2.31	6.74	10.7	3.89	9.40	7.52	11.6	11.3	7.52	5.04
U	(1)	0.94	1.44	1.77	2.84	1.44	2.79	2.93	0.79	1.81	1.99	0.82	2.76	1.75	3.06	2.80	1.28	1.51
(ppb)																		
Ir	(1)	<0.7	<1.1	<2.0	<1.6	<1.0	<1.6	<2.6	<0.9	<1.3	<3.1	<1.0	<2.4	<1.8	<1.3	<2.6	<1.3	<0.9
Au	(1)	<0.9	2.6	<1.4	<1.4	2.1	<1.3	<1.3	<1.1	0.4	0.7	0.2	0.6	<0.7	<0.8	1.0	0.4	1.7

(*Continued*)

TABLE A1. WHOLE-ROCK CHEMICAL COMPOSITIONS OF SAMPLES FROM THE EYREVILLE A AND B DRILL CORES (*Continued*)

Sample		CB6 064	CB6 065	CB6 066	CB6 067	CB6 068	CB6 069	CB6 070	CB6 071	CB6 072	W 035	CB6 073	W 036a	CB6 074	CB6 075	CB6 076	W 037	W 038
Core		A	A	A	B	B	B	B	B	B	B	B	B	B	B	B	B	B
Depth (m)		904.6	915.8	940.3	989.2	1007.3	1036.8	1065.7	1073.4	1096.8	1105.9	1118.0	1123.8	1123.9	1140.5	1147.5	1161.3	1166.6
Type*		sb/ gray-wacke	sb/ gray-wacke	sb/ gray-wacke	sb/ gray-wacke	sb/ mud-stone	sb/ mud-stone	sb/ silt-stone	sb/ sand-stone	gran-ite	gran-ite	Gran-ite	gran-ite gneiss	peg	gran-ite gneiss	xeno	gran-ite gneiss	gran-ite gneiss
(wt%)																		
SiO_2		87.1	73.0	74.1	66.0	60.4	59.6	64.8	86.5	71.8	71.8	71.5	73.5	69.8	74.9	55.8	72.6	76.0
TiO_2		0.29	0.62	1.12	1.01	0.91	0.94	0.95	0.12	0.30	0.24	0.29	0.73	0.11	0.19	3.12	0.27	0.19
Al_2O_3		5.5	12.6	12.9	15.8	17.1	17.4	16.6	7.0	14.4	14.4	14.7	12.8	15.2	12.4	13.8	14.5	12.2
Fe_2O_3	†	2.14	2.66	2.97	5.42	6.36	6.17	6.05	0.74	2.07	1.88	2.24	3.72	1.33	1.12	13.7	1.95	1.46
MnO		0.10	0.03	0.05	0.04	0.11	0.09	0.04	0.01	0.03	0.03	0.04	0.06	0.01	0.03	0.22	0.04	0.02
MgO		0.25	0.94	0.89	1.30	1.62	1.61	1.60	0.22	0.53	0.51	0.55	0.74	0.19	0.25	3.25	0.50	0.19
CaO		0.38	0.68	1.12	1.09	0.90	0.95	1.35	0.27	1.55	2.04	1.94	2.48	0.20	0.41	3.28	1.87	0.61
Na_2O		0.51	0.76	0.87	0.77	0.84	0.86	1.19	0.37	2.82	3.16	3.23	3.88	1.44	1.69	2.24	3.61	1.95
K_2O		1.84	2.74	2.17	2.60	2.22	2.15	2.33	2.87	4.73	4.66	4.73	1.09	10.3	7.63	3.19	3.91	6.59
P_2O_5		<0.01	0.10	0.10	0.12	0.08	0.09	0.26	0.01	0.07	0.05	0.08	0.09	0.02	0.01	0.50	0.03	0.01
SO_3		<0.1	<0.1	<0.1	0.1	<0.1	<0.1	<0.1	<0.1	<0.1	<0.1	<0.1	<0.1	<0.1	<0.1	<0.1	<0.1	<0.1
LOI		1.8	5.7	3.4	5.0	8.9	9.5	4.8	1.8	0.8	0.6	0.6	0.6	0.6	0.7	0.4	0.5	0.6
Total		99.91	99.83	99.69	99.25	99.44	99.36	99.97	99.91	99.10	99.37	99.90	99.69	99.20	99.33	99.50	99.78	99.82
(ppm)	m#																	
Sc	(1)	4.39	9.21	12.3	16.1	19.7	20.2	19.3	2.39	3.72	2.99	3.59	11.7	3.26	6.32	35.2	9.37	2.80
V	(2)	29	86	90	103	131	137	116	25	32	21	35	76	21	<15	267	29	22
Cr	(1)	18.7	40.9	45.7	57.3	72.7	74.4	75.4	13.5	11.0	10.0	11.3	9.82	7.28	8.29	18.8	11.2	8.58
Co	(1)	5.63	13.0	5.43	12.3	18.9	18.3	14.7	2.19	2.78	2.58	2.69	4.99	3.29	0.74	29.6	2.40	0.59
Ni	(2)	20	25	23	28	29	29	30	17	24	25	23	29	31	29	85	33	31
Cu	(2)	<30	<30	<30	<30	<30	<30	35	<30	<30	<30	<30	<30	<30	<30	<30	<30	<30
Zn	(1)	18	84	31	65	97	100	79	<4.2	44	38	50	84	22	35	387	60	23
As	(1)	39.1	4.75	1.07	2.66	3.38	1.44	1.20	0.95	<0.8	0.57	<0.8	0.8	<0.5	<0.6	<1.0	0.91	0.45
Se	(1)	<1.1	1.75	<2.2	1.84	<2.7	<2.9	<2.7	0.11	<1.2	<1.0	<1.2	<1.5	<1.0	<1.3	<2.7	<1.4	<1.0
Br	(1)	16	8.0	4.5	4.6	6.1	12	4.4	5.7	<0.6	0.7	<0.6	0.3	0.8	<0.7	<1.2	0.5	0.5
Rb	(1)	46.3	83.2	63.5	95.0	105	109	116	78.8	224	216	242	128	471	346	454	205	297
Sr	(2)	126	179	196	190	183	193	223	183	232	241	257	121	156	103	48	176	98
Y	(2)	16	24	28	39	41	47	43	<10	41	39	43	96	79	73	116	111	85
Zr	(2)	111	263	702	431	238	273	300	90	252	235	266	222	18	214	282	249	236
Nb	(2)	<10	<10	<10	10	<10	10	<10	<10	13	<10	10	41	<10	19	26	<10	<10
Mo	(2)	<10	<10	<10	<10	<10	<10	<10	<10	<10	<10	<10	<10	<10	<10	<10	<10	<10
Sb	(1)	0.26	0.42	0.25	0.31	0.43	0.46	0.27	0.11	0.06	<0.1	<0.1	<0.1	0.04	0.05	0.29	<0.1	0.05
Cs	(1)	0.56	1.86	1.24	3.08	4.99	5.75	4.82	1.11	2.30	2.65	3.25	5.13	4.87	4.94	27.3	4.09	3.83
Ba	(2)	399	597	508	591	492	472	474	672	946	979	1105	109	1021	701	465	750	773
La	(1)	9.10	26.6	27.4	39.6	43.6	43.7	40.1	6.45	83.9	80.6	93.0	37.5	12.1	39.2	26.0	96.0	41.6
Ce	(1)	19.7	55.0	58.1	82.0	91.3	91.4	81.8	11.9	150	148	166	85.1	29.1	79.3	60.1	180	90.2
Nd	(1)	9.11	25.2	25.4	36.2	39.6	40.0	35.6	4.91	48.2	46.9	50.0	42.5	14.0	34.5	34.7	58.8	39.0
Sm	(1)	1.67	4.77	5.55	7.68	8.13	8.23	7.71	0.96	6.54	6.67	6.93	9.79	4.15	6.20	7.98	10.4	8.09
Eu	(1)	0.41	1.31	1.25	1.85	2.01	2.00	2.00	0.34	1.09	1.16	1.13	0.97	0.83	0.95	2.33	1.37	1.07
Gd	(1)	1.85	4.14	5.01	7.51	8.06	8.46	7.71	0.80	6.47	3.2	8.55	12.0	3.66	6.02	10.0	11.8	8.25
Tb	(1)	0.36	0.71	0.85	1.17	1.21	1.35	1.22	0.16	0.57	0.56	0.61	2.02	0.51	1.03	1.92	1.84	1.58
Tm	(1)	0.30	0.36	0.52	0.64	0.69	0.69	0.58	0.14	0.39	0.29	0.45	1.06	0.33	0.51	1.15	0.91	0.55
Yb	(1)	2.28	2.23	3.00	3.72	3.66	4.03	3.91	0.79	1.17	1.07	1.44	7.60	2.08	3.03	7.43	6.22	3.35
Lu	(1)	0.35	0.36	0.46	0.57	0.58	0.63	0.60	0.13	0.21	0.21	0.21	1.20	0.30	0.45	1.11	0.98	0.49
Hf	(1)	2.25	6.56	16.1	10.1	7.18	7.40	7.40	1.82	6.38	6.04	7.25	7.82	0.15	6.63	8.95	6.70	7.85
Ta	(1)	0.40	0.88	1.31	1.25	1.13	1.19	1.10	0.25	1.61	1.83	1.44	4.47	1.36	1.99	1.93	1.93	1.04
W	(1)	<0.5	1.0	1.5	1.1	2.6	1.3	3.1	0.4	0.9	<2.3	1.1	<2.7	0.91	n.d.§	n.d.§	<3.4	<2.4
Pb	(2)	<15	<15	<15	15	<15	<15	<15	<15	28	19	24	<15	57	47	<15	27	47
Th	(1)	2.59	8.03	9.38	10.4	11.8	12.2	10.3	2.50	34.9	44.9	43.5	22.3	6.84	17.5	8.17	57.3	18.9
U	(1)	0.65	3.76	2.61	3.23	3.79	3.96	2.75	0.77	4.84	5.19	6.21	7.92	34.4	3.49	2.66	6.18	3.16
(ppb)																		
Ir	(1)	<1.0	<1.6	<2.2	<2.3	<2.8	<3.0	<2.7	<0.7	<1.6	<1.7	<1.8	<1.9	<0.9	<1.1	<2.4	0.75	<1.6
Au	(1)	<0.5	0.4	0.5	0.7	1.1	0.8	0.8	0.2	<1.0	<1.3	<1.1	<1.5	0.3	<0.7	0.5	<1.3	<1.1

(*Continued*)

TABLE A1. WHOLE-ROCK CHEMICAL COMPOSITIONS OF SAMPLES FROM THE EYREVILLE A AND B DRILL CORES (*Continued*)

Sample		CB6 077	CB6 078	W 039a	W 039b	W 040	CB6 079	CB6 080	W 041	CB6 081	W 042a	W 042b	W 043	CB6 082	W 044	CB6 083	W 045	W 046
Core		B	B	B	B	B	B	B	B	B	B	B	B	B	B	B	B	B
Depth (m)		1174.0	1175.1	1175.2	1175.2	1206.1	1212.4	1221.3	1233.2	1240.1	1252.0	1252.0	1263.8	1276.3	1289.5	1294.8	1312.7	1329.0
Type*		peg	xeno	granite gneiss	xeno	granite gneiss	granite gneiss	granite	granite	granite	peg	granite gneiss	granite	granite	granite	granite	granite	granite
(wt%)																		
SiO_2		73.7	49.8	76.1	51.2	73.8	74.7	72.6	70.8	76.3	72.5	69.9	71.9	71.4	71.8	71.4	71.9	71.3
TiO_2		0.17	2.52	0.14	2.52	0.18	0.17	0.27	0.33	0.13	0.18	0.70	0.25	0.28	0.26	0.30	0.32	0.30
Al_2O_3		14.5	15.2	13.2	15.8	13.2	13.3	14.0	14.7	12.2	14.7	13.3	14.6	14.6	14.7	14.7	14.2	14.7
Fe_2O_3†		1.09	11.5	1.63	11.2	1.76	1.51	1.38	2.42	1.18	0.69	6.46	1.83	2.06	1.89	2.14	1.90	2.11
MnO		0.02	0.16	0.02	0.16	0.05	0.03	0.04	0.04	0.02	0.02	0.08	0.04	0.04	0.04	0.04	0.04	0.04
MgO		0.10	5.69	0.18	5.37	0.25	0.15	0.30	0.59	0.10	0.14	0.47	0.44	0.48	0.46	0.52	0.42	0.54
CaO		1.76	5.35	2.34	5.08	0.83	0.93	1.51	2.03	0.84	1.27	2.28	1.85	1.89	1.87	2.11	1.61	2.01
Na_2O		4.20	1.05	4.04	1.62	2.78	2.92	3.35	3.14	2.41	2.89	3.78	3.34	3.28	3.34	3.33	3.03	3.24
K_2O		3.54	3.79	1.61	3.84	6.21	5.57	5.07	4.88	5.71	6.56	2.47	4.92	4.68	4.81	4.70	5.45	4.59
P_2O_5		0.01	1.16	0.01	1.16	0.01	0.01	0.07	0.09	0.01	0.03	0.17	0.07	0.07	0.07	0.09	0.17	0.08
SO_3		<0.1	<0.1	<0.1	<0.1	<0.1	<0.1	<0.1	<0.1	<0.1	<0.1	<0.1	<0.1	<0.1	<0.1	<0.1	<0.1	<0.1
LOI		0.8	3.0	0.5	1.3	0.4	0.4	0.6	0.5	0.6	0.2	0.2	0.3	0.5	0.5	0.6	0.4	0.5
Total		99.89	99.22	99.77	99.25	99.47	99.69	99.19	99.52	99.50	99.18	99.81	99.54	99.28	99.74	99.93	99.44	99.41
(ppm)	m#																	
Sc	(1)	2.22	17.2	4.22	15.0	11.9	9.55	5.24	3.63	1.63	1.56	6.64	3.25	3.62	4.00	8.84	6.66	3.72
V	(2)	<15	199	13	177	18	15	25	32	<15	16	47	33	24	33	23	28	26
Cr	(1)	9.74	60.9	8.94	54.8	7.9	10.1	9.64	8.70	10.8	6.14	10.1	8.34	8.26	8.65	13.9	8.67	10.0
Co	(1)	8.09	35.2	1.20	36.1	1.03	1.05	1.39	3.31	0.67	0.65	3.47	2.23	2.89	2.44	2.74	2.41	2.96
Ni	(2)	24	81	25	40	34	32	29	23	23	23	24	24	24	24	25	26	23
Cu	(2)	109	<30	<30	<30	<30	37	<30	<30	<30	<30	<30	<30	<30	<30	38	<30	<30
Zn	(1)	38	203	29	185	59	53	49	65	31	20	132	49	59	56	73	53	58
As	(1)	0.51	0.51	<0.8	0.60	0.56	<0.7	878	<1.2	<0.6	0.32	0.44	0.88	<0.8	0.64	0.28	0.08	0.53
Se	(1)	1.04	<2.1	<1.1	<1.8	<1.3	<1.4	<1.3	<1.7	<1.0	<0.7	<1.4	<1.1	<1.2	<1.1	<1.4	<1.8	<1.2
Br	(1)	<0.9	<1.1	0.4	0.4	0.4	<0.9	<0.9	<1.1	<0.7	0.6	0.6	0.4	<1.0	0.6	<1.0	<0.7	0.4
Rb	(1)	145	321	63	333	251	237	273	217	231	241	137	242	231	218	220	234	230
Sr	(2)	152	647	420	838	82	73	257	269	151	200	155	221	232	226	231	229	250
Y	(2)	39	63	50	61	99	91	72	39	38	39	39	49	41	42	41	67	39
Zr	(2)	68	297	195	354	230	205	206	341	168	21	666	242	243	254	264	300	289
Nb	(2)	14	25	<10	<10	<10	13	14	<10	<10	<10	23	<10	13	<10	13	<10	<10
Mo	(2)	11	<10	<10	12	<10	<10	<10	<10	<10	<10	<10	<10	<10	<10	<10	<10	<10
Sb	(1)	0.07	0.22	<0.1	0.17	<0.1	0.05	0.06	<0.1	<0.1	0.05	<0.1	<0.1	0.07	<0.1	<0.1	<0.1	<0.1
Cs	(1)	4.57	19.5	1.44	17.8	3.46	2.81	5.01	2.73	1.59	2.92	3.11	3.75	3.02	3.12	3.31	3.71	3.44
Ba	(2)	442	1274	376	1409	786	715	845	1173	643	629	257	832	937	886	1009	849	936
La	(1)	40.1	98.2	35.7	104	48.9	49.4	71.6	117	44.1	6.64	65.6	69.5	88.3	74	94.2	84.0	87.2
Ce	(1)	75.6	197	77.9	205	107	102	133	209	87.7	12.8	130	129	155	136	166	156	158
Nd	(1)	28.8	84.9	34.1	87.1	48.9	46.3	47.4	65.0	37.0	5.52	51.2	41.1	50.5	41.8	52.3	56.6	50.4
Sm	(1)	5.23	13.9	7.49	13.4	9.55	8.79	7.08	9.23	6.28	1.10	9.16	6.67	6.46	5.86	6.64	10.4	7.20
Eu	(1)	1.07	4.92	1.03	2.71	1.29	1.26	1.50	1.40	1.19	0.91	1.31	1.06	1.26	1.10	1.30	1.53	1.24
Gd	(1)	4.51	9.80	8.88	8.80	11.2	9.21	6.32	5.50	4.95	1.20	6.02	3.8	5.87	2.9	5.37	7.87	3.30
Tb	(1)	0.69	1.45	1.47	1.40	1.91	1.61	1.10	0.62	0.75	0.13	0.99	0.64	0.61	0.48	0.73	1.29	0.58
Tm	(1)	0.37	0.45	0.61	0.66	0.93	0.76	0.57	0.23	0.26	0.07	0.51	0.28	0.30	0.24	0.25	0.34	0.24
Yb	(1)	1.72	2.70	3.91	2.34	6.13	4.97	3.24	1.14	1.38	0.59	2.77	1.32	1.36	0.93	1.07	2.00	1.08
Lu	(1)	0.26	0.38	0.62	0.32	0.97	0.74	0.47	0.16	0.20	0.08	0.50	0.20	0.22	0.14	0.16	0.22	0.16
Hf	(1)	1.69	7.08	6.04	7.76	6.79	6.32	5.69	8.51	5.54	1.03	17.8	6.23	6.94	5.98	7.03	7.32	7.55
Ta	(1)	2.36	1.86	2.42	3.22	0.86	1.06	2.09	1.17	0.37	1.05	2.61	2.37	1.74	1.12	1.01	1.42	1.42
W	(1)	n.d.§	n.d.§	1.7	5.6	<2.0	n.d.§	n.d.§	<2.6	n.d.§	<1.8	<2.7	<3.3	n.d.§	<2.5	n.d.§	<1.5	<2.7
Pb	(2)	34	<15	18	<15	32	29	39	26	41	43	21	32	23	34	32	33	23
Th	(1)	22.4	6.85	16.2	8.44	18.6	17.2	29.5	45.8	18.3	4.63	32.6	41.1	39.6	30.6	32.5	39.4	39.0
U	(1)	7.06	3.03	5.75	3.3	2.71	5.25	4.78	3.20	2.51	2.52	6.90	7.34	4.13	2.42	2.23	2.52	3.10
(ppb)																		
Ir	(1)	<0.9	<0.4	<1.5	<1.9	<1.7	<1.2	<1.1	<0.8	<0.8	<0.9	<2.0	<1.8	<1.0	<1.8	<1.2	<0.9	<2.0
Au	(1)	0.5	1.6	<1.7	1.2	<1.3	<0.9	0.5	1.1	<0.7	<1.2	<1.5	<1.4	0.6	<1.4	<0.9	0.9	<1.7

(*Continued*)

TABLE A1. WHOLE-ROCK CHEMICAL COMPOSITIONS OF SAMPLES FROM THE EYREVILLE A AND B DRILL CORES (*Continued*)

Sample		W 047	CB6 084	CB6 085	W 048	W 049a	W 049b	CB6 086	CB6 087	CB6 088	W 050	CB6 089	W 051	RG 001	CB6 090	W 052	RG 002	RG 003
Core		B	B	B	B	B	B	B	B	B	B	B	B	B	B	B	B	B
Depth (m)		1336.4	1346.4	1355.3	1360.1	1367.9	1367.9	1369.0	1371.1	1371.4	1371.8	1375.6	1377.4	1378.2	1382.5	1383.1	1384.4	1387.5
Type*		gran-ite	gran-ite	gran-ite	gran-ite	gran-ite	peg	gran-ite	sand-stone	sand-stone	sand-stone	sand-stone	amph	amph	amph	amph	amph	amph
(wt%)																		
SiO_2		71.5	72.0	71.7	71.8	71.9	72.7	71.5	83.6	86.9	84.9	86.0	46.2	44.8	47.0	46.3	44.5	44.4
TiO_2		0.27	0.28	0.27	0.30	0.29	0.03	0.28	0.30	0.20	0.19	0.13	1.14	1.26	1.20	1.15	1.17	2.45
Al_2O_3		14.6	14.1	14.5	14.4	14.6	13.9	14.5	8.1	6.8	7.5	6.3	18.4	18.5	19.1	18.8	18.2	17.3
Fe_2O_3†		1.99	1.99	2.02	2.05	1.99	0.78	2.02	1.56	1.01	1.29	1.72	13.6	11.5	11.9	12.3	10.5	10.8
MnO		0.04	0.04	0.04	0.04	0.03	0.29	0.04	0.02	0.01	0.02	0.01	0.14	0.31	0.14	0.14	0.27	0.32
MgO		0.45	0.36	0.45	0.47	0.47	0.09	0.50	0.36	0.20	0.21	0.34	6.06	5.34	6.18	6.49	6.16	5.13
CaO		1.90	1.31	1.76	1.72	1.77	2.59	1.93	0.36	0.21	0.28	0.28	7.93	8.36	8.23	7.85	10.8	7.78
Na_2O		3.44	2.92	3.26	3.16	3.15	4.46	3.24	0.57	0.26	0.25	0.32	2.28	1.93	2.58	2.58	3.00	3.38
K_2O		4.72	5.77	4.89	5.15	4.49	2.53	4.57	2.27	2.09	2.64	2.72	0.25	0.97	0.21	0.23	0.30	3.02
P_2O_5		0.07	0.08	0.07	0.07	0.07	<0.01	0.07	0.05	0.01	0.01	<0.01	0.24	0.18	0.14	0.14	0.15	0.34
SO_3		<0.1	<0.1	<0.1	<0.1	<0.1	<0.1	<0.1	<0.1	<0.1	<0.1	<0.1	0.1	0.1	0.2	0.3	0.1	0.8
LOI		0.5	0.5	0.3	0.4	1.0	2.4	1.1	2.4	1.6	1.9	1.4	3.5	6.6	3.0	3.3	4.0	3.8
Total		99.48	99.35	99.26	99.56	99.76	99.77	99.75	99.59	99.29	99.19	99.22	99.84	99.85	99.88	99.58	99.15	99.52
(ppm)	m#																	
Sc	(1)	3.62	3.43	3.89	3.59	3.59	12.0	3.55	4.37	3.05	2.83	3.52	25.3	n.d.§	27.1	26.7	n.d.§	n.d.§
V	(2)	28	21	28	34	33	<15	24	36	23	28	33	173	190	186	178	178	182
Cr	(1)	9.75	11.4	8.78	9.1	9.82	6.81	8.82	17.8	14.1	16.4	16.9	148	n.d.§	160	151	n.d.§	n.d.§
Co	(1)	2.52	1.56	2.54	2.34	2.54	0.90	2.58	5.80	3.80	3.45	1.37	46.1	n.d.§	56.3	54.2	n.d.§	n.d.§
Ni	(2)	25	23	24	27	21	41	23	21	19	18	18	93	46	98	105	41	39
Cu	(2)	<30	<30	<30	<30	<30	<30	<30	<30	<30	<30	<30	37	41	65	42	39	70
Zn	(1)	52	50	72	54	58	41	60	42	17	14	14	77	n.d.§	102	98	n.d.§	n.d.§
As	(1)	0.9	<0.7	0.22	<0.8	0.69	<0.8	<0.6	1.63	1.41	1.81	0.13	<1.3	n.d.§	<0.8	<1.1	n.d.§	n.d.§
Se	(1)	0.6	<1.2	<1.3	<1.5	<1.1	0.57	<1.2	<1.1	<1.0	<1.0	<1.0	<2.6	n.d.§	<2.2	<2.7	n.d.§	n.d.§
Br	(1)	0.6	<0.8	<0.9	0.5	0.5	0.7	<0.7	2.3	3.5	1.9	5.2	0.6	n.d.§	0.7	0.6	n.d.§	n.d.§
Rb	(1)	254	207	262	233	220	316	216	104	60.1	71.9	80.6	17.9	n.d.§	12.6	25.5	n.d.§	n.d.§
Sr	(2)	231	290	225	221	238	34	234	88	96	144	137	317	287	328	343	406	210
Y	(2)	45	35	43	54	40	108	39	25	10	<10	15	<10	21	<10	<10	<10	61
Zr	(2)	290	297	231	307	291	<15	236	160	108	481	67	50	94	82	56	88	218
Nb	(2)	<10	<10	18	<10	<10	85	14	<10	<10	<10	<10	<10	<10	<10	<10	<10	46
Mo	(2)	<10	12	<10	<10	<10	<10	<10	<10	<10	<10	<10	<10	<10	<10	<10	<10	<10
Sb	(1)	<0.1	<0.1	0.05	<0.1	<0.1	<0.1	0.05	0.13	0.12	0.10	0.07	0.09	n.d.§	0.08	0.09	n.d.§	n.d.§
Cs	(1)	3.86	2.06	5.04	3.63	3.76	4.27	3.70	3.20	1.39	1.43	1.70	1.64	n.d.§	2.11	2.13	n.d.§	n.d.§
Ba	(2)	854	1039	849	955	908	<30	912	408	422	631	601	50	177	76	69	80	1042
La	(1)	92.8	157	101	87.1	107	4.84	106	36.9	12.6	9.81	8.70	5.08	n.d.§	4.97	4.58	n.d.§	n.d.§
Ce	(1)	174	291	177	162	195	14.0	187	72.7	26.5	20.1	19.0	12.5	n.d.§	12.4	11.0	n.d.§	n.d.§
Nd	(1)	57.1	90.8	56.9	52.1	59.5	5.31	60.4	27.0	11.3	7.75	8.38	6.48	n.d.§	8.06	6.28	n.d.§	n.d.§
Sm	(1)	8.20	11.6	7.76	7.50	8.68	2.68	7.64	4.36	1.92	1.79	1.67	2.00	n.d.§	2.05	1.85	n.d.§	n.d.§
Eu	(1)	1.27	2.09	1.30	1.30	1.32	0.22	1.29	0.85	0.55	0.49	0.59	0.92	n.d.§	0.98	0.85	n.d.§	n.d.§
Gd	(1)	4.10	7.95	7.48	4.50	3.60	3.59	7.16	3.89	1.99	1.28	1.67	n.d.	n.d.§	<1.42	n.d.	n.d.§	n.d.§
Tb	(1)	0.68	0.78	0.75	0.72	0.61	0.99	0.61	0.66	0.36	0.23	0.30	0.44	n.d.§	0.52	0.43	n.d.§	n.d.§
Tm	(1)	0.31	0.24	0.41	0.39	0.28	1.15	0.34	0.30	0.22	0.16	0.21	0.20	n.d.§	0.28	0.20	n.d.§	n.d.§
Yb	(1)	1.16	1.06	1.62	1.94	1.18	8.86	1.29	1.98	1.45	0.90	1.44	1.29	n.d.§	1.46	1.20	n.d.§	n.d.§
Lu	(1)	0.22	0.15	0.21	0.30	0.21	1.50	0.18	0.32	0.23	0.15	0.24	0.21	n.d.§	0.22	0.19	n.d.§	n.d.§
Hf	(1)	7.84	7.51	6.81	7.34	7.49	1.56	6.61	4.19	2.69	2.59	1.33	1.93	n.d.§	1.94	1.84	n.d.§	n.d.§
Ta	(1)	2.17	0.69	3.15	1.42	2.67	8.69	2.25	0.98	0.45	0.31	0.24	0.48	n.d.§	0.69	0.64	n.d.§	n.d.§
W	(1)	<3.5	n.d.§	n.d.§	71.5	<3.3	3.2	n.d.§	n.d.§	n.d.§	<1.7	n.d.§	<5.8	n.d.§	n.d.§	0.5	n.d.§	n.d.§
Pb	(2)	26	33	34	23	20	<15	25	<15	<15	<15	<15	<15	<15	<15	<15	<15	<15
Th	(1)	47.4	51.1	49.1	38.9	49.3	6.92	47.9	14.0	3.22	2.92	3.03	0.77	n.d.§	0.79	0.84	n.d.§	n.d.§
U	(1)	5.96	3.01	10.2	4.77	6.47	6.43	8.92	2.75	1.22	1.12	0.95	<0.5	n.d.§	0.25	<0.4	n.d.§	n.d.§
(ppb)																		
Ir	(1)	<2.1	<1.0	<1.0	<2.0	<1.9	0.3	<1.0	<1.0	<0.8	<0.8	<0.8	<2.6	n.d.§	<2.1	<2.8	n.d.§	n.d.§
Au	(1)	<1.5	0.6	0.3	<1.8	0.7	<1.7	0.5	0.2	<0.4	0.4	0.1	<1.3	n.d.§	<1.0	<1.1	n.d.§	n.d.§

(*Continued*)

TABLE A1. WHOLE-ROCK CHEMICAL COMPOSITIONS OF SAMPLES FROM THE EYREVILLE A AND B DRILL CORES (*Continued*)

Sample		CB6 091	W 053a	W 053b	W 2-14	CB6 092	W 054	W 055	CB6 093	CB6 094	W 056a	CB6 095	W 057	W 058	KB 2	W 059	W 060	KB 3
Core		B	B	B	B	B	B	B	B	B	B	B	B	B	B	B	B	B
Depth (m)		1390.4	1390.4	1390.5	1395.3	1396.5	1396.7	1397.4	1399.2	1399.7	1400.1	1401.3	1401.7	1402.3	1402.9	1403.2	1403.6	1404.4
Type*		sand-stone	sand-stone	sand-stone	schist/ catacl.	sand-stone	sand-stone	sv	sv	sv	sv	sv	sv	imr	imr	imr	imr	imr
Unit**								SU	SU	SU	SU	SU	SU	M2	M2	M2	M2	M2
(wt%)																		
SiO_2		89.4	85.7	85.6	68.1	79.1	77.4	69.9	69.7	68.5	69.6	68.9	69.1	70.0	70.0	69.6	70.6	67.2
TiO_2		0.20	0.25	0.18	0.91	0.52	0.55	0.81	0.81	0.83	0.82	0.83	0.83	0.82	0.65	0.81	0.76	0.81
Al_2O_3		5.4	6.8	7.4	14.4	10.3	10.7	13.8	13.6	14.7	13.6	14.0	14.5	14.3	12.8	14.2	13.9	12.7
Fe_2O_3†		0.91	1.54	1.33	6.70	2.64	3.01	4.59	5.10	5.15	5.24	4.93	4.98	5.51	4.96	4.84	4.66	4.83
MnO		0.01	0.01	0.02	0.10	0.02	0.03	0.05	0.05	0.05	0.06	0.07	0.05	0.07	0.05	0.05	0.04	0.05
MgO		0.17	0.30	0.30	1.91	0.89	0.95	1.54	1.51	1.51	1.45	1.37	0.99	0.99	0.85	0.98	0.94	0.90
CaO		0.23	0.32	0.32	1.40	0.45	0.58	1.37	1.38	1.36	1.56	1.89	1.92	1.64	1.35	1.80	1.69	1.60
Na_2O		0.18	0.41	0.29	0.80	0.74	0.74	1.93	1.62	1.53	1.40	1.65	1.56	1.12	1.46	1.34	1.20	1.32
K_2O		1.67	2.45	2.72	1.56	2.75	2.53	2.88	3.39	3.33	3.31	3.50	3.48	3.50	2.00	3.58	3.51	3.29
P_2O_5		0.02	<0.01	0.01	0.17	0.05	0.06	0.13	0.13	0.13	0.13	0.12	0.12	0.12	0.11	0.12	0.12	0.11
SO_3		<0.1	<0.1	<0.1	n.d.§	<0.1	0.1	<0.1	<0.1	<0.1	<0.1	<0.1	<0.1	<0.1	n.d.§	<0.1	<0.1	n.d.§
LOI		1.3	1.5	1.6	3.3	2.4	2.6	2.4	2.5	2.6	2.3	2.2	2.2	1.7	4.4	1.9	2.2	5.6
Total		99.49	99.28	99.77	99.35	99.86	99.25	99.40	99.79	99.69	99.47	99.46	99.73	99.77	98.63	99.22	99.62	98.41
(ppm)	m#																	
Sc	(1)	2.40	2.39	2.59	14.4	7.37	8.06	12.6	11.9	12.2	12.0	12.9	12.5	n.d.§	12.8	12.7	11.9	n.d.§
V	(2)	25	46	32	110	71	61	97	99	101	90	109	94	94	77	86	87	77
Cr	(1)	16.4	14.2	14.5	122	36.1	39.1	63.1	58.8	61.9	59.0	68.3	63.6	n.d.§	63.6	63	62.7	n.d.§
Co	(1)	4.56	2.90	2.74	16.7	9.57	10.4	15.5	14.5	13.2	14.3	14.9	14.9	n.d.§	14.9	14.2	14.0	n.d.§
Ni	(2)	20	19	23	57	28	28	31	33	33	30	33	29	30	18	31	30	27
Cu	(2)	<30	<30	<30	<30	<30	<30	32	36	31	33	30	32	<30	<30	<30	<30	<30
Zn	(1)	20	12	10	77	29	31	39	42	40	49	113	111	n.d.§	84	111	73	n.d.§
As	(1)	0.98	0.85	1.12	1.21	6.68	6.69	12.1	18.4	11.8	11.5	6.83	8.61	n.d.§	26.0	22.4	31.0	n.d.§
Se	(1)	<0.9	<1	<0.9	<1.5	<1.3	<1.6	<1.9	<1.6	<1.7	0.46	<2	<1.4	n.d.§	<1.5	<1.4	<1.4	n.d.§
Br	(1)	6.8	2.4	1.6	6.7	5.2	1.5	3.3	10	4.1	1.3	7.5	0.7	n.d.§	0.5	0.9	0.7	n.d.§
Rb	(1)	57.6	65.6	70.3	101	125	114	134	147	142	134	136	150	n.d.§	143	136	127	n.d.§
Sr	(2)	68	127	155	172	118	134	185	177	191	194	236	221	172	199	204	196	202
Y	(2)	15	<10	<10	30	40	38	45	45	42	45	45	42	46	29	42	40	33
Zr	(2)	109	142	114	273	218	256	238	228	219	253	234	239	247	224	259	238	241
Nb	(2)	<10	<10	<10	16	<10	<10	<10	11	10	<10	10	<10	<10	11	<10	<10	13
Mo	(2)	<10	<10	<10	n.d.§	<10	<10	<10	<10	<10	<10	<10	<10	<10	n.d.§	<10	<10	n.d.§
Sb	(1)	0.16	0.12	0.13	0.25	0.88	1.03	2.27	2.59	1.28	2.41	1.06	2.32	n.d.§	2.99	3.44	2.14	n.d.§
Cs	(1)	1.19	1.22	1.31	3.20	11.8	11.6	9.27	9.13	8.28	6.04	3.70	5.84	n.d.§	10.8	7.00	7.47	n.d.§
Ba	(2)	280	490	603	467	413	405	492	448	482	465	444	516	508	418	503	491	306
La	(1)	16.3	8.84	9.21	45.1	43.5	33.3	38.3	32.2	33.7	33.1	32.8	35.5	n.d.§	33.9	33.0	30.2	n.d.§
Ce	(1)	34.3	17.4	17.7	91.8	83.0	67.1	75.9	66.2	68.8	67.5	67.6	70.7	n.d.§	68.1	66.5	63.7	n.d.§
Nd	(1)	15.2	7.06	8.28	38.6	35.7	28.3	31.0	29.6	30.2	28.4	29.6	33.4	n.d.§	30.9	30.6	29.0	n.d.§
Sm	(1)	2.74	1.56	1.45	8.02	7.01	5.49	6.50	5.76	5.49	5.56	5.60	6.18	n.d.§	7.47	6.17	5.73	n.d.§
Eu	(1)	0.64	0.44	0.46	1.79	1.51	1.27	1.60	1.43	1.42	1.42	1.42	1.48	n.d.§	1.41	1.37	1.35	n.d.§
Gd	(1)	3.17	n.d.§	n.d.§	6.37	7.15	n.d.§	n.d.§	5.86	5.33	n.d.§	5.15	n.d.§	n.d.§	6.83	7.28	6.73	n.d.§
Tb	(1)	0.48	0.27	0.23	1.02	1.10	0.94	1.03	1.02	0.91	0.90	0.91	0.99	n.d.§	0.96	0.88	0.88	n.d.§
Tm	(1)	0.24	0.16	0.14	0.51	0.43	0.41	0.48	0.46	0.43	0.40	0.50	0.46	n.d.§	0.48	0.44	0.43	n.d.§
Yb	(1)	1.55	1.07	1.18	3.40	2.91	2.86	3.11	2.95	3.03	3.15	3.07	2.95	n.d.§	3.08	2.78	2.63	n.d.§
Lu	(1)	0.24	0.16	0.18	0.43	0.44	0.42	0.50	0.46	0.47	0.49	0.47	0.45	n.d.§	0.47	0.43	0.42	n.d.§
Hf	(1)	2.42	3.74	2.35	8.00	5.34	6.07	6.29	5.89	5.80	6.47	5.62	6.34	n.d.§	5.86	6.29	5.52	n.d.§
Ta	(1)	0.59	0.38	0.30	1.41	1.03	1.14	1.29	1.23	1.09	1.11	1.06	1.31	n.d.§	1.14	1.11	1.06	n.d.§
W	(1)	n.d.§	0.7	0.5	2.3	n.d.§	2.3	3.9	n.d.§	2.1	3.7	1.7	3.7	n.d.§	1.8	1.8	1.5	n.d.§
Pb	(2)	<15	<15	<15	n.d.§	<15	<15	<15	<15	17	16	18	16	<15	n.d.§	16	<15	n.d.§
Th	(1)	4.44	3.11	2.6	13.7	8.68	9.2	11.2	10.9	11.0	10.4	10.1	11.2	n.d.§	11.1	11.2	11.6	n.d.§
U	(1)	1.46	1.18	1.07	2.76	2.65	2.51	2.76	2.93	2.49	2.43	2.27	2.84	n.d.§	2.80	2.63	2.5	n.d.§
(ppb)																		
Ir	(1)	<0.8	<1.0	<0.8	<1.6	<1.1	<1.7	<1.9	<1.4	<1.7	<1.8	<2.0	<1.4	n.d.§	<1.7	<1.6	<1.6	n.d.§
Au	(1)	<0.4	0.2	0.2	1.3	0.5	<0.9	<1.2	0.7	<1.1	<0.8	0.4	0.6	n.d.§	0.8	0.8	0.6	n.d.§

(*Continued*)

TABLE A1. WHOLE-ROCK CHEMICAL COMPOSITIONS OF SAMPLES FROM THE EYREVILLE A AND B DRILL CORES (*Continued*)

Sample		KB 4	W 062	CB6 096	W 065a	CB6 097	KB 5	RG 018	W 066	W 067	CB6 098	W 069	CB6 099	W 070	W 071a	CB6 100	W 073	CB6 101
Core		B	B		B	B	B	B	B	B	B	B	B	B	B	B	B	B
Depth (m)		1405.7	1407.5	1409.3	1411.7	1412.8	1412.9	1413.8	1415.4	1416.4	1418.8	1421.2	1421.7	1422.5	1424.3	1427.0	1429.7	1431.1
Type*		imr	imr	sv	sv	sv	sv	sv	sv	sv	sv	sv	sv	sv	sv	sv	sv	sv
Unit**		M2	M2	S3	S3	S3	S3	S3	S3	S3	S3	S3	S3	S3	S3	S3	S3	S3
(wt%)																		
SiO_2		68.4	68.9	68.1	65.2	69.8	66.2	63.5	66.7	68.6	64.3	65.1	65.9	68.0	66.3	67.7	64.7	68.1
TiO_2		0.76	0.82	0.82	0.77	0.75	0.78	1.08	0.80	0.82	0.96	0.83	0.89	0.79	0.75	0.70	0.88	0.87
Al_2O_3		13.8	14.2	14.4	15.2	13.7	13.5	16.8	14.7	13.8	14.8	15.1	14.9	14.2	14.9	13.8	13.7	14.4
Fe_2O_3†		5.51	5.44	5.08	5.07	4.22	4.86	6.71	5.81	5.28	6.35	5.62	5.73	5.00	5.24	5.30	6.91	4.82
MnO		0.08	0.06	0.08	0.11	0.06	0.07	0.08	0.08	0.07	0.10	0.08	0.08	0.08	0.08	0.07	0.06	0.08
MgO		1.10	1.03	1.43	1.94	1.41	1.38	2.52	1.66	1.78	2.76	1.96	2.09	1.88	1.92	1.57	2.13	2.10
CaO		1.56	1.90	1.92	2.01	1.69	1.54	0.75	1.54	1.69	1.67	1.77	1.72	1.70	1.93	1.55	2.15	1.27
Na_2O		1.39	1.48	2.00	2.70	2.24	1.85	1.28	1.92	1.94	2.24	2.26	1.97	2.04	2.24	2.61	1.96	2.07
K_2O		3.07	3.61	3.59	4.64	3.15	3.09	3.66	3.00	2.83	2.56	2.82	2.69	2.80	2.66	2.73	0.25	3.21
P_2O_5		0.13	0.13	0.12	0.15	0.12	0.13	0.17	0.11	0.11	0.14	0.12	0.12	0.12	0.12	0.12	0.11	0.14
SO_3		n.d.§	<0.1	<0.1	<0.1	<0.1	n.d.§	<0.1	0.1	<0.1	0.4	0.1	<0.1	<0.1	0.1	0.4	0.2	0.1
LOI		2.3	1.9	2.4	2.0	2.5	5.4	3.1	2.8	3.0	3.1	4.1	3.4	3.0	3.6	3.2	6.6	2.5
Total		98.10	99.47	99.94	99.79	99.64	98.80	99.65	99.22	99.92	99.38	99.86	99.49	99.61	99.84	99.75	99.65	99.66
(ppm)	m#																	
Sc	(1)	13.0	13.0	12.2	15.3	10.9	11.9	n.d.§	12.0	12.7	18.6	13.9	13.2	12.4	12.4	11.4	8.71	14.8
V	(2)	78	101	105	99	96	88	113	95	101	134	102	108	100	106	91	79	105
Cr	(1)	102	71.6	56.4	32.9	53.8	57.9	n.d.§	57.7	61.1	96.1	72.2	65.4	63.6	62.9	51.2	41.1	83.8
Co	(1)	14.6	14.3	13.7	15.3	12.5	13.3	n.d.§	12.3	15.6	17.6	15.5	14.3	14.6	14.4	17.6	11.5	14.8
Ni	(2)	49	30	31	30	29	32	41	29	28	34	33	30	31	29	29	40	33
Cu	(2)	<30	34	31	<30	<30	<30	31	36	<30	<30	32	33	32	<30	<30	31	<30
Zn	(1)	78	73	92	96	89	93	n.d.§	104	63	113	120	127	120	130	86	63	100
As	(1)	15.6	15.0	5.52	24.1	9.81	8.74	n.d.§	11.6	18.7	13.5	5.52	6.21	5.51	5.35	31.2	39.1	5.75
Se	(1)	<1.5	<1.5	<1.7	<1.5	<1.9	<1.3	n.d.§	<1.5	<2.0	<2.8	<1.3	<1.7	<1.2	<1.3	<2.2	<1.2	<2.4
Br	(1)	<0.7	0.7	7.5	1.2	6.7	5.2	n.d.§	1.3	1.6	5.5	2.8	8.8	1.7	1.7	7.7	2.9	4.9
Rb	(1)	139	135	140	171	123	139	n.d.§	118	105	115	136	116	125	122	113	27	145
Sr	(2)	161	198	243	251	225	221	105	221	220	194	248	247	198	234	219	555	181
Y	(2)	32	44	41	47	36	28	54	41	37	42	42	37	41	34	34	22	38
Zr	(2)	222	241	235	220	215	217	328	242	217	206	245	245	232	230	198	378	215
Nb	(2)	14	<10	<10	<10	<10	14	17	<10	<10	<10	<10	11	<10	<10	<10	<10	11
Mo	(2)	n.d.§	<10	<10	<10	<10	n.d.§	<10	<10	<10	<10	<10	<10	<10	<10	<10	<10	<10
Sb	(1)	2.85	3.06	1.29	1.97	1.12	1.66	n.d.§	1.32	1.63	1.43	1.19	0.78	1.14	0.91	3.61	8.46	0.57
Cs	(1)	9.83	6.75	3.28	4.72	5.18	7.08	n.d.§	10.1	8.21	11.5	12.1	9.66	10.3	11.3	8.14	12.9	6.67
Ba	(2)	521	620	462	893	417	434	635	444	394	396	421	403	409	398	469	<30	429
La	(1)	32.5	29.3	31.6	34.2	27.4	29.4	n.d.§	31.9	28.3	31.9	38.8	31.8	33.6	31.0	29.0	24.1	30.2
Ce	(1)	66.3	59.9	65.1	70.2	57.3	63.2	n.d.§	65.7	56.6	66.6	82.3	65.7	71.8	64.9	60.8	50.3	64.3
Nd	(1)	27.5	24.8	26.0	34.0	23.1	27.4	n.d.§	28.1	24.0	29.4	34.5	28.7	30.7	28.1	25.2	22.1	26.7
Sm	(1)	6.15	5.75	5.29	7.06	4.33	5.46	n.d.§	6.45	5.25	5.98	7.99	5.21	7.05	6.69	5.01	5.88	5.21
Eu	(1)	1.42	1.32	1.39	1.52	1.24	1.30	n.d.§	1.31	1.19	1.66	1.59	1.39	1.52	1.42	1.33	1.24	1.41
Gd	(1)	5.23	6.41	5.34	6.32	4.39	4.78	n.d.§	6.00	5.12	6.03	8.33	5.48	6.75	6.69	5.16	6.25	5.09
Tb	(1)	0.93	0.84	0.86	0.95	0.77	0.83	n.d.§	0.83	0.75	1.03	1.11	0.87	1.00	0.97	0.84	0.90	0.91
Tm	(1)	0.55	0.42	0.43	0.51	0.39	0.38	n.d.§	0.43	0.38	0.52	0.62	0.46	0.56	0.54	0.42	0.49	0.46
Yb	(1)	3.05	2.53	2.98	3.19	2.55	2.63	n.d.§	2.59	2.34	3.32	3.28	2.78	3.06	2.90	2.80	2.30	2.89
Lu	(1)	0.48	0.41	0.47	0.51	0.41	0.44	n.d.§	0.42	0.37	0.52	0.42	0.46	0.39	0.36	0.43	0.29	0.45
Hf	(1)	6.03	5.65	5.67	5.82	5.14	5.67	n.d.§	5.61	4.84	5.26	6.23	6.08	5.69	5.44	4.97	7.63	5.66
Ta	(1)	1.24	0.99	1.13	1.15	1.00	1.19	n.d.§	1.20	0.99	1.20	1.40	1.25	1.29	1.33	1.03	1.23	1.25
W	(1)	3.0	1.7	1.5	1.6	<1.7	3.0	n.d.§	1.5	2.1	4.3	3.1	2.2	1.9	2.1	2.2	2.6	<1.7
Pb	(2)	n.d.§	15	<15	43	28	n.d.§	<15	27	<15	27	26	51	16	26	18	<15	19
Th	(1)	10.7	9.50	10.2	9.84	8.80	10.5	n.d.§	10.6	8.9	11.3	13.2	10.5	11.3	10.4	10.2	11.8	9.90
U	(1)	2.22	2.18	2.63	2.05	1.68	2.09	n.d.§	2.51	2.05	2.70	3.00	2.72	2.76	2.88	2.55	2.65	2.21
(ppb)																		
Ir	(1)	<1.8	<1.7	<1.7	<1.6	<1.9	<1.4	n.d.§	<1.7	0.4	<2.9	<1.5	<1.7	<1.4	<1.5	<2.2	<1.3	<2.4
Au	(1)	2.5	1.4	0.7	0.7	<1.3	3.2	n.d.§	0.5	0.4	0.5	0.8	0.4	0.3	<0.8	<1.2	1.7	<1.5

(*Continued*)

TABLE A1. WHOLE-ROCK CHEMICAL COMPOSITIONS OF SAMPLES FROM THE EYREVILLE A AND B DRILL CORES (*Continued*)

Sample		W 074	W 076	CB6 102	W 077	CB6 103	W 079	W 080a	CB6 104	W 081a	CB6 105	CB6 106	W 082	W 083	CB6 107	W 2-18	W 084	CB6 108
Core		B	B	B	B	B	B	B	B	B	B	B	B	B	B	B	B	B
Depth (m)		1431.4	1433.9	1436.6	1437.0	1440.0	1441.3	1443.1	1443.7	1444.6	1445.8	1447.0	1447.1	1448.7	1449.8	1450.4	1450.7	1451.0
Type*		sv	sv	sv	sv	sv	sv	sv	sv	sv	sv	sv	sv	sv	sv	imr	imr	sv
Unit**		S3	S2	S2	S2	S2	S2	S2	S2	S2	S2	S2	S2	S2	S2	M1	M1	S1
(wt%)																		
SiO_2		68.6	63.2	72.2	62.6	65.3	63.0	63.9	66.5	66.3	63.8	65.8	66.9	65.8	67.2	63.0	66.5	70.9
TiO_2		0.80	0.65	0.74	0.98	0.74	0.94	0.80	0.82	0.73	0.92	0.83	0.69	0.88	0.99	0.90	0.89	0.92
Al_2O_3		14.1	16.9	13.0	16.3	15.1	16.1	15.8	14.8	14.9	15.2	14.5	13.3	14.6	15.9	15.1	14.5	14.2
Fe_2O_3†		4.52	3.91	3.90	5.99	4.62	7.04	5.80	5.38	4.72	6.68	5.47	4.39	5.79	5.32	6.65	5.72	4.86
MnO		0.07	0.12	0.06	0.10	0.11	0.12	0.10	0.10	0.09	0.10	0.11	0.11	0.08	0.07	0.06	0.08	0.07
MgO		1.73	1.79	1.29	2.24	1.78	2.27	2.19	2.07	1.92	2.60	2.51	1.94	2.22	1.75	1.75	1.99	1.36
CaO		1.45	2.56	0.93	1.38	2.22	1.41	1.69	1.59	1.67	1.89	2.05	2.97	1.56	1.13	1.34	1.45	1.08
Na_2O		2.19	4.91	1.74	1.95	3.29	1.48	2.11	2.16	2.70	2.28	2.38	2.46	1.77	0.75	0.87	1.47	0.66
K_2O		3.36	3.36	3.00	4.34	3.33	3.73	3.98	3.80	3.81	2.73	3.28	3.31	2.71	3.53	2.03	2.55	3.55
P_2O_5		0.13	0.13	0.08	0.14	0.12	0.11	0.12	0.13	0.13	0.13	0.12	0.12	0.14	0.16	0.16	0.13	0.13
SO_3		<0.1	<0.1	<0.1	0.1	<0.1	0.2	0.1	0.2	0.1	0.1	<0.1	0.1	<0.1	<0.1	n.d.§	<0.1	0.1
LOI		2.8	1.9	2.5	3.2	2.6	3.4	3.1	2.2	2.9	3.4	2.6	3.5	4.0	2.4	6.0	3.9	1.4
Total		99.75	99.43	99.44	99.32	99.21	99.80	99.69	99.75	99.97	99.83	99.65	99.79	99.55	99.20	97.86	99.18	99.23
(ppm)	m#																	
Sc	(1)	13.0	11.5	10.8	17.3	11.2	16.8	14.3	13.8	11.0	14.7	14.0	12.8	13.3	15.5	12.7	13.4	12.9
V	(2)	101	74	87	122	111	117	106	102	95	115	113	95	103	116	98	105	102
Cr	(1)	60.7	24.1	65.2	86.7	52.4	84.9	73.8	71.2	62.7	77.7	80.0	65.6	68.5	68.6	87.0	70.8	66.9
Co	(1)	12.2	10.0	12.5	19.5	11.6	21.0	16.4	15.0	12.6	16.6	15.8	12.8	14.7	17.1	15.5	15.8	15.1
Ni	(2)	30	24	29	35	29	38	36	33	34	34	35	33	35	33	39	33	33
Cu	(2)	<30	<30	<30	33	35	<30	36	<30	31	32	30	<30	30	31	<30	30	<30
Zn	(1)	169	89	65	119	71	115	129	103	80	102	97	65	127	129	112	130	118
As	(1)	3.86	1.87	3.11	4.61	2.12	4.4	3.27	3.27	2.35	4.00	1.88	3.35	4.27	34.5	47.3	12.4	35.8
Se	(1)	<0.9	<1.2	<2.2	<1.4	<2.1	<1.5	<1.3	<2.4	<2.4	<2.5	<2.3	<1.2	<1.3	<2.5	<1.4	<1.3	<2.3
Br	(1)	2.7	0.8	8.0	2.7	13	2.0	1.5	6.9	2.7	12	9.3	2.1	3.8	1.9	2.2	3.2	1.2
Rb	(1)	148	119	121	204	125	184	174	159	137	111	129	133	123	130	53.7	115	127
Sr	(2)	171	254	127	157	233	127	190	162	163	246	196	212	303	193	188	232	158
Y	(2)	40	43	39	53	38	51	46	45	44	39	45	38	44	51	38	41	41
Zr	(2)	231	262	279	278	223	240	215	226	230	265	238	202	259	247	246	250	252
Nb	(2)	<10	<10	10	<10	<10	17	17	11	<10	10	11	<10	12	11	15	15	13
Mo	(2)	<10	<10	<10	<10	<10	<10	<10	<10	<10	<10	<10	<10	<10	<10	n.d.§	<10	<10
Sb	(1)	0.73	0.35	0.37	1.02	0.22	0.29	0.72	0.28	0.41	0.53	0.18	0.34	1.29	2.26	4.85	2.84	3.41
Cs	(1)	6.28	2.48	11.3	15.6	7.49	8.66	8.5	5.40	4.29	5.43	3.66	3.46	9.41	10.2	10.6	10.9	7.82
Ba	(2)	473	1041	450	503	523	478	512	471	549	395	581	486	406	541	283	408	570
La	(1)	33.7	38.6	34.5	45.1	32.2	42.8	41.6	34.3	33.0	37.2	34.5	29.0	42.0	45.9	39.0	39.7	40.0
Ce	(1)	68.5	80.2	70.4	92.9	65.1	88.0	85.4	70.9	64.4	76.4	70.3	60.5	85.4	93.3	76.3	80.6	83.0
Nd	(1)	29.7	32.9	28.5	38.1	26.5	36.3	34.8	29.0	26.2	30.9	28.7	25.6	36.4	40.4	31.4	33.7	35.8
Sm	(1)	6.82	7.43	5.20	9.30	4.79	8.32	7.83	5.76	5.63	6.23	5.72	5.83	8.02	7.76	7.79	7.91	6.70
Eu	(1)	1.45	1.66	1.46	2.01	1.44	1.84	1.71	1.53	1.34	1.56	1.47	1.35	1.74	1.84	1.63	1.72	1.68
Gd	(1)	6.11	7.04	5.28	8.20	4.78	8.40	6.89	5.57	5.60	5.54	6.15	4.95	7.90	7.37	7.52	7.41	6.28
Tb	(1)	0.92	1.06	0.91	1.28	0.83	1.20	1.08	0.97	0.81	0.98	0.99	0.81	1.11	1.25	1.16	1.13	1.08
Tm	(1)	0.51	0.58	0.43	0.71	0.41	0.66	0.57	0.47	0.37	0.50	0.50	0.45	0.60	0.56	0.67	0.59	0.51
Yb	(1)	2.99	3.36	2.97	3.82	2.80	3.61	3.11	3.13	2.60	3.17	3.40	2.62	3.41	3.81	3.53	3.36	3.29
Lu	(1)	0.37	0.44	0.47	0.48	0.42	0.44	0.40	0.50	0.33	0.50	0.52	0.34	0.44	0.58	0.44	0.42	0.50
Hf	(1)	5.85	6.46	7.37	7.47	5.72	6.56	5.67	6.12	5.51	6.92	6.13	4.87	6.58	6.52	6.79	6.36	6.67
Ta	(1)	1.24	1.35	1.14	1.64	1.03	1.60	1.25	1.17	0.99	1.28	1.18	0.91	1.25	1.46	1.36	1.35	1.39
W	(1)	1.6	<1.9	1.7	2.4	3.7	<2.9	2.2	1.0	<4.0	1.9	1.4	0.7	2.1	<2.4	2.2	2.4	2.4
Pb	(2)	<15	<15	<15	<15	<15	16	22	<15	<15	<15	<15	<15	21	25	n.d.§	32	27
Th	(1)	10.7	14.0	9.60	15.3	9.10	14.3	11.4	10.7	9.52	11.1	10.7	9.41	11.8	15.2	12.5	12.7	12.0
U	(1)	2.62	2.84	2.03	4.01	2.08	3.20	2.50	2.37	1.73	2.50	2.14	1.93	2.98	4.58	3.37	3.15	3.39
(ppb)																		
Ir	(1)	<1.0	<1.3	<2.3	<1.6	<2.1	<1.7	<1.5	<2.4	<1.3	<2.7	<2.4	<1.4	<1.4	<2.6	<1.5	<1.5	<2.4
Au	(1)	<0.9	0.7	<1.3	1.1	<1.3	0.8	<0.9	0.9	0.8	<1.3	<1.3	0.6	1.2	0.5	1.0	0.7	<1.1

(*Continued*)

TABLE A1. WHOLE-ROCK CHEMICAL COMPOSITIONS OF SAMPLES FROM THE EYREVILLE A AND B DRILL CORES (*Continued*)

Sample		CB6 109	W 085a	W 086a	CB6 110	CB6 111	W 088a	CB6 113	W 089a	CB6 114	W 090b	W 2-19	CB6 115	CB6 116	CB6 117	W 092	CB6 118	W 2-21
Core		B	B	B	B	B	B	B	B	B	B	B	B	B	B	B	B	B
Depth (m)		1452.3	1452.6	1454.2	1455.2	1458.2	1461.3	1464.0	1464.3	1467.4	1470.4	1471.4	1473.5	1480.8	1481.7	1481.4	1484.1	1484.4
Type*		sv	sv	sv	sv	sv	sv	sv	sv	sv	sv	sv	sv	sv	sv	sv	sv	sv
Unit**		S1	S1	S1	S1	S1	S1	S1	S1	S1	S1	S1	S1	P4	P4	P4	P4	P4
(wt%)																		
SiO_2		67.8	64.2	66.9	68.5	68.6	69.2	61.3	67.8	70.0	67.7	60.6	62.6	61.9	62.0	69.6	60.8	64.6
TiO_2		0.95	1.02	0.98	0.95	0.90	0.83	1.35	0.94	0.81	0.99	0.94	1.01	0.92	0.96	0.66	1.36	0.88
Al_2O_3		14.6	16.3	15.1	14.5	14.2	14.1	15.0	14.3	13.2	14.6	14.2	16.8	17.1	16.7	13.5	17.3	15.3
Fe_2O_3†		6.21	7.78	5.88	4.97	5.40	4.81	7.08	5.69	4.54	5.42	6.92	6.34	6.74	6.07	4.24	7.04	5.80
MnO		0.08	0.09	0.06	0.06	0.08	0.08	0.13	0.06	0.07	0.08	0.06	0.06	0.09	0.07	0.06	0.09	0.06
MgO		1.56	1.92	1.59	1.35	1.41	1.17	2.25	1.42	1.16	1.63	1.71	1.98	3.39	2.44	1.76	2.33	1.35
CaO		1.36	1.53	1.29	1.03	1.09	0.68	3.12	1.38	1.08	1.09	1.36	1.75	1.01	0.81	0.77	1.04	0.51
Na_2O		0.86	0.94	0.87	0.81	0.74	0.97	1.40	0.94	0.86	0.90	1.18	1.19	1.13	1.33	1.01	0.83	0.55
K_2O		2.06	1.99	2.64	3.50	3.12	4.15	2.79	2.36	3.35	3.24	2.17	2.16	4.07	5.37	4.56	4.19	3.93
P_2O_5		0.13	0.16	0.15	0.15	0.14	0.11	0.34	0.13	0.12	0.15	0.15	0.14	0.10	0.12	0.12	0.20	0.14
SO_3		0.1	<0.1	<0.1	0.1	0.1	<0.1	<0.1	<0.1	0.1	<0.1	n.d.§	<0.1	<0.1	0.1	0.1	0.3	n.d.§
LOI		3.6	3.7	3.8	3.5	4.0	3.5	5.0	4.9	4.3	4.1	9.8	5.3	3.4	3.2	3.0	4.2	7.2
Total		99.31	99.63	99.26	99.42	99.78	99.60	99.76	99.92	99.59	99.91	99.09	99.33	99.85	99.17	99.38	99.68	100.32
(ppm)	m#																	
Sc	(1)	12.3	14.4	12.5	12.4	12.8	12.4	15.8	12.2	10.7	13.1	12.5	14.1	14.9	16.1	n.d.§	16.7	13.4
V	(2)	98	110	109	109	101	90	131	97	93	120	107	105	120	120	84	138	106
Cr	(1)	65.3	69.7	61.4	60.5	59.7	63.5	82.8	61.1	52.5	66.6	61.9	65.7	112	107	n.d.§	83.5	69.8
Co	(1)	17.9	17.7	15.3	14.6	14.4	16.2	22.4	14.4	10.5	17.5	14.7	20.4	19.4	19.7	n.d.§	18.1	13.7
Ni	(2)	31	35	33	34	33	38	36	30	31	36	30	39	39	40	33	39	53
Cu	(2)	<30	30	<30	32	<30	<30	39	<30	<30	57	<30	44	<30	<30	<30	37	<30
Zn	(1)	102	120	116	151	109	455	114	95	99	122	103	107	99	116	n.d.§	136	130
As	(1)	44.6	24.5	23.1	23.1	22.7	28.1	26.0	18.7	14.0	21.4	12.5	33.4	7.70	11.3	n.d.§	21.9	29.7
Se	(1)	<2.3	<1.4	<1.3	<2.4	<1.7	<1.7	<2.3	<1.6	<1.9	<1.6	<1.4	<1.7	<2.1	<1.6	n.d.§	<2.4	<1.5
Br	(1)	3.2	1.0	1.5	5.3	8.0	2.0	2.7	3.4	2.8	2.4	4.3	<1.1	0.9	1.7	n.d.§	4.9	8.3
Rb	(1)	83	74.0	112	161	159	223	115	117	144	161	95.2	99.1	141	228	n.d.§	197	202
Sr	(2)	303	232	209	151	147	237	300	242	143	160	265	361	124	108	106	149	106
Y	(2)	33	44	43	51	46	57	40	37	44	52	35	41	45	61	48	59	35
Zr	(2)	301	278	307	262	233	231	238	265	255	254	231	275	255	236	213	371	247
Nb	(2)	11	16	13	11	11	<10	13	11	11	11	14	10	13	13	<10	16	16
Mo	(2)	<10	<10	<10	<10	<10	<10	<10	<10	<10	<10	n.d.§	<10	<10	<10	<10	<10	n.d.§
Sb	(1)	3.80	4.96	4.18	3.10	2.44	6.09	2.27	2.23	2.19	2.67	1.90	1.77	0.33	1.47	n.d.§	2.32	3.69
Cs	(1)	12.8	13.6	14.1	19.7	14.3	15.7	13.5	12.3	10.7	14.3	9.52	8.09	4.01	13.9	n.d.§	15.3	15.0
Ba	(2)	350	371	329	444	374	434	590	325	377	416	264	278	646	528	536	543	495
La	(1)	37.6	47.5	37.9	39.5	36.3	38.1	38.9	31.3	30.6	38.7	35.5	46.2	42.6	48.4	n.d.§	53.4	42.0
Ce	(1)	75.1	97.2	78.1	80.9	74.4	77.2	78.8	65.4	60.8	78.6	71.3	89.0	81.1	93.4	n.d.§	104	83.8
Nd	(1)	30.6	42.6	35.3	36.1	32.6	28.4	38.7	28.6	27.1	31.5	29.5	38.9	33.2	42.2	n.d.§	44.2	35.0
Sm	(1)	6.32	9.69	7.53	6.56	6.36	7.28	7.28	6.25	5.04	7.29	6.78	7.28	6.33	7.74	n.d.§	8.19	7.30
Eu	(1)	1.58	1.95	1.53	1.61	1.48	1.56	1.83	1.41	1.23	1.65	1.46	1.73	1.30	1.89	n.d.§	1.98	1.73
Gd	(1)	6.56	9.56	6.80	6.97	6.26	6.90	6.77	4.90	4.92	7.10	6.02	7.34	5.25	6.48	n.d.§	6.95	7.30
Tb	(1)	1.07	1.36	1.20	1.11	1.04	1.15	1.14	0.92	0.82	1.14	1.00	1.17	0.91	1.16	n.d.§	1.25	1.03
Tm	(1)	0.47	0.68	0.49	0.50	0.54	0.49	0.53	0.50	0.42	0.49	0.45	0.50	0.48	0.58	n.d.§	0.58	0.60
Yb	(1)	3.16	3.94	3.47	3.21	3.17	3.39	3.06	2.92	2.67	3.28	3.01	3.11	3.11	3.66	n.d.§	3.97	3.17
Lu	(1)	0.50	0.48	0.53	0.49	0.49	0.50	0.47	0.45	0.42	0.52	0.38	0.49	0.47	0.55	n.d.§	0.63	0.51
Hf	(1)	7.55	7.29	7.75	6.17	6.05	6.07	6.03	6.93	6.03	6.53	6.11	6.75	6.32	6.67	n.d.§	9.84	6.73
Ta	(1)	1.34	1.42	1.40	1.35	1.41	1.35	1.36	1.3	1.02	1.29	1.19	1.43	1.23	1.37	n.d.§	1.53	1.49
W	(1)	2.8	2.5	4.5	2.0	2.8	4.4	n.d.§	4.5	n.d.§	4.5	13	2.2	n.d.§	n.d.§	n.d.§	n.d.§	3.6
Pb	(2)	25	28	31	74	40	75	19	24	41	37	n.d.§	28	<15	<15	23	17	n.d.§
Th	(1)	13.1	14.0	12.9	12.4	12.5	12.5	8.9	12.7	9.80	12.2	11.9	13.0	12.2	13.4	n.d.§	15.1	12.9
U	(1)	3.68	3.66	4.21	3.16	3.89	4.16	2.75	3.74	2.59	3.56	2.71	3.64	2.65	3.20	n.d.§	4.17	3.24
(ppb)																		
Ir	(1)	<2.5	<1.6	<1.6	<2.6	0.5	<2.2	<2.3	<1.9	<1.7	<1.9	<1.4	<1.8	<2.1	<1.6	n.d.§	<2.4	<1.6
Au	(1)	0.9	0.5	<1.0	0.8	1.3	<1.1	0.6	<1.1	0.7	1.5	1.3	<1.3	<1.4	<1.5	n.d.§	0.8	<1.2

(*Continued*)

TABLE A1. WHOLE-ROCK CHEMICAL COMPOSITIONS OF SAMPLES FROM THE EYREVILLE A AND B DRILL CORES (*Continued*)

Sample		W 093	CB6 119	W 095	CB6 120	W 096a	CB6 121	CB6 124	W 099	W 100a	W 101	W 102a	CB6 126	W 104a	CB6 127	CB6 128	W 105a	W 106
Core		B	B	B	B	B	B	B	B	B	B	B	B	B	B	B	B	B
Depth (m)		1484.8	1494.0	1499.7	1504.3	1505.2	1508.5	1516.2	1517.1	1521.9	1523.9	1527.6	1529.3	1533.1	1535.4	1536.5	1537.5	1541.3
Type*		sv	gn/ catacl.	gn/ catacl.	sv	sv	sv	gn/ catacl.	gn/ catacl.	sv	sv	sv	sv	sv	sv	plib	plib	gn/ catacl.
Unit**		P4	B4	B4	P3	P3	P3	B3	B3	P2	P2	P2	P2	P2	P2	P2	P2	B2
(wt%)																		
SiO_2		63.0	65.2	64.7	68.1	64.8	61.5	59.5	70.4	61.8	62.3	63.6	65.6	66.7	63.3	64.7	63.6	69.4
TiO_2		0.91	0.92	0.92	0.89	0.90	1.35	0.93	0.70	1.11	1.08	1.04	0.99	0.90	0.97	1.05	0.91	0.88
Al_2O_3		15.5	15.1	15.1	13.8	15.7	15.8	15.7	11.9	17.2	16.0	15.9	14.9	14.6	15.6	15.8	15.4	13.5
Fe_2O_3†		5.76	5.98	6.06	5.59	6.18	7.61	6.56	5.14	6.74	6.87	6.62	6.22	5.78	6.09	6.04	6.25	5.89
MnO		0.10	0.08	0.09	0.08	0.07	0.07	0.13	0.08	0.08	0.08	0.08	0.08	0.08	0.09	0.08	0.09	0.06
MgO		2.30	2.89	2.95	1.63	1.86	2.50	3.28	2.51	2.11	2.09	2.00	1.83	1.78	1.84	1.80	1.87	2.32
CaO		1.26	1.16	1.77	0.86	0.97	2.34	3.63	2.01	1.11	1.22	1.35	1.38	0.98	1.72	1.00	1.52	0.49
Na_2O		1.41	1.39	1.96	0.92	0.94	1.80	3.27	1.53	0.85	0.98	0.85	0.85	1.15	1.04	1.02	1.03	1.26
K_2O		5.09	3.75	3.09	3.27	3.24	0.31	2.18	2.32	3.25	3.31	3.08	3.23	3.39	3.74	3.86	3.60	2.87
P_2O_5		0.14	0.16	0.18	0.13	0.12	0.15	0.11	0.13	0.17	0.27	0.15	0.16	0.16	0.15	0.16	0.15	0.11
SO_3		0.1	<0.1	<0.1	0.1	<0.1	<0.1	0.1	<0.1	0.2	0.2	<0.1	0.1	<0.1	0.2	<0.1	0.4	<0.1
LOI		3.6	3.0	2.8	4.1	4.9	6.3	4.1	2.9	5.1	4.9	5.1	4.4	3.9	4.8	4.4	4.6	2.9
Total		99.17	99.63	99.62	99.47	99.68	99.73	99.49	99.62	99.72	99.30	99.77	99.74	99.42	99.54	99.91	99.42	99.68
(ppm)	m#																	
Sc	(1)	13.5	14.9	14.6	12.1	13.5	9.80	17.1	11.7	15.8	16.0	15.8	13.4	14.4	14.6	15.5	13.7	12.5
V	(2)	114	109	115	92	122	108	113	79	116	111	119	121	104	112	126	107	93
Cr	(1)	91	117	115	63.8	69.8	40.3	124	91.6	72.6	75.3	75.9	66.3	73.2	74.1	85.9	69.3	90.4
Co	(1)	16.0	17.5	17.9	15.7	17.2	15.0	19.6	15.1	18.7	19.0	18.2	14.5	17.6	16.9	17.8	15.8	16.1
Ni	(2)	40	39	67	33	35	24	49	33	39	62	37	35	34	34	34	37	37
Cu	(2)	<30	<30	<30	30	<30	<30	32	<30	55	42	<30	<30	<30	31	<30	<30	<30
Zn	(1)	110	97	98	144	131	52	112	85	136	156	160	142	131	127	152	103	89
As	(1)	13.4	3.91	4.19	27.1	21.6	7.86	1.6	0.95	34.3	29.5	20.5	25.8	24.1	35.0	31.6	28.5	42.3
Se	(1)	<1.7	<2.2	<1.3	<2	<1.8	<1.9	<2.3	<1.6	<1.8	<2.1	<1.7	<2.1	<1.6	<2.2	<2.2	<2.6	<1.6
Br	(1)	3.4	0.8	0.4	3.3	3.5	8.7	1.0	0.8	3.6	6.3	3.2	5.7	2.5	5.0	3.2	6.2	0.7
Rb	(1)	220	138	128	163	168	23.6	88.3	95	179	193	177	161	195	178	197	171	122
Sr	(2)	142	126	232	351	400	474	223	134	284	320	265	143	136	122	109	110	97
Y	(2)	63	56	50	47	52	22	40	37	56	57	50	47	48	53	56	55	52
Zr	(2)	246	306	309	257	251	269	270	234	281	291	273	285	246	254	293	229	289
Nb	(2)	12	15	<10	10	11	11	12	10	12	<10	13	12	12	13	13	12	15
Mo	(2)	<10	<10	<10	<10	<10	<10	<10	<10	10	<10	<10	<10	<10	<10	<10	<10	<10
Sb	(1)	1.21	0.33	0.18	2.77	2.26	2.24	0.11	0.05	3.85	1.47	1.77	2.89	2.30	2.32	2.74	3.08	0.22
Cs	(1)	9.16	3.96	3.42	10.7	14.4	4.62	2.52	2.39	16.0	15.8	15.4	13.7	14.9	12.5	13.7	14.0	7.45
Ba	(2)	568	533	467	386	442	68	654	610	400	446	438	416	465	521	524	457	381
La	(1)	42.8	45.9	48.1	39.2	39.3	20.1	45.2	37.6	42.9	46.9	48.0	42.3	38.6	39.5	45.2	46.9	37.0
Ce	(1)	86.8	90.2	100	75.8	79.3	42.8	87.2	83.2	92.2	98.9	102	79.7	84.4	77.3	87.4	94.1	79.4
Nd	(1)	36.7	41.5	41.5	32.2	36.0	21.5	38.7	36.1	39.7	44.4	42.9	36.5	37.6	34.7	36.8	36.0	32.5
Sm	(1)	7.86	8.00	9.33	6.02	7.31	4.70	7.29	7.36	8.33	10.4	8.62	7.13	8.18	6.86	7.61	8.97	7.08
Eu	(1)	1.68	1.70	1.92	1.57	1.68	1.04	1.81	1.62	1.83	2.31	1.88	1.58	1.85	1.62	1.80	1.80	1.52
Gd	(1)	5.8	7.03	8.10	6.03	6.80	4.84	7.12	6.93	8.50	9.79	8.06	6.45	8.60	6.71	7.01	8.10	6.20
Tb	(1)	1.03	1.26	1.44	1.00	1.07	0.86	1.26	1.15	1.29	1.58	1.29	1.06	1.33	1.15	1.26	1.24	1.12
Tm	(1)	0.44	0.61	0.58	0.50	0.46	0.31	0.61	0.60	0.56	0.80	0.70	0.49	0.72	0.53	0.61	0.61	0.58
Yb	(1)	3.30	3.98	4.24	3.24	3.43	1.96	3.92	3.19	3.46	4.08	3.78	3.36	3.64	3.46	3.96	3.19	3.30
Lu	(1)	0.5	0.59	0.61	0.49	0.51	0.29	0.60	0.50	0.58	0.61	0.58	0.51	0.54	0.53	0.61	0.41	0.51
Hf	(1)	6.52	7.97	8.04	7.03	6.55	5.85	7.42	6.27	7.46	7.20	7.78	7.17	7.20	6.52	8.39	6.08	7.29
Ta	(1)	1.22	1.34	1.42	1.23	1.23	1.26	1.50	1.15	1.61	1.81	1.55	1.31	1.56	1.31	1.68	1.20	1.21
W	(1)	<5.6	n.d.§	<6	n.d.§	5.2	n.d.§	n.d.§	2.1	4.5	4.1	3.9	n.d.§	3.1	n.d.§	n.d.§	<2.9	3.1
Pb	(2)	26	<15	17	43	24	<15	<15	<15	33	36	40	42	18	16	29	23	<15
Th	(1)	12.3	13.3	14.7	11.7	12.6	10.4	13.4	12.1	15.7	19.5	15.1	12.7	14.2	11.7	14.2	12.0	11.3
U	(1)	3.10	3.13	3.41	3.22	3.67	2.22	2.87	2.44	4.46	4.66	4.19	3.58	3.59	3.17	4.12	2.55	2.30
(ppb)																		
Ir	(1)	<2.2	<2.3	<1.7	<1.9	<2.2	<1.8	<2.3	<1.6	<1.6	<1.9	<1.6	0.8	<1.4	<2.1	<2.2	<1.4	<2.1
Au	(1)	<1.2	<1.5	<1.2	<1.4	<1.1	0.1	0.6	0.3	1.2	1.1	1.2	<1.5	0.8	0.9	0.8	1.0	<0.8

(*Continued*)

TABLE A1. WHOLE-ROCK CHEMICAL COMPOSITIONS OF SAMPLES FROM THE EYREVILLE A AND B DRILL CORES (*Continued*)

Sample		CB6 129	W 2-29	W 107	RG 076	CB6 130	W 109	W 112	W 113a	W 113b	W 2-23	W 114	CB6 132	W 115	CB6 133	W 116	CB6 134	CB6 135
Core		B	B	B	B	B	B	B	B	B	B	B	B	B	B	B	B	B
Depth (m)		1542.7	1543.9	1545.0	1545.3	1547.4	1548.5	1554.1	1555.6	1555.6	1559.1	1559.2	1559.5	1560.2	1560.3	1563.2	1570.3	1576.8
Type*		gn/ catacl.	gn/ catacl.	gn/ catacl.	gn/ catacl.	gn/ catacl.	sv	schist/ catacl.	plib dike	schist	schist	schist	schist/ catacl.	schist	schist	schist	schist	schist
Unit**		B2	B2	B2	B2	B2	P1											
(wt%)																		
SiO_2		71.2	65.0	67.1	67.4	63.5	63.1	61.8	64.7	52.7	58.4	72.5	78.0	77.9	59.2	62.2	60.2	56.6
TiO_2		0.89	0.90	0.97	0.87	0.89	1.10	0.85	0.84	0.94	0.83	0.66	0.38	0.66	0.85	0.91	0.93	0.85
Al_2O_3		14.0	14.9	15.6	14.6	17.2	16.0	16.2	14.2	20.6	18.7	10.3	9.6	10.7	18.3	18.3	20.0	19.5
Fe_2O_3†		4.61	5.81	4.41	5.78	5.50	6.64	5.28	5.23	5.58	7.86	3.72	2.67	2.43	7.03	6.72	5.82	7.03
MnO		0.05	0.10	0.05	0.07	0.08	0.09	0.07	0.09	0.05	0.08	0.07	0.06	0.04	0.06	0.05	0.06	0.05
MgO		1.25	1.49	1.25	2.69	2.75	2.32	2.05	1.69	3.04	1.43	1.19	0.84	0.76	2.25	2.44	2.82	2.74
CaO		0.41	1.42	0.70	0.96	0.95	1.09	1.36	1.70	0.41	1.94	3.61	1.40	0.50	1.38	0.55	0.88	1.02
Na_2O		0.77	0.87	1.50	1.34	1.15	1.15	1.27	1.24	0.83	1.61	0.96	0.83	1.07	1.89	1.66	1.18	1.24
K_2O		3.32	3.60	3.34	2.79	4.61	3.86	3.78	3.28	5.06	3.62	2.43	2.17	2.42	4.17	3.30	3.91	4.14
P_2O_5		0.06	0.16	0.11	0.14	0.11	0.14	0.09	0.09	0.06	0.13	0.06	0.03	0.03	0.04	0.03	0.06	0.07
SO_3		<0.1	n.d.§	<0.1	<0.1	<0.1	<0.1	<0.1	<0.1	<0.1	n.d.§	<0.1	<0.1	<0.1	0.2	0.1	<0.1	<0.1
LOI		3.3	5.1	4.8	3.2	3.1	4.4	7.2	6.1	10.1	5.8	4.2	4.0	2.7	4.2	3.7	4.0	6.1
Total		99.86	99.35	99.83	99.84	99.84	99.89	99.95	99.16	99.37	100.40	99.70	99.98	99.21	99.57	99.96	99.86	99.34
(ppm)	m#																	
Sc	(1)	13.2	13.6	15.5	n.d.§	13.7	17.9	16.6	14.4	n.d.§	12.3	8.54	6.83	7.45	17.0	18.4	23.1	19.1
V	(2)	98	105	102	103	98	137	118	106	144	81	65	54	69	133	136	151	190
Cr	(1)	67.9	66.4	73.4	n.d.§	102	94.4	91.9	78.8	n.d.§	67.8	46.2	45.3	44	97.7	101	113	103
Co	(1)	13.5	15.4	12.2	n.d.§	14.3	19.5	15.7	16.7	n.d.§	20.5	7.78	8.43	9.05	18.6	17.1	11.1	22.0
Ni	(2)	27	40	29	39	40	37	67	32	93	28	26	23	26	38	37	30	36
Cu	(2)	<30	<30	<30	<30	161	32	<30	<30	40	34	<30	<30	<30	31	32	<30	<30
Zn	(1)	85	101	81	n.d.§	93	120	104	96	n.d.§	74	46	33	42	94	95	129	118
As	(1)	0.69	18.5	2.6	n.d.§	<1.4	17	6.76	8.34	n.d.§	2.33	0.31	0.99	3.80	0.35	<1.0	<0.6	<0.7
Se	(1)	<2.0	<1.5	<1.7	n.d.§	<2.1	0.18	1.79	<1.3	n.d.§	<1.3	<1.4	<1.5	<1.1	<2.0	<1.6	<2.3	<2.2
Br	(1)	1.0	6.1	0.9	n.d.§	1.1	2.2	2.7	2.5	n.d.§	3.6	1.3	0.8	3.2	1.1	0.5	0.7	1.3
Rb	(1)	146	175	119	n.d.§	168	185	188	155	n.d.§	141	83.0	94	122	210	146	167	165
Sr	(2)	66	85	90	104	99	112	114	150	60	100	85	78	86	117	113	111	123
Y	(2)	44	38	44	47	62	55	54	50	60	24	28	24	37	50	43	46	50
Zr	(2)	380	241	314	300	335	249	251	250	196	174	247	144	250	175	193	189	160
Nb	(2)	14	15	12	13	22	12	13	<10	12	11	<10	<10	<10	11	14	13	11
Mo	(2)	<10	n.d.§	<10	<10	<10	<10	<10	<10	<10	n.d.§	<10	<10	<10	<10	<10	<10	22
Sb	(1)	0.18	2.27	0.58	n.d.§	0.11	1.33	0.65	0.51	n.d.§	0.26	0.07	0.12	0.13	0.08	0.14	0.09	0.06
Cs	(1)	7.21	16.2	5.54	n.d.§	4.33	13.6	17.1	15.7	n.d.§	11.1	5.91	9.91	13.3	7.98	9.12	11.9	11.7
Ba	(2)	575	489	578	529	736	523	537	460	691	518	496	312	349	611	469	581	569
La	(1)	38.0	37.2	36.9	n.d.§	58.6	40.4	40.4	33.5	n.d.§	26.8	23.6	19.7	29.0	36.1	36.4	39.1	37.4
Ce	(1)	72.6	75.7	77.3	n.d.§	112	85.1	84.1	69.0	n.d.§	54.9	49.1	40.6	61.8	73.1	74.4	77.9	73.9
Nd	(1)	30.3	33.0	31.3	n.d.§	45.0	37.0	34.9	29.7	n.d.§	23.8	20.7	17.5	24.8	31.5	29.9	31.3	30.8
Sm	(1)	6.03	7.08	7.07	n.d.§	8.05	8.01	7.84	6.48	n.d.§	4.90	4.27	3.11	4.87	6.43	5.72	6.16	5.82
Eu	(1)	1.28	1.82	1.50	n.d.§	1.91	1.76	1.71	1.49	n.d.§	1.07	0.86	0.84	1.14	1.55	1.41	1.69	1.45
Gd	(1)	5.64	6.03	6.70	n.d.§	8.81	6.90	6.70	5.80	n.d.§	5.01	3.90	3.24	5.27	5.38	6.29	6.81	5.53
Tb	(1)	1.03	1.11	1.17	n.d.§	1.46	1.21	1.21	0.95	n.d.§	0.71	0.69	0.53	0.78	0.92	0.92	1.08	0.93
Tm	(1)	0.54	0.61	0.61	n.d.§	0.77	0.65	0.64	0.58	n.d.§	0.44	0.39	0.30	0.41	0.45	0.49	0.54	0.49
Yb	(1)	3.56	3.63	3.47	n.d.§	5.03	3.18	3.50	3.01	n.d.§	2.41	2.05	1.76	2.56	2.89	3.08	3.26	3.09
Lu	(1)	0.55	0.54	0.54	n.d.§	0.73	0.55	0.55	0.46	n.d.§	0.38	0.33	0.21	0.40	0.34	0.49	0.39	0.39
Hf	(1)	10.4	6.40	8.51	n.d.§	9.51	6.81	6.81	5.78	n.d.§	4.68	5.66	3.48	6.32	4.90	5.53	5.34	4.27
Ta	(1)	1.51	1.28	1.42	n.d.§	2.66	1.54	1.48	1.20	n.d.§	1.04	0.91	0.63	1.25	1.15	1.40	1.29	1.01
W	(1)	n.d.§	4.0	6.3	n.d.§	n.d.§	3.2	3.4	3.0	n.d.§	2.4	1.3	n.d.§	2.2	n.d.§	<3.0	n.d.§	n.d.§
Pb	(2)	<15	n.d.§	<15	<15	<15	25	19	17	15	n.d.§	<15	<15	<15	<15	16	18	<15
Th	(1)	13.2	11.7	12.9	n.d.§	30.4	12.3	14.0	10.9	n.d.§	9.44	7.49	5.90	9.87	12.1	13.0	13.2	11.3
U	(1)	3.28	2.67	2.89	n.d.§	6.11	3.59	3.16	2.56	n.d.§	1.82	1.52	1.14	1.98	4.09	2.9	4.12	6.48
(ppb)																		
Ir	(1)	<1.9	<1.7	<2.2	n.d.§	<2.1	<2.4	<2.4	<1.7	n.d.§	<1.4	<1.8	<1.5	<1.1	<0.7	<1.7	<2.4	<2.3
Au	(1)	<1.3	1.1	0.4	n.d.§	0.6	0.8	0.6	0.8	n.d.§	1.9	<0.7	<1	0.3	<1.5	<1.4	<1.4	0.5

(*Continued*)

TABLE A1. WHOLE-ROCK CHEMICAL COMPOSITIONS OF SAMPLES FROM THE EYREVILLE A AND B DRILL CORES (*Continued*)

Sample		W 117	RG 070	W 118	CB6 136	W 119	CB6 137	RG 068	W 120	CB6 138	W 121	RG 064	W 122	W 2-24	W 123a	W 123b	CB6 139	W 124
Core		B	B	B	B	B	B	B	B	B	B	B	B	B	B	B	B	B
Depth (m)		1576.8	1578.8	1579.0	1592.3	1595.4	1597.2	1597.7	1603.3	1603.6	1604.1	1604.8	1606.8	1607.4	1607.9	1607.9	1609.4	1609.5
Type*		schist	schist	schist	peg/ catacl.	peg	schist	schist	gran- ite	sv dike	sv dike	schist	schist	sv dike	gran- ite	catacl. br dike	catacl. br dike	catacl. br dike
(wt%)																		
SiO_2		54.9	50.8	52.8	73.3	83.5	52.9	54.7	75.0	58.4	59.4	48.5	56.0	70.5	69.8	60.7	55.6	56.0
TiO_2		0.94	0.85	0.81	0.01	0.03	1.04	0.89	0.02	0.78	0.76	1.00	0.78	0.52	0.02	0.73	0.91	0.88
Al_2O_3		19.9	19.9	21.1	13.4	10.3	23.0	20.3	15.9	18.2	18.4	20.8	18.6	10.0	13.9	19.0	20.5	19.5
Fe_2O_3†		7.67	9.03	6.96	0.45	0.17	7.25	7.86	0.52	8.11	7.85	9.45	9.16	3.65	0.11	4.68	6.76	7.48
MnO		0.06	0.14	0.12	0.10	0.02	0.02	0.03	0.04	0.06	0.05	0.12	0.05	0.04	0.10	0.05	0.06	0.07
MgO		2.90	4.60	3.17	0.09	0.11	1.55	2.20	0.14	1.33	1.28	1.15	2.04	0.79	0.08	0.96	1.40	1.50
CaO		1.63	2.84	3.23	3.23	0.65	0.64	0.80	0.59	1.14	1.16	4.50	0.55	2.21	5.06	1.60	1.70	1.67
Na_2O		1.66	1.97	2.10	4.04	1.76	2.06	2.04	3.06	2.00	2.17	4.53	0.88	1.57	5.65	1.76	1.94	1.51
K_2O		3.61	3.19	3.91	1.73	1.95	5.40	3.34	2.96	3.75	3.83	2.34	4.03	2.63	1.31	4.42	4.34	4.16
P_2O_5		0.06	0.08	0.05	0.01	0.30	0.04	0.08	0.05	0.13	0.12	0.04	0.07	0.18	0.04	0.08	0.10	0.10
SO_3		0.2	0.2	0.1	<0.1	<0.1	0.1	<0.1	<0.1	<0.1	0.3	0.1	<0.1	n.d.§	<0.1	0.2	0.2	0.5
LOI		6.3	6.0	5.5	3.4	1.1	5.7	7.1	1.8	5.5	4.2	6.9	7.5	6.0	3.4	5.8	6.3	6.1
Total		99.83	99.60	99.85	99.76	99.89	99.70	99.34	100.08	99.40	99.52	99.43	99.66	98.09	99.47	99.98	99.81	99.47
(ppm)	m#																	
Sc	(1)	19.5	n.d.§	19.3	0.40	0.56	23.7	n.d.§	0.65	15.2	14.1	n.d.§	19.0	15.9	0.43	14.7	19.4	17.6
V	(2)	177	154	166	<15	<15	212	219	<15	139	138	160	193	148	<15	160	177	161
Cr	(1)	110	n.d.§	100	11.6	6.67	113	n.d.§	5.2	70.8	64.0	n.d.§	85.2	74.4	17.8	79.7	96.3	83.9
Co	(1)	21.4	n.d.§	18.9	0.33	0.26	20.5	n.d.§	0.19	15.7	16.2	n.d.§	30.1	19.6	0.16	18.0	19.2	19.0
Ni	(2)	37	43	44	19	24	37	43	23	36	35	37	105	43	19	42	39	42
Cu	(2)	<30	37	43	<30	<30	<30	48	<30	<30	<30	36	41	42	<30	32	<30	<30
Zn	(1)	143	n.d.§	115	35	30	92	n.d.§	112	101	111	n.d.§	137	120	18	105	135	127
As	(1)	0.42	n.d.§	0.29	<0.6	0.03	<0.7	n.d.§	0.81	<0.8	<2.0	n.d.§	18.7	1.52	<1.1	0.56	0.32	3.11
Se	(1)	0.29	n.d.§	1.36	<0.9	1.24	1.43	n.d.§	1.75	0.77	1.66	n.d.§	7.29	1.4	<1.1	1.57	1.63	1.66
Br	(1)	1.4	n.d.§	1.1	0.7	0.5	0.7	n.d.§	0.6	2.7	8.3	n.d.§	4.1	5.9	<0.8	2.8	1.5	2.8
Rb	(1)	179	n.d.§	289	129	166	315	n.d.§	176	248	247	n.d.§	208	264	82.3	275	288	298
Sr	(2)	161	172	156	38	31	156	128	30	104	102	224	74	102	53	97	118	102
Y	(2)	54	57	74	12	61	73	64	39	57	56	56	60	31	16	69	62	68
Zr	(2)	180	160	152	19	<15	162	174	47	140	133	183	135	141	42	134	150	141
Nb	(2)	13	15	29	<10	13	14	13	11	20	22	15	20	26	11	18	31	19
Mo	(2)	19	14	12	<10	<10	26	31	<10	11	11	25	25	n.d.§	<10	14	19	35
Sb	(1)	0.10	n.d.§	0.16	<0.1	0.03	0.13	n.d.§	0.08	0.07	0.15	n.d.§	0.39	0.17	0.06	0.26	0.09	0.17
Cs	(1)	14.6	n.d.§	22.0	3.58	3.02	19.5	n.d.§	7.57	16.5	15.9	n.d.§	21.7	17.1	2.31	23.9	18.8	19.1
Ba	(2)	526	648	570	<30	<30	570	514	<30	309	347	108	554	363	<30	385	419	393
La	(1)	42.6	n.d.§	39.7	1.22	4.08	50.5	n.d.§	4.55	33.3	32.3	n.d.§	43.6	36.1	3.58	34.2	42.6	38.1
Ce	(1)	86.5	n.d.§	80.1	2.78	14.0	99.9	n.d.§	16.5	66.9	63.6	n.d.§	87.2	76.0	8.64	67.5	84.5	78.9
Nd	(1)	37.8	n.d.§	32.6	1.37	8.43	42.9	n.d.§	10.4	29.1	29.6	n.d.§	44.1	30.9	4.05	31.4	37.1	34.9
Sm	(1)	7.16	n.d.§	6.84	0.36	4.61	8.10	n.d.§	3.83	5.65	6.51	n.d.§	9.11	6.94	1.36	7.16	7.61	6.57
Eu	(1)	1.76	n.d.§	1.82	0.11	0.18	2.00	n.d.§	0.13	1.19	1.15	n.d.§	1.50	1.51	0.58	1.30	1.65	1.47
Gd	(1)	7.05	n.d.§	6.49	<0.9	5.96	7.67	n.d.§	2.65	5.24	5.85	n.d.§	7.32	5.48	1.47	6.94	7.38	6.59
Tb	(1)	1.09	n.d.§	1.09	0.04	1.42	1.21	n.d.§	0.49	0.87	0.86	n.d.§	1.29	0.98	0.26	0.98	1.11	1.02
Tm	(1)	0.54	n.d.§	0.64	n.d.	0.77	0.58	n.d.§	0.29	0.58	0.58	n.d.§	0.70	0.45	0.18	0.48	0.69	0.59
Yb	(1)	3.77	n.d.§	4.00	0.31	2.80	3.90	n.d.§	2.08	3.05	2.85	n.d.§	4.40	3.13	0.89	2.97	3.35	3.55
Lu	(1)	0.58	n.d.§	0.61	0.05	0.29	0.48	n.d.§	0.31	0.39	0.39	n.d.§	0.52	0.53	0.10	0.38	0.40	0.61
Hf	(1)	5.07	n.d.§	4.40	0.26	0.80	4.64	n.d.§	2.86	4.44	3.79	n.d.§	4.18	3.90	1.21	3.60	4.69	5.00
Ta	(1)	1.45	n.d.§	6.72	5.46	6.71	1.35	n.d.§	11.9	3.49	4.85	n.d.§	19.0	4.62	2.65	2.81	4.40	4.36
W	(1)	3.2	n.d.§	5.2	n.d.§	3.5	n.d.§	n.d.§	1.4	n.d.§	4.6	n.d.§	11	5.9	1.6	5.0	n.d.§	6.4
Pb	(2)	20	<15	19	57	37	<15	21	52	26	30	49	<15	n.d.§	71	31	31	17
Th	(1)	14.2	n.d.§	13.4	0.15	0.65	15.6	n.d.§	1.90	10.9	10.3	n.d.§	13.8	12.5	0.97	11.3	13.5	12.5
U	(1)	7.98	n.d.§	7.85	3.30	4.85	6.00	n.d.§	42.9	9.04	7.19	n.d.§	8.25	7.31	2.36	7.75	7.82	7.73
(ppb)																		
Ir	(1)	<1.8	n.d.§	<1.8	<0.8	<0.5	<2.3	n.d.§	<0.5	0.47	<1.4	n.d.§	<1.2	<1.7	<0.6	<1.4	<2.5	<1.3
Au	(1)	<1.5	n.d.§	<1.2	<1.5	<0.6	<1.7	n.d.§	<1.4	<1.6	0.2	n.d.§	0.8	<1.2	0.7	0.6	0.7	0.8

(*Continued*)

TABLE A1. WHOLE-ROCK CHEMICAL COMPOSITIONS OF SAMPLES FROM THE EYREVILLE A AND B DRILL CORES (*Continued*)

Sample		W 125a	W 125b	RG 061	W 126	W 127a	W 127b	CB6 140	W 128	W 129	CB6 141	W 130	CB6 142	RG 054	W 131a	RG 053	W 132	W 133
Core		B	B	B	B	B	B	B	B	B	B	B	B	B	B	B	B	B
Depth (m)		1611.0	1611.0	1611.9	1617.6	1619.8	1619.8	1622.9	1623.7	1627.0	1627.8	1630.4	1635.2	1639.0	1639.8	1641.8	1645.6	1645.7
Type*		peg	catacl. br dike	gran-ite	schist	gran-ite	schist	gran-ite	peg	schist	schist	schist	schist	schist	schist	schist	epido-site	epido-site
(wt%)																		
SiO_2		74.8	60.6	73.0	59.7	66.9	59.3	75.1	67.5	44.7	49.6	56.4	56.2	40.4	57.2	62.4	43.3	45.7
TiO_2		0.03	0.66	0.15	0.72	0.13	0.77	0.05	0.01	1.27	1.24	1.05	0.97	1.67	1.14	0.79	0.83	0.46
Al_2O_3		14.6	18.5	14.3	15.2	17.1	20.4	14.5	18.0	18.7	15.7	19.6	19.4	23.7	20.4	16.4	14.8	14.3
Fe_2O_3†		0.27	5.55	1.41	6.79	2.41	4.01	0.64	0.04	12.6	12.5	9.75	9.46	18.8	8.74	4.48	7.26	6.65
MnO		0.08	0.06	0.11	0.11	0.05	0.07	0.06	0.02	0.10	0.11	0.04	0.04	0.04	0.07	0.08	0.30	0.41
MgO		0.11	1.24	0.29	1.53	0.35	0.87	0.22	0.05	6.86	7.51	1.48	0.96	3.26	1.90	1.00	1.98	1.04
CaO		1.06	1.35	2.47	4.28	2.23	2.56	1.42	0.42	4.73	2.62	0.38	1.06	1.93	0.45	2.96	25.6	24.7
Na_2O		5.88	2.18	2.05	3.10	3.71	1.42	3.22	4.01	2.78	1.91	1.26	1.19	3.92	0.80	1.64	0.37	0.11
K_2O		1.33	4.06	2.43	1.90	2.95	4.96	2.43	9.26	2.18	2.53	4.12	4.19	0.85	3.98	3.15	0.23	0.04
P_2O_5		0.03	0.06	0.03	0.05	0.05	0.09	0.10	0.07	0.36	0.16	0.07	0.06	0.02	0.13	0.14	0.11	0.07
SO_3		<0.1	0.1	0.1	0.7	0.3	0.3	<0.1	<0.1	0.7	0.5	0.2	<0.1	<0.1	0.5	0.2	<0.1	<0.1
LOI		1.4	5.6	3.6	5.2	3.5	4.7	2.0	0.4	4.3	4.9	4.9	6.0	4.8	4.3	6.0	4.6	5.7
Total		99.59	99.96	99.94	99.28	99.68	99.45	99.74	99.78	99.28	99.28	99.25	99.53	99.39	99.61	99.24	99.38	99.18
(ppm)	m#																	
Sc	(1)	0.75	14.5	n.d.§	13.6	3.33	14.9	0.86	0.20	21.0	37.4	21.4	21.3	n.d.§	21.4	n.d.§	8.19	10.7
V	(2)	<15	153	18	119	30	159	<15	<15	155	228	216	179	260	205	105	65	93
Cr	(1)	77.2	76.0	n.d.§	88.1	15.2	79.2	10.6	5.52	305	213	91.7	104	n.d.§	93.1	n.d.§	71.3	75.3
Co	(1)	0.54	17.2	n.d.§	16.6	1.43	10.8	0.52	0.43	48.1	60.2	27.3	31.3	n.d.§	32.5	n.d.§	13.9	9.43
Ni	(2)	21	39	29	34	26	41	24	35	156	160	58	60	56	45	36	30	24
Cu	(2)	<30	<30	<30	33	<30	33	<30	<30	117	52	36	27	114	<30	40	<30	<30
Zn	(1)	70	123	n.d.§	155	68	180	47	20	200	114	298	130	n.d.§	320	n.d.§	468	295
As	(1)	<0.8	3.02	n.d.§	<1.3	<0.8	<0.5	<0.5	<0.8	<1.3	<0.9	1.1	<0.9	n.d.§	<1.1	n.d.§	0.96	0.65
Se	(1)	0.85	3.57	n.d.§	2.47	3.14	1.31	1.79	0.23	<4.1	<3.3	<3.0	<1.5	n.d.§	<3.3	n.d.§	<2.3	<1.1
Br	(1)	1.4	11	n.d.§	0.8	0.6	2.4	0.6	0.5	1.2	0.6	0.7	0.6	n.d.§	1.5	n.d.§	1.0	0.7
Rb	(1)	126	323	n.d.§	135	266	394	207	772	233	191	206	275	n.d.§	219	n.d.§	<5.3	9.54
Sr	(2)	42	91	84	166	54	112	38	38	257	135	126	220	247	80	112	107	102
Y	(2)	18	74	52	32	40	89	40	109	34	30	53	65	50	53	49	26	<10
Zr	(2)	43	132	98	129	27	142	42	<15	112	98	170	159	232	202	211	173	90
Nb	(2)	23	28	57	13	55	30	31	<10	11	<10	<10	12	18	17	10	<10	20
Mo	(2)	<10	20	<10	15	<10	<10	<10	<10	<10	<10	34	26	63	<10	<10	<10	<10
Sb	(1)	0.05	0.19	n.d.§	<0.1	0.06	<0.1	<0.1	0.15	<0.2	0.70	0.12	0.13	n.d.§	<0.1	n.d.§	1.45	0.69
Cs	(1)	3.64	19.7	n.d.§	10.2	5.55	11.2	5.21	24.8	85.2	97.8	12.1	18.7	n.d.§	34.6	n.d.§	0.24	1.90
Ba	(2)	<30	322	n.d.§	194	61	351	<30	<30	286	146	606	677	154	508	193	<30	<30
La	(1)	3.16	34.8	n.d.§	35.7	5.63	37.9	2.80	0.36	9.32	11.4	51.0	56.9	n.d.§	44.3	n.d.§	20.4	35.0
Ce	(1)	10.9	70.4	n.d.§	68.7	11.5	72.2	13.6	0.89	19.6	24.1	102	112	n.d.§	96.3	n.d.§	40.6	78.6
Nd	(1)	5.72	35.0	n.d.§	28.0	5.10	34.3	8.6	n.d.§	10.5	12.4	46.1	54.4	n.d.§	43.5	n.d.§	23.4	44.5
Sm	(1)	1.51	7.73	n.d.§	6.47	1.35	7.10	2.46	0.13	2.40	3.08	9.43	11.4	n.d.§	8.20	n.d.§	6.46	8.34
Eu	(1)	0.24	1.31	n.d.§	2.05	0.40	1.47	0.17	0.14	1.09	1.09	2.19	2.35	n.d.§	1.87	n.d.§	1.62	1.29
Gd	(1)	0.97	6.13	n.d.§	5.40	<0.70	6.79	1.35	0.15	2.21	3.72	7.62	10.5	n.d.§	6.15	n.d.§	5.83	4.28
Tb	(1)	0.16	0.97	n.d.§	0.82	0.20	0.92	0.26	0.02	0.44	0.70	1.35	1.58	n.d.§	1.03	n.d.§	1.16	0.61
Tm	(1)	<0.40	0.59	n.d.§	0.31	<1.0	0.58	n.d.§	<0.05	0.21	0.54	0.58	0.67	n.d.§	0.48	n.d.§	0.60	0.26
Yb	(1)	1.20	3.36	n.d.§	1.91	0.86	2.48	1.84	0.17	1.36	2.18	3.84	4.59	n.d.§	2.94	n.d.§	3.59	1.76
Lu	(1)	0.27	0.49	n.d.§	0.27	0.08	0.29	0.42	n.d.§	0.18	0.27	0.62	0.55	n.d.§	0.37	n.d.§	0.48	0.32
Hf	(1)	1.61	3.76	n.d.§	3.29	0.51	3.65	1.30	0.89	3.07	2.69	5.79	5.10	n.d.§	5.45	n.d.§	4.12	3.43
Ta	(1)	9.40	7.43	n.d.§	1.21	22.4	7.81	12.8	2.81	1.58	0.43	1.50	1.60	n.d.§	1.69	n.d.§	0.71	1.85
W	(1)	1.6	5.1	n.d.§	5.4	6.1	9.6	n.d.§	<2.3	0.7	n.d.§	5.9	n.d.§	n.d.§	2.7	n.d.§	6.5	71
Pb	(2)	64	29	33	39	44	<15	78	200	<15	<15	<15	19	28	29	<15	<15	<15
Th	(1)	1.88	11.9	n.d.§	11.2	1.58	11.3	2.62	0.09	1.37	1.29	15.6	16.4	n.d.§	13.0	n.d.§	4.91	16.4
U	(1)	20.6	11.9	n.d.§	3.81	3.73	5.73	32.3	1.08	0.60	0.35	7.52	8.48	n.d.§	2.50	n.d.§	5.94	4.96
(ppb)																		
Ir	(1)	<0.6	<1.3	n.d.§	<1.3	<0.9	<1.0	<0.9	<0.5	<2.4	<9.0	<2.4	<2.5	n.d.§	<1.7	n.d.§	<1.3	<1.3
Au	(1)	1.0	0.9	n.d.§	0.7	0.9	0.3	0.4	<1.3	0.9	<1.8	<2.4	<1.6	n.d.§	0.7	n.d.§	0.4	0.7

(*Continued*)

TABLE A1. WHOLE-ROCK CHEMICAL COMPOSITIONS OF SAMPLES FROM THE EYREVILLE A AND B DRILL CORES (*Continued*)

Sample		W 134	CB6 143	CB6 144	W 135	W 136a	W 136b	W 137	CB6 145	W 138	CB6 146	RG 044	W 139a	W 139b	W 140	W 141	RG 040	RG 039
Core		B	B	B	B	B	B	B	B	B	B	B	B	B	B	B	B	B
Depth (m)		1647.8	1649.2	1655.9	1659.4	1661.2	1661.2	1665.4	1667.8	1669.7	1671.7	1672.1	1679.1	1679.1	1681.9	1682.1	1687.1	1688.6
Type*		epido-site	schist	peg	peg	peg/ catacl.	catacl. br dike	schist	schist	schist	gran-ite	schist	schist	schist	peg	schist	gran-ite	schist
(wt%)																		
SiO_2		62.8	62.5	67.4	64.7	76.3	55.5	49.0	53.5	45.5	72.5	52.2	54.7	52.3	85.1	52.1	74.4	63.2
TiO_2		0.25	0.86	0.01	0.03	0.01	1.13	0.88	0.81	1.10	0.15	0.86	0.86	0.85	0.03	1.22	0.13	0.78
Al_2O_3		7.2	16.5	14.8	20.7	12.8	16.3	20.2	17.8	24.6	14.4	18.5	18.3	18.5	7.8	24.9	15.3	17.4
Fe_2O_3†		5.65	4.53	0.09	0.93	0.09	12.0	9.37	7.64	6.59	0.63	7.12	10.6	12.7	0.56	5.33	1.27	6.10
MnO		0.19	0.17	0.01	0.02	0.01	0.07	0.06	0.06	0.06	0.03	0.08	0.05	0.04	0.03	0.06	0.09	0.05
MgO		0.69	1.04	0.04	0.13	0.06	1.16	0.65	0.99	1.39	0.21	0.99	0.78	0.73	0.31	1.84	0.29	1.71
CaO		14.3	2.28	0.51	1.23	0.39	2.17	2.60	3.01	2.56	1.29	5.11	1.95	1.13	0.85	0.78	1.21	0.53
Na_2O		0.11	1.91	3.62	7.66	3.29	2.60	4.29	1.53	2.27	4.69	0.58	0.67	0.71	0.86	0.59	2.74	1.10
K_2O		0.15	3.87	6.86	3.61	5.51	2.60	2.20	3.77	4.84	1.85	4.29	3.85	1.47	1.71	6.51	2.71	4.50
P_2O_5		1.09	0.22	0.04	0.04	0.04	0.54	0.06	0.05	0.06	0.05	0.05	0.05	0.05	<0.01	0.06	0.03	0.05
SO_3		<0.1	0.1	<0.1	<0.1	<0.1	0.5	0.2	0.4	0.2	<0.1	1.2	0.4	<0.1	<0.1	<0.1	<0.1	0.1
LOI		7.2	5.3	5.9	0.9	1.0	4.8	10.0	9.5	10.1	3.7	8.4	7.4	10.7	2.2	6.0	1.8	4.5
Total		99.63	99.28	99.28	99.95	99.50	99.37	99.51	99.06	99.27	99.50	99.38	99.61	99.18	99.45	99.39	99.97	100.02
(ppm)	m#																	
Sc	(1)	8.34	19.3	0.86	3.01	0.30	10.0	18.2	19.8	24.9	5.28	n.d.§	19.4	14.4	2.47	23	n.d.§	n.d.§
V	(2)	42	113	<15	<15	<15	108	195	200	280	20	191	194	172	28	262	24	193
Cr	(1)	82.5	77.8	7.96	11.1	10.2	47.6	96.4	101	107	11.9	n.d.§	94.5	89.4	45.9	144	n.d.§	n.d.§
Co	(1)	25.8	14.0	0.31	0.59	0.34	9.48	26.3	25.1	17.5	0.99	n.d.§	22.4	3.35	0.81	14.3	n.d.§	n.d.§
Ni	(2)	27	33	33	32	25	46	104	40	47	27	42	72	80	24	40	29	41
Cu	(2)	<30	45	<30	<30	<30	<30	58	<30	41	<30	46	<30	42	<30	<30	<30	<30
Zn	(1)	219	74	10	15	11	130	270	123	157	63	n.d.§	115	99	11	146	n.d.§	n.d.§
As	(1)	0.74	0.99	<0.6	<1.4	<0.7	0.91	0.76	<0.9	<0.9	<0.9	n.d.§	<1.1	<1.0	<0.8	<1.1	n.d.§	n.d.§
Se	(1)	<1.1	<2.1	<0.9	2.37	<0.2	0.97	2.25	<2.2	1.04	0.46	n.d.§	1.11	2.36	1.39	<1.9	n.d.§	n.d.§
Br	(1)	2.7	0.7	0.5	<1.2	5.2	20	2.9	0.7	<0.9	0.7	n.d.§	1.7	7.6	<0.6	0.9	n.d.§	n.d.§
Rb	(1)	20.7	167	561	283	357	195	182	226	283	178	n.d.§	210	85.9	170	493	n.d.§	n.d.§
Sr	(2)	231	105	45	63	52	144	386	170	163	84	106	80	110	99	115	71	85
Y	(2)	18	51	81	79	58	44	51	45	90	67	54	57	31	36	97	62	72
Zr	(2)	150	247	23	65	16	225	157	133	191	110	156	140	145	41	221	74	148
Nb	(2)	<10	11	<10	50	<10	23	11	11	16	45	12	11	18	29	34	45	14
Mo	(2)	<10	<10	<10	<10	<10	15	25	25	34	<10	13	23	65	<10	255	<10	23
Sb	(1)	0.10	0.13	<0.1	<0.1	<0.1	0.14	<0.2	<0.1	<0.1	<0.1	n.d.§	<0.1	0.05	<0.1	0.22	n.d.§	n.d.§
Cs	(1)	4.92	14.3	9.07	5.56	7.54	12.0	19.9	15.5	17.0	4.19	n.d.§	12.3	8.77	5.66	23.7	n.d.§	n.d.§
Ba	(2)	32	324	111	<30	<30	274	260	441	742	64	516	470	134	74	699	83	428
La	(1)	29.3	30.1	1.14	9.90	1.10	51.8	47.3	39.8	60.2	36.0	n.d.§	45.9	37.6	7.51	56.1	n.d.§	n.d.§
Ce	(1)	58.5	62.2	2.80	26.9	3.66	102	91.2	80.7	116	75.2	n.d.§	87.7	70.5	16.2	115	n.d.§	n.d.§
Nd	(1)	28.3	30.4	0.82	16.6	2.34	45.5	41.8	36.0	51.3	39.1	n.d.§	39.3	32.1	8.88	49.2	n.d.§	n.d.§
Sm	(1)	7.24	5.90	0.40	6.15	0.90	10.8	10.2	7.56	12.9	7.96	n.d.§	9.15	8.72	3.17	9.68	n.d.§	n.d.§
Eu	(1)	1.33	1.50	0.19	0.28	0.11	1.67	1.91	2.33	2.49	0.59	n.d.§	1.61	1.21	0.44	2.05	n.d.§	n.d.§
Gd	(1)	5.05	5.96	0.32	6.53	0.64	7.33	6.66	8.23	8.09	8.19	n.d.§	8.35	6.88	3.01	9.11	n.d.§	n.d.§
Tb	(1)	0.85	1.09	0.07	0.81	0.11	1.04	1.14	1.64	1.68	1.29	n.d.§	1.06	1.02	0.43	1.24	n.d.§	n.d.§
Tm	(1)	0.41	0.51	n.d.§	<1.20	<0.30	0.53	0.53	0.92	0.93	0.78	n.d.§	0.57	0.59	0.27	0.62	n.d.§	n.d.§
Yb	(1)	2.09	3.54	0.34	4.72	0.34	3.13	3.35	7.04	6.17	4.56	n.d.§	3.71	3.44	1.84	3.70	n.d.§	n.d.§
Lu	(1)	0.31	0.43	0.06	0.68	0.05	0.54	0.57	0.87	0.98	0.73	n.d.§	0.56	0.55	0.24	0.64	n.d.§	n.d.§
Hf	(1)	4.04	6.60	0.56	3.91	0.35	6.44	4.53	4.25	6.09	4.80	n.d.§	4.48	4.39	1.58	6.21	n.d.§	n.d.§
Ta	(1)	1.17	1.07	1.59	21.2	2.53	5.22	1.29	1.24	1.89	6.33	n.d.§	1.23	5.77	7.08	1.95	n.d.§	n.d.§
W	(1)	3.0	n.d.§	n.d.§	1.8	<1.7	9.0	2.3	n.d.§	8.3	n.d.§	n.d.§	7.7	7.6	1.7	6.1	n.d.§	n.d.§
Pb	(2)	<15	<15	78	61	97	19	35	16	34	46	<15	<15	42	18	43	40	<15
Th	(1)	6.78	10.4	0.50	12.9	0.81	7.04	11.3	12.8	18.9	33.6	n.d.§	12.6	12.3	8.42	19.7	n.d.§	n.d.§
U	(1)	2.46	2.42	2.82	31.0	6.66	14.7	6.76	8.87	11.6	38.8	n.d.§	6.39	11.6	13.3	10.7	n.d.§	n.d.§
(ppb)																		
Ir	(1)	<1.2	<2.1	<0.8	<0.9	<0.3	<1.2	<1.6	<2.3	<1.8	<1.4	n.d.§	<1.5	<1.7	<0.8	<2	n.d.§	n.d.§
Au	(1)	0.9	<1.6	<1.1	1.4	0.7	0.9	1.5	0.6	1.3	<1.7	n.d.§	1.2	1.1	0.6	<1.5	n.d.§	n.d.§

(*Continued*)

TABLE A1. WHOLE-ROCK CHEMICAL COMPOSITIONS OF SAMPLES FROM THE EYREVILLE A AND B DRILL CORES (*Continued*)

Sample		CB6 147	W 142	RG 038	CB6 148	W 143	W 146	W 147	CB6 149	W 148	W 149	W 150	CB6 150
Core		B	B	B	B	B	B	B	B	B	B	B	B
Depth (m)		1689.0	1691.8	1693.4	1700.2	1704.9	1728.7	1738.2	1741.0	1744.7	1754.3	1764.9	1766.1
Type*		schist	peg	schist	peg	peg	peg	peg	peg	peg	peg	peg	peg
(wt%)													
SiO_2		58.5	77.6	55.4	71.6	74.4	73.3	73.9	73.9	75.1	76.8	74.0	73.3
TiO_2		0.90	0.01	0.62	0.02	0.03	0.02	0.06	0.02	0.01	0.06	0.02	0.05
Al_2O_3		19.5	12.1	15.4	15.9	15.1	14.5	14.8	14.9	14.6	13.1	15.4	14.9
Fe_2O_3†		6.63	0.02	15.8	0.14	0.53	0.85	0.79	0.38	0.31	0.88	0.36	0.71
MnO		0.05	0.01	0.09	0.01	0.07	0.15	0.05	0.05	0.06	0.03	0.01	0.02
MgO		2.12	0.03	1.36	0.05	0.12	0.05	0.11	0.04	0.04	0.07	0.05	0.14
CaO		0.58	0.22	1.29	0.45	0.97	0.85	0.89	0.86	1.00	0.96	1.38	0.54
Na_2O		1.26	2.29	0.61	4.78	6.00	4.88	4.54	5.03	5.37	5.33	6.09	3.22
K_2O		4.39	6.52	3.19	6.01	1.90	3.64	3.65	3.40	2.72	1.76	1.45	5.60
P_2O_5		0.02	0.05	0.13	0.05	0.04	0.01	0.01	<0.01	<0.01	<0.01	<0.01	0.01
SO_3		0.1	<0.1	<0.1	<0.1	<0.1	<0.1	<0.1	<0.1	<0.1	<0.1	<0.1	<0.1
LOI		5.3	0.4	5.6	0.3	0.8	1.0	0.6	0.8	0.6	0.4	0.8	0.7
Total		99.35	99.25	99.49	99.31	99.96	99.25	99.40	99.38	99.81	99.39	99.56	99.19
(ppm)	m#												
Sc	(1)	18.2	0.32	n.d.§	0.10	1.11	5.29	6.42	9.43	6.39	3.18	8.06	16.6
V	(2)	204	<15	151	<15	<15	<15	19	<15	<15	22	<15	<15
Cr	(1)	97.2	5.62	n.d.§	13.5	28.3	23.9	7.20	11.3	30.7	66.0	46.7	9.16
Co	(1)	16.1	0.24	n.d.§	0.18	0.52	0.81	0.45	0.27	0.33	0.43	0.27	0.18
Ni	(2)	36	27	69	26	23	37	28	29	27	25	25	43
Cu	(2)	<30	<30	290	<30	<30	<30	<30	<30	<30	<30	<30	<30
Zn	(1)	127	32	n.d.§	9	60	30	63	46	22	11	30	37
As	(1)	<0.9	<0.6	n.d.§	<0.5	<1.0	<1.4	<1.0	<1.0	<0.9	<1.4	<1.5	<1.1
Se	(1)	1.03	0.23	n.d.§	<0.7	0.64	2.81	0.56	1.00	0.38	0.73	<0.8	<2
Br	(1)	0.8	0.5	n.d.§	<0.1	<0.9	<1.1	0.6	0.7	<0.9	<1.1	<1.1	0.8
Rb	(1)	259	433	n.d.§	383	156	368	320	341	221	132	114	505
Sr	(2)	125	33	65	39	40	25	25	22	21	26	21	19
Y	(2)	62	64	47	49	37	116	71	76	56	37	50	148
Zr	(2)	171	<15	96	<15	40	42	<15	23	28	41	23	37
Nb	(2)	16	<10	10	<10	22	100	65	100	50	90	33	70
Mo	(2)	25	<10	24	<10	<10	<10	<10	<10	<10	<10	<10	<10
Sb	(1)	<0.1	0.07	n.d.§	<0.1	<0.1	<0.1	<0.1	<0.1	<0.1	<0.1	<0.1	<0.1
Cs	(1)	15.8	6.56	n.d.§	5.84	3.65	4.46	2.98	3.51	2.15	1.38	1.16	3.61
Ba	(2)	455	80	412	34	<30	205	<30	<30	<30	<30	<30	<30
La	(1)	57.9	0.35	n.d.§	0.63	2.43	10.6	3.52	9.34	5.24	19.7	8.94	9.71
Ce	(1)	113	1.48	n.d.§	2.04	11.6	26.5	10.2	23.7	13.8	40.5	18.9	25.3
Nd	(1)	51.3	0.84	n.d.§	1.33	8.88	19.4	5.18	16.2	6.74	28.1	11.7	14.4
Sm	(1)	9.67	0.38	n.d.§	0.43	3.57	5.63	2.32	5.23	3.02	9.60	4.76	5.19
Eu	(1)	2.07	0.11	n.d.§	0.12	0.11	0.16	0.14	0.12	0.13	0.17	0.19	0.18
Gd	(1)	8.28	0.35	n.d.§	<0.5	1.97	6.41	3.90	<1.0	3.43	3.77	4.75	7.27
Tb	(1)	1.40	0.06	n.d.§	0.02	0.40	1.42	0.65	0.87	0.60	0.65	0.91	1.52
Tm	(1)	0.63	0.05	n.d.§	n.d.§	0.42	<1.0	0.45	0.64	0.51	0.34	0.49	0.92
Yb	(1)	3.79	0.31	n.d.§	0.09	2.66	5.51	2.91	3.20	2.68	1.60	3.24	6.06
Lu	(1)	0.45	0.03	n.d.§	<0.01	0.41	0.77	0.46	0.36	0.48	0.20	0.47	0.72
Hf	(1)	5.91	0.25	n.d.§	0.09	1.32	3.14	2.17	1.02	1.37	2.13	0.70	2.11
Ta	(1)	2.16	2.23	n.d.§	0.65	6.67	25.3	7.30	6.00	5.70	8.69	1.46	5.54
W	(1)	n.d.§	1.6	n.d.§	n.d.§	3.0	<4.1	<2.8	n.d.§	<2.3	<4.3	<4.7	n.d.§
Pb	(2)	18	129	<15	170	74	37	45	32	38	18	28	52
Th	(1)	16.7	0.54	n.d.§	0.78	3.09	8.21	6.84	13.9	6.74	5.03	10.3	22.6
U	(1)	7.35	3.27	n.d.§	<0.36	28.2	16.3	8.82	14.2	4.27	7.95	7.40	15.3
(ppb)													
Ir	(1)	<2.4	<0.3	n.d.§	<0.7	<0.6	<0.8	<0.8	<1.4	<0.9	<0.9	<1.0	0.6
Au	(1)	<1.6	<0.8	n.d.§	<0.7	1.2	0.3	<1.4	<1.6	1.3	1.1	1.1	<1.7

*Abbreviations: amph—amphibolite, br—breccia, catacl.—cataclastic, Ex br—Exmore breccia (diamicton), gn—gneiss, imr—impact melt rock, peg—pegmatite, plib—polymict lithic impact breccia, post-Ex br—post-Exmore breccia transition zone, sb—sedimentary block, sv—suevite, xeno—xenolith of megablock. LOI—loss on ignition.

†Total Fe as Fe_2O_3.

§n.d.—not determined.

#m—analytical method for trace elements: 1—instrumental neutron activation analysis (INAA), 2—X-ray fluorescence (XRF).

**Subdivision of subunits after Horton et al. (this volume).

TABLE A2. CORRELATION COEFFICIENT *r* FOR SELECTED ELEMENT PAIRS FOR THE MAJOR ROCK TYPES OF THE EYREVILLE A AND B DRILL CORES

A. EXMORE BRECCIA (DIAMICTON) (*n* = 73)

	Depth	SiO_2	TiO_2	Al_2O_3	Fe_2O_3	MgO	CaO	Na_2O	K_2O	P_2O_5	LOI	V	Cr	Co	Ni	Rb	Sr	Zr	Ba
SiO_2	0.13																		
TiO_2	0.26	–0.69																	
Al_2O_3	0.16	–0.73	0.89																
Fe_2O_3	–0.17	–0.90	0.55	0.57															
MgO	–0.13	–0.86	0.62	0.77	0.84														
CaO	–0.12	–0.74	0.43	0.41	0.75	0.72													
Na_2O	0.27	–0.16	0.42	0.34	0.03	0.14	0.05												
K_2O	–0.08	0.20	–0.44	–0.48	–0.07	–0.31	0.10	–0.10											
P_2O_5	–0.15	–0.66	0.27	0.22	0.68	0.50	0.78	–0.06	0.20										
LOI	–0.09	–0.80	0.42	0.40	0.68	0.54	0.50	0.08	–0.11	0.67									
V	–0.07	–0.81	0.72	0.80	0.74	0.82	0.59	0.07	–0.34	0.45	0.53								
Cr	–0.09	–0.83	0.47	0.54	0.83	0.75	0.63	–0.05	–0.14	0.66	0.74	0.74							
Co	0.15	–0.49	0.62	0.62	0.46	0.52	0.28	0.16	–0.33	0.15	0.35	0.51	0.46						
Ni	–0.09	–0.31	0.36	0.48	0.33	0.54	0.29	–0.04	–0.29	0.04	0.01	0.44	0.31	0.48					
Rb	–0.04	–0.48	0.18	0.25	0.59	0.51	0.56	–0.08	0.18	0.57	0.30	0.46	0.62	0.29	0.33				
Sr	–0.55	0.08	–0.39	–0.25	0.01	0.03	0.16	–0.19	0.21	0.10	–0.13	–0.08	–0.06	–0.25	0.05	0.12			
Zr	0.04	–0.26	0.55	0.64	0.18	0.37	0.14	0.24	–0.37	–0.10	–0.01	0.48	0.13	0.47	0.39	–0.01	–0.11		
Ba	–0.15	0.69	–0.55	–0.63	–0.65	–0.75	–0.47	–0.01	0.42	–0.33	–0.51	–0.72	–0.70	–0.44	–0.35	–0.38	0.32	–0.25	
ΣREE	0.01	–0.74	0.67	0.73	0.71	0.75	0.54	0.07	–0.28	0.49	0.52	0.74	0.76	0.57	0.47	0.56	–0.16	0.42	–0.66

B. GRANITE OF THE MEGABLOCK (*n* = 18)

	Depth	SiO_2	TiO_2	Al_2O_3	Fe_2O_3	MgO	CaO	Na_2O	K_2O	P_2O_5	LOI	V	Cr	Co	Ni	Rb	Sr	Zr	Ba
SiO_2	–0.04																		
TiO_2	0.15	–0.43																	
Al_2O_3	0.04	–0.72	0.31																
Fe_2O_3	0.04	–0.80	0.76	0.62															
MgO	–0.21	–0.78	0.55	0.69	0.83														
CaO	–0.07	–0.79	0.20	0.78	0.53	0.76													
Na_2O	0.10	–0.26	–0.31	0.43	–0.09	–0.07	0.36												
K_2O	–0.12	0.58	–0.09	–0.52	–0.36	–0.63	–0.69	–0.26											
P_2O_5	0.19	–0.26	0.80	0.47	0.62	0.39	0.33	0.03	0.17										
LOI	–0.15	0.07	0.03	–0.01	0.09	0.31	0.15	–0.18	–0.47	–0.08									
V	–0.03	0.08	0.19	0.34	0.14	0.14	–0.14	–0.03	0.18	0.11	–0.17								
Cr	–0.14	0.08	0.08	–0.07	0.21	0.19	0.02	–0.32	–0.07	0.15	0.54	–0.23							
Co	–0.17	–0.85	0.56	0.65	0.82	0.91	0.72	–0.02	–0.67	0.43	0.05	–0.07	0.05						
Ni	–0.13	0.17	–0.01	–0.23	–0.22	–0.23	–0.05	0.42	0.30	0.06	–0.25	–0.09	–0.15	–0.09					
Rb	–0.08	0.16	–0.13	–0.10	–0.17	–0.37	–0.29	0.43	0.31	0.02	–0.28	0.36	–0.24	–0.28	0.46				
Sr	–0.19	–0.22	0.32	0.16	0.36	0.41	0.27	–0.12	–0.27	0.45	0.41	–0.33	0.41	0.29	–0.29	–0.31			
Zr	0.31	–0.26	0.74	0.33	0.49	0.29	0.15	–0.25	0.06	0.70	–0.22	0.33	0.27	0.18	–0.06	–0.24	0.26		
Ba	–0.14	–0.52	0.54	0.39	0.74	0.74	0.50	–0.28	–0.24	0.50	0.23	–0.11	0.56	0.51	–0.17	–0.50	0.60	0.51	
ΣREE	0.55	–0.34	0.51	0.22	0.53	0.27	0.20	–0.18	–0.18	0.56	0.32	–0.10	0.16	0.32	–0.34	–0.29	0.48	0.57	0.50

(*Continued*)

TABLE A2. CORRELATION COEFFICIENT *r* FOR SELECTED ELEMENT PAIRS FOR THE MAJOR ROCK TYPES OF THE EYREVILLE A AND B DRILL CORES (*Continued*)

C. GRANITIC GNEISS OF THE MEGABLOCK (*n* = 8)

	Depth	SiO_2	TiO_2	Al_2O_3	Fe_2O_3	MgO	CaO	Na_2O	K_2O	P_2O_5	LOI	V	Cr	Co	Ni	Rb	Sr	Zr	Ba
SiO_2	–0.14																		
TiO_2	–0.38	–0.72																	
Al_2O_3	0.49	–0.58	0.02																
Fe_2O_3	0.19	–0.81	0.59	0.56															
MgO	–0.47	–0.73	0.90	0.13	0.67														
CaO	0.00	–0.33	0.28	0.39	0.76	0.36													
Na_2O	0.10	–0.21	0.11	0.43	0.69	0.22	0.98												
K_2O	0.00	0.33	–0.27	–0.37	–0.76	–0.35	–0.99	–0.98											
P_2O_5	0.10	–0.62	0.86	0.48	0.88	0.82	0.67	0.57	–0.43										
LOI	–0.86	0.48	0.17	–0.68	–0.52	0.16	–0.26	–0.30	0.29	–0.09									
V	–0.36	–0.79	0.99	–0.02	0.71	0.89	0.32	0.11	–0.32	0.88	0.21								
Cr	0.16	–0.54	0.35	0.76	0.52	0.25	0.53	0.51	–0.52	0.66	–0.33	0.33							
Co	–0.03	–0.67	0.56	0.53	0.91	0.66	0.90	0.83	–0.89	0.86	–0.30	0.67	0.60						
Ni	–0.05	–0.05	–0.20	0.19	–0.19	–0.04	–0.41	–0.45	0.42	–0.21	–0.03	–0.21	–0.11	–0.32					
Rb	–0.10	0.21	–0.10	–0.41	–0.69	–0.21	–0.98	–0.99	0.98	–0.33	0.34	–0.11	–0.49	–0.82	0.46				
Sr	–0.21	–0.12	0.23	0.26	0.43	0.39	0.60	0.67	–0.60	0.52	0.09	0.11	0.38	0.57	–0.53	–0.67			
Zr	0.14	–0.71	0.69	0.25	0.52	0.60	–0.05	–0.12	0.05	–0.67	–0.26	0.64	0.29	0.23	0.09	0.12	0.12		
Ba	0.17	0.21	–0.41	–0.01	–0.43	–0.33	–0.69	–0.64	0.69	–0.41	–0.05	–0.43	–0.34	–0.67	0.83	0.64	–0.50	0.17	
ΣREE	0.48	–0.74	0.28	0.75	0.60	0.30	0.12	0.10	–0.12	0.52	–0.67	0.32	0.55	0.33	0.41	–0.10	0.00	0.74	0.33

D. IMPACTITE (SUEVITE, IMPACT MELT ROCK, POLYMICT LITHIC IMPACT BRECCIA; *n* = 75 FOR MAJOR ELEMENTS AND *n* = 71 FOR TRACE ELEMENTS)

	Depth	SiO_2	TiO_2	Al_2O_3	Fe_2O_3	MgO	CaO	Na_2O	K_2O	P_2O_5	LOI	V	Cr	Co	Ni	Rb	Sr	Zr	Ba
SiO_2	–0.55																		
TiO_2	0.62	–0.59																	
Al_2O_3	0.49	–0.80	0.63																
Fe_2O_3	0.51	–0.77	0.80	0.66															
MgO	0.40	–0.78	0.47	0.67	0.61														
CaO	–0.45	–0.04	–0.32	–0.08	–0.11	0.08													
Na_2O	–0.56	0.02	–0.58	–0.16	–0.33	0.24	0.68												
K_2O	0.08	–0.01	–0.06	0.22	–0.20	0.02	–0.24	–0.08											
P_2O_5	0.50	–0.43	0.68	0.50	0.49	0.30	–0.20	–0.40	–0.01										
LOI	0.64	–0.55	0.50	0.23	0.57	0.25	–0.24	–0.41	–0.37	0.36									
V	0.53	–0.65	0.76	0.73	0.64	0.66	–0.16	–0.22	0.15	0.51	0.29								
Cr	0.39	–0.47	0.50	0.50	0.52	0.51	–0.29	–0.24	0.24	0.29	0.17	0.61							
Co	0.50	–0.54	0.70	0.59	0.65	0.53	–0.30	–0.33	0.10	0.39	0.32	0.65	0.68						
Ni	0.53	–0.53	0.58	0.52	0.58	0.50	–0.39	–0.39	0.27	0.43	0.38	0.53	0.69	0.66					
Rb	0.33	–0.11	0.17	0.27	–0.01	0.04	–0.50	–0.29	0.78	0.19	0.05	0.30	0.37	0.28	0.45				
Sr	–0.13	–0.11	–0.02	–0.03	0.10	0.04	0.47	0.26	–0.56	–0.06	0.17	–0.15	–0.33	–0.08	–0.26	–0.48			
Zr	0.39	–0.25	0.60	0.36	0.44	0.11	–0.19	–0.48	–0.16	0.43	0.34	0.25	0.09	0.18	0.26	–0.02	0.13		
Ba	–0.09	–0.05	–0.15	0.21	–0.16	0.12	0.04	0.15	0.73	0.01	–0.50	0.10	0.25	0.07	0.20	0.40	–0.44	–0.17	
ΣREE	0.61	–0.53	0.64	0.71	0.52	0.37	–0.47	–0.52	0.28	0.53	0.33	0.59	0.60	0.69	0.65	0.47	–0.20	0.45	0.14

(*Continued*)

TABLE A2. CORRELATION COEFFICIENT *r* FOR SELECTED ELEMENT PAIRS FOR THE MAJOR ROCK TYPES OF THE EYREVILLE A AND B DRILL CORES (*Continued*)

E. CATACLASTIC/FELSIC GNEISS OF THE IMPACT BRECCIA SECTION (*n* = 10 FOR MAJOR ELEMENTS AND *n* = 9 FOR TRACE ELEMENTS)

	SiO_2	TiO_2	Al_2O_3	Fe_2O_3	MgO	CaO	Na_2O	K_2O	P_2O_5	LOI	V	Cr	Co	Ni	Rb	Sr	Zr	Ba
TiO_2	–0.58																	
Al_2O_3	–0.85	0.73																
Fe_2O_3	–0.60	0.27	0.23															
MgO	–0.68	0.19	0.45	0.80														
CaO	–0.52	0.15	0.17	0.56	0.68													
Na_2O	–0.37	0.37	0.25	0.44	0.63	0.71												
K_2O	–0.20	0.27	0.41	–0.24	–0.22	–0.42	–0.55											
P_2O_5	–0.25	0.09	0.02	0.50	0.44	0.57	0.32	0.13										
LOI	–0.16	0.41	0.33	–0.28	–0.41	–0.11	–0.29	0.18	–0.25									
V	–0.68	0.69	0.55	0.69	0.60	0.49	0.42	0.05	0.58	0.15								
Cr	–0.58	0.30	0.46	0.72	0.93	0.57	0.72	–0.22	0.29	–0.42	0.47							
Co	–0.55	0.21	0.10	0.98	0.85	0.63	0.57	–0.40	0.54	–0.35	0.61	0.70						
Ni	–0.86	0.30	0.54	0.79	0.80	0.64	0.38	0.00	0.58	–0.12	0.72	0.86	0.81					
Rb	–0.03	–0.18	0.06	–0.17	–0.30	–0.42	–0.82	0.80	0.17	0.22	0.03	–0.45	–0.27	0.06				
Sr	–0.44	0.09	0.20	0.64	0.88	0.77	0.86	–0.46	0.50	–0.57	0.45	0.83	0.83	0.61	–0.38			
Zr	0.02	0.28	0.39	–0.36	–0.17	–0.66	–0.33	0.54	–0.32	0.03	0.03	–0.48	–0.60	–0.21	0.79	–0.32		
Ba	–0.25	0.13	0.48	–0.32	0.15	0.19	0.18	0.03	–0.43	0.28	–0.19	0.19	–0.19	–0.07	–0.10	0.10	0.15	
ΣREE	–0.68	0.03	0.48	0.60	0.85	0.48	0.42	0.17	0.49	–0.50	0.34	0.78	0.53	0.74	0.02	0.77	–0.03	0.22

F. SCHIST OF THE BASAL CRYSTALLINE SECTION (*n* = 37 FOR MAJOR ELEMENTS AND *n* = 28 FOR TRACE ELEMENTS)

	Depth	SiO_2	TiO_2	Al_2O_3	Fe_2O_3	MgO	CaO	Na_2O	K_2O	P_2O_5	LOI	V	Cr	Co	Ni	Rb	Sr	Zr	Ba
SiO_2	–0.32																		
TiO_2	0.17	–0.61																	
Al_2O_3	0.09	–0.61	0.63																
Fe_2O_3	0.35	–0.66	0.42	0.21															
MgO	–0.31	–0.25	0.42	0.30	0.15														
CaO	0.07	–0.30	–0.13	–0.14	0.09	–0.11													
Na_2O	–0.16	–0.32	0.28	0.28	0.17	0.30	0.43												
K_2O	0.13	0.04	0.19	0.42	–0.28	0.09	–0.41	–0.31											
P_2O_5	0.03	–0.03	0.07	–0.04	0.13	0.16	0.14	0.01	0.04										
LOI	0.28	–0.54	0.11	0.29	0.28	–0.20	0.16	–0.02	0.15	0.13									
V	0.57	–0.63	0.63	0.59	0.47	0.17	–0.19	0.09	0.34	–0.05	0.34								
Cr	0.29	–0.64	0.77	0.50	0.36	0.60	0.05	0.29	0.32	0.09	0.17	0.59							
Co	0.24	–0.57	0.53	0.23	0.75	0.33	0.02	0.27	0.12	0.41	0.25	0.54	0.47						
Ni	0.34	–0.63	0.38	0.24	0.65	0.17	–0.03	–0.01	0.04	0.30	0.45	0.49	0.38	0.61					
Rb	0.48	–0.54	0.48	0.69	0.14	0.21	–0.02	0.16	0.75	0.10	0.23	0.65	0.54	0.38	0.44				
Sr	0.08	–0.55	0.47	0.40	0.36	0.24	0.42	0.79	–0.20	–0.09	0.15	0.38	0.62	0.42	0.15	0.40			
Zr	–0.34	0.25	0.23	0.20	–0.47	0.08	–0.27	0.03	0.10	–0.06	–0.13	–0.18	–0.16	–0.43	–0.38	–0.16	–0.09		
Ba	–0.25	–0.05	0.19	0.41	–0.16	0.30	–0.36	–0.21	0.72	0.07	0.17	0.18	0.34	0.13	0.04	0.47	–0.06	0.23	
ΣREE	0.56	–0.38	0.40	0.68	0.16	–0.12	–0.42	–0.14	0.67	–0.13	0.52	0.72	0.30	0.25	0.32	0.62	0.26	0.15	0.58

Note: n—number of analyses; REE—rare earth element; LOI—loss on ignition.

The Geological Society of America
Special Paper 458
2009

Search for a meteoritic component in impact breccia from the Eyreville core, Chesapeake Bay impact structure: Considerations from platinum group element contents

Iain McDonald
School of Earth, Ocean and Planetary Sciences, Cardiff University, Park Place, Cardiff CF10 3YE, UK

Katerina Bartosova
Christian Koeberl*
Department of Lithospheric Research, University of Vienna, Althanstrasse 14, Vienna, A-1090, Austria

ABSTRACT

This paper documents an attempt to detect a meteoritic component in both wash-back (resurge) crater-fill breccia (the so-called Exmore breccia) and in suevites from the Eyreville core hole, which was drilled several kilometers from the center of the 85-km-diameter Chesapeake Bay impact structure, Virginia, USA. Determining the presence of an extraterrestrial component and, in particular, the projectile type for this structure, which is the largest impact structure currently known in the United States, is of importance because it marks one of several large impact events in the late Eocene, during which time the presence of extraterrestrial ^{3}He and multiple impact ejecta layers provide evidence for a comet or asteroid shower. Previous work has indicated an ordinary chondritic projectile for the largest of the late Eocene craters, the Popigai impact structure in Siberia. The exact relation between the Chesapeake Bay impact event and siderophile element anomalies documented in late Eocene ejecta layers from around the world is not clear. The only clear indication for an extraterrestrial component related to this structure has been the discovery of a meteoritic osmium isotopic signature in impact melt rocks recovered from a hydrogeologic test hole located on Cape Charles near the center of the structure, and confirmation of a similar signature in suevitic rocks would have been desirable in order to place constraints on the type of projectile involved in formation of the Chesapeake Bay crater. Unfortunately, the current data show no discernible differences in the contents of the platinum group elements (PGEs) among the suevite, the Exmore breccia, and several crystalline basement rocks, all from the Eyreville core hole. Abundances of PGEs are uniformly low (e.g., <0.1 ppb Ir), and chondrite-normalized abundance patterns are nonchondritic. These data do not allow unambiguous verification of an extraterrestrial signature. Thus, the nature of the Chesapeake Bay projectile remains ambiguous.

*christian.koeberl@univie.ac.at

McDonald, I., Bartosova, K., and Koeberl, C., 2009, Search for a meteoritic component in impact breccia from the Eyreville core, Chesapeake Bay impact structure: Considerations from platinum group element contents, *in* Gohn, G.S., Koeberl, C., Miller, K.G., and Reimold, W.U., eds., The ICDP-USGS Deep Drilling Project in the Chesapeake Bay Impact Structure: Results from the Eyreville Core Holes: Geological Society of America Special Paper 458, p. 469–479, doi: 10.1130/2009.2458(21).

INTRODUCTION AND GEOLOGICAL BACKGROUND

The late Eocene Chesapeake Bay impact structure, which is the source crater of the North American tektite strewn field (Koeberl et al., 1996; Deutsch and Koeberl, 2006) (Fig. 1), is among the largest and best preserved of the known impact craters on Earth. It is the largest impact structure currently known in the United States. The age of the structure is ca. 35.4 Ma (e.g., Poag and Aubry, 1995; Horton and Izett, 2005; Pusz et al., 2009), and it has a diameter of 85 km with an "inverted sombrero"–shape cross section. The International Continental Scientific Drilling Program (ICDP) and the U.S. Geological Survey (USGS) completed one shallow and two deep core holes to a composite depth of almost 1.8 km into the Chesapeake Bay impact structure. Field operations began in July 2005 with site preparations at Eyreville Farm in Northampton County, Virginia; subsequently, three core holes were drilled at the Eyreville site. Eyreville hole A was cored between depths of 125 m and 941 m from September through early October 2005. Problems with lost mud circulation and swelling clays in Eyreville A led to deviation of the bit from Eyreville A to a new hole, Eyreville B, at a depth of 738 m. Eyreville B was cored from that depth to a final depth of 1766 m from October through December 2005. Postimpact sediments were cored from land surface to 140 m depth in the Eyreville C hole (April–May 2006).

The cored impactite section is composed of five major lithologic units. The lowest unit consists of ~216 m of fractured mica schist, granite, and granite pegmatite, and also carries several impact breccia veins. These rocks could represent the autochthonous crater floor, or they could be parautochthonous basement blocks. Above these rocks, there are ~157 m of suevitic impact breccias that are considered fallback and (or) ground-surge deposits. Above these breccias, a thin interval of quartz sand (22 m) contains an amphibolite block and other lithic clasts of centimeter to decimeter size. This sand occurs below a 275-m-thick granite megablock, which appears unshocked and thus must have been transported for tens of kilometers during the cratering process. The uppermost and thickest impactite unit consists of ~652 m of deformed sediment megablocks and overlying sedimentary clast breccia (Exmore beds). The Exmore beds contain clasts of target sediments and crystalline rock, as well as a small component of impact melt; these are mostly shard-shaped impact melt particles plus some shocked clasts and minerals, which are enriched in the depth interval between 457.7–467.3 m (Reimold et al., this volume). This unit is interpreted to represent late-stage collapse of the marine water column and its catastrophic flow back into the crater (Edwards et al., this volume; Horton et al., this volume, Chapter 2).

The present paper focuses on new geochemical studies of suevite samples from the Eyreville drill core into the Chesapeake Bay impact structure, which were analyzed with the aim of detecting an extraterrestrial meteoritic component and using it to further constrain the type of projectile involved.

METEORITIC COMPONENTS IN IMPACTITES

The detection and verification of an extraterrestrial component in impact-derived melt rocks or breccias can provide confirming evidence for an impact origin of a geological structure (see the reviews by Koeberl, 1998, 2007). In principle, a very small amount of meteoritic melt or vapor is mixed with a much larger quantity of target rock vapor and melt, and this mixture later is incorporated into impact melt rocks or melts breccias, suevite, or impact glass. In most cases, the extraterrestrial contribution to these impactite lithologies is very small—mostly much less than one percent by weight. The detection of such small amounts of meteoritic matter is extremely difficult, and only elements that have high abundances in meteorites, but correspondingly low abundances in terrestrial crustal rocks, (e.g., siderophile elements such as Ni, Cr, and the platinum group elements [PGEs]) are commonly used in such studies. Distinctly higher siderophile element contents in impact melts, compared to target rock abundances, can be indicative of the presence of either a chondritic or an iron meteoritic component (e.g., Palme et al., 1978; Evans et al., 1993; McDonald et al., 2001). Complications may arise because: (1) meteorites have a range of compositions within each class, and some classes are better constrained than others (cf. McDonald, 2002); (2) target rocks may have variable siderophile element concentrations; or (3) concentrations of siderophile elements retained in the impactites are very low. Furthermore, the contribution of the target rock (the indigenous component) to the composition of impactites can only be well understood if a well-constrained mixing relationship exists between the composition of the impactor and the target rocks that results in a reliable regression and a lower intercept reflecting the average PGE concentration in the target rocks (e.g., McDonald et al., 2001; Tagle and Claeys, 2005). Alternatively, all contributing target rocks must have been identified, and their relative contributions to the melt mixture must be known—something that is extremely difficult to achieve in practice.

A separate and independent method involves the use of the Os and Cr isotope systems, either of which can be used to establish the presence of a meteoritic component in impactites. Both methods are based on the observation that the isotopic compositions of the elements Os and Cr, respectively, are different between most meteorites and terrestrial rocks and that these differences are sufficiently large to permit detection of meteoritic Os or Cr present in the impact rock (for applications of the Os and Cr systems, see reviews by Koeberl and Shirey, 1997; Koeberl, 1998, 2007; Shukolyukov and Lugmair, 1998). In terms of sensitivity, the Os isotopic method allows detection of very small amounts of an extraterrestrial component (on the order of 0.1%) and is restricted to chondrites and iron meteorites, but it does not allow distinction between meteorite types. The Cr isotopic system requires larger amounts of extraterrestrial components (at least 2%), but it has the advantage of being able to distinguish between some meteorite types, including achondrites (but

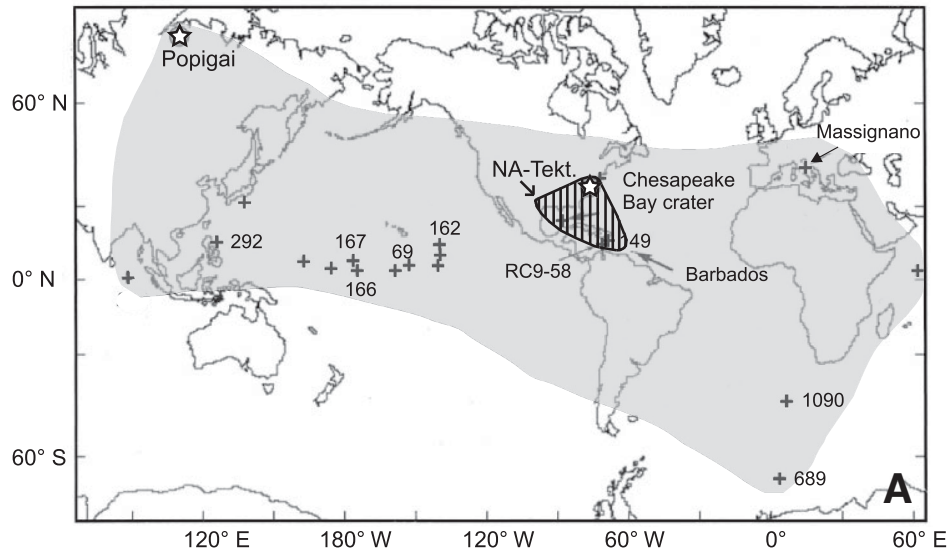

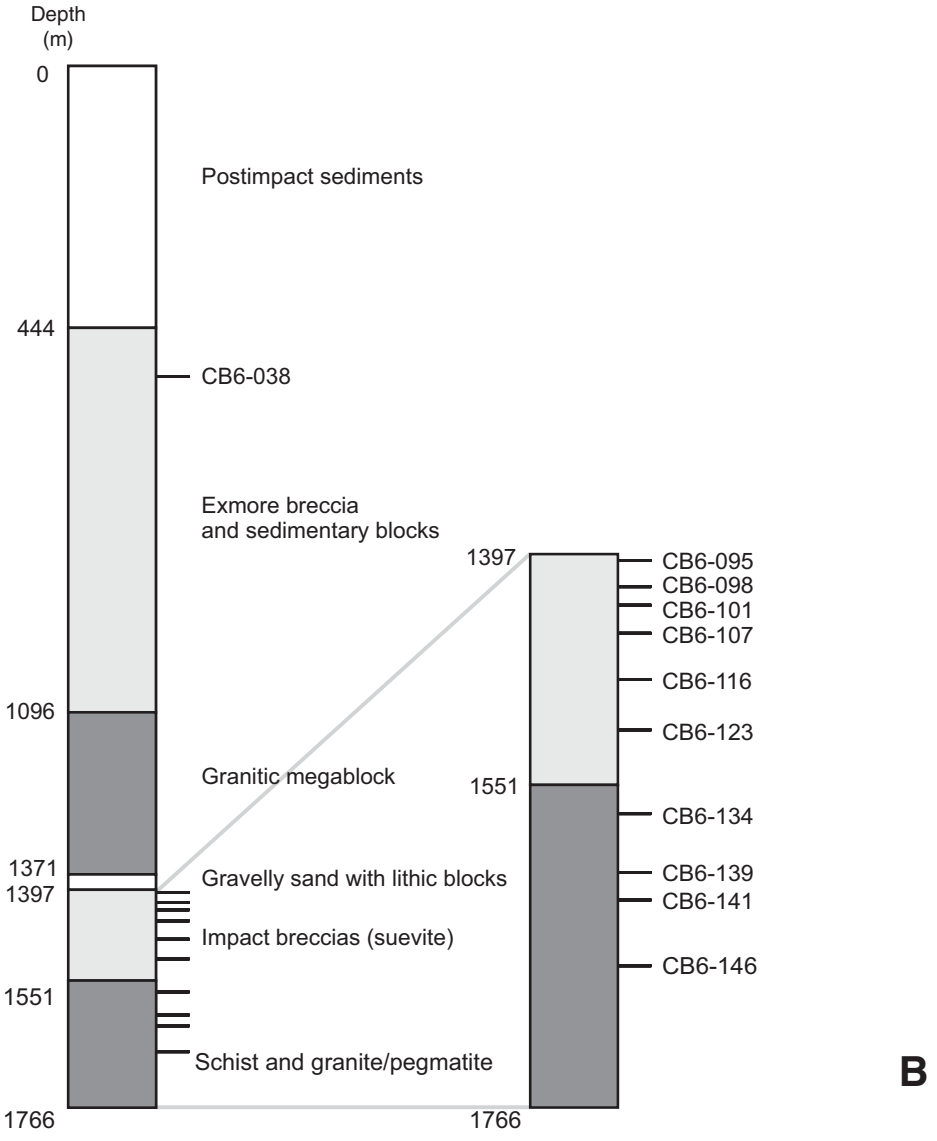

Figure 1. (A) Locations of Chesapeake Bay and Popigai impact craters, as well as the North American tektite strewn field (NA-Tekt.) and locations of distal ejecta (crosses) that contain evidence for an extraterrestrial component. (B) Diagram of the Eyreville core showing the exact depths from which the samples studied here were derived.

excluding most iron meteorites). A recent application of the Cr isotopic method to the determination of impact types was given by Koeberl et al. (2007).

IMPORTANCE OF THE SEARCH FOR A METEORITIC COMPONENT AT THE CHESAPEAKE BAY IMPACT STRUCTURE

The late Eocene was a period of major changes, characterized by an accelerated global cooling (e.g., Zachos et al., 2001; Miller et al., 2008, and references therein), a sharp temperature drop of ~2 °C near the Eocene-Oligocene (E-O) boundary, and significant stepwise floral and faunal turnovers. These global climate changes are commonly attributed to the expansion of the Antarctic ice cap following its gradual isolation from other continental masses (see previous references). However, multiple bolide impact events (e.g., Farley et al., 1998; Montanari and Koeberl, 2000, and references therein) over a duration of ~2 Ma may also have played an important role in the deterioration of the global climate at the end of the Eocene Epoch. Initial global cooling due to the late Eocene impact events has been suggested (e.g., Vonhof et al., 2000; Bodiselitsch et al., 2004).

There is abundant evidence for multiple impact events in the late Eocene, in terms of both impact craters and ejecta layers (Fig. 1). There are currently at least five impact craters known that are of late Eocene age, a relatively large number within a short time span. The two large impact structures Popigai, Russia, and Chesapeake Bay, USA, with respective diameters of 100 and 85 km, and respective ages of 35.7 ± 0.8 Ma (Bottomley et al., 1997) and 35.3 ± 0.2 Ma (Poag and Aubry, 1995; Obradovich et al., 1989; Horton and Izett, 2005), represent the largest post–Cretaceous-Tertiary (K-T) boundary impact events. Two smaller impact craters are known to be of comparable, but as yet poorly constrained, age, namely, Mistastin, Canada (38 ± 4 Ma, 28 km; Mak et al., 1976), and Wanapitei, Canada (37 ± 2 Ma, 7.5 km; Winzer et al., 1976). The 17-km-diameter Logoisk (Belarus) impact structure, which was earlier dated at 40 ± 5 Ma, has now been provisionally redated at 42.3 ± 1.1 Ms (Sherlock et al., 2006), and thus may not be part of the same event. In addition, Sherlock et al. (2005) reevaluated the age for the Haughton impact structure from new Ar-Ar data to be around 39 Ma; however, Haughton has thus far been assumed to have formed at around 23 Ma, and the older age is not yet confirmed. The multiple impact hypothesis predicts an even larger occurrence of smaller impacts that may have played a role in the alteration climate conditions at a global scale.

These impact craters are accompanied by tektites and clinopyroxene (cpx)-bearing spherules (microkrystites) in Upper Eocene marine deposits, some of which contain an iridium anomaly (e.g., Montanari et al., 1993; Kyte and Liu, 2002). Specifically, Upper Eocene marine sediments around the world contain evidence for at least two closely spaced impactoclastic layers, i.e., layers containing impact debris, such as tektites and microtektites and shocked minerals and rock fragments (for references, see, e.g., Montanari and Koeberl, 2000). Initially, only one layer was known from the eastern U.S. coast, the Caribbean, and the Gulf of Mexico, and it was correlated with the North American tektite strewn field. This layer contains microtektites (i.e., glassy, not recrystallized spherules), shocked minerals, and high-pressure phases (e.g., coesite), but no marked siderophile element anomaly (Glass et al., 1998). The presence of crystalline spherules composed mostly of clinopyroxene was detected in the same deep-sea sediments, and initially these spherules were also considered to belong to the North American tektite strewn field. The clinopyroxene spherules were found not only in the Caribbean and the Gulf of Mexico but also in the Pacific Ocean (e.g., Glass, 2002; Glass et al., 2004a).

The microtektite layer and the microkrystite (cpx-rich) layer are in fact separated from each other by up to 25 cm at sites in the Caribbean Sea or the Gulf of Mexico, with the microkrystite layer being the lower (i.e., older) one (Glass, 1989, 2002; Glass and Burns, 1987). The separation between the two layers amounts to ~10–20 ka (e.g., see review in Glass, 2002). Microtektites and tektite fragments at Deep Sea Drilling Project (DSDP) Site 612 (located at 38°49.21′N, 72°46.73′W, on the continental slope west of New Jersey) show chemical and isotopic similarities with other North American tektites. The microkrystite layer has been found at numerous locations, indicating that it has a more or less global distribution, and it seems to be associated at several locations with enhanced Ir abundances (e.g., Glass et al., 1982; Glass, 2002). Impact debris was also found at the late Eocene site at Massignano, Italy (Montanari and Koeberl, 2000; Glass et al., 2004b), but the relationship between this and the other two layers is not yet fully understood.

The Chesapeake Bay impact is thought to have been responsible for the younger of the two impact layers (which has definitely been found in the North American region, Caribbean, and Gulf of Mexico, but which may have a global distribution). There is a second large crater with an age indistinguishable from that of the Chesapeake Bay structure and the two ejecta layers, namely the 100-km-diameter Popigai impact structure in Siberia. The Popigai structure is exposed in Archean crystalline rocks of the Anabar Shield, with overlying Proterozoic to Mesozoic sedimentary sequences, and it is the largest Cenozoic crater on Earth. It is now commonly assumed that the global Upper Eocene microkrystite layer originated from the Popigai impact event; this link has been tentatively confirmed by isotope geochemical methods, as radiometric age determinations cannot resolve age differences of 10 or 20 ka (e.g., Whitehead et al., 2000; Deutsch and Koeberl, 2006).

It is also interesting to note that enhanced levels of ^{3}He were found to coincide with the two Upper Eocene impactoclastic layers. This isotope is a proxy for the influx of extraterrestrial dust and is interpreted as indicating that, during the late Eocene, there was a time of enhanced collision activity in the inner solar system, probably resulting in a higher impact rate than usual (e.g., Farley et al., 1998). The data were interpreted to represent a 2.2 Ma increased flux of interplanetary dust particles (IDPs).

The observed higher impact rate and the enhanced flux of IDPs during that time can be explained by (1) the arrival of long-period comets to the center of the solar system, bound to a perturbation of the Oort Cloud (Farley et al., 1998), or (2) the occurrence of an asteroid shower, triggered by a major collision in the asteroid belt (Tagle and Claeys, 2004).

Thus, there is evidence for the presence of an extraterrestrial component in late Eocene impact ejecta layers, although a strong PGE anomaly, such as that found at the Cretaceous-Tertiary boundary, is not observed. This may be the result of one or more factors, including: loss (erosion) of the PGE-bearing fraction from the impact layer at the sites sampled; an impact velocity and geometry that led to a large amount of projectile becoming retained in the crater instead of being released as ejecta (e.g., at the Morokweng impact structure; McDonald et al., 2001); or an achondrite projectile with low concentrations of PGE. Notably, the melt rocks of the Popigai impact structure show enrichments in characteristic siderophile trace elements, the ratios of which may point toward an ordinary chondrite projectile, possibly of the L chondrite type (e.g., Tagle and Claeys, 2005). Tagle and Claeys (2005) used regression techniques on PGE data to derive evidence of an L-chondritic projectile for Popigai. Goderis et al. (2007) noted that the PGE characteristics of melt rocks from the 7.5-km-diameter Wanapitei (37 ± 2 Ma) structure also indicate an ordinary chondrite, which suggests that the projectiles for these two impact structures were of the same general type.

Thus, it appears that two of the Upper Eocene impact craters were thus formed by the same type of projectile. This hypothesis is supported by chromium isotope analyses of several samples from Ocean Drilling Program (ODP) Site 709C (Kyte et al., 2004). The positive $\delta^{53}Cr$ results exclude carbonaceous chondrites, which make cometary sources less likely. Collisions in the main asteroid belt would result in an increase of the terrestrial impact rate, in the form of asteroid showers lasting 2–30 Ma (Zappalà et al., 1998). This would also be consistent with an asteroid shower between ca. 37 and 34 Ma (as proposed by Tagle and Claeys, 2004). However, the association of the layers studied by Kyte et al. (2004) with either Popigai or Chesapeake Bay is not exactly clear. Independent confirmation of a meteoritic component in the Upper Eocene ejecta layers comes from a study by Paquay et al. (2008), who used the Os isotopic record of marine sediments to derive the projectile sizes.

At the Chesapeake Bay impact structure, the situation is less clear cut. The North American tektites do not seem to contain any distinct enrichment in siderophile elements, and analyses of drill core samples from within the structure have yielded a range of results. Most analyses (e.g., Koeberl et al., 1996) were below detection limit for Ir (1 ppb). The highest content of Ir found by Lee et al. (2006) in a clast of impact melt rock from the Science and Technology Park (STP) test hole at Cape Charles, at the center of the Chesapeake Bay structure, was 0.466 ppb. Lee et al. (2006) reported on osmium isotope ratios and PGE concentrations of impact melt rocks. They found that the $^{187}Os/^{188}Os$ ratios of impact melt rocks range from 0.151 to 0.518, and PGE concentrations of some of these rocks are much higher than concentrations in basement gneiss. Together with the osmium isotopes, these data indicate a measurable meteoritic component (0.01%–0.1%) in some impact melt rocks. However, because the PGE abundances in the impact melt rocks are dominated by the target materials, the interelemental PGE ratios of the impact melt rocks are highly variable and nonchondritic (Lee et al., 2006). Due to the limitations of the Os isotopic method, the projectile type for the Chesapeake Bay impact structure cannot be constrained by these analyses.

The completion of the Eyreville core hole, which sampled suevites and an extensive section of the Exmore beds with their associated fragments of impact melt, affords a new opportunity to reassess the extent of meteoritic contamination in the Chesapeake Bay impact rocks. The purpose of this study is to characterize the geochemistry, and particularly the PGE concentrations, of a suite of suevites and breccias along with samples of the basement rock. If a meteoritic component can be resolved above the background contribution from the basement target rocks, it may be possible to use PGE and other elemental ratios to constrain the type of impactor that formed the Chesapeake Bay structure in a similar manner to other impact craters (e.g., McDonald et al., 2001; Tagle and Claeys, 2005; Koeberl et al., 2007).

SAMPLES FROM EYREVILLE CORE HOLE FOR PGE STUDY

Eleven samples from the Eyreville core hole at Chesapeake Bay impact structure were analyzed for major- and trace-element compositions, as well as for the PGE contents. The samples included one example of Exmore breccia, five suevites, one suevite dike, one cataclasite, and three crystalline basement rocks. Short descriptions of these samples are given in Table 1. The sample numbers CB6-X correspond to the numbers CK-X as they were originally recorded in the core sampling.

EXPERIMENTAL METHODS

Thin sections of all samples were investigated using optical microscopy. Modal point counting was performed for the five suevite samples (CB6-095, CB6-098, CB6-101, CB6-107, CB6-116) in order to determine the proportion of the different clasts (i.e., monomineral and rock) and hence the mineralogical balance of the sample. On average, 155 points per thin section were counted. The area of each thin section was investigated with 2 mm space in between each point counted; mineral grains (free in the matrix) and rock clasts (without distinguishing individual minerals within rock clasts) as well as melt particles were characterized; grains/clasts less than 0.2 mm apparent diameter were counted as matrix. For the more fine-grained polymict samples—the sample of Exmore breccia (CB6-038; depth = 526.69 m) and suevitic dike (CB6-139; depth = 1609.36 m)—similar, but more detailed, point counting was performed, with spacing of 0.3 × 1 mm and limit for matrix of 0.05 mm; over 2000 points were counted per thin section.

TABLE 1. PETROGRAPHIC DESCRIPTION OF THE ANALYZED SAMPLES FROM THE EYREVILLE DRILL CORE

Sample	Depth (m)	Lithology	Minerals	Petrographic description
CB6-038	526.69	Exmore breccia	Qtz, Kfs, calcite, glauconite, Ms, Bt, Chl in clasts, Pl, opaque minerals, accessories (garnet, staurolite)*	Typical sample of Exmore breccia, but very melt rich. It contains abundant altered melt (18 vol% determined by thin-section point counting), which is partly replaced by carbonate. There are some clusters of allotriomorph opaque minerals. The sample contains abundant small rock clasts of, e.g., fine-grained sedimentary clasts, polycrystalline quartz, schist, phyllite, granite, and sandstone.
CB6-095	1401.31	Suevite	Qtz, Kfs, Ms, Bt, Pl, opaque minerals, apatite	Suevite with greenish-gray clastic matrix from the upper part of the suevitic impact breccia section. It contains 6.2 vol% of melt (determined by point counting). There are angular to subangular clasts of siltstone <1 cm, rounded clasts of crystalline basement <1 cm, minor dark-purple melt particles <0.8 cm, yellowish weathered clasts or melt particles <2 cm, and large clast (3 cm) of arkose (with rounded gray and white grains).
CB6-098	1418.81	Melt-rich suevite	Qtz, Bt, Ms, feldspar, opaque minerals, carbonate	Melt-rich suevite with gray clastic matrix from the upper part of the suevitic impact breccia section. It contains angular to subrounded gray clasts of siltstone <2 cm; yellowish amoeboidal altered clasts, reddish subangular clast of granite 0.5 cm; large (5-cm) yellowish clast of sandstone, partly melted and altered; white elongated clasts of melt 1 cm; melt particle 2 cm long with olive green altered core. The proportion of the melt particles (determined by point counting) is 34.4 vol%.
CB6-101	1431.10	Melt-poor suevite	Qtz, Kfs, Pl, Ms, Bt, Chl, opaque minerals, titanite, and epidote	Suevite with gray matrix, rich in clasts; with rare melt and abundant crystalline clasts. There are clasts of polycrystalline quartz; angular to subangular clasts of siltstone <0.7 cm; white to gray subangular clasts of schist <2 cm; large yellowish melt particle with partly melted crystalline clast; some dark olive crystals and green pigment, amoeboid, 4.5 cm; abundant small vesicles. The proportion of the melt particles is 0.6 vol% (determined by point counting).
CB6-107	1449.81	Melt-rich suevite	Qtz, feldspar, Ms, Bt, opaque minerals	Suevite with gray matrix, rich in clasts; angular to subangular, often irregularly shaped clasts of mudstone <2 cm; angular brown clasts, amoeboid <3 cm, some with bands; and subrounded clasts of polycrystalline quartz <2 cm. It contains many different melt particles, and the proportion of the melt particles (determined by point counting) is 45.6 vol%.
CB6-116	1480.81	Melt-poor suevite	Qtz, feldspar, Ms, chlorite, opaque minerals	This melt-poor suevite with gray clastic matrix contains mostly fractured clasts of schist/gneiss. One part of the sample consists of gray clasts of schist/gneiss, subangular, <2 cm, in lighter gray matrix; black angular clast of mudstone 1.2 cm; other part is weathered, porous, with ocher pigment in abundant vesicles. The melt particles are rare (constitute about 1.8 vol% of the sample, determined by point counting) and are altered.
CB6-123	1514.30	Mafic cataclasite	Qtz, Kfs, Pl, amphibole (tremolite), Chl, Ms, opaque minerals, carbonate	Cataclasite of mafic rock, very fractured and altered. The rock is dark greenish and contains chlorite and amphibole (tremolite determined by X-ray diffraction). There are abundant clusters of opaque minerals, and fractures are often filled with carbonate.
CB6-134	1570.27	Sillimanite–mica schist	Qtz, Bt, Ms, feldspar, sillimanite, opaque minerals, and tourmaline	Schist with bands of mica and quartz and feldspar grains in between. There are some patches of sillimanite-fibrolite.
CB6-139	1609.36	Suevite dike	Qtz, Ms, Kfs, Bt, Pl, opaque minerals, Chl, and accessories (tourmaline)*	Fine-grained suevite dike, with abundant small melt particles, and mineral and crystalline rock clasts. There are small clasts of schist, granite, and polycrystalline quartz. Melt constitutes about 5.9 vol% (determined by point counting), and there is a large proportion of matrix (71 vol%).
CB6-141	1627.81	Graphite-biotite schist	Bt, Chl, Qtz, Kfs, Pl, opaque minerals, accessories (zircon, apatite)	The schist contains abundant bands of biotite, some mylonitic textures.
CB6-146	1671.74	Granite	Qtz, Pl, Kfs, Ms, carbonate, opaque minerals	Medium- to fine-grained granite, some parts very altered. Opaque minerals are very rare and small.

Note: Qtz—quartz, Kfs—K-feldspar, Pl—plagioclase, Ms—muscovite, Bt—biotite, Chl—chlorite (Kretz, 1983).
*Minerals in order of abundance were determined by point counting; in other cases, the order of abundance is only estimated.

Representative aliquots, weighing ~60 g, were cut, crushed to smaller pieces, and powdered in an agate mill. In the Exmore breccia and suevite samples, we tried to avoid larger clasts. Abundances of major and some trace elements (Ba, Ce, Co, Cr, Cu, Mo, Nb, Ni, Pb, Rb, Sr, Th, U, V, Y, Zn, Zr) were determined by X-ray fluorescence spectrometry (XRF) at the Museum of Natural History, Berlin (Germany) with a SIEMENS SRS 3000 instrument on glass tablets. More details about the method can be found in Schmitt et al. (2004). For loss on ignition (LOI), ~1 g of pulverized sample material was heated in porcelain crucibles in a furnace for 4 h at 1000 °C. LOI was calculated using the weight difference before and after heating. The contents of some major elements (Na, K, Fe) and most trace elements, including rare earth elements (REEs), were determined by instrumental neutron activation analysis (INAA) at the Center for Earth Sciences, University of Vienna (Austria). About 130 mg of each sample powder were sealed in polyethylene capsules. Three international rock standards were used for reference: the carbonaceous chondrite Allende (Smithsonian Institution, Washington, USA; Jarosewich et al., 1987), granite ACE (Centre de Recherche Petrographique et Geochimique, Nancy, France; Govindaraju, 1994), and Devonian Ohio shale SDO-1 (U.S. Geological Survey; Govindaraju, 1989). The standards and samples were irradiated in the 250 kW Triga reactor of the Atomic Institute of the Austrian Universities for 8 h at a neutron flux of 2.10^{12} n cm^{-2} s^{-1}. For more details of the instrumentation and method, see Koeberl (1993) or Son and Koeberl (2005). For major elements, XRF data are reported, and for trace elements, data acquired by the more precise method for each element were used. The major- and trace-element contents of the samples studied for PGEs are given in Table 2.

The contents of PGEs and Au were determined in Cardiff by inductively coupled plasma–mass spectrometry (ICP-MS) after Ni-sulfide fire assay with Te co-precipitation, using signal intensity calibration. All details regarding the procedures for these analyses, as well as related precision and accuracy values, are given in Huber et al. (2001) and McDonald and Viljoen (2006) and in Table 3.

RESULTS AND DISCUSSION

The results of the major- and trace-element compositions for the 11 samples (Table 2), and the results of the PGE analyses by ICP-MS of the samples (Table 3) show that for abundances of the siderophile elements Cr, Co, and Ni, little difference exists between the various sample types. The highest abundances of these elements are found for the cataclasite and one of the schist samples, not for a suevite. Indeed, most samples show contents that are similar to those found in average continental crust (see discussion in Koeberl, 2007). As for the PGEs, the abundances are all relatively low, with Ir contents from 0.03 to 0.09 ppb. The same samples that have elevated Cr, Co, and Ni contents (cataclasite CB6-123 and schist CB6-141) also have the highest Ir contents, whereas the suevites all have Ir contents of 0.03–0.06 ppb. The other PGEs are also generally low, and only Au values show a wider range, probably due to the higher mobility of Au compared to PGEs. There is no correlation between the amount of melt in suevites and the PGE content, indicating that impact melt in Chesapeake Bay suevite is not the carrier of a significant siderophile element component.

The chondrite-normalized PGE and Au abundance patterns for these samples (Fig. 2) show that all samples—irrespective of lithology—have fairly similar patterns, all of which are fractionated and nonchondritic. The lowest abundances are found for those PGEs with the highest volatilization temperature, and the patterns show a reasonably steep slope (over two orders of magnitude) from the left to the right of the diagram. These pattern shapes are typical of many crustal rocks, including many sediments and soils (e.g., Schmidt et al., 1997; McDonald et al., 2001). These patterns are different from those observed for suevites at the Bosumtwi crater (McDonald et al., 2007), which show a positive Pt anomaly in the normalized abundances, similar to basic magmas and associated sulfide mineralization where Pt is enriched over Rh (e.g., Barnes et al., 1985; Schmidt et al., 1997; McDonald et al., 2001; Kinnaird, 2005; Sproule et al., 2007). The absence of any relatively high Ir and other PGE contents, along with the fact that normalized PGE patterns are fractionated relative to chondrite, does not provide any unambiguous evidence for the presence of an extraterrestrial component. In contrast, some low-temperature mobility of PGEs might have influenced the distribution patterns (e.g., Colodner et al., 1993). No clear-cut distinction exists between the impact breccia and basement samples.

The normalized PGE contents of the suevite samples are somewhat variable, similar to those of the basement samples. The PGE and Au contents of all samples are only very slightly higher than those of average continental crust (Schmidt et al., 1997; Peucker-Ehrenbrink and Jahn, 2001). We did not observe values as high as those noted by Lee et al. (2006), who found Ir contents from 0.03 to almost 0.5 ppb in melt rock clasts, and similarly enriched PGE contents. They also noted fractionated PGE patterns in all of their impact melt rocks and breccias containing impact melt clasts. However, in our samples, no distinction exists in the contents and the overall normalized abundance patterns between the suevite and other breccia samples and basement samples. This similarity makes it impossible to calculate and subtract any indigenous siderophile component. Thus, our data do not indicate the presence of a meteoritic component in suevites from the Eyreville core hole at the Chesapeake Bay impact structure.

SUMMARY AND CONCLUSIONS

A search for a meteoritic component in suevites and Exmore breccia samples of the Chesapeake Bay impact structure was carried out. This involved analyzing the PGE contents of five suevites, one suevite dike, one cataclasite, one Exmore breccia, and three crystalline basement rocks. Unfortunately, the current data show no discernible differences in the contents of the platinum group

TABLE 2. MAJOR- AND SELECTED TRACE-ELEMENT DATA FOR THE SAMPLES FROM EYREVILLE CORE THAT WERE ANALYZED FOR PLATINUM GROUP ELEMENT CONTENTS

Sample no.	CB6-038	CB6-095	CB6-098	CB6-101	CB6-107	CB6-116	CB6-123	CB6-134	CB6-139	CB6-141	CB6-146
Depth (m)	526.69	1401.31	1418.81	1431.10	1449.81	1480.81	1514.30	1570.27	1609.36	1627.81	1671.74
Lithology	Exmore	Suevite	Suevite	Suevite	Suevite	Suevite	Cataclasite	Schist	Suevite dike	Schist	Granite
(wt%)											
SiO_2	70.5	68.9	64.3	68.1	67.2	61.9	46.0	60.2	55.6	49.6	72.5
TiO_2	0.72	0.83	0.96	0.87	0.99	0.92	1.44	0.93	0.91	1.24	0.15
Al_2O_3	12.3	14.0	14.8	14.4	15.9	17.1	17.0	20.0	20.5	15.7	14.4
Fe_2O_3	4.02	4.93	6.35	4.82	5.32	6.74	10.9	5.82	6.76	12.50	0.63
MnO	0.07	0.07	0.10	0.08	0.07	0.09	0.27	0.06	0.06	0.11	0.03
MgO	1.30	1.37	2.76	2.10	1.75	3.39	6.59	2.82	1.4	7.51	0.21
CaO	2.46	1.89	1.67	1.27	1.13	1.01	7.06	0.88	1.7	2.62	1.29
Na_2O	1.48	1.65	2.24	2.07	0.75	1.13	2.91	1.18	1.94	1.91	4.69
K_2O	2.41	3.50	2.56	3.21	3.53	4.07	2.09	3.91	4.34	2.53	1.85
P_2O_5	0.12	0.12	0.14	0.14	0.16	0.10	0.15	0.06	0.1	0.16	0.05
SO_3	<0.1	<0.1	0.4	0.1	<0.1	<0.1	0.2	<0.1	0.2	0.5	<0.1
LOI	4.3	2.2	3.1	2.5	2.4	3.4	5.1	4.0	6.3	4.9	3.7
Total	99.68	99.46	99.38	99.66	99.20	99.85	99.71	99.86	99.81	99.28	99.50
(ppm)											
Sc	9.92	12.9	18.6	14.8	15.5	14.9	36.0	23.1	19.4	37.4	5.28
V	80	109	134	105	116	120	223	151	177	228	20
Cr	58.9	68.3	96.1	83.8	68.6	112	262	113	96.3	213	11.9
Co	11.5	14.9	17.6	14.8	17.1	19.4	44.5	11.1	19.2	60.2	0.99
Ni	29	33	34	33	33	39	123	30	39	160	27
Cu	<30	30	<30	<30	31	<30	54	<30	<30	52	<30
Zn	78	113	113	100	129	99	130	129	135	114	63
As	6.33	6.83	13.5	5.75	34.5	7.70	15.2	<0.6	0.32	<0.9	<0.9
Se	<1	<2	<2.8	<2.4	<2.5	<2.1	<3	<2.3	1.63	<3.3	0.46
Br	12.9	7.53	5.53	4.87	1.86	0.91	1.15	0.71	1.47	0.62	0.76
Rb	77.7	136	115	145	130	141	86.0	167	288	191	178
Sr	168	236	194	181	193	124	447	111	118	135	84
Y	30	45	42	38	51	45	21	46	62	30	67
Zr	211	234	206	215	247	255	110	189	150	98	110
Nb	<10	10	<10	11	11	13	<10	13	31	<10	45
Mo	<10	<10	<10	<10	<10	<10	<10	<10	19	<10	<10
Sb	0.55	1.06	1.43	0.57	2.26	0.33	0.37	0.09	0.09	0.70	<0.1
Cs	2.96	3.70	11.5	6.67	10.2	4.01	3.67	11.9	18.8	97.8	4.19
Ba	433	444	396	429	541	646	244	581	419	146	64
La	24.0	32.8	31.9	30.2	45.9	42.6	9.0	39.1	42.6	11.4	36.0
Ce	49.7	67.6	66.6	64.3	93.3	81.1	19.5	77.9	84.5	24.1	75.2
Nd	20.6	29.6	29.4	26.7	40.4	33.2	10.8	31.3	37.1	12.4	39.1
Sm	4.03	5.60	5.98	5.21	7.76	6.33	2.84	6.16	7.61	3.08	7.96
Eu	1.21	1.42	1.66	1.41	1.84	1.30	1.31	1.69	1.65	1.09	0.59
Gd	4.09	5.15	6.03	5.09	7.37	5.25	3.63	6.81	7.38	3.72	8.19
Tb	0.69	0.91	1.03	0.91	1.25	0.91	0.63	1.08	1.11	0.70	1.29
Tm	0.39	0.50	0.52	0.46	0.56	0.48	0.31	0.54	0.69	0.54	0.78
Yb	2.34	3.07	3.32	2.89	3.81	3.11	2.19	3.26	3.35	2.18	4.56
Lu	0.37	0.47	0.52	0.45	0.58	0.47	0.34	0.39	0.40	0.27	0.73
Hf	5.11	5.62	5.26	5.66	6.52	6.32	2.52	5.34	4.69	2.69	4.80
Ta	0.84	1.06	1.20	1.25	1.46	1.23	0.40	1.29	4.40	0.43	6.33
W	<4.1	1.68	4.29	<1.7	<2.4	n.d.	n.d.	n.d.	n.d.	n.d.	n.d.
Ir (ppb)	<1.3	<2.0	<2.9	<2.4	<2.6	<2.1	<3.1	<2.4	<2.5	<9.0	<1.4
Au (ppb)	<1.1	0.4	0.5	<1.5	0.5	<1.4	<1.9	<1.4	0.7	<1.8	<1.7
Pb	<15	18	27	19	25	<15	<15	18	31	<15	46
Th	7.54	10.1	11.3	9.89	15.2	12.2	0.91	13.2	13.5	1.29	33.6
U	2.09	2.27	2.70	2.21	4.58	2.65	<0.6	4.12	7.82	0.35	38.8

Note: n.d.—not determined; LOI—loss on ignition.

TABLE 3. DATA FOR PLATINUM GROUP ELEMENTS AND Au BY INDUCTIVELY COUPLED PLASMA–MASS SPECTROMETRY (ICP-MS; CARDIFF), FOR SAMPLES FROM CORE LB-07A AND IN REFERENCE MATERIALS WITS-1 (SEE MCDONALD AND VILJOEN, 2006) AND TDB-1 (SEE GOVINDARAJU, 1994; PEUCKER-EHRENBRINK ET AL., 2003)

	CB6-038	CB6-095	CB6-098	CB6-101	CB6-107	CB6-116	CB6-123	CB6-134	CB6-139	CB6-141	CB6-146	Wits-1	TDB-1	Wits-1	TDB-1
Depth (m)	526.69	1401.31	1418.81	1431.10	1449.81	1480.81	1514.30	1570.27	1609.36	1627.81	1671.74	Literature	Literature	Measured	Measured
	Exmore	Suevite	Suevite	Suevite	Suevite	Suevite	Cataclasite	Schist	Suevite dike	Schist	Granite				
Ir	0.03	0.04	0.04	0.03	0.03	0.03	0.09	0.08	0.06	0.09	0.04	1.4 ± 0.3	0.15	1.39	0.10
Ru	0.16	0.16	0.24	0.17	0.15	0.23	0.35	0.34	0.24	0.18	0.22	3.9 ± 0.8	0.30	3.94	0.28
Rh	0.04	0.04	0.07	0.07	0.12	0.08	0.10	0.08	0.05	0.09	0.06	1.1 ± 0.2	0.70	1.13	0.61
Pt	0.81	0.49	0.95	0.23	0.93	0.82	0.64	0.44	0.44	0.40	0.39	5.7 ± 1.6	5.8 ± 1.1	5.98	5.38
Pd	0.72	0.54	0.71	0.70	0.85	0.69	0.56	0.77	1.47	0.53	0.42	5.0 ± 1.2	22.4 ± 1.4	5.10	22.14
Au	0.47	0.72	0.42	0.27	1.07	0.18	0.13	0.59	0.81	0.12	0.06	4.9 ± 2.6	6.3 ± 1.3	8.44	5.66

Note: All data are in ppb.

elements (PGEs) among the suevite, the Exmore breccia, and several crystalline basement rocks, all from the Eyreville core hole. Abundances of the PGEs are uniformly low (e.g., <0.1 ppb Ir), and chondrite-normalized abundance patterns are nonchondritic. These data do not allow any unambiguous verification of an extraterrestrial signature. Thus, the only clear indication for an extraterrestrial component related to this structure remains the earlier detection (Lee et al., 2006) of a meteoritic osmium isotopic signature in impact melt rocks from the STP hydrogeologic test hole on Cape Charles, near the center of the structure. However, the Os isotopic method does not allow specification of

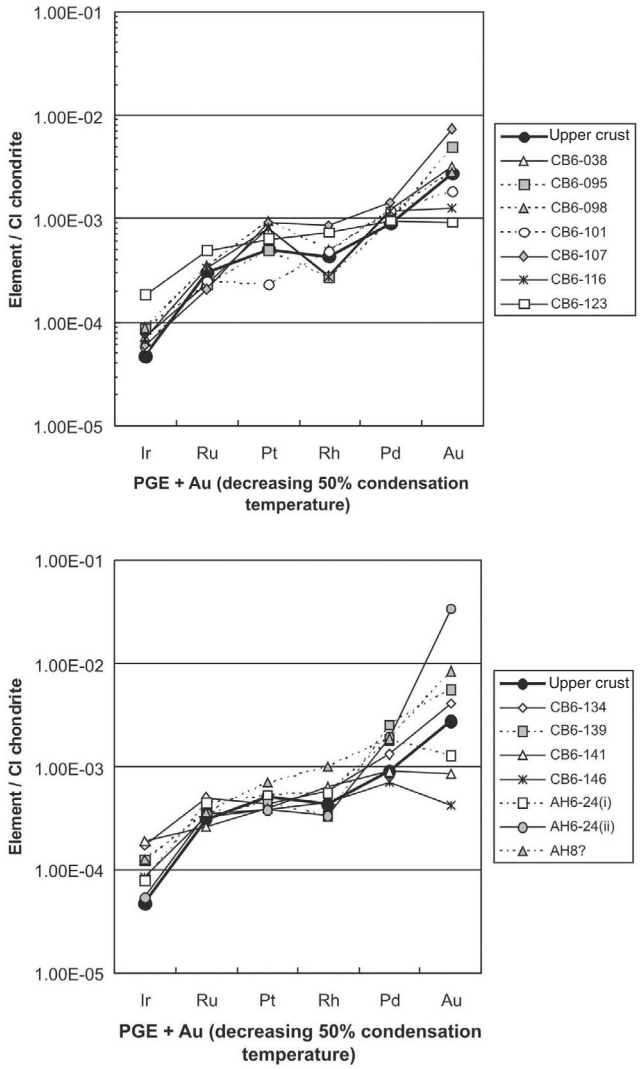

Figure 2. Chondrite-normalized abundances of the platinum group elements (PGEs) and Au for samples of suevitic breccia, Exmore breccia, and basement rocks from the Eyreville core hole, Chesapeake Bay impact structure. Upper crust values are from Peucker-Ehrenbrink and Jahn (2001), except Rh (Wedepohl, 1995) and Au (Schmidt et al., 1997). Chondrite normalization factors are from Lodders (2003).

the projectile type. Thus, the nature of the Chesapeake Bay projectile remains ambiguous. In contrast to the situation at impact craters such as Morokweng and Clearwater East, where an obvious meteoritic signature is recorded by PGE contents and ratios in the impact melt rocks, Cr isotopes, and even rare fragments of projectile (McDonald et al., 2001; McDonald, 2002; Maier et al., 2006), the determination of the type of impactor at Chesapeake Bay remains elusive. Constraints on the impactor type would be helpful in the discussion of the evidence of an asteroid versus a comet shower during the late Eocene, and in general to determine if the various late Eocene impact events had a common source or if the large impact events were just coincidental.

ACKNOWLEDGMENTS

The drilling at Eyreville was supported by the International Continental Scientific Drilling Program (ICDP), the U.S. Geological Survey (USGS), and the National Aeronautics and Space Administration (NASA). DOSECC, Inc., conducted the administrative and operational management of the deep drilling project. We thank the Buyrn family for use of their land as a drilling site, and the scientific and technical staff of the Chesapeake Bay Impact Structure Drilling Project for their many contributions. The present work was supported by the Austrian Science Foundation FWF, project P18862-N10 (to Koeberl). We appreciate helpful and constructive reviews by Philippe Claeys, an anonymous reviewer, and editor Ken Miller.

REFERENCES CITED

Barnes, S.-J., Naldrett, A.J., and Gorten, M.P., 1985, Origin of the fractionation of platinum-group elements in terrestrial magmas: Chemical Geology, v. 53, p. 197–214, doi: 10.1016/0009-2541(85)90076-2.

Bodiselitsch, B., Montanari, A., Koeberl, C., and Coccioni, R., 2004, Delayed climate cooling in the late Eocene caused by multiple impacts: High-resolution geochemical studies at Massignano, Italy: Earth and Planetary Science Letters, v. 223, p. 283–302, doi: 10.1016/j.epsl.2004.04.028.

Bottomley, R., Grieve, R., York, D., and Masaitis, V., 1997, The age of the Popigai impact event and its relation to events at the Eocene/Oligocene boundary: Nature, v. 388, p. 365–368, doi: 10.1038/41073.

Colodner, D.C., Boyle, E.A., and Edmond, J.M., 1993, Determination of rhenium and platinum in natural waters and sediments and iridium in sediments by flow injection isotope dilution inductive coupled plasma mass spectrometry: Analytical Chemistry, v. 65, p. 1419–1425, doi: 10.1021/ac00058a019.

Deutsch, A., and Koeberl, C., 2006, Establishing the link between the Chesapeake Bay impact structure and the North American tektite strewn field: The Sr-Nd isotopic evidence: Meteoritics and Planetary Science, v. 41, p. 689–703.

Evans, N.J., Gregoire, D.C., Grieve, R.A.F., Goodfellow, W.D., and Veizer, J., 1993, Use of platinum-group elements for impactor identification: Terrestrial impact craters and Cretaceous-Tertiary boundary: Geochimica et Cosmochimica Acta, v. 57, p. 3737–3748, doi: 10.1016/0016-7037(93)90152-M.

Farley, K.A., Montanari, A., Shoemaker, E.M., and Shoemaker, C.S., 1998, Geochemical evidence for a comet shower in the late Eocene: Science, v. 280, p. 1250–1253, doi: 10.1126/science.280.5367.1250.

Glass, B.P., 1989, North American tektite debris and impact ejecta from DSDP Site 612: Meteoritics, v. 24, p. 209–218.

Glass, B.P., 2002, Upper Eocene impact ejecta/spherule layers in marine sediments: Chemie der Erde, v. 62, p. 173–196, doi: 10.1078/0009-2819-00017.

Glass, B.P., and Burns, C.A., 1987, Late Eocene crystal-bearing spherules: Two layers or one?: Meteoritics, v. 22, p. 265–279.

Glass, B.P., DuBois, D.L., and Ganapathy, R., 1982, Relationship between an Ir anomaly and the North American microtektite layer in Core RC9-58 from the Caribbean Sea: Journal of Geophysical Research, v. 87, p. A425–A428, doi: 10.1029/JB087iS01p0A425.

Glass, B.P., Koeberl, C., Blum, J.D., and McHugh, C.M.G., 1998, Upper Eocene tektite ejecta layer on the continental slope off New Jersey: Meteoritics and Planetary Science, v. 33, p. 229–241.

Glass, B.P., Huber, H., and Koeberl, C., 2004a, Geochemistry of Cenozoic microtektites and clinopyroxene-bearing spherules: Geochimica et Cosmochimica Acta, v. 68, p. 3971–4006, doi: 10.1016/j.gca.2004.02.026.

Glass, B.P., Liu, S.B., and Montanari, A., 2004b, Impact ejecta in Upper Eocene deposits at Massignano, Italy: Meteoritics and Planetary Science, v. 39, p. 589–597.

Goderis, S., Tagle, R., and Claeys, P., 2007, Current situation on the characterization of the late Eocene impact structures using platinum group element (PGE) ratios, *in* Montanari, A., Koeberl, C., Coccioni, R., and Hilgen, F., eds., Penrose Conference "The Late Eocene Earth: Hothouse, Icehouse, and Impacts," Italy, Abstract volume: Frontale di Apiro, Italy, Osservatorio Geologico di Coldigioco, p. 27–28.

Govindaraju, K., 1989, 1989 compilation of working values and sample description for 272 geostandards: Geostandards Newsletter, v. 13, p. 1–113, doi: 10.1111/j.1751-908X.1989.tb00476.x.

Govindaraju, K., 1994, 1994 compilation of working values and sample description for 383 geostandards: Geostandards Newsletter, v. 18, p. 1–158.

Horton, J.W., Jr., and Izett, G.E., 2005, Crystalline-rock ejecta and shocked minerals of the Chesapeake Bay impact structure, USGS-NASA Langley core, Hampton, Virginia, with supplemental constraints on the age of impact, *in* Horton, J.W., Jr., Powars, D.S., and Gohn, G.S., eds., Studies of the Chesapeake Bay Impact Structure—The USGS-NASA Langley Corehole, Hampton, Virginia, and Related Coreholes and Geophysical Surveys: U.S. Geological Survey Professional Paper 1688, p. E1–E30.

Horton, J.W., Jr., Gibson, R.L., Reimold, W.U., Wittmann, A., Gohn, G.S., and Edwards, L.E., 2009, this volume, Chapter 2, Geologic columns for the ICDP-USGS Eyreville B core, Chesapeake Bay impact structure: Impactites and crystalline rocks, 1766 to 1096 m depth, *in* Gohn, G.S., Koeberl, C., Miller, K.G., and Reimold, W.U., eds., The ICDP-USGS Deep Drilling Project in the Chesapeake Bay Impact Structure: Results from the Eyreville Core Holes: Geological Society of America Special Paper 458, doi: 10.1130/2009.2458(02).

Huber, H., Koeberl, C., McDonald, I., and Reimold, W.U., 2001, Geochemistry and petrology of Witwatersrand and Dwyka diamictites from South Africa: Search for an extraterrestrial component: Geochimica et Cosmochimica Acta, v. 65, p. 2007–2016, doi: 10.1016/S0016-7037(01)00569-5.

Jarosewich, E., Clarke, R.S., Jr., and Barrows, J.N., 1987, The Allende meteorite reference sample: Smithsonian Contributions to the Earth Sciences, v. 27, p. 1–49.

Kinnaird, J.A., 2005, Geochemical evidence for multiphase emplacement in the southern Platreef: Transactions of the Institution of Mining and Metallurgy–Section B. Applied Earth Science, v. 114, p. 225–242, doi: 10.1179/037174505X82152.

Koeberl, C., 1993, Instrumental neutron activation analysis of geochemical and cosmochemical samples: A fast and reliable method for small sample analysis: Journal of Radioanalytical and Nuclear Chemistry, v. 168, p. 47–60, doi: 10.1007/BF02040877.

Koeberl, C., 1998, Identification of meteoritic components in impactites, *in* Grady, M.M., Hutchison, R., McCall, G.J.H., and Rothery, D.A., eds., Meteorites: Flux with Time and Impact Effects: Geological Society of London Special Publication 140, p. 133–153.

Koeberl, C., 2007, The geochemistry and cosmochemistry of impacts, *in* Davis, A., ed., Treatise of Geochemistry, Volume 1 (online edition): Elsevier, p. 1.28.1–.28.52, doi: 10.1016/B978-008043751-4/00228-5.

Koeberl, C., and Shirey, S.B., 1997, Re-Os isotope systematics as a diagnostic tool for the study of impact craters and distal ejecta: Palaeogeography, Palaeoclimatology, Palaeoecology, v. 132, p. 25–46, doi: 10.1016/S0031-0182(97)00045-X.

Koeberl, C., Poag, C.W., Reimold, W.U., and Brandt, D., 1996, Impact origin of Chesapeake Bay structure and the source of North American tektites: Science, v. 271, p. 1263–1266, doi: 10.1126/science.271.5253.1263.

Koeberl, C., Shukolyukov, A., and Lugmair, G.W., 2007, Chromium isotopic studies of terrestrial impact craters: Identification of meteoritic components at Bosumtwi, Clearwater East, Lappajärvi, and Rochechouart: Earth and Planetary Science Letters, v. 256, p. 534–546, doi: 10.1016/j.epsl.2007.02.008.

Kretz, R., 1983, Symbols for rock-forming minerals: The American Mineralogist, v. 68, p. 277–279.

Kyte, F.T., and Liu, S., 2002, Iridium and spherules in late Eocene impact deposits: Houston, Texas, Lunar and Planetary Institute, Lunar and Planetary Science, v. 33, abstract 1981 (CD-ROM).

Kyte, F.T., Shukolyukov, A., Hildebrand, A.R., and Lugmair, G.W., 2004. Initial Cr-isotopic and iridium measurements of concentrates from late-Eocene cpx-spherule deposits: Houston, Texas, Lunar Planetary Institute, Lunar and Planetary Science, v. 35, abstract no. 1824 (CD-ROM).

Lee, S.R., Horton, J.W., Jr., and Walker, R.J., 2006, Confirmation of a meteoritic component in impact-melt rocks of the Chesapeake Bay impact structure, Virginia, USA—Evidence from osmium isotopic and PGE systematics: Meteoritics and Planetary Science, v. 41, p. 819–833.

Lodders, K., 2003, Solar system abundances and condensation temperatures of the elements: The Astrophysical Journal, v. 591, p. 1220–1247, doi: 10.1086/375492.

Maier, W.D., Andreoli, M.A.G., McDonald, I., Higgins, M.D., Boyce, A.J., Shukolyukov, A., Lugmair, G.W., Ashwal, L.D., Gräser, P., Ripley, E., and Hart, R., 2006, Discovery of a 25-cm asteroid clast in the giant Morokweng impact crater, South Africa: Nature, v. 441, p. 203–206, doi: 10.1038/nature04751.

Mak, E.K.C., York, D., Grieve, R.A.F., and Dence, M.R., 1976, The age of the Mistastin Lake crater, Labrador, Canada: Earth and Planetary Science Letters, v. 31, p. 345–357, doi: 10.1016/0012-821X(76)90116-3.

McDonald, I., 2002, Clearwater East structure: A re-interpretation of the projectile type using new platinum-group element data from meteorites: Meteoritics and Planetary Science, v. 37, p. 459–464.

McDonald, I., and Viljoen, K.S., 2006, Platinum-group element geochemistry of mantle eclogites: A reconnaissance study of xenoliths from the Orapa kimberlite, Botswana: Transactions of the Institution of Mining and Metallurgy–Section B. Applied Earth Science, v. 115, p. 81–93, doi: 10.1179/174327506X138904.

McDonald, I., Andreoli, M.A.G., Hart, R.J., and Tredoux, M., 2001, Platinum-group elements in the Morokweng impact structure, South Africa: Evidence for the impact of a large ordinary chondrite projectile at the Jurassic-Cretaceous boundary: Geochimica et Cosmochimica Acta, v. 65, p. 299–309, doi: 10.1016/S0016-7037(00)00527-5.

McDonald, I., Peucker-Ehrenbrink, B., Coney, L., Ferrière, L., Reimold, W.U., and Koeberl, C., 2007, Search for a meteoritic component in drill cores from the Bosumtwi impact structure Ghana: Platinum-group element contents and osmium isotopic characteristics: Meteoritics and Planetary Science, v. 42, p. 743–753.

Miller, K.G., Browning, J.V., Aubry, M.-P., Wade, B.S., Katz, M.E., Kulpecz, A.A., and Wright, J.D., 2008, Eocene–Oligocene global climate and sea-level changes: St. Stephens Quarry, Alabama: Geological Society of America Bulletin, v. 120, p. 34–53, doi: 10.1130/B26105.1.

Montanari, A., and Koeberl, C., 2000, Impact Stratigraphy: The Italian Record: Lecture Notes in Earth Sciences, Volume 93: Heidelberg, Springer-Verlag, 364 p.

Montanari, A., Asaro, F., Michel, H.V., and Kennett, J.P., 1993, Iridium anomalies of late Eocene age at Massignano (Italy) and ODP Site 689B, Maud Rise, Antarctica: Palaios, v. 8, p. 420–437, doi: 10.2307/3515017.

Obradovich, J.D., Snee, L.W., and Izett, G.A., 1989, Is there more than one glassy impact layer in the late Eocene?: Geological Society of America Abstracts with Programs, v. 21, no. 6, p. A134.

Palme, H., Janssens, M.J., Takahashi, H., Anders, E., and Hertogen, J., 1978, Meteorite material at five large impact craters: Geochimica et Cosmochimica Acta, v. 42, p. 313–323, doi: 10.1016/0016-7037(78)90184-9.

Paquay, F.S., Ravizza, G.E., Dalai, T.K., and Peucker-Ehrenbrink, B., 2008, Determining chondritic impactor size from the marine osmium isotope record: Science, v. 320, p. 214–218, doi: 10.1126/science.1152860.

Peucker-Ehrenbrink, B., and Jahn, B.-m., 2001, Rhenium-osmium isotope systematics and platinum group element concentrations: Loess and the upper continental crust: Geochemistry, Geophysics, Geosystems, v. 2, p. 2001, doi: 10.1029/2001GC000172.

Peucker-Ehrenbrink, B., Bach, W., Hart, S.R., Blusztajn, J.S., and Abbruzzese, T., 2003, Rhenium-osmium isotope systematics and platinum group element concentrations in oceanic crust from DSDP/ODP Sites 504 and 417/418: Geochemistry, Geophysics, Geosystems, v. 4, no. 7, p. 8911, doi: 10.1029/2002GC000414.

Poag, C.W., and Aubry, M.-P., 1995, Upper Eocene impactites of the U.S. East Coast: Depositional origins, biostratigraphic framework, and correlation: Palaios, v. 10, p. 16–43.

Pusz, A.E., Miller, K.G., Wright, J.D., Katz, M.E., Cramer, B.S., and Kent, D.V., 2009, Stable isotopic response to late Eocene extraterrestrial impacts, *in* Koeberl, C., and Montanari, A., eds., The Late Eocene Earth: Hothouse, Icehouse, and Impacts: Geological Society of America Special Paper 452, p. 83–95, doi: 10.1130/2009.2452(06).

Reimold, W.U., Bartosova, K., Schmitt, R.T., Hansen, B., Crasselt, C., Koeberl, C., Wittmann, A., and Powars, D.S., 2009, this volume, Petrographic observations on the Exmore breccia, ICDP-USGS Drilling at Eyreville, Chesapeake Bay impact structure, USA, *in* Gohn, G.S., Koeberl, C., Miller, K.G., and Reimold, W.U., eds., The ICDP-USGS Deep Drilling Project in the Chesapeake Bay Impact Structure: Results from the Eyreville Core Holes: Geological Society of America Special Paper 458, doi: 10.1130/2009.2458(29).

Schmidt, G., Palme, H., and Kratz, K.-L., 1997, Highly siderophile elements (Re, Os, Ir, Ru, Rh, Pd, Au) in impact melts from three European impact craters (Saaksjärvi, Mien and Dellen): Clues to the nature of the impacting bodies: Geochimica et Cosmochimica Acta, v. 61, p. 2977–2987, doi: 10.1016/S0016-7037(97)00129-4.

Schmitt, R.T., Wittmann, A., and Stoeffler, D., 2004, Geochemistry of drill core samples from Yaxcopoil-1, Chicxulub impact crater, Mexico: Meteoritics and Planetary Science, v. 39, p. 979–1001.

Schmitt, R.T., Bartosova, K., Reimold, W.U., Mader, D., Wittmann, A., Koeberl, C., and Gibson, R.L., 2009, this volume, Geochemistry of impactites and crystalline basement-derived lithologies from the ICDP-USGS Eyreville A and B drill cores, Chesapeake Bay impact structure, Virginia, USA, *in* Gohn, G.S., Koeberl, C., Miller, K.G., and Reimold, W.U., eds., The ICDP-USGS Deep Drilling Project in the Chesapeake Bay Impact Structure: Results from the Eyreville Core Holes: Geological Society of America Special Paper 458, doi: 10.1130/2009.2458(22).

Sherlock, S.C., Kelley, S.P., Parnell, J., Green, P., Lee, P., Osinski, G.R., and Cockell, C.S., 2005, Re-evaluating the age of the Haughton impact event: Meteoritics and Planetary Science, v. 40, p. 1777–1787.

Sherlock, S.C., Kelley, S.P., and Glazovkaya, L., 2006, A new age for the Logoisk impact structure, Belarus, and implications for the late Eocene comet shower, *in* First International Conference on Impact Cratering in the Solar System [abs.]: Noordwijk, the Netherlands, European Space Agency–European Space Research and Technology Centre, 1 p.

Shukolyukov, A., and Lugmair, G.W., 1998, Isotopic evidence for the Cretaceous-Tertiary impactor and its type: Science, v. 282, p. 927–929.

Son, T.H., and Koeberl, C., 2005, Chemical variation within fragments of Australasian tektites: Meteoritics and Planetary Science, v. 40, p. 805–815.

Sproule, R.A., Sutcliffe, R., Tracanelli, H., and Lesher, C.M., 2007, Palaeoproterozoic Ni-Cu-PGE mineralisation in the Shakespeare Intrusion, Ontario, Canada: A new style of Nipissing gabbro-hosted mineralisation: Transactions of the Institution of Mining and Metallurgy–Section B. Applied Earth Science, v. 116, p. 188–200, doi: 10.1179/174327507X207492.

Tagle, R., and Claeys, P., 2004, Comet or asteroid shower in the late Eocene?: Science, v. 305, p. 492, doi: 10.1126/science.1098481.

Tagle, R., and Claeys, P., 2005, An ordinary chondrite impactor for the Popigai crater, Siberia: Geochimica et Cosmochimica Acta, v. 69, p. 2877–2889, doi: 10.1016/j.gca.2004.11.024.

Vonhof, H.B., Smit, J., Brinkhuis, H., Montanari, A., and Nederbragt, A.J., 2000, Global cooling accelerated by early late Eocene impacts?: Geology, v. 28, p. 687–690, doi: 10.1130/0091-7613(2000)28<687:GCABEL>2.0.CO;2.

Wedepohl, K.H., 1995, The composition of the continental crust: Geochimica et Cosmochimica Acta, v. 59, p. 1217–1232, doi: 10.1016/0016-7037(95)00038-2.

Whitehead, J., Papanastassiou, D.A., Spray, J.G., Grieve, R.A.F., and Wasserburg, G.J., 2000, Late Eocene impact ejecta: Geochemical and isotopic connections with the Popigai impact structure: Earth and Planetary Science Letters, v. 181, p. 473–487, doi: 10.1016/S0012-821X(00)00225-9.

Winzer, S.R., Lum, R.K.L., and Schuhmann, S., 1976, Rb, Sr and strontium isotopic composition, K/Ar age and large ion lithophile trace element abundances in rock and glasses from the Wanapitei Lake impact structure: Geochimica et Cosmochimica Acta, v. 40, p. 51–57, doi: 10.1016/0016-7037(76)90193-9.

Zachos, J., Pagani, M., Sloan, L., Thomas, E., and Billups, K., 2001, Trends, rhythms, and aberrations in global climate 65 Ma to present: Science, v. 292, p. 686–693, doi: 10.1126/science.1059412.

Zappalà, V., Cellino, A., Gladman, B.J., Manley, S., and Migliorini, F., 1998, Asteroid showers on Earth after family breakup events: Icarus, v. 134, p. 176–179, doi: 10.1006/icar.1998.5946.

Manuscript Accepted by the Society 3 March 2009 Printed in the USA

APPENDIX 4. LIST OF SAMPLES FROM THE EYREVILLE DRILL CORES, CHESAPEAKE BAY IMPACT STRUCTURE, STUDIED IN THE THESIS

Sample	Hole A/B	Box	Slot	Run	Midpoint (m)	Midpoint (feet)	Lithology
CB6-001	A	277	1	123	444.05	1456.85	mudstone
CB6-002	A	277	1	123	444.25	1457.52	siltstone
CB6-003	A	277	2	123	444.61	1458.7	sandstone
CB6-004	A	282	2	126	451.77	1482.17	Exmore breccia
CB6-005	A	283	2	126	452.6	1484.92	Exmore breccia
CB6-006	A	286	2	128	457.72	1501.71	Exmore breccia
CB6-007	A	288	1	129	459.49	1507.53	Exmore breccia (+ mudstone clast)
CB6-008	A	289	1	129	460.39	1510.48	siltstone
CB6-009	A	289	1	129	460.74	1511.61	graywacke
CB6-010	A	292	1	130	464.09	1522.6	Exmore breccia
CB6-011	A	295	1	132	467.33	1533.23	Exmore breccia
CB6-012	A	298	1	133	470.76	1544.5	Exmore breccia
CB6-013	A	299	2	133	472.65	1550.69	Exmore breccia
CB6-014	A	302	1	135	476.14	1562.15	Exmore breccia
CB6-015	A	303	2	136	478.7	1570.55	Exmore breccia
CB6-016	A	306	1	137	481.6	1580.05	Exmore breccia
CB6-017	A	308	2	138	484.3	1588.89	Exmore breccia
CB6-018	A	313	1	139	489.31	1605.34	Exmore breccia
CB6-019	A	314	1	140	490.83	1610.34	Exmore breccia
CB6-020	A	315	2	140	492.68	1616.39	Exmore breccia
CB6-021	A	318	1	141	494.96	1623.89	Exmore breccia
CB6-022	A	322	2	143	499.61	1639.15	Exmore breccia
CB6-023	A	323	2	144	500.66	1642.6	Exmore breccia
CB6-024	A	324	2	144	501.87	1646.55	Exmore breccia
CB6-025	A	325	2	145	503.45	1651.75	Exmore breccia
CB6-026	A	327	2	146	507.14	1663.85	clast in Exmore breccia
CB6-027	A	329	1	147	508.59	1668.6	Exmore breccia
CB6-028	A	332	2	148	512.56	1681.63	clast in Exmore breccia
CB6-029	A	333	1	148	513.02	1683.15	Exmore breccia
CB6-030	A	334	1	148	514.17	1686.9	Exmore breccia
CB6-031	A	335	1	149	515.41	1690.97	Exmore breccia
CB6-032	A	339	1	151	519.38	1703.99	Exmore breccia (+ mylonitic clast)
CB6-033	A	340	2	152	521.38	1710.55	Exmore breccia (+ impact melt clast?)
CB6-034	A	341	1	152	521.74	1711.75	Exmore breccia
CB6-035	A	341	1	152	522.02	1712.65	Exmore breccia
CB6-036	A	342	1	152	523.28	1716.8	Exmore breccia
CB6-037	A	343	2	153	524.33	1720.25	Exmore breccia
CB6-038	A	346	1	154	526.69	1728.0	Exmore breccia
CB6-039	A	346	2	154	527.81	1731.66	graywacke
CB6-040	A	355	2	157	537.27	1762.7	graywacke
CB6-041	A	359	2	159	542.32	1779.25	clay/mudstone
CB6-042	A	378	1	166	563.83	1849.85	Exmore breccia
CB6-043	A	381	1	167	567.51	1861.9	clay/mudstone
CB6-044	A	384	2	168	571.36	1874.55	Exmore breccia
CB6-045	A	395	1	172	583.14	1913.2	Exmore breccia (+ sandstone clast)
CB6-046	A	404	1	176	591.56	1940.8	red clay
CB6-047	A	410	2	179	599.0	1965.24	Exmore breccia
CB6-048	A	412	2	179	601.61	1973.8	graywacke
CB6-049	A	429	1	186	622.14	2041.15	sandstone
CB6-050	A	443	1	195	644.55	2114.65	red clay

APPENDIX 4. *CONTINUED* LIST OF SAMPLES FROM THE EYREVILLE DRILL CORES, CHESAPEAKE BAY IMPACT STRUCTURE, STUDIED IN THE THESIS

Sample	Hole A/B	Box	Slot	Run	Midpoint (m)	Midpoint (feet)	Lithology
CB6-051	A	452	1	198	655.12	2149.35	arkose
CB6-052	A	466	2	207	678.68	2226.65	siltstone
CB6-053	A	466	2	208	680.31	2232.0	clay/mudstone
CB6-054	A	473	2	210	688.23	2257.98	graywacke
CB6-055	A	491	1	217	710.24	2330.2	graywacke
CB6-056	A	500	1	222	721.4	2366.8	red clay
CB6-057	A	514	3	230	743.39	2438.95	graywacke
CB6-058	A	521	3	236	760.23	2494.2	siltstone
CB6-059	A	522	1	236	761.79	2499.3	vitrinite
CB6-060	A	539	1	253	802.97	2634.43	graywacke
CB6-061	A	546	2	259	822.28	2697.77	graywacke
CB6-062	A	554	2	266	841.61	2761.2	mudstone
CB6-063	A	563	1	273	863.15	2831.85	Exmore breccia
CB6-064	A	579	3	289	904.59	2967.82	graywacke
CB6-065	A	584	2	294	915.8	3004.59	graywacke
CB6-066	A	593	4	304	940.34	3085.1	graywacke
CB6-067	B	85	1	98	989.18	3245.35	graywacke
CB6-068	B	91	1	104	1007.3	3304.77	mudstone
CB6-069	B	100	1	116	1036.76	3401.45	mudstone
CB6-070	B	109	3	126	1065.72	3496.45	siltstone/graywacke
CB6-071	B	112	1	129	1073.4	3521.65	gravelly sand
CB6-072	B	119	4	137	1096.78	3598.37	medium-grained granite
CB6-073	B	127	1	149	1118.02	3668.03	medium-grained granite
CB6-074	B	129	2	151	1123.89	3687.3	pegmatite/coarse-grained granite
CB6-075	B	135	5	158	1140.52	3741.85	coarse granite/granitic gneiss
CB6-076	B	138	3	163	1147.47	3764.65	xenolith
CB6-077	B	146	4	193	1174.01	3851.75	pegmatite/coarse-grained granite
CB6-078	B	147	2	194	1175.07	3855.22	xenolith
CB6-079	B	162	4	227	1212.36	3977.55	granitic gneiss
CB6-080	B	166	1	235	1221.33	4007.0	coarse-grained granite
CB6-081	B	172	5	247	1240.06	4068.45	fine-grained granite
CB6-082	B	186	3	273	1276.32	4187.4	medium-grained granite
CB6-083	B	193	4	282	1294.81	4248.05	medium-grained granite
CB6-084	B	211	4	311	1346.38	4417.25	medium-grained granite
CB6-085	B	214	5	315	1355.31	4446.56	medium-grained granite
CB6-086	B	220	1	326	1369.02	4491.53	medium-grained granite
CB6-087	B	221	1	327	1371.13	4498.45	gravelly sand
CB6-088	B	221	2	327	1371.37	4499.25	gravelly sand
CB6-089	B	222	4	329	1375.61	4513.15	gravelly sand
CB6-090	B	225	1	334	1382.53	4535.85	amphibolite
CB6-091	B	227	5	336	1390.35	4561.5	gravelly sand
CB6-092	B	230	1	339	1396.54	4581.83	gravelly sand with reworked suevite
CB6-093	B	231	1	340	1399.22	4590.62	melt-rich suevite
CB6-094	B	231	2	340	1399.73	4592.28	melt-rich suevite
CB6-095	B	231	5	340	1401.31	4597.48	suevite
CB6-096	B	234	3	343	1409.3	4623.7	melt-rich suevite
CB6-097	B	235	4	344	1412.75	4635.0	melt-rich suevite
CB6-098	B	237	5	346	1418.81	4654.9	melt-rich suevite
CB6-099	B	238	5	347	1421.65	4664.2	melt-rich suevite
CB6-100	B	240	4	350	1427.01	4681.8	suevite

APPENDIX 4. *CONTINUED* LIST OF SAMPLES FROM THE EYREVILLE DRILL CORES, CHESAPEAKE BAY IMPACT STRUCTURE, STUDIED IN THE THESIS

Sample	Hole A/B	Box	Slot	Run	Midpoint (m)	Midpoint (feet)	Lithology
CB6-101	B	241	5	352	1431.1	4695.2	melt-poor suevite
CB6-102	B	243	5	354	1436.56	4713.12	melt-poor suevite
CB6-103	B	245	1	355	1440.0	4724.4	melt-poor suevite
CB6-104	B	246	3	356	1443.65	4736.4	melt-poor suevite
CB6-105	B	247	2	357	1445.76	4743.3	melt-poor suevite
CB6-106	B	247	4	357	1446.95	4747.2	melt-poor suevite
CB6-107	B	248	3	359	1449.81	4756.6	melt-rich suevite
CB6-108	B	248	5	360	1451.01	4760.54	melt-rich suevite/impact melt rock
CB6-109	B	249	3	360	1452.33	4764.86	melt-rich suevite
CB6-110	B	250	3	360	1455.22	4774.34	melt-rich suevite
CB6-111	B	251	3	361	1458.22	4784.2	melt-poor suevite
CB6-112	B	251	4	361	1459.2	4787.4	conglomerate clast in suevite
CB6-113	B	253	3	362	1463.98	4803.1	melt-rich suevite
CB6-114	B	254	4	362	1467.37	4814.2	melt-poor suevite
CB6-115	B	256	5	364	1473.46	4834.18	melt-rich suevite
CB6-116	B	259	2	366	1480.81	4858.3	melt-poor suevite
CB6-117	B	259	3	366	1481.74	4861.35	melt-poor suevite
CB6-118	B	260	3	367	1484.13	4869.2	melt-poor suevite
CB6-119	B	263	4	369	1494.04	4901.7	cataclastic gneiss
CB6-120	B	267	2	372	1504.25	4935.2	melt-rich suevite
CB6-121	B	268	5	373	1508.49	4949.12	melt-rich suevite
CB6-122	B	270	1	373	1511.86	4960.18	cataclastic gneiss
CB6-123	B	270	5	374	1514.3	4968.16	mafic cataclasite
CB6-124	B	271	4	374	1516.23	4974.51	cataclastic gneiss
CB6-125	B	273	4	375	1522.72	4995.8	conglomerate clast in suevite
CB6-126	B	275	5	376	1529.27	5017.3	melt-poor suevite
CB6-127	B	277	5	377	1535.4	5037.4	melt-poor suevite
CB6-128	B	278	2	377	1536.51	5041.05	polymict lithic breccia
CB6-129	B	280	3	379	1542.65	5061.2	cataclastic schist/gneiss
CB6-130	B	281	5	381	1547.41	5076.8	cataclastic schist/gneiss
CB6-131	B	283	1	382	1551.49	5090.18	graphitic breccia
CB6-132	B	285	2	385	1559.51	5116.5	graphitic breccia
CB6-133	B	285	3	385	1560.3	5119.1	mica schist
CB6-134	B	287	4	392	1570.27	5151.8	sillimanite mica schist
CB6-135	B	288	5	396	1576.79	5173.2	biotite-muscovite schist
CB6-136	B	292	2	405	1592.34	5224.2	cataclastic pegmatite
CB6-137	B	293	4	408	1597.21	5240.2	mica schist
CB6-138	B	295	3	413	1603.58	5261.1	suevite dike
CB6-139	B	297	2	416	1609.36	5280.05	cataclastic breccia dike
CB6-140	B	300	4	424	1622.88	5324.4	granite
CB6-141	B	302	3	426	1627.81	5340.59	graphite-biotite schist
CB6-142	B	304	5	430	1635.15	5364.66	graphite-sillimanite mica schist
CB6-143	B	309	5	434	1649.18	5410.7	muscovite-biotite schist
CB6-144	B	312	2	437	1655.9	5432.75	pegmatite
CB6-145	B	316	2	442	1667.8	5471.8	mica schist
CB6-146	B	317	5	444	1671.74	5484.7	granite
CB6-147	B	323	4	451	1688.96	5541.2	mica schist
CB6-148	B	327	3	455	1700.17	5578.0	pegmatite
CB6-149	B	341	1	481	1740.99	5711.9	pegmatite
CB6-150	B	350	2	497	1766.1	5794.3	pegmatite

APPENDIX 4. *CONTINUED* LIST OF SAMPLES FROM THE EYREVILLE DRILL CORES, CHESAPEAKE BAY IMPACT STRUCTURE, STUDIED IN THE THESIS

Sample	Hole A/B	Box	Slot	Run	Midpoint (m)	Midpoint (feet)	Lithology
KB-1	B	228	4	337	1393.12	4570.6	suevite boulder
KB-2	B	232	2	341	1402.83	4602.65	impact melt rock
KB-3	B	232	5	341	1404.35	4607.58	impact melt rock
KB-4	B	233	2	342	1405.71	4611.9	impact melt rock
KB-5	B	235	4	344	1412.87	4635.6	suevite
KB-6	B	255	1	367	1468.65	4818.5	conglomerate clast in suevite
KB1-09	B	222	1	328	1373.75	4507.25	gravelly sand
KB2-09	B	222	2	328	1374.54	4509.95	gravelly sand
KB3-09	B	222	4	329	1375.46	4512.65	gravelly sand
KB4-09	B	227	4	336	1389.84	4559.85	gravelly sand
KB5-09	B	227	5	336	1390.88	4563.25	gravelly sand
KB6-09	B	228	1	337	1391.4	4564.95	gravelly sand
KB7-09	B	228	3	337	1392.23	4567.7	gravelly sand
KB8-09	B	228	4	337	1393.48	4571.8	cataclastic gneiss
KB9-09	B	221	3	328	1372.29	4502.3	gravelly sand
KB10-09	B	221	5	328	1373.27	4505.65	gravelly sand

CURRICULUM VITAE

KATERINA BARTOSOVA

Personal:
born: 6. 12. 1979
nationality: Czech
marital status: married

Address:
Högelmüllergasse 6/13
A-1050 Vienna, Austria

EDUCATION:

2007–now**:** PhD at the University of Vienna, Department of Lithospheric Research
Impact research, Petrography, Geochemistry
Reseach topic: Petrographic and geochemical investigations of impactites from the Chesapeake Bay impact structure
Supervisor: Prof. Dr. Christian Koeberl

Masters degree: 1999–2004
Charles University Prague
Faculty of Natural Sciences
Master's degree in Geology with a specialization in Geochemistry
Diploma work: Chemical resistance of continuous basalt fibers
Supervisor: RNDr. Petr Jakes PhD.

High school: 1994–1998
Grammar school in Dobruska

WORK EXPERIENCE:

2005–2006
Celtic Surveys, Dunshaughlin, Ireland – geodesy/survey assistant

2004–2005
MDI-Technologies, Prague, Czech Republic – part time scientist – experimental processing and testing of continuous basalt fibers

PARTICIPATION AT CONFERENCES, COURSES, AND WORKSHOPS:

72nd Annual Meeting of the Meteoritical Society, Nancy, France, July 13–18, 2009. Student travel grant.

NIR – PhD-student workshop and excursion, Gardnos– Gol, Norway, June 8–11, 2009.

Rapid Environmental/Climate Changes and Catastrophic Events in Late Cretaceous and Early Paleogene, Gams, Austria, April 24–28, 2009.

European Geosciences Union (EGU) General Assembly 2009, Vienna, Austria, April 19–24, 2009.

Large meteorite impacts and planetary evolution IV, Vredefort Dome, South Africa, August 17–21, 2008. Student travel grant.

71st Annual Meeting of Meteoritical Society, Matsue, Japan, July 28 – August 1, 2008. Student travel grant.

Pangeo conference, Vienna, Austria, September 22–25, 2008.

European Geosciences Union (EGU) General Assembly 2008, Vienna, Austria, April 13–18, 2008.

2007 GSA Annual Meeting and Exposition, Denver, Colorado, USA, October 28–31, 2007.

Hothouse, Icehouse, and Impacts: The Late Eocene Earth, Geological Society of America Penrose Conference, Monte Cònero (Ancona), Italy, October 3–6, 2007.

6th EMU School, Spectroscopic methods in Mineralogy, Vienna, Austria, August 30 – September 8, 2004.

Melts, Glasses, Magmas, led by Prof. Dingwell, Munich, Germany, 2003.

AWARDS:
Synthesys project supported a two weeks stay at the Museum of Natural History in Berlin, where I used an electron microprobe to analyze melt in the impact breccias from the Eyreville drill core, Chesapeake Bay impact structure.

PRESENTATIONS:
Bartosova K. et al. Chesapeake Bay impact structure, Investigations of the ICDP-USGS Eyreville drill core. Museum of Natural History (Mineralogy), Leibniz-Institute at Humboldt University Berlin, Berlin, Germany. 19. March 2009. The talk was part of my research stay in Berlin sponsored by Synthesys.

JOURNAL REVIEWER:
Geological Society of America Special Paper – 1 review (2009)

LIST OF PUBLICATIONS:

Papers published in refereed journals:

Bartosova K., Ferrière L., Koeberl C., Reimold W. U., and Gier S. 2009. Petrographic and shock metamorphic studies of the impact breccia section (1397 – 1551 m depth) of the Eyreville drill core, Chesapeake Bay impact structure, USA. In *The ICDP-USGS deep drilling project in the Chesapeake Bay impact structure: Results from the Eyreville core holes,* edited by Gohn G. S., Koeberl C., Miller K. G., and Reimold W. U. *Geological Society of America Special Paper* 458: 317–348.

Bartosova K., Mader D., Schmitt R. T., Ferrière L., Koeberl C., Reimold W. U., and Brandstätter F. 2009. Geochemistry of the impact breccia section (1397 – 1551 m depth) of the Eyreville drill core, Chesapeake Bay impact structure, USA. In *The ICDP-USGS deep drilling project in the Chesapeake Bay impact structure: Results from the Eyreville core holes,* edited by Gohn G. S., Koeberl C., Miller K. G., and Reimold W. U. *Geological Society of America Special Paper* 458: 397–433.

Reimold W. U., **Bartosova K.**, Schmitt R. T., Hansen B., Crasselt C., Koeberl C., Wittmann A., and Powars D. 2009. Petrographic observations on the Exmore breccia, ICDP-USGS Drilling at Eyreville, Chesapeake Bay impact Structure, USA. In *The ICDP-USGS deep drilling project in the Chesapeake Bay impact structure: Results from the Eyreville core holes,* edited by Gohn G. S., Koeberl C., Miller K. G., and Reimold W. U. *Geological Society of America Special Paper* 458: 655–698.

Schmitt R. T., **Bartosova K.,** Reimold W. U., Mader D., Wittmann A., Koeberl C., and Gibson R. L. 2009. Geochemistry of impactites and crystalline basement derived lithologies from the ICDP-USGS Eyreville A and B drill cores, Chesapeake Bay impact structure, Virginia/USA. In *The ICDP-USGS deep drilling project in the Chesapeake Bay impact structure: Results from the Eyreville core holes,* edited by Gohn G. S., Koeberl C., Miller K. G., and Reimold W. U. *Geological Society of America Special Paper* 458: 481–541.

McDonald I., **Bartosova K.**, and Koeberl C. 2009. Search for a meteoritic component in impact breccia from the Eyreville core, Chesapeake Bay impact structure: Considerations from platinum-group element contents. In *The ICDP-USGS deep drilling project in the Chesapeake Bay impact structure: Results from the Eyreville core holes,* edited by Gohn G. S., Koeberl C., Miller K. G., and Reimold W. U. *Geological Society of America Special Paper* 458: 469–479.

Townsend G. N., Gibson R. L., Horton J. W. Jr., Reimold W. U., Schmitt R. T., and **Bartosova K.** 2009. Petrographic and geochemical comparisons between the lower crystalline basement-derived section and the upper granite and amphibolite megablocks of the Eyreville-B core, Chesapeake Bay impact structure, USA. In *The ICDP-USGS deep drilling project in the Chesapeake Bay impact structure: Results from the Eyreville core holes,* edited by Gohn G. S., Koeberl C., Miller K. G., and Reimold W. U. *Geological Society of America Special Paper* 458: 255–276.

Papers submitted to refereed journals:

Bartosova K., Hecht L., Koeberl C., Libowitzky E., and Reimold W. U. Melt in the impact breccias from the Eyreville drill core, Chesapeake Bay impact structure, USA. Submitted to *Meteoritics and Planetary Science*.

Bartosova K., Gier S., Horton J. W. Jr., Koeberl C., Mader D, and Dypvik H. Petrography, mineralogy, and geochemistry of deep gravelly sand in the Eyreville core, Chesapeake Bay impact structure. Submitted to *Meteoritics and Planetary Science*.

Bartosova K. and Koeberl C. Shock-metamorphism investigations of quartz grains in clasts from impact breccia of the Eyreville drill core, Chesapeake Bay impact structure, USA. Submitted to *Meteoritics and Planetary Science*.

Abstracts published:

Horton J. W. Jr., **Bartosova K.**, Edwards L. E., Gibson R. L., Gohn G. S., Koeberl C., Powars D. S., Reimold W. U., and Wittmann A. 2009. Insights into impact processes and basement rocks of the Chesapeake Bay impact structure from the ICDP-USGS Eyreville cores. GSA Abstracts with Programs, v. 41, no. 7, p. 596.

Bartosova K., Hecht L., Czaja P., Libowitzky E., and Koeberl C. 2009. Melt in the impact breccias from the Eyreville drill core, Chesapeake Bay impact structure – microprobe analyses. Meteoritics and Planetary Science, v. 44, p. A31.

Bartosova K., Koeberl C., and Mader D. 2009. The Late Eocene impact ejecta layer: Chesapeake Bay impact structure (Virginia, USA), and comparison with the K-T event. Rapid Environmental/Climate Changes and Catastrophic Events in Late Cretaceous and Early Paleogene (RECCCE) Workshop, IGCP 555 European Group Meeting. Abstracts and Excursion Guide, p. 7.

Bartosova K., Ferrière L., Koeberl C., and Reimold W. U. 2009. Shock metamorphic studies on suevite from the ICDP-USGS Eyreville drill core, Chesapeake Bay impact structure, Virginia, USA. Geophysical Research Abstracts, v. 11, EGU2009-3412, 2009.

Koeberl C., **Bartosova K.**, and Brandstätter F. 2009. Melt particles in the Chesapeake Bay impact structure Eyreville drillcore – A progress report. Lunar and Planetary Science Conference 40, Abstract no. 1715.

Ferrière L., Koeberl C., Reimold W. U., Hecht L., and **Bartosova K.** 2009. The origin of "toasted quartz" in impactites revisited. Lunar and Planetary Science Conference 40, Abstract no. 1751.

Bartosova K., Ferrière L., Koeberl C., and Brandstätter F. 2008. Melt particles from the impact breccia section, Eyreville B drill core, Chesapeake Bay impact structure, USA. GSA Joint Annual Meeting 2008. GSA Abstracts with programs, v. 40, no. 6, p. 407.

Bartosova K., Ferrière L., Mader D., Koeberl C., Schmitt R. T., and Reimold W. U. 2008. Petrographic and geochemical studies of impact breccia from the Eyreville drill core, Chesapeake Bay impact structure, USA. Journal of Alpine Geology, v. 49, p. 7.

Bartosova K., Koeberl C., and Reimold W. U. 2008. Stratigraphy of the impactite section (1397-1551 m) from the Eyreville drillcore, Chesapeake Bay impact structure, USA. Large Meteorite Impacts and Planetary Evolution IV, Conference Program and Abstract Volume, LPI Contribution no. 1423, p. 44–45.

Bartosova K., Mader D., Schmitt R. T., Koeberl C., and Reimold W. U. 2008. Alteration of impactites from the Chesapeake Bay impact structure, USA. Meteoritics and Planetary Science, v. 43, p. A22.

Bartosova K., Koeberl C., Schmitt R. T., and Brandstätter F. 2008. Investigations of suevite from the Eyreville drillcore, ICDP-USGS Chesapeake Bay impact structure deep drilling project, Virginia, USA. Geophysical Research Abstracts, vol. 10, EGU2008-A-01782, 2008.

Bartosova K., Koeberl C., Schmitt R. T., Reimold W. U., and Ferrière L. 2008. A petrographical, geochemical, and shock metamorphic study of suevite from the Eyreville drillcore, Chesapeake Bay impact structure, USA, Lunar and Planetary Science Conference 39, Abstract no. 1065.

Schmitt R. T., **Bartosova K.**, Reimold W. U., Mader D., Koeberl C., Wittmann A., and Gibson R. L. 2008. Whole-rock geochemistry of impactites and crystalline basement-derived lithologies from the ICDP-USGS Eyreville drill cores, Chesapeake Bay impact structure, Virginia/USA. 86th Annual Meeting of the German Mineralogical Society, Berlin, Germany, abstract #27, 1p.

Bartosova K., Ferrière L., Koeberl C., Reimold W. U., Gibson R., and Schmitt R. T. 2007. Lithological, petrographical, and geochemical investigations of suevite from the Eyreville core, Chesapeake Bay impact structure, GSA Abstracts with Programs, v. 39, no. 6, p. 451.

Bartosova K., Ferrière L., Koeberl C., and Reimold W. U. 2007. Investigations of melt particles in suevite from the Eyreville B core, Chesapeake Bay impact structure, GSA Abstracts with Programs, v. 39, no. 6, p. 314.

Mader D., **Bartosova K.**, Koeberl C., and Reimold W. U. 2007. Stable carbon isotope studies of impact breccia clasts from the Eyreville core, Chesapeake Bay impact structure, Virginia, USA, GSA Abstracts with Programs, v. 39, no. 6, p. 314.

Reimold W. U., Kenkmann T., Gibson R. L., **Bartosova K.**, Schmitt R. T., Hecht L., Koeberl C., and Horton J. W. Jr. 2007. Dike breccias in the deep basement-derived section of the Eyreville B core, Chesapeake Bay impact structure, GSA Abstracts with Programs, v. 39, no. 6, p. 451.

Reimold W. U., **Bartosova K.**, Schmitt R. T., Wittek A., and Koeberl C. 2007. First observations on Exmore breccia from the ICDP-USGS Eyreville core, Chesapeake Bay impact structure, GSA Abstracts with Programs, v. 39, no. 6, p. 314.

Schmitt R. T., Reimold W. U., **Bartosova K.**, and Koeberl C. 2007. Chemical composition of rock types from the Eyreville A and B drill cores, Chesapeake Bay impact structure, Virginia/USA, GSA Abstracts with Programs, v. 39, no. 6, p. 315.

Bartosova K., Koeberl C., Reimold W. U., Gohn G. S., Miller K. G. 2007. Scientific drilling at the Chesapeake Bay Impact Structure, Virginia, USA, Hothouse, Icehouse, and Impacts: The Late Eocene Earth, Geological Society of America Penrose conference, Monte Cònero (Ancona), Italy, 2007, Abstracts with Program and Field Trip Guide, p. 11–13.